frontiers | Research Topics

Abiotic stress alleviation in plants: Morpho-physiological and molecular aspects

Edited by
Diaa Abd El Moneim, Mehdi Rahimi, Mahmoud Magdy and Mohammad Golam Mostofa

Published in
Frontiers in Plant Science

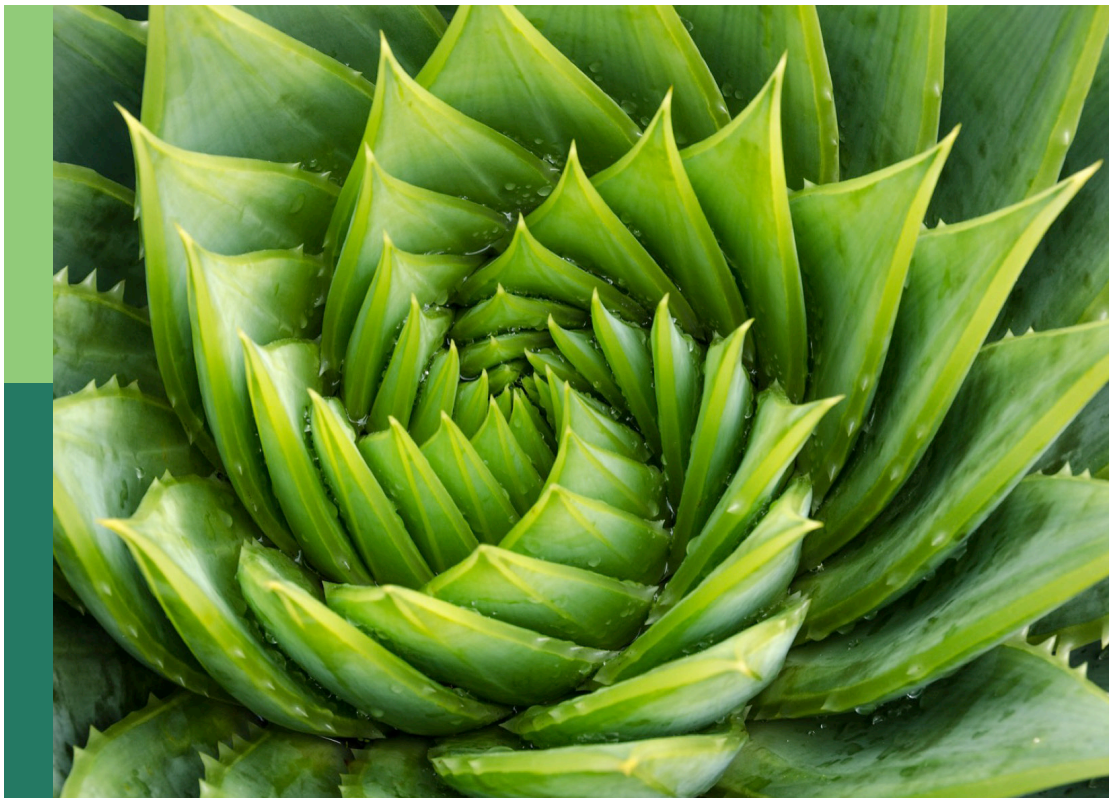

FRONTIERS EBOOK COPYRIGHT STATEMENT

The copyright in the text of individual articles in this ebook is the property of their respective authors or their respective institutions or funders. The copyright in graphics and images within each article may be subject to copyright of other parties. In both cases this is subject to a license granted to Frontiers.

The compilation of articles constituting this ebook is the property of Frontiers.

Each article within this ebook, and the ebook itself, are published under the most recent version of the Creative Commons CC-BY licence. The version current at the date of publication of this ebook is CC-BY 4.0. If the CC-BY licence is updated, the licence granted by Frontiers is automatically updated to the new version.

When exercising any right under the CC-BY licence, Frontiers must be attributed as the original publisher of the article or ebook, as applicable.

Authors have the responsibility of ensuring that any graphics or other materials which are the property of others may be included in the CC-BY licence, but this should be checked before relying on the CC-BY licence to reproduce those materials. Any copyright notices relating to those materials must be complied with.

Copyright and source acknowledgement notices may not be removed and must be displayed in any copy, derivative work or partial copy which includes the elements in question.

All copyright, and all rights therein, are protected by national and international copyright laws. The above represents a summary only. For further information please read Frontiers' Conditions for Website Use and Copyright Statement, and the applicable CC-BY licence.

ISSN 1664-8714
ISBN 978-2-8325-3732-9
DOI 10.3389/978-2-8325-3732-9

About Frontiers

Frontiers is more than just an open access publisher of scholarly articles: it is a pioneering approach to the world of academia, radically improving the way scholarly research is managed. The grand vision of Frontiers is a world where all people have an equal opportunity to seek, share and generate knowledge. Frontiers provides immediate and permanent online open access to all its publications, but this alone is not enough to realize our grand goals.

Frontiers journal series

The Frontiers journal series is a multi-tier and interdisciplinary set of open-access, online journals, promising a paradigm shift from the current review, selection and dissemination processes in academic publishing. All Frontiers journals are driven by researchers for researchers; therefore, they constitute a service to the scholarly community. At the same time, the *Frontiers journal series* operates on a revolutionary invention, the tiered publishing system, initially addressing specific communities of scholars, and gradually climbing up to broader public understanding, thus serving the interests of the lay society, too.

Dedication to quality

Each Frontiers article is a landmark of the highest quality, thanks to genuinely collaborative interactions between authors and review editors, who include some of the world's best academicians. Research must be certified by peers before entering a stream of knowledge that may eventually reach the public - and shape society; therefore, Frontiers only applies the most rigorous and unbiased reviews. Frontiers revolutionizes research publishing by freely delivering the most outstanding research, evaluated with no bias from both the academic and social point of view. By applying the most advanced information technologies, Frontiers is catapulting scholarly publishing into a new generation.

What are Frontiers Research Topics?

Frontiers Research Topics are very popular trademarks of the *Frontiers journals series*: they are collections of at least ten articles, all centered on a particular subject. With their unique mix of varied contributions from Original Research to Review Articles, Frontiers Research Topics unify the most influential researchers, the latest key findings and historical advances in a hot research area.

Find out more on how to host your own Frontiers Research Topic or contribute to one as an author by contacting the Frontiers editorial office: frontiersin.org/about/contact

Abiotic stress alleviation in plants: Morpho-physiological and molecular aspects

Topic editors

Diaa Abd El Moneim — Arish University, Egypt

Mehdi Rahimi — Graduate University of Advanced Technology, Iran

Mahmoud Magdy — Ain Shams University, Egypt

Mohammad Golam Mostofa — Michigan State University, United States

Citation

Abd El Moneim, D., Rahimi, M., Magdy, M., Mostofa, M. G., eds. (2023). *Abiotic stress alleviation in plants: Morpho-physiological and molecular aspects*. Lausanne: Frontiers Media SA. doi: 10.3389/978-2-8325-3732-9

Table of contents

07 Editorial: Abiotic stress alleviation in plants: morpho-physiological and molecular aspects
Mahmoud Magdy, Mohammad Golam Mostofa, Mehdi Rahimi and Diaa Abd El Moneim

12 The significance of calcium-sensing receptor in sustaining photosynthesis and ameliorating stress responses in plants
Rui Bai, Chunming Bai, Xiaori Han, Yifei Liu and Jean Wan Hong Yong

20 Effects of hydrogen peroxide priming on yield, photosynthetic capacity and chlorophyll fluorescence of waterlogged summer maize
Shouran Wang, Juan Hu, Baizhao Ren, Peng Liu, Bin Zhao and Jiwang Zhang

35 Sprayed biodegradable liquid film improved the freezing tolerance of cv. Cabernet Sauvignon by up-regulating soluble protein and carbohydrate levels and alleviating oxidative damage
Xing Han, Fei Yao, Ting-ting Xue, Zhi-lei Wang, Ying Wang, Xiao Cao, Miao Hui, Dong Wu, Yi-han Li, Hua Wang and Hua Li

54 Arbuscular mycorrhiza mitigates zinc stress on *Eucalyptus grandis* through regulating metal tolerance protein gene expression and ionome uptake
Li-Na Han, Si-Jia Wang, Hui Chen, Ying Ren, Xian-An Xie, Xing-Yang Wang, Wen-Tao Hu and Ming Tang

67 Overexpression of *Pyrus sinkiangensis* HAT5 enhances drought and salt tolerance, and low-temperature sensitivity in transgenic tomato
Xiaoyan Liu, Aowei Li, Saisai Wang, Chengfang Lan, Yize Wang, Jin Li and Jianbo Zhu

81 PIN1 regulates epidermal cells development under drought and salt stress using single-cell analysis
George Bawa, Zhixin Liu, Rui Wu, Yaping Zhou, Hao Liu, Susu Sun, Yumeng Liu, Aizhi Qin, Xiaole Yu, Zihao Zhao, Jincheng Yang, Mengke Hu and Xuwu Sun

95 An uncharacterized gene *Lb1G04794* from *Limonium bicolor* promotes salt tolerance and trichome development in *Arabidopsis*
Xiangmei Jiao, Boqing Zhao, Baoshan Wang and Fang Yuan

109 CARK3-mediated ADF4 regulates hypocotyl elongation and soil drought stress in Arabidopsis
Lu Peng, Juan He, Huan Yao, Qin Yu, Qian Zhang, Kexuan Li, Yaling Huang, Li Chen, Xufeng Li, Yi Yang and Xiaoyi Li

121 Low red to far-red light ratio promotes salt tolerance by improving leaf photosynthetic capacity in cucumber
Yanxiu Miao, Xingxing Gao, Bin Li, Wenjiao Wang and Longqiang Bai

134 OsGLP participates in the regulation of lignin synthesis and deposition in rice against copper and cadmium toxicity
Xiangchao ShangGuan, Ying Qi, Aiguo Wang, Yingnan Ren, Yu Wang, Tengwei Xiao, Zhenguo Shen, Qi Wang and Yan Xia

148 Transcriptome profiling disclosed the effect of single and combined drought and heat stress on reprogramming of genes expression in barley flag leaf
Krzysztof Mikołajczak, Anetta Kuczyńska, Paweł Krajewski, Michał Kempa and Maria Nuc

169 Proteomics approach to investigating osmotic stress effects on pistachio
Rambod Pakzad, Foad Fatehi, Mansour Kalantar and Mahmood Maleki

184 H^+-pyrophosphatases enhance low nitrogen stress tolerance in transgenic *Arabidopsis* and wheat by interacting with a receptor-like protein kinase
Huijuan Zhang, Ming Chen, Chengjie Xu, Rongbang Liu, Wensi Tang, Kai Chen, Yongbin Zhou, Zhaoshi Xu, Jun Chen, Youzhi Ma, Weiguo Chen, Daizhen Sun and Hua Fan

195 Rice DST transcription factor negatively regulates heat tolerance through ROS-mediated stomatal movement and heat-responsive gene expression
Yanfei Ding, Mei Zhou, Ke Wang, Aili Qu, Shanshan Hu, Qiong Jiang, Keke Yi, Feijuan Wang, Chong Cai, Cheng Zhu and Zhixiang Chen

214 Enriching drought resistance in *Solanum lycopersicum* using Abscisic acid as drought enhancer derived from *Lygodium japonicum*: A new-fangled computational approach
Kahkashan Perveen, Alanoud T. Alfagham, Sandip Debnath, Najat A. Bukhari, Dong-Qing Wei, Najla A. Alshaikh and Aisha Saleh Alwadai

223 A novel gene *SpCTP3* from the hyperaccumulator *Sedum plumbizincicola* redistributes cadmium and increases its accumulation in transgenic *Populus* × *canescens*
Shaocui Li, Renying Zhuo, Miao Yu, Xiaoyu Lin, Jing Xu, Wenmin Qiu, Haiying Li and Xiaojiao Han

237 A HD-Zip I transcription factor from physic nut, *JcHDZ21*, confers sensitive to salinity in transgenic Arabidopsis
Yuehui Tang, Jingrui Peng, Jin Lin, Miaomiao Zhang, Yun Tian, Yaqian Shang, Shuying Chen, Xinxin Bao and Qiyuan Wang

248 Transcriptome analysis provides insights into the response of *Lotus corniculatus* roots to low-phosphorus stress
Xin Zhao, Ke-ke Chen, Lei-ting Wang, Li-Li Zhao and Pu-Chang Wang

261 *SiNCED1*, a 9-cis-epoxycarotenoid dioxygenase gene in *Setaria italica*, is involved in drought tolerance and seed germination in transgenic Arabidopsis
Yuan Huang, Yang Jiao, Sha Yang, Dandan Mao, Feng Wang, Liangbi Chen and Manzhong Liang

273 Genome-wide identification of bHLH transcription factors and their response to salt stress in *Cyclocarya paliurus*
Zijie Zhang, Jie Fang, Lei Zhang, Huiyin Jin and Shengzuo Fang

288 ZnO nanoparticles efficiently enhance drought tolerance in *Dracocephalum kotschyi* through altering physiological, biochemical and elemental contents
Zahra Karimian and Leila Samiei

302 *De novo* transcriptome sequencing and gene co-expression reveal a genomic basis for drought sensitivity and evidence of a rapid local adaptation on Atlas cedar (*Cedrus atlantica*)
Irene Cobo-Simón, Jèssica Gómez-Garrido, Anna Esteve-Codina, Marc Dabad, Tyler Alioto, Julin N. Maloof, Belén Méndez-Cea, José Ignacio Seco, Juan Carlos Linares and Francisco Javier Gallego

326 Low nitrogen stress-induced transcriptome changes revealed the molecular response and tolerance characteristics in maintaining the C/N balance of sugar beet (*Beta vulgaris* L.)
Jiajia Li, Xinyu Liu, Lingqing Xu, Wangsheng Li, Qi Yao, Xilong Yin, Qiuhong Wang, Wenbo Tan, Wang Xing and Dali Liu

343 OsOLP1 contributes to drought tolerance in rice by regulating ABA biosynthesis and lignin accumulation
Jianpei Yan, Vincent Ninkuu, Zhenchao Fu, Tengfeng Yang, Jie Ren, Guangyue Li, Xiufen Yang and Hongmei Zeng

357 Transcriptome analysis showed that tomato-rootstock enhanced salt tolerance of grafted seedlings was accompanied by multiple metabolic processes and gene differences
Xiaolei Wu, Ding Yuan, Xinyu Bian, Ruixiao Huo, Guiyun Lü, Binbin Gong, Jingrui Li, Sichao Liu and Hongbo Gao

376 Metabolomics reveals the response of hydroprimed maize to mitigate the impact of soil salinization
Enying Zhang, Xingjian Zhu, Wenli Wang, Yue Sun, Xiaomin Tian, Ziyi Chen, Xinshang Mou, Yanli Zhang, Yueheng Wei, Zhixuan Fang, Neil Ravenscroft, David O'Connor, Xianmin Chang and Min Yan

391 Transcriptomic and metabolomic analyses reveal the potential mechanism of waterlogging resistance in cotton (*Gossypium hirsutum* L.)
Anane Gideon Owusu, Yin-Ping Lv, Man Liu, Yong Wu, Cheng-Lin Li, Ning Guo, Da-Hui Li and Jun-Shan Gao

408 CdWRKY2 transcription factor modulates salt oversensitivity in bermudagrass [*Cynodon dactylon* (L.) Pers.]
An Shao, Xiao Xu, Erick Amombo, Wei Wang, Shugao Fan, Yanling Yin, Xiaoning Li, Guangyang Wang, Hongli Wang and Jinmin Fu

423 Acetic acid positively modulates proline metabolism for mitigating PEG-mediated drought stress in Maize and Arabidopsis
Sakil Mahmud, Mohammad Kamruzzaman, Sabarna Bhattacharyya, Khadiga Alharbi, Diaa Abd El Moneim and Mohammad Golam Mostofa

437 Warming appears as the main risk of non-adaptedness for western Mediterranean relict fir forests under expected climate change scenarios
Belén Méndez-Cea, Isabel García-García, Juan Carlos Linares and Francisco Javier Gallego

frontiers | Frontiers in Plant Science

TYPE Editorial
PUBLISHED 03 October 2023
DOI 10.3389/fpls.2023.1295638

Check for updates

OPEN ACCESS

EDITED AND REVIEWED BY
Simone Landi,
University of Naples Federico II, Italy

*CORRESPONDENCE
Mahmoud Magdy
m.elmosallamy@agr.asu.edu.eg
Diaa Abd El Moneim
dabdelmoniem@aru.edu.eg

RECEIVED 16 September 2023
ACCEPTED 25 September 2023
PUBLISHED 03 October 2023

CITATION
Magdy M, Mostofa MG, Rahimi M and Abd El Moneim D (2023) Editorial: Abiotic stress alleviation in plants: morpho-physiological and molecular aspects. *Front. Plant Sci.* 14:1295638. doi: 10.3389/fpls.2023.1295638

COPYRIGHT
© 2023 Magdy, Mostofa, Rahimi and Abd El Moneim. This is an open-access article distributed under the terms of the Creative Commons Attribution License (CC BY). The use, distribution or reproduction in other forums is permitted, provided the original author(s) and the copyright owner(s) are credited and that the original publication in this journal is cited, in accordance with accepted academic practice. No use, distribution or reproduction is permitted which does not comply with these terms.

Editorial: Abiotic stress alleviation in plants: morpho-physiological and molecular aspects

Mahmoud Magdy[1,2]*, Mohammad Golam Mostofa[3,4], Mehdi Rahimi[5] and Diaa Abd El Moneim[6]*

[1]Genetics Department, Faculty of Agriculture, Ain Shams University, Cairo, Egypt, [2]Plant Biology Department, Faculty of Biology, Murcia University, Murcia, Spain, [3]Department of Energy Plant Research Laboratory, Michigan State University, East Lansing, MI, United States, [4]Department of Biochemistry and Molecular Biology, Michigan State University, East Lansing, MI, United States, [5]Department of Biotechnology, Institute of Science and High Technology and Environmental Sciences, Graduate University of Advanced Technology, Kerman, Iran, [6]Department of Plant Production (Genetic Branch), Faculty of Environmental Agricultural Sciences, Arish University, El-Arish, Egypt

KEYWORDS

plant resilience, abiotic stressors, molecular strategies, physiological adaptation, global agriculture, environmental challenges, ecosystem sentinels, thematic research collection

Editorial on the Research Topic

Abiotic stress alleviation in plants: morpho-physiological and molecular aspects

Research topic overview

Plants, our ecosystem's guardians, endure amidst ever-changing environmental challenges. Abiotic stresses, including drought and temperature extremes, continually test their resilience. Unraveling the mechanisms of abiotic stress tolerance in plants through molecular and physiological lenses is central to contemporary plant research. Within this scientific realm, understanding abiotic stress response is crucial. Each article in this Research Topic offers insights, sketching the diverse tactics plants deploy for survival. These pieces highlight the molecular pathways and physiological shifts plants use to counter abiotic adversities. In this editorial, we traverse a vibrant mosaic of research, organizing articles into themes highlighting plants' varied coping mechanisms. Beyond these insights awaits a realm of potential. The repercussions of our findings reach beyond academic realms, influencing global agriculture, food availability, and environmental balance. As we navigate the intricate labyrinth of abiotic stress adaptation, the featured articles shed light on the multifaceted dimensions of plant reactions. While particular articles seamlessly align with our designated sub-thematic clusters, others straddle multiple themes, underscoring the complexity of this research paradigm. Our editorial consortium has endeavored to contextualize each article based on the work's primary focus within the most apt sub-theme, as delineated below:

Sub-theme 1: investigating physiological, biochemical, and metabolic responses to abiotic stressors: implications for plant adaptive mechanisms

In the realm of plant science, understanding plants' responses to abiotic stressors like drought and heat is crucial. As these challenges threaten food security, research focuses on plants' multifaceted survival tactics. The ensuing studies illuminate a range of physiological, genetic, and agronomic strategies, revealing intricate metabolic pathways that equip plants to navigate these adversities.

A group of the published articles predominantly focused on plants' visible and immediate response to stress. In the context of drought amelioration strategies, Mahmud et al. elucidated an innovative tactic. They discovered that after acetic acid priming and subsequent exposure to drought stress induced by PEG, maize seeds manifested remarkable resilience. Such seeds displayed enhanced growth parameters, predominantly in shoot and root elongation. Concurrently, there was a notable augmentation in the plant's inherent water conservation strategies and photosynthetic efficiency, underscoring acetic acid's potential to fortify drought resilience via molecular and physiological avenues. The indispensable role of proteins in abiotic stress defense mechanisms was highlighted by (Yan et al.). They emphasized the significance of the OsOLP1 osmotin-like protein in rice, which, upon overexpression, conferred remarkable drought resistance. The treated plants displayed enhanced stomatal regulation, impressive leaf water conservation, and superior survivability, fundamentally supported by an escalation in lignin and proline concentrations. This insinuates that the strategic management of such proteins could be paramount in enhancing crop resilience. Ding et al. probed the thermotolerance mechanisms in rice by evaluating the hst1 mutant, steered by the DST transcription factor. A pronounced thermotolerance was discerned, attributed to elevated ROS concentrations, which stimulated heat shock protein expression. Such proteins are pivotal in cellular homeostasis during thermal stress, accentuating the DST transcription factor's potential in fortifying plant resistance amidst diverse abiotic challenges. Wang et al. underscored the potential of H_2O_2 priming to mitigate the detrimental impacts of waterlogging in maize, revealing enhancements in photosynthetic efficiency and overall plant vitality, suggesting applicative prospects in inundated terrains.

Under the same sub-theme, additional works dived into several plants' underlying genetic and molecular strategies. Gene expression plays a quintessential role in abiotic stress resistance. Shao et al. explored the CdWRKY2 gene in bermudagrass, a species distinguished for its innate stress resilience. There was a conspicuous association between the CdWRKY2 gene expression and its susceptibility to salt and ABA. A nuanced interplay in lateral root responses, striking a balance between ABA sensitivity and auxin accumulation, was associated with this gene, hinting at the prospects of genetic engineering for augmented salinity tolerance in agronomic crops. Zhang et al. probed into the molecular dynamics of plant responses, unveiling the critical role of H+-pyrophosphatases during nitrogen-deficient conditions. The study spotlighted the relevance of AtAVP1 in Arabidopsis and EdVP1 in *Elymus dahuricus*, exposing a potential regulatory circuit influencing plant acclimatization to nitrogen-scarce settings, thus suggesting possible avenues for enhancing nitrogen assimilation in crops. Li et al. delved into the molecular adaptability of sugar beet (*Beta vulgaris* L.) under nitrogen paucity. Employing transcriptome profiling, they discerned a meticulous balance between energy preservation and oxidative damage defense, suggesting adaptive strategies for other crops under nitrogen constraints. Bai et al. delineated the intricate regulatory dynamics of calcium ion signaling and its receptors in plants, elucidating the multifaceted interactions of these entities in orchestrating plant responses to diverse stressors and suggesting pathways for optimizing plant resilience in adversarial environments.

More works have emphasized agronomic and adaptive practices and techniques to improve plant stress resistance. Wu et al. accentuated the merits of grafting by juxtaposing grafted and non-grafted tomato variants under saline conditions. The grafted variants manifested superior salinity resilience and a more harmonized gene expression trajectory, signifying the potentiality of grafting as a modality to confer salt resistance and decipher key metabolic conduits and transcriptional regulators. Karimian et al. illuminated the efficacy of nano fertilizers in bolstering drought resistance in *Dracocephalum kotschyi*. Their findings suggested that zinc nanoparticle amendments could maintain resilience by modulating pivotal biochemical markers, hinting at a promising direction for drought amelioration in diverse plant species. Miao et al. explored the intricate nexus between light quality and saline stress, proposing a strategy to fine-tune light spectra to alleviate salt stress in cucumber plants. Their empirical findings intimate that modulation of red to far-red light ratios can potentially mitigate the adverse repercussions of salt stress, outlining an avant-garde tactic for enhancing salinity resistance.

The array of studies showcased reveals the multifaceted strategies underpinning plant resilience. Researchers are amplifying our arsenal to strengthen crops amidst a shifting climate by intertwining physiological, molecular, and agronomic approaches. This fusion of methodologies could be pivotal for safeguarding food security and ecological harmony in the future.

Sub-theme 2: molecular responses of stress-related genes and pathways for plant growth regulation and development under abiotic stress conditions

Molecular biology's frontier vibrantly probes the genetic orchestration behind plant resilience amidst growing abiotic challenges. Grasping these genetic pathways is vital for boosting crop robustness and understanding ecological evolution in shifting climates. The highlighted studies unveil specific stress-linked genes and the overarching molecular tactics guiding plant evolution under diverse stress conditions.

Several articles in on this topic presented works that concentrate on a particular gene and its influence on abiotic stress resistance. Huang et al. delved deep into the genomic landscapes of the cereal *Setaria italica L.*, highlighting the significance of the SiNCED1 gene. Markedly upregulated under a gamut of abiotic stressors, including abscisic acid (ABA), osmotic perturbations, and saline conditions, the SiNCED1 gene, when overexpressed, induced a plethora of adaptive responses. These ranged from augmented drought resistance, orchestrated by elevated ABA concentrations and strategic stomatal closure, to influencing a complex network of ABA-responsive stress genes. Transitioning from cereal to medicinal trees, Zhang et al. provided a comprehensive genomic analysis of *Cyclocarya paliurus*. Their investigation unraveled a constellation of 159 basic helix-loop-helix (bHLH) transcription factors, pivotal regulators in plant stress responses. Systematic classification delineated these genes into 26 nuanced subfamilies, and subsequent functional assays under varied salt gradients spotlighted 12 genes demonstrating heightened responsiveness. CpbHLH36/68/146 emerged as paramount nodes in the salt tolerance regulatory network. Tang et al. spotlighted the HD-Zip transcription factor. Their inquiry into the *JcHDZ21* gene, a constituent of the HD-Zip I gene family in physic nut, revealed intriguing genetic dynamics. Transgenic plants showcasing JcHDZ21 overexpression presented heightened sensitivity to saline conditions, offering pivotal insights for potential breeding programs targeting stress-tolerant variants. Concluding this molecular journey, Jiao et al. focused on the salt-resistant halophyte *Limonium bicolor*. The epicenter of their research was the Lb1G04794 gene, intricately associated with salt gland development and resistance. Overexpression studies emphasized accelerated salt gland maturation in *L. bicolor* and elicited an array of beneficial adaptive responses in *Arabidopsis*, underpinning the gene's paramount role in breeding salt-resilient cultivars.

Within the sub-theme frame, two additional studies focused on broader mechanisms or adaptations plants utilize under stress conditions. Cobo-Simón et al. ventured into the evergreen realm of *Cedrus atlantica*. Through a strategic analysis of seedlings subjected to diverse drought scenarios, their study unearthed potential loci of local adaptations. Astoundingly, the plant's genomic responses showcased a spectrum ranging from immediate genomic recalibrations to more protracted alterations, complemented by post-drought recovery strategies. Their magnum opus discovery spotlighted specific genomic variances, mainly single nucleotide polymorphisms (SNPs) associated with transposable elements, earmarking drought-resilient phenotypes. Zeroing in on the metal-responsive gene pathways, Li et al. illuminated the genomic strategies of *Sedum plumbizincicola* under cadmium (Cd) stress. Central to their findings was the cadmium tolerance protein SpCTP3. Remarkably, genetic overexpression of SpCTP3 heralded an enhanced phytoremediation potential, elevating cadmium accumulation in the plant's aerial and root architecture compared to wild types. These genetically manipulated plants also exhibited altered cadmium intracellular distribution paradigms and augmented antioxidative enzyme activities under Cd-induced stress.

Molecular research reveals the multifaceted intricacies of plant responses to abiotic adversities. From gene-focused analyses to comprehensive, adaptive strategies, nature's resilience emerges from a rich interplay of genetic, cellular, and physiological narratives. This depth of understanding highlights an essential reality: decoding the molecular conversations within plants paves the way for a resilient and sustainable agricultural future.

Sub-theme 3: comprehensive omics-based analyses to dissect abiotic stress coping mechanisms in plants

With the rapid advancements in omics technologies, researchers increasingly focus on an integrated understanding of plant responses at molecular, proteomic, transcriptomic, and metabolomic levels to dissect their adaptive mechanisms under various abiotic stresses. This multifaceted approach aids in elucidating the underlying mechanisms, revealing potential biomarkers, and suggesting innovative breeding and biotechnological strategies. Here, we cluster the research studies under this sub-theme based on their primary focus.

Under the effect of heavy metals on plants, the comprehensive analysis that can be conducted through the emerging omics approaches to understand the molecular mechanisms plants employ to tolerate such stresses is paramount. ShangGuan et al. elucidated the role of Germin-like proteins (GLPs) in *Oryza sativa* subjected to heavy metal stresses from Copper (Cu) and Cadmium (Cd). Utilizing hydroponic systems, their findings highlighted that GLP gene knockouts amplified the toxicological effects of Cd and Cu. Such mutants exhibited enhanced metal accumulation relative to wild-type (WT) plants. Intriguingly, altered sequestration patterns of Cu and Cd in the cell walls of these mutants were observed. Enhanced expression of the OsGLP8-2 gene bolstered lignin biosynthesis, crucial for maintaining cell wall structure, and concurrently upregulated antioxidative defense mechanisms against metalliferous stress.

In their evolutionary journey, plants have developed intricate physiological and developmental processes to cope with varying environmental stresses. Peng et al. delineated the pivotal role of Actin depolymerization factors (ADFs) in plant health and adaptative stress responses. Their investigations revealed that the CARK3 protein, via interaction with ADF4, modulates hypocotyl morphogenesis and functions as an intermediary in actin filament dynamics vis-à-vis drought stress. Distinct phenotypic alterations were evident in plants with targeted genetic perturbations in these proteins. Liu et al. investigated the implications of homeodomain-leucine zipper proteins, emphasizing HAT5 derived from *Pyrus sinkiangensis*, across diverse stress scenarios. Their empirical evidence indicated that the heterologous expression of this gene in *Solanum lycopersicum* conferred augmented tolerance against drought and salinity but, conversely, heightened susceptibility to cold stress.

When subjected to environmental stresses, metabolism shifts and growth regulation adaptations in plants provide unique insights into their survival strategies. Zhang et al. executed a holistic metabolomic examination of *Zea mays*, probing the merits of

hydropriming in augmenting its salt stress resistance. Their findings underscored specific metabolic pathways and growth mediators that become predominant during stress, revealing potential strategies for fortifying maize's stress resilience. Zhao et al. embarked on an in-depth analysis of the adaptive responses of *Lotus corniculatus* under phosphorus-deficient settings. They demarcated crucial molecular pathways and genetic determinants pivotal for this adaptation, offering prospects for breeding strategies focused on optimizing phosphorus utilization.

Delving deep into the genomic blueprints of plants, researchers can elucidate the genetic orchestration and subsequent adaptive mechanisms under diverse abiotic stress conditions. Owusu et al. examined *Gossypium* spp.'s genomic dynamics under extended hypoxic waterlogging-induced conditions. Their combined transcriptomic and metabolomic evaluations pinpointed pivotal genetic elements and metabolic cascades operative under sustained hypoxia, suggesting potential molecular targets to enhance Gossypium's adaptability against such adversities. Pakzad et al. unraveled the adaptive proteomic and metabolic pathways in *Pistacia vera* when subjected to osmotic stress due to salinity or drought. Their findings emphasized essential proteins and molecular cascades imperative for osmotic stress adaptation, suggesting innovative approaches for improving osmotic stress resilience in this species. Mikołajczak et al. presented an intricate analysis of *Hordeum vulgare*'s molecular responses, focusing on its flag leaf, under simultaneous drought and thermal stresses. Their analytical insights revealed the intricate molecular strategies this species employs to navigate co-occurring environmental hardships, which are valuable for subsequent breeding efforts to enhance *Hordeum vulgare*'s resilience.

The accumulated evidence from these diverse studies underscores the immense potential of leveraging omics-based approaches to gain a holistic understanding of plant responses under abiotic stresses. Such insights enrich our fundamental knowledge and pave the way for innovative approaches to enhance plant resilience in the face of mounting environmental challenges.

Sub-theme 4: biotechnological interventions of abiotic stress tolerance mechanisms for improvement of crop stress resistance to abiotic stresses

Enhancing crop resilience against abiotic stresses is crucial in the ever-evolving realm of agricultural science. Biotechnological tools provide a window to refine plant adaptability. This sub-theme bridges advanced biotechnological methods with plant responses, revealing molecular intricacies, evolutionary strategies, and symbiotic affiliations. Together, these studies highlight biotechnology's role in fortifying crops against environmental challenges, steering a path for sustainable agriculture in a dynamic global landscape.

The intricacies of molecular and genetic dynamics offer profound insights into plant adaptability amidst adverse environmental conditions, presenting an avenue for the augmentation of stress resilience through precise biotechnological interventions. In an analytical endeavor focusing on *Solanum lycopersicum*, a crop of global agronomic significance, Perveen et al. emphasized the implications of biotechnological tools to bolster drought resilience. Their methodological approach, incorporating advanced in silico models and contemporary sequencing paradigms, delineated the cardinal role of WRKY gene families, which function as quintessential transcriptional regulators in psychophysiological processes and stress-mediated responses. A notable discovery encompassed the molecular interaction dynamics between the phytohormone abscisic acid, synthesized in stress-induced scenarios, and WRKY protein structures, suggesting avenues for enhancing drought adaptability via biotechnological interventions. Delving into the evolutionary intricacies of plant adaptive mechanisms, Bawa et al. characterized the operational dynamics of the auxin efflux carrier, PINFORMED1 (PIN1), within the cellular plasmalemma. Their investigative focus revolved around the modulatory impact of PIN1 on pavement cells (PCs) and guard cells (GCs) in response to abiotic stressors such as desiccation and salinity. Their observations elucidated the differential morphogenesis of PCs and GCs predicated on distinct environmental challenges, accentuating the pivotal role of PIN1 in orchestrating epidermal cell development and proffering potential biotechnological interventions for plant resilience in hostile ecological milieus. The empirical exploration by Méndez-Cea et al. delineated the genetic landscape governing drought resilience in endogenous fir species, specifically *Abies pinsapo* and *Abies marocana*. Leveraging the ddRAD-seq genotypic platform, they discerned the underlying genetic architecture and identified loci potentially under environmental selective pressures. Identifying proteins intrinsic to abiotic stress responses, combined with genotype-environment association analyses, highlighted the potential vulnerabilities of these arboreal species amidst evolving climatic perturbations, setting the stage for targeted biotechnological strategies for conserving these relic taxa.

The synergism between plants and symbiotic organisms and innovative external treatments, epitomizes a paradigm shift in strategies to fortify plant robustness against environmental perturbations. Han et al. provided a comprehensive treatise on the symbiotic affiliations between plants and arbuscular mycorrhizal (AM) fungi, elucidating their role in promoting zinc (Zn) homeostasis in Eucalyptus grandis. Through comparative analyses between mycorrhized and non-mycorrhized specimens under differential Zn exposures, they observed enhanced vegetative metrics in symbiotically associated plants under elevated Zn regimes. In conjunction, the AM fungal consortium facilitated the absorption kinetics of essential ionome nutrients, with a concomitant genetic upregulation underpinning the beneficial role of this symbiotic association in Zn stress mitigation. In a subsequent investigative endeavor, Han et al. probed innovative methodologies to enhance cryogenic tolerance in *Vitis vinifera* L., particularly emphasizing the efficacy of Biodegradable Liquid Film (BLF). Their empirical analyses displayed a significant reduction in plant morbidity metrics in BLF-treated specimens. Concurrent biochemical profiling

attributed this heightened cryotolerance to the amplification of specific osmoprotective agents and a diminution of oxidative perturbations. Furthermore, a discernible genetic modulation in response to cryogenic stress post-BLF application suggested its potentiality as a protective adjunct in horticultural practices.

In the face of growing environmental challenges, biotechnological advances promise enhanced resilience in vital crops. Leveraging genetics, molecular insights, and symbiotic partnerships amplifies the possibility of creating hardier crops. The data presented in this sub-theme highlights critical avenues for future research endeavors.

Conclusion

These 30 articles collectively shed light on the intricate web of interactions within plants confronting various abiotic stress, offering new horizons for agriculture and deepening our understanding of plant stress adaptation mechanisms. This Research Topic provides a comprehensive overview of plants' multifaceted landscape of abiotic stress adaptation. It unravels the intricate mechanisms governing plant responses to stressors, spanning physiological, biochemical, molecular, and biotechnological dimensions. This compilation underscores the importance of continued research and collaboration in plant science to address the pressing challenges posed by abiotic stressors in agriculture. We can bolster crop yields and food security by harnessing the insights gleaned from these studies and contribute to sustainable agriculture practices in a changing climate. Further exploration in this field holds the potential to shape the future of plant stress adaptation and pave the way for innovative solutions in the agriculture sector.

Author contributions

MM: Writing – review & editing, Conceptualization, Data curation, Resources, Validation, Visualization, Writing – original draft. MM: Conceptualization, Project administration, Resources, Supervision, Writing – review & editing. MR: Project administration, Resources, Supervision, Writing – review & editing, Conceptualization. DM: Conceptualization, Project administration, Resources, Supervision, Writing – review & editing.

Conflict of interest

The authors declare that the research was conducted in the absence of any commercial or financial relationships that could be construed as a potential conflict of interest.

Publisher's note

All claims expressed in this article are solely those of the authors and do not necessarily represent those of their affiliated organizations, or those of the publisher, the editors and the reviewers. Any product that may be evaluated in this article, or claim that may be made by its manufacturer, is not guaranteed or endorsed by the publisher.

frontiers | Frontiers in Plant Science

TYPE Mini Review
PUBLISHED 11 October 2022
DOI 10.3389/fpls.2022.1019505

Check for updates

OPEN ACCESS

EDITED BY
Mahmoud Magdy,
Ain Shams University, Egypt

REVIEWED BY
Congming Lu,
Shandong Agricultural University, China
Shoaib Munir,
Huazhong Agricultural University, China

*CORRESPONDENCE
Yifei Liu
yifeiliu6@hotmail.com;
liuyifei@syau.edu.cn

†These authors have contributed equally to this work

SPECIALTY SECTION
This article was submitted to Plant Abiotic Stress, a section of the journal Frontiers in Plant Science

RECEIVED 15 August 2022
ACCEPTED 22 September 2022
PUBLISHED 11 October 2022

CITATION
Bai R, Bai C, Han X, Liu Y and Yong JWH (2022) The significance of calcium-sensing receptor in sustaining photosynthesis and ameliorating stress responses in plants.
Front. Plant Sci. 13:1019505.
doi: 10.3389/fpls.2022.1019505

COPYRIGHT
© 2022 Bai, Bai, Han, Liu and Yong. This is an open-access article distributed under the terms of the Creative Commons Attribution License (CC BY). The use, distribution or reproduction in other forums is permitted, provided the original author(s) and the copyright owner(s) are credited and that the original publication in this journal is cited, in accordance with accepted academic practice. No use, distribution or reproduction is permitted which does not comply with these terms.

The significance of calcium-sensing receptor in sustaining photosynthesis and ameliorating stress responses in plants

Rui Bai[1†], Chunming Bai[2,3†], Xiaori Han[1], Yifei Liu[1,3,4,5*] and Jean Wan Hong Yong[4,6]

[1]College of Land and Environment, National Engineering Research Center for Efficient Utilization of Soil and Fertilizer Resources, Northeast China Plant Nutrition and Fertilization Scientific Observation and Research Center for Ministry of Agriculture and Rural Affairs, Key Laboratory of Protected Horticulture of Education Ministry and Liaoning Province, Shenyang Agricultural University, Shenyang, China, [2]National Sorghum Improvement Center, Liaoning Academy of Agricultural Sciences, Shenyang, China, [3]The University of Western Australia (UWA) Institute of Agriculture, The University of Western Australia, Perth, WA, Australia, [4]School of Biological Sciences, The University of Western Australia, Perth, WA, Australia, [5]School of Agriculture and Environment, The University of Western Australia, Perth, WA, Australia, [6]Department of Biosystems and Technology, Swedish University of Agricultural Sciences, Alnarp, Sweden

Calcium ions (Ca^{2+}) regulate plant growth and development during exposure to multiple biotic and abiotic stresses as the second signaling messenger in cells. The extracellular calcium-sensing receptor (CAS) is a specific protein spatially located on the thylakoid membrane. It regulates the intracellular Ca^{2+} responses by sensing changes in extracellular Ca^{2+} concentration, thereby affecting a series of downstream signal transduction processes and making plants more resilient to respond to stresses. Here, we summarized the discovery process, structure, and location of CAS in plants and the effects of Ca^{2+} and CAS on stomatal functionality, photosynthesis, and various environmental adaptations. Under changing environmental conditions and global climate, our study enhances the mechanistic understanding of calcium-sensing receptors in sustaining photosynthesis and mediating abiotic stress responses in plants. A better understanding of the fundamental mechanisms of Ca^{2+} and CAS in regulating stress responses in plants may provide novel mitigation strategies for improving crop yield in a world facing more extreme climate-changed linked weather events with multiple stresses during cultivation.

KEYWORDS

abiotic stress, photosynthesis, calcium, biological functionality, calcium-sensing receptor

Introduction

Calcium, a crucial macronutrient for plants, has important physiological functions such as maintaining cell morphology and regulating ion balance and osmotic pressure. Interestingly, it is also a key component for several early signaling pathways involved in plant–environmental stresses interactions (Lambers and Oliveira, 2019; Song et al., 2020; Wu et al., 2020). Most elemental calcium in plant cells exists in ionic forms, which contribute to forming microtubules in the cytoskeleton and maintaining the fluidity of cell membranes (Kong et al., 2020; Liu, 2021). In addition, calcium signals assist in the integration of various signaling pathways to coordinate plants' growth response to multiple environmental signals (Edel and Kudla, 2016; Kudla et al., 2018; Luan and Wang, 2021; Kim et al., 2022). The extracellular calcium-sensing receptor (CAS) is an important protein that specifically exists in plants and has specific regulatory functions. These proteins regulate intracellular Ca^{2+} responses by sensing changes in extracellular Ca^{2+} concentration, thereby affecting a series of downstream signaling activities and fine-tuning plants' responses to environmental perturbations. We summarized the research progress of Ca^{2+} and CAS in regulating photosynthesis and stress responses. Here, we focused on the fundamental role of CAS in regulating growth and signal transduction in response to the external environment.

Structural characteristics of the calcium-sensing receptor

Discovery and location of CAS

The extracellular Ca^{2+} receptor gene was cloned for the first time using the functional gene screening method in *Arabidopsis thaliana* and named as the calcium-sensing receptor (CAS) (Li et al., 2022). With the aid of fluorescence imaging and proteomics technologies, the CAS was located on the chloroplast thylakoid membrane of *Arabidopsis thaliana*, spinach, and green algae (Allmer et al., 2006; Naumann et al., 2007; Nomura et al., 2008; Weinl et al., 2008). Interestingly, the CAS was also detected within the purified eyespot of green algae (Trippens et al., 2017). Yamano et al. (2018) fused the CAS-Clover with high-resolution fluorescence imaging to coincide with the eyespot, which also verified the existence of CAS. In addition, high-resolution fluorescence images of CAS were obtained using the sensitive hybrid detector and image deconvolution technology, and its cellular localization on the thylakoid membrane was authenticated and observed with greater clarity.

Structural features of CAS

The carboxyl-terminal of CAS is located within the cell and has two domains (Vainonen et al., 2008); one of which is a non-catalytic thiocyanate domain with high homology, and the other is related to protein interaction which can interact with the 14-3-3 and FHA (forkhead-associated) domain. Under light conditions, the CAS light-regulated kinase STN8 is targeted for phosphorylation at Thr-380 (Vainonen et al., 2008). The amino terminal of CAS is located outside the cell membrane, which may plausibly be the Ca^{2+} binding region, although its conserved sequence has not been found. It was later verified that the binding site of Ca^{2+} in CAS was the amino end rather than the carboxyl end in *Arabidopsis* and *Chlamydomonas* (Wang et al., 2016a).

CAS and stomatal functionality

The pair of guard cells have a fundamental role in regulating gas exchange between plants and the atmosphere, and biotic infection (Melotto et al., 2008; Chen et al., 2012; Sawinski et al., 2013; Sun et al., 2014; Murata et al., 2015; Agurla et al., 2016; Bharath et al., 2021). Generally, Ca^{2+} plays an important role in regulating guard cell turgor and the movements of guard cells. Ca^{2+} ions affect stomatal conductance to water vapor and CO_2 by regulating the pore size. Peng et al. (2022) discovered that an exogenous application of 18 Mm Ca^{2+} could increase the stomatal conductance of *Paris polyphylla* under high temperatures and strong light conditions. The CO_2-induced stomatal closure process is also calcium-dependent and the CPK (calcium-dependent protein kinase) has a role in signal transduction and regulating the ion channels of guard cells. In the pentaploid mutant plants with *cpk3/5/6/11/23*, the stomatal movements were significantly impaired, suggesting that CPK has important functions in facilitating stomatal movement and is plausibly regulated by CO_2 concentration (Schulze et al., 2021). Jakobson et al. (2016) confirmed that there were significant differences in stomatal phenotypes among *cas* mutants with different alleles and the *cas* overexpression of *Arabidopsis* transformants promoted stomatal closure. Li et al. (2017) also demonstrated that the deletion of the CAS gene could disrupt stomatal closure and this phenomenon was attributed to high levels of extracellular Ca^{2+}. It was later verified that the extracellular high Ca^{2+} in CAS gene-deficient mutants could not induce stomatal closure, indicating that CAS was essential for extracellular Ca^{2+}-induced stomatal closure in *Arabidopsis* (Qi et al., 2018).

Interestingly, it was also found that CAS has an important role in elevating intracellular Ca^{2+} concentration when induced by extracellular Ca^{2+}. These studies provided evidence for *Arabidopsis* chloroplasts in regulating extracellular Ca^{2+}-induced

intracellular Ca^{2+} concentration increases and subsequent stomatal closure (Nomura et al., 2008; Li et al., 2022). Wang et al. (2016b) found that the chloroplastic regulation of stomatal closure required the reduction of quinone, foliar production of H_2O_2, and the phosphorylation of CAS and LHCII during exposure to unfavorable perturbation. It was confirmed that stomatal movement was associated with NO and the NO acted downstream of the H_2O_2 step in regulating stomatal movement (Bright et al., 2006). Specifically, the stomatal closure induced by H_2O_2 and NO requires the involvement of extracellular Ca^{2+} and the accumulation of H_2O_2 and NO in guard cells (Li et al., 2009; Zhao et al., 2011). Tang et al. (2007) suggested that CAS might regulate the stomatal closure process through the Ca^{2+}-CAS-IP signaling pathway. Subsequently, Wang et al. (2012) found that the extracellular Ca^{2+} induced H_2O_2 and NO accumulation through CAS in *Arabidopsis thaliana*, which induced transient changes in cytoplasmic Ca^{2+} concentration and was able to regulate stomatal movement. In addition, *Arabidopsis* plants expressing $PH_{PLC\delta}$-GFP protein were used for $PH_{PLC\delta}$-GFP imaging of guard cells, which indicated that H_2O_2 and NO were involved in the CAS-IP_3 signaling pathway (Wang, 2013). Li et al. (2017) found that H_2O_2 might directly or indirectly regulate CAS activity and serve as redox signaling molecules, thereby regulating stomatal closure. Interestingly, the data also revealed that the exogenous NO-induced stomatal closure of CAS guard cells was facilitated by exogenous NO bypassing the damaged CAS. Furthermore, it was indicative that NO has a downstream role relative to CAS in the signal transduction pathway. Recent studies suggested that stomatal movement induced by extracellular Ca^{2+} was the culmination of multiple interactions among CAS, H_2O_2, and NO signals (Zhang et al., 2018; Li et al., 2022). Li et al. (2017) used multi-disciplinary approaches to examine the responses of different mutants to extracellular Ca^{2+} in guard cells. It was found that there was a cascade of H_2O_2, ABA, and NO in the CAS signaling pathway. With further studies, it was confirmed that seed germination and stomatal closure of mutant cau1 transformants were excessively sensitive to ABA. In addition to extracellular Ca^{2+}, the CAU1-CAS could also respond to ABA through interaction, and ABA and CAUI could also regulate stomatal closure (Ueda and Seki, 2020), although the specific role of CAS in this process required further clarification. Li et al. (2017) found that ABA in *CASas* mutant plants was able to induce stomatal closure, indicating that the ABA-induced signal transduction pathway was not dependent on CAS; here, *CASas* refers to the CAS antisense line of *Arabidopsis*. Based on these studies, the signal transduction cascade is summarized accordingly in a scheme (Figure 1).

CAS and photosynthesis

Photosynthesis is one of the most important biological processes on earth (Liu et al., 2011; Stael et al., 2012; Lambers and Oliveira, 2019). Calcium is involved in regulating various photosynthetic processes, such as CO_2 fixation and protein phosphorylation in chloroplasts (Rocha and Vothknecht, 2012; Liu, 2020). Hu et al. (2022) found that low calcium levels caused the decline in photosynthesis of *Taxus wallichiana* varieties, but this negative effect could be reversed by applying supplementary calcium nutrition, which was consistent with previous findings in grape and cucumber (He et al., 2018; Duan et al., 2020). Harnessing the pull-down analysis (network database GeneCAT) combined with proteomics and gene co-expression method, Wang (2013) found that 52% of the CAS co-expression genes in *Arabidopsis* were related to photosynthesis. Combining photosynthetic indexes, chloroplast structural observation and gene expression profiling, these observations verified that the photosynthetic level and biomass accumulation of *Arabidopsis CASas* plants were significantly reduced. Specifically, the inhibition of CAS caused the transcription level of photosynthetic electron-related genes to be down-regulated (Wang et al., 2014). Navazio et al. (2020) found that the transcription expression of the CAS gene in *Arabidopsis* was up-regulated under strong light conditions, and the CAS transcription level under dark and weak light conditions was also significantly up-regulated compared with that under normal light conditions. Petroutsos et al. (2011) confirmed that CAS played a role in maintaining PSII functionality and helping plants to adapt to strong light. Additionally, Li (2021) found three *AtCAS* homologous genes in some shade plants such as ginseng, and two *AtCAS* homologous genes in the non-shade plant such as tomato. As CAS is a phosphorylated protein regulated by light intensity; it is plausible that CAS may be closely related to light adaptability. The stomatal movement of terrestrial plants regulates CO_2 entry and exit through HTI protein kinase and carbonic anhydrase (Hu et al., 2010), and aquatic plants maintained stable photosynthesis through the CO_2-concentration mechanism (CCM). Studies have indicated that Ca^{2+} and CAS are related to CCM. In response to low CO_2 concentration, the CAS can be transferred to the protein nucleus, and then mediate the chloroplastic retrograde signaling to maintain the expression of HLA3 (high-light activated 3) and LCIA (low-CO_2-inducible gene A) (Wang et al., 2016a). Yamano et al. (2018) obtained interesting CAS-Clover high-resolution fluorescence images using a sensitive mixed detector coupled with image deconvolution technology. It was found that CAS moved along the thylakoid membrane in response to low concentration CO_2, and gathered spatially in the protein nucleus during the CCM mechanism. As a chloroplastic thylakoid membrane protein, CAS functionality was examined during de-etiolation and chloroplast development in *Arabidopsis thaliana* (Huang et al., 2012). The thylakoid-localized CAS protein could assist in the production of cytosolic calcium transients, and the activation of the MPK3/MPK6 signal system. Subsequently, the activated MPK3/MPK6 was involved

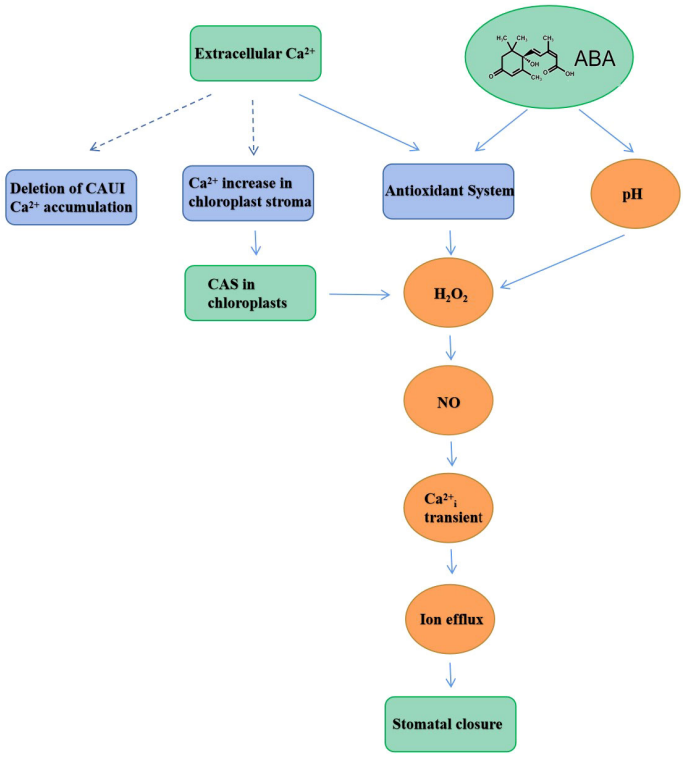

FIGURE 1
A simplified scheme illustrating the salient signal transduction steps leading to stomatal closure.

in the nucleus-induced phosphorylation of ABI4. The activation of ABI4 at both the transcriptional and posttranslational levels induced the inhibition of LHCB (Gao et al., 2016). These results showed that the cystoid-located CAS was involved in the retrograde signaling pathway from chloroplast to nucleus (Li et al., 2022).

Protein phosphorylation is vital for photosynthesis and adaptation to multiple environmental stresses (Vener, 2007; Fristedt et al., 2010). Vainonen et al. (2008) found that CAS could be phosphorylated by STN8, and the phosphorylation intensity increased with light intensity enhancement. At the same time, a new phosphorylation site Thr-367 was also found in the CAS of green algae (Lemeille et al., 2010). Cutolo et al. (2019) conducted proteomics analysis and phosphorylation determination of *CASas*, and identified Thr-376, Ser-378, and Thr-380 as the main phosphorylation sites of STN kinase. Protein phosphorylation is also important to regulate photosynthetic electron transport efficiency (Reiland et al., 2011). The cyclic electron transport (CET) process is involved in chloroplast energy regulation and redox metabolism, which is particularly important for photosynthesis. The studies demonstrated that CET has two pathways, PGR5/PGRL1-mediated pathway and the NDH-mediated pathway (Johnson et al., 2014; Ma et al., 2021a). The protein interaction between CAS and PGRL1 was confirmed in *Chlamydomonas reinhardtii*, indicating that there is a link between CAS and CET (Terashima et al., 2012; Ma et al., 2021b). Chen et al. (2015) found that Ca^{2+} controlled the biosynthesis of lipids induced by chloroplastic nitrogen starvation by promoting the expression of CAS in the PGRL1-mediated CET pathway.

CAS, stress resilience, and plant defense

When plants are exposed to environmental stresses, they will improve their resilience by self-regulating several *in vivo* processes (e.g. changes in intracellular calcium concentration) to cope with these perturbations (Liu, 2020). Salinity is an important environmental factor, which has a negative impact on plant growth and photosynthesis (Acosta-Motos et al., 2017; Ma et al., 2022). Similarly, Ca^{2+} is also crucial in mediating stress responses (Park et al., 2016). It was verified that Ca^{2+} can enhance the salt tolerance of plants by improving water

balance, regulating sodium secretion, and enhancing membrane integrity (Ahmed et al., 2021). In addition, Ca^{2+} also enhances resilience to chilling stress. Liu et al. (2013) found that exogenous Ca^{2+} could mitigate the significant decline in peanut photosynthesis and biomass accumulation during exposures to low night temperatures. It was also confirmed that exogenous Ca^{2+} ameliorated night chilling-dependent feedback inhibition of photosynthesis by improving sink demand and facilitating nonstructural carbohydrate export from chloroplasts, to restore peanut growth, dry matter production, and leaf photosynthetic capacity (Shi et al., 2020; Song et al., 2020; Wu et al., 2020). Sun et al. (2022) reported that the Ca^{2+} mediated-CAS was crucial for alleviating photoinhibition in peanut growing under conditions of moderate phosphorus deficiency. In addition, Zhao et al. (2015) confirmed that *OsCAS* could improve drought tolerance in *Arabidopsis*. When drought and heat stresses were imposed on the creeping bentgrass (*Agrostis stolonifera*), the expression of CAS was down-regulated, indicating that the calcium sensitivity to drought and heat stress responses was reduced (Xu and Huang, 2018). The molecular mechanism of proline metabolism regulation under drought also revealed a new drought tolerance pathway mediated by CAU1 (Fu et al., 2018). Huang et al. (2012) provided further evidence to support the role of Ca^{2+} and CAS in leaf re-greening and chloroplast development of *Arabidopsis*. Zheng et al. (2017) screened a chloroplast protein QUA1 by harnessing the large-scale forward genetic method. It is plausible that the CAS-mediated salt and drought tolerance of plants through the calcium signaling-linked QUA1 that influence the stability of CAS. It was further suggested that CAS has a regulatory role in the downstream of QUA1. Interestingly, there are some pieces of evidence to indicate that CAS is a prerequisite for chloroplast Ca^{2+} to induce light response and light-dark transition (Nomura et al., 2012). The expression of *cas* in *Arabidopsis thaliana* was significantly reduced under high-temperature treatment. It is plausible that the heat-sensing ability of chloroplasts was partially dependent on CAS during high-temperature exposure (Lenzoni and Knight, 2019).

Plant defense against invasive pathogens is dependent on the dual innate immune system. Meta-analysis indicated that CAS regulated the expression of flg22-induced immune genes through $^1O_2$-mediated retrograde signaling; flg22 is a peptide derived from bacterial flagellins. These studies revealed that the weakened signals, chloroplasts, and superoxide anions were collectively involved in the innate immune system (Sano et al., 2014; Stael et al., 2015). In the study of plant-pathogen interaction mediated by small molecules during the invasion of *Fusarium graminearum*, Jia et al. (2019) found that the fungal infection or the use of exogenous fusaoctaxin A inhibited the expression of three CAS-like genes and chloroplast genes. Thus, the lowered susceptibility of wheat to *Fusarium* A, and the inhibition of photosynthesis provided some evidence that chloroplasts might play a key role in regulating early immune responses (de Torres Zabala et al., 2015). *Sclerotinia sclerotiorum* is a well-known necrotizing fungus that attacks many crops (Bolton et al., 2006). The CAS is involved in the defense response of *Arabidopsis thaliana* to *S. sclerotiorum*, and actively regulates the accumulation of salicylic acid (SA) by promoting the expression of SA biosynthesis-related genes, thereby enhancing the resistance of plants to *S. sclerotiorum* (Tang et al., 2020). HopAU1 is an immune inducer existing in *Pseudomonas syringae pv. actinidiae* (Psa) which can interact with *NbCAS* in tobacco. Thus, silencing the *NbCAS* by RNAi in *N. benthamiana* greatly attenuated HopAU1-triggered cell death, suggesting that HopAU1 targets CAS and enhances plant immunity. Further study showed that the overexpression of *NbCaS* in *N. benthamiana* significantly improved plant resistance against *Sclerotinia sclerotiorum* and *Phytophthora capsici* (Zhang et al., 2022). Taken together, the CAS also serves as a promising resistant-related gene for breeding new disease-resistant varieties.

Future outlook

The CAS has an important role in facilitating Ca^{2+}-mediated stomatal closure and is associated with several signaling molecules. As a specific protein located on the chloroplast thylakoid membrane, the CAS functions as the first messenger along the signal transduction pathway in plants. There is some evidence that CAS may participate in various photosynthetic processes such as CO_2 fixation and protein phosphorylation. With further research, we could gain insights into the Ca^{2+}-induced signaling pathway and the functional characteristics of CAS in plant cells. In the future, it is important to further explore the following: (i) the various relationships between CAS and the other calcium-linked signals; (ii) the potential cross-talk between CAS and light signaling at the chloroplast thylakoid membranes; (iii) the CAS and its specific role in facilitating plant abiotic and biotic stress responses using advanced techniques/tools (proteomics, transcriptomics, and bioinformatics, etc.); (iv) extrapolating the understanding of CAS in model plants to non-model plants such as the legumes and horticultural crops, etc.

Author contributions

YL, RB, CB, XH, and JY are responsible for the general review described in the manuscript. YL, XH, and JY provided further discussion and edited the manuscript. All authors reviewed and approved the final version of the submitted manuscript.

Funding

This research was funded by the National Natural Science Foundation of China (project nos. 31772391 and 31301842), ARC-Linkage Project (project no. LP200100341), and the Scientific Research Project of the Education Department of Liaoning Province, China (project no. LJKZ0661).

Acknowledgments

We sincerely thank the reviewers for all their valuable comments and recommendations to improve the manuscript.

Conflict of interest

The authors declare that the research was conducted in the absence of any commercial or financial relationships that could be construed as a potential conflict of interest.

Publisher's note

All claims expressed in this article are solely those of the authors and do not necessarily represent those of their affiliated organizations, or those of the publisher, the editors and the reviewers. Any product that may be evaluated in this article, or claim that may be made by its manufacturer, is not guaranteed or endorsed by the publisher.

References

Acosta-Motos, J., Ortu-no, , Bernal-Vicente, M., Diaz-Vivancos, A. P., Sanchez-Blanco, M., Hernandez, J., et al (2017). Plant responses to salt stress: Adaptive mechanisms. *Agronomy* 7 (18), 1–38. doi: 10.3390/agronomy7010018

Agurla, S., Gayatri, G., and Raghavendra, A. S. (2016). Nitric oxide (NO) measurements in stomatal guard cells. *Method. Mol. Biol.* 1424, 49–56. doi: 10.1007/978-1-4939-3600-7_5

Ahmed, M. Z., Hussain, T., Gulzar, S., Adnan, M. Y., and Khan, M. A. (2021). Calcium improves the leaf physiology of salt treated *Limonium stocksii*: A floriculture crop. *Sci. Hortic.* 285 (3), 110190. doi: 10.1016/j.scienta.2021.110190

Allmer, J., Naumann, B., Markert, C., Zhang, M., and Hippler, M. (2006). Mass spectrometric genomic data mining: Novel insights into bioenergetic pathways in Chlamydomonas reinhardtii. *Proteomics* 6 (23), 6207–6220. doi: 10.1002/pmic.200600208

Bharath, P., Gahir, S., and Raghavendra, A. S. (2021). Abscisic acid-induced stomatal closure: An important component of plant defense against abiotic and biotic stress. *Front. Plant Sci.* 12. doi: 10.3389/fpls.2021.615114

Bolton, M. D., Thomma, B., and Nelson, B. D. (2006). *Sclerotinia sclerotiorum* (lib.) de bary: biology and molecular traits of a cosmopolitanpathogen. *Mol. Plant Pathol.* 7 (1), 1–16. doi: 10.1111/j.1364-3703.2005.00316.x

Bright, J., Desikan, R., Hancock, J. T., Weir, I. S., and Neill, S. J. (2006). ABA-induced no generation and stomatal closure in *Arabidopsis* are dependent on H_2O_2 synthesis. *Plant J.* 45 (1), 113–122. doi: 10.1111/j.1365–313X.2005.02615.x

Chen, H., Hu, J., Qiao, Y., Chen, W., Rong, J., Zhang, Y., et al. (2015). Ca^{2+}-regulated cyclic electron flow supplies ATP for nitrogen starvation-induced lipid biosynthesis in *green alga*. *Sci. Rep.* 5, 15117. doi: 10.1038/srep15117

Chen, D. H., Wang, M., Wang, H. G., and Zhang, W. (2012). A type of voltage-dependent Ca^{2+} channel on *Vicia faba* guard cell plasma membrane outwardly permeates k^+. *Protoplasma* 249 (3), 699–708. doi: 10.1007/s00709-011-0313-2

Cutolo, E., Parvin, N., Ruge, H., Pirayesh, N., and Vothknecht, U. C. (2019). The high light response in *Arabidopsis* requires the calcium sensor protein CAS, a target of STN7- and STN8-mediated phosphorylation. *Front. Plant Sci.* 10. doi: 10.3389/fpls.2019.00974

de Torres Zabala, M., Littlejohn, G., Jayaraman, S., Studholme, D., Bailey, T., Lawson, T., et al. (2015). Chloroplasts play a central role in plant defense and are targeted by pathogen effectors. *Nat. Plants.* 1, 15074–15074. doi: 10.1038/nplants.2015.74

Duan, S. Y., Wu, Y.S., Zhang, C.J., Wang Song, L. S. R., and Ma, C. (2020). Differential regulation of enzyme activities and physio-anatomical aspects of calcium nutrition in grapevine. *Sci. Hort.* 272, 109423. doi: 10.1016/j.scienta.2020.109423

Edel, K. H., and Kudla, J. (2016). Integration of calcium and ABA signaling. *Curr. Opin. Plant Biol.* 33, 83–91. doi: 10.1016/j.pbi.2016.06.010

Fristedt, R., Granath, P., and Vener, A. V. (2010). A protein phosphorylation threshold for functional stacking of plant photosynthetic membranes. *PloS One* 5 (6), e10963. doi: 10.1371/journal.pone.0010963

Fu, Y., Ma, H., Chen, S., Gu, T., and Gong, J. (2018). Control of proline accumulation under drought *via* a novel pathway comprising the histone methylase CAU1 and the transcription factor ANAC055. *J. Exp. Bot.* 69 (3), 579–588. doi: 10.1093/jxb/erx419

Gao, G. L., Zhang, X. Y., Chang, Z. Q., Yu, T. F., and Zhao, H. (2016). Environmental response simulation and the up-scaling of plant stomatal conductance. *Acta Ecol. Sinica.* 36 (06), 1491–1500. doi: 10.5846/stxb201408211652

He, L. Z., Yu, L., Li, B., Du, N. S., and Guo, S. R. (2018). The effect of exogenous calcium on cucumber fruit quality, photosynthesis, chlorophyll fluorescence, and fast chlorophyll fluorescence during the fruiting period under hypoxic stress. *BMC Plant Biol.* 18, 180–190. doi: 10.1186/s12870-018-1393-3

Huang, S. S., Chen, J., Dong, X. J., Patton, J., Pei, Z. M., and Zheng, H. L. (2012). Calcium and calcium receptor CAS promote *Arabidopsis thaliana* de-etiolation. *Physiol. Plant* 144 (1), 73–82. doi: 10.1111/j.1399-3054.2011.01523.x

Hu, H., Boisson-Dernier, A., Israelsson-Nordstrom, M., Bohmer, M., Xue, S., Ries, A., et al. (2010). Carbonic anhydrases are upstream regulators of CO_2-controlled stomatal movements in guard cells. *Nat. Cell Biol.* 12(1), 87–93. doi: 10.1038/ncb2009

Hu, W. J., Liu, T. W., Zhu, C. Q., Wu, Q., Chen, L., Lu, H. L., et al (2022). Physiological, proteomic analysis, and calcium-related gene expression reveal taxus wallichiana var. mairei adaptability to acid rain stress under various calcium levels. *Front. Plant Sci.* 13, 845107. doi: 10.3389/fpls.2022.845107

Jakobson, L., Vaahtera, L., Toldsepp, K., Nuhkat, M., Brosche, M., Wang, C., et al. (2016). Natural variation in *Arabidopsis* cvi-0 accession reveals an important role of MPK12 in guard cell CO_2 signaling. *PloS Biol.* 14 (12), e2000322. doi: 10.1371/journal.pbio.2000322

Jia, L. J., Tang, H. Y., Wang, W. Q., Yuan, T. L., Wei, W. Q., Pang, B., et al. (2019). A linear nonribosomal octapeptide from *Fusarium graminearum* facilitates cell-to-cell invasion of *wheat*. *Nat. Commun.* 10 (1), 922. doi: 10.1038/s41467-019-08726-9

Johnson, X., Steinbeck, J., Dent, R. M., Takahashi, H., Richaud, P., Ozawa, S., et al. (2014). Proton gradient regulation 5-mediated cyclic electron flow under ATP- or redox-limited conditions: A study of ΔATPase pgr5 and ΔrbcL pgr5 mutants in the green alga *Chlamydomonas reinhardtii*. *Plant Physiol.* 165 (1), 438–452. doi: 10.1104/pp.113.233593

Kim, N. H., Jacob, P., and Dangl, J. L. (2022). Con-$Ca2^+$-tenating plant immune responses via calcium-permeable cation channels. *New Phytol.* 234, 813–818. doi: 10.1111/nph.18044

Kong, X. P., Xu, L. H., and Jamieson, P. (2020). Plant sense: the rise of calcium channels. *Trends Plant Sci.* 25, 838–841. doi: 10.1016/j.tplants.2020.06.002

Kudla, J., Becker, D., Grill, E., Hedrich, R., Hippler, M., Kummer, U., et al. (2018). Advances and current challenges in calcium signaling. *New Phytol.* 2182, 414–431. doi: 10.1111/nph.14966

Lambers, H., and Oliveira, R. S. (2019). "Photosynthesis, respiration, and long-distance transport: photosynthesis," in *Plant physiological ecology* (Cham: Springer), 111–114.

Lemeille, S., Turkina, M. V., Vener, A. V., and Rochaix, J. D. (2010). Stt7-dependent phosphorylation during state transitions in the green alga *Chlamydomonas reinhardtii*. *Mol. Cell. Proteomics.* 9 (6), 1281–1295. doi: 10.1074/mcp.M000020-MCP201

Lenzoni, G., and Knight, M. R. (2019). Increases in absolute temperature stimulate free calcium concentration elevations in the chloroplast. *Plant Cell Physiol.* 60 (3), 538–548. doi: 10.1093/pcp/pcy227

Li, H. (2021). *Mechanism of the calcium receptor protein (CAS) involved in nitrogen regulation of flowering time in arabidopsis* (Jilin, China: Jilin University). doi: 10.27162/d.cnki.gjlin.2021.004485

Li, Q., Wang, Y. J., Liu, C. K., Pei, Z. M., and Shi, W. L. (2017). The crosstalk between aba, nitric oxide, hydrogen peroxide, and calcium in stomatal closing of arabidopsis thaliana. *Biologia* 72, 1140–1146. doi: 10.1515/biolog-2017-0126

Liu, J. (2021). Research progress of calcium Ion on plant growth and development. *Mod. Salt Chem. Indust.* 48, 137–39. doi: 10.19465/j.cnki.2095-9710.2021.05.062

Li, B., Hou, L. Y., Song, C. G., Wang, Z. B., Xue, Q. Y., Li, Y. Y., et al. (2022). The biological function of calcium-sensing receptor (CAS) and its coupling calcium signaling in plants. *Plant Physiol. Biochem.* 180, 74–80. doi: 10.1016/j.plaphy.2022.03.032

Li, J. H., Liu, Y. Q., Lu, P., Lin, H. F., Bai, Y., Wang, X. C., et al. (2009). A signaling pathway linking nitric oxide production to heterotrimeric G protein and hydrogen peroxide regulates extracellular calmodulin induction of stomatal closure in *Arabidopsis*. *Plant Physiol.* 150 (1), 114–124. doi: 10.1104/pp.109.137067

Liu, Y. F. (2020). Calcium chemical priming might play a significant role in relieving overnight chilling-dependent inhibition of photosynthesis in crops: A review. *Bas. Clin. Pharmacol. Toxicol.* 126. doi: 10.3389/fpls.2020.607029

Liu, Y. F., Han, X. R., Zhan, X. M., Yang, J. F., Wang, Y. Z., Song, Q. B., et al. (2013). Regulation of calcium on peanut photosynthesis under low night temperature stress. *J. Integr. Agric.* 12, 2172–2178. doi: 10.1016/S2095-3119(13)60411-6

Liu, Y. F., Qi, H. Y., Bai, C. M., Qi, M. F., Xu, C. Q., Hao, J. H., et al. (2011). Grafting helps improve photosynthesis and carbohydrate metabolism in the leaves of muskmelon. *Int. J. Biol. Sci.* 7, 1161–1170. doi: 10.7150/ijbs.7.1161

Luan, S., and Wang, C. (2021). Calcium signaling mechanisms across kingdoms. *Annu. Rev. Cell Dev. Biol.* 37, 311–340. doi: 10.1146/annurev-cellbio-120219-035210

Ma, M. Z., Liu, Y. F., Bai, C., Yang, Y. H., Sun, Z. Y., Liu, X. Y., et al. (2021b). The physiological functionality of PGR5/PGRL1-dependent cyclic electron transport in sustaining photosynthesis. *Front. Plant Sci.* 12. doi: 10.3389/FPLS.2021.702196

Ma, M., Liu, Y., Bai, C., and Yong, J. W. H. (2021a). The significance of chloroplast NAD(P)H dehydrogenase complex and its dependent cyclic electron transport in photosynthesis. *Front. Plant Sci.* 12. doi: 10.3389/fpls.2021.661863

Ma, Z., Zhao, X., He, A., Cao, Y., Han, Q., Lu, Y., et al. (2022). Mycorrhizal symbiosis reprograms ion fluxes and fatty acid metabolism in wild jujube during salt stress. *Plant Physiol.* 189, kiac239. doi: 10.1093/plphys/kiac239

Melotto, M., Underwood, W., and He, S. Y. (2008). Role of stomata in plant innate immunity and foliar bacterial diseases. *Annu. Rev. Phytopathol.* 46, 101–122. doi: 10.1146/annurev.phyto.121107.104959

Murata, Y., Mori, I. C., and Munemasa, S. (2015). Diverse stomatal signaling and the signal integration mechanism. *Annu. Rev. Plant Biol.* 66 (1), 369–392. doi: 10.1146/annurev-arplant-043014-114707

Naumann, B., Busch, A., Allmer, J., Ostendorf, E., Zeller, M., Kirchhoff, H., et al. (2007). Comparative quantitative proteomics to investigate the remodeling of bioenergetic pathways under iron deficiency in *Chlamydomonas reinhardtii*. *Proteomics* 7 (21), 3964–3979. doi: 10.1002/pmic.200700407

Navazio, L., Formentin, E., Cendron, L., and Szabò, I. (2020). Chloroplast calcium signaling in the spotlight. *Front. Plant Sci.* 11. doi: 10.3389/fpls.2020.00186

Nomura, H., Komori, T., Kobori, M., Nakahira, Y., and Shiina, T. (2008). Evidence for chloroplast control of external Ca^{2+}-induced cytosolic Ca^{2+} transients and stomatal closure. *Plant J.* 53 (6), 988–998. doi: 10.1111/j.1365-313X.2007.03390.x

Nomura, H., Komori, T., Uemura, S., Kanda, Y., Shimotani, K., Nakai, K., et al. (2012). Chloroplast-mediated activation of plant immune signaling in *Arabidopsis*. *Nat. Commun.* 3, 926. doi: 10.1038/ncomms1926

Park, H. J., Kim, W. Y., and Yun, D. J. (2016). A New Insight of Salt Stress Signaling in Plant. *Mol. Cell.* 39 (6), 447–459. doi: 10.14348/molcells.2016.0083

Peng, Y., Hu, Z. T., Zhong, F. G., and Li, S. H. (2022). Effects of calcium on physiology and photosynthesis of *paris polyphylla* SM. under high temperature and strong light stress. *Pak. J. Bot.* 54 (3), 809–816. doi: 10.30848/PJB2022-3(27

Petroutsos, D., Busch, A., Janssen, I., Trompelt, K., Bergner, S. V., Weinl, S., et al. (2011). The chloroplast calcium sensor CAS is required for photoacclimation in *Chlamydomonas reinhardtii*. *Plant Cell.* 23 (8), 2950–2963. doi: 10.1105/tpc.111.087973

Qi, J. S., Song, C. P., Wang, B. S., Zhou, J. M., Kangasjarvi, J., Zhu, J. K., et al. (2018). Reactive oxygen species signaling and stomatal movement in plant responses to drought stress and pathogen attack. *J. Integr. Plant Biol.* 60 (09), 805–826. doi: 10.1111/jipb.12654

Reiland, S., Finazzi, G., Endler, A., Willig, A., Baerenfaller, K., Grossmann, J., et al. (2011). Comparative phosphoproteome profiling reveals a function of the STN8 kinase in fine-tuning of cyclic electron flow (CEF). *Proc. Natl. Acad. Sci. U. S. A.* 108 (31), 12955–12960. doi: 10.1073/pnas.1104734108

Rocha, A. G., and Vothknecht, U. C. (2012). The role of calcium in the chloroplasts-an intriguing and unresolved puzzle. *Protoplasma* 249 (4), 957–966. doi: 10.1007/s00709-011-0373-3

Sano, S., Aoyama, M., Nakai, K., Shimotani, K., Yamasaki, K., Sato, M. H., et al. (2014). Light-dependent expression of flg22-induced defense genes in *Arabidopsis*. *Front. Plant Sci.* 5. doi: 10.3389/fpls.2014.00531

Sawinski, K., Mersmann, S., Robatzek, S., and Bohmer, M. (2013). Guarding the green: pathways to stomatal immunity. *Mol. Plant-Microbe Interact.* 26 (6), 626–632. doi: 10.1094/MPMI-12-12-0288-CR

Schulze, S., Dubeaux, G., Ceciliato, P., Munemasa, S., Nuhkat, M., Yarmolinsky, D., et al (2021). A role for calcium dependent protein kinases in differential CO2-and ABA-controlled stomatal closing and low CO2-induced stomatal opening in Arabidopsis. *New Phytol.* 229 (5), 2765–2779. doi: 10.1111/nph.17079

Shi, Q. W., Pang, J. Y, Yong, J. W. H., Bai, C. M., and Lambers, H. (2020). Phosphorus-fertilisation has differential effects on leaf growth and photosynthetic capacity of Arachis hypogaea L.. *Plant Soil* 447, 99–116. doi: 10.1007/s11104-019-04041-w

Song, Q. B., Liu, Y. F., Pang, J. Y., Yong, J. W. H., Chen, Y. L., Bai, C. M., et al. (2020). Supplementary calcium restores peanut (*Arachis hypogaea*) growth and photosynthetic capacity under low nocturnal temperature. *Front. Plant Sci.* 10. doi: 10.3389/fpls.2019.01637

Stael, S., Kmiecik, P., Willems, P., van der Kelen, K., Coll, N. S., Teige, M., et al. (2015). Plant innate immunity-sunny side up? *Trends Plant Sci.* 20 (1), 3–11. doi: 10.1016/j.tplants.2014.10.002

Stael, S., Rocha, A. G., Wimberger, T., Anrather, D., Vothknecht, U. C., and Teige, M. (2012). Cross-talk between calcium signaling and protein phosphorylation at the thylakoid. *J. Exp. Bot.* 63 (4), 1725–1733. doi: 10.1093/jxb/err403

Sun, Z. Y., Liu, X. Y., Zhang, S. W., Ma, M. Z., Bai, R., Liu, H., et al (2022). Mechanism of Exogenous Calcium Alleviating Sub - low Phosphorus Photosynthesis Obstacle in Peanut. *J. Plant Nutri. Fertil.* 28 (6), 1055–1066. doi: 10.11674/zwyf.2021514

Sun, Z. Y., Jin, X. F., Albert, R., and Assmann, S. M. (2014). Multi-level modeling of light-induced stomatal opening offers new insights into its regulation by drought. *PloS Comput. Biol.* 10 (11), e1003930. doi: 10.1371/journal.pcbi.1003930

Tang, R. H., Han, S. C., Zheng, H. L., Cook, C. W., Choi, C. S., Woerner, T. E., et al. (2007). Coupling diurnal cytosolic Ca^{2+} oscillations to the CAS-IP_3 pathway in *Arabidopsis*. *Science* 315 (5817), 1423–1426. doi: 10.1126/science.1134457

Tang, L. G., Yang, G. G., Ma, M., Liu, X. F., Li, B., Xie, J. T., et al. (2020). An effector of a necrotrophic fungal pathogen targets the calcium-sensing receptor in chloroplasts to inhibit host resistance. *Mol. Plant Pathol.* 21 (5), 686–701. doi: 10.1111/mpp.12922

Terashima, M., Petroutsos, D., Hüdlg, M., Tolstygina, I., Trompelt, K., Gäbelein, P., et al. (2012). Calcium-dependent regulation of cyclic photosynthetic electron transfer by a CAS, ANR1, and PGRL1 complex. *Proc. Natl. Acad. Sci. U. S. A.* 109 (43), 17717–17722. doi: 10.1073/pnas.1300172110

Trippens, J., Reißenwebe, T., and Kreimer, G. (2017). The chloroplast calcium sensor protein CAS affects phototactic behavior in *Chlamydomonas reinhardtii* (Chlorophyceae) at low light intensities. *Phycologia* 56 (3), 261–270. doi: 10.2216/16-67.1

Ueda, M., and Seki, M. (2020). Histone modifications form epigenetic regulatory networks to regulate abiotic stress response. *Plant Physiol.* 182 (1), 15–26. doi: 10.1104/pp.19.00988

Vainonen, J. P., Sakuragi, Y., Stael, S., Tikkanen, M., Allahverdiyeva, Y., Paakkarinen, V., et al. (2008). Light regulation of CAS, a novel phosphoprotein in the thylakoid membrane of *Arabidopsis thaliana*. *FEBS J.* 275 (8), 1767–1777. doi: 10.1111/j.1742-4658.2008.06335.x

Vener, A. V. (2007). Environmentally modulated phosphorylation and dynamics of proteins in photosynthetic membranes *Biochim. Biophys. Acta-Bioenerg.* 1767 (6), 449–457. doi: 10.1016/j.bbabio.2006.11.007

Wang, W. H. (2013). *Studies on signal transduction and CAS function involved in plant calcium receptor CAS* (Xiamen: University of XiaMen). Available at: http://dspace.xmu.edu.cn:8080/dspace/handle/2288/78689.

Wang, W. H., Chen, J., Liu, T. W., Chen, J., Han, A. D., Simon, M., et al. (2014). Regulation of the calcium-sensing receptor in both stomatal movement and photosynthetic electron transport is crucial for water use efficiency and drought tolerance in *Arabidopsis*. *J. Exp. Bot.* 65 (1), 223–234. doi: 10.1093/jxb/ert362

Wang, W. H., He, E. M., Chen, J., Guo, Y., Chen, J., Liu, X., et al. (2016b). The reduced state of the plastoquinone pool is required for chloroplast-mediated stomatal closure in response to calcium stimulation. *Plant J.* 86, 132–144. doi: 10.1111/tpj.13154

Wang, L. Y., Yamano, T., Takane, S., Niikawa, Y., Toyokawa, C., Ozawa, S. I., et al. (2016a). Chloroplast-mediated regulation of CO_2-concentrating mechanism by Ca^{2+}-binding protein CAS in the green alga *Chlamydomonas reinhardtii*. *Proc. Natl. Acad. Sci. U. S. A.* 113 (44), 12586–12591. doi: 10.1073/pnas.1606519113

Wang, W. H., Yi, X. Q., Han, A. D., Liu, T. W., Chen, J., Wu, F. H., et al. (2012). Calcium-sensing receptor regulates stomatal closure through hydrogen peroxide and nitric oxide in response to extracellular calcium in *Arabidopsis*. *J. Exp. Bot.* 63 (1), 177–190. doi: 10.4161/psb.18882

Weinl, S., Held, K., Schlucking, K., Steinhorst, L., Kuhlgert, S., Hippler, M., et al. (2008). A plastid protein crucial for Ca^{2+}-regulated stomatal responses. *New Phytol.* 179 (3), 675–686. doi: 10.1111/j.1469-8137.2008.02492.x

Wu, D., Liu, Y., Pang, J., Yong, J. W. H., Chen, Y., Bai, C., et al. (2020). Exogenous calcium alleviates nocturnal chilling-induced feedback inhibition of photosynthesis by improving sink demand in peanut (*Arachis hypogaea*). *Front. Plant Sci.* 11. doi: 10.3389/fpls.2020.607029

Xu, Y., and Huang, B. (2018). Comparative transcriptomic analysis reveals common molecular factors responsive to heat and drought stress in *Agrostis stolonifera*. *Sci. Rep.* 8 (1), 15181. doi: 10.1038/s41598-018-33597-3

Yamano, T., Toyokawa, C., and Fukuzawa, H. (2018). High-resolution suborganellar localization of Ca^{2+}-binding protein CAS, a novel regulator of CO_2-concentrating mechanism. *Protoplasma* 255 (4), 1015–1022. doi: 10.1007/s00709-018-1208-2

Zhang, J., Fang, H., Huo, J. Q., Huang, D. J., Wang, B., and Liao, W. B. (2018). Involvement of calcium and calmodulin in nitric oxide-regulated senescence of cut lily flowers. *Front. Plant Sci.* 9. doi: 10.3389/fpls.2018.01284

Zhang, J. L., Zhou, M. X., Liu, W., Nie, J. J., and Huang, L. L.. (2022). Pseudomonas syringae pv. actinidiae effector HopAU1 interacts with calcium-sensing receptor to activate plant immunity. *Int. J. Mol. Sci.* 23 (1), 508. doi: 10.3390/ijms23010508

Zhao, X., Wang, Y. J., Wang, Y. L., Wang, X. L., and Zhang, X. (2011). Extracellular Ca^{2+} alleviates NaCl-induced stomatal opening through a pathway involving H_2O_2-blocked na^+ influx in *Vicia* guard cells. *J. Plant Physiol.* 168 (9), 903–910. doi: 10.1016/j.jplph.2010.11.024

Zhao, X., Xu, M. M., Wei, R. R., and Liu, Y. (2015). Expression of OsCAS (Calcium-sensing receptor) in an *Arabidopsis* mutant increases drought tolerance. *PloS One* 10 (6), e0131272. doi: 10.1371/journal.pone.0131272

Zheng, Y., Liao, C., Zhao, S., Wang, C., and Guo, Y. (2017). The glycosyltransferase QUA1 regulates chloroplast-associated calcium signaling during salt and drought stress in *Arabidopsis*. *Plant Cell Physiol.* 58 (2), 329–341. doi: 10.1093/pcp/pcw192

frontiers | Frontiers in Plant Science

TYPE Original Research
PUBLISHED 21 October 2022
DOI 10.3389/fpls.2022.1042920

Check for updates

OPEN ACCESS

EDITED BY
Mehdi Rahimi,
Graduate University of Advanced Technology, Iran

REVIEWED BY
Honghai Luo,
Shihezi University, China
Wei Hu,
Nanjing Agricultural University, China
Jia Gao,
China Agricultural University, China

*CORRESPONDENCE
Jiwang Zhang
jwzhang@sdau.edu.cn

†These authors have contributed equally to this work

SPECIALTY SECTION
This article was submitted to Plant Abiotic Stress, a section of the journal Frontiers in Plant Science

RECEIVED 13 September 2022
ACCEPTED 07 October 2022
PUBLISHED 21 October 2022

CITATION
Wang S, Hu J, Ren B, Liu P, Zhao B and Zhang J (2022) Effects of hydrogen peroxide priming on yield, photosynthetic capacity and chlorophyll fluorescence of waterlogged summer maize. *Front. Plant Sci.* 13:1042920. doi: 10.3389/fpls.2022.1042920

COPYRIGHT
© 2022 Wang, Hu, Ren, Liu, Zhao and Zhang. This is an open-access article distributed under the terms of the Creative Commons Attribution License (CC BY). The use, distribution or reproduction in other forums is permitted, provided the original author(s) and the copyright owner(s) are credited and that the original publication in this journal is cited, in accordance with accepted academic practice. No use, distribution or reproduction is permitted which does not comply with these terms.

Effects of hydrogen peroxide priming on yield, photosynthetic capacity and chlorophyll fluorescence of waterlogged summer maize

Shouran Wang†, Juan Hu†, Baizhao Ren, Peng Liu, Bin Zhao and Jiwang Zhang*

State Key Laboratory of Crop Biology and College of Agronomy, Shandong Agricultural University, Tai'an, Shandong, China

Extreme rainfall events during the summer maize growth and development periods, which have induced losses in summer maize production. There was a completely randomized block experiment being designed with four treatments: waterlogging for 6 days at the V3 stage (C-W), H_2O_2-priming + non-waterlogging (H-CK), H_2O_2-priming + waterlogging for 6 days at the V3 stage (H-W) and control (C-CK). This study investigated the effects of H_2O_2 priming on yield and photosynthetic parameters of (*Zea mays*. L) summer maize hybrid DengHai605 (DH605) by measuring the leaf area index (LAI), soil and plant analyzer development (SPAD) value, stomatal morphology, gas exchange parameters, and chlorophyll fluorescence parameters. The results showed that the net photosynthetic rate (Pn) was decreased after waterlogging through the stomatal limitation of CO_2 supply and reduction of PSII photochemical efficiency, which led to the decrease in dry matter accumulation and grain yield. H_2O_2 priming increased the number of opening stomas, the stomatal length, and width, thus increasing Ci by 12.1%, which enhanced the Pn by 37.5%. Additionally, H_2O_2 priming could improve the energy of dark reaction carbohydrates by increasing the light energy absorption and utilization, alleviating the function of PSII reaction centers, protecting the PSII receptor and donor side, and the electron transport chain. The φEo, φPo, φRo, and Ψo of H-W were increased by 89.9%, 16.2%, 55.4%, and 63.9% respectively, and the φDo was decreased by 23.5%, compared with C-W. Therefore, H_2O_2 priming significantly enhanced the PSII photochemical efficiency, and increased the CO_2 supply in dark reactions to promote carbon assimilation, alleviating the waterlogging-induced damage to maize plant growth and grain yield.

KEYWORDS

summer maize, H2O2 priming, photosynthesis characteristics, waterlogging stress, grain yield

1 Introduction

In recent years, due to anthropogenic contributions including industrialization and urbanization, the environmental conditions have deteriorated, causing waterlogging disasters to occur frequently all over the world (Pan, 2022; Voesenek and Bailey-Serres, 2015). Waterlogging, as one of the main abiotic stresses for the normal growth and development of summer maize, seriously harmed crop production in nearly 16% of the world's agricultural production areas (Seng et al., 2012; Zhou et al., 2020). In the Huang huai hai region, the seedling stage (especially in the V3 stage) of summer maize coincided with the period of frequent rainfall (Yu, 2015). The Huang huai hai Plain was the main summer maize producing area in China, whose planting area and yield accounted for more than 1/3 of all maize planting areas in China (Gao, 2018), and 70% of annual precipitation was concentrated during the growing period of summer maize. Such a large amount of precipitation would lead to frequent rainfall-induced waterlogging, which could seriously affect the yield and quality of summer maize (Ren et al., 2015). It is thus desirable to explore effective management to mitigate the waterlogging damages to maize production.

When water content exceeded 80% of the maximum field water capacity, plant growth and development of summer maize were significantly inhibited, and the greatest impact occurred at the V3 stage (Ren et al., 2017). From the point of view of phenotypic characteristics: The leaves turn yellow and lose their green colour, which decreased the leaf area index and SPAD values, and reduced the production capacity by optical contraction (Ren et al., 2015). From the physiological point of view: Waterlogging stress resulted in stomatal closure, thus blocking the CO_2 uptake, which significantly reduced the photosynthetic rate of summer maize, and inhibited the ability of photosynthetic assimilation ability (Ren et al., 2018). With the prolonged waterlogging duration, the PSII system of summer maize was damaged, photosynthetic electron transport was blocked, and carbon assimilation was inhibited (Hu et al., 2020; Ren et al., 2020; Yu et al., 2021). So, when the plants encountered waterlogging stress, the stomatal performance and the PSII photoinhibition of leaves were limited, which further reduced production capacity and reduced the grain yield finally.

Chemical priming could improve the plant plasticity to abiotic stresses (Kaori et al., 2020). Plant priming was related to stress "memory" which as a potential way of improving cross-tolerance (When the plants were exposed to a mild stress, the subsequence severe stresses were improved) (Munné-Bosch and Alegre, 2013). H_2O_2, as one of the chemical priming agents, played an important role in the stress signal transduction pathway that was essential for crop growth and adaptation to adversity (Gao et al., 2010; Hossain et al., 2015). H_2O_2 played a wide role in plants responding to abiotic stresses by regulating a multitude of physiological processes such as acquiring resistance, antioxidant defense, photosynthesis, and stomatal opening (Petrov and Breusegem, 2012; Gdsa et al., 2020). Previous studies have demonstrated that pretreatments with 70 mM H_2O_2 favored the increase in net physiological rate, PSII efficiency, plant biomass, and antioxidant activity of leaves in soybean (*Glycine max* [L.] Merr.) (Andrade et al., 2018). It has been well summarized in several reviews that H_2O_2 priming could enhance plant tolerance to abiotic stress (Perez and Brown, 2014; Ayano et al., 2015; Kaori et al., 2020). Recent publications have reported that exogenous treatment of H_2O_2 could preserve plants from low temperature (Wahid et al., 2007), drought (Zhang et al., 2022), salt (Gondim et al., 2009), waterlogging (Andrade et al., 2018), and other stresses. Nonetheless, the use of H_2O_2 as a chemical priming agent has been rarely studied under waterlogging stress, especially in H_2O_2 alleviating the effects of waterlogging stress on photosynthetic characteristics (Perez & Brown, 2014; Ayano et al., 2015). As one of the most basic physiological activities of plants, photosynthesis which provided material and energy for plant life activities was also one of the important indicators of the ability of plants to withstand adversity and stress. The photosynthesis in the leaves decreased under waterlogging pressure, which would reduce crop yield and quality (Ashraf and Harris, 2013; Tian et al., 2019). This study was to investigate the effects of H_2O_2 priming on the yield and photosynthetic characteristics of summer maize subjected to waterlogging stress, thus providing theoretical and technical support for the chemical regulation of summer maize under waterlogging stress.

2 Materials and methods

2.1 Experimental materials and design

This experiment was conducted in 2020 and 2021 to explore the effects of H_2O_2 priming on waterlogged summer maize at the Shandong Agricultural University experimental farm (36.10°N, 117.09°E). Summer maize hybrid Denghai605 (DH605) was used as experimental materials. DH605 was approved by the approval committee of China in 2010 which was suitable for planting with in Shandong province and widely grown in China (Hu et al., 2020). Seed soaking for 12 h with 0.1% H_2O_2 [relevant literature showed that 0.1% H_2O_2 significantly promoted the germination of maize seeds (Zhang, 1996)]. Summer maize was sown on June 9 in 2020 and 2021 with the density of 67500 plants ha^{-1}, and waterlogging at the V3 stage for 6 days (Extreme rainfall events were frequent in the Huang huai hai region from June to July which was the V3 stage of summer maize (Supplementary Figure 1). At the same time, the plant growth and development of summer maize were significantly inhibited

TABLE 1 Waterlogging treatments for summer maize in the field from 2020 to 2021.

Abbreviation	Treatment
C-CK	Non-waterlogging treatment
C-W	Waterlogging at V3 stage
H-CK	H_2O_2 priming – Non-waterlogging treatment
H-W	H_2O_2 priming - Waterlogging at V3 stage

after waterlogging, and the greatest impact occurred at the V3 stage (Ren et al., 2017)). For details, see (Table 1). N, P, and K fertilizers were applied as base fertilizers: 210 kg ha^{-1} N (urea, 46% N), 52.5 kg ha^{-1} P_2O_5 (calcium superphosphate, 17% P_2O_5), and 67.5 kg ha^{-1} K_2O (muriate of potash, 60% K_2O). Management of other diseases, insects, grasses, and pests by reference to high-yield fields. The details were shown in (Hu et al., 2021). Complete randomized block design. Plot planting test was used in this experiment. A square plot was formed by 4 pieces of PVC board with 4 m × 4 m to form a 16 m^2 reservoir. Each piece of PVC plate was a length 4 m and width 2.3 m, which was used to bury 2.0 m below the underground and 0.3m above ground to facilitate the formation of a 2-3 cm water layer. The climatic conditions of the maize growing season in 2020 and 2021 are shown in (Supplementary Figure 1). The total annual precipitations were 805.8 and 939.1mm in 2020 and 2021, and mean temperatures were 25.1 and 25.3°C during the summer maize growth cycles in the two years.

2.2 Leaf area index

After 6 days of continuous waterlogging, six representative plant samples were signed from each plot (H-CK, H-W, C-CK, C-W) to measure and calculate leaf area. LAI was calculated as follows (Ren et al., 2016).

Leaf area (cm^2)=L (cm)×W (cm)×0.75

LAI=(leaf area per plant×plant number per plot)/plot area

2.3 Soil and plant analyzer development value

After 6 days of continuous waterlogging, a chlorophyll meter (SPAD-502, Soil-plant Analysis Development Section, MinoltaMinolta-CameraCo., Osaka, Japan) was used to measure 12 times of each plot to obtain the leaf SPAD value.

2.4 Dry matter accumulation

After 6 days of continuous waterlogging, three typical plant samples were selected from each plot. The samples were placed in the oven at 105°C in a force-draft oven for 30 min, and then dried to constant weight at 80°C and weighed separately. Refer to the specific method as follows (Ren et al., 2017).

2.5 Stomatal phenotypic characteristics of leaves

After 6 days of continuous waterlogging, the stomatal samples were collected during 9:00-11:00 am. First of all, we collected stomatal imprints from the middle section of the new fully expanded leaf using colorless transparent nail polish. Three leaves were selected for each plot and two replicates per leaf. After drying, the leaf was cut with scissors and then pasted with colorless transparent tape on the leaf with nail polish to be tested on the slide (Zheng et al., 2013; Yan et al., 2021). The imprints were observed and photographed in the laboratory with a microscope (Biological microscope, Nikon of Japan, Ni-u). A total of 30 photos (3 × 2 × 5) were taken from 5 randomly selected fields of vision at 200 × for stomatal density (SD, number of pores per unit area) and proportion of open stomata (POS), and 30 photos were taken at 400 × for open stomatal length (SL), width (SW), perimeter (SP) and area (SA) measurement and recording (Li et al., 2018).

2.6 Leaf gas exchange parameters

After 6 days of continuous waterlogging, the leaf gas exchange parameters: the net photosynthetic rate (Pn), stomatal conductance (Gs), intercellular CO_2 concentration (Ci), and transpiration rate (Tr) of ear leaves were measured between 10:00-12:00 am under saturating irradiance using a portable infrared gas analyzer (CIRAS-3, PP System, Hanstaech, U.K) and then calculated the pore limit value (Ls). Leaves with consistent growth and good light exposure under different treatments were selected. Five leaves were measured randomly for each treatment. Measurement conditions were kept consistent: LED light source and photosynthetically available radiation (PAR) of 1600 μmol m^{-2}. CO_2 concentration was maintained at a constant level of 360 μmol mol-1 using a CO_2 injector with a high-pressure liquid CO_2 cartridge.

Ls=(Ca-Ci)/Ca, in this formula, Ci was intercellular CO_2 concentration and Ca was environmental CO_2 concentration (Berry, 1982; Seng et al., 2012).

2.7 Chlorophyll fluorescence parameters

After 6 days of continuous waterlogging, photo-induced transients' photoinduced transients (Supplementary Table 1) of Fo, Fm, Fv/Fm, Wk, Vj, TRo/CSm, ETo/CSm, DIo/CSm, ABS/CSm, ψO, φDo, φEo, φPo, PI_{ABS} of the five typical leaves each plot was measured by M-PEA (Multi-Function Plant Efficiency Analyser, Hansatech Instruments Limited, U.K). See (Strasser, 2004) for the specific meanings of the parameters. The M-PEA data version was 1.10, the measurement duration was 10.0s, the number of data points was 145, and the red-light intensity was 3000 μmol m^{-2} s^{-1}. The determination time was consistent with that of photosynthetic parameters. The leaves should be dark-treated with clamps for 20 min before determination. Representative plants with good growth should be selected, with 5 plants in each treatment.

2.8 Grain yield

At R6, 30 ears harvested continuously selected from three rows were used to determine yield and ear traits. Grain yield was calculated as follows (Ren et al., 2016).

Grain yield (kg ha^{-1}) = Harvest ear (ears ha^{-1})×Number of kernel per ear×1,000-grain weight (g/1000 grains)/10^6×(1-moisture content%)/(1-14%)

2.9 Statistical analysis

Microsoft Excel 2016 (Microsoft, Redmond, WA, USA) was used for data processing and analysis. IBM SPSS Statistics 18.0 (IBM Cor-poration, Armonk, NY, USA) was used for data analysis. Analysis of variance (ANOVA) and LSD (Least significant difference) tests was used for comparisons analysis. The coefficient of pearson was used for the analysis of correlation. The significant differences are at $P<0.05$. The data were plotted using Origin 2021 (OriginLab Corporation, MA, USA) and Sigmaplot 12.5 (Systat Software, Inc., Richmond, CA, USA) software.

3 Results

3.1 Effects of H_2O_2 priming on summer maize yield under waterlogging stress at the V3 stage

3.1.1 Yield

The summer maize yield was significantly reduced after waterlogging, but H_2O_2 priming could increase the yield of waterlogged summed maize (Table 2). In 2020, the grain yield of summer maize in C-W and H-W decreased by 24.3% and 12.4% compared with C-CK (Control treatment) respectively, C-W was 15.7% lower than H-W. The two-year results were basically consistent. The increase in grain number per ear was responsible for the significantly greater yields obtained from H_2O_2 priming waterlogged plants (Table 2). In 2020, the grain number per ear of H-W was 12.4% higher than C-W, C-W and H-W decreased by 16.5% and 6.3% compared with C-CK. The two-year results were basically consistent.

3.1.2 Dry matter weight

Waterlogging reduced the dry matter accumulation of summer maize, while H_2O_2 priming could significantly alleviate waterlogging damages on the weight of dry matter. In 2020, compared with C-CK, waterlogging significantly decreased dry matter weight by respectively 28.7% and 23.9% on C-W and H-W respectively, and H-W was 6.7% higher than C-W. The two-year results were basically consistent (Figure 1).

3.2 Stomatal features of maize leaves

Stomatal density, stomatal length-width ratio, and stomatal shape index of summer maize increased significantly after waterlogging, while the proportion of opening stomas, stomatal length, and width was significantly decreased. H_2O_2

TABLE 2 Effects of H_2O_2 seed soaking on yield of summer maize under waterlogging stress at the seedling stage.

Year	Treatment	Ear number (ears ha^{-1})	Grains per ear	1000-kernel weight (g)	Yield (kg ha^{-1})
2020	C-CK	63125	562a	402a	14269a
	C-W	62500	469c	369b	10805c
	H-CK	62500	582a	406a	14752a
	H-W	64375	527b	372b	12505b
2021	C-CK	67500	527a	363a	12914b
	C-W	63125	437c	321c	8861d
	H-CK	67500	535a	364a	13142a
	H-W	65625	466b	349b	10682c

Values Followed by a different small letter within a column are significantly different at the 0.05 probability level. Differences between treatments were calculated within the hybrids. The same as below.

10.3389/fpls.2022.1042920

priming alleviated the effect on the stomatal performance of waterlogged summer maize (Table 3). In 2020, the stomatal density (SD) of C-W was increased by 44.3% compared with C-CK, H-W decreased by 11.0% compared with C-CK, and H-W were decreased by 36.4% compared with C-W, but there was no significant difference between H-CK and C-CK. The stomatal length-width ratio (SL/SW) of H-W were decreased by 22.9% compared with C-W. The stomatal opening ratio (POS) of H-W was increased by 137.1% compared with the C-W. The two-year results were basically consistent. Additionally, the stomatal arrangement pattern was irregular, and stomatal density and the number of opening stomas were harmed after waterlogging stress at the V3 stage. H_2O_2 priming could significantly alleviate waterlogging damages on the stomatal arrangement pattern, density, and size of summer maize. It could be seen that the stomatal size and the degree of the stomatal opening of C-W were significantly smaller, and the open stomas were slender and flat, than those of C-CK. After priming with H_2O_2, the size and the degree of stomatal opening were significantly increased (Figure 2). The two-year results were basically consistent.

3.3 Photosynthetic characteristics

3.3.1 Leaf area index

The leaf area index (LAI) was decreased significantly after waterlogging, but H_2O_2 priming could alleviate the negative effects on LAI after waterlogging. In 2020, the LAI of H-W was increased by 9.4% compared with C-W, the C-W and H-W was decreased by 48.6% and 43.7% than C-CK. The two-year results were basically consistent (Figures 3A, B).

3.3.2 Soil and plant analyzer development value

Soil and Plant Analyzer Development (SPAD) value was decreased significantly after waterlogging, but H_2O_2 priming could significantly alleviate the effects of waterlogging on SPAD. In 2020, pretreatment with H_2O_2 significantly increased the SPAD (around 8.0%) compared with C-W. The two-year results were basically consistent (Figures 3C, D).

3.3.3 Leaf gas exchange parameters

Leaf Pn, Gs, Ci, and Tr were significantly decreased after waterlogging. In 2020, a reduction in Pn (around 51.1%), Gs

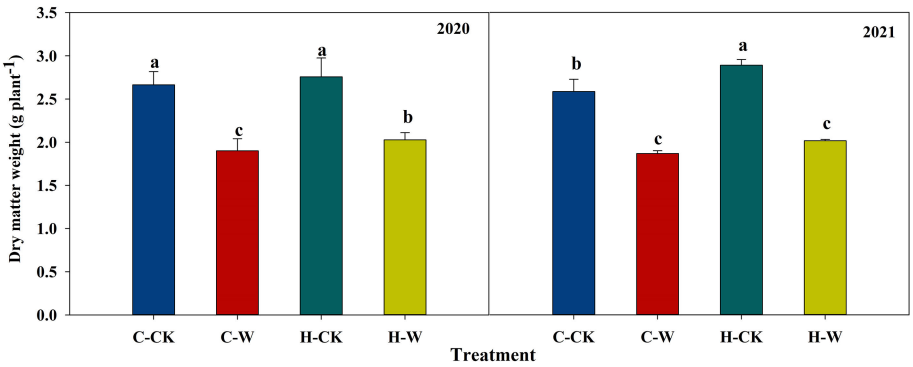

FIGURE 1
Effects of H_2O_2 priming on dry matter accumulation of summer maize under waterlogging stress at the seedling stage. *Note:* C-CK: Control treatment, C-W: Waterlogging for 6 days at the V3 stage; H-CK: H_2O_2-priming + non-waterlogging; H-W: H_2O_2-priming + waterlogging for 6 days at the V3 stage. The same as below.

TABLE 3 Effects of H_2O_2 priming on leaf stomatal morphology of summer maize under waterlogging stress at the seedling stage.

Year	Treatment	SD (No mm^{-2})	SL (μm)	SW (μm)	SL/SW	SP (μm)	SA (μm)	POS (%)
2020	C-CK	28.75b	37.22b	22.74bc	1.65c	99.87c	692.40c	86.03a
	C-W	41.50a	31.21c	20.58c	1.53c	85.24d	510.17d	32.24c
	H-CK	28.20b	49.46a	23.81ab	2.08a	127.27a	968.64a	86.54a
	H-W	26.40b	48.37a	25.69a	1.88b	118.12b	892.98b	76.43b
2021	C-CK	23.20b	37.33bc	25.59ab	1.48b	105.86bc	812.32b	91.63a
	C-W	34.20a	34.25c	23.71c	1.46b	101.67c	678.32c	39.69c
	H-CK	26.40b	45.72a	26.17ab	1.75a	117.95a	934.54a	93.93a
	H-W	32.40a	39.70b	26.45a	1.50b	108.74b	825.34b	74.35b

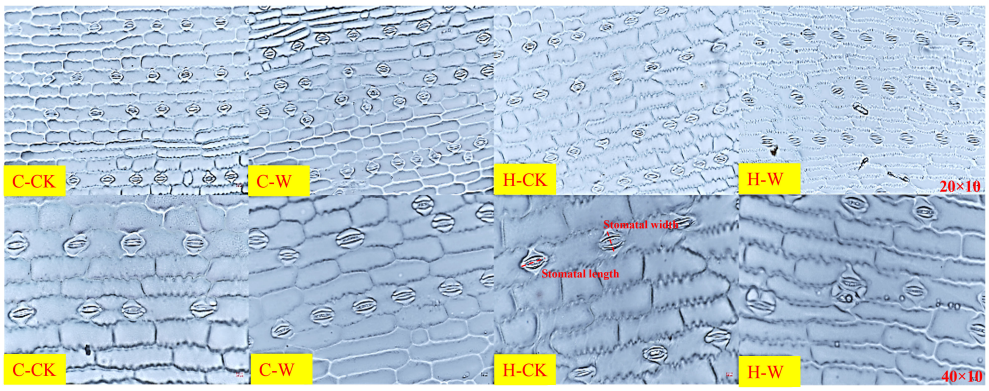

FIGURE 2
Effects of H_2O_2 priming on stomatal morphological characteristics of summer maize under waterlogging stress at the seedling stage.

(around 69.5%), Ci (around 14.8%), and Tr (around 46.3%) was observed in C-W treatment compared with C-CK. Pretreatment with H_2O_2 increased the Pn (around 37.5%), Gs (around 80.4%), Ci (around 12.1%), and Tr (around 46.3%) of summer maize compared with C-W. The two-year results were basically consistent (Figure 4). The stomatal limitation (Ls) of summer maize increased significantly after waterlogging stress, and H_2O_2 priming could significantly reduce the Ls of waterlogged maize. In 2020, the stomatal limitation of H-W decreased by 15.7% compared with C-W. The two-year results were basically consistent (Figure 4).

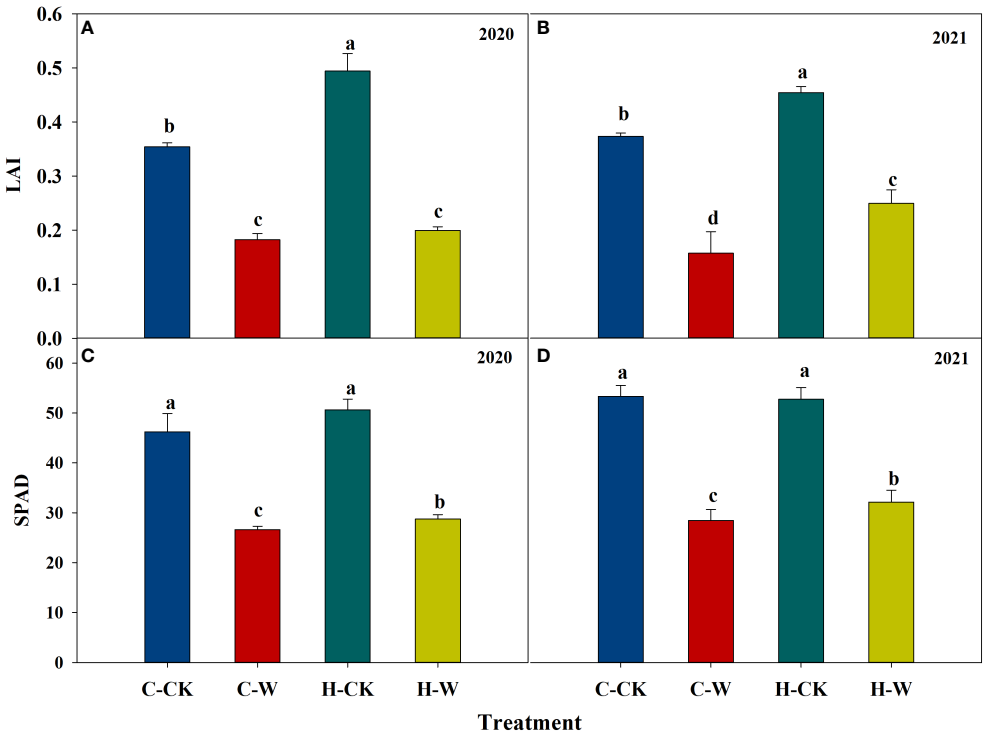

FIGURE 3
Leaf area index and Soil and plant analyzer development (SPAD) value. **(A, B)** Leaf area index in 2020 and 2021; **(C, D)** Soil and plant analyzer development (SPAD) value in 2020 and 2021.

10.3389/fpls.2022.1042920

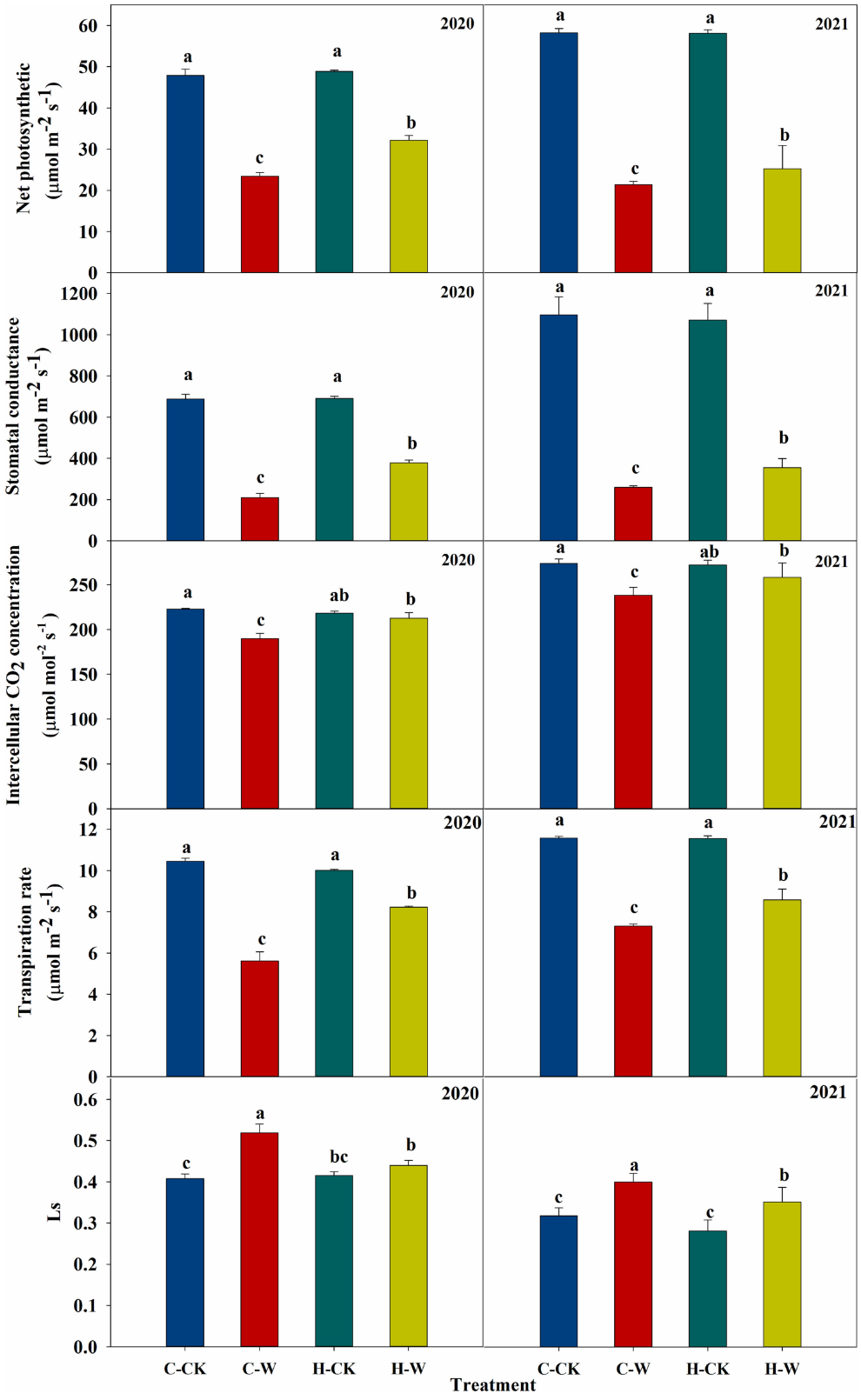

FIGURE 4
Effects of H_2O_2 priming on gas exchange parameters of summer maize under waterlogging stress at the seedling stage.

3.4 Chlorophyll fluorescence parameters

3.4.1 Changes in PSII donor/acceptor sides

The shape of the Vt curve was obviously changed after waterlogging stress. As was shown in (Figure 5), the K and J step were significantly increased after waterlogging. The Wk of H-W was decreased by 14.6% compared with that of C-W. The Vj of H-W was 25.7% lower than that of C-W. The two-year results were basically consistent (Figure 5).

3.4.2 PSII biophysical parameters derived by the JIP-test equations

3.4.2.1. Phenomenological energy fluxes (per exciting cross-section - CS)

Under waterlogging stress, electron transport flux per excited CS (ETo/CSo) in maize leaves was significantly decreased, but the heat dissipation per unit area (DIo/CSo) was significantly increased. H_2O_2 priming significantly increased ETo/CSo and decreased DIo/CSo (Figure 6A). In 2020, ETo/CSo of H-W was increased by 55.3% compared with that of C-W. DIo/CSo of H-W was decreased by 37.6% compared with that of C-W. The two-year results were basically consistent (Figure 6A). There was a decrease in trapping flux per excited CS (TRo/CSm) (blue arrow), electron transport flux per excited CS (ETo/CSm) (purple arrow), absorption flux per excited CS (ABS/CSm) (yellow arrow), but an increase in dissipated energy flux per excited CS (DIo/CSm) (red arrow) in waterlogged maize (Figures 6A, B). In 2020, ETo/CSm of H-W was increased 102.7% compared with that of C-W; DIo/CSm of H-W was decreased 18.7% compared with that of C-W. The two-year results were basically consistent (Figures 6A, B).

3.4.2.2 Specific energy fluxes (per Q_A reducing PSII reaction center – RC)

Waterlogging stress significantly reduced electron transport flux per RC (ETo/RC) and increased dissipated energy flux per RC (DIo/RC) in maize seedling leaves, while H_2O_2 priming significantly increased ETo/RC and decreased DIo/RC (Figures 6A, C). In 2020, RC/CSm of C-W and H-W were decreased by 42.6% and 15.6% compared with that of C-CK, respectively, and H-W was increased by 47.0% compared with that of C-W; ETo/RC of H-W was increased by 41.0% compared with that of C-W; DIo/RC of H-W was decreased by 43.1% compared with that of C-W (Figures 6A, C). The two-year results were basically consistent (Figures 6A, C).

3.4.2.3 Quantum yields and efficiencies/probabilities

The probability (at t = 0) that a trapped exciton moves an electron into the electron transport chain beyond Q_A^- (Ψo), the quantum yield of electron transport (φEo), and the maximum quantum yield of primary photochemistry (φPo) were decreased significantly and the quantum ratio (φDo) was increased significantly after waterlogging, while H_2O_2 priming significantly increased Ψo, φEo, φPo and significantly decreased φDo (Figure 6A). In 2020, φEo of H-W was increased by 89.9% compared with that of C-W; φPo of H-W was increased 16.2% compared with that of C-W; φDo of H-W was decreased by 23.5% compared with that of C-W (Figure 6A). In 2020, PI_{ABS} of H-W was increased by 352.8% compared with that of C-W (Figure 6A).

3.5 Correlation analysis

Correlation analysis showed that the net photosynthetic rate of summer maize was related to stomatal factors and non-stomatal factors. Pn was positively correlated with POS, Gs, and Ci. From the perspective of chlorophyll fluorescence, Pn was significantly positively correlated with φPo, φEo, φRo, and PI_{ABS}, but negatively correlated with φDo (Figure 7). The decrease in grain yield of waterlogged summer maize was significantly correlated with the decreases of 1000-grain weight

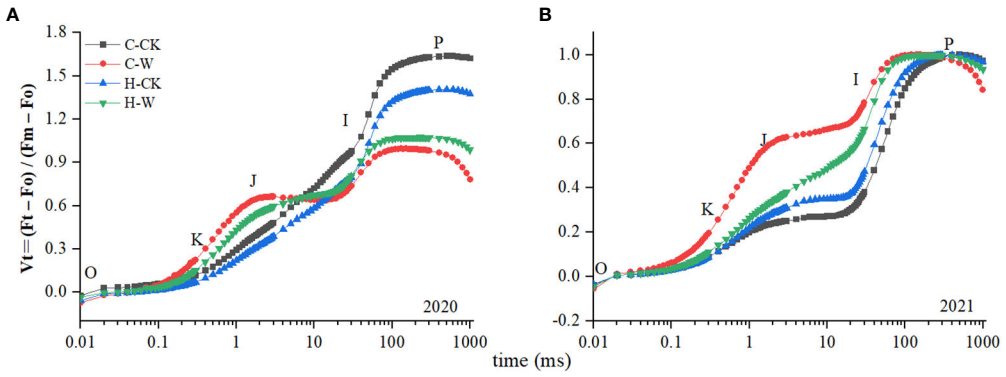

FIGURE 5
Changes in PS II donor/acceptor sides. **(A, B)** Vt curves in 2020 and 2021.

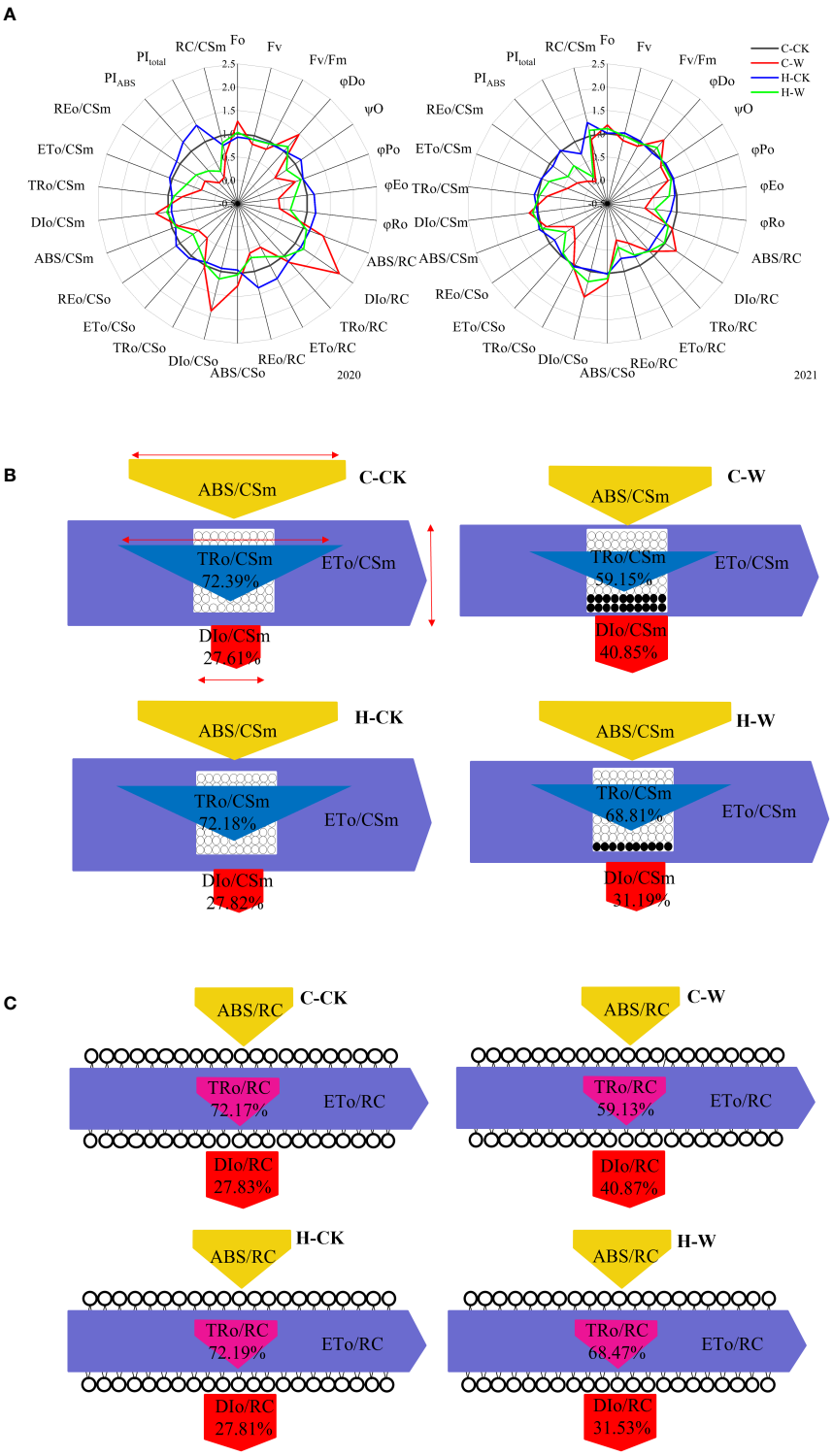

FIGURE 6
PSII biophysical parameters derived by the JIP-test equations. **(A)** Changes of JIP parameter radar images in 2020 and 2021. *Note:* The values were calculated relative to the C-CK, taken as 1, and the fluorescence parameters of other treatments were transformed into the percentage of C-CK fluorescence parameters. **(B)** Energy pipeline models of phenomenological fluxes (per cross-section, CSm) in 2020. The decrease in absorption (yellow), trapping (cyan), and electron transport (purple), can be seen as changes in the width of each arrow (red arrow = scale). The active reaction center is represented by a white circle, and the inactive reaction center is represented by a black circle. **(C)** Specific energy flux (membrane model) in 2020.

and grain number per spike. From the perspective of stomata, grain number per ear, 1000-grain weight, and yield were significantly negatively correlated with stomatal density (SD), but positively correlated with the proportion of open stomata (POS). Grain number per ear, 1000-grain weight, and yield was significantly positively correlated with Gs, Ci, Tr and Pn. From the perspective of chlorophyll fluorescence, grain number per ear, 1000-grain weight, and yield were significantly positively correlated with φPo, φEo, φRo, and PI_{ABS}, but significantly negatively correlated with φDo (Figure 7).

4 Discussion

4.1 The mitigation effect of H_2O_2 priming on photosynthetic characteristics of waterlogged summer maize at the seedling stage

4.1.1 H_2O_2 priming improved the stomatal performance improving photosynthetic characteristics

The leaves photosynthetic characteristics are closely related to the leaf structures. The stomatal conductance and photosynthetic rate were affected by the stomata, one of the important leaf structures. The stomatal conductance was positively correlated with stomatal size and negatively correlated with stomatal density (Wu et al., 2014; Haworth et al., 2015). To better adapt to waterlogging stress, stomata would become smaller in size and larger in number which might be related to the decrease of leaf area (Xu, 1997; Yu et al., 2003; Wang et al., 2010; Jurczyk et al., 2016; Ploschuk et al., 2018; Hu et al., 2019). In this study, the stomatal length, width, and the proportion of open stomata of waterlogged summer maize leaves were markedly decreased. Additionally, the stomas of plant leaves altered from regular arrangement to random distribution in waterlogged plants, thereby enhancing the CO_2 diffusion distance from stomas to photosynthetic parts. Accordingly, Gs and Ci of C-W were considerably decreased, while Ls were significantly increased, demonstrating that the decrease of Pn was predominantly caused by stomatal limitation factors. These results suggested that waterlogging had a grave effect on stomach traits of plants which blocked the uptake of CO_2, and here impeding the photosynthesis, and reducing the dry matter accumulation eventually. It has been demonstrated that H_2O_2 priming was conducive to regulate stomatal characteristics, thus improving the gas exchange characteristics of leaves under waterlogging conditions (Castro-Duque et al., 2020). This study showed that the stomatal density of leaves reduced considerably and the stomatal size increased significantly in H_2O_2 priming/waterlogging-stress plants. Additionally, the proportion of opening stomata was significantly increased, and the stomata were arranged in H-W, thus enhancing the uptake of CO_2. As a result, the Gs, Ci were increased by H_2O_2 priming, leading to a higher photosynthetic rate (Figure 8).

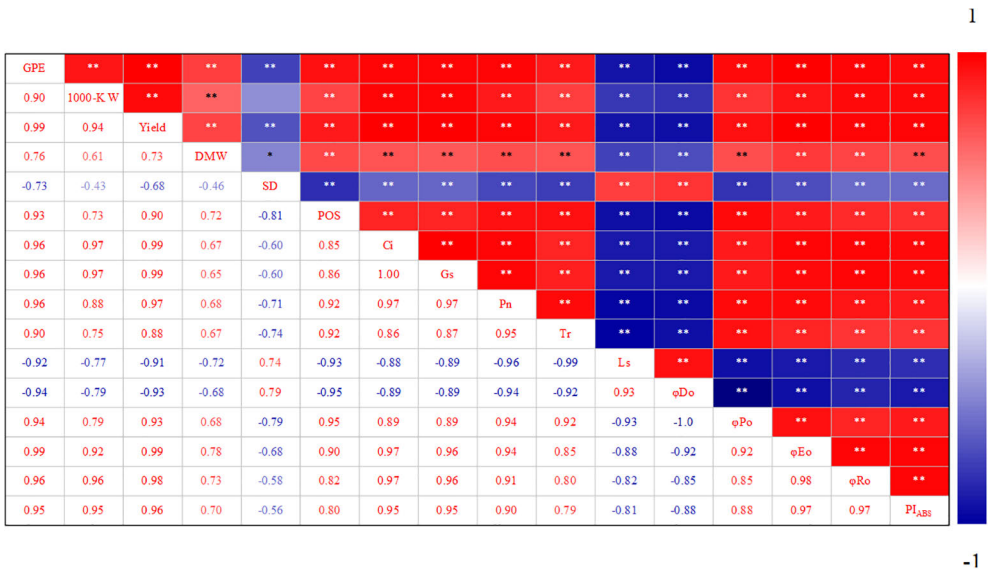

FIGURE 7
Correlation analysis of photosynthetic characteristics of soaking seeds with H_2O_2 under waterlogging stress. GPE: Grains per ear; 1000-K W: 1000-kernel weight; DMW: Dry matter weight; SD: Stomatal density; POS: Proportion of open stomata; Ci: Intercellular CO_2 concentration; Gs: Stomatal conductance; Pn: The net photosynthetic rate; Tr: Transpiration rate; Ls: Calculate the pore limit value; φDo: Quantum yield of electron transport (at t = 0); φPo: The maximum quantum yield of primary photochemistry (at t = 0); φEo: Quantum yield of electron transport (at t = 0); φRo: Quantum yield for reduction of end electron acceptors at the PSI acceptor side (RE) (at t = 0); PI_{ABS}: The performance index for energy conservation from exciton to the reduction of intersystem electron acceptors.

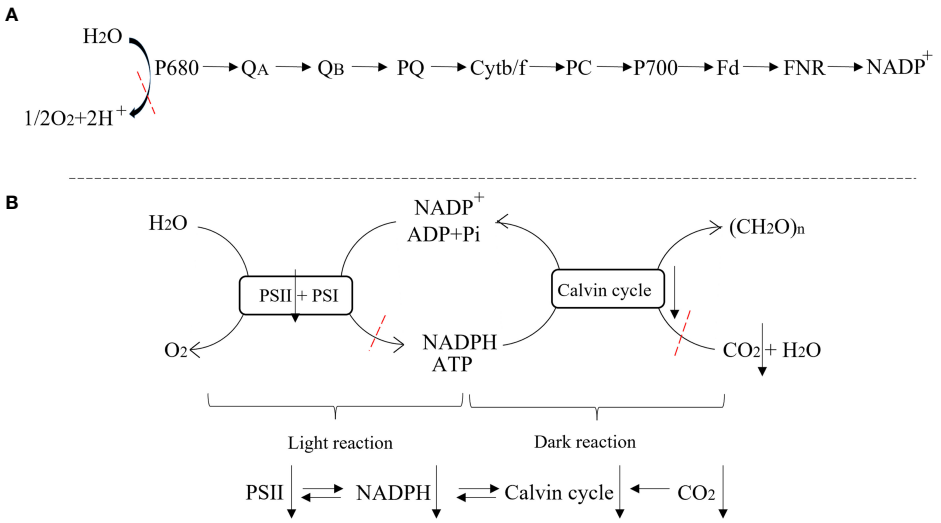

FIGURE 8
Schematic diagram of photosynthesis process. **(A)** Photosynthetic electron transport process; **(B)** Light and dark reaction.

4.1.2 H_2O_2 priming improved the light capture and conversion improving photosynthetic

Chlorophyll fluorescence induction kinetics is a sensitive probe to study the absorption, transformation, transmission, and distribution of sunlight energy in plants. The changes in chlorophyll fluorescence parameters can effectively reflect the characteristics of light reaction in photosynthesis (Strasserf and Srivastava, 1994; Yang et al., 2004; Kalaji et al., 2014; Li et al., 2020). PSII reaction centers were damaged and the number of active reaction centers was decreased after waterlogging (Li et al., 2005). The PSII reaction center converted the captured light energy into excitation energy. Most of the excitation energy was used to promote carbon assimilation, and the excess excitation energy was lost in the form of heat dissipation (Zuo et al., 2019). The number of RC/CSm was decreased after waterlogging, which damaged the PSII reaction centers and the antenna pigment structure. At the same time, Ro/CSm and ETo/CSm were decreased, but the DIo/CSm was increased, thus, the utilization rate of light energy per cross area, the share of energy devoted to electron transport were reduced, and heat dissipation was increased (Li et al., 2013; Liu et al., 2016). A similar conclusion could be drawn from quantum yields. Thus, waterlogging stress by decreasing the utilization of light energy and increased heat dissipation to limit the PSII photosynthetic electron transport chain. The level of electron transport inhibition at the donor or acceptor was closely related to PSII apparent activation energies (Chen et al., 2013; Sunil et al., 2020; Xing et al., 2021). This research showed that waterlogging stress significantly enhanced the K-step of summer maize, implying that the oxygen release complex (OEC) was damaged, the existence time of strong oxidant $P680^+$ was prolonged, and the D_1 protein in the reaction center of PSII was destroyed by oxidation, so as to damage the photosynthetic organs and decrease the photosynthetic activity. Additionally, the J-point was also significantly raised by waterlogging stress, indicating that the electron transfer from Q_A to Q_B was also significantly impeded, and reduced Q_A was accumulated, resulting in the singlet oxygen $^1O_2$ formation and biofilm lipid peroxidation being increased.

Studies have shown that exogenous H_2O_2 could be used as a signal molecule to alleviate the effects of waterlogging on plants by regulating PSII efficiency and protecting chloroplasts (Castro-Duque et al., 2020; Hasanuzzaman et al., 2020). H_2O_2 priming significantly increased the RC/CSm, indicating that H_2O_2 priming protected the PSII reaction center. At the same time, H_2O_2 priming enhanced the electron transfer at the PSII reaction center and the donor/acceptor side of maize, decreasing the waterlogging induced raise of K and J steps, which effectively promoted the photosynthetic electron transport chain, reduced the oxidant $P680^+$ and $^1O_2$, protected the photosystem from oxidative damages and reduced the damage of membrane lipid peroxidation. Additionally, H_2O_2 priming significantly reduced DIo/CSm, indicating that the absorption and transfer of PSII light energy were improved. Accordingly, H_2O_2 priming increased the PI_{ABS}, and the photochemical properties were improved, which alleviated the electron transport coupled photosynthetic phosphorylation process, and boosted the Calvin cycle. In summary, H_2O_2 priming effectively improved the capture, conversion, and transmission of light energy, protecting plants from photoinhibition and enhancing the carbon assimilation processes (Figure 8).

4.2 Yield

The decrease in grain yield was significantly associated with the decrease in 1000-grain weight and grain number ear (Ren et al., 2016). The accumulation of photosynthetic substances depends on the strength of photosynthesis, and the formation of yield was determined by the accumulation and transport of photosynthetic substances (Ren et al., 2015). The results of this study showed that waterlogging stress could significantly reduce the yield of summer maize, and its 1000-grain weight and grain number per ear were significantly affected, with grain number per ear being the most affected. Dry matter accumulation was blocked after waterlogging, resulting in insufficient assimilation for grain development, thus leading to a reduction in grain yield (Ren et al., 2014). In summary, this study showed that waterlogging stress significantly reduced photosynthetic rate through damaging stomatal performance, PSII photoinhibition, and the light capture and conversion, and the LAI and SPAD were decreased, resulting in a blockage in dry matter accumulation, and the yield was decreased finally. However, H_2O_2 priming could significantly mitigate the waterlogging damages on stomatal characteristic and photosystems, protecting chloroplasts and other photosynthetic organs from oxidative damage to increase the photosynthetic rate, and increase the biomass accumulation rate and grain yield of waterlogged summer maize (Figures 8, 9).

5 Conclusions

Waterlogging stress inhibited the light and dark response of the leaves. Waterlogging decreased Pn through stomatal limitation of CO_2 supply and reduction of PSII photochemical efficiency by limiting the donor and acceptor side of PSII and the activity of the reaction center, which would lead to the decrease

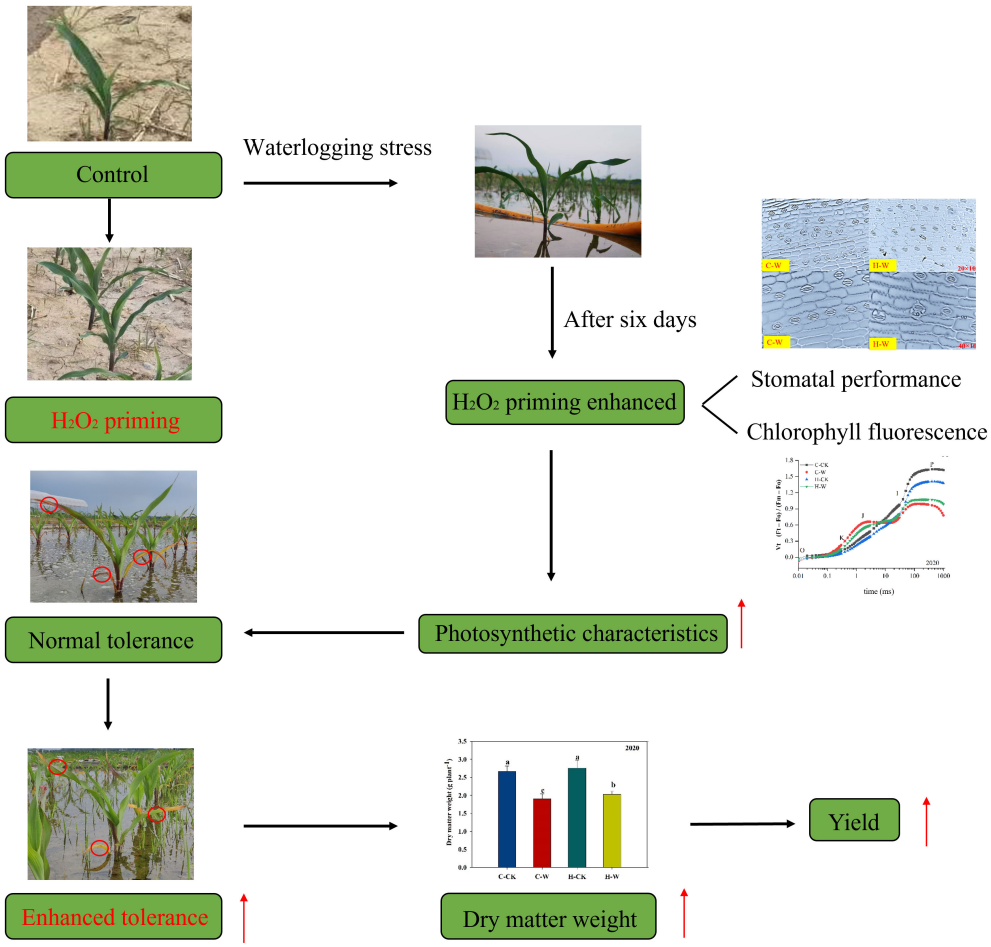

FIGURE 9
The mechanism of H_2O_2 priming could enhance the photosynthetic characteristics of summer maize. *Note:* Red circles indicated H_2O_2 priming versus flooded maize leaves, and red arrows indicated that H_2O_2 priming alleviates flooding stress.

of dry matter weight and grain yield. H_2O_2 priming could alleviate the negative effects of on waterlogged summer maize by increasing the CO_2 supply for carbon fixation, protecting PSII reaction centers, and enhancing electron transport to promote energy supply for carbon fixation. As a result, the photosynthetic capacity of waterlogged summer maize was significantly increased by H_2O_2 priming, dry matter weight and grain yield were increased eventually. In summary, H_2O_2 priming could modulate the waterlogging stress tolerance of summer maize: insights from photosynthetic.

Data availability statement

The original contributions presented in the study are included in the article/Supplementary Material. Further inquiries can be directed to the corresponding author.

Author contributions

SW: Conceptualization, Formal analysis, Investigation, Methodology, Writing – original draft.; JH: Conceptualization, Investigation, Methodology, Writing - Review and Editing; BR: Investigation, Resources, Writing – review and editing; BZ: Investigation, Resources, Writing – review and editing; PL: Investigation, Resources, Writing – review and editing; JZ: Conceptualization, Funding acquisition, Data curation, Supervision, Writing – review and editing. All authors contributed to the article and approved the submitted version.

Funding

This work was supported by the Shandong Province key research and development plan (2021LZGC014-2), National Natural Science Foundation of China (32172115), the earmarked fund for CARS (CARS-02-21) and the Shandong Agricultural Application Technology Innovation Project (Grant numbers SD2019ZZ013).

Acknowledgments

We acknowledge the support of the State Key Laboratory of Crop Biology and College of Agronomy, Shandong Agricultural University.

Conflict of interest

The authors declare that the research was conducted in the absence of any commercial or financial relationships that could be construed as a potential conflict of interest.

Publisher's note

All claims expressed in this article are solely those of the authors and do not necessarily represent those of their affiliated organizations, or those of the publisher, the editors and the reviewers. Any product that may be evaluated in this article, or claim that may be made by its manufacturer, is not guaranteed or endorsed by the publisher.

Supplementary material

The Supplementary Material for this article can be found online at: https://www.frontiersin.org/articles/10.3389/fpls.2022.1042920/full#supplementary-material

SUPPLEMENTARY FIGURE 1
The details of meteorological data during maize waterlogging periods.

SUPPLEMENTARY TABLE 1
Jip-test specifies the parameter term.

References

Andrade, C. A., Souza, K. R. D., Santos, M.d. O., Silva, D. M., and Alves, J. D. (2018). Hydrogen peroxide promotes the tolerance of soybeans to waterlogging. *Sci. Hortic.* 232, 40–45. doi: 10.1016/j.scienta.2017.12.048

Ashraf, M., and Harris, P. J. C. (2013). Photosynthesis under stressful environments: An overview. *Photosynthetica* 51, 163–190. doi: 10.1007/s11099-013-0021-6

Ayano, M., Kani, T., Kojima, M., Sakakibara, H., and Ashikari, M. (2015). Gibberellin biosynthesis and signal transduction is essential for internode elongation in deepwater rice. *Plant Cell Environ.* 37, 2313–2324. doi: 10.1111/pce.12377

Berry, J. A. (1982). Environmental regulation of photosynthesis. *Photosynthesis* 263–343. doi: 10.1016/b978-0-12-294302-7.50017-3

Castro-Duque, N. E., Chavez-Arias, C. C., and Restrepo-Diaz, H. (2020). Foliar glycine betaine or hydrogen peroxide sprays ameliorate waterlogging stress in cape gooseberry. *Plants (Basel)* 9, 644. doi: 10.3390/plants9050644

Chen, X. L., Li, G., Liu, P., Gao, H. Y., Dong, S. T., Wang, Z. L., et al. (2013). Effects of exogenous hormone 6-BenzylAdenine (6-BA) on photosystem II performance of maize during process of leaf senescence under different nitrogen fertilization levels. *Acta Agron. Sin.* 39, 1111–1118. doi: 10.3724/SP.J.1006.2013.01111

Gao, F. (2018). Effect of 4-PBA on the growth and yield of summer maize under flooding stress. PhD dissertation. *J. Henan Agric. Univ.*

Gao, Y., Guo, Y.-K., Lin, S.-H., Fang, Y.-Y., and Bai, J.-G. (2010). Hydrogen peroxide pretreatment alters the activity of antioxidant enzymes and protects chloroplast ultrastructure in heat-stressed cucumber leaves. *Sci. Hortic.* 126, 20–26. doi: 10.1016/j.scienta.2010.06.006

Gdsa, A., Pm, A., Skdpp, B., Edcm, B., Ldsl, A., Ecm, A., et al. (2020). H_2O_2 priming promotes salt tolerance in maize by protecting chloroplasts ultrastructure and primary metabolites modulation. *Plant Sci* 303, 110774. doi: 10.1016/j.plantsci.2020.110774

Gondim, F. A., Gomes-Filho, E., Lacerda, C. F., Prisco, J. T., and Marques, E. C. (2009). Pretreatment with H_2O_2 in maize seeds: Effects on germination and seedling acclimation to salt stress. *Braz. J. Plant Physiol.* 22, 103–112. doi: 10.1590/S1677-04202010000200004

Hasanuzzaman, M., Bhuyan, M., Zulfiqar, F., Raza, A., Mohsin, S. M., Mahmud, J. A., et al. (2020). Reactive oxygen species and antioxidant defense in plants under abiotic stress: Revisiting the crucial role of a universal defense regulator. *Antioxid. (Basel)* 9, 681. doi: 10.3390/antiox9080681

Haworth, M., Killi, D., Materassi, A., and Raschi, A. (2015). Coordination of stomatal physiological behavior and morphology with carbon dioxide determines stomatal control. *Am. J. Bot* 102, 677–688. doi: 10.3732/ajb.1400508

Hossain, M. A., Bhattacharjee, S., Armin, S. M., Qian, P., Xin, W., Li, H. Y., et al. (2015). Hydrogen peroxide priming modulates abiotic oxidative stress tolerance: insights from ROS detoxification and scavenging. *Front. Plant Sci.* 6. doi: 10.3389/fpls.2015.00420

Hu, J., Ren, B. Z., Dong, S. T., Liu, P., Zhao, B., and Zhang, J. W. (2020). Comparative proteomic analysis reveals that exogenous 6-benzyladenine (6-BA) improves the defense system activity of waterlogged summer maize. *BMC Plant Biol.* 20, 44. doi: 10.1186/s12870-020-2261-5

Hu, J., Ren, B. Z., Dong, S. T., Liu, P., Zhao, B., and Zhang, J. W. (2021). Poor development of spike differentiation triggered by lower photosynthesis and carbon partitioning reduces summer maize yield after waterlogging. *Crop J.* 10, 478–489. doi: 10.1016/j.cj.2021.08.001

Hu, X. Y., Yu, H. Y., Cui, Y. F., Fan, S. Q., Bi, Q. X., Li., Y. C., et al. (2019). Response of stomatal distribution characteristics on leaves of xanthocera sorbifolia from different provenances to water stress. *For. Res.* 32, 169–174. doi: 10.13275/j.cnki.lykxyj.2019.01.023

Jurczyk, B., Pociecha, E., Janowiak, F., Kabala, D., and Rapacz, M. (2016). Variation in waterlogging-triggered stomatal behavior contributes to changes in the cold acclimation process in prehardened lolium perenne and festuca pratensis. *Plant Physiol. Biochem.* 109, 280–292. doi: 10.1016/j.plaphy.2016.10.012

Kalaji, H. M., Oukarroum, A., Alexandrov, V., Kouzmanova, M., Brestic, M., Zivcak, M., et al. (2014). Identification of nutrient deficiency in maize and tomato plants by *in vivo* chlorophyll a fluorescence measurements. *Plant Physiol. Biochem.* 81, 16–25. doi: 10.1016/j.plaphy.2014.03.029

Kaori, S., Mai, N. H., and Motoaki, S. (2020). Advances in chemical priming to enhance abiotic stress tolerance in plants. *Plant Cell Physiol* 119. doi: 10.1093/pcp/pcaa119

Li, P. M., Gao, H. Y., and Strasser, R. J. (2005). Application of rapid chlorophyll fluorescence induction kinetics analysis in photosynthesis studies. *J. Plant Physiol. Mol. Biol.* 31, 8. doi: 10.3321/j.issn:1671-3877.2005.06.001

Li, X. X., Liu, B. X., Guo, Z. T., Chang, Y. X., He, L., Chen, F., et al. (2013). Effects of NaCl stress on photosynthesis characteristics and fast chlorophyll fluorescence induction dynamics of pistacia chinensis leaves. *Chin. J. Appl. Ecol.* 24, 6. doi: doi: CNKI: SUN: YYSB.0.2013-09-013

Li, F., Liu, L., Zhang, H., Wang, Q. T., Guo, L. L., Hao, L. H., et al. (2018). Effects of CO_2 concentrations on stomatal traits and gas exchange in leaves of soybean. *Acta Agron. Sin.* 44, 1212–1220. doi: 10.3724/SP.J.1006.2018.01212

Liu, Q. Q., Ma, S. B., Feng, X. H., Sun, Y., Yi, Y. J., and Liu, W. X. (2016). Effects of grafting on the fast chlorophyll fluorescence induction dynamics of pepper seedlings under temperature stress. *Acta Hortic. Sin.* 43, 885–896. doi: 10.16420/j.issn.0513-353x.2015-0970

Li, Y. T., Xu, W. W., Ren, B. Z., Zhao, B., Zhang, J. W., Liu, P., et al. (2020). High temperature reduces photosynthesis in maize leaves by damaging chloroplast ultrastructure and photosystem II. *J. Agron. Crop Sci.* 206, 548–564. doi: 10.1111/jac.12401

Munné-Bosch, S., and Alegre, L. (2013). Cross-stress tolerance and stress "memory" in plants: an integrated view. *Environ. Exp. Bot.* 94, 1–2. doi: 10.1016/j.envexpbot.2013.02.002

Pan, B. H. (2022). The global climate will continue to deteriorate in 2021. *Ecol. Econ.* 38, 1–4.

Perez, I. B., and Brown, P. J. (2014). The role of ROS signaling in cross-tolerance: from model to crop. front. *Plant Sci.* 5. doi: 10.3389/fpls.2014.00754

Petrov, V. D., and Breusegem, F. V. (2012). Hydrogen peroxide–a central hub for information flow in plant cells. *AoB Plants* (0), pls014–pls014. doi: 10.1093/aobpla/pls014

Ploschuk, R. A., Miralles, D. J., Colmer, T. D., Ploschuk, E. L., and Striker, G. G. (2018). Waterlogging of winter crops at early and late stages: Impacts on leaf physiology, growth and yield. *Front. Plant Sci.* 9. doi: 10.3389/fpls.2018.01863

Ren, B. Z., Hu, J., Zhang, J. W., Dong, S. T., Liu, P., and Zhao, B. (2020). Effects of urea mixed with nitrapyrin on leaf photosynthetic and senescence characteristics of summer maize (Zea mays L.) waterlogged in the field. *J. Integr. Agric.* 19, 1586–1595. doi: 10.1016/S2095-3119(19)62725-5

Ren, B. Z., Zhang, J. W., Dong, S. T., Liu, P., and Zhao, B. (2016). Effects of waterlogging on leaf mesophyll cell ultrastructure and photosynthetic characteristics of summer maize. *PloS One* 11 (9), e0161424. doi: 10.1371/journal.pone.0161424

Ren, B. Z., Zhang, J. W., Dong, S. T., Liu, P., and Zhao, B. (2018). Exogenous 6-benzyladenine improves antioxidative system and carbon metabolism of summer maize waterlogged in the field. *J. Agron. Crop Sci.* 204, 175–184. doi: 10.1371/journal.pone.0161424

Ren, B. Z., Zhang, J. W., Dong, S. T., Zhao, B., and Liu, P. (2017). Effect of waterlogging at early period on canopy structure andphotosynthetic characteristics of summer maize. *Sci. Agric. Sin.* 50, 2093–2103. doi: 10.3864/j.issn.0578-1752.2017.11.015

Ren, B. Z., Zhang, J. W., Li, X., Dong, S. T., and Liu, P. (2014). Effect of waterlogging on nutrient uptake and transport of summer maize. *J. Plant Nutr. Fert.* 20, 11. doi: 10.11674/zwyf.2014.0205

Ren, B. Z., Zhu, Y. L., Li, X., Fan, X., Dong, S. T., Zhao, B., et al. (2015). Effects of waterlogging on photosynthetic characteristics of summer maize under field conditions. *Acta Agron. Sin.* 4 (1), 329–338. doi: 10.3724/SP.J.1006.2015.00329

Seng, S. S., Wang, Q., Zhang, Y. E., Li, C. H., Liu, T. X., Zhao, L. F., et al. (2012). Effects of exogenous spermidine on physiological regulatory of maize after waterlogging stress. *Acta Agron. Sin.* 38, 1042–1050. doi: 10.3724/SP.J.1006.2012.01042

Strasser, R. J. (2004). *Analysis of the chlorophyll a fluorescence transient* (Dordrecht: Springer). doi: 10.1007/978-1-4020-3218-9_12

Strasserf, R. J., and Srivastava, A. (1994). Polyphasic chlorophyll a fluorescence transient in plants and cyanobacteria. *Photochem. Photobiol.* 61, 32–42. doi: 10.1111/j.1751-1097.1995.tb09240.x

Sunil, B., Strasser, R. J., and Raghavendra, A. S. (2020). Targets of nitric oxide (NO) during modulation of photosystems in pea mesophyll protoplasts: studies using chlorophyll a fluorescence. *Photosynthetica* 58, 452–459. doi: 10.32615/ps.2019.183

Tian, L. X., Li, J., Bi, W. S., Zuo, S. Y., Li, L. J., Li, W. L., et al. (2019). Effects of waterlogging stress at different growth stages on the photosynthetic characteristics and grain yield of spring maize (*Zea mays* l.) under field conditions. *Agric. Water Manage* 218, 250–258. doi: 10.1016/j.agwat.2019.03.054

Voesenek, L., and Bailey-Serres, J. (2015). Flood adaptive traits and processes: an overview. *New Phytol.* 206, 57–73. doi: 10.1111/nph.13209

Wahid, A., Perveen, M., Gelani, S., and Basra, S. M. (2007). Pretreatment of seed with H_2O_2 improves salt tolerance of wheat seedlings by alleviation of oxidative damage and expression of stress proteins. *J. Plant Physiol.* 164, 283–294. doi: 10.1016/j.jplph.2006.01.005

Wang, Y. J., Fu, Q. S., Zheng, H., Wen, C. L., Cheng., L., Zhao, B., et al. (2010). Effects of drought stress on growth, photosynthetic physiologica features and stomata characters of cucumber seedlings. *J. China Agric. Univ.* 15, 12–18.

Wu, B. J., Chow, W. S., Liu, Y. J., Shi, L., and Jiang, C. D. (2014). Effects of stomatal development on stomatal conductance and on stomatal limitation of photosynthesis in *Syringa oblata* and *Euonymus japonicus* thunb. *Plant Sci.* 229, 23–31. doi: 10.1016/j.plantsci.2014.08.009

Xing, Y. M., Wan, Y. T., Liu, Y. L., Wang, P. F., Fan, Z., Zhao, Y. X., et al. (2021). Effects of extracts from paecilomyces variotii on chlorophyll fluorescence transient in leaves of maize under waterlogging stress. *J. Irrig. Drain.* 40, 52–57. doi: 10.13522/j.cnki.ggps.2021108

Xu, D. Q. (1997). Some problems in stomatal limitation analysis of photosynthesis. *Plant Physiol. Commun.* 33, 241–244. doi: 10.13592/j.cnki.ppj.1997.04.001

Yang, X. Q., Zhang, Z. Q., Liang, Z. S., and Shan, Y. (2004). Effects of water stress on chlorophyll fluorescence parameters of different drought resistance winter wheat cultivars seedlings. *Acta Bot. Boreal. –Occident. Sin.* 24, 5. doi: 10.3321/j.issn:1000-4025.2004.05.010

Yan, R. J., Li, F., Zhang, Q. Q., Zhang, Y. X., Wu, H. X., Hao, L. H., et al. (2021). Effects of irrigation and fertilization on the morphological traits and distribution pattern of stomata of maize leaves under straw returning. *Water Sav. Irrig.* 000, 71–77. Available at: https://kns.cnki.net/kcms/detail/42.1420.TV.20210909.1900.008.html.

Yu, W. D. (2015). Research on the effect of waterlogging on the growth and yield of summer maize and it's temporal-spatial distribution in Huang huai hai region. PhD dissertation. *China Agric. Univ.* Beijing, China

Yu, H. Q., Wu, Z. H., Shem, X. Y., and Xu, K. Z. (2003). Changes of stomatal density, size and microstructure in maize leaves under water stress. *J. Jilin Agric. Univ.* 25, 239–242. doi: 10.13327/j.jjlau.2003.03.001

Yu, W. Z., Zhang, X. C., Hu, J., Shao, J. Y., Liu, P., Zhao, B., et al. (2021). Combined effects of shade and waterlogging on yield and photosynthetic characteristics of summer maize. *Acta Agron. Sin.* 54, 3834–3846. doi: 10.3864/j.issn.0578-1752.2021.18.004

Zhang, D. X. (1996). Effect of hydrogen peroxide on germination of rice and maize seeds. *Plant Physiol. J.* 32, 115–117. doi: 10.13592/j.cnki.ppj.1996.02.008

Zhang, X. H., Zhang, L., Ma, C., Su, M., Wang, J., Zheng, S., et al. (2022). Exogenous strigolactones alleviate the photosynthetic inhibition and oxidative damage of cucumber seedlings under salt stress. *Sci. Hortic.* 297, 110962. doi: 10.1016/j.scienta.2022.110962

Zheng, Y. P., Xu, M., Hou, R. X., Shen, R. C., Qiu, S., and Ouyang, Z. (2013). Effects of experimental warming on stomatal traits in leaves of maize (*Zea mays* l.). *Ecol. Evol.* 3, 3095–3111. doi: 10.1002/ece3.674

Zhou, W. G., Chen, F., Meng, Y. J., Chandrasekaran, U., Luo, X. F., Yang, W. Y., et al. (2020). Plant waterlogging/flooding stress responses: From seed germination to maturation. *Plant Physiol. Biochem.* 148, 228–236. doi: 10.1016/j.plaphy.2020.01.020

Zuo, G. Q., Wang, S. Y., Feng, N. J., Wang, X. X., Mou, B. M., and Zheng, D. F. (2019). Effects of uniconazole on photosynthetic physiology and phenotype of soybean under flooding stress. *Chin. J. Ecol.* 38, 2702–2708. doi: 10.13292/j.1000-4890.201909.029

frontiers | Frontiers in Plant Science

TYPE Original Research
PUBLISHED 01 November 2022
DOI 10.3389/fpls.2022.1021483

Check for updates

OPEN ACCESS

EDITED BY
Mehdi Rahimi,
Graduate University of Advanced Technology, Iran

REVIEWED BY
Xiangnan Li,
Northeast Institute of Geography and Agroecology (CAS), China
Ozkan Kaya,
Erzincan Horticultural Research Institute, Turkey

*CORRESPONDENCE
Hua Wang
wanghua@nwafu.edu.cn
Hua Li
lihuawine@nwafu.edu.cn

SPECIALTY SECTION
This article was submitted to Plant Abiotic Stress, a section of the journal Frontiers in Plant Science

RECEIVED 17 August 2022
ACCEPTED 12 October 2022
PUBLISHED 01 November 2022

CITATION
Han X, Yao F, Xue T-t, Wang Z-l, Wang Y, Cao X, Hui M, Wu D, Li Y-h, Wang H and Li Y-H (2022) Sprayed biodegradable liquid film improved the freezing tolerance of cv. Cabernet Sauvignon by up-regulating soluble protein and carbohydrate levels and alleviating oxidative damage. *Front. Plant Sci.* 13:1021483. doi: 10.3389/fpls.2022.1021483

COPYRIGHT
© 2022 Han, Yao, Xue, Wang, Wang, Cao, Hui, Wu, Li, Wang and Li. This is an open-access article distributed under the terms of the Creative Commons Attribution License (CC BY). The use, distribution or reproduction in other forums is permitted, provided the original author(s) and the copyright owner(s) are credited and that the original publication in this journal is cited, in accordance with accepted academic practice. No use, distribution or reproduction is permitted which does not comply with these terms.

Sprayed biodegradable liquid film improved the freezing tolerance of cv. Cabernet Sauvignon by up-regulating soluble protein and carbohydrate levels and alleviating oxidative damage

Xing Han[1], Fei Yao[1], Ting-ting Xue[2], Zhi-lei Wang[1], Ying Wang[1], Xiao Cao[1], Miao Hui[1], Dong Wu[1], Yi-han Li[1], Hua Wang[1,3,4,5]* and Hua Li[1,3,4,5]*

[1]College of Enology, Northwest A & F University, Yangling, China, [2]School of Wine, Ningxia University, Yinchuan, China, [3]China Wine Industry Technology Institute, Yinchuan, China, [4]Shaanxi Engineering Research Center for Viti-Viniculture, Yangling, China, [5]Engineering Research Center for Viti-Viniculture, National Forestry and Grassland Administration, Yangling, China

Most cultivars of *Vitis vinifera* L. are very sensitive to cold. As an exogenous protectant, Biodegradable Liquid Film (BLF) is considered to protect winegrapes from low temperatures and dry winds for safe overwintering. This study aimed to reveal the physiological and biochemical mechanisms of BLF regulating the freezing tolerance of wine grapes. Groups of ten-year-old vines (Cabernet Sauvignon) were sprayed with BLF in November 2020 and 2021, or left untreated as a control treatment, and field plant mortality after overwintering were investigated. Branch samples were collected monthly for determination of biochemical indicators. Dormant two-year-old cuttings (Cabernet Sauvignon) were also used for the determination of relative expression levels of key genes. The results showed that the application of BLF reduced the branch semi-lethal temperature in January and February samples compared with control, and reduced the mortality of above-ground parts, branches and buds. The physiological status of shoots was greatly affected by the climatic conditions of the year, but BLF treatment increased the levels of soluble protein and soluble sugar, and also decreased the content of superoxide anion and malondialdehyde at most sampling times. Correlation analysis showed that the differences in freezing tolerance between BLF and no treated overwintering(CK) vines were mainly related to peroxidase activity, soluble sugar, reducing sugar and starch content. Low temperature stress activated the over expression of *ICE1*, *CBF1*, and *CBF3*, especially for 12h. BLF

treatment significantly increased the expression levels of *CBF1* and *CBF3* under low temperature stress. Overall, these results demonstrate that BLF treatment protects vines from freezing damage by upregulating osmo-regulatory substances and alleviating oxidative damage.

KEYWORDS

biodegradable liquid film (BLF), low temperature stress, freezing tolerance, mortality, antioxidant system, osmoregulation, C-repeat binding factor

Introduction

Low temperature stress is one of the most important abiotic stresses, adversely affecting plant growth and development, restricting the geographic distribution of plant species, and reducing global crop yields (Lv et al., 2010; Kaya, 2020a; Kaya and Kose, 2020; Kaya, 2020b). Plants have evolved sophisticated mechanisms to withstand cold stress, such as cold acclimation, a process by which plants acquire increased freezing tolerance upon prior exposure to nonlethal low temperature (Guy, 1990; Thomashow, 1999; Chinnusamy et al., 2007). Under low temperature stress, the cell membrane system induces and transmits signals to the cell, prompting physiological and biochemical changes in the cell environment. The first is the leakage of electrolytes caused by the phase transition of the cell membrane (Lyons, 1973). In response to osmotic stress, soluble proteins, amino acids, soluble sugars and other substances are mass synthesized in cells (Bhowmik et al., 2006; Soloklui et al., 2012; Abeynayake et al., 2015). In addition, a large number of reactive oxygen species and free radicals will accumulate in cells after low temperature stress, as signal molecules, induce plants to respond to stress and generate oxidative stress, and malondialdehyde as a product of membrane lipid peroxidation is often used to evaluate this a process (Rende et al., 2018). In the process of cellular antioxidant, enzymatic systems including superoxide dismutase (SOD), peroxidase (POD), catalase (CAT) play an important role (Lee and Chen, 1992; Hasanuzzaman et al., 2020), ascorbic acid (ASA) and glutathione (GSH) also help resist plant stress by acting as a circulating peroxide ion scavenging system (Anjum et al., 2012; Pei, 2012).

Among the numerous low temperature-responsive signaling pathways, the CBF-COR signaling pathway is the most complete one described. C-repeat binding factor/dehydration-responsive element-binding protein 1 (CBF/DREB 1) is induced by low temperature and play a key role in plant low temperature acclimation (Stockinger et al., 1997). CBFs protein directly binds to CORs promoter and induces its expression, thereforeimproving the low temperature tolerance of plants (Stockinger et al., 1997; Liu et al., 1998; Siddiqua and Nassuth, 2011). CORs mainly encode osmotic regulator synthases and cryoprotective proteins, including a series of functional genes such as COR, LTI and KIN (Yamaguchi-Shinozaki and Shinozaki, 1994; Shi et al., 2018). Inducer of CBF expression 1 (ICE1) is a MYC-like bHLH transcription factor that encodes a protein that activates the expression of CBFs at low temperature by binding to the MYC site (CANNTG) in the CBF1-3 promoter (Chinnusamy et al., 2003; Kim et al., 2015).

As a perennial plant, fruit trees are more at risk of freezing damage than other crops (Snyder et al., 2005; Kaya et al., 2020). As one of the earliest and largest fruit trees planted in the world, most commercial grape varieties are sensitive to cold, and to survive the winter safely in many cool continental climates, grapevines must be buried under the soil (Zhang et al., 2012). This method is commonly used in cold climates like Eastern Europe, Northern China, Minnesota, and Quebec (Khanizadeh et al., 2005). Soil-burial increases labor intensity and costs, can cause cane damage and disease, restricts mechanized production, and can damage the ecological environment when there is no cover crop between rows (Pierquet et al., 1977; Jolivet and Dubois, 2000; Wang, 2015; Han et al., 2021). Therefore, studies of the feasibility of other winter protective measures are needed to support the development of the wine industry in such regions.

Biodegradable liquid film (BLF) was used in this experiment is a humic acid film, which was originally developed as an environmentally friendly soil structure conditioner. BLF can improve the soil structure, regulate the physical and chemical properties of the soil, facilitate the growth and development of crops, promote a good growth and reproduction environment for microorganisms, promote the transformation and accumulation of soil organic matter, and enhance soil fertility (Wang et al., 2010; Lan et al., 2013). The humic acid component in BLF can enhance the ability of plants to resist stress, and has obvious cold-resistant and growth-promoting effects (Lu, 2006). The use of plastic mulch results in the accumulation of large amounts of polystyrene nanoplastics in agricultural soils, affecting plant growth and stress resistance. Recent studies have shown that polymethylmethacrylate nanoplastics can penetrate cell walls and accumulate in plant cells, limiting photosynthesis in barley, resulting in decreased activities of

carbohydrate metabolism-related enzymes and antioxidant enzymes, reducing its low temperature tolerance (Wang et al., 2022). The unique benefit is that the application of BLF is environmentally friendly and it can be naturally degraded under the action of sunlight and soil microorganisms, therefore its use does not damage the ecological environment (Wang et al., 2007a; Xue, 2019a). Recently, Xue et al., (2019b) found that BLF can be used as an exogenous antifreeze for plants. After being sprayed on the surface of grape plants, it solidifies and forms a film, which improves the survival rate of multiple varieties in the winter without soil-burial (Xue et al., 2019b).

In this study, BLF was used as an exogenous protectant to protect grapevines from freezing damage during overwintering. The protective effect of BLF on vines in the field trial was evaluated by investigating mortality after overwintering and measuring electrolyte leakage. The levels of biochemical indexes and the relative expression of cold resistance-related genes were also determined to explore the mechanism of BLF. These results will verify the effect of BLF on vines under low temperature stress, and provide a theoretical basis for overwintering strategies in cold regions.

Materials and methods

Material, vineyard site and treatments

This field study was conducted in 2020 and 2021, on 10-year-old 'Vitis vinifera L. cv. Cabernet Sauvignon' grapevines grown in a commercial vineyard in Xia County, Shanxi Provience (lat. 35°24′N, long. 111°17′E, alt. 433 m), China. Xia County is located in a continental semi-humid monsoon climate zone, with an average annual temperature of 12.8°C, a frost-free period of about 205 days, and an annual sunshine duration of 2293.4 h However, the winter temperatures may plunge to −15° C or even lower, causing serious damage to grape dormant buds

Grapevines were planted with a spacing of 1.0 m between grapevines and 2.7 m between rows, and were trained using a crawled cordon training system. The vines used in the experiment were not pruned after the fall of leaves in autumn, but were instead pruned one week before the bleeding period in spring, leaving three buds on each shoot. The vines were divided into two treatment groups: no treated overwintering (CK) and BLF sprayed in November (BLF). A completely randomized design was adopted, with three replications, with 24 vigorous vines per experimental unit. The treated vines were from two neighboring plots, allowing direct comparison of differences among treatments in the same soil and climate conditions. One-year-shoots samples were collected on December 20, 2020, January 15, February 7, March 3, December 23, 2021 and January 17, February 13, March 9, 2022. For both CK and BLF treatments, 20 one-year-shootswere collected in each of 3 experimental repeat units. The samples collected in the field were divided into two groups, one group was used for the determination of moisture content and electrolyte leakage immediately after being brought back to the laboratory, and the other group was stored in a -80 °C refrigerator for the determination of other biochemical indicators.

Two-year-old cuttings of Cabernet Sauvignon cuttings were also used for the experiments. Grape seedlings were cultivated in substrates composed of garden soil, perlite and humus (2:1:1, v/v/v) and 16 h light in a greenhouse at 24/18°C (day/night)/ 8hdark photoperiod, the photosynthetic photon flux density is 160 μmol m^{-2}·s^{-1}. In October 2021, the cuttings were transferred to the field for cultivation until natural dormancy. The cuttings were divided into two groups, which were treated with no treatment (CK) and sprayed with BLF (BLF) in November. Electrolyte leakage from annual dormant shoots of cutting from both treatments was determined. The cutting of the two treatments were divided into 4 groups, and each group was placed in a high and low temperature alternating test chamber (Shanghai Lanhao Instrument Equipment Co., Ltd., China, YSGJS-408) with low temperature stress of -10 °C for 3h, 6h, 12h, and 24h respectively. After the low temperature treatment, the one-year-shootsof the cuttings were quickly cut off, frozen in liquid nitrogen, and stored in a -80 °C refrigerator for gene expression analysis. A completely randomized trial was used, with three biological replicates for each experimental group, with 24 grapevine plants per experimental unit.

The biodegradable liquid film used in the experiment is a commercial product that purchased from Shaanxi Yang Ling Mingrui Technology Company. It's brown and creamy and forms a thin, brown, multi-molecular chemical protection film that wraps and encloses the one-year-shootssurface. The BLF protects the one-year-shootsin winter and gradually degrades in spring (Xue et al., 2019b). The amount of BLF sprayed per hectare was 150 kg, which was diluted at the ratio of BLF: water = 1:3 (v/v) when used, and a gasoline sprayer was used for spraying. In this study, the film was applied to the one-year-shoots to be retained in the following year, trunks, and furrow soils.

Mortality of vine, one-year-shoot and bud

The daily minimum and maximum temperature and monthly precipitation data were collected for the experiment site from December to March (Figure 1). And the mortality rates of whole vine, above-ground parts, one-year-shoots, and buds of vines under the two overwintering treatments were determined in April 2021 and 2022. During the investigation, the buds did not germinate, and the branches without sap flow in the tissue after cutting were counted as dead. To measure branch mortality, the germination of all one-year-shoots was determined for 10 randomly selected germinating trees. Bud

10.3389/fpls.2022.1021483

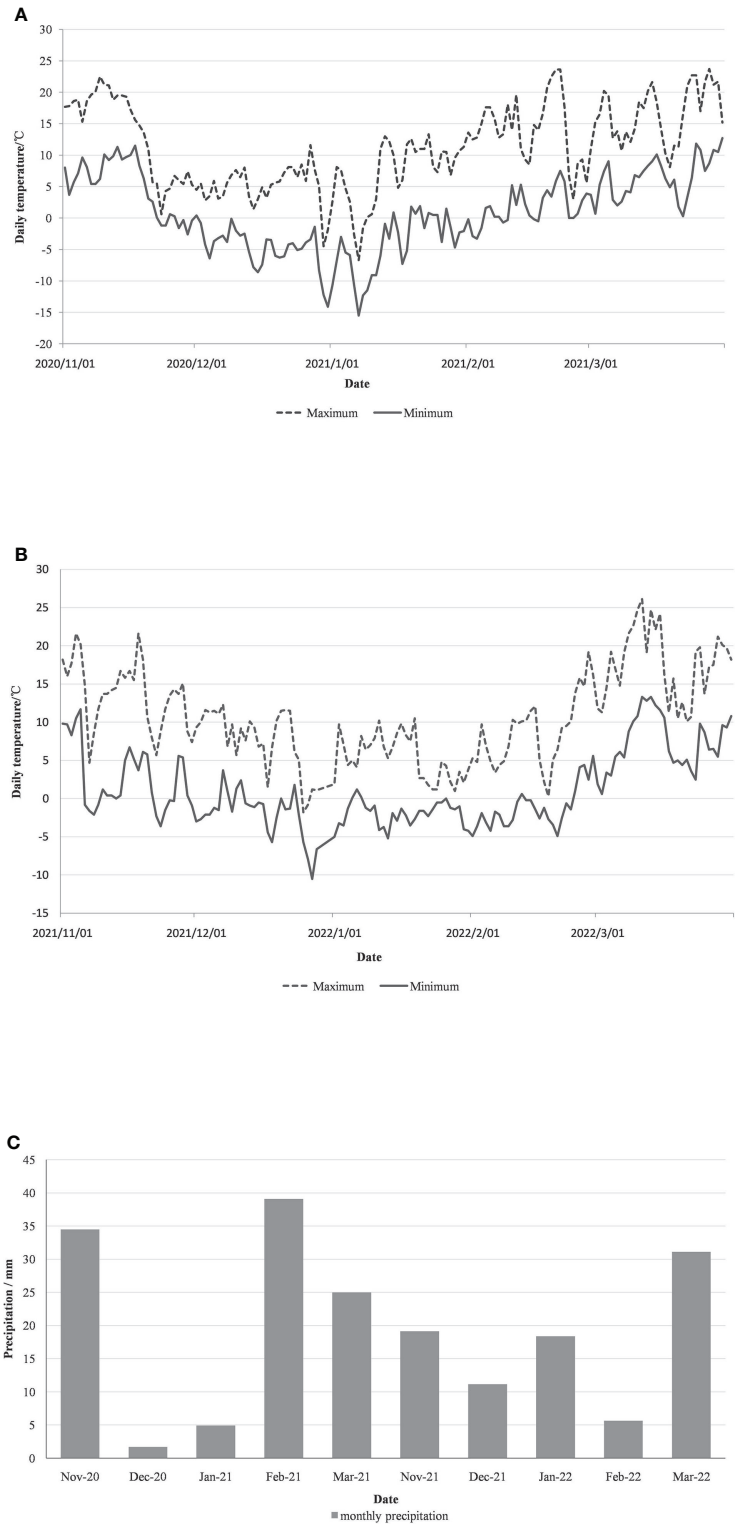

FIGURE 1
Daily maximum temperature, minimum temperature **(A, B)** and monthly precipitation **(C)** during the overwintering period (December to March) in 2020 and 2021 in Xia County.

mortality was measured by determining the germination of 10 randomly selected germinating one-year-shoots The mortality rate of each part is calculated according to Equation1-4:

$$\text{Death rate of whole vine (\%)} = \frac{\text{the number of vines with dead above ground parts and no sprouting roots}}{\text{total number of vines}} \times 100\% \quad (1)$$

$$\text{Above ground part mortality rate (\%)} = \frac{\text{the number of vines whose roots are sprouting but the above ground part is dead}}{\text{total number of vines}} \times 100\ \% \quad (2)$$

$$\text{Average one–year–shoot mortality rate (\%)} = \frac{\text{the number of dead branches on 10 trees}}{\text{total number of branches on 10 trees}} \times 100\% \quad (3)$$

$$\text{Average bud mortality rate (\%)} = \frac{\text{the number of dead buds on 10 branches}}{\text{total number of buds on 10 branches}} \times 100\ \% \quad (4)$$

Freezing procedure

Low temperature treatment was carried out using a high and low temperature alternating test chamber (YSGJS-408). Treatment temperatures for determination of electrolyte leakage were 4, -6, -10, -14, -18, -22 and -26°C, with a cooling rate of 4°C per hour. Samples were maintained at the set temperature for 12h The temperature was then restored to 4°C at 4°C per hour. The samples were maintained at 4°C to recover for 12hbefore removal from the chamber and recovery to room temperature to measure electrolyte leakage (Wang et al., 2007b; Hashempour et al., 2014). The procedure of low temperature stress for cutting was to drop from room temperature to -10 °C at a rate of 4 °C/h, and keep at -10 degrees for 3h, 6h, 12h, and 24h, and then collect the samples.

Determination of electrolyte leakage

The relative electrical conductivity was determined and the lethal temperature (LT) at which 50% of the total electrolyte leakage occurred in branch tissues (EL-LT50) was calculated according to the method of Wang et al. (2007b) with slight modifications. To avoid the influence of BLF materials, the one-year-shootsfor both treatments were cut off the epidermis, and cut into 0.3-0.5 cm thick slices. Samples (weighing 2.0 g) of the branches were cut and placed into a 25 mL test tube with a stopper. Next, 20 mL of distilled water was added, the tube was stoppered and then shaken in a shaker for 12 h before the conductivity ($\mu S \bullet cm^{-1}$) was measured using a conductivity meter (DDS-307A). The test tubes were then boiled for 40 min, allowed to stand for 2 h, and then the conductivity value was re-measured. The relative conductivity was measured according to Equation 5:

$$\text{Relative electrical conductivity (\%)} = \frac{\text{conductivity value before boiling}}{\text{conductivity value after boiling}} \times 100\ \% \quad (5)$$

The improved logistic equation was used to fit the conductivity values (Equation 6):

$$Y = \frac{K}{1 + ae^{-bx}} \quad (6)$$

The second derivative of the equation was obtained and set equal to zero, where K=100. The inflection point of the equation curve X=lna/b, and X is the EL-LT50 of the branch.

Determination of branch water content

The total water content was determined by the drying method. Collected branches were cut into 3 cm sections, accurately weighed, and killed by baking at 105°C for 0.5 h. The samples were then baked at 80°C for 16 h to achieve constant weight and the tissue water content was determined.

Free water content was measured according to the method of Chen et al. (2014). Collected branches were cut into slices of about 1 mm. Three 0.5g samples were transferred into three weighing bottles, accurately weighed, and 5mL of 65% sucrose solution was added before accurate weighing again to calculate the weight of the sugar solution. The sucrose-containing bottles were incubated in the dark for 4-6h, with occasional shaking before measurement of the sugar concentration using an pocket refractometer (PAL-1) to determine the concentration of sugar solution. The free water content was calculated according to the sucrose concentration before and after soaking, and the bound water content was the difference between the total water content and the free water content.

Determination of oxidative stress indices

Superoxide anion (O^{2-}) production was estimated as described by Elstner and Heupel (Elstner and Heupel, 1976).

Malondialdehyde (MDA) content was determined by thiobarbituric acid-reactive substances method (Hodges et al., 1999). Branch sample (2.0 g) was homogenized in 15 mL 0.1% TCA and then centrifuged at 5,000 rpm for 10 min. Next, 5 ml of 5% TCA containing 0.5% TBA was added to 1 mL of the supernatant, followed by incubation in boiling water for 10 min and then transfer to ice water to stop the reaction. MDA absorption was measured spectrophotometrically at 450, 532, and 600 nm.

Determination of anti-oxidative enzymes activities

Branch samples (1.25 g) from the two treatment groups were ground in a chilled mortar with 1% (w/v) polyvinylpolypyrrolidone, homogenized with 30 mL of 50 mM potassium phosphate buffer (pH 7.8), and then centrifuged at 10,000 rpm for 15 min. The supernatant after centrifugation was used for the determination of antioxidant enzyme activities. The supernatant after centrifugation was assayed for antioxidant enzyme activity. Superoxide dismutase (SOD; EC 1.15.1.1) activity was estimated by NBT and was expressed as $U{\cdot}g^{-1}FW{\cdot}h^{-1}$ (Giannopolitis and Ries, 1977). Catalase (CAT; EC 1.11.1.6) activity was evaluated according to the decomposition rate of hydrogen peroxide and was expressed as $U{\cdot}g^{-1}FW{\cdot}min^{-1}$ (Aebi, 1984). Peroxidase (POD; EC 1.11.1.7) activity was measured by guaiacol and was expressed as $\mu g{\cdot}g^{-1}FW{\cdot}h^{-1}$ (Rao et al., 1996).

Determination of osmoregulation substances

The extraction of soluble protein was according to the same procedure used to extract the antioxidant enzymes. The resulting supernatants were assayed for soluble protein content by Coomassie brilliant blue method, using bovine serum albumin as a standard (Bradford, 1976) and detection of protein at 525 nm.

Proline content was measured based on the method of (Bates et al., 1973). A branch sample (0.5 g) was placed into 5 mL of 3% aqueous sulfosalicylic acid, incubated in a boiling water bath for 30 min, cooled to room temperature, and centrifuged at 8,000 rpm for 5 min. Next, 1.0 mL of the supernatant extract was mixed with 2 mL ninhydrin and 2 mL acetic acid, maintained for 30 min in a boiling water bath, and then cooled to room temperature. Next, 5 mL of toluene was added, and the tube was turned upside down and mixed well before being placed in the dark for 3 h. The colored product with toluene was detected at 520 nm.

Determination of carbohydrate

Collected branch samples were dried to a constant weight and then crushed for the determination of sugar content. Reducing sugar content was measured using the 3,5-dinitrosalicylic acid method to determine the absorbance at 520 nm and calculated based on the standard curve of glucose (Gao, 2006). The soluble sugar content was determined by anthrone colorimetry at 620 nm and calculated according to the standard curve of glucose (Yemm and Willis, 1954). The reducing sugar extract was hydrolyzed with 6 mol/L hydrochloric acid and then neutralized with sodium hydroxide for the determination of sucrose content using 3,5-dinitrosalicylic acid method (Gao, 2006). The residue left after the extraction of reducing sugar was hydrolyzed with hydrochloric acid and then neutralized with sodium hydroxide for the determination of starch content. The starch content was determined using the 3,5-dinitrosalicylic acid method, as was conductedto measure reducing sugar content (Gao, 2006).

Transcriptional analysis of genes by real-time quantitative polymerase chain reaction

Branch tissue (100 mg), previously ground in liquid N^2, was used for total RNA extraction. Total RNA was extracted from each sample with Quick RNA Isolation Kit (Huayueyang, Beijing, China), following the manufacturer's instructions. The integrity and purity of the RNA were detected by the 2100 bioanalyzer and photometer (Agilent,USA). Afterward, cDNA was synthesised from 1 μg of total RNA using HiScript III 1st Strand cDNA Synthesis Kit (Vazyme, Nanjing, China). Real-time PCR analysis was performed with ChamQ Universal SYBR qPCR Master Mix (Vazyme, Nanjing, China) using 2 μL cDNA in a final reaction volume of 20 μL per well. The 20μL reaction system includes: 2×ChamQ Universal SYBR qPCR Masher Mix (10.0μL), Primer1 (10μM, 0.4μL), Primer2 (10μM, 0.4μL), cDNA (2μL), ddH2O (7.2μL). The qPCR was conducted on a qTOWER3G (Analytik Jena, Jena, Germany). The reaction procedure was ① 95°C for 3 min; ② 95°C for 10 s, then 60°C for 30 s, and step ② for 40 cycles; ③ 95°C for 15s, 60°C for 60s, and 95°C for 15s. Genes selected for further analysis included *VvICE1* (inducer of *CBF* expression 1), *VvCBF1* (c-repeat binding factor 1), *VvCBF3* (c-repeat binding factor 3). *Actin* was used as the internal control. Primer sequences designed by Primer 5 are shown in Table 1. Specific gene amplification was confirmed by melting curve, agarose gel and sequencing analysis. The expression values were normalised by the average of the expression of the reference genes and calculated using the $2^{-\Delta\Delta Ct}$ method (Livak and Schmittgen, 2001).

Statistical analysis

All data were evaluated by one-way ANOVA. Multiple comparisons tests were taken only between treatments with Duncan's multiple comparison test, where differences were considered significant at $P \leq 0.05$. And graphs were performed by GraphPad prism software 6.0 (Graph Pad Software, San Diego, CA, USA).

The Pearson's coefficient of correlation analysis was determined between the levels of each indicator, correlation significance was defined at the 0.05 level. The graph was created

TABLE 1 Sequences for primers used in qRT-PCR.

Gene	Primer sequencece (5'- 3')
Actin	F: 5'-GTGCCTGCCATGTATGTTGCC-3' R: 5'-GCAAGGTCAAGACGAAGGATA-3'
VvICE1 inducer of CBF expression 1	F:5'- GCCAAGGGTTGAAGTGA-3' R:5'- CCGCCTGTTGAACGTCTAG-3'
VvCBF1 c-repeat binding factor 1	F:5'-GGGGCGAAGGTCGTGTT-3' R:5'- GTCCCATCGTTTCCATTTT-3'
VvCBF3 c-repeat binding factor 3	F:5'- GCATAAGCGGAAAGCAG-3' R:5'- CCGCACTTCGCATACCC-3'

by the genescloud tools, a free online platform for data analysis (https://www.genescloud.cn).

Results

Climatic conditions and mortality in the field trial

The field experiment was conducted in two wintering periods of 2020-2021 and 2021-2022. The daily extreme temperature and monthly precipitation of the experiment site were provided by the Great Winery. The minimum temperature during the wintering season in 2020 is -15.5°C, and the precipitation is mainly in November, February, and March, and there is almost no precipitation in December. The minimum temperature during the wintering period in 2021 is only -10.5°C, with precipitation in every month, and the climate is milder than that in 2020.

The survival of vines under the two treatments was investigated in 2021 and 2022, with measurement of whole tree, above-ground, branch, and bud mortality. During the investigation, vines for both treatment groups were in the germination period. There was no whole tree mortality in either treatment, but higher mortality of above-ground parts for the untreated plants for two years. The mortality of branch and bud of vinesprotected by BLF is obviously lower in 2020 (Table 2). The difference in bud mortality between the two treatments in winter 2021 was not large, probably because the minimum temperature in winter was higher, which did not cause serious freezing damage (Figure 1).

Electrolyte leakage of branches in the field trial

The EL-LT50 value was calculated based on the relative electrical conductivities. During the overwintering period, the EL-LT50 values of the branches for both treatments first decreased and then increased, reaching the minimum value in January, corresponding to the maximum freezing tolerance (Table 3). The EL-LT50 of BLF-treated branches in January was significantly lower than that of CK both 2020 and 2021. There was no significant difference between the two treatments of EL-LT50 in March, which may be related to the natural degradation of the BLF material and the release of dormancy.

Water content of branches in the field trial

The water content composition of the branches was measured during the overwintering period and the results are shown in Figure 2. Under the influence of the continental monsoon climate, the dry and cold wind caused water loss of vines and the total water content gradually decreased. However, there was less water loss of the BLF-treated plants than that of the control, and this trend became more obvious over time between CK-2020 and BLF-2020. There was no significant difference in the total water content of the two treatments in the early overwintering period, but there was higher total water content in the branches sprayed with BLF in the late overwintering period, with a significant difference on March 3, 2021 (Figure 2A).

During the overwintering period, the moisture composition of the vine branches have significantly difference between two years. The content of free water decreased in December, January, and February, but increased in March, while the bound water content exhibited the opposite trend during 2020 winter period. Except for December 20, 2020, there were no significant differences in the free water content, bound water content, and free water/bound water of the two treatments (Figure 2). There was no significant difference in the water composition of the two treatments in the 2021 overwintering period except for the bound water content in December 2021 and January 2022 (Figure 2).

TABLE 2 The effect of spraying BLF on vine, one-year-shoot, and bud mortality.

Treatment	Whole vine mortality	Above-ground part mortality	One-year-shoot mortality	Bud mortality
CK-2020	0	10.00%	6.38%	25.93%
BLF-2020	0	1.75%	5.45%	10.71%
CK-2021	0	4.00%	4.00%	9.52%
BLF-2021	0	2.00%	2.00%	8.70%

10.3389/fpls.2022.1021483

TABLE 3 Effect of spraying BLF on the EL-LT50 value (°C) of one-year-shoots (estimated by relative electrical conductivities).

Treatment	December	January	February	March
CK-2020	-12.72a	-14.27b	-14.05a	-13.35a
BLF-2020	-12.24a	-16.92a	-14.76a	-12.38a
CK-2021	-13.93a	-16.8b	-11.85b	-9.82a
BLF-2021	-14.68a	-17.87a	-13.09a	-10.11a

Mean values for each parameter (EL-LT50) followed by the same lower-case letters in each column are not significantly different at $P \leq 0.05$ by Duncan's multiple range test.

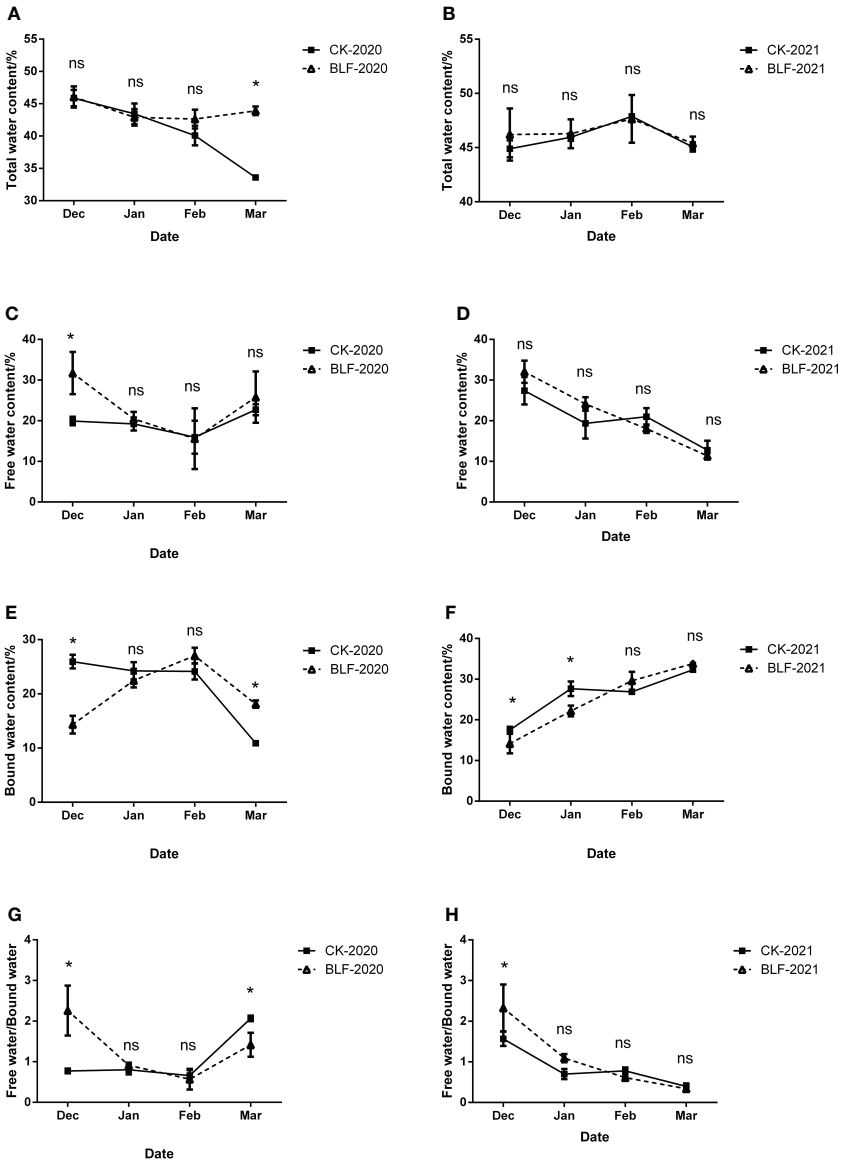

FIGURE 2
The effect of spraying BLF on the content of total water **(A, B)**, free water **(C, D)**, bound water **(E, F)**, and the ratio of free water to bound water **(G, H)** on 2020 and 2021. "*" means that the average value of each parameter is significant between the two treatments ($p<0.05$), and ns means no significance by Duncan's multiple range test.

Oxidative damage of branches in the field trial

Low temperature stress increased the degree of membrane lipid peroxidation in cells, which was reflected in the increase of superoxide anion and malondialdehyde content during overwintering. There was no significant difference between the two treatments in December and March, but in January and February, the superoxide anion content of the control plants was significantly higher than the plants that received the BLF treatment both of two years (Figures 3A, B). Compared with that of CK, the maximum decrease of superoxide anion content in BLF treatment at two years was 44.12% (Figure 3A) and 59.16% (Figure 3B), respectively. As shown in Figure 3C, except for February, the MDA content was always higher for the CK plants than for the plants that received the BLF treatment during the wintering period in 2020. During the overwintering period in 2021, the MDA content of BLF treatment was also significantly lower than that of CK in January and March (Figure 3D). During the wintering period of 2020, the MDA content basically showed an upward trend, while in 2021 it first increased and then decreased, which may be related to the temperature difference between the two years. The extreme minimum temperature of the wintering period in 2020 reached -15.5°C, and the oxidative damage to the cell membrane has been accumulating. The minimum temperature of the wintering period in 2021 is only -10.5°C, and the cell membrane gradually recovers its activity in the late winter.

Antioxidant enzyme activity and antioxidant content of branches in the field trial

To evaluate the effect of BLF treatment, the activities of superoxide dismutase (SOD), peroxidase (POD), and catalase (CAT) were measured, as shown in Figure 4. In both years, the activity of SOD reached the highest in February, and the SOD activity of BLF treatment was significantly higher than that of CK, and there was no significant difference at other times (Figures 4A, B). The trend in POD activity was very consistent between the two years, regardless of CK or BLF treatment (Figures 4C, D). The POD activity of BLF treatment first increased and then decreased in both wintering periods, and reached the highest in January, while the CK treatment has been in a downward trend. The POD activity was significantly higher in the BLF treatment than for CK in January and February. The trend of CAT activity in two years was basically opposite (Figures 4E, F,).

Antioxidants are key to the non-enzymatic reaction system, and ascorbic acid (ASA) and reduced glutathione (GSH) were measured in this study (Figure 5). During overwintering period in 2020, there was no significant difference in ASA content for the two treatments in December and January, but BLF increased more than CK, with a significant difference in February and March (Figure 5A). The content of GSH also increased sharply in the late over-wintering period. The difference was that the BLF treatment continued to increase, while the CK treatment decreased slightly in March (Figure 5B). There was only a significant difference between the two treatments in February and March. In 2021, the changing trends of both ASA and GSH have changed, with ASA content increasing over time and reaching the highest level in March, while GSH content reaching the highest level in February and dropping sharply in March (Figures 5C, D). However, the contents of ASA and GSH of BLF treatment in December and February were significantly higher than those of CK.

Osmoregulation substances of branches in the field trial

Substances that allow osmotic adjustment are part of the stress response in plants, including free proline, soluble protein, and soluble sugar, etc. Measurements of the soluble protein and free proline content for the two treatments during the overwintering period are shown in Figure 6. BLF treatment up-regulated the soluble protein content of the branches in most cases, especially in 2020, the soluble protein content of BLF was significantly higher than that of CK throughout the wintering period (Figure 6A). However, the change trend of soluble protein content in the two years was different (Figures 6A, B). The free proline content increased first and then decreased for the two treatments in 2020 (Figure 6C). Initially, the proline content of BLF-treated plants was higher, but in February and March in the late overwintering period, the level was significantly higher for the CK-treated plants. During the overwintering period in 2021, the changes in the proline content of BLF treatment were similar to those in 2020, which also showed a trend of first increasing and then decreasing, while the proline content of CK was basically stable (Figure 6D).

Carbohydrate content of branches in the field trial

The content of soluble sugar showed a trend of increasing first and then decreasing during the wintering period, with the highest value in January in both of two years (Figures 7A, B). The range of soluble sugar changes in BLF treatment was greater than that of CK, and the two were significantly different in January during 2020 wintering period, but not so much in 2021. In general, the change trend of reducing sugar content was similar to that of soluble sugar, with the maximum value in January (Figures 7C, D). There was no significant difference between the two treatments in December and January. Except for March, the reducing sugar content of BLF treatment was

10.3389/fpls.2022.1021483

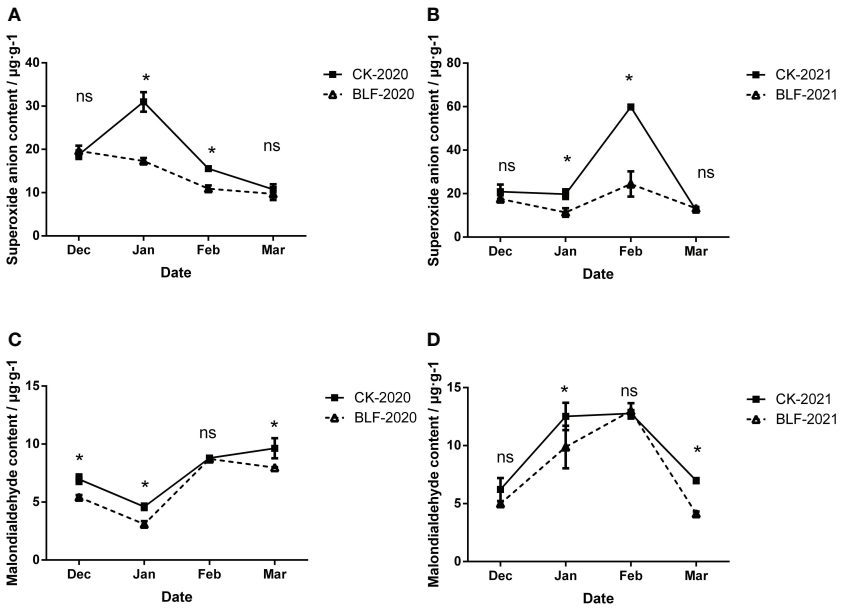

FIGURE 3
Effect of spraying BLF on superoxide anion **(A, B)** and malondialdehyde **(C, D)** on 2020 and 2021. "*" means that the average value of each parameter is significant between the two treatments ($p<0.05$), and ns means no significance by Duncan's multiple range test.

always lower than that of CK. During the wintering period, the sucrose content first decreased and then increased, reaching the minimum in February except for CK-2020 (Figures 7E, F). During the overwintering period in 2020, the sucrose content of BLF was always higher than that of CK except in December, and the difference was not significant in March. During the overwintering period in 2021, the sucrose content of BLF treatment was also significantly lower than that of CK in December, and significantly higher in February and March. Similar to the soluble sugar content, the change in starch content of BLF treatment was much greater than that of CK, with a significant difference between the two in January both of two years (Figures 7G, H). The starch content of BLF-2021 was also significantly lower than that of CK-2021 in March (Figure 7H).

Correlation analysis between freezing tolerance and biochemical indicators

The person correlation coefficient between the level of each physiological and biochemical index and EL-LT50 was analyzed (Figures 8A, B). During wintering period in 2020, free water/bound water, MDA, ascorbic acid, and starch were significantly positively correlated with EL-LT50, indicating that the higher their level, the larger the value of EL-LT50. The value of EL-LT50 is a negative number, and the larger the value, the higher the semi-lethal temperature and the poor freezing tolerance. However, POD, soluble sugar and reducing sugar were all significantly negatively correlated with EL-LT50, indicating that the higher their content, the lower the value of EL-LT50, and the better the freezing tolerance. During wintering period in 2021, bound water, ascorbic acid, and starch were significantly positively correlated with EL-LT50, and more indicators were significantly negatively correlated with EL-LT50, including free water, free water/bound water, soluble protein, POD, CAT, soluble sugar, reducing sugar and sucrose. The correlation analysis results of the two years are quite different, especially the composition of moisture content, because it is affected by climatic conditions such as precipitation. Nevertheless, the activities of antioxidant enzymes, especially POD, were significantly negatively correlated with EL-LT50 in both years, indicating that it plays a key role in alleviating oxidative stress. The correlations of carbohydrates in the two years were very consistent. Soluble and reducing sugars have always been significantly negatively correlated with EL-LT50, sucrose also showed a significant negative correlation in 2021, and starch was always significantly positively correlated with EL-LT50. This indicated that the effect of BLF on plant freezing tolerance was mainly related to antioxidant enzyme activity and carbohydrate content.

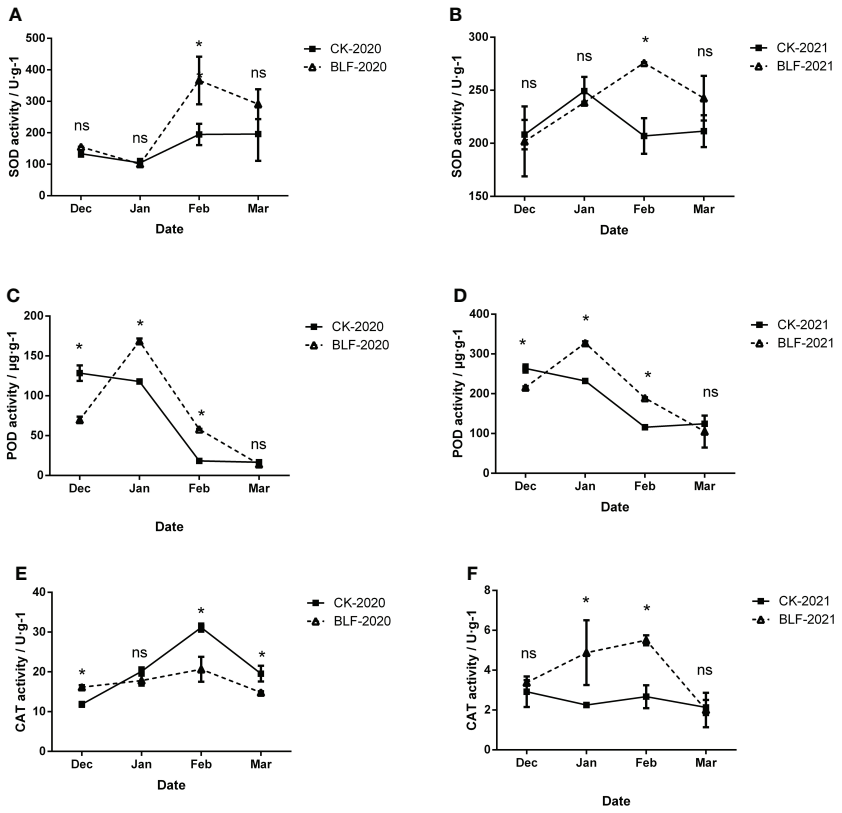

FIGURE 4
Effect of spraying BLF on superoxide dismutase **(A, B)**, peroxidase **(C, D)**, and catalase **(E, F)** activities on 2020 and 2021. "*" means that the average value of each parameter is significant between the two treatments ($p<0.05$), and ns means no significance by Duncan's multiple range test.

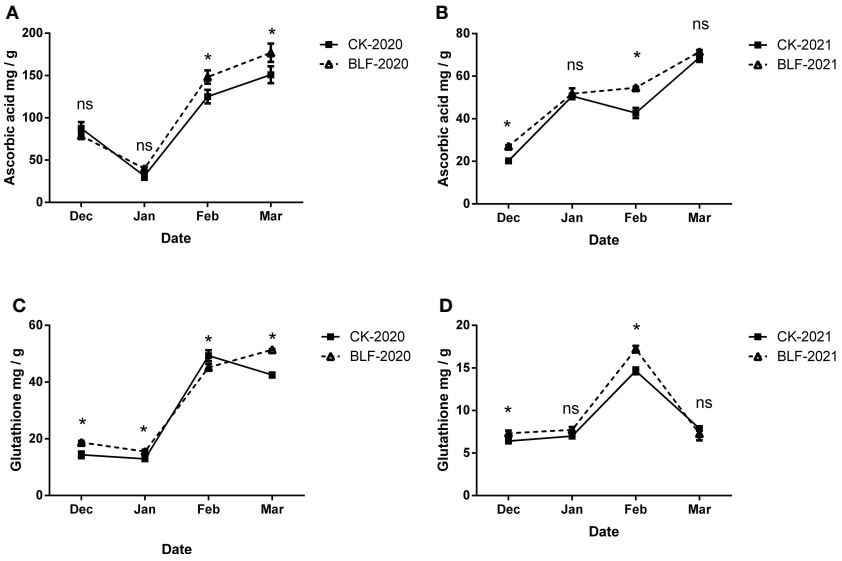

FIGURE 5
Effect of spraying BLF on the content of ascorbic acid **(A, B)** and glutathione **(C, D)** on 2020 and 2021. "*" means that the average value of each parameter is significant between the two treatments ($p<0.05$), and ns means no significance by Duncan's multiple range test.

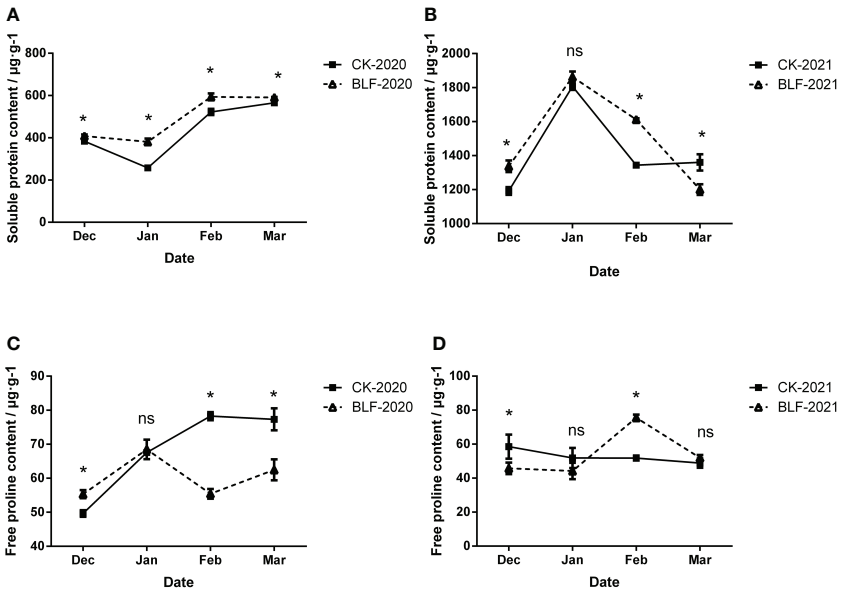

FIGURE 6
Effect of spraying BLF on the content of soluble protein **(A, B)** and free proline **(C, D)** on 2020 and 2021. "*" means that the average value of each parameter is significant between the two treatments ($p<0.05$), and ns means no significance by Duncan's multiple range test.

Relative expression levels of the genes under low temperature stress

Due to the difference in growth vigor, age and cultivation environment, the freezing tolerance of cuttings and perennial vines in the field was very different. The electrolyte leakage of dormant cuttings branches was first measured in this study (not shown in the figure and table), the EL-LT50 of CK was -9.84°C, and that of BLF treatment was -11.70°C, so -10°C was selected as the low temperature stress temperature to simulate field conditions. Under freezing temperature stress, the expression levels of CBF1 and CBF3 were basically the same with the stress time. Both CK and BLF treatments reached the peak at 12h and decreased at 24h, which may be due to prolonged extreme stress leading to plant death, cell membrane rupture, and intracellular transcription and metabolism disorders (Figure 9). The effect of BLF on the expression levels of CBF1 and CBF3 was very significant, except for CBF1 at 3h. At 6h, 12h and 24h, the relative expression of CBF1 in BLF-treated branches was 71.88, 34.32, and 14.53 times that of CK, respectively. Similarly, at 3h, 6h, 12h and 24h, the relative expression of CBF3 in BLF-treated branches was 19.66, 43.91, 10.48, and 5.56 times that of CK, respectively. The relative expression of ICE1 in the branches of the two treatments only showed significant difference at 12h, and the BLF treatment was significantly higher than that of the CK.

Discussion

Under low temperature stress, plants need to maintain cell membrane stability and biologically active protein structures to survive in unfavorable environments (Chen et al., 2018; Kaya et al., 2021a; Kaya et al., 2021b). Cold acclimation is an important process enabling many plants to cope with low temperature stress. Acclimation includes many physiological and biochemical changes in cells driven by shortened sunlight and reduced temperature. There is an interaction between low temperature exposure and short-day sunlight (Zhang et al., 2002), low temperature further increases the bud freezing tolerance of photoperiod-responsive genotypes and can also induce dormancy and domestication of non-photoperiod-responsive varieties (Meiering et al., 1980; Schnabel and Wample, 1987).

BLF treatment reduced water loss and electrolyte leakage of overwintering vines

Exposure of plants to sub-zero temperatures can cause plant tissues to freeze (Puhakainen et al., 2004). Ice crystals first form in the extracellular space of plant cells, reducing the water potential of the apoplast solution, causing water to flow out of the cell, so freezing stress at the cellular level is usually accompanied by

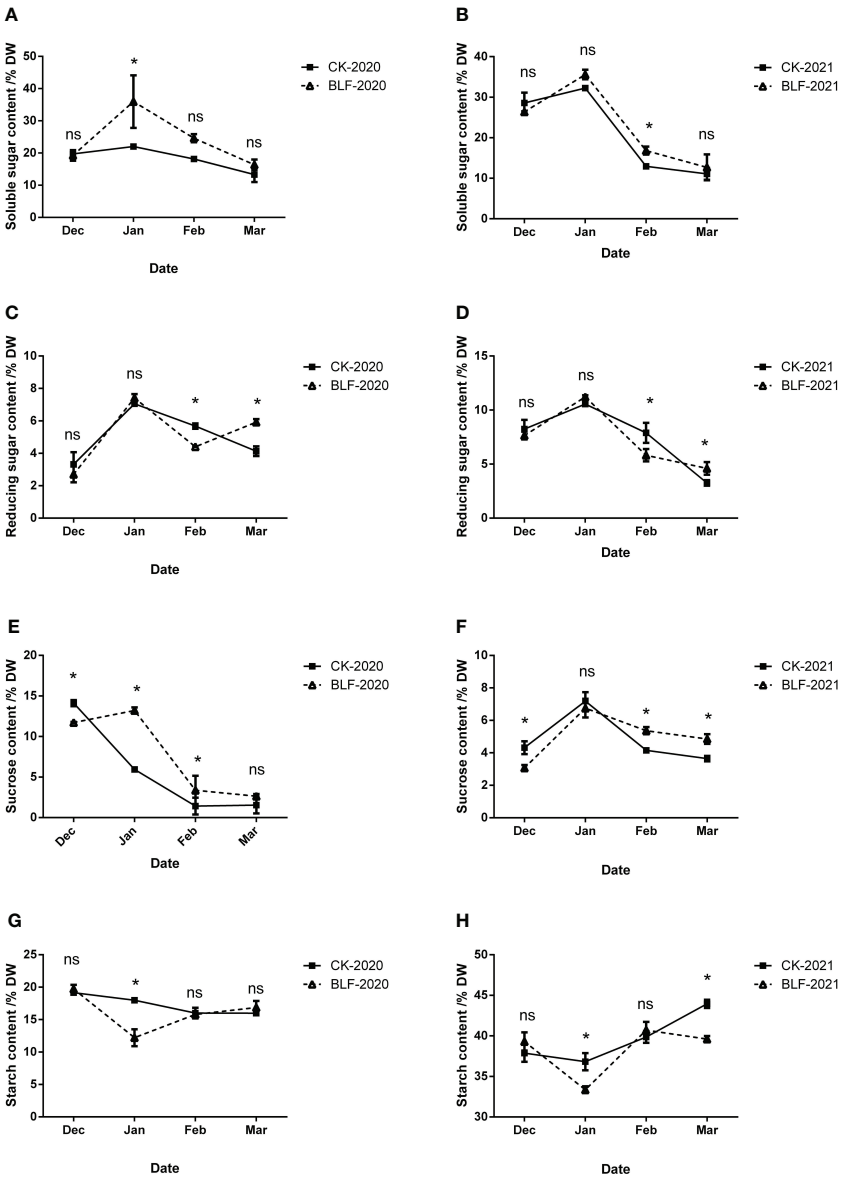

FIGURE 7
Effect of spraying BLF on the content of soluble sugar **(A, B)**, reducing sugar **(C, D)**, sucrose **(E, F)** and starch **(G, H)** on 2020 and 2021. "*" means that the average value of each parameter is significant between the two treatments ($p<0.05$), and ns means no significance by Duncan's multiple range test.

dehydration stress (Ritonga and Chen, 2020). Ice crystals can increase electrolyte leakage and membrane lipid phase changes (Vadim et al., 2014). In this study, controlled laboratory freezing tests were used to simulate the cooling process, during which there was electrolyte leakage and LT50 were calculated based on the relative electric conductivity (Table 3). With cold acclimation, the EL-LT50 showed a decreasing trend in the early overwintering period, demonstrating that the freezing tolerance of plants gradually increased, reaching maximum value in January. With the increase of temperature in February and March, deacclimation occurred and the freezing tolerance of plants was gradually lost, as seen in many previous studies (Yang et al., 2015; Haghi et al., 2019).

The hydrophobic film formed by BLF may also help to slow the formation of ice crystals. The general melting point of frozen plants is close to 0°C, but studies on various crops have shown changes in the freezing point of plants or supercooling capacity (Chen et al., 1995). Surface water contributes to the formation of early ice nuclei in plants (Fuller and Grice, 1998; Fuller and Wisniewski, 1998), and free water promotes the

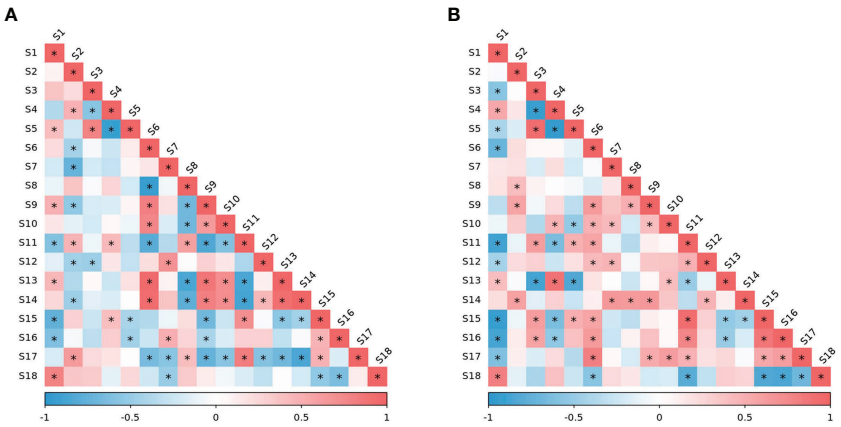

FIGURE 8
Pearson correlation values between the EL-LT50 (in °C) of vine one-year-shoots and other indicators under BLF and CK treatments in overwintering period of 2020 **(A)** and 2021 **(B)**. S_1: EL-LT50; S_2: total water; S_3: free water; S_4: bound water; S_5: free water/bound water; S_6: soluble protein; S_7: free proline; S_8: superoxide anion; S_9: malondialdehyde; S_{10}: superoxide dismutase; S_{11}: peroxidase; S_{12}: catalase; S_{13}: ascorbic acid; S_{14}: reduced glutathione; S_{15}: soluble sugar; S_{16}: reducing sugar; S_{17}: sucrose; S_{18}: starch. "*" means that the correlation between the two indicators is significant at the 0.05 level.

activity of ice nuclei in the leaf plane. Fuller et al. (2003) studied potatoes and showed that the hydrophobic granular film can prevent the formation of ice nuclei of leaves by delaying the ice penetration of frozen droplets on the leaf surface. A similar study of tomato plants reached the same conclusion (Wisniewski et al., 2002). Further tests of the effect of BLF on tissue icing are still needed.

Decreased water content is associated with increased bud hardiness in grapevine (Bourne and Moore, 1991; Salzman et al., 1996; Ershadi et al., 2016), but severe water loss may cause plant death (Chai and Wang, 1996). Under natural low temperature stress, the bound water content of plants increases and the free water content decreases, so the ratio of bound water to free water increases. This ratio is typically positively correlated with the cold resistance of plants (Chen et al., 2014). In China's viticulture areas with continental monsoon climate, dry winds in winter are one of the main causes of death of grape plants (Liu et al., 2004; Li, 2015). Increased water retention capacity of grape branches can enable survival of winter. The use of BLF can significantly reduce the water loss rate of isolated branches by 3.12% (Xue et al., 2019b). In this study, the use of BLF significantly increased the total water content of the branches in the late overwintering period of 2020, and this effect may be related to the formation of a hydrophobic protective layer after BLF film formation. BLF limits gas exchange between the branches and the environment and slows the evaporation of water from the plants. There was lower mortality of the above-ground parts, branches, and buds of the plants treated with BLF compared to the control plants (Table 2), which may be related to changes in water retention.

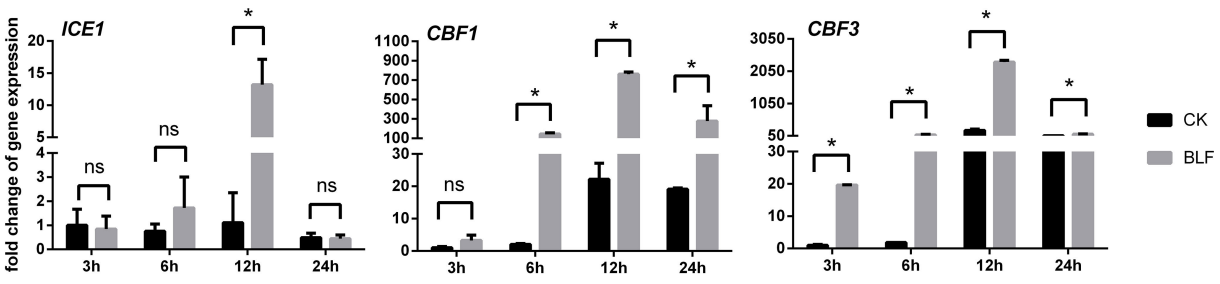

FIGURE 9
Effect of spraying BLF on the relative expression levels of genes associated with freezing tolerance. "*" means that the average value of each parameter is significant between the two treatments ($p<0.05$), and ns means no significance by Duncan's multiple range test.

BLF treatment alleviated oxidative stress in overwintering vines by improving antioxidant systems

Significant damage can be caused by reactive oxygen species under low temperature stress. To cope with oxidative damage, plants have evolved a complete antioxidant defense system, including antioxidant enzymes (such as SOD, CAT, POD, APX, etc.) and antioxidants (such as AsA, GSH, sulfhydryl compounds, phytochelatins) (Liu et al., 2022). SOD converts O^{2-} into H_2O_2 and is considered the first line of defense against oxidative damage (Kaya and Köse, 2017). Then H_2O_2 can be converted to H_2O by POD, CAT, and APX (Hasanuzzaman et al., 2020). In this study, BLF treatment reduced the O^{2-} and MDA content in branches during the overwintering period suggested that vines under low temperature stress treated with BLF maintained higher cell membrane integrity (Figure 3).

The scavenging enzymes are a key protein fraction in the acquisition of FT in plants (Lee and Chen, 1992). Plants under low temperature stress can alleviate reactive oxygen species damage by enhancing their antioxidant defense systems. The results of this study showed that the activity of antioxidant enzymes in grapevines tended to increase during cold acclimation, reaching a peak in January and February with cooler temperatures and decreasing during de-acclimation (Figure 4). This is consistent with many previous studies (Hashempour et al., 2014; Haghi et al., 2019) . ASA and GSH are also important components of the oxidative defense system, acting as antioxidant protection substances and maintaining the balance between ROS generation and scavenging by participating in the ASA-GSH cycling pathway (Anjum et al., 2012). In this study, the contents of ASA and GSH both increased significantly in the late overwintering period (Figure 5). Due to the variability of field climate and complex experimental conditions, the correlation analysis between oxidative damage and antioxidant system of branches during overwintering did not show a consistent law. However, the value of EL-LT50 was negatively correlated with the activities of POD and CAT in both years (Figure 8), indicating that the difference in FT between BLF and CK treatments may be mainly related to the scavenging of H_2O_2 by POD and CAT.

BLF treatment increased the contents of Osmoregulation substances of overwintering vines

The changes that occur in plants under cold stress prepare cells and organs to tolerate apoplastic freezing and its dehydration consequences (Weiser, 1970; Uemura and Steponkus, 1994; Grossnickle and South, 2014). Soluble protein can improve the water holding capacity of cells, protect the plasma membrane structure, and increase the concentration of cell fluid to lower the freezing point and improve the cold resistance of plants (Li et al., 2011). The soluble protein content of BLF treatment in this study was consistently higher than that of CK except in March 2022 (Figures 6A, B).

Under cold stress, polysaccharides are hydrolyzed into soluble sugars, therefore increasing the osmotic potential of the cytoplasm and lowering the freezing temperature. Soluble sugars can increase the osmotic concentration of cells, reduce water potential, and increase water retention capacity, therefore lowering the freezing point to function as a protective agent for ice, with a protective effect on protoplasts, mitochondria, and sensitive coupling factors on membranes (Wisniewski et al., 2003; Ren et al., 2013; Ling et al., 2015). Ling et al. (2015) studied cold resistance of Olea europaea and found increased soluble sugar content in the detached leaves with the decrease of the stress temperature, but a larger increase in varieties with strong cold resistance. The study on vines also proved that the total soluble sugar content of the branches was significantly correlated with LT50 value (Ershadi et al., 2016; Zhao et al., 2020). In this study, the content of soluble sugar was highest in January, and was higher in BLF treated plants than in CK-treated plants in January 2021 and February 2022 (Figure 7A), with a significant negative correlation with EL-LT50 both years (Figure 8). The change in starch content shows the opposite trend (Figures 7G, H), and starch content in both years was significantly positively correlated with EL-LT50 (Figure 8), which may be due to the large amount of soluble sugar produced by the hydrolysis of starch. The concentrations of fructose, glucose, sucrose, raffinose, and stachyose in buds are strongly correlated with EL-LT50 (Grant and Dami, 2015), and sucrose is considered to be closely related to cold resistance (Guy et al., 1992). Sucrose and reducing sugar contents were also negatively correlated with EL-LT50 both years (Figure 8), and these results suggest that carbohydrates play an important role in the improvement of FT by BLF treatment. Sucrose also act as a signal molecule and can induce or inhibit gene expression to alter the physiological adaptability of plants (Koch, 1996; Smeekens and Rook, 1997). Future work should examine the content change and transformation mechanism of different soluble sugars during the wintering period of grapevines under BLF treatment.

BLF treatment improved the freezing tolerance of grape cuttings by up-regulating the expression of CBFs

DREB is one of the main subfamilies of the AP2/ERF family, which is involved in the synergistic or antagonistic regulation of a variety of abiotic stresses, and plays a key role in the response of plants to various stresses such as cold, heat, drought, and high salinity (Licausi et al., 2013). The CBF/DREB1 transcription factors have been characterized as a regulatory hub in freezing

tolerance in plant systems (Thomashow, 2010; Theocharis et al., 2012). Xiao et al., 2006; Xiao et al., 2008) reported that ABA and low temperature up-regulated the expression of CBF/DREB1 gene in grape leaves and seedlings. Rubio et al. (2018) found that the expression levels of VvCBFs genes were associated with the cold tolerance of grape dormant buds. In addition, heterologous overexpression of the VvCBF4 gene also reduced freezing-induced electrolyte leakage and improved freezing survival in non-cold-acclimated vines (Tillett et al., 2012). In this study, low temperature (LT) also up-regulated the expression of *CBF1* and *CBF3* genes in dormant cuttings, and due to the combined action of BLF and LT, the expression of VvCBF/DREB1 transcription factor was greatly increased, which reduced the electrolyte leakage caused by freezing in the branches. The accumulation of soluble sugars is a common biochemical process during cold acclimation of plants, but some studies have shown that overexpression of CBFs can also lead to changes in sugars. Gilmour et al. (2000) found that CBF3-overexpressing Arabidopsis plants had elevated levels of total soluble sugars, including sucrose, raffinose, glucose, and fructose. The increase of soluble sugar, reducing sugar and sucrose content in BLF-treated vines in this experiment may also be related to the up-regulation of CBFs. Ectopic expression of *VvICE1a* and *VvICE1b* isolated from 'Muscat Hamburg' grapevine activated the expression levels of *AtRD29A* and *AtCOR47* transcripts in transgenic Arabidopsis, enhancing tolerance to cold, drought, salinity, and cold-drought stress (Li et al., 2014). Dong et al. (2013) reported the inducer of CBF expression 1 (*ICE1*) from Vitis amurensis is strongly induced in leaves, roots, stems, and petioles by cold temperature and transgenic tobacco over-expressing VaICE1 has higher chilling tolerance and survival ability by improving the activities of superoxide dismutase, peroxidase, and catalase, as well as the chlorophyll yield. In this study, low temperature did not show a significant up-regulation of *ICE1*, and the relative expression of *ICE1* between BLF treatment and CK only showed a significant difference at 12 h of low temperature stress.

Conclusion

Low temperature during overwintering resulted in the damage of grapevine manifested as the increase of O^{2-} and MDA, and the death of above-ground parts, branches and buds after overwintering. BLF treatment reduced mortality in all parts of the field vines after overwintering, and reduced the electrolyte leakage of branches in January. BLF treatment improved the antioxidant system by increasing POD and CAT activities, and decreased O^{2-} and MDA levels. BLF treatment increased the content of soluble protein and soluble carbohydrates, and alleviated the osmotic stress caused by low temperature and water loss during overwintering. BLF treatment up-regulated the expression levels of *CBF1* and *CBF3* in cuttings under low temperature stress, therefore improving freezing resistance. This study provide a theoretical basis for the study of winter protection measures for wine grapes in cold regions.

Data availability statement

The original contributions presented in the study are included in the article/supplementary material. Further inquiries can be directed to the corresponding author.

Author contributions

All authors contributed signifificantly to this manuscript. HL, HW, and XH conceived the project and designed the experiments. This article was primarily organized by XH, who participated in the entire process from experimental design to sample collection, indicators determination, data analysis, and article1 writing. FY, Y-HL, Z-LW, YW, XC, MH and DW made contributions to the determination of indicators, and T-TX made contributions to experimental treatment and sample collection. All authors have read and agreed to the published version of the manuscript.

Funding

This research was supported by the National Key Research and Development Project (2019YFD1002500) and Key Research and Development Project of Shaanxi Province (2020ZDLNY07-08).

Acknowledgments

The authors are grateful to the two engineers Huaitang Zheng and Xinyi Dong of the Great Winery for their help and support in the field trials.

Conflict of interest

The authors declare that the research was conducted in the absence of any commercial or financial relationships that could be construed as a potential conflict of interest.

Publisher's note

All claims expressed in this article are solely those of the authors and do not necessarily represent those of their affiliated organizations, or those of the publisher, the editors and the reviewers. Any product that may be evaluated in this article, or claim that may be made by its manufacturer, is not guaranteed or endorsed by the publisher.

References

Abeynayake, S. W., Etzerodt, T. P., Jonaviciene, K., Byrne, S., Asp, T., and Boelt, B. (2015). Fructan metabolism and changes in fructan composition during cold acclimation in perennial ryegrass. *Front. Plant Science*. 6. doi: 10.3389/fpls.2015.00329

Aebi, H. (1984). Catalase *in vitro*. *Methods Enzymol*. 105, 121–126. doi: 10.1016/s0076-6879(84)05016-3

Anjum, N. A., Ahmad, I., Mohmood, I., Pacheco, M., Duarte, A. C., Pereira, E., et al. (2012). Modulation of glutathione and its related enzymes in plants' responses to toxic metals and metalloids–a review. *Environ. Exp. Botany* 75, 307–324. doi: 10.1016/j.envexpbot.2011.07.002

Bates, L. S., Waldren, R. P., and Teare, I. D. (1973). Rapid determination of free proline for water-stress studies. *Plant Soil.* 39, 205–207. doi: 10.1007/BF00018060

Bhowmik, P. K., Tamura, K. I., Sanada, Y., Tase, K., and Yamada, T. (2006). Sucrose metabolism of perennial ryegrass in relation to cold acclimation. *Z. Für Naturforschung C J. Biosciences.* 61 (1-2), 99–104. doi: 10.1515/znc-2006-1-218

Bourne, T. F., and Moore, J. N. (1991). Cold hardiness in grape cultivar development. *Fruit Varieties J.* 45, 26–28.

Bradford, M. M. (1976). A rapid and sensitive method for the quantitation of microgram quantities of protein utilizing the principle of protein-dye binding. *Analytical Biochem.* 72, 248–254. doi: 10.1006/abio.1976.9999

Chai, C. J., and Wang, M. Z. (1996). Effects of cold-resistant rootstocks on moisture changes and safety of overwintering grape vines in open fields. *Tianjin Agric. Sci.* 2, 20–21.

Chen, T. H. H., Burke, M. J., and Gusta, L. V. (1995). *Freezing tolerance in plants: an overview* (St Paul, Minnesota: APS Press).

Chen, L., Y., Z., Xu, S., Zhang, Z., Xu, Y., and Zhang, J. (2018). OsMADS57 together with OsTB1 coordinates transcription of its target *OsWRKY94* and *D14* to switch its organogenesis to defense for cold adaptation in rice. *New Phytol.* 218, 219–231. doi: 10.1111/nph.14977

Chen, B. H., Zhang, B., Mao, J., Hao, Y., Yang, R., Cai, X. H., et al. (2014). The relationship between the changing of water content and the cold resistance of grape branches. *Plant Physiol. J.* 50, 535–541. doi: 10.13592/j.cnki.ppj.2013.0441

Chinnusamy, V., Ohta, M., Kanrar, S., Lee, B., Hong, X., Agarwal, M., et al. (2003). ICE1: a regulator of cold-induced transcriptome and freezing tolerance in arabidopsis. *Genes Dev.* 17, 1043–1054. doi: 10.1101/gad.1077503

Chinnusamy, V., Zhu, J., and Zhu, J. K. (2007). Cold stress regulation of gene expression in plants. *Trends Plant Sci.* 12 10, 444–451. doi: 10.1016/j.tplants.2007.07.002

Dong, C., Zhang, Z., Ren, J. P., Qin, Y., Huang, J. F., Wang, Y., et al. (2013). Stress-responsive gene ICE1 from *Vitis amurensis* increases cold tolerance in tobacco. *Plant Physiol. Biochem.* 71, 212–217. doi: 10.1016/j.plaphy.2013.07.012

Elstner, E. F., and Heupel, A. (1976). Inhibition of nitrite formation from hydroxylammoniumchloride: a simple assay for superoxide dismutase. *Analytical Biochem.* 70 2, 616–620. doi: 10.1016/0003-2697(76)90488-7

Ershadi, A., Karimi, R., and Mahdei, K. N. (2016). Freezing tolerance and its relationship with soluble carbohydrates, proline and water content in 12 grapevine cultivars. *Acta Physiologiae Plantarum.* 38, 2. doi: 10.1007/s11738-015-2021-6

Fuller, M. P., and Grice, P. L. (1998). A chamber for the simulation of radiation freezing of plants. *Ann. Appl. Biol.* 133, 111–121. doi: 10.1111/j.1744-7348.1998.tb05807.x

Fuller, M. P., Hamed, F., Wisniewski, M., and Glenn, D. M. (2003). Protection of plants from frost using hydrophobic particle film and acrylic polymer. *Ann. Appl. Biol.* 143, 93–98. doi: 10.1111/j.1744-7348.2003.tb00273.x

Fuller, M. P., and Wisniewski, M. (1998). The use of infrared thermal imaging in the study of ice nucleation and freezing of plants. *J. Thermal Biol.* 23 (2), 81–89. doi: 10.1016/S0306-4565(98)00013-8

Gao, J. F. (2006). *Experimental guidance for plant physiology* (Beijing, China: Higher Education Press).

Giannopolitis, C. N., and Ries, S. K. (1977). Superoxide dismutases: I. occurrence in higher plants. *Plant Physiol.* 59, 309–314. doi: 10.1104/pp.59.2.309

Gilmour, S. J., Audrey, M., Maite, P., Everard, J. D., and Thomashow, M. F. (2000). Overexpression of the arabidopsis CBF3 transcriptional activator mimics multiple biochemical changes associated with cold acclimation. *Plant Physiol.* 124 (4), 1854–1865. doi: 10.1104/pp.124.4.1854

Grant, T., and Dami, I. E. (2015). Physiological and biochemical seasonal changes in vitis genotypes with contrasting freezing tolerance. *Am. J. Enology Viticulture.* 66, 195 -203. doi: 10.5344/ajev.2014.14101

Grossnickle, S. C., and South, D. B. (2014). Fall acclimation and the lift/store pathway: effect on reforestation. *Open For. Sci. J.* 714 1, 1–20. doi: 10.2174/1874398601407010001

Guy, C. L. (1990). Cold acclimation and freezing stress tolerance: role of protein metabolism. *Annu. Rev. Plant Physiol. Plant Mol. Biol.* 41, 187–223. doi: 10.1146/annurev.pp.41.060190.001155

Guy, C. L., Huber, J. L., and Huber, S. (1992). Sucrose phosphate synthase and sucrose accumulation at low temperature. *Plant Physiol.* 100, 502–508. doi: 10.1104/pp.100.1.502

Haghi, H., Rabiei, V., Ershadi, A., and Razavi, F. (2019). Effects of late season foliar application of calcium chloride on cold hardiness in grapevines (*Vitis vinifera* 'Thompson seedless'). *Horticulture J.* 88, 347–353. doi: 10.2503/hortj.UTD-056

Han, X., Xue, T. T., Liu, X., Wang, Z. L., Zhang, L., Wang, Y., et al. (2021). A sustainable viticulture method adapted to the cold climate zone in China. *Horticulturae* 7, 150. doi: 10.3390/horticulturae7060150

Hasanuzzaman, M., Bhuyan, M. H. M. B., Zulfiqar, F., Raza, A., Al Mahmud, J., Fujita, M., et al. (2020). Reactive oxygen species and antioxidant defense in plants under abiotic stress: revisiting the crucial role of a universal defense regulator. *Antioxidants.* 9, 681. doi: 10.3390/antiox9080681

Hashempour, A., Ghasemnezhad, M., Ghazvini, R. F., and Sohani, M. M. (2014). Olive (*Olea europaea* l.) freezing tolerance related to antioxidant enzymes activity during cold acclimation and non acclimation. *Acta Physiologiae Plantarum.* 36, 3231–3241. doi: 10.1007/s11738-014-1689-3

Hodges, D. M., DeLong, J. M., Forney, C. F., and Prange, R. K. (1999). Improving the thiobarbituric acid-reactive-substances assay for estimating lipid peroxidation in plant tissues containing anthocyanin and other interfering compounds. *Planta.* 207, 604–611. doi: 10.1007/s004250050524

Jolivet, Y., and Dubois, J. M. M. (2000). Evaluation of hilling efficiency as a method of protection of vine against winter cold in québec. *J. Int. Des. Sci. la Vigne du vin.* 3, 83–92. doi: 10.20870/oeno-one.2000.34.3.1001

Kaya, O. (2020a). Defoliation alleviates cold-induced oxidative damage in dormant buds of grapevine by up-regulating soluble carbohydrates and decreasing ROS. *Acta Physiologiae Plantarum* 42 (7), 1–10. doi: 10.1007/s11738-020-03093-1

Kaya, O. (2020b). Bud death and its relationship with lateral shoot, water content and soluble carbohydrates in four grapevine cultivars following winter cold. *Erwerbs-Obstbau* 62 (1), 43–50. doi: 10.1007/s10341-020-00495-w

Kaya, Ö., and Köse, C. (2017). Determination of resistance to low temperatures of winter buds on lateral shoot present in karaerik (Vitis vinifera l.) grape cultivar. *Acta Physiologiae Plantarum* 39 (9), 1–9. doi: 10.1007/s11738-017-2513-7

Kaya, O., and Kose, C. (2020). How pretest temperatures change the cold hardiness of grapevine (Vitis vinifera l. cv. karaerik) dormant buds? *Int. J. Fruit Sci.* 20 (Suppl 3), S1470–S1482. doi: 10.1080/15538362.2020.1804516

Kaya, O., Kose, C., Donderalp, V., Gecim, T., and Taskın, S. (2020). Last updates on cell death point, bud death time and exothermic characteristics of flower buds for deciduous fruit species by using differential thermal analysis. *Scientia Hortic.* 270, 109403. doi: 10.1016/j.scienta.2020

Kaya, O., Kose, C., Esitken, A., Gecim, T., Donderalp, V., Taskin, S., et al. (2021). Frost tolerance in apricot (*Prunus armeniaca* l.) receptacle and pistil organs: how is the relationship among amino acids, minerals, and cell death points? *Int. J. Biometeorology* 65 (12), 2157–2170. doi: 10.1007/s00484-021-02178-x

Kaya, O., Kose, C., Esıtken, A., Turan, M., and Utku, O. (2021). Can organic acid and sugar compositions be used to predict cell death point limits? receptacle and pistil organs of apricot (*Prunus armeniaca* l.). *Rendiconti Lincei. Sci. Fisiche e Naturali* 32 (3), 493–509. doi: 10.1007/s12210-021-01007-y

Khanizadeh, S., Rekika, D., Levasseur, A., Groleau, Y., and Fisher, H. (2005). The effects of different cultural and environmental factors on grapevine growth, winter hardiness and performance, in three locations, in Canada. *Small Fruits Rev.* 4, 3–28. doi: 10.1300/J301v04n03_02

Kim, Y. S., Lee, M., Lee, J. H., Lee, H. J., and Park, C. M. (2015). The unified ICE-CBF pathway provides a transcriptional feedback control of freezing tolerance during cold acclimation in arabidopsis. *Plant Mol. Biol.* 89 (1-2), 187–201. doi: 10.1007/s11103-015-0365-3

Koch, K. E. (1996). Carbohydrate-modulated gene expression in plants. *Annu. Rev. Plant Physiol. Plant Mol. Biol.* 47, 509–540. doi: 10.1146/annurev.arplant.47.1.509

Lan, Y. C., Shen, L. X., and Li, R. F. (2013). Effects of different film mulching on soil temperature and moisture. *Chin. Agric. Sci. Bulletin.* 29, 120–126.

Lee, S. P., and Chen, T. H. H. (1992). Molecular biology of plant cold hardiness development. *In (eds) Adv. Plant Cold hardiness. CRC Press Boca Raton* pp, 1–30.

Li, H. (2015). *Crawled cordon training: A new grapevine shaping and pruning system for the soil-bury over-wintering zone in China* (Yangling, Shaanxi: NWSUAF Press).

Licausi, F., Ohme-Takagi, M., and Perata, P. (2013). APETALA2/Ethylene responsive factor (AP2/ERF) transcription factors: mediators of stress responses and developmental programs. *N Phytologist.* 199, 639–649. doi: 10.1111/nph.12291

Li, C. Y., Chen, S. S., Xu, W., Li, D. S., Gu, X., Zhu, X. K., et al. (2011). Effect of low temperature at seedling stage on antioxidation enzymes and cytoplasmic osmoticum of leaves in wheat cultivar yangmai 16. *Acta Agronomica Sinica.* 37, 2293–2298. doi: 10.3724/SP.J.1006.2011.02293

Ling, F., Jiao, J., Li, C. Z., Jin, Q. X., and Zhao, M. L. (2015). Physiological reaponse and comprehensive evaluation of cold resistance under cold stress for different varieties of olea europaea. *Acta Botanica Boreali Occidentalia Sinica.* 35, 0508–0515. doi: 10.7606/j.issn.1000-4025.2015.03.0508

Liu, Q., Kasuga, M., Sakuma, Y., Abe, H., Miura, S., Yamaguchi –Shinozaki, K., et al. (1998). Two transcription factors, DREB1 and DREB2, with an EREBP/AP2 DNA binding domain separate two cellular signal transduction pathways in drought- and low-temperature-responsive gene expression, respectively, in arabidopsis. *Plant Cell.* 10 (8), 1391–1406. doi: 10.1105/tpc.10.8.1391

Liu, L., Li, S. X., Guo, J. H., Li, N., Jiang, M., and Li, X. N. (2022). Low temperature tolerance is depressed in wild-type and abscisic acid-deficient mutant barley grown in cd-contaminated soil. *J. Hazardous Materials* 430, 128489. doi: 10.1016/j.jhazmat.2022.128489

Liu, J., Wang, X. W., Wei, X. P., Lu, R. Q., and Gao, Z. Q. (2004). Achievement and prospect of world cold-resistance grape breeding. *J. Fruit Sci.* 21, 461–466. doi: 10.1007/BF02873091

Livak, K. J., and Schmittgen, T. D. (2001). Analysis of relative gene expression data using real-time quantitative PCR and the 2^{-CT} method. *Methods.* 25, 402–408. doi: 10.1006/meth.2001.1262

Li, J. T., Wang, L. N., Zhu, W., Wang, N. A., Xin, H. P., and Li, S. H. (2014). Characterization of two VvICE1 genes isolated from 'Muscat hamburg' grapevine and their effect on the tolerance to abiotic stresses. *Scientia Hortic.* 165, 266–273. doi: 10.1016/j.scienta.2013.11.002

Lu, M. (2006). Effect of humic acid as special organic fertilizer for eucalyptus on cold resistance and growth stimulation of eucalyptus dunnii. *J. Zhejiang Forestry College.* 23, 501–506.

Lv, D. K., Xi, B., Yong, L., Ding, X. D., Ge, Y., Cai, H., et al. (2010). Profiling of cold-stress-responsive miRNAs in rice by microarrays. *Gene.* 459, 39–47. doi: 10.1016/j.gene.2010.03.011

Lyons, J. M. (1973). Chilling injury in plants. *Annu. Rev. Plant Physiol.* 24, 445–466. doi: 10.1146/annurev.pp.24.060173.002305

Meiering, A. G., Paroschy, J. H., Peterson, R. L., Hostetter, G., and Neff, A. (1980). Mechanical freezing injury in grapevine trunks. *Am. J. Enology Viticulture.* 31, 81–89.

Pei, D. L. (2012). The progress of GSTs in plant defense. *Chin. Agric. Sci. Bull.* 28, 185–188.

Pierquet, P., Stushnoff, C., and Burke, M. J. (1977). Low temperature exotherms in stem and bud tissues of vitis riparia michx. *J. Am. Soc. Hortic. Sci. Am. Soc. Hortic. Sci.* 102, 54–55. doi: 10.21273/JASHS.102.1.54

Puhakainen, T., Li, C. Y., Boije-Malm, M., Heino, P., and Palva, E. T. (2004). Short-day potentiation of low temperature-induced gene expression of a c-Repeat-Binding factor-controlled gene during cold acclimation in silver birch. *Plant Physiol.* 136 4, 4299–4307. doi: 10.1104/pp.104.047258

Rao, M., Paliyath, G., and Ormrod, D. P. (1996). Ultraviolet-b- and ozone-induced biochemical changes in antioxidant enzymes of arabidopsis thaliana. *Plant Physiol.* 110, 125–136. doi: 10.1104/pp.110.1.125

Rende, M., Kose, C., and Kaya, O. (2018). An assessment of the relation between cold-hardiness and biochemical contents of winter buds of grapevine cv.'Karaerik'in acclimation-hardening-deacclimation phases. *Mitt. Klosterneuburg Rebe und Wein Obstbau und Früchteverwertung* 68 (2), 67–81.

Ren, J., Huang, Z. L., Zeng, L. X., and Shi, Z. (2013). A review of physiological reaction mechanism of plants exposed to low temperature stress. *World Forestry Res.* 26, 15–20. doi: 10.13348/j.cnki.sjlyyj.2013.06.011

Ritonga, F. N., and Chen, S. (2020). Physiological and molecular mechanism involved in cold stress tolerance in plants. *Plants.* 9 (5), 560. doi: 10.3390/plants9050560

Rubio, S., Noriega, X., and Pérez, F. J. (2018). Abscisic acid (ABA) and low temperatures synergistically increase the expression of CBF/DREB1 transcription factors and cold-hardiness in grapevine dormant buds. *Ann. Botany.* 123, 681–689. doi: 10.1093/aob/mcy201

Salzman, R. A., Bressan, R. A., Hasegawa, P. M., Ashworth, E. N., and Bordelon, B. P. (1996). Programmed accumulation of LEA-like proteins during desiccation and cold acclimation of overwintering grape buds. *Plant Cell Environment.* 19, 713–720. doi: 10.1111/j.1365-3040.1996.tb00406.x

Schnabel, B. J., and Wample, R. L. (1987). Dormancy and cold hardiness in vitis vinifera l. cv. white Riesling as influenced by photoperiod and temperature. *Am. J. enology viticulture.* 38, 265–272.

Shi, Y. T., Ding, Y. L., and Yang, S. H. (2018). Molecular regulation of CBF signaling in cold acclimation. *Trends Plant Sci.* 23 (7), 623–637. doi: 10.1016/j.tplants.2018.04.002

Siddiqua, M., and Nassuth, A. (2011). Vitis CBF1 and vitis CBF4 differ in their effect on arabidopsis abiotic stress tolerance, development and gene expressionpce. *Plant Cell Environment.* 34, 1345–1359. doi: 10.1111/j.1365-3040.2011.02334.x

Smeekens, S., and Rook, F. (1997). Sugar sensing and sugar-mediated signal transduction in plants. *Plant Physiol.* 115 >1, 7–13. doi: 10.1104/pp.115.1.7

Snyder, R. L., Melo-Abreu, J. P. D., and Matulich, S. (2005). *Frost protection: fundamentals, practice and economics* (Rome, Italy: Food and Agriculture Organization of the United Nations).

Soloklui, A. A. G., Ershadi, A., and Fallahi, E. (2012). Evaluation of cold hardiness in seven Iranian commercial pomegranate (Punica granatum l.) cultivars. *Hortscience.* 47, 1821–1825. doi: 10.21273/HORTSCI.47.12.1821

Stockinger, E. J., Gi lmour, S. J., and Thomashow, M. F. (1997). Arabidopsis thaliana *CBF1* encodes an AP2 domain-containing transcriptional activator that binds to the c-repeat/DRE, a cis-acting DNA regulatory element that stimulates transcription in response to low temperature and water deficit. *Proc. Natl. Acad. Sci. U. S. A.* 94 (3), 1035–1040. doi: 10.1073/pnas.94.3.1035

Theocharis, A., Clement, C., and Barka, E. A. (2012). Physiological and molecular changes in plants grown at low temperatures. *Planta.* 235 6, 1091–1105. doi: 10.1007/s00425-012-1641-y

Thomashow, M. F. (1999). PLANT COLD ACCLIMATION: Freezing tolerance genes and regulatory mechanisms. *Annu. Rev. Plant Physiol. Plant Mol. Biol.* 50, 571–599. doi: 10.1146/annurev.arplant.50.1.571

Thomashow, M. F. (2010). Molecular basis of plant cold acclimation: insights gained from studying the CBF cold response pathway. *Plant Physiol.* 154, 571–577. doi: 10.1104/pp.110.161794

Tillett, R. L., Wheatley, M. D., Tattersall, E. A., Schlauch, K. A., Cramer, G. R., and Cushman, J. C. (2012). The vitis vinifera c-repeat binding protein 4 (*VvCBF4*) transcriptional factor enhances freezing tolerance in wine grape. *Plant Biotechnol. J.* 10, 105–124. doi: 10.1111/j.1467-7652.2011.00648.x

Uemura, M., and Steponkus, P. L. (1994). A contrast of the plasma membrane lipid composition of oat and rye leaves in relation to freezing tolerance. *Plant Physiol.* 104, 479–496. doi: 10.1104/pp.104.2.479

Vadim, D., Darya, S., Medvedev, S. S., Pozhvanov, G. A., Anatoliy, S., and Vladimir, Y. (2014). Stress-induced electrolyte leakage: the role of k+-permeable channels and involvement in programmed cell death and metabolic adjustment. *J. Exp. Botany.* 65, 1259–1270. doi: 10.1093/jxb/eru004

Wang, S. (2015). *Effect of shoots windbreak on vineyard ecotope in the soil-buried cold-proof period* (Yangling, China: Northwest A&F University).

Wang, Z. S., Li, S. X., Jian, S. L., Ye, F., Wang, T. Y., Gong, L., et al. (2022). Low temperature tolerance is impaired by polystyrene nanoplastics accumulated in cells of barley (*Hordeum vulgare* l.) plants. *J. Hazardous Materials* 426, 127826. doi: 10.1016/j.jhazmat.2021.127826

Wang, H. T., Ma, X. F., and Zhang, J. Z. (2010). The application of humic acid in soil and fertilizer. *Heilongjiang Sci.* 1, 59–62.

Wang, X., Xu, G. B., Ren, Z. G., Zhang, Z. J., Jian, Y. F., and Zhang, Y. M. (2007a). Effects of environment-friendly degradable films on corn growth and soil environment. *Chin. J. Eco-Agriculture.* 15, 78–81.

Wang, W. J., Zhang, Y. H., Niu, J. F., and Wang, Z. P. (2007b). Study on cold tolerance of table grape cultivars by measuring the conductivity. *J. Fruit Science.* 24, 34–37. doi: 10.13925/j.cnki.gsxb.2007.01.008

Weiser, C. J. (1970). Cold resistance and injury in woody plants. *Science.* 169, 1269–1278. doi: 10.1126/science.169.3952.1269

Wisniewski, M., Bassett, C., and Gusta, L. V. (2003). An overview of cold hardiness in woody plants: Seeing the forest through the trees. *Hortscience.* 38, 952–959. doi: 10.21273/HORTSCI.38.5.952

Wisniewski, M., Glenn, D. M., and Fuller, M. P. (2002). Use of a hydrophobic particle film as a barrier to extrinsic ice nucleation in tomato plants. journal of the American society for. *Hortic. Science.* 127, 358–364. doi: 10.21273/JASHS.127.3.358

Xiao, H., Siddiqua, M., Braybrook, S., and Nassuth, A. (2006). Three grape CBF / DREB1 genes respond to low temperature, drought and abscisic acid. *Plant Cell Environment.* 29, 1410–1421. doi: 10.1111/j.1365-3040.2006.01524.x

Xiao, H., Tattersall, E., Siddiqua, M., Cramer, G., and Nassuth, A. (2008). *CBF4* is a unique member of the CBF transcription factor family of vitis vinifera and vitis riparia. *Plant Cell Environment.* 31 1, 1–10. doi: 10.1111/j.1365-3040.2007.01741.x

Xue, T. T. (2019a). *Research of free-buried mode based on biodegradable liquid film in grapevine soil-burial areas* (Yangling, China: Northwest A&F University).

Xue, T. T., Han, X., Zhang, H. J., Wang, Y., Wang, H., and Li, H. (2019b). Effects of a biodegradable liquid film on winter chill protection of winegrape cultivars. *Scientia Hortic.* 246, 398–406. doi: 10.1016/j.scienta.2018.11.013

Yamaguchi-Shinozaki, K., and Shinozaki, K. (1994). A novel cis-acting element in an arabidopsis gene is involved in responsiveness to drought, low-temperature, or high-salt stress. *Plant Cell.* 6 (2), 251–264. doi: 10.1105/tpc.6.2.251

Yang, Y., Jia, Z. K., Chen, F. J., Sang, Z. Y., and Ma, L. Y. (2015). Comparative analysis of natural cold acclimation and deacclimation of two magnolia species with different winter hardiness. *Acta Physiologiae Plantarum.* 37, 129. doi: 10.1007/s11738-015-1883-y

Yemm, E. W., and Willis, A. J. (1954). The estimation of carbohydrates in plant extracts by anthrone. *Biochem. J.* 57, 508–514. doi: 10.1042/bj0570508

Zhang, G., Ryyppo, A., and Repo, T. (2002). The electrical impedance spectroscopy of scots pine needles during cold acclimation. *Physiologia Plantarum* 115, 385–392. doi: 10.1034/j.1399-3054.2002.1150308.x

Zhang, J., Wu, X., Niu, R., Liu, Y., Liu, N., Xu, W., et al. (2012). Cold-resistance evaluation in 25 wild grape species. *Vitis.* 51 4, 153–160.

Zhao, Y., Wang, Z. X., Yang, Y. M., Liu, H. S., and Ai, J. (2020). Analysis of the cold tolerance and physiological response differences of amur grape (Vitis amurensis) germplasms during overwintering. *Scientia Horticulturae.* 259, 1–9. doi: 10.1016/j.scienta.2019.108760

frontiers | Frontiers in Plant Science

TYPE Original Research
PUBLISHED 07 November 2022
DOI 10.3389/fpls.2022.1022696

Check for updates

OPEN ACCESS

EDITED BY
Diaa Abd El Moneim,
Arish University, Egypt

REVIEWED BY
Boutasknit Abderrahim,
Cadi Ayyad University, Morocco
Mohammad Etemadi,
Shiraz University, Iran

*CORRESPONDENCE
Ming Tang
tangmingyl@163.com

SPECIALTY SECTION
This article was submitted to Plant Abiotic Stress, a section of the journal Frontiers in Plant Science

RECEIVED 18 August 2022
ACCEPTED 17 October 2022
PUBLISHED 07 November 2022

CITATION
Han L-N, Wang S-J, Chen H, Ren Y, Xie X-A, Wang X-Y, Hu W-T and Tang M (2022) Arbuscular mycorrhiza mitigates zinc stress on *Eucalyptus grandis* through regulating metal tolerance protein gene expression and ionome uptake.
Front. Plant Sci. 13:1022696.
doi: 10.3389/fpls.2022.1022696

COPYRIGHT
© 2022 Han, Wang, Chen, Ren, Xie, Wang, Hu and Tang. This is an open-access article distributed under the terms of the Creative Commons Attribution License (CC BY). The use, distribution or reproduction in other forums is permitted, provided the original author(s) and the copyright owner(s) are credited and that the original publication in this journal is cited, in accordance with accepted academic practice. No use, distribution or reproduction is permitted which does not comply with these terms.

Arbuscular mycorrhiza mitigates zinc stress on *Eucalyptus grandis* through regulating metal tolerance protein gene expression and ionome uptake

Li-Na Han, Si-Jia Wang, Hui Chen, Ying Ren, Xian-An Xie, Xing-Yang Wang, Wen-Tao Hu and Ming Tang*

Guangdong Laboratory for Lingnan Modern Agriculture, State Key Laboratory of Conservation and Utilization of Subtropical Agro-bioresources, College of Forestry and Landscape Architecture, South China Agricultural University, Guangzhou, China

Arbuscular mycorrhizal (AM) fungi are symbionts of most terrestrial plants and enhance their adaptability in metal-contaminated soils. In this study, mycorrhized and non-mycorrhized *Eucalyptus grandis* were grown under different Zn treatments. After 6 weeks of treatment, the growing status and ionome content of plants as well as the expression patterns of metal tolerance proteins and auxin biosynthesis–related genes were measured. In this study, mycorrhized *E. grandis* showed higher biomass and height at a high level of Zn compared with non-mycorrhized plants. In addition, AM plants accumulated P, Mg, and Mn in roots and P, Fe, and Cu in shoots, which indicate that AM fungi facilitate the uptake of ionome nutrients to promote plant growth. In addition, mycorrhiza upregulated the expression of *EgMTP1* and *EgMTP7*, whose encoding proteins were predicted to be located at the vacuolar membrane. Meanwhile, Golgi membrane transporter *EgMTP5* was also induced in AM shoot. Our results suggest that AM likely mitigates Zn toxicity through sequestrating excess Zn into vacuolar and Golgi. Furthermore, the expression of auxin biosynthesis–related genes was facilitated by AM, and this is probably another approach for Zn tolerance.

KEYWORDS

***Eucalyptus grandis*, auxin biosynthesis–related genes, arbuscular mycorrhiza, metal tolerance protein, nutrient uptake, zinc stress**

Introduction

Zinc (Zn) was an utmost important micronutrient for all living organisms, and it acted as catalytic and structural component in a large number of enzymes and regulatory proteins (Maret, 2009; Zhang et al., 2018; Kaur and Garg, 2021; Bae et al., 2022). Zn played an important role in regulating plant growth and development, which involves modulating a wide range of physiological processes: cell proliferation, respiration, auxin biosynthesis, and antioxidative defenses (Broadley et al., 2007; Zhang et al., 2018; Kaur and Garg, 2021; Bae et al., 2022). However, high concentration of Zn can be toxic. Excess Zn strongly decreased fresh weight and inhibited net photosynthetic rate, transpiration, and stomatal conductance in bean seedlings (Vassilev et al., 2011). In rice, a high level of Zn induced the lateral root formation through modulating the redistribution of auxin in root tips (Zhang et al., 2018) as well as inhibited the root-to-shoot translocation and distribution of P into new leaves by downregulating P transporter genes (Ding et al., 2021).

To maintain the intracellular Zn level within physiological limit, plants had developed a dynamic system involving Zn uptake, efflux, transport, and sequestration *via* particular transporters (Clemens et al., 2002; Stephens et al., 2011; Sinclair and Krämer, 2012). Zn transporters in plant included zinc/iron-regulated transporter-like proteins (ZIP), metal tolerance protein (MTP), heavy metal ATPases (HMA), natural resistance-associated macrophage protein (NRAMP), yellow stripe-like transporter family (YSL), ATP-binding cassette transporters (ABC), zinc-induced facilitator 1 proteins (ZIF1), and plant cadmium resistance proteins (PCR) (Sinclair and Krämer, 2012; Neeraja et al., 2018; Kaur and Garg, 2021). Zn toxicity resulted in suppressed expression of *ZmZIP4*, *ZmZIP5*, *ZmZIP7*, and *ZmZIP8* in shoots and *ZmZIP3* in maize roots (Li et al., 2013). In response to Zn stress, upregulation of *MsZIP2* was a detoxification mechanism to store excess Zn in xylem parenchyma cells of *Medicago sativa* (Cardini et al., 2021). Enhanced expression of *ZIF1* by excess Zn had also been verified in *Arabidopsi thaliana* (Haydon and Cobbett, 2007). Moreover, the transcript amount of *HMA4* was elevated in the roots and shoots of *M. sativa* exposed to surplus Zn (Cardini et al., 2021).

MTP family as divalent cation transporters involved in metal ion efflux from the cytoplasm into subcellular compartments or to extracellular space (Sinclair and Krämer, 2012) and played a pivotal role in alleviating heavy metal toxicity. Previously, MTP family had been investigated at the genomic level in *A. thaliana*, *Oryza sativa*, *Citrus sinensis*, *Populus trichocarpa*, and *Glycine max* (Gustin et al., 2011; Fu et al., 2017; Gao et al., 2020; Haque et al., 2022). According to substrate specificity, the members of MTP family were phylogenetically classified into three subfamily: Zn-CDF (to transport Zn, Cd, Ni, and Co), Zn/Fe-CDF (to transfer Fe, Zn, Cd, Ni, and Co), and Mn-CDF (mostly, to target Mn) (Montanini et al., 2007). In *A. thaliana*, five MTPs had been reported to transport Zn: AtMTP1, AtMTP2, AtMTP3, AtMTP5, and AtMTP12 (Desbrosses-Fonrouge et al., 2005; Arrivault et al., 2006; Fujiwara et al., 2015; Sinclair et al., 2018).

Arbuscular mycorrhizal (AM) fungi were obligate biotrophic fungi, which formed mutualistic symbiosis with more than 70% of terrestrial vascular plants (Brundrett and Tedersoo, 2018; Tedersoo et al., 2020). In addition, AM fungi were eco-friendly and effective in alleviating heavy metal stress of plants (Ferrol and Tamayo, 2016; Nuria et al., 2016; Tedersoo et al., 2020; Riaz et al., 2021). For example, when plants were cultivated in soils containing toxic amount of Zn, AM fungi symbiosis induced higher phosphorus (P) concentration and lower Zn concentration in shoots than those grown in control conditions (Díaz et al., 1996). In addition, mycorrhization increased the total chlorophyll content of plant grown in metal-polluted soil but diminished the concentration of H_2O_2 and activity of glutathione reductase (GR), catalase (CAT), guaiacol peroxidase (POD) and ascorbate peroxidase (APX) (Fernández-Fuego et al., 2017). Glomalin-related soil protein, a kind of glycoprotein produced by AM fungi, was able to combine with metal ions to sequester them in soil, consequently, to mitigate metal uptake by plants (Yang et al., 2017). AM fungi increased the resistance of host to Zn stress by upregulating the expression of ZNT:4, COPT/Ctr:2, YSL:3, and CE:1 (Wang et al., 2022).

Eucalypts was well known for its fast growth and superior hardwood, and it had been widely planted as economical tree. Furthermore, eucalypts was popular for reclamation of degraded land in coal mines, because of its ability to uptake heavy metals from contaminated soil (Maiti and Rana, 2017). Previous studies showed that *Eucalyptus grandis* can form symbiosis relationships with AM fungi in both plantation and natural woodland community, and symbiosis protected it from potential damage of heavy metals (Adams et al., 2006; Chen et al., 2007; Canton et al., 2016). With the publication of *E. grandis* genome (Myburg et al., 2014), molecular mechanisms of *E. grandis* on metals stress need further exploration.

To get further insight into the role of *E. grandis* MTP on Zn homeostasis, we analyzed their expression patterns with/without AM fungi under different Zn treatments. We also assess the effects of Zn and AM fungi on ionome content and expression of auxin biosynthesis–related genes in *E. grandis*. This study will be helpful to the development of molecular markers for cultivar breeding of *E. grandis* with a high Zn tolerance.

Materials and methods

Biological materials and growth conditions

Rhizophagus irregularis DAOM197198 was used as the mycorrhizal fungus and was propagated on *Zea mays*. After

inoculation for 3 months, roots were treated with drought for another 2 months. Spores of *R. irregularis* were collected by modified sucrose-gradient centrifugation (Charoenpakdee et al., 2010).

The roots containing spores were broken with a blender; then, the roots were filtered through 710-, 200-, and 45-μm pore sieves. After backwashing the contents of 45-μm sieve into a 50-ml centrifuge tube, an equal volume of 50% (w/v) sucrose solution was gently added into the centrifuge tube. Then, the tubes were centrifuged at 2,000 rpm for 1 min with bench centrifuge. The spores were collected on 45-μm pore sieve and washed thoroughly to remove traces of sugar solution. Last, spores were backwashed into tube.

One milliliter of the liquid containing spores collected by sucrose-gradient centrifugation was dropped onto Miracloth (Calbiochem). The number of spores on Miracloth was counted with microscope, and the total number of spores was calculated according to the volume of the mixing liquid. Thus, we calculated the volume of liquid containing about 500 spores.

Eucalyptus grandis was used as host plant in this study. Seeds were surface-sterilized with 1.5% sodium hypochlorite for 15 min and washed with sterile water for three times and then were cultured in a quarter-strength Murashige and Skoog medium (pH 5.9) with 3 g L^{-1} agar. After 4 weeks, the seedlings were transferred to pots that contained sterile sands (the sands were sterilized three times for 2 h at 121°C) and inoculated with or without *R. irregularis* (about 500 spores per plant). The seedlings were cultivated in a greenhouse at 24°C/18°C day/night temperature under 16-h daylight and 50%–60% humidity. Moreover, the seedlings were fertilized with modified Long-Ashon solution (30 μM KH_2PO_4; Hewitt, 1966) every 3 days. After 5 weeks, mycorrhiza formation was checked following the MYCOCALC program (http://www2.dijon.inra.fr/mychintec/Mycocalc-prg/download.html). Then, the seedlings were fertilized with the abovementioned modified Long-Ashon solution containing 5, 50, and 150 μM Zn once a week for 6 weeks, respectively (Fu et al., 2017; Gao et al., 2020; Wang et al., 2021). Before harvest, fresh weight and length of root and shoot were measured. Then, roots and shoots were separated and frozen immediately in liquid nitrogen and then were stored in −80°C refrigerator.

Elemental concentration analyses

To measure Zn, P, Mg, Fe, Cu, and Mn concentrations in *E. grandis*, the roots and shoots were dried in vacuum lyophilizer (Christ, Germany). After fine grounding, the samples were weighed and then were digested in 1 ml of 6 M nitric acids at 90°C for 2 h. The digested product was diluted with equal volume of sterile water and then was filtered. After a further dilution (1:10), the element concentrations were analyzed with inductively coupled plasma optical emission spectrometry (710-ES, VARIAN, USA) (Xie et al., 2021, 2022).

Phylogenetic analyses

The MTP sequences of *A. thaliana*, *O. sativa*, *G. max*, *C. sinensis*, *P. trichocarpa*, and *E. grandis* were obtained from the NCBI (www.ncbi.nlm.nih.gov) and Phytozome database (phytozome-next.jgi.doe.gov) (Gustin et al., 2011; Fu et al., 2017; Gao et al., 2020; Haque et al., 2022). The sequences of identified MTP were listed in Table S1. The sequences were aligned with Clustal W. MEGA 7.0 was used to construct neighbor-joining tree with 1,000 bootstrap trials, and the evolutionary distance was analyzed with the Poisson correction method (Qi et al., 2022).

Gene expression analyses

Total RNA was extracted from the roots and shoots of *E. grandis* based on the modified CTAB-LiCl approach (Singh et al., 2015). cDNA was synthesized from 1 μg of total RNA with HiScript III RT SuperMix for qPCR (+gDNA wiper) kit (Vazyme, Nanjing, China), and then, it was three-fold diluted with sterile water. Real-time PCR were performed using Bio-Rad iQ5 and ChamQ Universal SYBR qPCR Master Mix (Vazyme, Nanjing, China). The relative expression level of MTP in both roots and shoots of *E. grandis*, as well as auxin biosynthesis–related genes in roots, were normalized with the normalization factor *EgUBI3* and presented as $2^{-\Delta\Delta Ct}$ (Livak and Schmittgen, 2001). For the expression of *EgMTPs*, the expression level in NM roots with 5 μM Zn was defined as 1. The gene-specific primers for real-time PCR were summarized in Table S2.

Mycorrhizal colonization

Fresh AM roots were fixed in 10% KOH (W/V) solution for 2 weeks under 37°C, and the solution was renewed every 3 days. After washing with sterile water, the roots were neutralized with 2% HCl (W/V) for 15 min. After another washing twice with sterile water, the roots with WGA-Alexa Fluor 488 (WGA488) then stained for 2 h at room temperature (Xie et al., 2021). Mycorrhizal colonization was quantified following the MYCOCALC program. We also launched confocal microscopy analysis performed with Zeiss 780 laser scanning confocal microscope.

Statistical analyses

Data were analyzed by SPSS software version 19.0 (Chicago, USA). The effects of mycorrhization and Zn on gene expression and ionome concentrations were evaluated by one-way analysis of variance. Results were indicated as mean ± standard error of at least three biological replicates. Statistical differences were

calculated using the Student's *t*-test with $P < 0.05$ as the significance thresholds. In addition, GraphPad Prism (version 8.0), TBtools (Chen et al., 2020), and iTOL were used to display graphics.

Results

Effect of Zn and mycorrhiza on the growth of *E. grandis*

Regarding the effects of Zn stress on non-mycorrhizal (NM) plants, Zn treatment led to decrease of root and shoot fresh weight (Figures 1A, B). Inoculation with AM fungi improved both roots and shoots fresh weight of *E. grandis*, especially under 150 μM Zn treatment (Figures 1A, B). Considering AM plants, Zn stress on the fresh weight of roots was prominent, whereas it was not indistinctive for the shoots.

With the increase of Zn concentrations, the plant height was suppressed in NM plants, whereas AM fungi inoculation eased the suppression on the height of *E. grandis* from Zn (Figure 1C, D). However, mycorrhiza cannot completely eliminate the inhibition by Zn stress on plant height: The height of AM plants at 50 and 150 μM Zn was still significantly lower than at 5 μM Zn (Figure 1C, D).

Effect of Zn and mycorrhiza on the ionome of *E. grandis*

Nutrient interactions in plants, in response to variable environmental stresses, significantly affect plant survival and development. With Zn treatment, Zn accumulated in NM roots, whereas the contents of P, Mg, Fe, and Cu decreased (Figure 2A). Meanwhile, Zn accumulation also occurred in NM shoots, but the concentrations of P, Mg, Fe, and Mn declined (Figure 2B). Moreover, the concentration of Mn in roots and Cu in shoots was unaffected.

Compared with NM roots, the concentration of Zn, P, Mg, and Mn was much higher in AM roots; nevertheless, Fe decreased, and Cu remained unaffected (Figure 2A). On the other hand, Zn and Mn contents were lower in AM shoots than that in NM shoots; P, Fe, and Cu were accumulated in AM shoots (Figure 2B).

MTPs of E. grandis

MTP sequences of *A. thaliana* were used as queries to search against *E. grandis* genome in Phytozome database to identify the MTP genes of *E. grandis*. After the conserved domain analysis, a total number of 16 MTP encoding genes were identified: *EgMTP1*, *EgMTP2*, *EgMTP3.1*, *EgMTP3.2*, *EgMTP4*, *EgMTP5*,

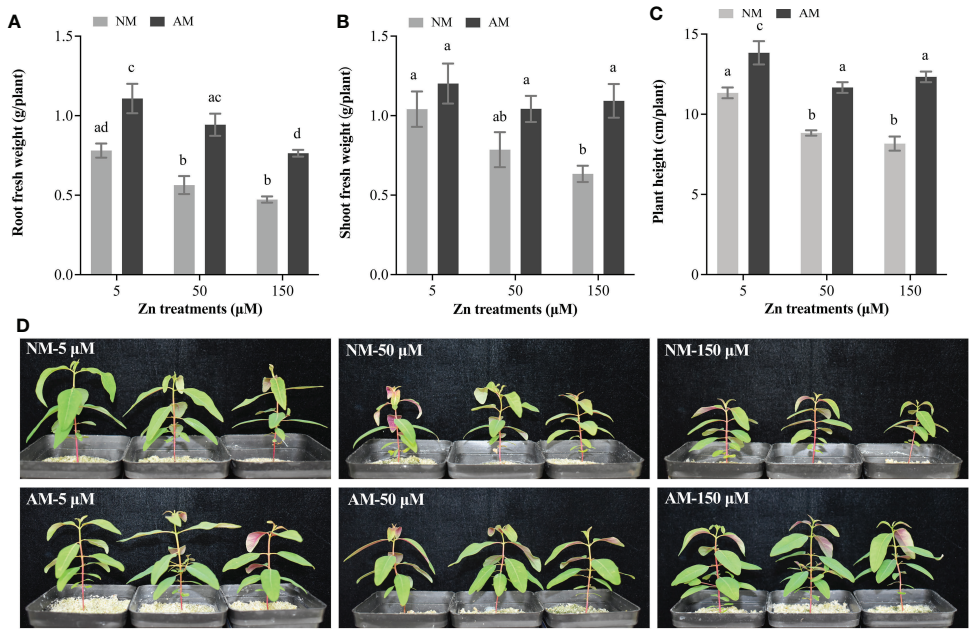

FIGURE 1
Effects of Zn and AM fungi on the growth of *E. grandis*. **(A)** Root fresh weight; **(B)** shoot fresh weight; **(C)** plant height; **(D)** the phenotype of *E. grandis* with or without AM fungi under 5, 50, and 150 μM Zn treatment. NM, non-mycorrhizal plants; AM, mycorrhizal plants. Values were indicated as mean ± SE of six biological replicates. Different letters above bars indicated significant differences at $P < 0.05$.

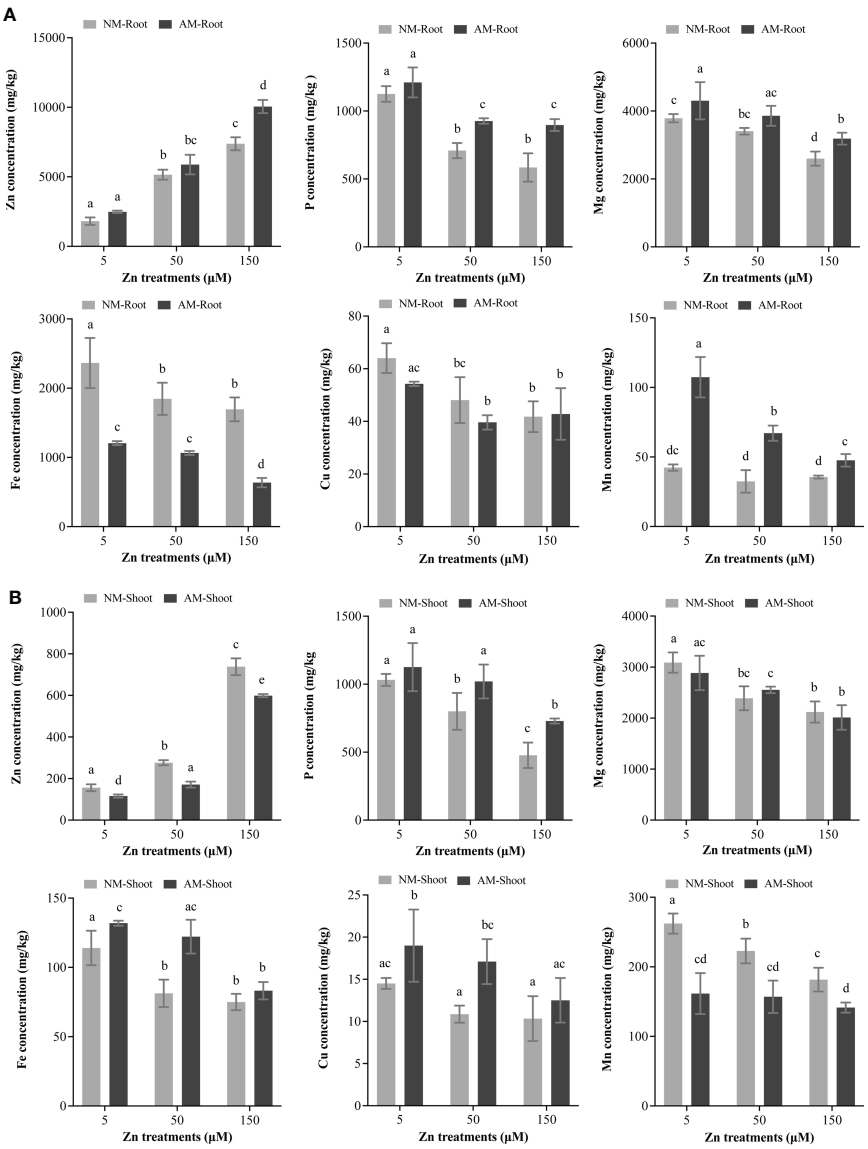

FIGURE 2
Total mineral element concentrations. The microelements (Zn, Fe, Cu, and Mn) and macroelements (P and Mg) of roots and shoots were analyzed by ICP-OES. NM, non-mycorrhizal plant; AM, mycorrhizal plant. **(A)** Total mineral concentration in root. **(B)** Total mineral concentration in shoot. Values were indicated as mean ± SE. Different letters above the bars indicated significant differences between treatments ($P < 0.05$).

EgMTP6, *EgMTP7*, *EgMTP8.1*, *EgMTP8.2*, *EgMTP9.1*, *EgMTP9.2*, *EgMTP10*, *EgMTP11.1*, *EgMTP11.2*, and *EgMTP12* (Figure 3).

To better understand the evolutionary characteristics and possible functions of the MTP family in *E. grandis*, a neighbor-joining tree consisting of 84 MTPs (including 12 MTPs from *A. thaliana*, 10 from *O. sativa*, 12 from *G. max*, 12 from *C. sativus*, 22 from *P. trichocarpa*, and 16 from *E. grandis*) was constructed (Figure 3). As previously reported, these proteins were divided into Zn-CDF, Zn/Fe-CDF, and Mn-CDF clusters (Montanini et al., 2007; Gustin et al., 2011), with seven (EgMTP1 to EgMTP5 and EgMTP12), two (EgMTP6 and EgMTP7), and seven (EgMTP8.1 to EgMTP11.2) MTP members, respectively (Figure 3).

Effect of Zn and mycorrhiza on the expression of *EgMTPs*

Previously, the expression of *ZIP2* was upregulated by excess Zn and downregulated by AM symbiosis both in *Medicago*

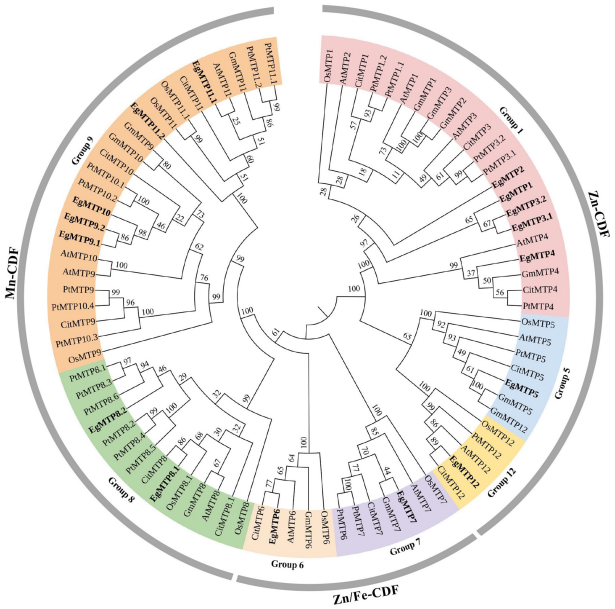

FIGURE 3
Phylogenetic relationships of MTP. The neighbor-joining tree was generated using MEGA 7.0 with 1,000 bootstrap replicates. *E. grandis* MTP proteins were in bold. At, *Arabidopsis thaliana*; Os, *Oryza sativa*; Gm, *Glycine max*; Pt, *Populus trichocarpa*; Cit, *Citrus sinensis*; Eg, *Eucalyptus grandis*.

truncatula and *Astragalus sinicus* (Burleigh et al., 2003; Xie et al., 2021). Herein, we analyzed the expression patterns of MTPs in NM and AM plants supplied with different concentrations of Zn.

In NM roots, the expression of *EgMTP1*, *EgMTP5*, and *EgMTP7* were significantly repressed by high-Zn treatment, whereas *EgMTP2* presented an overall upward trend, and no significant difference was detected in *EgMTP3.1*, *EgMTP3.2*, *EgMTP4*, *EgMTP6*, and *EgMTP12* (Figure 4A). As for AM root, Zn mostly reduced the expression of *EgMTPs*, except for *EgMTP7*. However, compared with NM roots, mycorrhiza induced the expression of *EgMTP1*, *EgMTP5*, and *EgMTP7* (Figure 4A). Regarding to NM shoots, the expression pattern of *EgMTP3.1* showed a downward trend with increased Zn concentration, whereas *EgMTP1*, *EgMTP4*, *EgMTP5*, *EgMTP6*, and *EgMTP7* were upregulated (Figure 4B). In AM shoots, Zn treatment induced the expression of *EgMTP1*, *EgMTP2*, *EgMTP3.1*, and *EgMTP5*, and upregulated *EgMTP1* and *EgMTP5* compared with that in NM shoots (Figure 4B). Overall, mycorrhiza induced the expression of *EgMTP1*, *EgMTP5*, and *EgMTP7* in roots and *EgMTP1* and *EgMTP5* in shoots.

Effect of Zn and mycorrhiza on the expression of the auxin biosynthesis–related gene

To further investigate the effects of Zn stress on auxin biosynthesis in *E. grandis*, we analyzed the expression patterns of *EgAAO3*, *EgYUC2*, *EgYUC3*, and *EgAMI1*. *EgAAO3* was strongly induced at 50 and 150 μM Zn (Figure 5A). Meanwhile, *EgYUC2* and *EgYUC3* significantly expressed at 150 μM Zn (Figures 5B, C), and the expression of *EgAMI1* was unaffected under any Zn concentration (Figure 5D).

Chareesri et al. (2020) and Wang et al.(2021) demonstrated that, compared to the NM roots, the content of auxin in the mycorrhizal rice and tomato roots significantly increased. To elucidate how mycorrhiza increased auxin accumulation in AM roots, we evaluated the transcript level of *EgAAO3*, *EgYUC2*, *EgYUC3*, and *EgAMI1*. Compared with NM roots, the expression of *EgYUC2* and *EgYUC3* was induced in AM roots (Figures 5B, C), whereas *EgAAO3* was repressed at 150 μM Zn treatment (Figure 5A).

Mycorrhizal colonization

To analyze the effect of Zn stress on AM fungi development in *E. grandis*, we quantified the mycorrhizal colonization rates in roots inoculated with *R. irregularis*. Plants grown with 5, 50, and 150 μM Zn showed similar mycorrhizal frequency (Figure 6A), based on the percentage of roots colonized by AM fungi in the whole roots. Although symbiosis had already existed for 5 weeks before the Zn treatment, mycorrhizal intensity was lower in AM roots grown at 50 and 150 μM Zn compared with that at 5 μM Zn (Figure 6B). Moreover, the arbuscule numbers decreased in AM roots exposed to a high level of Zn (Figure 6C). Roots exposed to

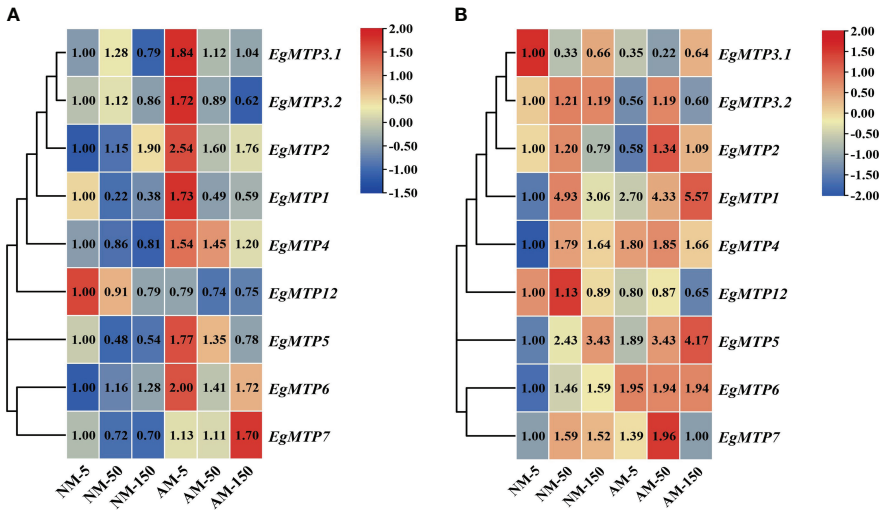

FIGURE 4
Expression profiles of *EgMTP*. The heat map was generated using the expression fold changes of *EgMTP* family. Relative gene expression was calculated by the $2^{-\Delta\Delta CT}$ method using the *EgUBI3* as a normalizer. For each gene, the expression level in NM roots with 5 μM Zn was defined as 1. **(A)** The expression profiles of *EgMTPs* in root. **(B)** The expression profiles of *EgMTPs* in shoot.

5 μM Zn had normal arbuscules, with full hyphal branches in the cortical cells, but fewer arbuscules were formed with high-Zn treatment (Figure 6D). In addition, intraradical hyphae at 150 μM Zn contained more septa (Figure 6D), which was a morphological signature of degradation of AM fungi. Intraradical hyphae was the channel for transporting nutrients in AM fungi, and the formation of septa prevented transport of nutrients to arbuscule, which led to the death of the arbuscule. In a nutshell, high-Zn treatments disturbed the arbuscule development through forming more septa in intraradical hyphae.

Discussion

Mycorrhiza promotes the growth of *E. grandis* under Zn stress

AM fungi were beneficial symbionts of plants that increased host resistance to various environmental stresses. Mycorrhizal *Betula pubescens* had higher fresh and dry weight than NM plants in metal-polluted industrial soil (Fernández-Fuego et al., 2017). In Cu-contaminated soils, symbiosis facilitated Cu tolerance of maize with increasing fresh weight (Gómez-Gallego et al., 2022). In our study, significantly higher biomass and height were detected in mycorrhizal *E. grandis* (Figure 1). AM fungi absorbed nutrients beyond the depletion zone that develops around the roots through external mycelium and then delivers them to host roots (Wang et al., 2017; Xie et al., 2021; Gómez-Gallego et al., 2022). This was a quite effective way to promote plant growth, and higher biomass further enhances the Zn tolerance of plants.

Zn and mycorrhiza affect the uptake of mineral elements

The growth and development of higher plants needed at least 17 essential elements, among which P and Mg were known as macroelements; Fe, Zn, Cu, and Mn were regarded as microelements; and the interactions between macro- and microelement were one of the key processes in the life cycle of plants (Xie et al., 2019; Fan et al., 2021; Kumar et al., 2021). Previous studies indicated that excess Zn triggered P starvation in lettuce and rice (Bouain et al., 2014; Ding et al., 2021). Similarly, we observed Zn increasing and P decreasing in both root and shoot of *E. grandis* along with elevation of Zn treatment (Figure 2). High Zn downregulated the expression of uptake and transporter-related genes of P (Ding et al., 2021), which inhibited the uptake and translocation of P; thus, less P was transported to shoots under high-Zn treatment (Figure 2). Consisting with the case of rapeseed seedlings (Wang et al., 2009), the concentrations of Fe and Mg in roots and shoots of *E. grandis* decreased with surplus Zn (Figure 2). On the other hand, when maize was grown in high-Zn condition, the concentrations of K, Ca, Mg, Fe, Mn, Ni, and Co significantly decreased in root, and Mn and Cu diminished in shoot along with the increase of S, Mg, and Mo (Bokor et al., 2015). Excessive Zn affected the level of Fe sensing, resulting in Fe deficiency (Leskova et al., 2017).

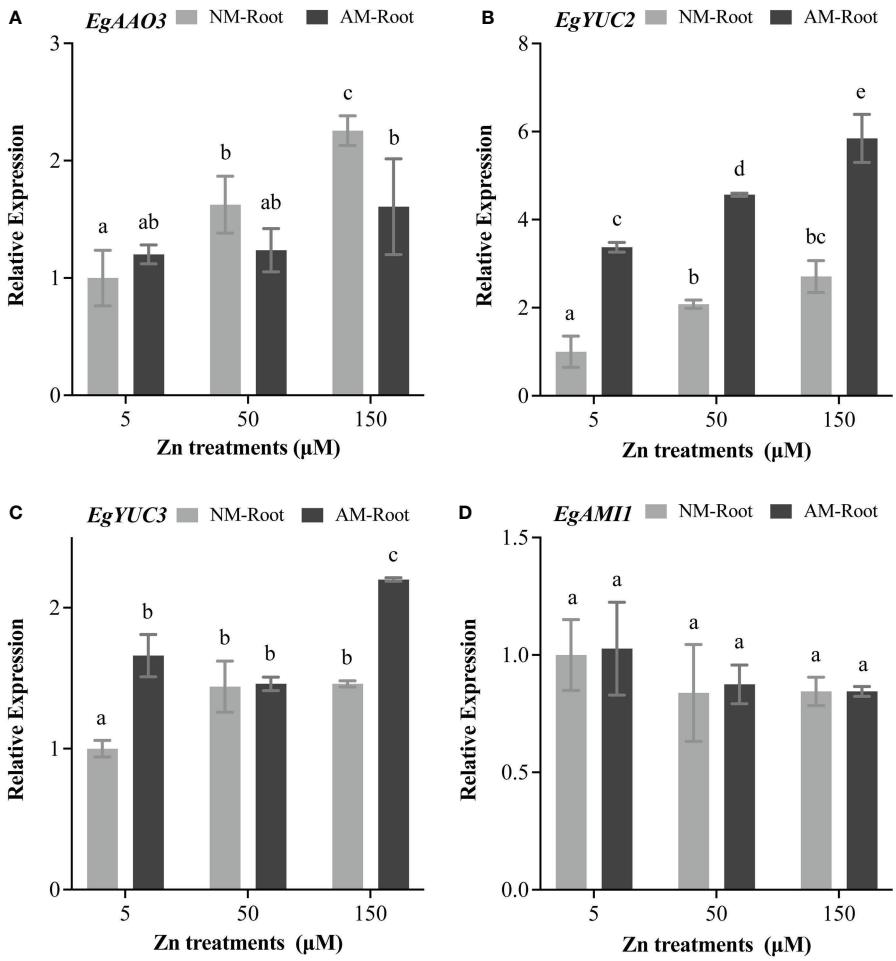

FIGURE 5
Expression profiles of auxin biosynthesis–related genes. The relative expression of *EgAAO3* **(A)**, *EgYUC2* **(B)**, *EgYUC3* **(C)**, and *EgAMI1* **(D)** was calculated by the $2^{-\Delta\Delta CT}$ method using the *EgUBI3* as a normalizer. For each gene, the expression level in NM roots with 5 μM Zn was defined as 1. NM-Root, the root of non-mycorrhizal plants; AM-Root, the root of mycorrhizal plants. Values were indicated as mean ± SE. Different letters on the histograms indicated significant differences ($P < 0.05$).

However, Cu content reduced in roots and Mn increased in shoots of *E. grandis* with a high level of Zn (Figure 2). Cross-talks between mineral nutrients involved with complicated mechanisms; therefore, multi-level interactions among nutrient elements needed further explore to better understand their availability.

AM fungi can improve shoot biomass and retain metals in roots to restrict their translocation to aerial parts under heavy metal stress (Huang et al., 2018; Janeeshma and Puthur, 2020; Riaz et al., 2021). In our study, more Zn was accumulated in AM roots; less Zn, therefore, was transferred to AM shoots (Figure 2). Moreover, AM fungal hyphal network functionally extended the root system of hosts, granting the hosts the ability to uptake mineral nutrients from enlarged soil volume to enhance the metal tolerance of hosts (Göhre and Paszkowski, 2006; Wang et al., 2017; Gómez-Gallego et al., 2022). For example, *Thlaspi praecox* grew in soils highly contaminated by Cd, Zn, and Pb, the concentrations of P, S, Ni, and Cu in both AM shoots and roots were found to be increased (Vogel-Mikuš et al., 2006). AM fungi improved the nutritional (P, N, Mg, and Fe) and water status, and stimulated proline biosynthesis of hosts, which enhanced the tolerance to Cd and Zn (Garg and Singh, 2018). In addition, concentrations of P, K, Mg, and Ca in mycorrhizal maize grown in Cu-contaminated soil were often higher than that in NM plants (Gómez-Gallego et al., 2022). Mycorrhiza significantly increased the concentrations of P, Mg, and Mn in *E. grandis* roots, as well as P, Fe, and Cu in shoots. However, Fe concentration in AM roots was lower than that in NM roots but higher in AM shoots than that in NM shoots (Figure 2), probably because the effect of Zn accumulation was dominant and stimulates Fe transporting from root to shoot.

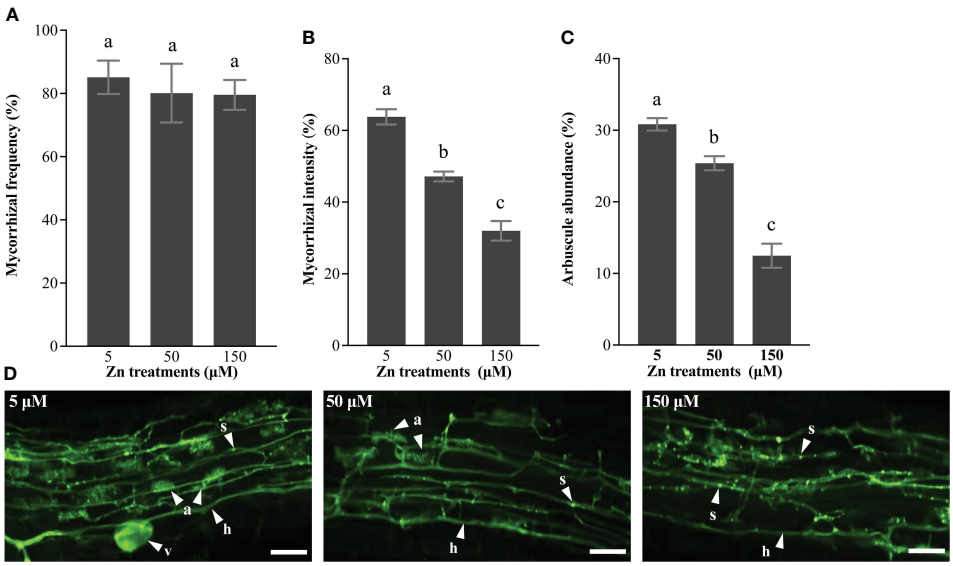

FIGURE 6
Mycorrhizal colonization. **(A)** Mycorrhizal frequency, **(B)** mycorrhizal intensity, and **(C)** arbuscule abundance were quantified using the MYCOCALC program. Values were indicated as mean ± SE. Different letters on the histograms indicated that the means significant differences ($P < 0.05$). **(D)** a, arbuscule; h, hyphae; v, vesicles; s, septa; bar, 50 μm.

To sum up, high Zn threatens plant growth by disturbing the homeostasis of nutrient elements, and AM fungi eases the stress to some extent.

Zn and mycorrhiza regulate the expression of *EgMTPs*

MTPs played vital roles in exporting excess metal ions into subcellular compartments or to extracellular space (Desbrosses-Fonrouge et al., 2005; Arrivault et al., 2006; Fujiwara et al., 2015; Migocka et al., 2018; Sinclair et al., 2018; Gao et al., 2020). Because MTPs of Mn-CDF cluster mostly transported Mn (Montanini et al., 2007), we analyzed the expression patterns of MTPs of Zn-CDF and Zn/Fe-CDF clusters. As showed in Figure 3, EgMTP1, EgMTP2, EgMTP3.1, EgMTP3.2, EgMTP4, EgMTP5, EgMTP12, and EgMTP7 of *E. grandis* had high similarity with MTPs of *A. thaliana*, *G. max*, *P. trichocarpa*, and *C. sinensis*, which implied that they shared comparable functions. Previous studies reported that AtMTP1 and AtMTP3 were vacuolar membrane transporters (Desbrosses-Fonrouge et al., 2005; Arrivault et al., 2006), and MTP1, MTP3, MTP4, and MTP7 of *G. max*, *P. trichocarpa*, and *C. sinensis* were also predicted to be located at vacuole (Fu et al., 2017; Gao et al., 2020; Haque et al., 2022). AtMTP5, AtMTP12, and CsMTP5 were localized at the Golgi compartment (Fujiwara et al., 2015; Migocka et al., 2018), whereas AtMTP2 and EgMTP6 were endoplasmic reticulum membrane proteins (Sinclair et al., 2018; Han et al., 2022). According to the grouping in the tree (Figure 3), we thus assumed that EgMTP1, EgMTP3.1, EgMTP3.2, EgMTP4, and EgMTP7 were located at vacuole; EgMTP2 and EgMTP6 were localized in the endoplasmic reticulum membrane; and EgMTP5 and EgMTP12 were membrane transporters of Golgi apparatus.

Desbrosses-Fonrouge et al. (2005) found that AtMTP1 acted to exclude excess Zn into vacuoles and driven Zn accumulation in young leaves. In this study, the expression of *EgMTP1* was suppressed in root but induced in NM shoot under Zn treatment (Figure 4); the expression pattern was similar with that of *PtrMTP1* (Gao et al., 2020). As Zn can enter plant cell non-specifically through plasma membrane transport proteins (Arrivault et al., 2006), the overaccumulated Zn in root suppressed the expression of *EgMTP1* and enhanced the transfer of Zn from root to shoot; then, excessive Zn in shoot upregulated the expression of *EgMTP1* to promote the storage of Zn in shoot vacuole. AtMTP3 mostly expressed in root and functioned in the immobilization of Zn in root vacuoles, restricting the movement of Zn from root into shoot (Arrivault et al., 2006). The expression of *EgMTP3.1* in NM shoot was reduced under Zn oversupply, indicating that EgMTP3.1 mediated Zn exclusion from shoot. Conversely, *EgMTP4* in NM shoot was induced under Zn oversupply (Figure 4). We speculated that EgMTP4 and MTP3 had difference physiological functions, and EgMTP4 promoted the Zn storage in shoot vacuoles. The expression level of *EgMTP7* was strongly intensified by Zn in NM shoot (Figure 4), a case similar with *PtMTP7* (Gao et al., 2020), suggesting that EgMTP7 transported Zn into shoot vacuole to remit the Zn toxicity.

AtMTP5 and AtMTP12 formed functional heterodimer to load Zn into Golgi, but the expression of *AtMTP12* was irrelevant to Zn concentration (Fujiwara et al., 2015). Similarly, the expression of *EgMTP12* in NM plants was not affected by Zn (Figure 4). In cucumber, CsMTP5 and CsMTP12 also functioned as a heterodimeric complex, which involved in transporting Zn into Golgi compartment, and the expression of *CsMTP5* was obviously upregulated with low-Zn treatment (Migocka et al., 2018). Conversely, a high level of Zn increased the expression of *EgMTP5* in both NM roots and shoots (Figure 4). Therefore, we propose that the heterodimeric complex EgMTP5-EgMTP12 functions to deliver excess Zn to Golgi compartment and is regulated by zinc at the level of *EgMTP5* transcription.

AtMTP2 contributed to the root-to-shoot Zn translocation through plasmodesmus (Sinclair et al., 2018). The high transcriptional level of *EgMTP2* in NM roots responded to excess Zn (Figure 4); therefore, more Zn was transferred to the shoot through symplast pathway. In addition, our previous study found that the expression of *EgMTP6* was irrelevant to Zn concentration, and heterologous expression of EgMTP6 in *zrc1*-mutant yeast enhanced the Zn tolerance of *zrc1Δ*, which cannot grow in high-Zn condition (Han et al., 2022). Thus, EgMTP6 mediated the sequestration of Zn to endoplasmic reticulum in the non-transcript level.

Recently, Gómez-Gallego et al. (2022) found an enhanced expression of the vacuolar membrane transporters *ZmHMA3a* and *ZmHMA4* in AM plants under Cu stress. Mycorrhiza promoted sequestering Cu into vacuole of root and shoot to reduce Cu translocation to aerial part by regulating the genes of Cu transporters (Gómez-Gallego et al., 2022). In *Astragalus sinicus*, mycorrhiza downregulated the expression of *AsZIP2* to reduce absorbing excessive Zn (Xie et al., 2021). It seems that mycorrhiza downregulates genes involved in metal uptake and upregulates genes related to exportation to protect host plant from metals toxicity. With Zn oversupply, mycorrhiza increased the expression of *EgMTP1* and *EgMTP7* in roots, as well as *EgMTP1* and *EgMTP5* in shoots, to facilitate the transport of excess Zn into vacuole and Golgi for plant detoxifying.

Zn and mycorrhiza affect the expression of auxin biosynthesis–related genes

In recent years, the alterations of auxin biosynthesis and transport induced by heavy metals stimuli had been intensively explored (Jiang et al., 2018; López-Ruiz et al., 2020; Angulo-Bejarano et al., 2021; Wang et al., 2021). For instance, toxic Cu, Al, Fe, and Ni disturbed auxin biosynthesis and distribution in root tips to inhibit root growth and development (Wu et al., 2014; Li et al., 2015; Song et al., 2017; Leškovï et al., 2020). Different from excess Se that decreased the auxin biosynthesis *via* reducing the expression of *YUCCA1* and *YUCCA3* in rice plants (Malheiros et al., 2019), excess Zn enhanced the expression of *EgAAO3*, *EgYUC2*, and *EgYUC3* (Figure 5). Previously, a comparative transcriptomic investigation indicated that 24-h treatment of 200 μM Zn significantly induced the expression of auxin biosynthesis genes (ATP SULFURYLASE ARABIDOPSIS1, SUPERROOT1, TRYPTOPHAN AMINOTRANSFERASE OF ARABIDOPSIS1, YUC2, YUC3, CYTOCHROME P450, and AAO3) (Zhang et al., 2018). On the other hand, Cu toxicity was found to inhibit auxin biosynthesis *via* reducing the expression of *TAA1* and *YUCCA* (Song et al., 2017). In contrast, transcriptomic analyses of auxin biosynthetic-related genes, including auxin amide synthase and tryptophan synthase, showed that Cu induced their expression (Zhao et al., 2009). The discrepancies in results might be related to differences in experimental exposure time and treatment approach. However, excess Zn promoted the expression of *AAO3*, *YUC2*, and *YUC3* in *E. grandis*.

AM fungi had a positive effect on the regulation of the auxin levels in plants under salt stress, drought, and biotic stress, and auxin concentration in mycorrhizal plants was higher than nonmycorrhizal plants (He et al., 2017; Liu et al., 2016; Chareesri et al., 2020). Moreover, the activity of synthetic auxin-inducible promoter DR5 increased in roots colonized by *R. irregularis*, mainly in cells containing arbuscules (Etemadi et al., 2014). Mycorrhiza is thus likely to promote auxin synthesis. Our results showed that *EgYUC2* and *EgYUC3* were upregulated in AM roots (Figure 5). Furthermore, the positive correlation between auxin content and arbuscule abundance suggested that maintaining cellular auxin homoeostasis was involved in finely tuning AM symbiosis (Hanlon and Coenen, 2011). The auxin content with denser AM fungi colonization was higher than those with sparser colonization in rice (Chareesri et al., 2020). According to this study, the arbuscule number at 150 μM Zn was significantly lower than at 5 μM and 50 μM Zn, but the expression of *EgYUC2* and *EgYUC3* was higher. The result reveals that, although Zn restrains the growth of mycorrhiza, it remarkably promotes the expression of auxin synthesis genes.

Conclusion

To sum up, we herein propose a mechanism of Zn detoxification in *E. grandis* (Figure 7): EgMTP1, EgMTP3.1, EgMTP3.2, EgMTP4, and EgMTP7 involve in sequestering Zn in vacuole; EgMTP2 and EgMTP6 mediate the Zn transport into endoplasmic reticulum; and EgMTP5 and EgMTP12 load Zn into Golgi. AM fungi inoculation enhances the expression of two putative tonoplast transporters (EgMTP1 and EgMTP7) and one Golgi transporter (EgMTP5) in *E. grandis* under Zn toxicity, indicating that mycorrhiza facilitates the transfer of Zn into vacuole and Golgi. In addition, mycorrhiza promotes mineral nutrient uptake to improve the growth of *E. grandis* and induces the expression of auxin biosynthesis–related genes to improve mycorrhizal colonization to enhance the Zn tolerance. The

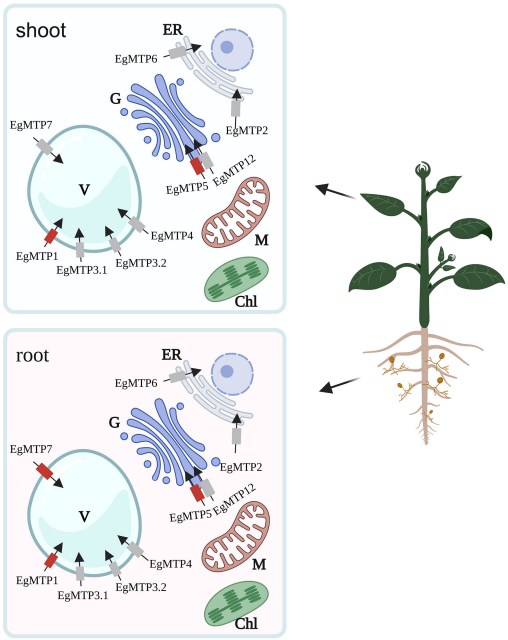

FIGURE 7
Schematic representation of the major changes induced by Zn in *EgMTP* expression in mycorrhizal and *E. grandis*. Red transporters, upregulated *EgMTPs* by mycorrhizal; ER, endoplasmic reticulum; V, vacuole; G, golgi; Chl, chloroplast; M, mitochondrion.

results will be valuable to the development of molecular markers for cultivar breeding of eucalyptus with a high Zn tolerance. Further functional investigations were required to better understand their role of EgMTPs to alleviate Zn toxicity.

Data availability statement

The raw data supporting the conclusions of this article will be made available by the authors, without undue reservation.

Author contributions

L-NH: Conceptualization, methodology, data analysis and curation, visualization, writing, and editing. S-JW, YR, and X-YW: Methodology and data analysis. X-AX and W-TH: Methodology. HC and MT: Conceptualization, editing, and funding acquisition. All authors contributed to the article and approved the submitted version.

Funding

This work was supported by the Key Projects of Guangzhou of Science and Technology Plan (grant no. 201904020022), the Laboratory of Lingnan Modern Agriculture Project (grant no. NZ2021025), and the National Natural Science Foundation of China (grant nos. 31800092 and 32071639).

Acknowledgments

We particularly thank Lei Duan of South China Botanical Garden, Chinese Academy of Sciences for refining the text.

Conflict of interest

The authors declare that the research was conducted in the absence of any commercial or financial relationships that could be construed as a potential conflict of interest.

Publisher's note

All claims expressed in this article are solely those of the authors and do not necessarily represent those of their affiliated organizations, or those of the publisher, the editors and the reviewers. Any product that may be evaluated in this article, or claim that may be made by its manufacturer, is not guaranteed or endorsed by the publisher.

Supplementary material

The Supplementary Material for this article can be found online at: https://www.frontiersin.org/articles/10.3389/fpls.2022.1022696/full#supplementary-material

References

Adams, F., Reddell, P., Webb, M. J., and Warren, S. A. (2006). Arbuscular mycorrhizas and ectomycorrhizas on *Eucalyptus grandis* (Myrtaceae) trees and seedlings in native forests of tropical north-eastern Australia. *Aust. J. Bot.* 54, 271–281. doi: 10.1071/BT05028

Angulo-Bejarano, P. I., Puente-Rivera, J., and Cruz-Ortega, R. (2021). Metal and metalloid toxicity in plants: an overview on molecular aspects. *Plants* 10 (4), 635. doi: 10.3390/plants10040635

Arrivault, S., Toralf, S., and Krämer, U. (2006). The arabidopsis metal tolerance protein AtMTP3 maintains metal homeostasis by mediating zn exclusion from the shoot under fe deficiency and zn oversupply. *Plant J.* 46, 861–879. doi: 10.1111/j.1365-313X.2006.02746

Bae, B., Park, H., and Kang, S. (2022). Quantitative estimation of synergistic toxicity of Cu and zn on growth of *Arabidopsis thaliana* by isobolographic method. *Toxics* 10 (4), 195. doi: 10.3390/toxics10040195

Bokor, B., Bokorová, S., Ondoš, S., Švubová, R., Lukačová, Z., Hýblová, M., et al. (2015). Ionome and expression level of Si transporter genes (*Lsi1*, *Lsi2*, and *Lsi6*) affected by zn and Si interaction in maize. *Environ. Sci. pollut. Res.* 22, 6800–6811. doi: 10.1007/s11356-014-3876-6

Bouain, N., Kisko, M., Rouached, A., Dauzat, M., Lacombe, B., Belgaroui, N., et al. (2014). Phosphate/zinc interaction analysis in two lettuce varieties reveals contrasting effects on biomass, photosynthesis, and dynamics of pi transport. *J. Biomed. Biotechnol.* 3), 548254. doi: 10.1155/2014/548254

Broadley, M. R., Philip, W. J., John, H. P., Ivan, Z., and Lux, A. (2007). Zinc in plants. *New Phytol.* 173, 677–702. doi: 10.1111/j.1469-8137.2007.01996

Brundrett, M. C., and Tedersoo, L. (2018). Evolutionary history of mycorrhizal symbioses and global host plant diversity. *New Phytol.* 220, 1108–1115. doi: 10.1111/nph.14976

Burleigh, S. H., Kristensen, B. K., and Bechmann, I. E. (2003). A plasma membrane zinc transporter from *Medicago truncatula* is up-regulated in roots by zn fertilization, yet down-regulated by arbuscular mycorrhizal colonization. *Plant Mol. Biol.* 52, 1077–1088. doi: 10.1023/A:1025479701246

Canton, G. C., Bertolazi, A. A., Cogo, A. J. D., Eutrópio, F. J., Melo, J., de Souza, S. B., et al. (2016). Biochemical and ecophysiological responses to manganese stress by ectomycorrhizal fungus *Pisolithus tinctorius* and in association with *Eucalyptus grandis*. *Mycorrhiza* 26, 475–487. doi: 10.1007/s00572-016-0686-3

Cardini, A., Pellegrino, E., White, P. J., Mazzolai, B., Mascherpa, M. C., and Ercoli, L. (2021). Transcriptional regulation of genes involved in zn transport after foliar zn application to *Medicago sativa*. *Plants* 10 (3), 476. doi: 10.3390/plants10030476

Chareesri, A., De Deyn, G. B., Sergeeva, L., Polthanee, A., and Kuyper, T. W. (2020). Increased arbuscular mycorrhizal fungal colonization reduces yield loss of rice (*Oryza sativa* l.) under drought. *Mycorrhiza* 30, 315–328. doi: 10.1007/s00572-020-00953-z

Charoenpakdee, S., Phosri, C., Dell, B., and Lumyong, S. (2010). The mycorrhizal status of indigenous arbuscular mycorrhizal fungi of physic nut (*Jatropha curcas*) in Thailand. *Mycosphere* 1 (2), 167–181.

Chen, C. J., Chen, H., Zhang, Y., Thomas, H. R., Frank, M. H., He, Y. H., et al. (2020). TBtools: an integrative toolkit developed for interactive analyses of big biological data. *Mol. Plant* 13, 1194–1202. doi: 10.1016/j.molp.2020.06.009

Chen, Y. L., Liu, S., and Dell, B. (2007). Mycorrhizal status of *Eucalyptus* plantations in south China and implications for management. *Mycorrhiza* 17, 527–535. doi: 10.1007/s00572-007-0125-6

Clemens, S., Palmgren, M., and Kraemer, U. (2002). A long way ahead: understanding and engineering plant metal accumulation. *Trends Plant Sci.* 7 (7), 309–315. doi: 10.1016/S1360-1385(02)02295-1

Desbrosses-Fonrouge, A. G., Voigt, K., Schröder, A., Arrivault, S., Thomine, S., and Krämer, U. (2005). *Arabidopsis thaliana* MTP1 is a zn transporter in the vacuolar membrane which mediates zn detoxification and drives leaf zn accumulation. *FEBS Lett.* 579, 4165–4174. doi: 10.1016/j.febslet.2005.06.046

Díaz, G., Azcón-Aguilar, C., and Honrubia, M. (1996). Influence of arbuscular mycorrhizae on heavy metal (Zn and Pb) uptake and growth of *Lygeum spartum* and *Anthyllis cytisoides*. *Plant Soil* 180, 241–249. doi: 10.1007/bf00015307

Ding, J. L., Liu, L., Wang, C., Shi, L., Xu, F. S., and Cai, H. M. (2021). High level of zinc triggers phosphorus starvation by inhibiting root-to-shoot translocation and preferential distribution of phosphorus in rice plants. *Environ. pollut.* 277, 116778. doi: 10.1016/j.envpol.2021.116778

Etemadi, M., Gutjahr, C., Couzigou, J. M., Zouine, M., Lauressergues, D., and Timmers, A. (2014). Auxin perception is required for arbuscule development in arbuscular mycorrhizal symbiosis. *Plant Physiol.* 166 (1), 281–292. doi: 10.1104/pp.114.246595

Fan, X. N., Zhou, X. Q., Chen, H., Tang, M., and Xie, X. A. (2021). Cross-talks between macro- and micronutrient uptake and signaling in plants. *Front. Plant Sci.* 122076. doi: 10.3389/fpls.2021.663477

Fernández-Fuego, D., Keunen, E., Cuypers, A., Bertrand, A., and González, A. (2017). Mycorrhization protects *Betula pubescens* ehr. from metal-induced oxidative stress increasing its tolerance to grow in an industrial polluted soil. *J. Hazard Mater.* 336, 119–127. doi: 10.1016/j.jhazmat.2017.04.065

Ferrol, N., and Tamayo, E. (2016). The heavy metal paradox in arbuscular mycorrhizas: from mechanisms to biotechnological applications. *J. Exp. Bot.* 67 (22), 6253–6265. doi: 10.1093/jxb/erw403

Fujiwara, T., Kawachi, M., Sato, Y., Mori, H., Kutsuna, N., and Hasezawa, S. (2015). A high molecular mass zinc transporter MTP12 forms a functional heteromeric complex with MTP5 in the golgi in *Arabidopsis thaliana*. *FEBS J.* 282, 1965–1979. doi: 10.1111/febs.13252

Fu, X. Z., Tong, Y. H., Zhou, X., Ling, L. L., Chun, C. P., Cao, L., et al. (2017). Genome-wide identification of sweet orange (*Citrus sinensis*) metal tolerance proteins and analysis of their expression patterns under zinc, manganese, copper, and cadmium toxicity. *Gene* 629, 1–8. doi: 10.1016/j.gene.2017.07.072

Gao, Y. F., Yang, F. M., Liu, J. K., Xie, W., Zhang, L., Chen, Z. H., et al. (2020). Genome-wide identification of metal tolerance protein genes in *Populus trichocarpa* and their roles in response to various heavy metal stresses. *Int. J. Mol. Sci.* 21 (5), 1680. doi: 10.3390/ijms21051680

Garg, N., and Singh, S. (2018). Arbuscular mycorrhiza *Rhizophagus irregularis* and silicon modulateg growth, proline biosynthesis and yield in *Cajanus cajan* l. millsp. (pigeonpea) genotypes under cadmium and zinc stress. *J. Plant Growth Regul.* 37, 46–63. doi: 10.1007/s00344-017-9708-4

Göhre, V., and Paszkowski, U. (2006). Contribution of the arbuscular mycorrhizal symbiosis to heavy metal phytoremediation. *Planta* 223 (6), 1115–1122. doi: 10.1007/s00425-006-0225-0

Gómez-Gallego, T., Valderas, A., van Tuinen, D., and Ferrol, N. (2022). Impact of arbuscular mycorrhiza on maize P1B-ATPases gene expression and ionome in copper-contaminated soils. *Ecotoxicol. Environ. Saf.* 234, 113390. doi: 10.1016/j.ecoenv.2022.113390

Gustin, J. L., Zanis, M. J., and Salt., D. E. (2011). Structure and evolution of the plant cation diffusion facilitator family of ion transporters. *BMC Evol. Biol.* 11, 76. doi: 10.1186/1471-2148-11-76

Hanlon, M. T., and Coenen, C. (2011). Genetic evidence for auxin involvement in arbuscular mycorrhiza initiation. *New Phytol.* 189, 701–709. doi: 10.1111/j.1469-8137.2010.03567.x

Han, L. N., Xie, X. A., Chen, H., and Tang, M. (2022). Molecular characteristics and function analyses of EgMTP6 in *Eucalyptus grandis*. *Scienta sylvae sinicae* 5 (58), 93–101. doi: 10.11707/j.1001-7488.20220500

Haque, M., Rahman, A., Urmi, D., Rahman, M., Elseehy, M. M., El-shehawi, A. M., et al. (2022). Changes in physiological responses and MTP (metal tolerance protein) transcripts in soybean (*Glycine max*) exposed to differential iron availability. *Plant Physiol. Biochem.* 179, 1–9. doi: 10.1016/j.plaphy.2022.03.007

Haydon, M. J., and Cobbett, C. S. (2007). A novel major facilitator superfamily protein at the tonoplast influences zinc tolerance and accumulation in *Arabidopsis*. *Plant Physiol.* 143 (4), 1705–1719. doi: 10.1104/pp.106.092015

He, L., Li, C., and Liu, R. (2017). Indirect interactions between arbuscular mycorrhizal fungi and *Spodoptera exigua* alter photosynthesis and plant endogenous hormones. *Mycorrhiza* 27 (6), 525–535. doi: 10.1007/s00572-017-0771-2

Hewitt, E. J. (1966). Sand and water culture methods used in the study of plant nutrition. *Commonwealth Agric. Bureaux* (UK) 547.

Huang, X., Wang, L., Zhu, S., Ho, S. H., Wu, J., Kalita, P. K., et al. (2018). Unraveling the effects of arbuscular mycorrhizal fungus on uptake, translocation, and distribution of cadmium in *Phragmites australis* (Cav.) trin. ex steud. *Ecotoxicol. Environ. Saf.* 149, 43–50. doi: 10.1016/j.ecoenv.2017.11.011

Janeeshma, E., and Puthur, J. T. (2020). Direct and indirect influence of arbuscular mycorrhizae on enhancing metal tolerance of plants. *Arch. Microbiol.* 202 (1), 1–16. doi: 10.1007/s00203-019-01730-z

Jiang, J., Rodriguez-Furlan, C., Wang, J. Z., de Souza, A., Ke, H., Pasternak, T., et al. (2018). Interplay of the two ancient metabolites auxin and MEcPP regulates adaptive growth. *Nat. Commun.* 9, 1. doi: 10.1038/s41467-018-04708-5

Kaur, H., and Garg, N. (2021). Zinc toxicity in plants: a review. *Planta* 253, 129. doi: 10.1007/s00425-021-03642-z

Kumar, S., Kumar, S., and Mohapatra, T. (2021). Interaction between macro- and micro-nutrients in plants. *Front. Plant Sci.* 12. doi: 10.3389/fpls.2021.665583

Leskova, A., Giehl, R. F. H., Hartmann, A., Fargasova, A., and von Wiren, N. (2017). Heavy metal induces iron deficiency responses at different hierarchic and regulatory levels. *Plant Physiol.* 174, 1648–1668. doi: 10.1104/pp.16.01916

Lešković, A., Zvarï, K. M., Araya, T., and Giehl, R. F. H. (2020). Nickel toxicity targets cell wall related processes and pin2-mediated auxin transport to inhibit root elongation and gravitropic responses in *Arabidopsis*. *Plant Cell Physiol.* 61 (3), 519–535. doi: 10.1093/pcp/pcz217

Li, G., Song, H., Li, B., Kronzucker, H. J., and Shi, W. (2015). Auxin Resistant1 and PINFORMED2 protect lateral root formation in *Arabidopsis* under iron stress. *Plant Physiol.* 169 (4), 2608–2623. doi: 10.1104/pp.15.00904

Liu, H. G., Wang, Y. J., Hart, M., Chen, H., and Tang, M. (2016). Arbuscular mycorrhizal symbiosis regulates hormone and osmotic equilibrium of *Lycium barbarum* l. under salt stress. *Mycosphere* 7 (6), 828–843. doi: 10.5943/mycosphere/7/6/14

Livak, K. J., and Schmittgen, T. D. (2001). Analysis of relative gene expression data using real-time quantitative PCR and the $2^{-\Delta\Delta CT}$ method. *Methods* 25, 402–408. doi: 10.1006/meth.2001.1262

Li, S., Zhou, X., Huang, Y., Zhu, L., Zhang, S., Zhao, Y., et al. (2013). Identification and characterization of the zinc-regulated transporters, iron-regulated transporter-like protein (ZIP) gene family in maize. *BMC Plant Biol.* 13, 114. doi: 10.1186/1471-2229-13-114

López-Ruiz, B. A., Zluhan-Martínez, E., Sanchez, M. P., Alvarez-Buylla, E. R., and GarayArroyo, A. (2020). Interplay between hormones and several abiotic stress

conditions on *Arabidopsis thaliana* primary root development. *Cells* 9 (12), 2576. doi: 10.3390/cells9122576

Maiti, S. K., and Rana, V. (2017). Assessment of heavy metals contamination in reclaimed mine soil and their accumulation and distribution in *Eucalyptus* hybrid. *Bull. Environ. Contam. Toxicol.* 98, 97–104. doi: 10.1007/s00128-016-1966-5

Malheiros, R. S., Costa, L. C., Avila, R. T., Pimenta, T. M., Teixeira, L. S., Brito, F. A., et al. (2019). Selenium downregulates auxin and ethylene biosynthesis in rice seedlings to modify primary metabolism and root architecture. *Planta* 250, 333–345. doi: 10.1007/s00425-019-03175-6

Maret, W. (2009). Molecular mspects of human cellular zinc homeostasis: redox control of zinc potentials and zinc signals. *Biometals* 22, 149–157. doi: 10.1007/s10534-008-9186-z

Migocka, M., Małas, K., Maciaszczyk-Dziubinska, E., Posyniak, E., Migdal, I., and Szczech, P. (2018). Cucumber golgi protein CsMTP5 forms a zn-transporting heterodimer with high molecular mass protein CsMTP12. *Plant Sci.* 277, 196–206. doi: 10.1016/j.plantsci.2018.09.011

Montanini, B., Blaudez, D., Jeandroz, S., Sanders, D., and Chalot, M. (2007). Phylogenetic and functional analysis of the cation diffusion facilitator (CDF) family: improved signature and prediction of substrate specificity. *BMC Genomics* 8, 107. doi: 10.1186/1471-2164-8-107

Myburg, A. A., Grattapaglia, D., Tuskan, G. A., Hellsten, U., Hayes, R. D., Grimwood, J., et al. (2014). The genome of *Eucalyptus grandis*. *Nature* 510, 356–362. doi: 10.1038/nature13308

Neeraja, C. N., Kulkarni, K. S., Babu, P. M., Rao, D. S., Surekha, K., and Babu, V. R. (2018). Transporter genes identified in landraces associated with high zinc in polished rice through panicle transcriptome for biofortification. *PloS One* 13 (2), e0192362. doi: 10.1371/journal.pone.0192362

Nuria, F., Tamayo, E., and Vargas, P. (2016). The heavy metal paradox in arbuscular mycorrhizas: from mechanisms to biotechnological applications. *J. Exp. Bot.* 67, 6253–6265. doi: 10.1093/jxb/erw403

Qi, D. Z., Wang, L. M., Liang, M. X., Zhang, Q., Tang, X. L., Geng, B., et al. (2022). Genome-wide analyses of metal tolerance protein genes in apple (*Malus domestica*): Identification, characterization, expression and response to various metal ion stresses. *Environ. Exp. Bot.* 201, 104948. doi: 10.1016/j.envexpbot.2022.104948

Riaz, M., Kamran, M., Fang, Y. Z., Wang, Q. Q., Cao, H. Y., Yang, G. L., et al. (2021). Arbuscular mycorrhizal fungi-induced mitigation of heavy metal phytotoxicity in metal contaminated soils: A critical review. *J. Hazard Mater.* 402, 123919. doi: 10.1016/j.jhazmat.2020.123919

Sinclair, S. A., and Krämer, U. (2012). The zinc homeostasis network of land plants. *BBA-Mol. Cell Res.* 1823, 1553–1567. doi: 10.1016/j.bbamcr.2012.05.016

Sinclair, S. A., Senger, T., Talke, I. N., Cobbett, C. S., Haydon, M. J., and Krämer, U. (2018). Systemic upregulation of MTP2- and HMA2-mediated zn partitioning to the shoot supplements local zn deficiency responses. *Plant Cell* 30 (10), 2463–2479. doi: 10.1105/tpc.18.00207

Singh, N. V., Saminathan, T., Chandra, R., Awachare, C., Babu, D. K., Mundewadikar, D. M., et al. (2015). RNA Isolation from high polyphenol containing tissues of pomegranate. *Indian J. Hortic.* 72 (2), 273–277. doi: 10.5958/0974-0112.2015.00051.1

Song, Y., Zhou, L., Yang, S., Wang, C., Zhang, T., and Wang, J. (2017). Dose-dependent sensitivity of *Arabidopsis thaliana* seedling root to copper is regulated by auxin homeostasis. *Environ. Exp. Bot.* 139, 23–30. doi: 10.1016/j.envexpbot.2017.04.003

Stephens, B. W., Cook, D. R., and Grusa, M. A. (2011). Characterization of zinc transport by divalent metal transporters of the ZIP family from the model legume *Medicago truncatula*. *Biometals* 24, 51–58. doi: 10.1007/s10534-010-9373-6

Tedersoo, L., Bahram, M., and Zobel, M. (2020). How mycorrhizal associations drive plant population and community. *Science* 367 (6480), eaba1223. doi: 10.1126/science.aba1223

Vassilev, A., Nikolova, A., Koleva, L., and Lidon, F. (2011). Effects of excess zn on growth and photosynthetic performance of young bean plants. *J. Phytol.* 3 (6), 58–62. doi: 10.1111/plb.13307

Vogel-Mikuš, K., Pongrac, P., Kump, P., Nečemer, M., and Regvar, M. (2006). Colonisation of a zn, cd and Pb hyperaccumulator *Thlaspi praecox* wulfen with indigenous arbuscular mycorrhizal fungal mixture induces changes in heavy metal and nutrient uptake. *Environ. pollut.* 139, 362–371. doi: 10.1016/j.envpol.2005.05.005

Wang, X. Y., Liang, J. W., Liu, Z. Y., Kuang, Y. X., Han, L. N., Chen, H., et al. (2022). Transcriptional regulation of metal metabolism- and nutrient absorption-related genes in *Eucalyptus grandis* by arbuscular mycorrhizal fungi at different zinc concentrations. *BMC Plant Biol.* 22, 76. doi: 10.1186/s12870-022-03456-5

Wang, J. H., Moeen-ud-din, M., and Yang, S. H. (2021). Dose-dependent responses of *Arabidopsis thaliana* to zinc are mediated by auxin homeostasis and transport. *Environ. Exp. Bot.* 189, 104554. doi: 10.1016/j.envexpbot.2021.104554

Wang, W. X., Shi, J. C., Xie, Q. J., Jiang, Y. N., Yu, N., and Wang, E. T. (2017). Nutrient exchange and regulation in arbuscular mycorrhizal symbiosis. *Mol. Plant* 10, 1147–1158. doi: 10.1016/j.molp.2017.07.012

Wang, C., Song, H. Z., Pei, F. W., Hou, J., Wen, J. Z., Li, W., et al. (2009). The effect of excess zn on mineral nutrition and antioxidative response in rapeseed seedlings. *Chemosphere* 75 (11), 1468–1476. doi: 10.1016/j.chemosphere.2009.02.033

Wang, Y., Zhang, W. Z., Liu, W. K., Ahammed, G. J., Wen, W. X., Guo, S. R., et al. (2021). Auxin is involved in arbuscular mycorrhizal fungi-promoted tomato growth and *NADP-malic enzymes* expression in continuous cropping substrates. *BMC Plant Biol.* 21, 48. doi: 10.1186/s12870-020-02817-2

Wu, D., Shen, H., Yokawa, K., and Baluska, F. (2014). Alleviation of aluminium-induced cell rigidity by overexpression of OsPIN2 in rice roots. *J. Exp. Bot.* 65 (18), 5305–5315. doi: 10.1093/jxb/eru292

Xie, X. A., Fan, X. N., Chen, H., and Tang, M. (2021). Phosphorus starvation-and zinc excess-induced *Astragalus sinicus* Aszip2 zinc transporter is suppressed by arbuscular mycorrhizal symbiosis. *J. Fungi* 7, 829. doi: 10.3390/jof7110892

Xie, X. A., Hu, W. T., Fan, X. N., Chen, H., and Tang, M. (2019). Interactions between phosphorus, zinc, and iron homeostasis in nonmycorrhizal and mycorrhizal plants. *Front. Plant Sci.* 10. doi: 10.3389/fpls.2019.01172

Xie, X. A., Lai, W. Z., Che, X. R., Wang, S. J., Ren, Y., Hu, W. T., et al. (2022). A SPX domain-containing phosphate transporter from *Rhizophagus irregularis* handles phosphate homeostasis at symbiotic interface of arbuscular mycorrhizas. *New Phytol.* 234 (2), 650–671. doi: 10.1111/nph.17973

Xie, K., Ren, Y., Chen, A. Q., Yang, C. F., Zheng, Q. S., Chen, J., et al. (2021). Plant nitrogen nutrition: The roles of arbuscular mycorrhizal fungi. *J. Plant Physiol.* 269, 153591. doi: 10.1016/j.jplph.2021.153591

Yang, Y. R., He, C. J., Huang, L., Ban, Y. H., and Tang, M. (2017). The effects of arbuscular mycorrhizal fungi on glomalin-related soil protein distribution, aggregate stability and their relationships with soil properties at different soil depths in lead-zinc contaminated area. *PloS One* 12 (8), e0182264. doi: 10.1371/journal.pone.0182264

Zhang, P., Sun, L. L., Qin, J., Wan, J. P., Wang, R. L., Li, S., et al. (2018). cGMP is involved in zn tolerance through the modulation of auxin redistribution in root tips. *Environ. Exp. Bot.* 147, 22–30. doi: 10.1016/j.envexpbot.2017.10.025

Zhao, C. R., Ikka, T., Sawaki, Y., Kobayashi, Y., Suzuki, Y., Hibino, T., et al. (2009). Comparative transcriptomic characterization of aluminum, sodium chloride, cadmium and copper rhizotoxicities in *Arabidopsis thaliana*. *BMC Plant Biol.* 9 (1), 1–15. doi: 10.1186/1471-2229-9-32

frontiers | Frontiers in Plant Science

TYPE Original Research
PUBLISHED 07 November 2022
DOI 10.3389/fpls.2022.1036254

Check for updates

OPEN ACCESS

EDITED BY
Diaa Abd El Moneim,
Arish University, Egypt

REVIEWED BY
Mohammed Ali Abd Elhammed Abd Allah,
Desert Research Center, Egypt
Deepak Kumar,
Banaras Hindu University, India

*CORRESPONDENCE
Jianbo Zhu
shzu_zhujianbo@yeah.net
Jin Li
lijin@shzu.edu.cn

†These authors have contributed equally to this work

SPECIALTY SECTION
This article was submitted to Plant Abiotic Stress, a section of the journal Frontiers in Plant Science

RECEIVED 04 September 2022
ACCEPTED 07 October 2022
PUBLISHED 07 November 2022

CITATION
Liu X, Li A, Wang S, Lan C, Wang Y, Li J and Zhu J (2022) Overexpression of *Pyrus sinkiangensis* HAT5 enhances drought and salt tolerance, and low-temperature sensitivity in transgenic tomato.
Front. Plant Sci. 13:1036254.
doi: 10.3389/fpls.2022.1036254

COPYRIGHT
© 2022 Liu, Li, Wang, Lan, Wang, Li and Zhu. This is an open-access article distributed under the terms of the Creative Commons Attribution License (CC BY). The use, distribution or reproduction in other forums is permitted, provided the original author(s) and the copyright owner(s) are credited and that the original publication in this journal is cited, in accordance with accepted academic practice. No use, distribution or reproduction is permitted which does not comply with these terms.

Overexpression of *Pyrus sinkiangensis* HAT5 enhances drought and salt tolerance, and low-temperature sensitivity in transgenic tomato

Xiaoyan Liu†, Aowei Li†, Saisai Wang, Chengfang Lan, Yize Wang, Jin Li* and Jianbo Zhu*

Key Laboratory of Agricultural Biotechnology, College of Life Sciences, Shihezi University, Shihezi, China

The homeodomain-leucine zipper protein HAT belongs to the homeodomain leucine zipper subfamily (HD-Zip) and is important for regulating plant growth and development and stress tolerance. To investigate the role of *HAT5* in tolerance to drought, salt, and low temperature stress, we selected a *HAT* gene from *Pyrus sinkiangensis Yü (Pyrus sinkiangensis* T.T. Yu). The sequences were analyzed using ioinformatics, and the overexpressed tomato lines were obtained using molecular biology techniques. The phenotypes, physiological, and biochemical indexes of the wild-type and transgenic tomato lines were observed under different stress conditions. We found that the gene had the highest homology with *PbrHAT5*. Under drought and NaCl stress, osmotic regulatory substances (especially proline) were significantly accumulated, and antioxidant enzyme activities were enhanced. The malondialdehyde level and relative electrical conductivity of transgenic tomatoes under low temperature (freezing) stress were significantly higher than those of wild-type tomatoes. The reactive oxygen species scavenging system was unbalanced. This study found that *PsHAT5* improved the tolerance of tomatoes to drought and salt stress by regulating proline metabolism and oxidative stress ability, reducing the production of reactive oxygen species, and maintaining normal cell metabolism. In conclusion, the *PsHAT5* transcription factor has great potential in crop resistance breeding, which lays a theoretical foundation for future excavation of effective resistance genes of the HD-Zip family and experimental field studies.

KEYWORDS

HD-ZIP, transcription factor, *Agrobacterium*-mediated method, tolerance, transgenic tomato

Introduction

Global warming is a well-known phenomenon; extreme weather changes cause irreversible damage to plant growth. When plants are subjected to abiotic stresses, such as drought, salinity, and low temperature, the germination cycle of seeds will be changed (Huang et al., 2018), reactive oxygen species will be accumulated in large quantities, and the normal metabolic balance will be upset (Girousse et al., 2018; Lodeyro et al., 2021). These will affect normal crop growth and development, and the resulting reduced crop yields and changed crop quality (DaMatta et al., 2018; Rotundo et al., 2019) pose a serious threat to food security and wood supply (Shao et al., 2022). Therefore, over a long evolution, plants have developed complex regulatory mechanisms to defend against habitat changes, with transcription factors being important regulatory factors. Transcription factors play a crucial role in the transcriptional regulation of genes (Wani et al., 2021). They participate in defense responses by interacting with Cis-regulatory elements (CREs) in the promoter regions of various biotic and abiotic stress-responsive genes (Liu et al., 1999), regulating the expression of downstream adversity stress-responsive target genes at the transcriptional level, and prompting plants to regulate at molecular, physiological, and biochemical levels to adapt with various stresses (Toledo-Ortiz et al., 2003; Ma et al., 2022).

Homeodomain leucine zipper (HD-Zip) is a plant-specific transcription factor encoding an HD-Zip protein, which contains a highly conserved HD and a leucine zipper domain (LZ) (Elhiti and Stasolla, 2009). HD motifs can bind DNA specifically, and Zip acts as a dimerization conserved sequence element (Yang et al., 2022). HD-Zip proteins are divided into four subfamilies (I–IV) (Agalou et al., 2008). An increasing number of studies have shown that HD-Zip transcription factors are involved in a wide range of plant life processes, including cell differentiation, growth and development, morphogenesis, and biotic and abiotic stress response (Belamkar et al., 2014; Gong et al., 2019; Sharif et al., 2021).

Vollbrecht et al. (1991) identified the first *HB* genes in plants and isolated them from maize. Subsequently, many *HB* genes were identified and isolated from monocots and dicots. *AtHB12* and *AtHB7* are a pair of paralogous homologs of the HD-Zip I subfamily, both of which can respond to ABA and drought stress (Olsson et al., 2004; Ré et al., 2014). Ectopic expression of *AtHB12* revealed that the transgenic yeast cells showed enhanced tolerance to NaCl, which led to the speculation that *AtHB12* might be involved in NaCl stress response in plants (Shin et al., 2004). The expression level of the *Zmhdz10* gene, a member of the HD-Zip I family, was strongly induced by exogenous ABA and salt stress, and maize lines exhibited stronger drought and salt stress tolerance than wild types (Zhao et al., 2014). The *MtHB1* gene is a member of the HD-Zip I family in alfalfa and is strongly induced by salt stress. The *MtHB1* gene could indirectly inhibit the formation of lateral roots and reduce the degree of damage to the plant by the external environment (Ariel et al., 2010).

The *GmHAT5* gene, a member of the HD-Zip I family in soybean, was greatly elevated by salt stress, and the overexpression of *GmHAT5* significantly enhanced the salt tolerance of *Centella asiatica* (Belamkar et al., 2014; Cao et al., 2016). HD-Zip I transcription factor *MdHB7-like* improves salt tolerance in *Malus domestica* (Zhao et al., 2021). *PsHDZ63* enhances salt stress tolerance in *Populus tremuloides* by combining effective stress elements with transgenic lines to improve reactive oxygen species scavenging capacity (Guo et al., 2021). *AtHB6* may act downstream of the signal transduction pathway in ABI1 and ABI2, mediating drought stress responses (Söderman et al., 1999; Himmelbach et al., 2002). Chickpea (*Cicer arietinum* Linn.) WRKY70 regulates the expression of transcription factor *CaHDZ12*, which confers abiotic stress tolerance to transgenic tobacco to enhance drought and salt tolerance (Sen et al., 2017). *GhHB12*, a cotton stress-responsive HD-Zip transcription factor, negatively regulates cotton resistance by repressing jasmonic acid-response genes (He et al., 2018). The homologous structural domain LZ ranscription factors *HaHB1* and *AtHB13* enhance tolerance to drought and salinity stresses by inducing proteins that stabilize the cell membrane (Cabello et al., 2012; Cabello and Chan, 2012).

Overexpression of the *CaHB12* transcription factor in cotton (*Gossypium hirsutum*) improves drought tolerance (Basso et al., 2021). Sunflower *Hahb-4* is a novel component of the ethylene signaling pathway and induces a significant delay in senescence (Dezar et al., 2005; Manavella et al., 2006). In summary, HD-Zip family genes are widely involved in regulating various growth and developmental processes and abiotic stress responses in plants. HD-Zip genes play an important regulatory role in drought and salt resistance, indicating that this family of genes has great potential to be used in developing new varieties of stress-resistant crops. Strangely, there is almost no information about this HD-Zip family gene in *P. sinkiangensis*, and functional studies are even less available.

Processed tomato (*Solanum Lycopersicum* L.) is an annual or perennial herb in the Solanaceae family and is a warm-loving vegetable. Originally from South America, tomatoes are grown in many parts of the world (Hanssen and Lapidot, 2012); they were rapidly developed in China in the early 1950s, becoming one of the major fruit vegetables. However, global warming has become an unavoidably hot issue and challenge for the international community (Sultan et al., 2019; Sun et al., 2019). Extreme environmental changes have seriously affected crop yield and quality and hindered the potential of agricultural production (Fatima et al., 2020; Epule et al., 2021; Laudien et al., 2022). Therefore, practical guidance is important for

improving the resilience of processed tomatoes to adapt with extreme weather changes, which is an urgent issue for agricultural development.

Recent experimental results have shown that HD-Zip genes play important regulatory functions in processes such as drought and salt resistance in crops, which predicts that this family of genes has great potential for application in breeding new varieties of stress-resistant crops (Ariel et al., 2010; Cabello et al., 2017; Zhao et al., 2017). Most HD-Zip-related gene studies have focused on the model plant *Arabidopsis thaliana*. However, *PsHAT5*, a transcription factor of the HD-Zip family, has been little studied. Therefore, in this study, the *PsHAT5* transcription factor encoding the HAT5 protein was cloned from *P. sinkiangensis*. The gene sequence was analyzed using bioinformatics to construct a plant overexpression vector and expression pattern. The transgenic tomato lines were obtained through the *Agrobacterium*-mediated infestation method, and the role of transgenic tomatoes in abiotic stress response (drought, low temperature, and salt) was investigated. This study generated a new series of drought-and salt-tolerant tomato plants. It provided some insights into the molecular regulatory mechanisms of drought and salt tolerance in tomatoes.

Materials and methods

Experimental materials and growth conditions

The P. sinkiangensis used in this study were nursed by the pear variety resource preservation garden of the Institute of Agricultural Science, Second Agricultural Division, Kulle, Xinjiang Uygur Autonomous Region (41°49'34.621" N and 86° 12'2.317"E). "Yaxin 87-5" wild-type tomato seeds Provided by Yaxin Seed Co. Ltd, (Shihezi, China). Wild-type tomato seeds were Sterilized with 10% NaClO for 10 min and then sown on 1/2 MS medium. After 3 days of dark culture and 4 days of light culture, they were grown to obtain sterile seedlings. The hypocotyls of the seedlings were cut, about 1.0 cm long, and cultured in the dark for 2 days in the pre-culture medium. *Agrobacterium tumefaciens* (OD 0.6–0.8) was suspended in MS liquid medium to prepare a recombinant bacterial solution. The pre-cultured tomato stem segments were infested with bacterial fluid for 15 min. Then the bacterial solution on the surface of the explants was sucked dry with filter paper and transferred to a co-culture medium. After 2 days of co-culture, the transformed tomato stem segment callus was transferred sequentially to the screening medium containing 100 mg/mL kanamycin (kan) for about 60 days. After differentiation, the seedlings were transferred to the rooting medium, and the roots were formed after 30 days of induction. Then, they were transplanted into pots after domestication for normal cultivation management. The volume ratio of cultivated soil, peat, vermiculite, and perlite used was 3:1:2. The culture conditions were: 25–28 °C, relative humidity 65–70%, light intensity 8000 lx, light/dark period 16/8 h. MS medium, Sucrose, and Agar strips were purchased from Shenggong Bioengineering Co. Ltd. (Shanghai, China). The medium used in the plant tissue culture process and the regeneration process of the intact plant are both found in the supplementary material (Supplementary Figures S1-5).

Bioinformatics analysis of *PsHAT5* transcription factor

Sequence analysis was done at NCBI (http://www.ncbi.nlm.nih.gov/) and DNAMAN. Multiple comparisons were performed with ClustalW, a phylogenetic tree of *PsHAT5* gene was constructed using MEGA 7.0 with NJ (Neighbor-Joining) method.

Cloning of *PsHAT5* transcription factor and construction of plant overexpression vector

Total RNA was extracted from the bast *P. sinkiangensis* using RNAisoPlus kit (TaKaRa) containing on-column DNase I according to the manufacturer's instructions. First-strand cDNA was synthesized from the total RNA using oligo (dT) primers and PrimeScript®RTase (TaKaRa). The sequence of white pear (*Pyrus×bretschneideri*) PbHAT5 protein (GenBank accession number: XP_009369353.1) published on the NCBI website was used to finally obtain the *PsHAT5* sequence of *P. sinkiangensis* after comparing with the genome database of *P. sinkiangensis* (unpublished) in our laboratory. Based on the sequence information of *PsHAT5*, specific primers were designed using Premier 5.0 software (Supplementary Table S1), and PCR amplification of *PsHAT5* transcription factor was performed using cDNA as template. The PCR amplification procedure was: 95°C for 5 min; 95°C for the 30 s, 60°C for 30 s, 72°C for 1 min for 30 s, 35 cycles; And finally, 72°C for 10 min. The purified PCR product was ligated to the pMD®19-T Vector and the ligated product was transformed into E. coli DH5-Alpha competent cells. The correctly sequenced T-PsHAT5 recombinant plasmid was inserted into the plant expression vector pCAMBIA2300 by double digestion to construct the pCAMBIA2300-PsHAT5 overexpression vector. After verified by digestion and sequencing, the recombinant plasmid was transferred into *Agrobacterium tumefaciens* GV3101 using the electroshock method for genetic transformation of tomato, Finally, the plant overexpression vector carrying *PsHAT5* transcription factor was constructed.

Acquisition and identification of transgenic tomatoes

To obtain transgenic tomato plants, wild-type tomato plants were transformed with a plasmid containing PsHAT5 by an *Agrobacterium*-mediated method. The specific methods are described in the "2.1 Experimental materials and growth conditions" section. First, we extracted DNA from the leaves of wild-type tomatoes and transformed tomato plants using the CTAB method, and used the leaf DNA of wild-type tomato plants as a negative control and the recombinant plasmid as a positive control for their PCR identification. Secondly, we used EasyPure Plant RNA Extraction Kit (Transgen Biotech, China) to extract total tomato RNA by referring to the operating instructions of the kit. First-strand cDNA was generated from RNA by using a reverse transcription system (Takara Biotechnology, Kusamatsu, Japan). The expression levels of *PsHAT5* transcription factors were determined by qPCR in 10 μL reactions using the Roche LightCycle® 480 System (Salt Lake City, UT, USA) and SYBR Green Real-Time PCR Master Mix (KAPA Biosystems, Wilmington, DE, USA). Contain 5 μL 2× SYBR Green Real MasterMix (SYBR Green, Applied Biosystems), 0.5 μL cDNA, 0.5 μL each of upstream and downstream primers for *PsHAT5* transcription factor (Table S1), and the rest was made up to 10 μL with ddH_2O. The amplification procedures were as follows: 95°C for 5 min, 95°C for the 30 s, 60°C for 30 s, 72°C for 30 s, 25 cycles; Finally, 72°C for 10 min, Using GAPDH as an internal reference. We selected T0 generation tomatoes for PCR identification and T1 tomatoes for qPCR identification (146bp), and through analysis, we selected two independent T2 generation homozygous strains (OE-2, and OE-4) for subsequent experiments.

Evaluation of stress tolerance

We selected 4-week-old wild-type and transgenic tomatoes of uniform size and good growth status from the same period and subjected them to drought and low temperature as well as salt stress treatments. Drought stress was performed as follows: Wild-type and transgenic tomatoes were watered fully and no longer watered during the period of continuous drought. Samples were taken on the 14th day and normal-watered tomatoes were used as control. Then, the tomatoes were watered for 7 d after drought stress. The specific methods of salt stress were as follows: wild-type and transgenic tomato plants of the same growth period were taken and watered with 200 mL of 200 mM NaCl and 250 mM NaCl solution every 3 d for 14 d. The control group was replaced with an equal amount of water; after the salt stress was over, the recovery test was conducted with normal watering for 7 d. The low temperature stress treatments were as follows: wild-type and transgenic tomatoes were subjected to low temperature stress treatments at 4°C for 8 h and -2°C for 6 h, respectively, in an artificial low temperature climatic chamber, using the 25°C treatment as a control. After the stress, 25°C was recovered. The growth status of wild-type and transgenic tomatoes at each treatment stage was observed and recorded by taking photographs with a camera. For each of the above stress treatments, three plants per treatment and three replications were performed.

Determination of relevant physiological and biochemical indexes

After each stress treatment, we tried to select tomato leaves from the same parts for subsequent physiological and biochemical indexes. Relative water content (RWC) was determined according to the method of Jun Cui et al. (Cui et al., 2018). Relative electrolyte leakage (REL) was determined according to the method of Wang et al. (Wang et al., 2014). MDA content was assessed according to the method of Jun Ma et al. (Ma et al., 2015). We used the method of Liu et al. (Liu et al., 2020) to determine the soluble sugar, soluble protein, and proline contents. For determining antioxidant enzyme activity: 0.5 g of fresh tomato leaves were accurately weighed on an analytical balance and ground in 50 mM/L cold PBS buffer (pH 7.8) with 1.0 mM/L EDTA-Na_2 and 2% (w/v) polyvinyl pyrrolidone (PVP) in an ice bath to make a homogenate, followed by centrifugation at 4000 r at 4°C. After centrifuging the samples for 15 min, the supernatant was retained as the crude extract for the enzyme activity assay. Specific activity assays of superoxide dismutase (SOD), peroxidase (POD), and catalase (CAT) were carried out according to the description of Muhammad Ali Khan et al. (Khan et al., 2022). Three biological replicates were performed for each indicator.

Statistical analysis

All measured data were subjected to three biological replicates, and statistical analysis was completed using SPSS and GraphPad Prism 8.3 software. * $P < 0.05$ (weak significant difference), ** $P < 0.01$ (significant difference), *** $P < 0.001$ (strong significant difference), and **** $P < 0.0001$ (very strong significant difference) are used to indicate significance. In addition, NS indicates that there is no significant difference between the two.

Results

Bioinformatics analysis of *PsHAT5* transcription factor

PsHAT5 had the highest homology with white pear *PbrHAT5* (GenBank: XM_009371078.3) using BlastP analysis on the NCBI

website, indicating that the *PsHAT5* transcription factor has the closest genetic relationship with white pear *PbrHAT5*. The next highest homology was with *Pyrus betulifolia bunge* (Chr6.g51268), *Pyrus ussuriensis x Pyrus communis* (KAB2633474.1), *Malus domestica* (NM_001328891.1), *Prunus avium* (XP_ 021808346.1), *Prunus mume* (XM_008241624.1), *Prunus persica* (XP_007209345.1), *Prunus dulcis* (XM_034359186.1), *Rosa chinensis* (XM_024315270.2), and *Gossypium hirsutum* (XP_040939127.1). These species have high homology of HAT5 protein, and all have two highly conserved functional structural domains (Figure 1A). The above results strongly suggest that the *PsHAT5* transcription factor is a member of the HD-Zip transcription factor family. The final cloned cDNA sequence of 1089 bp in length was analyzed using DNAMAN software, and the fragment was found to contain a 975 bp open reading frame (ORF) encoding 324 amino acids. A phylogenetic tree of different HAT5 proteins was constructed using MEGA 7.0 software (Figure 1B).

Construction of plant overexpression vectors and acquisition of transgenic tomatoes

To generate the pCAMBIA2300-PsHAT5 recombinant plasmid, the *PsHAT5* ORF was cloned into the pCAMBIA2300 vector under the control of the CaMV35S promoter. The insert was released from pMD19-T- PsHAT5 through BamH I and Xbal I digestion and then ligated into pCAMBIA2300-35S-PsHAT5-Nos. The construct was introduced into *Agrobacterium* GV3101 by electroporation to complete the construction of the overexpression vector (Figures 2A–D). *PsHAT5* transgenic tomato plant lines were generated and selected to assess the significance and effect of the *PsHAT5* transcription factor on the physiology of transgenic tomato plants under low temperature, drought, and salt stress. *Agrobacterium*-mediated infection of wild-type tomatoes and screening of T0 transgenic seeds on MS medium containing 200 mg/L kanamycin was used to obtain *PsHAT5*-transformed tomato plants. The genomic DNA of tomato leaves was extracted using the CTAB method, and PCR was performed on the transformed tomato plants using DNA as a template. The agarose gel electrophoresis results showed that eight transgenic tomato plants had been obtained (Figure 2E) after a preliminary determination of the specific band at 1089 bp. Finally, we selected OE-2 and OE-4 overexpressing transgenic tomato plants for qPCR analysis, which showed that the relative expression levels of *PsHAT5* in OE-2 and OE-4 were significantly higher than those in wild-type tomatoes (Figure 2F). Based on these results, we determined that the *PsHAT5* transcription factor had been successfully transformed into tomato plants, and we selected OE-2 and OE-4 strains for subsequent experiments.

Overexpression of *PsHAT5* transcription factor enhances drought tolerance in transgenic tomato

In our indoor cultivation experiments, we found that transgenic tomatoes sown in seedling trays showed better drought tolerance than the wild-type (Figure 3A). To further investigate the role of the *PsHAT5* transcription factor in drought, we subjected the obtained transgenic and wild-type tomatoes to drought stress treatment (Figures 3B1, B2). It was found that the growth of wild-type and transgenic tomatoes was almost identical when watered normally, and there were almost no significant differences between wild-type and transgenic tomato plants when analyzed for physiological and biochemical indicators. When the drought treatment was applied at 16 days, wild-type tomato leaves showed non-extreme wilting and water loss in phenotype, with severe wilting of the apical part and subsequent loss of some lateral branches. Still, the transgenic tomatoes remained upright with bright green leaves (Figures 3C1, C2). The results of the physiological and biochemical data showed

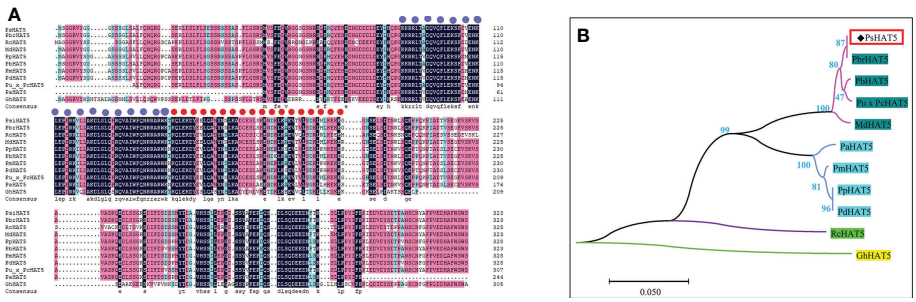

FIGURE 1
Homologous sequence alignment and phylogenetic analysis of *PsHAT5* transcription factor. **(A)** Sequence comparison results of *PsHAT5* with homologous proteins in other species (The purple circles represent the HD domain, and the red circles represent the LZ domain.). **(B)** Phylogenetic tree of *PsHAT5* (The phylogenetic tree was built using MEGA 7.0 by the Neighbor-Joining method with 1000 bootstrap replicates).

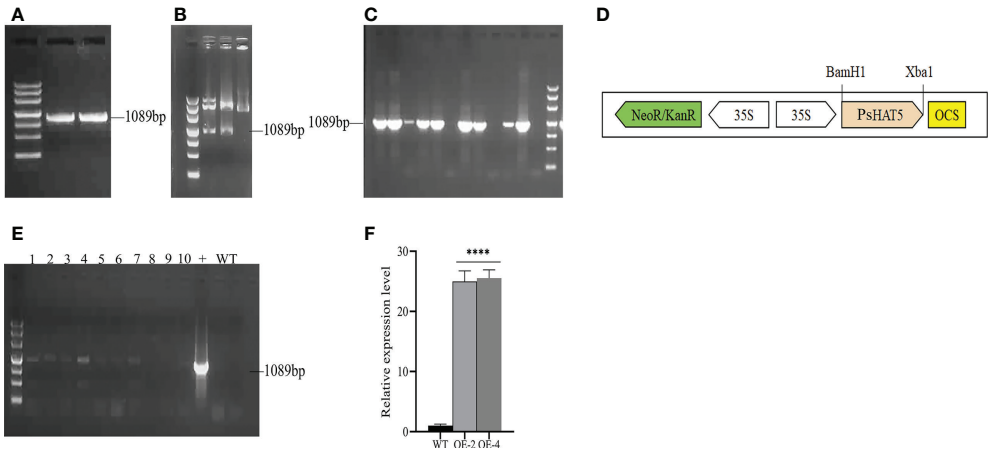

FIGURE 2
(A-D): The plant Overexpression vector construct of *PsHAT5*. **(A)** Cloning of *PsHAT5* gene. **(B)** The recombinant plasmid pCAMBIA2300-35S-PsHAT5-Nos was identified by restriction enzyme digestion. **(C)** Identification of *PsHAT5* gene by *Agrobacterium tumefaciens* GV3101. **(D)** pCAMBIA2300-35S-PsHAT5-Nos Expression Frame. **(E, F)** PCR identification of transgenic tomatoes with PsHAT5 gene. **(E)** PCR identification of transgenic plants. Numbers 1-10 indicate individual transgenic plant lines, the "+" plasmid was used as a positive control, and WT were used as negative controls. **(F)** Relative expression levels of transgenic tomatoes. (****P < 0.0001 for comparisons between the transgenic lines and wildtypeplants by Student's t-tests).

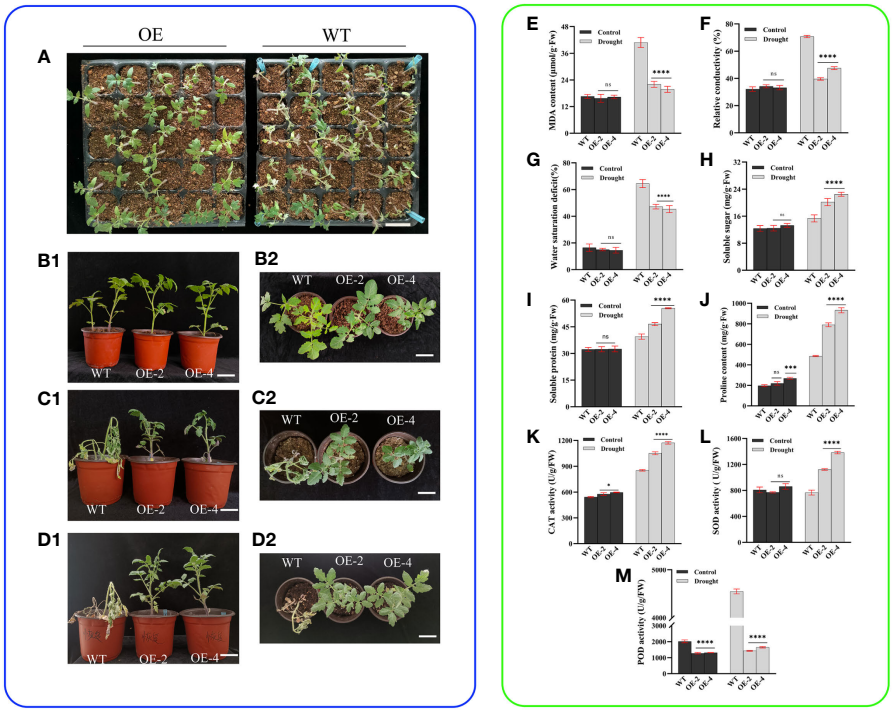

FIGURE 3
Phenotypic and physiological data of wild-type and transgenic tomatoes under drought stress. **(A)** The overall growth of wild type and transgenic tomatoes seedling trays under drought stress for 7 days. **(B1)** (Main view) and **(B2)** (top view) Growth status of wild-type and transgenic tomatoes at 4 weeks of age after normal watering. **(C1)** (Main view) and **(C2)** (top view): Morphological differences of 4 weeks tomatoes under drought stress for 16 days. **(D1)** (Main view) and **(D2)** (top view): The growth status of C1or C2 after 7 days of rehydration. **(E)** MDA content. **(F)** Relative conductivity content. **(G)** Water saturation deficit. **(H)** Soluble sugar content. **(I)** soluble protein content. **(J)** Proline content. **(K)** CAT activity. **(L)** SOD activity. **(M)** POD activity. Data are means ± SD of three replicates. (7.2 cm inner diameter, 11.5 cm high). (Ns > 0.05, *P < 0.05, ***P < 0.001, and ****P < 0.0001 for comparisons between the transgenic lines and wild-type plants by Student's t-tests).

that the malondialdehyde content, water saturation deficit, and relative conductivity of wild-type tomatoes were significantly higher, and the content of osmoregulatory substances (soluble sugars, soluble proteins, and proline) was significantly lower than those of transgenic tomatoes (Figures 3E–J). Malondialdehyde, the final breakdown product of membrane lipid peroxidation, and relative conductivity reflecting the permeability of cell membranes are important indicators of damage to the membrane system, and the levels of malondialdehyde and conductivity can directly reflect the extent of plant damage from adversity. The short-term changes in water saturation deficit reflect the regulation mechanism between various water saturations and affect the photosynthesis of plants. The larger the value, the stronger the resistance of plants to dehydration. The increase in the content of osmoregulatory substances such as soluble sugars, soluble proteins, and proline maintains the dynamic balance of the internal and external cellular environment.

CAT, SOD, and POD are the main enzymes in the antioxidant system, and they act synergistically to maintain the free radical content in plants at homeostatic levels. Notably, the enzyme activities of CAT and SOD were significantly higher in transgenic tomatoes than in the wild-type, indicating that the transgenic strains were less damaged by membrane lipid peroxidation (Figures 3K–M). The level of POD activity can reflect plant growth and development and intrinsic metabolism and serve as a physiological indicator of tissue aging. We found that POD enzyme activity was significantly lower than in the wild-type under normal watering treatment and drought treatment, probably due to POD's ability to convert certain carbohydrates contained in tissues into lignin, increasing lignification and delaying aging. Thus, the antioxidant enzyme system played an important role throughout the drought. Subsequently, we conducted re-watering tests on wild-type and transgenic tomatoes after drought stress. After 7 days of re-watering, wild-type plants did not recover and gradually wilted and died, while transgenic tomato strains had bright green leaves, upright stalks, and vigorous growth, with an increase in plant height and stem thickness of 2.2 cm and 41 mm (average), respectively (Figures 3D1, D2). These findings indicate that the overexpression of the *PsHAT5* transcription factor significantly improved drought tolerance in transgenic tomatoes.

Overexpression of *PsHAT5* transcription factor enhances salt tolerance in transgenic tomato

To investigate whether the *PsHAT5* transcription factor can regulate the tolerance of tomato plants to salt stress, we conducted a salt tolerance assay. The results showed that phenotypically, both wild-type and transgenic tomatoes grew vigorously and branched well under normal watering conditions (Figures 4A1, A2; D1, D2). When treated with 200 mM and 250 mM NaCl stress, the leaves of wild-type and transgenic plants yellowed, but wild-type tomato leaves showed a large number of yellow dead spots, and after rehydration, wild-type and transgenic tomatoes showed very different growth states (Figures 4B1, B2; E1, E2). After rehydration of tomatoes after 250 mM NaCl stress, the vast majority of leaves and petioles of both wild-type and transgenic tomatoes fell off, but the main stems of transgenic tomatoes still survived (Figures 4C1, C2; F1, F2). After 7 days of rehydration, the transgenic tomato could maintain a good growth state after 200 mM NaCl stress, while the control plants were wilted and greened until death.

In terms of physiological indicators, malondialdehyde content can directly reflect the level of cell membrane damage in plants under stress conditions. We found that the malondialdehyde content of wild-type tomatoes was higher than that of transgenic tomatoes under 200 mM NaCl treatment, indicating that wild-type and transgenic tomato plants were damaged to different degrees after NaCl stress treatment. With the increase in salt treatment concentration, cell membrane damage remained significantly higher in wild-type tomatoes than in transgenic tomatoes under 250 mM treatment. Analysis of the relative conductivity data revealed that the relative conductivity content of wild-type tomatoes was significantly higher than that of transgenic tomatoes under 200 mM and 250 mM NaCl stress. However, at 250 mM treatment, the relative conductivity content of both wild-type and transgenic tomatoes exceeded 90% (Figures 4G, H). This indicated that the cell membrane was severely damaged, membrane permeability was almost lost, and intracellular electrolytes leaked out, thus contributing significantly to the eventual death of wild-type and transgenic tomatoes in subsequent recovery experiments.

The water saturation deficit did not differ between wild-type and transgenic tomatoes under NaCl stress but was increased compared to tomatoes treated with normal watering; soluble sugars and proline were important physiological osmoregulatory substances (Figures 4I–L). Under NaCl stress, the content of soluble sugars increased significantly in the transgenic tomatoes compared to the wild-type, which improved the water retention capacity of plant cells; the accumulation of proline was also significantly higher in the transgenic plants compared to the wild-type, which effectively improved the ability of cells to absorb and retain water in salt stress; soluble protein is not only a nutrient but also an important osmoregulator. The increase and accumulation of soluble protein in plants can also improve the water retention capacity of cells. Under normal watering treatment, wild-type and transgenic tomato plants maintained a high soluble protein content, which decreased with increasing salt stress concentration in both wild-type and transgenic plants but remained significantly higher in transgenic plants than in wild-type. This indicated that the osmoregulatory substances, soluble sugars, proline, and soluble protein, play an important role in conferring salt tolerance in tomatoes.

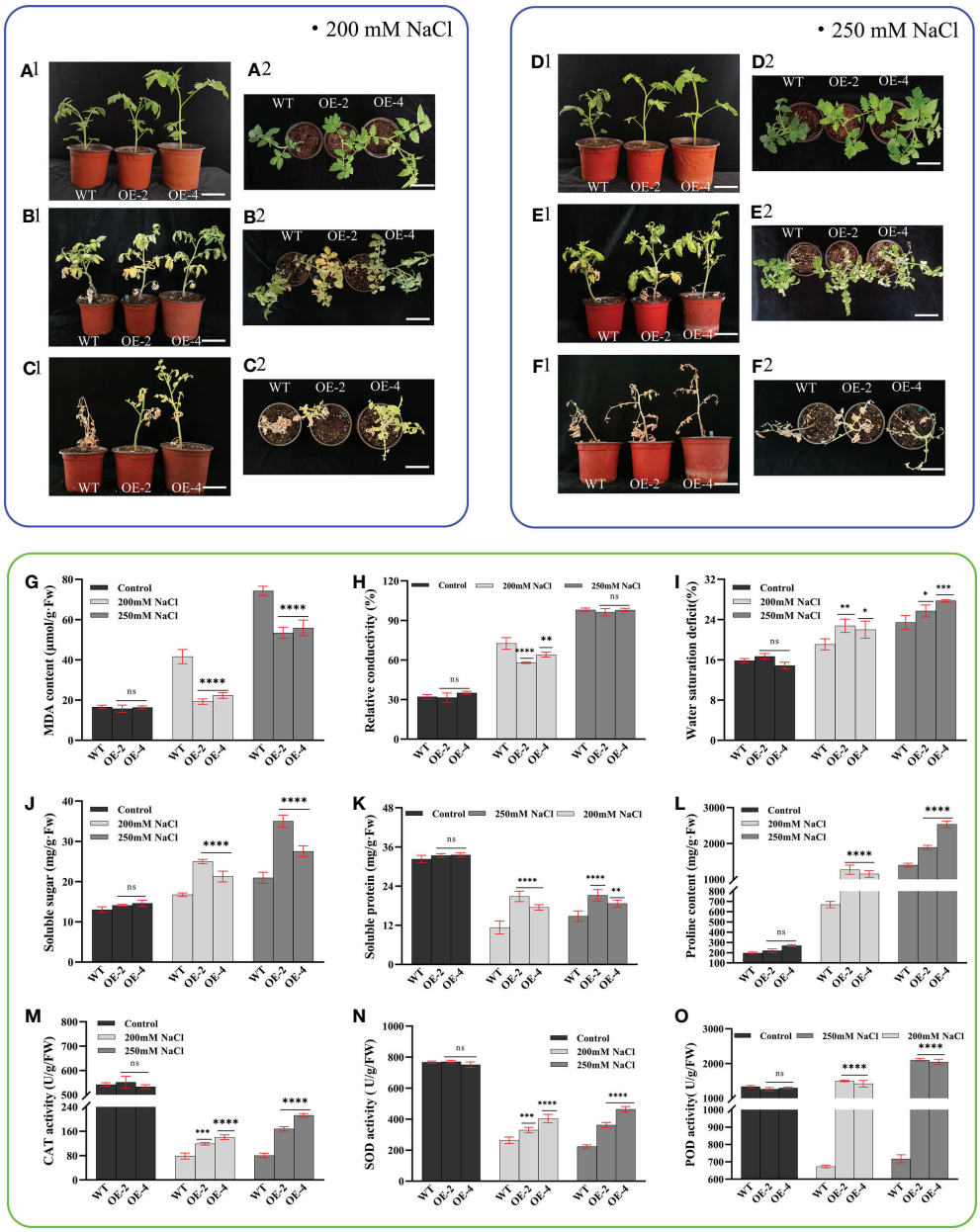

FIGURE 4
Phenotypic and physiological data of wild-type and transgenic tomatoes under NaCl stress (200mM NaCl and 250mM NaCl). **(A1)** (Main view) and **(A2)** (Top view): The growth status of wild-type and transgenic tomato at 4 weeks of age under normal watering. **(B1)** (Main view) and **(B2)** (Top view): Wild-type and transgenic tomato growth status after 14 days of 200 mM NaCl treatment. **(C1)** (Main view) and **(C2)** (Top view): The growth status of B1 or B2 after 7 days of normal watering. **(D1)** (Main view) and **(D2)** (Top view): The growth status of wild-type and transgenic tomato at 4 weeks of age under normal watering. **(E1)** (Main view) and **(E2)** (Top view): Wild-type and transgenic tomato growth status after 14 days of 200 mM NaCl treatment. **(F1)** (Main view) and **(F2)** (Top view): The growth status of E1 or E2 after 7 days of normal watering. **(G)** MDA content. **(H)** Relative conductivity content. **(I)** Water saturation deficit. **(J)** Soluble sugar content. **(K)** soluble protein content. **(L)** Proline content. **(M)** CAT activity. **(N)** SOD activity. **(O)** POD activity. Data are means ± SD of three replicates. (7.2 cm inner diameter, 11.5 cm high). (Ns > 0.05, *P < 0.05, **P < 0.01, ***P < 0.001, and ****P < 0.0001 for comparisons between the transgenic lines and wild-type plants by Student's t-tests).

POD, CAT, and SOD are all important members of the plant antioxidant enzyme system. POD enzyme activity increased with increasing NaCl stress concentration but overall was significantly higher in transgenic tomatoes than in the wild-type. CAT and SOD enzyme activities decreased in wild-type and transgenic tomatoes under NaCl stress compared to normally watered tomatoes. However, CAT and SOD enzyme activities were significantly higher in transgenic tomatoes than in the wild-type (Figures 4M–

O). Under NaCl stress, the accumulation of oxygen radicals was excessive, the degree of membrane lipid peroxidation was severe, more lipid membrane peroxidation products were also produced, and the structure and integrity of membranes were disrupted, causing physiological and biochemical disorders and leading to plant death. This may also be one of the reasons for the poor growth status and eventual death of tomatoes after rehydration. The above findings suggest that the overexpression of the *PsHAT5* transcription factor enhances salt tolerance in transgenic tomatoes.

Overexpression of the *PsHAT5* transcription factor increases the low temperature sensitivity of transgenic tomatoes (mainly freeze sensitive)

As a cold-sensitive crop, a short period of low temperature stress can induce significant phenotypic damage changes in tomatoes. We subjected the transgenic tomatoes to low temperature stress to investigate whether the PsHAT5 transcription factor plays a regulatory role at low temperatures. At room temperature, wild-type and transgenic tomatoes grew almost identically with bright green leaves (Figures 5A1, A2, D1, D2). After 8 h of cold treatment at 4°C, phenotypically, transgenic tomato leaves were dehydrated with curled edges and drooping tips. In contrast, wild-type tomatoes were almost identical to their pre-treatment state without wilting. Thus, wild-type tomatoes showed stronger cold tolerance (Figures 5B1, B2). After 24 h of recovery at room temperature, both wild-type and transgenic tomatoes returned to their pre-treatment growth status (Figures 5C1, C2).

When the -2°C freezing treatment was applied for 6 h, the transgenic tomato leaves lost water severely and had a touch of freezing. The top leaves of the plants were completely frozen and showed many obvious dead spots, while the wild-type tomato leaves also showed partial water loss with wilting and yellow dead spots (Figures 5E1, E2). After a 24-h room temperature recovery experiment, the transgenic tomato plants were severely dehydrated and died eventually. However, the main stems of the wild-type tomato plants remained upright with some green leaves (Figures 5F1, F2). This indicates that the freezing sensitivity of transgenic tomato is increased. From the physiological and biochemical indices, malondialdehyde content, relative conductivity, and water saturation deficit all increased to decreasing treatment temperature. However, wild-type tomatoes were significantly lower than transgenic tomatoes, and when the temperature dropped to -2°C, the relative conductivity of transgenic tomatoes reached more than 90% (Figures 5G–I).

Soluble sugar, soluble protein, and proline contents all showed increasing trends with decreasing treatment temperatures. The contents were significantly higher in wild-type tomatoes than in transgenic tomatoes (Figures 5J–L). When the temperature decreased to -2°C, it showed a decreasing trend, but wild-type tomatoes were significantly higher than transgenic tomatoes. Soluble sugars, soluble proteins, and proline all play an important role in the osmoregulation of plants as osmoregulatory substances, thus alleviating the damage to plant biofilms caused by low temperature environments; they show a certain trend of complementarity with each other. There was no significant difference in the enzyme activities of CAT, SOD, and POD among the plants at room temperature (Figures 5M–O). As the treatment temperature decreased, the CAT, SOD, and POD activities of wild-type and transgenic tomato plants first increased and then decreased. However, the overall trend was that the enzyme activity of wild-type tomatoes was significantly higher than that of transgenic tomatoes. The above results indicated that introducing the *PsHAT5* transcription factor increased the sensitivity of tomatoes under low temperature treatment.

Discussion

HD-Zip transcription factors are a class of transcription factors encoding homologous heterotypic domain LZ proteins unique to plants that recognize and bind to specific regulatory elements in the promoter regions of target genes to regulate plant growth and development processes involved in plant responses to adverse environmental conditions. Adverse conditions can affect plant growth and development and directly determine plant survival in severe cases. In this study, we increased the drought and salt tolerance of transgenic tomatoes by overexpressing the *PsHAT5* transcription factor into tomatoes to enhance the activity of antioxidant enzymes (CAT, SOD, POD) system and increase the water retention capacity of osmoregulatory substances (soluble sugars, soluble proteins, proline content). Conversely, CAT, SOD, and POD enzyme activities were significantly reduced in low temperature stress, especially freezing stress. The decrease in enzyme activities was greater in transgenic tomatoes, increasing the freezing sensitivity of overexpressed tomatoes.

Relative conductivity is an important physiological and biochemical index reflecting the condition of the plant membrane system. When plants are subjected to adversity or other damage, the cell membrane tends to rupture, and the intracellular material exudates, increasing relative conductivity (Du et al., 2019). Therefore, relative conductivity can reflect the osmoregulatory ability of the plasma membrane under abiotic stress (Hasanuzzaman et al., 2020). Therefore, conductivity studies have become an accurate and practical method to identify the strength of plant stress resistance in crop resistance cultivation and breeding (Ma et al., 2017). In our

10.3389/fpls.2022.1036254

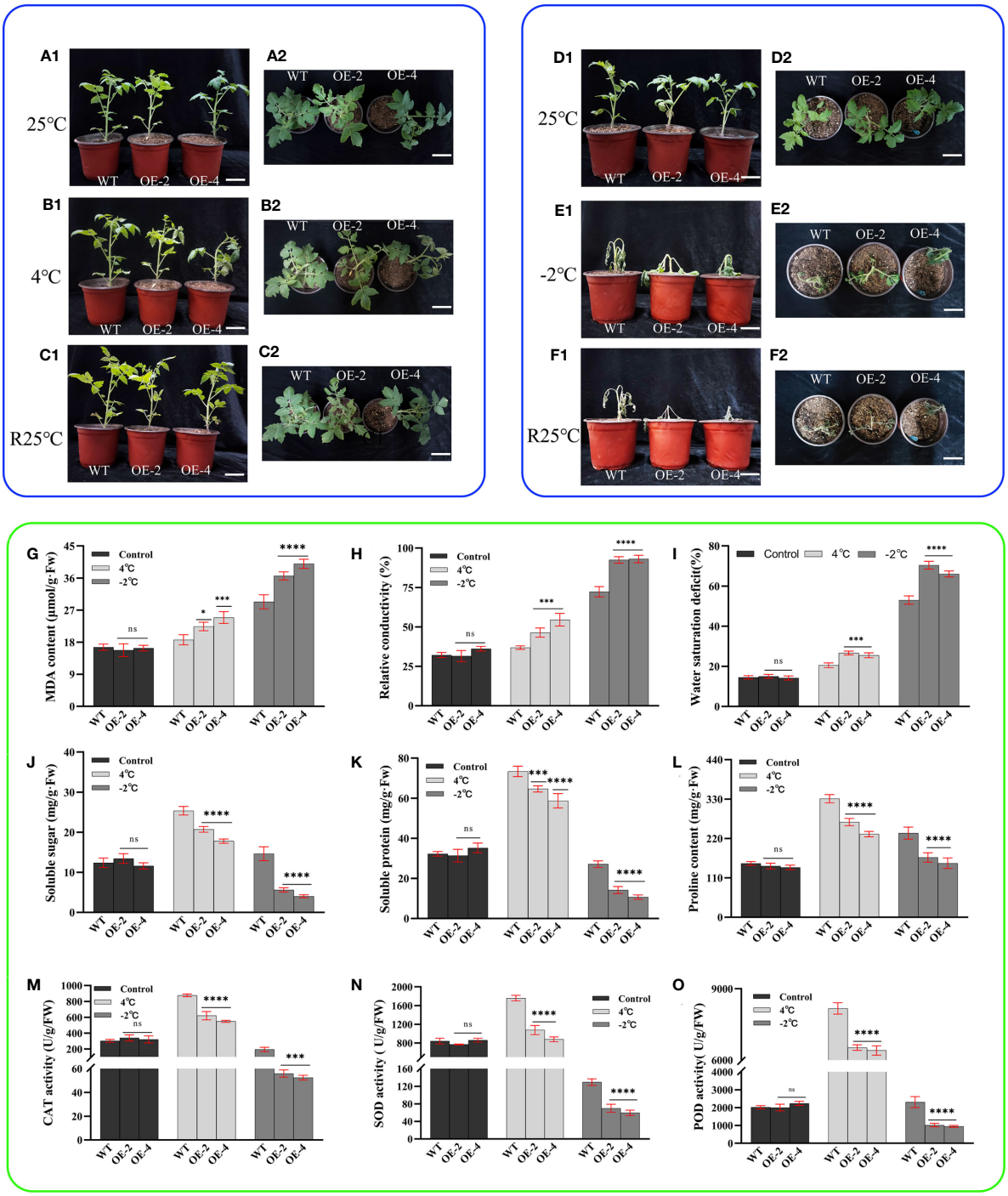

FIGURE 5

Phenotype and physiology of wild-type and transgenic tomatoes under low temperature (cold and freezing) stress. **(A1)** (Main view) and **(A2)** (Top view): Growth status of wild-type and transgenic tomatoes 4-week-old at room temperature. **(B1)** (Main view) and **(B2)** (Top view): The growth status of wild-type and transgenic tomatoes treated at 4°C for 8h. **(C1)** (Main view) and **(C2)** (Top view): The growth status of B1or B2 after 24 h of room temperature recovery. **(D1)** (Main view) and **(D2)** (Top view): Growth status of wild-type and transgenic tomatoes 4-week-old at room temperature. **(E1)** (Main view) and **(E2)** (Top view): The growth status of wild-type and transgenic tomatoes treated at -2°C for 6h. **(F1)** (Main view) and **(F2)** (Top view): The growth status of E1or E2 after 24 h of room temperature recovery. **(G)** MDA content. **(H)** Relative conductivity content. **(I)** Water saturation deficit. **(J)** Soluble sugar content. **(K)** soluble protein content. **(L)** Proline content. **(M)** CAT activity. **(N)** SOD activity. **(O)** POD activity. Data are means ± SD of three replicates. (7.2cm inner diameter, 11.5cm high.). (Ns > 0.05, *P < 0.05, ***P < 0.001, and ****P < 0.0001 for comparisons between the transgenic lines and wild-type plants by Student's t-tests).

study, after drought, salt, and low temperature stress treatments, the relative conductivity content of wild-type and transgenic tomatoes increased significantly after each stress treatment compared with those treated normally. Also, 250 mM NaCl and -2°C treatments directly exceeded 90% of the relative conductivity content. The plants did not recover even after 7 days of rehydration at a later stage but gradually dried out and died. The higher the relative conductivity, the greater the permeability of the cell membrane (Li et al., 2014), and the greater the damage to the plant, which exceeds the recovery capacity of the plant. Even if irrigation is carried out, recovery is difficult, and the plant will eventually dry up and die. The research of Menachem Moshelion, Tom Eeckhaut, and Leon V Kochian et al. (Eeckhaut et al., 2013; Kochian et al., 2015; Moshelion et al., 2015) also confirms this point. Their studies pointed out that, in general, abiotic stress in the short term would make the plant leaves lose their green color and wilt, and with timely rehydration, the plant would quickly return to its original growth condition. Different plants have significantly different stress tolerance and behave differently to external drought (Dietz, 2014; Seo, 2014).

In this experiment, the MDA accumulation of transgenic tomatoes after drought and NaCl treatment was relatively less, and the relative conductivity was significantly lower than that of the wild-type, which significantly alleviated the degree of oxidative damage and increased the responsiveness of transgenic tomatoes to drought and salt. MDA is a final product of unsaturated fatty acid peroxidation in phospholipids (Bokhorst et al., 2010; Bresson et al., 2018). Its content can reflect lipid peroxidation or cell membrane damage in plant tissues, affecting protein synthesis (Khan et al., 2021b). The results of Zhao H, Liu Z, and Zhang T et al. also demonstrated that malondialdehyde content accumulates substantially after abiotic stress in plants, aggravating the degree of membrane lipid peroxidation (Zhang et al., 2020; Liu et al., 2022; Zhao et al., 2022). When plants are subjected to osmotic stress, many plants accumulate proline in response to these stresses (Chen et al., 2013).

Proline, a water-soluble amino acid (Naliwajski and Skłodowska, 2021), is a typical osmoprotectant that prevents dehydration and denaturation of proteins under osmotic stress conditions, maintains the osmotic balance inside and outside the cell, and prevents water dissipation. For plants, proline accumulates over time and effectively has the ability of osmotic protection (Aganchich et al., 2009; Ben Ahmed et al., 2009). Our study also found that plants can reduce the osmotic potential of cells under stress by accumulating proline, soluble sugar, and soluble protein, enhancing the water retention and water absorption capacity of plant cells and alleviating the damage of abiotic stress to plants. The accumulation of these substances in transgenic tomatoes is significantly higher than that of wild-type tomatoes, giving them more drought and salt tolerance. Munsif et al. (2021) also revealed that abiotic stress significantly reduced the accumulation of substances such as soluble sugars and proteins.

When plants suffer from stress, the plant antioxidant enzyme system can activate self-defense function, balance reactive oxygen species metabolism, protect the membrane system, and enhance the resilience of plants (Miller et al., 2010; Raza et al., 2021; Sun et al., 2021). Our results showed that the changes in CAT, SOD, and POD enzyme activities did not show obvious synchronization under drought stress. The activities of CAT and SOD were significantly higher than those of the wild type, while the activity of POD was significantly lower than that of the wild type. The possible reason is that these three enzymes may have a coordinated relationship in plant adaptation to stress, which was also proved by Liu et al. (Khare et al., 2015; Liu et al., 2016). Under most environmental stresses, the change in antioxidant enzyme activity appears "first rising then falling" with the increase of stress intensity (Farhangi-Abriz and Torabian, 2017; Khan et al., 2021a; Wang et al., 2021). This is different from our results.

Our results showed that the levels of antioxidant enzymes in wild-type and transgenic lines showed a downward trend under NaCl and freezing stress. In this regard, we have made a possible conjecture and speculation. As a whole, the physiological functions of plants are interrelated, and the antioxidant enzyme system is only one aspect of plant adaptation and resistance to adversity. After exceeding the endurance capacity of cells, prolonged and excessive environmental stress will lead to a deeper degree of membrane lipid peroxidation and enhanced damage to cells, so the activity of antioxidant enzymes will decrease (Sihag et al., 2019; Li et al., 2020). The experiment of Fatma Bejaoui et al. also showed that the change in antioxidant enzyme activity was related to membrane damage index, plant growth cycle, photosynthesis, and secondary metabolite synthesis (Bejaoui et al., 2016; Tian et al., 2018; Liu et al., 2019). It also confirmed the reliability of our research results. These results indicated that the PsHAT5 transcription factor increased drought tolerance, salt tolerance, and low temperature sensitivity in transgenic tomatoes.

Conclusion

In this study, we cloned the HD-Zip family transcription factor *PsHAT5* from *P. sinkiangensis* and functionally validated it in overexpressing tomatoes. Phenotypic observations and related stress resistance physiological and biochemical indices revealed that overexpression of transgenic tomatoes increased resistance to drought and salt stress by increasing osmoregulatory substances and enhancing antioxidant enzyme

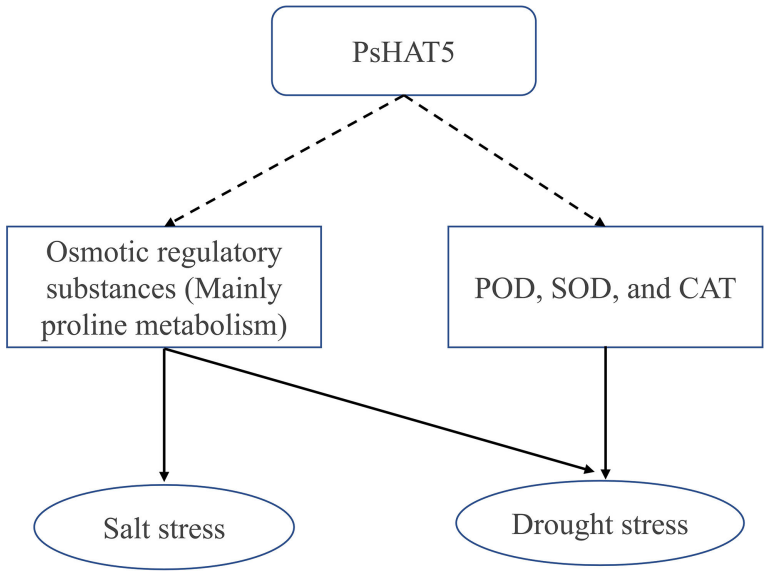

FIGURE 6
A pictorial representation of the role of *PsHAT5* transcription factors in the regulation of drought and salt stress in tomatoes. Dotted lines indicate events that have not yet clearly occurred and are subject to further study, and the solid lines represent events that occur.

activities while freezing sensitivity was increased in transgenic tomatoes (Figure 6). Our results suggest that the *PsHAT5* transcription factor has potential applications in drought and salt tolerance breeding.

Data availability statement

The datasets presented in this study can be found in online repositories. The names of the repository/repositories and accession number(s) can be found in the article/ Supplementary Material.

Author contributions

XL and AL were co-first authors of the present paper and co-wrote paper. CL and YW completed the preparation of the trial materials and acquisition of data, SW completed the analysis of the trial data. JL and JZ are the co-corresponding authors of this paper and directed the experimental design. All authors reviewed the manuscript. All authors contributed to the article and approved the submitted version.

Funding

National Natural Science Foundation of China (32160061) [Entry name: Study on improving water use efficiency of Saussurea involucrata (SIPIP2;7) through chloride ion signal pathway].

Acknowledgments

We are grateful for the support of the research group during this research work.

Conflict of interest

The authors declare that the research was conducted in the absence of any commercial or financial relationships that could be construed as a potential conflict of interest.

Publisher's note

All claims expressed in this article are solely those of the authors and do not necessarily represent those of their affiliated organizations, or those of the publisher, the editors and the reviewers. Any product that may be evaluated in this article, or claim that may be made by its manufacturer, is not guaranteed or endorsed by the publisher.

Supplementary material

The Supplementary Material for this article can be found online at: https://www.frontiersin.org/articles/10.3389/fpls.2022.1036254/full#supplementary-material

References

Agalou, A., Purwantomo, S., Overnäs, E., Johannesson, H., Zhu, X., Estiati, A., et al. (2008). A genome-wide survey of HD-zip genes in rice and analysis of drought-responsive family members. *Plant Mol. Biol.* 66, 87–103. doi: 10.1007/s11103-007-9255-7

Aganchich, B., Wahbi, S., Loreto, F., and Centritto, M. (2009). Partial root zone drying: Regulation of photosynthetic limitations and antioxidant enzymatic activities in young olive (*Olea europaea*) saplings. *Tree Physiol.* 29, 685–696. doi: 10.1093/treephys/tpp012

Ariel, F., Diet, A., Verdenaud, M., Gruber, V., Frugier, F., Chan, R., et al. (2010). Environmental regulation of lateral root emergence in *Medicago truncatula* requires the HD-zip I transcription factor HB1. *Plant Cell* 22, 2171–2183. doi: 10.1105/tpc.110.074823

Basso, M. F., Costa, J. A., Ribeiro, T. P., Arraes, F. B. M., Lourenço-Tessutti, I. T., Macedo, A. F., et al. (2021). Overexpression of the CaHB12 transcription factor in cotton (*Gossypium hirsutum*) improves drought tolerance. *Plant Physiol. Biochem.* 165, 80–93. doi: 10.1016/j.plaphy.2021.05.009

Bejaoui, F., Salas, J. J., Nouairi, I., Smaoui, A., Abdelly, C., Martínez-Force, E., et al. (2016). Changes in chloroplast lipid contents and chloroplast ultrastructure in *Sulla carnosa* and *Sulla coronaria* leaves under salt stress. *J. Plant Physiol.* 198, 32–38. doi: 10.1016/j.jplph.2016.03.018

Belamkar, V., Weeks, N. T., Bharti, A. K., Farmer, A. D., Graham, M. A., and Cannon, S. B. (2014). Comprehensive characterization and RNA-seq profiling of the HD-zip transcription factor family in soybean (*Glycine max*) during dehydration and salt stress. *BMC Genomics* 15, 950. doi: 10.1186/1471-2164-15-950

Ben Ahmed, C., Ben Rouina, B., Sensoy, S., Boukhriss, M., and Ben Abdullah, F. (2009). Saline water irrigation effects on antioxidant defense system and proline accumulation in leaves and roots of field-grown olive. *J. Agric. Food Chem.* 57, 11484–11490. doi: 10.1021/jf901490f

Bokhorst, S., Bjerke, J. W., Davey, M. P., Taulavuori, K., Taulavuori, E., Laine, K., et al. (2010). Impacts of extreme winter warming events on plant physiology in a sub-Arctic heath community. *Physiol. Plant* 140, 128–140. doi: 10.1111/j.1399-3054.2010.01386.x

Bresson, J., Bieker, S., Riester, L., Doll, J., and Zentgraf, U. (2018). A guideline for leaf senescence analyses: From quantification to physiological and molecular investigations. *J. Exp. Bot.* 69, 769–786. doi: 10.1093/jxb/erx246

Cabello, J. V., Arce, A. L., and Chan, R. L. (2012). The homologous HD-zip I transcription factors HaHB1 and AtHB13 confer cold tolerance *via* the induction of pathogenesis-related and glucanase proteins. *Plant J.* 69, 141–153. doi: 10.1111/j.1365-313X.2011.04778.x

Cabello, J. V., and Chan, R. L. (2012). The homologous homeodomain-leucine zipper transcription factors HaHB1 and AtHB13 confer tolerance to drought and salinity stresses *via* the induction of proteins that stabilize membranes. *Plant Biotechnol. J.* 10, 815–825. doi: 10.1111/j.1467-7652.2012.00701.x

Cabello, J. V., Giacomelli, J. I., Gómez, M. C., and Chan, R. L. (2017). The sunflower transcription factor HaHB11 confers tolerance to water deficit and salinity to transgenic *Arabidopsis* and alfalfa plants. *J. Biotechnol.* 257, 35–46. doi: 10.1016/j.jbiotec.2016.11.017

Cao, L., Yu, Y., DuanMu, H., Chen, C., Duan, X., Zhu, P., et al. (2016). A novel *Glycine soja* homeodomain-leucine zipper (HD-zip) I gene, Gshdz4, positively regulates bicarbonate tolerance and responds to osmotic stress in arabidopsis. *BMC Plant Biol.* 16, 184. doi: 10.1186/s12870-016-0872-7

Chen, J. B., Yang, J. W., Zhang, Z. Y., Feng, X. F., and Wang, S. M. (2013). Two P5CS genes from common bean exhibiting different tolerance to salt stress in transgenic *Arabidopsis*. *J. Genet.* 92, 461–469. doi: 10.1007/s12041-013-0292-5

Cui, J., Jiang, N., Zhou, X., Hou, X., Yang, G., Meng, J., et al. (2018). Tomato MYB49 enhances resistance to phytophthora infestans and tolerance to water deficit and salt stress. *Planta* 248, 1487–1503. doi: 10.1007/s00425-018-2987-6

DaMatta, F. M., Avila, R. T., Cardoso, A. A., Martins, S. C. V., and Ramalho, J. C. (2018). Physiological and agronomic performance of the coffee crop in the context of climate change and global warming: A review. *J. Agric. Food Chem.* 66, 5264–5274. doi: 10.1021/acs.jafc.7b04537

Dezar, C. A., Gago, G. M., Gonzalez, D. H., and Chan, R. L. (2005). Hahb-4, a sunflower homeobox-leucine zipper gene, is a developmental regulator and confers drought tolerance to *Arabidopsis thaliana* plants. *Transgenic Res.* 14, 429–440. doi: 10.1007/s11248-005-5076-0

Dietz, K. J. (2014). Redox regulation of transcription factors in plant stress acclimation and development. *Antioxid. Redox Signal* 21, 1356–1372. doi: 10.1089/ars.2013.5672

Du, B., Zhao, W., An, Y., Li, Y., Zhang, X., Song, L., et al. (2019). Overexpression of an alfalfa glutathione s-transferase gene improved the saline-alkali tolerance of transgenic tobacco. *Biol. Open* 8. doi: 10.1242/bio.043505

Eeckhaut, T., Lakshmanan, P. S., Deryckere, D., Van Bockstaele, E., and Van Huylenbroeck, J. (2013). Progress in plant protoplast research. *Planta* 238, 991–1003. doi: 10.1007/s00425-013-1936-7

Elhiti, M., and Stasolla, C. (2009). Structure and function of homodomain-leucine zipper (HD-zip) proteins. *Plant Signal Behav.* 4, 86–88. doi: 10.4161/psb.4.2.7692

Epule, T. E., Chehbouni, A., Dhiba, D., Etongo, D., Driouech, F., Brouziyne, Y., et al. (2021). Vulnerability of maize, millet, and rice yields to growing season precipitation and socio-economic proxies in Cameroon. *PloS One* 16, e0252335. doi: 10.1371/journal.pone.0252335

Farhangi-Abriz, S., and Torabian, S. (2017). Antioxidant enzyme and osmotic adjustment changes in bean seedlings as affected by biochar under salt stress. *Ecotoxicol. Environ. Saf.* 137, 64–70. doi: 10.1016/j.ecoenv.2016.11.029

Fatima, Z., Ahmed, M., Hussain, M., Abbas, G., Ul-Allah, S., Ahmad, S., et al. (2020). The fingerprints of climate warming on cereal crops phenology and adaptation options. *Sci. Rep.* 10, 18013. doi: 10.1038/s41598-020-74740-3

Girousse, C., Roche, J., Guerin, C., Le Gouis, J., Balzegue, S., Mouzeyar, S., et al. (2018). Coexpression network and phenotypic analysis identify metabolic pathways associated with the effect of warming on grain yield components in wheat. *PloS One* 13, e0199434. doi: 10.1371/journal.pone.0199434

Gong, S., Ding, Y., Hu, S., Ding, L., Chen, Z., and Zhu, C. (2019). The role of HD-zip class I transcription factors in plant response to abiotic stresses. *Physiol. Plant* 167, 516–525. doi: 10.1111/ppl.12965

Guo, Q., Jiang, J., Yao, W., Li, L., Zhao, K., Cheng, Z., et al. (2021). Genome-wide analysis of poplar HD-zip family and over-expression of PsnHDZ63 confers salt tolerance in transgenic *Populus simonii* × *p.nigra*. *Plant Sci.* 311, 111021. doi: 10.1016/j.plantsci.2021.111021

Hanssen, I. M., and Lapidot, M. (2012). Major tomato viruses in the Mediterranean basin. *Adv. Virus Res.* 84, 31–66. doi: 10.1016/b978-0-12-394314-9.00002-6

Hasanuzzaman, M., Bhuyan, M., Parvin, K., Bhuiyan, T. F., Anee, T. I., Nahar, K., et al. (2020). Regulation of ROS metabolism in plants under environmental stress: A review of recent experimental evidence. *Int. J. Mol. Sci.* 21(22):8659. doi: 10.3390/ijms21228695

He, X., Wang, T., Zhu, W., Wang, Y., and Zhu, L. (2018). GhHB12, a HD-ZIP I transcription factor, negatively regulates the cotton resistance to verticillium dahliae. *Int. J. Mol. Sci.* 19(12):3997. doi: 10.3390/ijms19123997

Himmelbach, A., Hoffmann, T., Leube, M., Höhener, B., and Grill, E. (2002). Homeodomain protein ATHB6 is a target of the protein phosphatase ABI1 and regulates hormone responses in *Arabidopsis*. *EMBO J.* 21, 3029–3038. doi: 10.1093/emboj/cdf316

Huang, Z., Footitt, S., Tang, A., and Finch-Savage, W. E. (2018). Predicted global warming scenarios impact on the mother plant to alter seed dormancy and germination behaviour in *Arabidopsis*. *Plant Cell Environ.* 41, 187–197. doi: 10.1111/pce.13082

Khan, I., Awan, S. A., Ikram, R., Rizwan, M., Akhtar, N., Yasmin, H., et al. (2021a). Effects of 24-epibrassinolide on plant growth, antioxidants defense system, and endogenous hormones in two wheat varieties under drought stress. *Physiol. Plant* 172, 696–706. doi: 10.1111/ppl.13237

Khan, R., Ma, X., Zhang, J., Wu, X., Iqbal, A., Wu, Y., et al. (2021b). Circular drought-hardening confers drought tolerance *via* modulation of the antioxidant defense system, osmoregulation, and gene expression in tobacco. *Physiol. Plant* 172, 1073–1088. doi: 10.1111/ppl.13402

Khan, M. A., Yasmin, H., Shah, Z. A., Rinklebe, J., Alyemeni, M. N., and Ahmad, P. (2022). Co Application of biofertilizer and zinc oxide nanoparticles upregulate protective mechanism culminating improved arsenic resistance in maize. *Chemosphere* 294, 133796. doi: 10.1016/j.chemosphere.2022.133796

Khare, T., Kumar, V., and Kishor, P. B. (2015). Na^+ and cl^- ions show additive effects under NaCl stress on induction of oxidative stress and the responsive antioxidative defense in rice. *Protoplasma* 252, 1149–1165. doi: 10.1007/s00709-014-0749-2

Kochian, L. V., Piñeros, M. A., Liu, J., and Magalhaes, J. V. (2015). Plant adaptation to acid soils: The molecular basis for crop aluminum resistance. *Annu. Rev. Plant Biol.* 66, 571–598. doi: 10.1146/annurev-arplant-043014-114822

Laudien, R., Schauberger, B., Waid, J., and Gornott, C. (2022). A forecast of staple crop production in Burkina Faso to enable early warnings of shortages in domestic food availability. *Sci. Rep.* 12, 1638. doi: 10.1038/s41598-022-05561-9

Li, C., Han, Y., Hao, J., Qin, X., Liu, C., and Fan, S. (2020). Effects of exogenous spermidine on antioxidants and glyoxalase system of lettuce seedlings under high temperature. *Plant Signal Behav.* 15, 1824697. doi: 10.1080/15592324.2020.1824697

Liu, T., Du, Q., Li, S., Yang, J., Li, X., Xu, J., et al. (2019). GSTU43 gene involved in ALA-regulated redox homeostasis, to maintain coordinated chlorophyll synthesis of tomato at low temperature. *BMC Plant Biol.* 19, 323. doi: 10.1186/s12870-019-1929-1

Liu, Z., Ma, C., Hou, L., Wu, X., Wang, D., Zhang, L., et al. (2022). Exogenous SA affects rice seed germination under salt stress by regulating Na(+)/K(+) balance and endogenous GAs and ABA homeostasis. *Int. J. Mol. Sci.* 23. doi: 10.3390/ijms23063293

Liu, Z. H., Wang, D. M., Fan, S. F., Li, D. W., and Luo, Z. W. (2016). Synergistic effects and related bioactive mechanism of *Potentilla fruticosa* l. leaves combined with *Ginkgo biloba* extracts studied with microbial test system (MTS). *BMC Complement Altern. Med.* 16, 495. doi: 10.1186/s12906-016-1485-2

Liu, L., White, M. J., and MacRae, T. H. (1999). Transcription factors and their genes in higher plants functional domains, evolution and regulation. *Eur. J. Biochem.* 262, 247–257. doi: 10.1046/j.1432-1327.1999.00349.x

Liu, C., Zhao, Y., Zhao, X., Dong, J., and Yuan, Z. (2020). Genome-wide identification and expression analysis of the CLC gene family in pomegranate (*Punica granatum*) reveals its roles in salt resistance. *BMC Plant Biol.* 20, 560. doi: 10.1186/s12870-020-02771-z

Li, L., Zhang, H., Zhang, L., Zhou, Y., Yang, R., Ding, C., et al. (2014). The physiological response of *Artemisia annua* l. @ to salt stress and salicylic acid treatment. *Physiol. Mol. Biol. Plants* 20, 161–169. doi: 10.1007/s12298-014-0228-

Lodeyro, A. F., Krapp, A. R., and Carrillo, N. (2021). Photosynthesis and chloroplast redox signaling in the age of global warming: Stress tolerance, acclimation, and developmental plasticity. *J. Exp. Bot.* 72, 5919–5937. doi: 10.1093/jxb/erab270

Ma, J., Du, G., Li, X., Zhang, C., and Guo, J. (2015). A major locus controlling malondialdehyde content under water stress is associated with *Fusarium* crown rot resistance in wheat. *Mol. Genet. Genomics* 290, 1955–1962. doi: 10.1007/s00438-015-1053-3

Manavella, P. A., Arce, A. L., Dezar, C. A., Bitton, F., Renou, J. P., Crespi, M., et al. (2006). Cross-talk between ethylene and drought signalling pathways is mediated by the sunflower hahb-4 transcription factor. *Plant J.* 48, 125–137. doi: 10.1111/j.1365-313X.2006.02865.x

Ma, Y., Yang, C., He, Y., Tian, Z., and Li, J. (2017). Rice OVATE family protein 6 regulates plant development and confers resistance to drought and cold stresses. *J. Exp. Bot.* 68, 4885–4898. doi: 10.1093/jxb/erx309

Ma, G., Zelman, A. K., Apicella, P. V., and Berkowitz, G. (2022). Genome-wide identification and expression analysis of homeodomain leucine zipper subfamily IV (HD-ZIP IV) gene family in *Cannabis sativa* l. *Plants (Basel)* 11, 1037. doi: 10.3390/plants11101307

Miller, G., Suzuki, N., Ciftci-Yilmaz, S., and Mittler, R. (2010). Reactive oxygen species homeostasis and signalling during drought and salinity stresses. *Plant Cell Environ.* 33, 453–467. doi: 10.1111/j.1365-3040.2009.02041.x

Moshelion, M., Halperin, O., Wallach, R., Oren, R., and Way, D. A. (2015). Role of aquaporins in determining transpiration and photosynthesis in water-stressed plants: crop water-use efficiency, growth and yield. *Plant Cell Environ.* 38, 1785–1793. doi: 10.1111/pce.12410

Munsif, F., Kong, X., Khan, A., Shah, T., Arif, M., Jahangir, M., et al. (2021). Identification of differentially expressed genes and pathways in isonuclear kenaf genotypes under salt stress. *Physiol. Plant* 173, 1295–1308. doi: 10.1111/ppl.13253

Naliwajski, M., and Skłodowska, M. (2021). The relationship between the antioxidant system and proline metabolism in the leaves of *Cucumber* plants acclimated to salt stress. *Cells* 10, 609. doi: 10.3390/cells10030609

Olsson, A. S., Engström, P., and Söderman, E. (2004). The homeobox genes ATHB12 and ATHB7 encode potential regulators of growth in response to water deficit in *Arabidopsis*. *Plant Mol. Biol.* 55, 663–677. doi: 10.1007/s11103-004-1581-4

Raza, A., Su, W., Gao, A., Mehmood, S. S., Hussain, M. A., Nie, W., et al. (2021). Catalase (CAT) gene family in rapeseed (*Brassica napus* l.): Genome-wide analysis, identification, and expression pattern in response to multiple hormones and abiotic stress conditions. *Int. J. Mol. Sci.* 22, 4281. doi: 10.3390/ijms22084281

Ré, D. A., Capella, M., Bonaventure, G., and Chan, R. L. (2014). *Arabidopsis* AtHB7 and AtHB12 evolved divergently to fine tune processes associated with growth and responses to water stress. *BMC Plant Biol.* 14, 150. doi: 10.1186/1471-2229-14-150

Rotundo, J. L., Tang, T., and Messina, C. D. (2019). Response of maize photosynthesis to high temperature: Implications for modeling the impact of global warming. *Plant Physiol. Biochem.* 141, 202–205. doi: 10.1016/j.plaphy.2019.05.03

Sen, S., Chakraborty, J., Ghosh, P., Basu, D., and Das, S. (2017). Chickpea WRKY70 regulates the expression of a homeodomain-leucine zipper (HD-zip) I transcription factor CaHDZ12, which confers abiotic stress tolerance in transgenic tobacco and chickpea. *Plant Cell Physiol.* 58, 1934–1952. doi: 10.1093/pcp/pcx126

Seo, P. J. (2014). Recent advances in plant membrane-bound transcription factor research: emphasis on intracellular movement. *J. Integr. Plant Biol.* 56, 334–342. doi: 10.1111/jipb.12139

Shao, J., Li, G., Li, Y., and Zhou, X. (2022). Intraspecific responses of plant productivity and crop yield to experimental warming: A global synthesis. *Sci. Total Environ.* 840, 156685. doi: 10.1016/j.scitotenv.2022.156685

Sharif, R., Raza, A., Chen, P., Li, Y., El-Ballat, E. M., Rauf, A., et al. (2021). HD-ZIP gene family: Potential roles in improving plant growth and regulating stress-responsive mechanisms in plants. *Genes (Basel)* 12(8):1256. doi: 10.3390/genes12081256

Shin, D., Koo, Y. D., Lee, J., Lee, H. J., Baek, D., Lee, S., et al. (2004). Athb-12, a homeobox-leucine zipper domain protein from *Arabidopsis* thaliana, increases salt tolerance in yeast by regulating sodium exclusion. *Biochem. Biophys. Res. Commun.* 323, 534–540. doi: 10.1016/j.bbrc.2004.08.127

Sihag, S., Brar, B., and Joshi, U. N. (2019). Salicylic acid induces amelioration of chromium toxicity and affects antioxidant enzyme activity in *Sorghum bicolor* l. *Int. J. Phytoremed.* 21, 293–304. doi: 10.1080/15226514.2018.1524827

Söderman, E., Hjellström, M., Fahleson, J., and Engström, P. (1999). The HD-zip gene ATHB6 in *Arabidopsis* is expressed in developing leaves, roots and carpels and up-regulated by water deficit conditions. *Plant Mol. Biol.* 40, 1073–1083. doi: 10.1023/a:1006267013170

Sultan, B., Defrance, D., and Iizumi, T. (2019). Evidence of crop production losses in West Africa due to historical global warming in two crop models. *Sci. Rep.* 9, 12834. doi: 10.1038/s41598-019-49167-0

Sun, Q., Miao, C., Hanel, M., Borthwick, A. G. L., Duan, Q., Ji, D., et al. (2019). Global heat stress on health, wildfires, and agricultural crops under different levels of climate warming. *Environ. Int.* 128, 125–136.10 doi: 10.1016/j.envint.2019.04.025

Sun, Y., Zhou, J., and Guo, J. (2021). Advances in the knowledge of adaptive mechanisms mediating abiotic stress responses in *Camellia sinensis*. *Front. Biosci. (Landmark Ed)* 26, 1714–1722. doi: 10.52586/5063

Tian, N., Liu, F., Wang, P., Yan, X., Gao, H., and Zeng, X. (2018). Overexpression of BraLTP2, a lipid transfer protein of *Brassica napus*, results in increased trichome density and altered concentration of secondary metabolites. *Int. J. Mol. Sci.* 19, 1733. doi: 10.3390/ijms19061733

Toledo-Ortiz, G., Huq, E., and Quail, P. H. (2003). The *Arabidopsis* basic/helix-loop-helix transcription factor family. *Plant Cell* 15, 1749–1770. doi: 10.1105/tpc.013839

Vollbrecht, E., Veit, B., Sinha, N., and Hake, S. (1991). The developmental gene knotted-1 is a member of a maize homeobox gene family. *Nature* 350, 241–243. doi: 10.1038/350241a0

Wang, G., Cai, G., Kong, F., Deng, Y., Ma, N., and Meng, Q. (2014). Overexpression of tomato chloroplast-targeted DnaJ protein enhances tolerance to drought stress and resistance to *Pseudomonas solanacearum* in transgenic tobacco. *Plant Physiol. Biochem.* 82, 95–104. doi: 10.1016/j.plaphy.2014.05.011

Wang, X., Wu, Z., Zhou, Q., Wang, X., Song, S., and Dong, S. (2021). Physiological response of soybean plants to water deficit. *Front. Plant Sci.* 12. doi: 10.3389/fpls.2021.809692

Wani, S. H., Anand, S., Singh, B., Bohra, A., and Joshi, R. (2021). WRKY transcription factors and plant defense responses: Latest discoveries and future prospects. *Plant Cell Rep.* 40, 1071–1085. doi: 10.1007/s00299-021-02691-8

Yang, S., de Haan, M., Mayer, J., Janacek, D. P., Hammes, U. Z., and Poppenberger, B. (2022). A novel chemical inhibitor of polar auxin transport promotes shoot regeneration by local enhancement of HD-ZIP III transcription. *New Phytol.* 235, 1111–1128. doi: 10.1111/nph.1819

Zhang, T., Li, Z., Li, D., Li, C., Wei, D., Li, S., et al. (2020). Comparative effects of glycinebetaine on the thermotolerance in codA- and BADH-transgenic tomato plants under high temperature stress. *Plant Cell Rep.* 39, 1525–1538. doi: 10.1007/s00299-020-02581-5

Zhao, P., Cui, R., Xu, P., Wu, J., Mao, J. L., Chen, Y., et al. (2017). ATHB17 enhances stress tolerance by coordinating photosynthesis associated nuclear gene and ATSIG5 expression in response to abiotic stress. *Sci. Rep.* 7, 45492. doi: 10.1038/srep45492

Zhao, S., Gao, H., Jia, X., Wei, J., Mao, K., and Ma, F. (2021). MdHB-7 regulates water use efficiency in transgenic apple (*Malus domestica*) under long-term moderate water deficit. *Front. Plant Sci.* 12. doi: 10.3389/fpls.2021.740492

Zhao, H., Liu, H., Jin, J., Ma, X., and Li, K. (2022). Physiological and transcriptome analysis on diploid and polyploid *Populus ussuriensis* kom. under salt stress. *Int. J. Mol. Sci.* 23, 7529. doi: 10.3390/ijms23147529

Zhao, Y., Ma, Q., Jin, X., Peng, X., Liu, J., Deng, L., et al. (2014). A novel maize homeodomain-leucine zipper (HD-zip) I gene, Zmhdz10, positively regulates drought and salt tolerance in both rice and *Arabidopsis*. *Plant Cell Physiol.* 55, 1142–1156. doi: 10.1093/pcp/pcu054

frontiers | Frontiers in Plant Science

TYPE Original Research
PUBLISHED 14 November 2022
DOI 10.3389/fpls.2022.1043204

Check for updates

OPEN ACCESS

EDITED BY
Mohammad Golam Mostofa,
Michigan State University,
United States

REVIEWED BY
Shaojun Dai,
Shanghai Normal University, China
Maksymilian Zienkiewicz,
University of Warsaw, Poland

*CORRESPONDENCE
Xuwu Sun
sunxuwussd@sina.com

†These authors have contributed equally to this work

SPECIALTY SECTION
This article was submitted to Plant Abiotic Stress, a section of the journal Frontiers in Plant Science

RECEIVED 13 September 2022
ACCEPTED 18 October 2022
PUBLISHED 14 November 2022

CITATION
Bawa G, Liu Z, Wu R, Zhou Y, Liu H, Sun S, Liu Y, Qin A, Yu X, Zhao Z, Yang J, Hu M and Sun X (2022) PIN1 regulates epidermal cells development under drought and salt stress using single-cell analysis.
Front. Plant Sci. 13:1043204.
doi: 10.3389/fpls.2022.1043204

COPYRIGHT
© 2022 Bawa, Liu, Wu, Zhou, Liu, Sun, Liu, Qin, Yu, Zhao, Yang, Hu and Sun. This is an open-access article distributed under the terms of the Creative Commons Attribution License (CC BY). The use, distribution or reproduction in other forums is permitted, provided the original author(s) and the copyright owner(s) are credited and that the original publication in this journal is cited, in accordance with accepted academic practice. No use, distribution or reproduction is permitted which does not comply with these terms.

PIN1 regulates epidermal cells development under drought and salt stress using single-cell analysis

George Bawa†, Zhixin Liu†, Rui Wu†, Yaping Zhou, Hao Liu, Susu Sun, Yumeng Liu, Aizhi Qin, Xiaole Yu, Zihao Zhao, Jincheng Yang, Mengke Hu and Xuwu Sun*

State Key Laboratory of Cotton Biology, Key Laboratory of Plant Stress Biology, School of Life Sciences, Henan University, Kaifeng, China

Over the course of evolution, plants have developed plasticity to acclimate to environmental stresses such as drought and salt stress. These plant adaptation measures involve the activation of cascades of molecular networks involved in stress perception, signal transduction and the expression of stress related genes. Here, we investigated the role of the plasma membrane-localized transporter of auxin PINFORMED1 (PIN1) in the regulation of pavement cells (PCs) and guard cells (GCs) development under drought and salt stress conditions. The results showed that drought and salt stress treatment affected the development of PCs and GCs. Further analysis identified the different regulation mechanisms of PIN1 in regulating the developmental patterns of PCs and GCs under drought and salt stress conditions. Drought and salt stress also regulated the expression dynamics of PIN1 in *pif1/3/4/5* quadruple mutants. Collectively, we revealed that PIN1 plays a crucial role in regulating plant epidermal cells development under drought and salt stress conditions, thus contributing to developmental rebustness and plasticity.

KEYWORDS

abiotic stress, arabidopsis, epidermal cells, leaf development, PINFORMED1

Introduction

As a result of global warming and possible climate anomalies, plants often encounter a high level of biotic and abiotic stresses, which engage them in challenging moments that affect their survival and yield (Ramegowda and Senthil-Kumar, 2015; Wang et al., 2021b). During such conditions, plants tend to fine-tune their developmental process and environmental response *via* changes in several transcriptional and metabolic programs (Sun et al., 2007; Sun et al., 2010; Meng et al., 2016; Bawa et al., 2019; Guo et al., 2019;

Tang et al., 2019; Sun et al., 2020; Li et al., 2021; Zhou et al., 2021; Liu et al., 2022b; Mostofa et al., 2022; Wu et al., 2022a; Yeshi et al., 2022). For example, drought and salt stress regulate plant growth and development (Li et al., 2016; Devkar et al., 2020; Zelm et al., 2020; Zhang et al., 2020; Karimi et al., 2021; Zhang et al., 2022), and a large number of plants respond to drought stress *via* reducing water loss through stomatal closure (Daszkowska-Golec and Szarejko, 2013; Pirasteh-Anosheh et al., 2016) as well as decreasing rate of leaf expansion under salt stress condition (Rasool et al., 2013; Muchate et al., 2016; Ullah et al., 2020). Drought and salt stress induce osmotic stress, limiting plant normal functions and developmental process, and tolerance to these stresses by plants is of major concern to current agriculture development. Several studies have identified the effects of drought and salt stress on the development and function of plant leaves (Sinha et al., 2016; Ji et al., 2018; Yang and Guo, 2018; López-Serrano et al., 2019; Devkar et al., 2020; Chowdhury et al., 2021). The plant cell wall promotes or impedes plant growth development depending on its mechanical properties, as it often responds to external stimuli, which regulate cell or tissue morphology (Cosgrove, 2017; Sampathkumar, 2020). Many studies have established the link between the development of leaf epidermal cells and leaf morphology (Ferreira et al., 2017; Fujiwara et al., 2018; Zhu et al., 2019). Leaf epidermis plays several key functions including regulating the exchange of gases, water, and nutrients with the surroundings (Zuch et al., 2021). However, the development and function of leaf epidermal cells, such as pavement cells (PCs) and guard cells (GCs), are sometimes disrupted by external environmental factors (Kebbas et al., 2015; Dong et al., 2018; Liu et al., 2022b).

The role of phytohormone's response to drought and salt stress has been well studied (Ullah et al., 2018; Jalil and Ansari, 2019; Yu et al., 2020; Rehman et al., 2021), among which auxin is a critical hormone (Pandey et al., 2019; Ribba et al., 2020) in the regulation of plant leaf formation (Reinhardt et al., 2003). Interestingly, in the plant epidermal cells, the plasma membrane-localized transporter of auxin PINFORMED1 (PIN1) is the main efflux transporter of auxin that controls the formation and development of leaves and flowers (Reinhardt et al., 2003; Heisler et al., 2005; Heisler et al., 2010). Also, auxin is involved in the regulation of cell polarization, such as the polar distribution of the auxin efflux PIN1 proteins to the plasma membrane and the regulation of root hair initiation areas in the root epidermal cells (Fischer et al., 2006; Dhonukshe et al., 2008); hence it is not surprising that PIN1 regulates the development of leaves in response to auxin signaling (Li et al., 2011; Adamowski and Friml, 2015; Xiong and Jiao, 2019). While the plasticity of plant morphological traits, such as leaf vein pattern development has been linked with varying auxin distribution resulting from changes in PIN1 protein localization (Dhakal et al., 2021), no mechanism has yet been proposed for the role of PIN1 in PCs and GCs development under drought and salt stress conditions.

To study the mechanism of epidermal cells development under drought and salt stress, we previously identified the role of *PHYTOCHROME INTERACTING FACTOR (PIF) 1*, *PIF3*, *PIF4*, and *PIF5* genes in PCs and GCs development under drought and salt stress conditions using single-cell RNA-seq analysis (Wu et al., 2022b). However, the mechanism underlying the role of PIN1 in PCs and GCs development under drought and salt stress conditions required further exploration. In the current study, we investigated the role of PIN1 in epidermal cells' response to drought and salt stress. These results demonstrate that PIN1 is critical in regulating the developmental response of PCs and GCs to drought and salt stress.

Materials and methods

Plant materials and growth conditions

Wild type (WT) Arabidopsis (Arabidopsis thaliana) Columbia ecotype (Col-0) was used in this study. The *pif1 pif3 pif4 pif5* quadruple mutant (*pif1-1*, *pif3-7*, *pif4-2*, *pif5-3*), *PIN1pro*:GUS, *pin1-5*, and *35S::PIN1* were obtained from the Arabidopsis Biological Resource Center (ABRC). All mutants and WT Arabidopsis were grown in an artificial climate chamber under the growth conditions of 21-23 ℃, 100 μmol photons $m^{-2}s^{-1}$ (normal light treatment), 16 h light/8 h dark and 60%-70% humidity. For NaCl and Mannitol treatments, the seedlings were grown on 1/2MS medium plates containing 100 mM NaCl or 150 mM Mannitol for 1-7 days.

GUS staining and histological analysis

Histochemical GUS staining was performed as previously described (Liu et al., 2022b). Samples were fixed in 90% acetone at –20°C, rinsed four times with 0.1M sodium phosphate buffer (pH 7.4), and then incubated in X-Gluc solution [0.1M sodium phosphate (pH 7.4), 3 mM potassium ferricyanide, 0.5 mM potassium ferrocyanide, 0.5 g l^{-1} 5-bromo-4-chloro-3-indolyl-β-d-glucuronide cyclohexilammonium salt] at 37°C. After staining, samples were incubated in methanol to remove chlorophyll and then mounted in the clearing solution (a mixture of chloral hydrate, water, and glycerol in a ratio of 8:2:1). Observation was performed using a stereomicroscope (MZ16F, Leica Microsystems, Germany) or a microscope equipped with Nomarski optics (BX51, Olympus Co., Tokyo, Japan).

Confocal microscopy

The seedlings were stained with 10 g/mL Propidium (PI) (Sigma) for 1 min before imaging. For confocal microscopy,

fluorescence in roots was detected using a confocal laser scanning microscope (Zeiss, LSM980). PI signal was visualized using wavelengths of 610 to 630 nm.

Identification of the genes highly expressed in the corresponding cell type

The average expression and dispersion were briefly calculated for all genes, which were subsequently placed into 9 bins based on expression. Principal component analysis (PCA) was performed to reduce the dimensionality on the log-transformed gene-barcode matrices of the most variable genes. Cells were clustered *via* a graph-based approach and visualized in two dimensions using t-distributed stochastic neighbor embedding (tSNE). A likelihood ratio test, which simultaneously tests for changes in mean expression and percentage of cells expressing a gene, was used to identify significantly differentially expressed genes (DEGs) between clusters. We used the FindAllMarkers function (test.use = bimod, logfc.thresold = 0, min.pct = 0.25) in Seurat to identify DEGs of each cluster. For a given cluster, FindAllMarkers identified positive markers compared with all other cells.

Total RNA extraction and qPCR analysis

Total RNA was extracted with FastPure Plant Total RNA Extraction kit (Cat. No. DC104, Vazyme; Nanjing, China). Total RNA was treated with DNaseI (Vazyme; Nanjing, China) for 30 min to remove the remaining DNA; then the cDNA was synthesized with HiScript II One-Step RT-PCR Kit (Cat. No. P611, Vazyme; Nanjing, China); qRT-PCR was performed with the corresponding primers (Supplemental Table 1). qPCR run was performed on a CFX 96 (Bio-Rad, Herculesm, CA, USA) with the following cycle parameter: 95°C for 30 s, 35 cycles of 95°C for 30 s, 55–56°C for 15 s and 72°C for 15s.

Results

Analysis of the expression of PIN1 in different cell types by scRNA-seq

To determine the possible regulators of PCs and GCs development under drought and salt stress, we first determined the cell types based on previously produced scRNA-seq data (Wu et al., 2022b). The following cell types, PC, guard mother cell (GMC), GC, meristemoid mother cell (MMC), early stage meristemoid (EM), late stage meristemoid (LM), young guard cell (YGC), and mesophyll cell (MPC) were identified based on the known marker genes for the corresponding cell type. A cell cluster without a known marker gene was annotated as unknown (u.k.). We screened the DEGs in the corresponding cell types. During the analysis of the expression patterns of the DEGs, we found that *PIN1* was highly expressed in PC and stomatal lineage cell populations, such as MPC, LM, and EM (Figure 1), indicating PIN1's role in the development of PCs and GCs.

Detection of the specific expression of pif1/3/4/5 in epidermal cells

In order to analyze the temporal and spatial expression dynamics of *PIN1* under normal, drought, and salt treatment conditions, we used transgenic plants expressing *PIN1pro:GUS* and observed the expression changes of *PIN1* at day 1, 3, 5 and 6 by GUS staining. As shown in Figure 2A, under normal growth conditions, there was no significant change in the expression level of *PIN1pro:GUS* in whole cotyledons from day 1 to day 6. Under NaCl treatment conditions, compared with the control, the GUS signal of *PIN1pro: GUS* in whole cotyledon was significantly decreased on day 5, and there was no significant change on the sixth day. Under mannitol treatment conditions, the GUS signal of *PIN1pro:GUS* increased gradually with treatment time. Compared with the control group, the GUS signal of *PIN1pro:GUS* in the cotyledons of day 5 was significantly decreased, and the GUS signal of *PIN1pro:GUS* in the cotyledons of day 6 was not significantly changed, while the GUS signal of *PIN1pro:GUS* was significantly enhanced in the veins of the cotyledons (Figure 2A). These results indicated that NaCl and mannitol treatment inhibited the expression of *PIN1pro:GUS* in cotyledons on day 5 before germination and promoted the expression of *PIN1pro:GUS* in vein (Figure 2A).

The expression of *PIN1* in *pif1/3/4/5* quadruple mutant under NaCl and mannitol treatment conditions was analyzed by q-PCR. Compared with the control group, NaCl treatment significantly down-regulated the expression of *PIN1* in *pif1/3/4/5* quadruple mutant, but there was no significant change in WT plants (Figure 2B). At the same time, mannitol treatment also reduced *PIN1* expression in WT and *pif1/3/4/5* quadruple mutant compared with the control group (Figure 2B). Under mannitol treatment conditions, the levels of *PIN1* in *pif1/3/4/5* quadruple mutant on day 1 were significantly higher than WT (Figure 2B). Over time, the levels of *PIN1* in *pif1/3/4/5* quadruple mutant were gradually lower than WT (Figure 2B).

Drought and salt stress affect the development of leaf morphology

In order to analyze the potential role of PIN1 in regulating plant leaves under drought and salt stress, we analyzed the development of seedlings of *pin1-5* mutant and *35S::PIN1*, the WT was used as control. As shown in Figure 3A, compared with

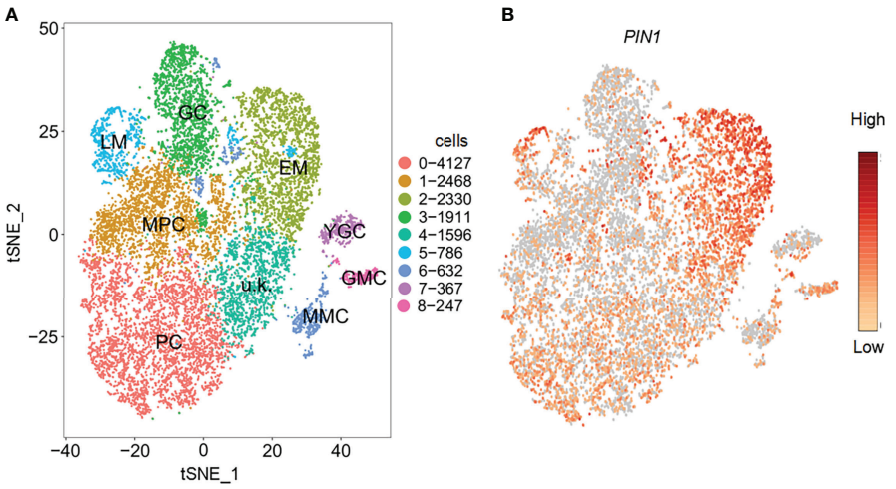

FIGURE 1
Identification of cell types with representative marker genes. **(A)** Distribution of cell types on tSNE plot; corresponding cell types are annotated on the plot. **(B)** Feature plot showing the expression pattern of *PIN1*. PC, pavement cell; GMC, guard mother cell; GC, guard cell; MMC, meristemoid mother cell; EM, early stage meristemoid; LM, late stage meristemoid; YGC, young guard cell; MPC, mesophyll cell; u.k., unknown.

WT, *pin1-5* mutant seedlings under normal growth conditions had significantly shorter petioles and a higher leaf length–width (L–W) ratio. Under normal conditions, the leaf development of *35S::PIN1* seedlings was slow in the early stage and faster in the late stage. Between days 7 and 14 after treatment, the leaf area of WT seedlings increased 2 times; the *pin1-5* mutant increased 1.2 times, while the *35S::PIN1* increased 4.5 times. Under NaCl treatment conditions, petiole length of WT was significantly shortened, and L-W ratio of leaves was also decreased (Figures 3A, B). Compared with the WT, under drought and NaCl treatment conditions, the leaf area and petiole length of *pin1-5* mutant was significantly shortened, while the ratio of L–W was significantly increased. The petiole length of the *35S::PIN1* was significantly lower than that of WT, while the L–W ratio was significantly higher than that of WT after 7 days of stress treatment (Figure 3B).

PIN1 is involved in regulating the developmental patterns of GC and PC

To understand the role of PIN1 in the development of PC and GC, we analyzed the developmental dynamics of PC and GC in seedlings of *pin1-5* mutant, *35S::PIN1* and WT during early seedling development. As shown in Figures 4A, C, compared with the WT, the growth rate that was characterized by the roots length of *pin1-5* mutant seedlings was faster than that of WT, but the subsequent growth was slower under normal conditions. The germination and subsequent growth of *35S::PIN1* seedlings were slower than that of WT. Figure 2B shows the development of PCs and GCs along with the growth time from day 1 to day 7. Statistical analysis showed that in WT, the size of PCs increased rapidly from day 1 to day 7, leading to a gradual decrease in the intensity of PCs (Figures 4D, E). Compared with WT, the size of PCs of *pin1-5* mutant showed a similar growth trend to WT from day 1 to day 5, but after day 5, the size of PCs was smaller than WT, resulting in a slightly higher intensity of PCs in *pin1-5* mutant than WT (Figures 4D, E). The trend of the size of PCs in *35S::PIN1* was similar to that of *pin1-5* mutant, and the overall size of PCs was smaller than in WT, so the intensity of PCs per unit area was higher than in WT (Figures 4D, E). The intensity of GCs per unit area in WT increased rapidly until day 4 before decreasing (Figure 4F). Compared with WT, the intensity of GCs per unit area of *pin1-5* mutant was slightly lower, while the intensity of GCs per unit area of *35S::PIN1* was higher (Figure 4F).

Drought and salt stress regulate the developmental patterns of GCs and PCs through PIN1

To analyze whether PIN1 was also involved in regulating the differentiation and development of PCs and GCs under NaCl and drought conditions, we analyzed the growth, development and differentiation dynamics of WT, *pin1-5* mutant and *35S::PIN1* seedlings. As shown in Figures 5A, C, *pin1-5* mutant and *35S::PIN1* seedlings' growth was slightly slower than WT from day 1 to day 7 under NaCl treatment conditions. Figure 5B shows the developmental dynamics of PCs and GCs in WT, *pin1-5* mutant and *35S::PIN1* seedlings from day 1 to day 7 under NaCl treatment conditions. Statistical analysis showed that under NaCl treatment conditions, the size of PCs in WT

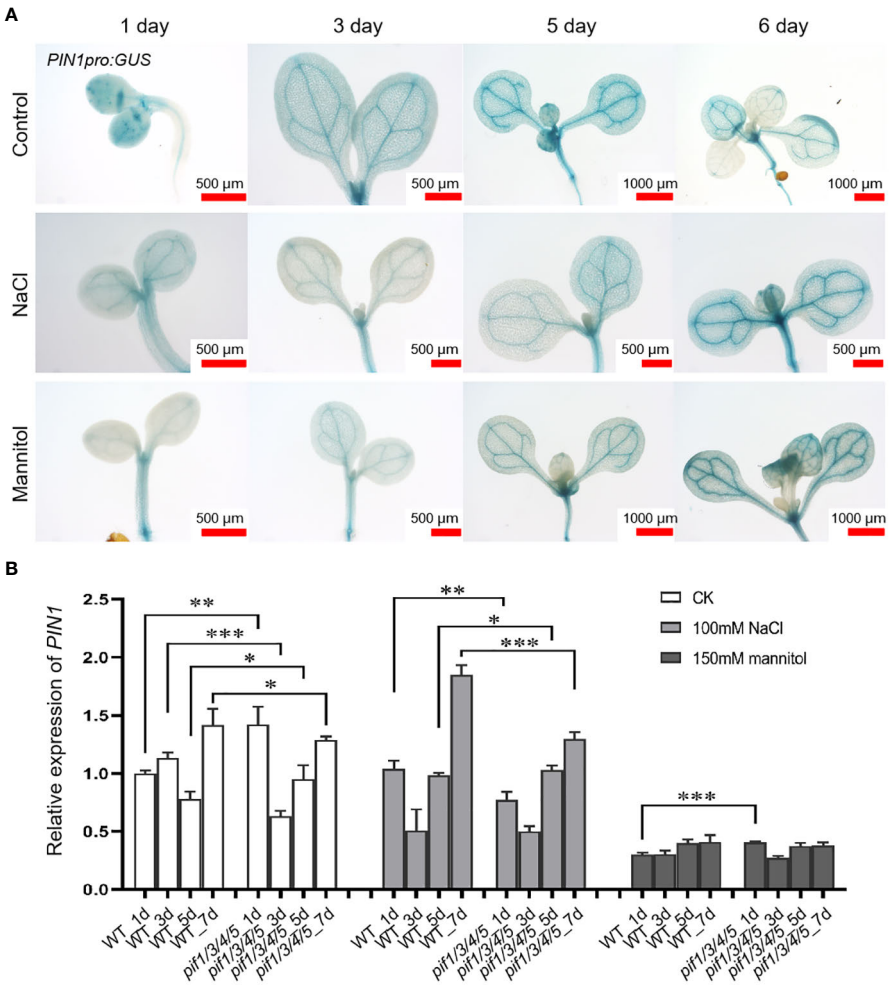

FIGURE 2
Analysis of the expression of *PIN1pro: GUS* and PIN1 gene after being treated with NaCl and mannitol. **(A)** Analysis of the expression of *PIN1pro: GUS* in whole cotyledons (up panel) during the development of seedlings grown under control, NaCl, and mannitol conditions, respectively. The seedlings of *PIN1pro:GUS* were grown in 1/2 MS plates plus 100 mM NaCl or 150 mM mannitol for 1, 3, 5, and 6 days, respectively; the seedlings of *PIN1pro:GUS* grown in normal 1/2 MS plates were used as controls. Then the seedlings were harvested and used for detecting the GUS activities by GUS staining, as described in Materials and Methods. **(B)** qPCR analysis of the relative expression of *PIN1* under control, NaCl, and mannitol conditions, respectively. Relative expression indicates the mean value (± SD) of three independent experiments. The black stars represent student's t-test of pif1/3/4/5 vs WT. *p < 0.05; **p < 0.01; ***p < 0.001.

seedlings increased gradually from day 1 to day 6 (Figure 5D), and the intensity of PCs in WT decreased continuously from day 1 to day 7 (Figure 5E). The changing trend of size and intensity of PCs in seedlings of *pin1-5* mutant was similar to that of WT (Figures 5D, E). However, the size of PCs in *35S::PIN1* seedlings increased slowly from day 1 to day 7, and was lower than WT (Figures 5D, E). The intensity of PCs in *35S::PIN1* seedlings was always higher than WT (Figures 5D, E).

Analysis of the intensity of GCs showed that under NaCl treatment conditions, the intensity of GCs in WT increased rapidly from day 1 to day 3 and gradually decreased from day 3 until day 7 (Figure 5F). Compared with WT, the intensity of GCs in *pin1-5* mutant seedlings had little change and began to stabilize after day 4. The intensity of GCs in *35S::PIN1* seedlings showed a rapid increase from day 1 to day 2 and then gradually decreased from day 2 to day 7 (Figure 5F).

Compared with the control group, the growth of WT, *pin1-5* mutant, and *35S::PIN1* seedlings was significantly inhibited under mannitol treatment conditions, and the growth rate of *pin1-5* mutant and *35S::PIN1* seedlings was significantly slower than that of WT (Figures 6A, C). Compared with WT, under mannitol treatment conditions, the germination rate of *pin1-5* mutant seedlings was faster, but the subsequent growth rate was slower. Both germination and growth of the *35S::PIN1* were inhibited (Figure 6A). Under mannitol treatment conditions, the size of PCs in WT seedlings increased gradually from day 1 to

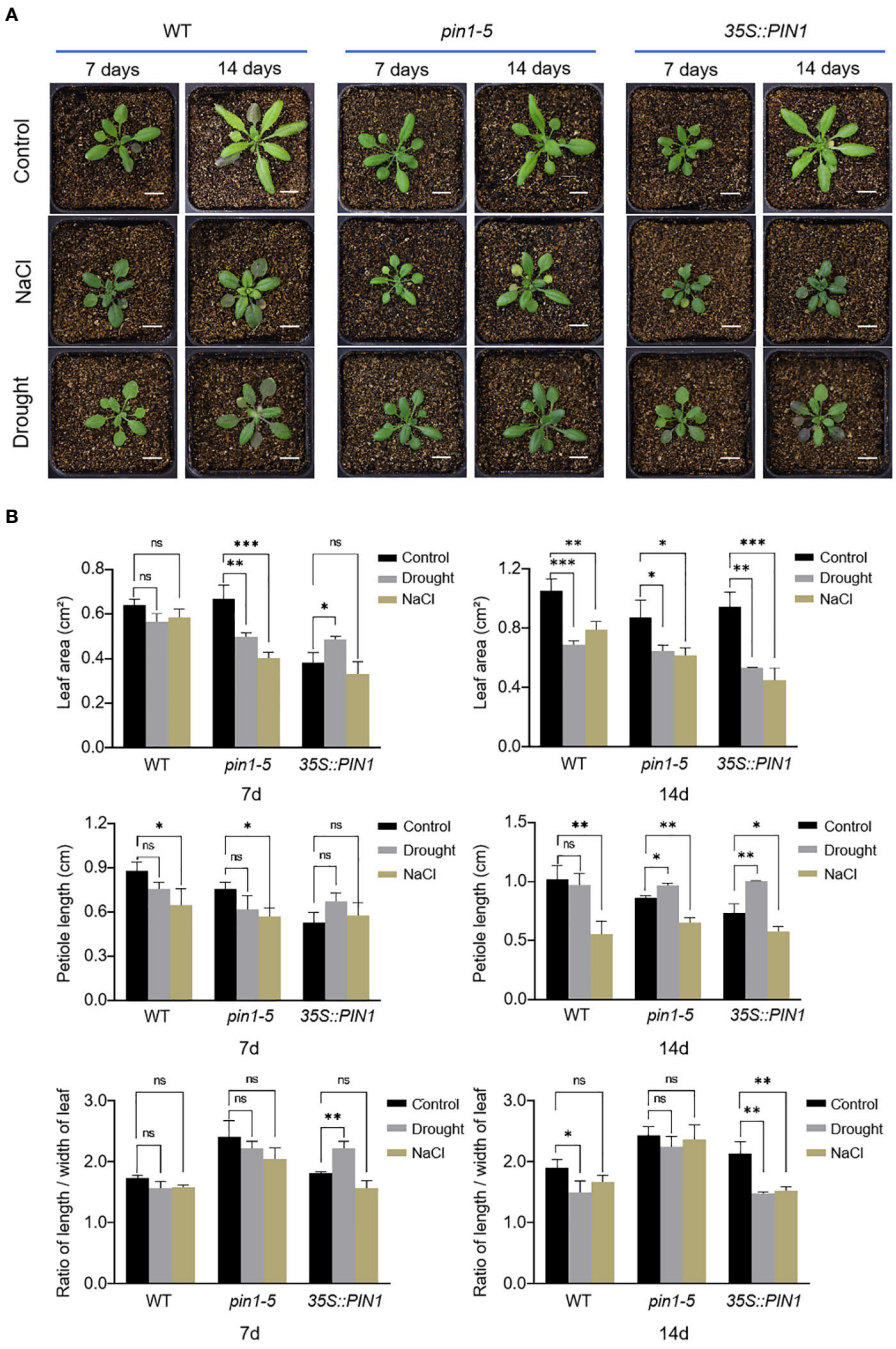

FIGURE 3
The leaves' shape changes in response to NaCl and drought stresses. **(A)** *pin1-5*, *35S::PIN1* and WT were grown in soil for drought and NaCl treatment for 7 days and 14 days, respectively; the growth phenotypes were recorded by a camera; untreated seedlings were used as controls. Scale bar: 1 cm. **(B)** Statistical analysis of leaf area, petiole length and ratio of length/width of leaf in *pin1-5*, *35S::PIN1* and WT seeding. The data were analyzed by one-way ANOVA following Brown–Forsythe test. ns: $p > 0.05$; *$p < 0.05$; **$p < 0.01$; ***$p < 0.001$.

day 6 and stabilized on day 7 (Figure 6D). The intensity of PCs showed a gradual decline from day 1 to day 7 (Figure 6E). Compared with WT, the size of PCs in seedlings of *35S::PIN1* increased gradually from day 1 to day 7 under mannitol treatment conditions, and the changing trend of the size of PCs in seedlings of *pin1-5* mutant was similar to WT (Figure 6D). The intensity of PCs in seedlings of WT, *pin1-5* mutant, and *35S::PIN1* showed an opposite trend with the area of PCs (Figures 6D, E). Overall, the intensity of PCs in seedlings of *35S::PIN1* was significantly higher than WT, while the

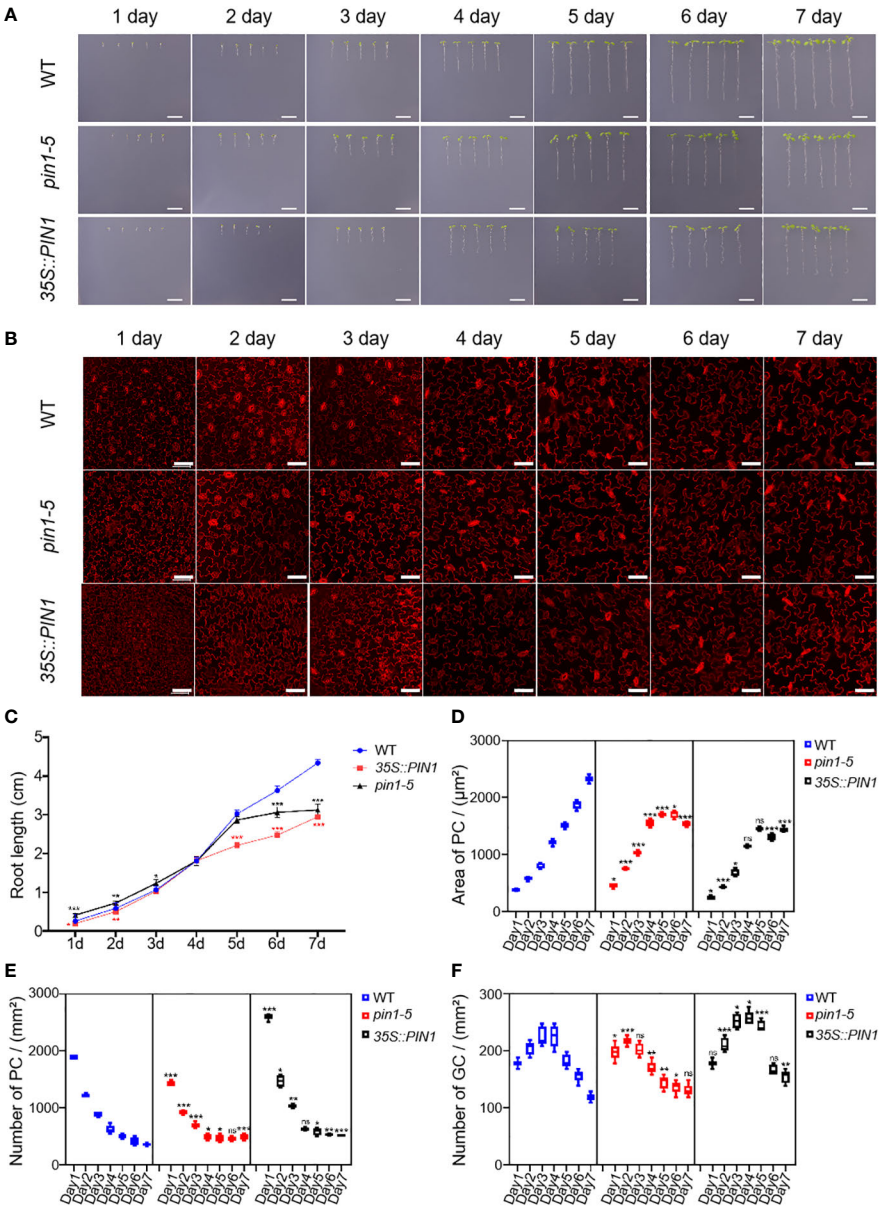

FIGURE 4
Pavement cells (PCs) and guard cells (GCs) development analysis of *pin1-5*, *35S::PIN1*, and WT under normal conditions. Analysis of the growth of *pin1-5*, *35S::PIN1* and WT under control conditions. **(A)** The seeding of *pin1-5*, *35S::PIN1* and WT were grown on 1/2MS medium for 7 days. The seedlings born 1-7 were photographed continuously by a camera to record their developmental and growth phenotypes. Untreated seedlings were used as controls. Scale bar: 1 cm. **(B)** The development of PC and GC was measured under the following conditions: *pin1-5*, *35S::PIN1* and WT seedlings were cultured in 1/2 MS medium for 1-7 days, then harvested and stained with propyl chloride (PI) for 30 min to stain the membrane. After PI staining, PC and GC's were detected under a confocal laser microscope. Scale bar: 50 μm. **(C)** Statistical analysis of the root length of seedlings of *pin1-5*, *35S::PIN1* and WT (n = 5). **(D)** Statistical analysis of the size of PCs in the lower epidermis of cotyledons of seedlings of *pin1-5*, *35S::PIN1* and WT (n = 5). **(E)** Statistical analysis of the intensity of PCs in the lower epidermis of cotyledons of seedlings of *pin1-5*, *35S::PIN1* and WT (n = 5). **(F)** Statistical analysis of the intensity of GCs in the lower epidermis of cotyledons of seedlings of *pin1-5*, *35S::PIN1* and WT (n = 5). The data were analyzed by one-way ANOVA following Brown–Forsythe test. ns: $p > 0.05$; *$p < 0.05$; **$p < 0.01$; ***$p < 0.001$.

intensity of PCs in seedlings of *pin1-5* was lower than WT (Figure 6E).

From day 1 to day 4, the intensity of GCs in WT seedlings gradually increased and began to decrease after day 4 (Figure 6F). Compared with WT, under mannitol treatment conditions, the intensity of GCs in *pin1-5* mutant and *35S::PIN1* seedlings showed the same trend, gradually increasing from day 1 to day 4 (Figure 6E). In general, the intensity of GCs in *pin1-5*

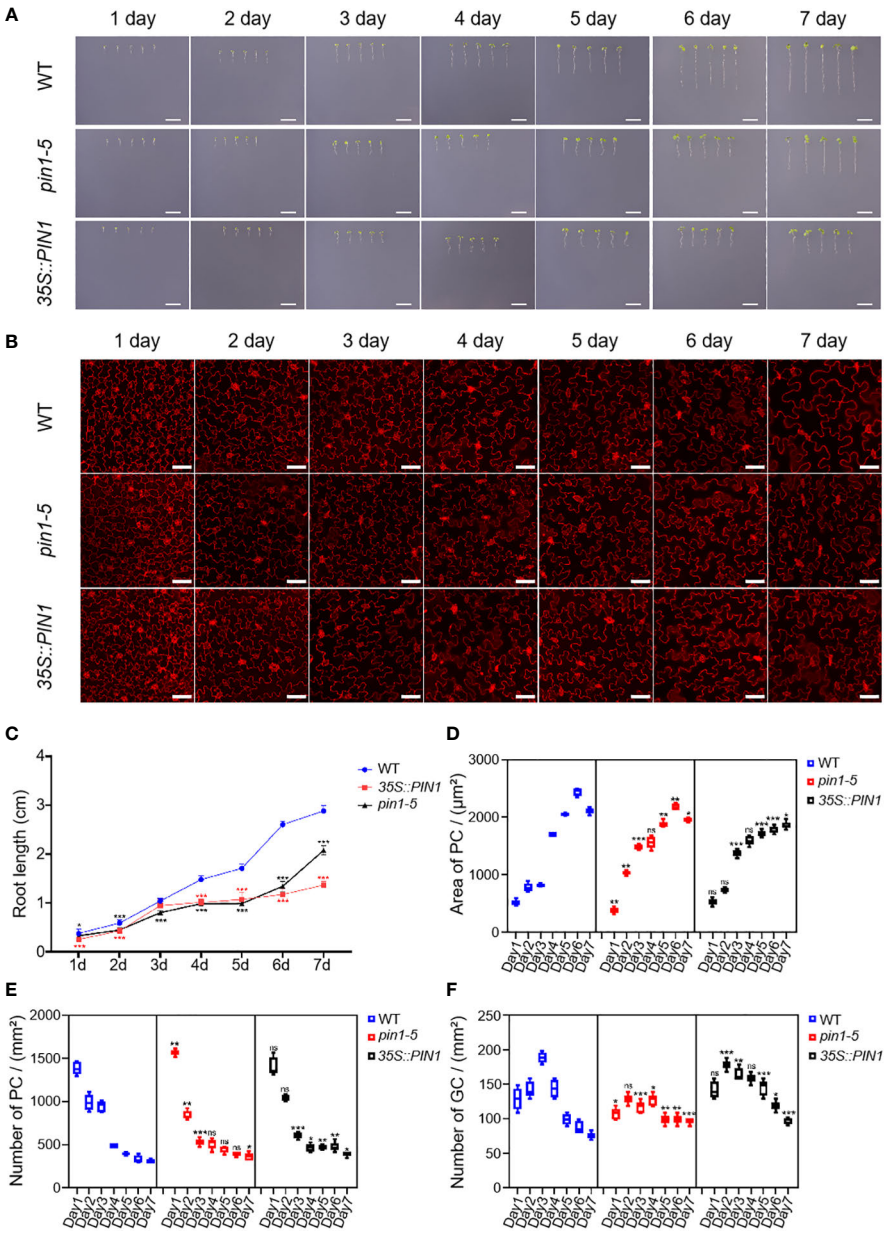

FIGURE 5
Analysis of PC and GC development in *pin1-5*, *35S::PIN1* and WT under NaCl conditions. Analysis of the growth of *pin1-5*, *35S::PIN1* and WT under control conditions. **(A)** The seeding of *pin1-5*, *35S::PIN1* and WT were grown in 1/2 MS plates plus 100 mM NaCl for 7 days. The seedlings grown for 1~7 days were photographed continuously by a camera to record their developmental and growth phenotypes, and untreated seedlings were used as controls. Scale bar: 1 cm. **(B)** The development of PC and GC was measured under the following conditions: *pin1-5*, *35S::PIN1* and WT seedlings were grown in 1/2 MS plates plus 100 mM NaCl for 1~7 days, then harvested and stained with PI for 30 min to stain the membrane. After PI staining, PC and GC's were detected under a confocal laser microscope. Scale bar: 50 μm. **(C)** Statistical analysis of the root length of seedlings of *pin1-5*, *35S::PIN1* and WT (n = 5). **(D)** Statistical analysis of the size of PCs in the lower epidermis of cotyledons of seedlings of *pin1-5*, *35S::PIN1* and WT (n = 5). **(E)** Statistical analysis of the intensity of PCs in the lower epidermis of cotyledons of seedlings of *pin1-5*, *35S::PIN1* and WT (n = 5). **(F)** Statistical analysis of the intensity of GCs in the lower epidermis of cotyledons of seedlings of *pin1-5*, *35S::PIN1* and WT (n = 5). The data were analyzed by one-way ANOVA following Brown–Forsythe test. ns: $p > 0.05$; *$p < 0.05$; **$p < 0.01$; ***$p < 0.001$.

mutant and *35S::PIN1* seedlings was significantly lower than that in WT (Figure 6E).

Considering the defects in stomatal development caused by NaCl and mannitol treatment, it may be that these treatments influenced cotyledon development and altered the expression of *ROP1*, *ROP2*, *RIC1*, *RIC4*, *ERH3* and *CLASP*. To analyze the effects of drought and salt stress on cotyledon development, we analyzed the cotyledon development of WT, *pin1-5* mutant and

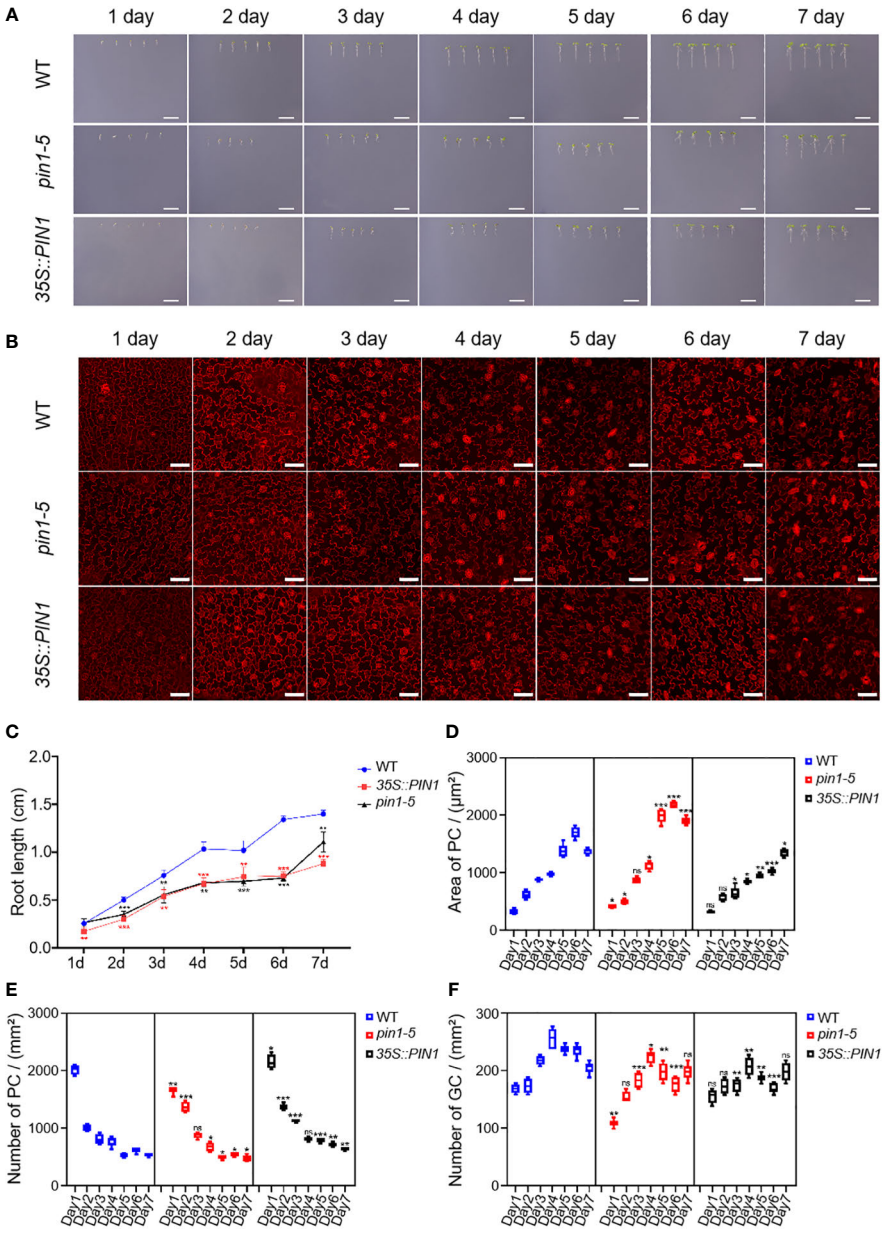

FIGURE 6
Analysis of PC and GC development in *pin1-5*, *35S::PIN1* and WT under drought conditions. Analysis of the growth of *pin1-5*, *35S::PIN1* and WT under control conditions. **(A)** The seeding of *pin1-5*, *35S::PIN1* and WT were grown in 1/2 MS plates plus 150 mM mannitol for 7 days. The seedlings born 1-7 were photographed continuously by a camera to record their developmental and growth phenotypes, and untreated seedlings were used as controls. Scale bar: 1 cm. **(B)** The development of PC and GC was measured under the following conditions: *pin1-5*, *35S::PIN1* and WT seedlings were grown in 1/2 MS plates plus 150 mM mannitol for 1–7 days, then harvested and stained with PI for 30 min to stain the membrane. After PI staining, PC and GC's were detected under a confocal laser microscope. Scale bar: 50 μm. **(C)** Statistical analysis of the root length of seedlings of *pin1-5*, *35S::PIN1* and WT (n = 5). **(D)** Statistical analysis of the size of PCs in the lower epidermis of cotyledons of seedlings of *pin1-5*, *35S::PIN1* and WT (n = 5). **(E)** Statistical analysis of the intensity of PCs in the lower epidermis of cotyledons of seedlings of *pin1-5*, *35S::PIN1* and WT (n = 5). **(F)** Statistical analysis of the intensity of GCs in the lower epidermis of cotyledons of seedlings of *pin1-5*, *35S::PIN1* and WT (n = 5). The data were analyzed by one-way ANOVA following Brown–Forsythe test. ns: $p > 0.05$; *$p < 0.05$; **$p < 0.01$; ***$p < 0.001$.

35S::PIN1 seedlings under control, NaCl and mannitol treatment conditions (Figure 7A). As shown in Figure 7A, compared with WT, *35S::PIN1* seedlings under normal growth conditions had significantly reduced aspect ratio relative to wild-type cotyledons, whereas the *pin1-5* mutant remained similar to the wild type. Under NaCl conditions, the cotyledon aspect ratio of WT increased (Figures 7A, B). Compared with WT, the cotyledon aspect ratio of *pin1-5* mutant and *35S::PIN1* did not

change significantly under mannitol treatment conditions (Figures 7A, B). However, under NaCl treatment conditions, the cotyledon aspect ratio of *pin1-5* mutant and *35S::PIN1* was significantly reduced compared with WT. To examine whether PIN could regulate the expression of *ROP1*, *ROP2*, *RIC1*, *RIC4*, *ERH3* and *CLASP*, qPCR analysis was performed. Compared with the control group, NaCl treatment resulted in significantly up-regulated expressions of *ROP1*, *ROP2*, *RIC4* and *ERH3* in WT but not in *pin1-5* mutant seedlings (Figures 7C, D, F, G). Meanwhile, mannitol treatment enhanced the expression of *ROP1*, *ROP2*, *RIC4*, and *ERH3* in WT and *pin1-5* mutant compared with the control group (Figures 7C, D, F, G). The levels of *ROP1*, *ROP2*, *RIC4* and *ERH3* in the *pin1-5* mutant were also higher than WT under mannitol treatment conditions (Figures 7C, D, F, G). For *RIC1*, compared with the control group, its expression was significantly decreased under NaCl and mannitol treatment conditions (Figure 7E). As for the expression of *CLASP*, it was found that under NaCl and mannitol treatment conditions, its expression in WT, *pin1-5* mutant, and *35S::PIN1* was significantly increased (Figure 7H).

Discussion

Drought and salt stresses affect the developmental pattern of leaf epidermal cells

Plants have developed several mechanisms to respond and adapt to different types of abiotic stress enacted by external environmental factors as part of their evolution. How and where plants sense changes in water levels in the root has been well studied. It has been demonstrated that the PLASMA MEMBRANE INTRINSIC PROTEINS (PIPs), a subfamily of plasma membrane-localized aquaporin channels, enhance water movement in plant roots (Dietrich, 2018). Similarly, in salt stress, phosphatidic acid is a minor membrane phospholipid required for plant growth response to salt stress. Phosphatidic acid binds to PINOID (PID) to promote PID-dependent PIN phosphorylation under salt stress (Wang et al., 2019). But the mechanisms underlying how leaf epidermal cells respond to drought and salt stress require further attention. Leaf development can be controlled by multiple regulatory networks. Environmental factors such as drought and salt stress (Chun et al., 2018; Gambetta et al., 2020) affect plants critical developmental processes, such as leaf development. These unfavorable factors invoke changes in plant growth patterns, regulating cell form and function, which plays a role in plant growth style. Although we previously analyzed the role of PHYTOCHROME INTERACTING FACTOR (PIF) 1, PIF3, PIF4, and PIF5 in PCs and GCs development under drought and salt stress (Liu et al., 2022b), no mechanism has yet been proposed for the role of PIN1 in PCs and GCs development under drought and salt stress conditions. Here, we investigated the role of PIN1 in drought and salt stress regulation of the developmental patterns of PCs and GCs in *Arabidopsis* leaves. The data showed that drought and salt stress highly regulated plant leaf morphology *via* decreased leaf area and petiole length in WT, *pin1-5* mutant and *35S::PIN1* seedlings (Figure 3). In agreement with these findings, several other studies reported on how drought and salt regulate plant physiology and morphology (Bartels and Sunkar, 2005; Ma and Qin, 2014). The functioning and development of these leaves' epidermal cells largely depend on each other. More often, the growth and development of the leaf depend on the conditions of these epidermal cells (Bar and Ori, 2014), suggesting that PCs and GCs developmental dynamics are critical for plant response to drought and salt stress conditions.

PIN1 regulates the development of leaf morphology and epidermal cells under drought and salt stress conditions

Besides biochemical manipulations, mechanical stress induced at the tissue scale influences microtubules to align with the maximal direction of stress, hence regulating cell and tissue level morphogenesis (Hamant et al., 2008; Hervieux et al., 2016; Takatani et al., 2020). Signals from environmental stress induce the expression of temporary regulatory networks, which promotes an overall defense process in plants. A large number of studies have uncovered major genes that regulate leaf epidermal cells development in plants subjected to drought and salt stress (Fricke et al., 2006; Maricle et al., 2009; Taleisnik et al., 2009; Garrido et al., 2014; Zhang et al., 2018; Liu et al., 2022b). This study investigated the role of PIN1 in the development of plant epidermal cells under drought and salt stress. Firstly, we analyzed the developmental dynamics of *pin1-5* mutant, *35S::PIN1* and WT during early seedling development. We observed that the intensity of PCs of *pin1-5* mutant seedlings and *35S::PIN1* seedlings was higher than in WT (Figure 4), while the intensity of GCs of *35S::PIN1* seedlings was higher than in *pin1-5* mutant and WT seedlings (Figure 4). Our previous findings demonstrated that drought and salt stress regulate the developmental patterns of GCs and PCs (Liu et al., 2022b). Meanwhile, how drought and salt stress regulate the differentiation and developmental patterns of GCs and PCs through PIN1 signaling is not determined yet. In Figure 5, we observed that NaCl treatment inhibited the growth of *35S::PIN1* and *pin1-5* mutant seedlings. However, the PC size and number per unit area of *35S::PIN1* seedlings increased more than WT and *pin1-5* mutant seedlings. For GC development under NaCl treatment conditions, we observed that, compared with WT, The intensity of GCs in *35S::PIN1* seedlings showed a rapid increase from day 1 to day 2 and then gradually decreased from day 2 to day 7 (Figure 3), indicating that even during growth inhibition by abiotic stress, plants adaptations to cope with and adapt to these stresses have evolved over time, thus why we observed

10.3389/fpls.2022.1043204

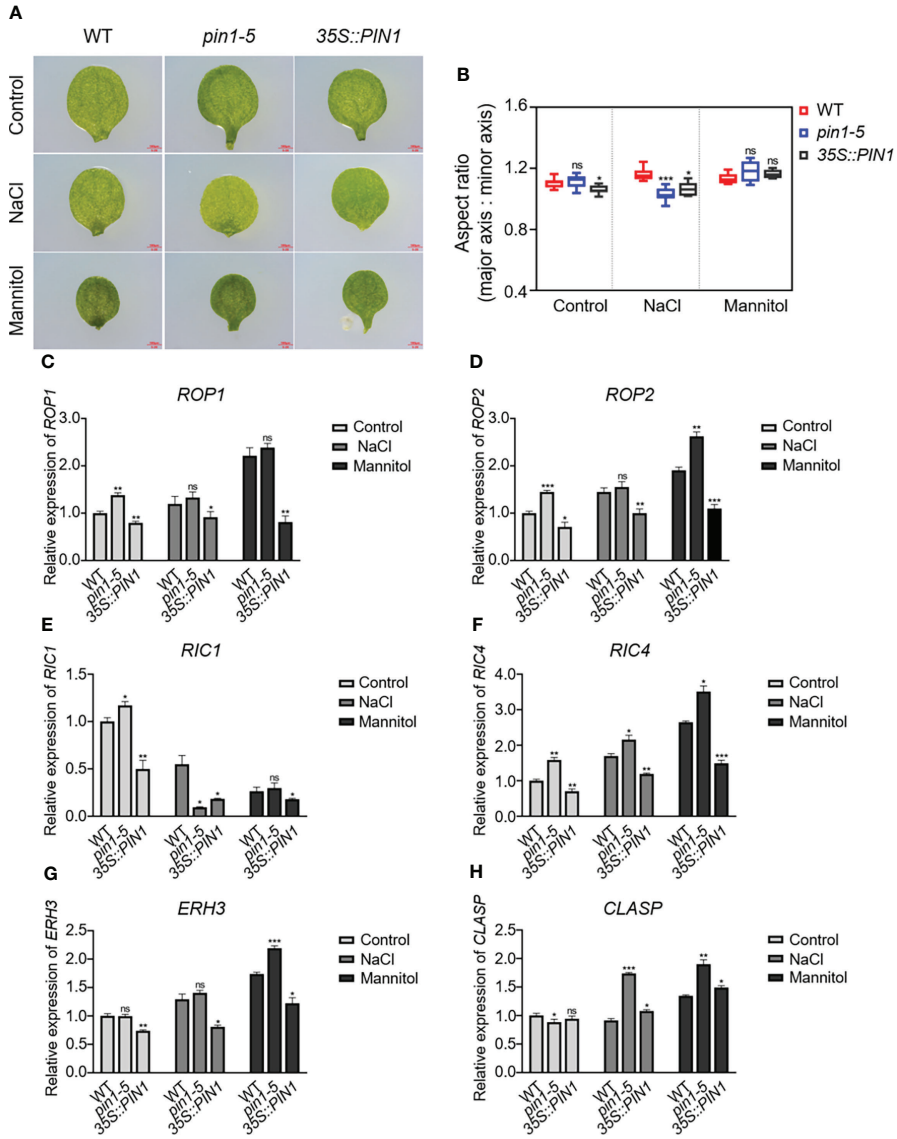

FIGURE 7
Effects of PIN1 on cotyledon morphological development. **(A)** The wild-type (WT) seedlings, *pin1-5* and *35S::PIN1*, were grown in 1/2 MS plates, 1/2 MS plates plus 100 mM NaCl, and 1/2 MS plates plus 150 mM mannitol for 7 days, and the development of cotyledons was observed on micrographs. Scale bars, 0.5 mm. n ≥ 8 cotyledons per genotype. **(B)** Boxplots represent the aspect ratio of WT and mutant cotyledons. **(C-H)** qPCR analysis of the relative expression of *ROP1*, *ROP2*, *RIC1*, *RIC4*, *ERH3*, and *CLASP* under control, NaCl, and mannitol conditions, respectively. Relative expression indicates the mean value (± SD) of three independent experiments. The data were analyzed by one-way ANOVA following Brown–Forsythe test. ns: $p > 0.05$; *$p < 0.05$; **$p < 0.01$; ***$p < 0.001$.

changes in the same organ responding to drought and salt stress, which also suggest that the plasma membrane-localized transporter of auxin PIN1 does not only control the formation and development of flowers and regulation of root hair initiation but also regulate PCs and GCs differentiation and development under salt stress tolerance.

Under mannitol treatment, compared with the control group, the growth of WT, *pin1-5* mutant and *35S::PIN1* seedlings was significantly inhibited. However, compared with WT and *pin1-5* mutant, the size of PCs of *35S::PIN1* seedlings increased. Although the intensity of PCs in WT, *pin1-5* mutant and *35S::PIN1* seedlings showed an opposite trend with the area of PCs, the overall intensity of PCs in *35S::PIN1* seedlings was significantly higher than in WT and *pin1-5* mutant (Figure 6). However, the intensity of GCs in *pin1-5* mutant and *35S::PIN1* seedlings was slightly increased, which highlights the involvement of PIN1 in PCs and GCs differentiation and development under drought stress tolerance.

Several genes involved in signaling and regulatory pathways or enzymes known to alleviate plant stress have been reported (Wang et al., 2003; Kim et al., 2010; Huang et al., 2012; Chen et al., 2021; Wang et al., 2021a; Liu et al., 2022a; Liu et al., 2022b). For example, several genes have been involved in the signaling network mediating cell fate determination of the epidermis and stomatal functioning (Pillitteri and Torii, 2012; Mckown and Bergmann, 2020). In addition, since PIN1 expression and distribution in plants is regulated by the auxin signaling pathway (Chen et al., 2011; Omelyanchuk et al., 2016; Guillory and Bonhomme, 2021), it is possible that PIN1 may regulate PCs and GCs development under drought and salt stress *via* auxin signaling. In Figure 1, using scRNA-seq analysis, we identified that PIN1 was highly expressed in PCs, suggesting a possible function of PIN1 in regulating PCs and GCs development. For further confirmation, we analyzed the temporal and spatial expression dynamics of PIN1 in *pif1/3/4/5* quadruple mutant under normal, drought, and salt treatment conditions using GUS staining and qPCR analysis (Figures 2A, B). The results showed that the expression level of PIN1 in *pif1/3/4/5* quadruple mutant changed under NaCl and mannitol treatments. Compared with the mock, the expression level of PIN1 in *pif1/3/4/5* quadruple mutant was down regulated under NaCl and mannitol treatments (Figure 2B). Together, the results demonstrate how NaCl and mannitol treatments regulate the expression of PIN1 in *pif1/3/4/5* quadruple mutant. Because cotyledon development in plants may be regulated by stomatal functioning, we analyzed the effects of drought and salt stress on cotyledon development. As shown in Figure 7, we observed that NaCl and mannitol treatments significantly regulated the cotyledon aspect ratio of *pin1-5* mutant and *35S::PIN1* seedlings compared to that of WT. We also determined whether PIN could regulate the expression of *ROP1*, *ROP2*, *RIC1*, *RIC4*, *ERH3* and *CLASP* using qPCR analysis. We found that compared to the control group, NaCl and mannitol treatments upregulated the expression of *ROP1*, *ROP2*, *RIC4* and *ERH3*. Compared with that of WT, the expression of *ROP1*, *ROP2*, *RIC4* and *ERH3* in the seedlings of *pin1-5* mutant was increased, but decreased in *35S::PIN1* seedlings, suggesting that PIN1 may be involved in regulating the cotyledon development by mediating the expression of these genes under drought and salt stress conditions. Collectively, these results suggest that temporally regulatory networks are crucial in leaf epidermal cell development and differentiation under drought and salt stress, among which PIN1 is a critical regulator.

Conclusion

In summary, PIN1 is critical in developing leaf epidermal cells under drought and salt stress conditions. PIN1 regulated plant morphology under drought and salt stress. PIN1 was constitutively involved in drought and salt stress regulation of PC and GC development. The determination of possible regulators of PC and GC development under drought and salt stress showed that PIN1 was highly expressed in PC and stomatal lineage cell populations, highlighting PIN1 as a critical regulator of PC and GC development under drought and salt stress. The gene expression analysis showed PIN1 expression dynamics in *pif1/3/4/5* quadruple mutant under drought and salt stress. Collectively, this work sheds light on the role of PIN1 in developing PCs and GCs under drought and salt stress, highlighting this gene as a promising candidate for breeding stress-tolerant crops.

Data availability statement

The original contributions presented in the study are included in the article/Supplementary material. Further inquiries can be directed to the corresponding author.

Author contributions

Conceptualization of the project: XS. Performance of specific experiments: RW, ZL, YZ, HL, SS, YL, AQ, XY, ZZ, JY, MH, and GB. Data analysis and writing of the first draft: XS and GB. Supervision and validation of the manuscript: XS. All authors approved the final version.

Acknowledgments

We are grateful to the Arabidopsis Biological Resource Center (ABRC) for the Arabidopsis seeds. This research was supported by the National Natural Science Foundation of China (31670233).

Conflict of interest

The authors declare that the research was conducted in the absence of any commercial or financial relationships that could be construed as a potential conflict of interest.

Publisher's note

All claims expressed in this article are solely those of the authors and do not necessarily represent those of their affiliated organizations, or those of the publisher, the editors and the reviewers. Any product that may be evaluated in this article, or claim that may be made by its manufacturer, is not guaranteed or endorsed by the publisher.

Supplementary material

The Supplementary Material for this article can be found online at: https://www.frontiersin.org/articles/10.3389/fpls.2022.1043204/full#supplementary-material

References

Adamowski, M., and Friml, J. (2015). PIN-dependent auxin transport: Action, regulation, and evolution. *Plant Cell* 27, 20–32. doi: 10.1105/tpc.114.134874

Bar, M., and Ori, N. (2014). Leaf development and morphogenesis. *Development* 141, 4219–4230. doi: 10.1242/dev.106195

Bartels, D., and Sunkar, R. (2005). Drought and salt tolerance in plants. *Crit. Rev. Plant Sci.* 24, 23–58. doi: 10.1080/07352680590910410

Bawa, G., Feng, L., Yan, L., Du, Y., Shang, J., Sun, X., et al. (2019). Pre-treatment of salicylic acid enhances resistance of soybean seedlings to fusarium solani. *Plant Mol. Biol.* 101, 315–323. doi: 10.1007/s11103-019-00906-x

Chen, X., Ding, Y., Yang, Y., Song, C., Wang, B., Yang, S., et al. (2021). Protein kinases in plant responses to drought, salt, and cold stress. *J. Integr. Plant Biol.* 63, 53–78. doi: 10.1111/jipb.13061

Chen, M., Liu, H., Jixiang, K., Yang, Y., Zhang, N., Li, R., et al. (2011). RopGEF7 regulates PLETHORA-dependent maintenance of the root stem cell niche in arabidopsis. *Plant Cell* 23, 2880–2894. doi: 10.1105/tpc.111.085514

Chowdhury, M. R., Ahamed, M. S., Mas-Ud, M. A., Islam, H., Fatamatuzzohora, M., Hossain, M. F., et al. (2021). Stomatal development and genetic expression in. *Heliyon* 7, e07889. doi: 10.1016/j.heliyon.2021.e07889

Chun, H. J., Baek, D., Cho, H. M., Jung, H. S., Jeong, M. S., Jung, W.-H., et al. (2018). Metabolic adjustment of arabidopsis root suspension cells during adaptation to salt stress and mitotic stress memory. *Plant Cell Physiol.* 60, 612–625. doi: 10.1093/pcp/pcy231

Cosgrove, D. J. (2017). Diffuse growth of plant cell walls. *Plant Physiol.* 176, 16–27. doi: 10.1104/pp.17.01541

Daszkowska-Golec, A., and Szarejko, I. (2013). Open or close the gate – stomata action under the control of phytohormones in drought stress conditions. *Front Plant Sci* 4, 138. doi: 10.3389/fpls.2013.00138

Devkar, V., Thirumalaikumar, V. P., Xue, G. P., Vallarino, J. G., Turečková, V., Strnad, M., et al. (2020). Multifaceted regulatory function of tomato SlTAF1 in the response to salinity stress. *New Phytol.* 225, 1681–1698. doi: 10.1111/nph.16247

Dhakal, S., Reiter, J. W., Laroche, A., and Schultz, E. A. (2021). Leaf vein pattern response to heat and drought requires genes that influence PINFORMED1 localization and is mimicked by ABA treatment. *Environ. Exp. Bot.* 185, 104426. doi: 10.1016/j.envexpbot.2021.104426

Dhonukshe, P., Tanaka, H., Goh, T., Ebine, K., Mähönen, A. P., Prasad, K., et al. (2008). Generation of cell polarity in plants links endocytosis, auxin distribution and cell fate decisions. *Nature* 456, 962–966. doi: 10.1038/nature07409

Dietrich, D. (2018). Hydrotropism - how roots search for water. *J. Exp. Bot.* 69, 2759–2771. doi: 10.1093/jxb/ery034

Dong, H., Bai, L., Zhang, Y., Zhang, G., Mao, Y., Min, L., et al. (2018). Modulation of guard cell turgor and drought tolerance by a peroxisomal acetate-malate shunt. *Mol. Plant* 11, 1278–1291. doi: 10.1016/j.molp.2018.07.008

Ferreira, C., Simioni, C., Schmidt, É.C., Ramlov, F., Maraschin, M., and Bouzon, Z. L. (2017). The influence of salinity on growth, morphology, leaf ultrastructure, and cell viability of the seagrass halodule wrightii ascherson. *Protoplasma* 254, 1529–1537. doi: 10.1007/s00709-016-1041-4

Fischer, U., Ikeda, Y., Ljung, K., Serralbo, O., Singh, M., Heidstra, R., et al. (2006). Vectorial information for arabidopsis planar polarity is mediated by combined AUX1, EIN2, and GNOM activity. *Curr. Biol.* 16, 2143–2149. doi: 10.1016/j.cub.2006.08.091

Fricke, W., Akhiyarova, G., Wei, W., Alexandersson, E., Miller, A., Kjellbom, P. O., et al. (2006). The short-term growth response to salt of the developing barley leaf. *J. Exp. Bot.* 57, 1079–1095. doi: 10.1093/jxb/erj095

Fujiwara, M. T., Yasuzawa, M., Kojo, K. H., Niwa, Y., Abe, T., Yoshida, S., et al. (2018). The arabidopsis arc5 and arc6 mutations differentially affect plastid morphology in pavement and guard cells in the leaf epidermis. *PloS One* 13, e0192380. doi: 10.1371/journal.pone.0192380

Gambetta, G. A., Herrera, J. C., Dayer, S., Feng, Q., Hochberg, U., and Castellarin, S. D. (2020). The physiology of drought stress in grapevine: Towards an integrative definition of drought tolerance. *J. Exp. Bot.* 71, 4658–4676. doi: 10.1093/jxb/eraa245

Garrido, Y., Tudela, J. A., Marín, A., Mestre, T., Martínez, V., and Gil, M. I. (2014). Physiological, phytochemical and structural changes of multi-leaf lettuce caused by salt stress. *J Sci Food Agric* 94, 1592–1599. doi: 10.1002/jsfa.6462

Guillory, A., and Bonhomme, S. (2021). Phytohormone biosynthesis and signaling pathways of mosses. *Plant Mol. Biol.* 107, 1–33. doi: 10.1007/s11103-021-01172-6

Guo, J., Zhou, Y., Li, J., Sun, Y., Shangguan, Y., Zhu, Z., et al. (2020). COE 1 and GUN1 regulate the adaptation of plants to high light stress. *Biochem. Biophys. Res. Commun.* 521, 184–189. doi: 10.1016/j.bbrc.2019.10.101

Hamant, O., Heisler, M. G., Jönsson, H., Krupinski, P., Uyttewaal, M., Bokov, P., et al. (2008). Developmental patterning by mechanical signals in arabidopsis. *Science* (New York, N.Y.) 322, 1650–1655. doi: 10.1126/science.1165594

Heisler, M. G., Hamant, O., Krupinski, P., Uyttewaal, M., Ohno, C., Jönsson, H., et al. (2010). Alignment between PIN1 polarity and microtubule orientation in the shoot apical meristem reveals a tight coupling between morphogenesis and auxin transport. *PloS Biol.* 8, e1000516. doi: 10.1371/journal.pbio.1000516

Heisler, M. G., Ohno, C., Das, P., Sieber, P., Reddy, G. V., Long, J. A., et al. (2005). Patterns of auxin transport and gene expression during primordium development revealed by live imaging of the arabidopsis inflorescence meristem. *Curr. Biol.* 15, 1899–1911. doi: 10.1016/j.cub.2005.09.052

Hervieux, N., Dumond, M., Sapala, A., Routier-Kierzkowska, A.-L., Kierzkowski, D., Roeder, A. h.K., et al. (2016). A mechanical feedback restricts sepal growth and shape in arabidopsis. *Curr. Biol.* 26, 1019–1028. doi: 10.1016/j.cub.2016.03.004

Huang, G. T., Ma, S. L., Bai, L. P., Zhang, L., Ma, H., Jia, P., et al. (2012). Signal transduction during cold, salt, and drought stresses in plants. *Mol. Biol. Rep.* 39, 969–987. doi: 10.1007/s11033-011-0823-1

Jalil, S., and Ansari, M. I. (2019). *Role of Phytohormones in Recuperating Salt Stress.*. Salt Stress, Microbes, and Plant Interactions: Mechanisms and Molecular Approaches M. S. Akhtar (Singapore, Springer Singapore), 2, 91–104.

Ji, T., Li, S., Li, L., Huang, M., Wang, X., Wei, M., et al. (2018). Cucumber phospholipase d alpha gene overexpression in tobacco enhanced drought stress tolerance by regulating stomatal closure and lipid peroxidation. *BMC Plant Biol.* 18, 355. doi: 10.1186/s12870-018-1592-y

Karimi, S. M., Freund, M., Wager, B. M., Knoblauch, M., Fromm, J., M. Mueller, H., et al. (2021). Under salt stress guard cells rewire ion transport and abscisic acid signaling. *The New phytologist* 231, 1040–1055. doi: 10.1111/nph.17376

Kebbas, S., Lutts, S., and Aid, F. (2015). Effect of drought stress on the photosynthesis of acacia tortilis subsp. raddiana at the young seedling stage. *Photosynthetica* 53, 288–298. doi: 10.1007/s11099-015-0113-6

Kim, D. Y., Jin, J. Y., Alejandro, S., Martinoia, E., and Lee, Y. (2010). Overexpression of AtABCG36 improves drought and salt stress resistance in arabidopsis. *Physiol. Plant* 139, 170–180. doi: 10.1111/j.1399-3054.2010.01353.x

Li, S., Fan, C., Li, Y., Zhang, J., Sun, J., Chen, Y., et al. (2016). Effects of drought and salt-stresses on gene expression in caragana korshinskii seedlings revealed by RNA-seq. *BMC Genomics* 17, 200. doi: 10.1186/s12864-016-2562-0

Li, H., Lin, D., Dhonukshe, P., Nagawa, S., Chen, D., Friml, J., et al. (2011). Phosphorylation switch modulates the interdigitated pattern of PIN1 localization and cell expansion in arabidopsis leaf epidermis. *Cell Res.* 21, 970–978. doi: 10.1038/cr.2011.49

Liu, Z., Guo, C., Wu, R., Hu, Y., Zhou, Y., Wang, J., et al. (2022a). FLS2– RBOHD–PIF4 module regulates plant response to drought and salt stress 23, 1080. doi: 10.3390/ijms23031080

Liu, Z., Guo, C., Wu, R., Wang, J., Zhou, Y., Yu, X., et al. (2022b). Identification of the regulators of epidermis development under drought- and salt-stressed conditions by single-cell RNA-seq. *Int. J. Mol. Sci.* 23, 2759. doi: 10.3390/ijms23052759

Li, T., Wu, R., Liu, Z., Wang, J., Guo, C., Zhou, Y., et al. (2021). GUN4 affects the circadian clock and seedlings adaptation to changing light conditions. *Int. J. Mol. Sci.* 23, 194. doi: 10.3390/ijms23010194

López-Serrano, L., Canet-Sanchis, G., Vuletin Selak, G., Penella, C., San Bautista, A., López-Galarza, S., et al. (2019). Pepper rootstock and scion physiological responses under drought stress. *Front Plant Sci* 10, 38. doi: 10.3389/fpls.2019.00038

Ma, Y., and Qin, F. (2014). "ABA regulation of plant responses to drought and salt stresses," in *Abscisic acid: Metabolism, transport and signaling*. Ed. D.-P. Zhang (Dordrecht: Springer Netherlands), 315–336.

Maricle, B. R., Koteyeva, N. K., Voznesenskaya, E. V., Thomasson, J. R., and Edwards, G. E. (2009). Diversity in leaf anatomy, and stomatal distribution and conductance, between salt marsh and freshwater species in the C(4) genus spartina (Poaceae). *New Phytol.* 184, 216–233. doi: 10.1111/j.1469-8137.2009.02903.x

Mckown, K. H., and Bergmann, D. C. (2020). Stomatal development in the grasses: lessons from models and crops (and crop models) 227, 1636–1648. doi: 10.1111/nph.16450

Meng, Y., Chen, F., Shuai, H., Luo, X., Ding, J., Tang, S., et al. (2016). Karrikins delay soybean seed germination by mediating abscisic acid and gibberellin biogenesis under shaded conditions. *Sci. Rep.* 6, 22073. doi: 10.1038/srep22073

Mostofa, M., Abdelrahman, M., Rahman, M., Cuong, T., Nguyen, K., Watanabe, Y., et al. (2022). Karrikin receptor KAI2 coordinates salt tolerance mechanisms in arabidopsis thaliana. *Plant Cell Physiol.* pcac121 doi: 10.1093/pcp/pcac121

Muchate, N. S., Nikalje, G. C., Rajurkar, N. S., Suprasanna, P., and Nikam, T. D. (2016). Plant salt stress: Adaptive responses, tolerance mechanism and

bioengineering for salt tolerance. *Botanical Rev.* 82, 371–406. doi: 10.1007/s12229-016-9173-y

Omelyanchuk, N., Kovrizhnykh, V., Oshchepkova, E. A., Pasternak, T., Palme, K., and Mironova, V. (2016). A detailed expression map of the PIN1 auxin transporter in arabidopsis thaliana root. *BMC Plant Biol.* 16, 5. doi: 10.1186/s12870-015-0685-0

Pandey, V., Bhatt, I. D., and Nandi, S. K. (2019). "Chapter 20 - role and regulation of auxin signaling in abiotic stress tolerance," in *Plant signaling molecules*. Eds. M. I. R. Khan, P. S. Reddy, A. Ferrante and N. A. Khan (Woodhead Publishing), 319–331.

Pillitteri, L. J., and Torii, K. U. (2012). Mechanisms of stomatal development. *Annual review of plant biology* 63, 591–614. doi: 10.1146/annurev-arplant-042811-105451

Pirasteh-Anosheh, H., Saed-Moucheshi, A., Pakniyat, H., and Pessarakli, M. (2016). Stomatal responses to drought stress. *Water Stress and Crop Plants* 24–40. doi: 10.1002/9781119054450.ch3

Ramegowda, V., and Senthil-Kumar, M. (2015). The interactive effects of simultaneous biotic and abiotic stresses on plants: Mechanistic understanding from drought and pathogen combination. *J. Plant Physiol.* 176, 47–54. doi: 10.1016/j.jplph.2014.11.008

Rasool, S., Hameed, A., Azooz, M., Muneeb, U., Siddiqi, T., and Ahmad, P. (2013). *Salt stress: Causes, types and responses of plants*. In book: Ecophysiology and Responses of Plants under Salt Stress. Eds. P. Ahmad, M.M. Azooz and M.N.V. Prasad (New York, NY, Springer New York) 1–24.

Rehman, A., Almas, H., Qayyum, A., Li, H., Peng, Z., Qin, G., et al. (2021). Role of phytohormones in drought stress. *Plant Growth Regulators for Climate-Smart Agriculture* 81–98. doi: 10.1201/9781003109013-6

Reinhardt, D., Pesce, E. R., Stieger, P., Mandel, T., Baltensperger, K., Bennett, M., et al. (2003). Regulation of phyllotaxis by polar auxin transport. *Nature* 426, 255–260. doi: 10.1038/nature02081

Ribba, T., Garrido-Vargas, F., and O'brien, J. A. (2020). Auxin-mediated responses under salt stress: from developmental regulation to biotechnological applications. *J. Exp. Bot.* 71, 3843–3853. doi: 10.1093/jxb/eraa241

Sampathkumar, A. (2020). Mechanical feedback-loop regulation of morphogenesis in plants. *Development* (Cambridge, England) 147, dev177964. doi: 10.1242/dev.177964

Sinha, R., Gupta, A., and Senthil-Kumar, M. (2016). Understanding the impact of drought on foliar and xylem invading bacterial pathogen stress in chickpea. *Front Plant Sci* 7, 902. doi: 10.3389/fpls.2016.00902

Sun, X., Fu, T., Chen, N., Guo, J., Ma, J., Zou, M., et al. (2010). The stromal chloroplast Deg7 protease participates in the repair of photosystem II after photoinhibition in arabidopsis. *Plant Physiol.* 152, 1263–1273. doi: 10.1104/pp.109.150722

Sun, Y., Liu, Z., Guo, J., Zhu, Z., Zhou, Y., Guo, C., et al. (2020). WRKY33-PIF4 loop is required for the regulation of H2O2 homeostasis. *Biochem. Biophys. Res. Commun.* 527, 922–928. doi: 10.1016/j.bbrc.2020.05.041

Sun, X., Peng, L., Guo, J., Chi, W., Ma, J., Lu, C., et al. (2007). Formation of DEG5 and DEG8 complexes and their involvement in the degradation of photodamaged photosystem II reaction center D1 protein in arabidopsis. *Plant Cell* 19, 1347–1361. doi: 10.1105/tpc.106.049510

Takatani, S., Verger, S., Okamoto, T., Takahashi, T., Hamant, O., and Motose, H. (2020). Microtubule response to tensile stress is curbed by NEK6 to buffer growth variation in the arabidopsis hypocotyl. *Curr. Biol.* 30, 1491–1503.e1492. doi: 10.1016/j.cub.2020.02.024

Taleisnik, E., Rodríguez, A. A., Bustos, D., Erdei, L., Ortega, L., and Senn, M. E. (2009). Leaf expansion in grasses under salt stress. *J. Plant Physiol.* 166, 1123–1140. doi: 10.1016/j.jplph.2009.03.015

Tang, Z.-Q., Shang, J., Zhang, L., Du, J.-B., Yang, H., Zeng, S.-H., et al. (2019). Characterization of synergy between cucumber mosaic virus and alternaria alternata in nicotiana tabacum. *Physiol. Mol. Plant Pathol.* 108, 101404. doi: 10.1016/j.pmpp.2019.03.001

Ullah, N., Basit, A., Ahmad, I., Ullah, I., Shah, S. T., Mohamed, H. I., et al. (2020). Mitigation the adverse effect of salinity stress on the performance of the tomato crop by exogenous application of chitosan. *Bull. Natl. Res. Centre* 44, 181. doi: 10.1186/s42269-020-00435-4

Ullah, A., Manghwar, H., Shaban, M., Khan, A. H., Akbar, A., Ali, U., et al. (2018). Phytohormones enhanced drought tolerance in plants: a coping strategy. *Environ. Sci. pollut. Res. Int.* 25, 33103–33118. doi: 10.1007/s11356-018-3364-5

Wang, Y., Huan, Q., Li, K., and Qian, W. (2021b). Single-cell transcriptome atlas of the leaf and root of rice seedlings. *J. Genet. Genomics* 48, 881–898. doi: 10.1016/j.jgg.2021.06.001

Wang, X., Niu, Y., and Zheng, Y. (2021a). Multiple functions of MYB transcription factors in abiotic stress responses. *International journal of molecular sciences* 22 (11), 6125. doi: 10.3390/ijms22116125

Wang, P., Shen, L., Guo, J., Jing, W., Qu, Y., Li, W., et al. (2019). Phosphatidic acid directly regulates PINOID-dependent phosphorylation and activation of the PIN-FORMED2 auxin efflux transporter in response to salt stress. *Plant Cell* 31, 250–271. doi: 10.1105/tpc.18.00528

Wang, W., Vinocur, B., and Altman, A. (2003). Plant responses to drought, salinity and extreme temperatures: Towards genetic engineering for stress tolerance. *Planta* 218, 1–14. doi: 10.1007/s00425-003-1105-5

Wu, R., Liu, Z., Wang, J., Guo, C., Zhou, Y., Bawa, G., et al. (2022a). COE2 is required for the root foraging response to nitrogen limitation. *Int. J. Mol. Sci.* 23, 861. doi: 10.3390/ijms23020861

Wu, R., Liu, Z., Wang, J., Li, W., Qin, A., Yu, X., et al. (2022b). Identification of two bZIP transcription factors that regulate development of pavement and trichome cells in arabidopsis thaliana by single-cell RNA-sequencing. *bioRxiv*. 2022.2004.2012.488054. doi: 10.1101/2022.04.12.488054

Xiong, Y., and Jiao, Y. (2019). The diverse roles of auxin in regulating leaf development. *Plants* 8, 243. doi: 10.3390/plants8070243

Yang, Y., and Guo, Y. (2018). Elucidating the molecular mechanisms mediating plant salt-stress responses. *The New phytologist* 217, 523–539. doi: 10.1111/nph.14920

Yeshi, K., Crayn, D., Ritmejerytė, E., and Wangchuk, P. (2022). Plant secondary metabolites produced in response to abiotic stresses has potential application in pharmaceutical product development. *Molecules* (Basel, Switzerland), 27 (1), 313. doi: 10.3390/molecules27010313

Yu, Z., Duan, X., Luo, L., Dai, S., Ding, Z., and Xia, G. (2020). How plant hormones mediate salt stress responses. *Trends Plant Sci.* 25, 1117–1130. doi: 10.1016/j.tplants.2020.06.008

van Zelm, E., Zhang, Y., and Testerink, C. (2020). Salt tolerance mechanisms of plants. *Annual review of plant biology* 71, 403–433. doi: 10.1146/annurev-arplant-050718-100005

Zhang, H., Sun, X., and Dai, M. (2022). Improving crop drought resistance with plant growth regulators and rhizobacteria: Mechanisms, applications, and perspectives. *Plant Commun.* 3, 100228. doi: 10.1016/j.xplc.2021.100228

Zhang, H., Xiang, Y., He, N., Liu, X., Liu, H., Fang, L., et al. (2020). Enhanced vitamin c production mediated by an ABA-induced PTP-like nucleotidase improves plant drought tolerance in arabidopsis and maize. *Mol. Plant* 13, 760–776. doi: 10.1016/j.molp.2020.02.005

Zhang, J., Zhang, H., Srivastava, A. K., Pan, Y., Bai, J., Fang, J., et al. (2018). Knockdown of rice MicroRNA166 confers drought resistance by causing leaf rolling and altering stem xylem development. *Plant Physiol.* 176, 2082–2094. doi: 10.1104/pp.17.01432

Zhou, W., Yang, Y., Zheng, C., Luo, X., Chandrasekaran, U., Yin, H., et al. (2021). Flooding represses soybean seed germination by mediating anaerobic respiration, glycometabolism and phytohormones biosynthesis. *Environ. Exp. Bot.* 188, 104491. doi: 10.1016/j.envexpbot.2021.104491

Zhu, X., Wang, L., Yang, R., Han, Y., Hao, J., Liu, C., et al. (2019). Effects of exogenous putrescine on the ultrastructure of and calcium ion flow rate in lettuce leaf epidermal cells under drought stress. *Horticul. Environment Biotechnol.* 60, 479–490. doi: 10.1007/s13580-019-00151-7

Zuch, D. T., Doyle, S. M., Majda, M., Smith, R. S., Robert, S., and Torii, K. U. (2021). Cell biology of the leaf epidermis: Fate specification, morphogenesis, and coordination. *Plant Cell* 34, 209–227. doi: 10.1093/plcell/koab250

frontiers | Frontiers in Plant Science

TYPE Original Research
PUBLISHED 08 December 2022
DOI 10.3389/fpls.2022.1079534

Check for updates

OPEN ACCESS

EDITED BY
Mehdi Rahimi,
Graduate University of Advanced Technology, Iran

REVIEWED BY
Lei Wang,
Xinjiang Institute of Ecology and Geography, Chinese Academy of Sciences (CAS), China
Weiqiang Li,
RIKEN, Japan
Jibiao Fan,
Yangzhou University, China

*CORRESPONDENCE
Baoshan Wang
bswang@sdnu.edu.cn
Fang Yuan
yuanfang@sdnu.edu.cn

†These authors have contributed equally to this work

SPECIALTY SECTION
This article was submitted to Plant Abiotic Stress, a section of the journal Frontiers in Plant Science

RECEIVED 25 October 2022
ACCEPTED 28 November 2022
PUBLISHED 08 December 2022

CITATION
Jiao X, Zhao B, Wang B and Yuan F (2022) An uncharacterized gene *Lb1G04794* from *Limonium bicolor* promotes salt tolerance and trichome development in *Arabidopsis*. *Front. Plant Sci.* 13:1079534. doi: 10.3389/fpls.2022.1079534

COPYRIGHT
© 2022 Jiao, Zhao, Wang and Yuan. This is an open-access article distributed under the terms of the Creative Commons Attribution License (CC BY). The use, distribution or reproduction in other forums is permitted, provided the original author(s) and the copyright owner(s) are credited and that the original publication in this journal is cited, in accordance with accepted academic practice. No use, distribution or reproduction is permitted which does not comply with these terms.

An uncharacterized gene *Lb1G04794* from *Limonium bicolor* promotes salt tolerance and trichome development in *Arabidopsis*

Xiangmei Jiao†, Boqing Zhao†, Baoshan Wang*and Fang Yuan*

Shandong Provincial Key Laboratory of Plant Stress, College of Life Sciences, Shandong Normal University, Ji'nan, Shandong, China

Halophytes can grow and reproduce in high-salinity environments, making them an important reservoir of genes conferring salt tolerance. With the expansion of saline soils worldwide, exploring the mechanisms of salt tolerance in halophytes and improving the salt tolerance of crops have become increasingly urgent. *Limonium bicolor* is a halophyte with salt glands that secrete excess Na^+ through leaves. Here, we identified an uncharacterized gene *Lb1G04794*, which showed increased expression after NaCl treatment and was high during salt gland development in *L. bicolor*. Overexpression of *Lb1G04794* in *L. bicolor* showed promoted salt gland development, indicating that this gene may promote salt gland differentiation. Transgenic Arabidopsis strains overexpressing *Lb1G04794* showed increased trichomes and decreased root hairs under normal conditions. Compared with wild type (WT), root growth in the transgenic lines was less inhibited by NaCl treatment. Transgenic seedlings accumulated less fresh/dry weight reductions under long-term salt treatment, accompanied by lower Na^+ and malondialdehyde accumulation than WT, indicating that these transgenic lines behave better growth and undergo less cellular damage under NaCl stress. These results were consistent with the low expression levels of salt-tolerance marker genes in the transgenic lines upon salt stress. We conclude that the unknown gene *Lb1G04794* positively regulated salt gland development, and promoted salt tolerance of Arabidopsis, offering a new direction for improving salt tolerance of non-halophytes and crops.

KEYWORDS

***Limonium bicolor*, *Arabidopsis thaliana*, root length, trichome, salt gland, salt tolerance, biomass**

1 Introduction

According to incomplete statistics from UNESCO and FAO, there are 953 million hectares of saline land in the world, 10% of which are in China. High ion concentrations and low water potential hinder normal plant growth and development, thus reducing crop yields and limiting food production (Boyer, 1982; Yuan et al., 2013). Saline lands affect the surrounding ecological environment, and intensifies with the expansion of human activities (Munns and Tester, 2008; Song et al., 2020; Zheng et al., 2020). The current decrease in arable land and the increase in the human population underscore the urgent need to effectively utilize saline land to expand usable land for the cultivation of adapted crops (Munns and Tester, 2008; Guo et al., 2017; Ma et al., 2020).

Although a number of physical and chemical methods such as salt washing, concealed pipe and chemical modification are currently used to remediate high-salinity soils, these methods are costly, have poor durability, and are prone to several environmental problems, which are likely to cause secondary salinization (Rasool et al., 2013). A more effective and sustainable transformation method should therefore call upon biological means of improving saline soils. Many salt tolerance genes have been isolated and introduced into various plant species to improve their tolerance to salt stress, which can be applied to valorize saline soils. Halophytes that can grow naturally on saline land have great potential in the biological improvement of saline-alkali land (Yuan et al., 2019b), which can be fueled by research on halophytes and their underlying salt tolerance mechanisms and associated key genes. The physiological response and adaptation mechanism of halophytes to soil salinity (Lu et al., 2022) have been extensively studied and confirmed.

Halophytes can improve the ecological environment and utilization degree of saline land by preserving soil and water, increasing vegetation coverage, and increasing the abundance of surface animals and microorganisms. Halophytes can complete their life cycle under conditions as extreme as 200 mM NaCl, using one of three strategies: secreting salt back into the environment (recretohalophytes), salt compartmentalization into cell vesicles (euhalophytes), or preventing salt from entering cells (pseudohalophytes) (Yuan et al., 2013; Song and Wang, 2015; Guo et al., 2020a). Among these three types of halophytes, recretohalophytes have a specific salt tolerance mechanism and can typically secrete Na^+ out of plant cells to avoid salt damage.

Several genes participating in salt tolerance and encoding proteins with distinct functional domains have been characterized in halophytes. *SUPER SENSITIVE TO ABA AND DROUGHT2* (*LbSAD2*) significantly increased salt resistance of Arabidopsis (*Arabidopsis thaliana*) seedlings by reducing root hair development and sensitivity to the abscisic acid (ABA), the physiological indexes of overexpressed lines were significantly better than those of WT under salt treatment (Xu et al., 2021). Similarly, *Limonium bicolor HELIX-LOOP-HELIX* (*LbHLH*) increased salt tolerance by reducing root hair development and increasing osmotic resistance when overexpressed in Arabidopsis (Wang et al., 2021). *TRIPTYCHON* (*LbTRY*) increased salt sensitivity when overexpressed in Arabidopsis by increasing root hair number and changing osmotic homeostasis (Leng et al., 2021). Analysis of salt tolerance mechanisms in the recretohalophyte *Limonium bicolor* established that the loss and modification of key genes initiating trichomes in other species have led to the development of salt glands instead of trichomes in this plant species (Yuan et al., 2022). Additional salt tolerance genes have been described in other species as well: The heterologous expression of *NAM, ATAF1/2, CUC2 17* (*LpNAC17*) from coral lily (*Lilium pumilum*) in *Nicotiana benthamiana* improved salt tolerance by shortening root length and line size (Cui, 2021), and *ALTERNATIVE OXIDASE2* from Chinese dwarf cherry (*Cerasus humilis*) (*ChAOX2*) transformation of *Arabidopsis thaliana* enhanced plant respiration, decreased ion leakage, increased proline content, and decreased the accumulation of reactive oxygen species to improve salt tolerance (Zhao, 2020). Protein–protein interaction can also significantly affect salt tolerance. For example, the transcription factors MdWRKY55 and MdNAC17-L from apple (*Malus domestica*) enhanced salt tolerance by activating the transcription of the Na^+/H^+ *exchanger 1* gene *MdNHX1* (Su et al., 2022). A network of salt tolerance genes is gradually emerging from the integration and exploration of the above genes and their mechanisms.

Analysis of the mechanisms involved in salt tolerance includes the characterization of proteins with unknown or poorly characterized functional domains. For example, the gene *Lb1G04202* conferred a stronger salt tolerance at the seedling stage when overexpressed in Arabidopsis and participated in salt tolerance by promoting proline biosynthesis (Wang et al., 2022). Mutants of *At5G45480* were more sensitive to osmotic stress; an analysis of differentially expressed genes between the mutant and WT revealed that the expression levels of genes related to substance biosynthesis and transport and related to protein translation and activity were closely related to *At5G45480* function (Zhu, 2014). The overexpression of *Lb2G14763* in *Arabidopsis thaliana* resulted in the greater accumulation of Na^+ and lower expression of salt-resistant genes compared to nontransgenic controls, resulting in the negative regulation of salt tolerance. Transgenic *Arabidopsis* lines overexpressing *Lb7G32827* and *Lb3G18904* showed more salt tolerance at the seedling stage than WT, and the expression of salt-tolerant marker genes was significantly increased, contributing to higher salt tolerance (Jing, 2021). A gene was isolated from an expressed sequenced tag (EST) library generated from mustard (*Brassica rapa*) exposed to 200 mM NaCl; The superepitope strain of this gene grew better than the WT under salt treatment (Wei, 2006). As more genes with

unknown function are discovered and characterized, the plant salt tolerance pathway becomes more complex.

Salt glands are a typical salt secretory epidermal structure that are present in 68 species, including sea lavender (*L. bicolor*) (Li et al., 2020; Lu et al., 2020). *L. bicolor* belongs to the Plumbaginaceae (Yuan et al., 2016a; Leng et al., 2018; Yuan et al., 2018; Leng et al., 2019a; Leng et al., 2019b; Guo et al., 2020b; Gao et al., 2021) and is a unique recretohalophyte with a sequenced genome that constitutes an essential genetic resource for improving salt tolerance in crops. Salt gland differentiation is the earliest visible sign on the epidermis, even before the development of stomata and other epidermal structures. Yuan et al. (2015) divided the differentiation and development time of epidermal cells into five stages, namely, undifferentiated stage (Stage A), salt gland differentiation stage (Stage B), stomatal differentiation stage (Stage C), pavement cell differentiation stage (Stage D) and maturation stage (Stage E) through observation on the first true leaf of *L. bicolor*. A previous transcriptome analysis of salt gland development and salt secretion (Yuan et al., 2015; Yuan et al., 2016b) identified the gene *Lb1G04794*, which encodes a protein with an uncharacterized domain, with high expression during salt gland development. As a typical halophyte with high salt tolerance and special salt secretion structure, *L. bicolor* has not been thoroughly studied. With the in-depth study of its transcriptome (Yuan et al., 2022), the mechanism of salt resistance will be further clarified. As an unknown gene, *Lb1G04794* is a further exploration of the mechanism of salt gland development and an effective means to perfect the mechanism of salt tolerance. To explore the function of this novel gene, we overexpressed *Lb1G04794* in Arabidopsis, which revealed its positive role in salt responses, suggesting that upregulated genes in response to *Lb1G04794* overexpression may be related to salt tolerance. *Lb1G04794* overexpression may therefore offer a means to improving salt tolerance in crops.

2 Materials and methods

2.1 Plant materials and growth conditions

Seeds of *L. bicolor* were collected from the saline inland environment (N37°20'; E118°36') in the Yellow River Delta, Shandong, China. The seeds were well dried and stored at 4°C until use. The seeds were washed with sterile deionized water after surface disinfection with 70% (v/v) ethanol for 5 min and 6% (v/v) sodium hypochlorite (Sigma, United States) for 15–20 min. Surface-sterilized seeds were then sown onto Murashige and Skoog (Murashige and Skoog, 1962) medium (MS medium; adjusted to pH 5.8 with KOH before autoclaving). The plates were incubated at 28 ± 3°C/23 ± 3°C (day/night cycle) under a light intensity of 600 μmol/m^2/s (15-h-light/9-h-dark photoperiod) and 70% relative humidity. Samples were collected and frozen in liquid nitrogen at the undifferentiated stage (5,000 leaves in stage A), the salt gland development stage (4,000 leaves in stage B), and the first true leaf was collected (Yuan et al., 2015). Total RNA was extracted for gene cloning.

The *Arabidopsis thaliana* accession Columbia-0 (Col-0) was used for heterologous overexpression of *Lb1G04794*. Seeds were first surface sterilized three times with 75% (v/v) ethanol for 4 min, during which a full eddy was applied, followed by 95% (v/v) ethanol for 1 min, repeated three times, with a full rinse with sterile water four times. The seeds were then sown onto half-strength MS medium (pH 5.8). After stratification at 4°C for 2 days, the plates were released at 22°C/18°C (day/night) under a light intensity of 150 mol/m^2/s, relative humidity of 70%, and a light cycle of 16 h light/8 h dark (Sui et al., 2017). Seedlings were transferred into small pots (10 cm in diameter and 8 cm in height) containing mixed soil (soil:vermiculite:perlite, 3:1:1) after 1 week and were allowed to grow under the same growth conditions for transformation and treatment.

2.2 Cloning of full-length cDNA and bioinformatic analysis of Lb1G04794

The first true leaves over the A-E period of *L. bicolor* leaf development were collected, frozen in liquid nitrogen, and stored at −80°C before total RNA extraction according to Yuan. (Yuan et al., 2015). A ReverTra Ace® qPCR RT Kit (Japan TOYOBO CO, LTD) was used for reverse transcription to obtain cDNA for each developmental stage. Based on Iso-seq transcriptome data from *L. bicolor*, the primers *Lb1G04794*-S and *Lb1G04794*-A for *Lb1G04794* were designed using Primer Premier 5.0, and the full-length coding sequence was amplified by PCR (Supplementary Table 1).

DNA and protein sequences were compared using DNAman and DNAstar. After BLAST with *Lb1G04794* as a query at the National Center for Biotechnology Information (NCBI), 33 related proteins were selected for phylogenetic tree construction, using MEGA and the ClustalX adjacency method. The percentage support at each node was determined from at least 1,000 bootstrap replicates. Using the ProtParam tool in ExPASy online software, the physicochemical properties of each protein were predicted. The hydrophilicity and hydrophobicity of all proteins were analyzed by prot-Scala in ExPASy. The software tools Signal4.14, ExPASy and Swiss-Model were used to predict the secondary and tertiary structures of the proteins and the presence of signal peptides.

2.3 Subcellular localization of Lb1G04794

A 2×Taq Plus Master Mix II and the primer pair *Lb1G04794* 1300-S and *Lb1G04794* 1300-A (Supplementary Table 1) were used to amplify the full-length coding sequences with

homologous terminal vectors. The *Lb1G04794* coding sequence was cloned into the pCAMBIA 1300 vector containing the cauliflower mosaic virus (CaMV) 35S promoter, the hygromycin resistance gene, and the green fluorescent protein sequence (*GFP*). The resulting pCAMBIA 1300-*Lb1G04794* vector was transformed into onion (*Allium cepa*) epidermal cells using Agrobacterium (*Agrobacterium tumefaciens*) strain GV3101 (Sun et al., 2007). The fluorescence signal of the GFP fusion protein was detected with a confocal microscope (TCS S8 MP two-photon confocal laser scanning microscope, Leica, Germany). Staining with 4′,6-diamidino-2-phenylindole (DAPI) was used to show the nucleus under 358-nm excitation.

2.4 Transcriptional activation assay of Lb1G04794 in yeast cells

ClonExpress® II was used to clone the coding sequence of *Lb1G04794* into the vector pGBKT7/BD *via* the NdeI restriction site (Supplementary Table 1). The three vector pairs pGADT7-T +pGBKT7-*Lb1G04794* (experimental group), pGADT7-T +pGBKT7-lam (negative control), and pGADT7-T+pGBKT7-53 (positive control) were introduced into Y2H Gold yeast cells through the yeast Maker transformation system. Yeast colonies were selected on synthetic defined (SD) medium lacking Trp (SD –Trp) for 3 days. Transcriptional activity was evaluated according to yeast growth on SD –Trp –Leu medium at 30°C for 2 days (Guo et al., 2013). β-Galactosidase activity was determined by growth on SD –Trp –Leu –Ade –His medium containing X-α-gal (Han et al., 2019).

2.5 Expression analysis in different tissues in *Limonium bicolor*

According to transcriptome deep sequencing (RNA-seq) results of *L. bicolo*r samples at different developmental stages, *Lb1G04794* was expressed at different levels across different developmental stages (Yuan et al., 2015). To validate these results, samples were collected from the first true leaf at the A and B stages (undifferentiated stage, 4–5 days after sowing; salt gland differentiation stage, 6–7 days after sowing, using 4,000 leaves), the C and D stages (stomatal differentiation, 8–10 days; epidermal cell differentiation stage, 11–13 days, 2,000 leaves), the E stage (mature young stage, 14 days, 500 leaves), old leaves (20 days) and the E stage petioles and roots. Meanwhile, we also collected true leaf materials treated with 300 mM NaCl for 14 days. Total RNA was extracted from the above materials. A separate set of seedlings was treated with 25 mg/L salicylic acid, 0.1 mg/L methyl jasmonate, or 300 mM NaCl, then sampled at 0, 6, 12, 24, 48, and 72 h. Beacon Designer Free Edition software (Version 7.8) was used to design the primers for quantitative PCR (qPCR) of *Lb1G04794*, using *LbTUBULIN* as internal control (Supplementary Table 1). PCR thermal cycling conditions were as follows: denaturation at 95°C for 5 min, followed by 40 cycles of denaturation at 94°C for 20 s, annealing at 58°C for 15 s, extension at 65°C for 15 s. Three biological replicates were analyzed. Relative expression levels were calculated according to the formula $2^{-\Delta\Delta C(T)}$.

2.6 Analysis of the tissue-specific expression of Lb1G04794 in Arabidopsis

The first true leaves of *L. bicolor* seedlings were collected, and genomic DNA was extracted by the cetyltrimethylammonium bromide (CTAB) method. The *Lb1G04794* promoter sequence was identified in the *L. bicolor* genome sequence (Lescot et al., 2002), and specific primers (*Lb1G04794*-P-S and *Lb1G04794*-P-A) were designed using Primer Premier 5.0 (Supplementary Table 1). The promoter fragment was amplified by PCR with a 2×Taq Plus Master Mix and cloned, as detailed below.

The CaMV 35S promoter in pCAMBIA3301-35S-GUS vector was excised by digestion with HindIII/NcoI to linearize the vector. The *Lb1G04794pro:GUS* reporter construct was obtained by linking the linearized vector and the *Lb1G04794* promoter with ClonExpress® II. The resulting construct was transformed into wild-type Arabidopsis plants by Agrobacterium-mediated transformation (strain GV3101). Transgenic plants were obtained by selection on basta. A GUS staining kit (Zhongkelitai Biological Technology Co, LTD; Cat No : RTU4032)was used for staining: a 50× X-Gluc concentrated solution was diluted 50 times with GUS staining buffer. The prepared materials were soaked in GUS staining solution overnight at 25–37°C. All materials were then transferred into anhydrous ethanol for chlorophyll clearing two to three times until the negative control material turned white. GUS staining was observed with the naked eye or under a microscope.

2.7 Vector construction and transformation of arabidopsis Col-0

After linearization of pCAMBIA3301-35S-GUS vector by digestion with NcoI to remove the 35S promoter coding sequence, the *Lb1G04794* coding sequence was amplified by PCR with the primers *Lb1G04794* 3301-S and *Lb1G04794* 3301-A (Supplementary Table 1) and cloned into the linearized vector with the ClonExpress® II recombination reaction system to generate *35S*: *Lb1G04794*. The resulting construct was introduced into Agrobacterium strain GV3101 and transformed into Arabidopsis Col-0 by Agrobacterium-mediated floral dipping (Clough and Bent, 1998). After three generations of selection for herbicide resistance, homozygous *35S:Lb1G04794* lines were identified. Genomic DNA was extracted for PCR with the primers pCAMBIA-S and *Lb1G04794*-A to confirm transgenic plants harboring the

overexpression construct (Supplementary Table 1). Total RNA of *35S:Lb1G04794* transgenic lines was extracted with a FastPure Plant Total RNA Isolation Kit (Vazyme, China). The expression levels of *Lb1G04794* were measured in the transgenic lines by RT-qPCR using *Lb1G04794* RT-S and *Lb1G04794* RT-A primers (Supplementary Table 1), using Arabidopsis *ACTIN2* as internal control (primers ACTIN2 sense and ACTIN2 anti). The expression of each transgenic line was repeated three times. The line with the lowest *Lb1G04794* expression level (line OE14) was used as the control (with relative expression level set to 1) to calculate the relative expression level of *Lb1G04794* in the other overexpression lines (Leng et al., 2021).

2.8 Overexpression transformation of Lb1G04794 in *Limonium bicolor*

pCAMBIA3301-35S-GUS and pCAMBIA3301-35S-*Lb1G04794*-GUS was transferred into *Agrobacterium* EHA105 and used to infect *L. bicolor* referring to Yuan et al. (2104). After the shoot regeneration, the regenerated leaves were transferred to the root regeneration medium. After screened in hygromycin for two weeks, the regenerated seedlings were used for qRT-PCR to verify the expression level in overexpression line. Then, the leaves were fixed in Carnoy (ethanol: acetic acid, 3:1) for 12 h and decolorized with 70% ethanol for 12 h, and finally decolorized with Hoyers' solution (chloral hydrate saturated with lactic acid solution). The structure and morphology of the salt glands were observed under the excitation light of 330–380 nm under the fluorescence microscope, and then the number of salt glands in a single leaf was counted.

2.9 Observation of root hairs and trichomes in transgenic lines under salt treatment

The phenotypes of one-week-old T_3 homozygous seedlings were observed using an anatomical microscope (Nikon, Japan). After the first pair of true leaves had fully expanded, the total number of trichomes was counted on the first pair of rosette leaves, with 20 seedlings analyzed for each line. The number and length of root hairs from five OE-*Lb1G04794* seedlings were scored, with 20 seedlings per line.

2.10 Effect of NaCl concentration on salt tolerance of different transgenic lines: Root length and physiological indicators

Three Arabidopsis transgenic lines overexpressing *Lb1G04794* at high, medium, or low expression levels, together with Arabidopsis wild-type Col-0, were treated with NaCl. All seeds were sown on half-strength MS medium alone or containing different concentrations of NaCl (50, 100, and 150 mM). After stratification for 2–3 days, the plates were released into tissue culture chambers. After 24 h, the germination percentage was scored as the emergence of the radicle through the seed coat. Thegermination percentage was calculated as follows: germination percentage (%) = number of germinated seeds/total seeds × 100%. Since the germination percentage of overexpressing lines was significantly lower than that of Col-0, the relative germination percentage of impermeable salt treatment was calculated as follows: (germination percentage under control − germination percentage under NaCl treatment)/germination percentage under control × 100% on half-strength MS medium.

All seeds were evenly sown on medium with different NaCl concentrations (0, 50, 100, and 150 mM) as three replicates. Seedlings were photographed after 5 days with an anatomical microscope, and root length was measured in ImageJ. As the relative inhibition rate of root length elongation was significantly lower than that of the WT, the relative shortening rate was also calculated. The relative inhibition rate of root length elongation was calculated as root length under control – root length under NaCl treatment)/root length under control × 100% on half-strength MS medium.

According to Han et al. (Han et al., 2019) and Guo et al. (Guo, 2017), 7-day-old Arabidopsis seedlings were transferred to nutrient soil and then treated with different concentrations of salt for 1 week. The fresh weight and various physiological indicators were determined after salt treatment for 1 week. The relative decrease in fresh weight was calculated as (fresh weight under control – fresh weight under NaCl treatment)/fresh weight under control × 100%. The relative reduction in dry weight was calculated as (dry weight under control – the dry weight under NaCl treatment)/dry weight under control × 100%. To determine the contents of various small molecules, 0.5 g of seedlings growing under different NaCl concentrations was collected and Na^+, K^+, malondialdehyde (MDA), and proline contents were measured. Ion concentrations were determined using a flame photometer (M410, Sherwood, United Kingdom). Five replicates were performed for each line.

2.11 Determination of plant hormone contents in Lb1G04794 transgenic Arabidopsis

Endogenous phytohormones were extracted from 7-day-old Arabidopsis seedlings by the isopropanol-water-hydrochloric acid method. Endogenous phytohormone contents were determined with an Agilent 1290 high-performance liquid chromatography (HPLC) tandem AB Sciex QTRAP 6500^+ mass spectrometer, and internal standard substances were added during extraction. Since the growth and development of overexpression lines were clearly weaker than those of the WT,

the contents of indole-3-acetic acid (IAA) and ABA were specifically targeted for determination.

2.12 Analysis of salt resistance marker gene expression in Lb1G04794 transgenic Arabidopsis

Total RNA was extracted from Arabidopsis seedlings grown on half-strength MS medium for 5 days and transplanted to soil for 2 weeks. The expression of six stress-related genes, *SALT OVERLY SENSITIVE1* (At2G01980, *AtSOS1*), *SOS2* (At1G01140), *SOS3* (At5G35410), *HIGH-AFFINITY* K^+ *TRANSPORTER1* (At4G1030, *AtHKT1*), Na^+/H^+ *EXCHANGER1* (At5G27150, *AtNHX1*), and *GST CLASS TAU5* (At2G29450, *AtGSTU5*), was determined by RT-qPCR (Supplementary Table 1). Three biological replicates were performed. The formula $2^{-\Delta\Delta C(T)}$ was used to calculate relative expression, with *ACTIN2* used as internal reference.

2.13 Statistical analysis

Statistical analysis was performed using SPSS at $P = 0.05$ (Duncan's multiple range tests). Analysis of variance (ANOVA) with orthogonal contrasts and mean comparison procedures was used to detect differences between the treatments.

3 Results

3.1 Characteristics and expression pattern of Lb1G04794

Based on the full-length sequence of *Lb1G04794*, we cloned a 1,074-bp open reading frame encoding a 357–amino acid protein with a predicted molecular weight of 39,928.25 Da and an isoelectric point (PI) of 6.36 (Supplementary Figure 1A). The gene sequence was verified to be consistent with the genomic data by sequencing. Of these 357 amino acids, 110 were hydrophobic, accounting for 30.8% of the total amino acid number, and 247 were hydrophilic (or 69.2%). The predicted protein had an aliphatic index of 65.01, indicating that the protein encoded by *Lb1G04794* is a hydrophilic protein without a transmembrane helical structure (Supplementary Figure 1B). We identified no homologous protein for Lb1G04794 in Arabidopsis. We thus used a BLAST search at NCBI with the predicted Lb1G04794 protein sequence as query (Supplementary Figure 2). We determined that the protein encoded by *Lb1G04794* is a hypothetical protein with no transmembrane domain (Supplementary Figure 1C), no signal peptide (Supplementary Figure 1D), and no conserved domain (Supplementary Figure 1E), making its function completely unknown. An analysis of the *Lb1G04794* promoter (2,000 bp upstream of the ATG) identified a core promoter element and a typical *cis*-element involved in light responses, a *cis*-element associated with methyl jasmonate (MeJA) responses (CGTCA-motif), a *cis*-acting element involved in salicylic acid (SA) reaction (TCA-element), and a *cis*-acting element involved in defense and stress response (TC-rich repeats) (Figure 1F). We generated transgenic Arabidopsis lines harboring the *Lb1G04794* promoter driving the transcription of the *β-GLUCURONIDASE* (*GUS*) reporter gene; we observed GUS staining in cotyledons and roots, especially in the root tip of these transgenic reporter lines (Figure 1E).

3.2 Lb1G04794 localizes to the nucleus and has self-activation activity

To determine the subcellular localization of the protein encoded by *Lb1G04794*, we transiently transformed onion epidermal cells with Agrobacterium harboring the vector p1300-*Lb1G04794*, encoding a fusion protein between GFP and the protein encoded by *Lb1G04794*. Observations with a two-photon fluorescence inverted microscope showed that GFP-*Lb1G04794* localizes specifically in the nucleus (Figure 1A), while the empty vector overexpressing free *GFP* resulted in green fluorescence in both the nucleus and the cytoplasm. We also studied the expression of *Lb1G04794* in *L. bicolor* at different developmental stages (Figure 1B) and under different treatments (Figure 1C). *Lb1G04794* was highly expressed during stages A and B, responded to salt treatment, and was most highly expressed in leaves compared to other tissues. We also observed that *Lb1G04794* expression responded to NaCl, SA, and MeJA treatments, with a peak in *Lb1G04794* transcript levels 6–12 h into the treatment, followed by a gradual decrease back to normal levels (Figure 1C). Finally, we determined that the protein encoded by *Lb1G04794* displays self-activation activity in yeast when fused to the GAL4 DNA-binding domain (Figure 1D).

3.3 *Lb1G04794* participated in salt gland development of *Limonium bicolor*

The *Lb1G04794* was overexpressed in *L. bicolor* (Figure 2), after expression level verification (Figure 2A), compared with the control transformed with the empty vector, overexpression of *Lb1G04794* can significantly enhanced salt gland development (Figures 2B, C). This indicated that *Lb1G04794* may participate in promoting salt gland differentiation.

3.4 Transgenic arabidopsis lines develop more trichomes and fewer root hairs

We isolated Arabidopsis transgenic lines overexpressing *Lb1G04794* from the cauliflower mosaic virus (CaMV) 35S

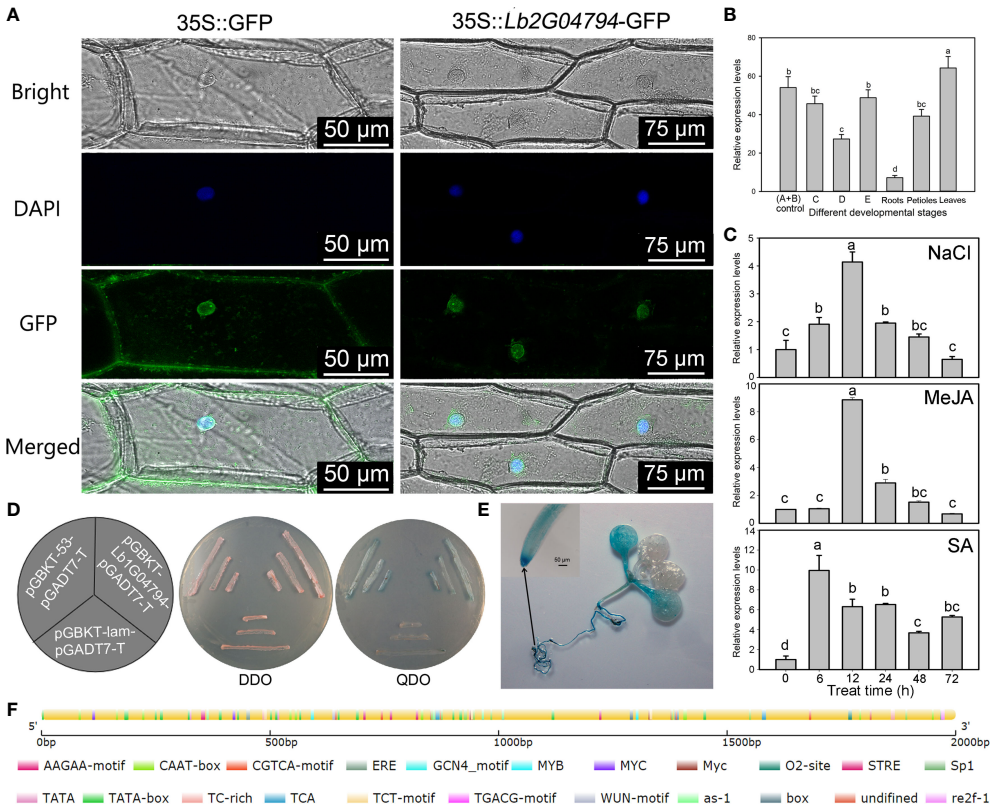

FIGURE 1
Expression pattern of *Lb1G04794* and subcellular localization of its encoded protein. **(A)** Subcellular localization of the protein encoded by the unknown gene *Lb1G04794* in onion epidermal cells transiently transformed with *35S:Lb1G04794-GFP via* Agrobacterium. pCAMBIA 1300-35S-sGFP (*35S:GFP*) was used as an empty control vector. Scale bar, 100 μm in *35S:GFP*, 250 μm in *35S:Lb1G04794-GFP*. **(B)** Expression of *Lb1G04794* in *L. bicolor* at different developmental stages. Stage A, undifferentiated, 4–5 days after sowing; stage B, salt gland differentiation, 6–7 days after sowing; stage C, stomatal differentiation, 8–10 days after sowing; stage D, epidermal differentiation, 11–16 days after sowing; stage E, mature, more than 17 days after sowing. Old leaves, >20 days old; petiole, base of stage-E leaf; root, root of stage-E seedling. Data are means of three replicates ± SD; different lowercase letters indicate significant differences at $P = 0.05$ according to Duncan's multiple range test. **(C)** Changes in *Lb1G04794* expression levels under different treatments: NaCl, MeJA, and SA for 6, 12, 24, 48, and 72 h. Data are means of three replicates ± SD; different lowercase letters indicate significant differences at $P = 0.05$ according to Duncan's multiple range test. **(D)** The protein encoded by *Lb1G04794* self-activates when expressed in yeast. Colonies were grown on synthetic defined (SD) medium −Trp −Leu (SD −Trp −Leu) and SD −Trp −Leu −Ade −His+X-α-gal. pGADT7-T+pGBKT7-*Lb1G04794*, experimental group; pGADT7-T+pGBKT7-53, positive control; pGADT7-T+pGBKT7-lam, negative control. **(E)** GUS staining results of the *Lb1G04794* promoter driving GUS expression in Arabidopsis transgenic lines (7 days after germination). **(F)** Schematic diagram of the *Lb1G04794* promoter, as predicted using PlantCARE (Lescot et al., 2002 (http://bioinformatics.psb.ugent.be/webtools/plantcare/html/); the map was drawn using CSDS 2.0 (Hu et al., 2015) (http://gsds.gao-lab.org/). Different colors indicate different *cis*-elements.

promoter. We confirmed the presence of the transgene by PCR and its expression by RT-qPCR (Supplementary Figure 3). We selected the overexpression lines OE-21, OE-1, and OE-4 as lines with high, medium, and low expression levels of the transgene for subsequent experiments (Supplementary Figure 3). As *Lb1G04794* was highly expressed during the development of salt glands in *L. bicolor*, we first characterized trichome and root hair development.

We counted the number of trichomes of the first fully extended true leaf of the Arabidopsis transgenic lines, which indicated that the overexpression lines have significantly more trichomes than the WT (Figures 3A, C). We identified *Lb1G04794* by screening for genes with high expression during salt gland development, underscoring the correlation between salt gland and trichome development. Similarly, we counted the number of root hairs over a 1-cm region from the root tip and observed that overexpression of *Lb1G04794* results in fewer root hairs, together with a shorter root, relative to the WT (Figures 3B, C).

3.5 Effect of NaCl treatment on the germination of Lb1G04794 overexpression Arabidopsis lines

Considering that *Lb1G04794* expression was induced by NaCl treatment (Figure 1C) and that fewer root hairs

10.3389/fpls.2022.1079534

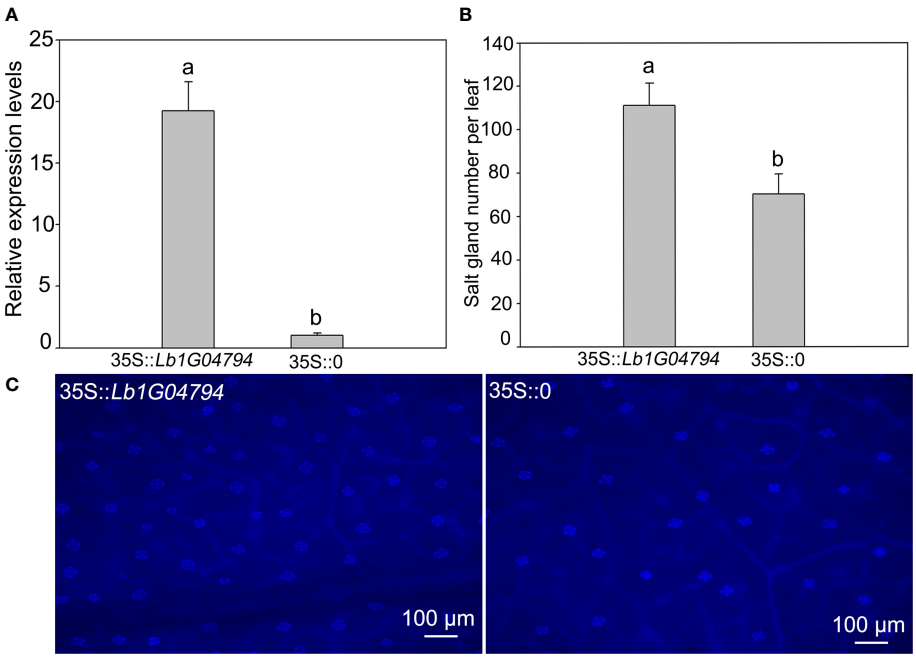

FIGURE 2
The salt gland phenotypes and quantification after overexpressing *Lb1G04794* in *L. bicolor*. **(A)** The expression level of overexpression line (35S::*Lb1G04794*) and control (35S::0). **(B)** The total number of salt glands per leaf. Data are means ± SD of three seedlings; different letters indicate significant differences at $P = 0.05$ according to Duncan's multiple range test. **(C)** The salt gland phenotypes in overexpression line and control under 330–380 nm microscope.

developed in *Lb1G04794* overexpression lines (Figure 3B), we explored salt tolerance–related indices at the germination stage in the transgenic lines. To this end, we sowed seeds from Arabidopsis and three transgenic lines onto medium containing different NaCl concentrations to determine the effect of NaCl on seed germination (Figure 4A). Notably, the germination of all *35S:Lb1G04794* overexpression lines was significantly lower under all conditions than in the WT of 24, 48, and 72 h after sowing, even when sown on control medium lacking added NaCl.

Although the germination percentage of the transgenic lines was lower than that of the WT (Figure 4B), the relative inhibition of root elongation (Figure 4C) was less affected by NaCl treatment than in the WT. These results indicated that germination and growth are inhibited upon overexpression of *Lb1G04794*, but the transgenic lines showed a greater salt tolerance than the WT under equivalent NaCl conditions.

The germination percentage of the transgenic lines was clearly inhibited under control (0 NaCl) conditions, which prompted us to measure the contents of endogenous phytohormones, with a focus on the three plant hormones IAA and ABA. We established that IAA contents in the overexpression lines are significantly lower than in the non-transgenic WT (Supplementary Figure 4), a result that was in agreement with the shorter roots of these lines, while the contents for ABA were similar between all genotypes. The lower IAA levels explained the shorter roots seen in the overexpression lines, indicating that *Lb1G04794* may negatively regulated IAA biosynthesis. These changes in plant hormone levels in the overexpression lines may reflect internal physiological changes of the overexpressing lines.

3.6 The effect of Lb1G04794 overexpression on salt tolerance at the seedling stage

We also investigated the long-term effect of NaCl treatment on the growth of Arabidopsis transgenic lines after a 2-week NaCl treatment in soil (Figure 5A). Although the biomass of the transgenic lines was lower than that of the WT, their relative dry and fresh weights appeared less affected by increasing NaCl concentrations than the WT (Figures 5B, C).

We also measured several physiological indices (Na^+, K^+, proline, and MDA contents) to explore the relationship between *Lb1G04794* and salt stress. Under 100 mM NaCl treatment, the proline contents of *35S:Lb1G04794* lines were lower than in WT. However, MDA contents in the overexpression lines under control conditions were higher than in the WT, suggesting that *Lb1G04794* overexpression imposes a degree of cellular stress in Arabidopsis. Na^+ and K^+ contents showed no

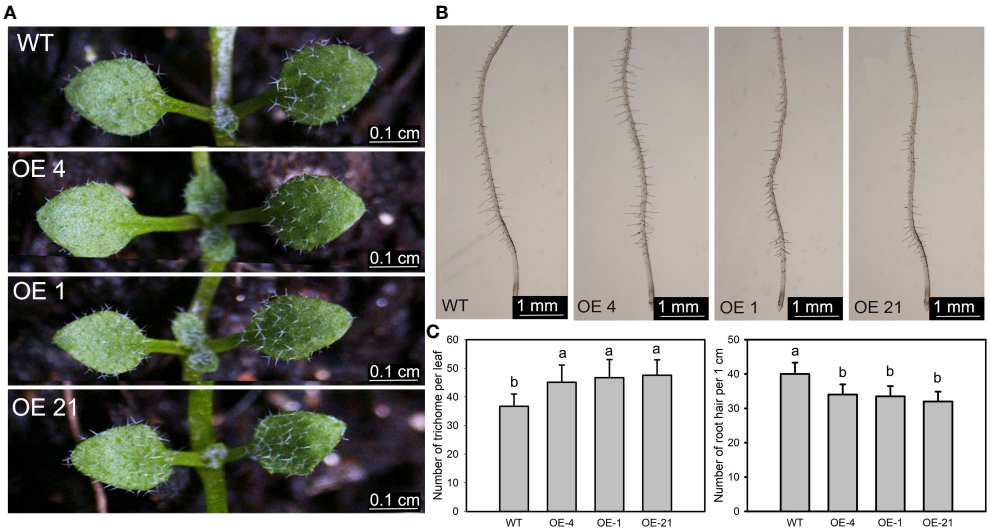

FIGURE 3
Trichome and root hair development in *35S:Lb1G04794* Arabidopsis lines. **(A)** Trichomes on the first two rosette leaves of the non-transgenic wild-type (WT, Col-0) and *35S:Lb1G04794* (OE 4, OE 1, and OE 21). Photographs show seedlings grown on half-strength MS medium for 7 days. Scale bar, 0.1 cm. **(B)** Root hairs in seedlings grown for 5 days on half-strength MS medium. Scale bar, 1 mm. **(C)** Number of trichomes per leaf (leaf) and root hairs (right) in WT and *35S:Lb1G04794* lines. Trichome number was counted in 10 seedlings. Root hair number was counted in the same region of each root (1 cm from root tip upward) for 10 seedlings per line. Data are means ± SD of 10 seedlings; different lowercase letters indicate significant differences at $P = 0.05$ according to Duncan's multiple range test.

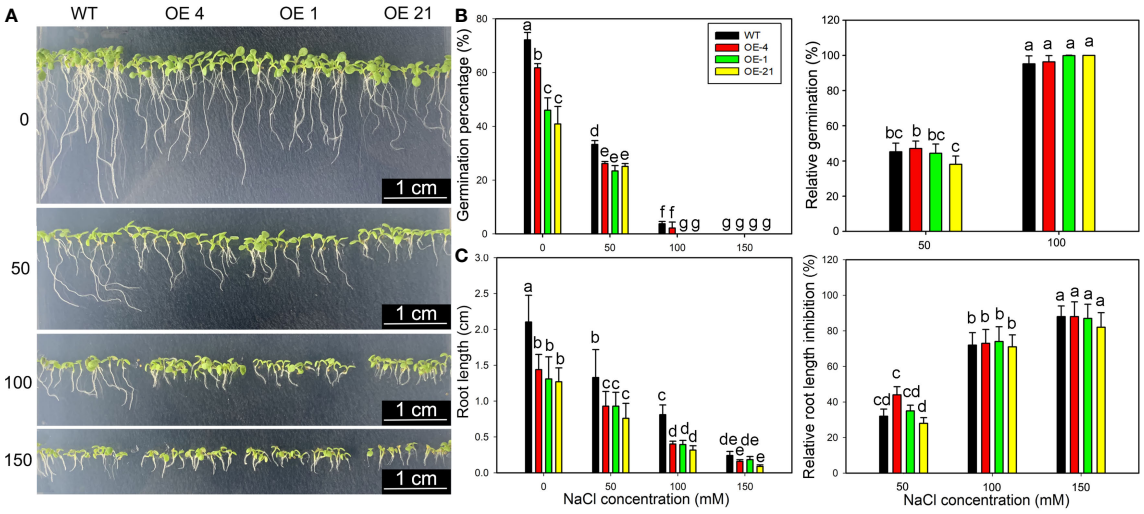

FIGURE 4
Growth characteristics of *35S:Lb1G04794* transgenic Arabidopsis lines following germination on different NaCl levels. **(A)** Phenotypes of WT and *35S:Lb1G04794* (OE 4, OE 1, and OE 21) Arabidopsis lines grown on half-strength MS medium (0) or different NaCl concentrations (50, 100, and 150 mM) for 5 days. **(B)** Germination percentages and germination inhibition percentages after 24 h at different concentrations of NaCl. The relative inhibition percentages of germination was calculated as (germination percentages under control − germination percentages under NaCl treatment)/germination percentages under control × 100%. **(C)** Root length and relative inhibition rate of root length elongation after 3 days at different concentrations of NaCl. The relative inhibition rate of root length elongation was calculated as (root length under control − root length under NaCl treatment)/root length under control × 100%. Fifty seeds per line were sown for each treatment, and three biological replicates were performed. The data for percentage germination are means ± SD. Root length of 5-day-old seedlings was measured in ImageJ. Data for root length are means ± SD of 10 seedlings per line; different lowercase letters indicate significant differences at $P = 0.05$ according to Duncan's multiple range test.

significant differences between genotypes when treated with 100 mM NaCl (Figure 5D). MDA contents in the *35S:Lb1G04794* lines increased to a lesser extent than in the WT when exposed to 100 mM NaCl (Figure 5E).

3.7 Expression of salt tolerance marker genes in transgenic Arabidopsis overexpressing Lb1G04794

We determined the expression levels of the six salt tolerance marker genes *AtSOS1*, *AtSOS2*, *AtSOS3*, *AtHKT1*, *AtNHX1*, and *AtGSTU5* by RT-qPCR. Notably, all of these genes displayed the similar trends (Figure 6). Under control conditions, all six genes showed the same expression levels in the WT and the overexpression lines, with little significant difference between genotypes. Upon treatment with 100 mM NaCl, however, the transcript levels of all salt stress–related marker genes increased significantly in all genotypes, although the expression levels in the overexpression lines were significantly lower than those in the WT.

4 Discussion

Recretohalophytes *L. bicolor* is a typical salt-secreting halophyte with epidermal salt glands and can grow under high-salt conditions (Yuan et al., 2018), providing a very important repertoire of potential salt tolerance genes (Zhang et al., 2022). Here, *Lb1G04794* was an uncharacterized gene cloned from *L. bicolor*, which was highly expressed during salt gland development and participate in promoting salt gland differentiation by overexpression (Figures 1, 2). The transgenic Arabidopsis lines have enhanced salt tolerance at the germination and seedling stage by reducing their salt sensitivity (Figures 4, 5). Lb1G04794 localized in the nucleus with self-activation activity, which may act as a transcription factor to regulate the expression of related genes and further regulate plant adaptation to stress, especially salt stress.

As the most important and special structure of *L. bicolor* resistant to salt stress (Yuan et al., 2022), salt gland development were proposed by various genes. The overexpression of *Lb1G04794* in *L. bicolor* induced enhanced salt gland development (Figure 2), indicating that this gene positively

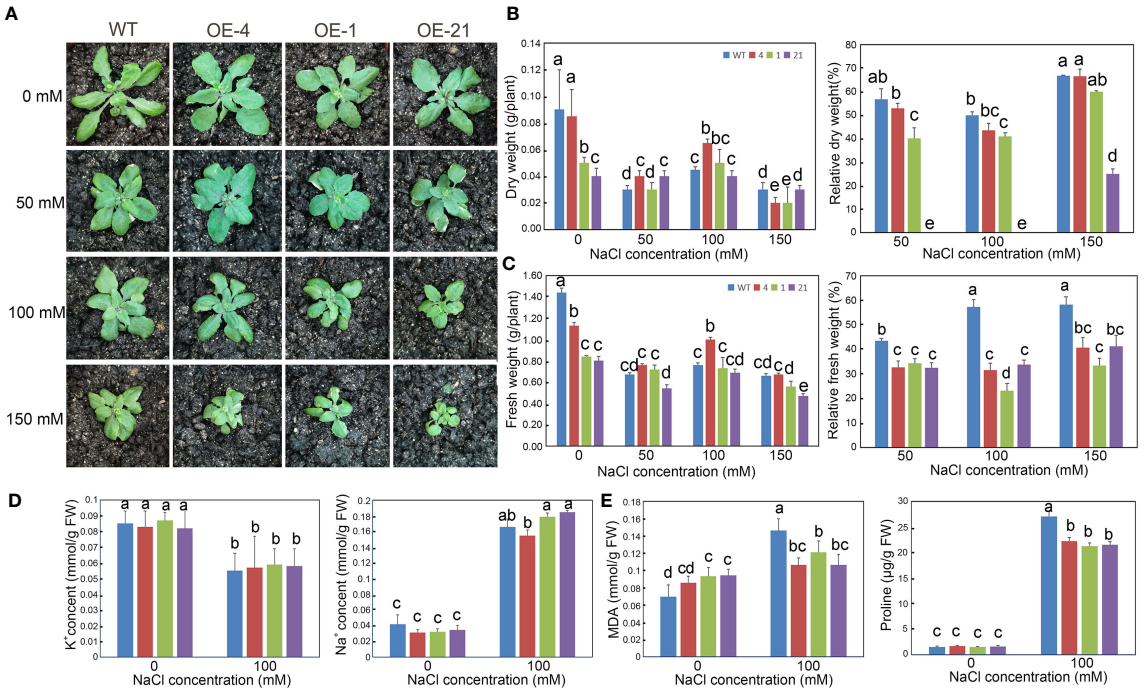

FIGURE 5
Growth status and determination of physiological indicators of Arabidopsis lines overexpressing *Lb1G04794* exposed to high-salt conditions. **(A)** Three-week-old plants of WT and 35S:*Lb1G04794* (OE 4, OE 1, and OE 21) lines under control conditions (0) or 50, 100, and 150 mM NaCl treatment. **(B, C)** Fresh **(C)** and dry weight **(B)** per plant of different lines under control conditions (0) or 50, 100, and 150 mM NaCl treatments. Relative reduction in fresh/dry weight per plant under control conditions (0) or 50, 100, and 150 mM NaCl treatments were also shown. **(D)** Na^+ and K^+ contents per plant under control conditions (0) or 100 mM NaCl treatment. **(E)** Contents for MDA or proline in each line under control conditions (0) or 100 mM NaCl treatment. Data are the means ± SD of three replicates; different lowercase letters indicate significant differences at $P = 0.05$ according to Duncan's multiple range test.

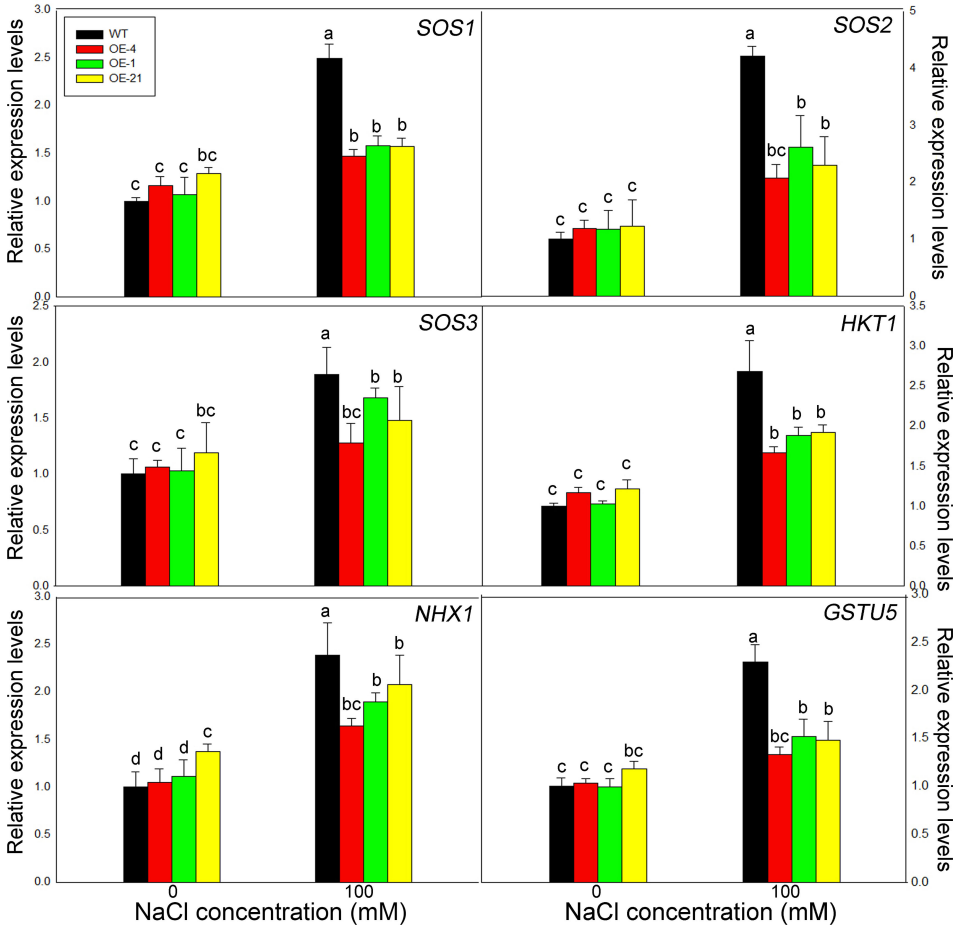

FIGURE 6
Expression levels of salt resistance–related marker genes in *Lb1G04794* transgenic Arabidopsis lines. Relative expression levels of *AtSOS1*, *AtSOS2*, *AtSOS3*, *AtHKT1*, *AtNHX1*, and *AtGSTU5*. WT and *35S:Lb1G04794* (OE 4, OE 1, and OE 21) Arabidopsis lines were grown for 7 days on half-strength MS medium (0) or with 100 mM NaCl. Data are means ± SD of three seedlings; different lowercase letters indicate significant differences at $P = 0.05$ according to Duncan's multiple range test.

regulate salt gland differentiation by promoting the initiation and development of salt glands to increase the number of salt glands in order to better adapt to high salt environment.

The salt resistance mechanisms of *Lb1G04794* were further verified in Arabidopsis by heterologous expression. At germination stage (Figure 4), although absolute indicators at the germination and seedling stages were lower than WT, a closer inspection of the results indicated that the transgenic lines exhibit the same phenotypes regardless of NaCl status, in contrast to the WT, whose germination percentage and root elongation were strongly and severely affected by high-salt treatment. By contrast, fewer root hairs in the overexpression lines limits the uptake of Na^+ under high-salinity conditions (Figure 3). Further determination of plant hormone contents indicated that IAA contents are lower in the overexpression lines, which would help explain the shorter roots observed in these lines. The repression of germination and growth of the transgenic lines could make them more adaptable to salt stress. However, the comparison of germination percentages at the seedling stage was established on the premise of similar germination conditions without salt treatment (Mwando et al., 2020). *Lb1G04794* clearly showed an effect on germination percentage when overexpressed even under normal growth conditions, which we interpret as a buffer and adaptation to adverse growth conditions. So *Lb1G04794* can down-regulate the root development of Arabidopsis in the germination stage and delay plant growth in order to reduce the salt absorption and promote the salt resistance of transgenic lines in order to make the individual better adapt to the salt stress.

At seedling stage (Figure 5), the overexpression strains also showed resistance to salt stress. Through the measurement of various physiological indexes, it was found that the overexpressed lines accumulated less Na^+, MDA and proline compared with WT under the same NaCl conditions. On the one hand, the less Na^+ accumulation may be related to the less

absorption due to fewer root hairs development (Figure 3) in overexpression lines. On the other hand, the physiological indicators were all consistent with the hypothesis that less Na^+ was taken up by the overexpression lines, while osmoregulatory substances accumulated to cope with salt stress. Interesting, we validated this result with the determination of expression levels for salt tolerance marker genes (Figure 6), which again were consistent with diminished responses to salt stress in the overexpression lines, likely caused by reduced salt uptake.

Notably, the overexpression of *Lb1G04794* in Arabidopsis resulted in an increase in the number of trichomes (Figure 3), which is reminiscent of other reports in which the overexpression of a gene encoding a WD40-repeat protein from *L. bicolor* increased salt resistance by promoting trichome development in Arabidopsis (Yuan et al., 2019a). The experimental results also confirm the evolutionary relatedness of salt glands and trichomes, forming salt glands or trichomes as two different options for gene regulation (Yuan et al., 2022). This result illustrates the close relationship between salt gland development and trichome formation. We propose that salt glands and trichomes constitute two possible developmental trajectories that share several key genes.

Lb1G04794, a gene of unknown function in *L. bicolor*, showed a correlation between salt gland and trichome development in Arabidopsis, in addition to several developmental roles. Based on the current report of *Lb1G04794* participating in salt gland development and salt resistance, more application and the characterization of more salt gland-related genes will continue to be explored in order to offer new ways to combat high salinity.

Data availability statement

The original contributions presented in the study are included in the article/Supplementary Material. Further inquiries can be directed to the corresponding authors.

Author contributions

FY designed the research; XJ and BZ performed the research; XJ and BZ analyzed the data; XJ and FY wrote the paper; FY and BW revised the paper. All authors contributed to the article and approved the submitted version.

Funding

This study was supported by the MOE Layout Foundation of Humanities and Social Sciences (21YJAZH108), and the National Natural Science Research Foundation of China (NSFC, project nos. 31770288 and 31600200).

Conflict of interest

The authors declare that the research was conducted in the absence of any commercial or financial relationships that could be construed as a potential conflict of interest.

Publisher's note

All claims expressed in this article are solely those of the authors and do not necessarily represent those of their affiliated organizations, or those of the publisher, the editors and the reviewers. Any product that may be evaluated in this article, or claim that may be made by its manufacturer, is not guaranteed or endorsed by the publisher.

Supplementary material

The Supplementary Material for this article can be found online at: https://www.frontiersin.org/articles/10.3389/fpls.2022.1079534/full#supplementary-material

SUPPLEMENTARY FIGURE 1
The sequence and bioinformatics characteristics of *Lb1G04794*.

SUPPLEMENTARY FIGURE 2
Phylogenetic tree of *Lb1G04794* and related unknown proteins identified by NCBI-BLAST.

SUPPLEMENTARY FIGURE 3
Screening of transgenic Arabidopsis lines by PCR and RT-qPCR. **(A)** Genotyping results of Arabidopsis transgenic lines harboring the *35S:Lb1G04794* transgene. M, DNA marker with standard molecular weight of 2,000; lanes 1–15, different *35S:Lb1G04794* Arabidopsis lines; lane 16, negative control, with Col-0 DNA as template. **(B)** Relative expression levels of *Lb1G04794* in the Arabidopsis transgenic lines, as determined by RT-qPCR in *35S:Lb1G04794* lines; OE numbers represent the different *35S:Lb1G04794* overexpression lines. Data are means of three replicates ± SD; different lowercase letters indicate significant differences at $P = 0.05$ according to Duncan's multiple range test.

SUPPLEMENTARY FIGURE 4
Determination of IAA and ABA contents. WT and *35S:Lb1G04794* (OE 4, OE 1, and OE 21) Arabidopsis seedlings were grown for 7 days on half-strength MS medium. Three biological replicates were performed. Data are means ± SD of three seedlings; different lowercase letters indicate significant differences at $P = 0.05$ according to Duncan's multiple range test.

SUPPLEMENTARY TABLE 1
Sequences of the primers used in this study.

References

Boyer, J. S. (1982). Plant productivity and environment. *Science* 218(4571), 443–448. doi: 10.1126/science.218.4571.443.

Clough, S. J., and Bent, A. F. (1998). Floral dip: a simplified method for agrobacterium -mediated transformation of arabidopsis thaliana. *Plant Journal* 16(6), 735–743. doi: 10.1046/j.1365-313x.1998.00343.x.

Cui, Y. (2021). *Cloning and salt resistance analysis of LpNAC17 gene from lilium pumilum* (Northeast Forestry University).

Gao, Y., Zhao, B., Jiao, X., Chen, M., Wang, B., and Yuan, F. (2021). Coupled development of salt glands, stomata, and pavement cells in limonium bicolor. *Front. Plant Sci.* 12, 745422. doi: 10.3389/fpls.2021.745422

Guo, J., Dong, X., Li, Y., and Wang, B. (2020a). NaCl Treatment markedly enhanced pollen viability and pollen preservation time of euhalophyte suaeda salsa *via* up regulation of pollen development-related genes. *J. Plant Res.* 133, 57–71. doi: 10.1007/s10265-019-01148-0

Guo, J., Li, Y., Han, G., Song, J., and Wang, B. S. (2017). NaCl Markedly improved the reproductive capacity of the euhalophyte suaeda salsa. *Funct. Plant Biol.* 44, 350–361. doi: 10.1071/fp17181.

Guo, J., Lu, C., Zhao, F., Gao, S., and Wang, B. (2020b). Improved reproductive growth of euhalophyte suaeda salsa under salinity is correlated with altered phytohormone biosynthesis and signal transduction. *Funct. Plant Biol.* 47, 170–183. doi: 10.1071/FP19215.

Guo, S., Xu, Y., Liu, H., Mao, Z., Zhang, C., Ma, Y., et al. (2013). The interaction between OsMADS57 and OsTB1 modulates rice tillering *via* DWARF14. *Nat. Commun.* 4, 1566. doi: 10.1038/ncomms2542.

Han, G., Yuan, F., Guo, J., Zhang, Y., Sui, N., and Wang, B. (2019). AtSIZ1 improves salt tolerance by maintaining ionic homeostasis and osmotic balance in arabidopsis. *Plant Sci.* 285, 55–67. doi: 10.1016/j.plantsci.2019.05.002

Hu, B., Jin, J., Guo, A.-Y., Zhang, H., Luo, J., and Gao, G. (2015). GSDS 2.0: an upgraded gene feature visualization server. *Bioinf. (Oxford England)* 31, 1296–1297. doi: 10.1093/bioinformatics/btu817

Jing, X. (2021). *Cloning and functional study of unknown genes Lb2G14763, Lb3G18904 and Lb7G32827 in limonium bicolor* (Shandong Normal University).

Leng, B., Geng, F., Dong, X., Yuan, F., and Wang, B. (2019a). Sodium is the critical factor leading to the positive halotropism of the halophyte limonium bicolor. *Plant Biosyst. - Int. J. Dealing all Aspects Plant Biol.* 153, 544–551. doi: 10.1080/11263504.2018.1508085

Leng, B., Wang, X., Yuan, F., Zhang, H., Lu, C., Chen, M., et al. (2021). Heterologous expression of the limonium bicolor MYB transcription factor LbTRY in arabidopsis thaliana increases salt sensitivity by modifying root hair development and osmotic homeostasis. *Plant Sci.* 302, 110704. doi: 10.1016/j.plantsci.2020.110704.

Leng, B. Y., Yuan, F., Dong, X. X., Wang, J., and Wang, B. S. (2018). Distribution pattern and salt excretion rate of salt glands in two recretohalophyte species of limonium (Plumbaginaceae). *South Afr. J. Of Bot.* 115, 74–80. doi: 10.1016/j.sajb.2018.01.002.

Leng, B., Zhao, P., Dong, X., Yuan, F., and Wang, B. (2019b). Study on the physiological mechanism of early flowering and low Male fertility of limonium bicolor mutant vrl15. *J. Plant Growth Regul.* 38, 1206–1214. doi: 10.1007/s00344-019-09925-w

Lescot, M., Déhais P, G., Thijs, G., Marchal, K., Moreau, Y., Van De Peer, Y., Rouzé, P., et al. (2002) PlantCARE, a database of plant cis-acting regulatory elements and a portal to tools for in silico analysis of promoter sequences. *Nucleic Acids Res* 30 (1362-4962), 7. doi: 10.1093/nar/30.1.325

Li, J., Yuan, F., Liu, Y., Zhang, M., Liu, Y., Zhao, Y., et al. (2020). Exogenous melatonin enhances salt secretion from salt glands by upregulating the expression of ion transporter and vesicle transport genes in limonium bicolor. *BMC Plant Biol.* 20, 493. doi: 10.1186/s12870-020-02703-x.

Lu, C., Feng, Z., Yuan, F., Han, G., Guo, J., Chen, M., et al. (2020). The SNARE protein LbSYP61 participates in salt secretion in limonium bicolor. *Environ. Exp. Bot.* 176. doi: 10.1016/j.envexpbot.2020.104076.

Lu, X., Liu, R., Liu, H., Wang, T., Li, Z., Zhang, L., et al. (2022). Experimental evidence from suaeda glauca explains why the species is not naturally distributed in non-saline soils. *Sci. Total Environ.* 817, 153028. doi: 10.1016/j.scitotenv.2022.153028

Ma, Y., Yang, Y., Liu, R., Li, Q., and Song, J. (2020). Adaptation of euhalophyte suaeda salsa to nitrogen starvation under salinity. *Plant Physiol. Biochem.* 146, 287–293. doi: 10.1016/j.plaphy.2019.11.025

Munns, R., and Tester, M. (2008). Mechanisms of salinity tolerance. *Annu Rev Plant Biol* 59, 651–681. doi: 10.1146/annurev.arplant.59.032607.092911

Murashige, T., and Skoog, F. (1962). A revised medium for rapid growth and bio assays with tobacco tissue cultures. *Physiol Plant* 15(3), 473–497. doi: 10.1111/j.1399-3054.1962.tb08052.x.

Mwando, E., Han, Y., Angessa, T. T., Zhou, G., Hill, C. B., Zhang, X. Q., et al. (2020). Genome-wide association study of salinity tolerance during germination in barley (Hordeum vulgare l.). *Front. Plant Sci.* 11, 118. doi: 10.3389/fpls.2020.00118.

Rasool, S., Hameed, A., Azooz, M. M., Muneeb U, R., Siddiqi, T. O., and Ahmad, P. (2013). "Salt stress: Causes, types and responses of plants," in *Ecophysiology and responses of plants under salt stress*, 1–24.

Song, Y., Li, J., Sui, Y., Han, G., Zhang, Y., Guo, S., et al. (2020). The sweet sorghum SbWRKY50 is negatively involved in salt response by regulating ion homeostasis. *Plant Mol. Biol.* 102, 603–614. doi: 10.1007/s11103-020-00966-4

Song, J., and Wang, B. (2015). Using euhalophytes to understand salt tolerance and to develop saline agriculture: Suaeda salsa as a promising model. *Ann. Bot.* 115 (3). doi: 10.1093/aob/mcu194.

Sui, N., Tian, S., Wang, W., Wang, M., and Fan, H. (2017). Overexpression of glycerol-3-Phosphate acyltransferase from suaeda salsa improves salt tolerance in arabidopsis 8 (14). doi: 10.3389/fpls.2017.01337

Sun, W., Cao, Z., Li, Y., Zhao, Y., and Zhang, H. (2007). A simple and effective method for protein subcellular localization using agrobacterium-mediated transformation of onion epidermal cells. *Biologia* 62, 529–532. doi: 10.2478/s11756-007-0104-6

Su, M., Wang, S., Liu, W., Yang, M., Zhang, Z., Wang, N., et al. (2022). Interaction between MdWRKY55 and MdNAC17-l enhances salt tolerance in apple by activating MdNHX1 expression. *Plant science* 320, 111282. doi: 10.1016/j.plantsci.2022.111282

Wang, X., Wang, B., and Yuan, F. (2022). Lb1G04202, an uncharacterized protein from recretohalophyte limonium bicolor, is important in salt tolerance. *Int. J. Mol. Sci.* 23 (10), 16. doi: 10.3390/ijms23105401

Wang, X., Zhou, Y., Xu, Y., Wang, B., and Yuan, F. (2021). A novel gene LbHLH from the halophyte limonium bicolor enhances salt tolerance *via* reducing root hair development and enhancing osmotic resistance. *BMC Plant Biol.* 21, 284. doi: 10.1186/s12870-021-03094-3

Wei, L. (2006). *Functional identification of an unknown gene in the EST database of saltmustard* (Shandong Normal University).

Xu, Y., Jiao, X., Wang, X., Zhang, H., Wang, B., and Yuan, F. (2021). Importin-β from the recretohalophyte limonium bicolor enhances salt tolerance in arabidopsis thaliana by reducing root hair development and abscisic acid sensitivity. *Front. Plant Sci.* 11, 2100. doi: 10.3389/fpls.2020.582459

Yuan, F., Chen, M., Leng, B. Y., and Wang, B. S. (2013). An efficient autofluorescence method for screening limonium bicolor mutants for abnormal salt gland density and salt secretion. *South Afr. J. Bot.* 88, 110–117. doi: 10.1016/j.sajb.2013.06.007.

Yuan, F., Guo, J., Shabala, S., and Wang, B. (2018). Reproductive physiology of halophytes: Current standing. *Front. Plant Sci.* 9, 1954. doi: 10.3389/fpls.2018.01954.

Yuan, F., Leng, B., and Wang, B. (2016a). Progress in studying salt secretion from the salt glands in recretohalophytes: How do plants secrete salt? *Front. Plant Sci.* 7, 977. doi: 10.3389/fpls.2016.00977.

Yuan, F., Leng, B., Zhang, H., Wang, X., Han, G., and Wang, B. (2019a). A WD40-repeat protein from the recretohalophyte limonium bicolor enhances trichome formation and salt tolerance in arabidopsis. *Front. Plant Sci.* 10, 1456. doi: 10.3389/fpls.2019.01456

Yuan, F., Liang, X., Li, Y., Yin, S., and Wang, B. (2019b). Methyl jasmonate improves tolerance to high salt stress in the recretohalophyte limonium bicolor. *Funct. Plant Biol.* 46, 82–92. doi: 10.1071/FP18120

Yuan, F., Lyu, M. J., Leng, B. Y., Zheng, G. Y., Feng, Z. T., Li, P. H., et al. (2015). Comparative transcriptome analysis of developmental stages of the limonium bicolor leaf generates insights into salt gland differentiation. *Plant Cell Environ.* 38, 1637–1657. doi: 10.1111/pce.12514.

Yuan, F., Lyu, M.-J. A., Leng, B.-Y., Zhu, X.-G., and Wang, B.-S. (2016b). The transcriptome of NaCl-treated limonium bicolor leaves reveals the genes controlling salt secretion of salt gland. *Plant Mol. Biol.* 91 (3), 241-256. doi: 10.1007/s11103-016-0460-0.

Yuan, F., Wang, X., Zhao, B., Xu, X., Shi, M., Leng, B., et al. (2022). The genome of the recretohalophyte limonium bicolor provides insights into salt gland development and salinity adaptation during terrestrial evolution. *Mol. Plant* 15, 1024–1044. doi: 10.1016/j.molp.2022.04.011

Zhang, M., Chen, Z., Yuan, F., Wang, B., and Chen, M. (2022). Integrative transcriptome and proteome analyses provide deep insights into the molecular mechanism of salt tolerance in limonium bicolor. *Plant Mol. Biol.* 108, 127–143. doi: 10.1007/s11103-021-01230-z

Zhao, X. (2020). *Preliminary study on the involvement of ChAOX2 gene in salt resistance* (Northeast Forestry University).

Zheng, H., Yang, Z., Wang, W., Guo, S., Li, Z., Liu, K., et al. (2020). Transcriptome analysis of maize inbred lines differing in drought tolerance provides novel insights into the molecular mechanisms of drought responses in roots. *Plant Physiol. Biochem.* 149, 11–26. doi: 10.1016/j.plaphy.2020.01.027.

Zhu, M. (2014). *A preliminary study of an unknown functional gene involved in osmotic stress response in arabidopsis thaliana* (Nanjing university).

frontiers | Frontiers in Plant Science

TYPE Original Research
PUBLISHED 21 December 2022
DOI 10.3389/fpls.2022.1065677

Check for updates

OPEN ACCESS

EDITED BY
Mahmoud Magdy,
Ain Shams University, Egypt

REVIEWED BY
Chun-Hai Dong,
Qingdao Agricultural University, China
Benjamin Karikari,
University for Development Studies, Ghana
Xiaoyun Li,
South China Normal University, China

*CORRESPONDENCE
Xiaoyi Li
lixiaoyi202@scu.edu.cn

†These authors have contributed equally to this work

SPECIALTY SECTION
This article was submitted to Plant Abiotic Stress, a section of the journal Frontiers in Plant Science

RECEIVED 10 October 2022
ACCEPTED 08 December 2022
PUBLISHED 21 December 2022

CITATION
Peng L, He J, Yao H, Yu Q, Zhang Q, Li K, Huang Y, Chen L, Li X, Yang Y and Li X (2022) CARK3-mediated ADF4 regulates hypocotyl elongation and soil drought stress in Arabidopsis. *Front. Plant Sci.* 13:1065677. doi: 10.3389/fpls.2022.1065677

COPYRIGHT
© 2022 Peng, He, Yao, Yu, Zhang, Li, Huang, Chen, Li, Yang and Li. This is an open-access article distributed under the terms of the Creative Commons Attribution License (CC BY). The use, distribution or reproduction in other forums is permitted, provided the original author(s) and the copyright owner(s) are credited and that the original publication in this journal is cited, in accordance with accepted academic practice. No use, distribution or reproduction is permitted which does not comply with these terms.

CARK3-mediated ADF4 regulates hypocotyl elongation and soil drought stress in Arabidopsis

Lu Peng†, Juan He†, Huan Yao, Qin Yu, Qian Zhang, Kexuan Li, Yaling Huang, Li Chen, Xufeng Li, Yi Yang and Xiaoyi Li*

Key Laboratory of Bio-Resources and Eco-Environment of Ministry of Education, State Key Laboratory of Hydraulics and Mountain River Engineering, College of Life Sciences, Sichuan University, Chengdu, China

Actin depolymerization factors (ADFs), as actin-binding proteins, act a crucial role in plant development and growth, as well as in response to abiotic and biotic stresses. Here, we found that CARK3 plays a role in regulating hypocotyl development and links a cross-talk between actin filament and drought stress through interaction with ADF4. By using bimolecular fluorescence complementation (BiFC) and GST pull-down, we confirmed that CARK3 interacts with ADF4 *in vivo* and *in vitro*. Next, we generated and characterized double mutant *adf4cark3-4* and OE-ADF4:*cark3-4*. The hypocotyl elongation assay indicated that the *cark3-4* mutant seedlings were slightly longer hypocotyls when compared with the wild type plants (WT), while *CARK3* overexpressing seedlings had no difference with WT. In addition, overexpression of *ADF4* significantly inhibited long hypocotyls of cark3-4 mutants. Surprisingly, we found that overexpression of *ADF4* markedly enhance drought resistance in soil when compared with WT. On the other hand, drought tolerance analysis showed that overexpression of *CARK3* could rescue *adf4* drought susceptibility. Taken together, our results suggest that CARK3 acts as a regulator in hypocotyl elongation and drought tolerance likely *via* regulating ADF4 phosphorylation.

KEYWORDS

hypocotyl elongation, drought tolerance, actin depolymerization factor, CARK3, phosphorylation

Introduction

Actin filaments (F-actin), as a scaffold in cells, play a fundamental role in numerous cellular processes, including morphogenesis, motility and cell elongation. In addition, the studies have shown that F-actin also functions in response to abiotic and biotic stresses in planta (Lin et al., 2014). The dynamic of F-actin is regulated by actin-binding proteins

(ABPs), including actin depolymerization factors (ADFs), formin family proteins and adenylyl cyclase-associated proteins (Liu et al., 2018; Jiang et al., 2019).

ABPs are involved in regulating a vast array of fundamental biological processes, such as the normal organism development (Ketelaar et al., 2004). For example, the actin-binding protein Rice Morphology Determinant (RMD) in rice (*Oryza sativa*) promotes statolith mobility in gravisensing endodermal cells, and for proper auxin distribution in light-grown shoots through reorganization of the actin cytoskeleton (Song et al., 2019). ADF7 and ADF10 directly modulate pollen tube elongation in Arabidopsis (Zheng et al., 2013; Jiang et al., 2017; Jiang et al., 2022). UV-B inhibits Arabidopsis hypocotyl elongation due to the fact that actin filaments shift from bundles to a loose arrangement (Du et al., 2020b). PRF4 and PRF5, as actin-binding proteins, could regulate vesicle trafficking and polarity establishment during pollen germination by enhancing the interaction between AtFH5 (Arabidopsis formin homology 5) and actin filaments (Liu et al., 2021). In the dark, *ADF4* mutants have longer hypocotyl and epidermal cells when compared with wild-type seedlings (Henty et al., 2011; Yao et al., 2022). However, the molecular mechanism of ADF4 is not uncovered in regulating the hypocotyl elongation.

In addition, ABPs have been implicated in integration of cellular responses to extracellular and intracellular signals during biotic and abiotic stresses. *GhVLN4* from cotton, as one type of major ABPs responsible for microfilament bundling, overexpression of which shows resistance to *Verticilium dahliae*, salt and drought stresses in Arabidopsis. (Ge et al., 2021). *Actin-depolymerizing factor 1* (ADF) is repressed by MYB73, which is known as a negative regulator in salt tolerance, and then regulates actin filaments organization (Wang et al., 2021). Additionally, ADF4 is mediated by CPK3 to control pathogen-induced actin reorganization during immune signaling, and phosphorylated by CKL2 to regulate actin filaments in stomata in response to dehydration (Guo et al., 2016; Lu et al., 2020). However, the recent studies have revealed that ADF5 has evolved F-actin-bundling activity, thus positively regulates drought stress (Qian et al., 2019). *DaADF3* from *Deschampsia antarctica* is induced by drought stress (Byun et al., 2021). Knockdown of *TaADF3* from wheat leads to *Puccinia striiformis* susceptibility, which is accompanied by increased ROS production (Tang et al., 2015). ADFs regulate the dynamics of actin filaments in response to environmental cues.

Our previous studies have shown that CAK3 kinase protein could form dimer to phosphorylate ABA (abscisic acid) receptors, and subsequently trigger ABA signaling pathway (Li et al., 2022). Here, we observed that *CARK3* T-DNA mutants exhibited long hypocotyl compared with the wild-type plants. Further, we found that CARK3 phosphorylates ADF4, and the association cooperatively mediates the hypocotyl growth in the dark. Moreover, the interaction between CARK3 and ADF4 led us to investigate a role of CARK3 during drought stress. The evaluation of drought tolerance reveals that overexpression of *ADF4* could resume *cark3-4* drought sensitivity in Arabidopsis.

Materials and methods

Plant materials and growth conditions

Plant materials and growth conditions Arabidopsis plants used in this study were all in the Columbia (Col-0) background. The *cark3-4* and *adf4* T-DNA insertion mutants, OE-*ADF4* #10, #17, #18 and *CARK3*-OE 2 overexpression plants were previously described (Wang et al., 2020; Yao et al., 2022). Plants were grown on soil-vermiculite mixtures at 22°C under 60% relative humidity with cycles of 16 h light and 8 h dark. For plate experiment, seeds were stratified in distilled water for 3 days at 4°C in dark. The imbibed seeds were surface sterilized with a 20% bleach solution for 15 min and then washed 5 times with sterilized water, and then sown on Murashige and Skoog (MS) medium containing 2% sucrose and 1.0% agar, pH 5.8.

Bimolecular fluorescence complementation (BiFC) assay

The ADF4-YFP^N and CARK3-YFP^C constructs were previously described (Wang et al., 2020; Yao et al., 2022). The constructs were transformed into Agrobacteria GV3101 stain. And then the indicated YFP^N/YFP^C combination were co-expressed in 4-week old tobacco leaves. After 2 days, the signals of YFP were observed with a Leica confocal laser scanning microscope (DM4 B). 3 leaves were observed each time and three biological repeats were performed.

GST pull-down assay

To test the interaction of CARK3 with ADF4 *in vitro*, GST-CARK3, GST and His-ADF4 were purified as previously described (Li et al., 2022; Yao et al., 2022). 5 μg GST-CARK3 or GST bound glutathione-agarose beads were incubated with His-ADF4 in binding buffer (50 mM Tris-HCl, pH 8.0, 200 mM NaCl, 10% glycerol, 0.1% Tween 20) at room temperature for 30 min and washed 10 times with binding buffer. The pulled-down compounds were eluted with 2× SDS sample buffer (24 mM Tris-Cl, pH 6.8, 10% glycerol, 0.8% SDS, and 2% 2-mercaptoethanol) and boiled at 98°C for 10 min. Next,

proteins were analyzed by immunoblotting with GST and His antibodies.

In vitro kinase assay

To investigate CARK3-mediated phosphorylation of ADF4, the purified ADF4 was incubated with His-CARK3-KD (Kinase domain) in kinase buffer (20 mM Tris, pH 7.5, 1 mM $MgCl_2$, 100 mM NaCl, and 1 mM DTT, 5 mM ATP), which was previously described (Wang et al., 2020). After incubation at 30°C for 30 min, the reaction mixture was terminated by adding an equal volume of 2 × SDS-PAGE (Sodium Dodecyl Sulfate, Polyacrylamide Gel Electrophoresis) loading buffer, and boiled at 98°C for 5 min. The proteins were separated by SDS–PAGE and analyzed with Anti-Phosphoserine/threonine Rabbit Polyclonal (Cell Signaling Technology).

Physiological analysis

To test the interaction of CARK3 with ADF4 in response to soil drought stress, we obtained the double mutant *adf4cark3-4* and OE-*ADF4*:*cark3-4* by crosses. For drought tolerance experiment, 7 d seedlings indicated genotypes were grown under the same conditions and then subjected to drought stress treatment by withholding water for 12 or 13 days. Then, 2 days after rehydration, the morphological changes of plants were recorded, including survival rate and fresh weight (FW).

For hypocotyl elongation assay, genotypes were grown in the dark for 4 d after germination and then representative seedlings were photographed. At least 20 seedlings per genotype were measured as one biological replicate using ImageJ software (http://imagej.nih.gov/ij/).

Stomatal aperture was carried out as previously described (Li et al., 2022). 3-week old leaves were peeled and then incubated in opening buffer (50 mM KCl, 10 μM $CaCl_2$, 10 mM MES pH 6.15) for 3 h to induce stomatal opening. For ABA treatment, 5 and 20 μM ABA was added to the opening buffer for 30 min or 2 h. Images were taken using Leica TCS SP5 II HCS confocal microscope.

For nitroblue tetrazolium (NBT) staining to test superoxides, 3-week-old leaves were treated with or without 50 μM ABA for 1 days, and then incubated in NBT buffer for overnight. Chlorophyll was removed with 95% ethanol.

Statistical analysis

In this study, statistical data were analyzed using GraphPad Prism version 8 software (GraphPad Software, La Jolla, CA, USA). Data were collected in triplicates and subjected to analysis of variance (ANOVA). *Post hoc* means separation was done with Tukey's test at $P < 0.05$.

Results

CARK3 is involved in hypocotyl elongation

In this study, we found that *cark3-4* T-DNA mutants and RNAi plants exhibited longer length of hypocotyl than WT (Figure 1). In addition, the overexpression of *CARK3* lines had markedly shorter hypocotyl when compared with the wild-type plants (Figure 1). These results suggest that CARK3 modulates hypocotyl growth in Arabidopsis.

CARK3 phosphorylates ADF4

In our previous study, we reported that 14-3-3κ coordinates ADF4 to regulate hypocotyl elongation (Yao et al., 2022). The 14-3-3 proteins usually interact with kinase proteins to mediate signal transduction by altering their activity, or affinity to other proteins (Paul et al., 2012). Thus, we proposed that CARK3 would interact with 14-3-3κ. However, the bimolecular fluorescence complementation (BiFC) assay showed that CARK3 could not interact with 14-3-3κ *in vivo*. Next, we tested the association of CARK3 with ADF4 using the BiFC assay. The yellow fluorescent signals were observed in tobacco cells when co-expression of ADF4-YFP^N and CARK3-YFP^C. However, no signal was found, when co-expression of ADF4-YFP^N and YFP^C or YFP^N and CARK3-YFP^C (Figure 2A). These results indicate that CARK3 interact with ADF4 *in vivo*.

To further confirm the physical interaction of CARK3 and ADF4, we then performed an *in vitro* pull-down assay using bacterially expressed purified proteins. GST and His-ADF4, GST-CARK3 and His-ADF4 were co-incubated with GST resin, respectively. The bound proteins were tested with anti-GST and anti-His antibodies, respectively. As indicated in Figure 2B, GST-CARK3 could pull-downed His-ADF4, while GST could not, indicating that CARK3 physically interacts with ADF4 *in vitro*.

CARK3 has been shown to phosphorylate ABA receptors to mediate ABA signaling pathway (Li et al., 2022). ADF4 has revealed to be phosphorylated by CKL2 (*Arabidopsis thaliana* casein kinase 1-like protein 2) and CPK3 (Arabidopsis calcium-dependent protein kinase 3), showing multiple potential Ser/Thr phosphorylation sites (Guo et al., 2016; Lu

10.3389/fpls.2022.1065677

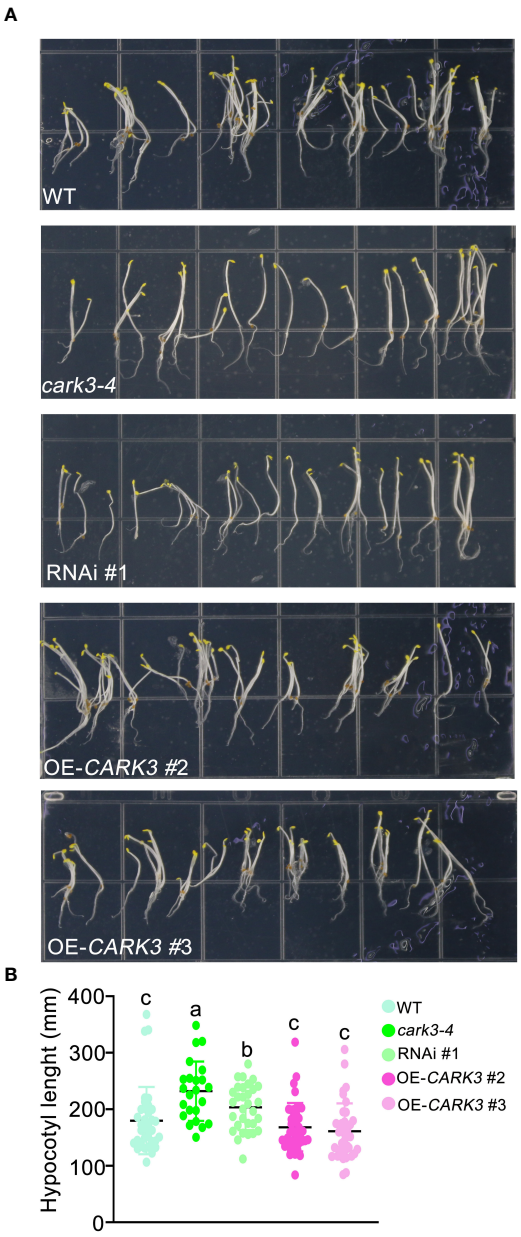

FIGURE 1
CARK3 is involved in hypocotyl elongation. **(A)** Seedlings from wild-type plants, CARK3 T-DNA insertion mutant (*cark3-4*), RNAi #1 plant and *CARK3*-overexpressing lines (*CARK3*-OE 2/3) grown on 1/2 MS growth medium in the dark for 4 d. **(B)** The graph shows the average hypocotyl length measured from a minimum of 20 seedlings. Each point represents an individual seedling. Lines and error bars represent the mean and 95% confidence interval for each genotype, respectively. Bars with different alphabets indicate significant difference by Tukey test at $P < 0.05$, while those with a common alphabet indicate no significant difference ($P > 0.05$).

et al., 2020). Thus, ADF4 could be a substrate of CARK3. To address this, an *in vitro* kinase assay was conducted. The phosphorylation band was observed, when ADF4 was incubated with CARK3. However, no band was detected in the gel without CARK3 (Figure 2C). The results suggest that CARK3 phosphorylates ADF4 *in vitro*.

CARK3-mediated ADF4 regulates hypocotyl elongation

To investigate ADF4 phosphorylated by CARK3 in regulation of hypocotyl elongation, we generated *adf4cark3-4* double mutant and OE-*ADF4*:*cark3-4* by crossing *cark3-4* with *adf4* and OE-*ADF4*, respectively (Yao et al., 2022). Next, sterilized seeds from WT, *adf4*, *cark3-4*, *adf4cark3-4* and OE-*ADF4*:*cark3-4* were plated on 1/2 MS plates grown vertically in the dark. After 4 d, we observed that *adf4cark3-4* double mutants displayed longer hypocotyls when compared with the *cark3-4* plants, and no significant difference with *adf4* or *cark3-4* (Figures 3A, B). On the other hand, the hypocotyl length in the *cark3-4* mutant was shorter than that of the OE-*ADF4*:*cark3-4* seedlings, which had longer hypocotyl length than OE-*ADF4* transgenic plants (Figures 3C, D). The hypocotyl length of the *adf4* seedlings exhibited longer than that of WT, which is consistent with the previous report (Henty et al., 2011; Yao et al., 2022). Considering that CARKs are involved in ABA signaling, we also investigated ABA-mediated hypocotyl growth in darkness. The results showed that *cark3-4* seedlings were insensitive to ABA (Figure S1), which may due to the fact that *cark3-4* plants have higher germination late that WT under ABA treatment (Wang et al., 2020). These results suggest that the phosphorylation of ADF4 by CARK3 mediates hypocotyl elongation in Arabidopsis.

Overexpression of *ADF4* enhances long-term drought tolerance

The previous studies have shown that CARK3 phosphorylates ABA receptors, triggers ABA binding, resulting in plant resistance to drought stress (Wang et al., 2020). In addition, ADF4 is also involved in stomatal closure through reorganization actin filaments (Guo et al., 2016). Thus, we proposed that CARK3 participates in drought tolerance, through regulation of ADF4 activity. To test this, we performed the drought tolerance assay in soil. The results showed that *CARK3*-OE plants had higher survival rate, while *cark3-4* mutants had lower when compared with the wild-type (WT) plants (Figures 4A, B). We further examined stomatal closure in response to ABA. The data showed that the *cark3-4* mutant was insensitive to ABA-induced stomatal closure under low (5 μM) and high (20 μM) concentration of ABA treatment (Figure 4C). Interestingly, we found that OE-*ADF4* lines were similar to WT, with 100% survival rate (Figures 5A, B), while the

10.3389/fpls.2022.1065677

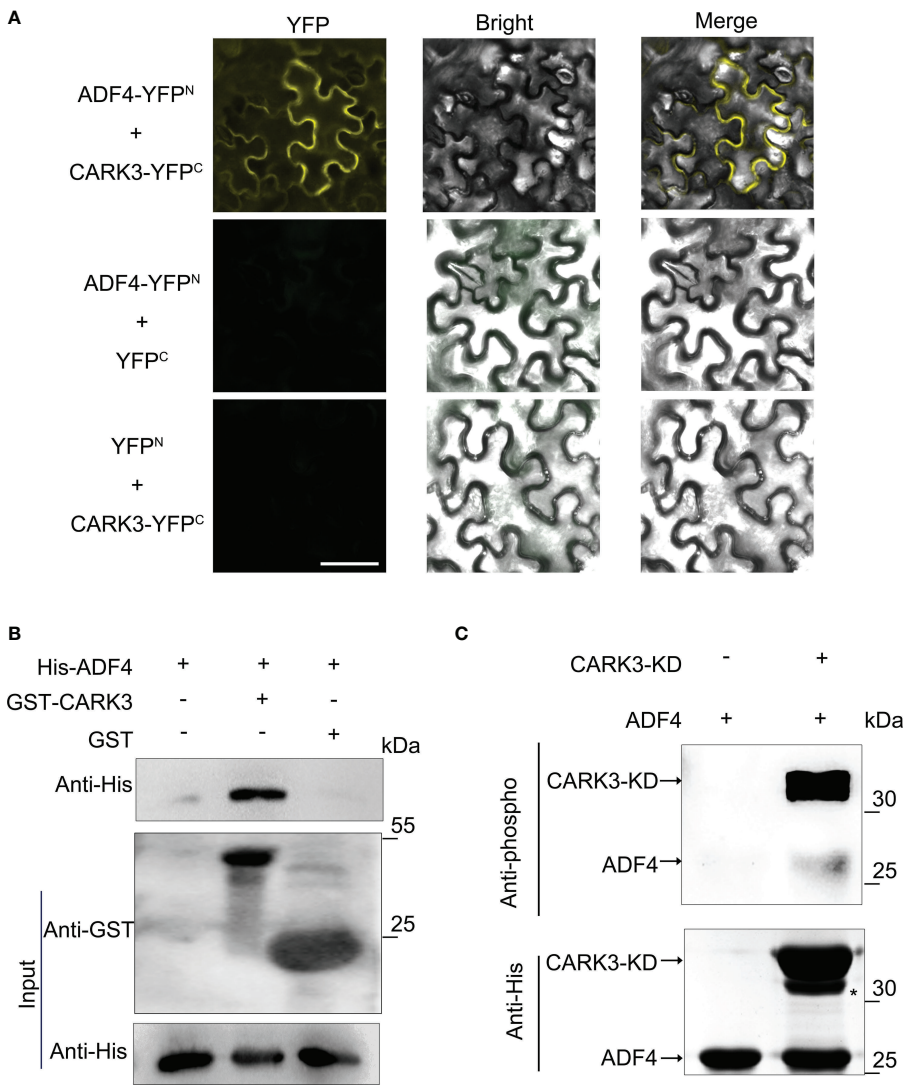

FIGURE 2
CARK3 interacts with ADF4. **(A)** BiFC assays showing interaction between CARK3 and ADF4 in tobacco leaves. Negative controls used were ADF4-YFP^N +YFP^C and YFP^N +CARK3-YFP^C. Scale bars = 50 μm. **(B)** Pull-down assays showing that GST-CARK3 interacts with His-ADF4. His-ADF4 pulled down by GST-CARK3 was detected by anti-His antibody. GST was used as a negative control and did not interact with His-ADF4. **(C)** *In vitro* phosphorylation of ADF4 by CARK3. Western blot assay with anti-phosphoserine/threonine antibody. Anti-His antibody was used to test loading.

percent survival of *adf4* was significantly lower than those of WT after drought treatment. The results of fresh weight also confirmed the phenotype analysis (Figure 5C). Additionally, the *adf4* mutant was sensitive to the low concentration of exogenous ABA (Figure 5D), which is consistent with the previous report (Guo et al., 2016). However, we here found that the *adf4* mutant was insensitive to ABA-induced stomatal closure, the plants overexpressing *ADF4* were sensitive under the high concentration of exogenous ABA treatment (Figure 5D). These data reveal that CARK3 and ADF4 are positive regulators in response to soil drought stress in Arabidopsis.

Drought resistance by CARK3 is dependent on ADF4

To determine the genetic relation of CARK3 with ADF4 in drought resistance, we performed drought tolerance experiment. The results showed that the *adf4cark3-4* double mutant had lower level of survival rate than WT, which had 100% survival rate and higher level than that of *adf4* or *cark3-4* genotype (Figures 6A, B). Similarly, WT plants had highest fresh weight after rewatered following 12-day dehydration (Figure 6C). ABA-induced stomatal closure assay also confirmed that the loss of *ADF4*

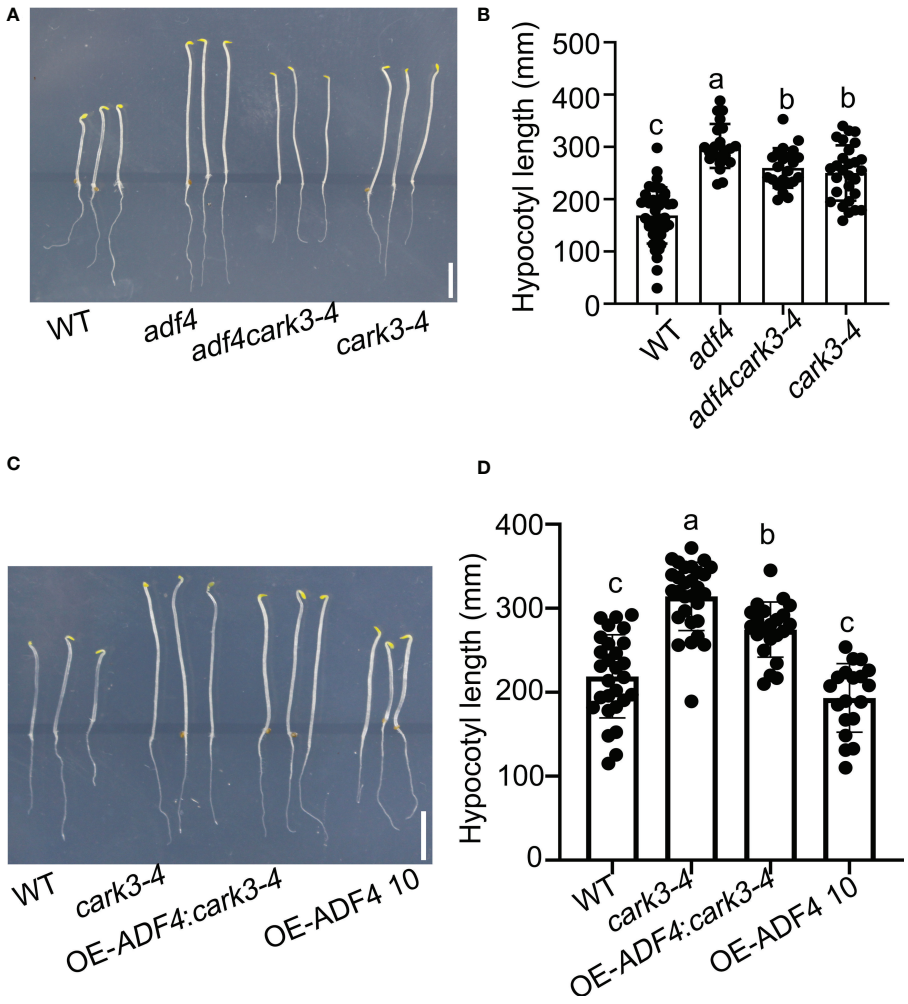

FIGURE 3
Overexpression of *ADF4* partially inhibited hypocotyl growth of c*ark3-4* mutants. **(A)** *adf4cark3-4* seedlings developed shorter hypocotyls when compared with *adf4* mutants. **(C)** OE-*ADF4*: *cark3-4* seedlings developed shorter hypocotyls than *cark3-4* mutants. **(B, D)** The graphs shows the average hypocotyl length measured from a minimum of 20 seedlings in **(A)** and **(C)**, respectively. Each point represents an individual seedling. Lines and error bars represent the mean and 95% confidence interval for each genotype, respectively. Bars with different alphabets indicate significant difference by Tukey test at $P < 0.05$, while those with a common alphabet indicate no significant difference ($P > 0.05$).

rescued the ABA insensitivity of *cark3-4* mutant under both low and high levels of exogenous ABA treatment (Figure 6D). Next, we analyzed OE-*ADF4*:*cark3-4* plants in drought tolerance compared with OE-*ADF4*, *cark3-4* and WT, respectively. The results showed that the percent survival rate of WT, OE-*ADF4* and OE-*ADF4*:*cark3-4* plants were indistinguishable (Figure 7A). However, OE-*ADF4*:*cark3-4* showed better and had higher level of fresh weight when compared WT OE-*ADF4* plants (Figures 7B, C). For ABA-induced stomatal aperture assay, we observed that the stomatal sensitivity of OE-*ADF4*:*cark3-4* plants to ABA recovered to that of the WT plants after low concentration of ABA treatment (Figure 7D). ABA induced-stomatal closure under drought stress also contributes to the production of hydrogen peroxide (H_2O_2) (An et al., 2019; Pei et al., 2022). In this study, we found that H_2O_2 accumulation in *adf4* mutants was higher than that in WT, while the *ADF4*-overexpressing line (#17) produced less H_2O_2 after ABA treatment (50 μM) (Figure S2). These phenotypic data indicate overexpression of *ADF4* mediates long-term drought tolerance through the its phosphorylation by CARK3.

Discussion

Plants need to respond to photomorphogenesis when grown in the light, and also undergo skotomorphogenesis in

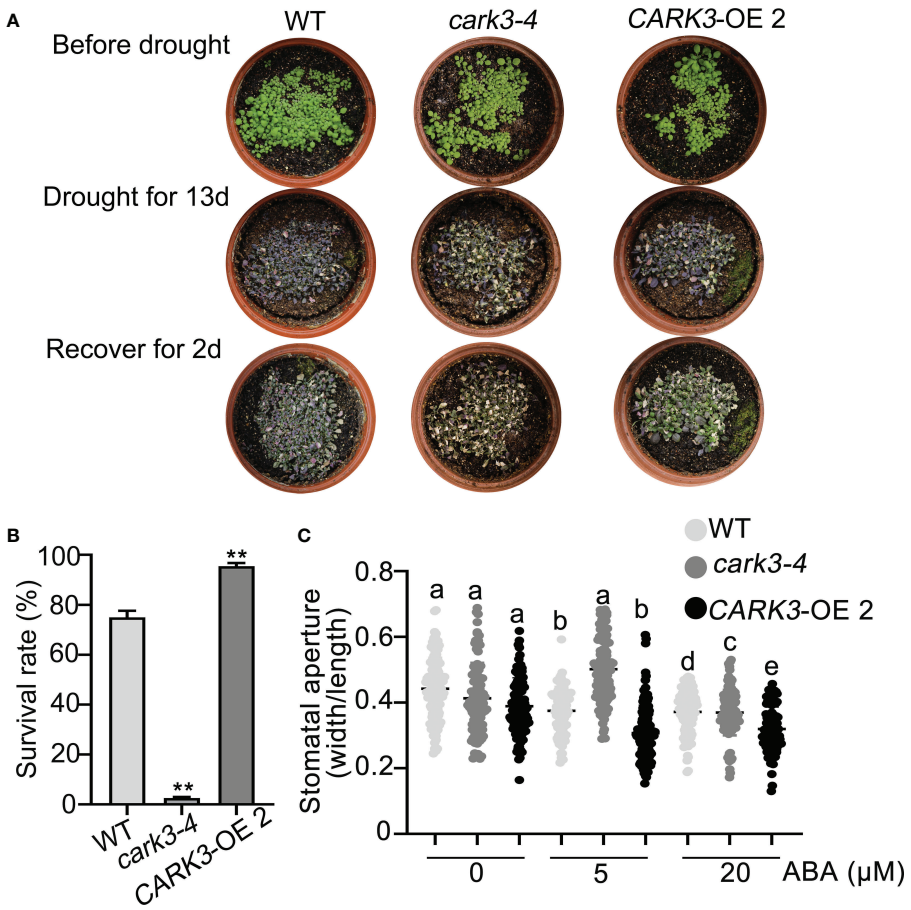

FIGURE 4
Overexpression of *CARK3* enhance Arabidopsis drought tolerance. **(A)** The representative images of the plants from WT, *cark3-4* and *CARK3*-OE that were grown for 7 days under normal conditions, then treated for 13 days with drought, and rewatered for 2 days. **(B)** Quantitative analysis of survival rates in **(A)**. Mean ± SEM, n = 3. $^{**}P < 0.05$, Student's *t*-test. The experiment was repeated three times, at least five pots at a time. **(C)** ABA-induced stomatal closure was measured with or without ABA treatment for 30 min. Low (5 μM) or high (20 μM) concentrations of ABA were added to the opening buffer. Each point represents some individual stomata, at least 50 stomata per genotype were measured. Bars with different alphabets indicate significant difference by Tukey test at $P < 0.05$, while those with a common alphabet indicate no significant difference ($P > 0.05$).

the dark, exhibiting long hypocotyls, as well as survive in response to multiple developmental and environmental cues. Hypocotyl length is usually controlled by cell elongation which is regulated by the dynamics of actin filaments (Fan et al., 2013; Zhao et al., 2015; Du et al., 2020b). In this study, we demonstrated that the phosphorylation of ADF4 mediated by CARK3 controls hypocotyl cell elongation and modulates soil dehydration in Arabidopsis.

Previous studies have revealed cross-talk between auxin and ABA signaling transduction (Emenecker et al., 2021). Auxin could induce reorganization of actin filaments (Du et al., 2020a). Loss of *AUX1* (auxin transporter AUXIN RESISTANT 1) leads to failure of actin reorganization in response to IAA treatment (Arieti and Staiger, 2020). ADF4 modulates auxin distribution and transport through regulating the dynamics of actin filaments, which is required for cell expansion (Deeks and Hussey, 2009; Jiang et al., 2020). Additionally, ABA receptors PYL8 (RCAR3) and PYL9 (RCAR1) could interact with the transcription factor PIF3 to regulate hypocotyl elongation (Qi et al., 2020). Our previous study shows that CARKs phosphorylate ABA receptors (Zhang et al., 2018). Thus, the interaction of ADF4 and CARK3 offers exciting new insights into the cross-talk between ABA signaling and actin filament in hypocotyl elongation.

The previous studies have revealed that *adf4* mutants have smaller stomatal aperture than the wild-type plants under 2 μM ABA treatment, indicating that ADF4 acts a negative

10.3389/fpls.2022.1065677

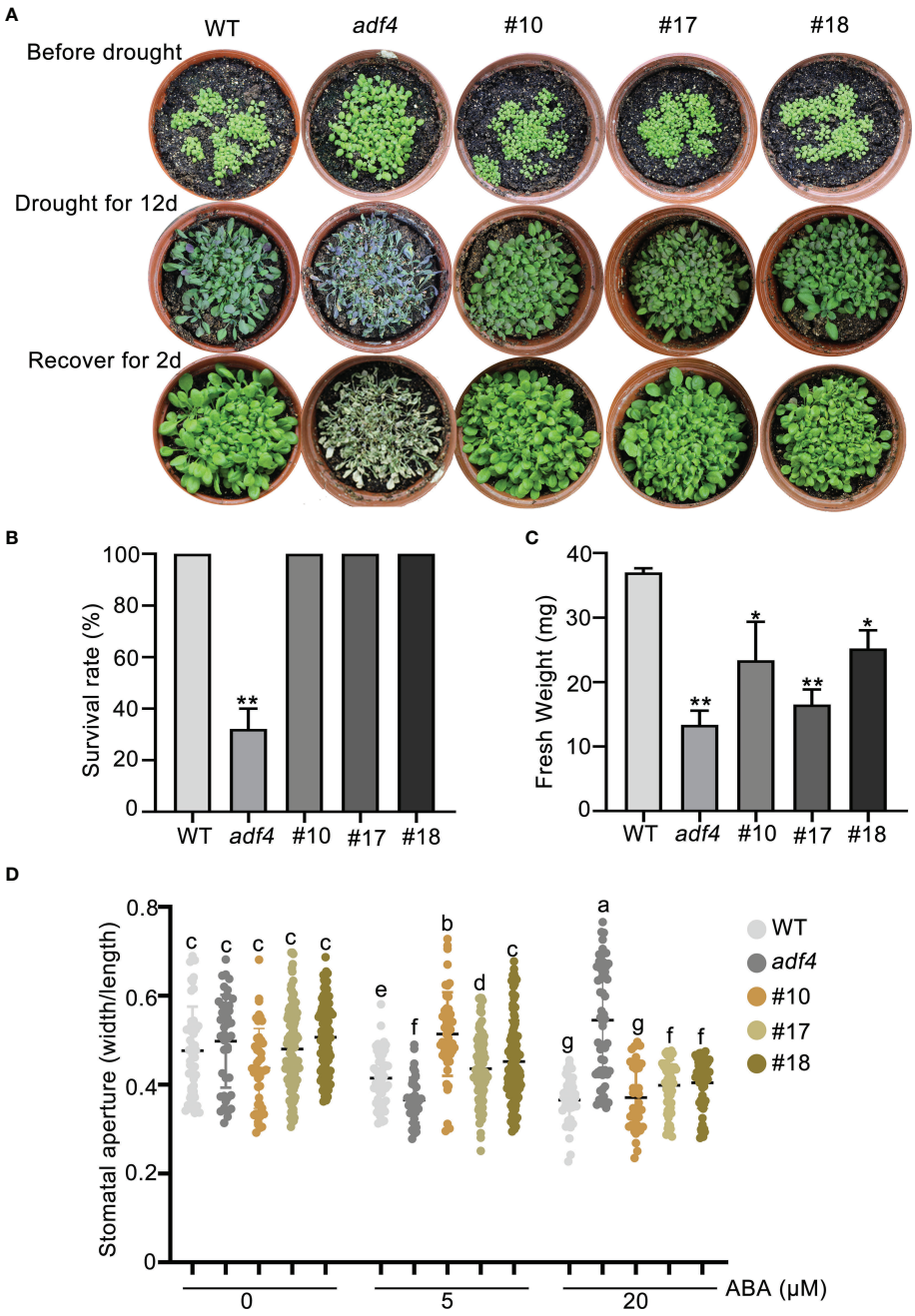

FIGURE 5
Overexpression of *ADF4* enhance Arabidopsis drought tolerance. **(A)** Images of plants before and after drought and after rewatering, including WT, *adf4* and OE-*ADF4* lines. The plants were grown for 7 days under normal conditions, then treated for 12 days without watering and rewatered for 2 days. **(B, C)** Quantities of survival rates and fresh weight of per pot from genotypes after rewatering in **(A)**. The error bars indicate the SEM from three replicates (n = 3). *$P < 0.05$, **$P < 0.01$, Student's *t*-test. The experiment was repeated three times, at least three pots at a time. **(D)** Stomatal aperture of WT, *adf4* and overexpression of *ADF4* plants. Four-week-old Arabidopsis leaves were treated with or without low (5 μM) and high (20 μM) concentrations of ABA for 2 h, respectively. Each point represents some individual stomata, at least 50 stomata per genotype were measured (the ratio of width to length). Bars with different alphabets indicate significant difference by Tukey test at $P < 0.05$, while those with a common alphabet indicate no significant difference ($P > 0.05$). #10, #17 and #18 represent the overexpression of *ADF4* lines in wild-type plants.

10.3389/fpls.2022.1065677

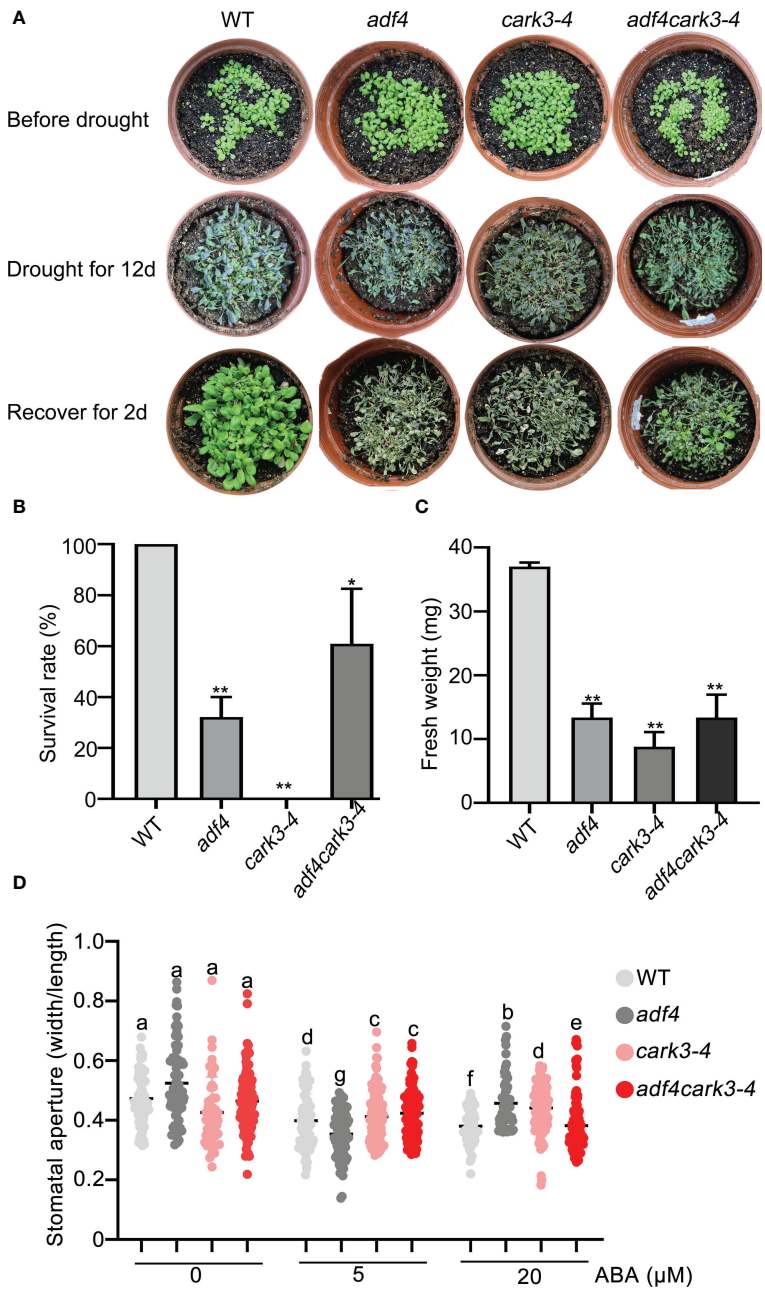

FIGURE 6
adf4 partially resumes *cark3* in response to soil drought stress. **(A)** Phenotypic comparison of WT, *cark3-4*, *adf4* and *adf4cark3-4* plants (upper) grown in soil after water was withheld for 12 days (middle) and the plants were then rewatered for 2 day (bottom). Three independent experiments were performed that yielded similar results; 5 pots per genotype for each time. **(B, C)** The survival rates and fresh weight were assessed in three replicates (n = 3). $*P < 0.05$, $**P < 0.05$, Student's *t*-test. **(D)** Stomatal closure (the ratio of stomatal width/length) was measured in WT, *cark3-4*, *adf4* and *adf4cark3-4* plants in response to 5 μM and 20 μM exogenous ABA. Each point represents some individual stomata, at least 50 stomata per genotype were measured. Bars with different alphabets indicate significant difference by Tukey test at $P < 0.05$, while those with a common alphabet indicate no significant difference ($P > 0.05$).

regulator in ABA-mediated drought tolerance (Guo et al., 2016). However, *adf4* mutants displayed lower survival rate compared with WT, when genotypes were subjected to long-term drought stress (Figure 5). We inferred that the inhibition of ADF4 activity by CARK3, leading to fail actin filament disassembly during stomatal closure. However, CKL2 inhibits ADF4 activity on severing actin filaments, leading to actin arrays being reorganized into

10.3389/fpls.2022.1065677

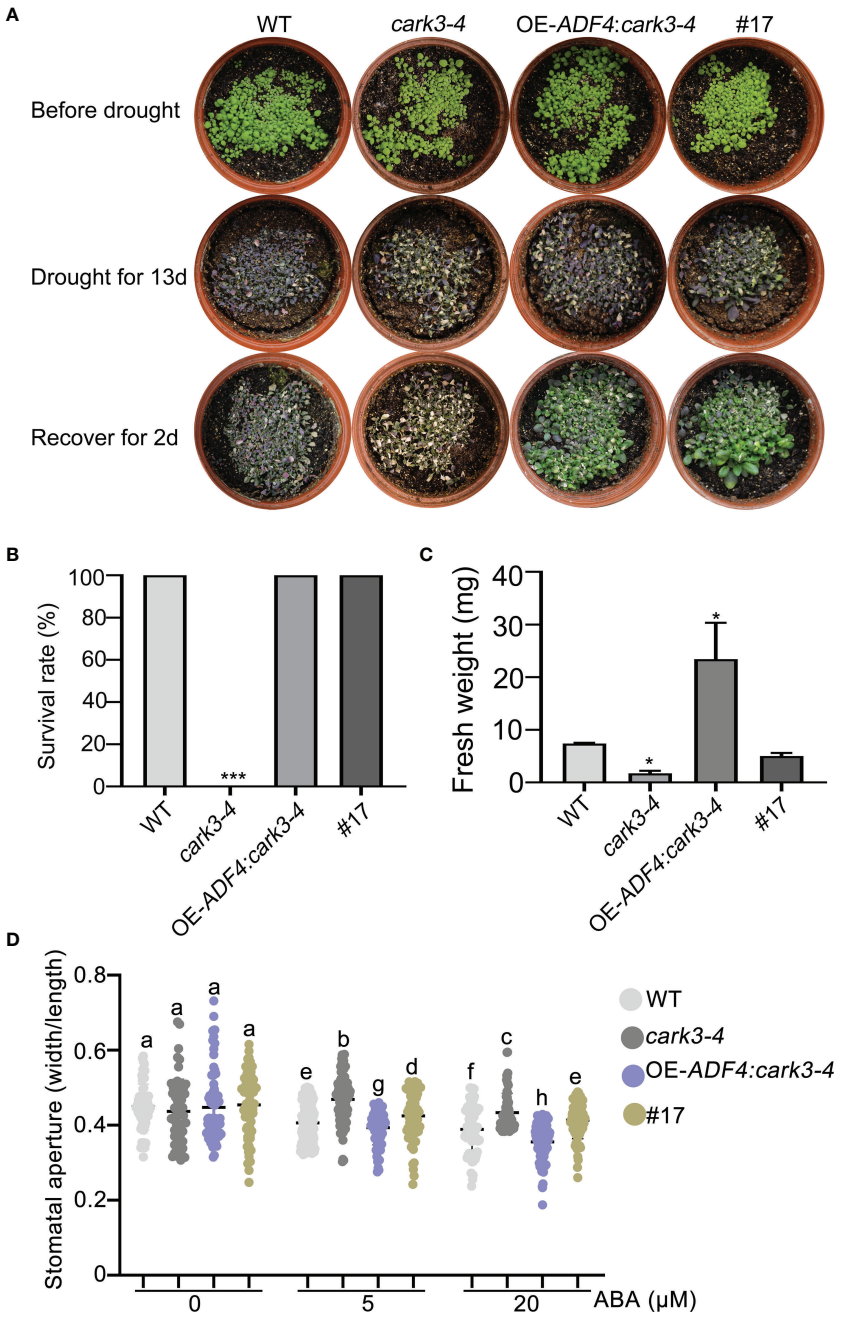

FIGURE 7
Overexpression of *CARK3* rescues *adf4* drought sensitivity. **(A)** Images of plants before and after drought and after rewatering, including WT, *cark3-4* and OE-*ADF4: cark3-4* genotypes. The plants were grown for 7 days under normal conditions, then treated for 13 days with drought, and rewatered for 2 days. **(B, C)** The survival rates and fresh weight were assessed in three replicates (n = 3). *$P < 0.05$, ***$P < 0.001$, Student's *t*-test. **(D)** ABA-induced stomatal closure was measured in each plant indicated under low (5 μM) and high (20 μM) concentrations of ABA treatment for 2 h. Each point represents some individual stomata, at least 50 stomata per genotype were measured. Bars with different alphabets indicate significant difference by Tukey test at $P < 0.05$, while those with a common alphabet indicate no significant difference ($P > 0.05$).

highly bundled long cables and maintain stomatal closure (Guo et al., 2016). The clade A PP2C phosphatase would inhibit CKL2 kinase activity, when water is supplied (Shi et al., 2021). Thus, overexpression of *ADF4* triggers F-actin in guard cell from cortical filaments to randomly distributed (Hwang and Lee, 2001), then CKL2 and CARK3 inhibit ADF4 activity, and then actin filaments changes to longitudinal direction, which stabilizes guard cells in closed stomata.

Similarly, CPK3-mediated ADF4 governs actin filaments organization and activate pattern- and effector-triggered immunity (Lu et al., 2020). In summary, ADF4 is mediated by upstream regulators during plant development and in response to abiotic and biotic stresses.

Data availability statement

The original contributions presented in the study are included in the article/Supplementary Material. Further inquiries can be directed to the corresponding author.

Author contributions

XYL and YY conceived and designed the experiment. LP and JH conducted the BiFC analysis. HY and QY preformed Arabidopsis crossing. KL, YH, and LC conducted drought tolerance experiments. XFL, YY, and XYL analyzed the results and wrote the paper. All authors contributed to the article and approved the submitted version.

Funding

This study was funded by the Science & Technology Department of Sichuan Province (2022NSFSC0162) and the Fundamental Research Funds for Central Universities (10822041A2018).

Conflict of interest

The authors declare that the research was conducted in the absence of any commercial or financial relationships that could be construed as a potential conflict of interest.

Publisher's note

All claims expressed in this article are solely those of the authors and do not necessarily represent those of their affiliated organizations, or those of the publisher, the editors and the reviewers. Any product that may be evaluated in this article, or claim that may be made by its manufacturer, is not guaranteed or endorsed by the publisher.

Supplementary material

The Supplementary Material for this article can be found online at: https://www.frontiersin.org/articles/10.3389/fpls.2022.1065677/full#supplementary-material

SUPPLEMENTARY FIGURE 1
Statistical analysis of hypocotyl length of seedlings in darkness. Seeds were sown on plants containing 0.1 μM ABA. Over 20 seedlings per genotype were measured after 4 d. Violin plot showing the average stomatal aperture (width/length). Student's *t*-test, $^{*}P < 0.05$.

SUPPLEMENTARY FIGURE 2
ABA-induced ROS accumulation. NBT staining indicates different levels of ABA-induced H_2O_2 production in leaves of the plants indicated. To detect O_2^-, 4-week-old plant leaves were staining with NBT after 2 days with or without 50 μM ABA.

References

An, J., Li, Q., Yang, J., Zhang, G., Zhao, Z., Wu, Y., et al. (2019). Wheat f-box protein TaFBA1 positively regulates plant drought tolerance but negatively regulates stomatal closure. *Front. Plant Sci.* 10. doi: 10.3389/fpls.2019.01242

Arieti, R. S., and Staiger, C. J. (2020). Auxin-induced actin cytoskeleton rearrangements require AUX1. *New Phytol.* 226, 441–459. doi: 10.1111/nph.16382

Byun, M. Y., Cui, L. H., Lee, A., Oh, H. G., Yoo, Y. H., Lee, J., et al. (2021). Abiotic stress-induced actin-depolymerizing factor 3 from deschampsia antarctica enhanced cold tolerance when constitutively expressed in rice. *Front. Plant Sci.* 12. doi: 10.3389/fpls.2021.734500

Deeks, M. J., and Hussey, P. J. (2009). "Plant actin biology," in *Encyclopedia of life sciences*.

Du, M., Spalding, E. P., and Gray, W. M. (2020a). Rapid auxin-mediated cell expansion. *Annu. Rev. Plant Biol.* 71, 379–402. doi: 10.1146/annurev-arplant-073019-025907

Du, M., Wang, Y., Chen, H., and Han, R. (2020b). Actin filaments mediated root growth inhibition by changing their distribution under UV-b and hydrogen peroxide exposure in arabidopsis. *Biol. Res.* 53, 54. doi: 10.1186/s40659-020-00321-3

Emenecker, R. J., Cammarata, J., Yuan, I., and Strader, L. C. (2021). Abscisic acid modulates auxin-responsive hypocotyl elongation. *Preprint*. doi: 10.1101/2021.04.25.441358

Fan, T., Zhai, H., Shi, W., Wang, J., Jia, H., Xiang, Y., et al. (2013). Overexpression of profilin 3 affects cell elongation and f-actin organization in arabidopsis thaliana. *Plant Cell Rep.* 32, 149–160. doi: 10.1007/s00299-012-1349-2

Ge, D., Pan, T., Zhang, P., Wang, L., Zhang, J., Zhang, Z., et al. (2021). GhVLN4 is involved in multiple stress responses and required for resistance to verticillium wilt. *Plant Sci.* 302, 110629. doi: 10.1016/j.plantsci.2020.110629

Guo, Y., Zhao, S., Jiang, Y., Zhao, Y., Huang, S., Yuan, M., et al. (2016). Casein Kinase1-like Protein2 regulates actin filament stability and stomatal closure *via* phosphorylation of actin depolymerizing factor. *Plant Cell* 28, 1422–1439. doi: 10.1105/tpc.16.00078

Henty, J. L., Bledsoe, S. W., Khurana, P., Meagher, R. B., Day, B., Blanchoin, L., et al. (2011). Arabidopsis actin depolymerizing factor4 modulates the stochastic dynamic behavior of actin filaments in the cortical array of epidermal cells. *Plant Cell* 23, 3711–3726. doi: 10.1105/tpc.111.090670

Hwang, J. U., and Lee, Y. (2001). Abscisic acid-induced actin reorganization in guard cells of dayflower is mediated by cytosolic calcium levels and by protein kinase and protein phosphatase activities. *Plant Physiol.* 125, 2120–2128. doi: 10.1104/pp.125.4.2120

Jiang, Y., Chang, M., Lan, Y., and Huang, S. (2019). Mechanism of CAP1-mediated apical actin polymerization in pollen tubes. *Proc. Natl. Acad. Sci. U.S.A.* 116, 12084–12093. doi: 10.1073/pnas.1821639116

Jiang, Y., Lu, Q., and Huang, S. (2022). Functional non-equivalence of pollen ADF isovariants in arabidopsis. *Plant J.* 110, 1068–1081. doi: 10.1111/tpj.15723

Jiang, H., Shui, Z., Xu, L., Yang, Y., Li, Y., Yuan, X., et al. (2020). Gibberellins modulate shade-induced soybean hypocotyl elongation downstream of the mutual promotion of auxin and brassinosteroids. *Plant Physiol. Biochem.* 150, 209–221. doi: 10.1016/j.plaphy.2020.02.042

Jiang, Y., Wang, J., Xie, Y., Chen, N., and Huang, S. (2017). ADF10 shapes the overall organization of apical actin filaments by promoting their turnover and ordering in pollen tubes. *J. Cell Sci.* 130, 3988–4001. doi: 10.1242/jcs.207738

Ketelaar, T., Allwood, E. G., Anthony, R., Voigt, B., Menzel, D., and Hussey, P. J. (2004). The actin-interacting protein AIP1 is essential for actin organization and plant development. *Curr. Biol.* 14, 145–149. doi: 10.1016/j.cub.2004.01.004

Lin, F., Qu, Y., and Zhang, Q. (2014). Phospholipids: molecules regulating cytoskeletal organization in plant abiotic stress tolerance. *Plant Signal Behav.* 9, e28337. doi: 10.4161/psb.28337

Liu, C., Zhang, Y., and Ren, H. (2018). Actin polymerization mediated by AtFH5 directs the polarity establishment and vesicle trafficking for pollen germination in arabidopsis. *Mol. Plant* 11, 1389–1399. doi: 10.1016/j.molp.2018.09.004

Liu, C., Zhang, Y., and Ren, H. (2021). Profi liu promotes formin-mediated actin filament assembly and vesicle transport during polarity formation in pollen. *Plant Cell* 33, 1252–1267. doi: 10.1093/plcell/koab027

Li, X., Xie, Y., Zhang, Q., Hua, X., Peng, L., Li, K., et al. (2022). Monomerization of abscisic acid receptors through CARKs-mediated phosphorylation. *New Phytol.* 235, 533–549. doi: 10.1111/nph.18149

Lu, Y. J., Li, P., Shimono, M., Corrion, A., Higaki, T., He, S. Y., et al. (2020). Arabidopsis calcium-dependent protein kinase 3 regulates actin cytoskeleton organization and immunity. *Nat. Commun.* 11, 6234. doi: 10.1038/s41467-020-20007-4

Paul, A. L., Denison, F. C., Schultz, E. R., Zupanska, A. K., and Ferl, R. J. (2012). 14-3-3 phosphoprotein interaction networks - does isoform diversity present functional interaction specification? *Front. Plant Sci.* 3. doi: 10.3389/fpls.2012.00190

Pei, D., Hua, D., Deng, J., Wang, Z., Song, C., Wang, Y., et al. (2022). Phosphorylation of the plasma membrane h+-ATPase AHA2 by BAK1 is required for ABA-induced stomatal closure in arabidopsis. *Plant Cell* 34, 2708–2729. doi: 10.1093/plcell/koac106

Qian, D., Zhang, Z., He, J., Zhang, P., Ou, X., Li, T., et al. (2019). Arabidopsis ADF5 promotes stomatal closure by regulating actin cytoskeleton remodeling in response to ABA and drought stress. *J. Exp. Bot.* 70, 435–446. doi: 10.1093/jxb/ery385

Qi, L., Liu, S., Li, C., Fu, J., Jing, Y., Cheng, J., et al. (2020). PHYTOCHROME-INTERACTING FACTORS interact with the ABA receptors PYL8 and PYL9 to orchestrate ABA signaling in darkness. *Mol. Plant* 13, 414–430. doi: 10.1016/j.molp.2020.02.001

Shi, Y., Liu, X., Zhao, S., and Guo, Y. (2021). The PYR-PP2C-CKL2 module regulates ABA-mediated actin reorganization during stomatal closure. *New Phytol.* 233, 2168–2184. doi: 10.1111/nph.17933

Song, Y., Li, G., Nowak, J., Zhang, X., Xu, D., Yang, X., et al. (2019). The rice actin-binding protein RMD regulates light-dependent shoot gravitropism. *Plant Physiol.* 181, 630–644. doi: 10.1104/pp.19.00497

Tang, C., Deng, L., Chang, D., Chen, S., Wang, X., and Kang, Z. (2015). TaADF3, an actin-depolymerizing factor, negatively modulates wheat resistance against puccinia striiformis. *Front. Plant Sci.* 6. doi: 10.3389/fpls.2015.01214

Wang, L., Qiu, T., Yue, J., Guo, N., He, Y., Han, X., et al. (2021). Arabidopsis ADF1 is regulated by MYB73 and is involved in response to salt stress affecting actin filament organization. *Plant Cell Physiol.* 62, 1387–1395. doi: 10.1093/pcp/pcab081

Wang, H.-H., Qiu, Y., Yu, Q., Zhang, Q., Li, X., Wang, J., et al. (2020). Close arrangement of CARK3 and PMEIL affects ABA-mediated pollen sterility in arabidopsis thaliana. *Plant. Cell Environ.* 43, 2699–2711. doi: 10.1111/pce.13871

Yao, H., Li, X., Peng, L., Hua, X., Zhang, Q., Li, K., et al. (2022). Binding of 14-3-3κ to ADF4 is involved in the regulation of hypocotyl growth and response to osmotic stress in arabidopsis. *Plant Sci.* 320. doi: 10.1016/j.plantsci.2022.111261

Zhang, L., Li, X., Li, D., Sun, Y., Li, Y., Luo, Q., et al. (2018). CARK1 mediates ABA signaling by phosphorylation of ABA receptors. *Cell Discovery* 4, 30. doi: 10.1038/s41421-018-0029-y

Zhao, S., Zhao, Y., and Guo, Y. (2015). 14-3-3 lambda protein interacts with ADF1 to regulate actin cytoskeleton dynamics in arabidopsis. *Sci. China Life Sci.* 58, 1142–1150. doi: 10.1007/s11427-015-4897-1

Zheng, Y., Xie, Y., Jiang, Y., Qu, X., and Huang, S. (2013). Arabidopsis actin-depolymerizing factor7 severs actin filaments and regulates actin cable turnover to promote normal pollen tube growth. *Plant Cell* 25, 3405–3423. doi: 10.1105/tpc.113.117820

frontiers | Frontiers in Plant Science

TYPE Original Research
PUBLISHED 06 January 2023
DOI 10.3389/fpls.2022.1053780

Check for updates

OPEN ACCESS

EDITED BY
Mohammad Golam Mostofa,
Michigan State University,
United States

REVIEWED BY
Baizhao Ren,
Shandong Agricultural University,
China
Abira Sahu,
Michigan State University,
United States

*CORRESPONDENCE
Yanxiu Miao
miaoyanxiu@163.com

†These authors contributed equally to this work and share first authorship

SPECIALTY SECTION
This article was submitted to Plant Abiotic Stress, a section of the journal Frontiers in Plant Science

RECEIVED 26 September 2022
ACCEPTED 30 November 2022
PUBLISHED 06 January 2023

CITATION
Miao Y, Gao X, Li B, Wang W and Bai L (2023) Low red to far-red light ratio promotes salt tolerance by improving leaf photosynthetic capacity in cucumber. *Front. Plant Sci.* 13:1053780. doi: 10.3389/fpls.2022.1053780

COPYRIGHT
© 2023 Miao, Gao, Li, Wang and Bai. This is an open-access article distributed under the terms of the Creative Commons Attribution License (CC BY). The use, distribution or reproduction in other forums is permitted, provided the original author(s) and the copyright owner(s) are credited and that the original publication in this journal is cited, in accordance with accepted academic practice. No use, distribution or reproduction is permitted which does not comply with these terms.

Low red to far-red light ratio promotes salt tolerance by improving leaf photosynthetic capacity in cucumber

Yanxiu Miao[1,2*†], Xingxing Gao[1†], Bin Li[1,2], Wenjiao Wang[1,2] and Longqiang Bai[1,2]

[1]College of Horticulture, Shanxi Agricultural University, Jinzhong, China, [2]Collaborative Innovation Center for Improving Quality and Increase profits of Protected Vegetables in Shanxi, Shanxi Agricultural University, Jinzhong, China

Soil salinity severely inhibits leaf photosynthesis and limits agricultural production. Red to far-red light ratio (R/FR) affects leaf photosynthesis under salt stress, however, its regulation mechanism is still largely unknown. This study investigated the effects of different R/FR on plant growth, gas exchange parameters, photosynthetic electron transport, Calvin cycle and key gene expression under salt stress. Cucumber seedlings were exposed to four treatments including 0 mM NaCl and R/FR=7 (L7, control), 0 mM NaCl and R/FR=0.7 (L0.7), 80 mM NaCl and R/FR=7 (H7) and 80 mM NaCl and R/FR=0.7 (H0.7) for 9 days in an artificial climate chamber. The results showed that compared to L7 treatment, H7 treatment significantly reduced relative growth rate (RGR), CO_2 assimilation rate (P_n), maximum photochemical efficiency PSII (F_v/F_m), most JIP-test parameters and total Rubisco activity, indicating that salt stress severely inhibited photosynthetic electron transport from PSII to PSI and blocked Calvin cycle in cucumber leaves. However, these suppressions were effectively alleviated by low R/FR addition (H0.7 treatment). Compared to H7 treatment, H0.7 treatment significantly increased RGR and P_n by 209.09% and 7.59%, respectively, enhanced F_v/F_m, maximum quantum yield for primary photochemistry (φ_{Po}), quantum yield for electron transport (φ_{Eo}) and total Rubisco activity by 192.31%, 17.6%, 36.84% and 37.08%, respectively, and largely up-regulated expressions of most key genes involved in electron transport and Calvin cycle. In conclusion, low R/FR effectively alleviated the negative effects of salt stress on leaf photosynthesis by accelerating photosynthetic electron transport from PSII to PQ pool and promoting Calvin cycle in cucumber plants. It provides a novel environmentally friendly light-quality regulation technology for high efficiency salt-resistant vegetable production.

KEYWORDS

red to far-red light ratio, salt stress, cucumber, photosynthetic electron transport, Calvin cycle

Introduction

Soil salinity, a global environmental problem, occurs in approximately 7% of the world's total land area and 20% of irrigated land (Shabala and Cuin, 2008). Salt stress not only negatively affects plant growth and production, but also induces a series of physiological and metabolic disorders, especially photosynthesis (Kalaji et al., 2011; Zhang J. et al., 2016). Salt stress-induced osmotic stress decreases water absorption in root, causes water loss in leaves, and thus plays negative roles in leaf photosynthesis. Salt stress also stimulates synthesis of reactive oxygen species (ROS), which seriously destructs photosynthetic organs and components, and inhibits leaf photosynthetic characteristics, such as CO_2 assimilation rate, stomatal conductance, maximum photochemical efficiency PSII (F_v/F_m) (Ma et al., 2017; Niu et al., 2019; Gong et al., 2020). Therefore, it is necessary to improve salt tolerance by promoting leaf photosynthetic capacity.

Light quality participants in the regulation of growth, physiological and yield characteristics in vegetable crops. Red to far-red light ratio (R/FR), one of the important light environment factors, participants in seed germination, plant photomorphogenesis, physiological metabolism and gene expression (Demotes-Mainard et al., 2015; Holalu and Finlayson, 2017). R/FR is about 7 under light-emitting diode (LED) lamp, 1.14 under sunny condition and 0.09-0.7 under shade condition. Low R/FR induces shade avoidance syndrome (SAS) responses, such as increased internode, petiole, stem, leaf length and plant dry weight, apical dominance and early flowering (Franklin, 2008). Low R/FR also takes parts in several physiological changes, especially in leaf photosynthetic characteristics, it dramatically increases leaf net photosynthetic rate and effective photochemical quantum yield of PSII (Φ_{II}), accelerates cyclic electron transport around PSI, but decreases leaf chlorophyll *a*/*b* in horticultural crops, such as tomato, soybean and lettuce (Zhen and Iersel, 2017; Kalaitzoglou et al., 2019; Yang et al., 2020).

R/FR not only influences plant growth and physiological metabolism, but also effectively alleviates injuries caused by abiotic stresses, including salt, cold and drought stresses and so on (Courbier and Pierik, 2019; Ahres et al., 2020; Gyugos et al., 2021). Under salt stress, low R/FR increased the stability of Phytochrome interaction factor (PIF) and upregulated brassinosteroid and auxin signaling, thus promoted hypocotyl growth in Arabidopsis (Hayes et al., 2019). Low R/FR also up-regulated *SODCC.2*, *GPX1*, *APX2* and *CAT1* gene expressions and increased antioxidant enzyme (e.g., SOD, POD and CAT) activities, thus enhanced salt resistance in tomato plants (Cao et al., 2018; Wang Y. et al., 2021). Cockburn et al. (1996) found that under salt stress, low R/FR enhanced PEP carboxylase activity, and caused accumulation of CAM isoform of PEP carboxylase isozyme and increased terpineol and soluble carbohydrate contents, finally improved salt tolerance in *Mesembryanthemum crystallinum* plant. However, these researches on salt tolerance of R/FR basically focus on plant growth and antioxidant capacity, little is known about how R/FR regulates leaf photosynthetic responses to salt stress. It is of great research significance to explore the regulation roles of R/FR on specific processes of photosynthetic electron transport chain and Calvin cycle simultaneously under salt stress.

Cucumber (*Cucumis sativus* L.) is an important worldwide economic vegetable crop, and its growth and production are severely limited by salt stress (Miao et al., 2020; Wang W. et al., 2021). Cucumber is sensitive to light quality, and its photomorphogenesis and photosynthetic characteristics are easily regulated by R/FR (Shibuya et al., 2015; Miao et al., 2019; Jeong et al., 2020). In the present study, we investigated the effect of R/FR on leaf gas exchange parameters, photosynthetic electron transfer capacity, Calvin cycle and key gene expression in salt-stressed cucumber plants. According to the regulation mechanism of R/FR on leaf photosynthesis under salt stress, this study will provide a more theoretical basic and new light quality control method to improve salt tolerance in cucumber production.

Materials and methods

Plant materials and growth conditions

Cucumber (*Cucumis sativus* L.cv. 'Jinchun 4') seeds were germinated at 28°C, then sowed into a hydroponic tank in an artificial climate chamber. After the second true leaf has fully developed, all plants were exposed to four treatments, including 0 mM NaCl and R/FR=7 (L7, control), 0 mM NaCl and R/FR=0.7 (L0.7), 80 mM NaCl and R/FR=7 (H7) and 80 mM NaCl and R/FR=0.7 (H0.7). The hydroponic tank was filled with full strength Hoagland nutrient solution contained 0 mM or 80 mM NaCl, respectively. Red and far-red light were provided by LED lamps with maximum intensity at 660nm and 730nm, respectively. Red to far-red light ratio (R/FR) was calculated from photon irradiance for the bands 655-656 nm and 725-735nm according to Kotilainen et al. (2020). The light intensity and spectral distribution were determined by Avaspec-2048 fiber optic spectrometer (AVANTES, Netherlands) in the range 400-950nm with a spectral resolution of 1 nm (Figure 1). The day/night temperature, light intensity, photoperiod and relative humidity were 26°C/18°C, 250μmol·m^{2}·s^{-1}, 12h·d^{-1} and 60%-80%, respectively. The cucumber samples were harvested at day 9 after treatments and the experiments were repeated at least three times.

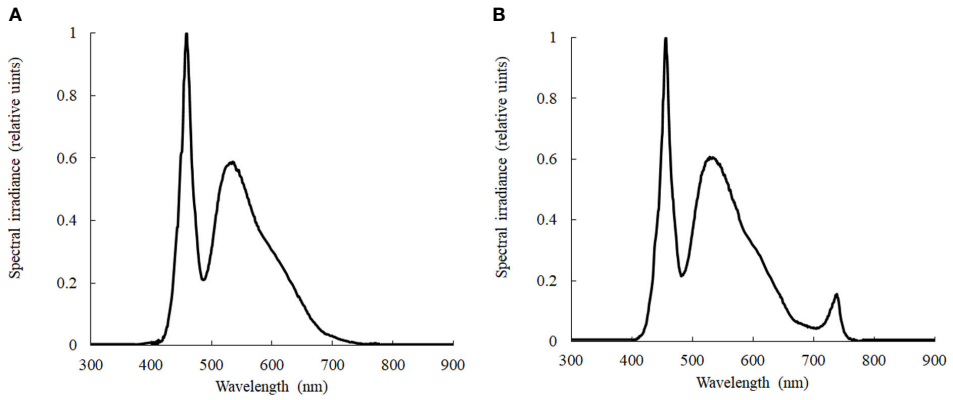

FIGURE 1
Relative spectral distribution in different light treatments. **(A)**, R/FR=7; **(B)**, R/FR=0.7.

Plant growth parameters

Four cucumber seedlings from each treatment were harvested on days 0 and 9 after treatments. Leaf area was measured using a LI-3000C portable leaf area meter (LI-COR, USA) and dry weight was fully dried at 80°C in an oven for 2 days. Relative growth rate (RGR), net assimilation rate (NAR), leaf area ratio (LAR), leaf dry weight ratio (LWR), and specific leaf area (SLA) were calculated according to Hunt (1978).

Leaf photosynthetic pigment and carbohydrate contents

The samples from second leaves were harvested to measure photosynthetic pigment and carbohydrate contents. The photosynthetic pigments, soluble sugar and starch contents was measured using the method of Zhao X. et al. (2022), fructose and sucrose content was determined by resorcinol spectrophotometry according to Gao (2006). Four cucumber seedlings were selected for each treatment.

Gas exchange parameters

Gas exchange parameters were determined on the fully expanded second leaves at a similar position. Cucumber leaves exposed to different R/FR were measured under their own light quality conditions with a LI-6800 gas exchange analyzer and a standard transparent leaf chamber (LI-COR, USA). When leaves were clamped and reached steady-state condition in leaf chamber, gas exchange parameters such as CO_2 assimilation rate (P_n), stomatal conductance (g_{sw}), intercellular CO_2 concentration (C_i) and transpiration rate (T_r) were measured. The light intensity was 250 μmol·m^{-2}·s^{-1}, leaf temperature was 26°C, relative humidity was 60%-70%, CO_2 concentration was 400 μmol·mol^{-1} in leaf chamber. Four cucumber seedlings were selected for each treatment.

The CO_2 response curve was measured with LI-6800 gas exchange analyzer using the same gas exchange parameters as described above. According to the procedure described by Long Bernacchi (2003), light intensity was 1500 μmol·m^{-2}·s^{-1}, CO_2 concentration in leaf chamber was initially 400 μmol·mol^{-1} for 5 min, then followed by 400, 300, 250, 200, 150, 100, 50, 400, 600, 800, 1000, 1200, 1500 and 1800 μmol·mol^{-1}. Three cucumber seedlings were selected for each treatment.

Chlorophyll fluorescence parameters

The maximum photochemical efficiency PSII (F_v/F_m) image was measured on the second leaves using a Maxi Imaging-pam fluorescence system (Walz, Germany). Details of procedure and measurement system were described in Perreault et al. (2010). After 30 min of dark adaptation, minimum fluorescence (F_o) was measured with a modulated light, then maximum fluorescence (F_m) was determined with a saturation pulse. F_v/F_m was calculated automatically using $F_v/F_m = (F_m-F_o)/F_m$.

The light induction transient of chlorophyll fluorescence (OJIP) curves were determined with a FluorPen FP 110 handheld chlorophyll fluorometer (Photon systems instruments, Czech Republic). After 30 min of dark adaptation, OJIP curve was induced by pulsed light of 3000 μmol·m^{-2}·s^{-1}. The relative variable fluorescence (V_t) was calculated as $V_t=(F_t-F_o)/(F_p-F_o)$ according to Suzuki et al. (2011). Where, V_t and F_t represent relative variable fluorescence and fluorescence intensity at time t, respectively, F_o and F_p represent initial and maximum fluorescence intensity, respectively. JIP-test parameters were calculated according to Strasser et al. (2004). The formulas are as follows: Maximum quantum yield for primary photochemistry, $\varphi_{Po}=TR_o/ABS=[1-$

(F_o/F_m)], quantum yield for electron transport, φ_{Eo}=ET_o/ABS=[1-(F_o-F_m)](1-V_J), quantum yield for reduction of end electron acceptors at the PSI acceptor side, φ_{Ro}=RE_o/ABS=[1-(F_o/F_m)](1-V_J), efficiency/probability that an electron moves further than Q_A^-, Ψ_{Eo}=ET_o/TR_o=1-V_J, efficiency/probability with which an electron from the intersystem electron carriers is transferred to reduce end electron acceptors at the PSI acceptor side, δ_{Ro}=RE_o/ET_o=(1-V_I)/(1-V_J), Q_A reducing RCs per PSII antenna Chl, RC/ABS=φ_{Po}(V_J/M_o), performance index (potential) for energy conservation from photons absorbed by PSII to the reduction of intersystem electron acceptors, PI_{ABS}=RC/ABS×[φ_{Po}/(1-φ_{Po})]×[Ψ_{Eo}/(1-Ψ_{Eo})], performance index (potential) for energy conservation from photons absorbed by PSII to the reduction of PSI end acceptors, PI_{total}=PI_{ABS}·δ_{Ro}/(1-δ_{Ro}). Four cucumber seedlings were selected for each treatment.

Rubisco activity

The second leaves of four plants from each treatment were selected and snap frozen in liquid nitrogen, then stored at -80°C in a refrigerator. The initial and total Ribulose 1,5-bisphosphate carboxylase/oxygenase (Rubisco) activity and protein content were determined and calculated according to Zhang et al. (2013) and Wang et al. (2016).

Quantitative real-time PCR analysis

Total RNA was extracted from the second leaves using TRIZOL reagent (Shanghai Blue Quarter Technology Development Co., Ltd., China) according to the method of Wang et al. (2009). Reverse transcription was performed with a CjamQTM Universal SYBR® qPCR Master Mix kit (Vazyme Biotech Co., Ltd, China) and real-time PCR (qPCR) was performed using a HiScript® III RT SuperMix kit (Vazyme Biotech Co., Ltd, China). The previously published primer sequences according to Miao et al. (2016) and Zhao H. et al. (2022) were used in this study (Table 1). Three cucumber seedlings were selected for each treatment.

Statistical analysis

All statistical analysis was carried out with SPSS 21.0 software (IBM Corporation, USA). The data were analyzed by one-way analysis of variance (ANOVA) and significant differences among means were assessed by Duncan's test ($P < 0.05$).

Results

Plant growth analysis

Generally, compared to L7 treatment, most plant parameters (e.g., Relative growth rate (RGR), net assimilation rate (NAR), leaf area ratio (LAR), specific leaf area (SLA) and total leaf area) were significantly increased by L0.7 treatment, while all plant parameters were significantly decreased by H7 and H0.7 treatments (Figure 2). Most plant parameters (e.g., RGR, NAR, LAR, LWR and total leaf area) were significantly higher for H0.7 treatment than for H7 treatment. These results indicated that salt stress seriously inhibited plant growth, however, the negative effects of salt stress on plant growth were effectively alleviated by low R/FR.

TABLE 1 Primers used for qPCR.

Gene name	Gene ID	Forward primer	Reverse primer
Actin	Csa6G484600.2	5'-ATGGCCGATGCCGAGGATAT-3'	5'-TAGGAGCATCATCACCAGCAAAAC-3'
***psb*A**	CsaUNG024230.1	5'-GTATTCCAGGCTGAGCACAACATC-3'	5'-TACCTAAAGCGGTGGACCAGATAC-3'
***psb*B**	Csa5G589930.1	5'-GGTATTTGGAGTTACGAAGGTGTG-3'	5'-CCCAACCCTGAGAGAAATAAATGA-3'
***psa*A**	Csa3G895840.1	5'-GATTTCTCATAGTTGGTGCTGCTG-3'	5'-TACAAACCAAAACTGTGAAAGCCT-3'
***psa*B**	CsaV3_UNG201530.1	5'-ATTTGGACATCTTGTTTGGGCTAC-3'	5'-TGATGTAGAGGCAATCAAGAAAGC-3'
rbcL	CsaV3_UNG203690.1	5'-TACTGATATCTTGGCAGCATTCCG-3'	5'-AAGATTCAGCAGCTACAGCGGC-3'
rbcS	Csa5G609710.1	5'-ATGGCTTCATCCATTCTCTCATCC-3'	5'-CCAGTGAATGGTGCTACCATGCTA-3'
Rca	Csa6G188680.2	5'-GAATATGGCAACATGCTCGTCATG-3'	5'-TCCAAGAGCAGCTTCGTTCAGAT-3'
TPI	Csa2G263900.1	5'-CTCTCTTTCACAACGTCCACTCACA-3'	5'-ACCAACGAAGAACTTGCCGGAG-3'
FBPase	Csa4G307350.1	5'-AATCTCTCGTTCTCTCTCTCGCCTC-3'	5'-CGCTATGCCTTCTATTTCCACGG-3'
SBPase	Csa5G198220.1	5'-CAGTGTCCTCCTCATACTTGGGTTG-3'	5'-CTGGGAAGAAAGATTGGGGAGAAA-3'
Rupe	Csa1G038360.2	5'-TCCCAAGTCAGTGGGTTTATCGGAG-3'	5'-AACCTTCTCCTCGAAACGGTAAGAG-3'
PRK	Csa3G638540.1	5'-ATCCACACCCTCATTCATTTCTCC-3'	5'-GCAGTTGAGGGAGTGAAGAAGAAGA-3'

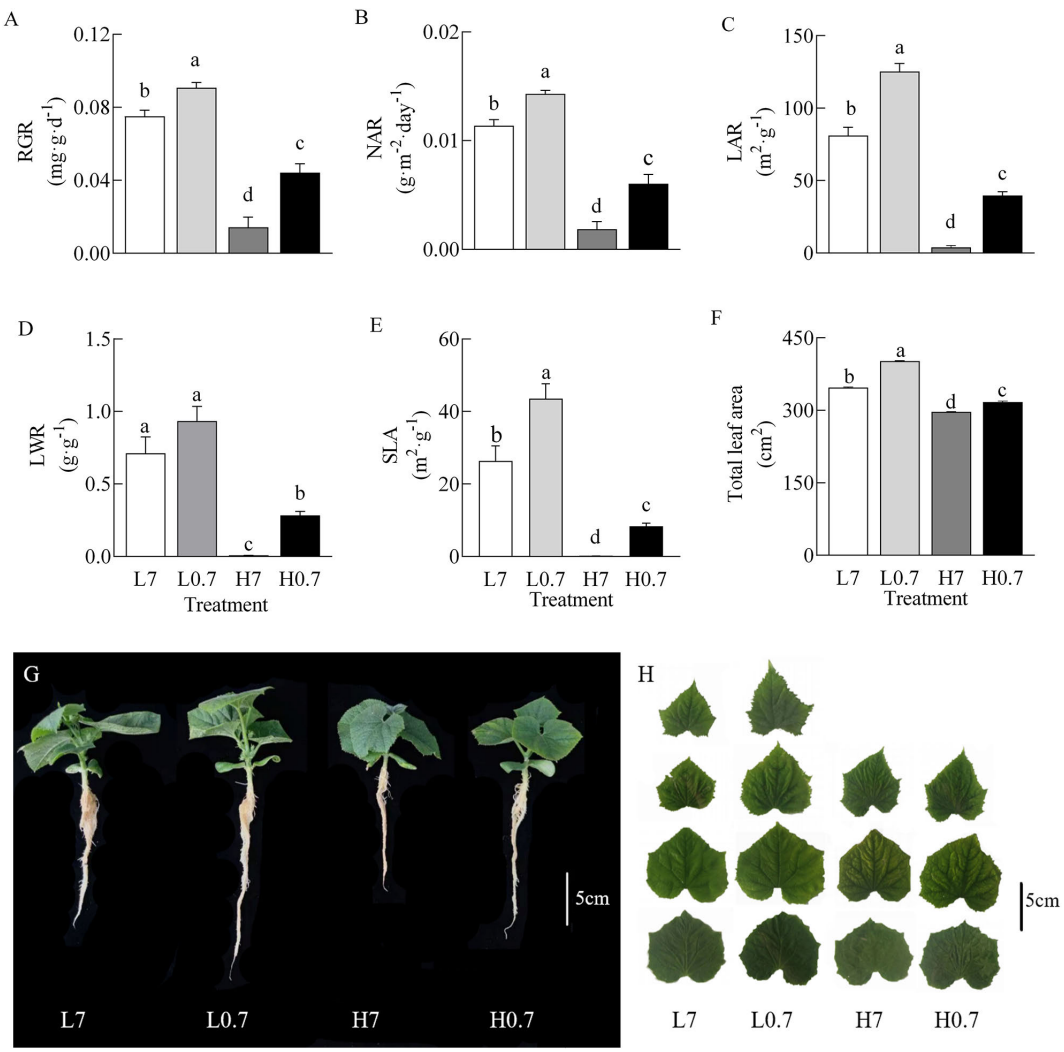

FIGURE 2
Effect of R/FR on growth parameters of cucumber seedlings under salt stress. **(A)**, RGR, relative growth rate; **(B)**, NAR, net assimilation rate; **(C)**, LAR, leaf area ratio; **(D)**, LWR, leaf dry weight ratio; **(E)**, SLA, specific leaf area; **(F)**, total leaf area; Cucumber seedlings **(G)** and total true leaves **(H)** on day 9 after treatment. L7, 0 mM NaCl and R/FR=7; L0.7, 0 mM NaCl and R/FR=0.7; H7, 80 mM NaCl and R/FR=7; H0.7, 80 mM NaCl and R/FR=0.7. Different letters indicate significant differences ($P< 0.05$; n= 4).

Leaf photosynthetic pigment and carbohydrate

Compared to L7 treatment, chlorophyll *a*, chlorophyll *b*, soluble sugar and starch contents were significantly increased by L0.7 treatment, however, all photosynthetic pigment and carbohydrate contents were significantly decreased by H7 treatment, chlorophyll *a*, soluble sugar, fructose and sucrose contents were significantly reduced by H0.7 treatments (Table 2). The chlorophyll *a* and all carbohydrate (e.g., soluble sugar, fructose, sucrose and starch) contents were significantly higher for H0.7 treatment than for H7 treatment. This indicated that the negative effects of salt stress on photosynthetic pigment and carbohydrate were dramatically reduced by low R/FR.

Leaf gas exchange parameter

Compared to L7 treatment, P_n and g_{sw} were significantly increased by L0.7 treatment, C_i was significantly enhanced by H0.7 treatment, while most gas exchange parameters (e.g., P_n, C_i and T_r) were significantly reduced by H7 treatment (Figure 3A–D). Compared to H7 treatment, P_n and T_r were significantly increased by H0.7 treatment.

TABLE 2 Effect of R/FR ratio on photosynthetic pigment and carbohydrate contents in cucumber leaves under salt stress.

Treatment	Chlorophyll *a* content (mg·g^{-1} FW)	Chlorophyll *b* content (mg·g^{-1} FW)	Carotenoid content (mg·g^{-1} FW)	Soluble sugar content (mg·g^{-1} FW)	Fructose content (mg·g^{-1} FW)	Sucrose content (mg·g^{-1} FW)	Starch content (mg·g^{-1} FW)
L7	0.45 ± 0.02 b	0.14 ± 0.01 b	0.09 ± 0.00 ab	2.25 ± 0.09 b	3.89 ± 0.04 a	3.49 ± 0.04 a	0.14 ± 0.01 b
L0.7	0.65 ± 0.01 a	0.16 ± 0.01 a	0.10 ± 0.01 a	2.55 ± 0.03 a	3.96 ± 0.09 a	3.54 ± 0.02 a	0.30 ± 0.03 a
H7	0.31 ± 0.01 d	0.11 ± 0.00 c	0.08 ± 0.00 c	0.50 ± 0.04 d	2.6 ± 0.08 c	2.71 ± 0.05 c	0.08 ± 0.01 c
H0.7	0.37 ± 0.02 c	0.12 ± 0.01 bc	0.09 ± 0.01 bc	1.75 ± 0.05 c	1.75 ± 0.05 b	3.33 ± 0.07 b	0.14 ± 0.01 b

L7, 0 mM NaCl and R/FR=7; L0.7, 0 mM NaCl and R/FR=0.7; H7, 80 mM NaCl and R/FR=7; H0.7, 80 mM NaCl and R/FR=0.7. Different letters within the same column represent significant differences ($P<0.05$, n=4).

For all treatments, CO_2 assimilation rate increased quickly with increasing C_i and reached maximum values when C_i was above 1000 μmol·mol^{-1} (Figure 3E). It was obvious that L0.7 treatment had the highest CO_2 assimilation rate, followed by L7, H0.7 and H7 treatments.

Leaf chlorophyll fluorescence parameter

The cucumber leaves in L7 and L0.7 treatments showed a homogeneous F_v/F_m distribution centred around an F_v/F_m of 0.80, while leaf in H7 treatment had a heterogeneous distribution with a high F_v/F_m around the veins and an extremely low level of F_v/F_m (0.26) between the veins, F_v/F_m distribution in H0.7 treatment was relative homogeneous around an F_v/F_m of 0.77 (Figure 4A and Table S1).

The typical polyphasic OJIP rise was found in L7 treatment (Figure 4B). The J (V_J, at 2ms) step was significantly higher for L0.7 treatment than for L7 treatment and was significantly higher for H0.7 treatment than for H7 treatment (Table S1). Compared to L7 treatment, φ_{Eo} and PI_{ABS} were significantly increased by L0.7 treatment, however, most JIP-test parameters (e.g., φ_{Po}, φ_{Eo}, φ_{Ro}, RC/ABS, PI_{ABS} and PI_{total}) were reduced by H7 treatment, and φ_{Po}, φ_{Eo} and PI_{ABS} were significantly decreased by H0.7 treatment (Figure 4C and Table S1). Compared with H7 treatment, φ_{Po} and φ_{Eo} were significantly increased by H0.7 treatment.

Rubisco activity

Compared with L7 treatment, total Rubisco activity was statistically increased by L0.7 treatment, while total Rubisco activity was significantly reduced by H7 treatments (Figure 5). Total Rubisco activity was much higher for H0.7 treatment than for H7 treatment.

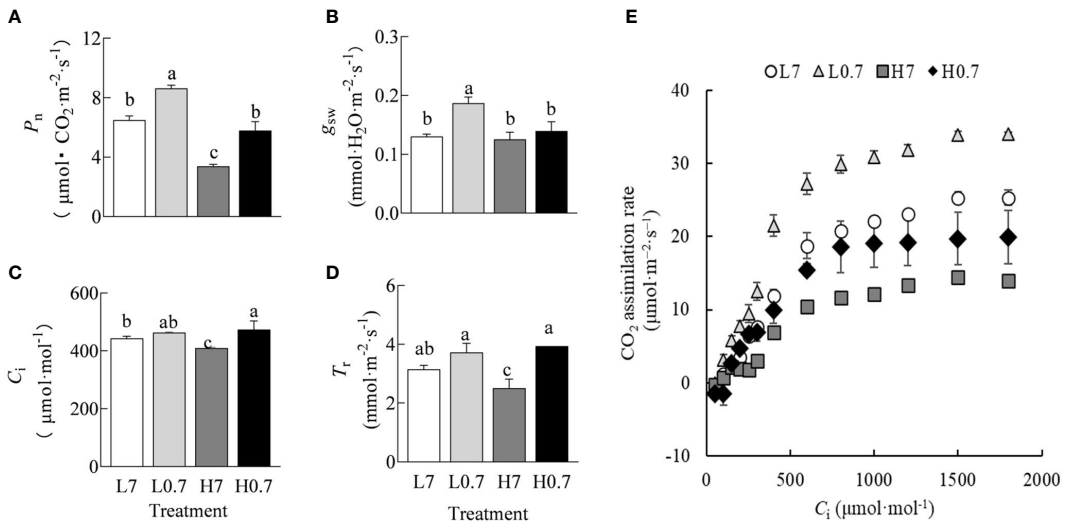

FIGURE 3
Effect of R/FR on gas exchange parameters in cucumber leaves under salt stress. **(A)**, P_n, CO_2 assimilation rate; **(B)**, g_{sw}, stomatal conductance; **(C)**, C_i, intercellular CO_2 concentration; **(D)**, T_r, transpiration rate; **(E)**, CO_2 response curve. All data in **(A–E)** were reported as the arithmetic mean ± standard error (n=4 and n=3, respectively).

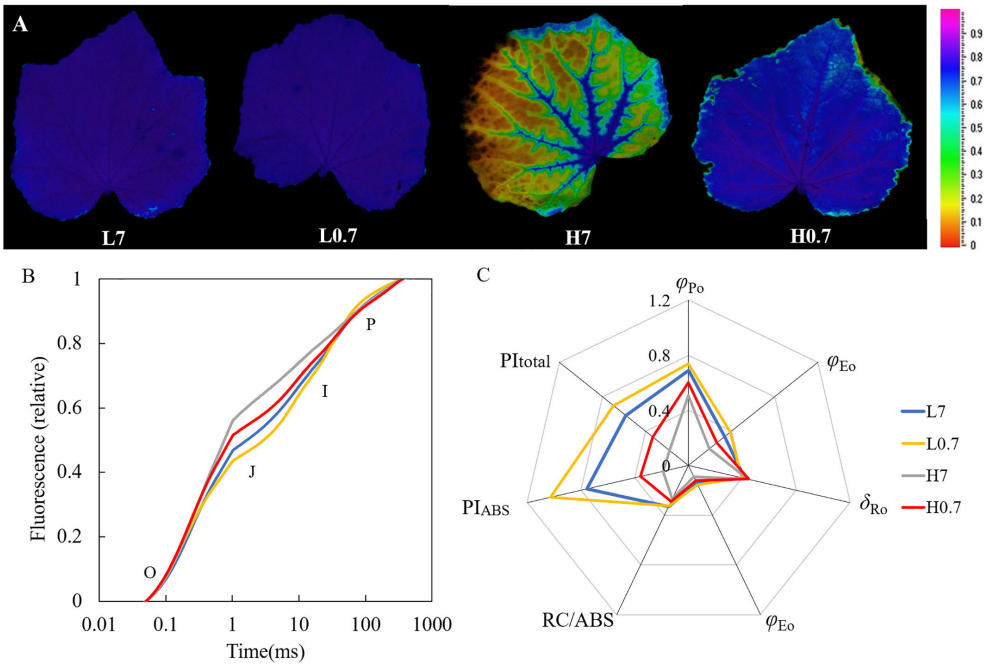

FIGURE 4
Effect of R/FR on chlorophyll fluorescence parameters in cucumber leaves under salt stress. **(A)**, maximal photochemical quantum yield of PSII (F_v/F_m) images of cucumber leaves; **(B)**, Chlorophyll *a* fluorescence transient (OJIP) curve; **(C)**, JIP-test parameters calculated according to OJIP curve. Different letters indicate significant differences (P< 0.05; n= 4).

Expression levels of key genes involved in electron transport and Calvin cycle

In general, compared to L7 treatment, expression levels of all key genes (e.g., *psbA*, *psbB*, *psaA*, *psaB*, *rbcL*, *rbcS*, *Rca*, *TPI*, *FBPase*, *SBPase*, *Rupe* and *PRK*) involved in photosynthetic electron transport and Calvin cycle were significantly up-regulated by L0.7 treatment, however, all gene expressions were obviously down-regulated by H7 treatment, only *Rca* gene expression was down-regulated by H0.7 treatments when compared to L7 treatment (Figure 6). The transcription levels of all genes except for *rbcL* and *TPI* were much higher in H0.7 treatment than H7 treatment.

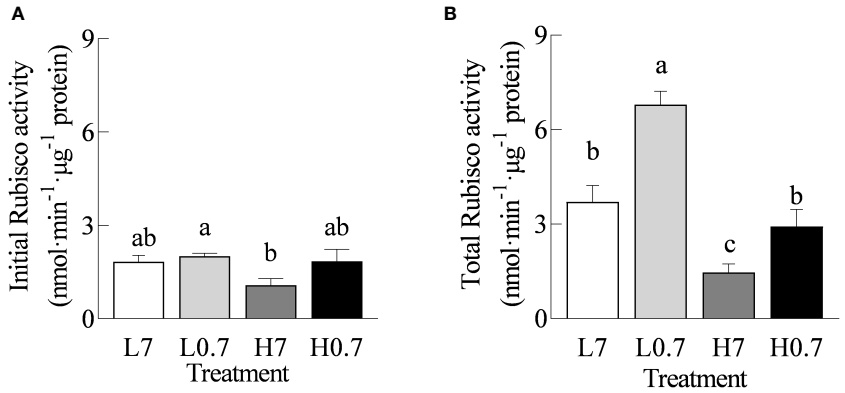

FIGURE 5
Effect of R/FR on Rubisco activity in cucumber leaves under salt stress. **(A)**, Initial Rubisco activity; **(B)**, Total Rubisco activity. Different letters indicate significant differences (P< 0.05; n= 4).

10.3389/fpls.2022.1053780

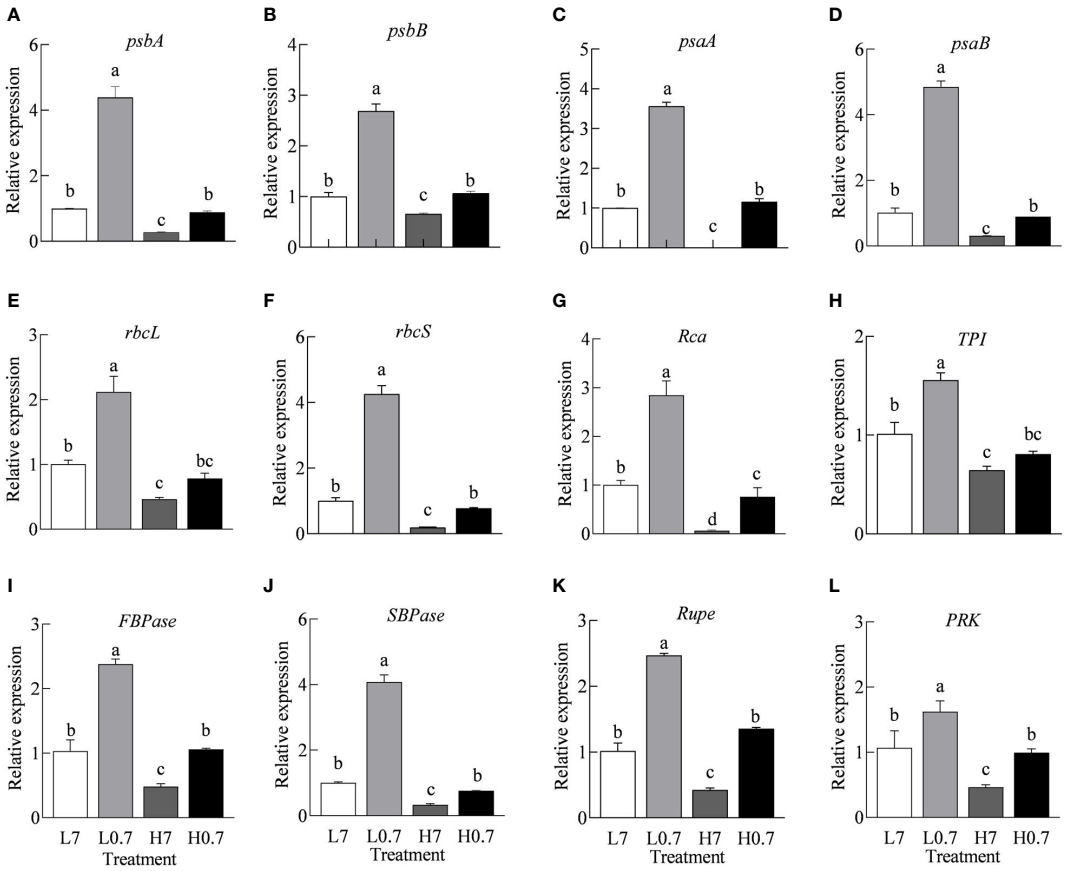

FIGURE 6
Effect of R/FR on relative expression levels of key genes involved in electron transport and Calvin cycle in cucumber leaves under salt stress. The relative expression levels of psbA **(A)**, psbB **(B)**, psaA **(C)** and psaB **(D)** genes involved in electron transport and relative expression levels of rbcL **(E)**, rbcS **(F)**, Rca **(G)**, TPI **(H)**, FBPase **(I)**, SBPase **(J)**, Rupe **(K)** and PRK **(L)** genes involved in Calvin cycle *rbcL*, ribulose-1,5-bisphosphate carboxylase/oxygenase large subunit; *rbcS*, ribulose-1,5-bisphosphate carboxylase/oxygenase small subunit; *Rca*, ribulose-1,5-bisphosphate carboxylase/oxygenase activase; *TPI*, propanosyl phosphate isomerase; *FBPase*, fructose-1,6-bisphosphatase; *SBPase*, scenic heptulose-1,7-bisphosphatase; *Rupe*, ribulose-5-phosphate epimerase; *PRK*, ribulose-5-phosphate kinase. Different letters indicate significant differences ($P< 0.05$; n= 3).

R/FR affects leaf photosynthesis under salt stress

Compared to L7 treatment, chlorophyll *a* and *b* contents, most JIP-test parameters, expressions of genes (e.g., *psbA*, *psbB*, *psaA* and *psaB*) encoding Photosystem II and I (PSII and PSI) reaction center proteins were significantly reduced by H7 treatment, indicating that salt stress delayed reduction of primary electron acceptor quinone molecule in PSII (Q_A), and electron transfer from Q_A^- to PQ pool until end acceptors (e.g., Fd, NADP) at PSI electron acceptor side, thus reduced photosynthetic electron transfer capacity (Figure 7); Meanwhile, expression levels of all key genes (e.g., *rbcL*, *rbcS*, *Rca*, *TPI*, *FBPase*, *SBPase*, *Rupe* and *PRK*) involved in Calvin cycle were statistically down-regulated, and Rubisco activity, sucrose and starch contents were significantly decreased by H7 treatments. These indicated that salt stress inhibited leaf photosynthesis mainly through disturbing photosynthetic electron transport and Calvin cycle.

L0.7 treatment had the highest chlorophyll *a* and *b* contents, φ_{Eo}, PI_{ABS}, *psbA*, *psbB*, *psaA* and *psaB* gene expressions in all treatments, suggesting that low R/FR accelerated electron transfer from Q_A^- to PQ pool, thus enhanced photosynthetic electron transport capacity; In the meanwhile, expression levels of all key genes (e.g., *rbcL*, *rbcS*, *Rca*, *TPI*, *FBPase*, *SBPase*, *Rupe* and *PRK*) involved in Calvin cycle, and Rubisco activity were highest in L0.7 treatment, contributing to accelerated Calvin cycle and increased starch content in cucumber leaf. In all, low R/FR enhanced leaf photosynthesis mainly through promoting photosynthetic electron transport and Calvin cycle.

Compared to H7 treatment, chlorophyll *a* content, φ_{Po}, φ_{Eo}, *psbA*, *psbB*, *psaA* and *psaB* gene expressions were significantly

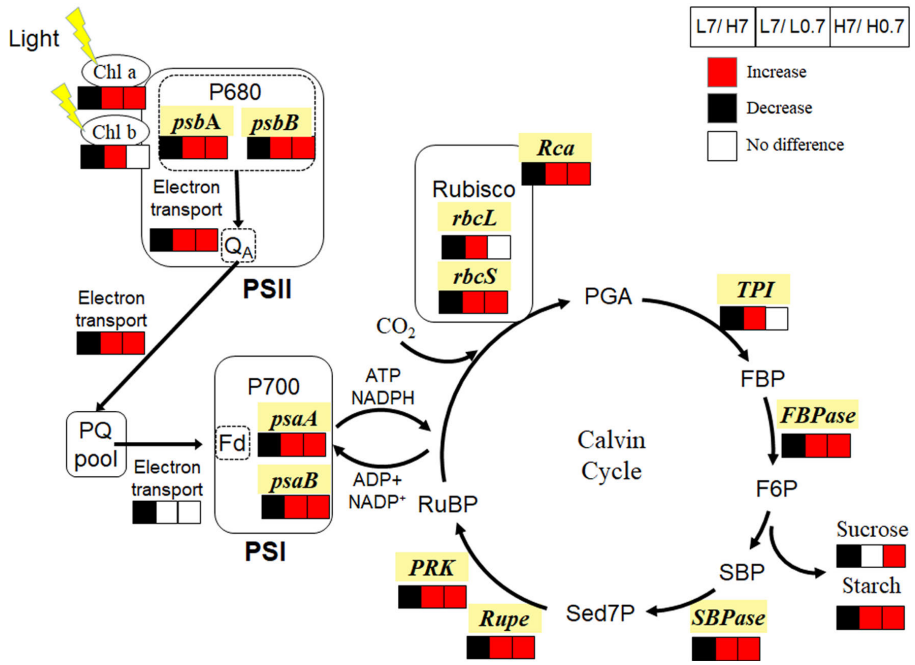

FIGURE 7
Effect of R/FR on photosynthetic electron transport and Calvin cycle in cucumber leaves under salt stress. Compared to L7 treatment, H7 treatment significantly decreased chlorophyll *a*, chlorophyll *b*, sucrose and starch contents, inhibited electron transport from PSII to PSI, and down-regulated expressions of genes (e.g., *psbA*, *psbB*, *psaA*, *psaB*, *rbcL*, *rbcS*, *Rca*, *TPI*, *FBPase*, *SBPase*, *Rupe* and *PRK*) involved in photosynthesis; While L0.7 treatment significantly increased chlorophyll *a*, chlorophyll *b* and starch contents, improved electron transport from PSII to PQ pool, and up-regulated expressions of genes (e.g., *psbA*, *psbB*, *psaA*, *psaB*, *rbcL*, *rbcS*, *Rca*, *TPI*, *FBPase*, *SBPase*, *Rupe* and *PRK*) involved in photosynthesis. Compared to H7 treatment, H0.7 treatment significantly enhanced chlorophyll *a*, sucrose and starch contents, promoted electron transport from PSII to PQ pool, and up-regulated expressions of genes (e.g., *psbA*, *psbB*, *psaA*, *psaB*, *rbcS*, *Rca*, *FBPase*, *SBPase*, *Rupe* and *PRK*) involved in photosynthesis. The red and black units represent enhancement and inhibition of photosynthesis apparatus or gene expression level, respectively, while white units represent no difference. Chl, chlorophyll; PSII, Photosystem II; P680, primary electron donor of PSII; Q_A, primary electron acceptor quinone molecule; PSI, Photosystem I; P700, primary electron Chl donor of PSI; PQ pool, plastoquinone pool; Rubisco, Ribulose-1,5-bisphosphate carboxylase-oxygenase; PGA, phosphoglycerate; FBP, fructose-1,6-bisphosphate; F6P, fructose-6-phosphate; SBP, Sedoheptulose-1, 7-bisphosphate; Sed7P, Sedoheptulose-7-bisphosphate; RuBP, ribulose-1,5-bisphosphate.

increased by H0.7 treatment, showing that low R/FR enhanced linear photosynthetic electron transport from PSII to PQ pool under salt stress; Simultaneously, expression levels of most genes (e.g., *rbcS*, *Rca*, *FBPase*, *SBPase*, *Rupe* and *PRK*) involved in Calvin cycle were up-regulated and Rubisco activity was enhanced by H0.7 treatment, resulting in increased sucrose and starch contents. In brief, low R/FR benefited leaf photosynthesis mainly through improving photosynthetic electron transport and Calvin cycle under salt stress.

Discussion

Salt stress severely inhibits leaf photosynthesis and plant growth, and it has become a challenge in vegetable production. R/FR, an important light environmental factor, takes an active part in regulating salt tolerance in plants. Recently, great progress has been made in physiological characteristics and molecular mechanism of vegetable crops under salt stress, however, the regulation roles of R/FR on leaf photosynthetic characteristics under salt stress is still largely unclear (Cao et al., 2018; Wang Y. et al., 2021). In this study, we emphasized that low R/FR promoted photosynthetic electron transport chain and Calvin cycle, finally improved leaf photosynthesis in salt-stressed cucumber plant.

Low R/FR promoted plant growth under salt stress

Growth parameters are common indicators of plant's response to salt stress. Salt stress inhibits plant tissues and organs growth, delays plant growth and development, and reduces yield and quality in many plant species, such as

tomato, lettuce, sorghum and so on (De Lacerda et al., 2005; Shao et al., 2015; Moncada et al., 2020; Wang W. et al., 2021). In the present study, both RGR and total leaf area were lower for H7 and H0.7 treatments than for L7 treatment, indicating that salt stress seriously inhibited cucumber plant growth (Figure 2). Low R/FR plays a vital role in regulating plant growth, it not only promotes cell wall extension which leads to increased leaf area, but also enhances leaf photosynthetic capacity, promotes dry matter accumulation and plant growth (Yang et al., 2020; Tan et al., 2022). In this study, H0.7 treatment had higher RGR and total leaf area than H7 treatment, suggesting that low R/FR alleviated the adverse effects of salt stress on plant growth.

Low R/FR increased leaf photosynthetic capacity in salt-stressed cucumber leaves

Photosynthesis is a crucial process of absorbing light energy and synthesizing inorganic substance into organic compound in plant. Salt stress usually induces the decline in photosynthetic characteristics in horticultural crops, such as *Ziziphus spina-christi* (L.) Willd., *Dianthus superbus* L. and *Coreopsis tinctoria* Nutt. (Ma et al., 2017; Gorai et al., 2019; Jiang et al., 2021). In the current study, P_n, C_i and T_r were significantly lower for H7 treatment than for L7 treatment, indicating that salt stress decreased photosynthetic characteristics (Figure 3A–D). Salt stress inhibits water absorption, i.e., insufficient photosynthetic raw materials, leading to a reduction in leaf photosynthesis; On the other hand, salt stress-induced ROS (e.g., $^1O_2$, O_2^-, H_2O_2 and HO) severely destroys chloroplast structure and metabolism through oxidation of membrane lipids and membrane proteins, thus adversely impacts photosynthetic capacity (Zhang M. et al., 2016). Furthermore, triose phosphate use (TPU) limitation is widely considered to be one of the main limiting factors of light-saturated photosynthetic rate (Long and Bernacchi, 2003). Interestingly, in CO_2 response curve, CO_2 assimilation rate plateaued or slightly declined at the higher CO_2 concentrations in H7 treatment, suggesting that salt stress significantly decreased rate of triose phosphate use, i.e., CO_2 utilization, leading to the reduction in sucrose and starch contents (Figure 3E and Table 2).

It is considered that low R/FR can largely increase superoxide dismutase (SOD), peroxidase (POD) and catalase (CAT) activity, effectively alleviate oxidative damage on chloroplast induced by salt stress (Wang Y. et al., 2021). In this study, H0.7 treatment had higher chlorophyll *a* content, gas exchange parameters (e.g., P_n, C_i and T_r) and carbohydrate (e.g., sucrose and starch) contents than H7 treatment, indicating that low R/FR had a positive effect on leaf photosynthesis in salt-stressed cucumber plants. This can be further proved by low R/FR-induced improved photosynthetic electron transport and Calvin cycle characteristics below.

Low R/FR enhanced photosynthetic electron transport capacity in salt-stressed cucumber leaves

Although achievements of photosynthetic characteristics under salt stress have been made in various plant species, effects of R/FR on photosynthetic electron transport capacity under salt stress are still largely unclear (Kalaji et al., 2011; Giorio and Sellami, 2021). Salt stress easily causes oxidation of oxygen-evolving complex (OEC), reaction center protein D1 and antenna protein CP47 in PSII, disrupts their structures and inactivates their function, resulting less electrons (Gururani Mayank et al., 2015). Our study found that F_v/F_m, V_J and most JIP-test parameters (e.g., φ_{Po}, φ_{Eo}, φ_{Ro}, RC/ABS, PI_{ABS} and PI_{total}) were significantly lower for H7 treatment than for L7 treatment (Figure 4 and Table S1). These results indicated that salt stress suppressed the reduction of Q_A in PSII, and electron transfer from Q_A^-, through PQ pool, to end acceptors (e.g., Fd, NADP) at PSI electron acceptor side, i.e., salt stress severely inhibited linear photosynthetic electron transport chain from PSII to PSI. In addition, salt stress largely down-regulated expression levels of *psbA* (encoding D1 protein in PSII), *psbB* (encoding CP47 protein in PSII), *psaA* and *psaB* (coding P700 core protein in PSI) genes, delayed the repair rate of PSII and decreased PSI activity, showing that salt stress played adverse roles in electron transport (Figure 6).

Studies have shown that R/FR could improve antioxidant enzyme activities, effectively relieve oxidative damage of salt stress, delay decomposition rate of proteins, eventually enhance leaf photosynthesis in plants (Cao et al., 2018). Our study clearly indicated that F_v/F_m, V_J in OJIP curve, φ_{Po} and φ_{Eo} were significantly increased by H0.7 treatment when compared to H7 treatment, suggesting that low R/FR effectively increased electron transport from primary electron acceptor to PQ pool through Q_A. Furthermore, owing to up-regulated expression levels of *psbA*, *psbB*, *psaA* and *psaB* genes, the synthesis rate and efficiency of PSII and PSI were also improved by low R/FR (Figure 6). These results indicated that low R/FR improved the structure and function of PSII and PSI under salt stress, thus benefited photosynthetic electron transport under stress. Moreover, low R/FR also generated abundant ATP and NADPH for Calvin cycle by exhibiting strong electron transport capacity.

Low R/FR accelerated Calvin cycle in salt-stressed cucumber leaves

The Calvin cycle is an important component of carbon assimilation in photosynthesis. Rubisco is the key rate-limiting enzyme in Calvin cycle (Sharwood, 2017). The *rbcL*, *rbcS*, and *Rca* genes encode for large subunit, small subunit and activase of Rubisco, respectively. Previous studies found that salt stress can decrease Rubisco activity (Lin et al., 2018), which is consistent with the phenomenon observed in the current study. Under salt stress, total Rubisco activity, expression levels of *rbcL*, *rbcS*, and *Rca* genes and most key genes (*TPI*, *FBPase*, *SBPase*, *Rupe* and *PRK*) involved in Calvin cycle were remarkedly reduced (Figures 5, 6). The decline in expression and catalytic activity of Rubisco enzyme and other key enzymes involved in Calvin cycle severely restricts the ability of carbon assimilation (Sobhanian et al., 2010).

The previous studies showed that Low R/FR could enhance leaf photosynthesis by promoting carbon assimilation (Tan et al., 2022). Zhou et al. (2021) have suggested that low R/FR improved leaf photosynthetic capacity by up-regulating *RBCS* (encoding for small subunit of Rubisco) gene expression under calcium nitrate stress. In this study, low R/FR increased total Rubisco activity and up-regulated expression of most key genes (*rbcS*, *Rca*, *FBPase*, *SBPase*, *Rupe* and *PRK*) involved in Calvin cycle. These observations were consistent with the observations in tomato (Zhou et al., 2021) and spinach (Tan et al., 2022). These changes illustrating that low R/FR promoted carbon assimilation under salt stress through upregulating the expression levels and activity of Rubisco and other Calvin cycle enzymes.

Conclusion

Salt stress severely reduced leaf chlorophyll content, inhibited leaf photosynthesis and delayed plant growth. However, Low R/FR largely alleviated the adverse effects of salt stress on photosynthesis, it not only effectively improved linear photosynthetic electron transport from PSII to PQ pool, but also increased Rubisco activity and accelerated Calvin cycle, improved leaf photosynthesis and accelerated plant growth. In conclusion, low R/FR enhanced leaf photosynthesis by improving photosynthetic electron transport and Calvin cycle in salt-stressed cucumber plants. Therefore, usage of low red to far-red light ratio under salt stress condition could be advantageous for vegetable production.

Data availability statement

The original contributions presented in the study are included in the article/Supplementary Materials. Further inquiries can be directed to the corresponding author.

Author contributions

YM and XG performed experimental design, experimentation, data collection and analysis, manuscript preparation. BL contributed to project leadership, funding. WW performed experimental design and data analysis. LB revised and edited the manuscript. All authors contributed to the article and approved the submitted version.

Funding

The research was financially supported by Shanxi Province Basic Research Program (20210302124242, 20210302123401), Shanxi Province Colleges and Universities' Innovative Projects (2019L0382, 2019L0354), Shanxi Province Key R&D Plan (201703D211001-04-03), National Natural Science Foundation of China (31902029), High-level Foreign Expert Introduction Program in Ministry of Science and Technology (G2021004010L).

Acknowledgments

We thank Dr. Xiangzhen Wen for contributing to the experimental design. We thank Dr. Yaling Li for technical support throughout the experiment.

Conflict of interest

The authors declare that the research was conducted in the absence of any commercial or financial relationships that could be construed as a potential conflict of interest.

Publisher's note

All claims expressed in this article are solely those of the authors and do not necessarily represent those of their affiliated organizations, or those of the publisher, the editors and the reviewers. Any product that may be evaluated in this article, or claim that may be made by its manufacturer, is not guaranteed or endorsed by the publisher.

Supplementary material

The Supplementary Material for this article can be found online at: https://www.frontiersin.org/articles/10.3389/fpls.2022.1053780/full#supplementary-material

References

Ahres, M., Gierczik, K., Boldizsár, Á, Vítámvás, P., and Galiba, G. (2020). Temperature and light-quality-dependent regulation of freezing tolerance in barley. *Plants.* 9 (1), 83. doi: 10.3390/plants9010083

Cao, K., Yu, J., Xu, D., Ai, K., Bao, E., and Zou, Z. (2018). Exposure to lower red to far-red light ratios improve tomato tolerance to salt stress. *BMC Plant Biol.* 18 (1), 92. doi: 10.1186/s12870-018-1310-9

Cockburn, W., Whitelam, G. C., Broad, A., and Smith, J. (1996). The participation of phytochrome in the signal transduction pathway of salt stress responses in *Mesembryanthemum crystallinum* l. *J. Exp. Bot.* 47 (298), 647–653. doi: 10.1093/jxb/47.5.647

Courbier, S., and Pierik, R. (2019). Canopy light quality modulates stress responses in plants. *iScience* 22, 441–452. doi: 10.1016/j.isci.2019.11.035

De Lacerda, C. F., Cambraia, J., Oliva, M. A., and Ruiz, H. A. (2005). Changes in growth and in solute concentrations in sorghum leaves and roots during salt stress recovery. *Environ. Exp. Bot.* 54 (1), 69–76. doi: 10.1016/j.envexpbot.2004.06.004

Demotes-Mainard, S., Péron, T., Corot, A., Bertheloot, J., Gourrierec, J. L., Pelleschi-Travier, S., et al. (2015). Plant responses to red and far-red lights, applications in horticulture. *Environ. Exp. Bot.* 309, S0098847215000933. doi: 10.1016/j.envexpbot.2015.05.010

Franklin, K. A. (2008). Shade avoidance. *New Phytol.* 179 (4), 930–944. doi: 10.1111/j.1469-8137.2008.02507.x

Gao, J. (2006). *Experimental guidance for plant physiology* (Beijing: Higher Education Press).

Giorio, P., and Sellami, M. H. (2021). Polyphasic OKJIP chlorophyll *a* fluorescence transient in a landrace and a commercial cultivar of sweet pepper (*Capsicum annuum*, l.) under long-term salt stress. *Plants* 10 (5), 887. doi: 10.3390/plants10050887

Gong, Z., Xiong, L., Shi, H., Yang, S., and Zhu, J. K. (2020). Plant abiotic stress response and nutrient use efficiency. *Sci. China Life Sci.* 63 (5), 635-674. doi: 10.1007/s11427-020-1683-x

Gorai, M., Romdhane, R., Maraghni, M., and Neffati, M. (2019). Relationship between leaf gas-exchange characteristics and the performance of *Ziziphus spina-christi* (L.) willd. seedlings subjected to salt stress. *Photosynthetica* 57 (3), 897–903. doi: 10.32615/ps.2019.093

Gururani Mayank, A., Venkatesh, J., and Tran, L. S. P. (2015). Regulation of photosynthesis during abiotic stress-induced photoinhibition. *Mol. Plant* 8 (9), 1304–1320. doi: 10.1016/j.molp.2015.05.005

Gyugos, M., Ahres, M., Gulyás, Z., Szalai, G., Darkó, É, Mednyánszky, Z., et al. (2021). Light spectrum modifies the drought-induced changes of glutathione and free amino acid levels in wheat. *Acta Physiol. Plant* 43 (6), 90. doi: 10.1007/s11738-021-03253-x

Hayes, S., Pantazopoulou, C. K., Van Gelderen, K., Reinen, E., Tween, A. L., Sharma, A., et al. (2019). Soil salinity limits plant shade avoidance. *Curr. Biol.* 29 (10), 1669–1676. doi: 10.1016/j.cub.2019.03.042

Holalu, S. V., and Finlayson, S. A. (2017). The ratio of red light to far red light alters *Arabidopsis* axillary bud growth and abscisic acid signalling before stem auxin changes. *J. Exp. Bot.* 68 (5), 943–952. doi: 10.1093/jxb/erw479

Hunt, R. (1978). *Plant growth analysis* (London: Edward Arnold).

Jeong, H. W., Lee, H. R., Kim, H. M., Kim, H. M., Hwang, H. S., and Hwang, S. J. (2020). Using light quality for growth control of cucumber seedlings in closed-type plant production system. *Plants* 9 (5), 639. doi: 10.3390/plants9050639

Jiang, H., Li, Z., Jiang, X., and Qin, Y. (2021). Effects of salt stress on photosynthetic fluorescence characteristics, antioxidant system, and osmoregulation of *Coreopsis tinctoria* nutt. *HortScience* 56 (9), 1066–1072. doi: 10.21273/HORTSCI15956-21

Kalaitzoglou, P., Van Ieperen, W., Harbinson, J., van der Meer, M., Martinakos, S., Weerheim, K., et al. (2019). Effects of continuous or end-of-day far-red light on tomato plant growth, morphology, light absorption, and fruit production. *Front. Plant Sci.* 10. doi: 10.3389/fpls.2019.00322

Kalaji, H. M., Bosa, K., Kościelniak, J., and Żuk-Gołaszewska, K. (2011). Effects of salt stress on photosystem II efficiency and CO_2 assimilation of two Syrian barley landraces. *Environ. Exp. Bot.* 73, 64–72. doi: 10.1016/j.envexpbot.2010.10.009

Kotilainen, T., Aphalo, P. J., Brelsford, C. C., Böök, H., Devraj, S., Heikkilä, A., et al. (2020). Patterns in the spectral composition of sunlight and biologically meaningful spectral photon ratios as affected by atmospheric factors. *Agric. For. Meteorol.* 291, 108041. doi: 10.1016/j.agrformet.2020.108041

Lin, J., Li, J. P., Yuan, F., Yang, Z., Wang, B. S., and Chen, M. (2018). Transcriptome profiling of genes involved in photosynthesis in *Elaeagnus angustifolia* l. under salt stress. *Photosynthetica* 56 (4), 998–1009. doi: 10.1007/s11099-018-0824-6

Long, S., and Bernacchi, C. (2003). Gas exchange measurements, what can they tell us about the underlying limitations to photosynthesis? procedures and sources of error. *J. Exp. Bot.* 54 (392), 2393–2401. doi: 10.1093/jxb/erg262

Ma, X., Zheng, J., Zhang, X., Hu, Q., and Qian, R. (2017). Salicylic acid alleviates the adverse effects of salt stress on *Dianthus superbus* (Caryophyllaceae) by activating photosynthesis, protecting morphological structure, and enhancing the antioxidant system. *Front. Plant Sci.* 8. doi: 10.3389/fpls.2017.00600

Miao, Y., Chen, Q., Qu, M., Gao, L., and Hou, L. (2019). Blue light alleviates 'red light syndrome'by regulating chloroplast ultrastructure, photosynthetic traits and nutrient accumulation in cucumber plants. *Sci. Hortic. (Amsterdam)* 257, 108680. doi: 10.1016/j.scienta.2019.108680

Miao, Y., Luo, X., Gao, X., Wang, W., Li, B., and Hou, L. (2020). Exogenous salicylic acid alleviates salt stress by improving leaf photosynthesis and root system architecture in cucumber seedlings. *Sci. Hortic. (Amsterdam)* 272, 109577. doi: 10.1016/j.scienta.2020.109577

Miao, Y., Wang, X., Gao, L., Chen, Q., and Qu, M. (2016). Blue light is more essential than red light for maintaining the activities of photosystem II and I and photosynthetic electron transport capacity in cucumber leaves. *J. Integr. Agr.* 15 (1), 87–100. doi: 10.1016/S2095-3119(15)61202-3

Moncada, A., Vetrano, F., and Miceli, A. (2020). Alleviation of salt stress by plant growth-promoting bacteria in hydroponic leaf lettuce. *Agronomy* 10 (10), 1523. doi: 10.3390/agronomy10101523

Niu, M., Sun, S., Nawaz, M. A., Sun, J., Cao, H., Lu, J., et al. (2019). Grafting cucumber onto pumpkin induced early stomatal closure by increasing ABA sensitivity under salinity conditions. *Front. Plant Sci.* 10. doi: 10.3389/fpls.2019.01290

Perreault, F., Oukarroum, A., Pirastru, L., Sirois, L., Matias, W. G., and Popovic, R. (2010). Evaluation of copper oxide nanoparticles toxicity using chlorophyll *a* fluorescence imaging in *Lemna gibba*. *J. Bot.* 2010 (4), 807–826. doi: 10.1155/2010/763142

Shabala, S., and Cuin, T. A. (2008). Potassium transport and plant salt tolerance. *Physiol. Plant* 133 (4), 651–669. doi: 10.1111/j.1399-3054.2007.01008.x

Shao, Q. S., Shu, S., Du, J., Xing, W. W., Guo, S. R., and Sun, J. (2015). Effects of NaCl stress on nitrogen metabolism of cucumber seedlings. *Russ. J. Plant Physiol.* 62 (5), 595–603. doi: 10.1134/S1021443715050155

Sharwood, R. E. (2017). Engineering chloroplasts to improve rubisco catalysis: P: rospects for translating improvements into food and fiber crops. *New Phytol.* 213 (2), 494–510. doi: 10.1111/nph.14351

Shibuya, T., Endo, R., Yuba, T., and Kitaya, Y. (2015). The photosynthetic parameters of cucumber as affected by irradiances with different red:Far-red ratios. *Biol. Plantarum* 59 (1), 198–200. doi: 10.1007/s10535-014-0473-y

Sobhanian, H., Motamed, N., Jazii, F. R., Nakamura, T., and Komatsu, S. (2010). Salt stress induced differential proteome and metabolome response in the shoots of *Aeluropus lagopoides* (Poaceae), a halophyte C4 plant. *J. Proteome Res.* 9 (6), 2882–2897. doi: 10.1021/pr900974k

Strasser, R., Tsimilli-Michael, M., and Srivastava, A. (2004). *Analysis of the chlorophyll a fluorescence transient* (Berlin. Berlin: Springer Netherlands).

Suzuki, K., Ohmori, Y., and Ratel, E. (2011). High root temperature blocks both linear and cyclic electron transport in the dark during chilling of the leaves of rice seedlings. *Plant Cell Physiol.* 52 (9), 1697–1707. doi: 10.1093/pcp/pcr104

Tan, T., Li, S., Fan, Y., Wang, Z., Ali Raza, M., Shafiq, I., et al. (2022). Far-red light: A regulator of plant morphology and photosynthetic capacity. *Crop J.* 10 (2), 300–309. doi: 10.1016/j.cj.2021.06.007

Wang, H., Gu, M., Cui, J. X., Shi, K., Zhou, Y. H., and Yu, J. (2009). Effects of light quality on CO_2 assimilation, chlorophyll-fluorescence quenching, expression of Calvin cycle genes and carbohydrate accumulation in *Cucumis sativus*. *J. Photoch. Photobio. B.* 96 (1), 30–37. doi: 10.1016/j.jphotobiol.2009.03.010

Wang, W., Cai, L., Long, Z., Zhang, X., and Zhao, F. (2021). Effects of non-uniform salt stress on growth, yield, and quality of tomato. *Soil Sci. Plant Nutr.* 67 (5), 545–556. doi: 10.1080/00380768.2021.1966834

Wang, X., Zhang, W., Miao, Y., and Gao, L. (2016). Root-zone warming differently benefits mature and newly unfolded leaves of *Cucumis sativus* l. seedlings under sub-optimal temperature stress. *PloS One* 11 (5), e0155298. doi: 10.1371/journal.pone.0155298

Wang, Y., Bian, Z., Pan, T., Cao, K., and Zou, Z. (2021). Improvement of tomato salt tolerance by the regulation of photosynthetic performance and antioxidant enzyme capacity under a low red to far-red light ratio. *Plant Physiol. Biochem.* 167, 806–815. doi: 10.1016/j.plaphy.2021.09.008

Yang, F., Liu, Q., Cheng, Y., Feng, L., Wu, X., Fan, Y., et al. (2020). Low red/far-red ratio as a signal promotes carbon assimilation of soybean seedlings by

increasing the photosynthetic capacity. *BMC Plant Biol.* 20 (1), 1–12. doi: 10.1186/s12870-020-02352-0

Zhang, J., Yang, D., Li, M., and Shi, L. (2016). Metabolic profiles reveal changes in wild and cultivated soybean seedling leaves under salt stress. *PloS One* 11 (7), e0159622. doi: 10.1371/journal.pone.0159622

Zhang, L., Zhang, L., Sun, J., Zhang, Z., Ren, H., and Sui, X. (2013). Rubisco gene expression and photosynthetic characteristics of cucumber seedlings in response to water deficit. *Sci. Hortic. (Amsterdam)* 161, 81–87. doi: 10.1016/j.scienta.2013.06.029

Zhang, M., Smith, J. A. C., Harberd, N. P., and Jiang, C. (2016). The regulatory roles of ethylene and reactive oxygen species (ROS) in plant salt stress responses. *Plant Mol. Biol.* 91 (6), 651–659. doi: 10.1007/s11103-016-0488-1

Zhao, H., Zhang, Z., Zhang, Y., Bai, L., Hu, X., Li, X., et al. (2022). Melatonin reduces photoinhibition in cucumber during chilling by regulating the Calvin-Benson cycle. *Sci. Hortic. (Amsterdam)* 299, 111007. doi: 10.1016/j.scienta.2022.111007

Zhao, X., Sui, X., Zhao, L., Gao, X., Wang, J., Wen, X., et al. (2022). Morphological and physiological response mechanism of lettuce (*Lactuca sativa* l.) to consecutive heat stress. *Sci. Hortic. (Amsterdam)* 301, 111112. doi: 10.1016/j.scienta.2022.111112

Zhen, S., and Iersel, M. V. (2017). Far-red light is needed for efficient photochemistry and photosynthesis. *J. Plant Physiol.* 209, 115–122. doi: 10.1016/j.jplph.2016.12.004

Zhou, X., Li, Z., He, J., Wang, X., Liu, Q., Huang, J., et al. (2021). Effects of red to far-red light ratio on growth and photosynthetic characteristics of tomato seedlings under calcium nitrate stress. *Photosynthetica* 59, 625–632. doi: 10.32615/ps.2021.052

frontiers | Frontiers in Plant Science

TYPE Original Research
PUBLISHED 12 January 2023
DOI 10.3389/fpls.2022.1078113

Check for updates

OPEN ACCESS

EDITED BY
Diaa Abd El Moneim,
Arish University, Egypt

REVIEWED BY
Amira Ibrahim,
Arish University, Egypt
Yasir Sharif,
Fujian Agriculture and Forestry University, China
Wasim Akhtar,
University of Azad Jammu and Kashmir, Pakistan

*CORRESPONDENCE
Yan Xia
yxia@njau.edu.cn
Qi Wang
qiwang8803@126.com
Zhenguo Shen
zgshen@njau.edu.cn

SPECIALTY SECTION
This article was submitted to Plant Abiotic Stress, a section of the journal Frontiers in Plant Science

RECEIVED 24 October 2022
ACCEPTED 19 December 2022
PUBLISHED 12 January 2023

CITATION
ShangGuan X, Qi Y, Wang A, Ren Y, Wang Y, Xiao T, Shen Z, Wang Q and Xia Y (2023) OsGLP participates in the regulation of lignin synthesis and deposition in rice against copper and cadmium toxicity.
Front. Plant Sci. 13:1078113.
doi: 10.3389/fpls.2022.1078113

COPYRIGHT
© 2023 ShangGuan, Qi, Wang, Ren, Wang, Xiao, Shen, Wang and Xia. This is an open-access article distributed under the terms of the Creative Commons Attribution License (CC BY). The use, distribution or reproduction in other forums is permitted, provided the original author(s) and the copyright owner(s) are credited and that the original publication in this journal is cited, in accordance with accepted academic practice. No use, distribution or reproduction is permitted which does not comply with these terms.

OsGLP participates in the regulation of lignin synthesis and deposition in rice against copper and cadmium toxicity

Xiangchao ShangGuan[1], Ying Qi[2], Aiguo Wang[3], Yingnan Ren[1], Yu Wang[1], Tengwei Xiao[1], Zhenguo Shen[1]*, Qi Wang[4]* and Yan Xia[1]*

[1]College of Life Sciences, Jiangsu Collaborative Innovation Center for Solid Organic Waste Resource, Nanjing Agricultural University, Nanjing, China, [2]College of Agronomy, Yunnan Research Center of Urban Agricultural Engineering and Technology, Kunming University, Kunming, China, [3]Key Laboratory of Ecological Environment and Tobacco Quality in Tobacco Industry, Zhengzhou Tobacco Research Institute of China National Tobacco Corporation, Zhengzhou, China, [4]School of Life Sciences, Zhengzhou University, Zhengzhou, China

Copper (Cu) and cadmium (Cd) are common heavy metal pollutants. When Cd and excessive Cu accumulate in plants, plant growth is reduced. Our previous study showed that Germin-like proteins (GLPs), which exist in tandem on chromosomes, are a class of soluble glycoproteins that respond to Cu stress. In this study, hydroponic cultures were carried out to investigate the effect of GLP on Cd and Cu tolerance and accumulation in rice. The results showed that knockout of a single *OsGLP8-2* gene or ten *OsGLP* genes (*OsGLP8-2* to *OsGLP8-11*) resulted in a similar sensitivity to Cd and Cu toxicity. When subjected to Cu and Cd stress, the *glp8-2* and *glp8-(2-11)* mutants displayed a more sensitive phenotype based on the plant height, root length, and dry biomass of the rice seedlings. Correspondingly, Cu and Cd concentrations in the *glp8-2* and *glp8-(2-11)* mutants were significantly higher than those in the wild-type (WT) and *OsGLP8-2*-overexpressing line. However, Cu and Cd accumulation in the cell wall was the opposite. Furthermore, we determined lignin accumulation. The overexpressing-*OsGLP8-2* line had a higher lignin accumulation in the shoot and root cell walls than those of the WT, *glp8-2*, and *glp8-(2-11)*. The expression of lignin synthesis genes in the *OsGLP8-2*-overexpressing line was significantly higher than that in the WT, *glp8-2*, and *glp8-(2-11)*. The SOD activity of *OsGLP8-2*, Diaminobe-nzidine (DAB), propidium iodide (PI) staining, and Malondialdehyde (MDA) content determination suggested that *OsGLP8-2* is involved in heavy metal-induced antioxidant defense in rice. Our findings clearly suggest that OsGLPs participate in responses to heavy metal stress by lignin deposition and antioxidant defense capacity in rice, and *OsGLP8-2* may play a major role in the tandem repeat gene clusters of chromosome 8 under heavy metal stress conditions.

KEYWORDS

***Oryza sativa* L., germin-like proteins, heavy metal, lignin accumulation, detoxification**

Highlights

- OsGLPs involved in Cd and Cu detoxification and tolerance in rice.
- OsGLPs regulate lignin deposition in cell wall by altering expression of lignin synthesis genes.
- *OsGLP8-2* may play a major role in the tandem repeat gene clusters of rice chromosome 8 when Cd and Cu exposure.

Introduction

Copper (Cu) is an essential micronutrient element for the normal growth and development of plants (Nazir et al., 2019). However, excessive copper exhibits high toxicity, causing oxidative stress, increasing the reactive oxygen species (ROS) content in plant cells, and destroying the integrity and function of cell membranes (Chrysargyris et al., 2019; Rather et al., 2020). Cadmium (Cd) is a common heavy metal pollutant that is absorbed by plant roots and enters the food chain, endangering human and animal health (Chen et al., 2019a; Zhang et al., 2020). In agriculture, excessive Cu and Cd have many adverse effects on crops, including reducing the germination rate of seeds, changing the growth and morphology of crops, and hindering the absorption of mineral nutrients (Zare et al., 2018; Napoli et al., 2019; Yue et al., 2021; Wang et al., 2021). These adverse effects lead to reduced crop yields and lower quality. The absorption of metal elements by plants is based on plant type and heavy metal. The absorption mechanisms include absorption, transport, accumulation, distribution, rejection, and osmotic adjustment (Ma et al., 2016a).

The cell wall is an important barrier that prevents the transfer of heavy metals into cells (Park and Chon, 2016; Fernández-Fuego et al., 2017; Liu et al., 2019). Previous studies have shown that heavy metals can affect the thickness of plant cell walls, pectin cross-linking, and enzyme activity (Douchiche et al., 2010), thereby affecting cell walls (Zhu et al., 2012; Jia et al., 2021). When subjected to biotic and abiotic stress, lignin metabolism can play a role in stress resistance (Do et al., 2007; Moura et al., 2010; Liu et al., 2018; Wang et al., 2022). Aluminium (Al) can induce lignin synthesis in rice roots, as well as the synthesis of other cell wall components (Mao et al., 2004), and the gene expression of 4-coumarate CoA ligase (4CL), cinnamon alcohol de oxidase (CAD), caffeoyl-CoA-*O*-methyltransferase (CCR), and other enzymes related to lignin synthesis increase (Mao et al., 2004; Mir Derikvand et al., 2008). Cd has a similar effect on soybean growth (Bhuiyan et al., 2007).

Germin-like proteins (GLPs) are a class of soluble glycoproteins that are highly homologous to the germin sequence of wheat (Majeed et al., 2018; Zhang et al., 2018). *GLP* genes have been identified in various plant species (Ilyas et al., 2016). GLPs, most of which are stable oligomers, exist in the extracellular matrix through ionic bonding (Bernier and Berna, 2001; Dunwell et al., 2008). GLPs showed enzymatic activities of oxalate oxidase (OXO), superoxide dismutase (SOD), and polyphenol oxidase (PPO) (Cheng et al., 2014; He et al., 2021). These proteins usually participate in the physiological activities of plants in the form of enzymes, receptors, and structural proteins (Lou and Baldwin, 2006; Dunwell et al., 2008). Earlier studies have shown that *GLPs* are an important class of genes involved in both biotic and abiotic stress responses (Bruno et al., 2014; Zhang et al., 2017; Liao et al., 2021; Zaynab et al., 2022). It has been reported that downregulation of *OsGLP1* sensitised rice to the pathogens of rice blast and sheath blight (Banerjee and Maiti, 2010). Transgenic tobacco plants overexpressing the soybean *GmGLP10* gene displayed enhanced resistance to *Sclerotinia sclerotiorum* infection (Zhang et al., 2017). In addition, these proteins have shown high resistance to salt stress (Hurkman et al., 1991; Barman and Banerjee, 2015; Takeuchi et al., 2016; Banerjee et al., 2017), drought stress (Ke et al., 2009), UV-B radiation (He et al., 2021), and various biological stressors. When exposed to Cu stress, several genes in rice *GLP* family showed higher transcription levels (Li et al., 2016). Similarly, rice treated with Cd also showed higher GLPs abundance (Wei et al., 2021). Zhou et al. (2009) found the GLP protein level of tomato was down-regulated under aluminum stress. However, there are still few studies on the relationship between GLPs and heavy metal tolerance in plants.

A previous study on rice proteomics by immobilised metal ion affinity chromatography-mass spectrometry (IMAC-MS) showed that heavy metal treatment significantly upregulated the abundance of OsGLP proteins (Song et al., 2013) and the transcriptional expression of some members of the *GLP* family (Li et al., 2016). Our current knowledge of the corresponding physiological functions and mechanisms of OsGLPs is still elusive. Here, we hypothesised that *OsGLP* genes are involved in Cd and Cu detoxification in rice. Crispr/Cas-9 technology, which has developed rapidly in recent years, can precisely edit plant genomes and obtain heritable plant material, providing an efficient technical tool for crop genetics (Ma et al., 2016b; Chen et al., 2019b). In this study, *OsGLP* transgenic rice lines, including knockout mutants of the single *OsGLP8-2* gene or ten genes (*OsGLP8-2 to OsGLP8-11*) and overexpressing *OsGLP8-2* transgenic rice, were constructed using Crispr/Cas-9 technology and the method of homologous recombination (Court et al., 2002). Furthermore, we functionally characterised OsGLPs responding to Cu and Cd stress in rice through detailed analysis, such as rice phenotype, heavy metal accumulation, lignin deposition in the cell wall, antioxidant defence capacity, and expression of lignin synthesis genes and members of the *OsGLP* family. This study aims to reveal the

10.3389/fpls.2022.1078113

relationship between rice OsGLPs and plant heavy metal tolerance, and further explains the mechanisms of plant response to heavy metal stress.

Materials and methods

Plant materials

Rice seeds were soaked in 10% sodium hypochlorite for 5 min under dark conditions. The seeds were then washed thoroughly, soaked in deionised water, and placed in an incubator at 37°C for germination. Uniformly emerging rice seedlings were evenly placed on a floating net and cultured in 0.5 mol L^{-1} $CaCl_2$ nutrient solution in the dark for two days to induce rooting. After $CaCl_2$ culture, rice seedlings were cultured with kimura B nutrient solution containing 0.18 $mmoL^{-1}$ KH_2PO_4, 0.36 $mmoL^{-1}$ $(NH_4)_2SO_4$, 0.54 $mmoL^{-1}$ $MgSO_4{\cdot}7H_2O$, 0.18 $mmoL^{-1}$ KNO_3, 0.36 $mmoL^{-1}$ $Ca(NO_3)_2{\cdot}4H_2O$, 46.25 μmoL^{-1} H_3BO_3, 0.32 μmoL^{-1} $CuSO_4{\cdot}5H_2O$, 0.76 μmoL^{-1} $ZnSO_4{\cdot}7H_2O$, 9.15 μmoL^{-1} $MnCl_2{\cdot}4H_2O$, 0.11μmoL^{-1} $H_2MoO_4{\cdot}H_2O$, 20 μmoL^{-1} EDTA–$FeSO_4$ (pH, 5.6).The nutrient solution was replaced every 2 days.

Two-week-old rice plants were cultured for 5 days under normal conditions, 10 µmol L^{-1} $CuSO_4$ treatment, or 25 µmol L^{-1} $CdCl_2$ treatment. A normal kimura B nutrient solution was used as the control. Four replicates were set, and each replicate was comprised of 5 rice seedlings. All rice seedlings were grown in a greenhouse under long-day conditions (14 h light/10 h dark) at 28°C/24°C. *Oryza sativa* cv 'Dongjin' was used as the wild type (WT) in this study.

Generation of transgenic plants

The CRISPR/Cas9 system was used to construct the rice mutants. Two sequences of 20 bp in exons of *GLP8-2* were selected as gRNAs. Primers were designed based on these sequences, and the annealed product was fused with the pRGEB31 vector. The coding sequences of *OsGLP8-2* were amplified from the cDNA of the WT (Dongjin, DJ). Two specific primers (CriOsGLP8-2F and CriOsGLP8-11R) were used to identify mutants, with 10 genes (*OsGLP8-2* to *OsGLP8-11*) knocked out. If a clear band was observed after 1% agarose gel electrophoresis (Supplementary Figure S1), this indicated that the multi-gene knockout mutant was successfully constructed. The coding region sequence of *OsGLP8-2* was fused with the pOx vector to form a recombinant plasmid (GLP8-2OE) driven by the 35S promoter. The primers used for vector construction are listed in Supplementary Table S1.

The recombinant plasmids were sequenced and introduced into *Agrobacterium tumefaciens* EHA105. The *A. tumefaciens*-mediated genetic transformation system was used to construct transgenic rice.

RNA-seq analysis of *OsGLP* Genes

Four-day-old WT rice seedlings were treated with 3 µmol L^{-1} $CuSO_4$ for 12 h. About 50 mg of root tips were collected and snap-frozen in liquid nitrogen to extract total RNA for transcriptome sequencing (GENE DENOVO Biotechnology Co., Ltd, Guangzhou, China). Bioinformatic analysis of the data was performed using the Omicsmart online real-time interactive platform. Each material was repeated three times. Fold change ≥ 2, and FDR ≤ 0.05.

Determination of Cu and Cd concentrations

The roots of the rice were washed with 20 mmol L^{-1} Na_2EDTA for 30 min to remove heavy metal ions attached to the surface of the roots. They were then placed in an oven at 80° C until a constant weight, and the dry weight was recorded. Dry plant samples or cell wall materials (0.2 g) were digested with 5.0 mL of guaranteed HNO_3:$HClO_4$ = 87:13 (*v*:*v*) mixed acid. Cd and Cu concentrations were determined using an inductively coupled plasma optical emission spectrometer (ICP-OES, PerkinElmer, Optima 8000, America). A plant standard [GBW10043 (GSB-21)] was purchased from the National Research Centre for Standards of China and used to ensure reliable results during the digestion and analysis processes.

Extraction of crude cell walls of rice seedlings

Extraction of crude cell walls was according to the methods of Yang et al. (2011) and Zhu et al. (2020). About 0.5 g of fresh samples of rice shoots and roots were ground with 10 times the volume of 95% ethanol to homogenise them. The mixture was centrifuged at 8,000×*g* for 5 min, and the supernatant was discarded. The pellet was washed 3 times with 95% ethanol. Finally, the pellet was washed twice with ethanol-hexane solution (*v*:*v*=1:2) and dried at room temperature to obtain the crude cell wall. The determination of heavy metals in the cell wall was performed as previously described in Determination of Cu and Cd concentrations section.

Histochemical and content determination of lignin

The stems of the rice plants were stained with Safranin O-Fast Green staining and paraffin sectioned by embedding

technology to determine lignin deposition in the cell walls (Wang et al., 2016; Han et al., 2021). The roots were placed on a Petri dish, and a few drops of 1% phloroglucinol ethanol solution were added. A drop of 35% HCl was added, and the roots were covered with cover glass. After volatilisation and colour development, the roots were placed on a type microscope and magnified four times for observation, and photos were taken.

Six milligrams of cell wall residue were transferred to a glass test tube, and 2.5 mL of 25% bromoacetyl-acetic acid solution (v/v=1:3) and 0.1 mL of 70% perchloric acid were added. The tube was covered, sealed, and placed in a water bath at 70°C for 30 min. The test tube was shaken every 10 min. After cooling, 10 mL of 2 mol L^{-1} NaOH solution was added, and the reaction mixture was diluted to 25 mL with glacial acetic acid. The mixture was centrifuged at 1000×*g* for 5 min. The absorbance of the supernatant was measured at 280 nm, with the reaction solution containing no sample as a blank control.

qRT-PCR

Total RNA from rice seedlings was extracted using an RNA Extraction Kit (TaKaRa, 9697, China). The cDNA was then obtained after inversion was used as a template, and the SYBR Green fluorescence quantitative kit (TaKaRa, RR420A, China) was used for fluorescence quantitative PCR amplification. The expression of the target gene was calculated using the $2^{-\Delta\Delta Ct}$ method (Gaonkar et al., 2018). The housekeeping gene *ACTIN1* (LOC_Os03g50885) was used as the internal control. Three biological replicates were used for qRT-PCR, and three technical replicates were set for each biological replicate. The primers used are listed in Supplementary Table S2.

Histochemical localisation of H_2O_2

The Diaminobenzidine (DAB) staining method was used for the quantitative detection of H_2O_2. DAB powder was dissolved in 50 mmol L^{-1} Tris-HCl (pH 6.0) to prepare a 1 mg mL^{-1} dye solution. Rice leaves (3–4 cm) were immersed in DAB dye solution, vacuumed for 2 hours until the leaves sank to the bottom of the tube, and placed in the dark for 12 hours. The dyed rice leaves were boiled in 95% ethanol for decolourisation. After bleaching was complete, the leaves were immersed in 70% ethanol, and pictures were taken using a stereo microscope (Nikon, SMZ1000, Japan).

Determination of MDA content

Leaf samples (0.1 g) were ground with 1.5 mL of trichloroacetic acid (TCA) on ice and centrifuged at 12,000×*g* for 15 min at 4°C. Then, 500 μL of the supernatant was transferred to a clean 2 mL centrifuge tube, and 1.5 mL of 0.5% thiobarbituric acid (TBA) was added and mixed well. The tubes were placed in a water bath at 90°C for 20 min. After cooling, the mixture was centrifuged at 10,000 rpm for 5 min. The absorbance of the supernatant was determined at 450, 532, and 600 nm. C (μmol L^{-1})=6.45×(A_{532}-A_{600})-0.56×A_{450}

Determination of the integrity of the root cell plasma membrane

Rice root tips (1 cm) were placed in 3 μg L^{-1} propidium iodide (PI) solution and soaked in the dark for 15 min. The root tips were removed from the dye solution and rinsed repeatedly with deionised water. Staining was observed with a fluorescence microscope (Zeiss, Axio Imager A1, Germany).

Statistical analysis

The data were analysed using Excel and SPSS25.0 for analysis of variance and LSD multiple comparison testing ($P \leq 0.05$). GraphPad Prism 6 was used to graph the data after processing. The values in the graph are the mean ± SD (n = 3). Different letters indicate the differences between several rice lines.

Results

Expression of *OsGLP* genes was induced by Cu stress

Thirty-two members of the *OsGLP* family were tandem repeat genes and were divided into 8 gene clusters located on chromosomes 1, 2, 3, 8, 9, and 12. Among them, the tandem repeat gene cluster on chromosome 8 was the largest, containing 11 *OsGLP* genes (*OsGLP8-1* to *OsGLP8-11*) (Li et al., 2016). Four-day-old WT seedlings were treated with 3 μmol L^{-1} $CuSO_4$ for 12 h. Total RNA was isolated from rice roots and used for transcriptome sequencing. The heat map showed that the expression of multiple *OsGLP* family genes, such as *OsGLP8-2*, *OsGLP8-5*, *OsGLP8-6*, *OsGLP8-7*, *OsGLP8-9*, *OsGLP8-10*, and *OsGLP8-11*, increased significantly after Cu treatment (Figure 1). It was inferred that some OsGLPs are Cu-responsive proteins.

Knockout of single *OsGLP8-2* or 10 *OsGLP* genes exhibits repressed growth

To understand the contribution of *OsGLPs* to heavy metal tolerance, we designed the primers for *OsGLP8-2* and *OsGLP8-*

11 to knock out multiple genes at the same time, and obtained the *glp8-2* and *glp8-(2-11)* mutants, respectively (Figure 2A; Supplementary Figure S2). Furthermore, we identified 6 overexpression lines and selected GLP8-2OE1 (hereinafter referred to as GLP8-2OE) with the highest expression of *OsGLP8-2* for subsequent experiments (Figure 2B).

The WT, two mutants *glp8-2* and *glp8-(2-11)*, and GLP8-2OE seedlings were treated with 10 μmol L^{-1} $CuSO_4$ or 25 μmol L^{-1} $CdCl_2$ for 5 days. Both the *glp8-2* and *glp8-(2-11)* mutants showed hypersensitivity to Cu and Cd toxicity compared with the WT seedlings (Figure 2C; Supplementary Figure S3). Excess Cu and Cd had a significant inhibitory effect on the shoot height and root elongation of *glp8-2* and *glp8-(2-11)* mutants, while *OsGLP8-2* overexpression increased heavy metal tolerance in rice (Figures 2D, E). Quantitative analysis further confirmed that the dry weights of *glp8-2* and *glp8-(2-11)* seedlings were significantly lower than those of WT and GLP8-2OE seedlings (Figures 2F, G). Overall, *OsGLP* knockout led to a decrease in chlorophyll content (Supplementary Figure S2). These results suggest that OsGLPs play an important role in regulating heavy metal tolerance in rice.

OsGLPs affect Cu and Cd accumulation in rice

To further investigate the mechanism of OsGLPs regulating heavy metal tolerance in rice, we measured the Cd and Cu concentrations in the shoots and roots, and in those of their cell walls. As shown in Figure 3, the Cd and Cu concentrations in both shoots and roots increased significantly with elevated heavy metal levels. At 3 and 10 μmol L^{-1}, *glp8-2* and *glp8-(2-11)* seedlings had higher Cu concentrations than the WT, while that in GLP8-2OE was lower. This was especially obvious when the rice seedlings were treated with 10 μmol L^{-1} $CuSO_4$ (Figures 3A, B). Cd accumulation in different rice seedlings at high levels of Cd (25 μmol L^{-1}) displayed a trend similar to Cu toxicity (Figures 3C, D). Cd and Cu concentrations in the roots were higher than those in the shoots of the different rice seedlings at the same level of heavy metals.

Cell walls are the main compartments that accumulate heavy metals (Krzeslowska, 2011; Wang et al., 2020; Yan et al., 2022). We determined Cd and Cd concentrations in the cell walls of different rice seedlings to investigate whether OsGLP changes the distribution of heavy metals. In contrast to the results of Cu concentrations in the shoots and roots, the *glp8-2* and *glp8-(2-11)* mutants accumulated less Cu in the cell wall than those of the WT and GLP8-2OE when exposed to 3 and 10 μmol L^{-1} $CuSO_4$ (Figures 4A, B). Similar to Cu concentration in the cell wall, the loss of *OsGLP8-2* resulted in lower Cd retention in the cell wall than the WT and overexpressing rice seedlings at high levels of $CdCl_2$ (25 μmol L^{-1}) (Figures 4C, D). However, there was no obvious difference in heavy metal concentrations of the cell wall between the *glp8-2* and *glp8-(2-11)* rice seedlings.

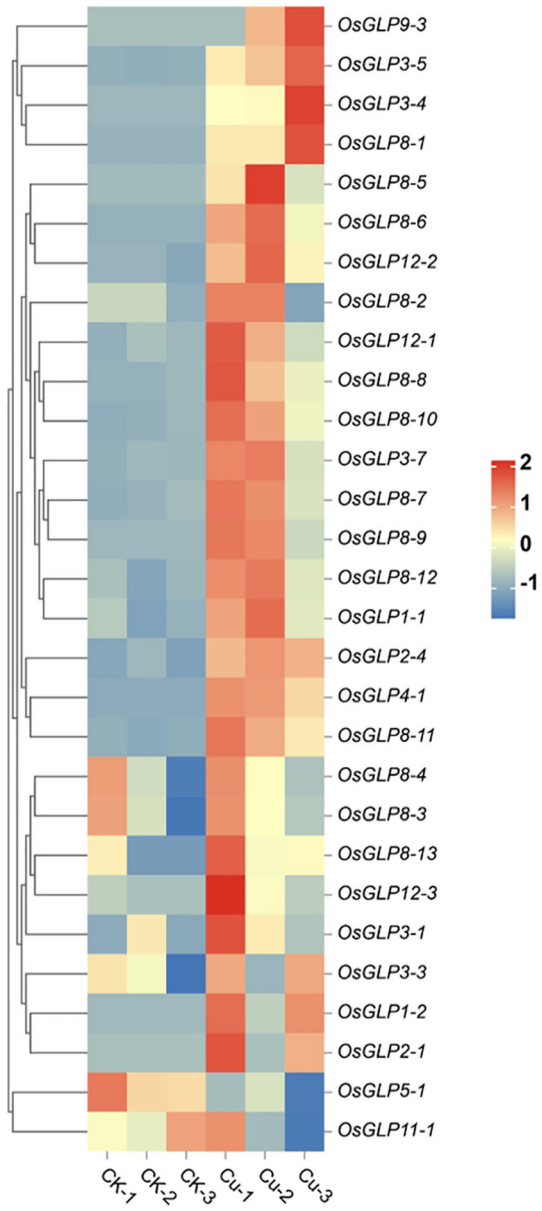

FIGURE 1
Cu toxicity induces the expression of *OsGLP8-2* in rice. Transcription levels of *OsGLPs* increased under heavy metal treatment. Total RNA was isolated from the roots of 4-day-old WT (wild type) rice seedlings treated with 3 μmol L^{-1} $CuSO_4$ for 12 h and used for transcriptome sequencing. Values are the mean ± SD; n = 3. Fold change ≥ 2 and FDR ≤ 0.05.

OsGLPs affect lignin accumulation in rice

Our previous studies reported that lignin may play a vital role in Cu and Cd stress (Liu et al., 2015; Xia et al., 2018; Su et al., 2020). To investigate the relationships among loss of *OsGLPs*, lignin synthesis, and heavy metal accumulation, we comparatively analysed lignin synthesis in different rice seedlings treated with elevated Cd and Cu levels. The Safranin O-Fast Green staining and

10.3389/fpls.2022.1078113

phloroglucinol-HCl staining in stems and roots showed that the lignin content in the *glp8-2* and *glp8-(2-11)* mutants was lower than that of the WT and GLP8-2OE rice (Figures 5A, B). To further confirm this, we quantitatively determined the lignin content in different rice seedlings treated with Cu and Cd using the acetyl bromide-soluble method (Van Acker et al., 2013; Jang and Lee, 2020). As expected, there was a decrease in the lignin content of the shoots and roots from the two *glp8-2* and *glp8-(2-11)* mutants under Cu and Cd stress, and the lignin content was about 4.6% lower than the WT (Figures 5C, D). The lignin content in the roots of OsGLP8-2OE induced by Cu and Cd was higher than that of the WT. A significant negative correlation between the heavy metal concentrations and lignin content was observed in rice roots ($p < 0.0001$ for Cu; $p = 0.0024$ for Cd) (Figures 5E, F).

OsGLPs positively regulate the expression of lignin synthesis-related genes

To determine whether the alteration of OsGLPs expression levels affects the lignin synthesis pathway, we tested the changes in the expression levels of lignin-related genes, including phenylalanine ammonia-lyase (PAL), 4-coumarate CoA ligase (4CL), caffeoyl-CoA-O-methyltransferase (CCoAoMT),

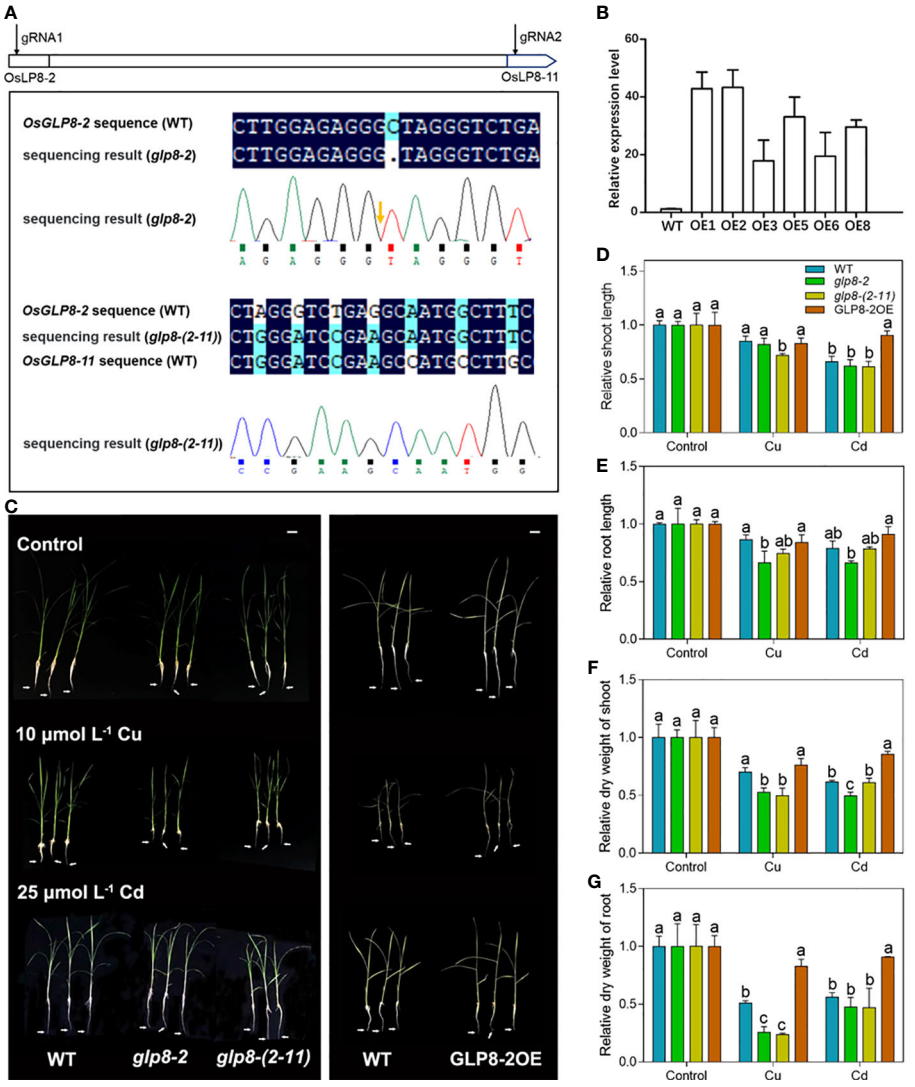

FIGURE 2
Knockout of *OsGLPs* results in the growth inhibition of rice seedlings. **(A)** Construction and identification of mutants. Two gRNAs were designed based on the exons of *OsGLP8-2* and *OsGLP8-11* near the ATG. Light blue and dark blue indicate successful sequence matching. Wavy lines are sequencing peaks. **(B)** Identification of *OsGLP8-2*-overexpressing lines. **(C)** Phenotypes of two-week-old WT (wild type) and transgenic seedlings grown for 5 days under normal conditions, 10 μmol L^{-1} $CuSO_4$ treatment, or 25 μmol L^{-1} $CdCl_2$ treatment. Scale bar = 3 cm. **(D, E)** Root elongation of WT and transgenic plants. **(F, G)** Dry weight of WT and transgenic plants. Values are the mean ± SD; n = 3. Different letters indicate a difference of $p \leq 0.05$ by the LSD test.

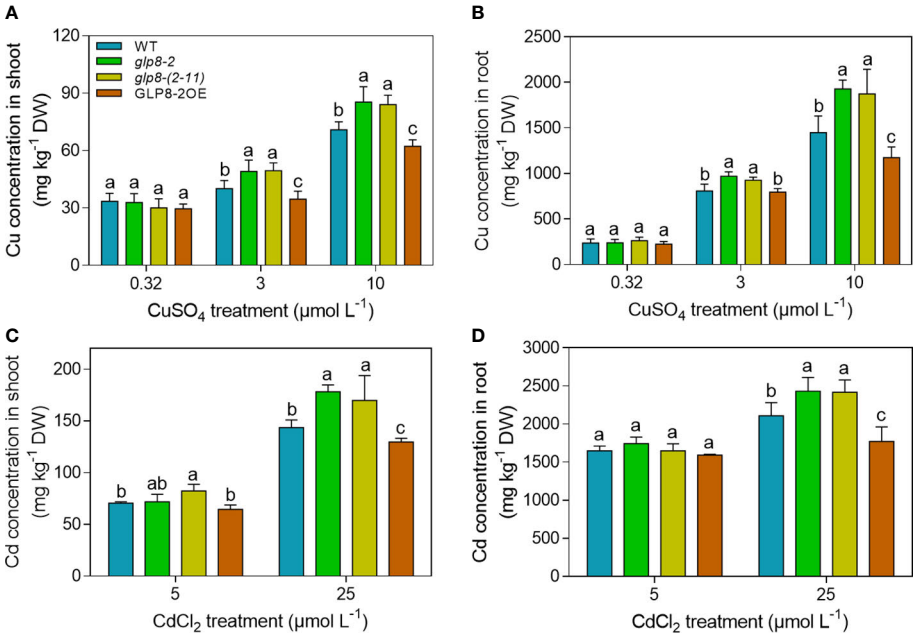

FIGURE 3
Knockout of OsGLPs affects heavy metal accumulation in rice. **(A, B)** Cu concentrations in the roots and shoots of two-week-old seedlings treated with 3 or 10 μmol L^{-1} $CuSO_4$ for 5 days. **(C, D)** Cd concentrations in the roots and shoots of two-week-old seedlings treated with 5 or 25 μmol L^{-1} $CdCl_2$ for 5 days. Values are the mean ± SD; n = 3. Different letters indicate a difference of $p \leq 0.05$ by the LSD test.

cinnamate-4-hydroxylase (C4H), and cinnamoyl-CoA reductase (CCR). Cu and Cd treatments significantly induced the expression of five lignin biosynthetic enzyme genes (PAL, 4CL, CCoAOMT, C4H, and CCR) (Figure 6). When treated with Cu and Cd, the expression levels of these five genes were reduced in the *glp8-2* and *glp8-(2-11)* mutants, especially in the *OsGLP8-(2-11)* mutants, but elevated significantly in the OsGLP8-2OE seedlings. The expression pattern of five lignin-related genes under Cu and Cd toxicity showed the same trend as lignin content in the roots and heavy metal accumulation in the cell wall.

OsGLPs participate in heavy metal-induced oxidative damage

To explore the role of *OsGLP*s in oxidative stress caused by heavy metal stress, we compared DAB staining in WT and transgenic rice lines. There was no significant difference in the leaf colour of the four lines in the absence of excess Cu and Cd. When exposed to Cu and Cd, the leaf colour was darker than that of the control and GLP8-2OE. Compared with the WT, the *glp8-2* and *glp8-(2-11)* mutants were darker, especially the *OsGLP8-(2-11)* mutant (Figure 7A). This indicates that OsGLPs participate in the elimination of active oxygen in rice cells and can reduce the accumulation of active oxygen caused by heavy metal stress, thereby alleviating the oxidative damage of rice.

Malondialdehyde (MDA) content indicates the degree of peroxidation of the cell membrane and is an important indicator of plant stress resistance (Yang et al., 2019). As shown in Figure 7B, Cu and Cd stress aggravated the peroxidation of membrane lipids and increased the MDA content. Loss of the function of OsGLPs led to increased MDA content, which was the opposite of the GLP8-2OE rice seedlings.

Propidium iodide (PI) is a nuclear fluorescent dye that indicates the integrity of the plasma membrane (Li et al., 2021). When the root tip cells are damaged, the permeability of the plasma membrane increases, PI can enter the cell and bind to DNA, and red fluorescence can be observed with a fluorescence microscope. In this study, PI was used to determine the integrity of the plasma membrane in the root tip. Cu and Cd treatments damaged the integrity of the plasma membrane in rice roots. By comparing the intensity of red fluorescence in different rice, the red fluorescence intensity of the *glp8-2* and *glp8-(2-11)* mutants were higher than that of the WT and OsGLP8-2OE (Figure 7C) when subjected to Cu and Cd stress, which was consistent with the H_2O_2 histochemical localisation and MDA content. This indicates that *OsGLP* genes play a certain role in maintaining the integrity of the plasma membrane.

OsGLP expression increases under Cu and Cd stress

The knockout mutant of 10 genes (*glp8-(2-11)*) and the mutant of *OsGLP8-2* (*glp8-2*) showed the same phenotypes, such as heavy metal tolerance and accumulation, lignin deposition

and gene expression levels, and antioxidant defence abilities. We speculated that *OsGLP8-2* may display the main contribution in the tandem repeat gene clusters on chromosome 8 in responding to heavy metal stress. The time course for expression levels of *OsGLP8-2*, *OsGLP8-3*, *OsGLP8-5*, *OsGLP8-7*, and *OsGLP8-11* genes on chromosome 8 were detected under Cu and Cd treatment. The expression of these five genes was significantly upregulated and reached a peak under Cu exposure for 3 h and Cd exposure for 12 h. Among these genes, Cd and Cu treatments upregulated the expression of *OsGLP8-2*, with the highest fold change. Its highest level was 71 times higher than that of the control under Cu stress and 11.3 times higher under Cd stress (Figure 8). These data demonstrate that OsGLP8-2 is more sensitive to Cu and Cd and is upregulated more than other tandem genes.

Discussion

Most GLPs have been reported to play three functions in plants, namely as enzymes, structural proteins, and signalling receptors (Bernier and Berna, 2001; Lou and Baldwin, 2006; Pei et al., 2019; Yuan et al., 2021; Zaynab et al., 2022). In this study, transcriptome analysis of rice under Cu stress was performed, in which the transcript levels of multiple genes of the *OsGLP* family showed significant differences compared with the control seedlings (Figure 1). Similarly, one member (*OsGLP8-7*) of the *OsGLP* family was identified, and its protein level was significantly upregulated under Cu stress (Chen et al., 2015). We speculated that the increased expression of *OsGLPs* may be a way for plants to cope with heavy metal toxicity.

Based on the unique distribution of the *OsGLP* genes on rice chromosome 8 (Li et al., 2016), gRNAs were designed for *OsGLP8-2* and *OsGLP8-11* genes to knock out the target genes, and two mutants, *glp8-2* and *glp8-(2-11)*, which were the mutants of the *OsGLP8-2* gene and ten genes (*OsGLP8-2 to OsGLP8-11*), respectively, were obtained. When treated with heavy metals, the loss of function of OsGLPs aggravated growth inhibition in rice (Figure 2) and led to higher heavy metal accumulation (Figure 3). This suggests that OsGLPs are important in response to heavy metal stress. In fact, studies have reported that two *AtGLP* genes in *Arabidopsis thaliana* L. were induced in large quantities when treated with Cd, indicating that AtGLPs play a role in Cd stress (van de Mortel et al., 2006).

The cell wall is the first barrier for metal ions to enter the plant cytoplasm across the membrane and has a strong ability to fix metal ions (Sun et al., 2013; Gao et al., 2021; Yan et al., 2022). In this study, when subjected to heavy metal stress, the heavy metal concentrations in the cell walls of the *OsGLP* mutants were significantly higher than those of the WT and overexpression line (Figure 4). However, the situation was reversed in the whole

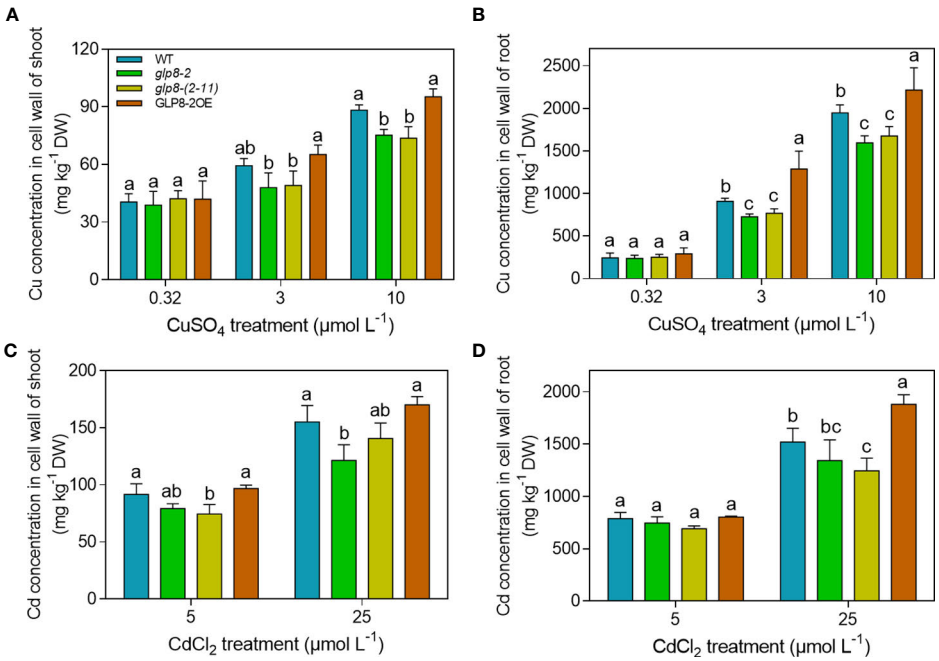

FIGURE 4
Knockout of OsGLPs affects heavy metal accumulation in the cell walls of rice. **(A, B)** Cu concentrations in the cell walls of roots and shoots of two-week-old seedlings treated with 3 or 10 μmol L^{-1} $CuSO_4$ for 5 days. **(C, D)** Cd concentrations in the cell walls of roots and shoots of two-week-old seedlings treated with 5 or 25 μmol L^{-1} $CdCl_2$ for 5 days. Values are the mean ± SD; n = 3. Different letters indicate a difference of $p \leq 0.05$ by the LSD test.

10.3389/fpls.2022.1078113

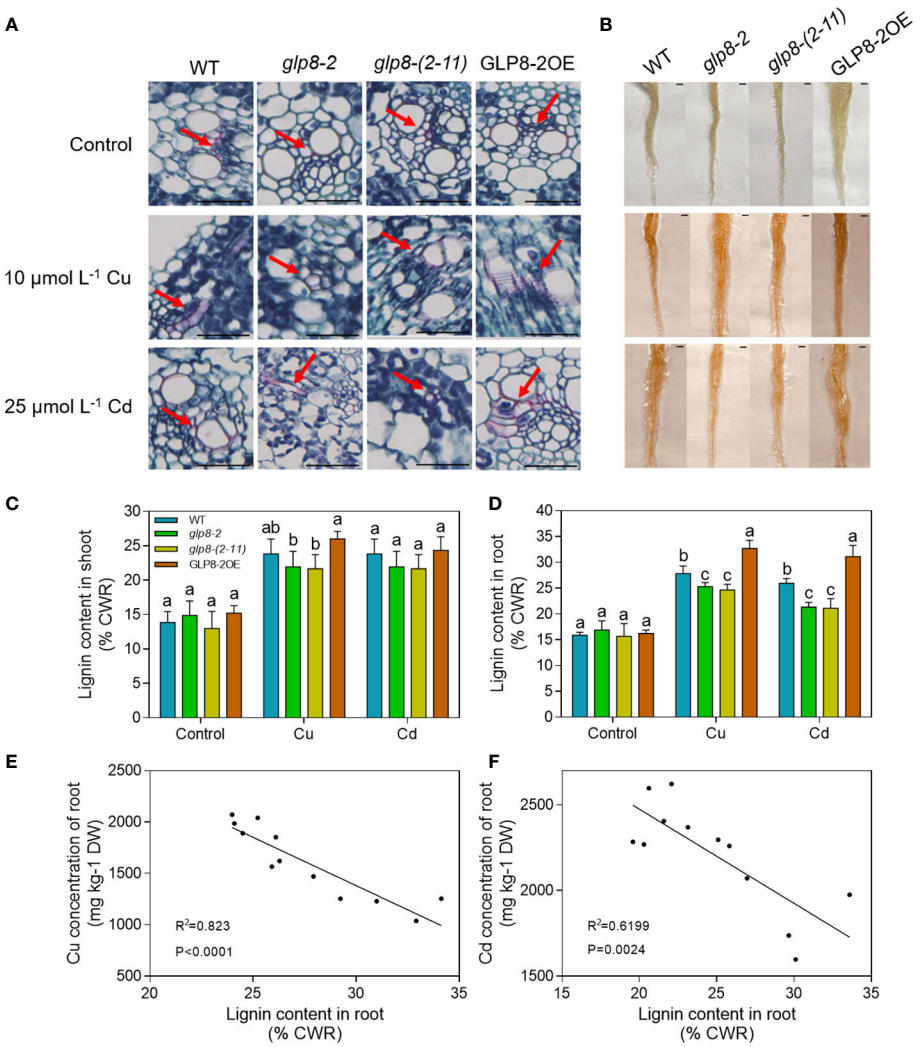

FIGURE 5
OsGLPs involved in lignin accumulation in rice. **(A)** Effects of Cu or Cd stress on lignin deposition in WT (wild type) and transgenic rice. Seedlings grew for 5 days under normal conditions, 10 μmol L^{-1} $CuSO_4$ treatment, or 25 μmol L^{-1} $CdCl_2$ treatment. The stems of the rice plants were stained with Safranin O-Fast Green, paraffin embedded, and sectioned. The magnification was 400×. Red indicates that the lignin was successfully dyed. **(B)** Histochemical localisation of lignin in primary roots of two-week-old seedlings grown for 5 days under normal conditions, 10 μmol L^{-1} $CuSO_4$ treatment, or 25 μmol L^{-1} $CdCl_2$ treatment. The roots were stained with phloroglucinol solution, sliced, and placed on a stereo microscope to take pictures. Scale bar = 1 cm. **(C, D)** The lignin content in the root and shoot cell walls of two-week-old seedlings grown for 5 days under normal conditions, 10 μmol L^{-1} $CuSO_4$ treatment, or 25 μmol L^{-1} $CdCl_2$ treatment. **(E, F)** Correlation between root Cu/Cd content in rice and lignin content in the root cell walls of rice. These seedlings were treated with 10 μmol L^{-1} $CuSO_4$ or 25 μmol L^{-1} $CdCl_2$ for 5 days. Values are the mean ± SD; n = 3. Different letters indicate a difference of $p \leq 0.05$ using the LSD test.

rice seedlings (Figure 3). The loss of OsGLPs led to a higher accumulation of heavy metals in rice; additionally, the ability of the cell wall to retain heavy metals was reduced, and the inward transport of heavy metals was increased. As a result, more heavy metals were enriched in the cytoplasm of the *glp8-2* and *glp8-(2-11)* seedlings, causing more serious toxicity and ultimately leading to a sensitive phenotype. The main components of the cell wall include cellulose, hemicellulose, lignin, and cell wall proteins (Zhao et al., 2019; Roig-Oliver et al., 2020). The abundance of lignin in the cell wall was second only to cellulose. It is a natural macromolecule polymerised by three monolignols: p-hydroxyphenyl (H), guaiacyl (G), and syringyl (S) units. Lignin is essential for maintaining the structural integrity of cell walls and the strength of roots and stems (Slabaugh et al., 2014; Zhao et al., 2020; Zhang et al., 2021). Lignin accumulation increases when plants are exposed to heavy metals, which causes the cell wall to thicken to fix and retard heavy metals, reducing their entry into the cell and causing toxic damage (Moura et al., 2010; Gao et al., 2012; Su et al., 2020; Pan et al., 2021). Therefore, lignin synthesis is a typical defence response of plants to environmental stress. Lignin deposition in the *glp8-2* and *glp8-(2-11)* seedlings was lower than that of the

10.3389/fpls.2022.1078113

WT and OsGLP8-2OE lines (Figure 5). It is generally believed that lignin enhances cell wall rigidification, inhibits root elongation (Xiong et al., 2015). When rice is subjected to heavy metal stress, GLPs can on the one hand increase lignin deposition, thereby inhibiting root growth; on the other hand, it can alleviate heavy metal toxicity, thus promoting root growth. In this study, there was a positive correlation between lignin content and root length, and a negative correlation between lignin content and heavy metal content. When *GLPs* was knocked down, the expression of lignin synthesis-related genes decreased (Figure 6). As functional proteins, GLPs may indirectly regulate the expression of these genes by regulating some transcription factors. Therefore, it was inferred that OsGLPs may participate in lignin synthesis.

GLPs mainly have the activities of three enzymes: SOD, OXO, and PPO (Cheng et al., 2014; Ilyas et al., 2020). The function of SOD is to disproportionate $O_2^{\cdot-}$ into H_2O_2 (Smirnoff and Arnaud, 2019). Researchers have shown that OsGLPs are localised to the cell wall. When OsGLPs perform the function of SOD, they cause an increase in the H_2O_2 content in the cell wall. The polymerisation of monolignols is the final step in lignin synthesis in the cell wall (Perkins et al., 2022; Zhang et al., 2022). We speculated that OsGLPs could affect lignin biosynthesis through the generated H_2O_2. Studies have shown that lignin polymerization is mediated by ROS (Poudel et al., 2019). Removal of H_2O_2 with KI (H_2O_2 scavenger) resulted in a sharp decrease in extracellular lignin content in *Picea abies* suspension cells (Karkonen et al., 2002). Diaminobenzidine (DAB) is a commonly used chromogenic substrate that reacts with H_2O_2 to form a brown precipitate in plant tissue. H_2O_2 accumulation can be determined by the shade of the brown substance (Graham and Karnovsky, 1966). However, DAB staining showed that *OsGLP8-2* overexpression reduced the H_2O_2 content (Figure 7A). On the one hand, the measurement of H_2O_2 deposition in the cell wall would explain the results better. On the other hand, when excessive H_2O_2 disrupts the

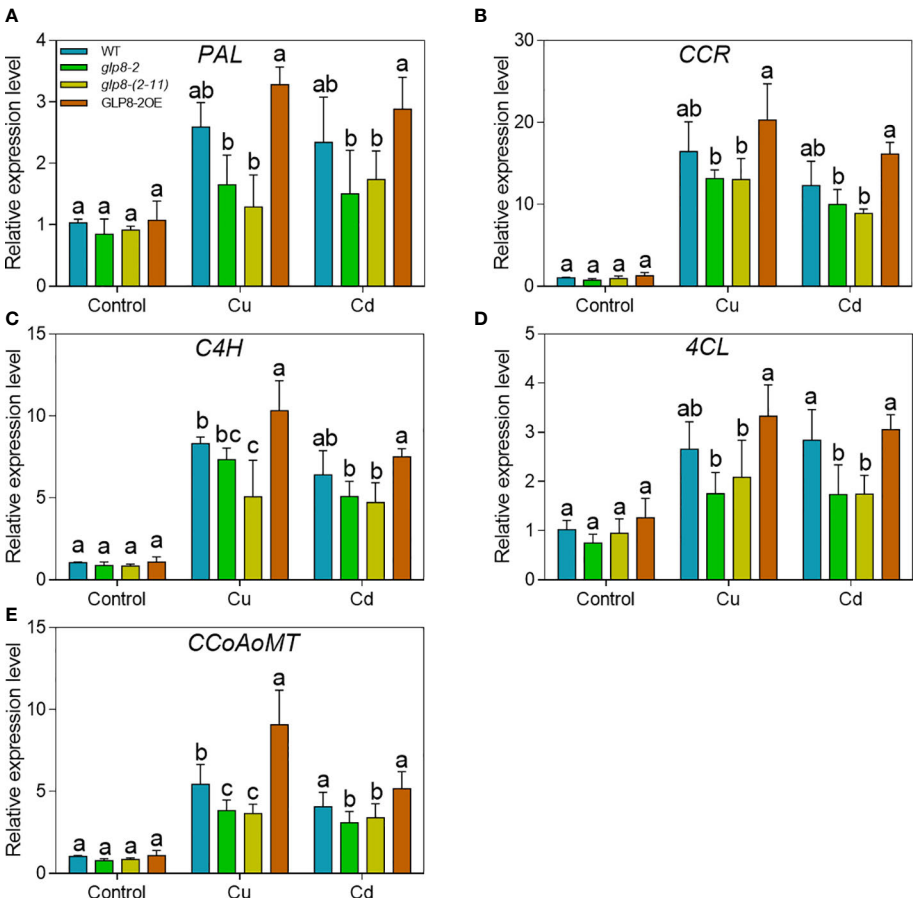

FIGURE 6
OsGLPs upregulate the expression of lignin synthesis-related genes using RT-qPCR. The expression of *PAL* **(A)**, *CCR* **(B)**, *C4H* **(C)**, *4CL* **(D)**, and *CCoAoMT* **(E)** in 2-week-old WT (wild type) and transgenic seedlings grown for 5 days under normal conditions, 10 μmol L^{-1} $CuSO_4$ treatment, or 25 μmol L^{-1} $CdCl_2$ treatment. *ACTIN1* (LOC_Os03g50885) was used as the internal control. The relative expression level was obtained by normalisation to the expression level in WT plants without heavy metal treatment. Values are the mean ± SD; n = 3. Different letters indicate a difference of $p \leq 0.05$ by the LSD test.

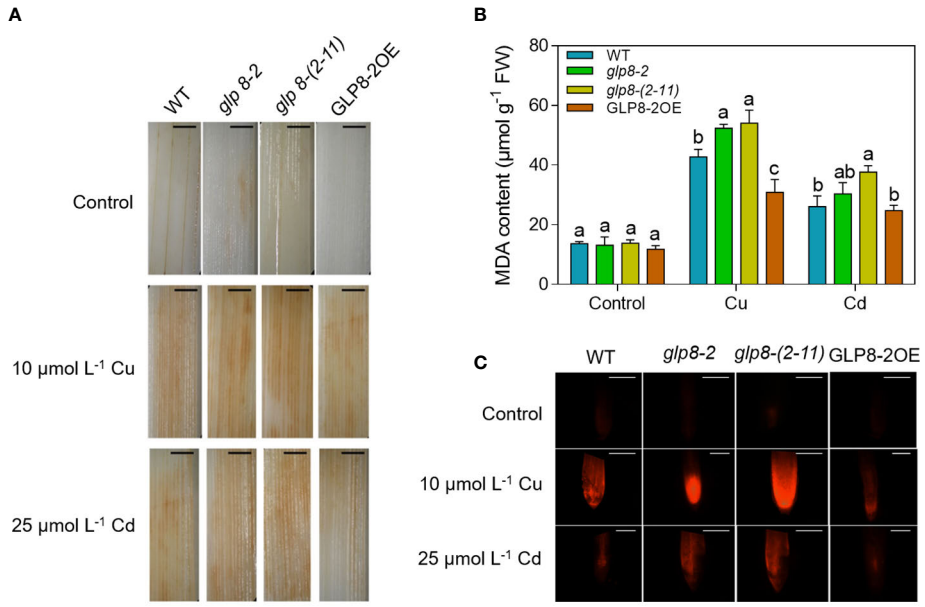

FIGURE 7
OsGLPs protect against heavy metal-induced oxidative stress. **(A)** Histochemical localisation of H_2O_2 in leaves of two-week-old WT (wild type) and transgenic seedlings grown for 5 days under normal conditions, 10 μmol L^{-1} $CuSO_4$ treatment, or 25 μmol L^{-1} $CdCl_2$ treatment. The shade of brown represents the amount of H_2O_2. Scale bar = 2 mm. **(B)** MDA content of leaves of two-week-old WT and transgenic seedlings grown for 5 days under normal conditions, 10 μmol L^{-1} $CuSO_4$ treatment, or 25 μmol L^{-1} $CdCl_2$ treatment. Values are the mean ± SD; n = 3. Different letters indicate a difference of $p \leq 0.05$ by the LSD test. **(C)** The integrity of the cell plasma membrane of rice roots of two-week-old WT and transgenic seedlings grown for 5 days under normal conditions, 10 μmol L^{-1} $CuSO_4$ treatment, or 25 μmol L^{-1} $CdCl_2$ treatment. Red represents the damage to the plasma membrane. The darker the red, the worse the integrity of the plasma membrane. Scale bar = 200 μm.

ROS balance, cells initiate a series of antioxidant enzymes to ensure oxidative homeostasis (Ding et al., 2020). Malondialdehyde (MDA) content indicates the degree of peroxidation of the cell membrane and is an important indicator of plant stress resistance (Yang et al., 2019). Propidium iodide (PI) is a nuclear fluorescent dye that indicates the integrity of the plasma membrane (Li et al., 2021). When the root tip cells are damaged, the permeability of the plasma membrane increases, PI can enter the cell and bind to DNA, and red fluorescence can be observed with a fluorescence microscope. In this study, H_2O_2 content, MDA content, and integrity of the plasma membrane in several materials indicate overexpressed GLP8-2 can alleviate the oxidative damage to rice caused by Cu and Cd (Figure 7). In addition, *StGLP* overexpression significantly increased the activity of related antioxidant enzymes in potato under heat stress (*Solanum tuberosum* L.) (Gangadhar et al., 2021). These findings imply that overexpression of *GLP* makes antioxidant related physiological activities more active in rice under Cu and Cd stress. Existing studies have shown that oxidation systems in the cell wall, such as peroxidase/H_2O_2 and laccase/$O_2^{\cdot-}$, are not only important components of the antioxidant protection system but also activate the polymerisation of monolignols to generate lignin polymers (Tobimatsu and Schuetz, 2019). When *OsGLP8-2* was overexpressed, the cell-wall-localised oxidation

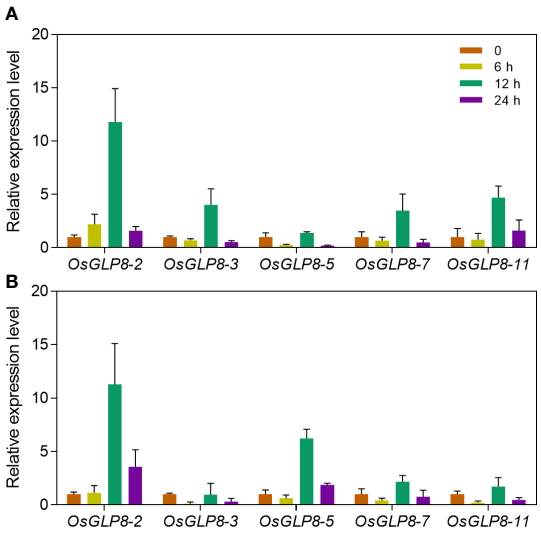

FIGURE 8
Expression levels of *OsGLPs* induced by heavy metal stress. The expression of *OsGLP8-2*, *OsGLP8-3*, *OsGLP8-5*, *OsGLP8-7*, and *OsGLP8-11* in two-week-old wild-type seedlings treated with 10 μmol L^{-1} $CuSO_4$ **(A)** or 25 μmol L^{-1} $CdCl_2$ **(B)** for 0, 6, 12, and 24 hours. Values are the mean ± SD; n = 3. Different letters indicate a difference of $p \leq 0.05$ by the LSD test.

system became active, thus enhancing lignin polymerisation. Further studies are needed to confirm the link between heavy metal-induced H_2O_2 production and lignin synthesis by H_2O_2 scavengers.

In addition, the *glp8-2* and *glp8-(2-11)* mutants did not show significant differences. qRT-PCR of 5 randomly selected genes on chromosome 8 showed that *OsGLP8-2* was more easily induced by Cu and Cd, and its upregulation was much greater than other tandem genes (Figure 8). This may explain why there was no obvious difference between the *glp8-2* and *glp8-(2-11)* mutants under heavy metal stress conditions.

Conclusion

Our findings suggest that OsGLPs play a critical role in heavy metal resistance for rice *via* lignin deposition in the cell wall and antioxidant defence capacity. OsGLP8-2 may play a main role in tandem repeat gene clusters on chromosome 8 in rice under heavy metal stress. Further studies on the physiological role of other OsGLP members, except for OsGLP8-2, in this tandem repeat gene cluster should be investigated to explain the diversity of GLP functions.

Data availability statement

The data presented in the study are deposited in the NCBI SRA repository, accession number PRJNA910469.

Author contributions

XS: Investigation, writing-original draft. YQ and AW: Investigation and methodology. YW and YR: Investigation. TX: Methodology. ZS: Funding acquisition. QW and YX: Supervision, project administration, writing - review & editing. All authors contributed to the article and approved the submitted version.

Funding

This work was financially supported by the Key Research and Development Program of Jiangsu (BE2021717), the National Natural Science Foundation of China (31672224).

Conflict of interest

Author AW was employed by the company CNTC.

The remaining authors declare that the research was conducted in the absence of any commercial or financial relationships that could be construed as a potential conflict of interest.

Publisher's note

All claims expressed in this article are solely those of the authors and do not necessarily represent those of their affiliated organizations, or those of the publisher, the editors and the reviewers. Any product that may be evaluated in this article, or claim that may be made by its manufacturer, is not guaranteed or endorsed by the publisher.

Supplementary material

The Supplementary Material for this article can be found online at: https://www.frontiersin.org/articles/10.3389/fpls.2022.1078113/full#supplementary-material

References

Banerjee, J., Gantait, S., and Maiti, M. K. (2017). Physiological role of rice germin-like protein 1 (OsGLP1) at early stages of growth and development in *indica* rice cultivar under salt stress condition. *Plant Cell Tiss. Org.* 131, 127–137. doi: 10.1073/pnas.1400975111

Banerjee, J., and Maiti, M. K. (2010). Functional role of rice germin-like protein1 in regulation of plant height and disease resistance. *Biochem. Biophy. Res. Commun.* 394, 178–183. doi: 10.1016/j.bbrc.2010.02.142

Barman, A. R., and Banerjee, J. (2015). Versatility of germin-like proteins in their sequences, expressions, and functions. *Funct. Integ R. Genomics* 15, 533–548. doi: 10.1007/s10142-015-0454-z

Bernier, F., and Berna, A. (2001). Germins and germin-like proteins: Plant do-all proteins. but what do they do exactly? *Plant Physiol. Biochem.* 39, 545–554. doi: 10.1016/S0981-9428(01)01285-2

Bhuiyan, N. H., Liu, W., Liu, G., Selvaraj, G., Wei, Y., and King, J. (2007). Transcriptional regulation of genes involved in the pathways of biosynthesis and supply of methyl units in response to powdery mildew attack and abiotic stresses in wheat. *Plant Mol. Bio.* 64, 305–318. doi: 10.1007/s11103-007-9155-x

Bruno, L., Spadafora, N. D., Iaria, D., Chiappetta, A., and Bitonti, M. B. (2014). Developmental stimuli and stress factors affect expression of *ClGLP1*, an emerging allergen-related gene in *Citrus limon*. *Plant Physio. Biochem.* 79, 31–40. doi: 10.1016/j.plaphy.2014.03.003

Chen, D., Chen, D., Xue, R., Long, J., Lin, X., Lin, Y., et al. (2019a). Effects of boron, silicon and their interactions on cadmium accumulation and toxicity in rice plants. *J. Hazard. Mater.* 367, 447–455. doi: 10.1016/j.jhazmat.2018.12.111

Cheng, X., Huang, X., Liu, S., Tang, M., Hu, W., and Pan, S. (2014). Characterization of germin-like protein with polyphenol oxidase activity from *Satsuma mandarine*. *Biochem. Biophys. Res. Commun.* 449, 313–318. doi: 10.1016/j.bbrc.2014.05.027

Chen, C., Song, Y. F., Zhuang, K., Li, L., Xia, Y., and Shen, Z. G. (2015). Proteomic analysis of copper-binding proteins in excess copper-stressed roots of

two rice (*Oryza sativa* l.) varieties with different Cu tolerances. *PloS One* 10, 0125367. doi: 10.1371/journal.pone.0125367

Chen, K., Wang, Y., Zhang, R., Zhang, H., and Gao, C. (2019b). CRISPR/Cas genome editing and precision plant breeding in agriculture. *Annu. Rev. Plant Biol.* 70, 667–697. doi: 10.1146/annurev-arplant-050718-100049

Chrysargyris, A., Papakyriakou, E., Petropoulos, S. A., and Tzortzakis, N. (2019). The combined and single effect of salinity and copper stress on growth and quality of *Mentha spicata* plants. *J. Hazard. Mater.* 368, 584–593. doi: 10.1016/j.jhazmat.2019.01.058

Court, D. L., Sawitzke, J. A., and Thomason, L. C. (2002). Genetic engineering using homologous recombination. *Annu. Rev. Genet.* 36, 361–388. doi: 10.1146/annurev.genet.36.061102.093104

Ding, H., Wang, B., Han, Y., and Li, S. (2020). The pivotal function of dehydroascorbate reductase in glutathione homeostasis in plants. *J. Exp. Bot.* 71, 3405–3416. doi: 10.1093/jxb/eraa107

Do, C. T., Pollet, B., Thévenin, J., Sibout, R., Denoue, D., Barrière, Y., et al. (2007). Both caffeoyl coenzyme a 3-*O*-methyltransferase 1 and caffeic acid *O*-methyltransferase 1 are involved in redundant functions for lignin, flavonoids and sinapoyl malate biosynthesis in arabidopsis. *Planta* 226, 1117–1129. doi: 10.1007/s00425-007-0558-3

Douchiche, O., Soret-Morvan, O., Chaïbi, W., Morvan, C., and Paynel, F. (2010). Characteristics of cadmium tolerance in 'Hermes' flax seedlings: Contribution of cell walls. *Chemosphere* 81, 1430–1436. doi: 10.1016/j.chemosphere.2010.09.011

Dunwell, J. M., Gibbings, J. G., Mahmood, T., and Naqvi, S. M. S. (2008). Germin and germin-like proteins: Evolution, structure, and function. *Crit. Rev. Plant Sci.* 27, 342–375. doi: 10.1080/07352680802333938

Fernández-Fuego, D., Bertrand, A., and González, A. (2017). Metal accumulation and detoxification mechanisms in mycorrhizal *Betula pubescens*. *Environ. pollut.* 231, 1153–1162. doi: 10.1016/j.envpol.2017.07.072

Gangadhar, B. H., Mishra, R. K., Kappachery, S., Baskar, V., Venkatesh, J., Nookaraju, A., et al. (2021). Enhanced thermo-tolerance in transgenic potato (*Solanum tuberosum* l.) overexpressing hydrogen peroxide-producing germin-like protein (GLP). *Genomics* 113, 3224–3234. doi: 10.1016/j.ygeno.2021.07.013

Gao, M. Y., Chen, X. W., Huang, W. X., Wu, L., Yu, Z. S., Xiang, L., et al. (2021). Cell wall modification induced by an arbuscular mycorrhizal fungus enhanced cadmium fixation in rice root. *J. Hazard. Mater.* 416, 125894. doi: 10.1016/j.jhazmat.2021.125894

Gaonkar, R., Shiralgi, Y., Lakkappa, D. B., and Hegde, G. (2018). Essential oil from *Cymbopogon flexuosus* as the potential inhibitor for HSP90. *Toxicol. Rep.* 5, 489–496. doi: 10.1016/j.toxrep.2018.03.014

Gao, L., Peng, K., Chen, Y., Wang, G., and Shen, Z. (2012). Roles of apoplastic peroxidases, laccases, and lignification in the manganese tolerance of hyperaccumulator *Phytolacca americana*. *Acta Physiol. Plant* 34, 151–159. doi: 10.1007/s11738-011-0813-x

Graham, R. C., and Karnovsky, M. J. (1966). The early stages of absorption of injected horseradish peroxidase in the proximal tubules of mouse kidney: Ultrastructural cytochemistry by a new technique. j. histochem. *Cytochem.* 14, 291–302. doi: 10.1177/14.4.291

Han, M. H., Yang, N., Wan, Q. W., Teng, R., Duan, A. Q., Wang, Y. H., et al. (2021). Exogenous melatonin positively regulates lignin biosynthesis in *Camellia sinensis*. *Int. J. Biol. Macromol.* 179, 485–499. doi: 10.1016/j.ijbiomac.2021.03.025

He, Z. D., Tao, M. L., Leung, D. W. M., Yan, X. Y., Chen, L., Peng, X. X., et al. (2021). The rice germin-like protein OsGLP1 participates in acclimation to UV-b radiation. *Plant Physiol.* 186, 1254–1268. doi: 10.1093/plphys/kiab125

Hurkman, W. J., Tao, H. P., and Tanaka, C. K. (1991). Germin-like polypeptides increase in barley roots during salt stress. *Plant Physiol.* 97, 366–374. doi: 10.1104/pp.97.1.366

Ilyas, M., Irfan, M., Mahmood, T., Hussain, H., Latif ur, R., Naeem, I., et al. (2020). Analysis of germin-like protein genes (OsGLPs) family in rice using various in silico approaches. *Curr. Bioinform.* 15, 17–33. doi: 10.2174/1574893614666190722165130

Ilyas, M., Rasheed, A., and Mahmood, T. (2016). Functional characterization of germin and germin-like protein genes in various plant species using transgenic approaches. *Biotechnol. Lett.* 38, 1405–1421. doi: 10.1007/s10529-016-2129-9

Jang, J. H., and Lee, O. R. (2020). Overexpression of ginseng patatin-related phospholipase *pPLAIIIβ* alters the polarity of cell growth and decreases lignin content in *Arabidopsis*. *J. Ginseng Res.* 44, 321–331. doi: 10.1016/j.jgr.2019.01.004

Jia, H. L., Wang, X. H., Wei, T., Wang, M., Liu, X., Hua, L., et al. (2021). Exogenous salicylic acid regulates cell wall polysaccharides synthesis and pectin methylation to reduce cd accumulation of tomato. *Ecotox. Environ. Safe.* 207, 111550. doi: 10.1016/j.ecoenv.2020.111550

Karkonen, A., Koutaniemi, S., Mustonen, M., Syrjanen, K., Brunow, G., Kilpelainen, I., et al. (2002). Lignification related enzymes in *Picea abies* suspension cultures. *Physiol. Plantarum* 114, 343–353. doi: 10.1034/j.1399-3054.2002.1140303.x

Ke, Y., Han, G., He, H., and Li, J. (2009). Differential regulation of proteins and phosphoproteins in rice under drought stress. *Biochem. Biophys. Res. Commun.* 379, 133–138. doi: 10.1016/j.bbrc.2008.12.067

Krzeslowska, M. (2011). The cell wall in plant cell response to trace metals: Polysaccharide remodeling and its role in defense strategy. *Acta Physiol. Plant* 33, 35–51. doi: 10.1007/s11738-010-0581-z

Liao, L. T., Hu, Z. Y., Liu, S. Q., Yang, Y. G., and Zhou, Y. (2021). Characterization of germin-like proteins (GLPs) and their expression in response to abiotic and biotic stresses in cucumber. *Hortic.* 7, 412. doi: 10.3390/horticulturae7100412

Liu, Q., Luo, L., and Zheng, L. (2018). Lignins: biosynthesis and biological functions in plants. *Int. J. Mol. Sci.* 19, 335. doi: 10.3390/ijms19020335

Liu, Y., Lv, H., Yang, N., Li, Y., Liu, B., Rensing, C., et al. (2019). Roles of root cell wall components and root plaques in regulating elemental uptake in rice subjected to selenite and different speciation of antimony. *Environ. Exp. Bot.* 163, 36–44. doi: 10.1016/j.envexpbot.2019.04.005

Liu, Q. Q., Zheng, L., He, F., Zhao, F. J., Shen, Z. G., and Zheng, L. Q. (2015). Transcriptional and physiological analyses identify a regulatory role for hydrogen peroxide in the lignin biosynthesis of copper-stressed rice roots. *Plant Soil* 387, 323–336. doi: 10.1007/s11104-014-2290-7

Li, L., Xu, X., Chen, C., and Shen, Z. (2016). Genome-wide characterization and expression analysis of the germin-like protein family in rice and arabidopsis. *Int. J. Mol. Sci.* 17, 1622. doi: 10.3390/ijms17101622

Li, Q., Zhao, Y., Zhu, X. M., and Xie, Y. L. (2021). Antifungal efficacy of paeonol on *Aspergillus flavus* and its mode of action on cell walls and cell membranes. *LWT-Food Sci. Technol.* 149, 111985. doi: 10.1016/j.lwt.2021.111985

Lou, Y., and Baldwin, I. T. (2006). Silencing of a germin-like gene in *Nicotiana attenuata* improves performance of native herbivores. *Plant Physiol.* 140, 1126–1136. doi: 10.1104/PP.105.073700

Majeed, N., Javaid, B., Deeba, F., Naqvi, S. M. S., and Douches, D. S. (2018). Enhanced *fusarium oxysporum* f. sp. *tuberosi* resistance in transgenic potato expressing a rice GLP superoxide dismutase gene. *Am. J. Potato Res.* 95, 383–394. doi: 10.1007/s12230-018-9639-z

Mao, C., Yi, K., Yang, L., Zheng, B., Wu, Y., Liu, F., et al. (2004). Identification of aluminium-regulated genes by cDNA-AFLP in rice (*Oryza sativa* l.): Aluminium-regulated genes for the metabolism of cell wall components. *J. Exp. Bot.* 55, 137–143. doi: 10.1093/jxb/erh030

Ma, Y., Rajkumar, M., Zhang, C., and Freitas, H. (2016a). Inoculation of *Brassica oxyrrhina* with plant growth promoting bacteria for the improvement of heavy metal phytoremediation under drought conditions. *J. Hazard. Mater.* 320, 36–44. doi: 10.1016/j.jhazmat.2016.08.009

Ma, X., Zhu, Q., Chen, Y., and Liu, Y. G. (2016b). CRISPR/Cas9 platforms for genome editing in plants: Developments and applications. *Mol. Plant* 9, 961–974. doi: 10.1016/j.molp.2016.04.009

Mir Derikvand, M., Sierra, J. B., Ruel, K., Pollet, B., Do, C. T., Thévenin, J., et al. (2008). Redirection of the phenylpropanoid pathway to feruloyl malate in *Arabidopsis* mutants deficient for cinnamoyl-CoA reductase 1. *Planta* 227, 943–956. doi: 10.1007/s00425-007-0669-x

Moura, J. C. M. S., Bonine, C. A. V., de Oliveira Fernandes Viana, J., Dornelas, M. C., and Mazzafera, P. (2010). Abiotic and biotic stresses and changes in the lignin content and composition in plants. *J. Integr. Plant Biol.* 52, 360–376. doi: 10.1111/j.1744-7909.2010.00892.x

Napoli, M., Cecchi, S., Grassi, C., Baldi, A., Zanchi, C. A., and Orlandini, S. (2019). Phytoextraction of copper from a contaminated soil using arable and vegetable crops. *Chemosphere* 219, 122–129. doi: 10.1016/j.chemosphere.2018.12.017

Nazir, F., Hussain, A., and Fariduddin, Q. (2019). Hydrogen peroxide modulate photosynthesis and antioxidant systems in tomato (*Solanum lycopersicum* l.) plants under copper stress. *Chemosphere* 230, 544–558. doi: 10.1016/j.chemosphere.2019.05.001

Pan, J., Guan, M., Xu, P., Chen, M., and Cao, Z. (2021). Salicylic acid reduces cadmium (Cd) accumulation in rice (*Oryza sativa* l.) by regulating root cell wall composition *via* nitric oxide signaling. *Sci. Total Environ.* 797, 149202. doi: 10.1016/j.scitotenv.2021.149202

Park, J. H., and Chon, H. T. (2016). Characterization of cadmium biosorption by *Exiguobacterium* sp isolated from farmland soil near Cu-Pb-Zn mine. *Environ. Sci. pollut. Res.* 23, 11814–11822. doi: 10.1007/s11356-016-6335-8

Pei, Y. K., Li, X. C., Zhu, Y. T., Ge, X. Y., Sun, Y., Liu, N. N., et al. (2019). GhABP19, a novel germin-like protein from *Gossypium hirsutum*, plays an important role in the regulation of resistance to verticillium and fusarium wilt pathogens. *Front. Plant Sci.* 10. doi: 10.3389/fpls.2019.00583

Perkins, M. L., Schuetz, M., Unda, F., Chen, K. T., Bally, M. B., Kulkarni, J. A., et al. (2022). Monolignol export by diffusion down a polymerization-induced concentration gradient. *Plant Cell* 34, 2080–2095. doi: 10.1093/plcell/koac051

Poudel, A., Navathe, S., Chand, R., Mishra, V. K., Singh, P. K., and Joshi, A. K. (2019). Hydrogen peroxide prompted lignification affects pathogenicity of hemibiotrophic pathogen *Bipolaris sorokiniana* to wheat. *Plant Pathol. J.* 35, 287–300. doi: 10.5423/PPJ.OA.09.2018.0180

Rather, B. A., Masood, A., Sehar, Z., Majid, A., Anjum, N. A., and Khan, N. A. (2020). Mechanisms and role of nitric oxide in phytotoxicity-mitigation of copper. *Front. Plant Sci.* 11. doi: 10.3389/fpls.2020.00675

Roig-Oliver, M., Bresta, P., Nadal, M., Liakopoulos, G., Nikolopoulos, D., Karabourniotis, G., et al. (2020). Cell wall composition and thickness affect mesophyll conductance to CO_2 diffusion in *Helianthus annuus* under water deprivation. *J. Exp. Bot.* 71, 7198–7209. doi: 10.1093/jxb/eraa413

Slabaugh, E., Davis, J. K., Haigler, C. H., Yingling, Y. G., and Zimmer, J. (2014). Cellulose synthases: New insights from crystallography and modeling. *Trends. Plant Sci.* 19, 99–106. doi: 10.1016/j.tplants.2013.09.009

Smirnoff, N., and Arnaud, D. (2019). Hydrogen peroxide metabolism and functions in plants. *N. Phytol.* 221, 1197–1214. doi: 10.1111/nph.15488

Song, Y. F., Cui, J., Zhang, H. X., Wang, G. P., Zhao, F. J., and Shen, Z. G. (2013). Proteomic analysis of copper stress responses in the roots of two rice (*Oryza sativa l.*) varieties differing in Cu tolerance. *Plant Soil* 366, 647–658. doi: 10.1007/s11104-012-1458-2

Su, N. N., Ling, F., Xing, A. M., Zhao, H. H., Zhu, Y. W., Wang, Y., et al. (2020). Lignin synthesis mediated by CCoAOMT enzymes is required for the tolerance against excess Cu in *Oryza sativa*. *Environ. Exp Bot.* 175, 104059. doi: 10.1016/j.envexpbot.2020.104059

Sun, J., Cui, J., Luo, C., Gao, L., Chen, Y., and Shen, Z. (2013). Contribution of cell walls, nonprotein thiols, and organic acids to cadmium resistance in two cabbage varieties. *Arch. Environ. Contam. Toxicol.* 64, 243–252. doi: 10.1007/s00244-012-9824-x

Takeuchi, K., Hasegawa, H., Gyohda, A., Komatsu, S., Okamoto, T., Okada, K., et al. (2016). Overexpression of *RSOsPR10*, a root-specific rice PR10 gene, confers tolerance against drought stress in rice and drought and salt stresses in bentgrass. *Plant Cell Tiss. Org.* 127, 35–46. doi: 10.1007/s11240-016-1027-0

Tobimatsu, Y., and Schuetz, M. (2019). Lignin polymerization: How do plants manage the chemistry so well? *Curr. Opin. Biotechnol.* 56, 75–81. doi: 10.1016/j.copbio.2018.10.001

Van Acker, R., Vanholme, R., Storme, V., Mortimer, J. C., Dupree, P., and Boerjan, W. (2013). Lignin biosynthesis perturbations affect secondary cell wall composition and saccharification yield in *Arabidopsis thaliana*. *Biotechnol. Biofuels* 6, 46. doi: 10.1186/1754-6834-6-46

van de Mortel, J. E., Almar Villanueva, L., Schat, H., Kwekkeboom, J., Coughlan, S., Moerland, P. D., et al. (2006). Large Expression differences in genes for iron and zinc homeostasis, stress response, and lignin biosynthesis distinguish roots of *Arabidopsis thaliana* and the related metal hyperaccumulator *Thlaspi caerulescens*. *Plant Physiol.* 142, 1127–1147. doi: 10.1104/pp.106.082073

Wang, X. S., Fu, H. I., Gong, F. Y., Zhang, Y., He, C. Y., and Yang, Z. Y. (2020). Lignin side chain region participates in cd detoxification related to the cultivar-dependent cd accumulation in *Brassica chinensis* l. *J. Hazard. Mater.* 392, 122264. doi: 10.1016/j.jhazmat.2020.122264

Wang, Y., Gui, C., Wu, J., Gao, X., Huang, T., Cui, F., et al. (2022). Spatio-temporal modification of lignin biosynthesis in plants: A promising strategy for lignocellulose improvement and lignin valorization. *Fron. Bioeng. Biotechnol.* 10. doi: 10.3389/fbioe.2022.917459

Wang, G. L., Huang, Y., Zhang, X. Y., Xu, Z. S., Wang, F., and Xiong, A. S. (2016). Transcriptome-based identification of genes revealed differential expression profiles and lignin accumulation during root development in cultivated and wild carrots. *Plant Cell Rep.* 35, 1743–1755. doi: 10.1007/s00299-016-1992-0

Wang, M., Hu, C., Xu, J., Jing, X., Rahim, H. U., and Cai, X. (2021). Facile combinations of thiosulfate and zerovalent iron synergically immobilize cadmium in soils through mild extraction and facilitated immobilization. *J. Hazard. Mater.* 407, 124806. doi: 10.1016/j.jhazmat.2020.124806

Wei, W., Peng, H., Xie, Y., Wang, X., Huang, R., Chen, H., et al. (2021). The role of silicon in cadmium alleviation by rice root cell wall retention and vacuole compartmentalization under different durations of cd exposure. *Ecotox. Environ. Safe.* 226, 112810. doi: 10.1016/j.ecoenv.2021.112810

Xia, Y., Liu, J., Wang, Y., Zhang, X. X., Shen, Z. G., and Hu, Z. B. (2018). Ectopic expression of *Vicia sativa* caffeoyl-CoA *O*-methyltransferase (*VsCCoAOMT*) increases the uptake and tolerance of cadmium in arabidopsis. *Environ. Exp. Bot.* 145, 47–53. doi: 10.1016/j.envexpbot.2017.10.019

Xiong, J., Yang, Y., Fu, G., and Tao, L. (2015). Novel roles of hydrogen peroxide (H_2O_2) in regulating pectin synthesis and demethylesterification in the cell wall of rice (*Oryza sativa*) root tips. *New Phytol.* 206, 118–126. doi: 10.1111/nph.13285

Yang, J., Lin, L. N., Zhang, X. B., Wu, Y., Bi, B., Zhang, G. C., et al. (2019). Sodium pheophorbide a has photoactivated fungicidal activity against *Pestalotiopsis neglecta*. *Pest. Biochem. Physiol.* 158, 25–31. doi: 10.1016/j.pestbp.2019.04.003

Yang, J. L., Zhu, X. F., Peng, Y. X., Zheng, C., Li, G. X., Liu, Y., et al. (2011). Cell wall hemicellulose contributes significantly to aluminum adsorption and root growth in. *Arabidopsis. Plant Physiol.* 155, 1885–1892. doi: 10.1104/pp.111.172221

Yan, L., Li, S., Cheng, J., Zhang, Y., and Jiang, C. (2022). Boron-mediated lignin metabolism in response to aluminum toxicity in citrus (*Poncirus trifoliata* (L.) raf.) root. *Plant Physiol. Bioch.* 185, 1–12. doi: 10.1016/j.plaphy.2022.05.018

Yuan, B., Yang, Y., Fan, P., Liu, J., Xing, H., Liu, Y., et al. (2021). Genome-wide identification and characterization of germin and germin-like proteins (GLPs) and their response under powdery mildew stress in wheat (*Triticum aestivum* l.). *Plant Mol. Biol. Rep.* 39, 821–832. doi: 10.1007/s11105-021-01291-w

Yue, Z., Chen, Y., Chen, C., Ma, K., Tian, E., Wang, Y., et al. (2021). Endophytic *Bacillus altitudinis* WR10 alleviates Cu toxicity in wheat by augmenting reactive oxygen species scavenging and phenylpropanoid biosynthesis. *J. Hazard. Mater.* 405, 124272. doi: 10.1016/j.jhazmat.2020.124272

Zare, A. A., Khoshgoftarmanesh, A. H., Malakouti, M. J., Bahrami, H. A., and Chaney, R. L. (2018). Root uptake and shoot accumulation of cadmium by lettuce at various Cd:Zn ratios in nutrient solution. *Ecotox. Environ. Safe.* 148, 441–446. doi: 10.1016/j.ecoenv.2017.10.045

Zaynab, M., Peng, J., Sharif, Y., Fatima, M., Albaqami, M., Al-Yahyai, R., et al. (2022). Genome-wide identification and expression profiling of germin-like proteins reveal their role in regulating abiotic stress response in potato. *Front. Plant Sci.* 12. doi: 10.3389/fpls.2021.831140

Zhang, Q., Cai, W., Ji, T. T., Ye, L., Lu, Y. T., and Yuan, T. T. (2020). WRKY13 enhances cadmium tolerance by promoting *D-CYSTEINE DESULFHYDRASE* and hydrogen sulfide production1. *Plant Physiol.* 183, 345–357. doi: 10.1104/pp.19.01504

Zhang, N., Guan, R., Yang, Y., Bai, Z., Ge, F., and Liu, D. (2017). Isolation and characterization of a *Fusarium oxysporum*-resistant gene *LrGLP1* from *Lilium regale* Wilson. *In Vitro Cell. Dev. Biol. Plant* 53, 461–468. doi: 10.1007/s11627-017-9829-2

Zhang, J., Liu, Y., Li, C., Yin, B., Liu, X., Guo, X., et al. (2022). PtomtAPX is an autonomous lignification peroxidase during the earliest stage of secondary wall formation in *Populus tomentosa* Carr. *Nat. Plants* 8, 828–839. doi: 10.1038/s41477-022-01181-3

Zhang, Y., Wang, X., Chang, X., Sun, M., Zhang, Y., Li, W., et al. (2018). Overexpression of germin-like protein GmGLP10 enhances resistance to *Sclerotinia sclerotiorum* in transgenic tobacco. *Biochem. Biophys. Res. Commun.* 497, 160–166. doi: 10.1016/j.bbrc.2018.02.046

Zhang, Q., Wang, L., Wang, Z., Zhang, R., Liu, P., Liu, M., et al. (2021). The regulation of cell wall lignification and lignin biosynthesis during pigmentation of winter jujube. *Hortic. Res.* 8, 238. doi: 10.1038/s41438-021-00670-4

Zhao, D., Luan, Y., Xia, X., Shi, W., Tang, Y., and Tao, J. (2020). Lignin provides mechanical support to herbaceous peony (*Paeonia lactiflora* pall.) stems. *Hortic. Res.* 7, 213. doi: 10.1038/s41438-020-00451-5

Zhao, Y. Y., Man, Y., Wen, J. L., Guo, Y. Y., and Lin, J. X. (2019). Advances in imaging plant cell walls. *Trends Plant Sci.* 24, 867–878. doi: 10.1016/j.tplants.2019.05.009

Zhou, S., Sauvé, R., and Thannhauser, T. W. (2009). Proteome changes induced by aluminium stress in tomato roots. *J. Exp. Bot.* 60, 1849–1857. doi: 10.1093/jxb/erp065

Zhu, X. F., Lei, G. J., Jiang, T., Liu, Y., Li, G. X., and Zheng, S. J. (2012). Cell wall polysaccharides are involved in p-deficiency-induced cd exclusion in *Arabidopsis thaliana*. *Planta* 236, 989–997. doi: 10.1007/s00425-012-1652-8

Zhu, X. F., Wu, Q., Meng, Y. T., Tao, Y., and Shen, R. F. (2020). AtHAP5A regulates iron translocation in iron-deficient *Arabidopsis thaliana*. *J. Integr. Plant Biol.* 62, 1910–1925. doi: 10.1111/jipb.12984

frontiers | Frontiers in Plant Science

TYPE Original Research
PUBLISHED 16 January 2023
DOI 10.3389/fpls.2022.1096685

Check for updates

OPEN ACCESS

EDITED BY
Diaa Abd El Moneim,
Arish University, Egypt

REVIEWED BY
Amal Harb,
Yarmouk University, Jordan
Damián Balfagón,
University of Jaume I, Spain

*CORRESPONDENCE
Krzysztof Mikołajczak
kmik@igr.poznan.pl

SPECIALTY SECTION
This article was submitted to Plant Abiotic Stress, a section of the journal Frontiers in Plant Science

RECEIVED 12 November 2022
ACCEPTED 14 December 2022
PUBLISHED 16 January 2023

CITATION
Mikołajczak K, Kuczyńska A, Krajewski P, Kempa M and Nuc M (2023) Transcriptome profiling disclosed the effect of single and combined drought and heat stress on reprogramming of genes expression in barley flag leaf.
Front. Plant Sci. 13:1096685.
doi: 10.3389/fpls.2022.1096685

COPYRIGHT
© 2023 Mikołajczak, Kuczyńska, Krajewski, Kempa and Nuc. This is an open-access article distributed under the terms of the Creative Commons Attribution License (CC BY). The use, distribution or reproduction in other forums is permitted, provided the original author(s) and the copyright owner(s) are credited and that the original publication in this journal is cited, in accordance with accepted academic practice. No use, distribution or reproduction is permitted which does not comply with these terms.

Transcriptome profiling disclosed the effect of single and combined drought and heat stress on reprogramming of genes expression in barley flag leaf

Krzysztof Mikołajczak*, Anetta Kuczyńska, Paweł Krajewski, Michał Kempa and Maria Nuc

Institute of Plant Genetics, Polish Academy of Sciences, Poznań, Poland

Despite numerous studies aimed at unraveling the genetic background of barley's response to abiotic stress, the modulation of the transcriptome induced by combinatorial drought and increased temperature remains largely unrecognized. Very limited studies were done, especially on the flag leaf, which plays an important role in grain filling in cereals. In the present study, transcriptome profiles, along with chlorophyll fluorescence parameters and yield components, were compared between barley genotypes with different flag leaf sizes under single and combined drought and heat stress. High-throughput mRNA sequencing revealed 2,457 differentially expressed genes, which were functionally interpreted using Gene Ontology term enrichment analysis. The transcriptomic signature under double stress was more similar to effects caused by drought than by elevated temperature; it was also manifested at phenotypic and chlorophyll fluorescence levels. Both common and stress-specific changes in transcript abundance were identified. Genes regulated commonly across stress treatments, determining universal stress responses, were associated, among others, with responses to drought, heat, and oxidative stress. In addition, changes specific to the size of the flag leaf blade were found. Our study allowed us to identify sets of genes assigned to various processes underlying the response to drought and heat, including photosynthesis, the abscisic acid pathway, and lipid transport. Genes encoding LEA proteins, including dehydrins and heat shock proteins, were especially induced by stress treatments. Some association between genetic composition and flag leaf size was confirmed. However, there was no general coincidence between SNP polymorphism of genotypes and differential expression of genes induced by stress factors. This research provided novel insight into the molecular mechanisms of barley flag leaf that determine drought and heat response, as well as their co-occurrence.

KEYWORDS

abiotic stress, combinatorial stresses, flag leaf, functional annotation, *Hordeum vulgare* L., mRNA sequencing, transcriptomics

Introduction

Today, it is known that understanding the transcriptome is important for interpreting the functional elements of the genome. Sustainable improvement of genetic and molecular techniques has facilitated a better exploration of plant genomes, including barley (Harb et al., 2020; Henry, 2020). Next generation sequencing (NGS), providing high-throughput analyses at the genome-wide level in a cost-effective manner, allowed us to unlock the barley genome (cv. Morex) in 2012, for the first time (IBGSC, 2012). In the following years, updated versions of the reference barley genome were published by Mascher et al. (2017) using chromosome conformation capture mapping and by Monat et al. (2019), who employed short-read sequencing data from multiple library types (TRITEX). Very recently, the newest version of barley genome assembly (MorexV3) was released using PacBio long-read sequencing (Mascher et al., 2021). Also, the first barley pan-genome concept was reported by Jayakodi et al. (2020), whereas Rapazote-Flores et al. (2019) released the barley gene reference transcript dataset (BaRTv1.0). Altogether, powerful resources for extensive research into the barley genome and its functioning under changing environmental conditions have been made available.

Climate extremes, like dryness and heat, have intensified in recent years due to global warming. The Intergovernmental Panel on Climate Change (a United Nations body) projected that warming of the Earth's atmosphere by every 0.5°C would result in more frequent and omnipresent drought episodes with a noticeable increase in their severity around the globe (the IPCC, 2021 report). Plants permanently struggle for survival under various environmental stressors and in field conditions, they are usually exposed to several hazards rather than just one (Suzuki et al., 2014). For instance, drought is often accompanied by high temperatures, and the molecular response of plants to combined stress cannot be easily deduced from the effect of each stress alone (Prasad et al., 2011). Some genes, i.e., those determining the trade-off between signaling pathways (e.g., phytohormones) or the underlying universal stress response (e.g., detoxification), can have the same regulatory status under different stresses (Prasch and Sonnewald, 2015). On the other hand, two different stress factors may induce a stress-specific strategy, sometimes requiring an opposite response from the plant. For instance, opening and closing of stomata are preferred by plants during exposure to heat and drought, respectively (Zandalinas et al., 2016; Hsu et al., 2021). Therefore, during their co-occurrence, the plant may generate a unique molecular response, too. The literature about the combined effects of abiotic stresses on barley is quite limited and mainly based on the physiological comparison of barley genotypes rather than the changes in gene expression profiles (Ahmed et al., 2013). Recognition of barley transcriptome modulation induced by combinatorial abiotic stresses, including drought and increased temperature, is still largely missing.

Response of plants to constrained conditions is a very complex phenomenon and involves reactions of a multitude of mechanisms. To date, many studies have focused on plants' molecular adaptation to environmental stresses, and numerous stress-induced genes have been reported, also in barley (Gürel et al., 2016; Zhao et al., 2020; Mareri et al., 2022). This includes the examination of the protective role of late embryogenesis-related proteins (LEA) during dehydration, and dehydrins belonging to group 2 of LEA are the most commonly studied in various plant species (Yu et al., 2018). Additionally, genes encoding group 3 of LEA proteins have been widely described as responsive to drought, salinity, heat, and cold stresses (Xiao et al., 2007; Kosová et al., 2014). Also, the regulatory network of abscisic acid (ABA), a prominent messenger of plant stress response, has been extensively studied (Ma et al., 2018); candidate genes for ABA biosynthesis and catabolism in barley have been proposed (Fidler et al., 2015). A large number of genes with potential roles in heat stress responses have been identified, with the central role being played by those encoding heat shock proteins (HSPs) (Chang et al., 2007). They play a role in the protection of intracellular proteins from denaturation and preserve their stability and function through protein folding; thus, they act as chaperones (Baniwal et al., 2004). Different HSP-encoding genes have been listed in barley (Reddy et al., 2014). A crucial role of heat stress factors (HSFs) in the induction of the heat stress response has also been confirmed in model plant studies, since they regulate thermal protection through interaction with HSPs (Scharf et al., 2012). Candidate genes encoding HSFs have been proposed in barley by phylogenetic analysis (Mishra et al., 2020).

Despite the large efforts made to study the complex regulatory mechanisms underlying plant response to stress factors, the genetic and environmental regulation of plant adaptations, including barley, to various conditions (e.g., drought, heat), remains largely unrecognized (dos Santos et al., 2022). Although the importance of the flag leaf in flowering and grain yield determination has been studied, relatively little research has been done on the molecular characterization of the flag leaf of barley. Abiotic stresses occurring at the reproductive stage limit the availability of nutrients translocated from photosynthetic and storage organs. At this developmental stage, the viability of the flag leaf and its efficient photosynthesis activity are of great importance (Verma et al., 2004). The flag leaf plays a fundamental role in grain filling in cereals. As the top-most leaf, it intercepts quite a lot of sunlight and feeds the spike by translocation of assimilates. When the flag leaf is lost or destroyed, grain yield is reduced (Ojanpera et al., 1992). Our previous studies demonstrated that a terminal water shortage imposed in the flag leaf stage was more devastating for yield components compared to the early stress in barley (Mikołajczak et al., 2017). Undoubtedly, profound molecular studies are needed to fill the gap about the flag leaf's behavior under environmental

stimuli. Most transcriptomics reports focus on younger leaf examination (e.g., Wehner et al., 2016; Zeng et al., 2016), less on roots (e.g., Janiak et al., 2019), and very limited studies about genome-wide expression changes in barley crown tissue have been reported (Svoboda et al., 2016; Mikołajczak et al., 2022). The sparse evidence corresponding to molecular characteristics of barley flag leaf is related mainly to metabolite profiling (Templer et al., 2017; Niu et al., 2022). Also, Hosseini et al. (2016) examined the effect of potassium treatment on primary metabolism and abscisic acid accumulation in barley flag leaf of two genotypes contrasted in stress tolerance and exposed to temporal drought. Additionally, the authors analyzed the expression changes of two ABA-related genes *via* real-time qPCR. In fact, the global transcriptome re-modeling in flag leaf, especially under combined drought and heat, has not been investigated in barley so far.

Hence, this study was aimed at deciphering the impact of drought and heat on genome-wide gene expression in the flag leaf of barley. We employed high-throughput sequencing of mRNA to identify genes that are associated with responses to drought or heat and their combinations. We assumed that changes in the transcriptome under a combined stress cannot be considered as the additive effects of the single stresses, however some subset of genes, e.g., with universal function, may react identically in different environments. Secondly, we hypothesized that stress-induced changes in gene expression depend also on the morphology of the flag leaf. However, we expected that although the morphology of the flag leaf is genetically determined, single nucleotide mutations do not have an unambiguous effect on the different expression of polymorphic genes under unfavorable conditions. Transcriptome data was analyzed along with the evaluation of phenotypes and chlorophyll fluorescence parameters of the flag leaf.

Material and methods

Plant material consisted of seven recombinant inbred lines (RILs, called MCam) of spring barley developed by crossing the cv. Maresi (European) and CamB1 (Syrian) breeding lines (Mikołajczak et al., 2016; Mikołajczak et al., 2017; Mikołajczak et al., 2020) in the Team of Cereal Phenomics, Institute of Plant Genetics, Polish Academy of Sciences. Accessions were classified into three groups according to flag leaf size: small (S), medium (M), and large (L) (Table 1, Figure 1). Five flag leaves of each genotype were used to define the average dimensions and calculate the leaf area (of the rectangle framing the leaf).

Abiotic stress application

Experiment was carried out in phytotrons under fully controlled conditions according to Kuczyńska et al. (2019) and Mikołajczak et al. (2022) with modifications. The 60%–70% of air humidity and 234 μmol m^{-2} s^{-1} PAR irradiance (Apollo 8 LED Grow Light) were applied. Each pot (H-LSR 4.5 L; 21 cm in diameter and 20 cm in height) was filled with a mixture of loamy soil and peat (3:1, *w*/*w*), then pots were arranged randomly on the phytotron benches. Ten seeds were sown in each pot, and the number of plants was reduced to five after germination. Firstly, all plants were grown at 8°/14° C and 12/12 h (night/day) photoperiod for one month and next at 16°/22° C and 8/16 h (night/day) photoperiod until the end of the vegetation season under optimal soil moisture, i.e., at above 70% field water capacity (FWC), with some changes in stressed variants. Overall, four environmental variants were applied with two temperature and water regimes: control conditions (C) as described above; drought (D)—soil moisture at 20% FWC and temperature as in C; high temperature (H)—20°/30° C (night/day) and optimal soil moisture; and combination of the stress treatments (HD)—20°/30° C (night/day) and 20% FWC. Abiotic stress was imposed at the flag leaf stage (39 BBCH, approx. 29–47 days after sowing depending on the genotype) and maintained for seven days. Biological samples (flag leaves) for molecular analyses were collected at two time points, i.e., on the third (T1) and seventh (T2) days of stress. Soil moisture was

TABLE 1 Grouping of barley genotypes with respect to the flag leaf size.

Genotype	Flag leaf dimensions (cm)				Area (rect., cm^2)	Rank	Group according to flag leaf size
	Length	s.e.m.	Width	s.e.m.			
MCam48	10.0	0.3536	0.84	0.02449	8.4	4	medium
MCam53	13.4	0.967	0.86	0.04	11.524	5	medium
MCam67	22.2	0.5148	0.98	0.03742	21.756	7	large
MCam71	16.3	0.7176	0.84	0.06	13.692	6	medium
MCam91	6.0	0.3536	0.62	0.03742	3.72	1	small
MCam99	7.8	0.3391	0.54	0.02449	4.212	2	small
MCam109	7.9	0.4	0.76	0.04	6.004	3	medium

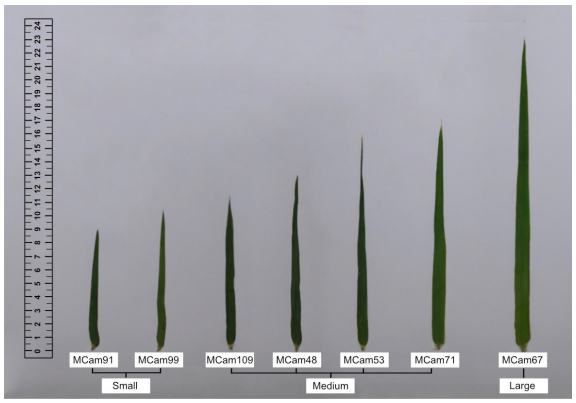

FIGURE 1
Flag leaves of seven barley accessions (RILs) classified into three groups according to flag leaf size: small, medium, and large.

controlled gravimetrically by the daily weighing of each pot. The number of pots was set to provide sufficient material for molecular studies and phenotyping.

Whole-genome expression analysis

Flag leaves of barley genotypes were collected from all experimental variants at two time points (T1 and T2), and they were immediately frozen in liquid nitrogen and stored at −80°C until analysis. Total RNA (1–2 µg) was extracted in triplicates using the Qiagen (RRID : SCR_008539, http://www.qiagen.com, Hilden, Germany) RNeasy Plant Mini Kit according to the manufacturer's instructions. Genomic DNA contamination was removed twice, i.e., on-column DNase digestion (RNase-Free DNase Set, Qiagen) and using the DNase Max Kit (Qiagen) during and after RNA isolation, respectively. Three flag leaves sampled from different plants of each genotype in a pot formed one replication, and three such replications were examined. RNA quantity, quality, and integrity were evaluated following the study by Mikołajczak et al. (2022). The construction of a cDNA library (TruSeq stranded mRNA) and mRNA sequencing were performed by Macrogen Inc. (RRID : SCR_014454, http://www.macrogen.com, Seoul, Republic of Korea) using an Illumina NovaSeq6000 platform with a 150-bp paired-end configuration and the number of read pairs ranging from 18.3 to 40.9 M per sample.

Phenotype characteristics

All plants were manually harvested after ripening (approximately 69–84 days after sowing depending on the genotype and treatment), and plant architecture-related traits along with yield components were measured. Both primary (main) and secondary (lateral) stems were examined, as well as the main phenological stages were noted; overall, 26 characteristics were evaluated (T1–T26). Additionally, nine chlorophyll fluorescence parameters (F1–F9) were measured using the FluorPen FP 110/D device (Photon System Instruments, PSI, Drásov, Czech Republic) on the flag leaf of plants at the third (T1) and seventh (T2) days of stress across treatments. After a 30-minute dark adaptation, employing detached leaf-clips, flag leaves were immediately exposed to a pulse of saturating light at an intensity of 3,000 µmol m^{-2} s^{-1} and all parameters were measured. Three replicates were used for the above-mentioned observations, each consisting of five plants from one pot. Full list of analyzed phenotypic traits and chlorophyll fluorescence parameters, with corresponding identifier/abbreviation, are given in Supplementary Table 9A and Supplementary Table 9B, respectively.

Data analysis

The IBSC_v2 *Hordeum vulgare* (Ensembl Plants rel. 48; RRID : SCR_008680, http://plants.ensembl.org/index.html) genome assembly was used as a reference for SNP and gene expression analyses. After removing adapter-related sequences and quality trimming using AdapterRemoval ver. 2.1.7 (RRID : SCR_011834, https://github.com/MikkelSchubert/adapterremoval, Schubert et al., 2016) (parameters: –minquality 20, –minlength 50), mRNA-seq reads were mapped into hi the reference sequence using TopHat ver. 2.1.1 (RRID : SCR_013035, http://ccb.jhu.edu/software/tophat/index.shtml, Kim et al., 2013) (parameters: maximum no. of mismatches = 1, –no-mixed, –no-discordant); the mapping efficiency was 61.8%–83.9%. Reads aligned to transcripts were counted using the featureCounts function in Bioconductor (RRID : SCR_006442, http://www.bioconductor.org/), R 3.6.1 (RRID: SCR_001905, http://www.r-project.org/, Rsubread library; Liao et al., 2019), and the resulting data were subjected to differential expression analysis in DESeq2 ver. 1.22.2 (RRID: SCR_015687, https://bioconductor.org/packages/release/bioc/html/DESeq2.html) (Love et al., 2014). Differentially expressed genes (DEGs) between treated and control samples were found among the genes characterized by a mean expression of at least 10 units (estimated in DESeq2), $|\log_2(FC| > 3$, and FDR <0.01. Principal coordinate analysis (PCoA) on $\log_2(FC)$ values for DEGs was based on the matrix of Euclidean distances. Gene Ontology term enrichment analysis was performed using GO Slim annotation and tools at geneontology.org (RRID : SCR_002811). A weighted gene co-reaction network analysis was performed using the WGCNA library (RRID : SCR_003302, http://www.genetics.ucla.edu/labs/horvath/CoexpressionNetwork/) in R (Langfelder and Horvath, 2008; Langfelder and Horvath, 2012) with the following parameters: beta = 10, complete link clustering method, cutHeight = 0.95, minsize = 20. SNP calling in

mRNA-seq data pooled from three biological replications separately for seven genotypes, in optimal conditions at T1, was performed using the samtools/bcftools pipeline (Li, 2011) (filtering parameters: %QUAL >60, MAF >0.10, DP >80). Venn diagrams were drawn using the "venn" package in R. SNP protein translation effects were predicted using the VEP tool (Ensembl Plants; McLaren et al., 2010). SNP data were analyzed using PCoA based on a matrix of simple matching similarity coefficients between genotypes and hierarchical clustering by complete link method. Statistical tests and analyses of phenotypic and chlorophyll fluorescence data were performed in GenStat 19 (RRID : SCR_014595, http://www.vsni.co.uk/products/genstat/) (VSN International, 2017). Principal component biplots were created after centering and normalizing the data. An analysis of variance was performed in a model containing fixed effects for treatment, flag leaf size group, time point, and the interactions of pairs these factors. A weighted trait correlation network analysis performed jointly for contrasts on phenotypic and expression data using the WGCNA library with the following parameters: beta = 6, complete link clustering method, cutHeight = 0.98, minsize = 10.

Results

Whole-genome expression analysis

Overall, 2,457 differentially expressed genes (DEGs) were detected in at least one of the 18 comparisons between the three treatments (H, D, and HD) and control conditions (C) for three flag leaf size groups at two time points (Supplementary Table 1). In general, accessions with a small size of the flag leaf (S) had a greater number of downregulated genes (with the exception of T1 and D), whereas in the large leaf group (L), upregulated genes were more numerous, independently of the type of stress and time of sampling; plants with a medium flag leaf size (M) had more upregulated genes in D and HD but less in H than downregulated ones at both time points. A larger number of genes showed induced expression in response to D and HD than to H, especially at T2 (Table 2). About 3-fold more DEGs were observed at the seventh day of stress (T2) than on the third day (T1) (Figure 2A), however in group M the number of DEGs in H treatment was similar at both time points (Table 2). Most of the DEGs at T1 (approx. 80%) were also present at T2. Genotypes in group S had 2-fold more common DEGs with plants in group M than with those in group L; significantly, 349 DEGs were shared between all classified groups (Figure 2B). There were 1,521 DEGs shared between D and HD, whereas 95 DEGs were shared across all stress conditions. Treatments D and HD affected the expression of ca. 9-fold more genes than H (Figure 2C).

Principal coordinate analysis (PCoA) of $\log_2$(FC) values for DEGs showed a lower variability in reaction of gene expression to applied stresses in flag leaves of group L than in group M, and transcriptomic reaction in group S was substantially different from the others (Supplementary Figure 1).

For the functional interpretation of differentially expressed genes, the Gene Ontology (GO Slim, geneontology.org) enrichment analysis was done for a set of DEGs significant in at least three contrasts (1,037 genes) (Supplementary Table 2). Mainly, overrepresented GO terms were related to "photosynthesis" and "response" to various factors; the term "response to abiotic stimulus" was the most significantly enriched in all cases (except for group L). Also, the term "response to abscisic acid" was significantly enriched in all cases (except for the H treatment). Within the groups defined by flag leaf size, the DEGs identified for group L determined the lowest number of enriched GO terms. A lower number of enriched GO terms was observed for H than for D and HD. However, GO terms shared across all treatments were more

TABLE 2 Number of down- and upregulated genes in genotypes classified to different groups according to flag leaf size, at time points T1 and T2, in comparisons between drought (D), heat (H), their combination (HD) v. control.

Group according to flag leaf size	Regulation status	T1			T2		
		D	H	HD	D	H	HD
Small	down	29	5	93	855	45	844
	up	47	2	41	767	22	614
	total	76	7	134	1622	67	1458
Medium	down	48	59	173	102	62	271
	up	290	21	281	727	18	613
	total	338	80	454	829	80	884
Large	down	0	4	3	182	11	222
	up	16	11	25	208	12	242
	total	16	15	28	390	23	464

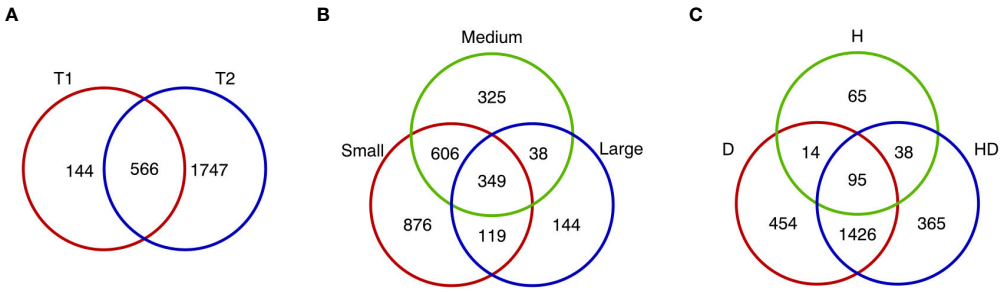

FIGURE 2
Venn diagrams visualizing the number of differentially expressed genes in flag leaves, specific and shared between: **(A)** time points (T1 and T2), **(B)** barley genotypes assigned to groups of different sizes of flag leaf (small, medium, and large), and **(C)** applied stress treatments (D, H, and HD).

significant in H than in other treatments, interestingly, including "response to osmotic stress" and "response to oxidative stress." In general, a set of enriched GO terms did not change over time (they were slightly more numerous in T2), and similar significance for each of them was observed between time points. A few enriched GO terms were specific to flag leaf size, stress variant, or time point (Supplementary Table 2). It is worth not that terms "response to heat," "response to oxidative stress," and "response to osmotic stress" were overrepresented in leaves of group M, whereas terms associated with phosphatase activity and dephosphorylation were specific to the second time point (T2).

Secondly, to interpret functionally a set of genes whose expression responded similarly to stress, we used $\log_2$(FC) values for 18 contrasts to construct the gene co-reaction network, which revealed 15 modules (M1–M15) (Supplementary Table 1, Supplementary Table 3). For a better summarization, the obtained modules were further grouped according to the similar response of DEGs assigned to each module (based on module eigengenes). On this basis, we selected three joined modules (MI–MIII) containing DEGs with the most similar expression (Table 3A), for which the GO Slim enrichment analysis was performed (Table 3B). In general, DEGs in module MI (86 genes) reacted positively in H relative to control condition C, whereas in D and HD gene expression was reduced or similar to that of condition C. These DEGs were numerously annotated as oxidoreductases, receptor-like protein kinase, and chlorophyll a/b binding proteins (according to the NR protein database). These findings were interrelated with GO term enrichment results, which revealed, i.e., that the terms photosynthesis and response to abiotic or to light stimuli were overrepresented in this set of DEGs.

DEGs assigned to module MII (225 genes) were strongly expressed in D and HD relative to C and H independently from the type of flag leaf in T2; it was also confirmed in T1, but only for genotypes belonging to group M. This module was, again, rich in oxidoreductase-related genes (NR protein database) and numerous hormone-related genes were observed, mainly corresponding to the abscisic acid regulatory pathway (Plant Reactome). We confirmed that the GO term "response to abscisic acid" was overrepresented within DEGs of module MII. Among the enriched GO terms we also found, i.e., the terms "response to cold" and "response to temperature stimulus."

Expression profiles of genes from module MIII (55 genes) were similar to those from module MII for all groups of flag leaf size over time, except for DEGs affected by D and HD in T1, which had rather positive regulation status compared to module MII in groups S and L. Genes associated with ABA biosynthesis and signal transduction and with the MAPK signaling pathway were particularly abundant in module MIII. However, only terms related to lipid catabolism were found to be overrepresented.

Next, GO term enrichment analysis (at geneontology.org) was applied to uncover functions of 349 DEGs common between all groups defined by flag leaf size (Figure 2B, Supplementary Table 4A) and 95 DEGs shared across stress treatments (Figure 2C, Supplementary Table 4B). In the first case, the biological process category contained the most enriched terms, mainly associated with responses to various factors, including water deprivation, temperature stimulus, and abscisic acid; the term "cold acclimation" had the highest fold enrichment. Three overrepresented GO terms were detected within the molecular function category (the term "carotenoid dioxygenase activity" enriched the strongest), but none of these terms was found for a cellular component. DEGs assigned to these GO terms were present in all modules defined by the gene co-reaction network (except for M4 and M7). For the set of DEGs shared between treatments (belonging to modules M6, M7, M9–M13), enriched GO terms were mostly similar to those mentioned above within the biological process category; additionally, "response to oxidative stress," "response to ROS," and some photosynthesis-related GO terms were overrepresented. Within the molecular function category, there were, among

10.3389/fpls.2022.1096685

TABLE 3A Joined co-reaction modules containing DEGs with the most similar expression reaction induced by stress.

Group according to flag leaf size	Time point	Treatment	MI	MII	MIII
S	T1	D	0.70	−0.17	0.41
M	T1	D	0.00	0.51	0.49
L	T1	D	0.38	−0.20	0.35
S	T2	D	−1.72	1.25	1.11
M	T2	D	−0.27	1.51	1.07
L	T2	D	−0.69	0.46	0.58
S	T1	H	0.84	−0.88	−0.37
M	T1	H	0.70	−1.05	−1.64
L	T1	H	0.91	−1.02	−1.16
S	T2	H	0.78	−0.92	−1.13
M	T2	H	0.94	−0.87	−1.31
L	T2	H	0.81	−0.94	−1.04
S	T1	HD	0.22	−0.46	0.17
M	T1	HD	−0.55	0.34	0.19
L	T1	HD	0.35	−0.44	0.00
S	T2	HD	−1.89	1.05	0.88
M	T2	HD	−0.83	1.36	0.96
L	T2	HD	−0.67	0.47	0.45

TABLE 3B GO Slim terms overrepresentation analysis of three joined co-reaction modules.

GO term|GO identifier	Overrepresentation score ($-\log_{10}$(q-value))		
	MI	MII	MIII
cellular lipid catabolic process|GO:0044242	–	–	1.88
generation of precursor metabolites and energy|GO:0006091	5.03	–	–
lipid catabolic process|GO:0016042	–	–	2.18
photosynthesis|GO:0015979	9.23	–	–
response to abiotic stimulus|GO:0009628	5.83	–	–
response to abscisic acid|GO:0009737	–	2.13	–
response to cold|GO:0009409	–	4.39	–
response to inorganic substance|GO:0010035	–	2.43	–
response to light stimulus|GO:0009416	7.63	–	–
response to lipid|GO:0033993	–	1.82	–
response to radiation|GO:0009314	7.56	–	–
response to stimulus|GO:0050896	1.87	–	–
response to temperature stimulus|GO:0009266	–	1.95	–

others, the terms "gibberellin 20-oxidase activity" and "binding of protein, tetrapyrrole, or chlorophyll". In general, terms associated with photosystems I and II as well as chloroplasts were enriched in the cellular component category.

Lastly, 365 genes whose expression was exclusively affected by combined drought and heat were used for GO term overrepresentation analysis. However, no significant results were found within the biological process, molecular function, and cellular component categories. Therefore, we additionally tested Panther Protein Class overrepresentation (at pantherdb.org) and discovered a few enriched enzyme-related terms, i.e., "oxygenase," "oxidoreductase," "metabolite interconversion enzyme," "hydrolase," and the term "transporter" (Figure 2C, Supplementary Table 4C).

Subset of DEGs assigned to selected functional GO annotations

We extracted GO terms annotating sets of DEGs (see the GO annotation in Supplementary Table 1) within which the distribution of genes, with respect to direction of up and downregulation, was significantly different from the calculated marginal distribution of all differential regulation events in the whole experiment (3,008 down/3,957 up). This approach enabled us to visualize for which GO term the expression of assigned genes was particularly increased or reduced under applied treatments (Figure 3, Supplementary Table 5); Furthermore, in this analysis one gene could be considered in several "differential expression events" (DE events) and could show different expression reactions across defined contrasts.

DEGs assigned to photosynthesis and closely related terms

In general, DEGs associated with photosynthesis and most of the terms closely related to it reacted negatively to stress factors relative to control. In fact, there were 53 DEGs assigned to photosynthesis whose expression was reduced in response to stress (189 DE events), excluding HORVU2Hr1G090070, which was exclusively upregulated in genotypes of group S under D in T2 (Supplementary Table 6). Almost 90% of these DEGs were observed for group S, especially in T2 for D and HD (including 11 genes specific to HD), whereas in T1 only HD induced some significant changes in gene expression. About 40% of DEGs were also identified for group M, mostly in HD at both time points. Only one gene, HORVU2Hr1G010690, had reduced expression in group L in D and T2. About 1/4 of photosynthetic DEGs were shared across treatments but no common DEGs between H and HD, being parallelly not significant in D, were identified. Interestingly, 4-fold more DEGs induced by H were detected in T1 than in T2. Genes encoding chlorophyll a/b binding proteins were the most numerously represented in this subset of DEGs. Few genes were associated with the photosystem I reaction center subunit.

On the other hand, there were some DEGs assigned to the terms "chloroplast" and "chloroplast thylakoid membrane"

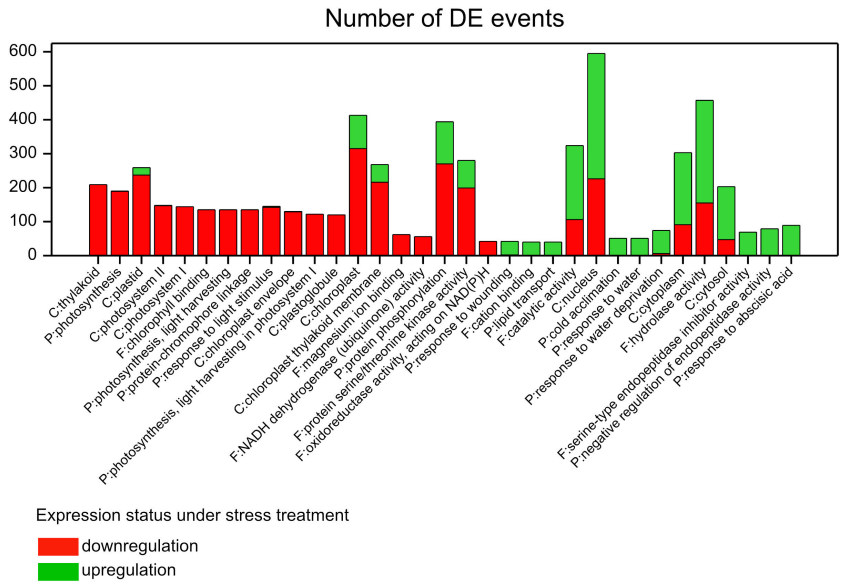

FIGURE 3
Enriched GO terms with assigned DE events whose distribution was significantly different than the marginal distribution of all DE events in the experiment (χ^2 test, P <0.001, |std. residual| >6); C, cellular component; F, molecular function; P, biological process.

(cellular components) whose expression reacted positively to stress; about 1/4 and 1/5 of all DE events were "upregulations," respectively (Figure 3, Supplementary Table 5). More than half DEGs were shared between D and HD being not significant in H. Interestingly, there was one upregulated DEG, HORVU2Hr1G038830, common between H and HD (not present in D) in group L in both time points and in group M in T1; it encoded ferredoxin-NADP reductase (Supplementary Table 6). The expression profile of downregulated genes assigned to both terms was similar to the above-mentioned photosynthesis related DEGs since they were partially shared between the two GO terms. Additionally, we found downregulated DEGs associated with ATP synthase CF1 epsilon subunit (six genes) and with NADH-plastoquinone oxidoreductase subunits 3, J, and K (12 genes), common between "chloroplast" and "chloroplast thylakoid membrane" terms, whose expression was specific to group S (in T2) in D and in D and HD, respectively. In turn, enhanced expression of genes was observed mostly in groups S and M under D and HD, especially in T2. Among them four genes encoded high molecular mass early light-inducible protein HV58. Several upregulated genes encoded unknown proteins (predicted proteins according to the NR protein database); however, using the Plant Reactome database, we uncovered that HORVU4Hr1G050510 was involved in the HSFA7/HSFA6B-regulatory network induced by drought and ABA, whereas HORVU2Hr1G005320 was related to arginine and proline metabolism. Also, one of them, HORVU3Hr1G070850, encodes the malic enzyme (EC:1.1.1.40). Three DEGs were found to have opposite regulation status in group M, i.e., gene expression was enhanced in D and HD in T2 but reduced in T1 in H. They encoded putative 9-cis-epoxycarotenoid dioxygenases (HORVU5Hr1G044510, HORVU5Hr1G054970), and HORVU5Hr1G092850 (a predicted protein) was involved in ABA biosynthesis and mediated signaling according to the Plant Reactome database (Supplementary Table 1).

DEGs assigned to drought response

One of the GO terms revealed above corresponds to "response to water deprivation," where 18 DEGs were assigned. Generally, they reacted positively in response to applied stress (Figure 3, Supplementary Table 5), mostly in D and HD in T2 in groups S and M, less in L; it was also confirmed for group M in T1 (Supplementary Table 6). Three DEGs were specific to D, one to H, and none to HD. The gene HORVU7Hr1G088140 encoding abscisic acid receptor PYL2 had reduced expression in HD, T1 in groups S and M, and in D, T2—group L. Another gene, HORVU6Hr1G080670, encoding bZIP transcription factor, was downregulated only in H (T1, group M). Eight of the detected DEGs were annotated to dehydrin (various types), and almost all of them were overexpressed in response to drought (D, HD) in T2 across flag leaf size groups. Significantly, they were also upregulated in T1 in group M. Gene HORVU5Hr1G092100 (dehydrin DHN2) was overexpressed only in group M in D, T2. Similarly, HORVU4Hr1G074130 encoding annexin D4-like was exclusively overexpressed in group M in T2 (D and HD). In contrast, another gene encoding annexin (D1), HORVU7Hr1G037080, had increased expression in groups S and L (but not in group M) in T2 in HD and D, respectively. Both genes were also annotated for heat response.

DEGs assigned to heat response

No GO term annotated to "response to heat" was found on the base of calculated marginal distribution of DEGs (Figure 3). Thus, to gain an overview of DEGs related to heat, we analyzed the regulation status of genes present in our dataset annotated as follows: "response to heat" (GO:0009408), "cellular response to heat" (GO:0034605), "regulation of cellular response to heat" (GO:1900034), "heat shock protein binding" (GO:0031072), "heat acclimation," and "positive regulation of transcription from RNA polymerase II promoter in response to heat stress" (GO:0061408) (Supplementary Table 6). This revealed 32 DEGs and nine of them were repeated within mentioned GO categories. The most numerous were genes encoding heat shock proteins (HSPs). Regulation status of heat-related DEGs was not uniform. Eight genes were downregulated and the most DE events were observed in group M in T2, mainly in H and/or HD. Four genes were shared between these treatments in group M over time. They encoded HSP23 (HORVU2Hr1G077710, HORVU6Hr1G077710), HSP70 (HORVU3Hr1G086500), and HSF (HORVU7Hr1G087690). In the same contrasts, gene HORVU5Hr1G094380 (putative HSF-type), was specifically underexpressed in response to H. In contrary, there were 11 upregulated genes, mainly in T2 in groups S and M in D, HD. However, HORVU4Hr1G063350 (HSP20-like chaperone) had increased expression only in T1 in group M across treatments. The expression of another gene encoding HSP20 (HORVU0Hr1G020420) was additionally increased in HD in group S and L (also in H in T2) in both time points. Interestingly, gene HORVU3Hr1G069590 encoding heat shock factor C1b showed enhanced expression always in response to D and HD in T2 in all groups of flag leaf size; it was also confirmed for group M in T1. In turn, gene HORVU7Hr1G088920 encoding heat shock factor C2b was upregulated specifically to group M in D and HD, T2, similarly to gene HORVU4Hr1G074130 encoding annexin D4-like as mentioned previously. Noteworthy, 13 DEGs within group M were found to have opposite regulation status dependent on time or stress treatment. They were upregulated in T1 mostly in D and/or HD, and not changed significantly in H (with two exceptions), whereas in T2 all of them were downregulated in H, and interestingly, they became not significant in D (with two exceptions). One of such gene, HORVU4Hr1G090090 encoding

heat-responsive transcription factor HSF85, was upregulated in D and HD but downregulated in H. Two genes encoding HSP20 (HORVU3Hr1G020500, HORVU3Hr1G020490) changed expression status also in response to HD, from positive in T1 to negative in T2. All significant DE events observed for groups S and L showed "upregulation" status.

DEGs assigned to abscisic acid

Sixteen DEGs annotated to "response to abscisic acid" were found whose expression was upregulated in reaction to stress factors with one exception, i.e., the drought-related gene HORVU7Hr1G085130 described above (Figure 3, Supplementary Table 5, Supplementary Table 6). In fact, most of the detected DEGs encoded dehydrins, and they were also assigned to drought responses, so the same behavior was observed. In turn, gene HORVU3Hr1G069590 (encoding HSFC1b) was annotated also to heat response. Additionally, we identified HORVU1Hr1G059950 (encoding Em protein CS41) as overexpressed across all groups defined by flag leaf size, mainly in D at both time points. Otherwise, HORVU6Hr1G058000 encoding ECERIFERUM 1-like had increased expression only in group S (D and HD, T2), whereas HORVU7Hr1G045630 encoding protein HVA22, was upregulated in groups M and L in D, HD in T2.

In contrast, there were few downregulated DEGs assigned to the GO term "abscisic acid-activated signaling pathway," including genes encoding the bZIP transcription factor and the abscisic acid receptor PYL2 mentioned above. Another gene, HORVU4Hr1G055220, encoding the abscisic acid receptor PYL4, had reduced expression in group S in D, HD in T2, and in group M in D over time (Supplementary Table 6).

Indeed, we found 19 additional DEGs encoding LEA proteins, based on the Interpro database, but they were not annotated to the ABA response (Supplementary Table 1). In general, they belonged to LEA1 and LEA2 subgroups and were overexpressed in groups S and M in response to D and HD in T2. However, two genes were downregulated in HD in T2 across groups of flag leaf size (except for group M for HORVU4Hr1G026770), and a third gene, HORVU7Hr1G012310 (encoding LEA1), had reduced expression only in group S in D, HD in T2. None of these genes were significantly affected by H.

DEGs assigned to lipid transport

Curiously, we identified the term "lipid transport" within GO categories with fully upregulated DEGs (Figure 3, Supplementary Table 5). All of them (with one exception) belonged to the family of lipid transfer protein (LTP) encoding genes, including ns-LTP6, the ns-LTP1 precursor, and three ns-LTP2-like genes. They were upregulated mainly in response to D and HD in groups S and M; however, HORVU5Hr1G109100 was exclusively overexpressed in H (group S in T2, group M in T1) (Supplementary Table 6).

DEGs assigned to leaf development

Due to the research on genotypes with different flag leaf sizes in our experiment, we decided to follow the reaction of DEGs assigned to the term "regulation of leaf development" (GO:2000024). Only one such DEG, HORVU1Hr1G046740, was found (Supplementary Table 6). It encoded the YABBY protein and showed reduced expression induced by individual drought in groups S and L in T2. No expression change was observed in group M. To expand the panel of genes involved in leaf development, we used the Plant Reactome database (Supplementary Table 1). This revealed 10 additional DEGs associated with the "regulation of leaf development" pathway, including six genes encoding enzymes. Four of them encoded cysteine protease, and in three cases the expression was increased in D and HD in T2 across all groups defined by flag leaf size; it was also confirmed in T1 in group M. Interestingly, a fourth gene, HORVU7Hr1G119930, was downregulated specifically in group S in D, HD in T2. Similar expression regulation was observed for two genes encoding cytochrome P450, i.e., HORVU5Hr1G057180 and HORVU5Hr1G081060 (downregulated additionally in group L). We detected one gene, HORVU5Hr1G097900, encoding putative TF RL9 (leaf rolling), which had reduced expression in D and HD in groups S and L in T2. None of the DEGs were significantly affected by H.

Single nucleotide polymorphism

SNP calling in mRNA-seq data revealed 17,261 polymorphic markers (homozygous), including 16,875 SNPs with some effects on protein translation assigned by the VEP tool (Table 4). There were 4,552 genes containing SNPs, whose number in a single gene ranged from 1 to 45 (Supplementary Table 7). SNP HIGH impact effects were the most abundant due to the introduction of stop codons (stop_gained_variant), whereas SNP MODIFIER effects were more numerous in 5' or 3' UTRs and less in introns or non-coding transcripts.

Some association between genetic composition and flag leaf size was confirmed by PCoA analysis, i.e., MCam67 with a large flag leaf was significantly distanced from the other group of genotypes, and MCam48 and MCam109, representing a group of medium flag leaf size, showed the closest similarity (Supplementary Figure 2).

Gene Ontology term enrichment analysis of genes with HIGH translation effects revealed overrepresented terms only within the molecular function category, mostly associated with the binding of different compounds; the largest fold enrichment was observed for the term "ABC-type transporter activity" (Supplementary Table 8).

Next, we analyzed whether DEGs, containing SNPs with HIGH translation effect and being polymorphic between groups of genotypes defined according to flag leaf size, reacted

TABLE 4 Classification of SNPs by the type of variant and type of predicted effect by VEP.

Type of variant	Effects predicted by VEP (Ensembl Plants)				
	HIGH	LOW	MODERATE	MODIFIER	Total
3_prime_UTR	0	0	0	3,131	3,131
5_prime_UTR	0	0	0	1,403	1,403
intron	0	0	0	750	750
missense	0	0	4,506	0	4,506
non_coding_transcript_exon	0	0	0	773	773
splice_acceptor	23	0	0	0	23
splice_donor	28	0	0	0	28
start_lost	31	0	0	0	31
stop_gained	71	0	0	0	71
stop_lost	16	0	0	0	16
stop_retained	0	10	0	0	10
synonymous_variant	0	6133	0	0	6,133
Total	169	6,143	4,506	6,057	16,875

differentially under stress or not. Among the 12 genes identified, only two seemed to have some relationship between genetic polymorphism and gene expression. Gene HORVU3Hr1G002550 (protein kinase domain) was polymorphic between plants of group M (allele C/C) and groups S and L (allele T/T); it was not differentially expressed in group M in any case, but it was downregulated in HD, T2 in groups S and L (also in D). Similarly, gene HORVU6Hr1G084070 (assigned to response to drought/ABA) showed SNP polymorphism between plants of groups M (allele T/T, with exception of MCam109) and S and L (allele C/C) but the only difference in expression was that in group M the gene was overexpressed in both time points in D, HD, whereas in groups S and L DEG was observed only in T2. Within DEGs assigned to another of selected GO terms mentioned above only one gene, HORVU7Hr1G101310, with SNP of HIGH translation effect was detected in subset annotated to lipid transport. However, despite the SNP polymorphism found between groups L (allele C/C) and S and M (allele G/G), there were no differences in the regulation of gene expression across genotypes.

Evaluation of phenotypes

The effects of applied stress factors on phenotype were similar in all three groups of genotypes. The mean effect of combined HD on the phenotype was more similar to the effect of D than H. In general, a negative effect of adverse conditions on studied traits was observed, excluding the number of tillers (T1) and basal internode length of the main stem (T5). The largest reduction under HD or D was found for grain-related traits (T15, T16, T19–T21). and the loss (by about max. 80%) was, in general, the greater the smaller the size of the flag leaf (Supplementary Figure 3A). Size leaf-dependent differences in phenology were noticeable for mean values of flag leaf and heading stages, i.e., with the increase in flag leaf size, plants reached the phase earlier, even by a dozen days; a slight stress-induced alternation was noted in both stages. On the other hand, D and HD caused the greatest delay in reaching full maturity (approximately 10 days) within group L relative to C and H. ANOVA confirmed the significant ($P < 0.001$) influence of flag leaf size on phenology (T24–T26) (Supplementary Table 9A). In turn, a significant effect of treatment ($P < 0.001$) and interaction of flag leaf size × treatment ($P < 0.01$) were observed only for full maturity (T26). An ANOVA revealed a significant effect of all sources of variation in the case of nine post-harvest traits (T3, T4, T8, T9, T13, T14, T19, T20, and T22). Treatment and flag leaf size had strong ($P < 0.001$) impact on most of traits, whereas their interaction affected significantly half of analyzed traits (at least at $P < 0.01$). The greatest stress-induced differentiation of mean values of chlorophyll fluorescence parameters was found for Pi_Abs and DI0_RC being, in general, reduced and increased, respectively, especially in T2 (Supplementary Figure 3B). Combined HD caused the strongest reduction of the Pi_Abs in all flag leaf size groups, with the greatest extent

(2.5-fold decrease relative to control) in group M. Parameter DI0_RC showed the largest positive reaction (2-fold increase), again in group M under D and HD. Other parameters were slightly affected by adverse conditions, excluding small flag leaf size genotypes exposed to H at the first time point (T1), where the greatest mean values of all parameters were identified (except for DI0_RC). An ANOVA revealed the significant effect of all sources of variation on most of the chlorophyll fluorescence parameters, mainly at P <0.001 (Supplementary Table 9B). The largest significant effects, on all traits, were observed for treatment and its interactions with time and flag leaf size (excluding Pi_Abs, significant at P <0.01). On the other hand, flag leaf size had the lowest impact on photosynthetic properties, and only Fv_Fm (P <0.001) and Pi_Abs (P <0.01) were significantly affected. The effect of time and interaction time × flag leaf size was significant for seven parameters.

Principal Component Analysis (PCA) confirmed the similar behavior of phenotypic (Figure 4A) and chlorophyll fluorescence (Figure 4B) traits within the two treatment groups, i.e., a similar effect of conditions C and H as well as a coincidence between D and HD impact.

We also conducted a correlation network analysis of phenotypic traits (post-harvest) and gene expression on contrasts between D, H, and HD v. C. This revealed a significant and negative relationship between reactions of expression of three genes, HORVU1Hr1G066100 (r = 0.65), HORVU2Hr1G026820 (r = 0.61), HORVU2Hr1G036720 (r = 0.65), and differences in grain weight per plant (T21), i.e., increased expression of each gene induced under D and HD and reduced grain weight relative to control, observed independently of flag leaf size (Supplementary Table 1, Figure 5).

Discussion

High-throughput sequencing of mRNA uncovered drought- and heat-responsive genes whose expression was differentially affected by individual and combined abiotic stress in barley flag leaf. In the global sense, the transcriptomic signature under double stress was more similar to effects caused by drought than by high temperature. Evidently, plants perceived drought as more severe than heat in our experimental setup. It was suggested that under co-occurrence of stressors, plants might prioritize the response strategy to the stress that impacts first or whose effect is perceived more intensely (Kumar Pandey et al., 2015). Prasch and Sonnewald (2015) pointed out four ways of plant response to combined stress: additivity, synergism, idiosyncrasy, and dominance, indicating that idiosyncrasy was the most often reported by researchers in various plant species exposed to multiple stressors. For example, a rather unique molecular response to simultaneous drought and heat compared to individual stresses was observed in *Arabidopsis* (Rasmussen et al., 2013), sorghum (Johnson et al., 2014), and wheat (Rampino et al., 2012). It was inconsistent with our study, where about 3/4 of all DEGs were common between D and HD. Therefore, we assumed that drought dominated during combinatorial stress treatments and the transcriptomic response was majorly shared than unique. This seems understandable as we applied severe drought and a moderate increase in temperature in the experiment. Similarly, Rizhsky et al. (2004) found that the transcriptomic response of *Arabidopsis* to combined drought and heat was more similar to that induced by single drought than heat, where about half of the transcripts were shared between drought and its combination. Concluding,

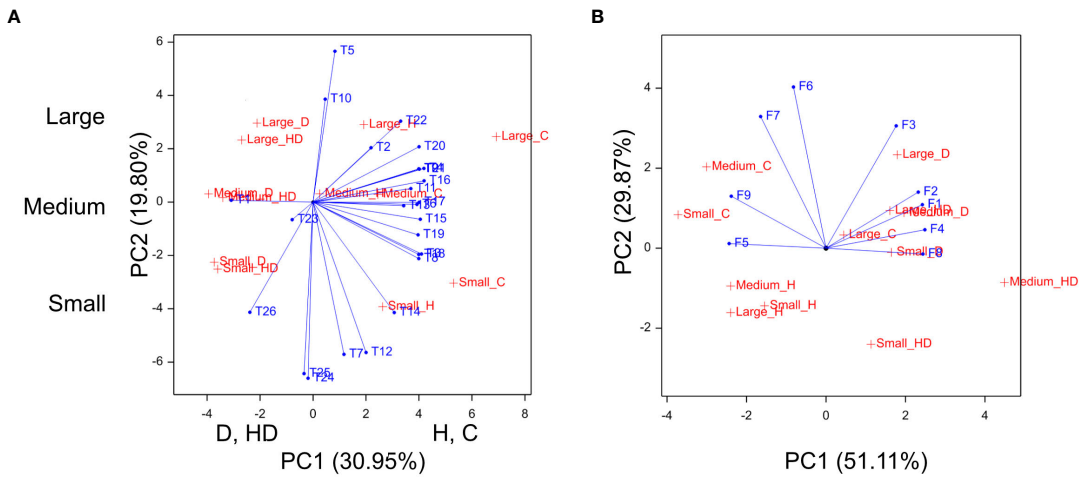

FIGURE 4
Biplots for phenotypic traits **(A)**, chlorophyll fluorescence parameters at T2 **(B)**. In **(A)**, axis PC1 discriminates treatments C, D, H, and HD, axis PC2—groups of genotypes classified according to the flag leaf size: large, medium, and small; T1–T26, phenotypic traits and phenological stages, F1–F9, chlorophyll fluorescence parameters.

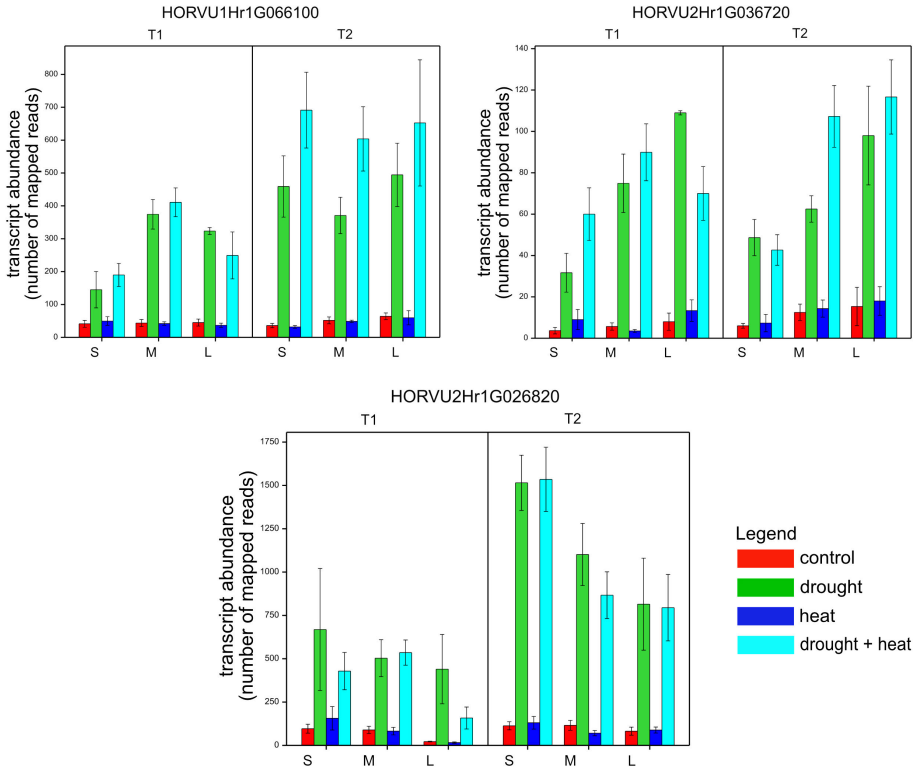

FIGURE 5
Mean expression levels (counts of mapped reads) for three genes in genotypes of different flag leaf size (S, small; M, medium; L, Large) in two time points (T1 and T2), whose reactions to stresses correlated with reaction with respect to grain weight per plant (T21).

plant responses to multiple stressors consisted of a combination of shared and unique transcriptomic changes, and their proportions depended on various factors like genotype or stress severity and duration.

Furthermore, expression co-reaction network analysis revealed that some DEGs playing various functions (e.g., genes associated with ABA signaling or lipid catabolism) had similar regulation under drought and under its combination with heat; on the other hand, the coincident expression of such DEGs was observed between heat and control conditions. Interestingly, among them, there were DEGs related to oxidoreductases that showed contrasting behavior, i.e., some were overexpressed and others were downregulated under D and HD in relation to H and C. It would seem that oxidoreductase-related genes should be generally upregulated in response to stressors, as indicated by Gharaghanipor et al. (2022), who observed increased abundance of oxidoreductase-coding transcripts in stress-sensitive barley genotypes under salinity. Also, Szurman-Zubrzycka et al. (2021) identified massive upregulation of peroxidases encoding genes in barley roots under low pH. However, in the same study, authors detected both down- and upregulated genes associated with peroxidases in response to aluminum treatment. Such opposite behavior of mentioned genes was also observed in leaves of sugarcane subjected to drought (Contiliani et al., 2022). Contrasting regulation of genes encoding oxidoreductases can be explained by the fact that they constitute a large family of enzymes with complex functions, and apart from defense against stress, they regulate cell homeostasis and plant development (Wang et al., 2018b).

We confirmed that gene expression was time-dependent, i.e., a four-day difference in exposition to adverse conditions had a large impact on transcriptome re-modeling since more DEGs were found on the seventh day compared to the third day of stress. Secondly, it was proved that stress-induced reaction of most of the early-responsive genes was maintained at the later period of plant exposition to stress. We claimed that stress severity was forcefully perceived by plants in the following days, therefore they needed more time for adjustment to adverse conditions. This situation was also observed for an increased temperature effect over time but to a lesser extent relative to other stress treatments, except for genotypes with medium flag leaf size.

Present study proved that stress-induced re-modeling of transcriptome depended also on the size of the flag leaf blade. It is well known that abiotic stresses affect leaves' morphology and physiology. Leaf rolling and limping as well as a decrease in

leaf size/area under drought have been reported in various species (Yang et al., 2021), including flag leaf modifications in wheat (Willick et al., 2018). Heat stress also causes the curling and wilting of leaves (Siddiqui et al., 2015). Hence, transcriptomic changes dependent on flag life size seem to be expected. We demonstrated that prolonged stress induced the most numerous changes in gene expression in genotypes of small size in the flag leaf. Perhaps the small flag leaf perceived the stress as stronger, and enhanced re-modeling of the transcriptome was required to protect leaf vitality under constrained conditions. Generally, the transcriptomic response of plants with small flag leaves was divergent from others with much more downregulated genes, but deeper insight into selected sets of DEGs showed that the reaction of plants in group S was much more like those belonging to group M than to group L. In turn, when considering only the early-responsive genes (T1 time point), most DEGs were specific to genotypes with medium flag leaf size, especially under D and HD. This group consisted of four genotypes, ensuring some genetic variability; thus, such a quick stress-induced reaction in gene expression can be attributed particularly to the medium size of flag leaf less and the genetic background. However, these findings had no significant effect on chlorophyll fluorescence parameters, and according to variance analysis, only two parameters were influenced by flag leaf size, including Fv_Fm. Parallelly, the maximum quantum efficiency of PSII photochemistry seemed to be the most constant parameter across stress treatments lasting for seven days; that can be expected since Fv_Fm was indicated as almost unaffected in barley leaves under early drought stress (Oukarroumet al., 2007). This is in accordance with the findings of Daszkowska-Golec et al. (2017), who did not observe significant changes in most chlorophyll fluorescence parameters in the barley cultivar Sebastian affected by the onset of drought. However, we found that the DI0_RC parameter responded positively, especially under HD in T2 in genotypes of medium flag leaf size. This may suggest that genotypes in group M can dissipate the excess energy more effectively than genotypes in other groups during stress treatment. On the other hand, genotypes in group M showed the strongest reduction of Pi_Abs. This integrative parameter was proved to be very sensitive to early stress scenarios and it corresponds to PSI and PSII efficiency providing quantitative information about plant status under adverse conditions (Strasser et al., 2004). We speculated that applied stresses can impair more strongly the assimilation of CO_2 in genotypes of group M because its positive correlation with Pi_Abs has been previously documented (e.g., van Heerden et al., 2007). The negative and additive effects of combined drought and heat on photosynthesis in wheat were reported by Perdomo et al. (2015), however they were not clearly evidenced by our evaluation of chlorophyll fluorescence parameters, probably due to the relatively short-term stress application (7 days).

It can be emphasized that some relationship between flag leaf size and phenotypic traits was identified. For example, plants with larger flag leaf size had slightly better grain yield (T21) under optimal conditions, and trait reduction induced by stress treatment (D, HD) was the greater the smaller the flag leaf size. It can be explained by the fact that larger leaves were able to produce, and transport assimilates to spikes more effectively, especially after re-watering and during the grain filling phase. Also, delayed heading was observed in plants with larger flag leaves, perhaps resulting from the plentiful introduction of heading-related alleles from Syrian parents instead of European parents used to develop the studied material (MCam lines), since the CamB1 genotype was earlier than the semi-dwarf genotype Maresi (Mikołajczak et al., 2017). As expected, abiotic stresses had a negative effect on phenotypic traits, mainly D and HD; however, tiller number and basal internode length increased. This agrees with our previous study on the effect on elevated temperature on barley phenotypes (Mikołajczak et al., 2022). Overall, evaluation of phenotypes and chlorophyll fluorescence parameters revealed the coincidence between effect of double stress and single drought as it was observed also at transcriptome level. Interestingly, the association network analysis revealed that increased expression of three genes corresponded significantly to reduced grain yield under drought and combined drought and heat. One of them encodes universal stress protein (USP), which is involved in a wide range of cellular responses and whose protective role against environmental stresses has been suggested (Chi et al., 2019). Loukehaich et al. (2012) reported that *UPS*-overexpressed tomato mutants had significantly increased ABA content. Therefore, it is tempting to speculate that overexpression of this gene in our study may correspond to an increased level of ABA under stress, and its overaccumulation may lead indirectly, e.g., *via* reduced photosynthesis, to reduced grain yield.

We inferred that the transcriptomic response to D and HD was functionally more concentrated than that of H, because in H the lowest number of enriched GO terms was observed. Functionally, the late response differed from the early ones mainly by activation of phosphorylation and dephosphorylation signaling. It plays one of the central roles in a plant's signalosome, since cascades of protein phosphorylation and dephosphorylation, mediated by kinases and phosphatases, transmit signals and influence gene expression to adapt the plant to stressors (Yang et al., 2021). Apparently, the defense mechanism of studied genotypes against stress was insufficient in the following days of stress, thus plants intensified the signal transduction *via* phosphorylation/dephosphorylation mechanism.

DEGs identified in most contrasts can be considered housekeeping genes required for plant functioning. Especially, genes regulated commonly across stress treatments can be suggested to be involved in the universal stress response, and thus they may constitute a promising target for plant

improvement under climate change (Prasch and Sonnewald, 2015). Based on GO enrichment analysis, we found that such genes were broadly associated with stress response, including drought, heat, oxidative stress, and response to reactive oxygen species, as well as with general processes like protein binding, or more specifically tetrapyrrole binding, and gibberellin 20-oxidase activity. These findings suggested that detoxification of reactive oxygen species mediated by tetrapyrroles (Busch and Montgomery, 2015) was the uniform mechanism to mitigate both drought and heat in our study. In turn, it is well documented that gibberellins (GAs) play a prominent role in whole-plant architecture formation, and GA signaling has been suggested to modulate stress tolerance, whereas GA-20-oxidases are crucial enzymes in the regulation of this phytohormone homeostasis (Kuczyńska et al., 2013; Colebrook et al., 2014). Hence it is justified that genes shared across stress treatments led to GA-20-oxidase term overrepresentation; furthermore, the fundamental role of *HvGa20ox2* linked to the *sdw1* locus has been widely discussed, and its paralogues have been identified in barley (Xu et al., 2017), and one was affected by elevated temperature (Mikołajczak et al., 2022). Photosynthesis-related genes were also identified here, as expected, since it is the most basic and critical process in green plants. Overall, the wide functional interpretation of genes affected by abiotic stress confirmed the enrichment of similar categories as for DEGs shared across treatments, and thus we concluded that the transcriptomic response of flag leaves was mainly concentrated on photosynthesis and adjustment to adverse conditions through numerous processes, including ABA signaling and scavenging of free radicals. Despite the large overlap between genes affected by combined stress and a single drought, a set of DEGs was found to be exclusively regulated during stress co-occurrence. Functionally, they were rather not concentrated, but the enrichment analysis suggested that the unique response to combined drought and heat could be partially determined by the specific activity of some enzymes (e.g., oxidoreductase) and transmembrane proteins (e.g., ion channels). Interpreting the set of DEGs assigned to selected functional GO annotations, we found more specific behavior in some genes. Stress-induced modulation of expression of photosynthesis-associated genes occurred more frequently in genotypes with the smallest flag leaf size, and they were majorly late-responsive to drought and combined stress. Several of them had modified expression only under HD. Transcriptomic changes in genotypes with medium flag leaf size were less numerous, but interestingly, they appeared in response to early stress and were maintained for the following days. These findings overlapped the overall conclusion driven from the whole-genome expression analysis, i.e., genotypes of group S perceived stronger the prolonged stress, while genotypes in group M responded quicker and, in that way, extended stress was not so perturbing at the transcriptome level. Noteworthy, part of this reaction of group M was exclusive, i.e., in terms of the oxidative, osmotic, and heat responses.

Most photosynthesis-related genes were downregulated under constrained conditions, but literally, those who had increased expression were of special interest since such genes can be the target of plant stress tolerance improvement. For example, Liang et al. (2019) proved that drought-tolerant mutants of *Arabidopsis* and *Brassica napus* overexpressed photosynthetic genes during exposition to stress. We found some of these DEGs being upregulated under elevated temperature treatment, especially in short-term stress, but note that heat was not as harmful to plants as drought in our study. Interestingly, we found the HORVU2Hr1G090070 gene, annotated to encode a PsbQ-like protein—a component of the oxygen evolving complex (OEC)—to be overexpressed specifically in genotypes of small flag leaf under late drought. OEC is an essential part of photosystem PSII and catalyzes the separation of molecular oxygen from the water; however, the influence of abiotic stress on OCE functioning has not attracted the relevant attention of researchers so far (Gupta, 2020). Daszkowska-Golec et al. (2019) observed decreased expression of genes encoding components of OEC, e.g., PsbO protein (HORVU2HR1G057700), in barley exposed to drought along with reduced photosynthesis efficiency. Hence, we assumed that upregulation of HORVU2Hr1G090070 can affect positively the photosynthetic activity and supposedly its overexpression may compensate partially the plentiful downregulation of photosynthetic-related genes in genotypes of group S under drought. Other genes upregulated under D and HD in genotypes of groups S and M were assigned to chloroplast GO term and encoded high molecular mass early light-inducible protein (ELIP) HV58, malic enzyme or unknow proteins involved in arginine and proline metabolism and HSFA7/HSFA6B-regulatory network-induced by drought and ABA. All of them have been shown to participate in the defense system against stress factors in various species; malic enzyme increases water use efficiency while improving photosynthesis (Sun et al., 2019); ELIP, although less recognized, has been indicated to protect *Arabidopsis* from photooxidative stress (Hutin et al., 2003). On the other hand, the unique overexpression of 9-cis-poxycarotenoid dioxygenase (*NCED*) encoding genes was found in group M (under D and HD), and it is worth mentioning that rice *NCED3*-overexpressing mutants had increased ABA content and enhanced drought and salt tolerance (Huang et al., 2018). These genes are not remarkably studied in barley, and our evidence may bring a new direction in the further improvement of cereals.

Next, we focused on DEGs assigned to drought and the ABA response, whose expression was mostly enhanced under long-term D and HD, independently of flag leaf size. Again, they were early-responsive to stress in genotypes in group M. They were the most numerously represented by dehydrin-encoding genes, which was reasonable due to the well-known multifunctional role of dehydrins in plants' adjustment to environmental hazards. It has been reported that some dehydrins can be

affected by ABA (Yang et al., 2015), so it was justified that DEGs of dehydrins identified in the present study were annotated to both drought- and ABA-related GO terms. Principally, dehydrins are responsible for stabilizing membranes and enzymes under abiotic stress. Dehydrin-overexpressed mutants of *Arabidopsis* showed enhanced tolerance to drought and salinity (Li et al., 2017). Thirteen dehydrin-encoding genes were identified in the barley genome (Tommasini et al., 2008); eight of these genes were found to be differentially expressed in our experiment, and their upregulation is consistent with the findings of Suprunova et al. (2004), who observed an increased abundance of dehydrin transcripts in wild barley exposed to drought. It is worth mentioning that overexpression of several genes encoding dehydrins was also detected in the flag leaf of the drought-tolerant barley cv. Yousef under conditions of water scarcity (Karami et al., 2013). Interestingly, gene HORVU4Hr1G074130 encoding annexin (D4-like) was exclusively upregulated in genotypes of group M under prolonged drought and its combination with heat, whereas HORVU7Hr1G037080 encoding annexin D1 was overexpressed specifically in genotypes of groups S and L. This may indicate that the inaction of the one gene can be compensated by the activity of the other. Drought-induced upregulation of HORVU7Hr1G037080 was also documented in the study of Harb et al. (2020). Annexins are an important component of Ca^{2+} signaling and alleviate oxidative stress. In *Arabidopsis*, enhanced expression of the annexin-1-encoding gene improved drought tolerance (Konopka-Postupolska et al., 2009). We found genotype-independent upregulation of HORVU3Hr1G069590 under drought, being the ortholog of the *EM1* gene of *Arabidopsis*, which was probably activated in an ABA-dependent manner, i.e., transcription factor ABI5 is known to interact with this gene (Carles et al., 2002); however, we did not observe *HvABI5* to be affected by stress treatments. Presumably, an alternative ABA-dependent regulator of the *EM1* gene may exist as suggested in *Arabidopsis* where *AtABI5* was active only in young seedlings (Yoshida et al., 2015). Additionally, post-translational modifications of ABI5 may occur (Zhou et al., 2015). Other known targets of *ABI5* are genes encoding HVA1 and HVA22 proteins of the LEA family, which ensure cell protection from water deprivation (Casaretto and Ho, 2003). Collin et al. (2020) confirmed upregulation of both genes in barley under drought, whereas we found the HVA22-encoding gene to be overexpressed under extended D and HD (excluding genotypes of group S). However, HORVU4Hr1G074710 putatively associated with HVA1—corresponding Interpro identifier (IPR004238) was assigned to HVA1 according to Uniprot database—had also enhanced expression in genotypes of groups S and M (also in T1) under D and HD in T2. This indicated that both genes were rather late-responsive to stress and their functioning could be interchangeable. Overall, consistent with previous reports, we observed several LEA proteins encoding genes to be upregulated under stress treatments, excluding heat. It was not surprising because LEA proteins were reported to be induced mainly by drought, salinity, and freezing (Kamarudin et al., 2019). Unexpectedly, three LEA-associated genes were downregulated, especially under combinatorial stress. Explanation of this phenomenon in the based on literature data remains enigmatic. Perhaps specific LEAs may play a unique role in response to multiple stresses that has not been discovered yet. Interestingly, decreased expression of genes encoding PYL (Pyrabactin Resistance-like) was found. It is the regulatory component of the ABA receptor that is the best characterized ABA perception mechanism in plants (Verma et al., 2019). Particularly interesting behavior of these genes was detected in genotypes of group S, i.e., HORVU7Hr1G088140 encoding PYL2 was induced by short-term HD, whereas HORVU4Hr1G055220 encoding PYL4 was late-responsive to D and HD. In response to abiotic stress, ABA biosynthesis is promoted in order to activate the expression of stress-responsive genes, but the balance of its level is required during plant adaptation to stress since too high an ABA content can have negative consequences, e.g., reduced photosynthesis efficiency (Wang et al., 2018a). We suggested that reduced expression of PYL encoding genes resulted from the need to limit ABA perception to maintain a certain equilibrium of hormone under constrained conditions. Our conclusion is supported by Xu and Zhu (2020), who examined ABA-deficient signaling mutants of *Arabidopsis* and reported that the negative impact of a high level of ABA was mitigated by blocking its signaling.

Enrichment analysis of GO terms revealed a set of heat-associated genes whose expression pattern was ambiguous. Most of them corresponded to heat shock proteins being, in general, upregulated in response to D and HD and not affected by H. Initially HSPs were believed to be stimulated by high temperature, but nowadays they are known to be induced by various stresses including biotic factors (Park and Seo, 2015). Nonetheless, the extraordinary reduction of several HSPs encoding genes was identified in genotypes of group M in T2 under single heat. Also, prolonged double stress caused the inversion of the regulatory status of two genes encoding HSP20, changing it from positive (early stress) to negative. These were unusual findings since HSP-encoding genes are commonly overexpressed under stress conditions; however, very incidental reports also confirmed the negative effect of heat on the regulation of HSP20 (reviewed by Ul Haq et al., 2019). HSPs' functioning is coordinated by heat shock factors; thus, in our study, downregulation of the above-mentioned genes could be associated with an overlapped decrease in HORVU4Hr1G090090 expression under heat, which encodes HSF (the putative ortholog of *Arabidopsis* HSFC1).

A multifunction of lipids has been documented, including maintenance of cell membrane integrity or signaling in response to stressors (Mamode Cassim et al., 2019), resulting in the

predominant overexpression of genes associated with lipid transport proteins (LTPs) under drought and combined stress. Seventy LTPs encoding genes distributed onto all chromosomes were found in barley; such omnipresence confirms their wide role in plant functioning (Zhang et al., 2019). Interestingly, three DEGs of LTP2-like genes were found in our study, and HORVU1Hr1G083170 was also identified by Duo et al. (2021), and it responded to drought, cold, and salinity in roots and in developing grain. In general, the expression of LTP2-encoding genes has been suggested to be specific to the barley aleurone layer (Opsahl-Sorteberg et al., 2004). Hence, our study provided novel data on stress-induced expression of *HvLTP2* in vegetative tissue of barley. Supposedly, heavy stress caused overproduction of LTP2 protein to be transported from the flag leaf to the developing spike, since the flag leaf is an important reservoir of compounds.

During the analysis of DEGs associated with leaf development, a curious behavior of genotypes in groups S and L was observed. Although their flag leaves were morphologically distant, the common regulatory status of three DEGs under prolonged stress was revealed, i.e., the *RL9* gene (the ortholog of *KANADI* in *Arabidopsis*) and genes encoding YABBY and cytochrome P450. All of them were downregulated under D or HD, and in fact, all may correspond to leaf rolling. Apart from known leaf rolling genes (e.g., *RL9*; Yan et al., 2008), the overexpression of the YABBY (key transcription factor affecting leaf blade and floral organ development; Romanova et al., 2021) encoded gene also resulted in leaf curling in *Arabidopsis* (Yang et al., 2019). In turn, cytochromes P450 belong to a large superfamily of enzymes involved in multiple regulatory mechanisms, including phytohormonal signaling, and therefore they influence plant development. Zhang et al. (2021) proved that cytochrome P450 influenced flag leaf shape in transgenic rice. Leaf rolling is a well-known defense phenomenon under drought to limit leaf area and decrease transpiration as a consequence (Kadioglu et al., 2012). Altogether, these results may indicate some disturbances in flag leaf rolling under stress treatments, which seems to be especially relevant for genotypes of group S where stronger perception of stress causes more intense re-modeling of the transcriptome, as we discussed above.

Afterwards, we attempted to deduce whether differential expression of genes can result from SNP polymorphisms between genotypes. We found that about 18% of DEGs contained at least one SNP mutation. Analyzing individual DEGs with SNPs of HIGH translation effect, we were not able to confirm such a relationship; it was incidental. Additionally, according to PCoA analysis on log2FC values for gene expression contrasts and PCoA on SNP markers there was no general coincidence between SNP polymorphism of genotypes and differential expression of genes induced by stress factors. Enrichment of GO terms of genes with SNPs of HIGH translation effects showed that the ABC-type transporter activity differentiated functionally genotypes the most. The ATP-binding cassette (ABC) transporters belong to a large protein family and execute a multitude of biological functions, constituting a fundamental part of the plant regulome (Kang et al., 2011). Despite the importance of ABC transporters, they have not been thoroughly studied in barley so far. Phylogenetic analysis of ABC transporters encoding genes in barley revealed 131 candidate genes, and the stress-induced expression of only several of them was evaluated by Zhang et al. (2020). The expansion of this research area of barley seems inevitable in the near future.

Conclusions

Genome-wide scale transcriptomics provided a pioneering insight into genes' behavior in barley flag leaf exposed to drought, elevated temperature, and their combination. Our study demonstrated that, under combined stress, drought was the dominant factor affecting gene expression. It was also confirmed for phenotypic traits and chlorophyll fluorescence parameters. Drought- and heat-responsive genes were identified, including those associated with photosynthesis, abscisic acid signaling, and lipid transport. Interestingly, our study provided novel data on stress-induced expression of *HvLTP2* genes in vegetative tissue of barley. A set of genes annotated to different functions were identified as being shared across stress treatments, e.g., genes encoding LEA proteins, including dehydrins and HSPs. They can determine the universal stress response and thus constitute a promising target for cereal improvement against multiple abiotic stresses. Likewise, regulation of genes involved in signal transduction mediated by phosphorylation and dephosphorylation may be an effective tool for adaptation to prolonged abiotic stress, as indicated in the present study. Genes encoding enzymes, transmembrane proteins, and regulating photosynthetic efficiency that were specifically affected by combined drought and heat can also pave the way for cereals' improvement against multiple abiotic stresses. Some relationship between flag leaf size and stress response was detected: we assumed that genotypes with a small flag leaf perceived stronger the prolonged stress, while genotypes with medium flag leaf responded quicker (e.g., dehydrin encoding genes), thus probably the extended stress was not so perturbing at transcriptome level; flag leaf-dependent reduction of grain yield confirmed this assumption. Stress-induced genes specific to flag leaf size were also found, e.g., genes encoding the OEC (group S) complex or *HvNCED* (group M). No general coincidence between SNP polymorphism of genotypes and differential expression of genes induced by stress factors was observed.

Data availability statement

The RNA-seq data presented in the study are deposited in the ArrayExpress repository, accession number E-MTAB-12438.

Author contributions

KM and AK conceived and designed the study. KM obtained of funding and administrated the project. KM, AK, and MK performed the experiments and collected the data. PK and MN processed the raw data and conducted statistical and bioinformatics analyses. KM interpreted the data, drafted, and revised the manuscript with subsequent critical input and approval by all authors. KM is responsible for the manuscript as a whole.

Funding

The research was financially supported by the National Science Centre, Poland, project Sonata 12 no. 2016/23/D/NZ9/00043. The funders had no role in study design, collection, analysis and interpretation of data, decision to publish, or preparation of the manuscript.

Acknowledgments

Computations were performed in part with the support of Poznań Supercomputing and Networking Centre (http://www.man.poznan.pl).

Conflict of interest

The authors declare that the research was conducted in the absence of any commercial or financial relationships that could be construed as a potential conflict of interest.

Publisher's note

All claims expressed in this article are solely those of the authors and do not necessarily represent those of their affiliated organizations, or those of the publisher, the editors and the reviewers. Any product that may be evaluated in this article, or claim that may be made by its manufacturer, is not guaranteed or endorsed by the publisher.

Supplementary material

The Supplementary Material for this article can be found online at: https://www.frontiersin.org/articles/10.3389/fpls.2022.1096685/full#supplementary-material

References

Ahmed, I. M., Cao, F., Zhang, M., Chen, X., Zhang, G., and Wu, F. (2013). Difference in yield and physiological features in response to drought and salinity combined stress during anthesis in Tibetan wild and cultivated barleys. *PLoS One* 8, e77869. doi: 10.1371/journal.pone.0077869

Baniwal, S. K., Bharti, K., Chan, K. Y., Fauth, M., Ganguli, A., Kotak, S., et al. (2004). Heat stress response in plants: a complex game with chaperones and more than twenty heat stress transcription factors. *J. Biosci.* 29, 471–487. doi: 10.1007/BF02712120

Busch, A. W. U., and Montgomery, B. L. (2015). Interdependence of tetrapyrrole metabolism, the generation of oxidative stress and the mitigative oxidative stress response. *Redox Biol.* 4, 260–271. doi: 10.1016/J.REDOX.2015.01.010

Carles, C., Bies-Etheve, N., Aspart, L., Leon-Kloosterziel, K. M., Koornneef, M., Echeverria, M., et al. (2002). Regulation of *Arabidopsis thaliana em* genes: role of *ABI5*. *Plant J.* 30, 373–383. doi: 10.1046/j.1365-313X.2002.01295.x

Casaretto, J., and Ho, T. D. (2003). The transcription factors HvABI5 and HvVP1 are required for the abscisic acid induction of gene expression in barley aleurone cells. *Plant Cell* 15, 271–284. doi: 10.1105/tpc.007096

Chang, H.-C., Tang, Y.-C., Hayer-Hartl, M., and Hartl, F. U. (2007). SnapShot: Molecular chaperones, part I. *Cell* 128, 212.e1–212.e2. doi: 10.1016/J.CELL.2007.01.001

Chi, Y. H., Koo, S. S., Oh, H. T., Lee, E. S., Park, J. H., Phan, K. A. T., et al. (2019). The physiological functions of universal stress proteins and their molecular mechanism to protect plants from environmental stresses. *Front. Plant Sci.* 10. doi: 10.3389/fpls.2019.00750

Colebrook, E. H., Thomas, S. G., Phillips, A. L., and Hedden, P. (2014). The role of gibberellin signalling in plant responses to abiotic stress. *J. Exp. Biol.* 217, 67–75. doi: 10.1242/jeb.089938

Collin, A., Daszkowska-Golec, A., Kurowska, M., and Szarejko, I. (2020). Barley *ABI5* (*Abscisic acid insensitive 5*) is involved in abscisic acid-dependent drought response. *Front. Plant Sci.* 11 1138. doi: 10.3389/fpls.2020.01138

Contiliani, D. F., de Oliveira Nebó, J. F. C., Ribeiro, R. V., Andrade, L. M., Peixoto Júnior, R. F., Lembke, C. G., et al. (2022). Leaf transcriptome profiling of contrasting sugarcane genotypes for drought tolerance under field conditions. *Sci. Rep.* 12 9153. doi: 10.1038/s41598-022-13158-5

Daszkowska-Golec, A., Collin, A., Sitko, K., Janiak, A., Kalaji, H. M., and Szarejko, I. (2019). Genetic and physiological dissection of photosynthesis in barley exposed to drought stress. *Int. J. Mol. Sci.* 20. doi: 10.3390/ijms20246341

Daszkowska-Golec, A., Skubacz, A., Marzec, M., Slota, M., Kurowska, M., Gajecka, M., et al. (2017). Mutation in *HvCBP20* (*Cap binding protein 20*) adapts barley to drought stress at phenotypic and transcriptomic levels. *Front. Plant Sci.* 8. doi: 10.3389/fpls.2017.00942

dos Santos, T. B., Ribas, A. F., de Souza, S. G. H., Budzinski, I. G. F., and Domingues, D. S. (2022). Physiological responses to drought, salinity, and heat stress in plants: A review. *Stresses* 2, 113–135. doi: 10.3390/stresses2010009

Duo, J., Xiong, H., Wu, X., Li, Y., Si, J., Zhang, C., et al. (2021). Genome-wide identification and expression profile under abiotic stress of the barley *non-specific lipid transfer protein* gene family and its qingke orthologues. *BMC Genomics* 22, 674. doi: 10.1186/s12864-021-07958-8

Fidler, J., Zdunek-Zastocka, E., Bielawski, W., and Bielawski, W. (2015). Regulation of abscisic acid metabolism in relation to the dormancy and germination of cereal grains. *Acta Soc Bot. Pol.* 84, 3–11. doi: 10.5586/asbp.2015.004

Gharaghanipor, N., Arzani, A., Rahimmalek, M., and Ravash, R. (2022). Physiological and transcriptome indicators of salt tolerance in wild and cultivated barley. *Front. Plant Sci.* 13 1039. doi: 10.3389/fpls.2022.819282

Gupta, R. (2020). The oxygen-evolving complex: A super catalyst for life on earth, in response to abiotic stresses. *Plant Signal. Behav.* 15, 1824721. doi: 10.1080/15592324.2020.1824721

Gürel, F., Öztürk, Z. N., Uçarlı, C., and Rosellini, D. (2016). Barley genes as tools to confer abiotic stress tolerance in crops. *Front. Plant Sci.* 7. doi: 10.3389/fpls.2016.01137

Harb, A., Simpson, C., Guo, W., Govindan, G., Kakani, V. G., and Sunkar, R. (2020). The effect of drought on transcriptome and hormonal profiles in barley genotypes with contrasting drought tolerance. *Front. Plant Sci.* 11 2060. doi: 10.3389/fpls.2020.618491

Henry, R. J. (2020). Innovations in plant genetics adapting agriculture to climate change. *Curr. Opin. Plant Biol.* 56, 168–173. doi: 10.1016/J.PBI.2019.11.004

Hosseini, S. A., Hajirezaei, M. R., Seiler, C., Sreenivasulu, N., and von Wirén, N. (2016). A potential role of flag leaf potassium in conferring tolerance to drought-induced leaf senescence in barley. *Front. Plant Sci.* 7. doi: 10.3389/fpls.2016.00206

Hsu, P., Dubeaux, G., Takahashi, Y., and Schroeder, J. I. (2021). Signaling mechanisms in abscisic acid-mediated stomatal closure. *Plant J.* 105, 307–321. doi: 10.1111/tpj.15067

Huang, Y., Guo, Y., Liu, Y., Zhang, F., Wang, Z., Wang, H., et al. (2018). 9-cis-Epoxycarotenoid dioxygenase 3 regulates plant growth and enhances multi-abiotic stress tolerance in rice. *Front. Plant Sci.* 9. doi: 10.3389/fpls.2018.00162

Hutin, C., Nussaume, L., Moise, N., Moya, I., Kloppstech, K., and Havaux, M. (2003). Early light-induced proteins protect *Arabidopsis* from photooxidative stress. *Proc. Natl. Acad. Sci.* 100, 4921–4926. doi: 10.1073/pnas.0736939100

Intergovernmental Panel on Climate Change (2021). Future global climate: Scenario-based projections and near-term information. in climate change 2021: The physical science basis. contribution of working group I to the sixth assessment report of the intergovernmental panel on climate change. *Cambridge Univ. Press*, 553–672.

International Barley Genome Sequencing Consortium, Mayer, K. F. X., Waugh, R., Brown, J. W. S., Schulman, A., Langridge, P., et al. (2012). A physical, genetic and functional sequence assembly of the barley genome. *Nature* 491, 711–716. doi: 10.1038/nature11543

Janiak, A., Kwasniewski, M., Sowa, M., Kuczyńska, A., Mikołajczak, K., Ogrodowicz, P., et al. (2019). Insights into barley root transcriptome under mild drought stress with an emphasis on gene expression regulatory mechanisms. *Int. J. Mol. Sci.* 20. doi: 10.3390/ijms20246139

Jayakodi, M., Padmarasu, S., Haberer, G., Bonthala, V. S., Gundlach, H., Monat, C., et al. (2020). The barley pan-genome reveals the hidden legacy of mutation breeding. *Nature* 588, 284–289. doi: 10.1038/s41586-020-2947-8

Johnson, S. M., Lim, F.-L., Finkler, A., Fromm, H., Slabas, A. R., and knight, M. R. (2014). Transcriptomic analysis of sorghum bicolor responding to combined heat and drought stress. *BMC Genomics* 15, 456. doi: 10.1186/1471-2164-15-456

Kadioglu, A., Terzi, R., Saruhan, N., and Saglam, A. (2012). Current advances in the investigation of leaf rolling caused by biotic and abiotic stress factors. *Plant Sci.* 182, 42–48. doi: 10.1016/J.PLANTSCI.2011.01.013

Kamarudin, Z. S., Yusop, M. R., Ismail, M. R., Tengku Muda Mohamed, M., Harun, A. R., Yusuff, O., et al. (2019). LEA gene expression assessment in advanced mutant rice genotypes under drought stress. *Int. J. Genomics* 2019, 8406036. doi: 10.1155/2019/8406036

Kang, J., Park, J., Choi, H., Burla, B., Kretzschmar, T., Lee, Y., et al. (2011). Plant ABC transporters. *Arab. B.* 9, e0153. doi: 10.1199/tab.0153

Karami, A., Shahbazi, M., Niknam, V., Shobbar, Z. S., Tafreshi, R. S., Abedini, R., et al. (2013). Expression analysis of dehydrin multigene family across tolerant and susceptible barley (Hordeum vulgare l.) genotypes in response to terminal drought stress. *Acta Physiol. Plant* 35, 2289–2297. doi: 10.1007/s11738-013-1266-1

Kim, D., Pertea, G., Trapnell, C., Pimentel, H., Kelley, R., and Salzberg, S. L. (2013). TopHat2: accurate alignment of transcriptomes in the presence of insertions, deletions and gene fusions. *Genome Biol.* 14, R36. doi: 10.1186/gb-2013-14-4-r36

Konopka-Postupolska, D., Clark, G., Goch, G., Debski, J., Floras, K., Cantero, A., et al. (2009). The role of annexin 1 in drought stress in *Arabidopsis*. *Plant Physiol.* 150, 1394–1410. doi: 10.1104/pp.109.135228

Kosová, K., Vítámvás, P., and Prášil, I. T. (2014). Wheat and barley dehydrins under cold, drought, and salinity - what can LEA-II proteins tell us about plant stress response? *Front. Plant Sci.* 5. doi: 10.3389/fpls.2014.00343

Kuczyńska, A., Cardenia, V., Ogrodowicz, P., Kempa, M., Rodriguez-Estrada, M. T., and Mikołajczak, K. (2019). Effects of multiple abiotic stresses on lipids and sterols profile in barley leaves (*Hordeum vulgare* l.). *Plant Physiol. Biochem.* 141, 215–24. doi: 10.1016/j.plaphy.2019.05.033

Kuczyńska, A., Surma, M., Adamski, T., Mikołajczak, K., Krystkowiak, K., and Ogrodowicz, P. (2013). Effects of the semi-dwarfing *sdw1/denso* gene in barley. *J. Appl. Genet.* 54, 381–390. doi: 10.1007/s13353-013-0165-x

Kumar Pandey, G., Varotto, S., Ramegowda, V., Pandey, P., and Senthil-Kumar, M. (2015). Shared and unique responses of plants to multiple individual stresses and stress combinations: physiological and molecular mechanisms. *Front. Plant Sci.* 6. doi: 10.3389/fpls.2015.00723. www.frontiersin.org.

Langfelder, P., and Horvath, S. (2008). WGCNA: an r package for weighted correlation network analysis. *BMC Bioinf.* 9, 559. doi: 10.1186/1471-2105-9-559

Langfelder, P., and Horvath, S. (2012)Fast r functions for robust correlations and hierarchical clustering. Available at: http://www.ncbi.nlm.nih.gov/23050260 (Accessed October 19, 2022).

Li, H. (2011). A statistical framework for SNP calling, mutation discovery, association mapping and population genetical parameter estimation from sequencing data. *Bioinformatics* 27, 2987–2993. doi: 10.1093/bioinformatics/btr509

Liang, Y., Kang, K., Gan, L., Ning, S., Xiong, J., Song, S., et al. (2019). Drought-responsive genes, late embryogenesis abundant group3 (*LEA3*) and vicinal oxygen chelate, function in lipid accumulation in *Brassica napus* and *Arabidopsis* mainly *via* enhancing photosynthetic efficiency and reducing ROS. *Plant Biotechnol. J.* 17, 2123–2142. doi: 10.1111/pbi.13127

Liao, Y., Smyth, G. K., and Shi, W. (2019). The r package rsubread is easier, faster, cheaper and better for alignment and quantification of RNA sequencing reads. *Nucleic Acids Res.* 47, e47–e47. doi: 10.1093/nar/gkz114

Li, Q., Zhang, X., Lv, Q., Zhu, D., Qiu, T., Xu, Y., et al. (2017). Physcomitrella patens dehydrins (PpDHNA and PpDHNC) confer salinity and drought tolerance to transgenic arabidopsis plants. *Front. Plant Sci.* 8 1316. doi: 10.3389/fpls.2017.01316

Loukehaich, R., Wang, T., Ouyang, B., Ziaf, K., Li, H., Zhang, J., et al. (2012). SpUSP, an annexin-interacting universal stress protein, enhances drought tolerance in tomato. *J. Exp. Bot.* 63, 5593–5606. doi: 10.1093/jxb/ers220

Love, M. I., Huber, W., and Anders, S. (2014). Moderated estimation of fold change and dispersion for RNA-seq data with DESeq2. *Genome Biol.* 15, 550. doi: 10.1186/s13059-014-0550-8

Ma, Y., Cao, J., He, J., Chen, Q., Li, X., and Yang, Y. (2018). Molecular mechanism for the regulation of ABA homeostasis during plant development and stress responses. *Int. J. Mol. Sci.* 19. doi: 10.3390/ijms19113643

Mamode Cassim, A., Gouguet, P., Gronnier, J., Laurent, N., Germain, V., Grison, M., et al. (2019). Plant lipids: Key players of plasma membrane organization and function. *Prog. Lipid Res.* 73, 1–27. doi: 10.1016/j.plipres.2018.11.002

Mareri, L., Parrotta, L., and Cai, G. (2022). Environmental stress and plants. *Int. J. Mol. Sci.* 23 5416. doi: 10.3390/ijms23105416

Mascher, M., Gundlach, H., Himmelbach, A., Beier, S., Twardziok, S. O., Wicker, T., et al. (2017). A chromosome conformation capture ordered sequence of the barley genome. *Nature* 544, 427–433. doi: 10.1038/nature22043

Mascher, M., Wicker, T., Jenkins, J., Plott, C., Lux, T., Koh, C. S., et al. (2021). Long-read sequence assembly: a technical evaluation in barley. *Plant Cell* 33, 1888–1906. doi: 10.1093/plcell/koab077

McLaren, W., Pritchard, B., Rios, D., Chen, Y., Flicek, P., and Cunningham, F. (2010). Deriving the consequences of genomic variants with the ensembl API and SNP effect predictor. *Bioinformatics* 26, 2069–2070. doi: 10.1093/bioinformatics/btq330

Mikołajczak, K., Kuczyńska, A., Krajewski, P., Sawikowska, A., Surma, M., Ogrodowicz, P., et al. (2017). Quantitative trait loci for plant height in maresi × CamB barley population and their associations with yield-related traits under different water regimes. *J. Appl. Genet.* 58, 23–35. doi: 10.1007/s13353-016-0358-1

Mikołajczak, K., Kuczyńska, A., Ogrodowicz, P., Kiełbowicz-Matuk, A., Ćwiek-Kupczyńska, H., Daszkowska-Golec, A., et al. (2022). High-throughput sequencing data revealed genotype-specific changes evoked by heat stress in crown tissue of barley *sdw1* near-isogenic lines. *BMC Genomics* 23, 177. doi: 10.1186/s12864-022-08410-1

Mikołajczak, K., Ogrodowicz, P., Ćwiek-Kupczyńska, H., Weigelt-Fischer, K., Mothukuri, S. R., Junker, A., et al. (2020). Image phenotyping of spring barley (*Hordeum vulgare* l.) RIL population under drought: Selection of traits and biological interpretation. *Front. Plant Sci.* 11. doi: 10.3389/fpls.2020.00743

Mikołajczak, K., Ogrodowicz, P., Gudyś, K., Krystkowiak, K., Sawikowska, A., Frohmberg, W., et al. (2016). Quantitative trait loci for yield and yield-related traits in spring barley populations derived from crosses between European and Syrian cultivars. *PLoS One* 11. doi: 10.1371/journal.pone.0155938

Mishra, S. K., Poonia, A. K., Chaudhary, R., Baranwal, V. K., Arora, D., Kumar, R., et al. (2020). Genome-wide identification, phylogeny and expression analysis of

HSF gene family in barley during abiotic stress response and reproductive development. *Plant Gene* 23, 100231. doi: 10.1016/J.PLGENE.2020.100231

Monat, C., Padmarasu, S., Lux, T., Wicker, T., Gundlach, H., Himmelbach, A., et al. (2019). TRITEX: chromosome-scale sequence assembly of *Triticeae* genomes with open-source tools. *Genome Biol.* 20, 284. doi: 10.1186/s13059-019-1899-5

Niu, Y., Chen, T., Zheng, Z., Zhao, C., Liu, C., Jia, J., et al. (2022). A new major QTL for flag leaf thickness in barley (*Hordeum vulgare* l.). *BMC Plant Biol.* 22, 305. doi: 10.1186/s12870-022-03694-7

Ojanpera, K., Sutinen, S., Pleijel, H., and Sellden, G. (1992). Exposure of spring wheat, *Triticum aestivum* l., cv. drabant, to different concentrations of ozone in open-top chambers: effects on the ultrastructure of flag leaf cells. *New Phytol.* 120, 39–48. doi: 10.1111/j.1469-8137.1992.tb01056.x

Opsahl-Sorteberg, H.-G., Divon, H. H., Nielsen, P. S., Kalla, R., Hammond-Kosack, M., Shimamoto, K., et al. (2004). Identification of a 49-bp fragment of the *HvLTP2* promoter directing aleurone cell specific expression. *Gene* 341, 49–58. doi: 10.1016/J.GENE.2004.06.059

Oukarroum, A., Madidi, S., Schansker, G., and Strasser, R. J. (2007). Probing the responses of barley cultivars (*Hordeum vulgare* l.) by chlorophyll a fluorescence OLKJIP under drought stress and re-watering. *Environ. Exp. Bot.* 60, 438–446. doi: 10.1016/J.ENVEXPBOT.2007.01.002

Park, C.-J., and Seo, Y.-S. (2015). Heat shock proteins: A review of the molecular chaperones for plant immunity. *Plant Pathol. J.* 31, 323–333. doi: 10.5423/PPJ.RW.08.2015.0150

Perdomo, J. A., Conesa, M.À., Medrano, H., Ribas-Carbó, M., and Galmés, J. (2015). Effects of long-term individual and combined water and temperature stress on the growth of rice, wheat and maize: relationship with morphological and physiological acclimation. *Physiol. Plant* 155, 149–165. doi: 10.1111/ppl.12303

Prasad, P. V. V., Pisipati, S. R., Momčilović, I., and Ristic, Z. (2011). Independent and combined effects of high temperature and drought stress during grain filling on plant yield and chloroplast EF-tu expression in spring wheat. *J. Agron. Crop Sci.* 197, 430–441. doi: 10.1111/j.1439-037X.2011.00477.x

Prasch, C. M., and Sonnewald, U. (2015). Signaling events in plants: Stress factors in combination change the picture. *Environ. Exp. Bot.* 114, 4–14. doi: 10.1016/J.ENVEXPBOT.2014.06.020

Rampino, P., Mita, G., Fasano, P., Borrelli, G. M., Aprile, A., Dalessandro, G., et al. (2012). Novel durum wheat genes up-regulated in response to a combination of heat and drought stress. *Plant Physiol. Biochem.* 56, 72–78. doi: 10.1016/J.PLAPHY.2012.04.006

Rapazote-Flores, P., Bayer, M., Milne, L., Mayer, C.-D., Fuller, J., Guo, W., et al. (2019). BaRTv1.0: an improved barley reference transcript dataset to determine accurate changes in the barley transcriptome using RNA-seq. *BMC Genomics* 20, 968. doi: 10.1186/s12864-019-6243-7

Rasmussen, S., Barah, P., Suarez-Rodriguez, M. C., Bressendorff, S., Friis, P., Costantino, P., et al. (2013). Transcriptome responses to combinations of stresses in *Arabidopsis*. *Plant Physiol.* 161, 1783–1794. doi: 10.1104/pp.112.210773

Reddy, P. S., Kavi Kishor, P. B., Seiler, C., Kuhlmann, M., Eschen-Lippold, L., Lee, J., et al. (2014). Unraveling regulation of the small heat shock proteins by the heat shock factor *HvHsfB2c* in barley: Its implications in drought stress response and seed development. *PloS One* 9, e89125. doi: 10.1371/journal.pone.0089125

Rizhsky, L., Liang, H., Shuman, J., Shulaev, V., Davletova, S., and Mittler, R. (2004). When defense pathways collide. the response of *Arabidopsis* to a combination of drought and heat stress. *Plant Physiol.* 134, 1683–1696. doi: 10.1104/pp.103.033431

Romanova, M. A., Maksimova, A. I., Pawlowski, K., and Voitsekhovskaja, O. V. (2021). *YABBY* genes in the development and evolution of land plants. *Int. J. Mol. Sci.* 22. doi: 10.3390/ijms22084139

Scharf, K. D., Berberich, T., Ebersberger, I., and Nover, L. (2012). The plant heat stress transcription factor (Hsf) family: Structure, function and evolution. *Biochim. Biophys. Acta - Gene Regul. Mech.* 1819, 104–119. doi: 10.1016/J.BBAGRM.2011.10.002

Schubert, M., Lindgreen, S., and Orlando, L. (2016). AdapterRemoval v2: Rapid adapter trimming, identification, and read merging. *BMC Res. Notes* 9, 88. doi: 10.1186/s13104-016-1900-2

Siddiqui, M. H., Al-Khaishany, M. Y., Al-Qutami, M. A., Al-Whaibi, M. H., Grover, A., Ali, H. M., et al. (2015). Morphological and physiological characterization of different genotypes of faba bean under heat stress. *Saudi J. Biol. Sci.* 22, 656–663. doi: 10.1016/J.SJBS.2015.06.002

Strasser, R. J., Tsimilli-Michael, M., and Srivastava, A. (2004). "Analysis of the chlorophyll a fluorescence transient," in *Chlorophyll a fluorescence: A signature of photosynthesis*. Eds. G. C. Papageorgiou and Govindjee, (New York: Springer), 321–362. doi: 10.1007/978-1-4020-3218-9_12

Sun, X., Han, G., Meng, Z., Lin, L., and Sui, N. (2019). Roles of malic enzymes in plant development and stress responses. *Plant Signal. Behav.* 14, e1644596. doi: 10.1080/15592324.2019.1644596

Suprunova, T., Krugman, T., Fahima, T., Chen, G., Shams, I., Korol, A., et al. (2004). Differential expression of dehydrin genes in wild barley, *Hordeum spontaneum*, associated with resistance to water deficit. *Plant Cell Environ.* 27, 1297–1308. doi: 10.1111/j.1365-3040.2004.01237.x

Suzuki, N., Rivero, R. M., Shulaev, V., Blumwald, E., and Mittler, R. (2014). Abiotic and biotic stress combinations. *New Phytol.* 203, 32–43. doi: 10.1111/nph.12797

Svoboda, P., Janská, A., Spiwok, V., Prášil, I. T., Kosová, K., Vítámvás, P., et al. (2016). Global scale transcriptional profiling of two contrasting barley genotypes exposed to moderate drought conditions: Contribution of leaves and crowns to water shortage coping strategies. *Front. Plant Sci.* 7. doi: 10.3389/fpls.2016.01958

Szurman-Zubrzycka, M., Chwiałkowska, K., Niemira, M., Kwaśniewski, M., Nawrot, M., Gajecka, M., et al. (2021). Aluminum or low pH – which is the bigger enemy of barley? transcriptome analysis of barley root meristem under Al and low pH stress. *Front. Genet.* 12. doi: 10.3389/fgene.2021.675260

Templer, S. E., Ammon, A., Pscheidt, D., Ciobotea, O., Schuy, C., McCollum, C., et al. (2017). Metabolite profiling of barley flag leaves under drought and combined heat and drought stress reveals metabolic QTLs for metabolites associated with antioxidant defense. *J. Exp. Bot.* 68, 1697–1713. doi: 10.1093/jxb/erx038

Tommasini, L., Svensson, J. T., Rodriguez, E. M., Wahid, A., Malatrasi, M., Kato, K., et al. (2008). Dehydrin gene expression provides an indicator of low temperature and drought stress: transcriptome-based analysis of barley (*Hordeum vulgare* l.). *Funct. Integr. Genomics* 8, 387–405. doi: 10.1007/s10142-008-0081-z

Ul Haq, S., Khan, A., Ali, M., Khattak, A. M., Gai, W.-X., Zhang, H.-X., et al. (2019). Heat shock proteins: Dynamic biomolecules to counter plant biotic and abiotic stresses. *Int. J. Mol. Sci.* 20. doi: 10.3390/ijms20215321

van Heerden, P. D. R., Swanepoel, J. W., and Krüger, G. H. J. (2007). Modulation of photosynthesis by drought in two desert scrub species exhibiting C3-mode CO2 assimilation. *Environ. Exp. Bot.* 61, 124–136. doi: 10.1016/J.ENVEXPBOT.2007.05.005

Verma, V., Foulkes, M. J., Worland, A. J., Sylvester-Bradley, R., Caligari, P. D. S., and Snape, J. W. (2004). Mapping quantitative trait loci for flag leaf senescence as a yield determinant in winter wheat under optimal and drought-stressed environments. *Euphytica* 135, 255–263. doi: 10.1023/B:EUPH.0000013255.31618.14

Verma, R. K., Santosh Kumar, V. V., Yadav, S. K., Pushkar, S., Rao, M. V., and Chinnusamy, V. (2019). Overexpression of ABA receptor *PYL10* gene confers drought and cold tolerance to indica rice. *Front. Plant Sci.* 10. doi: 10.3389/fpls.2019.01488

VSN International (2017). *Genstat for windows 19th edition* (UK: VSN Int. Hemel Hempstead).

Wang, M., Lee, J., Choi, B., Park, Y., Sim, H.-J., Kim, H., et al. (2018a). Physiological and molecular processes associated with long duration of ABA treatment. *Front. Plant Sci.* 9. doi: 10.3389/fpls.2018.00176

Wang, R.-S., Oldham, W. M., Maron, B. A., and Loscalzo, J. (2018b). Systems biology approaches to redox metabolism in stress and disease states. *Antioxid. Redox Signal.* 29, 953–972. doi: 10.1089/ars.2017.7256

Wehner, G., Balko, C., Humbeck, K., Zyprian, E., and Ordon, F. (2016). Expression profiling of genes involved in drought stress and leaf senescence in juvenile barley. *BMC Plant Biol.* 16, 3. doi: 10.1186/s12870-015-0701-4

Willick, I. R., Lahlali, R., Vijayan, P., Muir, D., Karunakaran, C., and Tanino, K. K. (2018). Wheat flag leaf epicuticular wax morphology and composition in response to moderate drought stress are revealed by SEM, FTIR-ATR and synchrotron X-ray spectroscopy. *Physiol. Plant* 162, 316–332. doi: 10.1111/ppl.12637

Xiao, B., Huang, Y., Tang, N., and Xiong, L. (2007). Over-expression of a *LEA* gene in rice improves drought resistance under the field conditions. *Theor. Appl. Genet.* 115, 35–46. doi: 10.1007/s00122-007-0538-9

Xu, Y., Jia, Q., Zhou, G., Zhang, X.-Q., Angessa, T., Broughton, S., et al. (2017). Characterization of the *sdw1* semi-dwarf gene in barley. *BMC Plant Biol.* 17, 11. doi: 10.1186/s12870-016-0964-4

Xu, Y., and Zhu, Z. (2020). Abscisic acid suppresses thermomorphogenesis in *Arabidopsis thaliana*. *Plant Signal. Behav.* 15, 1746510. doi: 10.1080/15592324.2020.1746510

Yang, X., Lu, M., Wang, Y., Wang, Y., Liu, Z., and Chen, S. (2021). Response mechanism of plants to drought stress. *Horticulturae* 7, 50. doi: 10.3390/horticulturae7030050

Yang, H., Shi, G., Li, X., Hu, D., Cui, Y., Hou, J., et al. (2019). Overexpression of a soybean *YABBY* gene, *GmFILa*, causes leaf curling in *Arabidopsis thaliana*. *BMC Plant Biol.* 19, 234. doi: 10.1186/s12870-019-1810-2

Yang, W., Zhang, L., Lv, H., Li, H., Zhang, Y., Xu, Y., et al. (2015). The K-segments of wheat dehydrin WZY2 are essential for its protective functions under temperature stress. *Front. Plant Sci.* 6. doi: 10.3389/fpls.2015.00406

Yan, S., Yan, C.-J., Zeng, X.-H., Yang, Y.-C., Fang, Y.-W., Tian, C.-Y., et al. (2008). *Rolled leaf 9*, encoding a GARP protein, regulates the leaf abaxial cell fate in rice. *Plant Mol. Biol.* 68, 239–250. doi: 10.1007/s11103-008-9365-x

Yoshida, T., Fujita, Y., Maruyama, K., Mogami, J., Todaka, D., Shinozaki, K., et al. (2015). Four *Arabidopsis* AREB/ABF transcription factors function predominantly in gene expression downstream of SnRK2 kinases in abscisic acid signalling in response to osmotic stress. *Plant Cell Environ.* 38, 35–49. doi: 10.1111/pce.12351

Yu, Z., Wang, X., and Zhang, L. (2018). Structural and functional dynamics of dehydrins: A plant protector protein under abiotic stress. *Int. J. Mol. Sci.* 19. doi: 10.3390/ijms19113420

Zandalinas, S. I., Balfagón, D., Arbona, V., Gómez-Cadenas, A., Inupakutika, M. A., and Mittler, R. (2016). ABA is required for the accumulation of APX1 and MBF1c during a combination of water deficit and heat stress. *J. Exp. Bot.* 67, 5381–5390. doi: 10.1093/jxb/erw299

Zeng, X., Bai, L., Wei, Z., Yuan, H., Wang, Y., Xu, Q., et al. (2016). Transcriptome analysis revealed the drought-responsive genes in Tibetan hulless barley. *BMC Genomics* 17, 386. doi: 10.1186/s12864-016-2685-3

Zhang, M., Kim, Y., Zong, J., Lin, H., Dievart, A., Li, H., et al. (2019). Genome-wide analysis of the barley non-specific lipid transfer protein gene family. *Crop J.* 7, 65–76. doi: 10.1016/J.CJ.2018.07.009

Zhang, Z., Tong, T., Fang, Y., Zheng, J., Zhang, X., Niu, C., et al. (2020). Genome-wide identification of barley *ABC* genes and their expression in response to abiotic stress treatment. *Plants (Basel Switzerland)* 9. doi: 10.3390/plants9101281

Zhang, X., Wang, Y., Zhu, X., Wang, X., Zhu, Z., Li, Y., et al. (2021). *Curled flag leaf 2*, encoding a cytochrome P450 protein, regulated by the transcription factor Roc5, influences flag leaf development in rice. *Front. Plant Sci.* 11 2297. doi: 10.3389/fpls.2020.616977

Zhao, J., Lu, Z., Wang, L., and Jin, B. (2020). Plant responses to heat stress: Physiology, transcription, noncoding RNAs, and epigenetics. *Int. J. Mol. Sci.* 22. doi: 10.3390/ijms22010117

Zhou, X., Hao, H., Zhang, Y., Bai, Y., Zhu, W., Qin, Y., et al. (2015). SOS2-like protein kinase5, an SNF1-related protein kinase3-type protein pinase, is important for abscisic acid responses in *Arabidopsis* through phosphorylation of abscisic acid insensitive5. *Plant Physiol.* 168, 659–676. doi: 10.1104/pp.114.255455

frontiers | Frontiers in Plant Science

TYPE Original Research
PUBLISHED 25 January 2023
DOI 10.3389/fpls.2022.1041649

Check for updates

OPEN ACCESS

EDITED BY
Mahmoud Magdy,
Ain Shams University, Egypt

REVIEWED BY
Juan De Dios Franco-Navarro,
Hospital Universitario Puerto Real, Spain
Aziz Ebrahimi,
Purdue University, United States
Mohamed Ahmed Abbas Mahmoud,
Ain Shams University, Egypt
Mohamed Mahmoud Aboul Fotouh,
Ain Shams University, Egypt

*CORRESPONDENCE
Foad Fatehi
ffatehi@pnu.ac.ir

SPECIALTY SECTION
This article was submitted to Plant Abiotic Stress, a section of the journal Frontiers in Plant Science

RECEIVED 11 September 2022
ACCEPTED 28 December 2022
PUBLISHED 25 January 2023

CITATION
Pakzad R, Fatehi F, Kalantar M and Maleki M (2023) Proteomics approach to investigating osmotic stress effects on pistachio.
Front. Plant Sci. 13:1041649.
doi: 10.3389/fpls.2022.1041649

COPYRIGHT
© 2023 Pakzad, Fatehi, Kalantar and Maleki. This is an open-access article distributed under the terms of the Creative Commons Attribution License (CC BY). The use, distribution or reproduction in other forums is permitted, provided the original author(s) and the copyright owner(s) are credited and that the original publication in this journal is cited, in accordance with accepted academic practice. No use, distribution or reproduction is permitted which does not comply with these terms.

Proteomics approach to investigating osmotic stress effects on pistachio

Rambod Pakzad[1], Foad Fatehi[2]*, Mansour Kalantar[1] and Mahmood Maleki[3]

[1]Department of Plant Breeding, Yazd Branch, Islamic Azad University, Yazd, Iran, [2]Department of Agriculture, Payame Noor University (PNU), Tehran, Iran, [3]Department of Biotechnology, Institute of Science and High Technology and Environmental Sciences, Graduate University of Advanced Technology, Kerman, Iran

Osmotic stress can occur due to some stresses such as salinity and drought, threatening plant survival. To investigate the mechanism governing the pistachio response to this stress, the biochemical alterations and protein profile of PEG-treated plants was monitored. Also, we selected two differentially abundant proteins to validate *via* Real-Time PCR. Biochemical results displayed that in treated plants, proline and phenolic content was elevated, photosynthetic pigments except carotenoid decreased and MDA concentration were not altered. Our findings identified a number of proteins using 2DE-MS, involved in mitigating osmotic stress in pistachio. A total of 180 protein spots were identified, of which 25 spots were altered in response to osmotic stress. Four spots that had photosynthetic activities were down-regulated, and the remaining spots were up-regulated. The biological functional analysis of protein spots exhibited that most of them are associated with the photosynthesis and metabolism (36%) followed by stress response (24%). Results of Real-Time PCR indicated that two of the representative genes illustrated a positive correlation among transcript level and protein expression and had a similar trend in regulation of gene and protein. Osmotic stress set changes in the proteins associated with photosynthesis and stress tolerance, proteins associated with the cell wall, changes in the expression of proteins involved in DNA and RNA processing occur. Findings of this research will introduce possible proteins and pathways that contribute to osmotic stress and can be considered for improving osmotic tolerance in pistachio.

KEYWORDS

dehydration, osmotic stress, pistachio, proteomics, stress response

Introduction

Since plants are sessile, they could not change their location and are continuously subjected to various stresses that threaten their survival. Osmotic stress, which results from abiotic stresses such as salinity, drought, and cold, and is one of the most common stresses in nature, is caused by a decrease in water potential in the environment around the roots (Xiong

and Zhu, 2002; Zang and Komatsu, 2007; Toorchi et al., 2009), which limits the plant's ability to absorb water and restricts water accessibility (Zang and Komatsu, 2007). Osmotic stress appears in various morphological, physiological, and biochemical dimensions in the plant. Tolerance to stress is a complicated phenomenon. To deal with this stress, plants trigger a variety of response mechanisms that require three steps of stress recognition, signal transduction, and the generation of related response components (Zang and Komatsu, 2007; Zhou et al., 2012). These responses enable plants to save water and reprogram cell metabolism for adaptation to stress (Ngara et al., 2018).

Plant survival against stress requires the rearrangement of many molecular processes and reregulation of many genes. Examination of mRNA expression is not sufficient to predict the events that occur in the plant during exposure to stress because there is a low correlation between the abundance of mRNAs and proteins (Wang et al., 2020). Moreover, proteins play important roles in all cellular processes such as gene regulation, transcription, translation, cell detoxification, protection of macromolecules, and osmotic adjustment (Pasaribu et al., 2021). Hence, studying the expression of proteins provides us with more information about plant behavior under stress. Numerous studies show that proteomics is a beneficial tool for analyzing osmotic stress induced changes. Zang and Komatsu (2007) showed that the accumulation of 15 proteins under stress was altered in rice, most of which were involved in lipid accumulation, proteasome regulatory pathway, and glyoxalase system. Applying osmotic stress, in addition to altering the expression of 37 proteins, including affeoyl-CoA-O-methyltransferase and 20S proteasome alpha subunit A, led to reduced root and hypocotyl lengths in soybean (Toorchi et al., 2009). It has been reported that some main stress-responsive genes and proteins involved in ROS scavenging, phytohormone and protein metabolism, membrane stability, transport and signaling were active under osmotic stress (Zhang and Shi, 2018; Wang et al., 2020).

Iran, as an origin area of pistachio and its largest producer, is located in the arid regions, where environmental stresses which cause osmotic stress, constantly threaten agriculture (Esmaeilpour et al., 2015). According to the report of the Food and Agriculture Organization (FAO), countries such as Iran, America, Turkey, China and Syria respectively have the largest production of pistachios in the world (FAO, 2020). Pistachio is one of the most important strategic products of Iran, which has decreased in recent years due to the increase of osmotic stresses such as salinity stresses (Rahimi et al., 2021). According to the FAO report, the amount of production of this valuable product in Iran has decreased from 575 thousand tons in 2016 to 190 thousand tons in 2020 (FAO, 2020). Iran is the principal exporter of pistachio crop in the world, which recently its production due to over salinity water and soil has been reduced. According to this fact, in the present study, our aim is to identify important pathways related to osmotic stress through investigating changes of the proteome profiling of pistachio leaves using 2DE-MS under osmotic stress.

Materials and methods

The seeds of *Pistacia vera* L. cv. Akbari were obtained from the Iranian Pistachio Research Institute (IPRI), Rafsanjan, Iran. The seeds were soaked in water for 24h and germinated for a week in 9cm petri dishes with double layers of Whatman filter paper. The germinated seeds were sown in 5L pots containing perlite and irrigated by Hoagland solution for 10 weeks in a controlled greenhouse (25°C, 16h light/8h dark photoperiod with 30% relative humidity) (Esmaeilpour et al., 2015). Then, plants were divided into two groups, control group and osmotic treatment group, each treatment with three replicates (three plants per pots and two pots per replication). Pre-experiments was conducted to select the osmotic treatment. The osmotic treatment (-1.5 MPa) was applied by adding polyethylene glycol 6000 (PEG6000) to Hoagland solution as described by Khoyerdi et al. (Khoyerdi et al., 2016) and maintained for two weeks. The fully expanded leaves from the tip of each plant were frozen in liquid nitrogen prior to being stored at -70°C for physiological measurements and proteomics study.

Biochemical assays

For three biological replicates of each treatment, proline was quantified following Carillo and Gibon (2011). Determining the concentration of phenolic compounds was performed according to Ainsworth and Gillespie (2007). Malondialdehyde (MDA) content were measured based on the study of Velikova et al. (Velikova et al., 2000). Photosynthetic pigment's assay (chlorophyll a, chlorophyll b, and carotenoids) was carried out according to the method of Lichtenthaler and Buschmann (2001).

Protein extraction

According to modified Hurkman and Tanaka (1986) method, after homogenizing 500mg of fresh leaves in liquid nitrogen for three biological replicates of each treatment, 1 mL of cold extraction buffer comprising of 20mM Tris–HCl, (pH 7.5), 1mM EGTA, 1mM PMSF, and 1mM DTT was prepared and added. Then, the sample was incubated at 4°C for 90 min and centrifuged at 20,000×g for 45 min. Four volumes of cold acetone containing 0.08% β-mercaptoethanol and 12% TCA was added to the supernatant as it was incubated at -10°C for 15h. After that, the sample was centrifuged at 20,000×g for 45min. The pellet was washed by cold acetone including 0.08% β-mercaptoethanol seven times at -10°C for 4h and then lyophilized. Finally, the pellet was resolved in lysis buffer comprising of 7M urea, 2M thiourea, 4% CHAPS, 35mM TRIS–HCl, 1% w/v DTT, and 1% v/v Ampholyte, pH 3.5–10) and incubated at 25°C for 1h and then centrifuged at 12,000×g for 15min. The supernatant containing proteins was stored at -80°C. Proteins amounts were assayed by Bradford (1976) method.

Detection of proteins by 2-dimensional gel electrophoresis

120μg protein was added to 320μg rehydration buffer including 8M urea, 2% CHAPS, 0.018M DTT, 2% IPG buffer (pH 3–10), and 0.002% bromophenol blue. Rehydration buffer was loaded to 17 cm IPG linear gradient strips (Bio-Rad) with pH 4–7 in a rehydration tray

at 25°C for 12–16h. Isoelectric focusing (IEF) was carried out on a Multiphor II electrophoresis system (Amersham Pharmacia Biotech) at 20°C pursuant to the following conditions: 150Vh at 0–300 V, 300Vh at 300–500 V, followed by 2000Vh at 500-3500 V and finally 39,500Vh at 3500V. A maximum of 50μA per strip was used for the electric current. Equilibrium buffer comprising of 50mM Tris-HCl (pH 8.8), 6M urea, 30% glycerol (v/v), 2% SDS, 1% DTT, and bromophenol blue was used for balancing IEF strips for 15 min. Afterwards, strips were put onto 12.5% SDS-PAGE gels on Protein II Xi Cell (Bio- Rad) apparatus. Gels were stained using silver nitrate according to Blum et al. (Blum et al., 1987) protocol. After staining, the gels were scanned using Bio-Rad's GS800 densitometer and then converted into TIF format using PDQuest software. Melanie software (version 7) was used for quantitative and qualitative evaluation of protein spots in different treatments (Fatehi et al., 2012; Fatehi et al., 2013). Only spots with reproducible alternations (at least 1.5-fold change) in three biological replicates were used in further analyzes.

In gel digestion and of protein Identification by MALDI/TOF/TOF MS

In-gel digestion and mass spectrometry were carried out according to Pakzad et al. (Pakzad et al., 2019). Briefly, ◦spot were manually excised from the gels and destined for 1 h at 28 C by fresh wash solution (50% acetonitrile 50 mM ammonium bicarbonate (50:50 v/v)). Then washing solution were eliminated and spots dried for 30 min at 37°C. Protein reclamation and alkylation were carried out by 10 mM dithiotreitol (DTT) and 55 mM iodoacetamide (IAA), respectively, and then tryptic digestion were done in 50mM ammonium bicarbonate (pH 8) using MassPREP automated digester station (PerkinElmer). Peptides were extracted using a solution containing 2% acetonitrile and 1% formic acid and lyophilized. Using a solution including of 0.1% TFA (trifluoroacetic acid) and 10% acetonitrile, lyophilized peptides were solved. The peptide mixed in 5 mg/mL of α-cyano-4-hydroxycinnamic acid (CHCA) (MALDI matrix), 50% acetonitrile, 6mM ammonium phosphate monobasic and 0.1% trifluoroacetic acid. The Mass Spectrometry information were obtained using an AB Sciex 5800 TOF/TOF System, MALDI/TOF/TOF (Framingham, MA, USA) with a 349 nm Nd : YLF OptiBeam On-Axis laser.

Protein characterization and classification

Mass spectrometry data was analyzed by MASCOT software (Version 2.2, Matrix Science, London, UK) against Swiss-Prot. Protein properties were gained from UniProt database (https://www.uniprot.org/). More information about the function of proteins was obtained from the scientific literature.

Bioinformatics analysis

The Gene Ontology (GO) analysis of identified proteins were investigated *via* Uniprot (http://www.uniprot.org) and string database (https://string-db.org). Protein–protein interaction was evaluated by the search tool for interactions of chemicals (STITCH) (http://stitch.embl.de).

Validate identified proteins using quantitative real-time PCR

Based on the proteomics results, we validated three identified proteins *via* q-PCR. Total RNA was extracted from control and treated pistachio leaf by RNX – plus kit (Sinaclon, Iran). Synthesis of cDNA and qRT-PCR were done as illustrated by Sadeghi, Mirzaei (Sadeghi et al., 2022). Primers were designed using Primer 3 software (Table 1). Three biological and technical replicates were considered for each sample. The *EF1α* gene was considered as an endogenous control (Moazzam Jazi et al., 2016) and normalization of the CT value of each gene was done by REST software (Relative Expression Software Tool). Change of transcription levels were quantified through the Pfaffl method (Pfaffl et al., 2002).

Statistical analysis

To evaluate the significant differences between mean values of control and osmotic treatment t-test were performed using SAS software v9.1 (SAS Institute Inc., Cary, NC, USA). The measurements are presented as mean ± standard deviation (SD) of 18 samples.

TABLE 1 The sequence of primers designed in this study.

Gene	Forward and Reverse primers sequence (5′ - 3′)	GC%	Annealing temperature (°C)	Amplicon size (bp)
Actin	F: GTCAGCCACACTGTCCCCAT	60	62.13	91
	R: GGGCGTCAGTAAGGTCACGA	60	61.87	
Catalase isozyme 1	F: CAGGCGGACAAATCACTGGG	60	61.31	135
	R: ACAGCAGTCATCCTTCCCGT	55	61.19	
Abscisic acid receptor PYL9	F: CCAAACCCAACCCAAAGGTGA	52.38	60.97	131
	R: CTCTGGGCTCGTGTCTGTGA	60	61.53	
Aspartokinase 2	F: AGTGAGTTGTGAGGGAGCGA	55	60.83	132
	R: CTCTCAGCAGAGGACACGGA	60	60.96	

10.3389/fpls.2022.1041649

Results

Biochemical parameters

MDA concentration was assayed as a lipid peroxidation product. Osmotic stress did not change its concentration, while it increased the level of phenolic compounds. Proline content was dramatically increased when osmotic stress was applied. Stress affected photosynthetic pigments except carotenoid, so that chlorophylls were degraded under stress (Figure 1).

Identification of differentially regulated proteins

In present study, for finding the impact of osmotic stress, pistachio seedlings were treated with PEG6000 to apply osmotic stress for two weeks. Then, proteins of three biological replicates for treatment and control were extracted from leaves and separated by 2-DE (Figure 2). Silver nitrate and Melanie software were used for gel staining and analyzing, respectively. Only differentially accumulated protein spots that represented reproducible alterations were used for further analysis by MS.

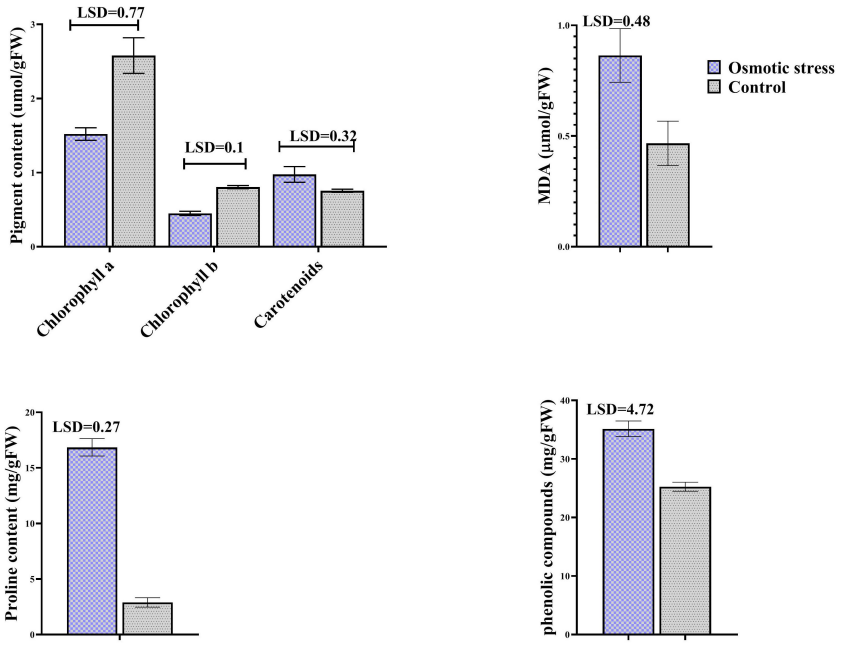

FIGURE 1
The effect of osmotic stress on photosynthetic pigments, MDA, proline and phenolic compounds in leaves of pistachio under osmotic stress compared with control. Bars indicated the SD (n = 3). Statistic were carried out at p = 0.05 according to the t test.

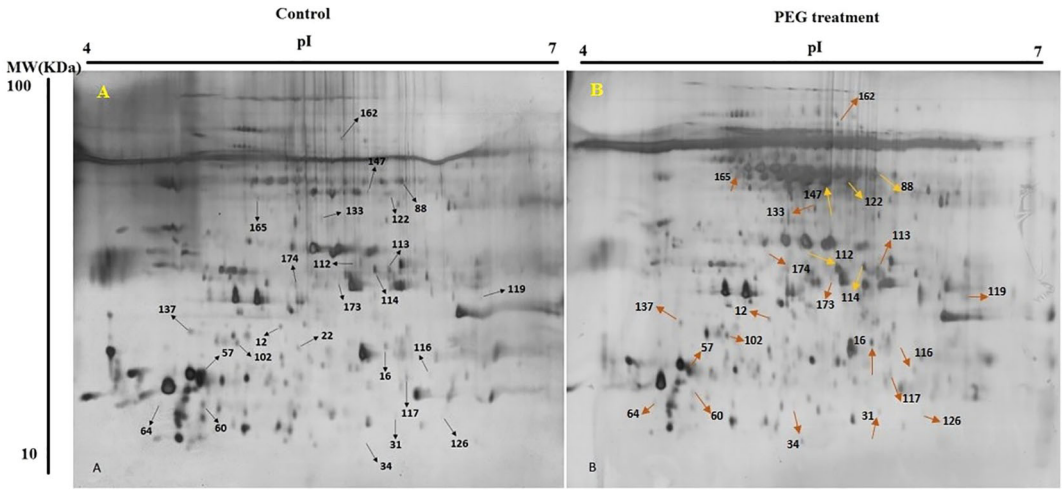

FIGURE 2
2-DE gel images of protein profiles from pistachio leaves. Control **(A)** and PEG treatment **(B)**. 17cm IPG strip (pH 7-14) was used for loading proteins and SDS-PAGE was done with a 12% gel. Gel was stained using CBB G-250. Proteins with differential regulation levels are marked by arrows.

10.3389/fpls.2022.1041649

Out of 280 detected spots, 25 protein spots were significantly altered in response to osmotic stress, accounting for about 8.9% of the detected spots. Among them, only four proteins (spots 57, 64, 102, and 137) were down-regulated and the others were up-regulated (Table 2).

MALDI-TOF/TOF MS was applied to distinguish possible identities of differentially expressed spots. Mascot search engine searched the Swiss-Prot database, while a higher score as well as higher sequence coverage was our criteria for selection.

The calculated pIs of nearly half of the identified proteins were in the acidic pH range and those of the other half were in the neutral and alkaline pH range. 64% of them were distributed in the range of 10,000 – 100,000 Da. whereas, monoisotopic mass of protein 31 was below 10,000 Da and those of proteins 60, 88, and 162 were above 100,000 Da.

TABLE 2 Protein properties of differentially expressed proteins of pistachio leaves under osmotic stress.

Annotations	Spot No.	Accession No.	Score	Coverage%	MW (Da)	pI	Accumulation Status
Photosynthesis and metabolism							
Ribulose bisphosphate carboxylase large chain	57	P28458	58	12	52115	5.91	_*
Ribulose bisphosphate carboxylase small subunit	64	P07180	58	28	20446	6.73	_
Oxygen-evolving enhancer protein 1	102	P85194	57	29	34487	5.4	_
Photosystem I assembly protein Ycf4	137	Q8WI09	60	24	21398	9.83	_
Aspartokinase 2, chloroplastic	133	O23653	62	22	60137	6.31	+*
Glyceraldehyde-3-phosphate dehydrogenase A	113	P19866	52	28	43338	7.62	+
Putative cytochrome c oxidase subunit II PS17	31	P84733	41	100	1707	9.62	+
Thiosulfate/3-mercaptopyruvate sulfurtransferase 1	112	O64530	48	16	42152	5.95	+
Cytosolic sulfotransferase 4	12	Q8RUC1	54	35	32368	8.68	+
Stress response							
Abscisic acid receptor PYL9	116	Q84MC7	41	31	21173	5.89	+
Phospholipase D alpha 3	122	P58766	41	7	93931	6.36	+
18.1 kDa class I heat shock	117	P19037	40	25	18123	6.77	+
Catalase-2	119	P25819	63	24	57237	6.63	+
Catalase isozyme 2	173	Q9XHH3	43	19	57141	7.71	+
Probable serine/threonine-protein kinase CST	34	P27450	51	19	46482	9.58	+
DNA and RNA processing							
DEAD-box ATP-dependent RNA helicase 7	16	Q39189	62	24	73187	9.29	+
DNA repair protein RAD50	162	Q9SL02	68	22	153632	5.98	+
Replication protein A 70 kDa DNA-binding subunit D	174	Q9FME0	58	33	70676	6.1	+
Protein argonaute MEL1	60	Q851R2	66	8	117987	9.34	+
Cell wall biosynthesis							
Prolyl 4-hydroxylase 5	147	Q24JN5	42	11	32842	7.75	+
Probable galacturonosyltransferase 3	165	Q0WQD2	58	15	78178	7.27	+
Transporting and movement							
Putative aluminum-activated malate transporter 11	22	Q3E9Z9	38	24	17149	9.55	+
Kinesin-like protein KIN-7H	88	F4JZ68	57	27	122375	5.53	+
Signal transduction							
Guanine nucleotide-binding protein alpha-1 subunit	126	P18064	59	32	44860	5.96	+
Other							
F-box/kelch-repeat protein At3g17530	114	Q9LUP5	48	26	44807	7.43	+

*+: Up-regulated expression, _: Down-regulated expression, ND, no data.

Functional classification of differentially regulated proteins

As shown in Figure 3, the study of biological functions of differentially accumulated proteins led to their classification into seven diverse groups. Most of them contributed to photosynthesis and metabolism accounting for 36% then followed by stress response (24%), DNA and RNA processing (16%), and cell wall biosynthesis (8%), transporting (8%). Furthermore, the remaining proteins were associated with signal transduction (4%) and other (4%).

Protein-chemical interaction

In this study, we evaluated the network of protein-protein/chemicals interactions involving in osmotic stress in pistachio leave using STITCH database against *Arabidopsis thaliana*. All of 25 identified proteins were detected with the STITCH database. The PCI network indicated a strong interaction network between identified proteins and several chemical compounds in different pathways (Figure 4). Identified chemical compounds related to plant response under osmotic stress were included proline, guanosine triphosphate, arginine, nicotinamide, H_2O_2, pectin, glucan, glutamate, phosphoglycerate kinase 1, phosphate, glucose, chitin, topoisomerase II, estradiol, malondialdehyde, cytochrome p450 72c1, cytochrome oxidase 2, cytochrome c oxidase subunit 3,1,4-beta-D-xylan synthase, allene oxide cyclase 2, putative nucleolar GTP-binding protein 1, ATP-dependent RNA helicase DHX8/PRP22, silencing defective, large subunit ribosomal protein L24e, cell wall-associated kinase, alpha-ketoglutarate-dependent dioxygenase alkB, ethylparaben, replication factor A1, G protein alpha subunit 1, magnesium chloride, hypersensitive to ABA1, pescadillo-related protein, putative xyloglucan glycosyltransferase 8, phosphoglycerate kinase 1. Also STITCH database were predicated that various pathways controlled by hormones and their crosstalk, consisting of brassinolide, gibberellin, ethylene, salicylic acid, ABA, auxin, and jasmonate.

Gene ontology analysis

According to the analyses of GO enrichment, investigated proteins were in various ranges of biological processes (Figure 5), included of metabolic process (16.78%), response to stimulus (16%), cellular component organization or biogenesis (9.48%), oxidation-reduction process (8%), DNA metabolic process (5.1%), meiotic cell cycle (4.38%), DNA repair (4.38%), reproduction (4.38%), carbohydrate biosynthetic process (4.38%), DNA recombination (3.65%), photosynthesis (3.65%), reductive pentose-phosphate cycle (2.2%), carbon fixation (2.2%), double-strand break repair (2.2%), meiotic nuclear division (2.2%), telomere maintenance (2.19%), reciprocal meiotic recombination (2.19%), meiosis I (2.19%) and mitotic recombination (1.46%).

Findings of the GO enrichment analyses displayed that identified proteins, under osmotic stress, mainly located in intracellular part (22%), intracellular membrane-bounded organelle (19.64%), cytoplasm (17.26%), macromolecular complex (6.54%), organelle envelope (5.35%), intracellular organelle lumen (4.16%), nuclear part (4.16%), thylakoid (3.57%), plastid envelope (3.75%), nuclear lumen (3.75%), chloroplast stroma (3.57%), stromule (2.97%), Mre11 complex (1.19%), heterotrimeric G-protein complex (1.19%) and cytoplasmic side of plasma membrane (1.19%) (Figure 5).

The enrichment of molecular functions illustrated the most processes related to catalytic activity (42.25%), ion binding (35.21%), oxidoreductase activity (15.49%), cytochrome-c oxidase activity (4.22%) and ribulose-bisphosphate carboxylase activity (2.81%) (Figure 5).

Evaluation of KEGG pathways demonstrated that differentially accumulated proteins enriched in metabolic pathways (35.29%), microbial metabolism in diverse environments (14.70%), Carbon fixation in photosynthetic organisms (11.76%), homologous recombination (11.76%), carbon metabolism (11.76%), glyoxylate and dicarboxylate metabolism (8.82%) and non-homologous end-joining (5.88%) (Figure 5).

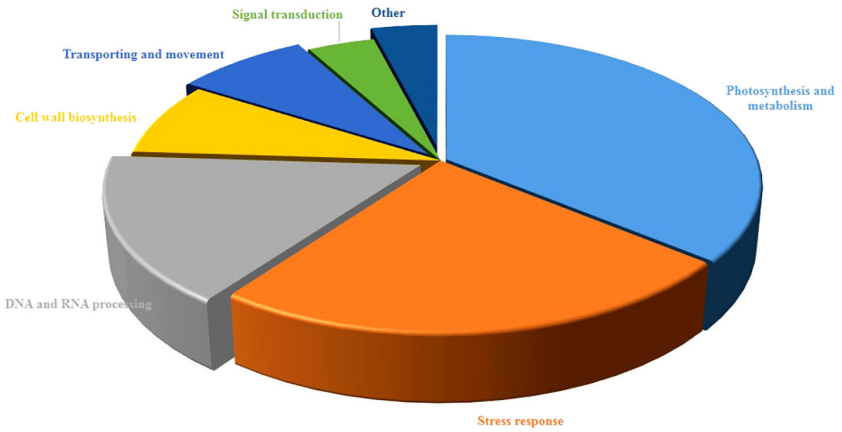

FIGURE 3
Functional classification of differentially regulated proteins of pistachio leaves under osmotic stress condition. The percentage of annotated proteins related to each pathway illustrated in pie charts.

FIGURE 4
Analysis of the network of protein – chemical of identified proteins using STITCH 5.0. AT2G44860, large subunit ribosomal protein L24e; AT3G17530, F-box and associated interaction domain-containing protein; WAK1, Serine/threonine-protein kinase; At5g14060, aspartokinase 2; SDE3, SILENCINGDEFECTIVE; AT1G11780, alpha-ketoglutarate-dependent dioxygenase alkB; ST4A, sulfotransferase 4A; AGO2, argonaute 2;P4H5, prolyl 4-hydroxylase 5; AOC2, allene oxide cyclase 2; THM1, thioredoxin M1, RPA1A, replication factor A1; YCF4, unfolded protein binding; GPA1, G protein alpha subunit 1; NBS1, nijmegen breakage syndrome 1; PLDALPHA3, phospholipase D; RBCS1A, ribulose bisphosphate carboxylase small chain 1A, AT4G35090, catalase 2; TOPII, topoisomerase II; AT4G17585, aluminum activated malate transporter family protein;HAB1, HYPERSENSITIVE TO ABA1; CSLD5, 1,4-beta-D-xylan synthase; AT5G14520, pescadillo-related protein; MST1, thiosulfate sulfurtransferase;COX1, cytochrome oxidase; AT3G26560, ATP-dependent RNA helicase DHX8/PRP22; RCAR1, abscisic acid receptor PYL9; RAD50, DNA repair protein RAD50; RBCL, ribulose-bisphosphate carboxylases;ATCSLC08, putative xyloglucan glycosyltransferase 8; GAUT3, galacturonosyltransferase 3; PGK1, phosphoglycerate kinase 1;PRH75, DEAD-box ATP-dependent RNA helicase 7; AT5G66310, ATP binding microtubule motor family protein; ATR, serine/threonine-protein kinase ATR;AGB1, GTP binding protein beta 1; CYP72C1, cytochrome p450 72c1; AT2G07687.1, cytochrome c oxidase subunit 3; COX3, cytochrome c oxidase subunit 3; MRE11, MEIOTIC RECOMBINATION 11; COX2, cytochrome oxidase 2; Hsp70-15, Heat shock protein 70.

Analysis of transcriptional expression change by qRT-PCR

Changes in the transcription level of three selected genes of differentially abundant proteins were investigated by qRT-PCR (Figure 6). Results of qRT-PCR analysis indicated that transcription level of genes related to spots 116 and 133 increased in response to osmotic stress. The change of the expression level of representative genes was the same as their protein expression.

Discussion

Plants have established numerous defense mechanisms against osmotic stress such as osmotic adjustment by ion transport

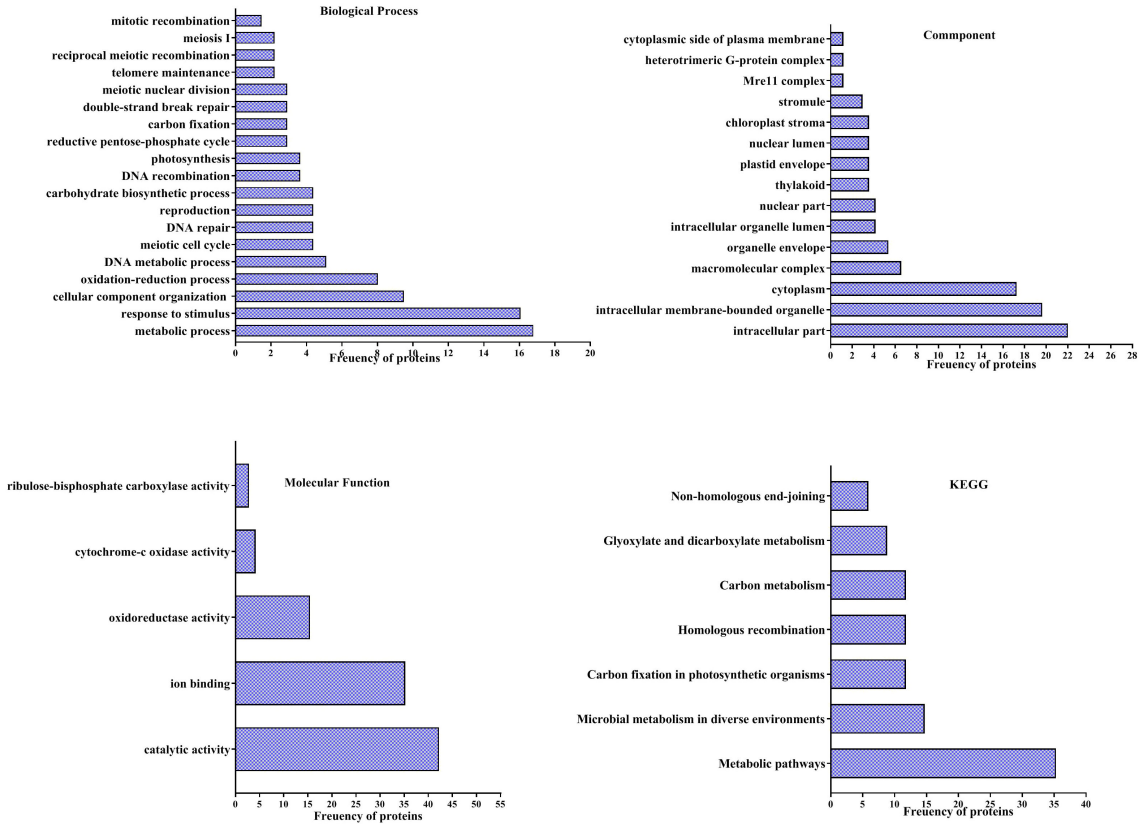

FIGURE 5
Analysis of Gene ontology (GO) of differentially accumulation proteins of pistachio leaves under osmotic condition. Pathways of four groups of functional enrichment consisting of biological process, cellular component, molecular function and KEGG were analyzed *via* the STITCH database.

reregulation and osmoprotectants synthesis, preservation of membrane stability, activation of antioxidant defense, reregulation of cell cycle, and metabolic changes (Xiong and Zhu, 2002; Zhang and Shi, 2018). Polyethylene glycol (PEG), which has no toxic effect on the plant, induces osmotic stress by withdrawing water from the protoplasm and apoplast (Toorchi et al., 2009). In this study, the altered contents of some biochemical compounds and several differences in protein expression patterns due to dehydration resulted from PEG were detected in pistachio.

Biochemical Parameters

Tolerant plants to osmotic stress have potency to sustain homeostasis of metabolic using increase of different solutes (Blum, 2017). In this study, accumulation of several organic solutes like proline and phenolics were increased, indicating a positive role of these compounds in the pistachio plant under osmotic stress. Proline acts not only as a compatible osmolyte but also as a ROS scavenger, a buffer for cellular redox potential, and a nutritional source under

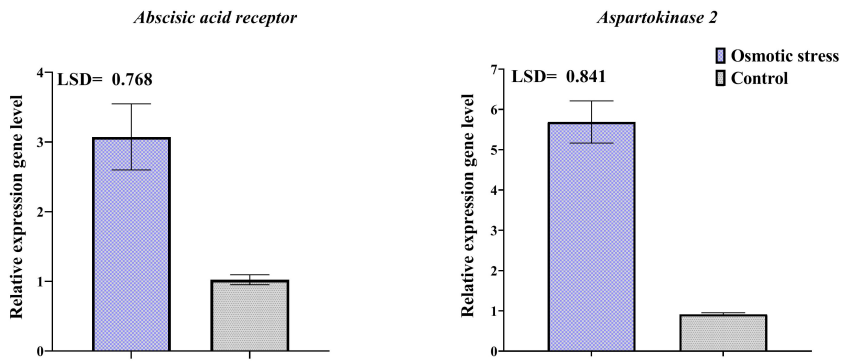

FIGURE 6
Transcriptional expression levels of two differentially abundant proteins in pistachio leaves in response to osmotic stress based on qRT-PCR analysis results. Error bars indicated the SD (n = 3) Statistic were carried out at p = 0.05 according to the LSD test.

stress (Hayat et al., 2012; Chun et al., 2018). An increase of about six-fold in proline content was observed here. An increase in proline accumulation as an osmolyte in response to dehydration has been observed in a wide range of plants (Skirycz et al., 2010; Benhassaini et al., 2012; Kim et al., 2016; Jungklang et al., 2017; Zegaoui et al., 2017; Koenigshofer and Loeppert, 2019; Mattioli et al., 2020). Pálet al. (Pál et al., 2018) had also confirmed the enhancement in the amount of proline under osmotic stress. Owing to ability to forgive hydrogen, decrease and extinguish radical oxygen, phenolics have oxidation virtues and have a main role as sweepers of ROS in plant under various stresses (Naikoo et al., 2019; Mechri et al., 2020). A potent relation exists among osmotic tolerance and increased accumulation of phenolic compounds (Dey and Bhattacharjee, 2020; Naikoo et al., 2019). Piwowarczyk et al. (Piwowarczyk et al., 2017) reported that concentration of phenols elevated in grass pea plant under PEG-induced osmotic stress, similar to our results. Several studies illustrated that concentration of proline and phenols increased under salinity and drought stress in pistachio plants (Khoyerdi et al., 2016; Akbari et al., 2018; Jamshidi Goharrizi et al., 2020). Therefore, considering the presented results and literature data, the increased accumulation of phenolics and proline may be propounded as a main elements related to the tolerance of pistachio to osmotic stress.

Lipid peroxidation of cell leading to produce malondialdehyde indicating severity of injury to the cell membrane (Morales and Munné-Bosch, 2019). Our data showed that malondialdehyde content did not changed that maybe due to the physiological adaptation and or elevated activity of antioxidant systems that diminished ROS levels and membrane injury. On the other hand, our result contradicts results of Khoyerdi et al. (Khoyerdi et al., 2016) and Goharrizi et al. (Goharrizi et al., 2020). The principal reason for this conflict is probably differences in type of reaction pistachio varieties to osmotic stress as well as differences in the way of implementing stress treatment.

The photosynthesis process and its severity rely on content of pigments such as Chl a, Chl b, and carotenoids and effect the biological productivity. Also, photosynthetic pigments harvest the light for photosynthesis process (Rahneshan et al., 2018; Lan et al., 2020). Osmotic condition can injury the chlorophyll content and prevent synthesis of chlorophyll pigments, therefore chlorophyll degradation is one of the subsequences of osmotic stress (Akbari et al., 2018; García-Morales et al., 2018). In this study, decline in chlorophyll content were observed under osmotic stress. In general, this reduction can be imputed to various factors, such as the sluggish synthesis or rapid degradation of the pigments in cells, decrease in synthesis of chlorophylls, derangement in the complex of pigment–protein and thought deficits in ions that are necessary for chlorophyll biosynthesis (Akbari et al., 2018; Behzadi Rad et al., 2021; Zhu et al., 2021). Lan et al. (Lan et al., 2020) reported that chlorophyll content remarkably reduced in wheat under PEG-induced osmotic stress, similar to our results. Also, our findings are in compliance with (Behzadi Rad et al., 2021) who reported that the chlorophyll content of pistachio leaves reduce under salinity condition. Carotenoids function as photoprotection by absorbing extreme light and protect chloroplasts from harmful ROS level therefore protect chlorophyll from major damage (Rahneshan et al., 2018). In this study, no change in carotenoids concentration was observed (Figure 1).

Photosynthesis and metabolism related proteins

The most important enzyme in photosynthesis is ribulose bisphosphate carboxylase (Rubisco), which consists of two types of large and small subunits, plays main role in the fixation of CO_2.

The alteration in photosynthesis of plants highly related to the Rubisco activity. It has been reported that drought stress had a harmful impact on the function of Rubisco in various plants, led to decrease of biosynthesis and degradation of subunits and finally diminution of photosynthesis (Zhang et al., 2016; Shayan et al., 2020). In this study, subunits of Rubisco down-regulated which was agreement with our pervious study (Pakzad et al., 2019). Also, Jamshidi Goharrizi et al. (Jamshidi Goharrizi et al., 2020) using analyzing the leaf proteome profiling of pistachio demonstrated that ribulose bisphosphate carboxylase/oxygenase large chains were down-regulated under salinity stress condition.

OEE1 is one of member of the PSII related to photoreactions, and plays a role in stabilizing the cluster of Mn in the PSII that is initial locate of water splitting. A loss of this protein leads to a full inability for evolve oxygen in PSII (Chaves et al., 2009; Dubey, 2018; Heide et al., 2004; Mayfield, 1999). The decreased levels of this protein were occurred under osmotic stress. In contrast to our results Buendig et al. (Buendig et al., 2016), reported a decrease in the abundance of OEE1 in potato genotypes under osmotic stress. A diminish in the accumulation of OEE1 maybe therefore due to harm to PSII and represents a considerable decrease of efficiency photosynthesis under osmotic stress (Chaves et al., 2009; Dubey, 2018). PSI assembly protein Ycf4 (YCF4) plays a significant role in the assembly of PSI and its firm hold to the thylakoid membrane (Nellaepalli et al., 2018; Hui-Hui et al., 2019). In this study, we found that the accumulation of YCF4 were reduced under osmotic stress, illustrating that osmotic stress reduce quantity and integrity of PSI protein. Cytochrome c oxidase subunit II PS17 is the final enzyme related to respiratory chain, oxidizing cytochrome c and make molecular water using transfer electrons to molecular oxygen. It has been reported that alterations in expression of the cytochrome c oxidase level were attended with alterations in the accumulation of proteins related to photosynthesis and carbohydrate metabolism under stress condition (Çulha Erdal et al., 2021). Increased accumulation of this protein has been reported by Çevik et al. (Çevik et al., 2019) and Çulha Erdal et al. (Çulha Erdal et al., 2021) under drought stress. Abundance of this protein was elevated by osmotic stress in pistachio, indicating that maybe help to generation of energy *via* respiratory chain, leading to improve photosynthesis and carbohydrate metabolism levels. Totally, the decrease in the expression of OEE1, Ycf4, and ribulose bisphosphate carboxylase, implicitly indicated destructive effect of osmotic stress on the photosynthesis process.

Glyceraldehyde-3-phosphate dehydrogenase (GAPDH) plays a vital role in the physiological plant function and energy production *via* glycolytic pathway and protect of photosystem II from ROS under stress condition (Fermani, 2007; Bertomeu et al., 2010). the study conducted by Kappachery et al. (Kappachery et al., 2021) indicated that Overexpression of gene encoding GAPDH in *Arabidopsis thaliana* transgenic elevate antioxidant enzymes, photosynthetic pigments and improve photosynthesis *via* increasing general PSII efficiency under salt stress. In our study, GAPDH accumulation elevated in pistachio leaves

treated with PEG6000, revealing that this enzyme may provide the way for obtaining extra energy for regulation of cellular homeostasis and also it maintain photosynthetic efficiency using protect photosystem II from adverse effect of osmotic stress.

Aspartate kinase (AK) is the primary and the most vital enzyme in phosphorylating L-aspartate, leading to biosynthesizing four necessary amino acids: methionine, threonine, lysine, and isoleucine (Jander and Joshi, 2009; Han et al., 2021). There are several evidences demonstrated AK involved in osmotic stress (Chefdor et al., 2006; Héricourt et al., 2013; Héricourt et al., 2016) and drought and nutritional stress (Curtis et al., 2018). In this study the increased accumulation of AK was determined, suggesting biosynthesis of numerous amino acid leading to improve plant adaption abilities under osmotic stress.

The function of the sulfotransferase superfamily is to transfer a sulfuryl group from the general donor, PAPS, to a hydroxyl group from a wide range of substrates, including glucosinolates, phenolic acids, flavonoids, brassinosteroids, coumarins, jasmonates, and terpenoids. They are involved in very diverse physiological functions such as a response to pathogen or detoxification (Hernàndez-Sebastiá et al., 2008; Hirschmann et al., 2014). In this study two proteins belong to sulfotransferase superfamily; Thiosulfate/3-mercaptopyruvate sulfurtransferase 1and sulfotransferase 4 was found to be increased under osmotic stress. It has been reported that sulfurtransferases play a main role in ROS, cyanide, and heavy metals detoxification and contribute to metabolism of sulfur and cysteine (Papenbrock and Schmidt, 2000; Nakamura et al., 2000; Most and Papenbrock, 2015; Yamasaki and Cohen, 2016). Proteomic profiling on lettuce was conducted by Leitão et al. (Leitão et al., 2021) indicated that accumulation of sulfurtransferase was increased under stress induced by pharmaceutical contamination. Also, several studied illustrated that sulfurtransferases play a main role in plant response to abiotic stress such as osmotic, salt and hormone stress (Jin et al., 2019). Overall, increased expression of cytosolic sulfotransferase 4 and thiosulfate/3-mercaptopyruvate sulfurtransferase 1 indicated a wide range of changes associated with osmotic stress.

Stress response related proteins

Phospholipase D is a most important enzyme involved in hydrolyzing membrane phospholipids, leading to generate phosphatidic acid which act as a signaling molecule so that promotes stomatal closure under osmotic stress (Saucedo-García et al., 2015; Rodas-Junco et al., 2021). Many evidences illustrate that PLD has an important role in plant tolerance under stress (Ji et al., 2018; Alferez et al., 2019; Gnanaraj et al., 2021; Wei et al., 2022) and adjust plant defense response to osmotic stress (Liu et al., 2021; Liu et al., 2022; Hong et al., 2008). Our findings indicated that abundance of Phospholipase D was increased under osmotic stress, similar to results of (Urban et al., 2021).

Osmotic stress induce the ABA level in various plants, which is a well-known reality (Haider et al., 2018; Kai etal., 2019; Xing et al., 2016). In this study, the up-regulation of abscisic acid receptor PYL9 was observed, indicating activation of pathway related to ABA signaling in pistachio plant toward response to osmotic stress. Transcriptomic analysis of grapevine leaves indicated that PYL9 induced under salt stress (Guan et al., 2018) Also, it Miao et al. (Miao et al., 2018) reported that PYL9 overexpression improves drought resistance.

Up-regulation HSPs, as chaperones, involved in facilitating protein conformation or refolding under stress conditions, because, denaturation of proteins occurs as a result of the reduction of water content in osmotic stress (Zang and Komatsu, 2007). The expressions of HSP genes are prompted by denatured or damaged proteins (Xiong and Zhu, 2002).Thus, their expressions are up-regulated in the stress or some stages of growth and development (Park and Seo, 2015).The elevated expression of a heat shock protein under osmotic stress was observed in the present study. This result is agreement to studies of Rahman et al. (Rahman et al., 2015) who reported increased accumulation of 18.1 kDa class I heat shock protein and other HSPs in transgenic sugarcane under drought stress induced with PEG.

Following many stresses, oxidative stress also occurs due to augmented ROS. Although ROS plays a key role in signaling and regulation of many genes (Xiong and Zhu, 2002), enhancing its concentration damages cellular structures seriously, so some mechanisms have been established in the plant to prevent the overproduction or to remove ROS (Toorchi et al., 2009), including catalase activation or biosynthesis, which sweeps away H_2O_2 by its activity. Increasing antioxidants as a common result of most abiotic stresses, improves plant stress tolerance. Abiotic stress induces genes for various catalase isoforms (Xiong and Zhu, 2002). Catalase in interaction with plant natriuretic peptide (PNP) triggers the regulation of ROS levels and cell redox homeostasis during the salinity or drought stress (Turek et al., 2020). In this study two spots (119 and 173) identified as catalase enzyme that their expression were increased under osmotic stress. Augmented activity of the antioxidant system due to increased expression of relevant proteins during osmotic stress has been observed in other studies, as well (Toorchi et al., 2009; Zhang and Shi, 2018).

Serine/threonine-protein kinase CST is a receptor-like cytoplasmic kinase that acts as an inhibitor in such a way that limits the extent of cell separation signaling, and causes cells to be separated only in designated areas in abscission zone (Burr et al., 2011). Several researches have been proven positive role of Serine/threonine-protein kinases under stress condition in different plants (Mao et al., 2010; Sun et al., 2013; Rampino et al., 2017; Mao et al., 2010). In this study, activation of Serine/threonine-protein kinase CST was increased. The role of this protein in response plant to biotic stress was proved (Ghorbani et al., 2019).

DNA and RNA processing related proteins

Plants to dominate the stable challenge from a swiftly altering environment have several particular adaptation mechanisms, among which DNA and RNA processing are main strategies (Wong et al., 2017; Song et al., 2021). In this study several proteins related to DNA and RNA processing were identified included of DEAD-box ATP-dependent RNA helicase 7, DNA repair protein RAD50, replication protein A 70 kDa DNA-binding subunit D, and argonaute MEL1 are proteins that participate in the processes assigned to DNA and RNA

(Nonomura et al., 2007; Takashi et al., 2009; Gherbi et al., 2001; Gallego et al., 2001; Aubourg et al., 1999). This display that plant to adapt under osmotic condition could increase several transcriptional and translation processes and seriously elevated the stability and variety of proteins (Aubourgrt al., 1999; Nonomura et al., 2007). The role of DNA and RNA processing has been indicated in studies related to various environmental stress (Gao et al., 2019; Li et al., 2020; Marondedze et al., 2020)

Cell wall biosynthesis related proteins

Like other results (Ngara et al., 2018; Zhang and Shi, 2018; Wang et al., 2020), we also recognized some proteins associated with cell wall construction, including prolyl 4-hydroxylase 5 and probable galacturonosyltransferase 3, since the cell wall is the protective barrier and the first front of defense against stress. Cell division, which requires the formation of a new cell wall, is also inhibited under osmotic stress (Xiong and Zhu, 2002). Hence, cell metabolism changes to guide plant status from optimal growth to stress-adapted growth, which requires alterations in the expression and the activity of many proteins assigned to the intercellular space and cell wall (Ngara et al., 2018). The synthesis of pectin, which is a component of the cell wall, requires the activity of galacturonosyltransferase (Boustani et al., 2017). 4-hydroxyproline, which is an important component of cell wall glycoproteins, is produced post-translationally by the activity of Prolyl 4-hydroxylase 5 on proline-rich sequences in glycoproteins (Velasquez et al., 2011). In this study proteins related to cell wall stabilization was increased, indicating that these proteins might help to the more consolidation of cell wall in pistachio and leads to more osmotic tolerance and plant could regulate the osmotic potential using changes to the cell wall.

Transporting and movement related proteins

Kinesin-like proteins are motors that perform microtubule-based movement, such as the transport of vesicles and organs, chromosome segregation, and signal transduction, thus play a key role in developmental and environmental processes (Ni et al., 2005). Changes in the expression of microtubule-related proteins may alter the morphology of stressed tissue. In this research, kinesin-like protein KIN-7H revealed higher abundance in the PEG treatment.

Aluminum-activated malate transporter, which belongs to the anion channels, is located in the membranes of different tissues and has a various and fundamental range of physiological functions such as aluminum resistance, signaling, anion homoeostasis, osmotic adjustment, stomata regulation, and abiotic stress tolerance *via* transporting malate or inorganic anions (Palmer et al., 2016; Ramesh et al., 2018; Hejri et al., 2021). Maintaining sufficient amounts of water is essential for plant growth and development (Pasaribu et al., 2021). Therefore, the plant controls the ionic balance in the cell to regulate the osmotic pressure during the osmotic stress. Thus, aluminum-activated malate transporter 11 can play a significant role in this process by transporting malate and inorganic anions. Scientific reports suggest that abiotic stresses such as salinity regulate transporters either at the protein or mRNA levels (Xiong and Zhu, 2002).

Signal transduction related protein

Under osmotic stress, plants sense the stress through signal transmission networks and as a result start to react. They adapt to stress conditions through different signaling pathways that affect a wide range of protein expression (Zandalinas et al., 2020). Alterations were reported in levels of various proteins related to signal transduction under stress condition (Shan et al., 2018; Meena et al., 2019; Zhang et al., 2019; Wang et al., 2022). A main protein to take a notice is guanine nucleotide-binding proteins, named G proteins or GTPases. These proteins *via* activity of moderator or transducers in different signaling systems located in transmembrane adjust many cellular processes such as secretion, transport etc. (Patel et al., 2020). G-proteins consisting of the Gα, Gβ, and Gγ subunits, Based on our findings, The Gα subunit up-regulated under osmotic stress. Gα subunit is the vital the member of G-protein signal transduction so that activation of G-protein and downstream signal depended on Gα (Liu et al., 2021; Liu et al., 2018; Pandey and Assmann, 2004). Similar to our findings, several studies illustrated that increased expression of the Gα subunit plays a significant role in plant resistance to various abiotic stress such as salt (Misra et al., 2007), drought (Ferrero-Serrano and Assmann, 2016), heat and cold (Chakraborty et al., 2015; Chakraborty et al., 2015; Ma et al., 2015; Guo et al., 2020).

Other protein

F-box kelch-repeat proteins can adjust biosynthesis of phenylpropanoid *via* regulating the turnover of phenylalanine ammonia-lyase and also play a main role in a main role in providing homeostasis *via* eliminating misfolded or injured proteins which could destroy cellular activations (Zhang et al., 2013; Kamireddy et al., 2021). In this study, the expression level of the F-box/Kelch-repeat protein (At3g17530) was elevated under stress. To date, the function of this protein is unclear but several studies indicated that proteins belong to F-box/Kelch-repeat protein family play an important role in improve of tolerance plant under stress condition (Curtis et al., 2013; Wang et al., 2017; Venkatesh et al., 2020).

STITCH and GO analysis

Protein–protein/chemical interactions can notably modulate different cellular activities, such as replication, transcriptional regulation, defense responses, growth and development, processes of signaling, and consonance of numerous metabolic pathways (Fukao, 2012; Braun et al., 2013). In this study, the interaction networks proteins-proteins/chemicals in pistachio leaves treated by PEG were analyzed using STITCH. The STITCH network predicted 33 proteins and small molecules interacted with identified proteins using proteomic technic. Also STITCH analysis indicated that all of proteins and small molecules regulation by a set of hormones and their crosstalk.

According to KEGG analysis, the most proteins involved in response to osmotic in pistachio leaves enriched in metabolic

pathways that was similar to proteomic findings, indicating the osmotic stress mostly impacts the metabolic pathways.

Conclusion

To better our knowledge about plant tolerance under osmotic stress and molecular mechanisms behind related responses, proteomics of pistachio leaves was performed. Osmotic stress imposed a change in the expression of 25 proteins. 21 proteins were highly expressed while four proteins were less expressed. These identified proteins function in several biological processes such as stress response, photosynthesis and metabolism, DNA and RNA processing, and cell wall biosynthesis which point out their roles in adaptation of pistachio under osmotic stress. Based on KEGG analysis, proteins related to metabolic pathways have the most vital role in pistachio response to osmotic stress. The decline in the expression of Rubisco, OEE1, and photosystem I assembly protein Ycf4 suggested the destructive effect of membrane dehydration resulted from osmotic stress on the photosynthesis process. Altered expression of some proteins associated with the cell wall was expected because the wall is the first defense barrier against stress, and cell division, which requires the formation of a new wall, is inhibited under stress as well. Some proteins involved in DNA and RNA processing were also overexpressed because osmotic stress activates signaling pathways such as the ABA-related pathway, which ultimately leads to altered gene expression and delayed cell division, and stress-induced ROS may also damage DNA.

Data availability statement

The datasets presented in this study can be found in online repositories. The names of the repository/repositories and accession number(s) can be found in the article/supplementary material.

Author contributions

RP performed the experiments, analyzed the data and wrote the original draft. FF conceived and designed the study, supervised all steps, review and edit the manuscript, approved the final version to be published. MK investigate and MM analyzed the data, review and edit the manuscript.

Funding

Research funding provided by FF and RP.

Conflict of interest

The authors declare that the research was conducted in the absence of any commercial or financial relationships that could be construed as a potential conflict of interest.

Publisher's note

All claims expressed in this article are solely those of the authors and do not necessarily represent those of their affiliated organizations, or those of the publisher, the editors and the reviewers. Any product that may be evaluated in this article, or claim that may be made by its manufacturer, is not guaranteed or endorsed by the publisher.

Supplementary material

The Supplementary Material for this article can be found online at: https://www.frontiersin.org/articles/10.3389/fpls.2022.1041649/full#supplementary-material

References

Ainsworth, E. A., and Gillespie, K. M. (2007). Estimation of total phenolic content and other oxidation substrates in plant tissues using folin–ciocalteu reagent. *Nat. Protoc.* 2 (4), 875–877. doi: 10.1038/nprot.2007.102

Akbari, M., Mahna, N., Ramesh, K., Bandehagh, A., and Mazzuca, S. (2018). Ion homeostasis, osmoregulation, and physiological changes in the roots and leaves of pistachio rootstocks in response to salinity. *Protoplasma* 255 (5), 1349–1362. doi: 10.1007/s00709-018-1235-z

Alferez, F., Wu, J., and Graham, J. H. (2019). Phospholipase d (PLD) response to water stress in citrus roots and leaves. *Agronomy* 10 (1), 45. doi: 10.3390/agronomy10010045

Aubourg, S., Kreis, M., and Lecharny, A. (1999). The DEAD box RNA helicase family in arabidopsis thaliana. *Nucleic Acids Res.* 27 (2), 628–636. doi: 10.1093/nar/27.2.628

Behzadi Rad, P., Roozban, M. R., Karimi, S., Ghahremani, R., and Vahdati, K. (2021). Osmolyte accumulation and sodium compartmentation has a key role in salinity tolerance of pistachios rootstocks. *Agriculture* 11 (8), 708. doi: 10.3390/agriculture11080708

Benhassaini, H., Fetati, A., Hocine, A. K., and Belkhodja, M. (2012). Effect of salt stress on growth and accumulation of proline and soluble sugars on plantlets of pistacia atlantica desf. subsp. atlantica used as rootstocks. *BASE.* 16 (2), 159–165.

Blum, A. (2017). Osmotic adjustment is a prime drought stress adaptive engine in support of plant production. *Plant Cell environment.* 40 (1), 4–10. doi: 10.1111/pce.12800

Blum, H., Beier, H., and Gross, H. J. (1987). Improved silver staining of plant proteins, RNA and DNA in polyacrylamide gels. *Electrophoresis* 8 (2), 93–99. doi: 10.1002/elps.1150080203

Boustani, A., Fatehi, F., and Azizinezhad, R. (2017). The proteome response of "Hordeum marinum" to long-term salinity stress. *Cereal Res. Commun.* 45 (3), 401–410. doi: 10.1556/0806.45.2017.020

Bradford, M. M. (1976). A rapid and sensitive method for the quantitation of microgram quantities of protein utilizing the principle of protein-dye binding. *Analytical Biochem.* 72 (1-2), 248–254. doi: 10.1016/0003-2697(76)90527-3

Braun, P., Aubourg, S., Van Leene, J., De Jaeger, G., and Lurin, C. (2013). Plant protein interactomes. *Annu. Rev. Plant Biol.* 64, 161–187. doi: 10.1146/annurev-arplant-050312-120140

Buendig, C., Jozefowicz, A. M., Mock, H.-P., and Winkelmann, T. (2016). Proteomic analysis of two divergently responding potato genotypes (Solanum tuberosum l.) following osmotic stress treatment *in vitro*. *J. Proteomics* 143, 227–241. doi: 10.1016/j.jprot.2016.04.048

Burr, C. A., Leslie, M. E., Orlowski, S. K., Chen, I., Wright, C. E., Daniels, M. J., et al. (2011). CAST AWAY, a membrane-associated receptor-like kinase, inhibits organ abscission in arabidopsis. *Plant Physiol.* 156 (4), 1837–1850. doi: 10.1104/pp.111.175224

Carillo, P., and Gibon, Y. (2011). Protocol: extraction and determination of proline. *PrometheusWiki* 2011, 1–5.

Çevik, S., Akpinar, G., Yildizli, A., Kasap, M., Karaosmanoğlu, K., and Ünyayar, S. (2019). Comparative physiological and leaf proteome analysis between drought-tolerant chickpea cicer reticulatum and drought-sensitive chickpea c. arietinum. *J. biosciences.* 44 (1), 1–13. doi: 10.1007/s12038-018-9836-4

Chakraborty, N., Sharma, P., Kanyuka, K., Pathak, R. R., Choudhury, D., Hooley, R., et al. (2015). G-Protein α-subunit (GPA1) regulates stress, nitrate and phosphate

response, flavonoid biosynthesis, fruit/seed development and substantially shares GCR1 regulation in a. thaliana. *Plant Mol. Biol.* 89 (6), 559–576. doi: 10.1007/s11103-015-0374-2

Chakraborty, N., Singh, N., Kaur, K., and Raghuram, N. (2015). G-Protein signaling components GCR1 and GPA1 mediate responses to multiple abiotic stresses in arabidopsis. *Front. Plant science.* 6, 1000. doi: 10.3389/fpls.2015.01000

Chaves, M., Flexas, J., and Pinheiro, C. (2009). Photosynthesis under drought and salt stress: regulation mechanisms from whole plant to cell. *Ann. botany.* 103 (4), 551–560. doi: 10.1093/aob/mcn125

Chefdor, F., Bénédetti, H., Depierreux, C., Delmotte, F., Morabito, D., and Carpin, S. (2006). Osmotic stress sensing in populus: components identification of a phosphorelay system. *FEBS letters.* 580 (1), 77–81. doi: 10.1016/j.febslet.2005.11.051

Chun, S. C., Paramasivan, M., and Chandrasekaran, M. (2018). Proline accumulation influenced by osmotic stress in arbuscular mycorrhizal symbiotic plants. *Front. Microbiol.* 9, 2525. doi: 10.3389/fmicb.2018.02525

Çulha Erdal, Ş, Eyidoğan, F., and Ekmekçi, Y. (2021). Comparative physiological and proteomic analysis of cultivated and wild safflower response to drought stress and re-watering. *Physiol. Mol. Biol. Plants.* 27 (2), 281–295. doi: 10.1007/s12298-021-00934-2

Curtis, T. Y., Bo, V., Tucker, A., and Halford, N. G. (2018). Construction of a network describing asparagine metabolism in plants and its application to the identification of genes affecting asparagine metabolism in wheat under drought and nutritional stress. *Food Energy security.* 7 (1), e00126. doi: 10.1002/fes3.126

Curtis, R. H., Powers, S. J., Napier, J., and Matthes, M. C. (2013). The arabidopsis f-box/Kelch-repeat protein At2g44130 is upregulated in giant cells and promotes nematode susceptibility. *Mol. Plant-Microbe interactions.* 26 (1), 36–43. doi: 10.1094/MPMI-05-12-0135-FI

Dey, N., and Bhattacharjee, S. (2020). Accumulation of polyphenolic compounds and osmolytes under dehydration stress and their implication in redox regulation in four indigenous aromatic rice cultivars. *Rice Science.* 27 (4), 329–344. doi: 10.1016/j.rsci.2020.05.008

Dubey, R. S. (2018). "Photosynthesis in plants under stressful conditions," in *Handbook of photosynthesis* (Boca Raton: CRC Press), 629–649.

Esmaeilpour, A., Van Labeke, M.-C., Samson, R., and Van Damme, P. (2015). Osmotic stress affects physiological responses and growth characteristics of three pistachio cultivars. *Acta Physiologiae Plantarum.* 37 (6), 1–14. doi: 10.1007/s11738-015-1876-x

FAO (2020). "FaAOotUN," in *FAOSTAT*, United Nations. vol. 2020.

Fatehi, F., Hosseinzadeh, A., Alizadeh, H., and Brimavandi, T. (2013). The proteome response of hordeum spontaneum to salinity stress. *Cereal Res. Commun.* 41 (1), 78–87. doi: 10.1556/CRC.2012.0017

Fatehi, F., Hosseinzadeh, A., Alizadeh, H., Brimavandi, T., and Struik, P. C. (2012). The proteome response of salt-resistant and salt-sensitive barley genotypes to long-term salinity stress. *Mol. Biol. Rep.* 39 (5), 6387–6397. doi: 10.1007/s11033-012-1460-z

Fermani, S., Sparla, F., Falini, G., Martelli, P., Casadio, R., Pupillo, P., et al. (2007). Molecular mechanism of thioredoxin regulation in photosynthetic A2B2-glyceraldehyde-3-phosphate dehydrogenase. *Proc. Natl. Acad. Sci.* 104 (26), 11109–11114. doi: 10.1073/pnas.0611636104

Ferrero-Serrano, Á, and Assmann, S. M. (2016). The α-subunit of the rice heterotrimeric G protein, RGA1, regulates drought tolerance during the vegetative phase in the dwarf rice mutant d1. *J. Exp. botany.* 67 (11), 3433–3443. doi: 10.1093/jxb/erw183

Fukao, Y. (2012). Protein–protein interactions in plants. *Plant Cell Physiol.* 53 (4), 617–625. doi: 10.1093/pcp/pcs026

Gallego, M. E., and White, C. I. (2001). RAD50 function is essential for telomere maintenance in arabidopsis. *Proc. Natl. Acad. Sci.* 98 (4), 1711–1716. doi: 10.1073/pnas.98.4.1711

Gao, Y., Cui, Y., Long, R., Sun, Y., Zhang, T., Yang, Q., et al. (2019). Salt-stress induced proteomic changes of two contrasting alfalfa cultivars during germination stage. *J. Sci. Food Agriculture.* 99 (3), 1384–1396. doi: 10.1002/jsfa.9331

García-Morales, S., Gómez-Merino, F., Trejo-Téllez, L., Tavitas-Fuentes, L., and Hernández-Aragón, L. (2018). Osmotic stress affects growth, content of chlorophyll, abscisic acid, na+, and k+, and expression of novel NAC genes in contrasting rice cultivars. *Biol. plantarum.* 62 (2), 307–317. doi: 10.1007/s10535-017-0761-4

Gherbi, H., Gallego, M. E., Jalut, N., Lucht, J. M., Hohn, B., and White, C. I. (2001). Homologous recombination in planta is stimulated in the absence of Rad50. *EMBO Rep.* 2 (4), 287–291. doi: 10.1093/embo-reports/kve069

Ghorbani, A., Tahmasebi, A., Izadpanah, K., Afsharifar, A., and Dietzgen, R. G. (2019). Genome-wide analysis of alternative splicing in zea mays during maize Iranian mosaic virus infection. *Plant Mol. Biol. Reporter.* 37 (5), 413–420. doi: 10.1007/s11105-019-01169-y

Gnanaraj, M., Baburajan, R., Sekar, T., Muneewaran, T., and Manoharan, K. (2021). Isolation and characterization of phospholipase d in response to abiotic stress from vigna radiata (L.) wilczek. *Plant Gene* 27, 100308. doi: 10.1016/j.plgene.2021.100308

Goharrizi, K. J., Baghizadeh, A., Kalantar, M., and Fatehi, F. (2020). Combined effects of salinity and drought on physiological and biochemical characteristics of pistachio rootstocks. *Scientia Horticulturae.* 261, 108970. doi: 10.1016/j.scienta.2019.108970

Guan, L., Haider, M. S., Khan, N., Nasim, M., Jiu, S., Fiaz, M., et al. (2018). Transcriptome sequence analysis elaborates a complex defensive mechanism of grapevine (Vitis vinifera l.) in response to salt stress. *Int. J. Mol. Sci.* 19 (12), 4019. doi: 10.3390/ijms19124019

Guo, X., Li, J., Zhang, L., Zhang, Z., He, P., Wang, W., et al. (2020). Heterotrimeric G-protein α subunit (LeGPA1) confers cold stress tolerance to processing tomato plants (Lycopersicon esculentum mill). *BMC Plant Biol.* 20 (1), 1–16. doi: 10.1186/s12870-020-02615-w

Haider, M. S., Kurjogi, M. M., Khalil-ur-Rehman, M., Pervez, T., Songtao, J., Fiaz, M., et al. (2018). Drought stress revealed physiological, biochemical and gene-expressional variations in 'Yoshihime'peach (Prunus persica l) cultivar. *J. Plant Interactions.* 13 (1), 83–90. doi: 10.1080/17429145.2018.1432772

Han, M., Zhang, C., Suglo, P., Sun, S., Wang, M., and Su, T. (2021). L-aspartate: An essential metabolite for plant growth and stress acclimation. *Molecules* 26 (7), 1887. doi: 10.3390/molecules26071887

Hayat, S., Hayat, Q., Alyemeni, M. N., Wani, A. S., Pichtel, J., and Ahmad, A. (2012). Role of proline under changing environments: a review. *Plant Signaling behavior.* 7 (11), 1456–1466. doi: 10.4161/psb.21949

Heide, H., Kalisz, H. M., and Follmann, H. (2004). The oxygen evolving enhancer protein 1 (OEE) of photosystem II in green algae exhibits thioredoxin activity. *J. Plant Physiol.* 161 (2), 139–149. doi: 10.1078/0176-1617-01033

Hejri, S., Salimi, A., Malboobi, M. A., and Fatehi, F. (2021). Comparative proteome analyses of rhizomania resistant transgenic sugar beets based on RNA silencing mechanism. *GM Crops Food.* 12 (1), 419–433. doi: 10.1080/21645698.2021.1954467

Héricourt, F., Chefdor, F., Bertheau, L., Tanigawa, M., Maeda, T., Guirimand, G., et al. (2013). Characterization of histidine-aspartate kinase HK1 and identification of histidine phosphotransfer proteins as potential partners in a populus multistep phosphorelay. *Physiologia Plantarum.* 149 (2), 188–199. doi: 10.1111/ppl.12024

Héricourt, F., Chefdor, F., Djeghdir, I., Larcher, M., Lafontaine, F., Courdavault, V., et al. (2016). Functional divergence of poplar histidine-aspartate kinase HK1 paralogs in response to osmotic stress. *Int. J. Mol. Sci.* 17 (12), 2061. doi: 10.3390/ijms17122061

Hernàndez-Sebastiá, C., Varin, L., and Marsolais, F. (2008). "Sulfotransferases from plants, algae and phototrophic bacteria," in *Sulfur metabolism in phototrophic organisms* (Dordrecht: Springer), 111–130.

Hirschmann, F., Krause, F., and Papenbrock, J. (2014). The multi-protein family of sulfotransferases in plants: composition, occurrence, substrate specificity, and functions. *Front. Plant science.* 5, 556. doi: 10.3389/fpls.2014.00556

Hong, Y., Pan, X., Welti, R., and Wang, X. (2008). Phospholipase Dα3 is involved in the hyperosmotic response in arabidopsis. *Plant Cell.* 20 (3), 803–816. doi: 10.1105/tpc.107.056390

Hui-Hui, Z., Guang-Liang, S., Jie-Yu, S., Xin, L., Ma-Bo, L., Liang, M., et al. (2019). Photochemistry and proteomics of mulberry (Morus alba l.) seedlings under NaCl and NaHCO3 stress. *Ecotoxicol. Environ. Saf.* 184, 109624. doi: 10.1016/j.ecoenv.2019.109624

Hurkman, W. J., and Tanaka, C. K. (1986). Solubilization of plant membrane proteins for analysis by two-dimensional gel electrophoresis. *Plant Physiol.* 81 (3), 802–806. doi: 10.1104/pp.81.3.802

Jamshidi Goharrizi, K., Amirmahani, F., and Salehi, F. (2020). Assessment of changes in physiological and biochemical traits in four pistachio rootstocks under drought, salinity and drought+ salinity stresses. *Physiologia plantarum.* 168 (4), 973–989. doi: 10.1111/ppl.13042

Jamshidi Goharrizi, K., Baghizadeh, A., Kalantar, M., and Fatehi, F. (2020). Assessment of changes in some biochemical traits and proteomic profile of UCB-1 pistachio rootstock leaf under salinity stress. *J. Plant Growth regulation.* 39 (2), 608–630. doi: 10.1007/s00344-019-10004-3

Jander, G., and Joshi, V. (2009). "Aspartate-derived amino acid biosynthesis in arabidopsis thaliana," in *The arabidopsis book/American society of plant biologists*, Rockville, MD. vol. 7.

Ji, T., Li, S., Li, L., Huang, M., Wang, X., Wei, M., et al. (2018). Cucumber phospholipase d alpha gene overexpression in tobacco enhanced drought stress tolerance by regulating stomatal closure and lipid peroxidation. *BMC Plant Biol.* 18 (1), 1–14. doi: 10.1186/s12870-018-1592-y

Jin, L., Ouyang, N., Huang, Y., Liu, C., and Ruan, Y. (2019). Genome-wide analysis of sulfotransferase genes and their responses to abiotic stresses in Chinese cabbage (Brassica rapa l.). *PloS One* 14 (8), e0221422. doi: 10.1371/journal.pone.0221422

Jungklang, J., Saengnil, K., and Uthaibutra, J. (2017). Effects of water-deficit stress and paclobutrazol on growth, relative water content, electrolyte leakage, proline content and some antioxidant changes in curcuma alismatifolia gagnep. cv. Chiang mai pink. *Saudi J. Biol. Sci.* 24 (7), 1505–1512. doi: 10.1016/j.sjbs.2015.09.017

Kai, W., Wang, J., Liang, B., Fu, Y., Zheng, Y., Zhang, W., et al. (2019). PYL9 is involved in the regulation of ABA signaling during tomato fruit ripening. *J. Exp. botany.* 70 (21), 6305–6319. doi: 10.1093/jxb/erz396

Kamireddy, K., Sonbarse, P. P., Mishra, S., Agrawal, L., Chauhan, P. S., Lata, C., et al. (2021). Proteomic approach to identify the differentially abundant proteins during flavour development in tuberous roots of decalepis hamiltonii Wight & arn. *3 Biotech.* 11 (4), 1–19. doi: 10.1007/s13205-021-02714-x

Kappachery, S., Sasi, S., Alyammahi, O., Alyassi, A., Venkatesh, J., and Gururani, M. A. (2021). Overexpression of cytoplasmic solanum tuberosum glyceraldehyde 3-phosphate dehydrogenase (GAPDH) gene improves PSII efficiency and alleviates salinity stress in arabidopsis. *J. Plant Interactions.* 16 (1), 398–410. doi: 10.1080/17429145.2021.1962420

Khoyerdi, F. F., Shamshiri, M. H., and Estaji, A. (2016). Changes in some physiological and osmotic parameters of several pistachio genotypes under drought stress. *Scientia horticulturae.* 198, 44–51. doi: 10.1016/j.scienta.2015.11.028

Kim, J., Liu, Y., Zhang, X., Zhao, B., and Childs, K. L. (2016). Analysis of salt-induced physiological and proline changes in 46 switchgrass (Panicum virgatum) lines indicates multiple response modes. *Plant Physiol. Biochem.* 105, 203–212. doi: 10.1016/j.plaphy.2016.04.020

Koenigshofer, H., and Loeppert, H.-G. (2019). The up-regulation of proline synthesis in the meristematic tissues of wheat seedlings upon short-term exposure to osmotic stress. *J. Plant Physiol.* 237, 21–29. doi: 10.1016/j.jplph.2019.03.010

Krech, K., Ruf, S., Masduki, F. F., Thiele, W., Bednarczyk, D., Albus, C. A., et al. (2012). The plastid genome-encoded Ycf4 protein functions as a nonessential assembly factor for

photosystem I in higher plants. *Plant Physiol.* 159 (2), 579–591. doi: 10.1104/pp.112.196642

Lan, C.-Y., Lin, K.-H., Chen, C.-L., Huang, W.-D., and Chen, C.-C. (2020). Comparisons of chlorophyll fluorescence and physiological characteristics of wheat seedlings influenced by iso-osmotic stresses from polyethylene glycol and sodium chloride. *Agronomy* 10 (3), 325. doi: 10.3390/agronomy10030325

Leitão, I., Leclercq, C. C., Ribeiro, D. M., Renaut, J., Almeida, A. M., Martins, L. L., et al. (2021). Stress response of lettuce (Lactuca sativa) to environmental contamination with selected pharmaceuticals: A proteomic study. *J. Proteomics.* 245, 104291. doi: 10.1016/j.jprot.2021.104291

Lichtenthaler, H. K., and Buschmann, C. (2001). Chlorophylls and carotenoids: Measurement and characterization by UV-VIS spectroscopy. *Curr. Protoc. Food analytical Chem.* 1 (1), F4. 3.1–F4. 3.8. doi: 10.1002/0471142913.faf0403s01

Li, H., Li, Y., Ke, Q., Kwak, S.-S., Zhang, S., and Deng, X. (2020). Physiological and differential proteomic analyses of imitation drought stress response in sorghum bicolor root at the seedling stage. *Int. J. Mol. Sci.* 21 (23), 9174. doi: 10.3390/ijms21239174

Liu, Q., Liu, R., Zhou, Y., Wang, W., Wu, G., and Yang, N. (2022). Phospholipase dδ and H2S increase the production of NADPH oxidase-dependent H2O2 to respond to osmotic stress-induced stomatal closure in arabidopsis thaliana. *J. Plant Physiol.* 270, 153617. doi: 10.1016/j.jplph.2022.153617

Liu, Y., Wang, X., Dong, D., Guo, L., Dong, X., Leng, J., et al. (2021). Research advances in heterotrimeric G-protein α subunits and uncanonical G-protein coupled receptors in plants. *Int. J. Mol. Sci.* 22 (16), 8678. doi: 10.3390/ijms22168678

Liu, C., Xu, Y., Feng, Y., Long, D., Cao, B., Xiang, Z., et al. (2018). Ectopic expression of mulberry G-proteins alters drought and salt stress tolerance in tobacco. *Int. J. Mol. Sci.* 20 (1), 89. doi: 10.3390/ijms20010089

Liu, Q., Zhou, Y., Li, H., Liu, R., Wang, W., Wu, W., et al. (2021). Osmotic stress-triggered stomatal closure requires phospholipase dδ and hydrogen sulfide in arabidopsis thaliana. *Biochem. Biophys. Res. Commun.* 534, 914–920. doi: 10.1016/j.bbrc.2020.10.074

Ma, Y., Dai, X., Xu, Y., Luo, W., Zheng, X., Zeng, D., et al. (2015). COLD1 confers chilling tolerance in rice. *Cell* 160 (6), 1209–1221. doi: 10.1016/j.cell.2015.01.046

Mao, G., Wang, R., Guan, Y., Liu, Y., and Zhang, S. (2011). Sulfurtransferases 1 and 2 play essential roles in embryo and seed development in arabidopsis thaliana. *J. Biol. Chem.* 286 (9), 7548–7557. doi: 10.1074/jbc.M110.182865

Mao, X., Zhang, H., Tian, S., Chang, X., and Jing, R. (2010). TaSnRK2. 4, an SNF1-type serine/threonine protein kinase of wheat (Triticum aestivum l.), confers enhanced multistress tolerance in arabidopsis. *J. Exp. botany.* 61 (3), 683–696. doi: 10.1093/jxb/erp331

Marondedze, C., Thomas, L., Lilley, K. S., and Gehring, C. (2020). Drought stress causes specific changes to the spliceosome and stress granule components. *Front. Mol. biosciences.* 6, 163. doi: 10.3389/fmolb.2019.00163

Mattioli, R., Palombi, N., Funck, D., and Trovato, M. (2020). Proline accumulation in pollen grains as potential target for improved yield stability under salt stress. *Front. Plant science.* 11, 582877. doi: 10.3389/fpls.2020.582877

Mayfield, S. P. (1991). Over-expression of the oxygen-evolving enhancer 1 protein and its consequences on photosystem II accumulation. *Planta* 185 (1), 105–110. doi: 10.1007/BF00194521

Mechri, B., Tekaya, M., Hammami, M., and Chehab, H. (2020). Effects of drought stress on phenolic accumulation in greenhouse-grown olive trees (Olea europaea). *Biochem. Systematics Ecology.* 92, 104112. doi: 10.1016/j.bse.2020.104112

Meena, M., Divyanshu, K., Kumar, S., Swapnil, P., Zehra, A., Shukla, V., et al. (2019). Regulation of l-proline biosynthesis, signal transduction, transport, accumulation and its vital role in plants during variable environmental conditions. *Heliyon* 5 (12), e02952. doi: 10.1016/j.heliyon.2019.e02952

Miao, C., Xiao, L., Hua, K., Zou, C., Zhao, Y., Bressan, R. A., et al. (2018). Mutations in a subfamily of abscisic acid receptor genes promote rice growth and productivity. *Proc. Natl. Acad. Sci.* 115 (23), 6058–6063. doi: 10.1073/pnas.1804774115

Misra, S., Wu, Y., Venkataraman, G., Sopory, S. K., and Tuteja, N. (2007). Heterotrimeric G-protein complex and G-protein-coupled receptor from a legume (Pisum sativum): role in salinity and heat stress and cross-talk with phospholipase c. *Plant J.* 51 (4), 656–669. doi: 10.1111/j.1365-313X.2007.03169.x

Moazzam Jazi, M., Ghadirzadeh Khorzoghi, E., Botanga, C., and Seyedi, S. M. (2016). Identification of reference genes for quantitative gene expression studies in a non-model tree pistachio (Pistacia vera l.). *PloS One* 11 (6), e0157467. doi: 10.1371/journal.pone.0157467

Morales, M., and Munné-Bosch, S. (2019). Malondialdehyde: facts and artifacts. *Plant Physiol.* 180 (3), 1246–1250. doi: 10.1104/pp.19.00405

Most, P., and Papenbrock, J. (2015). Possible roles of plant sulfurtransferases in detoxification of cyanide, reactive oxygen species, selected heavy metals and arsenate. *Molecules* 20 (1), 1410–1423. doi: 10.3390/molecules20011410

Muñoz-Bertomeu, J., Cascales-Miñana, B., Alaiz, M., Segura, J. A., and Ros, R. (2010). A critical role of plastidial glycolytic glyceraldehyde-3-phosphate dehydrogenase in the control of plant metabolism and development. *Plant Signaling Behavior.* 5 (1), 67–69. doi: 10.4161/psb.5.1.10200

Naikoo, M. I., Dar, M. I., Raghib, F., Jaleel, H., Ahmad, B., Raina, A., et al. (2019). "Role and regulation of plants phenolics in abiotic stress tolerance: An overview. *Plant signaling molecules*, (Cambridge: Woodhead Publishing) 157–168. doi: 10.1016/B978-0-12-816451-8.00009-5

Nakamura, T., Yamaguchi, Y., and Sano, H. (2000). Plant mercaptopyruvate sulfurtransferases: molecular cloning, subcellular localization and enzymatic activities. *Eur. J. Biochem.* 267 (17), 5621–5630. doi: 10.1046/j.1432-1327.2000.01633.x

Nellaepalli, S., Ozawa, S.-I., Kuroda, H., and Takahashi, Y. (2018). The photosystem I assembly apparatus consisting of Ycf3–Y3IP1 and Ycf4 modules. *Nat. Commun.* 9 (1), 1–10. doi: 10.1038/s41467-018-04823-3

Ngara, R., Ramulifho, E., Movahedi, M., Shargie, N. G., Brown, A. P., and Chivasa, S. (2018). Identifying differentially expressed proteins in sorghum cell cultures exposed to osmotic stress. *Sci. Rep.* 8 (1), 1–12. doi: 10.1038/s41598-018-27003-1

Ni, C. Z., Wang, H. Q., Xu, T., Qu, Z., and Liu, G. Q. (2005). AtKP1, a kinesin-like protein, mainly localizes to mitochondria in arabidopsis thaliana. *Cell Res.* 15 (9), 725–733. doi: 10.1038/sj.cr.7290342

Nonomura, K.-I., Morohoshi, A., Nakano, M., Eiguchi, M., Miyao, A., Hirochika, H., et al. (2007). A germ cell–specific gene of the ARGONAUTE family is essential for the progression of premeiotic mitosis and meiosis during sporogenesis in rice. *Plant Cell.* 19 (8), 2583–2594. doi: 10.1105/tpc.107.053199

Pakzad, R., Fatehi, F., Kalantar, M., and Maleki, M. (2019). Evaluating the antioxidant enzymes activities, lipid peroxidation and proteomic profile changing in UCB-1 pistachio rootstock leaf under drought stress. *Scientia Horticulturae.* 256, 108617. doi: 10.1016/j.scienta.2019.108617

Palmer, A. J., Baker, A., and Muench, S. P. (2016). The varied functions of aluminium-activated malate transporters–much more than aluminium resistance. *Biochem. Soc. Trans.* 44 (3), 856–862. doi: 10.1042/BST20160027

Pál, M., Tajti, J., Szalai, G., Peeva, V., Végh, B., and Janda, T. (2018). Interaction of polyamines, abscisic acid and proline under osmotic stress in the leaves of wheat plants. *Sci. Rep.* 8 (1), 1–12. doi: 10.1038/s41598-018-31297-6

Pandey, S., and Assmann, S. M. (2004). The arabidopsis putative G protein–coupled receptor GCR1 interacts with the G protein α subunit GPA1 and regulates abscisic acid signaling. *Plant Cell.* 16 (6), 1616–1632. doi: 10.1105/tpc.020321

Papenbrock, J., and Schmidt, A. (2000). Characterization of a sulfurtransferase from arabidopsis thaliana. *Eur. J. Biochem.* 267 (1), 145–154. doi: 10.1046/j.1432-1327.2000.00980.x

Park, C.-J., and Seo, Y.-S. (2015). Heat shock proteins: a review of the molecular chaperones for plant immunity. *Plant Pathol. J.* 31 (4), 323. doi: 10.5423/PPJ.RW.08.2015.0150

Pasaribu, S., Basyuni, M., Purba, E., and Hasanah, Y. (2021). "The estimated of 18.1 kDa class IV small heat shock protein (sHsp) from hevea brasiliensis using of PHYRE2 and SWISS-MODEL software," in *IOP conference series: Earth and environmental science* (Indonesia: IOP Publishing).

Patel, J. S., Selvaraj, V., Gunupuru, L. R., Kharwar, R. N., and Sarma, B. K. (2020). Plant G-protein signaling cascade and host defense. *3 Biotech.* 10 (5), 1–8. doi: 10.1007/s13205-020-02201-9

Pfaffl, M. W., Horgan, G. W., and Dempfle, L. (2002). Relative expression software tool (REST©) for group-wise comparison and statistical analysis of relative expression results in real-time PCR. *Nucleic Acids Res.* 30 (9), e36–e3e. doi: 10.1093/nar/30.9.e36

Piwowarczyk, B., Tokarz, K., Makowski, W., and Łukasiewicz, A. (2017). Different acclimatization mechanisms of two grass pea cultivars to osmotic stress in *in vitro* culture. *Acta Physiologiae Plantarum.* 39 (4), 1–5. doi: 10.1007/s11738-017-2389-6

Rahimi, B., Afzali, M., Farhadi, F., and Alamolhoda, A. A. (2021). Reverse osmosis desalination for irrigation in a pistachio orchard. *Desalination* 516, 115236. doi: 10.1016/j.desal.2021.115236

Rahman, M. A., Ren, L., Wu, W., and Yan, Y. (2015). Proteomic analysis of PEG-induced drought stress responsive protein in TERF1 overexpressed sugarcane (Saccharum officinarum) leaves. *Plant Mol. Biol. Reporter.* 33 (3), 716–730. doi: 10.1007/s11105-014-0784-3

Rahneshan, Z., Nasibi, F., and Moghadam, A. A. (2018). Effects of salinity stress on some growth, physiological, biochemical parameters and nutrients in two pistachio (Pistacia vera l.) rootstocks. *J. Plant Interact.* 13 (1), 73–82. doi: 10.1080/17429145.2018.1424355

Ramesh, S. A., Kamran, M., Sullivan, W., Chirkova, L., Okamoto, M., Degryse, F., et al. (2018). Aluminum-activated malate transporters can facilitate GABA transport. *Plant Cell.* 30 (5), 1147–1164. doi: 10.1105/tpc.17.00864

Rampino, P., De Pascali, M., De Caroli, M., Luvisi, A., De Bellis, L., Piro, G., et al. (2017). Td4IN2: A drought-responsive durum wheat (Triticum durum desf.) gene coding for a resistance like protein with serine/threonine protein kinase, nucleotide binding site and leucine rich domains. *Plant Physiol. Biochem.* 120, 223–231. doi: 10.1016/j.plaphy.2017.10.010

Rodas-Junco, B. A., Racagni-Di-Palma, G. E., Canul-Chan, M., Usorach, J., and Hernández-Sotomayor, S. T. (2021). Link between lipid second messengers and osmotic stress in plants. *Int. J. Mol. Sci.* 22 (5), 2658. doi: 10.3390/ijms22052658

Sadeghi, B., Mirzaei, S., and Fatehi, F. (2022). The proteomic analysis of the resistance responses in tomato during interaction with alternaria alternate. *Scientia Horticulturae.* 304, 111295. doi: 10.1016/j.scienta.2022.111295

Saucedo-García, M., Gavilanes-Ruíz, M., and Arce-Cervantes, O. (2015). Long-chain bases, phosphatidic acid, MAPKs, and reactive oxygen species as nodal signal transducers in stress responses in arabidopsis. *Front. Plant science.* 6, 55. doi: 10.3389/fpls.2015.00055

Shan, Z., Luo, X., Wei, M., Huang, T., Khan, A., and Zhu, Y. (2018). Physiological and proteomic analysis on long-term drought resistance of cassava (Manihot esculenta crantz). *Sci. Rep.* 8 (1), 1–12. doi: 10.1038/s41598-018-35711-x

Shayan, S., Norouzi, M., Vahed, M. M., Mohammadi, S. A., and Toorchi, M. (2020). Leaf proteome pattern of two bread wheat varieties under water deficit stress conditions. *Curr. Plant Biol.* 23, 100146. doi: 10.1016/j.cpb.2020.100146

Skirycz, A., De Bodt, S., Obata, T., De Clercq, I., Claeys, H., De Rycke, R., et al. (2010). Developmental stage specificity and the role of mitochondrial metabolism in the response of arabidopsis leaves to prolonged mild osmotic stress. *Plant Physiol.* 152 (1), 226–244. doi: 10.1104/pp.109.148965

Song, Z. T., Liu, J. X., and Han, J. J. (2021). Chromatin remodeling factors regulate environmental stress responses in plants. *J. Integr. Plant Biol.* 63 (3), 438–450. doi: 10.1111/jipb.13064

Sun, X.-L., Yu, Q.-Y., Tang, L.-L., Ji, W., Bai, X., Cai, H., et al. (2013). GsSRK, a G-type lectin s-receptor-like serine/threonine protein kinase, is a positive regulator of plant tolerance to salt stress. *J. Plant Physiol.* 170 (5), 505–515. doi: 10.1016/j.jplph.2012.11.017

Takashi, Y., Kobayashi, Y., Tanaka, K., and Tamura, K. (2009). Arabidopsis replication protein a 70a is required for DNA damage response and telomere length homeostasis. *Plant Cell Physiol.* 50 (11), 1965–1976. doi: 10.1093/pcp/pcp140

Toorchi, M., Yukawa, K., Nouri, M.-Z., and Komatsu, S. (2009). Proteomics approach for identifying osmotic-stress-related proteins in soybean roots. *Peptides* 30 (12), 2108–2117. doi: 10.1016/j.peptides.2009.09.006

Turek, I., Wheeler, J., Bartels, S., Szczurek, J., Wang, Y. H., Taylor, P., et al. (2020). A natriuretic peptide from arabidopsis thaliana (AtPNP-a) can modulate catalase 2 activity. *Sci. Rep.* 10 (1), 1–14. doi: 10.1038/s41598-020-76676-0

Urban, M. O., Planchon, S., Hoštičková, I., Vanková, R., Dobrev, P., Renaut, J., et al. (2021). The resistance of oilseed rape microspore-derived embryos to osmotic stress is associated with the accumulation of energy metabolism proteins, redox homeostasis, higher abscisic acid, and cytokinin contents. *Front. Plant Sci.* 1161. doi: 10.3389/fpls.2021.628167

Velasquez, S. M., Ricardi, M. M., Dorosz, J. G., Fernandez, P. V., Nadra, A. D., Pol-Fachin, L., et al. (2011). O-Glycosylated cell wall proteins are essential in root hair growth. *Science* 332 (6036), 1401–1403. doi: 10.1126/science.1206657

Velikova, V., Yordanov, I., and Edreva, A. (2000). Oxidative stress and some antioxidant systems in acid rain-treated bean plants: protective role of exogenous polyamines. *Plant science.* 151 (1), 59–66. doi: 10.1016/S0168-9452(99)00197-1

Venkatesh, J., Kang, M.-Y., Liu, L., Kwon, J.-K., and Kang, B.-C. (2020). F-box family genes, LTSF1 and LTSF2, regulate low-temperature stress tolerance in pepper (capsicum chinense). *Plants* 9 (9), 1186. doi: 10.3390/plants9091186

Wang, C.-F., Han, G.-L., Yang, Z.-R., Li, Y.-X., and Wang, B.-S. (2022). Plant salinity sensors: Current understanding and future directions. *Front. Plant Sci.* 13. doi: 10.3389/fpls.2022.859224

Wang, Y., Sang, Z., Xu, S., Xu, Q., Zeng, X., Jabu, D., et al. (2020). Comparative proteomics analysis of Tibetan hull-less barley under osmotic stress *via* data-independent acquisition mass spectrometry. *GigaScience* 9 (3), giaa019. doi: 10.1093/gigascience/giaa019

Wang, J., Yao, W., Wang, L., Ma, F., Tong, W., Wang, C., et al. (2017). Overexpression of VpEIFP1, a novel f-box/Kelch-repeat protein from wild Chinese vitis pseudoreticulata, confers higher tolerance to powdery mildew by inducing thioredoxin z proteolysis. *Plant Science.* 263, 142–155. doi: 10.1016/j.plantsci.2017.07.004

Wei, J., Shao, W., Liu, X., He, L., Zhao, C., Yu, G., et al. (2022). Genome-wide identification and expression analysis of phospholipase d gene in leaves of sorghum in response to abiotic stresses. *Physiol. Mol. Biol. Plants.* 28 (6), 1261–1276. doi: 10.1007/s12298-022-01200-9

Wong, M. M., Chong, G. L., and Verslues, P. E. (2017). "Epigenetics and RNA processing: connections to drought, salt, and ABA?," in *Plant stress tolerance* (New York: Springer), 3–21.

Xing, L., Zhao, Y., Gao, J., Xiang, C., and Zhu, J.-K. (2016). The ABA receptor PYL9 together with PYL8 plays an important role in regulating lateral root growth. *Sci. Rep.* 6 (1), 1–13. doi: 10.1038/srep27177

Xiong, L., and Zhu, J. K. (2002). Molecular and genetic aspects of plant responses to osmotic stress. *Plant Cell Environment.* 25 (2), 131–139. doi: 10.1046/j.1365-3040.2002.00782.x

Yamasaki, H., and Cohen, M. F. (2016). Biological consilience of hydrogen sulfide and nitric oxide in plants: gases of primordial earth linking plant, microbial and animal physiologies. *Nitric. Oxide* 55, 91–100. doi: 10.1016/j.niox.2016.04.002

Zandalinas, S. I., Fritschi, F. B., and Mittler, R. (2020). Signal transduction networks during stress combination. *J. Exp. Botany.* 71 (5), 1734–1741. doi: 10.1093/jxb/erz486

Zang, X., and Komatsu, S. (2007). A proteomics approach for identifying osmotic-stress-related proteins in rice. *Phytochemistry* 68 (4), 426–437. doi: 10.1016/j.phytochem.2006.11.005

Zegaoui, Z., Planchais, S., Cabassa, C., Djebbar, R., Belbachir, O. A., and Carol, P. (2017). Variation in relative water content, proline accumulation and stress gene expression in two cowpea landraces under drought. *J. Plant Physiol.* 218, 26–34. doi: 10.1016/j.jplph.2017.07.009

Zhang, X., Gou, M., and Liu, C.-J. (2013). Arabidopsis kelch repeat f-box proteins regulate phenylpropanoid biosynthesis *via* controlling the turnover of phenylalanine ammonia-lyase. *Plant Cell.* 25 (12), 4994–5010. doi: 10.1105/tpc.113.119644

Zhang, C., and Shi, S. (2018). Physiological and proteomic responses of contrasting alfalfa (Medicago sativa l.) varieties to PEG-induced osmotic stress. *Front. Plant Sci.* 9, 242. doi: 10.3389/fpls.2018.00242

Zhang, Y., Wei, M., Liu, A., Zhou, R., Li, D., Dossa, K., et al. (2019). Comparative proteomic analysis of two sesame genotypes with contrasting salinity tolerance in response to salt stress. *J. proteomics.* 201, 73–83. doi: 10.1016/j.jprot.2019.04.017

Zhang, F., Zhu, G., Du, L., Shang, X., Cheng, C., Yang, B., et al. (2016). Genetic regulation of salt stress tolerance revealed by RNA-seq in cotton diploid wild species, gossypium davidsonii. *Sci. Rep.* 6 (1), 1–15. doi: 10.1038/srep20582

Zhou, G., Yang, L.-T., Li, Y.-R., Zou, C.-L., Huang, L.-P., Qiu, L.-H., et al. (2012). Proteomic analysis of osmotic stress-responsive proteins in sugarcane leaves. *Plant Mol. Biol. reporter.* 30 (2), 349–359. doi: 10.1007/s11105-011-0343-0

Zhu, D., Luo, F., Zou, R., Liu, J., and Yan, Y. (2021). Integrated physiological and chloroplast proteome analysis of wheat seedling leaves under salt and osmotic stresses. *J. Proteomics.* 234, 104097. doi: 10.1016/j.jprot.2020.104097

frontiers | Frontiers in Plant Science

TYPE Original Research
PUBLISHED 27 January 2023
DOI 10.3389/fpls.2023.1096091

Check for updates

OPEN ACCESS

EDITED BY
Mehdi Rahimi,
Graduate University of Advanced Technology, Iran

REVIEWED BY
Guangjie Li,
Chinese Academy of Sciences, China
Shijuan Liu,
Qufu Normal University, China
Tingwu Liu,
Huaiyin Normal University, China
Yutong Jiang,
Shanghai Jiao Tong University, China

*CORRESPONDENCE
Daizhen Sun
sdz64@126.com
Hua Fan
jeanafan@163.com

†These authors have contributed equally to this work

SPECIALTY SECTION
This article was submitted to Plant Abiotic Stress, a section of the journal Frontiers in Plant Science

RECEIVED 11 November 2022
ACCEPTED 09 January 2023
PUBLISHED 27 January 2023

CITATION
Zhang H, Chen M, Xu C, Liu R, Tang W, Chen K, Zhou Y, Xu Z, Chen J, Ma Y, Chen W, Sun D and Fan H (2023) H^+-pyrophosphatases enhance low nitrogen stress tolerance in transgenic *Arabidopsis* and wheat by interacting with a receptor-like protein kinase.
Front. Plant Sci. 14:1096091.
doi: 10.3389/fpls.2023.1096091

COPYRIGHT
© 2023 Zhang, Chen, Xu, Liu, Tang, Chen, Zhou, Xu, Chen, Ma, Chen, Sun and Fan. This is an open-access article distributed under the terms of the Creative Commons Attribution License (CC BY). The use, distribution or reproduction in other forums is permitted, provided the original author(s) and the copyright owner(s) are credited and that the original publication in this journal is cited, in accordance with accepted academic practice. No use, distribution or reproduction is permitted which does not comply with these terms.

H^+-pyrophosphatases enhance low nitrogen stress tolerance in transgenic *Arabidopsis* and wheat by interacting with a receptor-like protein kinase

Huijuan Zhang[1,2†], Ming Chen[2†], Chengjie Xu[1,2†], Rongbang Liu[2], Wensi Tang[2], Kai Chen[2], Yongbin Zhou[2], Zhaoshi Xu[2], Jun Chen[2], Youzhi Ma[2], Weiguo Chen[1], Daizhen Sun[1*] and Hua Fan[1*]

[1]College of Agriculture, Shanxi Agricultural University, Shanxi, China, [2]Institute of Crop Sciences, Chinese Academy of Agricultural Sciences (CAAS)/National Key Facility for Crop Gene Resources and Genetic Improvement, Key Laboratory of Biology and Genetic Improvement of Triticeae Crops, Ministry of Agriculture, Beijing, China

Introduction: Nitrogen is a major abiotic stress that affects plant productivity. Previous studies have shown that plant H+-pyrophosphatases (H+-PPases) enhance plant resistance to low nitrogen stress. However, the molecular mechanism underlying H+-PPase-mediated regulation of plant responses to low nitrogen stress is still unknown. In this study, we aimed to investigate the regulatory mechanism of AtAVP1 in response to low nitrogen stress.

Methods and Results: AtAVP1 in Arabidopsis thaliana and EdVP1 in Elymus dahuricus belong to the H+-PPase gene family. In this study, we found that AtAVP1 overexpression was more tolerant to low nitrogen stress than was wild type (WT), whereas the avp1-1 mutant was less tolerant to low nitrogen stress than WT. Plant height, root length, aboveground fresh and dry weights, and underground fresh and dry weights of EdVP1 overexpression wheat were considerably higher than those of SHI366 under low nitrogen treatment during the seedling stage. Two consecutive years of low nitrogen tolerance experiments in the field showed that grain yield and number of grains per spike of EdVP1 overexpression wheat were increased compared to those in SHI366, which indicated that EdVP1 conferred low nitrogen stress tolerance in the field. Furthermore, we screened interaction proteins in Arabidopsis; subcellular localization analysis demonstrated that AtAVP1 and Arabidopsis thaliana receptor-like protein kinase (AtRLK) were located on the plasma membrane. Yeast two-hybrid and luciferase complementary imaging assays showed that the AtRLK interacted with AtAVP1. Under low nitrogen stress, the Arabidopsis mutants rlk and avp1-1 had the same phenotypes.

Discussion: These results indicate that AtAVP1 regulates low nitrogen stress responses by interacting with AtRLK, which provides a novel insight into the regulatory pathway related to H+-pyrophosphatase function in plants.

KEYWORDS

low nitrogen stress, receptor-like protein kinase, arabidopsis, transgenic wheat, H^+-pyrophosphatase

1 Introduction

Nitrogen (N) is an essential macronutrient for plants to achieve optimal growth and development; therefore, low nitrogen is often a major limiting factor for crop yield (Jones et al., 2013). In actual crop production systems, excessive nitrogen fertilizer is used to maintain high yields. The extensive application of nitrogen fertilizer not only increases the cost of crop production but also causes serious environmental problems (Guo et al., 2010). In fact, only 30–50% of applied nitrogen is absorbed by the crop plants (Zhu et al., 2018). Improving crop nitrogen use efficiency (NUE) can increase crop productivity with less nitrogen fertilizer input (Han et al., 2015). H^+-pyrophosphatases (H^+-PPases) can respond to various abiotic stresses, including low nitrogen stress. For example, overexpression of *Arabidopsis thaliana AVP1* (*AtAVP1*) has been reported to improve the NUE in *Romaine Lettuce* (Paez-Valencia et al., 2013).

H^+-PPases are hydrolases that use pyrophosphate (PPi) as a substrate. In plants, there are type I and type II H^+-PPases. At present, the composition and structure of H^+-PPase is mainly a vacuolar membrane topological model, consisting of a single oligopeptide chain (Maeshima, 2000). Type II H^+-PPase is mainly distributed in the Golgi apparatus, and the Type II H^+-PPase accounts for 0.2% of the total type I H^+-PPase. The type I H^+-PPase was mainly located in the vacuolar membranes, but in recent years type I H^+-PPases was also located on the plasma membrane (PM) in *Ricinus communis, cauliflower, Oryza sativa* and *Arabidopsis thaliana* (Serrano et al., 2007; Paez-Valencia et al., 2011). Preliminary studies show that H^+-PPases are generally expressed in young, growing tissues, and are highly expressed in *Arabidopsis thaliana* under drought and salt stress (Shiratake et al., 1997; Paez-Valencia et al., 2011). The lack of the a2 and a3 subunits of another tonoplast proton pump V-ATPase resulted in an increase in its nitrate reductase activity under 24 h light (Krebs et al., 2010). H^+-PPase acts as a proton pump along with vacuolar V-ATPase to maintain acidic pH within the vacuolar lumen (Yoichi et al., 2003). Further the functional and physical characteristics are different (Maeshima, 2000).The activity of tonoplast proton pump V-ATPase creates the proton gradient and the membrane potential that is used to transport compounds against their concentration or electrochemical gradients (Schumacher, 2007). And Li et al. showed that the absorption of NO_3^- concentrations regulated by *TaVP* (H^+-pyrophosphatase) were caused by increased root absorption area instead of alteration of Pi and NO_3^- acquisition kinetics (Li et al., 2014).

The overexpression of *AVP1* was also reported to improve salt tolerance and drought tolerance of transgenic *Arabidopsis* (Gaxiola et al., 2001). Additionally, the drought and salt tolerance of transgenic plants was significantly improved when H^+-PPases from different plants (including *Arabidopsis*), and other type I H^+-PPases were overexpressed in alfalfa (Bao et al., 2009; Su et al., 2019), barley (Schilling et al., 2014), cotton (Pasapula et al., 2011), and tobacco (Gao et al., 2006). H^+-PPases also respond to low phosphorus stress in plants. When H^+-PPase genes were expressed in tomato, rice (Yang et al., 2007), tobacco (Li et al., 2014) and alfalfa (Su et al., 2019), the plants grew better in low phosphorus environment than did wild type (WT). In addition, *AVP1* can improve low nitrogen tolerance in plants. *TaAVP* overexpressed in tobacco increased the nitrogen content in the transgenic plants to an extent more than that observed in WT tobacco (Li et al., 2014). In our previous study, we found that the *Elymus dahuricus* H^+-PPase gene (*EdVP1*) was induced by low potassium stress, and overexpression of *EdVP1* in wheat considerably increased the grain yield and potassium uptake in transgenic wheat under low potassium stress (Zhou et al., 2020). These findings show that H^+-PPases genes play an important role in plant response to various abiotic stresses. However, our understanding of the regulatory mechanisms related to H^+-pyrophosphatases is still very limited.

In this study, we aimed to investigate the regulatory mechanism of *AtAVP1* in response to low nitrogen stress. We found that the H^+-pyrophosphatase (*AVP1*) gene could significantly improve plant resistance to low nitrogen stress in *Arabidopsis*, and overexpression of the *Elymus dahuricus* homolog of *AtAVP1* in wheat could also significantly improve the resistance of transgenic wheat to low nitrogen stress in greenhouse and field conditions. Furthermore, we found that the receptor-like kinases in *Arabidopsis* (AtRLK) can interact with AtAVP1, and the *Arabidopsis* mutant *rlk* had similar sensitivity to low nitrogen stress as the *Arabidopsis* mutant *avp1-1*. Our study provides useful insights into genes that may contribute towards strengthening plant tolerance against abiotic stress, and would help to improve crop plant production and associated costs.

2 Material and methods

2.1 *Arabidopsis* plants and growth conditions

For phenotypic analysis of transgenic, mutant and WT *Arabidopsis thaliana* plants under stress, we used the *Arabidopsis* ecotype Columbia-0 as WT and the *avp1-1* (SALK_019677) and *rlk* (SALK_123639C) mutants, which were obtained from the *Arabidopsis* Biological

Resource Center (Ohio State University, Columbus, OH, USA). Mutants were screened *via* the triple primer method, using the T-DNA Primer Design tool (http://signal.salk.edu/tdnaprimers.2.html) (mutants represent T-DNA insertion). Quantitative reverse transcription-PCR (qRT-PCR) was used to detect the expression of *AtAVP1* and *AtRLK* (AT5G35370) in WT and transgenic plants. Transgenic *AtAVP1 Arabidopsis* (OE-*AtAVP1*) plants were obtained using the floral dip method (Clough and Bent, 1998). The coding sequence (CDS) of *AtAVP1* (AT1G15690) was retrieved from the TAIR website (https://www.Arabidopsis.org/). The CDS of *AtAVP1* was inserted into the binary vector pCAMBIA1302 driven by a CaMV35S promoter, following which the circular plasmids were digested with *Ncol I* , and the recombinant binary vector pCAMBIA1302-AtAVP1 was cloned into the *Agrobacterium tumefaciens* strain GV1301, which as then used to transform plants using the floral dip method (transgenes represent overexpression of the 35S promoter). Homozygous T_3 lines were identified *via* PCR detection. The primers used in this study are shown in Supplementary Table 1.

The seedlings of *Arabidopsis* (WT, OE-*AtAVP1*, *avp1-1*, and *rlk*) were sterilized with 10% sodium hypochlorite for 10 min and then washed with sterile water five times for 1 min each wash. Sterilized seeds were sown on MS_0 medium (Millipore Sigma, St. Louis, MO, USA) and placed in a growth chamber (16 h light/8 h dark, 22 °C, light intensity around 100 $\mu \cdot m^{-2} \cdot s^{-2}$) for 3 d before being transferred to 6 mM low NO_3^- (control), 1 mM low NO_3^-, or 0.2 mM NO_3^- (low nitrogen) medium (Ma et al., 2014), following which they were grown at a 30° angle. Low nitrogen media were prepared using Murashige & Skoog (MS) modified basal salt mixture (no nitrogen, phosphate, or potassium) reagent preparation M407 purchased from Phyto Technology Laboratories ^{TM}. For control medium, 6mM NO_3^- were applied to the medium without nitrogen, and 1 and 0.2 mM NO_3^- were applied externally to the treatment medium. Specific ingredients are shown in Supplementary Table 2. The seedlings were photographed when phenotypic differences were observed. Win RHIZO Pro 2012 root scanning software (Regent Instrument Inc., Ottawa, ON, Canada), EPSON flatbed scanner, and Expression 10000XL scanners were used to scan and measure root length, total root area, and lateral root number. Each treatment was conducted in triplicate, with each line tested in at least six plants.

The *Arabidopsis* ecotype Columbia-0 WT was used for gene expression analysis. First, the *Arabidopsis* seeds were sterilized and cultured as described above; then, the seedlings with uniform growth were transferred to a medium containing nitrogen, indole acetic acid (IAA) and salt (NaCl). For IAA and NaCl treatments, MS_0 medium containing the following (all from Millipore Sigma, St. Louis, MO, USA) were used. The final concentrations of IAA were 0 (MS_0), 1 μM, and 10 μM (Guo et al., 2002; Zheng et al., 2017). For the NaCl treatment, the final concentrations were 50 mM and 100 mM. Roots were harvested after 7 d of treatment to detect changes in gene expression in response to different stresses. These experiments were conducted in triplicate for each treatment.

2.2 Sequence alignment and phylogenetic tree construction of *AtAVP1*

The *AtAVP1* and *EdVP1* exon-intron substructures were mapped using the server (GSDS) program (http://gsds.cbi.pku.edu.cn/). Genome and protein sequences were obtained from the TAIR website (https://www.Arabidopsis.org/) through a keyword search for *AtAVP1*. The NCBI BLAST site (https://blast.ncbi.nlm.nih.gov/Blast.cgi) was used to find and download gramineous protein sequences highly homologous to AtAVP1. The AtAVP1 phylogenic tree was constructed using the neighbor-joining (NJ) method *via* the MEGAX software (https://www.megasoftware.net/dload_win_gui) as previously described (Kumar et al., 2016). Protein sequence alignment was performed using DNAMAN.

2.3 Analysis of low nitrogen tolerance in greenhouse-grown *EdVP1* transgenic wheat

The transgenic *EdVP1* wheat lines OE-8, OE-28, and OE-32 were previously constructed in the laboratory (Zhou et al., 2020). These lines were self-preserved in our laboratory. Genomic DNA was isolated from OE-EdVP1 lines and SHI366 wheat plants using the CTAB method (Kim et al., 2005) and then analyzed *via* PCR. Homozygous transgenic lines were screened using PCR. qRT-PCR was used to detect the expression of *EdVP1* in WT, OE-8, OE-28, and OE-32 lines. The primers used are shown in Supplementary Table 1.

In the hydroponic low nitrogen tolerance experiments, transgenic wheat seeds with consistent germination were selected and transplanted into the pots. The seedlings were cultivated in a greenhouse (60% relative humidity) with 14 h light at 25 °C and 10 h darkness at 20 °C. After 3 d, the seedlings were cultured hydroponically in nutrient solutions with a control medium concentration of 2 mM NO_3^- and a low nitrogen medium concentration of 0.2 mM NO_3^-. The nutrient solutions used for the hydroponic phase were used as described previously (Qu et al., 2015).The nutrient solution was changed daily. Five plants from each treatment were randomly selected for determining various indices after one week, including plant height, root length, aboveground fresh and dry weight, and underground fresh and dry weight. Each experiment was repeated thrice.

2.4 Analysis of low nitrogen tolerance in transgenic wheat under field conditions

The transgenic lines OE-28 and OE-32 showed better performance in the laboratory and, therefore, were selected for low nitrogen field experiments. All experiments were conducted at the Shun Yi experimental station of the Institute of Crop Sciences of the Chinese Academy of Agricultural Sciences in Beijing. Two consecutive field experiments were conducted in 2020-2021 using the transgenic T_4 generation and in 2021-2022 using the transgenic T_5 generation. Both experiments comprised two treatments, each with three replicates. Both treatments included 7.5 $g \cdot m^{-2}$ P in the form of superphosphate. The normal nitrogen treatment had 15.6 g $N \cdot m^{-2}$ in the form of urea with 8.9 g $N \cdot m^{-2}$ applied prior to sowing and 6.7 g $N \cdot m^{-2}$ applied at the stem elongation stage. The low nitrogen treatment had no nitrogen application. Plot size was 6 m^2 (4 m × 1.5 m), which included six rows spaced 25 cm apart; the sowing density was 300 germinating seeds per m^2. At maturity, twenty spikes in each plot were randomly collected to measure grain number per

spike, and the 1000-grain weight. Spike numbers in two 1-m rows of each plot were recorded, and the spike number per square meter was calculated. The yield was calculated using the actual grain weight of each plot by converting the plot area.

2.5 Yeast two-hybrid system for screening AtAVP1 protein interactions

The yeast two-hybrid system was used to screen the *Arabidopsis* cDNA library (Stagljar et al., 1998). The yeast library screening for this experiment was carried out by the Oyman Biotech company (Oebiotech, Shanghai, China). The CDS sequence of *AtAVP1* was amplified from the cDNA and ligated into the pBT3-STE vector to construct the bait vector. After validating the autoactivation activity of the vector, the cDNA library was screened; the *Arabidopsis* cDNA library plasmid was then cloned into NMY51 yeast cells. Blue/white screening for colonies was performed on an SD/-Leu-Trp-His-Ade medium containing X-α-gal. The sequences of blue yeast colonies were subjected to NCBI BLAST. Library screening and reagent preparation were performed according to the system method (http://www.dualsystems.com/).

The interaction between AtAVP1 and AtRLK was verified with the ubiquitin isolation system. The coding regions of *AtAVP1* were inserted into the bait vector pBT3-STE, and the full-length CDS of *AtRLK* was inserted into the capture vector pPR3N. The primers used are shown in Supplementary Table 1. The bait vector pBT3-STE : AtAVP1 and the capture vector pPR3N:AtRLK were co-transformed into NMY51 yeast cells. The yeast cells were spread onto SD/-Leu-Trp and SD/-Leu-Trp-His-Ade-deficient medium plates and cultured at 30 °C for 3-4 d. Unseeded plates were used as the corresponding negative controls.

2.6 Luciferase complementary imaging assay

The CDSs of *AtAVP1* and *AtRLK* were inserted into the pCAMBIA1300-nLUC and pCAMBIA1300-cLUC vectors to obtain nLUC-AtAVP1 and cLUC-AtRLK recombinant plasmids, respectively. The primers used are shown in Supplementary Table 1. These recombinant plasmids were cloned into *Agrobacterium tumefaciens* (GV3101) and cultured to a final concentration of OD_{600} = 0.2; the nLUC-AtAVP1/cLUC-AtRLK, nLUC/cLUC, nLUC-AtAVP1/cLUC, and nLUC/cLUC-AtRLK combinations of *A. tumefaciens* were then infiltrated into tobacco leaves. After 48 h, the leaves were analyzed with Night SHADE LB 985 (Berthold Technologies, Germany). These experiments were conducted at least three times.

2.7 Subcellular localization of AtAVP1 and AtRLK

The coding regions of *AtAVP1* and *AtRLK* (with the termination codon removed) were inserted into the p16318hGFP vector for GFP-protein fusion expression. The resultant 35S:AtAVP1-GFP and 35S: AtRLK-GFP vectors driven by a CaMV35S promotor were constructed and used for subcellular localization studies. The primers used are shown in Supplementary Table 1. The 35S: AtAVP1-GFP recombinant plasmid and mCherry vectors (the signals of mCherry proteins were located in the membrane) harboring membrane-localized proteins were co-transformed into *Arabidopsis* protoplasts as previously described (Abel and Theologis, 1994). respectively, and cultured at 25 °C under dark conditions for more than 18 h. The expression of the vectors was observed with a Zeiss LSM980 confocal laser scanning microscope.

2.8 RNA extraction and qRT-PCR

Total RNA was extracted according to the Plant RNA Extraction Kit manual (Zoman Biotechnology Co, Beijing, China). This RNA was used as a template for synthesizing cDNA using the TransScript One-Step gDNA Removal and cDNA Synthesis SuperMix Kit (TransGene, Beijing, China). A real-time fluorescence quantitative detection kit (TransGene, Beijing, China) and the ABI 7500 real-time quantitative PCR instrument (Thermo Fisher, Waltham, MA, USA) was used to detect the fluorescence signal. The primers used are shown in Supplementary Table 1. The *Arabidopsis* reference gene was AT3G18780.The $2^{-\triangle Ct}$ method was used to calculate the relative expression of genes according to the Ct value of each sample at a specific fluorescence threshold.

2.9 Data analysis

All data were analyzed *via* a one-way ANOVA using SPSS19, and the significance of differences between multiple groups of samples was analyzed using Duncan's multiple range test. Significance level was $p< 0.05$. All results are shown as mean ± standard deviation (SD).

3 Results

3.1 Characteristics of transgenic *AtAVP1* and mutant *avp1* plants under low nitrogen stress

To identify the function of *AtAVP1* under low nitrogen stress, we constructed homozygous transgenic *AtAVP1* (OE-AtAVP1) and mutant *avp1-1 Arabidopsis* lines (Supplementary Figure 1A, B). The homozygous mutant was screened by PCR according to the insertion location of T-DNA (Supplementary Figure 1E), gene expression was measured in T_3 generation transgenic plants using qRT-PCR (Supplementary Figure 1F). Results showed that the expression of *AtAVP1* was increased in the OE-AVP1 line under 6 mM NO_3^-, 1 mM NO_3^-, and 0.2 mM NO_3^- conditions, and the expression of *AtAVP1* in the mutant *avp1-1* was substantially decreased under 6 mM NO_3^-, 1 mM NO_3^-, and 0.2 mM NO_3^- conditions compared to that in WT plants (Supplementary Figure 1F). The growth of OE-AVP1 plants was higher under 1 mM NO_3^- and 0.2 mM NO_3^- conditions (Figures 1B, C), and the root length of OE-AVP1 plants was significantly higher than that of WT under the same conditions ($p< 0.05$) (Figure 1D). Under 0.2 mM NO_3^- conditions, total root area and

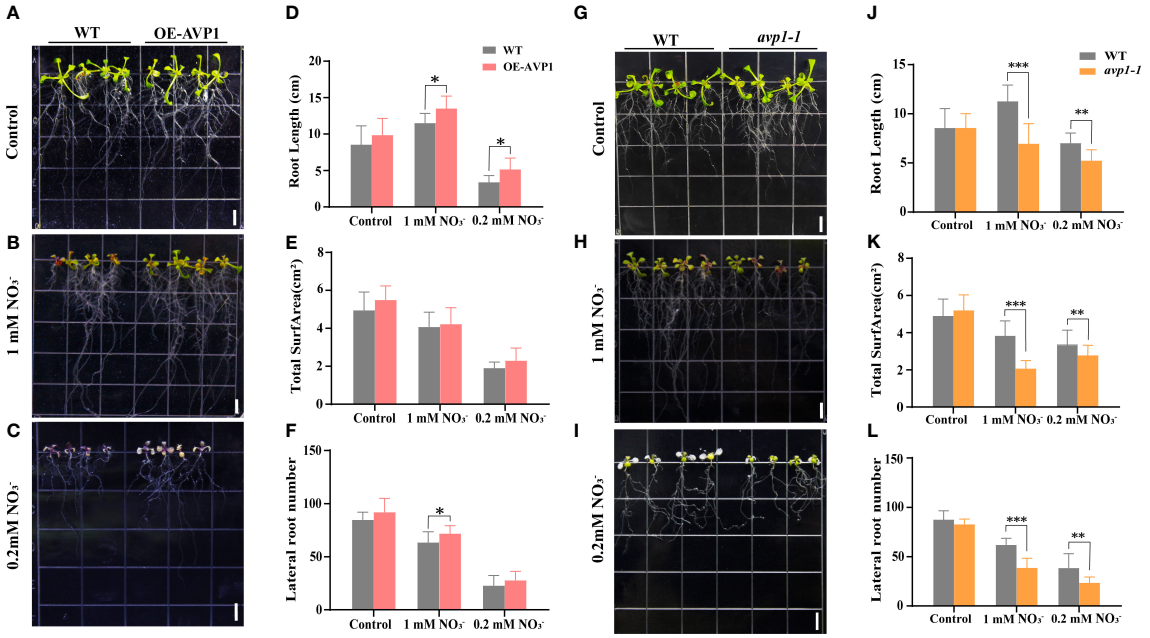

FIGURE 1
Functions of *AtAVP1* in *Arabidopsis* under normal conditions and different levels of nitrogen stress Phenotypic analysis of the transgenic *AtAVP1* *Arabidopsis* line OE-AVP1 grown under **(A)** 6 mM NO_3^- (control), **(B)** 1 mM NO_3^-, and **(C)** 0.2 mM NO_3^- (low nitrogen) conditions. Images were taken after 5 d of growth on different media. DIAN Win RHIZO Pro 2012 root scanning software and EPSON Flatbed and Expression 10000XL scanners were used to scan and measure the roots. **(D)** Root length, **(E)** total root surface, and **(F)** lateral root number of OE-AVP1 lines grown under different nitrogen treatment conditions. Phenotypic analysis of the mutant *avp1-1* under **(G)** 6 mM NO_3^- (control), **(H)** 1 mM NO_3^-, and **(I)** 0.2 mM NO_3^- medium conditions. Images were taken after 7 d of growth; the **(J)** root length, **(K)** total root surface, and **(L)** lateral root number of *avp1-1* lines grown under different nitrogen treatments were measured. All data represent mean ± standard deviation (n ≥ 6). (* $p< 0.05$, ** $p< 0.01$, *** $p< 0.001$, Duncan's multiple range test). Scale bars = 0.5 cm.

lateral root number were higher than those of WT (Figures 1E, F). Under 1 mM NO_3^- conditions, lateral root number were significantly higher than those of WT ($p< 0.05$) (Figure 1F). Conversely, the growth of mutant *avp1-1* plant was low under 1 mM NO_3^- and 0.2 mM NO_3^- conditions compared with that of WT (Figures 1H, I). After treatment with 0.2 mM NO_3^- and 1 mM NO_3^-, root length, total root area and lateral root number in the mutant *avp1-1* plants were significantly reduced compared to those in WT ($p< 0.01$) (Figures 1J–L); however, no significant differences were observed between WT and OE-AVP1 or between WT and mutant *avp1-1* under normal nitrogen conditions (Figures 1A, G). These findings indicate that *AtAVP1* positively regulates tolerance to nitrogen deficiency in *Arabidopsis*.

3.2 Transgenic *EdVP1* wheat seedlings have enhanced tolerance to low nitrogen stress under greenhouse conditions

We previously constructed transgenic *EdVP1* wheat plants and found that *EdVP1* from *Elymus dahuricus* improved low potassium tolerance in transgenic wheat grown in the field ((Zhou et al., 2020). In this study, we analyzed *AtAVP1* and *EdVP1* gene structures (Supplementary Figure 2A) and constructed a phylogenetic tree, which showed that EdVP1 had the closest homology with TaAVP1 (Supplementary Figure 2B). The protein sequence identity was 97.68% between EdVP1 and TaAVP1 (Supplementary Figure 2C). These results indicated that the *AVP1* sequence remained conserved during the evolution of gramineous crops. We further characterized the low nitrogen tolerance of the transgenic *EdVP1* wheat in greenhouse conditions.

We screened *EdVP1* T_3 homozygous transgenic lines using PCR and qRT-PCR, which showed that under 0.2 mM low nitrogen conditions, the transgenic wheat lines OE-8, OE-28, and OE-32 had higher *EdVP1* expression levels than did SHI366 (WT) (Supplementary Figure 3A, Figure 2B). We analyzed the transgenic wheat grown in the greenhouse and found that under the low nitrogen treatment (0.2 mM NO_3^-), the plant height of the line OE-28 was significantly higher than that of WT ($p< 0.05$) (Figures 2A, C). The root length, aboveground fresh and dry weight, and underground fresh and dry weight of transgenic wheat lines OE-28 and OE-32 were significantly increased compared with those of WT ($p< 0.05$) (Figures 2D-H). The plant height, root length, aboveground fresh and dry weight, and underground fresh and dry weight of the transgenic wheat line OE-8 were increased compared with those of WT (Figures 2C–H).

3.3 *EdVP1* overexpression enhances the yield of field-grown transgenic wheat under low nitrogen stress

To analyze the role of H^+-pyrophosphatases in field grown crops, we selected two optimal transgenic lines OE-28 and OE-32 and assessed their low nitrogen tolerance in the field. The low nitrogen tolerance experiments were conducted in Beijing for two consecutive

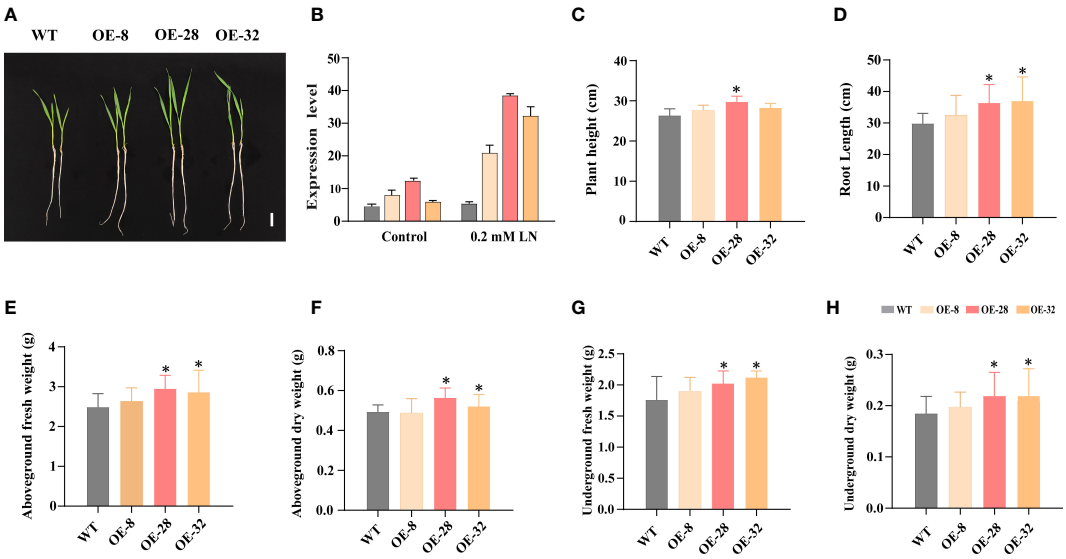

FIGURE 2
EdVP1 overexpression in wheat seedlings enhances low nitrogen stress tolerance **(A)** Phenotypes of the WT (SHI366) and transgenic *EdVP1*-overexpressing wheat lines OE-8, OE-28, and OE-32 grown under 0.2 mM low nitrogen (0.2 mM NO_3^-) conditions. Scale bars = 5 cm. **(B)** *EdVP1* expression in seedling roots of WT and T_3 transgenic *EdVP1*-overexpressing wheat lines grown under 0.2 mM NO_3^- and normal conditions. **(C)** Plant height, **(D)** root length, **(E)** aboveground fresh weight, **(F)** aboveground dry weight, **(G)** underground fresh weight, and **(H)** underground dry weight of WT (SHI366) and the transgenic *EdVP1*-overexpressing wheat lines OE-8, OE-28, OE-32 grown under 0.2 mM low nitrogen condition. Data represent mean ± standard deviation (n = 5), (*p< 0.05, Duncan's multiple range test).

years between 2020-2022. Under low nitrogen stress, OE-28 and OE-32 showed better growth and greener leaves than WT (wheat variety SHI366), while under normal conditions, the transgenic wheat lines OE-28, OE-32 showed similar growth to WT (Figures 3A–C). Analysis of the three main yield components revealed that under low nitrogen conditions, OE-28 and OE-32 showed a significant increase in the grain number per spike over WT (p< 0.05), while there was no significant difference in spike number and the 1000-grain weight (Figures 3D–G). Under low nitrogen stress, the grain yield of OE-28 increased by 10.10% and 9.16%, while that of OE-32 increased by 10.56% and 8.81% compared with that of WT, in 2021 and 2022, respectively (Figure 3G, Supplementary Table 3). These findings indicate that overexpression of *EdVP1* increased the yield of field-grown wheat under low nitrogen stress, which suggests that the H^+-pyrophosphatase gene has potential application in increasing grain yield under low nitrogen conditions.

3.4 Subcellular localization of AtAVP1 and AtRLK

We screened the proteins interacting with AtAVP1 using the yeast two-hybrid system; the results showed that yeast cells expressing the

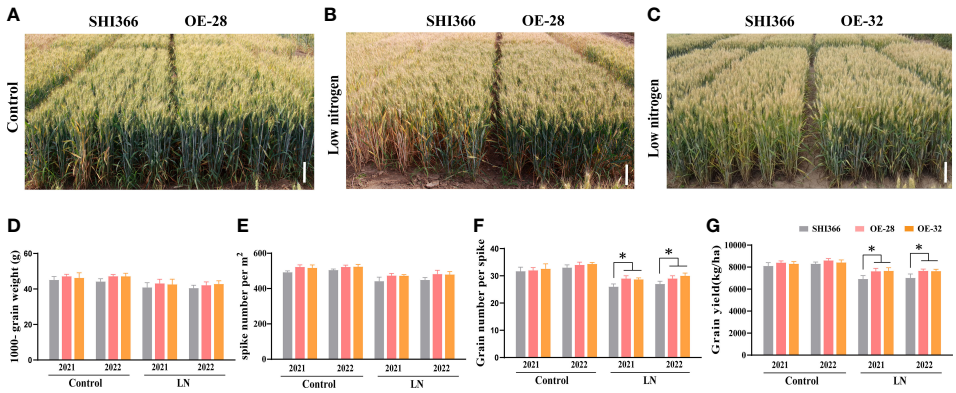

FIGURE 3
Low nitrogen stress tolerance analysis of *EdVP1* transgenic wheat grown in the field Phenotypes of OE-28 and SHI366 wheat plants grown under **(A)** normal and **(B)** low nitrogen conditions in 2022. **(C)** Phenotypes of OE-32 and SHI366 wheat plants grown under low nitrogen conditions in 2021. Scale bars = 10 cm **(D)** The 1000-grain weight, **(E)** spike number per m^2, **(F)** grain number per spike, and **(G)** grain yield of the OE-28 and OE-32-overexpressing lines and wild-type SHI366 plants grown under normal and low nitrogen conditions in 2021 and 2022. Data represent the mean of values from three biological replicates ± standard deviation. Asterisks indicate significant differences between the OE-28, OE-32, and SHI366 wheat plants, as assessed using Duncan's multiple range test (*p< 0.05, Duncan's multiple range test).

receptor-like protein kinase AtRLK and AtAVP1 interacted with each other in a heterologous system (Supplementary Table 4). Additionally, the expression profile analysis indicated that *AtRLK* was induced by low nitrogen stress in *Arabidopsis* (Supplementary Figure 1I).

We found that both AtAVP1 and AtRLK were highly expressed in the roots of *Arabidopsis* (Supplementary Figure 1D). To further determine subcellular AtAVP1 and AtRLK protein localization, the fusion constructs 35S:AtAVP1-GFP and 35S:AtRLK-GFP were transiently transformed into *Arabidopsis* protoplasts. The p16318hGFP vector served as a positive control for construct expression in the transient system. We observed that the GFP control was distributed throughout the cell, while AtAVP1 and AtRLK were expressed on the plasma membrane (Figure 4).

3.5 AtAVP1 directly interacts with AtRLK *in vivo* and *in vitro*

To further verify the interaction between AtAVP1 and AtRLK, we used the luciferase complementary imaging (LCI) assay in addition to the yeast two-hybrid assay, which showed a strong luminescence signal in the nLUC : AtAVP1/cLUC : AtRLK co-injection region. However, no signal was detected in the negative control co-injection region (Figure 5A). The yeast two-hybrid results showed that all the fused plasmids grew normally on SD/-Leu-Trp medium (Figure 5B), but only pBT3-STE : AtAVP1 and pPR3N:AtRLK could grow normally on the SD/-Leu-Trp-His-Ade selection medium (Figure 5C). These results indicate that AtAVP1 physically interacts with AtRLK.

3.6 *AtRLK* plays a positive role in the low nitrogen stress response

To investigate the function of *AtRLK* under low nitrogen stress, the homozygous mutant *rlk* was identified *via* PCR and qRT-PCR according to the insertion location of T-DNA (Supplementary Figures 1C, E, G) and grown under the same conditions as *avp1-1*. We found that as the nitrogen concentration decreased, the growth potential of WT and mutant *rlk* gradually weakened (Figures 6A–C). Under 1 mM NO_3^- conditions, the root surface area and the number of lateral roots were significantly lower in *rlk* plants than in WT ($p< 0.05$) (Figures 6E. F). Under the 0.2 mM NO_3^- conditions, the root length, root surface area, and number of lateral roots were significantly reduced compared to those in WT ($p< 0.05$) (Figures 6D–F). We observed no significant differences between the *rlk* mutant and WT plants under normal nitrogen conditions (Figure 6A).

4 Discussion

4.1 H^+-pyrophosphatase positively regulates the response of various plants to low nitrogen stress and other stresses

By analyzing the function of two H^+-PPases genes with high homology from *Arabidopsis* and *Elymus dahuricus* in response to low nitrogen stress, we showed that H^+-pyrophosphatase genes can significantly improve plant resistance to low nitrogen stress and

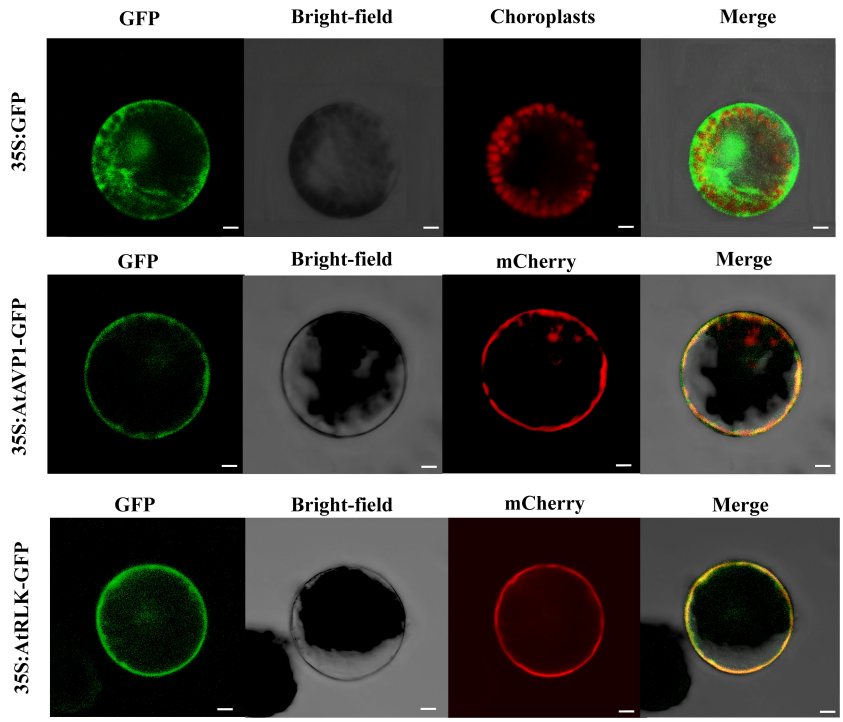

FIGURE 4
Subcellular AtAVP1 and AtRLK localization in *Arabidopsis* protoplasts The 35S:AtAVP1-GFP, 35S:AtRLK-GFP, and 35S:GFP control vectors were transiently expressed in *Arabidopsis* protoplasts. Compared to that of the 35S:GFP construct, the expression of 35S:AtAVP1-GFP and 35S:AtRLK-GFP was localized to the plasma membrane of the protoplasts. Fluorescence was observed using a Zeiss LSM980 confocal laser scanning microscope 16 h after transformation. Membrane marker protein (mCherry) was co-expressed with 35S:AtAVP1-GFP. Scale bars = 5 μm.

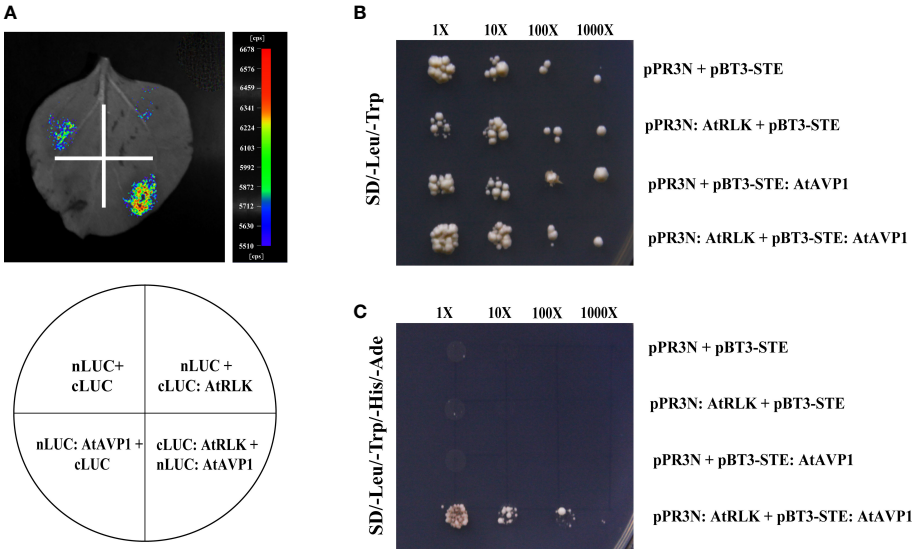

FIGURE 5
Identification of AtAVP1 interactions with AtRLK **(A)** Identification of an interaction between AtRLK and AtAVP1 using a luciferase complementary imaging (LCI) assay. The nLUC : AtAVP1/cLUC : AtRLK and negative control constructs were transfected into *Agrobacterium tumefaciens* and then injected into four different regions of a tobacco leaf. The leaves were analyzed for luminescence signal by Night SHADE LB 985. **(B, C)** Identification of an interaction between AtRLK and AtAVP1 using a yeast two-hybrid system. **(B)** The pBT3-STE : AtAVP1/pPR3N:AtRLK and negative control constructs were co-transformed into yeast cells and grown on SD/-Leu-Trp double deficiency medium. **(C)** The co-transformed pBT3-STE : AtAVP1/pPR3N:AtRLK and negative control into yeast cells were grown on SD/-Leu-Trp-His-Ade selective medium at 1×, 10×, 100×, and 1000× dilution gradients to test the interaction.

have a potentially important application in the field setting. The overexpression of H^+-PPases genes in *Arabidopsis thaliana* can improve nitrogen use efficiency and protein abundance of H^+-PPase in *Romaine Lettuce* (Paez-Valencia et al., 2011). Similarly, with the decrease of nitrogen concentration, the expression of *AVP1* increased (Supplementary Figure 1H). We used *Arabidopsis* transgenic lines overexpressing *AVP1* and T-DNA insertion mutant *avp1-1* to show that the growth of plants overexpressing *AVP1* in 1 mM NO_3^- and 0.2 mM NO_3^- media was higher than that of WT. Meanwhile, mutant *avp1-1* grew to a lesser extent than did WT (Figures 1B,C, H, I). We previously constructed transgenic wheat lines overexpressing *EdVP1* (Zhou et al., 2020). To investigate the response of transgenic *EdVP1* wheat to low nitrogen stress, we performed low nitrogen treatment experiments in the greenhouse and field. The greenhouse experiment showed that plant height, root length, aboveground fresh and dry weight, and underground fresh and dry weight were significantly higher than those of WT ($p < 0.05$) (Figure 2). The transgenic *EdVP1* lines in field experiments showed

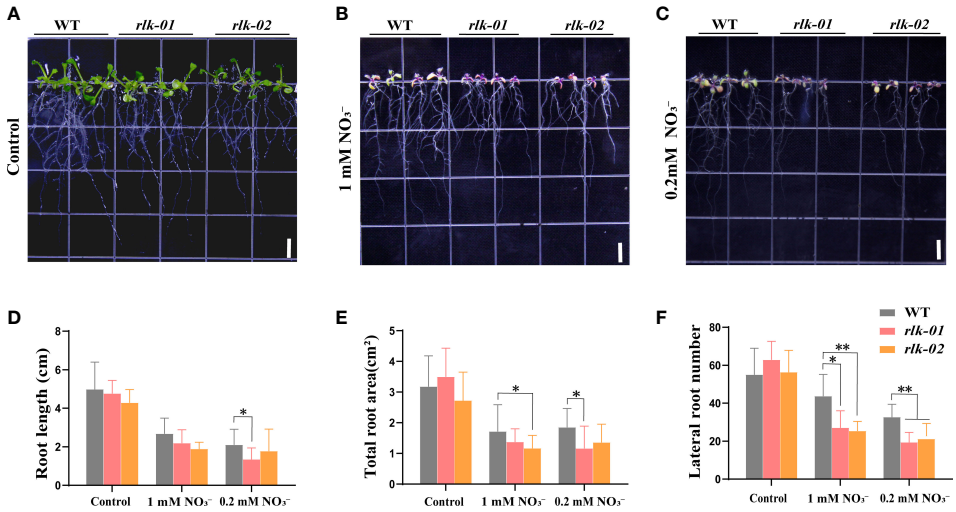

FIGURE 6
AtRLK plays a role in low nitrogen stress tolerance in *Arabidopsis* **(A–C)** Phenotypic analysis of mutant *rlk* and WT plants under control and nitrogen stress conditions. The *rlk*-01 and *rlk*-02 represent the same line plated out twice. **(D)** Root length, **(E)** total root surface, and **(F)** lateral root number in *rlk* mutant lines grown on 6 mM NO_3^- (control), 1 mM NO_3^-, and 0.2 mM NO_3^- media. All data represent mean ± standard deviation (n ≥ 6). Asterisks indicate significant differences compared to WT (* $p < 0.05$, ** $p < 0.01$, Duncan's multiple range test). Scale bars = 0.5 cm.

increased yield potential, as they had increased grain number per spike under low nitrogen stress (Figure 3). These results indicated that *AVP1* improved the low nitrogen tolerance of gramineous crops in the field.

Gramineous crops are the main food source for the global population. With the reduction in nitrogen fertilizer application being pushed world-wide, it is essential to ensure global food security by improving low nitrogen tolerance of gramineous crops. A previous study found that nitrogen starvation induced the expression of *Salicornia europaea VP1 (SeVP1)* and *SeVP2*. *Arabidopsis* and wheat plants expressing *SeVP1* or *SeVP2* were more tolerant to low nitrogen treatment than were WT, which indicated that the overexpression of H^+-PPase was conducive to the transport of photosynthates into the root system, thus promoting root growth and integrating nitrogen and carbon metabolism (Lv et al., 2015). These findings are consistent with our results, further indicating that H^+-pyrophosphatase has a promising potential for improving the resistance of *Arabidopsis* and gramineous crops to low nitrogen stress.

Salt stress is a ubiquitous abiotic stress that adversely affects plant growth and development. We found that *AVP1* also modulated salt stress. The relative expression of *AVP1* in *Arabidopsis* increased after treatment with salt (Supplementary Figure 1K); additionally, the survival rate of transgenic *EdVP1* wheat treated with 100 mM NaCl was higher than that of WT (Supplementary Figure 3B, C). Indeed, the *Arabidopsis* seedlings cultured with 50 and 100 mM NaCl showed enhanced H^+-PPase activity on the vacuolar membrane (Krebs et al., 2010). The greater salt tolerance observed in transgenic *AVP1* plants may be related to the fact that H^+-PPase can promote the accumulation of Na^+ in the vacuole, which inhibits the toxic effects of excess Na^+ on plant cells (Gaxiola et al., 2001; Shaheen et al., 2008). These results suggest that H^+-pyrophosphatase genes may play a role in plant responses to various abiotic stresses.

4.2 AtAVP1 interacting with AtRLK may associated with an auxin signaling pathway that enhances low nitrogen tolerance in plants

The receptor-like protein kinase (AtRLK) that interacts with AtAVP1 was selected using the yeast two-hybrid system. We found that both *AtAVP1* and *AtRLK* were highly expressed in roots (Supplementary Figure 1D), where the proteins are located on the plasma membrane (Figure 4). The interaction of AtRLK with AtAVP1 was further determined using yeast two-hybrid and luciferase complementary imaging (LCI) assays (Figure 5). To investigate whether *AtRLK* responds to low nitrogen stress, we further studied a T-DNA insertion mutant *rlk* line. Under low nitrogen (0.2 mM NO_3^-) conditions, the root length of the *rlk* mutant was shorter and the root surface area and number of lateral roots were lower than those of WT (Figure 6). These phenotypes were similar to those of the *avp1-1* mutant, leading to the hypothesis that the two proteins regulate plant responses to low nitrogen stress using the same signaling pathway.

Receptor-like protein kinases (RLK) are important signal transduction network members that play a role in plant response to various abiotic stresses. Moreover, RLK are widely involved in cell signal transduction and plant response to stress (Morris and Walker, 2003; Morillo and Tax, 2006; Lemmon and Schlessinger, 2010). Analysis of the expression profiles of the SsLRR RLK in the root and leaf transcriptomes of the two sugarcane cultivars ROC22 (resistant) and Badila (susceptible) under low nitrogen conditions showed that some genes in the SsLRR RLK gene family were highly expressed, indicating that *RLK* respond to low nitrogen stress (Cheng et al., 2021). RLK can recognize extracellular signals on the cell surface and activate downstream signaling pathways by phosphorylating specific target proteins (Shiu and Bleecker, 2001). We hypothesized that AtRLK functioned upstream of AtAVP1 to regulate the low nitrogen response.

Furthermore, we found that *AVP1* expression increased after exogenously adding different concentrations of IAA (Supplementary Figure 1J). It has been reported that plant V-H^+-PPase activity is involved in root regulation through auxin transport, and *AVP1* overexpression increases auxin transport. The *avp1* deletion mutation severely interferes with root/shoot development and reduces auxin transport (Li et al., 2005), and the *avp1* deletion mutation direct sequencing showed that the T-DNA insertion of this line localizes to the predicted fifth exon of the *AVP1* ORF. Transgenic *AVP1 Arabidopsis* had increased plasma membrane H^+-ATPase and Pin-formed 1 (PIN1) auxin effector protein activity and auxin content in the germ compared with that in WT (Li et al., 2005). *AVP1* was also found to regulate auxin transport by increasing plasma membrane H^+-ATPase activity. The root auxin content in *Agrostis stolonifera* expressing *AVP1* was significantly higher than that in WT (Li et al., 2010); based on current literature and our results, we hypothesize that *RLK* may activate the IAA signaling pathway through the phosphorylation of *AVP1* to improve plant tolerance to low nitrogen conditions. Further studies are needed to elucidate the role of *AVP1* in regulating low nitrogen stress through auxin related pathway. Our findings lay the foundation for further research on improving plant tolerance to low nitrogen stress.

Data availability statement

The datasets presented in this study can be found in online repositories. The names of the repository/repositories and accession number(s) can be found in the article/Supplementary Material.

Author contributions

HZ completed the experiments, wrote the manuscript, and analyzed the data. HZ, MC, and CX designed the experiments and edited the manuscript. CX helped with the experiments, RL helped with preparing the yeast two-hybrid screening library, YB provided the experimental materials, and WT, KC, ZX, JC, and YM provided the illustration for experiments. DS and HF coordinated the project and edited the manuscript. All authors contributed to the article and approved the submitted version.

Funding

This research was sponsored by the National Science and Technology Major Project of the Ministry of Science and Technology of China (SQ2022YFD1200002), Science and Technology Innovation Foundation of Shanxi Agricultural University (2020BQ42), and Agricultural Science and Technology Innovation Program of CAAS and National Natural Science Foundation of China (32272099, 31900256, and 32101719).

Conflict of interest

The authors declare that the research was conducted in the absence of any commercial or financial relationships that could be construed as a potential conflict of interest.

Publisher's note

All claims expressed in this article are solely those of the authors and do not necessarily represent those of their affiliated organizations, or those of the publisher, the editors and the reviewers. Any product that may be evaluated in this article, or claim that may be made by its manufacturer, is not guaranteed or endorsed by the publisher.

Supplementary material

The Supplementary Material for this article can be found online at: https://www.frontiersin.org/articles/10.3389/fpls.2023.1096091/full#supplementary-material

References

Abel, S., and Theologis, A. (1994). Transient transformation of arabidopsis leaf protoplasts: A versatile experimental system to study gene expression. *Plant J.* 5 (3), 421–427. doi: 10.1111/j.1365-313X.1994.00421.x

Bao, A.-K., Wang, S.-M., Wu, G.-Q., Xi, J.-J., Zhang, J.-L., and Wang, C.-M. (2009). Overexpression of the arabidopsis h^+-PPase enhanced resistance to salt and drought stress in transgenic alfalfa (Medicago sativa l.). *Plant Sci.* 176 (2), 232–240. doi: 10.1016/j.plantsci.2008.10.009

Cheng, W., Wang, Z., Xu, F., Ahmad, W., Lu, G., Su, Y., et al. (2021). Genome-wide identification of LRR-RLK family in saccharum and expression analysis in response to biotic and abiotic stress. *Curr. Issues Mol. Biol.* 43 (3), 1632–1651. doi: 10.3390/cimb43030116

Clough, S., and Bent, A. (1998). Floral dip: A simplified method for agrobacterium-mediated transformation of arabidopsis thaliana. *Plant J. Cell Mol. Biol.* 16 (6), 735–743. doi: 10.1046/j.1365-313x.1998.00343.x

Gao, F., Gao, Q., Duan, X., Yue, G., Yang, A., and Zhang, J. (2006). Cloning of an h +-PPase gene from thellungiella halophila and its heterologous expression to improve tobacco salt tolerance. *J. Exp. Bot.* 57 (12), 3259–3270. doi: 10.1093/jxb/erl090

Gaxiola, R. A., Jisheng, L., Undurraga, S., Dang, L., Gethyn, J., Allen,, et al. (2001). Drought- and salt-tolerant plants result from overexpression of the AVP1 h^+-pump. *Proc. Natl. Acad. Sci. United States America* 98 (20), 11444–11444. doi: 10.1073/pnas.191389398

Guo, J., Liu, X., Zhang, Y., Shen, J., Han, W., Zhang, W., et al. (2010). Significant acidification in major Chinese croplands. *Sci. (New York N.Y.)* 327 (5968), 1008–1010. doi: 10.1126/science.1182570

Guo, F., Wang, R., and Crawford, N. (2002). The arabidopsis dual-affinity nitrate transporter gene AtNRT1.1 (CHL1) is regulated by auxin in both shoots and roots. *J. Exp. Bot.* 53 (370), 835–844. doi: 10.1093/jexbot/53.370.835

Han, M., Okamoto, M., Beatty, P. H., Rothstein, S. J., and Good, A. G. (2015). The genetics of nitrogen use efficiency in crop plants. *Annu. Rev. Genet.* 49, 269–289. doi: 10.1146/annurev-genet-112414-055037

Jones, D. L., Clode, P. L., Kilburn, M. R., Stockdale, E. A., and Murphy, D. V. (2013). Competition between plant and bacterial cells at the microscale regulates the dynamics of nitrogen acquisition in wheat (Triticum aestivum). *New Phytol.* 200 (3), 796–807. doi: 10.1111/nph.12405

Kim, Y. O., Kim, J. S., and Kang, H. (2005). Cold-inducible zinc finger-containing glycine-rich RNA-binding protein contributes to the enhancement of freezing tolerance in arabidopsis thaliana. *Plant J.* 42 (6), 890–900. doi: 10.1111/j.1365-313X.2005.02420.x

Krebs, M., Beyhl, D., Gorlich, E., Al-Rasheid, K., Marten, I., Stierhof, Y., et al. (2010). Arabidopsis V-ATPase activity at the tonoplast is required for efficient nutrient storage but not for sodium accumulation. *Proc. Natl. Acad. Sci. United States America* 107 (7), 3251–3256. doi: 10.1073/pnas.0913035107

Kumar, S., Stecher, G., and Tamura, K. (2016). MEGA7: Molecular evolutionary genetics analysis version 7.0 for bigger datasets. *Mol. Biol. Evol.* 33 (7), 1870–1874. doi: 10.1093/molbev/msw054

Lemmon, M. A., and Schlessinger, J. (2010). Cell signaling by receptor tyrosine kinases. *Cell* 141 (7), 1117–1134. doi: 10.1016/j.cell.2010.06.011

Li, Z., Baldwin, C., Hu, Q., Liu, H., and Luo, H. (2010). Heterologous expression of arabidopsis h^+-pyrophosphatase enhances salt tolerance in transgenic creeping bentgrass (Agrostis stolonifera l.). *Plant Cell Environ.* 33 (2), 272–289. doi: 10.1111/j.1365-3040.2009.02080.x

Li, X., Guo, C., Gu, J., Duan, W., Zhao, M., Ma, C., et al. (2014). Overexpression of VP, a vacuolar h+-pyrophosphatase gene in wheat (Triticum aestivum l.), improves tobacco plant growth under pi and n deprivation, high salinity, and drought. *J. Exp. Bot.* 65 (2), 683–696. doi: 10.1093/jxb/ert442

Li, J., Yang, H., Ann Peer, W., Richter, G. L., Blakeslee, J. J. , Bandyopadhyay, A., et al. (2005). Arabidopsis h^+-PPase AVP1 regulates auxin-mediated organ development. *Science* 310, 121–125. doi: 10.1126/science.1115711

Lv, S., Jiang, P., Nie, L., Chen, X., Tai, F., Wang, D., et al. (2015). H(+) -pyrophosphatase from salicornia europaea confers tolerance to simultaneously occurring salt stress and nitrogen deficiency in arabidopsis and wheat. *Plant Cell Environ.* 38 (11), 2433–2449. doi: 10.1111/pce.12557

Maeshima, M. (2000). Vacuolar H^+-pyrophosphatase. *Biochimica et biophysica acta (BBA) - biomembranes* 1465(1-2), 37–51. doi: 10.1016/S0005-2736(00)00130-9

Ma, W., Li, J., Qu, B., He, X., Zhao, X., Li, B., et al. (2014). Auxin biosynthetic gene TAR2 is involved in low nitrogen-mediated reprogramming of root architecture in arabidopsis. *Plant J. Cell Mol. Biol.* 78 (1), 70–79. doi: 10.1111/tpj.12448

Morillo, S. A., and Tax, F. E. (2006). Functional analysis of receptor-like kinases in monocots and dicots. *Curr. Opin. Plant Biol.* 9 (5), 460–469. doi: 10.1016/j.pbi.2006.07.009

Morris, E. R., and Walker, J. C. (2003). Receptor-like protein kinases: The keys to response. *Curr. Opin. Plant Biol.* 6 (4), 339–342. doi: 10.1016/S1369-5266(03)00055-4

Paez-Valencia, J., Patron-Soberano, A., Rodriguez-Leviz, A., Sanchez-Lares, J., Sanchez-Gomez, C., Valencia-Mayoral, P., et al. (2011). Plasma membrane localization of the type I h(+)-PPase AVP1 in sieve element-companion cell complexes from arabidopsis thaliana. *Plant Sci. an Int. J. Exp. Plant Biol.* 181 (1), 23–30. doi: 10.1016/j.plantsci.2011.03.008

Paez-Valencia, J., Sanchez-Lares, J., Marsh, E., Dorneles, L. T., Santos, M. P., Sanchez, D., et al. (2013). Enhanced proton translocating pyrophosphatase activity improves nitrogen use efficiency in romaine lettuce. *Plant Physiol.* 161 (3), 1557–1569. doi: 10.1104/pp.112.212852

Pasapula, V., Shen, G., Kuppu, S., Paez-Valencia, J., Mendoza, M., Hou, P., et al. (2011). Expression of an arabidopsis vacuolar h^+-pyrophosphatase gene (AVP1) in cotton improves drought- and salt tolerance and increases fibre yield in the field conditions. *Plant Biotechnol. J.* 9 (1), 88–99. doi: 10.1111/j.1467-7652.2010.00535.x

Qu, B., He, X., Wang, J., Zhao, Y., Teng, W., Shao, A., et al. (2015). A wheat CCAAT box-binding transcription factor increases the grain yield of wheat with less fertilizer input. *Plant Physiol.* 167 (2), 411–423. doi: 10.1104/pp.114.246959

Schilling, R. K., Marschner, P., Shavrukov, Y., Berger, B., Tester, M., Roy, S. J., et al. (2014). Expression of the arabidopsis vacuolar h plus - pyrophosphatase gene (AVP1) improves the shoot biomass of transgenic barley and increases grain yield in a saline field. *Plant Biotechnol. J.* 12 (3), 378–386. doi: 10.1111/pbi.12145

Schumacher, P. K. (2007). Plant proton pumps. *FEBS Lett* 581. doi: 10.1016/j.febslet.2007.03.050

Serrano, A., Pérez-Castiñeira, J., Baltscheffsky, M., and Baltscheffsky, H. (2007). H +-PPases: yesterday, today and tomorrow. *IUBMB Life* 59 (2), 76–83. doi: 10.1080/15216540701258132

Shaheen, A., Zahid, M., Farhat, N., Amjad, H. J., Shahid, M., Yusuf, Z., et al. (2008). Silicon carbide whisker-mediated embryogenic callus transformation of cotton (Gossypium hirsutum l.) and regeneration of salt tolerant plants. *Mol. Biotechnol.* 40 (2), 161–169. doi: 10.1007/s12033-008-9072-5

Shiratake, K., Kanayama, Y., Maeshima, M., and Yamaki, S. (1997). Changes in h(+)-pumps and a tonoplast intrinsic protein of vacuolar membranes during the development of pear fruit. *Plant Cell Physiol.* 38 (9), 1039–1045. doi: 10.1093/oxfordjournals.pcp.a029269

Shiu, S. H., and Bleecker, A. B. (2001). Receptor-like kinases from arabidopsis form a monophyletic gene family related to animal receptor kinases. *Proc. Natl. Acad. Sci. United States America* 98 (19), 10763–10768. doi: 10.1073/pnas.181141598

Stagljar, I., Korostensky, C., Johnsson, N., and Teesen, S. (1998). A genetic system based on split-ubiquitin for the analysis of interactions between membrane. *Proc. Natl. Acad. Sci. United States America* 95 (9), 5187–5187. doi: 10.1073/pnas.95.9.5187

Su, J.-H., Bai, T.-H., Wang, F., and Bao, A.-K. (2019). Overexpression of arabidopsis h^+-pyrophosphatase improves the growth of alfalfa under long-term salinity, drought conditions and phosphate deficiency. *Czech J. Genet. Plant Breed. 55(No.* 4), 156–161. doi: 10.17221/134/2018-cjgpb

Yang, H., Knapp, J., Koirala, P., Rajagopal, D., Peer, W., Silbart, L., et al. (2007). Enhanced phosphorus nutrition in monocots and dicots over-expressing a phosphorus-responsive type I h^+-pyrophosphatase. *Plant Biotechnol. J.* 5 (6), 735–745. doi: 10.1111/j.1467-7652.2007.00281.x

Yoichi, N., Isamu, Y., and Masayoshi, M. (2003). Patch clamp analysis of a h+ pump heterologously expressed in giant yeast vacuoles. *J. Biochem.* 4), 615. doi: 10.1093/jb/mvg184

Zheng, K., Wang, Y., Zhang, N., Jia, Q., Wang, X., Hou, C., et al. (2017). Involvement of PACLOBUTRAZOL RESISTANCE6/KIDARI, an atypical bHLH transcription factor, in auxin responses in arabidopsis. *Front. Plant Sci.* 8. doi: 10.3389/fpls.2017.01813

Zhou, Y., Li, Y., Qi, X., Liu, R., Dong, J., Jing, W., et al. (2020). Overexpression of V-type h(+) pyrophosphatase gene EdVP1 from elymus dahuricus increases yield and potassium uptake of transgenic wheat under low potassium conditions. *Sci. Rep.* 10 (1), 5020. doi: 10.1038/s41598-020-62052-5

Zhu, Q., de Vries, W., Liu, X., Hao, T., Zeng, M., Shen, J., et al. (2018). Enhanced acidification in Chinese croplands as derived from element budgets in the period 1980-2010. *Sci. total Environ.* 618, 1497–1505. doi: 10.1016/j.scitotenv.2017.09.289

frontiers | Frontiers in Plant Science

TYPE Original Research
PUBLISHED 31 January 2023
DOI 10.3389/fpls.2023.1068296

Check for updates

OPEN ACCESS

EDITED BY
Mohammad Golam Mostofa,
Michigan State University, United States

REVIEWED BY
Syed Adeel Zafar,
University of California, Riverside, United States
Fugui Zhang,
Anhui Agricultural University, China
Tofazzal Islam,
Bangabandhu Sheikh Mujibur Rahman Agricultural University, Bangladesh

*CORRESPONDENCE
Cheng Zhu
pzhch@cjlu.edu.cn
Zhixiang Chen
zhixiang@purdue.edu

SPECIALTY SECTION
This article was submitted to Plant Abiotic Stress, a section of the journal Frontiers in Plant Science

RECEIVED 12 October 2022
ACCEPTED 18 January 2023
PUBLISHED 31 January 2023

CITATION
Ding Y, Zhou M, Wang K, Qu A, Hu S, Jiang Q, Yi K, Wang F, Cai C, Zhu C and Chen Z (2023) Rice DST transcription factor negatively regulates heat tolerance through ROS-mediated stomatal movement and heat-responsive gene expression.
Front. Plant Sci. 14:1068296.
doi: 10.3389/fpls.2023.1068296

COPYRIGHT
© 2023 Ding, Zhou, Wang, Qu, Hu, Jiang, Yi, Wang, Cai, Zhu and Chen. This is an open-access article distributed under the terms of the Creative Commons Attribution License (CC BY). The use, distribution or reproduction in other forums is permitted, provided the original author(s) and the copyright owner(s) are credited and that the original publication in this journal is cited, in accordance with accepted academic practice. No use, distribution or reproduction is permitted which does not comply with these terms.

Rice DST transcription factor negatively regulates heat tolerance through ROS-mediated stomatal movement and heat-responsive gene expression

Yanfei Ding[1], Mei Zhou[1], Ke Wang[1], Aili Qu[2], Shanshan Hu[3], Qiong Jiang[1], Keke Yi[4], Feijuan Wang[1], Chong Cai[1], Cheng Zhu[1]* and Zhixiang Chen[1,5]*

[1]Key Laboratory of Specialty Agri-product Quality and Hazard Controlling Technology of Zhejiang Province, College of Life Sciences, China Jiliang University, Hangzhou, China, [2]School of Biological and Chemical Engineering, Ningbo Institute of Technology, Ningbo, China, [3]College of Life Sciences, Zhejiang University, Hangzhou, China, [4]Key Laboratory of Plant Nutrition and Fertilizer, Ministry of Agriculture, Institute of Agricultural Resources and Regional Planning, Chinese Academy of Agricultural Science, Beijing, China, [5]Department of Botany and Plant Pathology, Purdue University, West Lafayette, IN, United States

Plants are frequently subjected to a broad spectrum of abiotic stresses including drought, salinity and extreme temperatures and have evolved both common and stress-specific responses to promote fitness and survival. Understanding the components and mechanisms that underlie both common and stress-specific responses can enable development of crop plants tolerant to different stresses. Here, we report a rice *heat stress-tolerant 1* (*hst1*) mutant with increased heat tolerance. *HST1* encodes the DST transcription factor, which also regulates drought and salinity tolerance. Increased heat tolerance of *hst1* was associated with suppressed expression of reactive oxygen species (ROS)-scavenging peroxidases and increased ROS levels, which reduced water loss by decreasing stomatal aperture under heat stress. In addition, increased ROS levels enhanced expression of genes encoding heat shock protein (HSPs) including HSP80, HSP74, HSP58 and small HSPs. HSPs promote stabilization of proteins and protein refolding under heat stress and accordingly mutation of *HST1* also improved reproductive traits including pollen viability and seed setting under high temperature. These results broaden the negative roles of DST in abiotic stress tolerance and provide important new insights into DST-regulated tolerance to diverse abiotic stresses through both shared and stress-specific mechanisms.

KEYWORDS

plant heat tolerance, DST transcription factor, reactive oxygen species, stomatal aperture, heat shock genes, reproductive traits under heat stress

Introduction

As sessile organisms, plants are constantly exposed to a variety of abiotic stresses such as drought, salinity and heat and have evolved complex and diverse responses to promote survival, growth and development under stress conditions (Zhu, 2016). Over the past several decades, important progress has been made in establishing the core mechanisms of responses and adaptation to major abiotic stresses in plants (Zhang et al., 2022). The best characterized mechanism of drought stress responses is the reduction of water loss through stomatal closure in response to water deficiency. The phytohormone abscisic acid (ABA), which is rapidly induced in leaves under drought stress, plays a central role in drought-induced stomatal closure by activating plasma membrane calcium ion (Ca^{2+}) channels, resulting in elevation of cytosolic Ca^{2+} levels (Pei et al., 2000; Jannat et al., 2011; Brandt et al., 2015). This Ca^{2+} elevation causes the efflux of K^+ and Cl^- and the removal of organic solutes from guard cells, resulting in reduced cellular turgor and rapid stomatal closing (Macrobbie, 2000; Schroeder et al., 2001; Song and Matsuoka, 2009). Under high salt levels (primarily Na^+), plants use the so-called Salt-Overly-Sensitive (SOS) pathway to promote salt tolerance. In this pathway, the Ca^{2+}-binding protein SOS3 senses salt stress-elicited Ca^{2+} signal and activates the SOS2 protein kinase, which in turn can phosphorylate and activate the SOS1 Na^+/H^+ antiporter at the plasma membrane to extrude Na^+ from root cells into the soil and into the xylem for long transport to leaves (Zhu, 2002; Quan et al., 2007; Zhu, 2016). Under high temperature, on the other hand, denatured and misfolded proteins accumulate and can lead to proteotoxicity (Izumi, 2019). An important part of heat stress responses universally found in different types of living organisms is the rapid expression of genes encoding heat shock proteins (HSPs) (Craig et al., 1993; Georgopoulos and Welch, 1993; Jakob et al., 1993; Arrigo, 2005; Latijnhouwers et al., 2010; Xu et al., 2012; Reddy et al., 2014). In plants, well-characterized HSPs include Hsp101, Hsp70 and small HSPs. These HSPs act as molecular chaperones that promote folding and refolding of nonnative proteins (Baniwal et al., 2007; Kotak et al., 2007; Von Koskull-Doring et al., 2007; Schramm et al., 2008). HSPs can also monitor misfolded/damaged proteins and target their degradation by the ubiquitin proteasome system, autophagy and other pathways (Arias and Cuervo, 2011; Amm et al., 2014).

Abiotic stresses can occur singularly or together, particularly under natural environmental conditions. Heat stress occurs often with drought and, therefore, has a special relationship with water status in plants (Fahad et al., 2017). Heat stress can also directly or indirectly perturb leaf water status and root hydraulic conductivity as observed in *Lotus creticus* and tomato guard cells (Morales et al., 2003; Banon et al., 2004). Different types of adverse environmental conditions may also cause the same or similar physiological stresses in plant cells and can induce common signaling pathways and responses. For example, both drought and salinity can induce hyperosmotic stress in plant cells, which induces Ca^{2+} signaling, ABA accumulation, stomatal closure and stress-responsive gene expression (Zhang et al., 2022). Various abiotic stresses are also associated with the production of reactive oxygen species (ROS), including superoxide and H_2O_2 (Mittler et al., 2022). ROS are produced from a variety of sources in plant cells under stress and are highly toxic at high levels. As a result, induction of ROS-scavenging activities is an important and common plant response to different stresses. However, ROS also play important role in stress signaling (Mittler et al., 2022). In guard cells, ROS including H_2O_2 act as second messengers for ABA in the regulation of stomatal movement by activating plasma membrane Ca^{2+} channels, resulting in elevation of cytosolic Ca^{2+} levels (Pei et al., 2000; Jannat et al., 2011; Brandt et al., 2015). Under heat stress, ROS, especially H_2O_2, are continuously produced in plant cells and the redox balance of cells is disturbed leading to oxidative damage (Apel and Hirt, 2004). On the other hand, heat-induced ROS can also trigger the mobilization and activation of heat shock transcription factor A to promote expression of heat-responsive genes including those encoding HSPs (Giesguth et al., 2015). ROS also regulate stomatal movement to control rates of transpiration, thereby reducing heat-induced water loss (Singh et al., 2017; Qi et al., 2018). Dissection of the complex mechanisms responsible for shared and coordinated stress responses could provide new insights into the comprehensive networks of plant stress responses. This knowledge is also necessary to engineer plants with tolerance to different abiotic stresses by targeting common mechanisms and core pathways of plant stress responses.

Rice is the most important grain that provides more than one-fifth of the calories consumed worldwide by humans. Even though rice thrives in hot climates, extreme heat can irreversibly damage the crop, particularly during germination and fertilization, causing loss in yield and grain quality. To identify genes required for rice heat tolerance, we have performed large-scale screens of a rice T-DNA insertion population for mutants with altered heat tolerance and isolated the *heat stress tolerance 1* or *hst1* mutant. Through positional cloning, we have isolated the *HST1* gene and found it encoding a Cys-2/His-2-type (C2H2) zinc finger transcription factor. Interestingly, rice *HST1* was isolated initially as *Drought and Salt Tolerance* (*DST*) for its negative role in drought and salt tolerance and more recently as *Regulator of Gn1a 1* (*REG1*) for its negative role in the regulation of grain number (Huang et al., 2009; Li et al., 2013b; Cui et al., 2015). Unlike the previously reported *dst1* and *reg1* mutants that still produce mutant DST proteins capable of binding DNA, *hst1* is a complete loss-of-function mutant. Based on the increased heat tolerance of the *hst1* mutant, we have hypothesized that HST1 is an important regulator of rice responses to multiple types of abiotic stresses through both common and distinct molecular mechanisms. To test this hypothesis, we have comprehensively characterized the *hst1* mutant for its role in heat tolerance at both seedling and reproductive stages. We have also analyzed the contribution of drought-related mechanisms such as ROS-mediated stomatal and water status (Huang et al., 2009; Cui et al., 2015) as well as heat-induced mechanisms to the enhanced heat tolerance of the *hst1* mutant. These studies have provided important new insights into the broad role of the transcription factor in rice stress tolerance.

Materials and methods

Rice growth and treatment

Rice cultivar Zhonghua 11 is a heat sensitive japonica variety and was used as WT throughout the study. The *hst1* mutant was isolated

from the T_7 generation of ZH 11 T-DNA insertion mutant lines. Rice seeds were sterilized with 10% (v/v) sodium hypochlorite for 15 min before rinsing five times with sterilized water, then soaked in the water at 37°C for 2 d in the dark. After germination in Petri dishes with wet filter paper at 37°C, the most uniformly germinated seeds were transferred to a 96-well plate, from which the bottom was removed. The plate was floated on water for 5 days in a growth chamber with a 13-h light (28°C)/11-h dark (23°C) photoperiod and 65% relative humidity. After 4 days, the seedlings were cultured with Yoshida's culture solution (Yoshida et al., 1976). For heat-tolerant screening, rice seedlings were subjected to treatment of heat stress at 42°C with a 13h light/11h dark photoperiod.

Analysis of heat and salt tolerance

For heat treatment at the vegetative stage, WT and *hst1* mutant seedlings that were grown hydroponically in 4.5 liters of Yoshida's culture solution were transferred to a chamber and treated for 3 days at 42°C with a 13h light/11h dark photoperiod. The plants were then transferred to the normal temperature for recovery. The daily loss of the volume of Yoshida's culture solution was very small (<5%) and was replenished with water daily during the heat treatment and recovery period. The heat tolerance phenotypes of the plants were examined, and plants were photographed after different days of recovery at normal temperature. For analysis of the effect of heat stress on reproductive performance, rice plants were moved to a growth chamber one day prior to heading and subjected to heat treatment for 7 days with a 13h light/11h dark photoperiod. The heat treatment (40°C) lasted for 6 hours daily during the light period from 9:00AM to 15:00PM. The plants were grown at 30°C for the remaining 7 hours (3 and 4 hours before and after heat treatment, respectively). Control plants were grown at 28°C during the 13-hour light period. All plants were grown at 23°C during the 11-hour dark period. Plants were grown under normal growth conditions after treatment and their reproductive traits were evaluated after they reached full maturity.

For salt treatment, WT and *hst1* mutant seedlings grown in pots under normal conditions were transferred to plastic containers containing Yoshida nutrient solution with 0.6% NaCl for 12 days. After the treatment, the plants were transferred to the normal nutrient solution for recovery.

Map-based cloning approach

The *hst1* mutant was crossed with IR29, a heat-sensitive indica rice variety. All F1 progeny showed a heat-sensitive phenotype. In the F2 population, heat-sensitive plants and heat tolerant plants segregated in a ratio close to 3 to one. Preliminary mapping with about 300 F2 plants located the *hst1* gene on chromosome 3 using PCR-based molecular markers (Supplemental Table 1). Further mapping placed the mutant gene in a region on chromosome 3. The *hst1* gene was putatively identified by sequencing the genes in the region and confirmed by complementation with the WT *HST1* gene.

HST1 gene cloning and rice transformation

For complementation of the *hst1* mutant, a 3970-bp DNA fragment of the full-length *HST1* genomic sequence was amplified from genomic DNA and cloned into pCAMBIA1301 with *Kpn* I and *Sal* I enzymes. Transgenic lines were achieved by co-cultivation of *hst1* rice calli with *Agrobacterium tumefaciens* strain EHA105 containing the *HST1* construct (Hiei et al., 1994). Positive T0 transgenic plants were screened using PCR analysis of *hpt* with genomic DNA from their leaves.

Production of recombinant DST proteins and EMSA

Full-length coding sequences of WT DST and mutant DST^{hst1} proteins were amplified by PCR using gene-specific primers and cloned into the expression vector pET-32a (Novagen) and transformed into *E. coli* strain BL21(DE3). Expression and purification of recombinant proteins were performed as previously described (Lai et al., 2011). EMSA was performed with purified recombinant proteins and ^{32}P-labeled double-stranded synthetic oligonucleotides as described previously (Lai et al., 2011).

Water loss and relative water content assay

Water loss from the detached leaves of WT plants and *hst1* mutants was measured according to the method described by (Tian et al., 2004) with minor modifications. Detached leaves were placed at 24°C with 40% relative humidity and their fresh weights were determined at various time points. Water loss was expressed as the percentage of initial fresh weight at each time point. The measurement of relative water content was performed as described (Ascenzi and Gantt, 1999) with slight modifications. Briefly, eight fully expanded leaves were detached from plants after various periods of heat treatment and immediately determined for the fresh weight. The leaves were then submerged in ddH_2O overnight. Water on the surface of the leaves was removed by quick blotting using filter papers and the turgid weight was determined immediately. The leaves were then dried at 105°C for 4 hours before their dry weight was determined.

Stomatal conductance and density measurement

For assays of stomatal conductance, 10-day-old plants were grown in a growth chamber. The stomatal conductance was measured using a portable photosynthesis system (LI-6400 LI-COR, Lincoln, USA). For stomatal density measurement, middle sections of fully expanded leaves were sampled from the same position of rice plants of WT and *hst1* mutant. A leaf surface imprint method was used. Nail polish was painted on the sample. After the nail polish was dry, the smear layer was obtained and spread onto the glycerin and

observed under a light microscope as previously described (Berger and Altmann, 2000).

Peroxidase activity, H_2O_2 and malondialdehyde level detection

The peroxidase activity was measured using a peroxidase assay kit from Nanjing Jiancheng Bioengineering Institute (Nanjing, China) as described previously (Li et al., 2013a). H_2O_2 content was measured using an Amplex® Red Hydrogen Peroxide/Peroxidase Assay Kit (Invitrogen) following the vendor's instructions. For sample preparation, 0.5g leaf segments of 10-day-old seedlings were ground in liquid nitrogen and thoroughly mixed with 10 volumes of 50 mM Na_3PO_4 (pH 7.4). After centrifugation at 12000 rpm for 20 minutes at 4 °C, the supernatants were used for the H_2O_2 assay. The levels of MDA were determined based on the spectrophotometer measurement of the product from the reaction of MDA and thiobarbituric acid as previously described (Li et al., 2013a).

RNA isolation and qRT-PCR analysis

Total RNA was isolated using Trizol reagent (Invitrogen) from WT and *hst1* mutant seedlings and flowers. Total RNA was treated with 5 U of RNase-free DNase I (TaKaRa) to remove any DNA contamination. DNase I-treated RNA was reverse transcribed using an oligo(dT) primer and a PrimeScript RT reagent kit (TaKara, Japan) to generate cDNA. Real-time PCR was carried out using SYBR Premix Ex Taq (TaKara, Japan) for detection of PCR products (parameters: 95°C for 1 min, followed by 40 cycles of 95°C for 15 s, 60°C for 15 s, and 72°C for 15 s). All reactions were performed in triplicate. Quantification of gene expression was done using the comparative Ct method. The gene encoding *ACTIN* (LOC_Os03g50885) was chosen as a reference gene. The primers used for qRT-PCR were shown in Supplemental Table 2.

Western blotting

Total proteins from rice leaf tissues were extracted with P-PER® Plant Protein Extraction Kit (Pierce, Cat # 89803). Proteins were fractionated by SDS-PAGE and the HSP70 protein levels were detected by western blotting for detection using an anti-HSP70 antibody (Abcam, Cat # ab5439). The Rubisco large subunit, which was detected with a Rubisco-specific antibody (Agrisera, Cat # AS07 259), was used an loading control. The antigen-antibody complexes were detected by enhanced chemiluminescence using luminal as substrate. The western blot films were scanned, and the intensities of protein bands were quantified using the Image J software. The quantification reflected the relative amounts as a ratio of each HSP protein band to the lane's Rubisco loading control.

Pollen viability assays

Pollen viability was tested with the peroxidase reaction method as described previously (Wang et al., 2012). Briefly, pollens were collected onto a glass slide and stained with two reagents (reagent I: 0.5% benzidine, 0.5% α-naphthol and 0.25% sodium carbonate at 1:1:1 ratio and reagent II: 0.3% hydrogen peroxide). After incubation at 30°C for 10 minutes, the pollen viability was examined under a microscope with viable pollens stained blue and unviable pollens stained colorless or yellowish.

Results

Isolation of the rice *hst1* mutant

To gain important insights into the genes and their network in controlling heat stress responses in rice, we performed a large-scale screen of the rice ZH11 T-DNA insertion lines for mutants with altered levels of wilting immediately after heat stress, or survival after recovery at normal temperature. We isolated several mutants that showed increased heat tolerance and retesting of these putative heat-stress-tolerant mutants confirmed one of them to be highly heat-tolerant in the subsequent generations and was named *heat-stress tolerant 1* (*hst1*). After heat treatment at 42°C for 3 days (13 h light/11h dark photoperiod), the *hst1* mutant seedlings showed less severe wilting than wild-type (WT) plants (data not shown). After 12 days of recovery at 25°C following the heat treatment, approximately 44% of the *hst1* mutant seedlings survived but almost all of WT seedlings died (Figure 1). Based on the wilting symptoms and survival rates after heat treatment, we concluded that the *hst1* mutant had substantially improved heat tolerance.

Cloning and characterization of *HST1*

Since the *hst1* mutant was isolated from a rice T-DNA insertion population, we first determined whether the mutation was caused by a T-DNA insertion. The T-DNA insertion in the binary vector contains a *hygromycin phosphotransferase* (*hpt*) gene as a selection marker that confers resistance to the antibiotic hygromycin. Therefore, we first determined resistance of *hst1* to hygromycin and, surprisingly, discovered that the mutant was as sensitive to the antibiotic as WT plants. To ensure that the hygromycin sensitivity was not due to silencing of the selection marker, we also performed PCR using *hpt*-specific primers but failed to amplify the antibiotic resistance gene from the mutant. Therefore, the *hst1* mutant plant is unlikely to be a T-DNA insertion line. To further determine the genetic nature of the *hst1* mutant, we crossed the mutant with WT plants and found *hst1* to be a recessive mutation based on phenotyping of their F1 and F2 progeny. These results collectively suggested that the *hst1* mutant resulted from a loss-of-function mutation rather than by a T-DNA insertion.

We then took a map-based cloning approach to isolate the *HST1* gene. We first crossed the *hst1* mutant (as female) with a heat sensitive Indica rice variety IR29 (as male parent). All F1 progeny showed a WT heat-sensitive phenotype based on the survival and recovered growth after heat treatment. In the F2 population, the ratio of the heat-sensitive plants to the heat-tolerant plants was close to 3 (220 heat-sensitive *vs.* 80 heat-tolerant; $x^2 = 0.444 < x^2_{0.5} = 0.455$; $P>0.5$), indicating that the *hst1* mutant was caused by a single recessive

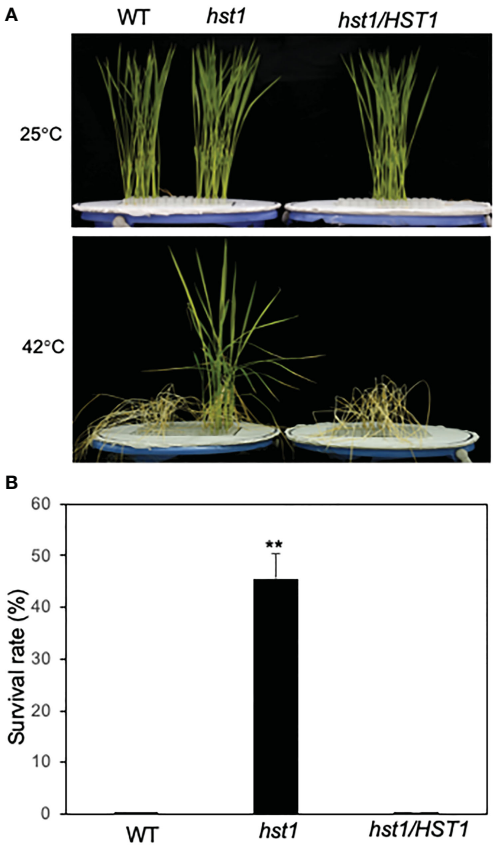

FIGURE 1
Enhanced heat tolerance of rice WT and *hst1* mutant. **(A)** Survival of rice plants after heat treatment. Ten-day old rice seedlings of WT, *hst1* mutant and *hst1* mutant containing a full length HST1 genome clone (*hst1/HST1*) were subjected to heat treatment for 3 days at 42°C. The pictures were taken after 12 days of recovery after heat treatment. The pictures of plants grown at 25°C are also shown for comparison. **(B)** Plant survival rates of WT, *hst1* mutant and *hst1* mutant containing a full length HST1 genome clone (*hst1/HST1*) after heat treatment. Means and SE were calculated from survival rates determined from three experiments with about 100 seedlings per experiment for each genotype. The statistical differences in the survival rate between WT and *hst1* mutant plants were tested using a Student *t* test (**P ≤ 0.01).

nuclear gene mutation. The *HST1* locus was fine-mapped to a region of approximately 80 kb on chromosome 3 (Supplemental Figure 1). The genes within the region were sequenced, and it was discovered that one of them (LOC_Os03g57240) contains a four-nucleotide insertion (TGGG) between the 194th and 195th nucleotides of its coding sequence in the *hst1* mutant (Figure 2A). The insertion would lead to a frameshift in translation after the first 64 amino acid residues (Figure 2). To confirm that LOC_Os03g57240 is *HST1*, we performed a complementation test. A 3966-nucleotide WT LOC_Os03g57240 genomic fragment containing both its promoter and coding region was amplified and cloned into the binary vector pCAMBIA1300. The recombinant vector pCAMBIA1300-*HST1* was transformed into the callus of the *hst1* mutant by an *Agrobacterium*-mediated method. Five positive transgenic *hst1/Hst1* lines were obtained and were as heat-sensitive as WT based on increased wilting and reduced survival rate when compared to the *hst1* mutant after heat treatment (Figure 1). Thus, the TGGG insertion in LOC_Os03g57240 is responsible for the increased heat-tolerant phenotype of the *hst1* mutant. These results indicate that HST1 has a negative role in heat tolerance in rice.

Interestingly, LOC_Os03g57240 was previously named *Drought and Salt Tolerance* (*DST*), which negatively regulates drought and salt tolerance in rice plants based on the analysis of a *dst* mutant (Huang et al., 2009; Cui et al., 2015). The *DST* gene encodes a 301-residue transcription factor containing a nuclear localization signal (NLS) and a C2H2-type zinc finger motif at the N-terminus. The C2H2-type zinc finger of DST is responsible for its sequence-specific DNA binding activity (Huang et al., 2009; Li et al., 2013b; Cui et al., 2015). The *dst* mutant is recessive with increased drought and salt tolerance due to a missense mutation that converted the codon for asparagine at residue 69 to a codon for threonine in the conserved C2H2 zinc finger motif (Figure 2B) (Huang et al., 2009). A second mutant, *reg1*, is semidominant with increased panicle branches and consequently improved grain number (Li et al., 2013b). The *reg1* mutant contains an A insertion between the 214th and 215th nucleotides of the *DST* cDNA, which leads to a frameshift after the first 72 amino acids (Figure 2B) (Li et al., 2013b). As a result, the NLS and C2H2 zinc finger motif at the N-terminus of DST^{reg1} are not altered but the remaining protein sequence is completely changed as a result of the frameshift (Figure 2B) (Li et al., 2013b). Both DST^{dst} and DST^{reg1} mutant proteins still contain the conserved C2H2 residues in the zinc finger motif and, as a result, still bind to the TGNTANN(A/T)T sequence, a *cis*-acting element called DST-binding sequence present

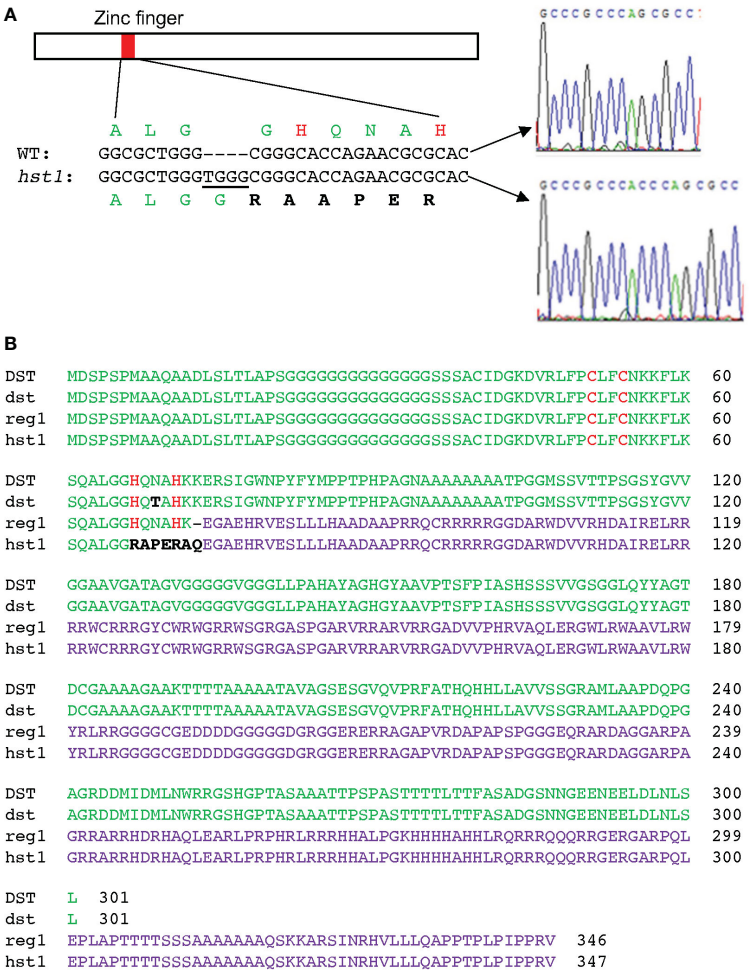

FIGURE 2
Positional cloning and gene product of the *hst1* mutant gene. **(A)** Identification of the *hst1* gene mutation. The *hst1* gene contains a four-nucleotide (TGGG) insertion at the nucleotide position 194, which leads to a frameshift of the translated protein at its CCHH zinc finger motif. **(B)** Comparison of WT DST protein with the three isolated mutant proteins: DST^{dst} (dst), DST^{reg1}(reg1) and DST^{hst1}(hst1). The dst protein contains a single amino acid substitution (N69T) between the two conserved H residues at the zinc finger motif. Both *reg1* and hst1 proteins result from frameshift mutations that alter a majority of the DST amino acid sequence. The reg1 protein still contains the intact zinc finger motif while the hst1 protein lost the conserved histidine H residues of the zinc finger motif due to the frameshift mutations. The conserved zinc-binding cysteine (C) and H residues of the zinc finger motif are in red. The unique amino acid residues in dst and hst1 from their respective mutations are in black. The altered C-terminal amino acid sequences from reading frame shifting in reg1 and hst1 proteins are in purple.

in DST target genes (Huang et al., 2009; Li et al., 2013b; Cui et al., 2015). By contrast, the two conserved histidine residues in the DNA-binding C2H2 zinc finger motif in our DST^{hst1} mutant protein are eliminated by the frameshift mutation in the *hst1* mutant (Figure 2), which would abolish its sequence-specific DNA-binding activity. To test this, we produced recombinant DST and DST^{hst1} proteins and analyzed them for sequence-specific DNA-binding activity using electrophoresis mobility shifting assays (EMSA). As shown in Figure 3, only WT DST but not the DST^{hst1} protein was able to bind DNA molecules containing the DST-binding sequence.

Expression analysis of rice *HST1(DST)*

To further analyze the role of the rice *DST* gene, we analyzed its tissue-specific expression using qRT-PCR. As shown in Figure 4A, although *DST* transcripts were detected in all tissues, their levels were relatively low in callus, root, stem, node and spike. On the other hand, high levels of *DST* transcripts were detected in leaves (Figure 4A). As a negative regulator of plant responses to a range of abiotic stresses, high levels of DST transcripts in rice leaves may be necessary to suppress induction of stress responses under normal conditions and promote other processes such as photosynthesis in the green tissues that are important for plant growth.

We also analyzed the expression pattern of *DST* in rice leaves in response to heat stress. qRT-PCR analysis showed that the levels of *DST* transcripts were rapidly down-regulated after 1 hour of heat treatment, followed by gradual recovery over the subsequent 6 hours (Figure 4B). During the first 6 hours of heat treatment, the transcript levels of *DST* in heat-treated leaves were generally lower than those in the leaves with heat treatment (Figure 4B). Thus, heat stress reduced expression of *DST* during the first 6 hours of heat treatment. After 6

10.3389/fpls.2023.1068296

FIGURE 3
Assays of DNA-binding activity of DST and DST^{hst1} proteins. Binding reactions (20 µl) contained no (-) or 0.5 µg indicated recombinant proteins, 2 ng labeled oligo DNA (GGCTATACTAACCGTGCtgctagccattagGCCCAAGTTAGT) and 5 µg polydeoxyinosinic-deoxycytidylic acid.

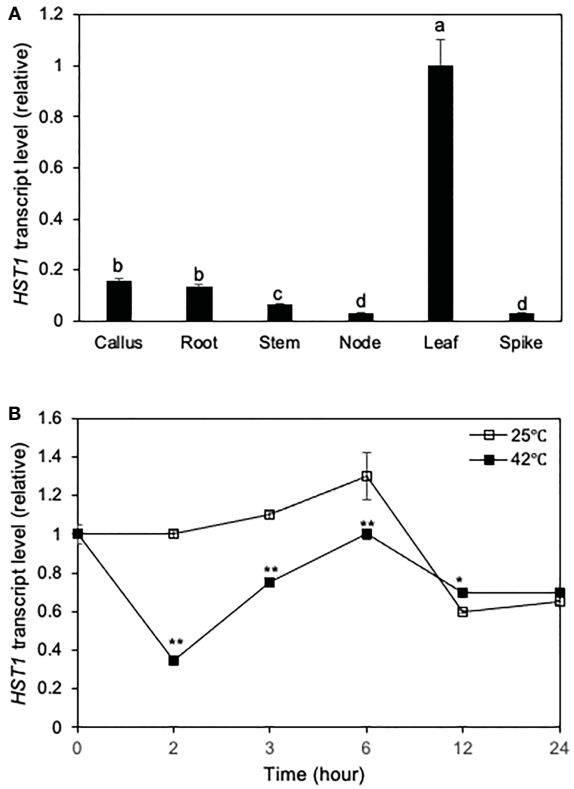

FIGURE 4
Tissue-specific and heat-regulated expression of *DST*. **(A)** Tissue-specific expression of *DST*. Total RNA was isolated from indicated tissues and transcript levels of *DST* were determined using qRT-PCR. Error bars indicate SE (n = 3). According to Duncan's multiple range test (P=0.01), means of the values do not differ if they are indicated with the same letter. **(B)** *DST* gene expression in response to heat treatment. Rice seedlings (10-days old) were placed in a 25°C or 42°C growth chamber and total RNA was isolated from leaf samples collected at indicated times. Transcript levels of *DST* were determined using qRT-PCR. Error bars indicate SE (n = 3). The statistical differences in the transcript levels between 25°C and 42°C were tested using a Student *t* test (*P ≤ 0.05; **P ≤ 0.01).

hours, the *DST* transcript levels decreased not only at 42°C but also at 25°C (Figure 4B). This reduction in *DST* transcripts was likely in response to the light-to-dark transition of the rice plants.

Altered water and stomatal status of *hst1* under heat stress

To understand the physiological basis of the reduced wilting phenotype of the *hst1* mutant during heat treatment, we analyzed the relative water content in the WT and *hst1* mutant plants. Detached WT and *hst1* mutant leaves were placed at 24°C under 40% relative humidity and water loss was measured after various hours. As shown in Figure 5A, WT rice leaves lost 20-38% more water during the first 4 hours. After 4 hours at the high temperature, water loss in the detached WT leaves was substantially reduced likely due to limited amounts of residual water in the leaves. In the *hst1* mutant, water loss also decreased after 4 hours under the heat stress but to a lesser extent than in WT probably due to higher levels of residual water in the mutant leaves (Figure 5A). We also subjected whole WT and *hst1* mutant plants to heat stress (42°C) and monitored the relative water content for 36 hours. As shown in Figure 5B, significant difference in relative water content between WT and *hst1* plants was first apparent after 24 hours under heat stress and became more pronounced in the next 12 hours. As a result, during the last 8-10 hours of the experiments, the *hst1* mutant plants steadily maintained about 10% more water than the WT plants (Figure 5B). Thus, the *hst1* mutant plants were more resistant to water loss than WT plants at the high temperature, which would allow for better survive under heat stress.

Stomata are vital for sensing and adapting to environmental changes including mitigating transpirational water loss under water or other stresses. Therefore, we investigated the stomatal conductance of the *hst1* mutant and WT plants. Even under normal temperature, the stomatal conductance of the *hst1* mutant was only about 60% of that of WT plants (Figure 5C). Under heat stress, the stomatal conductance of WT and the *hst1* mutant plants was reduced by about 30% and 20%, respectively, when compared to those under normal temperature (Figure 5C). Even with the relatively small reduction for the *hst1* mutant with elevated temperature, the stomatal conductance of the *hst1* mutant was still about 30% lower than that of WT plants under heat stress (Figure 5C). Furthermore,

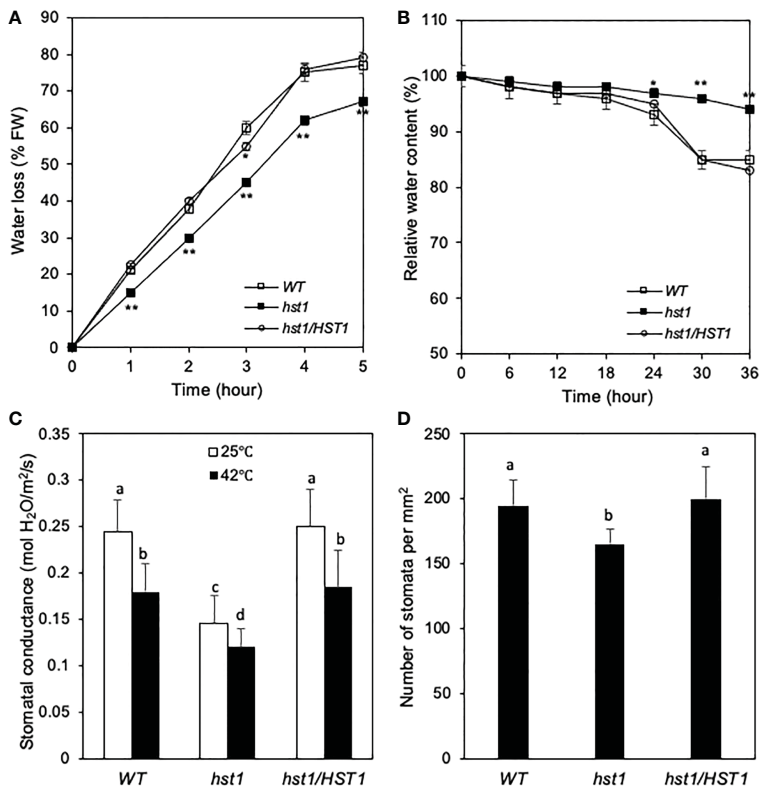

FIGURE 5
Effects of the *hst1* mutation on leaf stomata and water loss under heat stress. **(A)** Water loss of detached leaves. For each repeat, 10 fully expanded leaves of 10-day-old plants were detached from WT and the *hst1* mutant plants and placed at 24°C with 40% relative humidity in a triplicate experiment (n = 3). **(B)** Relative water content. Relative water content of WT and *hst1* mutant treated with heat (42°C) at 65% relative humidity using the fully expanded leaves of 10-day-old plants (n = 9). **(C)** Stomatal conductance. Seedlings were cultured in a growth chamber for 10 days, and the stomatal conductance was measured using a portable photosynthesis system (LI-6400 LI-COR, Lincoln, USA). The statistical differences in water loss or water content between WT and *hst1* mutant plants including the *hst1* mutant plants containing the full *HST1* genome clone (*hst1*/*HST1*) were tested using a Student *t* test (*P ≤ 0.05; **P ≤ 0.01). **(D)** Stomata number. Stomatal density of middle sections of leaves from WT and *hst1* mutant plants (n = 10) were determined from three random microscopic fields in each repeat. According to Duncan's multiple range test (P=0.01), means of the values do not differ if they are indicated with the same letter. The experiment was repeated three times with similar results.

we found that the stomatal density in the *hst1* mutant plants was 15% lower than that in WT plants (Figure 5D). Thus, the enhanced heat tolerance of *hst* mutants was associated with decreased stomatal density and low stomatal conductance, which would make the mutant retain more water and survive better than WT plants under heat stress.

To determine whether altered water status of the *hst1* mutant was caused by the *DST* gene mutation, we analyzed transgenic *hst1* lines containing the WT DST^{HST1} genomic fragment (*hst1/HST1*) for relative water content and water loss. Indeed, all transgenic *hst1/HST1* plants were similar to WT with reduced water content and increased water loss after heat treatment when compared to those of the *hst1* mutant (Figures 5A, B). Furthermore, the stomatal conductance and stomata number of the *hst1* mutant were restored to those of WT in the complemented lines (Figures 5C, D). These results further indicate that the TGGG insertion in the DST^{HST1} gene is responsible for the increased heat tolerance of the *hst1* mutant, demonstrating that the DST transcription factor is a negative regulator of heat tolerance in rice.

To determine whether the enhanced heat tolerance of the *hst1* mutant was entirely or partially due to its reduced stomatal conductance, which reduces water loss under heat stress, we compared survival rates of WT and *hst1* mutant plants after heat treatment under 65% and 100% of relatively air humidity. As shown in Figure 6, increased air humidity improved survival rates of both WT and *hst1* mutant plants after both 3 and 4 days of heat treatment. Furthermore, the differences in the survival rates after heat stress between WT and *hst1* mutant plants decreased when the air humidity was increased from 65% to 100% (Figure 6). It should be noted that at both 65% and 100% humidity, the rice plants were grown hydroponically in a large volume of growth medium (4.5 liters) that was replenished daily during the heat treatment and recovery period. Therefore, the differences in the survival rates after heat treatment between the two levels of air humidity and between WT and the *hst1* mutant were not caused by reduced water supply or drought. Instead, the substantial effect of relative air humidity on the heat tolerance was mostly through their effect on the water status of shoots above the ground, which is controlled not only by the water supply from the roots but also by water loss from transpiration. Furthermore, even with 100% air humidity, there were still significant differences in the survival rates between WT and *hst1* mutant after 3 or 4 days of heat stress (Figure 6). These results indicate that stomatal conductance plays an important role in increased heat tolerance of the *hst1* mutant but other factors also contribute to improved survival of *hst1* under high temperatures.

Reduced expression of ROS-scavenging *Prx24* target gene and altered H_2O_2 homeostasis in the *hst1* mutant

It has been previously shown that DST binds to the TGCTANNATTG elements in its target gene promoters by the C2H2 zinc finger motif and activates their transcription (Huang et al., 2009; Li et al., 2013b; Cui et al., 2015). Expression profile analysis using the Affymetrix Rice Genome Genechip has identified DST-dependent genes, some of which are related to reactive oxygen species (ROS) homeostasis (Huang et al., 2009). Among the genes directly targeted by DST is *Peroxidase 24 Precursor* (*Prx24*), which encodes a peroxidase that directly scavenges H_2O_2 (Huang et al., 2009). To determine whether the expression of *Prx24* was altered in the *hst1* mutant, we compared WT and the *hst1* mutant for the transcript levels of *Prx24* in response to heat stress using qRT-PCR. As shown in Figure 7A, the transcript levels of *Prx24* in WT were substantially higher than those in *hst1* even prior to heat treatment. Thus, the loss-of-function mutation in *DST* gene in the *hst1* mutant caused reduction in basal expression levels of *Prx24*. Upon heat treatment at 42°C, we observed rapid reduction in *Prx24* transcripts in both WT and *hst1* mutant during the first 0.5 and 1 hours at the high temperature (Figure 7A). Following the rapid reduction during the first hour, the transcript levels of *Prx24* became relatively stable or even increased slightly during the remaining hours of the experiments (Figure 7A). Throughout the 12 hours at the high temperature, however, the *Prx24* transcript levels in the *hst1* mutant were

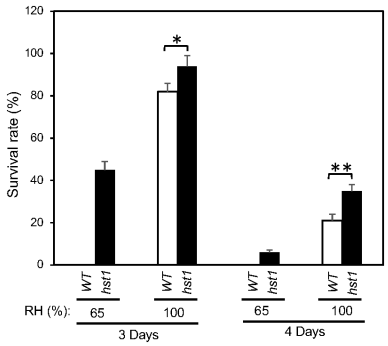

FIGURE 6
Effects of humidity on the heat tolerance of rice WT and *hst1* mutant. Ten-day old WT and *hst1* mutant plants were subjected to heat treatment at 42°C for 3 and 4 days under 65% and 100% relative air humidity. The survival rates were estimated after 10 days of recovery at the room temperature. Means and SE were calculated from survival rates determined from three experiments with about 50 seedlings per experiment for each genotype. The statistical differences in the maximum leaf width between WT and *hst1* mutant were tested using a Student *t* test (*P ≤ 0.05; **P ≤ 0.01).

10.3389/fpls.2023.1068296

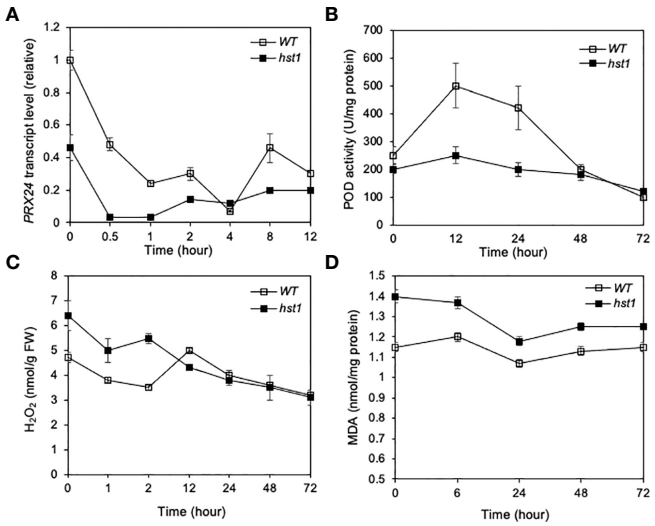

FIGURE 7
Effect of the *hst1* mutation on expression of ROS-scavenging *Prx24* target gene and levels of ROS and MDA under heat stress. **(A)** Expression of *Prx24*. Rice WT and *hst1* mutant seedlings (10-day old) were placed in a 42°C growth chamber and total RNA was isolated from leaf samples collected at indicated times. Transcript levels of *Prx24* were determined using qRT-PCR. Error bars indicate SE (n = 3). **(B)** Level of peroxidase (POD) activity. Heat treatment of rice seedlings was performed as in (c). One unit (U) POD activity is defined as the amount of enzyme which catalyzes 1 µg substrate in 20 seconds at 25°C. Means and SE were calculated from three experiments with five leaf samples per time point for each genotype. **(C)** Level of ROS. Heat treatment of rice seedlings was performed as in (a). Means and SE were calculated from three experiments with five leaf samples per time point for each genotype. **(D)** Level of MDA. Heat treatment of rice seedlings was performed as in (a). Means and SE were calculated from three experiments with five leaf samples per time point for each genotype. The statistical differences in the *Prx24* transcript level, POD activity, ROS or MDA level between WT and *hst1* mutant plants were tested using a Student *t* test (**P ≤ 0.01).

generally lower than those in WT, particularly during the first 0.5 to 1 hour under heat stress (Figure 7A). We also found that the levels of peroxidase activity was substantially lower in the *hst1* mutant than in WT during the first 24 hours under heat stress (Figure 7B).

To determine whether reduced expression of ROS-scavenging *Prx24* was associated with altered ROS levels in the *hst1* mutant, we compared WT and *hst1* for the H_2O_2 levels. As shown in Figure 7C, the *hst1* mutant had a significantly higher level of H_2O_2 than WT even prior to heat treatment. During the first two hours of treat stress, the H_2O_2 levels in the *hst1* mutant remained higher than those in WT (Figure 7C). By the 12th hour at the high temperature, the H_2O_2 levels became similar in WT and *hst1* mutants (Figure 7C). Thus, the loss-of-function *hst1* mutation elevated H_2O_2 levels prior to and during the early hours of heat treatment. We also compared WT and the *hst1* mutant for the levels of malondialdehyde (MDA), which results from lipid peroxidation of polyunsaturated fatty acids at elevated levels of ROS. Again, we observed that the basal levels of MDA in the *hst1* mutant prior to heat treatment were elevated when compared to those in WT (Figure 7D). During the first 6 hours at the high temperature, the MDA level remained significantly different between WT and *hst1* mutant plants (Figure 7C). The difference in the MDA levels between WT and the *hst1* mutant during the remaining hours of the experiments was also observed, albeit to a lesser extent (Figure 7D).

Rapid induction of *HSP* gene expression in the *hst1* mutants

Heat shock responses are found universally in cells that are characterized by rapid transcriptional activation of genes encoding HSPs, many of which act as molecular chaperones in protein quality control (Craig et al., 1993; Jakob et al., 1993). To determine whether enhanced heat tolerance of the *hst1* mutant was also associated with altered expression of genes associated with the heat shock response, we compared 45-day-old WT and the *hst1* mutant for the transcript levels of six *HSP* genes, which have been previously shown to be strongly responsive to heat shock treatment (Zou et al., 2009). In WT, all of these six *HSP* genes displayed rapid induction by heat treatment. Transcript levels for four of the six tested *HSP* genes (*Hsp17.0*, *Hsp24.1*, *Hsp26.7* and *Hsp74.8*) peaked after 1 or 2 hours at the high temperature (Figure 8). Rice *Hsp58.7* displayed relatively slow induction and continued to increase in its transcript level after 2 hours of heat treatment (Figure 8). Rice *Hsp80.2*, on the other hand, had relatively low induction in its transcript level, although its peak levels occurred quite rapidly at the first 0.5 hour after heat treatment (Figure 8). Importantly, the *hst1* mutant was more rapid and robust in induction of these *HSP* genes under heat treatment (Figure 8). As a result, the differences in the transcript levels for the six *HSP* genes

10.3389/fpls.2023.1068296

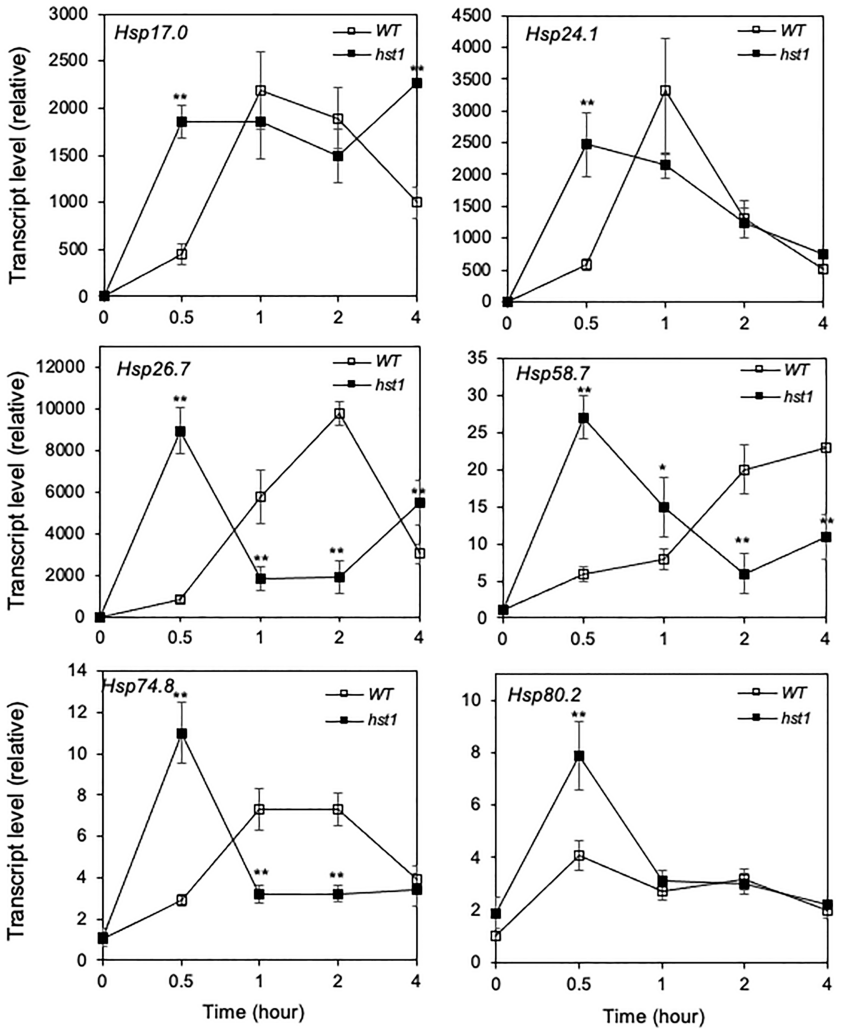

FIGURE 8
Heat-induced expression of *HSP* genes. WT and *hst1* mutant plants (45-day-old) were placed in a 42°C growth chamber and total RNA was isolated from leaf samples collected at indicated times. Transcript levels were determined using qRT-PCR. Error bars indicate SE (n = 3). The statistical differences in the transcript level between WT and *hst1* mutant were tested using a Student *t* test (*P ≤ 0.05; **P ≤ 0.01).

were most pronounced during the first half hour of heat treatment (Figure 8). The transcript levels of five of these six *HSP* genes peaked at 0.5 hour after heat treatment in the *hst1* mutant, which were 0.5 to 2 hour earlier than those in WT (Figure 8). Even though they peaked at 0.5 hour after heat treatment in both WT and the *hst1* mutant, the transcript levels of *Hsp80.2* were substantially higher in the *hst1* mutant than in WT at the initial hours of heat stress (Figure 8). We also analyzed heat-induced expression of the *HSP* genes in ten-day-old seedlings and found that the *hst1* mutant again displayed significantly faster and stronger induction of the *HSP* genes than WT (Supplemental Figure 2A). Furthermore, we performed western blotting using an anti-HSP70 antibody and found that the *hst1* mutant seedlings accumulated HSP70 proteins at rates significantly faster and stronger than those of WT plants during response to heat treatment (Figure 9). Thus, enhanced heat tolerance of the *hst1* mutant was also associated with rapid and increased induction of *HSP* gene expression and HSP protein accumulation, which would lead to enhanced heat shock responses.

Role of ROS in rapid heat induction of HSP genes in the *hst1* mutant

Several studies have shown that H_2O_2 is involved in heat shock responses (Miller and Mittler, 2006). Since the *hst1* mutant contained increased levels of H_2O_2, we investigated whether the elevated ROS is required for the more rapid and robust induction of rice *HSP* genes. For this purpose, we treated both 45-day-old WT and *hst1* mutant seedlings with diphenyleneiodonium chloride (DPI), an inhibitor of ROS production, and compared WT and *hst1* for the induction of the *HSP* genes during the first half hour of heat treatment, in which the differences in the transcript levels for the six *HSP* genes were most

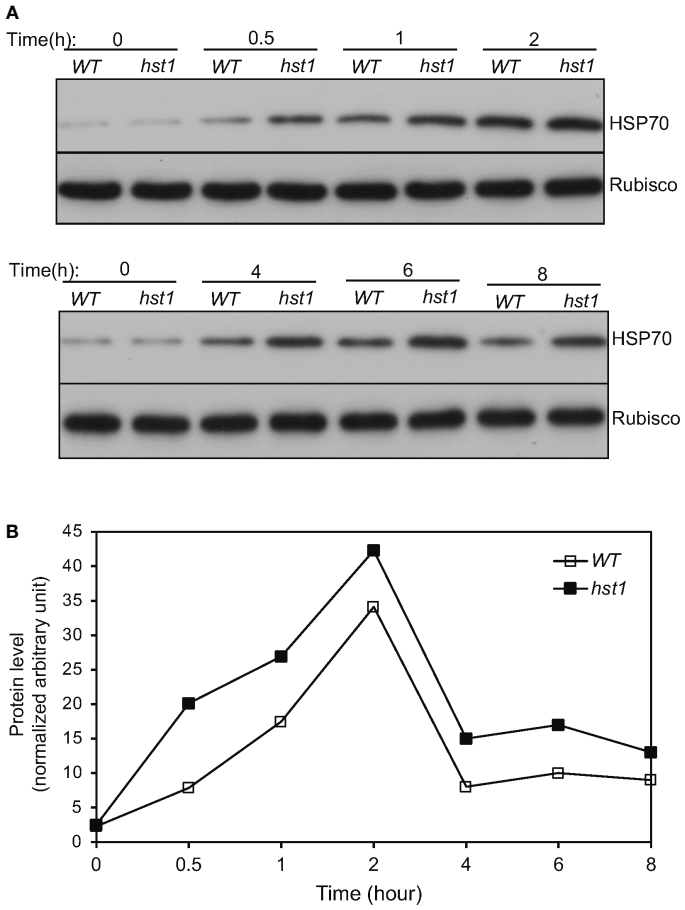

FIGURE 9
Heat-induced HSP70 accumulation in rice seedlings. **(A)** Ten-day old WT and *hst1* mutant seedlings were placed in a 42°C growth chamber and total proteins were isolated from leaf samples collected at indicated times. The HSP70 protein levels were analyzed by western blotting using anti-HSP70 polyclonal antibodies. Rubisco large subunit proteins, detected with an anti-Rubisco antibody, were used as a loading control. **(B)** HSP70 protein levels at the indicated times of heat treatment were determined from the band intensities of scanned western blots using Image J software. The quantification reflected the relative amounts as a ratio of each HSP protein band to the lane's Rubisco loading control. The HSP70 protein band intensities from different blots were normalized. The experiments were repeated twice with similar results.

pronounced (Figure 8). Indeed, treatment of DPI suppressed the induction of the *HSP* gene transcript levels in the *hst1* mutant to the levels similar to those in WT (Figure 10). Similar inhibitory effects of DPI on the stronger induction of *HSP* genes in the *hst1* mutant were also observed at the seedling stage (Supplemental Figure 2B). These results suggest that increased ROS levels in the *hst1* mutant are involved in the increased transcription of *HSP* genes in the *hst1* mutant.

Phenotypes of *hst1* in grain production and heat tolerance at reproductive stages

Heat stress at the flowering and grain-filling stages seriously affects rice grain quality and yield (Zafar et al., 2020a; Yan et al., 2021; Zafar et al., 2022). To determine the role of DST transcription factor in the rice heat tolerance at reproductive stages, we first analyzed the expression of *DST* in reproductive tissues. Rice plants at the heading and flowering stages were growth at grown at 28°C and 40°C and flowers were collected at various time points for determination of *DST* transcript levels in the reproductive tissues. As shown in Figure 11, there was a reduction of DST transcripts during the first hour of treatment at both at 28°C and 40°C. At 28°C, the reduced DST transcripts were largely restored over the next few hours and were largely maintained at the levels similar to those at the beginning of the experiments (Figure 11). At 40°C, the *DST* transcripts also recovered from the early reduction and displayed a 3- to 4-fold induction between the 3rd and 6th hours after treatment (Figure 11). As a result, the DST transcript levels were 2-4 times higher at 40°C than at 28°C throughout the 12 hours of the experiments (Figure 11). Thus, expression of *DST* appears to be more responsive to high temperature in the reproductive tissues than in the seedling leaves (Figure 4B).

We also compared grain production between WT and *hst1* mutant grown under the normal and heat stress conditions. Under normal growth conditions, grain production has been previously studied in another rice mutant for DST transcription factor, *reg1*, which contains a single nucleotide insertion that leads to a frameshift

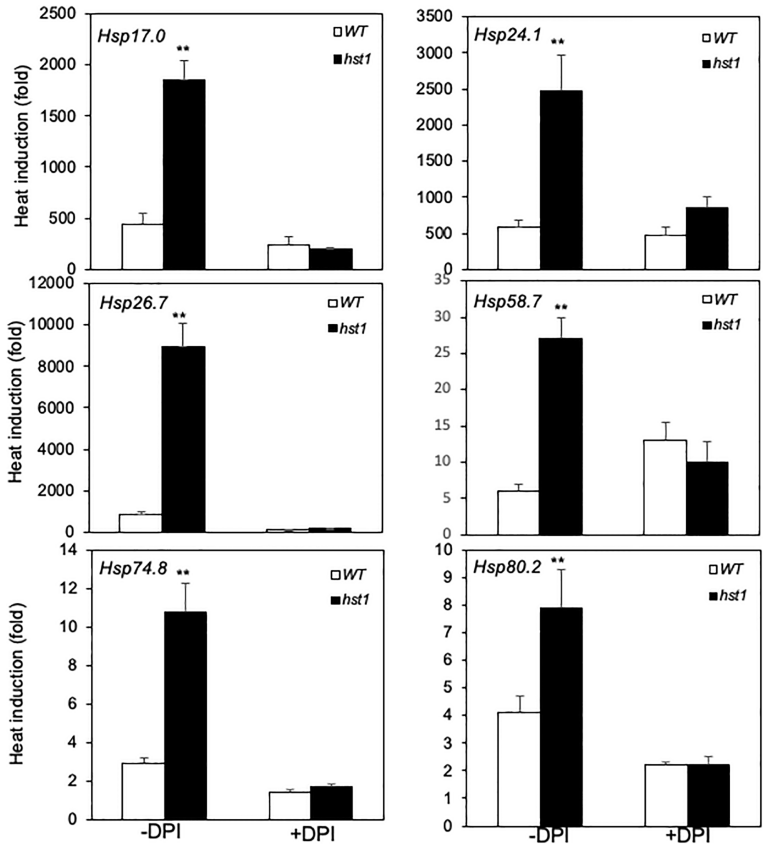

FIGURE 10
Effect of DPI on early induction of *HSP* gene expression by heat treatment. WT and *hst1* mutant plants (45-day-old) were transferred to the growth medium with (+) or without (-) 10 uM DPI. After 24-hour treatment, the plants were placed in a 42°C growth chamber and total RNA was isolated from leaf samples collected after 0.5 hour of heat treatment. Transcript levels were determined using qRT-PCR. Error bars indicate SE (n = 3). The statistical differences in heat induction of the indicated gene transcript with or without DPI treatment between WT and *hst1* mutant were tested using a Student *t* test (**P ≤ 0.01).

after the first 72 amino acids (Figure 2). As a result, the NLS and C2H2 zinc finger motif at the N-terminus of DST^{reg1} are not altered but the remaining protein sequence is completely changed (Figure 2B) (Li et al., 2013b). The *reg1* mutant is semi-dominant with increased panicle branches and consequently improved grain number (Li et al., 2013b). The *reg1* mutant contained about 14 primary and secondary branches per panicle, compared to about 10 branches in WT plants (Li et al., 2013b). As a result, grain number per main panicle in the *reg1* mutant was 63.8% higher than that of WT plants (Li et al., 2013b). The *hst1* mutant contains a four-base

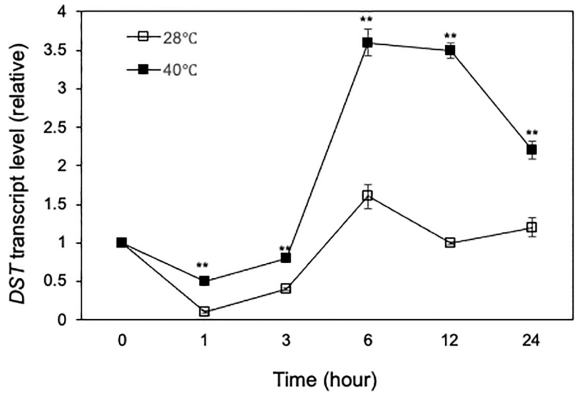

FIGURE 11
Heat-regulated expression of *DST*. Rice plants on the first day of heading and flowering were placed in a 28°C or 40°C growth chamber and total RNA was isolated from panicle/flower samples collected at indicated times. Transcript levels of *DST* were determined using qRT-PCR. Error bars indicate SE (n = 3). The statistical differences in the transcript levels between 28°C and 40°C were tested using a Student *t* test (**P ≤ 0.01).

insertion (tggg) between its 194th and 195th nucleotides in DST, which causes a frameshift after the first 64 amino acid residues (Figure 2). Therefore, the mutation in the *hst1* mutant not only disrupts the conserved C2H2 zinc finger motif but also alters the remaining protein sequence (Figure 2). Intriguingly, the *hst1* mutant had about 10 primary and secondary branches per panicle, similar to those of WT plants (Figure 12A). Furthermore, both the seed yield per plant and the grain number per main panicle in the *hst1* mutant were about 20% higher than that of WT, primarily due to significantly higher seed-setting rates in the *hst1* mutant (Figures 12B, C). Thus, the beneficial phenotypes of the *hst1* mutant in grain production were not as strong as the *reg1* mutant. Furthermore, unlike the semidominant nature of the *reg1* mutant, the slightly improved grain production in the *hst1* mutant was observed only in the *hst1/hst1* homozygous mutant, but not in the *Hst1/hst1* heterozygous plants (Figures 2A–C).

To determine the role of DST in rice heat tolerance at reproductive stages, we analyzed the effect of heat treatment on the seed yield of WT and hst1 mutant. As described in Materials and Methods, for heat treatment, rice plants at the heading and flowering stages were subjected to 6-hour daily heat treatment (40°C) during the daytime for 7 days and their seed yields were compared to those of rice plants without the daily heat treatment. As shown in Figure 12, under normal conditions, the seed yield per plant of *hst1* was about 20% higher than those of WT and *hst1* complemented with HST1 (*hst1/HST1*). This increase in seed yield in *hst1* was primarily resulted from the increase in the grain number per panicle (Figure 12). On the other hand, WT and *hst1* had similar numbers of branches per panicles. Daily heat treatment of 6 hours at 40°C for 7 days reduced seed yield and grain numbers by approximately 80-85% in WT and *hst1/HST1*, but only about 50% in *hst1* (Figure 12). Thus, *hst1* mutant was also more tolerant to heat stress at the reproductive stages than WT.

The negative effects on heat stress on the grain numbers and seed yield in WT and hst1 mutants were strongly correlated with the seed setting rates (Figure 12D). Under normal growth conditions, WT, *hst1* and *hst1/HST*1 had very similar seed setting rates of approximately 70% (Figure 12D). When grown under daily heat stress, the seed setting rates were reduced by 80-90% in WT and *hst1/HST1*, but only about 45% in *hst1* (Figure 12D). We also observed that heat stress has a stronger effect on the pollen viability of WT and *hst1/HST1* than on that of *hst1* (Figure 13). Heat treatment for 1 day resulted in reduction of pollen viability by 12% in WT and *hst1/HST1* but only by 7% in *hst1* (Figure 13). Interestingly, increasing daily heat treatment from 1 day to 5 days, led to a significant recovery in pollen viability and as a result, the pollen viability of WT and *hst1* was reduced only by 10 and 5%, respectively, when compared to those under normal growth conditions (Figure 13). These results collectively indicate that heat stress negatively impact reproductive processes, ultimately leading to reduction in grain formation and seed yield.

Mutant phenotypes of *hst1* in salt tolerance

As described earlier, two rice mutants, *dst* and *reg1*, for the rice *DST* gene have been previously reported with altered phenotypes in drought and salt tolerance and in grain production, respectively

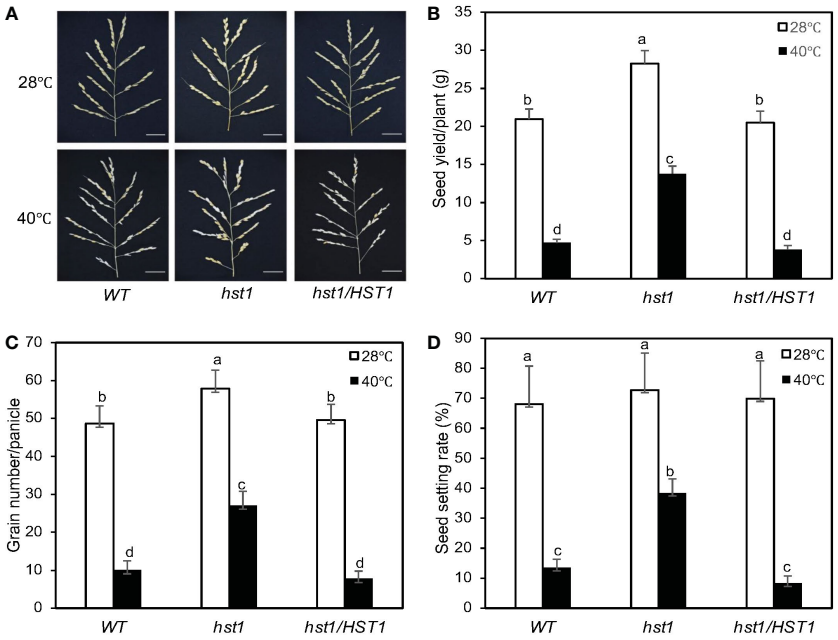

FIGURE 12
Enhanced reproductive performance of *hst1* under heat stress. Rice plants were moved to a growth chamber one day prior to heading and subjected to a heat treatment regimen (daily 6 hours at 40°C) for 7 days with a 13h light/11h dark photoperiod as described in Materials and Methods. Control plants were grown at 28°C during the 13-hour light period. Plants were grown under normal growth conditions after treatment and their reproductive traits including panicle numbers **(A)**, seed yield per plant **(B)**, grain numbers per panicle **(C)** and seed setting rates **(D)** were evaluated after they reached full maturity. Means and SE were calculated from 40 plants for each genotype. According to Duncan's multiple range test (P=0.01), means of the reproductive traits do not differ if they are indicated with the same letter. The experiment was repeated three times with similar results.

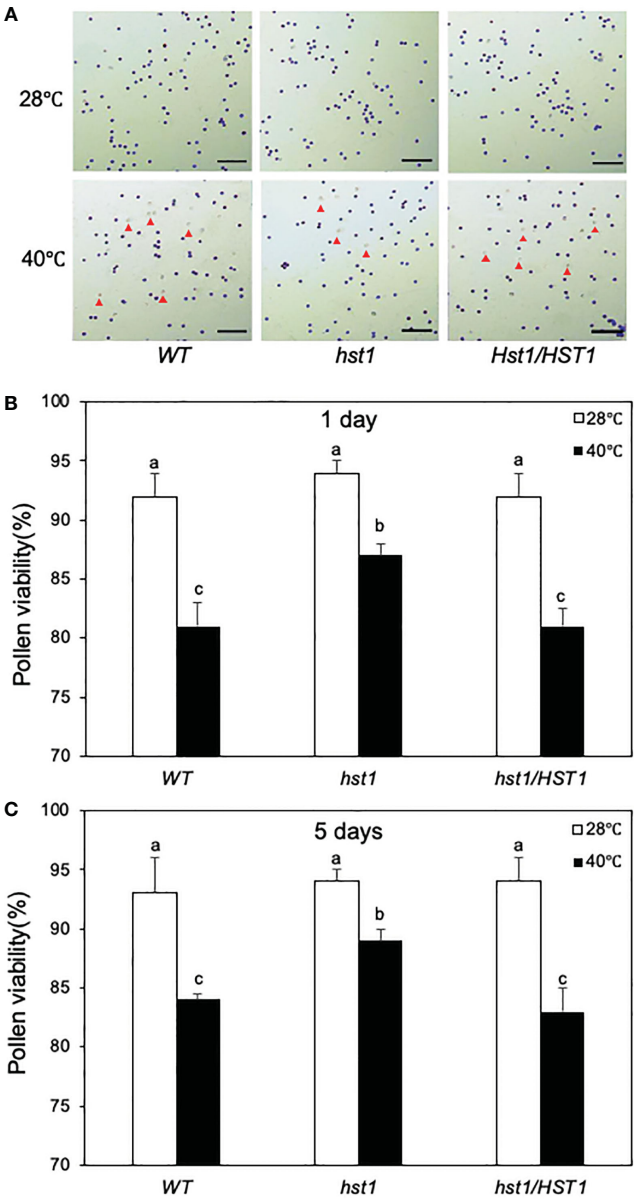

FIGURE 13
Enhanced pollen viability of *hst1* under heat stress. Rice plants were moved to a growth chamber one day prior to heading and subjected to the same heat treatment regimen as in Figure 12 and described in Materials and Methods. Pollen viability was assayed with a peroxidase activity staining procedure. Viable pollens stained blue and unviable pollens stained colorless or yellowish as indicated by red markers **(A)**. The percentages of viable pollens after 1 **(B)** and 5 **(C)** days of heat treatment were determined, Means and SE of viable pollen percentages were calculated from approximately 300 pollens from three microscope fields of view. According to Duncan's multiple range test (P=0.05), viable pollen percentage means do not differ if they are indicated with the same letter. The experiment was repeated three times with similar results.

(Huang et al., 2009; Li et al., 2013b; Cui et al., 2015). The *dst* mutant is recessive with increased drought and salt tolerance due to a missense mutation that causes the substitution of an asparagine (N) at residue 69 for a threonine (T) in the conserved C2H2 zinc finger motif (Figure 2B). Despite the substitution of a conserved amino acid in the C2H2 zinc finger motif, the sequence-specific DNA-binding activity of the DST^{dst} mutant protein was not altered and the enhanced drought and salt tolerance of the *dst* has been attributed to abolished or reduced transcription-acting activity of the mutant protein (Huang et al., 2009). Therefore, we also examined whether the *hst1* mutant was altered in tolerance to salt. When treated with 0.6% NaCl for 12 days, more than 50% of *hst1* mutant plants but only about 20% WT plants survived (Supplemental Figure 3). The enhanced salt tolerance was observed only in the *hst1/hst1* homozygous lines, but not in the *hst1* mutant complemented with the WT DST genomic fragment (*hst1/HST1*). Thus, the *dst* and *hst1* mutants share the same

phenotype of enhanced salt tolerance and as with the *dst* mutant, this salt-tolerant phenotype of the *hst1* mutant is recessive. Like the *dst* mutant, the leaf width of the *hst1* mutant was also substantially increased (Supplemental Figure 4).

Discussion

Analysis of two previously reported mutant alleles for DST have shown that the rice C2H2 transcription factor is an important regulator of plant stress tolerance and grain production (Huang et al., 2009; Li et al., 2013b). The *dst* recessive mutant displayed increased drought and salt tolerance due to a missense mutation that results in an amino acid substitution in the conserved C2H2 zinc finger motif (Huang et al., 2009). The semi-dominant *reg1* mutant has increased panicle branches and grain number due to a single nucleotide insertion that causes a frameshift immediately downstream of the C2H2 zinc finger (Figure 2B) (Li et al., 2013b). Both DST^{dst} and DST^{reg1} mutant proteins are still capable of sequence-specific DNA-binding (Huang et al., 2009; Li et al., 2013b). Our new *hst1* mutant allele, on the other hand, contains a 4-nucleotide insertion in *DST* that causes a frameshift at the first conserved histidine residue of the C2H2 motif and, as a result, disrupts the zinc finger (Figure 2) and abolishes the DNA-binding activity (Figure 3). Therefore, unlike the previously reported *dst* and *reg1* mutant alleles, *hst1* is a knockout mutant for the DST transcription factor. Comprehensive analysis of the *hst1* mutant revealed a critical and novel role of the DST transcription factor in rice heat tolerance through both common and heat-specific mechanisms of stress responses. Characterization of the *hst1* mutant also provided important new insights into the regulation of rice grain production that were not obvious from the previously reported *reg1* mutant.

The rice *hst1* mutant seedlings displayed increased heat tolerance based on its increased survival after heat treatment when compared to WT (Figure 1). Enhanced heat tolerance of the *hst1* mutant was associated with reduced water loss and wilting during the heat treatment at 42°C (Figure 5). Reduced water loss of the *hst1* mutant was further associated with reduced stomatal density and stomatal conductance of the mutant when compared with those of WT (Figure 5). These results provided strong evidence that the loss-of-function mutation of the *DST* gene in the *hst1* mutant enhanced heat tolerance in part by reducing heat-induced water loss in leaves. In support of this interpretation, the increased survival rates of the *hst1* mutant after heat treatment over those of WT was strongly influenced by air humidity (Figure 6). At 100% air humidity, in which transpirational water loss is eliminated, the survival rates of WT after heat treatment were much closer to those of the *hst1* mutant than at 65% humidity (Figure 6). These results point strongly to reduced water stress in the shoots under high temperatures as a critical mechanism for the increased heat tolerance of the *hst1* mutant.

Plant water stress is a critical factor in plant drought tolerance and, therefore, it can be argued that the heat tolerance of the *hst1* is merely a reflection of its drought tolerance. However, drought is a condition of water shortage, which was not present during the heat treatment of WT and the *hst1* mutant plants as they were grown in a large volume of growth medium (4.5 liters) that was replenished daily. Therefore, the reduced stomatal number and reduced stomatal conductance of the *hst1* mutant were likely to be primarily responsible for reduced transpirational water loss, thereby delaying wilting and improving survival under heat stress. Thus, even in the absence of drought, there could still be severe water stress in rice shoots caused by transpirational water loss under heat stress, which can cause severe damage or even death to plants. Accordingly, improving plant ability to reduce water loss under heat stress may be an effective means to improve plant heat tolerance.

The enhanced heat tolerance of the *hst1* mutant broadens the role of the DST C2H2 transcription factor in plant stress responses. Extreme temperature, drought and salinity are among the most important abiotic stresses that negatively impact plant growth, leading to loss of crop yield worldwide. Cross-tolerance to abiotic stresses is well known in plants, whereas exposure to one type of stress often leads to increased tolerance to a range of other abiotic stresses (Rizhsky et al., 2002; Perez and Brown, 2014). Despite the importance and potential in agriculture, the precise molecular mechanisms by which cross-tolerance develops are not fully understood. The demonstrated tolerance of the *dst/hst1* mutants to a broad range of abiotic stresses and shared mechanisms in coping with water stress under different abiotic stresses makes the DST transcription factor highly valuable for studying the molecular and physiological basis of plant cross-tolerance and associated signaling and transcriptional reprograming.

There was increased accumulation of H_2O_2 in the *hst1* mutant, associated with reduced expression of genes involved in ROS homeostasis including *Prx24* that encodes an important ROS-scavenging enzyme (Figure 7) (Huang et al., 2009; Cui et al., 2015). As H_2O_2 accumulation is known to regulate stomatal closure (Sierla et al., 2016), it appears that increased H_2O_2 as a result of reduced expression of ROS-scavenging genes acts as an early signaling molecule mediating heat-responsive stomatal closure that reduces water loss under high temperature. Interestingly, the rice RING finger ubiquitin E3 ligase OsHTAS, which plays a positive role in heat tolerance at the seedling stage, targets an isoform of rice ascorbate peroxidase, modulate H_2O_2 in shoots, alters the stomatal aperture and promotes ABA biosynthesis (Liu et al., 2016). A similar mode of action through modulation of H_2O_2 and ABA-mediated stomatal closure has also been proposed for the role of DST in regulation of plant responses to drought and salt (Huang et al., 2009; Cui et al., 2015). The SNAC1-targeted gene *OsSRO1c* modulates stomatal closure and oxidative stress tolerance by regulating H_2O_2 in rice (You et al., 2013; You et al., 2014). Therefore, the critical role of ROS in stress-induced and ABA-mediated stomatal closure appears to be a common theme in tolerance to a broad range of abiotic stresses in rice and possibly in other plants as well.

Even at 100% humidity, there was still a significant difference in the relative survival rates between WT and *hst1* mutant plants after heat treatment (Figure 6). Furthermore, the *hst1* mutant was more

heat-tolerant than WT not only at the seedling stages but also at the reproductive states characterized by increased grain number and seed yield when grown under heat stress conditions. Unlike at seedling stages, even WT plants displayed no wilting symptom at the reproductive stages under the heat stress condition used. Furthermore, the improved grain number and seed yield of the *hst1* mutant relative to those of WT were closely correlated with increased seed setting and pollen viability under high temperature (Figures 12 and 13), which cannot be directly attributed to altered stomatal number and behavior. These observations suggests that while leaf water stress plays a major role in increased heat tolerance of the *hst1* mutant, there are other factors that also contribute to its improved fitness and survival of *hst1* under heat stress. Indeed, heat induction of these *HSP* genes was more rapid and robust in the *hst1* mutant than in WT (Figure 8; Supplemental Figure 2A). Therefore, nuclear heat-responsive gene expression might also play a role in DST-regulated heat tolerance. Treatment with an inhibitor of ROS production reduced heat-induced expression of the *HSP* genes (Figure 10; Supplemental Figure 2B), indicating that ROS plays a critical role for effective induction of nuclear heat-responsive gene expression. Different classes of HSPs can cooperate to resolubilize protein aggregates after heat stress in plants (Ben-Zvi et al., 2004; Zwirowski et al., 2017). Small HSPs can also stabilize membranes and act as site-specific antioxidants to protect thylakoid membranes against heat stresses in photosynthetic organisms (Heckathorn et al., 2004). Therefore, DST-regulated ROS homeostasis plays an important role in plant heat responses through at least two distinct mechanisms: regulation of stomatal closure to modulate water loss and promotion of nuclear heat-responsive gene expression. Since plant responses to other types of abiotic stresses are also associated with nuclear gene reprogramming, it would be of great interest to determine whether the critical role of DST in plant tolerance to other abiotic stresses also involves ROS-mediated induction of stress-specific genes.

DST has been previously shown to regulate grain production in rice (Li et al., 2013b). This role of DST was revealed from the *reg1* mutant caused by a frameshift immediately downstream of the C2H2 zinc finger of DST (Li et al., 2013b). Our *hst1* mutant was caused by a frameshift in the C2H2 zinc finger of DST (Figure 2). As a result, the DST^{reg1} and DST^{hst1} differ only in seven amino acid residues in the C2H2 zinc finger, which is still intact in DST^{reg1} but disrupted in DST^{hst1} (Figure 2). The *reg1* mutant contained about 40% more primary and secondary branches per panicle and 63.8% more grains per main panicle than WT plants (Li et al., 2013b). Further analysis has revealed that DST directly regulates rice *Gn1a/OsCKX2* (*Grain number 1a/Cytokinin oxidase 2*) for a cytokinin oxidase in the reproductive meristem (Li et al., 2013b). It has been proposed that with its intact DNA-binding C2H2 zinc finger motif without the C-terminal transcription activation domain, the DST^{reg1} mutant protein acts as a dominant negative regulator that can perturb the direct regulation of *OsCKX2* expression by WT DST proteins in heterozygous *reg1/REG1* plants, leading to the semi-dominant nature of the *reg1* mutant (Li et al., 2013b). According to this model, we would expect that the homozygous *hst1* mutant display the levels of increase in panicle branches and grain number similar to those in the homozygous *reg1* mutant. However, we observed no increase in panicle branches and less than 20% increase in grain number per panicle in the *hst1* mutants (Figure 11), compared to about 40% increase in branch number and more than 60% increase in grain number in *reg1* (Li et al., 2013b). The difference in the phenotypes between the two mutants is unlikely to be caused by the different genetic backgrounds since DST^{reg1} can enhance grain production to similar extents in different indica and japonica rice varieties (Li et al., 2013b). We have also sequenced the promoter and coding regions of the *Gn1a/OsCKX2* gene in both WT and the *hst1* mutant and found no mutation (data not shown), thereby excluding the possibility that the relatively weak phenotype of *hst1* in grain production is due to impaired function or expression of the cytokinin catabolic gene. The difference in the phenotypes in grain production between the *reg1* and *hst1* mutants might be caused by different growth conditions. While this possibility cannot be completely ruled out, it is worthy to note that the difference of the *reg1* and *hst1* mutants in grain production was based on their difference to their respective WT plants, which had similar panicle branch and grain numbers from the two studies, suggesting similar growth conditions (Li et al., 2013b) (Figure 12). Another possibility for the substantial difference in grain production between the *reg1* and *hst1* mutants could be due to the presence of an additional negative regulator factor of rice grain production that recognizes same sequence as DST or the sequence that overlaps with the DST-binding site in the promoter of *OsCKX2* to activates its expression in reproductive meristem. The DST^{reg1} dominant negative protein would suppress the expression of *OsCKX2* by preventing binding of the *OsCKX2* promoter by WT DST and the new factor. On the other hand, due to lack of DNA-binding activity, DST^{hst1} is unable to prevent binding of the *OsCKX2* promoter by WT DST and the new factor and, therefore, would not inhibit the activation of *OsCKX2*. Thus, the mechanism for the regulation of *OsCKX2* gene expression in grain production could be more complicated than originally thought. Further research on the additional regulators of *OsCKX2* expression in reproductive meristem will help establish the signaling pathways and network of grain production in rice and other grain crops.

In summary, our study has expanded the analysis of HST1/DST as a novel negative regulator of rice tolerance to multiple abiotic stresses including drought, salt and heat stresses. Our comprehensive analysis has also revealed that the broad roles of HST1/DST in abiotic stress tolerance are mediated by both shared and stress-specific mechanisms. In particular, the water status is a critical factor not only for plant tolerance to drought, but also to heat. HST1/DST also negatively regulates rice grain production. These important properties of HST1/DST make it a potential target for genome editing to develop stress tolerant rice with improved yield (Zafar et al., 2020b).

Accession numbers

The identifiers for the rice genes described in this article are as follows: *HST1* (LOC_Os03g57240), *OsPrx24* (LOC_Os02g06630) and *OsCKX2* (LOC_Os01g10110).

Data availability statement

The original contributions presented in the study are included in the article/Supplementary Material. Further inquiries can be directed to the corresponding authors.

Author contributions

CZ, YD, ZC, and KY conceived the project. YD, MZ, and KW performed most of the work. AQ, SH, QJ, FW, and CC performed some of the work. YD, CZ and ZC analyzed the data and wrote the paper with input from the other authors. All authors contributed to the article and approved the submitted version.

Funding

This work was supported by grants from Zhejiang Provincial Natural Science Foundation of China (grant no. LZ22C130003 and LZ14C020001), and the National Natural Science Foundation of China (grant no. 31470368), the National Key Research and Development Project of China, the International Cooperation Project (2018YFE0111900).

Conflict of interest

The authors declare that the research was conducted in the absence of any commercial or financial relationships that could be construed as a potential conflict of interest.

Publisher's note

All claims expressed in this article are solely those of the authors and do not necessarily represent those of their affiliated organizations, or those of the publisher, the editors and the reviewers. Any product that may be evaluated in this article, or claim that may be made by its manufacturer, is not guaranteed or endorsed by the publisher.

Supplementary material

The Supplementary Material for this article can be found online at: https://www.frontiersin.org/articles/10.3389/fpls.2023.1068296/full#supplementary-material

References

Amm, I., Sommer, T., and Wolf, D. H. (2014). Protein quality control and elimination of protein waste: the role of the ubiquitin-proteasome system. *Biochim. Biophys. Acta* 1843, 182–196. doi: 10.1016/j.bbamcr.2013.06.031

Apel, K., and Hirt, H. (2004). Reactive oxygen species: metabolism, oxidative stress, and signal transduction. *Annu. Rev. Plant Biol.* 55, 373–399. doi: 10.1146/annurev.arplant.55.031903.141701

Arias, E., and Cuervo, A. M. (2011). Chaperone-mediated autophagy in protein quality control. *Curr. Opin. Cell Biol.* 23, 184–189. doi: 10.1016/j.ceb.2010.10.009

Arrigo, A. P. (2005). [Heat shock proteins as molecular chaperones]. *Medecine Sci. M/S* 21, 619–625. doi: 10.1051/medsci/2005216-7619

Ascenzi, R., and Gantt, J. S. (1999). Molecular genetic analysis of the drought-inducible linker histone variant in arabidopsis thaliana. *Plant Mol. Biol.* 41, 159–169. doi: 10.1023/A:1006302330879

Baniwal, S. K., Chan, K. Y., Scharf, K. D., and Nover, L. (2007). Role of heat stress transcription factor HsfA5 as specific repressor of HsfA4. *J. Biol. Chem.* 282, 3605–3613. doi: 10.1074/jbc.M609545200

Banon, S., Fernandez, J. A., Franco, J. A., Torrecillas, A., Alarcon, J. J., and Sachez-Blanco, H. J. (2004). Effects of water stress and night temperature preconditioning on water relations and morphological and anatomical changes of lotus creticus plants. *Sci. Hortic.* 101, 333–342. doi: 10.1016/j.scienta.2003.11.007

Ben-Zvi, A., De Los Rios, P., Dietler, G., and Goloubinoff, P. (2004). Active solubilization and refolding of stable protein aggregates by cooperative unfolding action of individual hsp70 chaperones. *J. Biol. Chem.* 279, 37298–37303. doi: 10.1074/jbc.M405627200

Berger, D., and Altmann, T. (2000). A subtilisin-like serine protease involved in the regulation of stomatal density and distribution in arabidopsis thaliana. *Genes Dev.* 14, 1119–1131. doi: 10.1101/gad.14.9.1119

Brandt, B., Munemasa, S., Wang, C., Nguyen, D., Yong, T., Yang, P. G., et al. (2015). Calcium specificity signaling mechanisms in abscisic acid signal transduction in arabidopsis guard cells. *Elife* 4, e03599. doi: 10.7554/eLife.03599

Craig, E. A., Gambill, B. D., and Nelson, R. J. (1993). Heat shock proteins: molecular chaperones of protein biogenesis. *Microbiological Rev.* 57, 402–414. doi: 10.1128/mr.57.2.402-414.1993

Cui, L. G., Shan, J. X., Shi, M., Gao, J. P., and Lin, H. X. (2015). DCA1 acts as a transcriptional Co-activator of DST and contributes to drought and salt tolerance in rice. *PloS Genet.* 11, e1005617. doi: 10.1371/journal.pgen.1005617

Fahad, S., Bajwa, A. A., Nazir, U., Anjum, S. A., Farooq, A., Zohaib, A., et al. (2017). Crop production under drought and heat stress: Plant responses and management options. *Front. Plant Sci.* 8, 1147. doi: 10.3389/fpls.2017.01147

Georgopoulos, C., and Welch, W. J. (1993). Role of the major heat shock proteins as molecular chaperones. *Annu. Rev. Cell Biol.* 9, 601–634. doi: 10.1146/annurev.cb.09.110193.003125

Giesguth, M., Sahm, A., Simon, S., and Dietz, K. J. (2015). Redox-dependent translocation of the heat shock transcription factor AtHSFA8 from the cytosol to the nucleus in arabidopsis thaliana. *FEBS Lett.* 589, 718–725. doi: 10.1016/j.febslet.2015.01.039

Heckathorn, S. A., Mueller, J. K., Laguidice, S., Zhu, B., Barrett, T., Blair, B., et al. (2004). Chloroplast small heat-shock proteins protect photosynthesis during heavy metal stress. *Am. J. Bot.* 91, 1312–1318. doi: 10.3732/ajb.91.9.1312

Hiei, Y., Ohta, S., Komari, T., and Kumashiro, T. (1994). Efficient transformation of rice (Oryza sativa l.) mediated by agrobacterium and sequence analysis of the boundaries of the T-DNA. *Plant J.* 6, 271–282. doi: 10.1046/j.1365-313X.1994.6020271.x

Huang, X. Y., Chao, D. Y., Gao, J. P., Zhu, M. Z., Shi, M., and Lin, H. X. (2009). A previously unknown zinc finger protein, DST, regulates drought and salt tolerance in rice *via* stomatal aperture control. *Genes Dev.* 23, 1805–1817. doi: 10.1101/gad.1812409

Izumi, M. (2019). Heat shock proteins support refolding and shredding of misfolded proteins. *Plant Physiol.* 180, 1777–1778. doi: 10.1104/pp.19.00711

Jakob, U., Gaestel, M., Engel, K., and Buchner, J. (1993). Small heat shock proteins are molecular chaperones. *J. Biol. Chem.* 268, 1517–1520. doi: 10.1016/S0021-9258(18)53882-5

Jannat, R., Uraji, M., Morofuji, M., Islam, M. M., Bloom, R. E., Nakamura, Y., et al. (2011). Roles of intracellular hydrogen peroxide accumulation in abscisic acid signaling in arabidopsis guard cells. *J. Plant Physiol.* 168, 1919–1926. doi: 10.1016/j.jplph.2011.05.006

Kotak, S., Larkindale, J., Lee, U., Von Koskull-Doring, P., Vierling, E., and Scharf, K. D. (2007). Complexity of the heat stress response in plants. *Curr. Opin. Plant Biol.* 10, 310–316. doi: 10.1016/j.pbi.2007.04.011

Lai, Z., Li, Y., Wang, F., Cheng, Y., Fan, B., Yu, J. Q., et al. (2011). Arabidopsis sigma factor binding proteins are activators of the WRKY33 transcription factor in plant defense. *Plant Cell* 23, 3824–3841. doi: 10.1105/tpc.111.090571

Latijnhouwers, M., Xu, X. M., and Moller, S. G. (2010). Arabidopsis stromal 70-kDa heat shock proteins are essential for chloroplast development. *Planta* 232, 567–578. doi: 10.1007/s00425-010-1192-z

Liu, J., Zhang, C., Wei, C., Liu, X., Wang, M., Yu, F., et al. (2016). The RING finger ubiquitin E3 ligase OsHTAS enhances heat tolerance by promoting H2O2-induced stomatal closure in rice. *Plant Physiol.* 170, 429–443. doi: 10.1104/pp.15.00879

Li, H. X., Xiao, Y., Cao, L. L., Yan, X., Li, C., Shi, H. Y., et al. (2013a). Cerebroside c increases tolerance to chilling injury and alters lipid composition in wheat roots. *PloS One* 8, e73380. doi: 10.1371/journal.pone.0073380

Li, S., Zhao, B., Yuan, D., Duan, M., Qian, Q., Tang, L., et al. (2013b). Rice zinc finger protein DST enhances grain production through controlling Gn1a/OsCKX2 expression. *Proc. Natl. Acad. Sci. U.S.A.* 110, 3167–3172. doi: 10.1073/pnas.1300359110

Macrobbie, E. A. (2000). ABA activates multiple Ca(2+) fluxes in stomatal guard cells, triggering vacuolar K(+)(Rb(+)) release. *Proc. Natl. Acad. Sci. U.S.A.* 97, 12361–12368. doi: 10.1073/pnas.220417197

Miller, G., and Mittler, R. (2006). Could heat shock transcription factors function as hydrogen peroxide sensors in plants? *Ann. Bot.* 98, 279–288. doi: 10.1093/aob/mcl107

Mittler, R., Zandalinas, S. I., Fichman, Y., and Van Breusegem, F. (2022). Reactive oxygen species signalling in plant stress responses. *Nat. Rev. Mol. Cell Biol* 23, 663–679. doi: 10.1038/s41580-022-00499-2

Morales, D., Rodriguez, P., Dell'amico, J., Nicolas, E., Torrecillas, A., and Sanchez-Blanco, M. J. (2003). High-temperature preconditioning and thermal shock imposition affects water relations, gas exchange and root hydraulic conductivity in tomato. *Biol. Plant* 47, 203–208. doi: 10.1023/B:BIOP.0000022252.70836.fc

Pei, Z. M., Murata, Y., Benning, G., Thomine, S., Klusener, B., Allen, G. J., et al. (2000). Calcium channels activated by hydrogen peroxide mediate abscisic acid signalling in guard cells. *Nature* 406, 731–734. doi: 10.1038/35021067

Perez, I. B., and Brown, P. J. (2014). The role of ROS signaling in cross-tolerance: from model to crop. *Front. Plant Sci.* 5, 754. doi: 10.3389/fpls.2014.00754

Qi, J., Song, C. P., Wang, B., Zhou, J., Kangasjarvi, J., Zhu, J. K., et al. (2018). Reactive oxygen species signaling and stomatal movement in plant responses to drought stress and pathogen attack. *J. Integr. Plant Biol.* 60, 805–826. doi: 10.1111/jipb.12654

Quan, R., Lin, H., Mendoza, I., Zhang, Y., Cao, W., Yang, Y., et al. (2007). SCABP8/CBL10, a putative calcium sensor, interacts with the protein kinase SOS2 to protect arabidopsis shoots from salt stress. *Plant Cell* 19, 1415–1431. doi: 10.1105/tpc.106.042291

Reddy, P. S., Kavi Kishor, P. B., Seiler, C., Kuhlmann, M., Eschen-Lippold, L., Lee, J., et al. (2014). Unraveling regulation of the small heat shock proteins by the heat shock factor HvHsfB2c in barley: its implications in drought stress response and seed development. *PloS One* 9, e89125. doi: 10.1371/journal.pone.0089125

Rizhsky, L., Liang, H., and Mittler, R. (2002). The combined effect of drought stress and heat shock on gene expression in tobacco. *Plant Physiol.* 130, 1143–1151. doi: 10.1104/pp.006858

Schramm, F., Larkindale, J., Kiehlmann, E., Ganguli, A., Englich, G., Vierling, E., et al. (2008). A cascade of transcription factor DREB2A and heat stress transcription factor HsfA3 regulates the heat stress response of arabidopsis. *Plant J. Cell Mol. Biol.* 53, 264–274. doi: 10.1111/j.1365-313X.2007.03334.x

Schroeder, J. I., Allen, G. J., Hugouvieux, V., Kwak, J. M., and Waner, D. (2001). Guard cell signal transduction. *Annu. Rev. Plant Physiol. Plant Mol. Biol.* 52, 627–658. doi: 10.1146/annurev.arplant.52.1.627

Sierla, M., Waszczak, C., Vahisalu, T., and Kangasjarvi, J. (2016). Reactive oxygen species in the regulation of stomatal movements. *Plant Physiol.* 171, 1569–1580. doi: 10.1104/pp.16.00328

Singh, R., Parihar, P., Singh, S., Mishra, R. K., Singh, V. P., and Prasad, S. M. (2017). Reactive oxygen species signaling and stomatal movement: Current updates and future perspectives. *Redox Biol.* 11, 213–218. doi: 10.1016/j.redox.2016.11.006

Song, X. J., and Matsuoka, M. (2009). Bar the windows: an optimized strategy to survive drought and salt adversities. *Genes Dev.* 23, 1709–1713. doi: 10.1101/gad.1834509

Tian, L., Dellapenna, D., and Zeevaart, J. (2004). Effect of hydroxylated carotenoid deficiency on ABA accumulation in arabidopsis. *Physiologia Plantarum* 122, 314–320. doi: 10.1111/j.1399-3054.2004.00409.x

Von Koskull-Doring, P., Scharf, K. D., and Nover, L. (2007). The diversity of plant heat stress transcription factors. *Trends Plant Sci.* 12, 452–457. doi: 10.1016/j.tplants.2007.08.014

Wang, Y. L., Guan, Z. Y., Chen, F. D., Fang, W. M., and Teng, N. J. (2012). Pollen viability, pistil receptivity, and embryo development in hybridization of nelumbo nucifera gaertn. *ScientificWorldJournal* 2012, 678706. doi: 10.1100/2012/678706

Xu, Q., Metzler, B., Jahangiri, M., and Mandal, K. (2012). Molecular chaperones and heat shock proteins in atherosclerosis. *Am. J. Physiol. Heart Circulatory Physiol.* 302, H506–H514. doi: 10.1152/ajpheart.00646.2011

Yan, H., Wang, C., Liu, K., and Tian, X. (2021). Detrimental effects of heat stress on grain weight and quality in rice (Oryza sativa l.) are aggravated by decreased relative humidity. *PeerJ* 9, e11218. doi: 10.7717/peerj.11218

Yoshida, S., Forno, D. A., Cook, J. H., and Gomez, K. A. (1976). "Routine procedures for growing rice plants in culture solution," in *Laboratory manual for physiological studies of rice*. Eds. S. Yoshida, D. A. Forno, J. H. Cook and K. A. Gomez. (Los Banos, Philippines: International Rice Research Institute), 61–66.

You, J., Zong, W., Du, H., Hu, H., and Xiong, L. (2014). A special member of the rice SRO family, OsSRO1c, mediates responses to multiple abiotic stresses through interaction with various transcription factors. *Plant Mol. Biol.* 84, 693–705. doi: 10.1007/s11103-013-0163-8

You, J., Zong, W., Li, X., Ning, J., Hu, H., Li, X., et al. (2013). The SNAC1-targeted gene OsSRO1c modulates stomatal closure and oxidative stress tolerance by regulating hydrogen peroxide in rice. *J. Exp. Bot.* 64, 569–583. doi: 10.1093/jxb/ers349

Zafar, S. A., Arif, M. H., Uzair, M., Rashid, U., Naeem, M. K., Rehman, O. U., et al. (2022). Agronomic and physiological indices for reproductive stage heat stress tolerance in green super rice. *Agronomy* 12, 1907. doi: 10.3390/agronomy12081907

Zafar, S. A., Hameed, A., Ashraf, M., Khan, A. S., Qamar, Z. U., Li, X., et al. (2020a). Agronomic, physiological and molecular characterisation of rice mutants revealed the key role of reactive oxygen species and catalase in high-temperature stress tolerance. *Funct. Plant Biol.* 47, 440–453. doi: 10.1071/FP19246

Zafar, S. A., Zaidi, S. S., Gaba, Y., Singla-Pareek, S. L., Dhankher, O. P., Li, X., et al. (2020b). Engineering abiotic stress tolerance *via* CRISPR/ cas-mediated genome editing. *J. Exp. Bot.* 71, 470–479. doi: 10.1093/jxb/erz476

Zhang, H., Zhu, J., Gong, Z., and Zhu, J. K. (2022). Abiotic stress responses in plants. *Nat. Rev. Genet.* 23, 104–119. doi: 10.1038/s41576-021-00413-0

Zhu, J. K. (2002). Salt and drought stress signal transduction in plants. *Annu. Rev. Plant Biol.* 53, 247–273. doi: 10.1146/annurev.arplant.53.091401.143329

Zhu, J. K. (2016). Abiotic stress signaling and responses in plants. *Cell* 167, 313–324. doi: 10.1016/j.cell.2016.08.029

Zou, J., Liu, A., Chen, X., Zhou, X., Gao, G., Wang, W., et al. (2009). Expression analysis of nine rice heat shock protein genes under abiotic stresses and ABA treatment. *J. Plant Physiol.* 166, 851–861. doi: 10.1016/j.jplph.2008.11.007

Zwirowski, S., Klosowska, A., Obuchowski, I., Nillegoda, N. B., Pirog, A., Zietkiewicz, S., et al. (2017). Hsp70 displaces small heat shock proteins from aggregates to initiate protein refolding. *EMBO J.* 36, 783–796. doi: 10.15252/embj.201593378

frontiers | Frontiers in Plant Science

TYPE Original Research
PUBLISHED 02 February 2023
DOI 10.3389/fpls.2023.1106857

Check for updates

OPEN ACCESS

EDITED BY
Mehdi Rahimi,
Graduate University of Advanced Technology, Iran

REVIEWED BY
Faez Iqbal Khan,
Xi'an Jiaotong-Liverpool University, China
Klára Kosová,
Crop Research Institute (CRI), Czechia
Deepu Pandita,
Government department of School Education, India

*CORRESPONDENCE
Kahkashan Perveen
kperveen@ksu.edu.sa
Sandip Debnath
sandip.debnath@visva-bharati.ac.in

†These authors have contributed equally to this work

SPECIALTY SECTION
This article was submitted to Plant Abiotic Stress, a section of the journal Frontiers in Plant Science

RECEIVED 24 November 2022
ACCEPTED 10 January 2023
PUBLISHED 02 February 2023

CITATION
Perveen K, Alfagham AT, Debnath S, Bukhari NA, Wei D-Q, Alshaikh NA and Alwadai AS (2023) Enriching drought resistance in *Solanum lycopersicum* using Abscisic acid as drought enhancer derived from *Lygodium japonicum*: A new-fangled computational approach.
Front. Plant Sci. 14:1106857.
doi: 10.3389/fpls.2023.1106857

COPYRIGHT
© 2023 Perveen, Alfagham, Debnath, Bukhari, Wei, Alshaikh and Alwadai. This is an open-access article distributed under the terms of the Creative Commons Attribution License (CC BY). The use, distribution or reproduction in other forums is permitted, provided the original author(s) and the copyright owner(s) are credited and that the original publication in this journal is cited, in accordance with accepted academic practice. No use, distribution or reproduction is permitted which does not comply with these terms.

Enriching drought resistance in *Solanum lycopersicum* using Abscisic acid as drought enhancer derived from *Lygodium japonicum*: A new-fangled computational approach

Kahkashan Perveen [1*†], Alanoud T. Alfagham [1†], Sandip Debnath [2*†], Najat A. Bukhari [1], Dong-Qing Wei [3], Najla A. Alshaikh [1] and Aisha Saleh Alwadai [1]

[1]Department of Botany & Microbiology, College of Science, King Saud University, Riyadh, Saudi Arabia, [2]Department of Genetics and Plant Breeding, Institute of Agriculture, Visva-Bharati University, Sriniketan, West Bengal, India, [3]Tianjin Institute of Bioinformatics and Drug Discovery (TIBDD), Tianjin Normal University, Tianjin, China

Introduction: Drought is the largest abiotic factor impacting agriculture. Plants are challenged by both natural and artificial stressors because they are immobile. To produce drought-resistant plants, we need to know how plants react to drought. A largescale proteome study of leaf and root tissue found drought-responsive proteins. Tomato as a vegetable is grown worldwide. Agricultural biotechnology focuses on creating drought-resistant cultivars. This is important because tomato drought is so widespread. Breeders have worked to improve tomato quality, production, and stress resistance. Conventional breeding approaches have only increased drought tolerance because of drought's complexity. Many studies have examined how tomatoes handle drought. With genomics, transcriptomics, proteomics, metabolomics, and modern sequencing technologies, it's easier to find drought-responsive genes.

Method: Biotechnology and in silico studies has helped demonstrate the function of drought-sensitive genes and generate drought-resistant plant types. The latest tomato genome editing technology is another. WRKY genes are plant transcription factors. They help plants grow and respond to both natural and artificial stimuli. To make plants that can handle stress, we need to know how WRKY-proteins, which are transcription factors, work with other proteins and ligands in plant cells by molecular docking and modeling study.

Result: Abscisic acid, a plant hormone generated in stressed roots, was used here to make plants drought-resistant. Abscisic acid binds WRKY with binding affinity -7.4kcal/mol and inhibitory concentration (Ki) 0.12 microM.

Discussion: This study aims to modulate the transcription factor so plants can handle drought and stress better. Therefore, polyphenols found to make Solanum lycopersicum more drought-tolerant.

KEYWORDS

phytochemicals, drought, MD simulation, molecular docking, drought tolerant, *Solanum lycopersicum*, Abscisic acid

10.3389/fpls.2023.1106857

Introduction

Crop production is confronted with a tremendous encounter in the shape of stress, salt and drought, two climate change effects that are particularly harmful to sustainable agriculture. The atmosphere, anticipated to grow substantially less favorable due to ongoing greenhouse gas emissions, would likely limit agricultural production. Evapo-transpiration, dryness, and soil salinity will increase as a result, as will the likelihood of pest and disease infestation. These poor conditions harm plant growth, plant survival, and harvest quality. It is commonly known that potatoes are a crop that suffers tremendously from drought. The fundamental reason is that tomatoes have weaker roots than other plants. When a plant does not get enough water, it experiences stress, which can lead to the death of leaf tissue. This death often occurs in bands that extend outward from the leaf's borders. Some individuals may get this confused with late blight. When plants are undergoing rapid development or experiencing other conditions that cause them to lose a greater quantity of water through transpiration, plants are particularly susceptible to the adverse effects of this stress. In these conditions, it may be challenging to formulate a plan that takes advantage of periods when the soil is moderately dry and moist enough. The rate at which water is lost through transpiration is slowed when the environment has a high humidity level. When huge plants are kept in confined containers, it is not straightforward to maintain an adequate soil moisture level. A physiological injury, as opposed to late blight, can be diagnosed by the absence of light green, wilted border tissue around leaf symptoms, the absence of pathogen development, and the absence of stem lesions. Extremely low or high temperatures, protracted droughts or floods, excessive salt in the soil, and other abiotic factors are some of the environmental causes that frequently result in low yields (Taheri et al., 2022). A common vegetable that might suffer from unfavorable conditions is the tomato, scientifically known as *Solanum lycopersicum* (Perez-Alfocea et al., 1996). Because they are nearer non-living factors than tomatoes cultivated in greenhouses, tomatoes grown in open fields are more prone to sustain damage from them, how drought and extreme heat affect crop production, the length of the growing season, and the area that may be used for crop cultivation. A plant's roots lose a lot of their capacity to transmit water when exposed to freezing temperatures. This thickens the water while also making the crucial membrane in the roots less conductive (Venema et al., 2005). As a result, plants absorb less water, which may cause water stress in the shoots. Thus, tomato leaves begin towards wane, and photosynthesis besides water loss are slackened (Ishiguro and Nakamura, 1994).

The WRKY transcription factor family comprehends 5936 members found in various plant systems (PlantTFDB 3.0). WRKY is the DNA-binding protein SPF1 from sweet potato, which may assist control of gene expression, as described for the first time (Ishiguro and Nakamura, 1994). The word "WRKY" denotes to their WRKY domain, which instigates with a relatively constant sequence of WRKYGQK at the N-terminus and ends with a Cx4-5Cx22-23HxH or Cx7Cx23HxC zinc-finger motif (Rushton et al., 1996; Zou et al., 2004). Much study has been conducted on the WRKY domain, mainly how it controls genes and communicates with other molecules within plant cells. WRKY transcription factors were initially assumed to be a part of a plant´s defense against pathogens (Zou et al., 2004; Rushton et al., 2010). However, the subsequent study has revealed that they are related to abiotic stresses (Rushton et al., 2010), seed dormancy and germination (Qiu and Yu, 2009; Akbudak and Filiz, 2020), and seed development (Alexandrova and Conger, 2002; Guo et al., 2004). Most WRKY proteins (Chen and Chen, 2000; Cormack et al., 2002; Zou et al., 2004) can be identified by their capacity to recognize TTGACC/T W-box sequences in the promoter region, although this does not imply that they all perform the same function. So, controlling the specificity of WRKY transcription factors requires more than just identifying the essential W box promoter components. This could be because of interactions with proteins involved in signal transduction, transcription, and chromatin remodeling. Earlier reports demonstrated the role of WRKY transcription factors as negative regulators of abiotic stresses through the constitutive countenance of the BcWRKY46 gene in transgenic tobacco under the CaMV35S promoter, which made the transgenic tobacco more susceptible to cold, abscisic acid (ABA), salt, and dehydration stresses (Xu et al., 2006). There is evidence that WRKY proteins can talk to calmodulin, a signaling molecule that binds Ca^{2+}. Recent proteomics research showed that WRKY and 14-3-3 proteins work together (Xu et al., 2006) (illustrated in Figure 1A).

The majority of ABA synthesis (illustrated in Figure 1B) takes place in the vascular tissues, and then it is delivered to the target tissues. Because this transport happens in both the xylem and the phloem, it makes it possible for substances to move between the roots and the shoots in either way. The abbreviation ABA was given that name because people used to believe that ABA was a part of the abscission process. Scientists have since discovered that this is only true for a small number of plant species. ABA is also critical to a plant's defense against environmental stress and disease. It accomplishes this by assisting in the transmission of signals. The order of the steps in the ABA production pathway and the plant genes that produce it have been determined. Some plant-harming fungi can also produce ABA *via* a different biosynthetic pathway than plants (Siewers et al., 2004; Wang et al., 2016). This stops the plant's growth and instructs the leaf precursors to produce scales to defend the buds while they snooze during the winter. ABA also impedes cell division in the vascular cambium. This permits the plant to reply to cold winter temperatures by halting mutually primary and secondary development (Wang et al., 2016). ABA can also be twisted in plant roots when there is less water in the soil (like when the soil is dry) or when the plant is stressed in some other way. Following that, ABA travels to the leaves, where it rapidly modifies the osmotic potential of stomatal guard cells, shrinking them and sealing the stomata. When there is insufficient water, the ABA causes the stomata to close.

This reduces transpiration and prevents the leaves from losing additional water. Water leaves the plant *via* the stomata during the transpiration process. A robust linear association was discovered between the amount of ABA detected in the leaves and how well the stomata let air in and out based on leaf area (stomatal resistance) (Steuer et al., 1988). The fern species Lygodium japonicum is known by the common names like vine fern (Bradley, 2022) and Japanese climbing fern. It is indigenous to eastern Asia, including Taiwan, Japan, Korea, southeast Asia, and India, as well as eastern Australia. The fern is an invasive species in the southeastern United States and Puerto Rico (Munger, 2005). This plant is harvested for its abscisic acid content (Ohishi et al., 2021). ABA is a hormone that has been

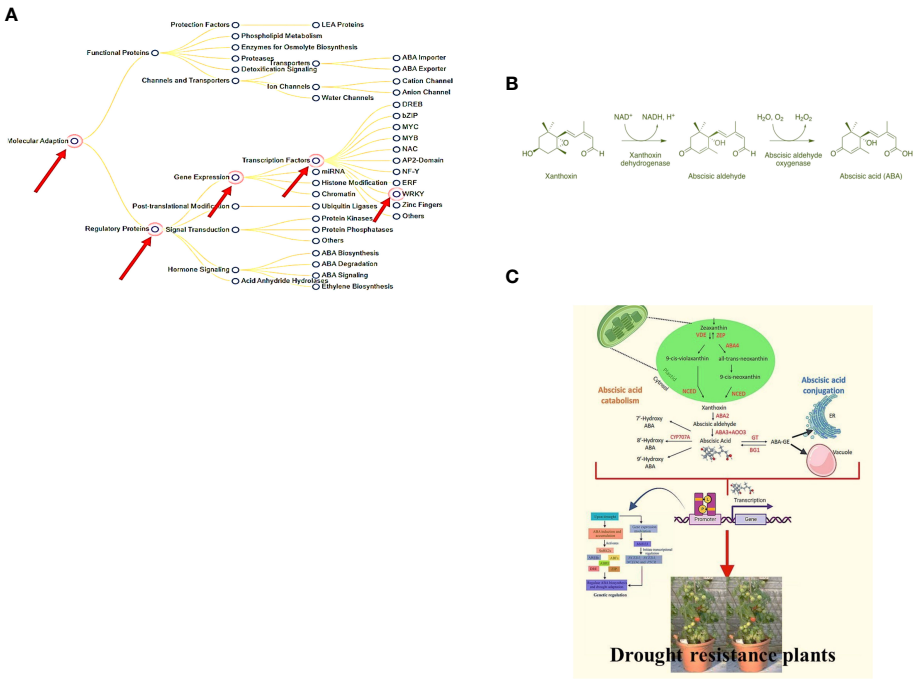

FIGURE 1
(A) Enhanced tolerance to drought & biotic stress and genes responsible (*Available from:* https://pgsb.helmholtz-muenchen.de/droughtdb/drought_db.html). **(B)** Abscisic acid bio-synthesis. **(C)** Role of Abscisic acid in enhancing drought resistance and improved fruits production (Created with Adobe Illustrator).

around for a long time. It dates back to the first living things, probably the ancestors of modern (ABA-producing) cyanobacteria, long before the plant and animal kingdoms were split. It has always worked as a signal that controls how cells respond to environmental changes. Nanomolar ABA controls how the metabolism of mammals responds to the availability of glucose by increasing energy expenditure in brown and white adipose tissue and turning on glucose uptake in skeletal muscle and adipose tissue in a way that doesn't require insulin. In contrast to insulin's activation of AMPK-inhibiting Akt, ABA's activation of AMP-dependent kinase (AMPK) causes white adipocytes to turn brown and increases muscle glucose uptake through GLUT4. People at risk for prediabetes and metabolic syndrome can improve their blood glucose, lipids, and morphometric parameters (waist circumference and body mass index) with a chronic dose of this amount of ABA. When people with standard or borderline glucose tolerance take in micrograms of ABA per kg of body weight, their glucose tolerance improves (Magnone et al., 2020) (–).-abscisic acid is the unnaturally occurring (1'R)- (-) enantiomer of abscisic acid, it functions as a hormone for plants. This substance is an enantiomer of (+)-abscisic acid (Ohishi et al., 2021). We found Abscisic acid as a product from plant self-hormone which shows a promising result in drought and plant stress tolerance.

Molecular docking is the most commonly applied technique in structure-based ligand design since it allows one to consider the action of small molecules in selected protein targets and predict the structure of the ligand-receptor complex (Meng et al., 2011; Ferreira et al., 2015). This study aimed to find a new compound (Abscisic acid) in the PubChem database that worked well against transcription factor in WRKY gene in enhancing drought resistance. Virtual screening and a structure-based docking approach were used to find the best compound for effective target inhibition. With the help of molecular dynamics simulation studies, this study also looked at the structural stability of the target compound and the best compound. The overall plan is to find a new compound that is a robust drought tolerance enhancer in *Solanum lycopersicum* to be used as a potential candidate against drought resistance (as illustrated in Figure 1C).

Resources and methods

Potential target preparation

Accessible from the RCSB protein data bank (PDB) (https://www.rcsb.org/2AYD) are 3D structures of the β-Secretase protein for study. The structure stayedexported using a freely accessible molecular editor (Discovery studio visualizer 4.0). Co-crystal ligands and heteroatoms were deleted before the structure was saved in.pdb format. The Chimera UCSF team employed a thousand-step steepest-descent and a thousand-step Conjugate gradient of energy minimization approach for this optimization. Abscisic acid (**ChemI. D: 643732**) was downloaded as a.sdf file from PubChem. National Center for Biotechnology Information, (2023). These.pdb files result from a ligand structure loaded into the Discovery Studio visualizer.

Virtual screening of selected compounds

The active site of an enzyme is a region of an enzyme that possesses an explicit profile that makes it possible for it to connect with a certain molecular substrate (Jorgensen et al., 1996; Mukerjee

et al., 2022). This binding then results in a chemical reaction that is caused by the enzyme. An enzyme's active site is a section of an enzyme that possesses a particular shape that enables the enzyme to bind with a particular molecular substrate. An active site can be described as a portion of an enzyme that contains this shape. AS ensures that the catalytic microenvironments are ideal and acceptable, and it helps chemical compounds develop adequate contact sites so that they can generate strong binding with the enzymes of choice. This allows the chemical compounds to catalyze reactions more effectively. Therefore, in order to establish a high binding affinity with our chemical, the active side of the protein was evaluated using BIOVIA Discovery Studio Visualizer v19.1.0.18287. This was done so that we could achieve our goal. In order to get a high degree of binding affinity, this step was taken. Utilizing the AutoDockvina, virtual screening tool allowed for the determination of the protein's binding site, which was then employed in the process of constructing the receptor grid. The virtual high throughput screening of 10 different compounds was carried out with the help of AutoDock vina 4.2.6. The compounds were chosen based on the best binding energy scores they achieved with the macromolecule with PDB ID: 2AYD. The best docked posture with the highest binding energies was chosen for re-docking and additional research out of the nine possible poses for each ligand, which were ranked from top to lowest according to the binding energies they produced.

Molecular docking studies

In the AutoDock MGL tool 1.5.6, the receptor protein to be utilized for docking was produced. To construct the receptor grid, residues around 2Å the 2AYD were linked to the co-crystal of Abscisic acid were utilized. Receptors and ligands were saved in.pdbqt format for future use with the MGL application, and vina was launched using the command line from a command prompt. The exhaustiveness was set to 8 and the default grid point spacing was 0.431 Å. The.pdbqt output files were processed using PyMol and the Discovery studio visualizer 2021. The co-crystallized ligand was used to validate and optimize the ligand binding.The molecular mechanism of the target protein (PDB ID: 2AYD) that is involved in the binding of Abscisic acid. The purpose of this work is to identify the most effective molecule, as determined by virtual screening, for interacting with 2AYD and to determine the inhibitory concentration of each candidate molecule. The structure of 2AYD was simplified by employing the steepest descent method (1000 steps), which was then followed by the incorporation of the AMBER ff4 force field. This was done before the docking research with the necessary ligands could begin. Before beginning the investigations into the interaction, the protonation states of the 2AYD that would be involved were checked for neutralization. Experiments on molecular docking were carried out with the help of AutoDock version 4.2.6 (Steuer et al., 1988; Bowers et al., 2006). Polar hydrogen bonds, Kollman and Gastieger charges, and other electrostatic forces were combined to produce not just the receptor but also the ligands. After merging the nonpolar hydrogens, the receptor and ligand molecules were finally saved in the.pdbqt format. With the values X=12, Y=20, and Z=30, with a spacing of 0.33 angstrom, a grid box was produced. Lamarckian Genetic Algorithm was used to dock protein-ligand complexes to get the lowest binding free energy (ΔG).

Molecular dynamic Simulations

Schrodinger, LLC's Desmond 2020.1 was utilized to conduct 100 ns MD simulations of the main protein, 2AYD, along with the ligand Abscisic acid. The explicit solvent model with SPC water molecules and the OPLS-2005 force field were utilized in this particular system (Martyna et al., 1992; Martyna et al., 1994; Shivakumar et al., 2010). To eliminate the charge, multiple Na+ ions were administered. In order to simulate the physiological environment, 0.15M NaCl solutions were added to the system. In each simulation, the NPT ensemble was generated by applying the Nose-Hoover chain coupling method (Goodsell et al., 1996; Ghosh et al., 2022). The simulations were conducted with the following parameters: a temperature of 300 K, a relaxation period of 1.0 ps, a pressure of 1 bar, and a subsequent time step of 2 ps. The Martyna–Tuckerman–Klein chain coupling system (Toukmaji and Board, 1996) barostat method was used, and the relaxation time was set to 2 picoseconds. This method was used to regulate the pressure. To predict long-range electrostatic interactions, the Colombian interaction radius was set to 9 and the particle mesh Ewald technique (Bowers et al., 2006) was employed. Utilizing the RESPA integrator, the unbonded forces were determined. The root mean square deviation was utilized to assess the ability of MD simulations to maintain stability.

Results

Virtual screening of compounds

Binding empathy of the complex, 2AYD-643732 posses-7.4kcal/mol score. The most promising molecule underwent additional reassembly in the binding cavity of 2AYD. A total of 10 ligands were investigated as potential binding partners for the 2AYD receptor protein shown in Table 1. This virtual screening based on binding energy gave us a vivid idea of best ligand having highest affinity with the targeted protein.

Molecular docking investigation

Molecular docking is a method that can be employed to ascertain the intermolecular framework that is optimally shaped by a macromolecule in conjunction with medication or added small molecular contender. At the outset, molecular docking research was conducted to screen for and locate the intermolecular interaction that would be most beneficial between the protein of interest and the phytochemical substances. PyRx instruments: To carry out molecular docking between 10 phytochemical compounds with a three-dimensional structure and desire protein, the AutoDock vina wizard has been used. Table 1 shows the binding affinities of 10 different phytochemicals. Molecular interaction in re-docking studies of ligand Abscisic acid with 2AYD displayed well defined binding

10.3389/fpls.2023.1106857

TABLE 1 Molecular Docking of 10 selected phyto-compounds.

Sl No.	Compound ID (CID)	Binding energy (Kcal/mol)
1.	CID_100332	-5.6
2.	CID_101389368	-5.5
3.	CID_119034	-6.4
4.	CID_15559069	-7.1
5.	CID_241572	-7.0
6.	**CID_643732**	**-7.4**
7.	CID_3981577	-6.9
8.	CID_5280343	-5.3
9.	CID_5280443	-7.0
10.	CID_5280445	-6.2

Ligand bound to the core of the pocket with lowest binding energy is indicated in bold.

pocket constituted of residues leucine, valine, proline, alanine, asparagine, serine, cystine, leucine, glycine where the ligand bound to the core of the pocket with binding energy (ΔG)-7.4kcal/mol and inhibitory concentration (Ki) 0.12microM.

Molecular dynamic simulation study

The ligand Abscisic acid (Chem ID:643732) and the 2AYD protein were subjected to MD simulation studies for one hundred nanoseconds to examine the overall quality and stability of the complex till convergence. The root means square deviation (RMSD) of the C-α, the backbone of 2AYD (depicted in Figure 2) with ligand coupled complex, revealed an extremely stable structure, with a fluctuation of only 1.99Å. On the other hand, the RMSD of the ligand Abscisic acid was slightly distorted in the beginning up. However, it remained stable until 100 ns without any significant variations (depicted in Figure 3. i). On the other hand, the root means square fluctuations (RMSF) of the different amino acids that make up the C-α backbone of 2AYD showed the most negligible fluctuations, which indicates that the protein structure is stable. The relative mean squared deviation of Abscisic acid-bound protein simulation trajectories across a timescale of 100 ns. Every piece of data is measured three times to ensure accuracy, and the Y-axis is shifted after each iteration. After a total of 100 ns, the final structure of 2AYD had significant deviations from the reference structure, with an average difference of 2 between it and residue positions 230-250. (depicted in Figure 3. ii). Figure 3. iii provides a visual representation of the typical number of hydrogen bonds established between Abscisic acid and the various proteins throughout the 100 ns simulation. The MD simulation of Abscisic acid and 2AYD revealed a significant number of hydrogen bonds. Throughout the simulation, a total of two hydrogen bonds were established. The increased number of hydrogen bonds between protein 2AYD and Abscisic acid has helped to strengthen the binding and enhancing the drought resistance, which has contributed to the simulation's success in maintaining its stability. In addition, the radius of gyration, also known as Rg, was calculated. Rg is an indicator of the size and compactness of the protein when it is in a state where it is attached to the ligand. Figure 3.iv depicts the Rg plots for the convenience. According to the Rg plot of the C-α backbone, the 2AYD protein displays Rg values ranging from 27.8 to 28.0 angstroms, suggesting significant compactness with an average of 0.3 angstroms from the start to the finish of the 100 ns simulation.

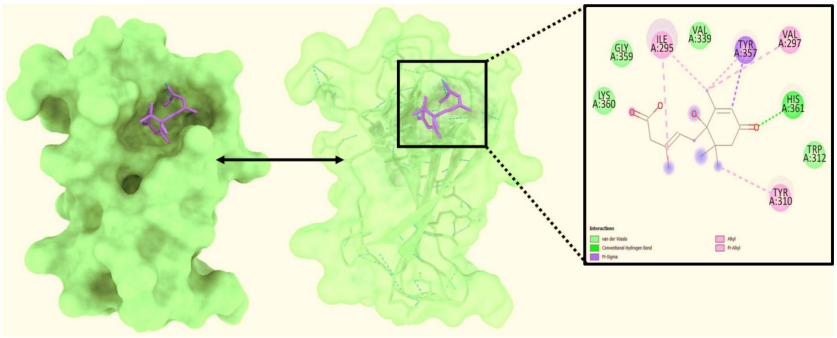

FIGURE 2
Analysis of the docked posture of 2AYD-643732; were displayed the ligand bound at the pocket of the receptor 2AYD and the binding pocket residues interacted with the ligand displayed.

10.3389/fpls.2023.1106857

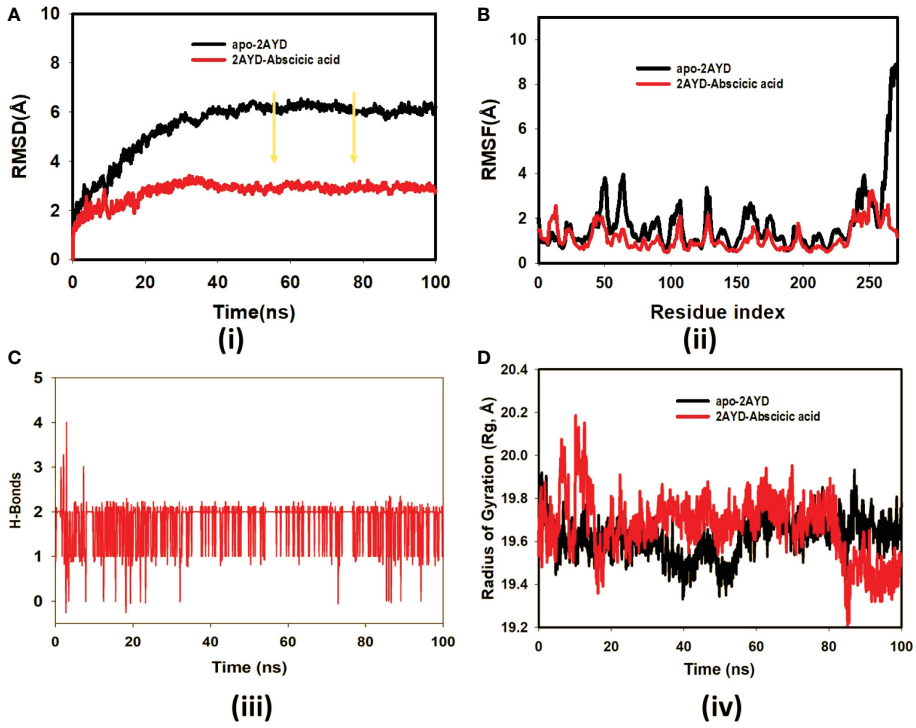

FIGURE 3
(A) RMSD of 2AYD and ligand Abscisic acid for 100 ns; **(B)** RMSF of 2AYD and ligand Abscisic acid for 100 ns; **(C)** Number of Hydrogen bindings of 2AYD and ligand Abscisic acid for 100 ns; **(D)** Radius of gyration of 2AYD and ligand Abscisic acid for 100 ns.

Ligand interaction of Abscisic acid with predicteddocked residues of 2AYDdemonstratedtheestablishment of substantial hydrogen bonds and apart from this, other non-bonded interactions such as hydrophobic interaction as well as water bridges (illustrated in Figure 4). These interactions interplayed critical role in making a stable complex between the protein and the ligand.

The illustration in Figure 5A highlights ligand characteristic such as RMSD, radius of gyration (rGyr), intra-molecular hydrogen bond, molecular surface area (MolSA), solvent accessible surface area (SASA), and polar surface area (PSA). In the ligand, no intra-molecular hydrogen was found. In Figure 5B, ligand torsion map shows the structural evolution of each rotatable bond (RB) over time (0.00 through 100.00 ns). Top: Two-dimensional graphic illustrating rotatable ligand linkages.

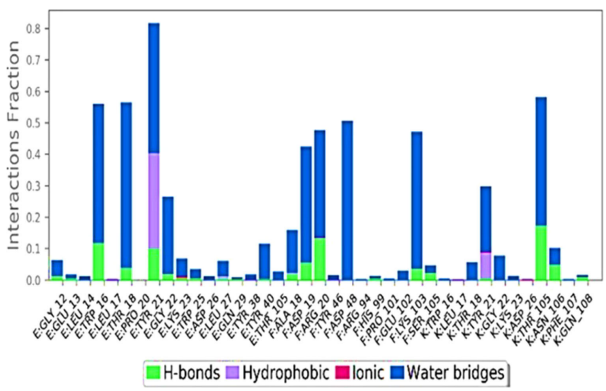

FIGURE 4
Types of bond formed in 100ns simulation run.

Dial plots and bar plots, both the same color, indicate rotatable bonds. As the simulation progresses, dial (or radial) charts depict the torsion's conformation. The simulation is traced in a circle from the display's center. Dial plots and bar charts depict the torsion's probability distribution. Infographic shows rotatable bond strength (if torsional potential information is given). Check the chart's left Y-axis for available values. When conducting this type of research, it's crucial to monitor the histogram, torsion potential, and protein's conformation strain to evaluate if the bound shape is maintained.

Discussion

Drought severity is the abiotic factor with the most significant impact on agricultural output. Because plants do not migrate from their fixed positions, they are vulnerable to natural and artificial pressures. More understanding of how plants react to drought is needed to devise breeding procedures that will make plants more drought-resistant. A thorough analysis of the proteome of leaf and root tissue revealed the presence of proteins that respond to drought in several unique ways depending on the genotype of the plant. WRKY genes are members of one of the most diverse plants transcription factor families, and they play an essential part in how plants respond to both natural and unnatural stimuli and how they grow and develop as a whole.

Furthermore, WRKY genes influence how plants respond to natural and manmade stimuli. Understanding how WRKY proteins interact with other proteins and ligands in plant cells is critical to creating plants that can withstand biotic and abiotic stressors. The utilization of abscisic acid, a hormone produced in plant roots when

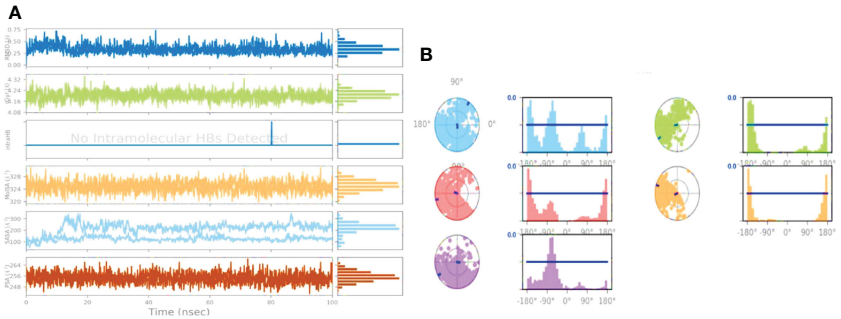

FIGURE 5
(A) The figure displayed shows ligand characteristics such as RMSD, RoG, Hydrogen bonding, MolSA, SASA, and polar surface area (PSA) of Abscisic acid; **(B)** Ligand torsion profile after 100 ns simulation.

stressed, is the focus of this research endeavour, which aims to make plants more drought-resistant and stress resistant by modulating the transcription factor (as illustrated in Figure 6).

Conclusion

Through molecular dynamics simulation, we investigated the expected structure's peculiar responses when placed in an aqueous environment. In addition, the structure can be used to evaluate the complexity of any ligand or molecule designed to interact with the WRKY transcription protein possessing a binding affinity of -7.4 kcal/mol. Abscisic acid has a high affinity for the WRKY protein. These polyphenols are a powerful component that, according to a study that used molecular docking and modeling, makes *Solanum lycopersicum* more drought tolerant. The binding energies of the ligand-target interaction are vital for characterizing the affinity with which the drug binds to the drought transcription factor-associated target. Finally, we are able to identify Abscisic acid as a potential phytoagent which can enhance drought tolerance in tomato plants.

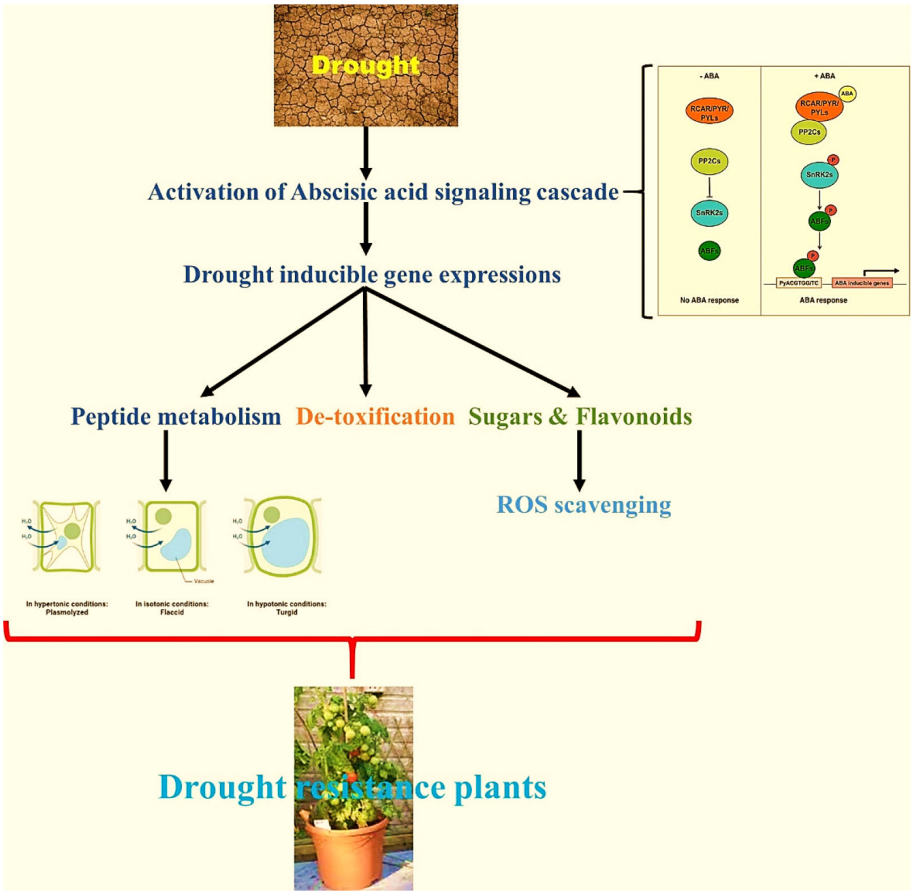

FIGURE 6
Research outcome in using Abscisic acid as drought resistance enhancer factor.

Data availability statement

The original contributions presented in the study are included in the article/supplementary material. Further inquiries can be directed to the corresponding authors.

Author contributions

KP, AA and SD: Conceptualization, designing experiment, Investigation, Data analysis, Supervision, Manuscript writing and editing. NB: Designing experiment, Data collection and analysis, Manuscript writing and editing. D-QW, NA and AA: Manuscript writing and revision editing. All authors contributed to the article and approved the submitted version.

Acknowledgments

The authors extend their appreciation to the Deputyship for Research & Innovation, Ministry of Education in Saudi Arabia for funding this research work through the project no. (IFKSURG-2-1592).

Conflict of interest

The authors declare that the research was conducted in the absence of any commercial or financial relationships that could be construed as a potential conflict of interest.

Publisher's note

All claims expressed in this article are solely those of the authors and do not necessarily represent those of their affiliated organizations, or those of the publisher, the editors and the reviewers. Any product that may be evaluated in this article, or claim that may be made by its manufacturer, is not guaranteed or endorsed by the publisher.

References

Akbudak, M. A., and Filiz, E. (2020). Genome-wide investigation of proline transporter (ProT) gene family in tomato: bioinformatics and expression analyses in response to drought stress. *Plant Physiol. Biochem.* 157, 13–22. doi: 10.1016/j.plaphy.2020.10.004

Alexandrova, K. S., and Conger, B. V. (2002). Isolation of two somatic embryogenesis-related genes from orchard grass (Dactylisglomerata). *Plant Sci.* 162, 301–307. doi: 10.1016/S0168-9452(01)00571-4

Bowers, K. J., Chow, D. E., Xu, H., Dror, R. O., Eastwood, M. P., Gregersen, B. A., et al. (2006). "Scalable algorithms for molecular dynamics simulations on commodity clusters," in *SC'06: Proceedings of the 2006 ACM/IEEE Conference on Supercomputing*, Tampa, FL, USA, (New York, NY: Association for Computing Machinery), 84–es. doi: 10.1145/1188455.1188544

Bradley, K. A. (2022). 'Lygodium japonicum (Japanese climbing fern)', CABI Compendium. *CABI Int.* doi: 10.1079/cabicompendium.31783

Chen, C., and Chen, Z. (2000). Isolation and characterization of two pathogen- and salicylic acid-induced genes encoding WRKY DNA-binding proteins from tobacco. *Plant Mol. Biol.* 42, 387–396. doi: 10.1023/A:1006399311615

Cormack, R. S., Eulgem, T., Rushton, P. J., Köchner, P., Hahlbrock, K., and Somssich, I. E. (2002). Leucine zipper containing WRKY proteins widen the spectrum of immediate early elicitor-induced WRKY transcription factors in parsley. *Biochim. Biophys. Acta (BBA)-Gene Structure and Expression* 1576 (1-2), 92–100. doi: 10.1016/S0167-4781(02)00298-1

Ferreira, L. G., dos Santos, R. N., Oliva, G., and Andricopulo, A. (2015). Molecular docking and structure-based drug design strategies. *Molecules* 20, 13384–13421. doi: 10.3390/molecules200713384

Ghosh, A., Chakraborty, D., Mukerjee, N., Baishya, D., Chigurupati, S., Felemban, S. G., et al. (2022). Target-based virtual screening and molecular interaction studies for lead identification of natural olive compounds against glioblastomamultiforme. *Environ. Sci. pollut. Res. Int.* doi: 10.1007/s11356-022-22401-5

Goodsell, D. S., Morris, G. M., and Olson, A. J. (1996). Automated docking of flexible ligands: applications of AutoDock. *J. Mol. Recognit* 9 (1), 1–5. doi: 10.1002/(SICI)1099-1352(199601)9:1<1::AID-JMR241>3.0.CO;2-6

Guo, Y., Cai, Z., and Gan, S. (2004). Transcriptome of arabidopsis leaf senescence. *Plant Cell Environ.* 27, 521–549. doi: 10.1016/S0083-6729(05)72007-0

Ishiguro, S., and Nakamura, K. (1994). Characterization of a cDNA encoding a novel DNA-binding protein, SPF1, that recognizes SP8 sequences in the 5' upstream regions of genes coding for sporamin and beta-amylase from sweet potato. *Mol. Gen. Genet.* 244, 563–571. doi: 10.1007/BF00282746

Jorgensen, W. L., Maxwell, D. S., and Tirado-Rives, J. (1996). Development and testing of the OPLS all-atom force field on conformational energetics and properties of organic liquids. *J. Am. Chem. Soc.* 118 (45), 11225–11236. doi: 10.1021/ja9621760

Magnone, M., Sturla, L., Guida, L., Spinelli, S., Begani, G., Bruzzone, S., et al. (2020). Abscisic acid: A conserved hormone in plants and humans and a promising aid to combat prediabetes and the metabolic syndrome. *Nutrients* 12 (6), 1724. doi: 10.3390/nu12061724

Martyna, G. J., Klein, M. L., and Tuckerman., M. (1992). Nose-hoover chains-the canonical ensemble *via* continuous dynamics. *J. Chem. Phys.* 97, 2635–2643. doi: 10.1063/1.463940

Martyna, G. J., Tobias, D. J., and Klein, M. L. (1994). Constant pressure molecular dynamics algorithms. *J. Chem. Phys.* 101, 4177–4189. doi: 10.1063/1.467468

Meng, X.-Y., Zhang, H.-X., Mezei, M., and Cui, M. (2011). Molecular docking: A powerful approach for structure-based drug discovery. *Curr. Comput. Aided Drug Des.* 7 (2), 146–157. doi: 10.2174/157340911795677602

Mukerjee, N., Das, A., Maitra, S., Ghosh, A., Khan, P., Alexiou, A., et al. (2022). Dynamics of natural product lupenone as a potential fusion inhibitor against the spike complex of novel semliki forest virus. *PloS One* 17 (2), e0263853. doi: 10.1371/journal.pone.0263853

Munger, G. T. (2005). "Lygodium," in *Fire effects information system* (U.S. Department of Agriculture, Forest Service, Rocky Mountain Research Station, Fire Sciences Laboratory). Available at : https://www.fs.usda.gov /database/feis/plants/fern/lygspp/all.html.

National Center for Biotechnology Information. (2023). PubChem Compound Summary for CID 643732, (-)-Abscisic acid. Retrieved January 14, 2023 from https://pubchem.ncbi.nlm.nih.gov/compound/Abscisic-acid.

Ohishi, N., Hoshika, N., Takeda, M., Shibata, K., Yamane, H., Yokota, T., et al. (2021). Involvement of auxin biosynthesis and transport in the antheridium and prothalli formation in *Lygodiumjaponicum*. *Plants (Basel)* 10 (12), 2709. doi: 10.3390/plants10122709

Perez-Alfocea, F., Balibrea, M. E., Santa-Curz, A., and Estan, M. T. (1996). Agronomical and physiological characterization of salinity tolerance in a commercial tomato hybrid. *Plant Soil* 180, 251–257. doi: 10.1007/BF00015308

Qiu, Y. P., and Yu, D. Q. (2009). Over-expression of the stress-induced OsWRKY45 enhances disease resistance and drought tolerance in arabidopsis. *Environ. Exp. Bot.* 65, 35–47. doi: 10.1016/j.envexpbot.2008.07.002

Rushton, P. J., Somssich, I. E., Ringler, P., and Shen, Q. J. (2010). WRKY transcription factors. *Trends Plant Sci.* 15, 247–258. doi: 10.1016/j.tplants.2010.02.006

Rushton, P. J., Torres, J. T., Parniske, M., Wernert, P., Hahlbrock, K., and Somssich, I. E. (1996). Interaction of elicitor induced DNA-binding proteins with elicitor response elements in the promoters of parsley PR1 genes. *EMBO J.* 15 (20), 5690–5700. doi: 10.1002/j.1460-2075.1996.tb00953.x

Shivakumar, D., Williams, J., Wu, Y., Damm, W., Shelley, J., and Sherman, W. (2010). Prediction of absolute solvation free energies using molecular dynamics free energy perturbation and the OPLS force field. *J. Chem. Theory Comput.* 6 (5), 1509–1519. doi: 10.1021/ct900587b

Siewers, V., Smedsgaard, J., and Tudzynski, P. (2004). The P450 monooxygenase BcABA1 is essential for abscisic acid biosynthesis in botrytis cinerea. *Appl. Environ. Microbiol.* 70 (7), 3868–3876. doi: 10.1128/AEM.70.7.3868-3876.2004

Steuer, B., Stuhlfauth, T., and Fock, H. P. (1988). The efficiency of water use in water stressed plants is increased due to ABA induced stomatal closure. *Photosynthesis Res.* 18 (3), 327–336. doi: 10.1007/BF0003483

Taheri, S., Gantait, S., Azizi, P., and Mazumdar, P. (2022). Drought tolerance improvement in solanumlycopersicum: an insight into "OMICS" approaches and genome editing. *3 Biotech.* 12 (3), 63. doi: 10.1007/s13205-022-03132-3

Toukmaji, A. Y., and Board, J. (1996). Ewald summation techniques in perspective: A survey. *Comput. Phys. Commun.* 95), 73–92. doi: 10.1016/0010-4655(96)00016-1

Venema, J. H., Linger, P., van Heusden, A. W., Hasselt, P. R., and Bruggemann, W. (2005). The inheritance of chilling tolerance in tomato (*Lycopersicon* spp.). *Plant Biol.* 7, 118–130. doi: 10.1055/s-2005-837495

Wang, D., Gao, Z., Du, P., Xiao, W., Tan, Q., Chen, X., et al. (2016). Expression of ABA metabolism-related genes suggests similarities and differences between seed dormancy and bud dormancy of peach (Prunuspersica). *Front. Plant Sci.* 6. doi: 10.3389/fpls.2015.01248

Xu, X. P., Chen, C., Fan, B., and Chen, Z. (2006). Physical and functional interactions between pathogen-induced arabidopsis WRKY18, WRKY40, and WRKY60 transcription factors. *Plant Cell* 18, 1310–1326. doi: 10.1105/tpc.105.037523

Zou, X., Jeffrey, R. S., Dawn, N., and Qingxi, J. S. (2004). AWRKY gene from creosote bush encodes an activator of the abscisic acid signaling pathway. *J. BiolChem* 279, 55770–55779. doi: 10.1074/jbc.M408536200

frontiers | Frontiers in Plant Science

TYPE Original Research
PUBLISHED 08 February 2023
DOI 10.3389/fpls.2023.1111789

Check for updates

OPEN ACCESS

EDITED BY
Diaa Abd El Moneim,
Arish University, Egypt

REVIEWED BY
Jagna Chmielowska-Bąk,
Adam Mickiewicz University, Poland
Ewa Joanna Hanus-Fajerska,
University of Agriculture in Krakow, Poland

*CORRESPONDENCE
Haiying Li
lihaiying_2004@163.com
Xiaojiao Han
hanxiaojiao1004@163.com

†These authors have contributed equally to this work

SPECIALTY SECTION
This article was submitted to Plant Abiotic Stress, a section of the journal Frontiers in Plant Science

RECEIVED 30 November 2022
ACCEPTED 25 January 2023
PUBLISHED 08 February 2023

CITATION
Li S, Zhuo R, Yu M, Lin X, Xu J, Qiu W, Li H and Han X (2023) A novel gene *SpCTP3* from the hyperaccumulator *Sedum plumbizincicola* redistributes cadmium and increases its accumulation in transgenic *Populus* × *canescens*. *Front. Plant Sci.* 14:1111789. doi: 10.3389/fpls.2023.1111789

COPYRIGHT
© 2023 Li, Zhuo, Yu, Lin, Xu, Qiu, Li and Han. This is an open-access article distributed under the terms of the Creative Commons Attribution License (CC BY). The use, distribution or reproduction in other forums is permitted, provided the original author(s) and the copyright owner(s) are credited and that the original publication in this journal is cited, in accordance with accepted academic practice. No use, distribution or reproduction is permitted which does not comply with these terms.

A novel gene *SpCTP3* from the hyperaccumulator *Sedum plumbizincicola* redistributes cadmium and increases its accumulation in transgenic *Populus* × *canescens*

Shaocui Li[1,2†], Renying Zhuo[1†], Miao Yu[1], Xiaoyu Lin[3], Jing Xu[1], Wenmin Qiu[1], Haiying Li[4*] and Xiaojiao Han[1*]

[1]State Key Laboratory of Tree Genetics and Breeding, Key Laboratory of Tree Breeding of Zhejiang Province, Research Institute of Subtropical Forestry, Chinese Academy of Forestry, Hangzhou, Zhejiang, China, [2]Forestry Faculty, Nanjing Forestry University, Nanjing, Jiangsu, China, [3]College of Life Sciences, Fujian Agriculture and Forestry University, Fuzhou, China, [4]Institute of Virology and Biotechnology, Zhejiang Academy of Agricultural Sciences, Hangzhou, Zhejiang, China

A cadmium (Cd) tolerance protein (*SpCTP3*) involved in the *Sedum plumbizincicola* response to Cd stress was identified. However, the mechanism underlying the Cd detoxification and accumulation mediated by *SpCTP3* in plants remains unclear. We compared wild-type (WT) and *SpCTP3*-overexpressing transgenic poplars in terms of Cd accumulation, physiological indices, and the expression profiles of transporter genes following with 100 μmol/L $CdCl_2$. Compared with the WT, significantly more Cd accumulated in the above-ground and below-ground parts of the *SpCTP3*-overexpressing lines after 100 μmol/L $CdCl_2$ treatment. The Cd flow rate was significantly higher in the transgenic roots than in the WT roots. The overexpression of *SpCTP3* resulted in the subcellular redistribution of Cd, with decreased and increased Cd proportions in the cell wall and the soluble fraction, respectively, in the roots and leaves. Additionally, the accumulation of Cd increased the reactive oxygen species (ROS) content. The activities of three antioxidant enzymes (peroxidase, catalase, and superoxide dismutase) increased significantly in response to Cd stress. The observed increase in the titratable acid content in the cytoplasm might lead to the enhanced chelation of Cd. The genes encoding several transporters related to Cd^{2+} transport and detoxification were expressed at higher levels in the transgenic poplars than in the WT plants. Our results suggest that overexpressing *SpCTP3* in transgenic poplar plants promotes Cd accumulation, modulates Cd distribution and ROS homeostasis, and decreases Cd toxicity *via* organic acids. In conclusion, genetically modifying plants to overexpress *SpCTP3* may be a viable strategy for improving the phytoremediation of Cd-polluted soil.

KEYWORDS

cadmium tolerance protein 3, *Sedum plumbizincicola*, cadmium stress, subcellular distribution, transgenic poplars

1 Introduction

Rapid economic and technological developments have resulted in the release of a relatively large amount of heavy metal waste, which has led to increased environmental pollution. In China, more than 1.3 × 10^5 km^2 of cultivated land has been polluted with cadmium (Cd) (MER and MLR, 2014; Jia et al., 2022). Soil degradation due to Cd contamination is becoming a major issue affecting food security and quality (Rehman et al., 2020). Heavy metal pollution has threatened the sustainable development of various industries (e.g., agriculture) (Yessica et al., 2020). Heavy metal pollution has attracted the attention of researchers in several disciplines (Li et al., 2018; Angulo-Bejarano et al., 2021). Cadmium is one of the most dangerous heavy metals because of its high toxicity and bioconcentration factor (Singh P et al., 2020; Cui et al., 2021) As a non-essential element in plants, Cd can disrupt plant metabolic activities, adversely affect photosynthesis, exacerbate the effects of nutrient deficiency as well as oxidative stress, and even inhibit cell proliferation and division (Rasafi et al., 2020; Shamelashvili et al., 2020; Yazdi, 2021). Cadmium stress can also inhibit plant growth in mild cases and cause plant death in severe cases (Yang et al., 2022). In heavily polluted areas, Cd can enter the human body through the food chain, with detrimental and irreversible effects on human health (Fu and Xi, 2020). Therefore, the remediation of Cd-contaminated soil is a major challenge that must be addressed (Wan et al., 2016; Han et al., 2020).

Phytoremediation has attracted widespread interest as an economically feasible and eco-friendly method for rescuing Cd-contaminated soils (Hamid et al., 2020; Raza et al., 2020). The Cd accumulation and detoxification capacities of plants are the main determinants of phytoremediation efficiency (Wang et al., 2021; Jia et al., 2022). The remediation of Cd-contaminated soil by hyperaccumulating plants is one of the most promising environmentally friendly remediation methods (Yaashikaa et al., 2022). It may be improved by increasing the absorption rate, transport, and accumulation of Cd in plants, which depends on the synergism between physiological and molecular mechanisms (Chai et al., 2020).

Elucidating the mechanisms regulating Cd tolerance and accumulation in plants is important for increasing the efficiency of the phytoremediation of Cd-polluted soil. Cadmium that is taken up by plants accumulates in the above-ground plant parts *via* the long-distance transport mediated by many transporters. Cd uptake, transport and distribution in plants depend on their metal transporters, such as zinc/iron-regulated transporter (ZRT/IRT-related ZRT-IRT-like proteins (ZIP)), heavy metal ATPase (HMA), Natural Resistance-Associated Macrophage Protein (NRAMP), and ATP-binding cassette (ABCC) (Zhang et al., 2013; Jiang et al., 2021; Yue et al., 2021). Cd in the external environment can be transported from the soil to the cell interior through the ZIP transporter on the plasma membrane (Viehweger, 2014). Then Cd^{2+} is transported to xylem through NRAMP, HMA, etc (He et al., 2015). The heterologous expression of *NRAMP3* from the hyperaccumulator *Sedum alfredii* in *Brassica juncea* reportedly does not significantly affect Cd tolerance, but it significantly increases the Cd content in the above-ground transgenic plant parts, implying that *SaNRAMP3* regulates the root-to-shoot translocation of Cd (Feng et al., 2018). *HMA* genes encode proteins that mediate the transport of metals from the roots to the shoots (Peng et al., 2017). In *Brassica rapa*, *HMA3* regulates Cd accumulation and increases the root-to-shoot Cd translocation rate (Zhang et al., 2019). In addition, some of the cadmium that enters the cytoplasm is transported into the vesicles by the action of ABC transporter and metal tolerance protein 1 (MTP1) (Lin and Aarts, 2012; Park et al., 2012).

The Cd tolerance of plants depends on physiological detoxification-related processes (Li et al., 2022). After passing through the cytoplasmic membrane, Cd is chelated with ligands to inhibit reactions between Cd and other cellular compounds. Plants often increase the accumulation of titratable acid to cope with heavy metal stress. When Cu was sprayed on leaves of *Hibiscus sabdariffa*, the contents of anthocyanin and titratable acid were increased significantly (Patricio et al., 2018). In lettuce, humic acid can stimulate production of organic acids by improving dark fixation of carbon dioxide or prevent the harmful effects of Cd, thereby increases titratable acidity of leaves (Haghighi et al., 2013). In response to lead stress, 5-aminolevulinic acid minimizes the potential for lead ions to inhibit metabolism by increasing the expression of genes encoding enzymes associated with malate and citrate metabolism, leading to the chelation of lead ions (Singh R et al., 2020).

Under heavy metal stress conditions, reactive oxygen species (ROS) levels increase substantially in plants. Heavy metal-tolerant plants then produce relatively large amounts of ROS-scavenging antioxidant enzymes to protect against heavy metal-induced oxidative stress (Dvorak et al., 2020). Superoxide dismutase (SOD) was inhibited under high Cd treatment, and excess ROS also led to significantly higher levels of oxidative damage (Zhang et al., 2020). A novel *Nicotiana tabacum* Cd transporter gene *NtNRAMP3* preventing chlorophyll degradation and reducing ROS accumulation under Cd stress conditions. Nevertheless, knockdown of the *NtNRAMP3* gene could increase the activities of SOD, POD and CAT thereby improving the Cd tolerance of tobacco to a great degree (Jia et al., 2022). Furthermore, *SaCu/Zn SOD* expression in *S. alfredii* is induced by Cd stress; the overexpression of this gene increases the resistance of transgenic *A. thaliana* plants to oxidative stress (Li et al., 2017).

New plant genes that may increase the efficiency of Cd phytoremediation were recently identified. For example, in *A. thaliana*, overexpressing the *IRON MAN* (*IMA*) gene encoding a small peptide improves Cd tolerance, whereas silencing *BRUTUS* (*BTS*) expression can increase the efficiency of the phytoremediation of Cd-contaminated soil (Zhu et al., 2020; Meng et al., 2022). Therefore, the functions of some key Cd stress-related genes in plants may be exploited to alleviate Cd toxicity and improve the Cd tolerance of plants. However, the physiological and molecular mechanisms underlying the functions of these novel genes related to Cd tolerance have not been precisely characterized, which is necessary for the sequential identification of novel genes. We previously detected five new proteins related to Cd tolerance or accumulation in the hyperaccumulator *Sedum plumbizincicola*, of which the production of Cadmium Tolerance Protein 3 (*SpCTP3*) is strongly induced by Cd treatments (Liu et al., 2019). Moreover, the expression of *SpCTP3*, which belongs to the *Nod19* superfamily, is up-regulated by stress. *Populus* × *canescens* (i.e., poplar species) is potentially useful for phytoremediations because of its fast growth rate and high biomass as well as the availability of an established

genetic transformation system. The genetic transformation of this poplar species with Cd hyperaccumulation-related candidate genes from *S. plumbizincicola* may generate transgenic plants capable of accumulating high Cd levels, making them relevant for the phytoremediation of Cd-contaminated soil. Hence, the mechanisms controlling Cd accumulation, subcellular distribution, and chemical morphology in *SpCTP3*-overexpressing poplar trees under Cd stress conditions should be clarified. In this study, we examined the effects of *SpCTP3* on Cd absorption, distribution, and detoxification to improve its utility for Cd phytoremediation. The data presented herein will provide researchers with the theoretical basis for applying *SpCTP3* in the remediation of Cd-polluted lands by transgenic woody plants.

2 Materials and methods

2.1 Vector construction and plant transformation

The *S. plumbizincicola SpCTP3* gene was cloned by a PCR amplification using the primers SpCTP3-F/R. The full-length *SpCTP3* sequence comprises 1,383 base pairs. The amplified *SpCTP3* was incorporated into the pBI121 vector *via* homologous recombination for the subsequent expression under the control of the CaMV 35S promoter. An *Agrobacterium tumefaciens*-mediated leaf disc transformation method was used to insert *SpCTP3* into *P.* × *canescens* plants (Wen et al., 2022). Transgenic plants were identified by a genomic PCR amplification using the primers SpCTP3-F/R and the positive lines were further analyzed by quantitative real-time PCR (qRT-PCR). The relative expression levels were calculated according to the $2^{-\Delta\Delta Ct}$ method (Jia et al., 2022). The *TUBU* (Beta tubulin) gene was selected as an internal control. Primer details are listed in Table S1. Four-week-old transgenic rooted poplar plants and the control group were grown for 4 weeks in Hoagland nutrient solution (i.e., hydroponic system). The nutrient solution was renewed every 3 days. For the heavy metal treatment experiments, plants were grown for 30 days in Hoagland nutrient solution supplemented with 100 µmol/L $CdCl_2$. The growth chamber conditions were set as follows: 16-h day (25°C)/8-h night (18°C), 50%–60% relative humidity, and a photon flux density of 120 µmol/m^2/s. Plants were photographed and their phenotypes were analyzed.

2.2 Determination of Cd elements

The Cd-treated lines were harvested separately and rinsed thoroughly with tap water. They were then soaked in 20 mmol/L EDTA for 20 min and washed three times with deionized water. The roots, stems, and leaves of each line were collected and dried at 70°C until they reached a constant weight. At least 0.2 g dried material was used to measure the Cd concentration. Briefly, the samples were ground to fine powder, and digested with a mixture consisting of HNO_3:$HClO_4$ (9:1, v/v) at 120–200°C in a microwave-accelerated reaction system (CEM, Matthews, NC, USA). The final volume was adjusted to 25 mL with distilled water. The Cd concentration was analyzed using the iCAP-7400 inductively coupled plasma optical emission spectroscopy (ICP-OES) system (Thermo Fisher Scientific, California, USA). The heavy metal translocation factor was calculated according to the following formula (Dineshkumar et al., 2019): heavy metal content in the aerial plant parts/heavy metal content in the roots.

2.3 Separation of subcellular components and analysis of the Cd content

Fresh leaves and roots (2.0 g) were homogenized using a precooled mortar and 20 mL precooled extraction solution [50 mmol/L Tris-HCl, 250 mmol/L sucrose, and 1.0 mmol/L $C_4H_{10}O_2S_2$ (pH 7.5)]. After centrifuging the samples at 1,250 × g for 15 min, the precipitate was collected as the cell wall component. The supernatant was centrifuged at 20,800 × g for 45 min to obtain the precipitate (organelles) and supernatant (soluble fraction). All steps were completed at 4°C. After the collected components were digested, their Cd concentrations were determined by ICP-OES.

2.4 Extraction and quantitative analysis of Cd chemical forms

Cadmium in different chemical forms was extracted as described by Ouyang et al. (2019). Inorganic titratable acid cadmium (Cd_E) was extracted with 80% ethanol, water-soluble cadmium (Cd_W) was extracted with deionized water, Cd integrated with pectin and protein (Cd_{NaCl}) was extracted with 1 mol/L NaCl, insoluble $CdHPO_4$, $Cd_3(PO_4)_2$, and other Cd-phosphate complexes (Cd_{HAC}) were extracted with 2% HAC, oxalic acid bound cadmium (Cd_{HCl}) was extracted with 0.6 mol/L HCl, and the rest was residual cadmium (Cdr). Approximately 0.5 g samples were shaken for the 22-h extraction at 25°C. The proportion of the sample weight and extraction solution volume was adjusted to 1:10 (w/v) before a centrifugation at 5,000 × g for 10 min. The precipitate was resuspended twice with the same extraction solution, shaken at 25°C for 2 h, and then centrifuged at 5,000 × g for 10 min. Finally, the supernatants after three centrifugations were combined. Each pooled solution was then evaporated on an electric plate to a constant weight. After digesting the materials, the Cd concentrations of the three parts were determined by ICP-OES.

2.5 Measurement of the Cd^{2+} net flux

To determine the net Cd^{2+} flow rate in different lines treated with Cd stress, nine fine roots (approximately 1.5 mm diameter) were selected from each Cd-treated transgenic line and the WT control. The Cd^{2+} net flux was measured according to the noninvasive micro-test (NMT) technique (NMT100 Series; Younger, USA LLC, Amherst, MA, USA) as previously described (He et al., 2015; Chen et al., 2017). Each fine root was equilibrated in the measurement solution (0.05mM $CdSO_4$, 0.25 mmol/L NaCl, 0.1 mmol/L Na_2SO_4, 0.05 mmol/L KCl, 0.15 mmol/L MES, pH6.0) for 30 min and then transferred to fresh measurement solution before determining the Cd^{2+} net flux. The root Cd^{2+} flow rate was analyzed by moving the electrode between two

points (30 μm) on the root surface to measure the voltage difference perpendicular to the root surface.

2.6 Analysis of antioxidants and antioxidative enzyme activities

To analyze antioxidant enzyme activities and the contents of ROS ($O^{2\cdot-}$ and H_2O_2), 1.0 g leaf and root samples were collected from the WT and transgenic plants and homogenized in 8 mL 50 mmol·L^{-1} sodium phosphate buffer (pH 7.8) using a prechilled mortar. The samples were then centrifuged at 10,000 × g for 15 min at 4°C. The supernatant was used to measure enzyme activities and the contents of ROS. The superoxide dismutase (SOD) activities were determined using NBT (Nitroblue tetrazolium) photoreduction method as absorbance 560 nm as described by Akbari et al. (2020). The peroxidase (POD) activity was assayed spectrophotometrically using hydrogen peroxide and guaiacol as extracts at 470 nm (Dai et al., 2020). Catalase (CAT) activity was tested in potassium phosphate buffer (pH 7.8) containing 3 mM H_2O_2 at 240 nm. The H_2O_2 content and the $O2\cdot^-$ level were determined as described by Alexieva et al. (2001) and Jing et al. (2020). H_2O_2 content was determined using trichloroacetic acid (0.1% w/v) at 630 nm (Alexieva et al., 2001). For determination of $O^{2\cdot-}$ level, supernatant was mixed with 10 mM of hydroxylamine hydrochloride and left for 20 min followed by the addition of sulfanilamide and naphthylamine. After 20 min of incubation at 25°C, absorbance was measured at 530 nm, and calculations were done using the standard curve of $NaNO_2$ (Jing et al., 2020).

2.7 Determination of titratable acid contents

For titratable acid assay, 0.1 g sample of each treatment was added to water and then ground into a homogenate. The final volume was adjusted to 5 mL for the extraction of titratable acid. The titratable acid content was determined by a titration using sodium hydroxide (0.1 mol/L) and phenolphthalein (1%) as the pH indicator (Huo et al., 2009).

2.8 Analysis of transporter gene expression profiles

Total RNA was extracted from Cd-treated and WT poplar samples using the RNAprep Pure Plant Plus Kit (TIANGEN, Beijing), after which 800 ng total RNA in 20 μL was used to synthesize cDNA. The qRT-PCR analysis was performed using SYBR Green Premix Ex Taq II (TAKARA, Japan). The primer sequence refers to He et al. (2015) and Ma et al. (2014). Information regarding the qRT-PCR primers is provided in Table S1. The qRT-PCR reaction mixture was prepared in a volume of 20 μL, with 10 μL of SYBR green master mix, cDNA template (2 μL), ddH_2O (6.8 μL), ROX Reference Dye 0.4μL and 0.4 μL of each of the primer. The qRT-PCR conditions were set as follows; 95°C for 30s, 40 cycles of 95°C for 5 s, and 60°C for 30 s, followed by melting of PCR products step: 95°C for 15 s, 60°C for 1 min, 95°C for 15 s. Each sample was analyzed using three technical replicates to ensure the results were reliable. Gene expression levels were calculated according to the $2^{-\Delta\Delta Ct}$ method, with *TUBU* selected as the reference gene. Relative gene expression levels were visualized in a heatmap on the basis of Z-score transformed values.

2.9 Statistical analysis

For each experiment, at least three plants were sampled. Statistical analyses were performed using the SPSS software (version 18.0). The significance of the differences between the treated and control samples was analyzed *via* a one-way ANOVA followed by Duncan's test ($p< 0.05$). Data are presented herein as the mean ± standard deviation (SD). The Kruskal Wallis test was used if the data did not meet the assumptions for ANOVA (equality of variances) according to Levene's test. A principal components analysis (PCA) was performed and the results were plotted using the ggbiplot package of R (version 3.6.4).

3 Results

3.1 Development of poplar lines overexpressing *SpCTP3*

Genomic DNA was extracted from the WT and transgenic lines using the CTAB method. The transgenic lines were verified using SpCTP3-F/R primers (Table S1). Of the 13 putatively transformed lines, 11 were confirmed as transgenic (Figure S1). The PCR results showed that *SpCTP3* was expressed in the transgenic poplar plants (Figure S1). Total RNA was extracted from some of the transgenic lines and reverse transcribed to cDNA for the qRT-PCR analysis. Three independent lines (OE-3, OE-6, and OE-7) with high *SpCTP3* expression levels were selected for the subsequent analyses.

3.2 *SpCTP3* has no effect on the biomass of the transgenic poplar under Cd treatment

There was no significant difference in the dry weights of the untreated WT and transgenic plants. After the Cd treatment, the dry weight of the above-ground parts of the transgenic and WT plants decreased by an average of 28.49% and 12.96% (relative to the control), respectively. The dry weight of the root system decreased slightly after the Cd treatment, but this decrease was not significant. Accordingly, *SpCTP3* expression has no effect of the biomass of transgenic poplar plants exposed to Cd stress (Figure 1).

3.3 *SpCTP3* overexpression increased the Cd accumulation in transgenic poplars

To further functionally characterize *SpCTP3*, we measured the Cd content of specific parts of the WT and transgenic plants treated with

10.3389/fpls.2023.1111789

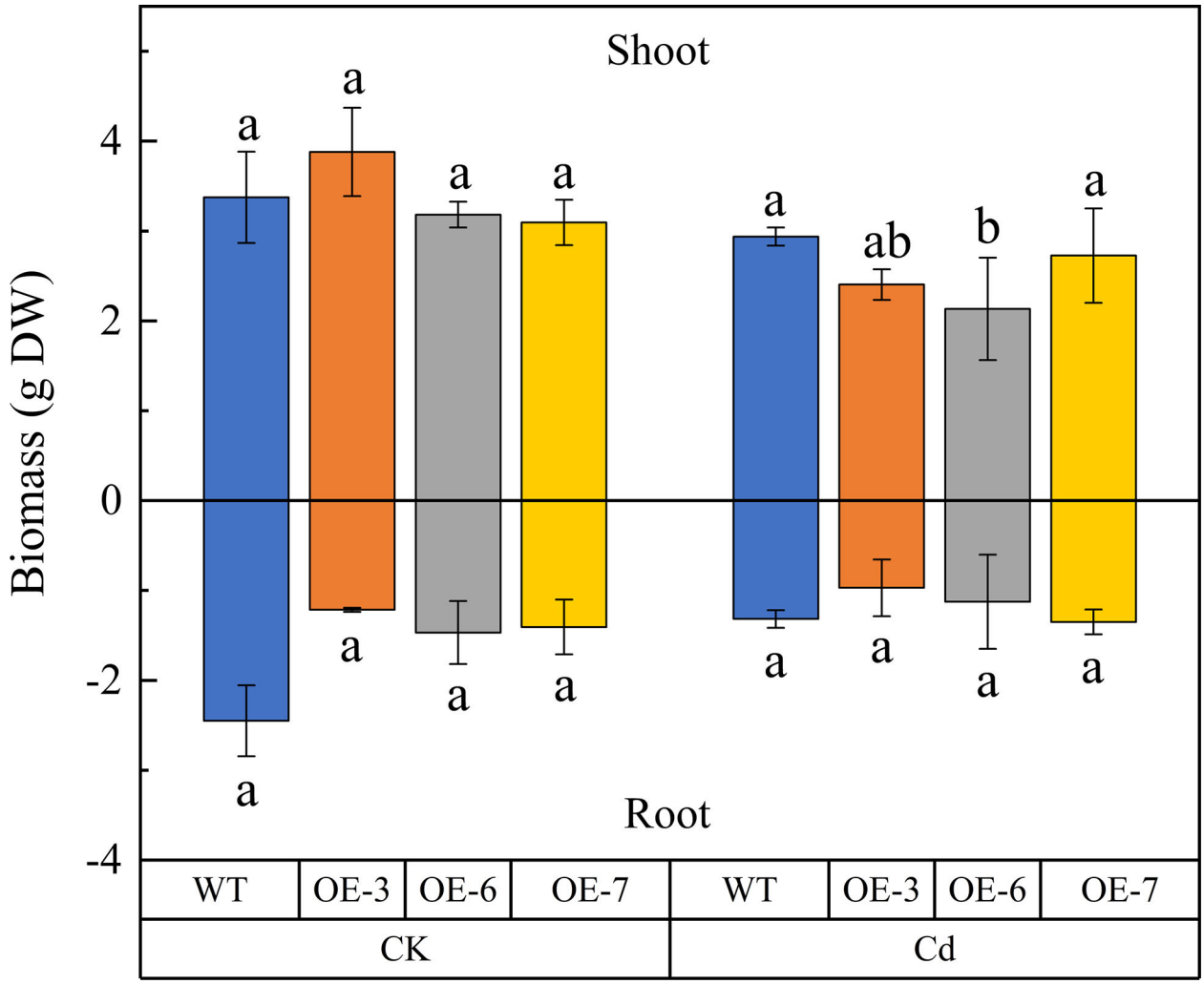

FIGURE 1
Effect of cadmium (Cd) stress on the shoot and root biomasses of *SpCTP3*-overexpressing transgenic and WT lines. Data are presented as the mean ± SD of three independent replicates. Different letters above bars indicate significant differences among treatments ($p < 0.05$; n = 3).

Cd for 30 days (Figure 2). Notably, the root and leaf Cd contents were higher for the *SpCTP3*-overexpressing transgenic lines than for the WT controls. In contrast, there were no obvious differences in the stem Cd contents. The distribution of Cd was in the order of roots, leaves, and stems. The leaf Cd content was 48.58%–82.49% higher for the transgenic lines than for the WT controls. Similarly, the translocation factor was higher for the transgenic lines than for the WT plants. These observations indicated that compared with the WT plants, the transgenic poplar plants were better able to transport Cd from the roots to the aerial parts.

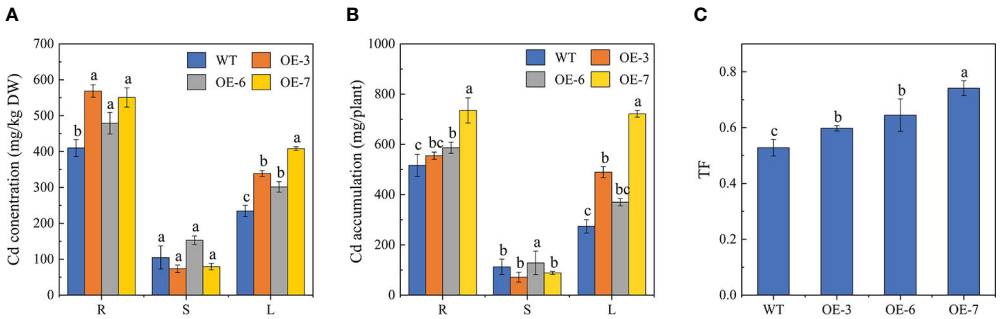

FIGURE 2
(A) Cd concentrations. **(B)** Cd accumulation. **(C)** Root-to-leaf Cd translocation factors (TFs).

10.3389/fpls.2023.1111789

3.4 Overexpression of *SpCTP3* altered the distribution and chemical forms of Cd in transgenic plants

In this study, Cd^{2+} was differentially distributed in various subcellular components. Most of the Cd in the roots and leaves of the transgenic lines was stored in the soluble fraction, followed by the cell wall and organelles (Figure 3). In the WT plants, 36.12% and 56.77% of the Cd were present in the cell wall and soluble fraction, respectively; the rest of the Cd was detected in the organelle fraction. In the WT leaves, 44.47% and 47.52% of the Cd content was distributed in the cell wall and soluble fraction, respectively. The cell wall Cd content was lower for the transgenic lines than for the WT plants, whereas the opposite pattern was observed for the Cd content in the soluble fraction.

Cadmium absorbed by plants is present in cells in diverse forms and affects plant growth and development. We extracted various forms of Cd and determined the Cd contents using an ICP-OES system. The Cd_W content was highest in the roots and leaves of the transgenic and WT plants (Figure 3). The Cd in the WT roots was mostly detected as Cd_W (59.19%), followed by Cd_{NaCl} (29.11%) and then Cd_{HCl}, Cd_{HAc}, and Cd_E. The Cd in the transgenic roots was also mostly detected as Cd_W (average of 75.59%), although the Cd_{HAc} content was also relatively high. The Cd in the leaves of the transgenic and WT plants was predominantly in the Cd_E, Cd_{NaCl}, and Cd_{HAc} forms. Compared with the WT control, the Cd treatment of the transgenic plants decreased the Cd_W and Cd_{NaCl} contents, while increasing the Cd_{HCl} and Cd_{HAc} contents. Hence, the overexpression of *SpCTP3* altered the Cd distribution and chemical forms in the transgenic plants.

3.5 Overexpression of *SpCTP3* enhanced the net flux of Cd^{2+} in poplar roots

To clarify the changes in Cd uptake by the roots of transgenic and WT poplar plants exposed to Cd stress, we used the NMT technique to analyze the Cd^{2+} flow rate at 120 µm from the root tip after the Cd treatment. The Cd^{2+} flow rate was 72.927–163.48 pmol/cm^2/s for the transgenic lines and 44.707–61.058 pmol/cm^2/s for the WT plants (Figure 4). The net influx of Cd^{2+} was higher for the transgenic roots than for the WT roots.

3.6 Overexpression of *SpCTP3* increased the ROS content and affected antioxidant enzyme activities

An exposure to Cd stress results in different degrees of oxidative stress in plants. The $O_2^{\cdot-}$ and H_2O_2 concentrations were compared between the WT and transgenic poplar plants (Figure 5). For both the WT and transgenic samples, the Cd treatment induced a significant H_2O_2 and $O_2^{\cdot-}$ burst. The leaf $O_2^{\cdot-}$ content was 2-times higher in the transgenic plants than in the WT plants. In the roots, the H_2O_2 and

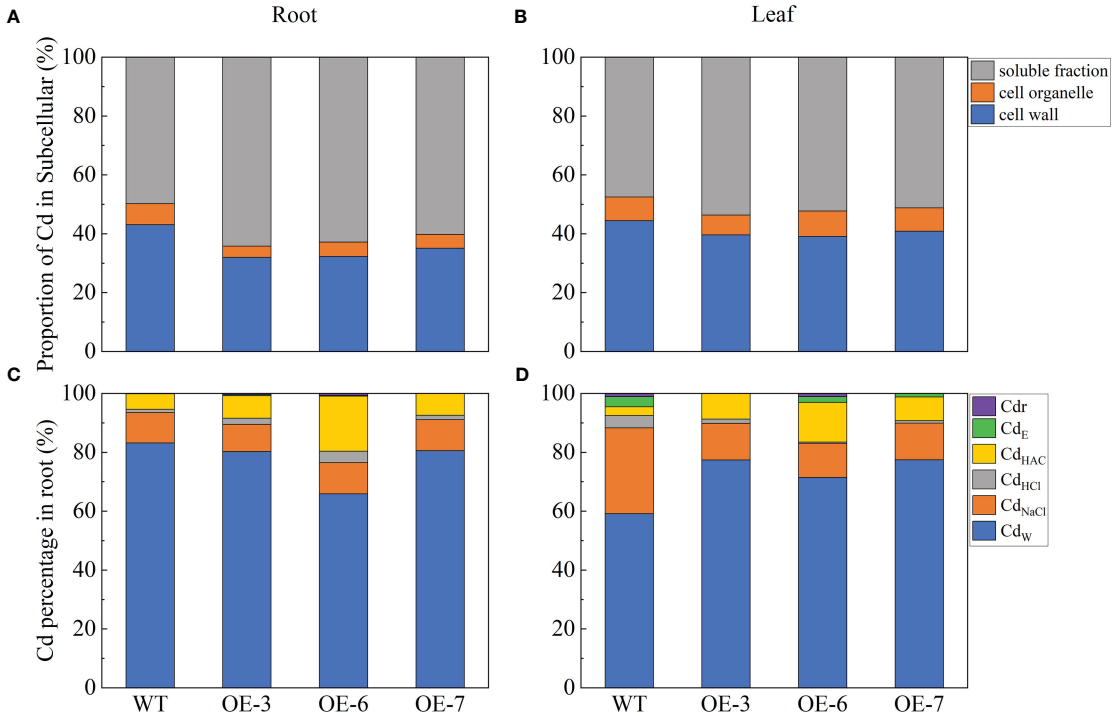

FIGURE 3
Cd subcellular distribution and Cd chemical forms in WT and *SpCTP3*-overexpressing poplar roots and leaves treated with 100 µmol·L^{-1} Cd for 30 days. **(A)** Cd subcellular distribution in the roots. **(B)** Cd subcellular distribution in the leaves. **(C)** Cd chemical forms in the roots. **(D)** Cd chemical forms in the leaves. Cd_E, inorganic Cd; Cd_W, water-soluble Cd; Cd_{NaCl}, pectate- and protein-integrated Cd; Cd_{HAc}, insoluble $CdHPO_4$, $Cd_3(PO_4)_2$, and other Cd-phosphate complexes; Cd_{HCl}, oxalic acid-bound Cd; Cdr, Cd in residues.

10.3389/fpls.2023.1111789

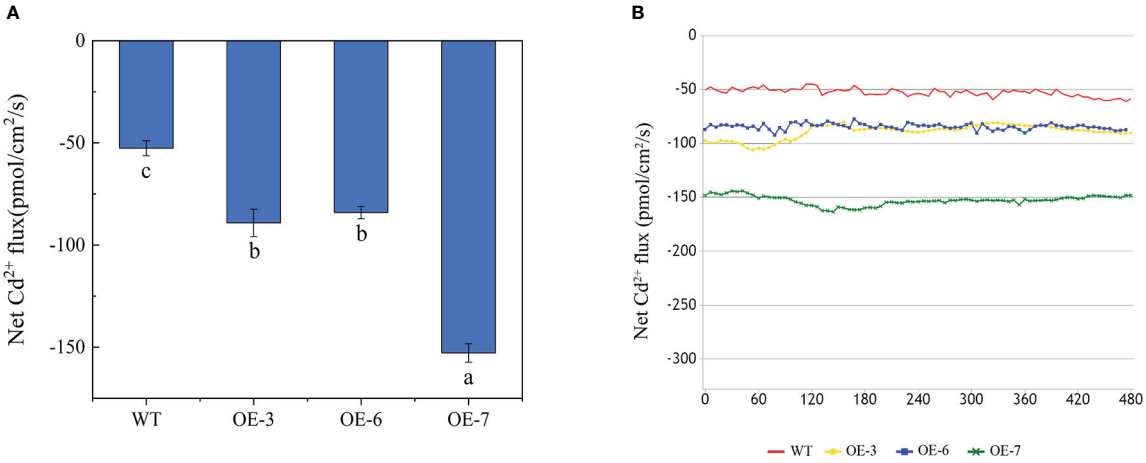

FIGURE 4
Effects of Cd treatments on the Cd^{2+} net flux in the roots of WT and transgenic lines. **(A)** Results of the statistical analysis of the steady-state Cd^{2+} net flux. **(B)** Time-course of the Cd^{2+} net flux at the root surface. Different letters on bars indicate significant differences in the Cd concentrations among lines ($p< 0.05$).

O_2^- contents increased in the transgenic plants by varying degrees, resulting in levels that were significantly higher than those in the WT plants. Additionally, H_2O_2 and O_2^- accumulated more in the leaves than in the roots, although this phenomenon was significantly less pronounced in the WT plants than in the transgenic plants.

Cadmium significantly affected the CAT, SOD, and POD activities (Figure 6). The CAT activity levels were significantly higher in the transgenic lines than in the WT plants after the Cd treatment. Compared with the WT control, the CAT activity was respectively 1.37-fold and 2.98-fold higher in the roots and leaves of the transgenic lines by Cd stress. Furthermore, there was no significant difference in the SOD activities of the Cd-treated transgenic and WT leaves, but the root SOD activities were slightly lower in the transgenic lines than in the WT control following the Cd treatment. In addition, the POD activity in the leaves was slightly higher in the transgenic lines than in the WT plants, but there was no significant difference in the root POD activity.

3.7 Overexpression of *SpCTP3* increased the titratable acid content of Cd-treated transgenic lines

Titratable acids are often considered to be important for the resistance of plants to heavy metal pollution because they contribute to the chelation of metal elements and convert metal ions to less toxic or non-toxic chelated states. Titratable acids were extracted from the *SpCTP3*-overexpressing and WT plants and the total organic acid content was determined *via* acid-base titration (Figure 7). The Cd treatment induced a substantial change in the titratable acid content. More specifically, the titratable acid content in the transgenic roots and leaves increased significantly, peaking at 20.76 $\mu mol \cdot g^{-1}$ in the roots (i.e., 31.87% higher than the titratable acid content of the control roots) and 30.81 $\mu mol \cdot g^{-1}$ in the leaves. Thus, the overexpression of *SpCTP3* increased the titratable acid content of transgenic lines under Cd stress conditions.

3.8 Expression of the genes involved in Cd^{2+} transport and detoxification

On the basis of the physiological data (Figure 8), differences in the Cd uptake by the roots and the subsequent translocation to the shoots may be a possible reason for diversity in the Cd accumulation between the WT and transgenic poplar plants. Therefore, we focused on the transcriptional regulation of some transporter genes involved in Cd^{2+} transport and detoxification. The expression levels of all 12 genes related to Cd transport and detoxification were differentially up-regulated in the roots after the Cd treatment (Figure 8). In the roots, the up-regulated expression of *ZIP2* (encoding zinc-regulated transporter 2), *ZIP6.2*, and *IRT* (encoding an iron-regulated transporter-related protein) was greater in the transgenic lines than in the WT control. Among the leaves, the most up-regulated genes were *IRT*, *YSL2* (encoding a yellow stripe-like protein), and *CAX* (encoding a cation exchanger). Moreover, the Cd treatment significantly up-regulated the expression of *HMA4* (encoding heavy metal ATPase 4) only in the transgenic roots. Similar expression trends were observed for other genes in the leaves and roots, in which *NAS* (encoding a nicotianamine synthase), *MTP1* (encoding metal tolerance protein 1), and *Nramp1.3* (encoding natural resistance-associated macrophage protein 1.3) expression levels increased significantly in the Cd-treated transgenic lines.

3.9 Principal component analysis of physiological responses

To determine the response patterns of the WT and transgenic poplar plants to Cd^{2+}, a PCA was conducted using the physiological data related to the exposure to Cd^{2+} (e.g., Cd concentration as well as ROS, antioxidant, and titratable acid contents) (Figure 9). The PCA results indicated that 88.11% of the total variance could be explained by the effects of the Cd stress on the WT and *SpCTP3*-overexpressing transgenic poplar plants, with principal components 1 and 2

respectively explaining 74.68% and 13.43% of the Cd-induced variance. There was a significant difference between the *SpCTP3*-overexpressing transgenic and WT poplar plants under Cd stress conditions.

4 Discussion

4.1 *SpCTP3* overexpression enhanced Cd accumulation by regulating subcellular components and Cd chemical forms

The soluble fraction of cells consists mainly of vesicles, which contain many proteins, sugars, and organic acids that bind to heavy metals to decrease their effects and limit the amount of heavy metals entering organelles, thereby protecting cells from Cd stress (Li et al., 2014; Ouyang et al., 2019). For example, in *Capsicum annuum* roots, the Cd content in the soluble fraction can be as high as 77%–87% (Xin and Huang, 2014). Additionally, Cd is mainly distributed in the soluble fraction of the leaves and roots of Cd-tolerant radish varieties (Xin et al., 2017). We obtained similar results. In the WT control, the soluble fraction had the highest Cd content (56.77%), followed by the cell wall. In the transgenic lines, the rank-order for the Cd content was as follows: soluble fraction > cell wall > organelle (Figure 3). This trend was also detected in the leaves. Plants absorb Cd and store most of it in the soluble fraction, followed by the cell wall. However, plant responses to Cd stress may vary among species and stress levels. The transgenic poplar plants had a higher Cd capacity than the WT controls. The accumulation of Cd in the cell wall and soluble fraction can effectively decrease Cd toxicity in plants. In the current study, the Cd content decreased in the cell walls of the transgenic roots and leaves, whereas it increased in the soluble fraction. Hence, in the *SpCTP3*-overexpressing transgenic poplar plants, Cd ions were separated and fixed in the cytoplasm in the form of relatively stable metal chelates/complexes. Compared with the WT plants, the overexpression of *SpCTP3* in the transgenic plants increased the Cd content of the roots and leaves, while also altering the subcellular distribution of Cd by increasing and decreasing the Cd proportions in the soluble fraction and cell wall, respectively. These findings reflect the importance of *SpCTP3* for minimizing the toxic effects of Cd in plants.

Under heavy metal stress conditions, multiple mechanisms may be activated in plants to prevent the excessive accumulation of metals in the cytosol and limit the toxicity of the metals. If heavy metals enter the soluble part of the cell, the internal heavy metal tolerance mechanism is activated, resulting in the production of metal chelators, including organic acids, amino acids, and binding proteins (Hall, 2002). Organic acids are an extremely important

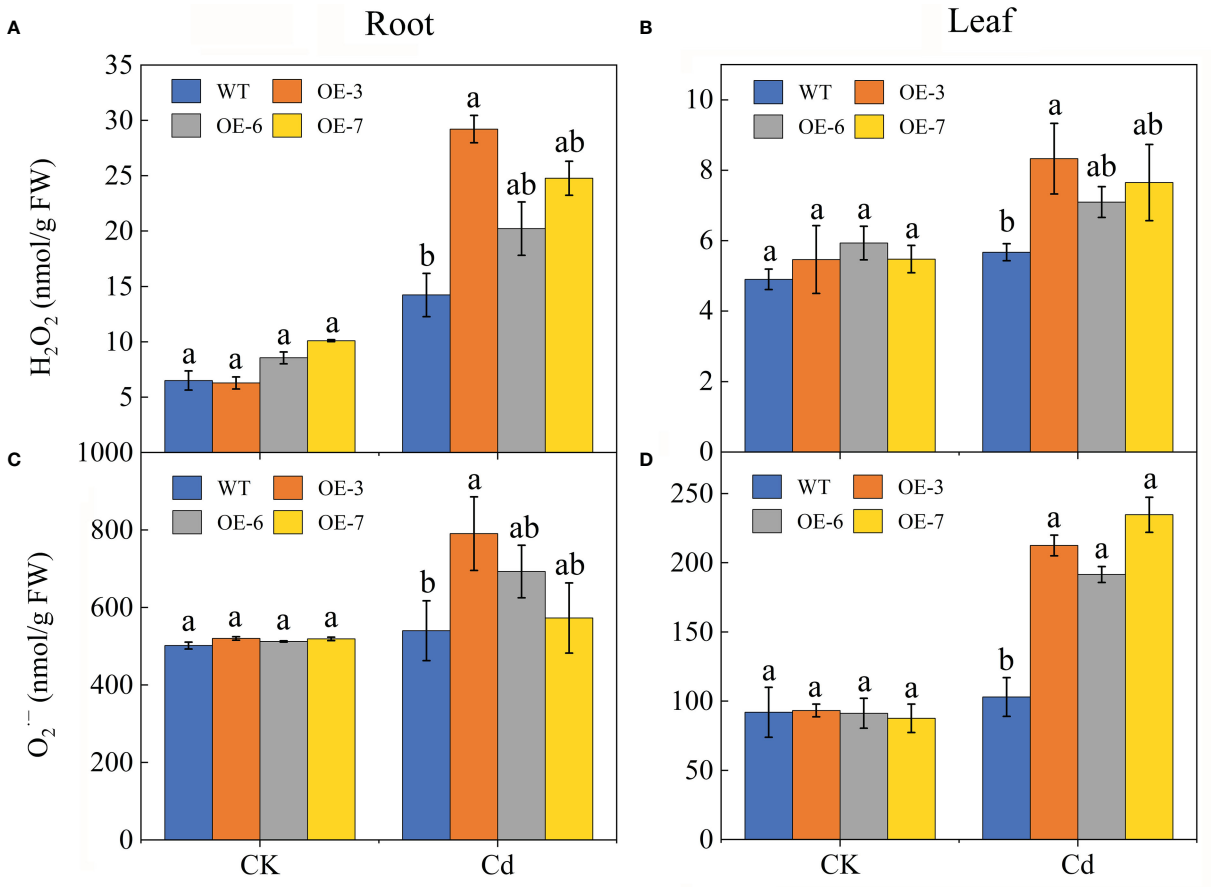

FIGURE 5
Effect of Cd stress on the ROS contents of the WT and *SpCTP3*-overexpressing transgenic poplar roots and leaves. **(A)** Root H_2O_2 concentrations. **(B)** Leaf H_2O_2 concentrations. **(C)** Root O_2^- concentrations. **(D)** Leaf O_2^- concentrations. Data are presented as the mean ± SD of three independent replicates. Different letters above bars indicate significant differences among treatments ($p < 0.05$).

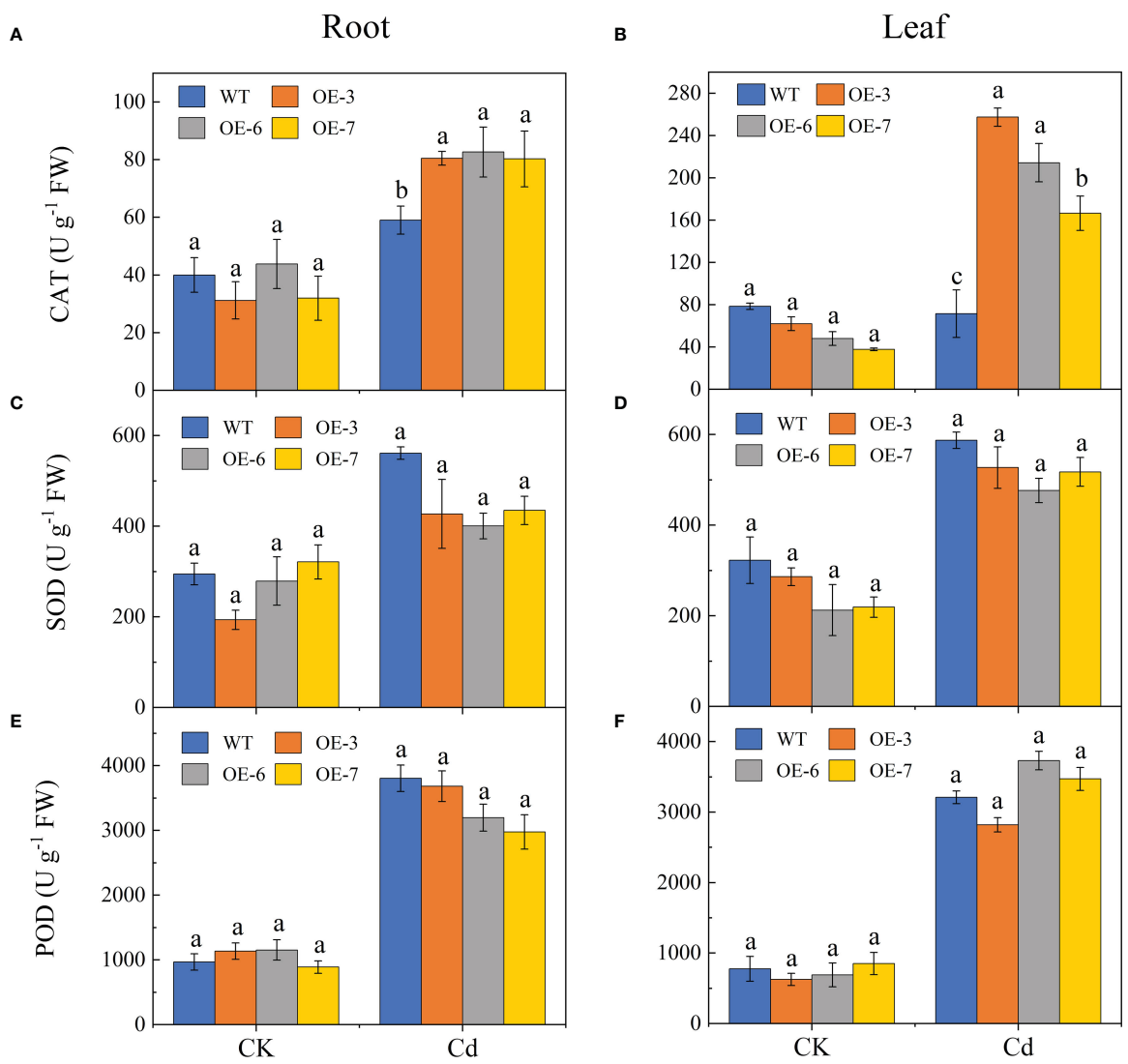

FIGURE 6
Effect of Cd stress on the antioxidant enzyme activities of the WT and *SpCTP3*-overexpressing poplar roots and leaves. **(A)** Root CAT activities. **(B)** Leaf CAT activities. **(C)** Root SOD activities. **(D)** Leaf SOD activities. **(E)** Root POD activities. **(F)** Leaf POD activities. Data are presented as the mean ± SD of three independent replicates. Different letters above bars indicate significant differences among treatments ($p < 0.05$).

class of metal ligands that are crucial for the absorption, transport, storage, and detoxification of heavy metals (Long et al., 2003). The proportion of the Cd content in the cell wall of the roots and leaves of the transgenic poplar plants decreased, which was in contrast to the increase in the proportion of the Cd content in the soluble fraction, implying that more Cd ions in cytoplasm need to be immobilized in the form of stable metal chelates/complexes in the transgenic poplar plants than in the WT plants. Accordingly, poplar plants can avoid the harmful effects of Cd stress by decreasing the free Cd concentration in the cytoplasm. In response to the 30-day Cd treatment in this study, the titratable acid content was significantly higher in the transgenic poplar plants than in the WT plants. This indicates that *SpCTP3* is critical for ameliorating the toxicity of Cd in plants.

The chemical form of Cd reflects the degree of migration and the toxicity of Cd (Kudo et al., 2021). Highly mobile inorganic and organic Cd compounds are usually more toxic than Cd_{HAc}, Cd_{HCl}, and Cd_{NaCl} (Wu et al., 2016). In our study, Cd_W was the dominant form in all transgenic lines. Additionally, the Cd_W content was lower in the roots of the transgenic lines than in the WT roots. The Cd_W form of Cd is converted to Cd_{HAc} and Cd_{HCl}. However, Cd_{HAc} is associated with Cd uptake, transport, and detoxification (Qiu et al., 2011). It is also indicative of the adaptive response of plants to an exposure to stress. Cd_W extracted as free inorganic Cd, and these free Cd^{2+} are not only easily localized in the organelles, but it is also transported to the above-ground tissues. Our analysis of leaves showed that Cd_W was more abundant in the transgenic lines than in the WT plants, indicating that the transgenic lines had considerably more free Cd^{2+} (Xin et al., 2017). The Cd content as well as the translocation factor were higher in the transgenic lines than in the WT plants, which is consistent with the results of a recent study (Lai et al., 2021). In the WT control, the proportion of Cd_{NaCl} increased, indicative of the increase in the binding between Cd and pectin or protein. Therefore, the leaf cell wall Cd content was higher for the WT plants than for the transgenic lines. Both Cd_{HAc} and Cd_{HCl} are mainly present in the cell wall and vesicles (Jiang et al., 2007). In the current

10.3389/fpls.2023.1111789

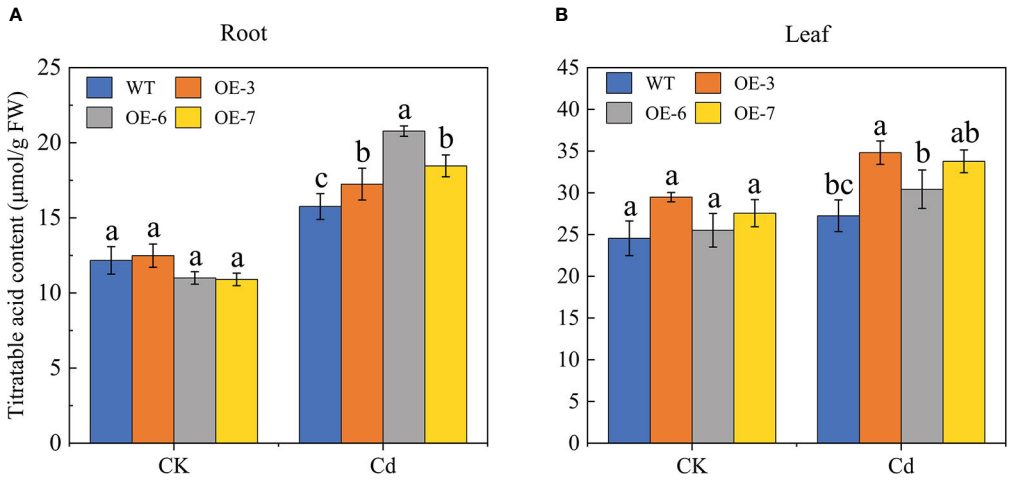

FIGURE 7
Titratable acid contents of the WT and *SpCTP3*-overexpressing transgenic poplar roots and leaves treated with 100 μmol·L^{-1} Cd for 30 days. **(A)** Root titratable acid contents. **(B)** Leaf titratable acid contents. Data are presented as the mean ± SD of three independent replicates. Different letters above bars indicate significant differences among treatments (p< 0.05).

study, Cd_{HAc} and Cd_{HCl} contents were higher in the transgenic lines than in the WT plants, which corresponds to the subcellular distribution of Cd. In summary, the conversion of Cd to Cd_{HAc}, Cd_{HCl}, and Cd_{NaCl} is an important mechanism related to the Cd uptake, translocation, and detoxification in plants.

4.2 *SpCTP3* induced oxidation reaction under cadmium treatment

Plants take up heavy metals from the soil primarily through their roots. Therefore, determining the Cd uptake and efflux from the roots is important for measuring plant Cd accumulation. Noninvasive micro-test techniques can measure real-time ion transport changes in living plant and animal tissues, cells, and internal/external environments. Our NMT analysis revealed that the Cd in-flow rate was significantly higher for the transgenic roots than for the WT roots. The overexpression of *SpCTP3* promoted the influx of Cd in root cells and the accumulation of Cd, indicating that the roots of the transgenic lines had a greater Cd uptake capacity than the WT roots, which is consistent with the findings of an earlier study by Zhang et al. (2021).

In our study, *SpCTP3* was induced to be expressed by the Cd treatment and Cd accumulation was increased in the transgenic lines. Then ROS levels were significantly elevated, which induced the up-regulated expression of *SpCTP3*, thereby promoting ROS detoxification. This is one of the reasons for the increased antioxidant enzyme activities in the *SpCTP3*-overexpressing

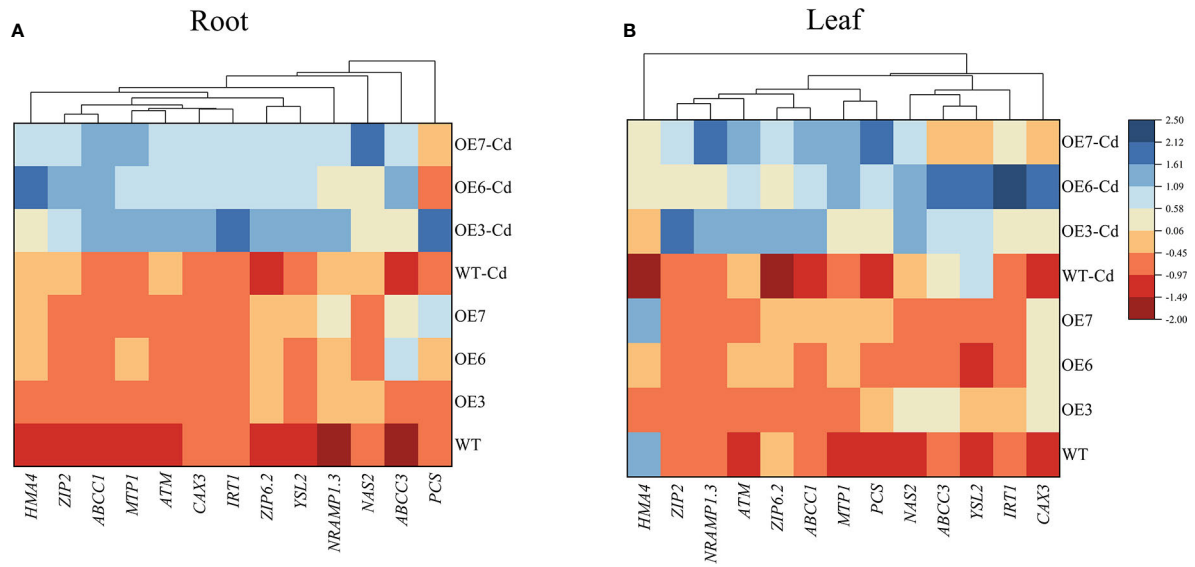

FIGURE 8
Expression levels of key transporter genes in the Cd-treated roots and leaves of WT and transgenic poplar lines treated with 0 or 100 μmol·L^{-1} Cd^{2+} for 30 days. **(A)** Root gene expression levels. **(B)** Leaf gene expression levels. Three biological replicates were analyzed. Red and blue respectively indicate negative and positive Z-scores for the gene expression levels.

transgenic lines. In addition, Cd induced the accumulation of ROS in the roots and leaves, ultimately resulting in oxidative stress, which is in accordance with the findings of recent studies involving other plant materials (Bari et al., 2019; Zhang et al., 2020a). In the current study, Cd stress induced the excessive accumulation of O_2^- in the roots and leaves. Moreover, the H_2O_2 content increased as the treatment duration increased. To protect against excessive ROS, plants employ a complex array of antioxidant defense mechanisms to prevent or mitigate the oxidative damage caused by abiotic stresses (Shafi et al., 2022). Because they are signaling compounds, the accumulation of H_2O_2 and O_2^- may increase the activities of CAT, SOD, POD, and other enzymes during plant responses to Cd stress (Wrzaczek et al., 2013). Superoxide dismutase activity is positively correlated with the intracellular ROS level within a certain range (Zhou et al., 2021). Under stress conditions, an increase in the ROS content increases the activities of SOD and other antioxidant enzymes (Gupta et al., 2017). In addition, SOD converts superoxide radicals into less toxic substances in reactions that produce H_2O_2 (Fujita and Hasanuzzaman, 2022). This may explain the observed accumulation of H_2O_2 in the transgenic poplar lines. Subsequently, CAT and POD are activated as H_2O_2 scavengers to maintain plant redox homeostasis (Tadjouri et al., 2022). In our study, the *SpCTP3*-overexpressing transgenic lines had significantly elevated CAT and POD activities after the Cd treatment, and the CAT activities were significantly higher in the Cd-treated transgenic lines than in the WT plants (Figure 6). Similarly, Cd stress reportedly causes the SOD, POD, and CAT activities in the above-ground parts of rice plants to increase to some extent to limit the toxic effects of Cd (Afzal et al., 2018). An exposure to Cd stress can significantly increase SOD, CAT, APX, and POD activities in marigold (*Calendula calypso*) by 150%, 79%, 97%, and 60%, respectively, leading to the conversion of H_2O_2 to non-toxic oxygen and water (Farooq et al., 2020).

4.3 *SpCTP3* overexpression enhanced Cd transport by up-regulating the expression of transporter genes

The physiological process leading to the accumulation of Cd in above-ground plant parts is divided into the following three stages: root

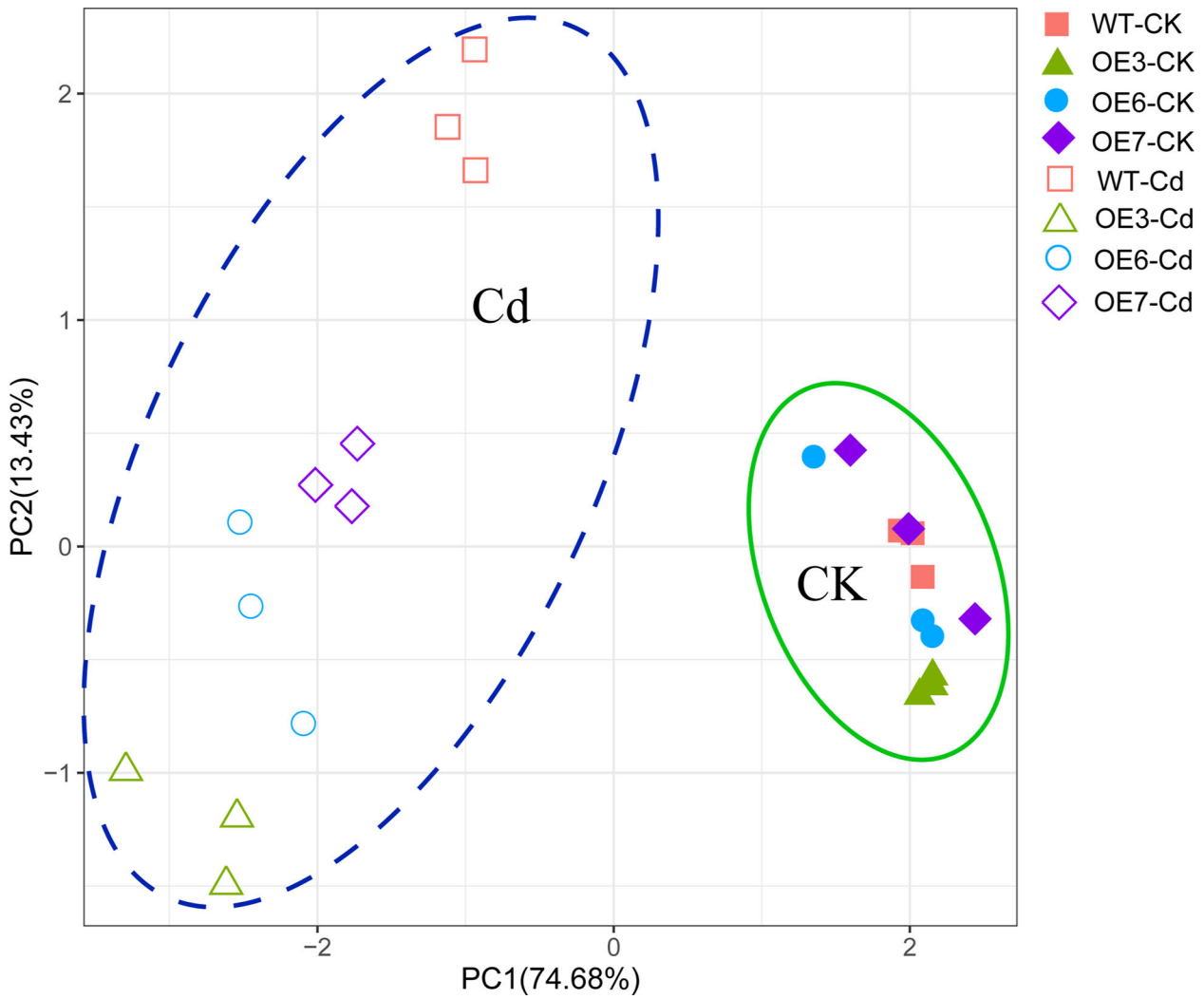

FIGURE 9
Principal component analysis plots of the Cd concentrations and ROS, antioxidant, and titratable acid contents in the roots and leaves of WT and transgenic plants.

cell absorption; ectoplastic pathway-, symplast pathway-, and apoplast pathway-mediated transport; and above-ground accumulation (Uraguchi et al., 2009). Cadmium is transported to the above-ground tissues *via* numerous transporter proteins. In plants, the NRAMP proteins form one of the heavy metal transporter families in monocotyledons and dicotyledons (Ishida and Corcino, 2022). Their functions have been demonstrated in rice (Chang et al., 2020), poplar (Chen et al., 2019), and other plants (Li et al., 2021).

The ability of roots to absorb Cd is the decisive factor influencing the accumulation of Cd in plant shoots (Chaney, 2015). The overexpression of the *S. alfredii SaNRAMP1H* gene significantly increases the Cd contents of tobacco plants (above-ground and below-ground parts), implying that *SaNRAMP1H* promotes Cd uptake and accumulation (Zhang et al., 2020). The ZIP family proteins also function as heavy metal transporters. A previous study showed that Cd^{2+} can enter plant root cells through the ZIP transporter, which regulates Cd uptake, sequestration, and translocation (Ma et al., 2014). In addition, the overexpression of the *Vicia sativa VsIRT1* gene in *A. thaliana* enhances the transport and accumulation of Cd (Zhang et al., 2020b). In poplar, *NRAMP1.3*, *ZIP2*, and *ZIP6.2* encode plasma membrane proteins that control the entry of Cd^{2+} into root cells. In the current study, the Cd treatment up-regulated the *NRAMP1*, *ZIP2*, and *ZIP6.2* expression levels and increased the cytoplasmic Cd content in the transgenic lines; the Cd content was higher in the transgenic lines than in the WT plants (Figure 8).

Cytosolic Cd^{2+} may bind to phytochelatins (PCs), which are synthesized from glutathione in a reaction catalyzed by PC synthase (PCS) (Liu et al., 2021). The generated PC–Cd complex can be transported to vesicles *via* ABC transporters (e.g., ABCC1 and ABCC2) (Feng et al., 2020). Cytoplasmic Cd^{2+} may also be transported into vesicles *via MTP1*, which is located in the vesicle membrane (Singh et al., 2021). In poplar, *PCS*, *ABCC1*, and *MTP1* are differentially expressed in response to Cd^{2+}. In the present study, *PCS*, *ABCC1*, and *MTP1* expression levels increased 3.7-fold, 7.4-fold, and 16.4-fold, respectively, in the Cd-treated transgenic poplar plants. Earlier research confirmed *HMA4* is localized to the plasma membrane, wherein it helps export divalent cations (e.g., Cd^{2+}/Zn^{2+}) from the cytoplasm and facilitates their transport into the xylem (He et al., 2015; Wang et al., 2020). A recent study indicated *HMA4* is responsible for the transport of Cd^{2+} through the central cylinder and xylem (Wiyono et al., 2021). In the root system, *HMA4* expression increased significantly in the transgenic lines exposed to Cd stress, which increased the transport of Cd from the roots to the above-ground parts. Moreover, *HMA4* expression was up-regulated in the roots, but not in the leaves. These results suggest that the substantial accumulation of Cd in the transgenic lines may have been due to enhanced heavy metal transport.

5 Conclusion

Transgenic poplar plants overexpressing *SpCTP3* accumulated more Cd in the above-ground tissues than the WT plants, likely because of changes to Cd distribution and chemical forms. The transgenic poplar lines also had a higher net influx of Cd^{2+} into the roots than the WT controls. Consistent with this observation, the expression levels of transporter genes (e.g., *ABCC1*, *MTP1*, and *ZIP6.2*) involved in Cd^{2+} transport and detoxification, were higher in the transgenic roots and leaves than in the WT roots and leaves after the Cd^{2+} treatment. Moreover, in response to the exposure to Cd stress, the $O_2^{\cdot-}$, H_2O_2, and titratable acid concentrations in the roots and leaves were higher for the transgenic lines than for the WT plants. These findings indicate that the overexpression of *SpCTP3* promoted the accumulation of Cd by increasing the organic acid content, up-regulating the expression of key transporter genes, and regulating oxidative homeostasis. The results of this study provide a theoretical basis for improving plant characteristics *via SpCTP3* expression to increase the utility of poplar plants for remediating Cd-contaminated soil.

Data availability statement

The original contributions presented in the study are included in the article/Supplementary Material. Further inquiries can be directed to the corresponding authors.

Author contributions

XH, SL and RZ designed the experiments. SL performed the experiments and conducted the data. SL and XH wrote the manuscript. XH contributed to manuscript revision. MY, XL, WQ, JX and HL analyzed the data. All authors contributed to the article and approved the submitted version.

Funding

This work was supported by National Key Research and Development Program of China (No 2021YFD2200201) and National Nonprofit Institute Research Grant of CAF (No. RISFZ-2021-01). The authors declared no competing financial interests.

Conflict of interest

The authors declare that the research was conducted in the absence of any commercial or financial relationships that could be construed as a potential conflict of interest.

Publisher's note

All claims expressed in this article are solely those of the authors and do not necessarily represent those of their affiliated organizations, or those of the publisher, the editors and the reviewers. Any product that may be evaluated in this article, or claim that may be made by its manufacturer, is not guaranteed or endorsed by the publisher.

Supplementary material

The Supplementary Material for this article can be found online at: https://www.frontiersin.org/articles/10.3389/fpls.2023.1111789/full#supplementary-material

References

Afzal, J., Hu, C., Imtiaz, M., Elyamine, A. M., Rana, M. S., Imran, M., et al. (2018). Cadmium tolerance in rice cultivars associated with antioxidant enzymes activities and Fe/Zn concentrations. *Int. J. Environ. Sci. Technol.* 16, 4241–4252. doi: 10.1007/s13762-018-2018-y

Akbari, M., Katam, R., Husain, R., Farajpour, M., and Mahna, N. (2020). Sodium chloride induced stress responses of antioxidative activities in leaves and roots of pistachio rootstock. *Biomolecules* 10, 189. doi: 10.3390/biom10020189

Alexieva, V., Sergiev, I., Mapelli, S., and Karanov, E. (2001). The effect of drought and ultraviolet radiation on growth and stress markers in pea and wheat. *Plant Cell Environ.* 24, 1337–1344. doi: 10.1046/j.1365-3040.2001.00778.x

Angulo-Bejarano, P. I., Puente-Rivera, J., and Cruz-Ortega, R. (2021). Metal and metalloid toxicity in plants: An overview on molecular aspects. *Plants (Basel)* 10, 635. doi: 10.3390/plants10040635

Bari, M. A., Akther, M. S., Reza, M. A., and Kabir, A. H. (2019). Cadmium tolerance is associated with the root-driven coordination of cadmium sequestration, iron regulation, and ROS scavenging in rice. *Plant Physiol. Biochem.* 136, 22–33. doi: 10.1016/j.plaphy.2019.01.007

Chai, H., Guo, J., Zhong, Y., Hsu, C. C., Zou, C., Wang, P., et al. (2020). The plasma-membrane polyamine transporter PUT3 is regulated by the Na^+/H^+ antiporter SOS1 and protein kinase SOS2. *New Phytol.* 226, 785–797. doi: 10.1111/nph.16407

Chaney, R. L. (2015). How does contamination of rice soils with cd and zn cause high incidence of human cd disease in subsistence rice farmers. *Curr. pollut. Rep.* 1, 13–22. doi: 10.1007/s40726-015-0002-4

Chang, J., Huang, S., Yamaji, N., Zhang, W., Ma, J., Zhao, F., et al. (2020). *OsNRAMP1* transporter contributes to cadmium and manganese uptake in rice. *Plant Cell Environ.* 43, 13843. doi: 10.1111/pce.13843

Chen, S., Han, X., Fang, J., Lu, Z., and Qiu, W. (2017). *Sedum alfredii SaNramp6* metal transporter contributes to cadmium accumulation in transgenic *Arabidopsis thaliana*. *Sci. Rep. Uk* 7, 13318. doi: 10.1038/s41598-017-13463-4

Chen, H., Wang, Y., Yang, H., Zeng, Q., and Liu, Y. (2019). *NRAMP1* promotes iron uptake at the late stage of iron deficiency in poplars. *Tree Physiol.* 39, 1235–1250. doi: 10.1093/treephys/tpz055

Cui, X., Mao, P., Sun, S., Huang, R., Fan, Y., Li, Y., et al. (2021). Phytoremediation of cadmium contaminated soils by amaranthus hypochondriacus l.: The effects of soil properties highlighting cation exchange capacity. *Chemosphere* 283, 131067. doi: 10.1016/j.chemosphere.2021.131067

Dai, L., Li, J., Harmens, H., Zheng, X., and Zhang, C. (2020). Melatonin enhances drought resistance by regulating leaf stomatal behaviour, root growth and catalase activity in two contrasting rapeseed (*Brassica napus* l.) genotypes. *Plant Physiol. Biochem.* 149, 86–95. doi: 10.1016/j.plaphy.2020.01.039

Dineshkumar, M., Sivalingam, A., and Thirumarimurugan, M. (2019). Phytoremediation potential of bacopa monnieri in the removal of heavy metals. *J. Environ. Biol.* 40, 753–757. doi: 10.22438/jeb/40/4(SI)/JEB_11

Dvorak, P., Krasylenko, Y., Zeiner, A., Samaj, J., and Takac, T. (2020). Signaling toward reactive oxygen species-scavenging enzymes in plants. *Front. Plant Sci.* 11. doi: 10.3389/fpls.2020.618835

Farooq, A., Nadeem, M., Abbas, G., Shabbir, A., Khalid, M. S., Javeed, H. M. R., et al. (2020). Cadmium partitioning, physiological and oxidative stress responses in marigold (*Calendula calypso*) grown on contaminated soil: Implications for phytoremediation. *Bull. Environ. Contam Toxicol.* 105, 270–276. doi: 10.1007/s00128-020-02934-6

Feng, T., He, X., Zhuo, R., Qiao, G., Han, X., Qiu, W., et al. (2020). Identification and functional characterization of ABCC transporters for cd tolerance and accumulation in *Sedum alfredii* hance. *Sci. Rep.* 10, 20928. doi: 10.1038/s41598-020-78018-6

Feng, Y., Wu, Y., Zhang, J., Meng, Q., Wang, Q., Ma, L., et al. (2018). Ectopic expression of *SaNRAMP3* from *Sedum alfredii* enhanced cadmium root-to-shoot transport in *Brassica juncea*. *Ecotoxicol Environ. Saf.* 156, 279–286. doi: 10.1016/j.ecoenv.2018.03.031

Fujita, M., and Hasanuzzaman, M. (2022). Approaches to enhancing antioxidant defense in plants. *Antioxidants* 11, 925. doi: 10.3390/antiox11050925

Fu, Z., and Xi, S. (2020). The effects of heavy metals on human metabolism. *Toxicol. Mech. Methods* 30, 167–176. doi: 10.1080/15376516.2019.1701594

Gupta, D. K., Pena, L. B., Romero Puertas, M. C., Hernández, A., Inouhe, M., Sandalio, L. M., et al. (2017). NADPH oxidases differentially regulate ROS metabolism and nutrient uptake under cadmium toxicity. *Plant Cell Environ.* 40, 509–526. doi: 10.1111/pce.12711

Haghighi, M., Kafi, M., and Khoshgoftarmanesh, A. (2013). Effect of humic acid application on cadmium accumulation by lettuce leaves. *J. Plant Nutr.* 36 (10), 1521–1532. doi: 10.1080/01904167.2013.799182

Hall, J. L. (2002). Cellular mechanisms for heavy metal detoxification and tolerance. *J. Exp. Bot.* 53, 1–11. doi: 10.1093/jexbot/53.366.1

Hamid, Y., Tang, L., Hussain, B., Usman, M., Lin, Q., Rashid, M. S., et al. (2020). Organic soil additives for the remediation of cadmium contaminated soils and their impact on the soil-plant system: A review. *Sci. Total Environ.* 707, 136121. doi: 10.1016/j.scitotenv.2019.136121

Han, X., Zhang, Y., Yu, M., Zhang, J., Xu, D., Lu, Z., et al. (2020). Transporters and ascorbate-glutathione metabolism for differential cadmium accumulation and tolerance in two contrasting willow genotypes. *Tree Physiol.* 40, 1126–1142. doi: 10.1093/treephys/tpaa029

He, J., Li, H., Ma, C., Zhang, Y., Polle, A., Rennenberg, H., et al. (2015). Overexpression of bacterial gamma-glutamylcysteine synthetase mediates changes in cadmium influx, allocation and detoxification in poplar. *New Phytol.* 205, 240–254. doi: 10.1111/nph.13013

Huo, Y., Hu, H., Peng, S., and Chen, Q. (2009). Contents and changes of organic acid in sand pears from different germplasm resources. *Scientia Agricultura Sin.* 42 (01), 216–223. doi: 10.3864/j.issn.0578-1752.2009.01.027

Ishida, J. K., and Corcino, D. (2022). Role of natural resistance-associated macrophage proteins in metal ion transport in plants. *Cation Transporters Plants* chapter 18, 337–356. doi: 10.1016/B978-0-323-85790-1.00003-8

Jiang, Y., Han, J., Xue, W., and Wang, J. (2021). Overexpression of *SmZIP* plays important roles in cd accumulation and translocation, subcellular distribution, and chemical forms in transgenic tobacco under cd stress. *Ecotoxicol Environ. Saf.* 214, 112097. doi: 10.1016/j.ecoenv.2021.112097

Jiang, H., Yang, J., and Zhang, J. (2007). Effects of external phosphorus on the cell ultrastructure and the chlorophyll content of maize under cadmium and zinc stress. *Environ. pollut.* 147, 750–756. doi: 10.1016/j.envpol.2006.09.006

Jia, H., Yin, Z., Xuan, D., Lian, W., Han, D., Zhu, Z., et al. (2022). Mutation of *NtNRAMP3* improves cadmium tolerance and its accumulation in tobacco leaves by regulating the subcellular distribution of cadmium. *J. Hazard Mater* 432, 128701. doi: 10.1016/j.jhazmat.2022.128701

Jing, X., Zhou, M., Nie, X., Zhang, L., and Chen, K. (2020). *OsGSTU6* contributes to cadmium stress tolerance in rice by involving in intracellular ROS homeostasis. *J. Plant Growth Regul.* 2021, 945–61. doi: 10.1007/s00344-020-10148-7

Kudo, H., Inoue, C., and Sugawara, K. (2021). Effects of growth stage and cd chemical form on cd and zn accumulation in *Arabidopsis halleri* ssp. gemmifera. *Int. J. Environ. Res. Public Health* 18, 4214. doi: 10.3390/ijerph18084214

Lai, J., Liu, Z., Li, C., and Luo, X. (2021). Analysis of accumulation and phytotoxicity mechanism of uranium and cadmium in two sweet potato cultivars. *J. Hazard Mater* 409, 124997. doi: 10.1016/j.jhazmat.2020.124997

Li, C., Dang, F., Cang, L., Zhou, C., and Zhou, D. (2014). Integration of metal chemical forms and subcellular partitioning to understand metal toxicity in two lettuce (*Lactuca sativa* l.) cultivars. *Plant Soil* 384, 201–212. doi: 10.1007/s11104-014-2194-6

Li, J., Duan, Y., Han, Z., Shang, X., Zhang, K., Zou, Z., et al. (2021). Genome-wide identification and expression analysis of the NRAMP family genes in tea plant (*Camellia sinensis*). *Plants (Basel)* 10, 1055. doi: 10.3390/plants10061055

Li, Z., Han, X., Song, X., Zhang, Y., Jiang, J., Han, Q., et al. (2017). Overexpressing the *Sedum alfredii* Cu/Zn superoxide dismutase increased resistance to oxidative stress in transgenic *Arabidopsis*. *Front. Plant Sci.* 8. doi: 10.3389/fpls.2017.01010

Li, X., Li, B., Zheng, Y., Luo, L., Qin, X., Yang, Y., et al. (2022). Physiological and rhizospheric response characteristics to cadmium of a newly identified cadmium accumulator *Coreopsis grandiflora* hogg. (Asteraceae). *Ecotoxicol Environ. Saf.* 241, 113739. doi: 10.1016/j.ecoenv.2022.113739

Lin, Y., and Aarts, M. (2012). The molecular mechanism of zinc and cadmium stress response in plants. *Cell Mol. Life Sci.* 69, 3187–3206. doi: 10.1007/s00018-012-1089-z

Liu, M., He, X., Feng, T., Zhuo, R., Qiu, W., Han, X., et al. (2019). cDNA library for mining functional genes in *sedum alfredii* hance related to cadmium tolerance and characterization of the roles of a novel *SaCTP2* gene in enhancing cadmium hyperaccumulation. *Environ. Sci. Technol.* 53, 10926–10940. doi: 10.1021/acs.est.9b03237

Liu, J., Zhang, J., Kim, S. H., Lee, H. S., Marinoia, E., Song, W., et al. (2021). Characterization of *Brassica rapa* metallothionein and phytochelatin synthase genes potentially involved in heavy metal detoxification. *PloS One* 16, e252899. doi: 10.1371/journal.pone.0252899

Li, C., Yang, X., Xu, Y., Li, L., and Wang, Y. (2018). Cadmium detoxification induced by salt stress improves cadmium tolerance of multi-stress-tolerant *Pichia kudriavzevii*. *Environ. pollut.* 242, 845–854. doi: 10.1016/j.envpol.2018.07.058

Long, X., Yang, X., and Zheng-Qian, Y. (2003). Metal chelators in hyperaccumulator and their application in phytoremedi- ation. *Plant Physiol. Commun.* 39, 71–77. doi: 10.1021/js980090u

Ma, Y., He, J., Ma, C., Luo, J., Li, H., Liu, T., et al. (2014). Ectomycorrhizas with *Paxillus involutus* enhance cadmium uptake and tolerance in *Populus* x *canescens*. *Plant Cell Environ.* 37, 627–642. doi: 10.1111/pce.12183

Meng, X., Li, W., Shen, R., and Lan, P. (2022). Ectopic expression of IMA small peptide genes confers tolerance to cadmium stress in *Arabidopsis* through activating the iron deficiency response. *J. Hazard Mater* 422, 126913. doi: 10.1016/j.jhazmat.2021.126913

MEP and MLR (2014). *Nationwide soil pollution survey report* (Ministry of Environment Protection and Ministry of Land Resources of the People' s Republic of China).

Ouyang, J., Li, B., Xue, W., Jiang, Y., Li, C., Shang, X., et al. (2019). Cadmium uptake and accumulation, subcellular distribution and chemical forms in young seedlings of *Salix babylonica* l. *Fresenius Environ. Bull.* 28, 3637–3648.

Park, J., Song, W., Ko, D., Eom, Y., and Lee, Y. (2012). The phytochelatin transporters *AtABCC1* and *AtABCC2* mediate tolerance to cadmium and mercury. *Plant J.* 69, 278–288. doi: 10.1111/j.1365-313X.2011.04789.x

Patricio, A. B., María del, C. R. G., Santos, M. E. P., and Montao, Y. A. R. (2018). Effect of foliar copper application on yield and anthocyanin concentration in hibiscus sabdariffa calyces. *Rev. Fac Cienc Agrar* 50 (2), 65–75.

Peng, J., Wang, Y., Ding, G., Ma, H., Zhang, Y., Gong, J., et al. (2017). A pivotal role of cell wall in cadmium accumulation in the crassulaceae hyperaccumulator *Sedum plumbizincicola*. *Mol. Plant* 10, 4. doi: 10.1016/j.molp.2016.12.007

Qiu, Q., Wang, Y., Yang, Z., and Yuan, J. (2011). Effects of phosphorus supplied in soil on subcellular distribution and chemical forms of cadmium in two Chinese flowering cabbage (*Brassica parachinensis* l.) cultivars differing in cadmium accumulation. *Food Chem. Toxicol.* 49, 2260–2267. doi: 10.1016/j.fct.2011.06.024

Rasafi, T. E., Oukarroum, A., Haddioui, A., Song, H., and Rinklebe, J. (2020). Cadmium stress in plants: A critical review of the effects, mechanisms, and tolerance strategies. *Crit. Rev. Environ. Sci. Technol.* doi: 10.1080/10643389.2020.1835435

Raza, A., Habib, M., Kakavand, S. N., Zahid, Z., Zahra, N., Sharif, R., et al. (2020). Phytoremediation of cadmium: Physiological, biochemical, and molecular mechanisms. *Biol. (Basel)* 9, 177. doi: 10.3390/biology9070177

Rehman, M. Z. U., Zafar, M., Waris, A. A., Rizwan, M., Shafaqat Ali, M. S., Sabir, M. , et al. (2020). Residual effects of frequently available organic amendments on cadmium bioavailability and accumulation in wheat - ScienceDirect. *Chemosphere* 244, 125548. doi: 10.1016/j.chemosphere.2019.125548

Shafi, A., Hassan, F., and Khanday, F. A. (2022). "Reactive oxygen and nitrogen species: Oxidative damage and antioxidative defense mechanism in plants under abiotic stress," (Apple Academic Press), 71–99.

Shamelashvili, K., Svenlana, O., and Shatorna, V. (2020). The toxic effect of cadmium on a living organism and its detoxification by zinc ions. *Modern Sci. — Moderní Věda* 3, 150–157.

Shi, W., Li, J., Kan, D., Yu, W., and Chen, X. (2022). Sulfur metabolism, organic acid accumulation and phytohormone regulation are crucial physiological processes modulating the different tolerance to pb stress of two contrasting poplars. *Tree Physiol.* 9), 9. doi: 10.1093/treephys/tpac033

Singh, R., Kesavan, A. K., Landi, M., Kaur, S., Thakur, S., Zheng, B., et al. (2020). 5-aminolevulinic acid regulates Krebs cycle, antioxidative system and gene expression in *Brassica juncea* l. *J. Biotechnol.* 323, 283–292. doi: 10.1016/j.jbiotec.2020.09.004

Singh, R., Misra, A. N., and Sharma, P. (2021). Differential responses of thiol metabolism and genes involved in arsenic detoxification in tolerant and sensitive genotypes of bioenergy crop *Ricinus communis*. *Protoplasma* 258, 391–401. doi: 10.1007/s00709-020-01577-y

Singh, P., Singh, I., and Shah, K. (2020). Alterations in antioxidative machinery and growth parameters upon application of nitric oxide donor that reduces detrimental effects of cadmium in rice seedlings with increasing days of growth - ScienceDirect. *South Afr. J. Bot.* 131, 283–294. doi: 10.1016/j.sajb.2020.02.022

Tadjouri, H., Medjedded, H., Nemmiche, S., Chadli, R., and Moulay, M. (2022). Stress response induced by cadmium in soybeans (*Glycine max* l.) and health risk assessment. *Plant Physiol. Rep.*, 1–8. doi: 10.1007/s40502-022-00663-y

Uraguchi, S., Mori, S., Kuramata, M., Kawasaki, A., Arao, T., Ishikawa, S, et al. (2009). Root-to-shoot cd translocation *via* the xylem is the major process determining shoot and grain cadmium accumulation in rice. *J. Exp. Bot.* 60, 2677–2688. doi: 10.1093/jxb/erp119

Viehweger, K. (2014). How plants cope with heavy metals. *Bot. Stud.* 55, 35. doi: 10.1186/1999-3110-55-35

Wang, J., Chen, X., Chu, S., You, Y., and Zhou, P. (2021). Comparative cytology combined with transcriptomic and metabolomic analyses of *Solanum nigrum* l. *J. Hazardous Materials* 423, 127168. doi: 10.1016/j.jhazmat.2021.127168

Wang, H., Chen, W., Sinumvayabo, N., Li, Y., and Zhang, Y. (2020). Phosphorus deficiency induces root proliferation and cd absorption but inhibits cd tolerance and cd translocation in roots of *Populus* × *euramericana*. *Ecotoxicol Environ. Saf.* 204, 111148. doi: 10.1016/j.ecoenv.2020.111148

Wan, X., Lei, M., and Chen, T. (2016). Cost-benefit calculation of phytoremediation technology for heavy-metal-contaminated soil. *Sci. Total Environ.* 563-564, 796–802. doi: 10.1016/j.scitotenv.2015.12.080

Wen, S., Ge, X., Wang, R., Yang, H., Bai, Y., Guo, Y., et al. (2022). An efficient agrobacterium-mediated transformation method for hybrid poplar 84K (*Populus alba*× *P. glandulosa*) using calli as explants. *Int. J. Mol. Sci.* 23, 2216. doi: 10.3390/ijms23042216

Wiyono, C., Inoue, C., and Chien, M. F. (2021). *HMA4* and *IRT3* as indicators accounting for different responses to cd and zn by hyperaccumulator *Arabidopsis halleri* ssp. gemmifera. *Plant Stress* 2, 100042. doi: 10.1016/j.stress.2021.100042

Wrzaczek, M., Brosché, M., and Kangasj Rvi, J. (2013). ROS signaling loops - production, perception, regulation. *Curr. Opin. Plant Biol.* 16, 575–582. doi: 10.1016/j.pbi.2013.07.002

Wu, H., Wang, J., Li, B., Ouyang, J., Wang, J., Shi, Q., et al. (2016). *Salix matsudana* koidz tolerance mechanisms to cadmium: Uptake and accumulation, subcellular distribution, and chemical forms. *Polish J. Environ. Stud.* 25, 1739–1747. doi: 10.15244/pjoes/62715

Xin, J., and Huang, B. (2014). Subcellular distribution and chemical forms of cadmium in two hot pepper cultivars differing in cadmium accumulation. *J. Agric. Food Chem.* 62, 508–515. doi: 10.1021/jf4044524

Xin, J., Zhao, X., Tan, Q., Sun, X., and Hu, C. (2017). Comparison of cadmium absorption, translocation, subcellular distribution and chemical forms between two radish cultivars (*Raphanus sativus* l.). *Ecotoxicol Environ. Saf.* 145, 258–265. doi: 10.1016/j.ecoenv.2017.07.042

Yaashikaa, P. R., Kumar, P. S., Jeevanantham, S., and Saravanan, R. (2022). A review on bioremediation approach for heavy metal detoxification and accumulation in plants. *Environ. pollut.* 301, 119035. doi: 10.1016/j.envpol.2022.119035

Yang, L., Li, N., Kang, Y., Liu, J., Wang, Y., Sun, H., et al. (2022). Selenium alleviates toxicity in *Amaranthus hypochondriacus* by modulating the synthesis of thiol compounds and the subcellular distribution of cadmium. *Chemosphere* 291, 133108. doi: 10.1016/j.chemosphere.2021.133108

Yazdi, M. E. T. Y. (2021). Bio-indicators in cadmium toxicity: Role of HSP27 and HSP70. *Environ. Sci. pollut. Res. Int.* 28, 26359–26379. doi: 10.1007/s11356-021-13687-y

Yessica, E. Z., Martinez-Nava, G., Reyes-Hinojosa, D., Mendoza-Soto, L., Fernandez-Torres, J., López-Reyes, A., et al. (2020). Impact of cadmium toxicity on cartilage loss in a 3D *in vitro* model. *Environ. Toxicol. Pharmacol.* 74, 103307. doi: 10.1016/j.etap.2019.103307

Yue, X., Song, J., Fang, B., Wang, L., Zou, J., Su, N., et al. (2021). *BcNRAMP1* promotes the absorption of cadmium and manganese in *Arabidopsis*. *Chemosphere* 283, 131113. doi: 10.1016/j.chemosphere.2021.131113

Zhang, Y., Chao, J., Li, X., Zhang, C., Khan, R., Du, S., et al. (2021). Comparative transcriptome combined with biochemical and physiological analyses provide new insights toward cadmium accumulation with two contrasting *Nicotiana* species. *Physiol. Plant* 173, 369–383. doi: 10.1111/ppl.13431

Zhang, H., Li, X., Xu, Z., Wang, Y., Teng, Z., An, M., et al. (2020). Toxic effects of heavy metals Pb and cd on mulberry (*Morus alba* l.) seedling leaves: Photosynthetic function and reactive oxygen species (ROS) metabolism responses. *Ecotoxicol Environ. Saf.* 195, 110469. doi: 10.1016/j.ecoenv.2020.110469

Zhang, X., Li, X., Zhang, X., Li, X., Tang, L., Guo, Y., et al. (2020b). The root iron transporter 1 governs cadmium uptake in *Vicia sativa* roots. *J. Hazard Mater* 398, 122873. doi: 10.1016/j.jhazmat.2020.122873

Zhang, L., Wu, J., Tang, Z., Huang, X., Wang, X., Wang, X. , et al. (2019). Variation in the *BrHMA3* coding region controls natural variation in cadmium accumulation in *Brassica rapa* vegetables. *J. Exp. Bot.* 70, 5865–5878. doi: 10.1093/jxb/erz310

Zhang, X., Yang, Z., Li, Z., Zhang, F., and Hao, L. (2020a). Effects of drought stress on physiology and antioxidative activity in two varieties of *Cynanchum thesioides*. *Braz. J. Bot.* 43, 1–10. doi: 10.1007/s40415-019-00573-8

Zhang, K., Yuan, J., Kong, W., and Yang, Z. (2013). Genotype variations in cadmium and lead accumulations of leafy lettuce (*Lactuca sativa* l.) and screening for pollution-safe cultivars for food safety. *Environ. Sci-Proc Imp* 15 (6), 1245–1255. doi: 10.1039/C3EM00158J

Zhang, J., Zhang, M., Song, H., Zhao, J., and Yang, X. (2020). A novel plasma membrane-based NRAMP transporter contributes to cd and zn hyperaccumulation in *Sedum alfredii* hance. *Environ. Exp. Bot.* 176, 104121. doi: 10.1016/j.envexpbot.2020.104121

Zhou, Y., Wang, Y., and Inyang, A. I. (2021). Ecophysiological differences between five mangrove seedlings under heavy metal stress. *Mar. pollut. Bull.* 172, 112900. doi: 10.1016/j.marpolbul.2021.112900

Zhu, Y., Du, W., Fang, X., Zhang, L., and Jin, C. (2020). Knockdown of BTS may provide a new strategy to improve cadmium-phytoremediation efficiency by improving iron status in plants. *J. Hazard Mater* 384, 121473. doi: 10.1016/j.jhazmat.2019.121473

frontiers | Frontiers in Plant Science

TYPE Original Research
PUBLISHED 15 February 2023
DOI 10.3389/fpls.2023.1097265

Check for updates

OPEN ACCESS

EDITED BY
Diaa Abd El Moneim,
Arish University, Egypt

REVIEWED BY
Yuri Shavrukov,
Flinders University, Australia
Fei Zhou,
Huazhong Agricultural University, China

*CORRESPONDENCE
Yuehui Tang
yhtang2005@163.com

SPECIALTY SECTION
This article was submitted to Plant Abiotic Stress, a section of the journal Frontiers in Plant Science

RECEIVED 13 November 2022
ACCEPTED 03 February 2023
PUBLISHED 15 February 2023

CITATION
Tang Y, Peng J, Lin J, Zhang M, Tian Y, Shang Y, Chen S, Bao X and Wang Q (2023) A HD-Zip I transcription factor from physic nut, *JcHDZ21*, confers sensitive to salinity in transgenic Arabidopsis. *Front. Plant Sci.* 14:1097265. doi: 10.3389/fpls.2023.1097265

COPYRIGHT
© 2023 Tang, Peng, Lin, Zhang, Tian, Shang, Chen, Bao and Wang. This is an open-access article distributed under the terms of the Creative Commons Attribution License (CC BY). The use, distribution or reproduction in other forums is permitted, provided the original author(s) and the copyright owner(s) are credited and that the original publication in this journal is cited, in accordance with accepted academic practice. No use, distribution or reproduction is permitted which does not comply with these terms.

A HD-Zip I transcription factor from physic nut, *JcHDZ21*, confers sensitive to salinity in transgenic Arabidopsis

Yuehui Tang[1*], Jingrui Peng[1], Jin Lin[1], Miaomiao Zhang[1], Yun Tian[1], Yaqian Shang[1], Shuying Chen[1], Xinxin Bao[2] and Qiyuan Wang[1]

[1]College of Life Science and Agronomy, Zhoukou Normal University, Henan, Zhoukou, China, [2]School of Journalism and Communication, Zhoukou Normal University, Henan, Zhoukou, China

HD-Zip is a plant-specific transcription factor that plays an important regulatory role in plant growth and stress response. However, there have been few reports on the functions of members of the physic nut HD-Zip gene family. In this study, we cloned a HD-Zip I family gene from physic nut by RT-PCR, and named *JcHDZ21*. Expression pattern analysis showed that *JcHDZ21* gene had the highest expression in physic nut seeds, and salt stress inhibited the expression of *JcHDZ21* gene. Subcellular localization and transcriptional activity analysis showed that JcHDZ21 protein is localized in the nucleus and has transcriptional activation activity. Salt stress results indicated that *JcHDZ21* transgenic plants were smaller and had more severe leaf yellowing compared to those of the wild type. Physiological indicators showed that transgenic plants had higher electrical conductivity and MDA content, and lower proline and betaine content compared with wild-type plants under salt stress. In addition, the expression of abiotic stress-related genes in *JcHDZ21* transgenic plants was significantly lower than that in wild type under salt stress. Our results showed that ectopic expression of *JcHDZ21* increased the sensitivity of transgenic Arabidopsis to salt stress. This study provides a theoretical basis for the future application of *JcHDZ21* gene in the breeding of physic nut stress-tolerant varieties.

KEYWORDS

HD-Zip gene family, salt stress, *JcHDZ21*, physic nut, arabidopsis

Introduction

Salinity is one of the main abiotic stress factors that limit crop yields. Plants can initiate a series of corresponding stress tolerance mechanisms to resist environmental stress under abiotic stress conditions. During this process, almost all plants showed changes in the expression levels of various functional genes and regulatory protein genes. Among these

genes, transcription factors can improve the tolerance of plants to extreme environmental stress by activating the expression of many downstream stress-resistant genes. The transcription factors related to abiotic stress discovered so far are mainly concentrated in the following gene family members, such as DREB, MYB, HD-Zip, WRKY and NAC (Dubos et al., 2010; Rushton et al., 2010; Harris et al., 2011; Javelle et al., 2011; Thirumalaikumar et al., 2018; Feng et al., 2020).

The HD-Zip family is a type of plant-specific transcription factor that contains a highly conserved homeodomain (HD) and a leucine zipper (LZ) domain (Johannesson et al., 2001). The HD-Zip protein forms a dimer through the LZ domain, and then acts as a transcription factor by combining its HD with a specific DNA sequence (Deng et al., 2002). According to the conservative and structural characteristics of the amino acid sequence, the family can be divided into 4 subfamilies, named HD-Zip I-IV (Henriksson et al., 2005). Most of the HD-Zip proteins related to plant stress response belong to HD-Zip I subfamily, and the expression of this family member is mainly affected by drought, salt, cold and osmotic pressure, and increasing the expression of these genes can change the tolerance of transgenic plants to extreme environmental stress (Harris et al., 2011). For example, overexpression of *ATHB-6* increases drought stress tolerance in transgenic maize by activating the expression of reactive oxygen species-related genes (Jiao et al., 2022), *PsnHDZ63* transgenic plants showed better phenotypic and physiological indicators under salt stress, indicating that increasing the expression of the *PsnHDZ63* gene altered the tolerance of transgenic plants to salt stress (Guo et al., 2021). Overexpression of maize *Zmhdz4* and *Zmhdz10* genes in rice increases the tolerance of transgenic plants to drought and salt stress (Zhang et al., 2012; Zhao et al., 2014). In addition to participating in abiotic stress regulation, HD-Zip family genes also play important roles in plant growth and development (Turchi et al., 2013; Preciado et al., 2022). *ABIG1* plays a role in leaf laminar growth as well as in adaxial-abaxial polarity establishment (Preciado et al., 2022). Overexpression of *ATHB13* affects cotyledon shape by inhibiting lateral expansion of epidermal cells in sugar-treated seedlings (Hanson et al., 2001). *OsHOX1* and *OsHOX28* regulate the local distribution of auxin by reducing endogenous auxin content, thereby regulating the size of the tiller angle (Hu et al., 2020). Although many HD-Zip genes have been cloned from different plants, the physiological and molecular mechanisms by which HD-Zip family genes regulate plant responses to salt stress, especially in salt-tolerant Euphorbiaceae species, need to be further studied.

Physic nut (*Jatropha curcas*), a Euphorbiaceae species, has high salinity tolerance, and rich in oils suitable for production of biodiesel, which is one of the most promising biomass energy plants (Montes and Melchinger, 2016). Although physic nut has strong salt tolerance, the molecular mechanism of how physic nut responds to salt stress tolerance is still unclear. In previous study, we notice that a HD-Zip I family transcription factor, we named *JcHDZ21*, which is strongly repressed expression by salinity stress (Tang et al., 2019). On this basis, we cloned the *JcHDZ21* gene and investigated its function in Arabidopsis. Up-regulation of *JcHDZ21* gene expression increases the sensitivity of transgenic Arabidopsis to salt stress, indicating that *JcHDZ21* acts as a negative regulator in the regulation of plant responses to salt stress. The results provide foundations for exploring roles of *JcHDZ21* gene in responses to salinity stress in physic nut.

Material and methods

Plant material and stress treatment

After the physic nut seeds germinated, the three-week-old physic nut seedlings with uniform growth were divided into three groups for abiotic stress, and each group contained twenty seedlings. Then, the physic nut seedlings in the first and second groups were used to irrigate 1/2 MS nutrient solution containing 150 mM NaCl for salinity stress treatment. After the stress treatment, the fourth leaves of five treatment time points (0 h, 2 h, 4 h, 12 h and 24 h) were selected for RNA extraction and gene expression detection. In addition, the roots, cortex stem, flowers, and leaves of the 3-week-old physic nut seedlings without stress treatment were taken for tissue expression analysis. The material was quickly frozen in liquid nitrogen and stored in a refrigerator at -80°C. The growth conditions of physic nut under normal growth and stress treatment were as follows: 16 h light/8 h dark, and the temperature was controlled at 28°C.

JcHDZ21 protein characterization and sequence alignment analysis

Download the amino acid sequence of Arabidopsis proteins from TAIR database (https://www.arabidopsis.org/). Download the amino acid sequence of *Oryza sativa* L. and *Zea mays* L. proteins from NCBI database (https://www.ncbi.nlm.nih.gov/). SMART online software and NCBI were used to detect the conserved domain of JcHDZ21 protein. We selected HD-Zip I group proteins with positive regulator function in abiotic stress for multiple sequence alignment analysis. Amino acid multiple sequence alignment analysis was performed using the software DNAMAN XL.

Subcellular localization of JcHDZ21 protein

Using physic nut leaf cDNA as a template, the full-length CDS sequence of the *JcHDZ21* gene (with the stop codon removed) was amplified by RT-PCR and verified by sequencing. Then connect the correct gene sequence to the subcellular localization vector to construct pBWA(V)HS-JcHDZ21-GLosgfp fusion expression vector. Finally, the constructed pBWA(V)HS-JcHDZ21-GLosgfp fusion expression vector and empty vector (control vector) were co-transformed into *Arabidopsis* protoplasts by PEG-mediated method. The isolation and extraction of *Arabidopsis* mesophyll protoplasts and the PEG-mediated transient transformation were

carried out according to the method in the previously reported paper (Yoo et al., 2007). Add 100 µL of plasmid DNA to the 100 µL of protoplast suspension. Add 200 µL of PEG4000 solution to the protoplast suspension, store the tube on room temperature for 30 min. Finally, add 1 mL of W5 solution to the mixture, and culture in the dark at 23°C for 16 h, and then the fluorescence was observed under a laser confocal microscope (LSM800, Carl Zeiss).

Transcriptional activity assay

The cDNA sequence of JcHDZ21 was combined with the GAL4 DNA binding domain on the pGBKT7 expression vector to construct the pGBKT7-JcHDZ21 recombinant expression vector. The recombinant expression vector was transferred into Y2HGold yeast competent cells by PEG/LiAc method, and cultured on SD/-Trp solid medium for 3-5 d. Then pick a single colony and inoculate it in SD/-Trp liquid medium. Taking 2.5 uL of pGBKT7-GAL4, pGBKT7, pGBKT7-JcHDZ21 bacterial solution dropwise on SD/-Trp, SD/-Trp/-His/X-a-gal and SD/-Trp/-His/-Ade/X-a-gal plates. Finally, verify transcriptional activity based on colony growth and whether it turns blue.

Construction of plant expression vector and selection of transgenic plants

Using physic nut root cDNA as a template, the full-length cDNA sequence of *JcHDZ21* was amplified by RT-PCR and verified by sequencing. Subsequently, the target gene and plant expression vector were digested by *Kpn* I and *Xba* I. After electrophoresis, gel excision, and recovery of DNA fragments, the target gene was ligated to the binary transformation vector pCAMBIA1301 by T4 DNA ligase, and the target gene was driven by the CaMV 35S promoter. The vector was transformed into *Agrobacterium* strain GV3101, and then we transformed the constructed vector into *Arabidopsis thaliana* (Columbia ecotype) by Agrobacterium-mediated transformation of Arabidopsis using the floral dip method (Zhang et al., 2006). Homozygous plants of the T3 generation were selected in hygromycin-resistant medium. The transgenic Arabidopsis was then identified by GUS staining and RT-PCR techniques. Finally, the effective three transgenic lines were used for subsequent functional analysis.

Analysis of salt tolerance of transgenic Arabidopsis

To avoid mechanical root damage of 4-day-old Arabidopsis seedlings during transferring for salinity treatment, sterile seeds were sown directly into 1/2 MS solid medium containing 100 mM NaCl in petri dishes for salinity stress. Then put them in the growing room to grow at 22 ± 2°C under a 16 h light/8 h dark photoperiod. After 25 days, observing the salt tolerance of wild-type and transgenic plants. Salt stress treatment experiments contained three biological replicates.

Determination of physiological indicators of wild-type and transgenic plants

Seeds of wild-type and transgenic plants were spotted into 1/2 MS solid medium containing 0 and 100 mM NaCl in petri dishes. The leaves of wild-type and transgenic plants growth in control and salt stress conditions for 15 days were taken, washed twice with deionized water, and then the surface water of the leaves was blotted with filter paper. Accurately weigh 0.1 g and cut into filaments and place in a test tube containing 10 mL of deionized water. The test tube was then placed in a vacuum pump for 30 min. After standing at room temperature for 1 h, we used a HANNA 546808 (Italy) conductivity meter to measure the initial conductivity value and named R1. Immediately after heating the test tube in boiling water for 30 min, the running water was cooled to room temperature and shaken well, the conductance value R2 was measured. Calculate the relative conductivity using the following formula: R1/R2×100%. The betaine content was detected by ELISA kit, the specific operation method is shown in the kit instructions. The detection methods of proline and MDA content refer to the papers published by the previous research group (Tang et al., 2019).

RNA isolation and qRT-PCR analysis

Seeds of wild-type and transgenic plants were spotted into 1/2 MS solid medium containing 0 and 100 mM NaCl in petri dishes. Then culture vessels containing the seeds were incubated at 22 ± 2° C under 16/8 h (light/dark) conditions. The leaves of wild-type and transgenic plants growth in control and salt-stressed conditions for 15 days were collected and used for qRT-PCR analysis. Plant RNA extraction kit (Magen, China) was used to extract the total RNA of each tissue in this study, and then the extracted RNA was synthesized into cDNA by TAKARA reverse transcription kit. TB Green® Fast qPCR Mix (TAKARA, Beijing) was used for real-time fluorescence quantitative PCR detection, and the BIO-RAD Mini Opticon fluorescence quantitative analyzer was used for qRT-PCR reaction and analysis. Each reaction contains 100 ng cDNA, primers (10 µmol/L) 0.4 µL, SuperMix 10 µL, PassiveDye 0.4 µL, add ddH_2O to 20 µL. The amplification program was initial denaturation at 94°C for 30 s, denaturation at 94°C for 5 s, annealing at 60°C for 15 s, extension at 72°C for 34 s, 40 cycles. All the above specific operating methods were carried out according to the kit instructions. Physic nut *JcActin* (GenBank Accession JQ806331) and Arabidopsis *Actin2* (GenBank Accession AT3G18780) were used as internal reference genes. Primer Premier 5 was used for the design of the gene-specific qRT-PCR primers. Primer sequences were shown in Supplementary Table 1. The specificity of qRT-PCR amplification was confirmed by melting curve analysis. Then using the $2^{-\Delta\Delta Ct}$ method to calculate the

10.3389/fpls.2023.1097265

relative expression of genes in different samples based on the Ct value of each sample at a specific fluorescence threshold.

Statistical analysis

The SPSS 25.0 software was used for data analysis. Significance analysis was performed using One-Way ANOVA for LSD testing of SPSS 25.0 data processing system (* P<0.05; ** P<0.01).

Results

JcHDZ21 encodes a HD-Zip protein belonging to HD-Zip I subfamily

In order to study the biological function of *JcHDZ21* gene, we cloned the gene by RT-PCR using physic nut leaf cDNA as template. Sequence analysis showed that the full-length open reading frame of *JcHDZ21* was 969 bp, encoding 322 amino acids. SMART analysis revealed that JcHDZ21 contained a highly conserved HD domain and an LZ domain.

We further analyzed the homology between JcHDZ21 and HD-Zip proteins of other species by DNAMAN XL software. Sequence alignment analysis showed that, like the reported HD-Zip proteins, JcHDZ21 also contained the same characteristic regions named homeodomain and leucine zipper domains (Figure 1). Results also showed that many amino acids residues distributed in the N-terminal and C-terminal of HD-Zip protein were variable. Taken together, these results indicated that the different functions of HD-Zip proteins in different species may be attributed to these highly variable amino acid residues.

Expression profile of *JcHDZ21* gene

To study the expression profile of *JcHDZ21* gene, we analyzed the expression of *JcHDZ21* gene in roots, stems and leaves of physic nut at six-leaf stage, flowers and seeds 35 days after pollination by qRT-PCR. The results showed that the expression of *JcHDZ21* gene could be detected in all tissues of physic nut, with the highest expression in seeds, followed by flowers and roots, and the lowest expression in stems (Figure 2A).

In order to analyze the expression characteristics of *JcHDZ21* gene under salt stress, we further detected the expression level of *JcHDZ21* gene under salt stress. The results showed that the expression of *JcHDZ21* under salt stress was significantly lower than that in the control group (Figure 2B). The above results suggest

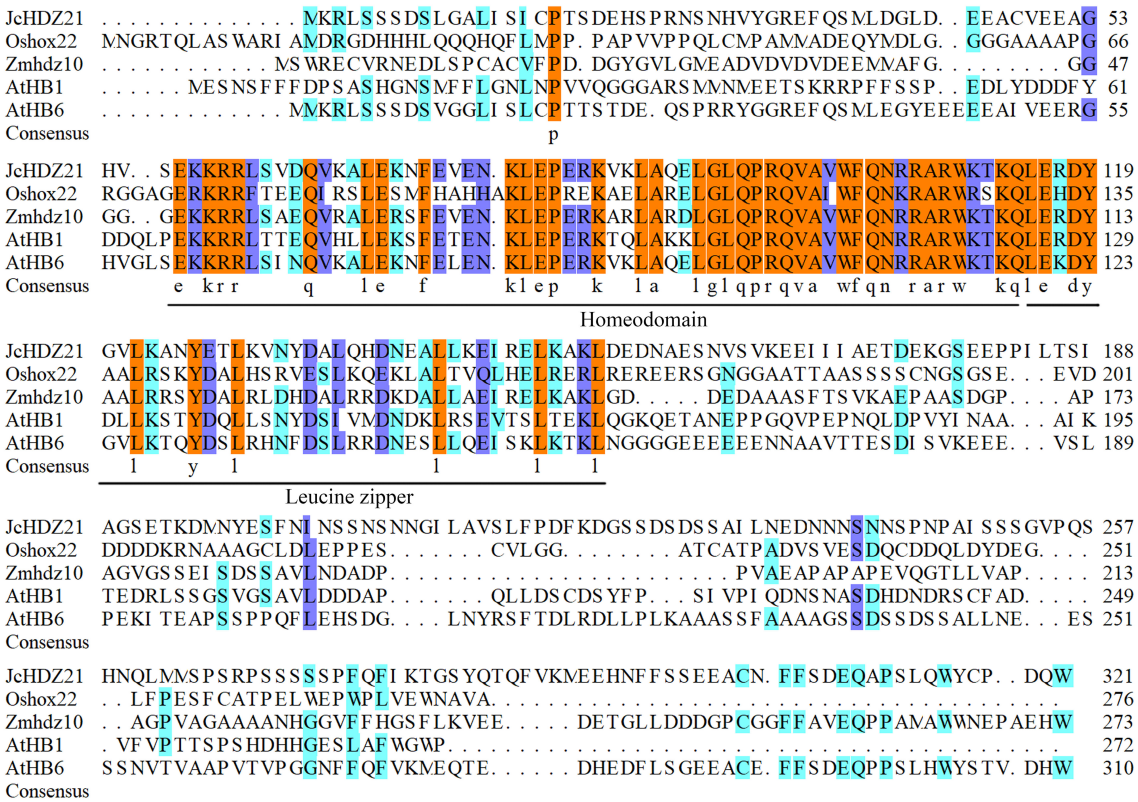

FIGURE 1
Sequence alignment analysis of JcHDZ21 and HD-Zip I family proteins that have been functionally studied. The DNAMAN XL software was used to perform the sequence alignment analysis.

10.3389/fpls.2023.1097265

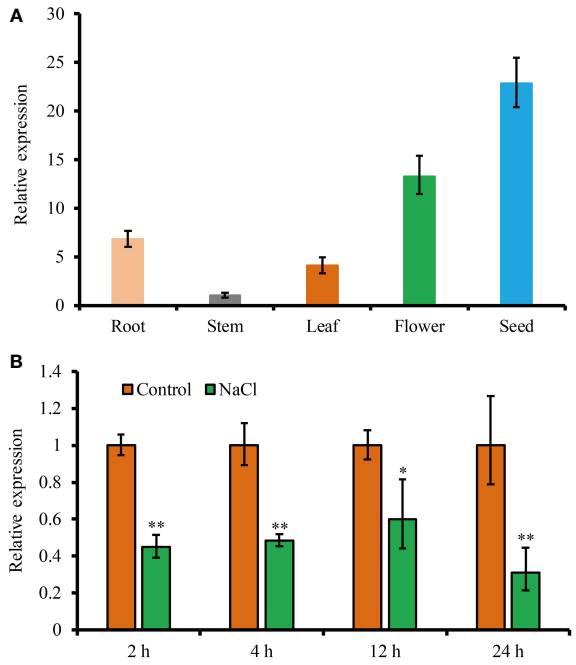

FIGURE 2
Expression level of *JcHDZ21* gene in physic nut growth in control and salt stress conditions. **(A)** Expression levels of *JcHDZ21* gene in different tissues of physic nut under normal growth conditions. **(B)** Expression level of *JcHDZ21* gene in physic nut leaves treated with 150 mM NaCl. Data are from three independent biological replicates, asterisks represent significant differences ($p<0.01$).

that the *JcHDZ21* gene can be inhibited by salt stress, indicating that the *JcHDZ21* gene may be involved in the regulation of plants to salt stress.

Subcellular localization of JcHDZ21 protein

To clarify the subcellular localization of JcHDZ21 protein, we transformed p16318hGFP-JcHDZ21 fusion expression vector and GFP empty vector plasmid into *Arabidopsis* protoplasts, and observed the subcellular localization of JcHDZ21-GFP fusion protein under laser confocal microscope. The result showed that the GFP empty control protein was expressed in all cells, while the JcHDZ21-GFP fusion protein suggested green fluorescence only in the nucleus (Figure 3), indicating that the JcHDZ21 protein is localized in the nucleus.

Analysis of JcHDZ21 protein transcriptional activity

In order to further explore the transcriptional activity of JcHDZ21 protein, we used the yeast two-hybrid system to detect the transcriptional activity of JcHDZ21 in yeast. The results showed

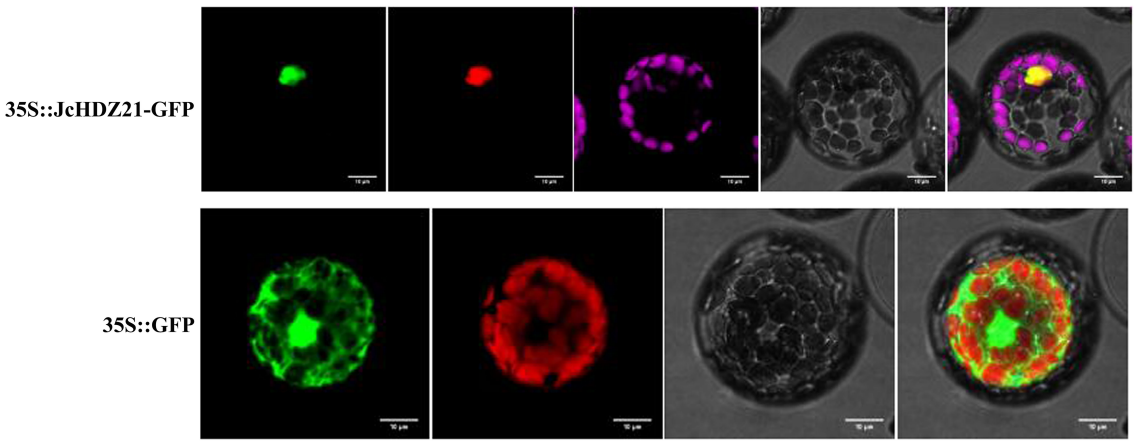

FIGURE 3
Subcellular localization of JcHDZ21 protein. 35S::JcHDZ21-GFP shows GFP, NLS-Cherry, Chlorophy II, Bright and Merge from left to right, whereas 35S::GFP shows GFP, Chlorophy II, Bright and Merge from left to right. Bars shows 10 μm.

that all the combined vectors could grow on SD/-Trp medium. On SD/-Trp/-His/X-a-gal medium, the negative control grew weakly and did not turn blue, but pGBKT7-JcHDZ21 recombinant expression vector and the pGBKT7-GAL4 plaques showed blue. However, on SD/-Trp/-His/-Ade/X-a-gal medium, the pGBKT7 vector could not grow, but the pGBKT7-JcHDZ21 recombinant expression vector and the pGBKT7-GAL4 could grow well and the plaques were blue (Figure 4). These results indicate that *JcHDZ21* acts as a transcriptional activator.

Phenotypic analysis of *JcHDZ21* transgenic plants

To verify the function of the *JcHDZ21* gene, we constructed a *JcHDZ21* overexpression vector and obtained *JcHDZ21* overexpressing transgenic Arabidopsis plants. Homozygous plants of the T3 generation were selected in hygromycin-resistant medium for further study. We further detected the expression of *JcHDZ21* gene in wild-type and transgenic plants by RT-PCR. The results showed that high expression levels of *JcHDZ21* were detected in transgenic plants, but no expression was detected in wild-type plants (Figure 5A). We selected 4-week wild-type and transgenic plants for phenotype observation. Phenotypic analysis showed that there was no significant difference in the growth of *JcHDZ21* transgenic plants and wild-type plants (Figures 5B, C). Statistical data showed that *JcHDZ21* transgenic plants had no significant difference in root length compared with wild-type plants (Figure 5D). We further analyzed the flowering time and yield per plant of *JcHDZ21* transgenic plants. The results showed that the flowering time and yield per plant of *JcHDZ21* transgenic plants were not significantly different from those of wild-type plants (Figures 5E, F), indicating that ectopic expression of *JcHDZ21* gene did not affect the growth and development of transgenic Arabidopsis.

JcHDZ21 negatively regulates the tolerance of transgenic Arabidopsis to salt stress

Salt stress can repress the expression of *JcHDZ21* gene, indicating that *JcHDZ21* might be involved in plant response to salt stress. To prove this hypothesis, we directly spread the sterilized transgenic and wild type Arabidopsis seeds onto 1/2 MS medium containing 100 mM NaCl for 25 days. The results showed that the leaves of transgenic and wild-type Arabidopsis showed different degrees of yellow and smaller symptoms, but the degree of yellow of wild-type plants leaves was significantly lower than that of transgenic Arabidopsis plants, and the leaves of transgenic Arabidopsis were smaller than that of wild-type plants (Figure 6A). The growth status and survival rate of transgenic Arabidopsis plants were significantly lower than those of wild-type plants. The survival rates of *JcHDZ21* transgenic plants were 22.58%, 21.24% and 19.27%, respectively, while the survival rate of wild-type plants reached 76.21%. The above results indicate that the heterologous expression of physic nut *JcHDZ21* gene significantly enhances the sensitivity of transgenic Arabidopsis to salt stress.

Some physiological indicators were also tested in transgenic and wild-type plants under normal growth and salt stress conditions. The results showed that salinity stress increased MDA, proline and betaine content, and relative electrolyte leakage, whereas wild-type plants had higher proline and betaine content, lower relative

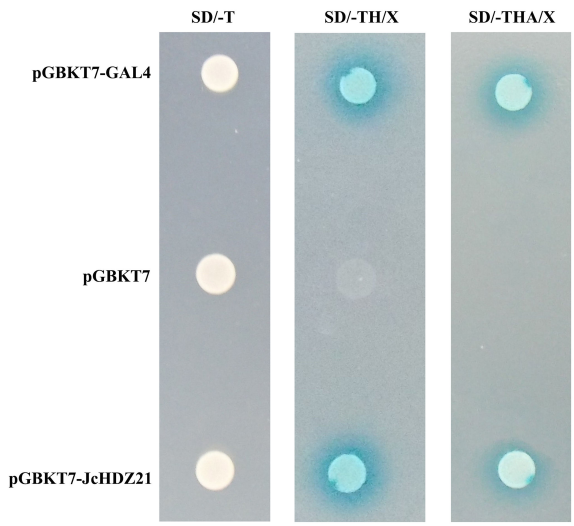

FIGURE 4
JcHDZ21 protein transcriptional activity. The left panel shows pGBKT7-GAL4, pGBKT7 and pGBKT7-JcHDZ21 grown on SD/-Trp plates for 4d, and the middle panel shows pGBKT7-GAL4, pGBKT7 and pGBKT7-JcHDZ21 grown on SD/-Trp/-His/X-a-gal plates for 4d, and the right panel shows pGBKT7-GAL4, pGBKT7 and pGBKT7-JcHDZ21 grown on SD/-Trp/-His/-Ade/X-a-gal plates for 4d.

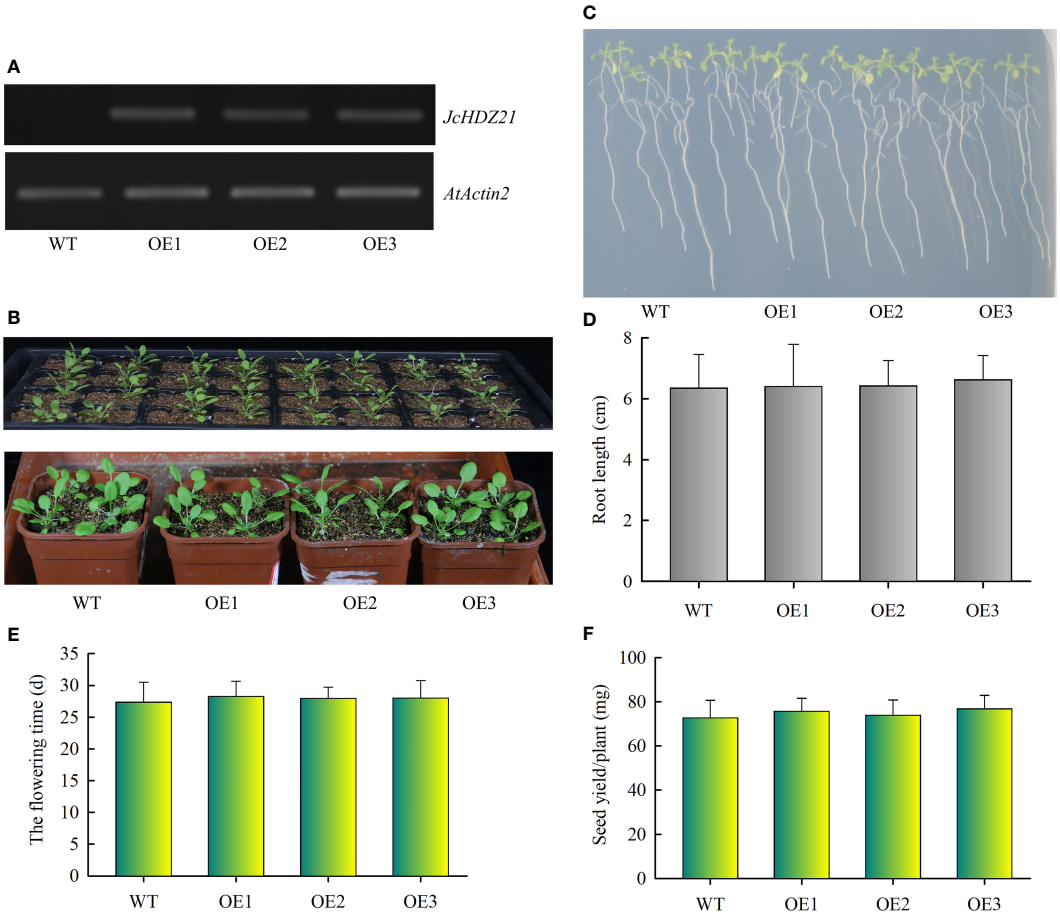

FIGURE 5
Phenotype of *JcHDZ21* transgenic Arabidopsis plants under normal growth condition. **(A)** Expression levels of *JcHDZ21* in wild-type and transgenic plants. **(B)** Growth status of wild-type and *JcHDZ21* transgenic plants at 25 days. **(C)** Root morphology of wild-type and *JcHDZ21* transgenic plants at day 10. The seeds of the sterilized wild-type and *JcHDZ21* transgenic plants were sown on 1/2 MS medium for vertical cultivation for 4 days, and the plants with consistent growth were selected and transferred to 1/2 MS medium for vertical growth for 6 days. **(D)** Root length of wild-type and *JcHDZ21* transgenic plants at day 10. Data in **(D)**: means of n = 20 ± SD from three independent experiments. **(E)** The flowering time of wild-type and JcHDZ21 transgenic plants. **(F)** Seed yield of wild-type and JcHDZ21 transgenic plants under normal growth conditions. Values represent means of n = 30 ± SD from three independent experiments.

electrolyte leakage and MDA content compared with transgenic plants under salinity stress (Figures 6B–E). In contrast, no significant differences in these stress response indicators between wild-type and transgenic plants were observed under non-stress conditions. The above results show that overexpression of *JcHDZ21* increases the sensitivity of transgenic Arabidopsis to salt stress, which may be partly caused by changing these physiological indicators. Taken together, these results strongly suggest that *JcHDZ21* acts as a negative regulator in responses to salt stress.

JcHDZ21 alters the expression of abiotic stress genes under salt stress

To clarify the molecular mechanism of *JcHDZ21* regulating Arabidopsis in response to salt stress, we further detected the expression levels of abiotic stress-related genes by qRT-PCR method, such as *AtP5CS1*, *AtNHX1*, *AtBADH* and *AtHKT1;1*. The results showed that plants growth in control condition, these abiotic stress-related genes had no significant differences among different plants. However, the expression of these abiotic stress-related genes was significantly downregulated in *JcHDZ21* transgenic plants compared to wild type when plants were exposed to salt stress (Figure 7).

Discussion

HD-Zip group I transcription factors, as the main type in the HD-Zip transcription factor family, can respond to abiotic stresses by participating in various biological processes (Gong et al., 2019; Zhao et al.,2021). The properties of HD-Zip transcription factors closely related to abiotic stress have been widely reported in the model plant Arabidopsis and other plants (Perotti et al., 2021). For example, ectopic expression of the Arabidopsis *AtHB6* gene increases drought stress tolerance in transgenic maize (Jiao et al.,

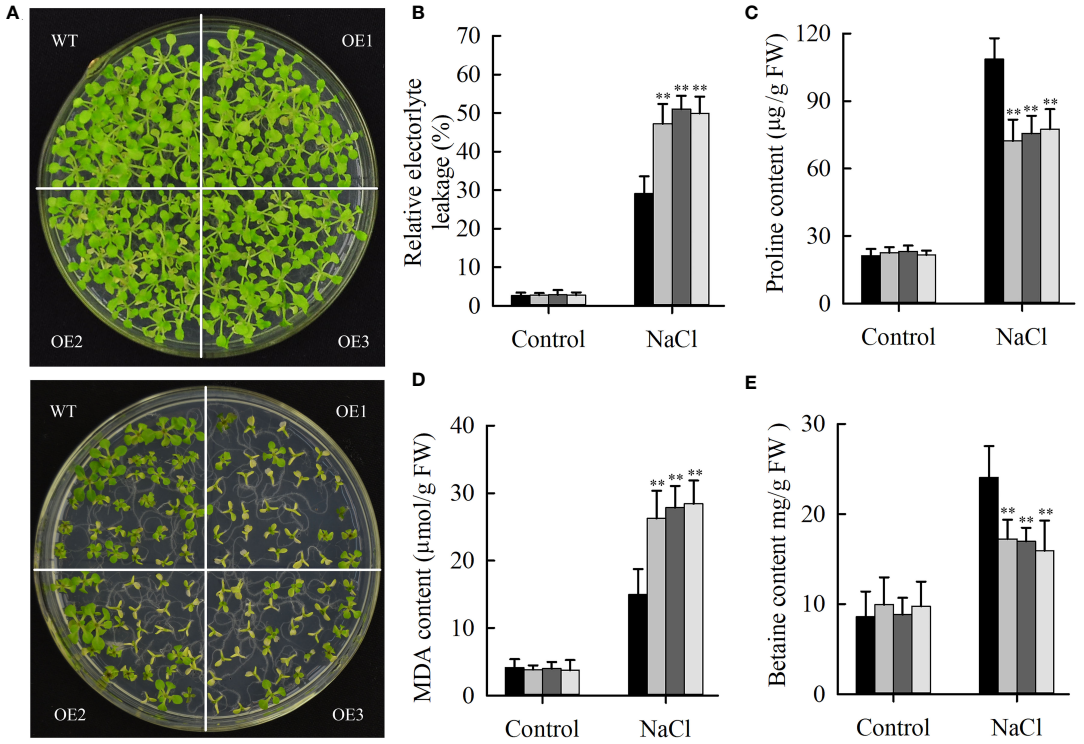

FIGURE 6
Phenotypic and physiological indicators analysis of wild-type and *JcHDZ21* transgenic plants growth in control and salt stress conditions. **(A)** Phenotypes of wild-type and *JcHDZ21* transgenic plants at 25 days growth in control and salt stress conditions. **(B)** Relative electrolyte leakage of leaves of wild-type and overexpressing plants after stress treatment and under non-stress conditions. **(C)** Proline content of leaves of wild-type and overexpressing plants after stress treatment and under non-stress conditions. **(D)** MDA content of leaves of wild-type and overexpressing plants after stress treatment and under non-stress conditions. **(E)** Betaine content of leaves of wild-type and overexpressing plants after stress treatment and under non-stress conditions. Data in **(B–E)**: means of n = 21 ± SD from three independent experiments, asterisks above the bars indicate significant differences from wild-type controls at $p < 0.01$according to Duncan's multiple range test.

2022); the expression of the maize HD-Zip transcription factor gene *Zmhdz10* and the cotton transcription factor gene *MdHB7-like* enhanced the salt tolerance of the transgenic plants (Zhao et al., 2014; Zhao et al., 2021). After the physic nut genome sequencing was completed, a total of 32 HD-Zip family genes were identified in physic nut (Wu et al., 2015), but little is known about the regulatory function of HD-Zip transcription factors in physic nut. To date, only a few genes related to HD-Zip transcription factors have been identified in physic nut, such as *JcHDZ16* (Tang et al., 2019), which both alter the ability of transgenic plants to tolerate abiotic stress. Therefore, we cloned a salt stress-responsive gene *JcHDZ21* in physic nut and analyzed the function of this gene in Arabidopsis. In future research, we will use CRISPR/Cas9 genome editing technology to construct *jchdz21* mutant physic nut plants to obtain more salt-tolerant physic nut species. Thus, our results may provide foundations to further promote application of *JcHDZ21* gene in physic nut breeding.

When plants are under salt stress, some substances that regulate osmotic pressure (such as proline and betaine) will be induced to synthesize to adapt to the stress. The accumulation of proline and betaine in plants under salt stress is an important physiological phenomenon that is beneficial to the growth of plants under stress (Ganjavi et al., 2021; Hosseinifard et al., 2022). Their contents are positively correlated with plant salt tolerance and can protect plant cell membrane systems from abiotic stress (Ganjavi et al., 2021; Hosseinifard et al., 2022). Maize transcription factor *ZmWRKY114* enhances the sensitivity of transgenic Arabidopsis to salt stress by regulating proline accumulation (Bo et al., 2020). *GmNAC06* alters the salt tolerance of transgenic soybean by promoting the accumulation of proline and betaine (Li et al., 2021). Similarly, our study found that increasing the expression of the *JcHDZ21* gene increased the sensitivity of transgenic Arabidopsis to salt stress, and the accumulation of proline and betaine in *JcHDZ21* transgenic plants induced by salt stress was significantly lower than that in wild-type plants (Figure 6), indicating that proline and betaine may be the factors that confer lower salt stress tolerance in *JcHDZ21* transgenic plants. Increases in malondialdehyde (MDA) and relative electrical conductivity caused by abiotic stress are also important indicators of plant oxidative damage (Xie et al., 2019). In our study, compared with wild type, the relative conductivity and MDA content of *JcHDZ21* transgenic plants induced by salt stress were significantly increased (Figures 6B–E). Therefore, we speculate that the increase in relative conductivity and MDA content induced by salt stress may be one of the reasons for the weaker salt stress tolerance of *JcHDZ21* transgenic plants. JcHDZ21 protein has transcriptional activation

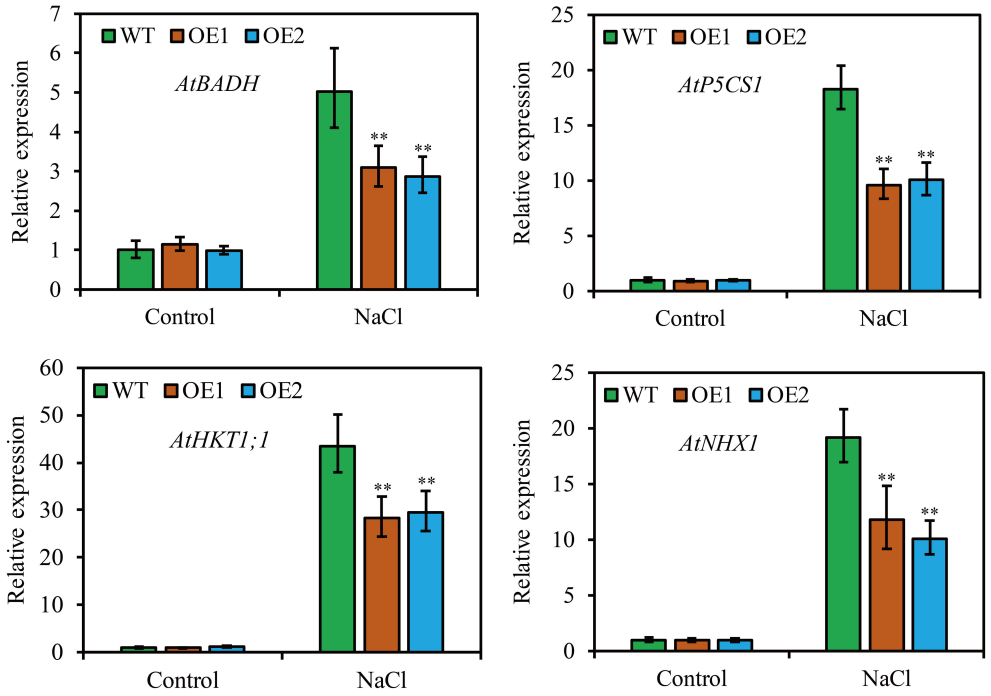

FIGURE 7
Expression levels of abiotic stress-related genes in wild-type and overexpressing plants under salt stress and non-stress conditions. Each experiment contains three biological replicates, and each with two technical replicates (means of n = 6 ± SD, asterisks above the bars indicate significant differences from wild-type controls at $p < 0.01$).

activity, suggesting that JcHDZ21 may interact with other transcriptional repressors to regulate the process of plant response to salt stress.

In addition to physiological indicators that can reflect the parameters of plants responding to adversity stress, some abiotic stress genes also play an important role in plant responses to abiotic stresses when plants encounter adversity stress. *AGL16* negatively regulates salt stress progression by altering the expression of abiotic stress-related genes (Zhao et al., 2021). *Oshox22* alters the tolerance of transgenic plants to salt stress by promoting the expression of abiotic stress-related genes (Zhang et al., 2012). Similarly, our study found that the expression of abiotic stress-related genes (*AtP5CS1*, *AtNHX1*, *AtBADH* and *AtHKT1;1*) in *JcHDZ21* transgenic plants was significantly lower than that in wild type under salt stress conditions (Figure 7). *P5CS1* has been identified as the major contributor to stress-induced proline accumulation (Feng et al., 2016), and ectopic expression of the Arabidopsis *P5CS1* gene increases salt stress tolerance in transgenic tobacco by regulating proline accumulation (Ibragimova et al., 2015). *AtHKT1;1* gene plays an important role in regulating the process of plant response to salt stress, and increasing the expression of this gene increases the tolerance of transgenic plants to salt stress (Plett et al., 2010). Increased expression of the *AtNHX1* gene alters the tolerance of transgenic plants to salt stress (Asif et al., 2011). *AtBADH* increases salt stress tolerance in transgenic plants by altering betaine content (Zhou et al., 2008). Taken together, *JcHDZ21* may affect the biosynthesis of proline and betaine by regulating the expression of proline and betaine metabolism genes under salt stress, thereby increasing the sensitivity of transgenic plants to salt stress. Another possibility is that *JcHDZ21* may alter the tolerance of transgenic plants to salt stress by regulating the expression of abiotic stress-related genes.

Conclusion

JcHDZ21 is a member of the HD-Zip I family, which is highly expressed in seeds and responds to salt stress. JcHDZ21 protein is localized to the nucleus and has transcriptional activity. Under the condition of salt stress, the damage degree of salt stress on *JcHDZ21* transgenic Arabidopsis was significantly higher than that of wild type. This study provides a reference for further research on the functions of the HD-Zip family genes in physic nut and other species, and also provides important candidate genes for the genetic breeding of physic nut.

Data availability statement

The original contributions presented in the study are included in the article/Supplementary Material. Further inquiries can be directed to the corresponding author.

Author contributions

YHT conceived and designed the experiments; JP, JL, MZ, YT, SC, and YS performed experiments; QW and MZ analyzed the data; XB provided research advice; YHT wrote and revised the manuscript. All authors contributed to the article and approved the submitted version.

Funding

This work was supported by the Innovation and Entrepreneurship Training Program for College Students of Henan Province (grant no. 202210478018, 202210478019), Zhoukou Normal University, and the Research and Innovation Fund for College Students of Zhoukou Normal University (grant no. ZKNUD2022014).

Acknowledgments

We thank the reviewers and editor-in-chief for their valuable comments on our paper.

Conflict of interest

The authors declare that the research was conducted in the absence of any commercial or financial relationships that could be construed as a potential conflict of interest.

Publisher's note

All claims expressed in this article are solely those of the authors and do not necessarily represent those of their affiliated organizations, or those of the publisher, the editors and the reviewers. Any product that may be evaluated in this article, or claim that may be made by its manufacturer, is not guaranteed or endorsed by the publisher.

Supplementary material

The Supplementary Material for this article can be found online at: https://www.frontiersin.org/articles/10.3389/fpls.2023.1097265/full#supplementary-material

References

Asif, M. A., Zafar, Y., Iqbal, J., Iqbal, M. M., Rashid, U., Ali, G. M., et al. (2011). Enhanced expression of *AtNHX1*, in transgenic groundnut (*Arachis hypogaea* l.) improves salt and drought tolerence. *Mol. Biotechnol.* 49, 250–256. doi: 10.1007/s12033-011-9399-1

Bo, C., Chen, H., Luo, G., Li, W., Zhang, X., Ma, Q., et al. (2020). Maize *WRKY114* gene negatively regulates salt-stress tolerance in transgenic rice. *Plant Cell Rep.* 39, 135–148. doi: 10.1007/s00299-019-02481-3

Deng, X., Phillips, J., Meijer, A. H., Salamini, F., and Bartels, D. (2002). Characterization of five novel dehydration-responsive homeodomain leucine zipper genes from the resurrection plant craterostigma plantagineum. *Plant Mol. Biol.* 49, 601–610. doi: 10.1023/a:1015501205303

Dubos, C., Stracke, R., Grotewold, E., Weisshaar, B., Martin, C., and Lepiniec, L. (2010). MYB transcription factors in arabidopsis. *Trends Plant Sci.* 15, 573–581. doi: 10.1016/j.tplants.2010.06.005

Feng, K., Hou, X. L., Xing, G. M., Liu, J. X., Duan, A. Q., Xu, Z. S., et al. (2020). Advances in AP2/ERF super-family transcription factors in plant. *Crit. Rev. Biotechnol.* 40, 750–776. doi: 10.1080/07388551.2020.1768509

Feng, X. J., Li, J. R., Qi, S. L., Lin, Q. F., Jin, J. B., and Hua, X. J. (2016). Light affects salt stress-induced transcriptional memory of *P5CS1* in arabidopsis. *Proc. Natl. Acad. Sci. U.S.A.* 113, 8335–8343. doi: 10.1073/pnas.1610670114

Ganjavi, A. S., Oraei, M., Gohari, G., Akbari, A., and Faramarzi, A. (2021). Glycine betaine functionalized graphene oxide as a new engineering nanoparticle lessens salt stress impacts in sweet basil (*Ocimum basilicum* l.). *Plant Physiol. Biochem.* 162, 14–26. doi: 10.1016/j.plaphy.2021.02.028

Gong, S., Ding, Y., Hu, S., Ding, L., Chen, Z., and Zhu, C. (2019). The role of HD-Zip class I transcription factors in plant response to abiotic stresses. *Physiol Plant.* 167, 516–525. doi: 10.1111/ppl.12965

Guo, Q., Jiang, J., Yao, W., Li, L., Zhao, K., Cheng, Z., et al. (2021). Genome-wide analysis of poplar HD-zip family and over-expression of *PsnHDZ63* confers salt tolerance in transgenic populus simonii × p.nigra. *Plant Sci.* 311, 111021. doi: 10.1016/j.plantsci.2021.111021

Hanson, J., Johannesson, H., and Engström, P. (2001). Sugar-dependent alterations in cotyledon and leaf development in transgenic plants expressing the HDZhdip gene *ATHB13*. *Plant Mol. Biol.* 45, 247–262. doi: 10.1023/a:1006464907710

Harris, J. C., Hrmova, M., Lopato, S., and Langridge, P. (2011). Modulation of plant growth by HD-zip class I and II transcription factors in response to environmental stimuli. *New Phytol.* 190, 823–837. doi: 10.1111/j.1469-8137.2011.03733.x

Henriksson, E., Olsson, A. S., Johannesson, H., Johansson, H., Hanson, J., Engström, P., et al. (2005). Homeodomain leucine zipper class I genes in arabidopsis. expression patterns and phylogenetic relationships. *Plant Physiol.* 139, 509–518. doi: 10.1104/pp.105.063461

Hosseinifard, M., Stefaniak, S., Ghorbani Javid, M., Soltani, E., Wojtyla, Ł., and Garnczarska, M. (2022). Contribution of exogenous proline to abiotic stresses tolerance in plants: A review. *Int. J. Mol. Sci.* 23, 5186. doi: 10.3390/ijms23095186

Hu, Y., Li, S., Fan, X., Song, S., Zhou, X., Weng, X., et al. (2020). OsHOX1 and OsHOX28 redundantly shape rice tiller angle by reducing HSFA2D expression and auxin content. *Plant Physiol.* 184, 1424–1437. doi: 10.1104/pp.20.00536

Ibragimova, S. M., Trifonova, E. A., Filipenko, E. A., and Shymny, V. K. (2015). Evaluation of salt tolerance of transgenic tobacco plants bearing with *P5CS1* gene of *Arabidopsis thaliana*. *Genetika* 51, 1368–1375. doi: 10.1134/S1022795415120078

Javelle, M., Klein-Cosson, C., Vernoud, V., Boltz, V., Maher, C., Timmermans, M., et al. (2011). Genome-wide characterization of the HD-ZIP IV transcription factor family in maize: Preferential expression in the epidermis. *Plant Physiol.* 157, 790–803. doi: 10.1104/pp.111.182147

Jiao, P., Jiang, Z., Wei, X., Liu, S., Qu, J., Guan, S., et al. (2022). Overexpression of the homeobox-leucine zipper protein ATHB-6 improves the drought tolerance of maize (*Zea mays* l.). *Plant Sci.* 316, 111159. doi: 10.1016/j.plantsci.2021.111159

Johannesson, H., Wang, Y., and Engström, P. (2001). DNA-Binding and dimerization preferences of arabidopsis homeodomain-leucine zipper transcription factors *in vitro*. *Plant Mol. Biol.* 45, 63–73. doi: 10.1023/a:1006423324025

Li, M., Chen, R., Jiang, Q., Sun, X., Zhang, H., and Hu, Z. (2021). GmNAC06, a NAC domain transcription factor enhances salt stress tolerance in soybean. *Plant Mol. Biol.* 105, 333–345. doi: 10.1007/s11103-020-01091-y

Montes, J. M., and Melchinger, A. E. (2016). Domestication and breeding of Jatropha curcas L. *Trends Plant Sci* 21, 1045–1057. doi: 10.1016/j.tplants.2016.08.008

Perotti, M. F., Arce, A. L., and Chan, R. L. (2021). The underground life of homeodomain-leucine zipper transcription factors. *J. Exp. Bot.* 72, 4005–4021. doi: 10.1093/jxb/erab112

Plett, D., Safwat, G., Gilliham, M., Skrumsager Møller, I., Roy, S., Shirley, N., et al. (2010). Improved salinity tolerance of rice through cell type-specific expression of AtHKT1;1. *PloS One* 5, e12571. doi: 10.1371/journal.pone.0012571

Preciado, J., Begcy, K., and Liu, T. (2022). The arabidopsis HDZIP class II transcription factor ABA INSENSITIVE TO GROWTH 1 functions in leaf development. *J. Exp. Bot.* 73, 1978–1991. doi: 10.1093/jxb/erab523

Rushton, P. J., Somssich, I. E., Ringler, P., and Shen, Q. J. (2010). WRKY transcription factors. *Trends Plant Sci.* 15, 247–258. doi: 10.1016/j.tplants.2010.02.006

Tang, Y., Wang, J., Bao, X., Liang, M., Lou, H., Zhao, J., et al. (2019). Genome-wide identification and expression profile of HD-ZIP genes in physic nut and functional

analysis of the *JcHDZ16* gene in transgenic rice. *BMC Plant Biol.* 19, 298. doi: 10.1186/s12870-019-1920-x

Thirumalaikumar, V. P., Devkar, V., Mehterov, N., Ali, S., Ozgur, R., Turkan, I., et al. (2018). NAC transcription factor JUNGBRUNNEN1 enhances drought tolerance in tomato. *Plant Biotechnol. J.* 16, 354–366. doi: 10.1111/pbi.12776

Turchi, L., Carabelli, M., Ruzza, V., Possenti, M., Sassi, M., Peñalosa, A., et al. (2013). Arabidopsis HD-zip II transcription factors control apical embryo development and meristem function. *Development* 140, 2118–2129. doi: 10.1242/dev.092833

Wu, P., Zhou, C., Cheng, S., Wu, Z., Lu, W., Han, J., et al (2015). Integrated genome sequence and linkage map of physic nut (Jatropha curcas L.), a biodiesel plant. *Plant J.* 81, 810–821. doi: 10.1111/tpj.12761

Xie, Y., Sun, X., Feng, Q., Luo, H., Wassie, M., Amee, M., et al. (2019). Comparative physiological and metabolomic analyses reveal mechanisms of Aspergillus aculeatus-mediated abiotic stress tolerance in tall fescue. *Plant Physiol. Biochem.* 142, 342–350. doi: 10.1016/j.plaphy.2019.07.022

Yoo, S. D., Cho, Y. H., and Sheen, J. (2007). Arabidopsis mesophyll protoplasts: A versatile cell system for transient gene expression analysis. *Nat. Protoc.* 2, 1565–1572. doi: 10.1038/nprot.2007.199

Zhang, S., Haider, I., Kohlen, W., Jiang, L., Bouwmeester, H., Meijer, A. H., et al. (2012). Function of the HD-zip I gene *Oshox22* in ABA-mediated drought and salt tolerances in rice. *Plant Mol. Biol.* 80, 571–585. doi: 10.1007/s11103-012-9967-1

Zhang, X., Henriques, R., Lin, S. S., Niu, Q. W., and Chua, N. H. (2006). Agrobacterium-mediated transformation of arabidopsis thaliana using the floral dip method. *Nat. Protoc.* 1, 641–646. doi: 10.1038/nprot.2006.97

Zhao, P. X., Zhang, J., Chen, S. Y., Wu, J., Xia, J. Q., Sun, L. Q., et al. (2021). Arabidopsis MADS-box factor AGL16 is a negative regulator of plant response to salt stress by downregulating salt-responsive genes. *New Phytol.* 232, 2418–2439. doi: 10.1111/nph.17760

Zhao, S., Wang, H., Jia, X., Gao, H., Mao, K., and Ma, F. (2021). The HD-zip I transcription factor MdHB7-like confers tolerance to salinity in transgenic apple (*Malus domestica*). *Physiol. Plant* 172, 1452–1464. doi: 10.1111/ppl.13330

Zhao, Y., Ma, Q., Jin, X., Peng, X., Liu, J., Deng, L., et al. (2014). A novel maize homeodomain-leucine zipper (HD-zip) I gene, *Zmhdz10*, positively regulates drought and salt tolerance in both rice and arabidopsis. *Plant Cell Physiol.* 55, 1142–1156. doi: 10.1093/pcp/pcu054

Zhou, S., Chen, X., Zhang, X., and Li, Y. (2008). Improved salt tolerance in tobacco plants by co-transformation of a betaine synthesis gene *BADH* and a vacuolar Na+/H+ antiporter gene *SeNHX1*. *Biotechnol. Lett.* 30, 369–376. doi: 10.1007/s10529-007-9548-6

frontiers | Frontiers in Plant Science

TYPE Original Research
PUBLISHED 01 March 2023
DOI 10.3389/fpls.2023.1089380

Check for updates

OPEN ACCESS

EDITED BY
Mehdi Rahimi,
Graduate University of Advanced Technology, Iran

REVIEWED BY
John Hammond,
University of Reading, United Kingdom
Anis M. Limami,
Université d'Angers, France

*CORRESPONDENCE
Li-Li Zhao
zhaolili_0508@163.com

SPECIALTY SECTION
This article was submitted to Plant Abiotic Stress, a section of the journal Frontiers in Plant Science

RECEIVED 04 November 2022
ACCEPTED 17 February 2023
PUBLISHED 01 March 2023

CITATION
Zhao X, Chen K-k, Wang L-t, Zhao L-L and Wang P-C (2023) Transcriptome analysis provides insights into the response of *Lotus corniculatus* roots to low-phosphorus stress.
Front. Plant Sci. 14:1089380.
doi: 10.3389/fpls.2023.1089380

COPYRIGHT
© 2023 Zhao, Chen, Wang, Zhao and Wang. This is an open-access article distributed under the terms of the Creative Commons Attribution License (CC BY). The use, distribution or reproduction in other forums is permitted, provided the original author(s) and the copyright owner(s) are credited and that the original publication in this journal is cited, in accordance with accepted academic practice. No use, distribution or reproduction is permitted which does not comply with these terms.

Transcriptome analysis provides insights into the response of *Lotus corniculatus* roots to low-phosphorus stress

Xin Zhao[1], Ke-ke Chen[1], Lei-ting Wang[1], Li-Li Zhao[1]* and Pu-Chang Wang[2]

[1]College of Animal Science, Guizhou University, Guiyang, China, [2]School of Life Sciences, Guizhou Normal University, Guiyang, China

Introduction: A lack of soil phosphorus (P) is a principal factor restricting the normal growth of *Lotus corniculatus* in the karst area of Guizhou Province, China, but the response mechanism of *L. corniculatus* under low-phosphorus stress remains unclear.

Methods: Therefore, we treated two selected *L. corniculatus* lines (low-P-intolerant line 08518 and low-P-tolerant line 01549) from 13 *L. corniculatus* lines with normal phosphorus (0.5 mmol/L KH_2PO_4, NP) and low phosphorus (0.005 mmol/L KH_2PO_4, LP) concentrations to study changes in morphological, physiological and transcriptome data under low-phosphorus stress.

Results: The low-P-tolerant line 01549 exhibited better performance under low-phosphorus stress. Compared with the NP treatment, all root morphological indicators of the low-P-tolerant line 01549 increased, and those of the low-P-intolerant line 08518 decreased under low-P stress. Compared with the NP treatment, acid phosphatase (ACP), catalase (CAT), superoxide dismutase (SOD), and peroxidase (POD) activities, and the malondialdehyde (MDA), soluble sugar (SS), soluble protein (SP) and proline (Pro) contents of the two *L. corniculatus* lines increased under low-P stress. A transcriptome analysis of *L. corniculatus* showed that a total of 656 and 2243 differentially expressed genes (DEGs) were identified in line 01549 and line 08518, respectively. Meanwhile, the main pathways, such as carbohydrate metabolism, acid phosphatases, phosphate transporters and biosynthesis of secondary metabolites, as well as related genes were also screened by performing a KEGG enrichment analysis.

Discussion: The findings provide an essential point of reference for studying the physiological and molecular mechanism of the response to low-P stress in *L. corniculatus*.

KEYWORDS

***Lotus corniculatus*, low-phosphorus stress, physiological, morphological, transcriptomic**

Introduction

Phosphorus (P), one of the essential elements for plants, plays a key role not only in promoting plant growth and development, but also in regulating physiological metabolism and resistance to stress (Ding et al., 2021; Zipfel and Oldroyd, 2017). The soil P concentration is high, but about 80% of the phosphorus is organic phosphorus which is difficult to be used by plants, while inorganic phosphate in soil is easily fixed by iron, aluminum and calcium ions to form insoluble phosphate which cannot be used by plants directly (Chiou et al., 2006). Usually, the concentration of available phosphate in soil does not exceed 2.0 uM, and even in fertile soils it rarely exceeds 10 uM, far from meeting the needs of normal plant growth(Yuan and Liu, 2008). In order to improve the efficiency of P acquisition and utilization by plants, many scholars have studied the mechanisms of plant adaptation and tolerance to low-P stress (Nilsson et al., 2010; Ried et al., 2021).

Plants have been shown to have evolved a range of complex and tightly controlled mechanisms for maintaining cellular Pi concentrations (Tesfaye et al., 2007). One of the most important mechanisms is the ability of the plant root system to improve phosphorus uptake from the soil and autologous phosphorus utilization through a series of collaborative processes involving changes in plant morphology, physiology and molecular biology (Verma et al., 2021). Some studies have reported that plant biomass decreases significantly under low-P conditions and that the root surface area, total root number, lateral root length, number of lateral roots and root volume increase, expanding the area of P uptake by the root system (Hernández et al., 2007; Raya-González et al., 2021). O'Rourke et al. (2013) found that when P is deficient in the soil, white lupin forms cluster roots, while the row roots secrete organic acids to activate the fixed P in the soil, thereby increasing the effective P concentration in the medium. Simultaneously, the plant activates the fixed phosphorus in the soil through its own physiological and biochemical changes, such as the secretion of organic acids, and increases the effective phosphorus content through chemical action (Plaxton and Tran, 2011; Ciereszko et al., 2011). Li et al. (2016) found that *Leymus chinensis* protected PSII against Pi-induced photooxidative stress in the organism by enhancing the activity of anti-reactive oxygenase. Under P-deprived conditions, chlorophyll contents, soluble protein contents and root vigor are reduced, while malondialdehyde (MDA), soluble sugar and free proline contents are increased, as are peroxidase (POD), superoxide dismutase (SOD) and catalase (CAT) activities (Rohman et al., 2019).

The morphological, physiological, and biochemical changes exhibited by plants under low-P stress are achieved by the synergistic expression of phosphate starvation-response (PSR) genes in plant tissues (Zhang H. et al., 2014). Sun and Zheng (2022) found *ZmPHT1;1*, *ZmPHT1;9* and Zmphytase 2 genes play a key role in phosphorus recovery in maize. Hu et al. (2021) found P deficit increases the expression of genes related to glycerolipid synthesis, while the expression of genes related to phospholipid breakdown is inhibited. An increase in the expression of the genes encoding the PSII protein complex, the cytochrome b/f protein complex, the PSI protein complex, photosynthetic electron transport proteins, and several members of the F-type ATPase family was observed. Müller et al. (2007) found that chronic low-P stress affected primary and secondary plant metabolism, disrupted the balance of carbon metabolism, inhibited the binding of proteins and chlorophyll a or b, and reduced the photosynthetic capacity of plants, while the expression of genes related to sucrose and glucose metabolism were upregulated. Jeong et al. (2017) studied the rice transcriptome under low-P stress and found that kinase and phosphotransferase-related genes were upregulated, and the expression of genes involved in ribosome composition, transcription and translation was downregulated. In addition, in-depth transcriptomics analyses of oil palm (Kong et al., 2021), barley (Ren et al., 2018), wheat (Wang et al., 2019) and sorghum (Zhang J. et al., 2019) under low-P stress have also been performed, and the corresponding drought stress-responsive genes have been identified.

Lotus corniculatus is a perennial herb of the genus *Lotus* with strong tolerance of cold, barren and drought, developed root system, creeping stem and branch growth, strong grip, wide coverage, and is an excellent grass species for karst ecological environment management (Knežević et al., 2021). Second, the stems and leaves of *L. corniculatus* are soft and juicy, rich in carbohydrates, with high yield, good palatability, a high saponin content and enrichment of condensed tannins, which may reduce the occurrence of swelling disease in livestock (Antonelli et al., 2021). Its root system has many rhizomes and has good nitrogen fixation, which can increase soil organic matter and improve soil structure, and is a high-quality forage plant resource and green manure (Jiang et al., 2021). Genetic diversity analysis of accession resources is the basis for new variety selection and breeding, and since the 1980s, some cultivars of *L. corniculatus* have been introduced from abroad in China, and production trials have shown that these varieties have strong adaptability and high production performance and are widely planted in northwest China (Xie et al., 2023). In the karst region of southwest China, the research on the selection and breeding of varieties of *L. corniculatus* is not systematic, and there are few new varieties of *L. corniculatus*. It is of great practical significance for the large-scale cultivation of *L. corniculatus* and the development of local ecological animal husbandry in karst mountainous areas of southwest China by introducing new excellent *L. corniculatus* line resources and breeding accession varieties suitable for different ecological zones and uses. Moreover, the karst region of southwest China with severe regional rock desertification and effective phosphorus deficiency, and low phosphorus concentrations can impair plant growth and development (Baghbani-Arani et al., 2021; Zhao et al., 2022a), it is of great significance and application value to cultivate phosphorus-efficient plants and improve the utilization of phosphorus in soil by plants. Therefore, in the present study, we used the line resources of *L. corniculatus* as the object of the study and established two treatments, normal and low P concentrations, to screen two line species of *L. corniculatus* that are tolerant or sensitive to low P

concentrations. The aim was to elucidate the adaptive mechanisms and identify the genes regulating the low-P tolerance in the two genotypes of *L. corniculatus*. And it is intended to provide a preliminary reference for the innovative utilization of excellent *L. corniculatus* line resources and the selection and breeding of new varieties.

Materials and methods

Accession selection

We conducted sand culture experiments to evaluate the P tolerance of 13 *L. corniculatus* lines (Table S1) provided by the National Germplasm Forage Medium Term Repository, Institute of Grassland Research, Chinese Academy of Agricultural Sciences. The experiment was performed at Guizhou University College of Animal Science from May to August 2021. For the tested *L. corniculatus* lines, 4-8 cm cuttings were planted in different pots, the plants were grown and divided, the roots were washed with distilled water, and the uniformly growing *L. corniculatus* lines was selected and planted in seedling trays filled with quartz sand (width: high: long = 28 cm: 7.5 cm: 54 cm) and precultured with 15 seedlings per tray in a nutrient solution on 14 h/10 h light/dark cycle at 26°C/22°C. Three trays were included for one treatment. The nutrient solution was prepared with deionised water, which was formulated as described in our previous research article (Zhao et al., 2022b). Plants were incubated with the complete nutrient solution for one week and then divided into two treatment groups consisting of normal (0.5 mmol/L KH_2PO_4, NP) and low phosphorus (0.005 mmol/L KH_2PO_4, LP) concentrations, with the nutrient solution replenished every 2 d. KH_2PO_4 was used as the phosphorus source, the K^+ concentration was balanced by K_2SO_4, and the pH of the nutrient solution was adjusted to 6.00 using NaOH and H_2SO_4. After 21 d, root tissues from the control and low-P stress groups were collected to measure their growth characteristics and whole plant P concentration.

Determination of morphological indices

A straightedge was used to measure the plant height. The aboveground and belowground sections of the plant were separated and the fresh weights were measured before these parts were placed in an oven at 105°C for 30 min and dried to a constant weight at 65°C to determine the dry weights of the aboveground and belowground portions. The molybdenum blue technique was used to measure the total P concentration of *L. corniculatus* (Chapman and Pratt, 1962). Fresh leaves and roots were scanned with an Epson Perfection V800 Photo scanner, and the resulting images were analyzed with WinFOLIA Pro 2015 and WinRHIZO Pro 2015 software (Regent Instructions, Canada Inc.) to obtain leaf indicators (surface area, length, width, length/width and perimeter) and root indicators (total length, total surface area, diameter, volume, tip number and hair number), respectively.

Evaluation of low-P tolerance

An evaluation of the low-P tolerance of different *L. corniculatus* lines was conducted. Low-P tolerance coefficients (based on root morphology, leaf morphology, biomass, plant height and whole plant P concentration of the different *L. corniculatus* lines under low-P stress) were first calculated, followed by a comprehensive evaluation using principal component analysis and affiliation function for low-P tolerance to eliminate differences related to the accessions (Zhu, 2018). The equations were as follows.

$$Low-P \quad tolerance \quad factor = LP \cdot Xi / NP \cdot Xi \tag{1}$$

$$\mu(X_j) = (X_j - X_{min})/(X_{max} - X_{min}) \quad j = 1, 2, 3...., n \tag{2}$$

$$W_j = P_j / \sum_{j=1}^{m} P_j \quad j = 1, 2, 3...., n \tag{3}$$

$$D = \sum_{j=1}^{n} [\mu(X_j) \times W_j] \quad j = 1, 2, 3...., n \tag{4}$$

Note that Xi denotes the mean value of an indicator, $\mu(X_j)$ denotes the affiliation function value of the jth composite indicator, X_j denotes the value of the jth composite indicator, X_{min} denotes the minimum value of the jth composite indicator, X_{max} denotes the maximum value of the jth composite indicator, W_j denotes the weight of the jth composite indicator to all composite indicators, and P_j denotes the contribution of the jth composite indicator. D denotes the composite evaluation value of the low-P tolerance of each *L. corniculatus* line.

Sand culture experiment using the two selected lines

The experimental design of the two screened *L. corniculatus* lines (01549 and 08518) was carried out according to the line Selection part, with 15 seedlings per pot and 3 replicates per treatment. After 7 d of low phosphorus stress, the seedlings were removed from the seedling tray, the roots were washed with distilled water and fresh tissue parts were obtained for the determination of physiological indexes and transcriptome sequencing.

Determination of physiological indices

Physiological indices, including MDA, soluble protein (SP), proline (Pro) and soluble sugar (SS) contents, as well as SOD, POD, CAT and acid phosphatase (ACP) activities, were determined using an assay kit from Beijing Solarbio Technology Co., Ltd., China.

Transcriptome sequencing and gene expression profiling

The methods for transcriptome sequencing and gene expression profiling were the same as those described in our previous study

(Zhao et al., 2022c). Briefly, total RNA was extracted from the root samples collected from lines 01549 and 08518, and cDNA libraries were constructed, followed by sequencing using the Illumina NovaSeq6000 platform with a PE150 sequencing strategy. Raw reads obtained from sequencing were quality controlled, and low-quality reads were removed. The quality-controlled clean reads were mapped to the *L. corniculatus* reference genome (Ensembl, http://www.kazusa.or.jp/lotus/summary3.0.html) using Bowtie2, and then the RSEM was used to count the number of reads mapped to each reference genome for each sample and to calculate the FPKM (fragments per kilobase of transcript per million mapped reads) for each gene. Paired-end reads from the same fragment were counted as one fragment to obtain the expression levels of genes and transcripts. A differential expression analysis was performed using the R package EdgeR. Genes with FDR (false discovery rate)< 0.05 and |log2FC (fold change)| >1 were defined as differentially expressed genes (DEGs). The GO enrichment analysis is an international standard classification system for gene function. DEGs were functionally annotated using the Gene Ontology database (http://www.geneontology.org/), and GO terms with FDR ≤ 0.05 were selected as significantly enriched GO entries for analysis. Functional annotation of DEGs was performed using the same approach with the KEGG database (http://www.genome.jp/kegg/pathway.html) to analyze pathways significantly correlated with DEGs. The number of genes in each pathway was then counted, and the significantly enriched pathways were analyzed using hypergeometric tests.

qRT-PCR validation

Eight DEGs (4 upregulated and 4 downregulated) were randomly selected for the experiment using the RNA obtained as described in Table S3 as the template to confirm the accuracy of the RNA-seq results. cDNA was synthesized from the same RNA samples used for transcriptome sequencing. We performed qRT-PCR on a CFX Connect™ Real-Time System (Applied Biosystems) using UltraSYBR mixture (CWBiotech). The thermocycle parameters were 10 min at 95°C, 40 cycles of 10 s at 95°C, 30 s at 60°C, and 32 s at 72°C, followed by 15 s at 95°C, 1 min at 60°C, 15 s at 95°C, and 15 s at 60°C, in a 20 μl reaction mixture (Zhao et al., 2022c). As an internal reference for normalization, the *Lotus corniculatus*-actin gene was used. Each sample was analyzed in triplicate.

Statistical analysis

Data were analyzed using Student's t test in SPSS 25.0 (IBM, Chicago, IL, USA), with a significance level of $p<0.05$. Relative root length=root length of plants under low-P stress/root length of the control plants, and all morphological and physiological parameters were obtained using similar methods. All data are presented as the means ± standard errors (SE) of three replicates and were plotted graphically using Origin 2021 software.

Results

Screening of the low-P-tolerant line (01549) and the low-P-intolerant line (08518)

Previous studies have shown that differences in plant line tolerance to low-P are due to their increased ability to acquire P. (Zhang J. et al., 2019). We speculate that low-P-tolerant plants will have higher P concentration under low-P treatment than low-P-intolerant plants. Thirteen *L. corniculatus* lines were cultured with the LP and NP treatments, which showed the whole-plant P concentration of all 13 *L. corniculatus* lines were significantly deceased ($P< 0.05$) in the range of 9.09%-140.74%, with 08518 (140.74%), 00116 (128.57%), and 01885 (85.71%) showing larger reductions and 01549 showing the smallest reduction (9.09%) under low phosphorus stress (Table S2). The value of the affiliation function of each composite indicator was computed using the formula, and the weight of the indicator was computed according to the contribution rate of each indicator. Finally, the comprehensive value of the low-P tolerance of each accession was obtained. The low-P tolerance of different *L. corniculatus* lines varied, where the low-P-tolerance line 01549 was strongest, and the low-P-intolerant line 08518 was weakest (Table S3). Therefore, we selected 01549 and 08518 as the low-P-tolerant and low-P-sensitive lines, respectively, for subsequent analyses. At the same time, the root morphology of each accession was examined. The relative P concentration in whole plants was significantly positively correlated with the relative length, relative volume and relative surface area of roots (Table 1), and most values of root morphology differed significantly between lines 01549 and 08518 under low phosphorus stress (Table 2).

Physiological and biochemical changes

The MDA, Pro, SS, and SP contents and SOD, POD, CAT and ACP activities of both lines 01549 and 08518 increased following LP treatment compared with NP treatment. Compared with those of line 01549, the MDA and SS contents and CAT activity of line 08518 increased under low-P stress, but only the MDA content significantly increased. The Pro and SP contents and SOD, POD and ACP activities of line 08518 were decreased under low-P stress, and the Pro content and SOD, POD and ACP activities were significantly decreased (Table 3).

DEGs identified in *L. corniculatus*

Twelve cDNA libraries were sequenced from the roots of lines 01549 and 08518 grown for 7 d under LP and NP treatments using Illumina high-throughput sequencing technology, generating a total of 554 million high-quality clean reads from three replicates of 12 libraries. The sequencing results were submitted to NCBI (**SRA accession: PRJNA871253**), and the Q30 values of the samples reached 93%. Approximately 80% of the total clean reads (Ensembl;

10.3389/fpls.2023.1089380

TABLE 1 Correlation analysis of root morphology and low-P tolerance.

	Relative root length	Relative root surface area	Relative root volume	Relative average root diameter	Relative root tip numbers	Relative root dry weight	Relative dry weight of the aboveground portion	Relative P concentration in the whole plant
Relative root length	1							
Relative root surface area	0.948**	1						
Relative root volume	0.907**	0.955*	1					
Relative average root diameter	-0.064	0.149	0.244	1				
Relative root tip numbers	0.114	-0.066	-0.111	-0.554*	1			
Relative root dry weight	0.681*	0.792**	0.786**	0.492	-0.402	1		
Relative dry weight of the aboveground portion	0.084	0.127	0.123	0.559*	-0.386	0.208	1	
Relative P concentration in the whole plant	0.695**	0.634*	0.653*	0.225	0.059	0.518	0.341	1

One and two asterisks indicate significant differences and highly significant differences between the LP and NP treatments, respectively ($p< 0.05$ and $p< 0.01$, respectively).

http://www.kazusa.or.jp/lotus/summary3.0.html) were mapped to the *L. corniculatus* reference sequence lotus/summary3.0 (Table S4). Eight DEGs were randomly chosen for qRT-PCR validation (Figure 1). Their expression profiles were significantly associated with the RNA-seq data FPKM, validating the trustworthiness of the transcriptomic data (Table S5).

When the transcripts of *L. corniculatus* were cultivated with the LP treatment 656 DEGs (243 upregulated and 413 downregulated) were identified in line 01549, and 2243 DEGs (1,455 upregulated and 788 downregulated) were identified in line 08518 compared with the NP treatment (Figure 2). Surprisingly, the number of DEGs in line 01549 was fewer than that in line 08518, regardless of whether they were upregulated or downregulated. A total of 5,596 DEGs (3,277 upregulated and 2,319 downregulated) were discovered in the low-P-tolerant line 01549 compared with the low-P-intolerant line 08518 under low-P stress. Only 58 common genes were discovered among these DEGs, indicating that these genes were considered valuable candidate genes for improving low-P tolerance (Figure 2B).

We performed GO and KEGG pathway enrichment analyses of the DEGs identified in *L. corniculatus*. In total, 278 of the 656 DEGs in line 01549, 1,055 of the 2,243 DEGs in line 08518 and 1,445 of the 5,595 DEGs in the comparison of lines 01549 and 08518 under low-P stress were identified in the GO database. All DEGs identified in the GO database from the three comparison groups were assigned to cellular components, biological processes and molecular functions. In addition, oxidoreductase activity and oxidation-reduction process were the two GO terms with the largest number of DEGs in the three comparison groups. Second, chlorophyllide oxygenase activity, tetrapyrrole binding, enzyme inhibitor activity, endopeptidase inhibitor activity, tetrapyrrole binding and heme binding were

TABLE 2 Effects of *L. corniculatus* lines on root morphology under low phosphorus stress.

P concentration	Accession	Total root length (cm)	Total root surface area (cm^2)	Root volume (cm^3)	Root diameter (cm)	Root tips
NP (0.5 mmol)	01549	175.14 ± 7.67b	30.89 ± 2.48b	0.44 ± 0.01b	0.54 ± 0.02a	377.67 ± 8.39c
	08518	171.49 ± 2.12b	28.45 ± 2.61b	0.38 ± 0.02b	0.53 ± 0.04a	423.00 ± 6.00b
LP (0.005 mmol)	01549	217.24 ± 6.56a	34.01 ± 1.20a	0.48 ± 0.02a	0.53 ± 0.03a	541.67 ± 7.77a
	08518	118.34 ± 1.82c	19.85 ± 0.14c	0.25 ± 0.04c	0.48 ± 0.01a	289.67 ± 1.53d

Values are means ± standard errors (n = 3). Different lowercase letters indicate significant differences ($P< 0.05$) within each index.

10.3389/fpls.2023.1089380

TABLE 3 Effect of low-P stress on the root physiological traits of *L. corniculatus* lines 01549 and 08518.

Accession	P concentration	MDA content (nmol·g^{-1})	Pro content (μg·g^{-1})	SS content (mg·g^{-1})	SP content (mg·g^{-1})	SOD activity (U·g^{-1}·min^{-1})	POD activity (U·g^{-1}·min^{-1})	CAT activity (U·g^{-1}·min^{-1})	ACP activity (μmol·h^{-1}·g^{-1})
01549	NP	53.75 ± 0.98d	92.28 ± 0.52c	47.84 ± 0.34b	23.93 ± 0.57c	47.15 ± 0.89c	5480.24 ± 59.89b	840.68 ± 21.06b	61.38 ± 1.11c
	LP	58.01 ± 0.64b	99.74 ± 0.47a	64.33 ± 0.44a	29.04 ± 0.23a	64.84 ± 0.94a	7107.44 ± 57.51a	1465.56 ± 27.24a	100.89 ± 0.83a
08518	NP	55.82 ± 0.44c	88.87 ± 0.69d	50.51 ± 1.77b	26.36 ± 1.21b	36.01 ± 0.41d	2831.97 ± 203.42d	642.81 ± 10.73c	51.46 ± 0.41d
	LP	70.48 ± 0.53a	96.77 ± 0.61b	67.12 ± 2.61a	27.82 ± 0.54a	48.96 ± 0.81b	5158.19 ± 79.51c	1485.19 ± 37.65a	72.57 ± 1.03b

Values are means ± standard errors (n = 3). Different lowercase letters indicate significant differences (P<no><</no> 0.05) within each index.

also significantly enriched in the three comparison groups (Table S6).

Ten, 24, and 17 significantly enriched pathways were identified among the enriched KEGG pathways for line 01549, 08518, and 01549 vs. 08518 under low-P stress, respectively (Table S7). As shown in Figures 3A-C, we screened the top 20 enriched KEGG pathways for the analysis of line 01549, line 08518 and lines 01549 vs. 08518 under low-P stress. For line 01549, phenylpropanoid biosynthesis (ko00940, 11 genes), stilbenoid, diarylheptanoid and gingerol biosynthesis (ko00945, 4 genes), and nitrogen metabolism (ko00910, 3 genes) were the three enriched pathways with the highest number of DEGs (Figure 3A). For line 08518, phenylpropanoid biosynthesis (ko00940, 43 genes), linoleic acid metabolism (ko00591, 12 genes), and ubiquinone and other terpenoid-quinone biosynthesis (ko00130, 11 genes) were the three main pathways with a large number of DEGs (Figure 3B). For the comparison of line 01549 with line 08518, phenylpropanoid biosynthesis (ko00940, 51 genes), stilbenoid, diarylheptanoid and gingerol biosynthesis (ko00945, 16 genes), and glycolysis/gluconeogenesis (ko00010, 30 genes) were the three main pathways (Figure 3C). The enriched KEGG pathways therefore revealed that genes in *L. corniculatus* were considerably differentially expressed, suggesting that the various lines activated various molecular mechanisms in response to low-P stress.

Identification of DEGs in plants under low-P stress

DEG-related acid phosphatases and phosphate transporters

From the transcriptome data, 6 differentially expressed acid phosphatase genes were identified; among those, 4 *PAP* genes (1 *PAP1*, 1 *PAP17*, 1 *PAP22* and 1 *PAP27*) were significantly upregulated in different lines, but 2 *APS1* genes were downregulated in the comparison of lines 01549 and 08518 under low-P stress. Eight differentially expressed phosphate transporter genes from 6 families were identified; among those, 2 *PHT1-3* genes,

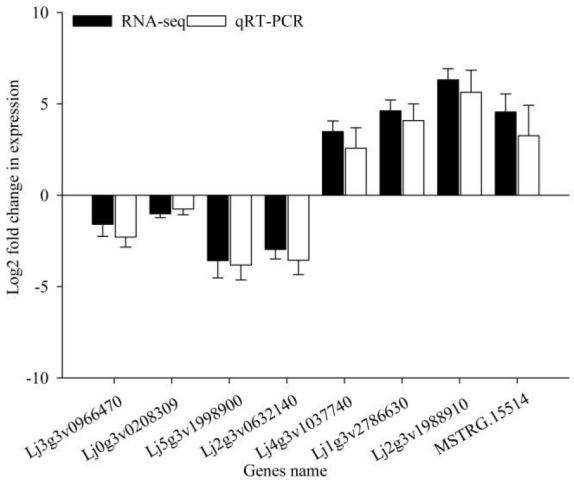

FIGURE 1
Validation of the transcript abundance of eight selected genes obtained from RNA-seq using qRT-PCR.

10.3389/fpls.2023.1089380

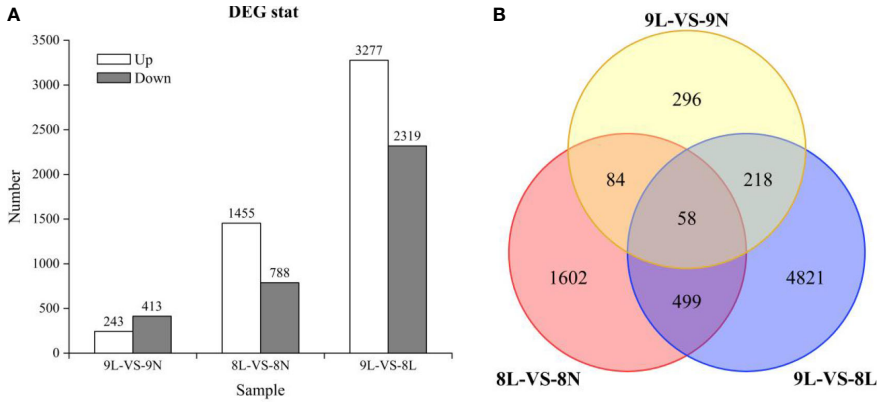

FIGURE 2
(A) The number of diferentially expressed genes in each comparison. **(B)** Venn diagram illustrating the genes of *L. corniculatus* in response to low-P stress.DEGs are shown in Venn diagrams. 9: Low-P-tolerant line 01549; 8: low-P-intolerant line 08518; L: low P; N: normal P.

2 *PHT1-4* genes, 1 *PHT1-7* gene, 1 *PHO1-H1* gene, and 1 *PHT1-11* gene were significantly upregulated, but 1 *PHO1-H10* gene was significantly downregulated in line 01549 compared with line 08518 under low-P stress (Figure 4 and Table S8).

DEGs related to plant hormone signal transduction

Sixty-one DEGs, including genes involved in auxin, abscisic acid, brassinosteroid, cytokinin, ethylene, gibberellin, jasmonic acid, and salicylic acid signal transduction, were discovered to be associated with plant hormones (Figure 5 and Table S9). In the auxin signaling pathway, 2 *ARF*, 3 *GH3* and 4 *SAUR* genes were significantly upregulated, but 1 *GH3* and 6 *SAUR* genes were significantly downregulated in line 01549 compared with line 08518 under low-P stress. Two *GH3*, 3 *SAUR* and 3 *IAA* genes were significantly upregulated, but 1 *GH3* and 2 *SAUR* genes were significantly downregulated in line 08518 under low-P stress. One *GH3* gene was significantly upregulated in line 01549 under low-P stress. In the abscisic acid signaling pathway, 1 *PYL* and 3 *SNRK* genes were significantly upregulated, while 2 *PP2C* and 1 *SNRK* genes were significantly downregulated in line 01549 compared with line 08518 under low-P stress. One *ABF* gene and 1 *PYL* gene

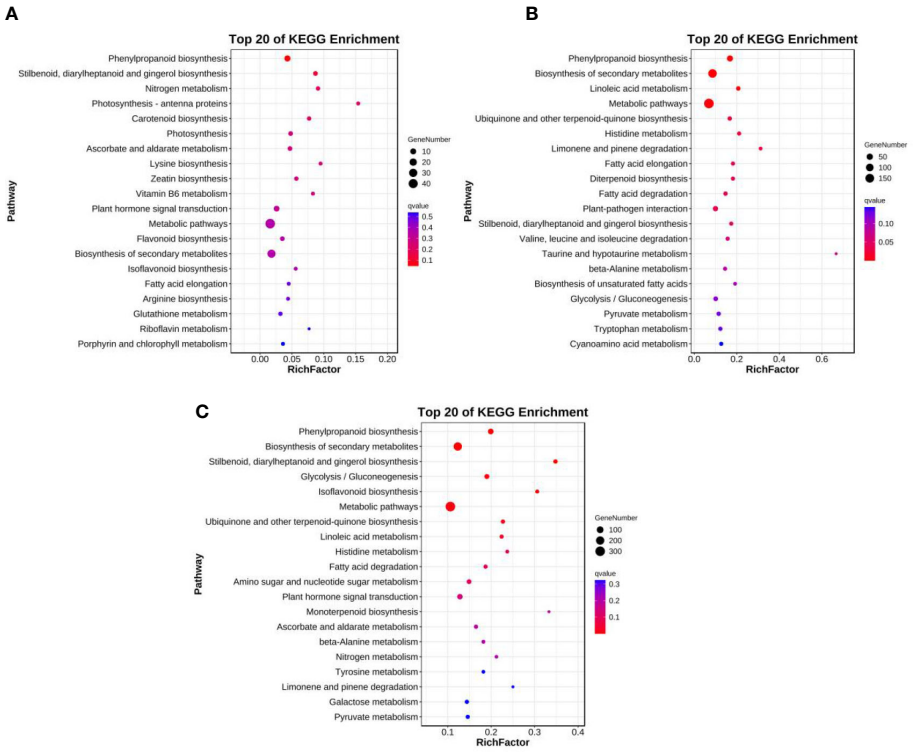

FIGURE 3
Top 20 enriched KEGG pathways in **(A)** line 01549, **(B)** line 08518, and **(C)** the comparison of lines 01549 and 08518 under low-P stress.

10.3389/fpls.2023.1089380

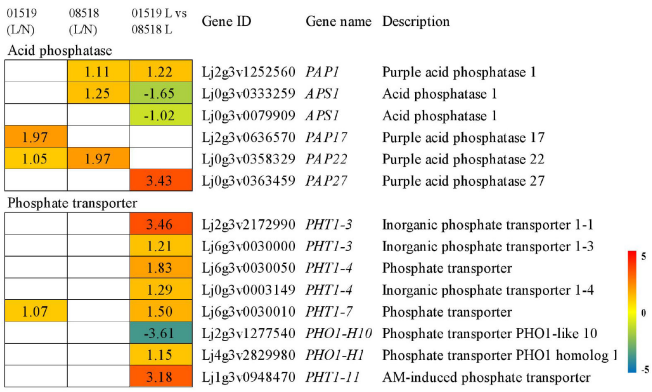

FIGURE 4
Acid phosphatase and phosphate transporter genes identified in the RNA-seq analysis that showed changes in expression during low-P stress. Log_2 (fold-changes) of the comparisons are shown by the numbers in the gray rectangles. The comparisons show that each of the genes in the picture is significantly differentially expressed.

were significantly upregulated in lines 01549 and 08518, respectively. In the brassinosteroid signaling pathway, 2 *BZR1_2* and 4 *TCH4* genes were significantly downregulated in line 01549 compared with line 08518 under low-P stress, and 1 *BZR1_2* and 3 *TCH4* genes were significantly downregulated in line 08518 under low-P stress. In the cytokinin signaling pathway, 1 *AHP* and 1 *ARR-A* gene were significantly upregulated in line 01549 compared with line 08518 under low-P stress, and 1 *AHP* gene was significantly upregulated and 1 *AHK2_3_4* gene was significantly downregulated in line 08518 under low-P stress. In the ethylene signaling pathway, 1 *ETR* and 2 *ERF1* genes were significantly upregulated, while 1 *EIN3* and 1 *ERF1* gene were significantly downregulated in lines 01549 and 08518 under low-P stress. One *ERF1* gene was significantly upregulated, while 1 *ERF1* gene was significantly downregulated in line 08518 under low-P stress. One *ERF1* gene was significantly downregulated in line 01549 under low-P stress. In the gibberellin signaling pathway, 1 *GID2* and 1 *PIF3* gene were significantly upregulated, while 1 *PIF4* gene was significantly downregulated in lines 01549 and 08518 under low-P stress, 1 *PIF4* gene was significantly downregulated in line 08518 under low-P stress, and 1 *DELLA* gene was significantly upregulated in line 01549 under low-P stress. In the jasmonic acid signaling pathway, 2 *JAZ* genes were significantly downregulated, while 1 *MYC2* and 1 *JAR1_4_6* gene were significantly upregulated in line 01549

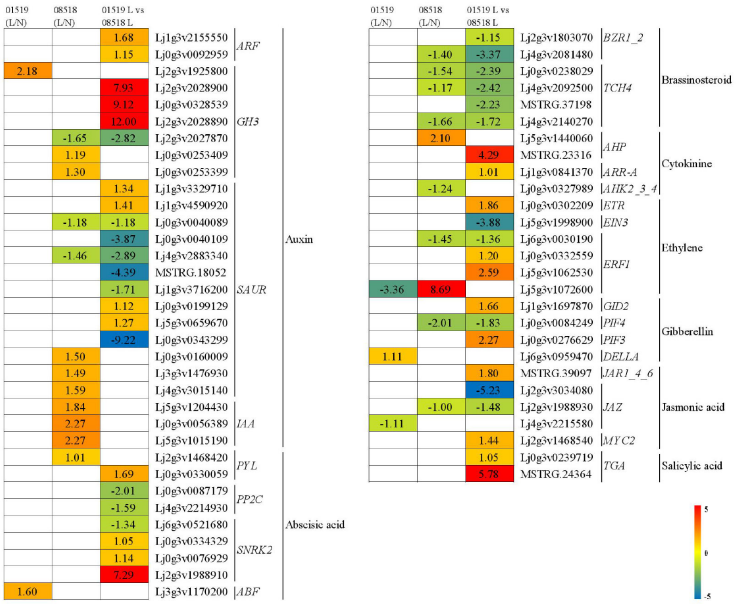

FIGURE 5
Plant hormone signal transduction-related genes identified in the RNA-seq analysis that showed changes in expression during low-P stress. Log_2 (fold-changes) of the comparisons are shown by the numbers in the gray rectangles. The comparisons show that each of the genes in the picture is significantly differentially expressed.

10.3389/fpls.2023.1089380

compared with line 08518 under low-P stress, 1 *JAZ* gene was significantly downregulated in line 08518 under low-P stress, and 1 *JAZ* gene was significantly downregulated in line 01549 under low-P stress. In the salicylic acid signaling pathway, 2 *TGA* genes were significantly upregulated in line 01549 compared with line 08518 under low-P stress.

DEGs related to the biosynthesis of secondary metabolites

In the phenylpropanoid, flavonoid and anthocyanin biosynthesis pathways, 29 genes, including *PAL*, *CYP73A*, *4CL*, *CHS*, *E5.5.1.6*, *DFR*, *E2.3.1.133*, *CYP98A*, *E2.1.1.104* and *BZ1*, were differentially accumulated in the *L. corniculatus* roots under low-P stress (Figure 6 and Table S10). Overall, the majority of the structural genes implicated in the pathways were significantly downregulated under low-P stress, repressing secondary metabolism in *L. corniculatus* roots. Among them, 3 *PAL*, 3 *CYP73A*, 4 *4CL*, 1 *CHS*, 1 *DFR*, 4 *E2.3.1.133*, 1 *CYP98A* and 1 *E2.1.1.104* genes were significantly downregulated, while 2 *E5.5.1.6*, 1 *E2.3.1.133* and 2 *E2.1.1.104* genes were significantly upregulated in line 01549 compared with 08518 under low-P stress. 2 *4CL*, 3 *CHS* and 2 *E2.3.1.133* were significantly downregulated, while 2 *PAL*, 1 *4CL*, 1 *CHS*, 1 *E2.3.1.133*, 1 *E2.1.1.104* and 1 *BZ1* genes were significantly upregulated in line 08518 under low-P stress. Two *CYP73A* and *2 E2.3.1.133* genes were significantly downregulated in line 01549 under low-P stress. These results imply that the defense mechanisms of *L. corniculatus* against low-P stress involved the induction of phenylpropanoid and secondary metabolism.

DEGs related to carbohydrate metabolism

In the glycolysis/gluconeogenesis and citrate cycle pathways, 41 enzyme genes, including *HK*, *GALM*, *E5.1.3.15*, *PFK*, *TPI*, *GAPDH*, *ENO*, *PK*, *aceE*, *PDC*, *ADH1_7*, *PGAM*, *DLAT*, *ACSS1_2*, *ALDH*, *AKR1A1*, *PFP* and *ACO*, were differentially accumulated in *L. corniculatus* roots under low-P stress (Figure 7 and Table S11). Among them, 2 *HK*, 1 *PFK*, 3 *GAPDH*, 2 *ENO*, 2 *PK*, 4 *ADH1_7* and 2 *AKR1A1* genes were significantly upregulated, while 1 *GALM*, 1 *E5.1.3.15*, 1 *PFK*, 1 *TPI*, 1 *ENO*, 2 *PK*, 2 *PDC*, 3 *ADH1_7* and 1 *ACO* genes were significantly downregulated in line 01549 compared with line 08518 under low-P stress. 1 *GALM*, 1 *GAPDH*, 2 *PK*, 1 *ADH1_7*, *1 PGAM*, 1 *DLAT* and 2 *ALDH* were significantly upregulated, while 1 *ENO*, 1 *PDC*, 3 *ADH1_7*, 1 *ACSS1_2* and 1 *ALDH* genes were significantly downregulated in line 08518 under low-P stress. The 1 *PFP* gene was significantly downregulated in line 01549 under low-P stress. These results imply that the reaction of *L. corniculatus* to low-P stress was mediated by activating the citrate cycle pathway and glycolysis/gluconeogenesis as defense mechanisms.

Discussion

Plant response to low-P stress is a complex process regulated by multiple genes interacting with each other, and therefore, manipulation of a set of genes or individual genes is not sufficient to study plant tolerance to low-P (Sun et al., 2021; Zhao et al., 2022b). In this study, two selected genotypes (01549 and 08518) of *L. corniculatus* seedlings to better highlight the differences in resistance between the two *L. corniculatus* genotypes by systematically studying the morphological, physiological, and transcriptional responses of *L. corniculatus* to low-P stress. In this study, low phosphorus stress caused extensive changes in morphological traits, physiological indicators, and gene expression in the *L. corniculatus* roots.

In the study, low-P stress increased the MDA content in the roots of both lines 01549 and 08518 compared to the NP treatment, and the MDA content of line 01549 was significantly lower than that of line 08518 during low-P treatment. Based on these results, low-P stress caused a large number of superoxide radicals to be produced in the *L. corniculatus* roots, which caused an imbalance in plant metabolic oxygen production and subsequent oxidative damage to the plant (Tarumoto et al., 2022). However, the membrane system of line 08518 was damaged to a greater extent by low-P stress. Plants scavenge the accumulated O^{2-} through the

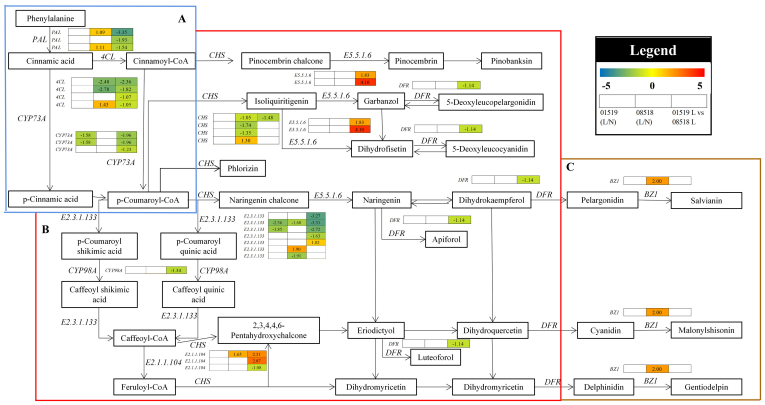

FIGURE 6
The pathways of phenylpropanoid biosynthesis **(A)**, flavonoid biosynthesis **(B)** and anthocyanin biosynthesis **(C)** enriched in the KEGG analysis. Log2 (fold-changes) of the comparisons are shown by the numbers in the gray rectangles. The comparisons show that each of the genes in the picture is significantly differentially expressed.

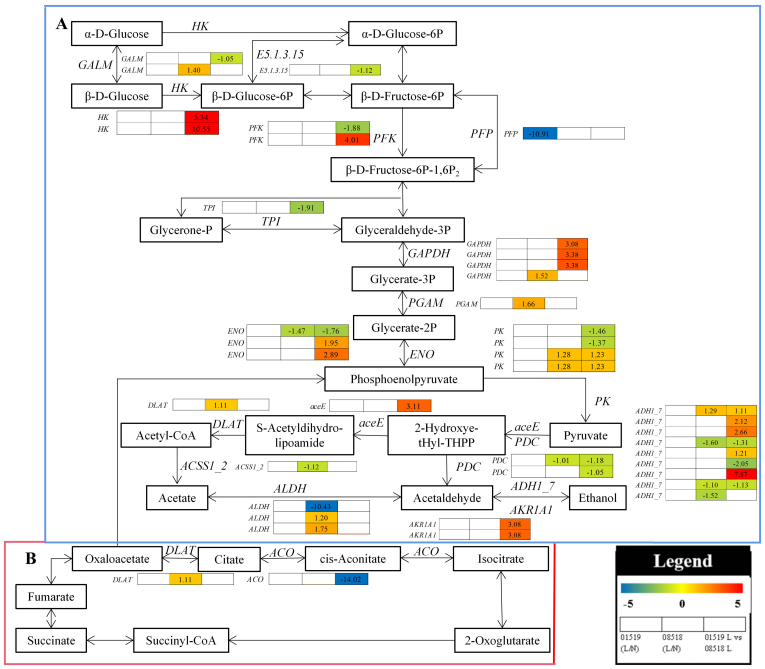

FIGURE 7
Analysis of the carbohydrate metabolism pathway in plants under low-P stress. **(A)** Glycolysis/gluconeogenesis. **(B)** Citrate cycle. Log_2(fold-changes) of the comparisons are shown by the numbers in the gray rectangles. The comparisons show that each of the genes in the picture is significantly differentially expressed.

antioxidant enzyme system consisting of SOD, CAT and POD to avoid cell membrane damage and keep the free radicals in plants at a low level under adverse conditions (Niu et al., 2013; Xu et al., 2018). In this study, we found that the antioxidant enzyme activities in both lines 01549 and 08518 were increased to enhance the adaptation to the low-P environment. Osmoregulatory substances in plants play an important role in reducing plant damage caused by stress(Anawar et al., 2018). In this study, we found that the proline, soluble sugar and soluble protein contents in lines 01549 and 08518 were increased under low phosphorus stress, indicating that the root cells of *L. corniculatus* were able to reduce the intracellular osmotic potential by regulating the content of their organic osmoregulatory substances, thus achieving self-protection and enhancing the tolerance to low phosphorus (Sun and Zheng, 2022). However, the antioxidant enzyme activities and osmoregulatory substance contents of line 01549 was higher than that of line 08518, indicating that line 01549 was more adapted to the low-P environment. Meanwhile, these data show very small differences in some cases between the two treatments in P treatment concentrations, this could be the different phosphorus uptake capacity and phosphorus utilization efficiency of different lines of *L. corniculatus*. However, the exact reasons need further analysis.

By studying the transcriptional responses of *L. corniculatus* to low-P stress, we have revealed different patterns of *L. corniculatus* to response low-P stress, including carbohydrate metabolism, acid phosphatases and phosphate transporters, biosynthesis of secondary metabolites, and plant hormone signal transduction.

Anthocyanin biosynthesis is catalyzed by phenylpropanoid and flavonoid biosynthetic pathways through related genes such as *PAL*, *CHS*, *CHI*, *F3H*, *DFR*, and *ANS* (Liu et al., 2016; Farooq et al., 2016). The expression of these genes involved in secondary metabolite biosynthesis were differentially expressed in *L. corniculatus* lines under low-P stress in the present study, with *PAL*, *4CL*, *CHS* and *DFR* expression downregulated in line 01549 compared with line 08518 under low-P stress, while line 08518 showed upregulated *PAL* expression and decreased total gene expression of the *4CL* and *CHS* genes in the anthocyanin biosynthetic pathway under low-P stress, and the *BZ1* gene was upregulated in line 08518 under low-P stress. Although the expression of these genes does not fully reflect the antioxidant characteristics of *L. corniculatus* and requires further verification in cells and *in vivo* tissues, it nevertheless provides an indication of the tolerance of *L. corniculatus*. Regardless of the comparative group, line 08518 was more sensitive to low-P stress, suggesting that a low P concentration may have suppressed gene transcription or translation in *L. corniculatus*.

Acid phosphatase and high-affinity phosphate transporter family genes play key roles in the activation of phosphorus uptake and efficient phosphorus transport under low-P stress (Kuerban et al., 2020). Phosphatase is an adaptation-inducible enzyme that promotes the mineralization and decomposition of soil organic P (Zhu et al., 2020). In our study, two acid phosphatase 1 (*APS1*) genes were downregulated in lines 01549 and 08518 under low-P stress, and four purple acid phosphatase (*PAP*) genes were significantly upregulated by low-P stress. Fita et al. (2012) found that *Cm-PAP10.1* and *Cm-PAP10.2*, genes encoding purple acid phosphatases, were upregulated in melon under low-P stress, indicating that the activity of APS secreted by plant roots under low-P stress was positively correlated with the degree of P

deficiency. Meanwhile, genes encoding phosphorus transporter proteins were screened in transcriptome data, among which eight DEGs of high-affinity phosphorus transporter systems (*Pht1* and *Pho1* families) were screened, all of which were differentially expressed to varying degrees in the two *L. corniculatus* lines treated with low P. Hu et al. (2021) found that the *PHO1* and *PHT1* genes were upregulated in the roots of *Zygophyllum xanthoxylum*, suggesting that these phosphorus transporter protein genes may play a vital role in regulating the distribution, transport and maintenance of dynamic homeostasis of P in the plant body during P deficiency (Hu et al., 2021), but their functions in response to low-P stress remain to be further investigated.

Several respiratory metabolic pathways have been identified in plants, including the glycolytic pathway (EMP), the tricarboxylic acid cycle (TCA), and the mitochondrial electron transport chain (Van Dongen et al., 2011). Plants produce ATP and CO_2 through the breakdown of photosynthetic products (e.g., glucose) by respiration to promote root growth and development or maintain root activity for nutrient and water uptake and translocation (Chen et al., 2021). The differential expression of 41 key glycolysis and TCA cycle-related genes was discovered in this study. Among these genes, the glycolytic pathway-related genes *HK, PFK, GAPDH, ENO, PK, ADH1 7*, and *AKR1A1* were elevated, whereas the TCA cycle-related aconitate hydratase gene *ACO3* was downregulated in line 01549 compared with line 08518 under low-P conditions. The expression of some genes related to the glycolytic pathway, namely, *GALM*, *PK*, *ADH1_7*, and *ALDH*, was downregulated, and the expression of *DLAT*, a pyruvate dehydrogenase E2 component of the TCA cycle, was upregulated in line 01549 compared with line 08518 under low-P stress, suggesting that low-P stress suppresses both pathways while increasing electron transport, and the *L. corniculatus* root maintains an ATP supply by constantly changing the transcript levels of genes encoding critical enzymes in the glycolytic/gluconeogenic pathway. (Du et al., 2020).

Low-P stress affects the synthesis and distribution of hormones in plants, which further regulates root conformation, such as root morphology and structure (Zhang Z. et al., 2014; Kumar et al., 2021; Martínez-Andújar et al., 2017). In this study, the expression genes involved in plant hormone signal transduction was significantly changed under low-P conditions, which may indicate that hormones play a crucial role in root development under low-P conditions (Zhang X. et al., 2019; Bhosale et al., 2018). In our study, the expression of the *ARF*, *GH3*, *PYL*, *SNRK2*, *ABF*, *AHP*, *ARR-A*, *ERF1*, *GID*, *PIF3*, *JAR1_4_6*, *MYC2* and *TGA* genes involved in in auxin, abscisic acid, cytokinin, ethylene, gibberellin, jasmonic acid and salicylic acid signaling, respectively, was upregulated in line 01549 compared with line 08518 under low-P stress, suggesting that these genes associated with phytohormone signaling are involved in regulating the root morphology of *L. corniculatus* in response to low-P stress. Gene expression was increased in line 01549, and the values of root morphological indicators were significantly higher in line 01549 than in line 08518, indicating that line 01549 regulates root development more quickly in response to stress. Brassinosteroids (BRs) are plant hormones that promote cell elongation and division and play an important role in plant growth and development (Planas-Riverola et al., 2019). In our study, the expression of all genes related to brassinosteroid signaling was downregulated, potentially due to the negative regulation of brassinosteroids in response to low-P stress in the root, but further analyses are needed to determine the exact cause. Similarly, transcription factors related to hormone metabolism and signal transduction play a crucial role. Studies have shown that the growth hormone-responsive transcription factor SAUR also regulates root morphology and promotes lateral root development (Xie et al., 2000). *Arabidopsis* RLK (receptor-like protein kinase) regulates root hair development (Wei and Li, 2018). In this study, *SAUR* genes were both upregulated and downregulated in line 01549 compared with line 08518 under low-P stress, indicating that both lines suffered from low-P stress, regardless of the accession. Two *SAUR* genes were downregulated in line 08518, and no difference in *SAUR* expression was identified in line 01549 under low-P stress, indicating that line 08518 has a reduced root morphology and requires the regulation of *SAUR* genes to respond to low-P stress.

By determining morphological and physiological features, we verified that the phosphorus-resistant genotype 01549 performed better under low-P stress, which was also highly supported by transcriptome data. However, previous studies have shown that these genes do not always coincide with changes in physiological indicators, and it is possible that other unknown genes are involved in the response of *L. corniculatus* to low-P stress.

Conclusions

Key KEGG pathways and their candidate genes were evaluated to explore changes in the morphological and physiological characteristics of the two *L. corniculatus* lines under low-P stress. We found that the root morphology of phosphorus-tolerant line 01549 increased and that of phosphorus-sensitive line 08518 decreased under low-P stress. *L. corniculatus* adapted to the low-P environment by increasing enzyme activity and the contents of osmoregulatory substances to rapidly regulate its physiological and metabolic functions as a mechanism to mitigate the injury. In addition, a multilevel analysis of changes in gene expression in *L. corniculatus* was conducted. Low-P stress activated important pathways, such as plant hormone signal transduction, and we identified key candidate genes, such as *PAP*, *PHT1* and *PHO1*. The combination of morphological, physiological, and transcriptome data reported in this work provides a theoretical foundation for future studies of the complex processes driving low-P responses in *L. corniculatus* and other plant species.

Data availability statement

The data presented in the study are deposited in the BCBI repository, accession number PRJNA870253.

Author contributions

XZ and K-KC: experimental design, experimental performance, experimental data collection, data analysis, manuscript writing and revision. L-LZ: seed provision, manuscript writing, resource provision and funding acquisition. L-TW: experimental performance, experimental data collection and data analysis. P-CW: manuscript writing and revision. All authors contributed to the article and approved the submitted version.

Funding

This work was financially supported by Guizhou Provincial Department of Education Natural Science Research Project (QJJ [2022]076), Guizhou Provincial Science and Technology Projects (QKHPTRC[2021]5636), and the National Natural Science Foundation of China (32060391, 31560664).

Conflict of interest

The authors declare that the research was conducted in the absence of any commercial or financial relationships that could be construed as a potential conflict of interest.

Publisher's note

All claims expressed in this article are solely those of the authors and do not necessarily represent those of their affiliated organizations, or those of the publisher, the editors and the reviewers. Any product that may be evaluated in this article, or claim that may be made by its manufacturer, is not guaranteed or endorsed by the publisher.

Supplementary material

The Supplementary Material for this article can be found online at: https://www.frontiersin.org/articles/10.3389/fpls.2023.1089380/full#supplementary-material

References

Anawar, H. M., Rengel, Z., Damon, P., and Tibbett, M. (2018). Arsenic-phosphorus interactions in the soil-plant-microbe system: Dynamics of uptake, suppression and toxicity to plants. *Environ. pollut. (Barking. Essex. 1987).* 233, 1003–1012. doi: 10.1016/j.envpol.2017.09.098

Antonelli, C. J., Calzadilla, P. I., Campestre, M. P., Escaray, F. J., and Ruiz, O. A. (2021). Contrasting response of two lotus corniculatus l. lines to combined waterlogging-saline stress. *Plant Biol. (Stuttgart. Germany).* 23 (2), 363–374. doi: 10.1111/plb.13216

Baghbani-Arani, A., Modarres-Sanavy, S. A. M., and Poureisa, M. (2021). Improvement the soil physicochemical properties and fenugreek growth using zeolite and vermicompost under water deficit conditions. *J. Soil Sci. Plant Nutr.* 21, 1213–1228. doi: 10.1007/s42729-021-00434-y

Bhosale, R., Giri, J., Pandey, B. K., Giehl, R., Hartmann, A., Traini, R., et al. (2018). A mechanistic framework for auxin dependent arabidopsis root hair elongation to low external phosphate. *Nat. Commun.* 9 (1), 1409. doi: 10.1038/s41467-018-03851-3

Chapman, H. D., and Pratt, P. F. (1962). Methods of analysis for soils, plants and waters. *Soil Sci.* 93, 68. doi: 10.1097/00010694-196201000-00015

Chen, W., Zhou, M., Zhao, M., Chen, R., Tigabu, M., Wu, P., et al. (2021). Transcriptome analysis provides insights into the root response of Chinese fir to phosphorus deficiency. *BMC Plant Biol.* 21 (1), 525. doi: 10.1186/s12870-021-03245-6

Chiou, T. J., Aung, K., Lin, S. I., Wu, C. C., Chiang, S. F., and Su, C. L. (2006). Regulation of phosphate homeostasis by MicroRNA in arabidopsis. *Plant Cell* 18 (2), 412–421. doi: 10.1105/tpc.105.038943

Ciereszko, I., Szczygla, A., and Zebrowska, E. (2011). Phosphate deficiency affects acid phosphatase activity and growth of two wheat varieties. *J. Plant Nutr.* 34 (6), 815–829. doi: 10.1080/01904167.2011.544351

Ding, W., Cong, W. F., and Lambers, H. (2021). Plant phosphorus-acquisition and -use strategies affect soil carbon cycling. *Trends Ecol. Evol.* 36 (10), 899–906. doi: 10.1016/j.tree.2021.06.005

Du, Y., Zhao, Q., Chen, L., Yao, X., Zhang, W., Zhang, B., et al. (2020). Effect of drought stress on sugar metabolism in leaves and roots of soybean seedlings. *Plant Physiol. Biochem.: PPB* 146, 1–12. doi: 10.1016/j.plaphy.2019.11.003

Farooq, M. A., Gill, R. A., Islam, F., Ali, B., Liu, H., Xu, J., et al. (2016). Methyl jasmonate regulates antioxidant defense and suppresses arsenic uptake in brassica napus l. *Front. Plant Sci.* 7. doi: 10.3389/fpls.2016.00468

Fita, A., Bowen, H. C., Hayden, R. M., Nuez, F., Picó, B., and Hammond, J. P. (2012). Diversity in expression of phosphorus (P) responsive genes in cucumis melo l. *PloS One* 7 (4), e35387. doi: 10.1371/journal.pone.0035387

Hernández, G., Ramírez, M., Valdés-López, O., Tesfaye, M., Graham, M. A., Czechowski, T., et al. (2007). Phosphorus stress in common bean: root transcript and metabolic responses. *Plant Physiol.* 144 (2), 752–767. doi: 10.1104/pp.107.096958

Hu, X., Zhang, L., Niu, D., Nan, S., Wu, S., Gao, H., et al. (2021). Transcriptome analysis of zygophyllum xanthoxylum adaptation strategies to phosphate stress. *Front. Plant Sci.* 12. doi: 10.3389/fpls.2021.723595

Jeong, K., Baten, A., Waters, D. L., Pantoja, O., Julia, C. C., Wissuwa, M., et al. (2017). Phosphorus remobilization from rice flag leaves during grain filling: an RNA-seq study. *Plant Biotechnol. J.* 15 (1), 15–26. doi: 10.1111/pbi.12586

Jiang, W., Ma, L., Yi, D., and Pang, Y. (2021).). the complete chloroplast genome sequence of lotus corniculatus l. mitochondrial DNA. *Part B. Resour.* 6 (1), 189–190. doi: 10.1080/23802359.2020.1860708

Knežević, M., Berić, T., Buntić, A., Delić, D., Nikolić, I., Stanković, S., et al. (2021). Potential of root nodule nonrhizobial endophytic bacteria for growth promotion of lotus corniculatus l. and dactylis glomerata l. *J. Appl. Microbiol.* 131 (6), 2929–2940. doi: 10.1111/jam.15152

Kong, S. L., Abdullah, S., Ho, C. L., Musa, M., and Yeap, W. C. (2021). Comparative transcriptome analysis reveals novel insights into transcriptional responses to phosphorus starvation in oil palm (Elaeis guineensis) root. *BMC Genomic. Data* 22 (1), 6. doi: 10.1186/s12863-021-00962-7

Kuerban, M., Jiao, W., Pang, J., Jing, J., Qiu, L. J., Ding, W., et al. (2020). Targeting low-phytate soybean genotypes without compromising desirable phosphorus-acquisition traits. *Front. Genet.* 11. doi: 10.3389/fgene.2020.574547

Kumar, S., Chugh, C., Seem, K., Kumar, S., Vinod, K. K., and Mohapatra, T. (2021). Characterization of contrasting rice (Oryza sativa l.) genotypes reveals the pi-efficient schema for phosphate starvation tolerance. *BMC Plant Biol.* 21 (1), 282. doi: 10.1186/s12870-021-03015-4

Li, L. Y., Yang, H. M., Ren, W. B., Liu, B., Cheng, D. M., Wu, X. H., et al. (2016). Physiological and biochemical characterization of sheepgrass (Leymus chinensis) reveals insights into photosynthetic apparatus coping with low-phosphate stress conditions[J]. *J. Plant Biol.* 59, 336–346. doi: 10.1007/s12374-016-0117-1

Liu, W., Yin, D., Li, N., Hou, X., Wang, D., Li, D., et al. (2016). Influence of environmental factors on the active substance production and antioxidant activity in potentilla fruticosa l. and its quality assessment. *Sci. Rep.* 6, 28591. doi: 10.1038/srep28591

Liu, X., Zhao, X., Zhang, L., Lu, W., Li, X., and Xiao, K. (2013). TaPht1;4, a high-affinity phosphate transporter gene in wheat (Triticum aestivum), plays an important role in plant phosphate acquisition under phosphorus deprivation. *Funct. Plant Biol. FPB.* 40 (4), 329–341. doi: 10.1071/FP12242

Martínez-Andújar, C., Ruiz-Lozano, J. M., Dodd, I. C., Albacete, A., and Pérez-Alfocea, F. (2017). Hormonal and nutritional features in contrasting rootstock-mediated tomato growth under low-phosphorus nutrition. *Front. Plant Sci.* 8. doi: 10.3389/fpls.2017.00533

Müller, R., Morant, M., Jarmer, H., Nilsson, L., and Nielsen, T. H. (2007). Genome-wide analysis of the arabidopsis leaf transcriptome reveals interaction of phosphate and sugar metabolism. *Plant Physiol.* 143 (1), 156–171. doi: 10.1104/pp.106.090167

Nilsson, L., Müller, R., and Nielsen, T. H. (2010). Dissecting the plant transcriptome and the regulatory responses to phosphate deprivation. *Physiol. Plant.* 139 (2), 129–143. doi: 10.1111/j.1399-3054.2010.01356.x

Niu, Y. F., Chai, R. S., Jin, G. L., Wang, H., Tang, C. X., and Zhang, Y. S. (2013). Responses of root architecture development to low phosphorus availability: a review. *Ann. Bot.* 112 (2), 391–408. doi: 10.1093/aob/mcs285

O'Rourke, J. A., Yang, S. S., Miller, S. S., Bucciarelli, B., Liu, J., Rydeen, A., et al. (2013). An RNA-seq transcriptome analysis of orthophosphate-deficient white lupin reveals novel insights into phosphorus acclimation in plants. *Plant Physiol.* 161 (2), 705–724. doi: 10.1104/pp.112.209254

Planas-Riverola, A., Gupta, A., Betegón-Putze, I., Bosch, N., Ibañes, M., and Caño-Delgado, A. I. (2019). "Brassinosteroid signaling in plant development and adaptation to stress," in *Development*, vol. 146. (England: Cambridge), dev151894. doi: 10.1242/dev.151894

Plaxton, W. C., and Tran, H. T. (2011). Metabolic adaptations of phosphate-starved plants. *Plant Physiol.* 156 (3), 1006–1015. doi: 10.1104/pp.111.175281

Raya-González, J., Ojeda-Rivera, J. O., Mora-Macias, J., Oropeza-Aburto, A., Ruiz-Herrera, L. F., López-Bucio, J., et al. (2021). MEDIATOR16 orchestrates local and systemic responses to phosphate scarcity in arabidopsis roots. *New Phytol.* 229 (3), 1278–1288. doi: 10.1111/nph.16989

Ren, P., Meng, Y., Li, B., Ma, X., Si, E., Lai, Y., et al. (2018). Molecular mechanisms of acclimatization to phosphorus starvation and recovery underlying full-length transcriptome profiling in barley (Hordeum vulgare l.). *Front. Plant Sci.* 9. doi: 10.3389/fpls.2018.00500

Ried, M. K., Wild, R., Zhu, J., Pipercevic, J., Sturm, K., Broger, L., et al. (2021). Inositol pyrophosphates promote the interaction of SPX domains with the coiled-coil motif of PHR transcription factors to regulate plant phosphate homeostasis. *Nat. Commun.* 12 (1), 384. doi: 10.1038/s41467-020-20681-4

Rohman, M. M., Islam, M. R., Monsur, M. B., Amiruzzaman, M., Fujita, M., and Hasanuzzaman, M. (2019). Trehalose protects maize plants from salt stress and phosphorus deficiency. *Plants (Basel. Switzerland).* 8 (12), 568. doi: 10.3390/plants8120568

Sun, T., Zhang, J., Zhang, Q., Li, X., Li, M., Yang, Y., et al. (2021). Transcriptome and metabolome analyses revealed the response mechanism of apple to different phosphorus stresses. *Plant Physiol. Biochem. PPB* 167, 639–650. doi: 10.1016/j.plaphy.2021.08.040

Sun, Y., and Zheng, H. (2022). Divergent molecular and physiological response of two maize breeding lines under phosphate deficiency. *Plant Mol. Biol. Rep.* 40, 197–207. doi: 10.1007/s11105-021-01310-w

Tarumoto, M. B., de Campos, M., Momesso, L., do Nascimento, C., Garcia, A., Coscolin, R., et al. (2022). Carbohydrate partitioning and antioxidant substances synthesis clarify the differences between sugarcane varieties on facing low phosphorus availability. *Front. Plant Sci.* 13. doi: 10.3389/fpls.2022.888432

Tesfaye, M., Liu, J., Allan, D. L., and Vance, C. P. (2007). Genomic and genetic control of phosphate stress in legumes. *Plant Physiol.* 144 (2), 594–603. doi: 10.1104/pp.107.097386

Van Dongen, J. T., Gupta, K. J., Ramírez-Aguilar, S. J., Araújo, W. L., Nunes-Nesi, A., and Fernie, A. R. (2011). Regulation of respiration in plants: a role for alternative metabolic pathways. *J. Plant Physiol.* 168 (12), 1434–1443. doi: 10.1016/j.jplph.2010.11.004

Verma, S. K., Sahu, P. K., Kumar, K., Pal, G., Gond, S. K., Kharwar, R. N., et al. (2021). Endophyte roles in nutrient acquisition, root system architecture development and oxidative stress tolerance. *J. Appl. Microbiol.* 131 (5), 2161–2177. doi: 10.1111/jam.15111

Wang, J., Qin, Q., Pan, J., Sun, L., Sun, Y., Xue, Y., et al. (2019). Transcriptome analysis in roots and leaves of wheat seedlings in response to low-phosphorus stress. *Sci. Rep.* 9 (1), 19802. doi: 10.1038/s41598-019-56451-6

Wei, Z., and Li, J. (2018). Receptor-like protein kinases: Key regulators controlling root hair development in arabidopsis thaliana. *J. Integr. Plant Biol.* 60 (9), 841–850. doi: 10.1111/jipb.12663

Xie, Q., Frugis, G., Colgan, D., and Chua, N. H. (2000). Arabidopsis NAC1 transduces auxin signal downstream of TIR1 to promote lateral root development. *Genes Dev.* 14 (23), 3024–3036. doi: 10.1101/gad.852200

Xie, W., Zhao, W., Wang, L., Zhao, L., and Wamg, P. (2023). Genetic diversity analysis of 22 lotus corniculatus germplasm resources based on phenotypic quantitative traits. *Acta agrestia sinica* 31(1), 173–179. doi: 10.11733/j.issn.1007-0435.2023.01.020

Xu, C., Zhang, H., Sun, J., Guo, Z., Zou, C., Li, W. X., et al. (2018). Genome-wide association study dissects yield components associated with low-phosphorus stress tolerance in maize. TAG. theoretical and applied genetics. *Theoretische. Und. Angewandte. Genetik.* 131 (8), 1699–1714. doi: 10.1007/s00122-018-3108-4

Yuan, H., and Liu, D. (2008). Signaling components involved in plant responses to phosphate starvation. *J. Integr. Plant Biol.* 50 (7), 849–859. doi: 10.1111/j.1744-7909.2008.00709.x

Zhang, J., Jiang, F., Shen, Y., Zhan, Q., Bai, B., Chen, W., et al. (2019). Transcriptome analysis reveals candidate genes related to phosphorus starvation tolerance in sorghum. *BMC Plant Biol.* 19 (1), 306. doi: 10.1186/s12870-019-1914-8

Zhang, Z., Liao, H., and Lucas, W. J. (2014). Molecular mechanisms underlying phosphate sensing, signaling, and adaptation in plants. *J. Integr. Plant Biol.* 56 (3), 192–220. doi: 10.1111/jipb.12163

Zhang, H., Uddin, M. S., Zou, C., Xie, C., Xu, Y., and Li, W. X. (2014). Meta-analysis and candidate gene mining of low-phosphorus tolerance in maize. *J. Integr. Plant Biol.* 56 (3), 262–270. doi: 10.1111/jipb.12168

Zhang, X., Wang, B., Zhao, Y., Zhang, J., and Li, Z. (2019). Auxin and GA signaling play important roles in the maize response to phosphate deficiency. *Plant Sci.* 283, 177–188. doi: 10.1016/j.plantsci.2019.02.011

Zhao, X., Huang, L. J., Sun, X. F., Zhao, L. L., and Wang, P. C. (2022c). Differential physiological, transcriptomic, and metabolomic responses of paspalum wettsteinii under high-temperature stress. *Front. Plant Sci.* 13. doi: 10.3389/fpls.2022.865608

Zhao, X., Huang, L. J., Zhao, L. L., Wang, P. C., and Sun, X. F. (2022b). Transcriptome analysis of sophora davidii leaves in response to low-phosphorus stress. *J. Plant Growth Regul.* 41, 1241–1253. doi: 10.1007/s00344-021-10382-7

Zhao, H., Wu, Y., Shen, L., Hou, Q., Wu, R., Li, Z., et al. (2022a). Cross-talk between transcriptome analysis and physiological characterization identifies the genes in response to the low phosphorus stress in malus mandshurica. *Int. J. Mol. Sci.* 23 (9), 4896. doi: 10.3390/ijms23094896

Zhu, T. Q. (2018). *Study on establishment of alfalfa phosphorus efficiency evaluation system and difference metabolism in nitrogen and phosphorus* (Gansu: Gansu Agricultural University).

Zhu, S., Chen, M., Liang, C., Xue, Y., Lin, S., and Tian, J. (2020). Characterization of purple acid phosphatase family and functional analysis of GmPAP7a/7b involved in extracellular ATP utilization in soybean. *Front. Plant Sci.* 11. doi: 10.3389/fpls.2020.00661

Zipfel, C., and Oldroyd, G. E. (2017). Plant signalling in symbiosis and immunity. *Nature* 543 (7645), 328–336. doi: 10.1038/nature22009

frontiers | Frontiers in Plant Science

TYPE Original Research
PUBLISHED 09 March 2023
DOI 10.3389/fpls.2023.1121809

Check for updates

OPEN ACCESS

EDITED BY
Mahmoud Magdy,
Ain Shams University, Egypt

REVIEWED BY
Agata Daszkowska-Golec,
University of Silesia in Katowice, Poland
Kenji Miura,
University of Tsukuba, Japan
Pooja Choudhary,
Jaypee Institute of Information Technology, India
Juan Wang,
Xinjiang Academy of Agricultural Sciences, China

*CORRESPONDENCE
Manzhong Liang
1962liang@163.com

SPECIALTY SECTION
This article was submitted to Plant Abiotic Stress, a section of the journal Frontiers in Plant Science

RECEIVED 12 December 2022
ACCEPTED 24 February 2023
PUBLISHED 09 March 2023

CITATION
Huang Y, Jiao Y, Yang S, Mao D, Wang F, Chen L and Liang M (2023) *SiNCED1*, a 9-cis-epoxycarotenoid dioxygenase gene in *Setaria italica*, is involved in drought tolerance and seed germination in transgenic Arabidopsis.
Front. Plant Sci. 14:1121809.
doi: 10.3389/fpls.2023.1121809

COPYRIGHT
© 2023 Huang, Jiao, Yang, Mao, Wang, Chen and Liang. This is an open-access article distributed under the terms of the Creative Commons Attribution License (CC BY). The use, distribution or reproduction in other forums is permitted, provided the original author(s) and the copyright owner(s) are credited and that the original publication in this journal is cited, in accordance with accepted academic practice. No use, distribution or reproduction is permitted which does not comply with these terms.

SiNCED1, a 9-cis-epoxycarotenoid dioxygenase gene in *Setaria italica*, is involved in drought tolerance and seed germination in transgenic Arabidopsis

Yuan Huang[1,2], Yang Jiao[2], Sha Yang[1], Dandan Mao[2,3], Feng Wang[2], Liangbi Chen[2,3] and Manzhong Liang[2,3]*

[1]College of Pharmacy, Guizhou University of Traditional Chinese Medicine, Guiyang, China, [2]College of Life Science, Hunan Normal University, Changsha, China, [3]Hunan Province Key Laboratory of Crop Sterile Germplasm Resource Innovation and Application, College of Life Science, Hunan Normal University, Changsha, China

Foxtail millet (*Setaria italica* L.) is a vital cereal food crop with promising development and utilization potential because of its outstanding ability to resist drought stress. However, the molecular mechanisms underlying its drought stress resistance remain unclear. In this study, we aimed to elucidate the molecular function of a 9-cis-epoxycarotenoid dioxygenase gene, *SiNCED1*, in the drought stress response of foxtail millet. Expression pattern analysis showed that *SiNCED1* expression was significantly induced by abscisic acid (ABA), osmotic stress, and salt stress. Furthermore, ectopic overexpression of *SiNCED1* could enhance drought stress resistance by elevating endogenous ABA levels and promoting stomatal closure. Transcript analysis indicated that *SiNCED1* modulated ABA-related stress responsive gene expression. In addition, we found that ectopic expression of *SiNCED1* delayed seed germination under normal and abiotic stress conditions. Taken together, our results show that *SiNCED1* plays a positive role in the drought tolerance and seed dormancy of foxtail millet by modulating ABA biosynthesis. In conclusion, this study revealed that *SiNCED1* is an important candidate gene for the improvement of drought stress tolerance in foxtail millet and could be beneficial in the breeding and investigation of drought tolerance in other agronomic crops.

KEYWORDS

foxtail millet, abscisic acid, SiNCED1, drought stress, seed germination

1 Introduction

Foxtail millet (*Setaria italica* L.) is an important cereal food crop that has been cultivated for over 8000 years (Zhang et al., 2012). This species is an ideal model plant because of its short life cycle, self-pollination, small diploid genome, prolific seed production, and small adult stature (Doust et al., 2009). Moreover, foxtail millet is a promising crop for the study of drought stress because of its outstanding ability to resist it (Barton et al., 2009). However, the genes underlying the foxtail millet drought stress response have not been studied extensively to date.

Abscisic acid (ABA) is an essential phytohormone that regulates plant development and modulates abiotic stress tolerance. The main functions of ABA in plant development include dormancy, the delaying of seed germination, and induction of stomatal closure (Yang et al., 2022). For example, ABA plays a critical role in the protection of seed dormancy and inhibition of seed germination through ABA metabolism, which is modulated by regulatory factors, the environment, and natural variations of ABA metabolism signal pathway related genes (Sano and Marion-Poll, 2021). Moreover, ABA promotes stomatal closure in a dual way by increasing its concentration in guard cells and decreasing water permeability in leaf vascular tissues (Pantin et al., 2013). During exposure to abiotic stresses, such as drought, salinity, heat, and cold, ABA can act as a dominant hormone to regulate abiotic stress signaling pathways. For instance, ABA promotes desiccation-tolerance by controlling stomatal closure, enabling plants to adapt to water stress (Shang et al., 2020). In addition, ABA participates in plant development, and abiotic-stress tolerance depends on ABA metabolism (biosynthesis and catabolism), perception, the core signaling pathway, and factors that trigger ABA-mediated transcription (Nambara et al., 2010).

Endogenous ABA levels in plants are positively regulated by ABA biosynthesis (Ng et al., 2014). ABA biosynthesis occurs in two sites, starting in the plastids and ending in the cytosol (Sah et al., 2016). ABA biosynthesis has two pathways, but in higher plants, ABA is synthesized *via* an indirect pathway, also called the mevalonic acid-independent pathway. Several enzymes that originate from the catalysis of carotenoid precursors participate in this pathway (Xu et al., 2013). To date, almost all biosynthetic genes have been identified through the isolation of nutritionally deficient mutants or the creation of specific gene-editing mutants (Eiji and Annie, 2005; Miao et al., 2013), including zeaxanthin epoxidase (*ZEP*), 9-cis-epoxycarotenoid dioxygenase (*NCED*), and abscisic aldehyde oxidase (*AAO*) (Andrew and Roger, 1992; Finkelstein, 2013). The NCED enzyme regulates the key limiting step of ABA biosynthesis by catalyzing the cleavage of 9-cis-violaxanthin or 9-cis-neoxanthin to xanthoxin (C15) (Ye et al., 2012).

The first *NCED* gene, *VP14*, was cloned and identified in maize (*Zea mays* L.) (Schwartz et al., 1997). Subsequently, *NCED* genes have been isolated and studied from multiple plant species in both dicotyledons and monocotyledons, such as Arabidopsis (*Arabidopsis thaliana* (L.) Heynh.) (Sato et al., 2018), peaches (*Prunus persica* L.) (Wang et al., 2021), cotton (*Gossypium hirsutum* L.) (Li et al., 2021), *Brassica napus* L. (Xu and Cai, 2017), tomatoes (*Solanum lycopersicum* L.) (Sun et al., 2012), rice (*Oryza sativa* L.) (Ye et al., 2011), wheat (*Triticum aestivum* L.) (Lang et al., 2021), and *Phaius tankervilliae* (Banks ex L'Hér.) Blume (Lee et al., 2018). The rice *NCED* gene family consists of five members (Ye et al., 2011), with the following functions: *OsNCED1*, the overexpression of which can improve the heat tolerance of rice by enhancing its antioxidant capacity (Zhou et al., 2022); *OsNCED3* and *OsNCED5*, which mediate multi-abiotic stress tolerance and leaf senescence by regulating endogenous ABA accumulation in rice (Huang et al., 2018; Huang et al., 2019); and *OsNCED3*, *OsNCED4*, and *OsNCED5*, whose ectopic expression in Arabidopsis can alter plant size and leaf morphology, delay seed germination, and advanced drought stress tolerance through the regulation of endogenous ABA content (Hwang et al., 2010; Hwang et al., 2018; Huang et al., 2019). In Arabidopsis, five *NCED* genes have been identified (Tan et al., 2003), which exhibit diverse expression patterns and share redundant functions. *AtNCED6* cooperates with *AtNCED9* to regulate seed germination and dormancy by controlling ABA levels in seeds. The transcription of *AtNCED3* and *AtNCED5* can be strongly induced by drought stress, which results in increased endogenous ABA levels and improved water stress tolerance (Hao et al., 2009; Frey et al., 2012). Two *NCED* isozymes, *PpNCED1* and *PpNCED5*, which have been identified in peach fruits, control fruit ripening and senescence by regulating ABA biosynthesis (Wang et al., 2021).

The above studies have shown that increasing the transcript levels of *NCED* could promote ABA biosynthesis and enhance ABA accumulation in plants, which play important roles during the various phases of the plant life cycle, including seed development and dormancy, and in plant responses to variable environmental stress (Koshiba, 2002). However, the functions of ABA biosynthesis genes for *NCED* in foxtail millet are still unknown. In this study, we cloned four *NCED* genes from the *Setaria italica* cultivated variety Jigu 42. The expression pattern and ectopic expression of *SiNCED1* in Arabidopsis was investigated. *SiNCED1* was strongly induced by ABA, osmotic stress, and salt stress. Furthermore, *SiNCED1* overexpression increased endogenous ABA contents to enhance drought stress tolerance and delay seed dormancy. Our findings indicate that *SiNCED1* can be an important candidate gene to improve drought stress tolerance and keep seed dormancy in foxtail millet and other agronomic crops.

2 Materials and methods

2.1 Plant growth conditions and treatment

Foxtail millet (*S. italica*, cultivar Jigu 42) seeds were germinated in distilled water for 3 d at 28°C. The seedlings were grown in Hoagland's culture solution (Li and Cheng, 2015) and cultured in growth chambers at 28°C under a 16 h light/8 h dark cycle. For abiotic stress, two-week-old seedlings were subjected to various stress treatments by placing them in a solution with a final

concentration of 20% PEG6000, 150 mM NaCl, and 100 μM ABA. All treatments were repeated more than three times. The shoots and roots were harvested for RNA extraction.

A. thaliana (Columbia-0 ecotype; Col) was used in this study. The seeds were surface-sterilized with 75% (v/v) ethanol and sown on either a 1/2 MS medium or soil at 22°C under a 16 h light/8 h dark cycle (Lu et al., 2017). To analyze the seed-germination rate, sterilized seeds were sown on a 1/2 MS medium with 150 mM NaCl, 275 mM mannitol, and 6% glucose. The seed germination rate were calculated according to opened cotyledons. For drought stress treatment, the Arabidopsis transgenic lines and Col were grown in soil for 25 d under the same growth conditions mentioned above; after which, water was withheld for 30 d, followed by watering for 7 d.

2.2 Phylogenetic relationship and multiple alignment analysis

The NCED protein sequences from four species, *A. thaliana*, *Oryza sativa*, *Zea mays*, and *Setaria italica*, were used for phylogenetic analysis. Phylogenetic tree analysis was performed using MEGA 7 software utilizing the maximum-likelihood method. Multiple sequence alignment was used to construct the phylogenetic tree in MEGA7 with the following parameter settings: Jones-Taylor-Thornton, pairwise deletion, and 1000 bootstrap replications.

The protein sequences of *NCED* genes used for multiple alignment were downloaded from the NCBI database (http://plants.ensembl.org/index.html). The multiple alignment was conducted using Bioedit software, applying ClustalW with the following parameters: full multiple alignment, number of bootstraps 1000, output clustal format with clustal consensus sequence generation.

2.3 Generation of *SiNCED1*-overexpressing lines

The *SiNCED1* open reading frame (ORF) was amplified through PCR using pHB-NCED1-F/R primers (Supplementary Table S1) and then inserted into the pHB binary vector with HindIII and XbaI restriction sites. The recombinant construct, 2×35S::*SiNCED1*, was transformed into Arabidopsis using the floral dip transformation method. The transgenic lines were planted on MS medium containing 50 μg hygromycin for 7 d. Homozygous lines with 100% resistance to hygromycin were selected and confirmed through semi-quantitative-PCR. Two genetically stable transgenic lines (OE3 and OE5) with high transcript levels of *SiNCED1* were selected for further analysis.

2.4 Quantitative real-time PCR analysis

Total RNA extraction was carried out for all samples using Trizol (Invitrogen, Shanghai, China) and was converted to cDNA using the Synthesis Kit (Thermo Fisher Scientific, USA) according to the manufacturer's instructions. Subsequently, quantitative real-time PCR (RT-qPCR) was performed using the SYBR Premix Ex Taq kit (Takara, Dalian, China) on an Applied Biosystems Quant Studio 5 (Thermo Fisher Scientific). Relative changes in gene expression levels were quantitated based on three biological replicates using the $2^{-\Delta\Delta Ct}$ method (Livak and Schmittgen, 2001). Each experiment included three technical replicates. The primer sequences used for RT-qPCR are listed in Supplementary Table S1.

2.5 Analysis of water loss rate, proline, electrolyte leakage and ABA content

The water loss rate was measured as described previously (Huang et al., 2018). The Arabidopsis rosette leaves of 25-day-old Col and *SiNCED1*-overexpressing lines were detached and placed in dishes with constant conditions. Fresh weight was measured at set times (0, 10, 20, 30, 40, 50, 60, 90,120, 150, and 180 min). The proportion of the initial fresh weight represented the water loss rate.

The proline content was measured according to previously described methods (Huang et al., 2018). Approximately 300 mg fresh leaf samples were homogenized in 3 mL of 3% aqueous sulfosalicylic acid and centrifuged at 4000 × *g* for 10 min. Then, 1 mL of supernatant was taken out and mixed with 1 mL of acid ninhydrin and 1 mL of glacial acetic acid in a new tube and then incubated in boiling water bath for 40 min. For every reaction, 2 mL toluene was added and oscillated for 30 min at room temperature. The proline content was measured using a spectrophotometer at 520 nm.

Relative electrolyte leakage was measured as previously described (Lou et al., 2017). The same number of detached leaf samples were placed in 20 mL of deionized water and then in a vacuum pump for 30 min. Samples were then sealed and placed in a 25 °C incubator for 6 h. The water conductance was measured using a conductivity meter.

ABA content was measured as previously described (Huang et al., 2019). Arabidopsis rosette leaves (300 mg) were collected from 25-day-old Col and *SiNCED1*-overexpressing lines and ground in liquid nitrogen. The internal standard was [$^2H_6$], and ABA content was quantified using UPLC–MS/MS with three independent biological replicates.

2.6 Measurement of stomatal aperture

Stomatal apertures were analyzed using *Arabidopsis* leaf epidermis samples under normal or drought stress conditions. Stomata were observed and photographed under a fluorescence microscope (BX51, Olympus, Japan). The size of stomatal apertures was measured using Image J software and a digital ruler. Three independent experiments were performed, which obtained similar results. Each experiment included at least 30 stomata from each epidermal sample.

2.7 Statistical analysis

All experiments were repeated at least three times for each treatment. Data were analyzed using SPSS software (version 13.0). Differences were considered statistically significant at $P < 0.05$, as determined using ANOVA analysis and Tukey's multiple comparisons test. All data are shown as mean ± SD from the three independent experiments.

3 Results

3.1 Molecular characterization of *NCED* in foxtail millet

Four 9-*cis*-epoxycarotenoid dioxygenase genes were found in the foxtail millet genome database (NCBI GenBank) and cloned (Supplementary Table S2). These genes were designated as *SiNCED1* (LOC101783411), *SiNCED3* (LOC101778945), *SiNCED4* (LOC101766978), and *SiNCED5* (LOC101770668). Among these, *SiNCED1* was further investigated because of its promoter, which may have a drought related cis-element, as assessed through plantCARE prediction analysis (Supplementary Table S3). The full-length *SiNCED1* CDS has a 1980 bp ORF, encoding 660 amino acids. To understand the phylogenetic relationship of SiNCED protein, a phylogenetic tree was constructed among SiNCED1, other SiNCEDs, and NCED proteins derived from Arabidopsis, rice, and maize. Based on the analysis, SiNCED proteins were clustered into two clades (Figure 1). SiNCED1 was separately clustered into a clade, while the other three SiNCEDs were aggregated into another clade. Alignment of the deduced protein sequences showed that SiNCED1 contains a large number of conserved amino acid residues in the NCED conserved domain RPE65, when compared with other NCED proteins (Figure 2). Therefore, SiNCED1 is homologous with NCED proteins from other species.

3.2 Expression pattern analysis of *SiNCED1* in multiple tissues and under ABA or abiotic stresses treatments

The temporal and spatial expression patterns of *SiNCED1* were observed through RT-qPCR. *SiNCED1* was constitutively expressed in the roots, young leaves, mature leaves, stems, and flowers but highly expressed in the roots, following by the stems, young leaves, mature leaves and flowers (Figure 3A).

To investigate the response of *SiNCED1* transcript levels under ABA, 20% PEG, and 150 mM NaCl treatments, RT-qPCR was performed to analyzed *SiNCED1* expression in the shoots and roots of seedlings. Compared with the normal conditions, *SiNCED1* was strongly induced in the shoots and roots of seedlings that underwent ABA treatment. We found that the expression levels of *SiNCED1* reached their peak at 4 h in the shoots but 0.5 h in the roots (Figures 3B, C). In roots and shoots that had undergone PEG treatment, the expression of *SiNCED1* was also induced, reaching their highest levels at 24 h in the shoots but 12 h in the roots (Figures 3D, E). Under high salt treatment, the level of *SiNCED1* showed a trend of first increasing and then decreasing in the shoots and roots and reached its highest level in both at 4 h (Figures 3F, G). These results suggest that *SiNCED1* plays a role in the tolerance of foxtail millet to multiple types of abiotic stress.

3.3 *SiNCED1* confers drought stress tolerance

The heterogeneous expression of *SiNCED1* in Arabidopsis was investigated to determine the function of *SiNCED1*. Semi-quantitative PCR analysis showed that *SiNCED1* expression was only detected in *SiNCED1*-overexpressing lines (SiOE1-3 and SiOE1-5) but not in Col (Figure 4A). Subsequently, *SiNCED1*-overexpressing plants and Col were analyzed to identify the ability of drought stress tolerance. The *SiNCED1*-overexpressing plants and Col were grown in soil for 25 d under well-watered conditions, and water-stress conditions (water withheld) for 15 d and 30 d. When water was withheld for 30d, almost all Col plants withered, but *SiNCED1*-overexpressing lines did not show any wilted leaves (Figure 4B).

Given that the altered physiological mechanism was possibly responsible for drought stress adaptation, we examined the water loss rate, proline content, and relative electrolyte leakage in detached Arabidopsis rosette leaves. We observed that Col rosette leaves lost water faster than those from the *SiNCED1*-overexpressing lines (Figure 4C). Meanwhile, the proline content and relative electrolyte leakage were not substantially different between Col plants and *SiNCED1*-overexpressing lines under

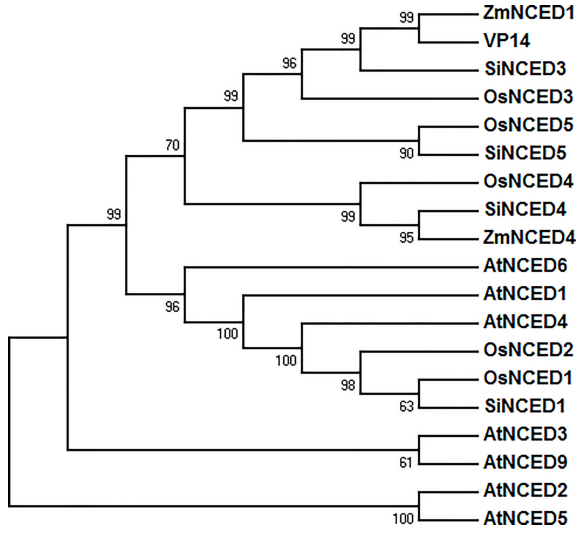

FIGURE 1
Phylogenetic tree analysis based on the amino acid sequences of SiNCED1 and other NCED from other plants. Nineteen amino acid sequences from four species were selected and analyzed by MEGA 7.

10.3389/fpls.2023.1121809

FIGURE 2
Multiple alignment of the deduced protein sequence of SiNCED1 and NCED proteins from other plants. Ten protein sequences from six species were selected and analyzed by Bioedit.

normal conditions. However, *SiNCED1*-overexpressing lines had higher proline content and lower relative electrolyte leakage than Col plants under drought stress (Figures 4D, E). These results indicate that *SiNCED1* could increase drought stress tolerance in foxtail millet.

We also investigated stomatal aperture to further assess the drought stress tolerance in Col and *SiNCED1*-overexpressing plants. Stomatal apertures were classified into three categories: completely open, partially open, and completely closed (Figure 5A). Under normal conditions, the percentage of completely open stomata in *SiNCED1*-overexpressing plants was slightly higher than that in Col plants, but the percentage of completely closed and partially open stomata showed no difference between *SiNCED1*-overexpressing and Col plants (Figure 5B). However, under drought stress conditions, 34% and 32.05% of stomata were completely closed in *SiNCED1*-overexpressing plants (SiOE1-3 and SiOE1-5, respectively), whereas only 20.97% were completely closed in Col plants. Furthermore, only 4.43% and 9.65% of stomata were completely open in *SiNCED1*-overexpressing plants (SiOE1-3 and SiOE1-5, respectively), whereas 14.92% were completely open in Col. Additionally, 64.11% of stomata were partially open in Col, and no marked differences were observed compared with 61.57% and 58.3% of partially open stomata in *SiNCED1*-overexpressing plants (SiOE1-3 and SiOE1-5, respectively) (Figure 5B). Consistent with these results, the stomatal apertures did not differ between Col and *SiNCED1*-overexpressing plants under normal conditions. However, the stomatal apertures of *SiNCED1*-overexpressing plants (SiOE1-3, SiOE1-5) were significantly smaller than those of Col plants under drought conditions (Figure 5C). These results indicate that *SiNCED1* may reduce stomatal apertures to inhibit water loss under drought stress conditions.

3.4 *SiNCED1* increases ABA accumulation and ABA-related stress-responsive gene expression under drought stress

Stomata movement acts as an important mechanism for plant resistance to drought stress through an ABA-dependent pathway. Moreover, NCED is a critical rate-limiting enzyme in ABA biosynthesis. To understand whether endogenous ABA is involved in altering drought stress tolerance, ABA levels were measured in Col and *SiNCED1*-overexpressing plants before and after drought stress treatment. We found that under normal conditions, ABA levels were not different between Col and *SiNCED1*-overexpressing plants (Figure 6A). However, ABA levels rapidly increased under drought stress condition in both

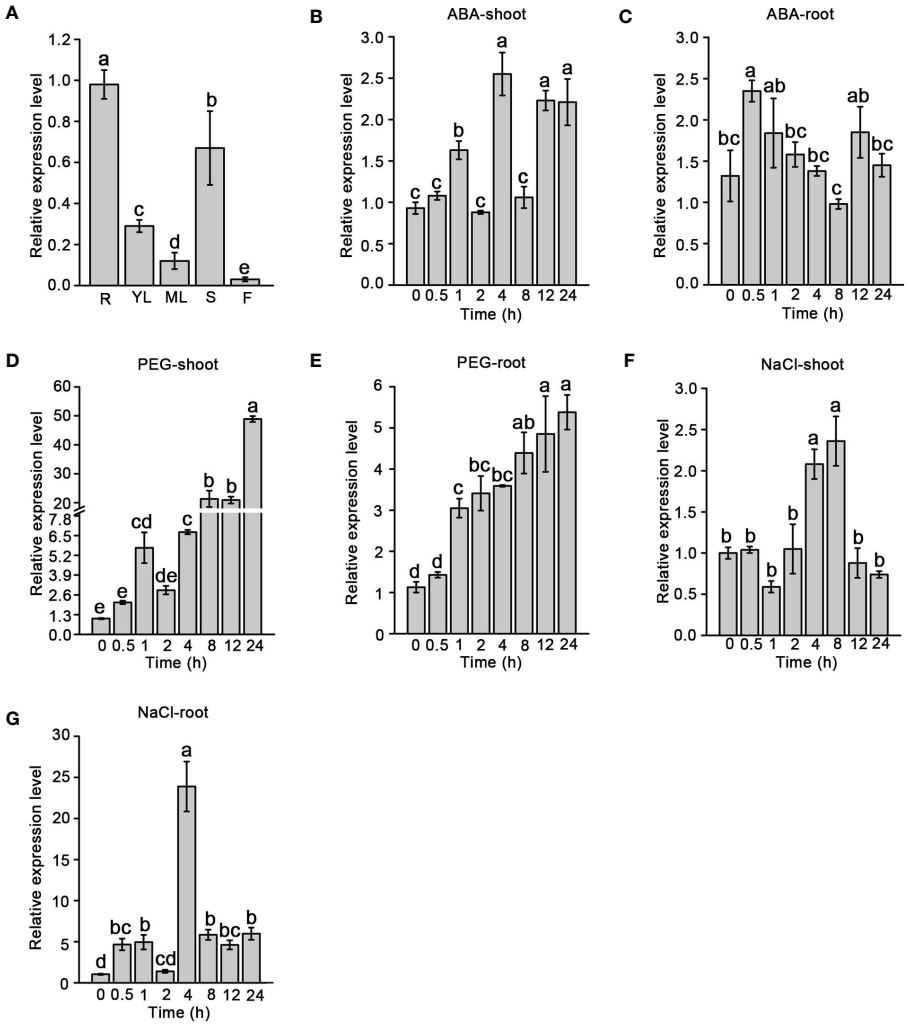

FIGURE 3
SiNCED1 gene expression pattern. **(A)** *SiNCED1* gene expression in different organs. R(root), YL(young leaf), ML(mature leaf), S(stem), F(flower). **(B–G)** The three-leaf stage seedlings were submitted to ABA and 20% PEG, 150 mM NaCl treatment. **(B, C)** Expression of *SiNCED1* under ABA treatment; **(D, E)** Expression of *SiNCED1* under 20% PEG stress; **(F, G)** Expression of *SiNCED1* under 150 mM NaCl stress. The shoot and root samples were collected for *SiNCED1* expression analysis. Data are the mean ± SD for three replicates. Different letters represent significant differences at $P<0.05$ (ANOVA analysis, Tukey's multiple comparisons test).

Col and *SiNCED1*-overexpressing plants, and the ABA levels in *SiNCED1*-overexpressing plants (SiOE1-3, 44.2 ng/g; SiOE1-5, 39 ng/g) were much higher than those in Col plants (31.8 ng/g) (Figure 6A). Therefore, *SiNCED1* increases drought stress tolerance by promoting endogenous ABA biosynthesis in plants.

We further determined the transcript levels of ABA-related stress-responsive genes under normal and drought stress conditions. Consistent with the changes in ABA content, the expression of *AtPP2C*, *AtCOR15A*, *AtRd29B*, *AtSOS1*, and *AtLTP3* did not differ between Col and *SiNCED1*-overexpressing plants under normal conditions. However, the expression levels of these genes were noticeably higher in *SiNCED1*-overexpressing plants than in Col plants (Figures 6B–F). These results suggest that *SiNCED1* up-regulated ABA-related stress-responsive genes under drought stress conditions.

3.5 Delayed seed germination of *SiNCED1*-overexpressing Arabidopsis

The above results show that *SiNCED1* regulates endogenous ABA biosynthesis. Since ABA plays pivotal roles in seed dormancy and germination, the seed germination rate of Col and *SiNCED1*-overexpressing lines were determined. The results showed that the seed germination rate of *SiNCED1*-overexpressing lines was slower and more inhibited than that of Col plants when the seeds were sown in normal MS medium (Figure 7A). Ectopic *SiNCED1*-overexpressing line seeds sown in MS medium containing high NaCl, mannitol, and glucose showed germination delay, which revealed that *SiNCED1*-overexpressing lines were more sensitive to high salt, high mannitol, and high glucose conditions than Col plants (Figures 7B–D). Furthermore, when we grew *SiNCED1*-

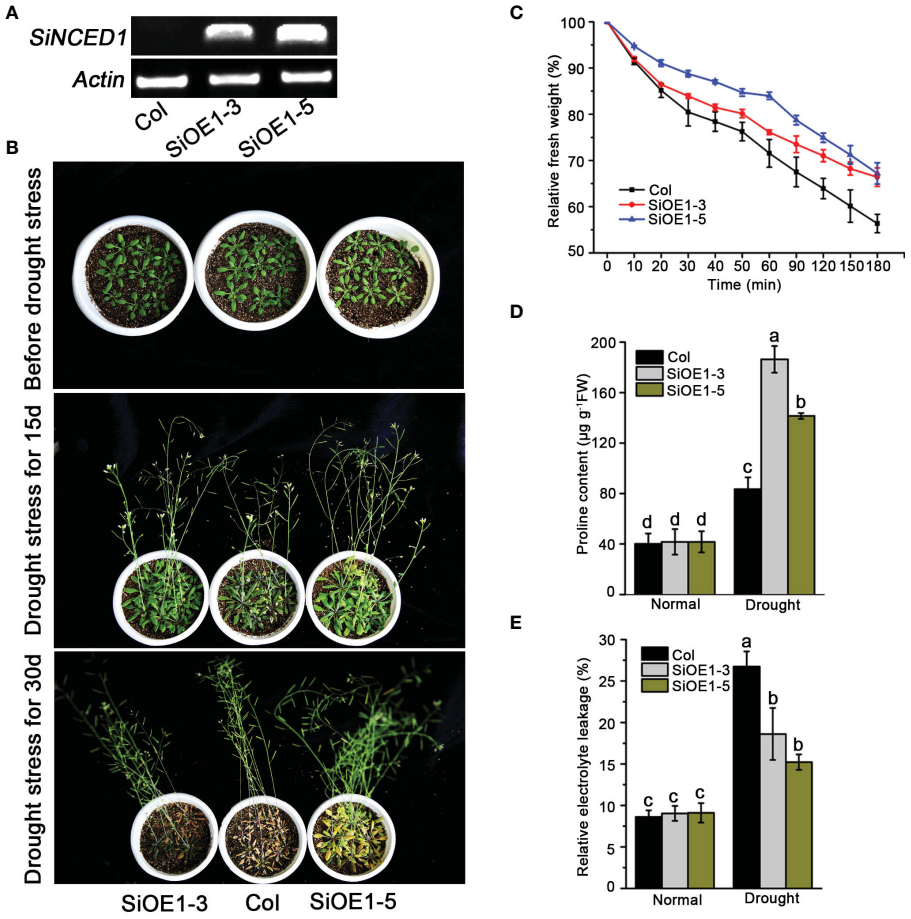

FIGURE 4
Drought stress tolerance of *SiNCED1* overexpression plants. **(A)** Semi-quantitative RT-PCR detection of *SiNCED1* expression in Col and SiOE1-3, SiOE1-5. **(B)** The phenotype of *SiNCED1*-overexpressing plants and Col seedlings under drought stress. **(C)** Measurement of water loss rate in Col and *siNCED1*-overexpressing seedlings. **(D)** Proline content determination after drought stress treatment **(E)** Relative electrolyte leakage determination after drought stress treatment. Data shown are mean ± SD from three independent replicates. Values are the mean ± SD (n = 6 plants). Similar results were obtained from three independent replicates. Different letters represent significant differences at $P<0.05$ (ANOVA analysis, Tukey's multiple comparisons test).

overexpressing lines and Col seeds for 7 d in normal MS media, the Col seeds all germinated, while only 87.58% and 85.60% of the seeds of *SiNCED1*-overexpressing lines OE1-3 and OE1-5 germinated, respectively (Figures 7A, 8A). Sowing the seeds in the MS medium containing high NaCl, mannitol, and glucose for 7 d, the phenotype of *SiNCED1*-overexpressing lines OE1-3 and OE1-5 showed that the seeds could not germinate as well as those of Col (Figures 8B–D).

4 Discussion

ABA is a key hormone in plants that regulates plant development, including seed germination, seedling growth, stomatal aperture, flowering, and senescence. Additionally, it also elevates the ability of plants to withstand multiple stresses (Finkelstein, 2013; Kumar et al., 2022). NCED is the key rate-limiting enzyme in ABA biosynthesis that modulates endogenous ABA homeostasis by oxidatively cleaving 9-*cis*-violaxanthin or 9-*cis*-neoxanthin to produce xanthoxin (Priya and Siva, 2015). Currently, the *NCED* gene has been cloned in many plants, and its biological functions have been reported. However, the biological function of *NCED* in foxtail millet remains unclear. In this study, four *SiNCED* genes were found in the NCBI database and cloned, after which homologous comparison were performed. The following biological functions of *SiNCED1* were identified: seed germination regulation, stomatal closure, and drought stress tolerance by modulating endogenous ABA synthesis.

NCED belongs to the *CCD* gene family, which ordinarily contains the conserved REP65 domain (Yue et al., 2022; Zhao et al., 2022). In our study, the phylogenetic tree and multiple alignment analysis showed that SiNCED1 was separately grouped into one cluster, while the other three SiNCEDs were aggregated into another cluster, but SiNCED1 was homologous with other NCED proteins and contains the conserved REP65 domain (Figures 1, 2). Members of the *NCED* subfamily are involved in the synthesis of ABA, which is involved in plant growth and development (Yang et al., 2022). *OsNCED2* was constitutively

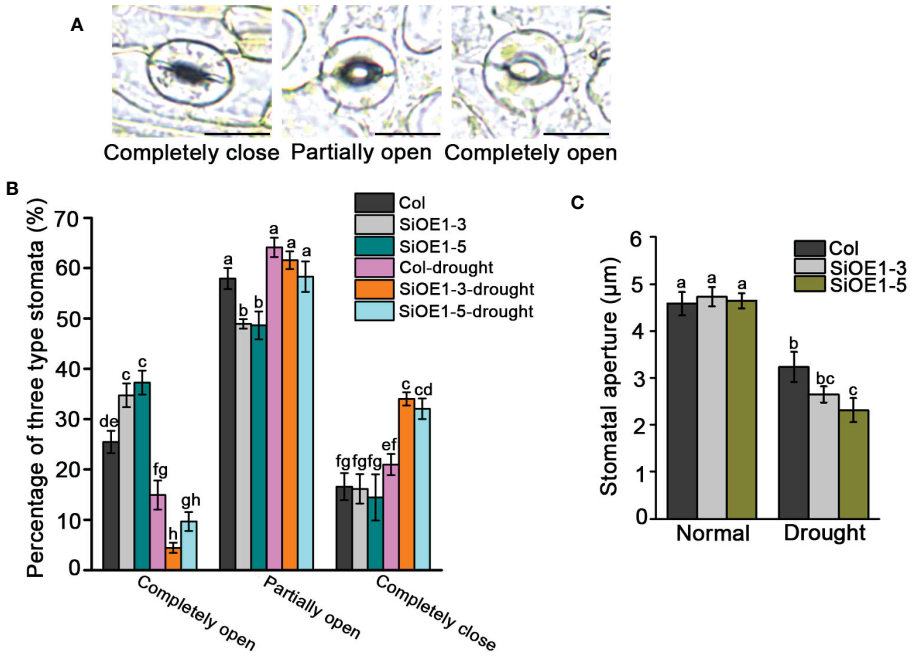

FIGURE 5
Stomata closure of *SiNCED1*-overexpressing plants under drought stress. **(A)** Images of three levels of stomatal apertures, Bars = 10 μm. **(B)** The percentage of three levels of stomatal apertures in *SiNCED1*-overexpressing plants and Col were calculated under normal and drought stress condition. **(C)** Comparison of stomatal apertures in *SiNCED1*-overexpressing plant and Col under normal and drought stress condition. Data shown are mean ± SD from there independent replicate. Each experiment includes at least 30 stomata from each epidermal peel. Different letters represent significant differences at $P<0.05$ (ANOVA analysis, Tukey's multiple comparisons test).

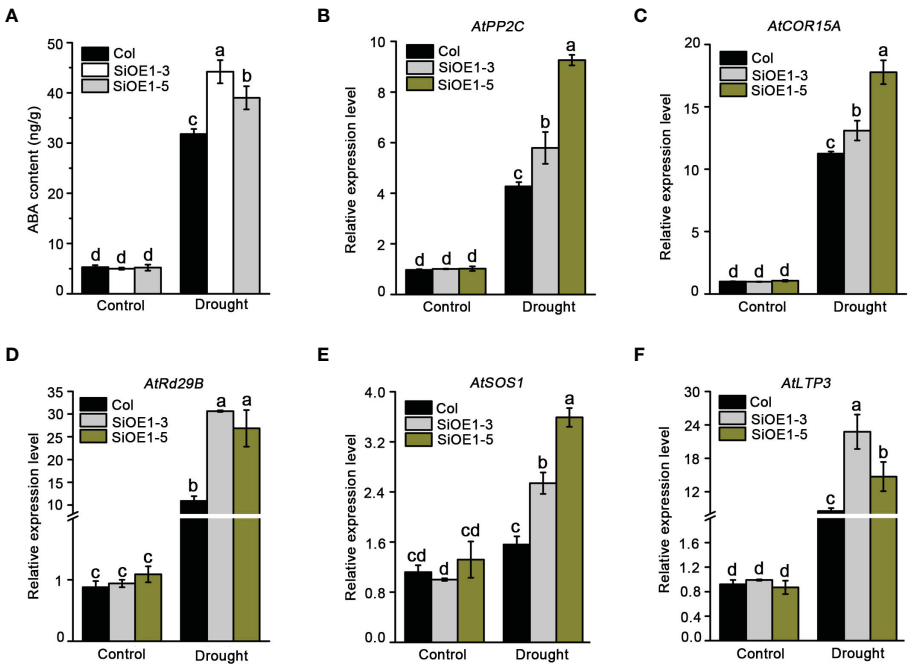

FIGURE 6
ABA content and abiotic stress related genes expression. **(A)** The ABA content in seedlings of Col and *SiNCED1*-overexpressing plants under drought stress. **(B–F)** The expression of ABA related stress responsive genes in Col and *SiNCED1*-overexpressing plants under drought stress for 7 d. Data shown are mean ± SD from there independent replicate. Different letters represent significant differences at $P<0.05$ (ANOVA analysis, Tukey's multiple comparisons test).

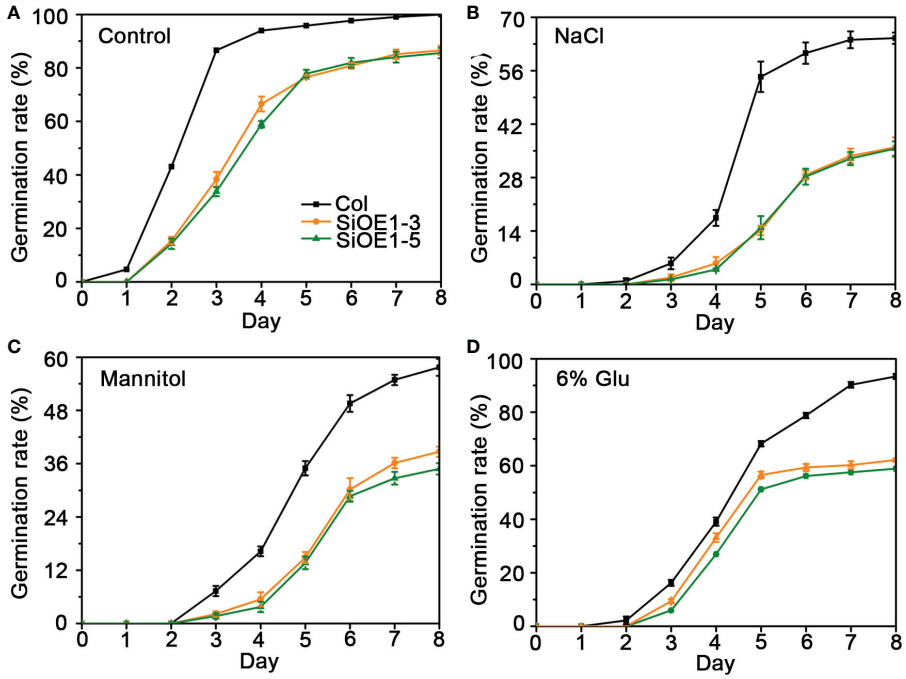

FIGURE 7
Germination rate of Col and *SiNCED1* transgenic seeds grown in MS, Mannitol, NaCl and Glucose media. **(A–D)** The germination rate of Col and *SiNCED1* transgenic seeds grown in MS media contain 150 mM NaCl, 275 mM Mannitol, or 6% Glucose. Data shown are mean ± SD from three independent replicates.

expressed in various tissues in rice plants; *osnced2* mutant seedlings with knockout of *OsNCED2* showed growth inhibition (Copenhaver et al., 2021). *OsNCED3* is expressed in multiple tissues, including embryo, coleoptile, root, leaf, culm, node, flower, stigma, and pollen, with especially high expression found in the flower and root. However, *nced3* mutant seedlings with a mutation in the *OsNCED3* gene showed a faster growth trend as well as longer roots and shoots compared with the wild type (Huang et al., 2018). Furthermore, *osnced2* and *nced3* mutants showed contrary seedling phenotypes. The regulation of endogenous ABA content was regarded as the main mechanism for the regulation of the growth and development of seedlings by *OsNCED2* and *OsNCED3*, which also confirms the dual regulatory effect of endogenous ABA on plant growth and development (Cheng et al., 2002). Expression pattern analysis showed that *SiNCED1* was expressed in multiple organs, especially the roots, which showed the highest expression (Figure 3A). However, the seedling growth and development of ectopic *SiNCED1*-overexpressing lines showed no difference from those of Col. Whether *SiNCED1* modulates the growth and development of foxtail millet needs to be investigated by constructing *nced1* mutants of foxtail millet. In addition, the transcript levels of *SiNCED1* were significantly induced by ABA, osmotic stress, and high salt stress (Figures 3B–G). *SiNCED1* is likely similar to other *NCEDs* in other vascular plants, such as *AtNCED3* in Arabidopsis and *OsNCED3* and *OsNCED4* in rice, which are significantly induced by high salt and osmotic stress (Huang et al., 2018; Hwang et al., 2018).

ABA is an important plant stress hormone. Under water stress, ABA can rapidly synthesize and regulate ABA-dependent signaling pathways to resist water stress, which are in turn regulated by *NCED* genes (Ye et al., 2012; Kavi Kishor et al., 2022). In our study, the ectopic overexpression of *SiNCED1* in Arabidopsis enhanced its ability to survive water stress (Figure 4B), and increased endogenous ABA levels under water stress (Figure 6A). *NCED* genes that participate in drought stress have also been reported in many plants. For instance, heterologous expression of *CrNCED1* in tobacco has indicated that this gene can enhance drought stress tolerance by increasing ABA levels and decreasing the levels of reactive oxygen species (Xian et al., 2014). Constitutively overexpressing *VaNCED1* in a drought-sensitive cultivar of *V. vinifera* increased ABA content and decreased stomatal density, thereby significantly strengthening drought resistance (He et al., 2018). *GhNCED3a/3c* participates in drought stress in cotton because *GhirNAC2* directly binds to its promoter to modulate ABA biosynthesis and stomatal closure (Shang et al., 2020). *AhNCED1*, cloned from peanuts, can control ABA content, and the negative feedback loop regulated by the transcription factor complex *AhAREB1* cooperates with *AhNAC2* under water stress (Liu et al., 2016). *AtNCED3* mediates drought stress by increasing endogenous ABA levels and promoting drought- and ABA-inducible genes expression. These signaling pathways are manipulated by NGATHA1, which binds directly to the *AtNCED3* promoter of the NBE cis-element (Sato et al., 2018). *OsNCED4* can also elevate ABA levels to increase drought tolerance through *OsbZIP23*, which is directly bound to its promoter cis-element, ABRE (Zong et al., 2016).

Under drought conditions, plants produce and accumulate ABA in their guard cells, which induces stomatal closure to

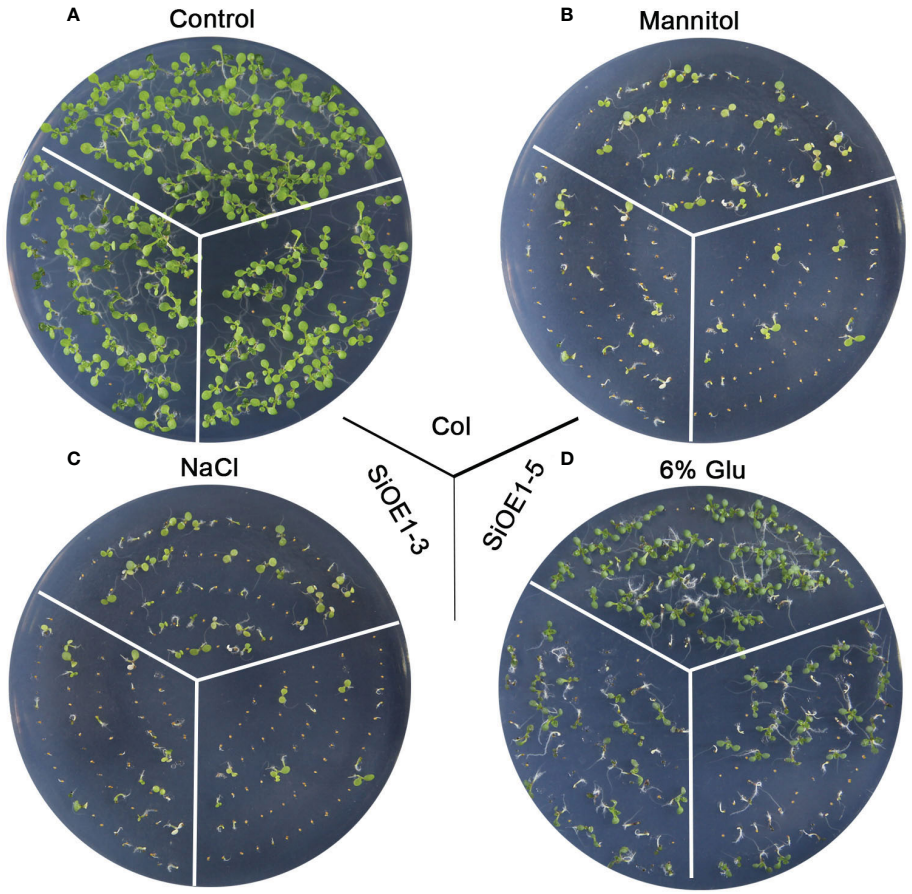

FIGURE 8
Phenotypic analysis of *SiNCED1* transgenic plants under MS, mannitol, NaCl and Glucose. **(A–D)** The phenotype of Col and *SiNCED1* transgenic seeds grown in MS (control), MS contain 275 mM Mannitol, 150 mM NaCl or 6% Glucose, respectively for 7 d.

reduce water loss (Lim et al., 2015; Wang et al., 2022). *NCED* genes have been identified as a major determinant of endogenous ABA levels by regulating ABA biosynthesis (Tan et al., 1997; Schwartz et al., 2003). Our results suggest that *SiNCED1* overexpression in Arabidopsis can reduce water loss by increasing the percentage of completely closed stomata and reducing stomata apertures under water stress (Figure 5). This is consistent with the modulation of ABA biosynthesis and stomatal closure by *GhNCED3a/3c* under drought stress (Shang et al., 2020) and *AtNCED3* expression induced by the small peptide CLE25 to enhance ABA levels and modulate stomatal movement to prevent water loss (Takahashi et al., 2018). In addition, proline content and electrolyte leakage are important physiological indices for the evaluation of plant resistance to water stress (Voetberg and Sharp, 1991; Jiang et al., 2016). The ectopic expression of *BnNCED3* in Arabidopsis or overexpression of *OsNCED5* in rice resulted in both exhibiting higher proline content and lower electrolyte leakage than the wild type following drought stress treatment (Xu and Cai, 2017; Huang et al., 2019). In the present study, *SiNCED1*-overexpressing transgenic lines had higher proline content and lower electrolyte leakage than Col under water stress (Figures 4D, F), which is reliable evidence for the role of *SiNCED1* in resistance to drought stress. Furthermore, high expression levels of ABA-related stress-responsive marker genes, such as *AtPP2C*, *AtCOR15A*, *AtRd29B*, *AtSOS1*, and *AtLTP3*, enhance resistance to drought stress in Arabidopsis (Guo et al., 2013; Yang et al., 2018; Lu et al., 2019). We found that the expression levels of these stress-responsive genes increased substantially in *SiNCED1* transgenic lines (Figures 6B–F), indicating that *SiNCED1* can also help to maintain a high resistance to water stress.

ABA has an important effect on seed dormancy, which relies on its biosynthesis and catabolism (Bentsink and Koornneef, 2008). Numerous studies have showed that the overexpression of ABA biosynthesis pathway genes, including *PtNCED1* (Lee et al., 2018), *AtNCED9* (Seo et al., 2016), *BdNCED1* (Barrero et al., 2012), *TaNCED2* (Izydorczyk et al., 2018), and *LeNCED1* (Tung et al., 2008), can promote seed dormancy by regulating endogenous ABA accumulation. In the present study, *SiNCED1* overexpression in transgenic lines exhibited the inhibition of seed germination under normal and abiotic stress conditions (Figures 7 and 8), which showed a similar phenotype to that in the above-mentioned reports. However, the molecular mechanism underlying the regulation of dormancy and germination processes in foxtail millet seeds by *SiNCED1* still requires further study.

In the present study, four *NCED* genes were identified and cloned into foxtail millet. The relative expression levels of *SiNCED1* were strongly induced in the shoots and roots under osmotic stress. Overexpression of *SiNCED* confers drought stress tolerance to Arabidopsis. This function is supported by the finding that *SiNCED1* regulates ABA biosynthesis to modulate stress-related physiological indices, stomatal closure, and ABA-related stress-responsive genes. Furthermore, *SiNCED1* promotes seed dormancy by increasing ABA accumulation. Thus, *SiNCED1* is likely crucial for improving the breeding of foxtail millet. The mechanisms by which *SiNCED1* cooperates with other *SiNCED* members and how transcription factors regulate its expression and affect developmental processes and abiotic stress could be novel research topics for future studies.

Data availability statement

The original contributions presented in the study are included in the article/Supplementary Material, further inquiries can be directed to the corresponding author.

Author contributions

Conceptualization, ML and LC. Formal analysis, SY and FW. Investigation, YH and YJ. Supervision, ML and LC. Writing—original draft, YH and SY. Writing—review and editing, ML and DM. All authors contributed to the article and approved the submitted version.

Funding

This study was supported by the National Natural Science Foundation of China (No. 8226140781), the Basic Scientific Research Program from Guizhou Science and Technology Agency (No. Qian Ke He Ji Chu-ZK [2021]522).

Conflict of interest

The authors declare that the research was conducted in the absence of any commercial or financial relationships that could be construed as a potential conflict of interest.

Publisher's note

All claims expressed in this article are solely those of the authors and do not necessarily represent those of their affiliated organizations, or those of the publisher, the editors and the reviewers. Any product that may be evaluated in this article, or claim that may be made by its manufacturer, is not guaranteed or endorsed by the publisher.

Supplementary material

The Supplementary Material for this article can be found online at: https://www.frontiersin.org/articles/10.3389/fpls.2023.1121809/full#supplementary-material

References

Andrew, D., and Roger, H. (1992). Abscisic acid biosynthesis in root. *Planta* 187, 185–191. doi: 10.1007/BF00201936

Barrero, J. M., Jacobsen, J. V., Talbot, M. J., White, R. G., Swain, S. M., Garvin, D. F., et al. (2012). Grain dormancy and light quality effects on germination in the model grass brachypodium distachyon. *New Phytol.* 193 (2), 376–386. doi: 10.1111/j.1469-8137.2011.03938.x

Barton, L., Newsome, S., Chen, F., Wang, H., Guilderson, T., and Bettinger, R. (2009). Agricultural origins and the isotopic identity of domestication in northern China. *Proc. Natl. Acad. Sci. U.S.A.* 106 (14), 5523–5528. doi: 10.1073/pnas.0809960106

Bentsink, L., and Koornneef, L. (2008). "Seed dormancy and germination," in *The arabidopsis book* 6, 1–18. doi: 10.1199/tab.0050

Cheng, W., Endo, A., Zhou, L., Penney, J., Chen, H., Arroyo, A., et al. (2002). A unique short-chain dehydrogenase/reductase in arabidopsis glucose signaling and abscisic acid biosynthesis and functions. *Plant Cell* 14 (11), 2723–2743. doi: 10.1105/tpc.006494

Copenhaver, G., Li, X., Yu, B., Wu, Q., Min, Q., Zeng, R., et al. (2021). OsMADS23 phosphorylated by SAPK9 confers drought and salt tolerance by regulating ABA biosynthesis in rice. *PloS Genet.* 17 (8), e1009699. doi: 10.1371/journal.pgen.1009699

Doust, A., Kellogg, E., Devos, K., and Bennetzen, J. (2009). Foxtail millet: a sequence-driven grass model system. *Plant Physiol.* 149 (1), 137–141. doi: 10.1104/pp.108.129627

Eiji, N., and Annie, M. (2005). Abscisic acid biosynthesis and catabolism. *Annu. Rev. Plant Biol.* 56, 165–185. doi: 10.1146/annurev.arplant.56.032604.144046

Finkelstein, R. (2013). Abscisic acid synthesis and response. *Am. Soc. Plant Biologists.* 11. doi: 10.1199/tab.0166

Frey, A., Effroy, D., Lefebvre, V., Seo, M., Perreau, F., Berger, A., et al. (2012). Epoxycarotenoid cleavage by NCED5 fine-tunes ABA accumulation and affects seed dormancy and drought tolerance with other NCED family members. *Plant J.* 70 (3), 501–512. doi: 10.1111/j.1365-313X.2011.04887.x

Guo, L., Yang, H. B., Zhang, X. Y., and Yang, S. H. (2013). Lipid transfer protein 3 as a target of MYB96 mediates freezing and drought stress in arabidopsis. *J. Exp. Bot.* 64 (6), 1755–1767. doi: 10.1093/jxb/ert040

Hao, G. P., Zhang, X. H., Wang, Y. Q., Wu, Z. Y., and Huang, C. L. (2009). Nucleotide variation in the *NCED3* region of *Arabidopsis thaliana* and its association study with abscisic acid content under drought stress. *J. Integr. Plant Biol.* 51 (2), 175–183. doi: 10.1111/j.1744-7909.2008.00786.x

He, R., Zhuang, Y., Cai, Y., Agüero, C. B., Liu, S., Wu, J., et al. (2018). Overexpression of 9-cis-epoxycarotenoid dioxygenase cisgene in grapevine increases drought tolerance and results in pleiotropic effects. *Front. Plant Sci.* 9 (970). doi: 10.3389/fpls.2018.00970

Huang, Y., Guo, Y., Liu, Y., Zhang, F., Wang, Z., Wang, H., et al. (2018). 9-cis-epoxycarotenoid dioxygenase 3 regulates plant growth and enhances multi-abiotic stress tolerance in rice. *Front. Plant Sci.* 9. doi: 10.3389/fpls.2018.00162

Huang, Y., Jiao, Y., Xie, N., Guo, Y., Zhang, F., Xiang, Z., et al. (2019). *OsNCED5*, a 9-cis-epoxycarotenoid dioxygenase gene, regulates salt and water stress tolerance and leaf senescence in rice. *Plant Sci.* 287, 110188. doi: 10.1016/j.plantsci.2019.110188

Hwang, S. G., Chen, H. C., Huang, W. Y., Chu, Y. C., Shii, C. T., and Cheng, W. H. (2010). Ectopic expression of rice *OsNCED3* in arabidopsis increases ABA level and alters leaf morphology. *Plant Sci.* 178 (1), 12–22. doi: 10.1016/j.plantsci.2009.09.014

Hwang, S. G., Lee, C. Y., and Tseng, C. S. (2018). Heterologous expression of rice 9-cis-epoxycarotenoid dioxygenase 4 (*OsNCED4*) in arabidopsis confers sugar oversensitivity and drought tolerance. *Botanical Stud.* 59 (1). doi: 10.1186/s40529-018-0219-9

Izydorczyk, C., Nguyen, T. N., Jo, S., Son, S., Tuan, P. A., and Ayele, B. T. (2018). Spatiotemporal modulation of abscisic acid and gibberellin metabolism and signalling mediates the effects of suboptimal and supraotimal temperatures on seed germination in wheat (*Triticum aestivum* l.). *Plant Cell Environ.* 41, 1022–1037. doi: 10.1111/pce.12949

Jiang, Y., Qiu, Y., Hu, Y., and Yu, D. (2016). Heterologous expression of *AtWRKY57* confers drought tolerance in *Oryza sativa*. *Front. Plant Sci.* 7. doi: 10.3389/fpls.2016.00145

Kavi Kishor, P. B., Tiozon, R. N., Fernie, A. R., and Sreenivasulu, N. (2022). Abscisic acid and its role in the modulation of plant growth, development, and yield stability. *Trends Plant Sci.* 27 (12), 1283–1295. doi: 10.1016/j.tplants.2022.08.013

Koshiba, M. (2002). Complex regulation of ABA biosynthesis in plants. *Trends Plant Sci.* 7 (1), 41–48. doi: 10.1016/s1360-1385(01)02187-2

Kumar, S., Shah, S. H., Vimala, Y., Jatav, H. S., Ahmad, P., Chen, Y., et al. (2022). Metabolism, transport, crosstalk with other plant growth regulators, and its role in heavy metal stress mitigation. *Front. Plant Sci.* 13. doi: 10.3389/fpls.2022.972856

Lang, J., Fu, Y. X., Zhou, Y., Cheng, M. P., Deng, M., Li, M. L., et al. (2021). *Myb10-d* confers *PHS-3D* resistance to pre-harvest sprouting by regulating *NCED* in ABA. *New Phytol.* 230, 1940–1952. doi: 10.1111/NPH.17312

Lee, Y. I., Chen, M. C., Lin, L., Chung, M. C., and Leu, W. M. (2018). Increased expression of 9- cis-epoxycarotenoid dioxygenase, *PtNCED1*, associated with inhibited seed germination in a terrestrial orchid, *Phaius tankervilliae*. *Front. Plant Sci.* 9. doi: 10.3389/fpls.2018.01043

Li, H. Z., and Cheng, Z. H. (2015). Hoagland nutrient solution promotes the growth of cucumber seedlings under light-emitting diode lingt. *Acta Agric. Scand. Sect. B Soil Plant Sci.* 65, 74–82. doi: 10.1080/09064710.2014.967285

Li, Q. H., Yu, X. T., Chen, L., Zhao, G., Li, S. Z., Zhou, H., et al. (2021). Genome-wide identification and expression analysis of the NCED family in cotton (*Gossypium hirsutum* l.). *PloS One* 16 (2), e0246021. doi: 10.1371/journal.pone.0246021

Lim, C. W., Baek, W. H., Jung, J. H., Kim, J. H., and Lee, S. C. (2015). Function of ABA in stomatal defense against biotic and drought stresses. *Int. J. Mol. Sci.* 16, 15251–15270. doi: 10.3390/ijms160715251

Liu, S., Li, M. J., Su, L. C., Ge, K., Li, L. M., Li, X. Y., et al. (2016). Negative feedback regulation of ABA biosynthesis in peanut (*Arachis hypogaea*): a transcriptioin factor complex inhibits *AhNCED1* expression during water stress. *Sci. Rep.* 6, 37943. doi: 10.1038/srep37943

Livak, K. J., and Schmittgen, T. D. (2001). Analysis of relative gene expression data using real-time quantitative PCR and the 2 (-DeltaDeltaC(T)). *Method Methods* 25, 402–408. doi: 10.1006/meth.2001.1262

Lou, D., Wang, H., Liang, G., and Yu, D.. (2017). OsSAPK2 confers abscisic acid sensitivity and tolerance to drought stress in rice. *Front. Plant Sci.* 8, 993. doi: 10.3389/fpls. 2017.00993

Lu, C. Q., Yu, F., Tian, L. F., Huang, X. Y., Tan, H., Xie, Z. J., et al. (2017). RPS9M, a mitochondrial ribosomal protein, is essential for central cell maturation and endosperm development in *Arabidopsis*. *Front. Plant Sci.* 8. doi: 10.3389/fpls.2017.02171

Lu, P., Magwanga, R. O., Kirungu, J. N., Hu, Y. G., Dong, Q., Cai, X. Y., et al. (2019). Overexpression of cotton a *DTX/MATE* gene enhances drought, salt, and cold stress tolerance in transgenic arabidopsis. *Front. Plant Sci.* 10. doi: 10.3389/fpls.2019.00299

Miao, J., Guo, D. S., Zhang, J. Z., Huang, Q. P., Qin, G. J., Zhang, X., et al. (2013). Targeted mutagenesis in rice using CRISPR-cas system. *Cell Res.* 23, 1233–1236. doi: 10.1038/cr.2013.123

Nambara, E., Okamoto, M., Tatematsu, K., Yano, R., Seo, M., and Kamiya, Y. (2010). Abscisic acid and the control of seed dormancy and germination. *Seed Sci. Res.* 20 (2), 55–67. doi: 10.1017/s0960258510000012

Ng, L. M., Melcher, K., Teh, B. T., and Xu, H. E. (2014). Abscisic acid perception and signaling: structural mechanisms and applications. *Acta Pharmacologica Sin.* 35 (5), 567–584. doi: 10.1038/aps.2014.5

Pantin, F., Monnet, F., Jannaud, D., Costa, J. M., Renaud, J., Muller, B., et al. (2013). The dual effect of abscisic acid on stomata. *New Phytol.* 197 (1), 65–72. doi: 10.1111/nph.12013

Priya, R., and Siva, R. (2015). Analysis of phylogenetic and functional diverge in plant nine–cis epoxycarotenoid dioxygenase gene family. *J. Plant Res.* 128, 519–534. doi: 10.1007/s10265-015-0726-7

Sah, S. K., Reddy, K. R., and Li, J. (2016). Abscisic ccid and abiotic stress tolerance in crop plants. *Front. Plant Sci.* 7. doi: 10.3389/fpls.2016.00571

Sano, N., and Marion-Poll, A. (2021). ABA metabolism and homeostasis in seed dormancy and germination. *Int. J. Mol. Sci.* 22 (10), 5069. doi: 10.3390/ijms22105069

Sato, H., Takasaki, H., Takahashi, F., Satoshi, L., Mitsuda, N., Ohme Takagi, M., et al. (2018). *Arabidopsis thaliana* NGATHA1 transcription factor induces ABA biosynthesis by activating *NCED3* gene during dehydration stress. *PNAS* 115, e11178–e11187. doi: 10.1073/pnas.1811491115

Schwartz, S. H., Qin, X., and Zeevaart, J. A. D. (2003). Elucidation of the indirect pathway of abscisic acid biosynthesis by mutants, genes, and enzymes. *Plant Physiol.* 131, 1591–1601. doi: 10.1104/pp.102.017921

Schwartz, S. H., Tan, B., Gage, D. A., Zeevaart, J. A. D., and McCarty, R. D. (1997). Specific oxidative cleavage of carotenoids by VP14 of maize. *Science* 276, 1872–1874. doi: 10.1126/science.276.5320.1872

Seo, M., Kanno, Y., Frey, A., North, H. M., and Marion-Poll, A. (2016). Dissection of arabidopsis *NCED9* promoter regulatory regions reveals a role for ABA synthesized in embryos in the regulation of GA-dependent seed germination. *Plant Sci.* 246, 91–97. doi: 10.1016/j.plantsci.2016.02.013

Shang, X. G., Yu, Y. J., Zhu, L. J., Liu, H. Q., Chai, Q. C., and Guo, W. Z. (2020). A cotton NAC transcription factor GhirNAC2 plays positive roles in drought tolerance *via* regulating ABA biosynthesis. *Plant Sci.* 296, 110498. doi: 10.1016/j.plantsci.2020.110498

Sun, L., Sun, Y. F., Zhang, M., Wang, L., Ren, J., Cui, M. M., et al. (2012). Suppression of 9-cis-epoxycarotenoid dioxygenase, which encodes a key enzyme in abscisic acid biosynthesis, alters fruit texture in transgenic tomato. *Plant Physiol.* 158, 283–298. doi: 10.1104/pp.111.186866

Takahashi, F., Suzuki, T., Osakabe, Y., Betsuyaku, S., Kondo, Y., Dohmae, N., et al. (2018). A small peptide modulates stomatal control *via* abscisic acid in long-distance signalling. *Nature* 556 (7700), 235–238. doi: 10.1038/s41586-018-0009-2

Tan, B. T., Joseph, L. M., Deng, W. D., Liu, L., Li, Q., Cline, K., et al. (2003). Molecular characterization of the arabidopsis 9-cis epoxycarotenoid dioxygenase gene family. *Plant J.* 33, 44–56. doi: 10.1046/j.1365-313x.2003.01786.x

Tan, B., Schwartz, S. H., Zeevaart, J. A. D., and McCarty, D. R. (1997). Genetic control of abscisic acid biosynthesis in maize. *Proc. Natl. Acad. Sci. U.S.A.* 94, 12235–12240. doi: 10.1073/pnas.94.22.12235

Tung, S. A., Smeeton, R., White, C. A., Black, C. R., Taylor, I. B., Hilton, H. W., et al. (2008). Over-expression of *LeNCED1* in tomato (*Solanum lycopersicum* l.) with the rbcS3C promoter allows recovery of lines that accumulate very high levels of abscisic acid and exhibit severe phenotypes. *Plant Cell Environ.* 31, 968–981. doi: 10.1111/j.1365-3040.2008.01812.x

Voetberg, G. S., and Sharp, R. E. (1991). Growth of the maize primary root at low water potentials III. role of increased proline deposition in osmotic adjustment. *Plant Physiol.* 96, 1125–1130. doi: 10.1104/pp.96.4.1125

Wang, P., Lu, S., Zhang, X., Hyden, B., Qin, L., Liu, L., et al. (2021). Double NCED isozymes control ABA biosynthesis for ripening and senescent regulation in peach fruits. *Plant Sci.* 304, 110739. doi: 10.1016/j.plantsci.2020.110739

Wang, P., Qi, S. J., Wang, X. H., Dou, L. R., Jia, M. A., Mao, T. L., et al. (2022). The OPEN STOMATA1-SPIRAL1 module regulates microtubule stability during abscisic acid-induced stomatal closure in arabidopsis. *Plant Cell* 35 (1), 260–278. doi: 10.1093/plcell/koac307

Xian, L., Sun, P., Hu, S., Wu, J., and Liu, J. (2014). Molecular cloning and characterization of *CrNCED1*, a gene encoding 9–cis–epoxycarotenoid dioxygenase in *Citrus reshni*, with functions in tolerance to multiple abiotic stresses. *Planta* 239, 61–77. doi: 10.1007/s00425-013-1963-4

Xu, P., and Cai, W. (2017). Functional characterization of the *BnNCED3* gene in *Brassica napus*. *Palnt Sci.* 256, 16–24. doi: 10.1016/j.plantsci.2016.11.012

Xu, Z. Y., Kim, D. H., and Hwang, I. (2013). ABA homeostasis and signaling involving multiple subcellular compartments and multiple receptors. *Plant Cell Rep.* 32 (6), 807–813. doi: 10.1007/s00299-013-1396-3

Yang, X. W., He, K., Chi, X. Y., Chai, G. H., Wang, Y. P., Jia, C. L., et al. (2018). *Miscanthus* NAC transcription factor MlNAC12 positively mediates abiotic stress tolerance in transgenic arabidopsis. *Plant Sci.* 277, 229–241. doi: 10.1016/j.plantsci.2018.09.013

Yang, X., Jia, Z., Pu, Q., Tian, Y., Zhu, F., and Liu, Y. (2022). ABA mediates plant development and abiotic stress *via* alternative splicing. *Int. J. Mol. Sci.* 23 (7). doi: 10.3390/ijms23073796

Ye, N. H., Jia, L. H., and Zhang, J. H. (2012). ABA signal in rice under stress conditions. *Rice* 5, 1. doi: 10.1186/1939-8433-5-1

Ye, N. H., Zhu, G. H., Liu, Y. G., Li, Y. X., and Zhang, J. H. (2011). Glucose-induced delay of seed germination in rice is mediated by the suppression of ABA catabolism rather than an enhancement of ABA biosynthesis. *Plant Cell Phsiology* 52 (4), 689–698. doi: 10.1093/pcp/pcp022

Yue, X. Q., Zhang, Y., Yang, C. K., Li, J. G., Rui, X., Ding, F., et al. (2022). Genome-wide identification and expression analysis of carotenoid cleavage oxygenase genes in litchi (*Litchi chinensis* sonn.). *BMC Plant Biol.* 22, 394. doi: 10.1186/s12870-022-03772-w

Zhang, G. Y., Liu, X., Quan, Z. W., Cheng, S. F., Xu, X., Pan, S. K., et al. (2012). Genome sequence of foxtail millet (*Setaria italica*) provides insights into grass evolution and biofuel potential. *Nat. Biotechnol.* 30 (6), 549–554. doi: 10.1038/nbt.2195

Zhao, X. L., Yang, Y. L., Xia, H. X., and Li, Y. (2022). Genome-wide analysis of the carotenoid cleavage dioxygenases gene family in *Forsythia suspensa*: Expression profile and cold and drought stress responses. *Front. Plant Sci.* 13. doi: 10.3389/fpls.2022.998911

Zhou, H., Wang, Y. F., Zhang, Y. J., Xiao, Y. H., Liu, X., Deng, H. B., et al. (2022). Comparative analysis of heat-tolerant and heat-susceptible rice highlights the role of *OsNCED1* gene in heat stress tolerance. *Plants* 11 (8), 1062. doi: 10.3390/plants11081062

Zong, W., Tang, N., Yang, J., Pang, L. P., Ma, S. Q., Yan, X., et al. (2016). Feedback regulation of ABA signaling and biosynthesis by a bZIP transcription factor targets drought-Resistance-Related genes. *Palnt Physiol.* 171, 2810–2825. doi: 10.1104/pp.16.00469

frontiers | Frontiers in Plant Science

TYPE Original Research
PUBLISHED 09 March 2023
DOI 10.3389/fpls.2023.1117246

Check for updates

OPEN ACCESS

EDITED BY
Mehdi Rahimi,
Graduate University of Advanced Technology, Iran

REVIEWED BY
Feng Xu,
Yangtze University, China
Leila Zarei,
Razi University, Iran

*CORRESPONDENCE
Shengzuo Fang
fangsz@njfu.edu.cn

SPECIALTY SECTION
This article was submitted to Plant Abiotic Stress, a section of the journal Frontiers in Plant Science

RECEIVED 06 December 2022
ACCEPTED 20 February 2023
PUBLISHED 09 March 2023

CITATION
Zhang Z, Fang J, Zhang L, Jin H and Fang S (2023) Genome-wide identification of bHLH transcription factors and their response to salt stress in *Cyclocarya paliurus*. *Front. Plant Sci.* 14:1117246. doi: 10.3389/fpls.2023.1117246

COPYRIGHT
© 2023 Zhang, Fang, Zhang, Jin and Fang. This is an open-access article distributed under the terms of the Creative Commons Attribution License (CC BY). The use, distribution or reproduction in other forums is permitted, provided the original author(s) and the copyright owner(s) are credited and that the original publication in this journal is cited, in accordance with accepted academic practice. No use, distribution or reproduction is permitted which does not comply with these terms.

Genome-wide identification of bHLH transcription factors and their response to salt stress in *Cyclocarya paliurus*

Zijie Zhang[1], Jie Fang[1], Lei Zhang[1,2], Huiyin Jin[1] and Shengzuo Fang[1,2]*

[1]College of Forestry, Nanjing Forestry University, Nanjing, China, [2]Co-Innovation Center for Sustainable Forestry in Southern China, Nanjing, China

As a highly valued and multiple function tree species, the leaves of *Cyclocarya paliurus* are enriched in diverse bioactive substances with healthy function. To meet the requirement for its leaf production and medical use, the land with salt stress would be a potential resource for developing *C. paliurus* plantations due to the limitation of land resources in China. The basic helix-loop-helix (bHLH) transcription factor protein family, the second largest protein family in plants, has been found to play essential roles in the response to multiple abiotic stresses, especially salt stress. However, the *bHLH* gene family in *C.paliurus* has not been investigated. In this study, 159 *CpbHLH* genes were successfully identified from the whole-genome sequence data, and were classified into 26 subfamilies. Meanwhile, the 159 members were also analyzed from the aspects of protein sequences alignment, evolution, motif prediction, promoter cis-acting elements analysis and DNA binding ability. Based on transcriptome profiling under a hydroponic experiment with four salt concentrations (0%, 0.15%, 0.3%, and 0.45% NaCl), 9 significantly up- or down-regulated genes were screened, while 3 genes associated with salt response were selected in term of the GO annotation results. Totally 12 candidate genes were selected in response to salt stress. Moreover, based on expression analysis of the 12 candidate genes sampled from a pot experiment with three salt concentrations (0%, 0.2% and 0.4% NaCl), *CpbHLH36/68/146* were further verified to be involved in the regulation of salt tolerance genes, which is also confirmed by protein interaction network analysis. This study was the first analysis of the transcription factor family at the genome-wide level of *C. paliurus*, and our findings would not only provide insight into the function of the *CpbHLH* gene family members involved in salt stress but also drive progress in genetic improvement for the salt tolerance of *C. paliurus*.

KEYWORDS

wheel wingnut, *bHLH* family genes, *CpbHLH* genes, salt tolerance, expression analysis, regulation networks

1 Introduction

Plants are constantly challenged by the environmental stresses, and it is estimated that up to 70% of plants can be affected by diverse abiotic stresses from which they cannot escape (Mantri et al., 2012a; Chen et al., 2021). Salinity stress, which affects 8.31 billion hm^2 of land, is one of the major abiotic stresses to impair plant growth (Li et al., 2020a; Zhang et al., 2020a; Liao et al., 2022). In order to maintain normal growth and survival, plants turned on or suppressed many genes by transcription factors (TFs) to regulate physiological and biochemical processes in response to changes in the external environment (Agarwal et al., 2006; Bhatnagar-Mathur et al., 2008). It has been noted that six major families of transcription factors (TFs) have vital regulatory functions in plant resistance to various abiotic stresses, including MYBs, basic helix-loop-helix (bHLHs), ethylene responsive element binding factor (ERFs), dehydration responsive element-binding (DREBs), WRKYs and basic region/leucine zipper motif members (bZIPs) (Kavas et al., 2016; Mao et al., 2017; Zhang et al., 2022a). As reported, the bHLH TFs are widespread in all eukaryotes and own the second largest number of TF families in plants (Pires and Dolan, 2010; Feller et al., 2011), while the bHLH members possess highly conserved bHLH domain constituted by two functionally diverse regions with approximately 60 amino acids (Toledo-Ortiz et al., 2003). The basic region, containing approximately 10-17 amino acids and a binding site to bind the specific E-box (CANNTG) DNA sequence, is located at the N-terminus. Inversely, at the C-terminus, the helix-loop-helix (HLH) region, consisting of roughly 40 amino acids and acting as a dimerization domain, is responsible for facilitating the dimerization between proteins (Atchley et al., 1999). On account of diverse binding elements, bHLH transcription factors in animals were organized into six groups (Wang et al., 2018b), whereas the classification of plant bHLH proteins has not been determined though 15-32 groups were suggested according to current studies (Pires and Dolan, 2010).

Over the years, many plant bHLH proteins have been identified and characterized. For example, there are 162 *bHLH* genes in *Arabidopsis thaliana* (Toledo-Ortiz et al., 2003), 188 in apple (*Malus* × *domestica*) (Mao et al., 2017), and 113 in strawberry (*Fragaria* × *ananassa*) (Zhao et al., 2018), 115 in spine grapes (*Vitis davidii*)(Li et al., 2021) and 206 in sweet osmanthus (*Osmanthus fragrans*) (Li et al., 2020b). Furthermore, some studies on the role of bHLH proteins revealed that the plant bHLH family participated in numerous processes including anthocyanin biosynthesis (Hou et al., 2017; Lim et al., 2017), growth and development (Sorensen et al., 2003; Carretero-Paulet et al., 2010) and response to stress (Babitha et al., 2013; Ji et al., 2016; Sum et al., 2021). Among the functions, regulating the stress tolerance by binding to the promoters of downstream genes has been well characterized in bHLH proteins (Cui et al., 2016). For instance, *MdbHLH104* was recognized to response to iron deficiency stress in apple by immediately binding to the P3 cis-acting element of the *MdAHA8* promoter (Zhao et al., 2016), while *ICE1 (AtbHLH116)*, could increase the cold tolerance in *A. thaliana* by activating expression the cold-responsive (COR) genes (Chinnusamy et al., 2003). Besides, gene *AtbHLH92* has been shown to have function in responses to osmotic stresses of plants (Jiang et al., 2009) and AtbHLH17 (AtAIB), a nuclear-localized bHLH-type protein, could confer the drought tolerance of transgenic plants *via* regulating of ABA signaling (Li et al., 2007). More interesting is some bHLH TFs could play essential role in the regulation of multiple abiotic stresses signaling simultaneously. For instance, *SlICE1a* (a tomato bHLH transcription factor) could enhance the resistance of cold, osmotic and salt stresses (Feng et al., 2013), while overexpressed *TabHLH39* in *A. thaliana* could increase freezing, salt, and drought tolerance (Zhai et al., 2016). It was also reported that ATNIG1 regulates downstream gene expression by specifically binding to E-box motifs (CANNTG) of salt stress-related gene promoters, thereby enhanced plant tolerance to salt stress (Kim and Kim, 2006).

Wheel wingnut (*Cyclocarya paliurus*), a multiple-fuction tree species, belongs to Juglandaceae family (Fang, 2022). Although now naturally distributed in sub-tropical mountain areas of China, *Cyclocarya* has a long fossil record of fruits in North America, Europe and eastern Asia, while went extinct in North America and Europe during the Cenozoic (Manchester et al., 2009; Wu et al., 2017). The leaves of *C. paliurus* has been used as tea, traditional food and medicine for thousands of years in China (Fang et al., 2006), and the leaves have been listed as new food raw material by National Health and Family Planning Commission of China since 2013 (Qin et al., 2021). Many studies have demonstrated that the extractives from *C. paliurus* leaves possess antioxidant activities, antiproliferative activities and antidiabetic activities (Kurihara et al., 2003; Yao et al., 2015; Zhai et al., 2018; Zhou et al., 2021), and some products derived from the leaves have been developed and put into the market. However, at present, the resources of *C. paliurus* are mainly distributed in natural forests whereas its plantations can only be established at the sites where the soil is relatively deep and loose, well-drained and moist fertile (Fang et al., 2011; Fang, 2022), resulting in that the amount of its leaves cannot meet the market demand (Qin et al., 2021). Therefore, a feasible option is to develop *C. paliurus* plantation with oriented cultivation on potential land resources such as coastal saline areas due to the limitation of land resources in China in order to meet the requirement for its leaf production and medical use. Our previous studies found that R2R3-MYB transcription factor family affected salt tolerance of *C. paliurus* (Zhang et al., 2022b), while some bHLH proteins could regulate the accumulation of flavonoid compounds under salt stress by promoting the expression of genes encoding related enzymes in *C. paliurus* (Zhang et al., 2021), which provide some evidences for the crucial role of TFs in plant resistance to salt stress. However, so far, no TF family has been systematically identified in the whole genome of *C. paliurus*. The recent release of high quality whole-genome sequence data of *C. paliurus* gives us the opportunity to investigate the *bHLH* gene family and to identify salt-responsive members. In this study, 159 bHLH transcription factors in *C. paliurus* were analyzed comprehensively and systematically, and some key *bHLH* genes associated with salt tolerance were identified. Results from this study would not only provide insight into the function of the *CpbHLH* gene family members involved in salt stress, but also drive progress in genetic improvement for the salt

tolerance of *C. paliurus* to develop *C. paliurus* plantation in the coastal saline areas of south-east China.

2 Materials and methods

2.1 Identification and sequence analysis of *CpbHLH* genes

The whole genome data of *C. paliurus* were available from the Genome Sequence Archive (GSA) database (https://ngdc.cncb.ac.cn/gsa) provided by our research group. The Hidden Markov Model (HMM) profile of the HLH domain (PF00010) was obtained from the Pfam database (version 30.0) (Finn et al., 2014), and was used as a query to search for all protein sequences with default E-values in the whole genome and to identify genes with specific conserved domains by HMMER software (version 3.3; http://hmmer.org/) (Johnson et al., 2010). All screened sequences were aligned and checked with the online tools Batch CD-search (https://www.ncbi.nlm.nih.gov/Structure/bwrpsb/bwrpsb.cgi) (Marchler-Bauer and Bryant, 2004), Pfam, and SMART (http://smart.embl-heidelberg.de) (Letunic et al., 2021) to verify the existence of the conserved bHLH domain. The ExPASy software (https://web.expasy.org/protparam/) was used to obtain basic physical and chemical characteristics of these *bHLH* genes respectively.

2.2 Phylogenetic analysis, multiple alignment analysis and chromosomal locations

The *A. thaliana* MYB sequences data were download from PlantTFDB database (http://planttfdb.cbi.pku.edu.cn/index). The construction of a phylogenetic tree consisted of proteins from *A. thaliana* and *C. paliurus* was performed with MEGA X (version 6.0) (Kumar et al., 2018) software using the neighbor-joining (NJ) method with 1000 bootstrap replicates. Multiple sequence alignment (MSA) of *C. paliurus* and *A. thaliana* bHLH proteins was performed using ClustalX 2.11 software (Thompson et al., 1997), and Weblogo3 (http://weblogo.threeplusone.com/create.cgi), while Jalview software (http://www.jalview.org/) was used to visualize and analyze the sequences of conserved domains in CpbHLH proteins. The GFF3 (Generic Feature Format Version 3) file, containing the positional and gene structure information of genes on the chromosomes, was obtained from whole genome data of *C. paliurus*. The TBtools software (version 1.098774) (Chen et al., 2020) was adopted to map the *CpbHLH* genes onto specific chromosomes.

2.3 Gene structure, conserved motif, and promoter analysis

The exon/intron structures of *CpbHLH* genes were visualized by TBtools software (version 1.098774) (Chen et al., 2018), whereas fifteen conserved motifs were obtained using the online software MEME (http://MEME-suite.org/) (upper limit of the recognition motif was 20, minimum motif width was 6, and maximum motif width was 50, zoops) (Bailey et al., 2009). The online tool PLACE (Higo et al., 1999) was used to analyze the cis-acting elements of *CpbHLH* genes.

2.4 RNA-seq data analysis, GO annotation and prediction of the protein interaction network

Raw data were obtained *via* RNA sequencing of leaves treated with different salt concentration in hydroponic experiment (Zhang et al., 2021). *CpbHLHs* with reads per kilobase of transcript per million mapped reads or fragments per kilobase of transcript per million mapped reads (RPKM and FPKM, respectively) > 1 were collected for further analyses of all of the transcriptome data. TBtools was performed to generate the heatmap (Chen et al., 2020). Gene ontology (GO) analysis was carried out by the Blast2GO program (Conesa et al., 2005), with selecting the NCBI database as the reference database. The results were divided into three categories, namely molecular function, biological process, and cellular component. The NCBI database (https://www.ncbi.nlm.nih.gov/) were used to search the functions of *AtbHLHs*, which were predicted to be orthologous genes of *CpbHLHs*. STRING (https://string-db.org/) (Szklarczyk et al., 2019) was performed to predict the functional interaction network of candidate genes with option value>0.7.

2.5 Plant materials and stress treatments

The experiment was carried out at Baima Experimental Base of Nanjing Forestry University (31°35′ N, 119°09′ E). *C. paliurus* seeds were collected from Jinzhongshan county (24° 58′ N latitude, 110° 09′ E longitude), Guangxi province, China, in October 2018. After treated by exogenous GA3 (gibberellin A3) and stratification method (Fang et al., 2006), the germinated seeds were sown in nonwoven containers (10.0 cm height, 8.0 cm diameter) in April 2019.

Hydroponic experiment: After three months, uniform size seedlings (height: 40 ± 2.79 cm) were selected and transplanted to polypropylene containers (50L) with 1/2-strength Hoagland's nutrient solution (pH 6.0 ± 0.2). Two weeks after hydroponic transplanting, four salt concentration (0%, 0.15%, 0.3%, and 0.45% NaCl) regimes were implemented in completely randomized design with three biological replicates for each treatment. The detailed information has been described in our previous study (Zhang et al., 2022a).

Pot experiment: After one-year growth in the nonwoven containers, the seedlings were transplanted into the big nonwoven containers (25 cm height, 20 cm diameter) and cut into 3-5 cm height in early spring in 2020. In February 2022, saplings with similar size were selected and all their stems were cut to 120 cm height, whereas in early April 2022, the selected saplings were transplanted from the nonwoven containers into plastic pots (26 cm height, 26 cm top diameter and 20 cm bottom diameter) containing peat: substrates of perlite: rotten bird dung: soil =5: 2:2:1 (v/v/v/v). The plastic pots were placed in plastic trays to prevent NaCl leaching. The substrate was a

loam with pH 6.4, and the contents of total N, total P, and total K in the soil were 79.7, 66.5, 2.40, and 9.7 g kg^{-1}, respectively.

Salt treatments were conducted in early May 2022, and a completely randomized design was adopted with three replications per treatment and six plants per replication. Based on previous research (Zhang et al., 2022b), three levels of NaCl concentration were set up: CK (control, distilled water), T1 (0.2% NaCl) and T2 (0.4% NaCl). 1L solution were gradually add to the soil every three days (Chen et al., 2021), and electrical conductivity in the substrate was also monitored to keep the soil salt concentration relatively stable. Six complete and mature leaves were respectively collected from the upper, middle and lower positions of each sampled tree at the 45 days after the treatments (obvious differences were observed) (Figure 1) and were immediately frozen in liquid nitrogen and stored at −80°C until needed for further analysis.

2.6 RNA extraction and real-time quantitative RT-PCR analysis

Plant materials were ground under RNase-free conditions. Trizol reagent kit (Invitrogen, Carlsbad, CA, USA) was used to extract RNA from 9 samples of the 3 treatments (CK, 0.2% NaCl and 0.4% NaCl); subsequently, MonScript RTIII All-in-One Mix with dsDNase kits (Monad, Nanjing, China) was used to acquire cDNA, following the manufacturer's instructions. The qRTPCRs were performed on BiosystemsTM 7500 Real-Time PCR Systems (Monad, China). Primer Premier 6.0 (Premier Biosoft International, Palo Alto CA, USA) was used to design qRT-PCR primers for 12 genes (Supplementary Table S1). SYBR Premix Ex Taq kit (Takara Biotechnology, Dalian, China) was applied to conduct qRT-PCR analysis. The cDNA diluted 20 times and an *18sRNA* gene (Chen et al., 2019) were selected as the template and the internal standard, respectively. PCR reaction conditions were as 95 °C for 3 min; denaturation 5 s at 95 °C; 60 °C for 30 s; 40 cycles. Three technical and three biological replicates were used for each sample. After reaction, the relative expression levels of target gene and internal reference gene were calculated with the $2^{-\Delta\Delta CT}$ method (Penfield, 2001).

2.7 Statistical analysis

One-way analysis of variance (ANOVA) was conducted to identify significant differences in the related gene expression among the treatments, followed by Duncan's test for multiple comparisons. All statistical analyses were performed using IBM SPSS Statistics Version 22 software package (SPSS Inc., IBM Company Headquarters, Chicago, IL, USA). Data were presented as means ± standard deviation (SD).

3 Results

3.1 Identification and sequence analysis of *CpbHLH* genes

Based on the Genome-wide data of *C. paliurus*, a total of 174 supposed CpbHLH proteins were discovered by using the HMMER software with default parameters. Subsequently, SMART and CD-

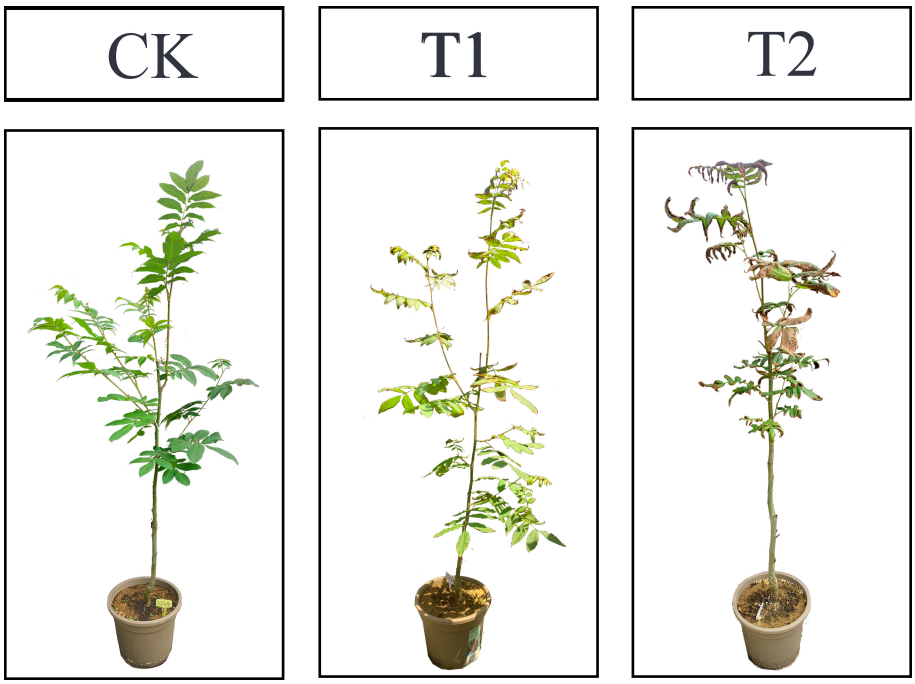

FIGURE 1
Phenotypes of *C. paliurus* seedlings at the sampling time under various salt treatments of the pot experiment.

Search were performed to confirm the existence of the conserved bHLH domain. After removing redundant sequences, 159 bHLH protein sequences of *C. paliurus* with typical complete bHLH domain were obtained and they were named *CpbHLH1* to *CpbHLH159* according to their location on chromosomes (Figure 2; Supplementary Table S2). Sequence analysis showed that the average length of the CpbHLH proteins was 354 amino acids. The relative molecular weight (Nw) ranged from 10454.72 Da (*CpbHLH39*) to 175494.7 Da (*CpbHLH86*), whereas the isoelectric point (pI) ranged from 4.65 (*CpbHLH48*) to 9.66 (*CpbHLH66*) (Supplementary Table S2).

3.2 Conserved residues and DNA-binding ability prediction of the *CpbHLH* genes

To gain in-depth knowledge of the function of CpbHLH family, the bHLH domains of the CpbHLH proteins were searched and the presence of the conserved amino acid residues were analyzed based on multiple sequence alignment. The alignment results (Figure 3) showed that the CpbHLH domains were composed of four conserved regions, namely one basic region, two helix regions and a loop region. Consistent with previous studies (Heim et al., 2003), the conservation of basic region and helix region is higher than that of the loop region. The bHLH domains of *C. paliurus* were made up of 79 amino acid residues, of which 24 were highly conserved (> 50% consensus ratio) and 8 were extremely conservative (> 75% consensus ratio). Among the 24 highly conserved amino acid residues, six conserved residues were found in the basic region (His-9, Ala-12, Glu-13, Arg-14, Arg-16, Arg-17), seven conserved residues were found in the first helix region (Ile-20, Asn-21, Arg-23, Leu-27, Leu-30, Val-31, Pro-32), one conserved residues were found in the loop region (Asp-64), and ten conserved residues were found in the second helix region (Lys-65, Ala-66, Ser-67, Leu-69, Ala-72, Ile-73, Tyr-75, Val-76, Lys-77, Leu-79).

It is generally believed that the basic region performs DNA binding functions, and is critical for the bHLH family to achieve its biological function (Carretero-Paulet et al., 2010). Therefore, the DNA-binding ability of the 159 CpbHLH proteins were predicted based on the conserved amino acid residues in the basic region (Supplementary Table S3). The remaining 159 CpbHLH members were classified into three categories: G-box (His/Lys-9, Glu-13 and Arg-17), E-box (Glu-13 and Arg-16) and non-E-box (Glu-13 and Arg-16 do not appear together) in accordance with the classification method reported previously (Katiyar et al., 2012). The predicted results revealed there were 93 G-box-binding proteins, 43 non-G-box-binding proteins and 23 non-E-box-binding proteins in 159 CpbHLHs (Supplementary Table S3).

3.3 Phylogenetic analysis and classification of the *CpbHLH* genes

In order to explore the evolutionary relationship among the CpbHLH members, the 159 CpbHLH proteins were aligned with 140 bHLH proteins from Arabidopsis, afterwards the phylogenetic tree was constructed using total 299 bHLH proteins based on the alignment (Figure 4). In accordance with the classification of bHLH proteins from Arabidopsis and other plants (Heim et al., 2003; Li et al., 2020b; Li et al., 2021), 299 bHLH protein sequences were

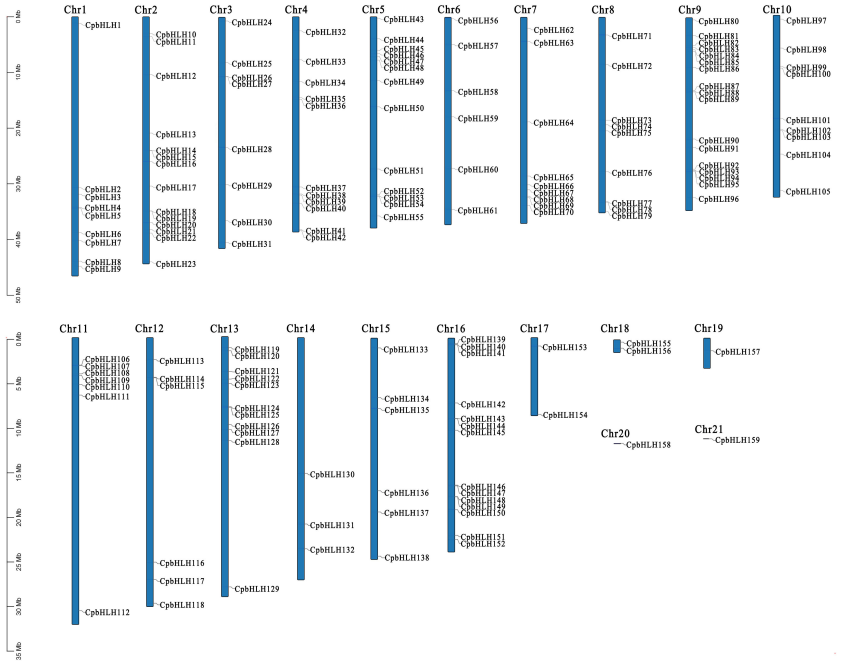

FIGURE 2
Chromosomal locations of the *CpbHLH* genes. The 159 *CpbHLH* genes were distributed on 21 pseudo-chromosomes of *C. paliurus* based on their physical positions.

10.3389/fpls.2023.1117246

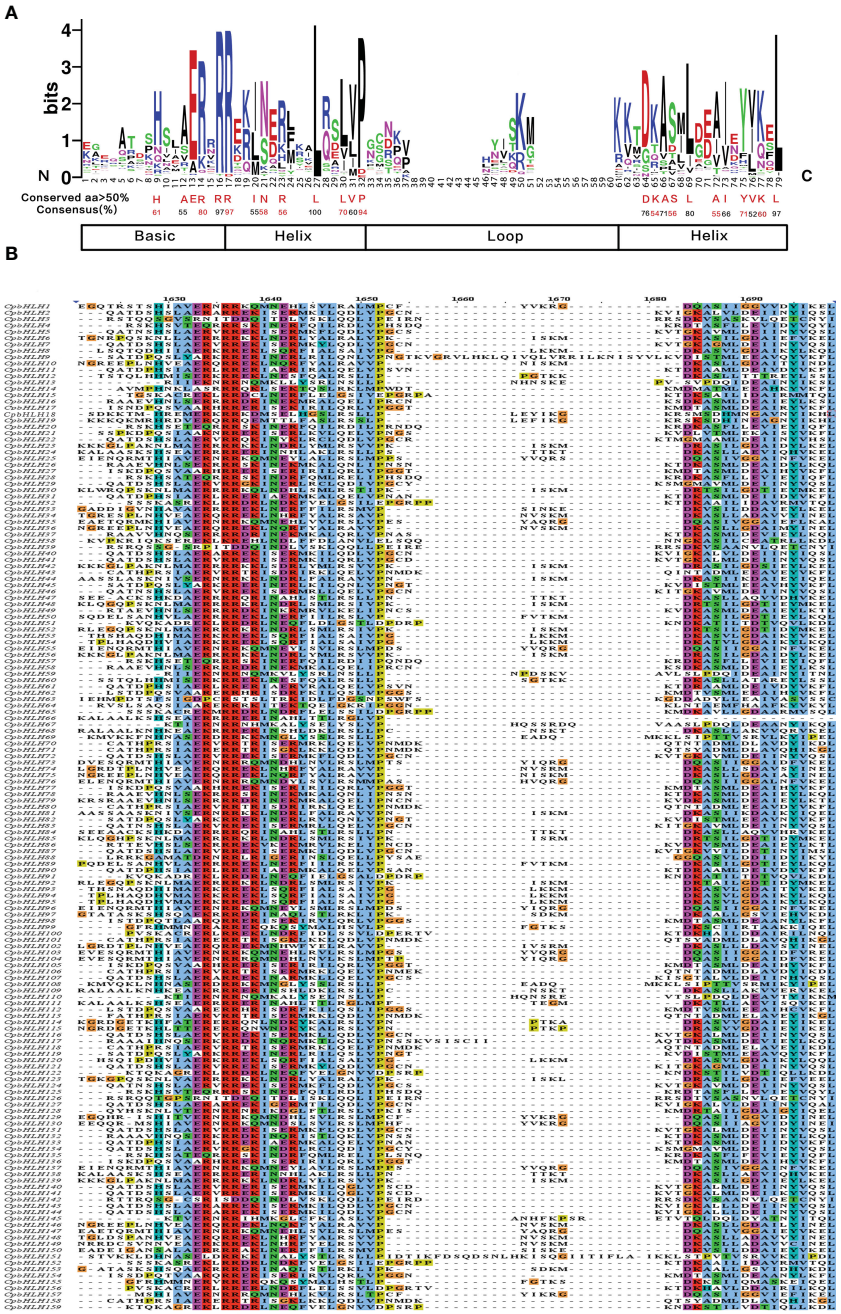

FIGURE 3
Multiple sequence alignments of the bHLH domains in CpbHLH proteins. **(A)** Visualization of conserved amino acids of bHLH domains of CpbHLH proteins. Amino acids with a conserved degree of more than 50 and their conserved degree were labeled using red and black colors for easy recognition which had no special meaning. **(B)** Multiple sequence alignments of the bHLH domains of 159 CpbHLH proteins, using the Clustal color scheme.

classified into 26 subfamilies, and were named from Ia to XV on the basis of the nomenclature of *AtbHLHs* proposed by Heim et al. (Heim et al., 2003). Figure 4 showed that the XII subfamily was the largest (contained 35 CpbHLH proteins), while the smallest subfamily (VI) contained only one CpbHLH protein. According to results from Heim et al. (Heim et al., 2003), CpbHLH proteins in the same subfamily would have similar functions, consequently, the clustering results of phylogenetic tree could contribute to predict the function of CpbHLH proteins.

3.4 Gene structure and conserved motif analysis of *CpbHLH* genes

Diversity of exon-intron structures, which could cause divergences in coding regions, is significant to the evolution of multiple gene families (Xu et al., 2012b). Hence, the gene structural characteristics of the *CpbHLH* family were investigated. The number of exons in the 159 *CpbHLH* genes varied from 1 to 13 (Figure 5C). In addition, 20 (12.6%) genes were intronless and

10.3389/fpls.2023.1117246

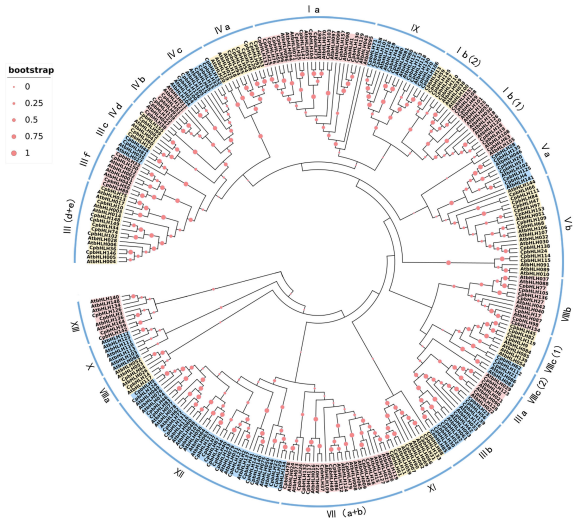

FIGURE 4
Phylogenetic tree and classification of bHLH subfamily proteins in *A. thaliana* and *C. paliurus*. The number of bHLH proteins of *A. thaliana* and *C. paliurus* is 140 and 159, respectively. The red dots represent boot values—the larger the dot, the larger the bootstrap value. Roman numerals line up with the bHLH subfamily.

distributed across subfamilies IIId, IIIe, VIIIa, VIIIb and VIIIc(2), while 13 (8.2%) genes contained one intron, and certainly the remaining genes had two or more introns. The 159 genes in different families varied widely in structure, including the number and relative location of introns and exons (Figure 5C). On the contrary, the intron/exon patterns of genes in the same subfamily had highly similarity, such as in subfamilies Ib(1) (five three-exon genes), Ib(2) (five three-exon genes), III(d+e) (nine one-exon genes), IVc (eight five-exon genes), and VIIIb (seven one-exon genes) (Figure 5C).

It is generally accepted that motifs figure prominently in interaction and signal transduction between different modules of the gene transcription process (Toledo-Ortiz et al., 2003). To further understand the evolutionary relationships among these CpbHLH proteins, the conserved motifs were analyzed by using MEME. Twenty motifs were identified and their sequences and length were counted (Figure 5B, Supplementary Table S4). In addition, eight of twenty motifs were annotated by Pfam and CD-search (Supplementary Table S4). Obviously, the composition patterns tended to be consistent with the results from our phylogenetic tree and gene structures, being resemble among genes within the same group, but varying greatly between groups (Figure 5). The number of motifs in 159 *CpbHLHs* ranged from one (*CpbHLH66*) to nine (*CpbHLH50*). All 159 *CpbHLH* genes contained motif 1 and motif 2, except *CpbHLH66*, only containing motif 1 (Figure 5B). Interestingly, some conserved motifs were nested in specific groups. For example, motif 13 only existed in group Ia, motif 16 in group VIIIb, motif 18 in group XII, and motif 19 in group IX respectively (Figure 5B). This phenomenon might be the reason why functions for CpbHLH proteins tend to be specific to a particular group.

3.5 GO annotation and cis-element analyses of the *CpbHLHs*

The highly differentiated sequences outside the conserved bHLH domain suggest that CpbHLH proteins may have a variety of biological functions. GO annotation of these 159 proteins was performed to understand the biological processes associated with *CpbHLH* genes. The results are shown in (Figure 6; Supplementary Table S5). The identified CpbHLH proteins were classified into three main Gene ontology (GO) terms, which were CC (cellular component), MF (molecular function), and BP (biological process). Within MF category, the majority of CpbHLH proteins were annotated for "molecular function" (139/159), "nucleic acid binding" and "DNA binding", respectively. These functions were closely related to the primary roles that TFs have. As for CC category, most of the CpbHLH proteins were assigned to cellular components and the nucleus (139/159). However, there were also a small number of CpbHLH proteins distributed in cytoplasm (8/159), organelle part (7/159), cytosol (4/159), symplast (*CpbHLH37/117/132*) and chloroplast (*CpbHLH68/109*) (Figure 6; Supplementary Table S5). Furthermore, the BP aspect showed that CpbHLH proteins participated in various biological processes. Proteins annotated to be related to multiple biosynthetic and metabolic possessed the largest number of *CpbHLHs* (141/159). Besides, CpbHLH proteins may function in regulating biological processed, such as regulation of cellular process (111/159), transcription (109/159), DNA-templated (109/159) and gene expression (109/159). The BP analysis also showed that many *CpbHLHs* could respond to stimuli (46/159), including different types of biotic and abiotic stressors, while *CpbHLH38/68/109* were predicted to be involved in respond to salt stress (Figure 6; Supplementary Table S5).

Conserved motifs located in gene promoter regions are recognition and binding sites for proteins. In this study, a large number of cis-regulatory elements (CREs) of *CpbHLH* genes were identified, and they were classified into three main categories (plant growth and development, phytohormone responsive, as well as abiotic and biotic stresses) according to their roles (Figure 7). Our result showed that CAT-box (105) and O2-site (86), which were involved in the meristem expression and zein metabolism regulation respectively were most frequently found motifs related to plant growth and development. On the contrary, the number of HD-Zip 1 (the differentiation of the palisade mesophyll cells), AACA-motif (involved in endosperm-specific negative expression) and MSA-like (cell cycle regulation) elements were 8, 3 and 2 respectively. Additionally, RY-element (seed-specific regulation) and GCN4_motif (endosperm expression) were also identified in the promoters of the *CpbHLH* genes (Figure 7). The most common elements in phytohormone responsive category were ABRE (the abscisic acid-responsive element), CGTCA-motif and TGACG-motif (elements involved in MeJA responsiveness) and the TCA element (SA-responsive element) (Figure 7). In the last category, a lot of important CREs related to plant abiotic stress were detected. Most abundant of these were the ABRE (drought

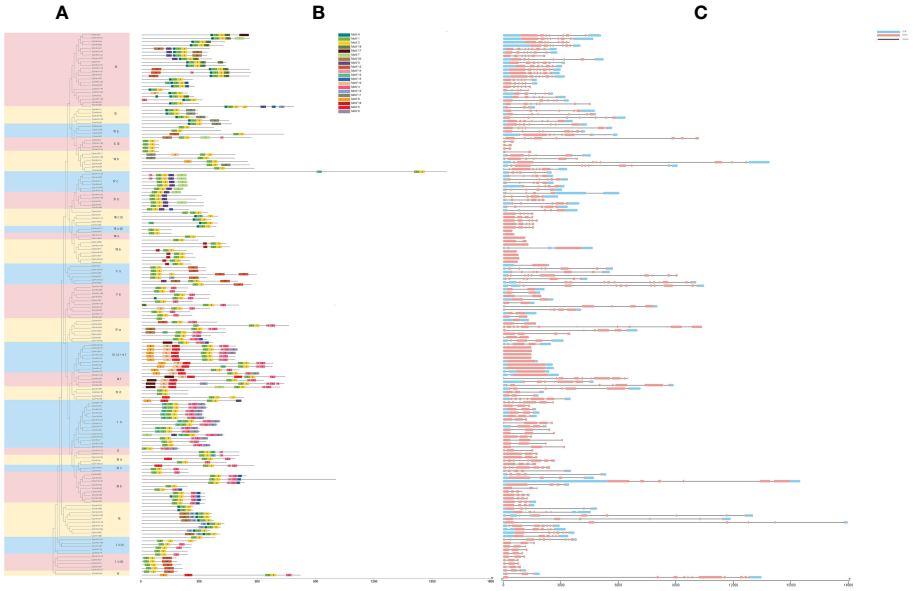

FIGURE 5
Analysis of conserved motifs and gene structure for 159 CpbHLH proteins. **(A)** Phylogenetic tree. **(B)** Distribution of conserved motifs. Twenty motifs were represented by twenty kinds of colored blocks. The position of each block represents the location of the motif. **(C)** organization of gene structure. The length of the gray line represents the length of a sequence relative to that of all the other sequences.

response element), ARE (anaerobic induced response element), MBS (drought induced response element) and LTR (low temperature response element). Other stress response CREs, such as GC-motif (anoxic specific inducibility element), TC-rich (defense and stress response element) and ERE elements (oxidative stress responsive elements were also identified (Figure 7).

3.6 Expression profiles of *CpbHLH* genes in salt stress under hydroponic experiment

Analysis of gene expression profiles is an effective way to determine gene functions. Hence, the leaves of *C. paliurus* treated with different salt concentrations (0%, 0.15%, 0.3%, and 0.45% NaCl) for 30 days in hydroponic experiment were sequenced and analyzed (Zhang et al., 2021). The raw sequencing data were submitted to the NCBI BioProject database under project number PRJNA700136. The RPKM (Reads Per Kilobase per Million mapped reads) values of 159 *CpbHLH* genes were obtained from the transcriptome data to estimate the expression levels of bHLH family members. However, *CpbHLH119/121/138/151* were not analyzed because of the absence or low level of expression in the transcriptome data. Figure 8 showed that 155 of these genes were expressed in all concentrations of NaCl treatments with different expression patterns, providing evidence that *CpbHLH* genes are significantly affected by salt stress.

Based on the similarity of expression patterns, the 155 *CpbHLH* genes were clustered into 8 clusters, named A1-A8 (Figure 8). The genes in cluster A1 were mainly expressed in the middle (0.30% NaCl) or high (0.45% NaCl) salinity condition and did not change significantly under low (0.15% NaCl) salinity condition. In contrast, *CpbHLHs* in cluster A6, A7 and A8 was strongly and preferentially expressed under low salt concentrations and down-regulated under high salt concentration. In cluster A2, the expression of *CpbHLH* genes did not change significantly under low and middle salt stress, but reached its highest value at high salinity treatment. However, expressions of most genes in cluster A4 varied with salt concentration treatments, and expression of these genes were all down-regulated under salt treatments and reached its lowest value at 0.45% NaCl treatment. However, very low expression levels of these genes in cluster A3 and A5 were observed at middle and high salt concentrations, respectively (Figure 8). In particular, among these 155 genes, the expression of some genes were strongly induced or inhibited under salt stress. For example, compared with the CK, the expressions of *CpbHLH36/74/75* in cluster A4 were down regulated by nearly folds of 3 in the low salinity treatment (0.15% NaCl), especially *CpbHLH74* down regulated by nearly folds of 9 in the high salinity treatment (0.45% NaCl). Similarly, seven differentially expressed genes (DEGs) (*CpbHLH68/69/71/108/146/152/158*) were identified in the A5, A6 and A7, indicating a response to salt stress (Figure 8).

3.7 Expression analysis of candidate genes in response to salt in pot experiment

Combining the results from both GO annotation and expression profiles analysis in hydroponic experiment, twelve salt-induced candidate genes (*CpbHLH36/38/68/69/71/74/75/108/109/146/152/158*) were selected for further qRT-PCR analysis using templates from pot experiment with three salt concentrations (0% NaCl, 0.2% NaCl and 0.4% NaCl) (Figure 9). Notably, eight candidate genes (*CpbHLH36/68/71/75/109/146/152/158*) were up

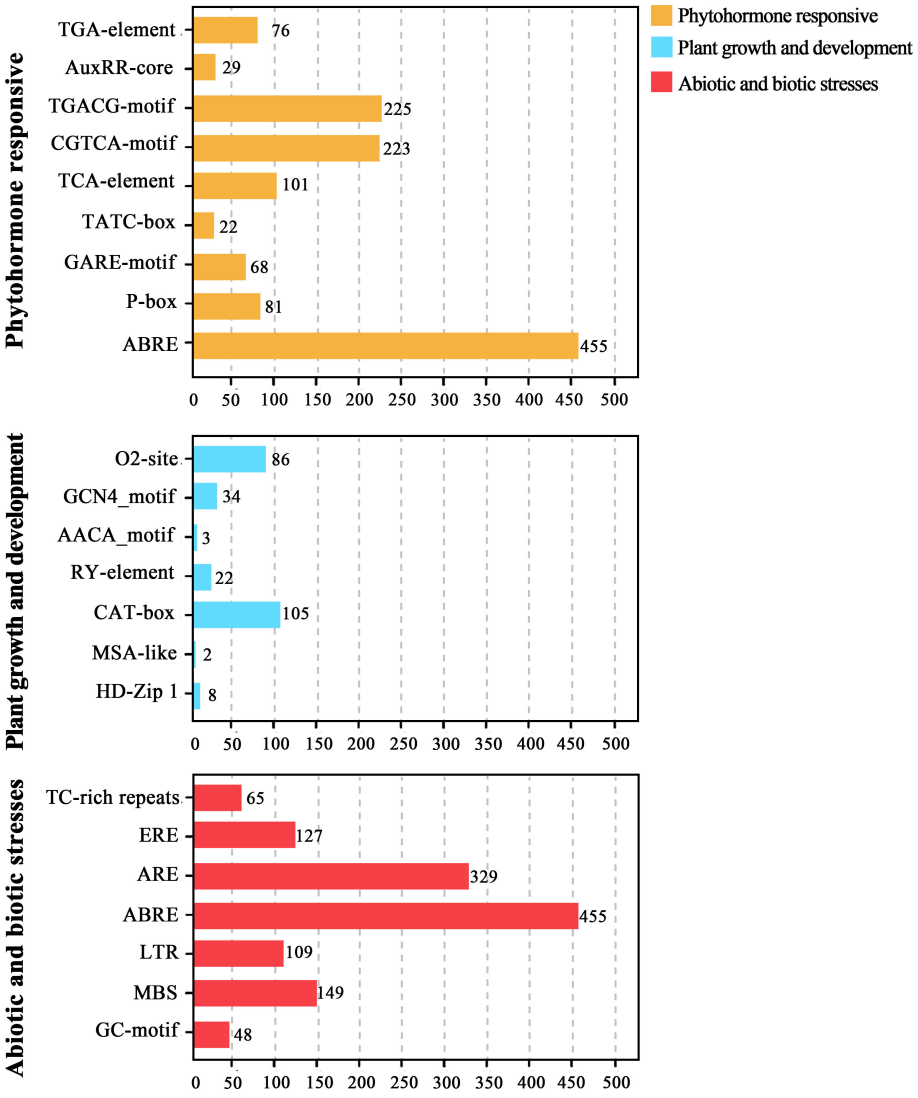

FIGURE 6
Gene ontology (GO) distribution of CpbHLH proteins. GO annotation using a cut-off value of $p \leq 0.05$ showed that GO items including molecular function (MF), biological process (BP), and cellular component (CC), while predominant GO items was selected to visualize the result.

regulated or decreased dramatically under different salt treatments, indicating that the expression of these genes was significantly induced or inhibited under salt stress (Figure 9). Among the eight genes, four genes (*CpbHLH36/146/152/158*) were down-regulated under salt stress, with three of these genes (*CpbHLH146/152/158*) being lowest expressed at 0.4% NaCl and one gene (*CpbHLH36*) being lowest expressed at 0.2% NaCl. On the contrary, three genes (*CpbHLH68/71/109*) were significantly induced by salt stress (Figure 9). In particular, three genes (*CpbHLH36/68/146*) responded strongly to salt treatments. Compared to the control, the variation trend of their expression in the pot experiment was highly consistent with that in the hydroponic experiment (Figure 8; Figure 9), indicating their vital functions in response to salt stress. For example, the expression level of *CpbHLH36* in both experiments was strongly inhibited under salt stress, whereas the inhibition degree was greater in low salt concentration than in high salt concentration.

3.8 Interaction network prediction of candidate genes

It was reported that bHLH proteins exert regulatory effects by forming homodimers or heterodimers between bHLH proteins or between bHLH and non-bHLH proteins (Herold et al., 2002; Hernandez et al., 2007). Thus, the interaction network of three candidate genes was predicted by STRING (Figure 10), based on the *CpbHLH* homologous genes in *A. thaliana*. The investigation of *CpbHLH146* (*MYC2* ortholog) showed that it was involved in light, abscisic acid (ABA), and jasmonic acid (JA) signaling pathways and controlled additively subsets of JA-dependent responses with *MYC3* and *MYC4* (Figure 10B, Supplementary Table S6). Among the proteins interacting with *MYC2*, those related to JA signaling pathway accounted for the majority, including *JAZ1*, *JAZ3*, *JAZ5*, *JAZ8*, *JAZ10*, *JAZ12* and *TILY7*. Besides, *PFT1* was determined as phytochrome and flowering time regulatory protein and the *EIN3*

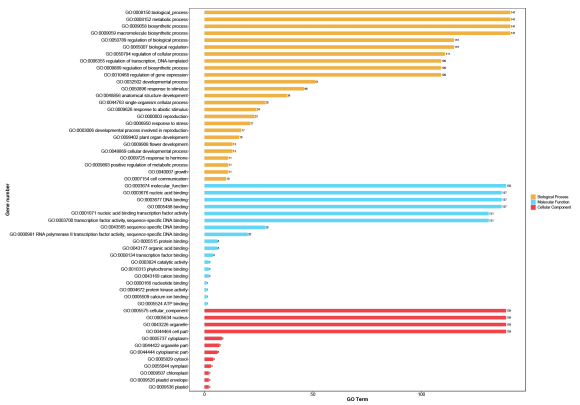

FIGURE 7
Cis-regulatory elements in the promoter region of *CpbHLH* genes. The figure represents the number of each type of motifs identified in the promoter sequence of *CpbHLH* genes.

probablely acted as a positive regulator in the ethylene response pathway (Figure 10A, Supplementary Table S6). The predicted network for *CpbHLH36* (*NIG* ortholog) showed that it plays central roles in regulating various proteins, and coincidently several of which were also involved in the jasmonic acid signaling pathway (*JAZ1* and *JAZ10*) (Figure 10A, Supplementary Table S6). Other proteins, *GSTU1* and *GSTU2*, could be involved in the conjugation of reduced glutathione to a wide number of exogenous and endogenous hydrophobic electrophiles and have a detoxification role against certain herbicides, whereas *bHLH11* and *TRFL8* both function in DNA binding (Figure 10A, Supplementary Table S6). Finally, the results of predicted network (Figure 10C, Supplementary Table S6) also indicated that *CpbHLH68* (ortholog of *bHLH106*) has crucial roles in DNA binding, whose function is the same as most of the proteins that interact with it. In addition, several interacting genes possibly regulate light responses, for example *CRY1* and *CPY2* are cryptochromes, and *UVR2* and *UVR3* involved in repair of UV radiation-induced DNA damage. However, *PRMT4B* has been identified as a positive regulator of oxidative stress tolerance that promotes the expression of antioxidant enzymes such as *APX1* and *GPX1* (Figure 10A, Supplementary Table S6). Overall, the results of the protein interaction network analysis indicated that the three candidate genes interact with proteins of various functions, making them crucial players in regulating plant growth and stress responses.

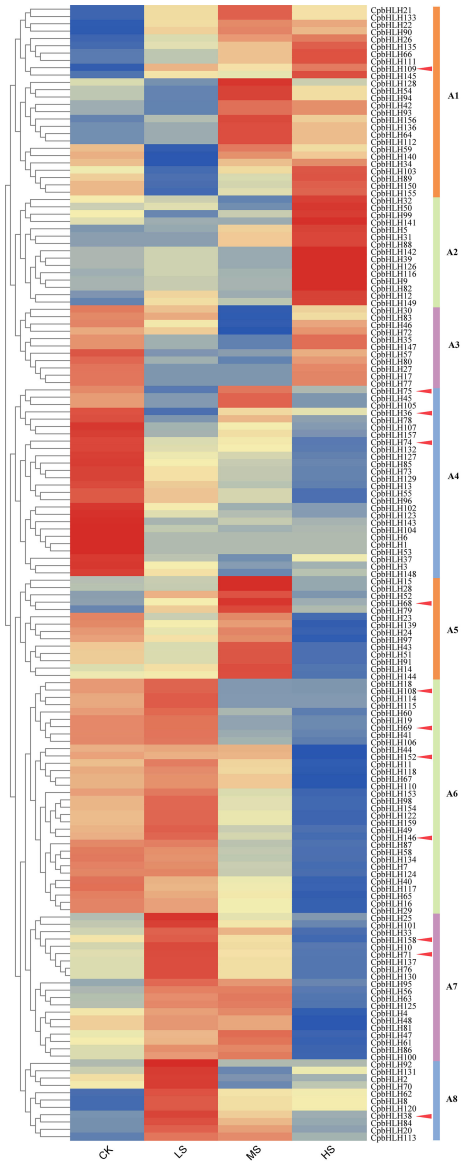

FIGURE 8
Clustering expression analysis of 159 *CpbHLH* genes in salt stress based on hydroponic experiments. The CK, LS, MS and HS represent the NaCl concentrations of 0%, 0.15%, 0.3% and 0.45% respectively. The transcript abundance level was normalized and hierarchically clustered by using the log 2 (FPKM + 1) comparison among genes of different treatments. The expression value is presented on the color scale, with red representing high expression and blue representing low expression. A1-A8 represent different clusters. In order to distinguish A1-A8 clusters more intuitively, lines of different colours were used in the right.

4 Discussion

4.1 Systematic and comprehensive genome-wide detection of *CpbHLHs* in *C paliurus*

Based on the whole genome of *C. paliurus*, 159 *bHLH* genes were systematically identified in the present study (Supplementary Table S2). The number of *CpbHLH* genes was the same as that identified in tomato (Sun et al., 2015), but smaller than that in Arabidopsis (162 genes) (Toledo-Ortiz et al., 2003) and apple (175 genes) (Yang et al., 2017), whereas greater than that in grape (94 genes) (Wang et al., 2018a), strawberry (113 genes) (Zhao et al., 2018) and jujube (92 genes) (Li et al., 2019). Overall, 159 CpbHLH proteins were further categorized into 26 subfamilies (Figure 4), according to the phylogenetic tree with the nomenclature protocol of bHLH proteins in *C. paliurus* and Arabidopsis (Heim et al., 2003), in agreement with results from previous studies (Pires and Dolan, 2010; Sun et al., 2015; Chu et al., 2018). However, the

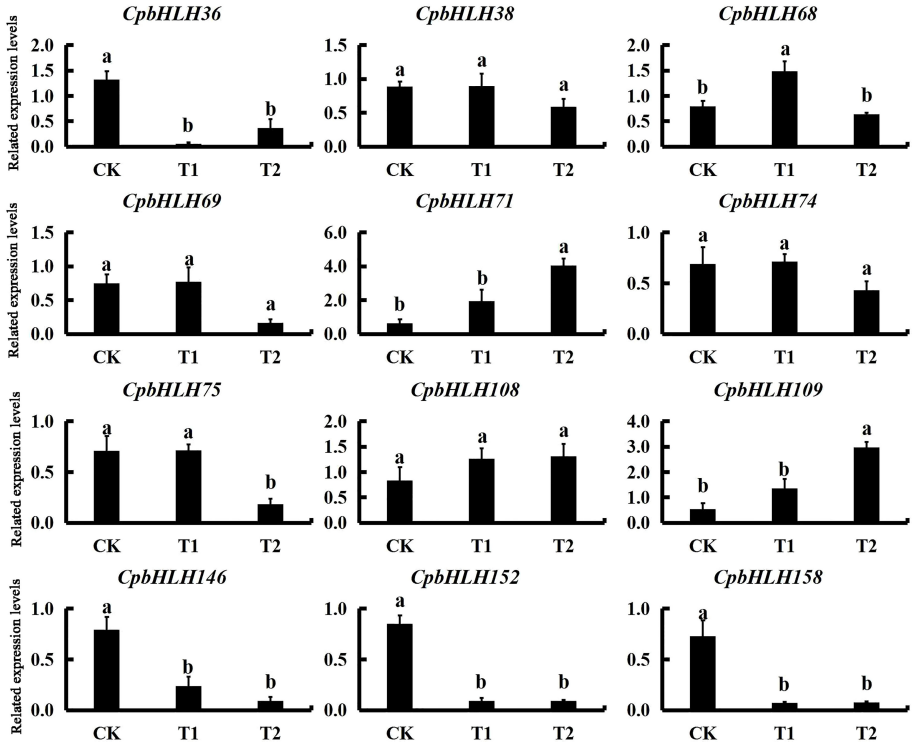

FIGURE 9
Expression profiles of the 12 candidate *CpbHLH* genes responding to salt stress treatments in pot experiment. The standard errors from three biological and three technical replications are presented as error bars. Following analysis of variance, significant differences identified by Duncan's test ($p < 0.05$), using SPSS v.22, are represented by different letters.

CpbHLHs were distributed almost evenly across 20 subfamilies, similar to *Camellia sinensis* (Sun et al., 2015) and *O. fragrans* (Li et al., 2020b). Moreover, our result indicated that no *CpbHLHs* were found in subfamily X, whereas the most *CpbHLH* members were detected in subfamily XII (Figure 4), with the number of members in this family increasing from 17 in Arabidopsis to 22 in *C. paliurus*. Differences in the numbers of *bHLH* genes among plant species may be due to gene replication events or genome size or gene loss during evolution (Flagel and Wendel, 2009; Li et al., 2020b).

Based on the analysis of the conserved motif and intron/exon (Figure 5B, C), the results showed that *CpbHLHs* in the same subfamily of the phylogenetic tree were similar in genetic and motif structures, further confirming the accuracy of subgroup classification of phylogenetic tree (Figure 4; Figure 5). Totally twenty motifs were identified in 159 CpbHLH proteins (Figure 5B). However, among them, motifs 1 and 2 existed in almost every CpbHLH protein and represented main components of the bHLH domain with high capability of conserved DNA binding, suggesting that the two motifs had very important implications about the functioning of *bHLH* genes (Zhang et al., 2020b). Nonetheless, the remaining 18 conserved non-bHLH domains can also feature separately in *CpbHLHs* in their

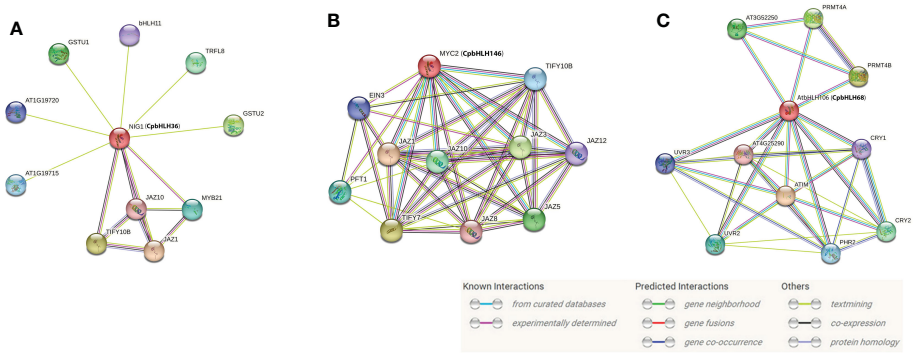

FIGURE 10
Interaction network analysis for *CpbHLH36* **(A)**, *CpbHLH146* **(B)** and *CpbHLH68* **(C)**. The predicted results are based on the orthologous gene in Arabidopsis. *CpbHLH* genes are shown in brackets.

respective subfamilies, similar to the other plant species (Chu et al., 2018; Li et al., 2020b). For example, most *bHLH* genes of subfamily III(d+e) in *Panax ginseng* (Chu et al., 2018) contained MYC-N structures (bHLH-MYC_N domain, Pfam : PF14215), which have been proved functioning in regulating the biosynthesis of phenylpropane. In this study, all *CpbHLHs* of III(d+e) also contained MYC-N structures (motif 5, 8, 10) (Figure 5B; Supplementary Table S4), implying that *CpbHLHs* of the same subgroup may have the similar roles. It was reported that gain/loss of exons and introns may result in the functional diversification of gene families (Xu et al., 2012a), whereas introns are related to gene evolution, and especieally the genes with few or no introns are more highly expressed in plants (Chung et al., 2006; Ren et al., 2006). In the present study, the intron-less *CpbHLHs* were distributed across subfamilies III (d+e) and VIIIb (Figure 5C), in accordance with the phenomenon in *P. ginseng* (Chu et al., 2018), apple (Yang et al., 2017) and Osmanthus (Li et al., 2020b), suggesting *CpbHLHs* of these subgroups could facilitates rapid and timely response to various stresses (Jeffares et al., 2008).

4.2 Functional prediction and identification of salt tolerance genes of *CpbHLHs*

Transcriptional regulation is a basic process of gene regulation in response to stress signals and a mass of TFs are involved in regulating plant responses to a given stress (Riechmann et al., 2000). The results of GO annotation in this study showed the functions of the *CpbHLH* genes are diverse (Figure 6; Supplementary Table S5), supporting that the bHLH TFs plays a crucial role in regulating plant growth, development and stress response (Shen et al., 2021). Several lines of evidence showed that salt stress had adverse effects on photosynthesis and the accumulation of secondary metabolites in *C. paliurus* (Zhang et al., 2021; Zhang et al., 2022a). Therefore, the detection of salt stress response genes from *CpbHLHs* will be helpful to achieve salt-tolerant breeding of *C. paliurus*.

The transcriptome sequencing analysis of salt treatments in the hydroponics provided specific expression data for the *CpbHLHs*, which makes it possible to further study the function of these genes. The RPKM values from our hydroponics showed that a large number of *CpbHLH* genes were induced/repressed under NaCl stress (Figure 8). According to the RPKM data, ten significantly differentially expressed genes (*CpbHLH36/68/69/71/74/75/108/146/152/158*) were predicted to function in responding to salt stress (Figure 8). Moreover, the molecular function annotations of 159 *CpbHLHs* indicated that three genes (*CpbHLH38/68/109*) strongly responded to salt stress (Supplementary Table S5). Thus, the 12 genes mentioned above were predicted to be candidate genes in response to salt stress and were selected for further qRT-PCR analysis, using salt-treated templates collected from our pot experiment. The qRT-PCR results showed that the expression of three genes (*CpbHLH36/68/146*) strongly responded to the salt treatments (Figure 9), and the variation trend of their expression levels was highly similar in the two salt stress experiments (Figure 8; Figure 9), indicating that these genes were specific for the regulation of salt tolerance in *C. paliurus*.

Phylogenetic analysis can be used to derive orthogonal relationships based on sequence similarity and protein structure, while the most closely related *bHLH* genes in the phylogenetic tree may share a similar function (Wang et al., 2021). The existed research indicated that *AtbHLH106* could enhance salt tolerance of plant by directly interacting with the G-box of salt tolerant genes (Ahmad et al., 2015), whereas the *CpbHLH68* was clustered in the same clade that possess high bootstrap value with *AtbHLH106* (Figure 4), suggesting *CpbHLH68* may be involved in response to salt stress. In addition, DNA sequences are decisive factors of the binding specificity between transcription factors and their genomic targets (Gordân et al., 2013), and our results from the DNA-binding ability of 159 *CpbHLHs* showed that *CpbHLH68* was G-box-binding protein (Supplementary Table S3), which further suggests that *CpbHLH68*, similar to *AtbHLH106*, may respond to salt stress by binding to G-box of target genes. Moreover, *AtbHLH6* (*ATMYC2*) has been reported to exhibit a significant response to salt and drought stresses (Abe et al., 1997; Aleman et al., 2016), while *AtNIG1* (a salt stress-responsive gene) was the first known TF participating in salt stress signal by binding calcium ions and bound to the E-box sequence (CANNTG) (Kim and Kim, 2006). Our study showed that *CpbHLH36* and *CpbHLH146* were clustered in the same clade with *AtbHLH6*(*MYC2*) and *AtbHLH28*(*AtNIG1*) (Figure 4), suggesting that *CpbHLH36* and *CpbHLH146* are also E-box proteins (Supplementary Table S3), and very likely to be involved in the regulation of salt stress signaling pathways.

In general, the function of a given gene can be inferred from its homologous genes (Yue et al., 2016; Qu et al., 2022). Therefore, Arabidopsis orthologs were used to predict the regulatory network of these three candidate genes (*CpbHLH36/68/146*) in this study. Some previous researches showed that *AtMYC2* was involved in the regulation of ABA-inducible genes under drought stress conditions (Gordân et al., 2013) and could provide a possible mechanistic link between ABA signaling and JA signaling (Abe et al., 1997; Zhang et al., 2021). The predicted interaction genes of *CpbHLH146* (*MYC2* ortholog) were mainly involved in the regulation of JA signaling (Figure 10A, Supplementary Table S6). The interaction of plant hormone ABA and JA played a major role in abiotic stress tolerance (Xiong et al., 2002; Zhang et al., 2012b) and ABA-dependent pathways the was one of important abiotic stress response signaling transduction pathways (Zhang et al., 2012a). The promoter region of most ABA regulatory genes contains many ABA responsive elements (Leonhardt et al., 2004; Yamaguchi-Shinozaki and Shinozaki, 2005; Fujita et al., 2011). In this study, a high occurrence of ABRE (ABA-responsive element) and CGTCA-motif (MeJA-responsive element) cis-acting elements was detected in the promoters of *CpbHLH146* (Figure 7). Thus, it can be inferred that this gene may have an important role in regulating stress resistance by regulating the expression of key genes in the ABA signaling pathway. Furthermore, most interaction genes of *CpbHLH36* (*AtNIG1* ortholog) and *CpbHLH68* (*bHLH106* ortholog) were mainly involved in DNA binding (Figure 10A, Supplementary Table S6), which further supports our hypothesis that these two genes regulate plant salt stress mainly *via* recognizing G-box of target genes. Moreover, *CpbHLH36* (*AtNIG1* ortholog) was also interacted with some JA signaling pathway proteins

(Figure 10A, Supplementary Table S6), and it was in the same cluster of the phylogenetic tree with *CpbHLH146* (*MYC2* ortholog) (Figure 4). Besides, the similar expression trend of *CpbHLH36* was observed between pot experiment and hydroponic experiment, the same as to *CpbHLH146* (Figure 8; Figure 9). Therefore, it could be concluded that there is an indirect interaction between *CpbHLH36* and *CpbHLH146* at the protein level and these two genes coordinately control the expression of downstream genes, whereas the plant salt tolerance may depend upon the co-expression of these two genes.

In short, combined with the above results, *CpbHLH36/68/146* could be the key putative candidates in response to salt stress in *C. paliurus*. However, characterizations of these three genes involved in the regulation of salt tolerance varied. *CpbHLH36/68/146* are all G-box proteins, and may respond to salt stress by binding to G-box of target genes. Secondly, *CpbHLH36* may participate in salt stress signal by binding calcium ions and regulating the expression of key genes in the JA signaling pathway. Thirdly, *CpbHLH146* was very likely to be involved in the regulation of salt stress in ABA signaling pathways. Moreover, it is noted that there exists an indirect interaction between *CpbHLH36* and *CpbHLH146* at the protein level, thus we guess the salt tolerance of *C. paliurus* may depend upon the co-expression of these two genes.

In conclusion, it is the first report to identify the TF family based on the whole genome of *C. paliurus*. A total of 159 *CpbHLH* genes were detected and divided into 26 subfamilies, according to their evolutionary characteristics. In addition to investigating their structures and DNA-binding abilities, expression analysis from both the pot and hydroponic experiments and the regulatory network were also performed to determine which genes are most active for salt stress responses in this species. A total of 12 candidate genes were selected in response to salt stress, whereas the 3 genes (*CpbHLH36/68/146*) were further verified to be involved in regulating the salt tolerance of *C. paliurus* based on a pot experiment and protein interaction network analysis. Our findings would not only provide a basis for further understanding regulatory mechanisms of bHLH proteins TFs, but also drive progress in genetic improvement for the salt tolerance of *C. paliurus*.

Data availability statement

The whole genome sequencing raw data including Illumina short reads, PacBio long reads, Hi-C interaction reads, and transcriptome data have been submitted to the Genome Sequence Archive at the National Genomics Data Center (NGDC), Beijing Institute of Genomics (BIG), Chinese Academy of Sciences (CAS) / China National Center for Bioinformation (CNCB) (GSA: CRA004671 and BioProject: PRJCA005987), and are publicly accessible at https://ngdc.cncb.ac.cn/gsa/.

Author contributions

ZZ: Conceptualization, writing-original draft, visualization, data analysis, bioinformatics analysis. JF: Participated in the pot experiment. SF: Methodology, writing-review & editing, funding acquisition. LZ: Participated in the hydroponic experiment HJ: Participated in the pot experiment. All authors contributed to the article and approved the submitted version.

Funding

This work was funded by The Key Research and Development Program of Jiangsu Province (BE2019388), and the National Natural Science Foundation of China (32071750).

Acknowledgments

The authors are grateful to Drs. Xulan Shang, Wanxia Yang, Caowen Sun and Jian Qin as well as Mr. Xiliang Yue in Nanjing Forestry University for their help in the experiments.

Conflict of interest

The authors declare that the research was conducted in the absence of any commercial or financial relationships that could be construed as a potential conflict of interest.

Publisher's note

All claims expressed in this article are solely those of the authors and do not necessarily represent those of their affiliated organizations, or those of the publisher, the editors and the reviewers. Any product that may be evaluated in this article, or claim that may be made by its manufacturer, is not guaranteed or endorsed by the publisher.

Supplementary material

The Supplementary Material for this article can be found online at: https://www.frontiersin.org/articles/10.3389/fpls.2023.1117246/full#supplementary-material

References

Abe, H., Yamaguchi-Shinozaki, K., Urao, T., Iwasaki, T., Hosokawa, D., and Shinozaki, K. (1997). Role of arabidopsis MYC and MYB homologs in drought- and abscisic acid-regulated gene expression. *Plant Cell* 9 (10), 1859–1868. doi: 10.1105/tpc.9.10.1859

Agarwal, P. K., Agarwal, P., Reddy, M. K., and Sopory, S. K. (2006). Role of DREB transcription factors in abiotic and biotic stress tolerance in plants. *Plant Cell Rep.* 25 (12), 1263–1274. doi: 10.1007/s00299-006-0204-8

Ahmad, A., Niwa, Y., Goto, S., Ogawa, T., Shimizu, M., Suzuki, A., et al. (2015). bHLH106 integrates functions of multiple genes through their G-box to confer salt tolerance on arabidopsis. *PloS One* 10 (5), e0126872. doi: 10.1371/journal.pone.0126872

Aleman, F., Yazaki, J., Lee, M., Takahashi, Y., Kim, A. Y., Li, Z., et al. (2016). An ABA-increased interaction of the PYL6 ABA receptor with MYC2 transcription factor: A putative link of ABA and JA signaling. *Sci. Rep.* 6, 28941. doi: 10.1038/srep28941

Atchley, W. R., Terhalle, W., and Dress, A. (1999). Positional dependence, cliques, and predictive motifs in the bHLH protein domain. *J. Mol. Evol.* 48 (5), 501–516. doi: 10.1007/PL00006494

Babitha, K. C., Ramu, S. V., Pruthvi, V., Mahesh, P., Nataraja, K. N., and Udayakumar, M. (2013). Co-Expression of *AtbHLH17* and *AtWRKY28* confers resistance to abiotic stress in arabidopsis. *Transgenic Res.* 22 (2), 327–341. doi: 10.1007/s11248-012-9645-8

Bailey, T. L., Boden, M., Buske, F. A., Frith, M., Grant, C. E., Clementi, L., et al. (2009). MEME SUITE: tools for motif discovery and searching. *Nucleic Acids Res.* 37, W202–W208. doi: 10.1093/nar/gkp335

Bhatnagar-Mathur, P., Vadez, V., and Sharma, K. K. (2008). Transgenic approaches for abiotic stress tolerance in plants: retrospect and prospects. *Plant Cell Rep.* 27 (3), 411–424. doi: 10.1007/s00299-007-0474-9

Carretero-Paulet, L., Galstyan, A., Roig-Villanova, I., Martínez-García, J. F., Bilbao-Castro, J. R., and Robertson, D. L. (2010). Genome-wide classification and evolutionary analysis of the bHLH family of transcription factors in arabidopsis, poplar, rice, moss, and algae. *Plant Physiol.* 153 (3), 1398–1412. doi: 10.1104/pp.110.153593

Chen, C., Chen, H., Zhang, Y., Thomas, H. R., Frank, M. H., He, Y., et al. (2020). TBtools: an integrative toolkit developed for interactive analyses of big biological data. *Mol. Plant* 13 (8), 1194–1202. doi: 10.1016/j.molp.2020.06.009

Chen, X., Mao, X., Huang, P., and Fang, S. (2019). Morphological characterization of flower buds development and related gene expression profiling at bud break stage in heterodichogamous *Cyclocarya paliurus* (Batal.) Iljinskaja. *Genes (Basel)* 10(10):818. doi: 10.3390/genes10100818

Chen, C., Xia, R., Chen, H., and He, Y. (2018). TBtools, a toolkit for biologists integrating various HTS-data handling tools with a user-friendly interface. *bioRxiv*. doi: 10.1101/289660

Chen, P., Yang, W., Minxue, W., Jin, S., and Liu, Y. (2021). Hydrogen sulfide alleviates salinity stress in *Cyclocarya paliurus* by maintaining chlorophyll fluorescence and regulating nitric oxide level and antioxidant capacity. *Plant Physiol. Biochem.* 167, 738–747. doi: 10.1016/j.plaphy.2021.09.004

Chinnusamy, V., Ohta, M., Kanrar, S., Lee, B. H., Hong, X., Agarwal, M., et al. (2003). ICE1: a regulator of cold-induced transcriptome and freezing tolerance in arabidopsis. *Genes Dev.* 17 (8), 1043–1054. doi: 10.1101/gad.1077503

Chu, Y., Xiao, S., Su, H., Liao, B., Zhang, J., Xu, J., et al. (2018). Genome-wide characterization and analysis of bHLH transcription factors in *Panax ginseng*. *Acta Pharm. Sin. B.* 8 (4), 666–677. doi: 10.1016/j.apsb.2018.04.004

Chung, B., Simons, C., Firth, A., Brown, C., and Hellens, R. (2006). Effect of 5'UTR introns on gene expression in *Arabidopsis thaliana*. *BMC Genomics* 7, 120. doi: 10.1186/1471-2164-7-120

Conesa, A., Götz, S., García-Gómez, J. M., Terol, J., Talón, M., and Robles, M. (2005). Blast2GO: a universal tool for annotation, visualization and analysis in functional genomics research. *Bioinformatics* 21 (18), 3674–3676. doi: 10.1093/bioinformatics/bti610

Cui, J., You, C., Zhu, E., Huang, Q., Ma, H., and Chang, F. (2016). Feedback regulation of DYT1 by interactions with downstream bHLH factors promotes DYT1 nuclear localization and anther development. *Plant Cell* 28 (5), 1078–1093. doi: 10.1105/tpc.15.00986

Fang, S. (2022). A review on the development history and the resource silviculture of *Cyclocarya paliurus* industry. *J. Nanjing For. Univ. (Nat. Sci. Ed.)* 46 (6), 115–126. doi: 10.12302/j.issn.1000-2006.202206019

Fang, S., Wang, J., Wei, Z., and Zhu, Z. (2006). Methods to break seed dormancy in *Cyclocarya paliurus* (Batal)Iljinskaja. *Sci. Hortic.* 110 (3), 305–309. doi: 10.1016/j.scienta.2006.06.031

Fang, S., Yang, W., Chu, X., Shang, X., She, C., and Fu, X. (2011). Provenance and temporal variations in selected flavonoids in leaves of *Cyclocarya paliurus*. *Food Chem.* 124 (4), 1382–1386. doi: 10.1016/j.foodchem.2010.07.095

Feller, A., Machemer, K., Braun, E. L., and Grotewold, E. (2011). Evolutionary and comparative analysis of MYB and bHLH plant transcription factors. *Plant J.* 66 (1), 94–116. doi: 10.1111/j.1365-313X.2010.04459.x

Feng, H. L., Ma, N. N., Meng, X., Zhang, S., Wang, J. R., Chai, S., et al. (2013). A novel tomato MYC-type ICE1-like transcription factor, SlICE1a, confers cold, osmotic and salt tolerance in transgenic tobacco. *Plant Physiol. Biochem.* 73, 309–320. doi: 10.1016/j.plaphy.2013.09.014

Finn, R. D., Bateman, A., Clements, J., Coggill, P., Eberhardt, R. Y., Eddy, S. R., et al (2014). Pfam: the protein families database. *Nucleic Acids Res.* 42, 222230. doi: 10.1093/nar/gkt1223

Flagel, L. E., and Wendel, J. F. (2009). Gene duplication and evolutionary novelty in plants. *New Phytol.* 183 (3), 557–564. doi: 10.1111/j.1469-8137.2009.02923.x

Fujita, Y., Fujita, M., Shinozaki, K., and Yamaguchi-Shinozaki, K. (2011). ABA-mediated transcriptional regulation in response to osmotic stress in plants. *J. Plant Res.* 124 (4), 509–525. doi: 10.1007/s10265-011-0412-3

Gordân, R., Shen, N., Dror, I., Zhou, T., Horton, J., Rohs, R., et al. (2013). Genomic regions flanking e-box binding sites influence DNA binding specificity of bHLH transcription factors through DNA shape. *Cell Rep.* 3 (4), 1093–1104. doi: 10.1016/j.celrep.2013.03.014

Heim, M. A., Jakoby, M., Werber, M., Martin, C., Weisshaar, B., and Bailey, P. C. (2003). The basic helix-loop-helix transcription factor family in plants: a genome-wide study of protein structure and functional diversity. *Mol. Biol. Evol.* 20 (5), 735–747. doi: 10.1093/molbev/msg088

Hernandez, J. M., Feller, A., Morohashi, K., Frame, K., and Grotewold, E. (2007). The basic helix loop helix domain of maize r links transcriptional regulation and histone modifications by recruitment of an EMSY-related factor. *Proc. Natl. Acad. Sci. U.S.A.* 104 (43), 17222–17227. doi: 10.1073/pnas.0705629104

Herold, S., Wanzel, M., Beuger, V., Frohme, C., Beul, D., Hillukkala, T., et al. (2002). Negative regulation of the mammalian UV response by myc through association with miz-1. *Mol. Cell* 10 (3), 509–521. doi: 10.1016/S1097-2765(02)00633-0

Higo, K., Ugawa, Y., Iwamoto, M., and Korenaga, T. (1999). Plant cis-acting regulatory DNA elements (PLACE) database: 1999. *Nucleic Acids Res.* 27 (1), 297–300. doi: 10.1093/nar/27.1.297

Hou, X. J., Li, J. M., Liu, B. L., and Wei, L. (2017). Co-Expression of basic helix–loop–helix protein (bHLH) and transcriptional activator-myb genes induced anthocyanin biosynthesis in hairy root culture of *Nicotiana tabacum l* and *Ipomea tricolor*. *Acta Physiol. Plant* 39 (2), 59. doi: 10.1007/s11738-017-2362-4

Jeffares, D. C., Penkett, C. J., and Bähler, J. (2008). Rapidly regulated genes are intron poor. *Trends Genet.* 24 (8), 375–378. doi: 10.1016/j.tig.2008.05.006

Ji, X., Nie, X., Liu, Y., Zheng, L., Zhao, H., Zhang, B., et al. (2016). A bHLH gene from *Tamarix hispida* improves abiotic stress tolerance by enhancing osmotic potential and decreasing reactive oxygen species accumulation. *Tree Physiol.* 36 (2), 193–207. doi: 10.1093/treephys/tpv139

Jiang, Y., Yang, B., and Deyholos, M. K. (2009). Functional characterization of the arabidopsis bHLH92 transcription factor in abiotic stress. *Mol. Genet. Genom.* 282 (5), 503–516. doi: 10.1007/s00438-009-0481-3

Johnson, L.S., Eddy, S.R., and Portugaly, E. (2010). Hidden Markov model speed heuristic anditerative HMM search procedure. *BMC Bioinformatics* 11, 431. doi: 10.1186/1471-2105-11-431

Katiyar, A., Smita, S., Lenka, S. K., Rajwanshi, R., Chinnusamy, V., and Bansal, K. C. (2012). Genome-wide classification and expression analysis of MYB transcription factor families in rice and arabidopsis. *BMC Genom.* 13, 544. doi: 10.1186/1471-2164-13-544

Kavas, M., Baloğlu, M. C., Atabay, E. S., Ziplar, U. T., Daşgan, H. Y., and Ünver, T. (2016). Genome-wide characterization and expression analysis of common bean bHLH transcription factors in response to excess salt concentration. *Mol. Genet. Genom.* 291 (1), 129–143. doi: 10.1007/s00438-015-1095-6

Kim, J., and Kim, H. Y. (2006). Functional analysis of a calcium-binding transcription factor involved in plant salt stress signaling. *FEBS Lett.* 580 (22), 5251–5256. doi: 10.1016/j.febslet.2006.08.050

Kumar, S., Stecher, G., Li, M., Knyaz, C., and Tamura, K. (2018). MEGA X: Molecular evolutionary genetics analysis across computing platforms. *Mol. Biol. Evol.* 35 (6), 1547–1549. doi: 10.1093/molbev/msy096

Kurihara, H., Fukami, H., Kusumoto, A., Toyoda, Y., Shibata, H., Matsui, Y., et al. (2003). Hypoglycemic action of *Cyclocarya paliurus* (Batal.) iljinskaja in normal and diabetic mice. *Biosci. Biotechnol. Biochem.* 67 (4), 877–880. doi: 10.1271/bbb.67.877

Leonhardt, N., Kwak, J. M., Robert, N., Waner, D., Leonhardt, G., and Schroeder, J. I. (2004). Microarray expression analyses of arabidopsis guard cells and isolation of a recessive abscisic acid hypersensitive protein phosphatase 2C mutant[W]. *Plant Cell* 16 (3), 596–615. doi: 10.1105/tpc.019000

Letunic, I., Khedkar, S., and Bork, P. (2021). SMART: recent updates, new developments and status in 2020. *Nucleic Acids Res.* 49 (D1), D458–d460. doi: 10.1093/nar/gkaa937

Li, H., Gao, W., Xue, C., Zhang, Y., Liu, Z., Zhang, Y., et al. (2019). Genome-wide analysis of the bHLH gene family in Chinese jujube (*Ziziphus jujuba* mill.) and wild jujube. *BMC Genom.* 20 (1), 568. doi: 10.1186/s12864-019-5936-2

Li, Y., Li, L., Ding, W., Li, H., Shi, T., Yang, X., et al. (2020b). Genome-wide identification of *Osmanthus fragrans* bHLH transcription factors and their expression analysis in response to abiotic stress. *Environ. Exp. Bot.* 172. doi: 10.1016/j.envexpbot.2020.103990

Li, H., Shi, J., Wang, Z., Zhang, W., and Yang, H. (2020a). H_2S pretreatment mitigates the alkaline salt stress on malus hupehensis roots by regulating $Na(^+)/K(^+)$ homeostasis and oxidative stress. *Plant Physiol. Biochem.* 156, 233–241. doi: 10.1016/j.plaphy.2020.09.009

Li, M., Sun, L., Gu, H., Cheng, D., Guo, X., Chen, R., et al. (2021). Genome-wide characterization and analysis of bHLH transcription factors related to anthocyanin biosynthesis in spine grapes (*Vitis davidii*). *Sci. Rep.* 11 (1), 6863. doi: 10.1038/s41598-021-85754-w

Li, H., Sun, J., Xu, Y., Jiang, H., Wu, X., and Li, C. (2007). The bHLH-type transcription factor AtAIB positively regulates ABA response in arabidopsis. *Plant Mol. Biol.* 65 (5), 655–665. doi: 10.1007/s11103-007-9230-3

Liao, Y., Zhang, P., Zhang, Q., and Li, X. (2022). Advances in salt-tolerant mechanisms of trees and forestation techniques on saline-alkali land. *J. Nanjing For. Univ. (Nat. Sci. Ed.)* 46 (6), 96–104. doi: 10.12302/j.issn.1000-2006.202209010

Lim, S. H., Kim, D. H., Kim, J. K., Lee, J. Y., and Ha, S. H. (2017). A radish basic helix-Loop-Helix transcription factor, RsTT8 acts a positive regulator for anthocyanin biosynthesis. *Front. Plant Sci.* 8. doi: 10.3389/fpls.2017.01917

Manchester, S. R., Chen, Z. D., Lu, A. M., and Uemura, K. (2009). Eastern Asian Endemic seed plant genera and their paleogeographic history throughout the northern hemisphere. *J. Syst. Evol.* 47, 1–2. doi: 10.1111/j.1759-6831.2009.00001.x

Mantri, N., Patade, V., Penna, S., Ford, R., and Pang, E. (2012a). Abiotic stress responses in plants: Present and future. *Springer New York* 1-19. doi: 10.1007/978-1-4614-0634-1_1

Mao, K., Dong, Q., Li, C., Liu, C., and Ma, F. (2017). Genome wide identification and characterization of apple bHLH transcription factors and expression analysis in response to drought and salt stress. *Front. Plant Sci.* 8. doi: 10.3389/fpls.2017.00480

Marchler-Bauer, A., and Bryant, S. H. (2004). CD-Search: protein domain annotations on the fly. *Nucleic Acids Res.* 32, W327–W331. doi: 10.1093/nar/gkh454

Penfield, S. (2001). MYB61 is required for mucilage deposition and extrusion in the arabidopsis seed coat. *Plant Cell* 13, 2777–2791. doi: 10.1105/tpc.13.12.2777

Pires, N., and Dolan, L. (2010). Origin and diversification of basic-helix-loop-helix proteins in plants. *Mol. Biol. Evol.* 27 (4), 862–874. doi: 10.1093/molbev/msp288

Qin, J., Yue, X., Fang, S., Qian, M., Zhou, S., Shang, X., et al. (2021). Responses of nitrogen metabolism, photosyntheticparameter and growth to nitrogen fertilization in *Cyclocarya paliurus*. *For. Ecol. Manage.* 502, 119715. doi: 10.1016/j.foreco.2021.119715

Qu, Y., Chen, X., Mao, X., Huang, P., and Fu, X. (2022). Transcriptome analysis reveals the role of GA_3 in regulating the asynchronism of floral bud differentiation and development in heterodichogamous *Cyclocarya paliurus* (Batal.) iljinskaja. *Int. J. Mol. Sci.* 23, 6763. doi: 10.3390/ijms23126763

Ren, X.-Y., Vorst, O., Fiers, M. W. E. J., Stiekema, W. J., and Nap, J.-P. (2006). In plants, highly expressed genes are the least compact. *Trends Genet.* 22 (10), 528–532. doi: 10.1016/j.tig.2006.08.008

Riechmann, J. L., Heard, J., Martin, G., Reuber, L., Jiang, C., Keddie, J., et al. (2000). Arabidopsis transcription factors: genome-wide comparative analysis among eukaryotes. *Science* 290 (5499), 2105–2110. doi: 10.1126/science.290.5499.2105

Shen, T., Wen, X., Wen, Z., Qiu, Z., Hou, Q., Li, Z., et al. (2021). Genome-wide identification and expression analysis of bHLH transcription factor family in response to cold stress in sweet cherry (*Prunus avium* l.). *Sci. Hortic.* 279, 109905. doi: 10.1016/j.scienta.2021.109905

Sorensen, A. M., Kröber, S., Unte, U. S., Huijser, P., Dekker, K., and Saedler, H. (2003). The *Arabidopsis ABORTED MICROSPORES (AMS)* gene encodes a MYC class transcription factor. *Plant J.* 33 (2), 413–423. doi: 10.1046/j.1365-313x.2003.01644.x

Sum, J., Guo, Y., Li, S., Zhou, C., Chiang, V., and Li, W. (2021). A functional study of bHLH106 transcription factor based on CRISPR/Cas9 in *Populus trichocarpa*. *J. Nanjing For. Univ. (Nat. Sci. Ed.)* 45 (6), 15–23. doi: 10.12302/j.issn.1000-2006.202107031

Sun, H., Fan, H. J., and Ling, H. Q. (2015). Genome-wide identification and characterization of the bHLH gene family in tomato. *BMC Genom.* 16 (1), 9. doi: 10.1186/s12864-014-1209-2

Szklarczyk, D., Gable, A. L., Lyon, D., Junge, A., Wyder, S., Huerta-Cepas, J., et al. (2019). STRING v11: protein-protein association networks with increased coverage, supporting functional discovery in genome-wide experimental datasets. *Nucleic Acids Res.* 47 (D1), D607–d613. doi: 10.1093/nar/gky1131

Thompson, J. D., Gibson, T. J., Plewniak, F., Jeanmougin, F., and Higgins, D. G. (1997). The CLUSTAL_X windows interface: flexible strategies for multiple sequence alignment aided by quality analysis tools. *Nucleic Acids Res.* 25 (24), 4876–4882. doi: 10.1093/nar/25.24.4876

Toledo-Ortiz, G., Huq, E., and Quail, P. H. (2003). The arabidopsis basic/helix-loop-helix transcription factor family. *Plant Cell* 15 (8), 1749–1770. doi: 10.1105/tpc.013839

Wang, P., Su, L., Gao, H., Jiang, X., Wu, X., Li, Y., et al. (2018a). Genome-wide characterization of bHLH genes in grape and analysis of their potential relevance to abiotic stress tolerance and secondary metabolite biosynthesis. *Front. Plant Sci.* 9. doi: 10.3389/fpls.2018.00064

Wang, Y., Zhang, Y., Fan, C., Wei, Y., Meng, J., Li, Z., et al. (2021). Genome-wide analysis of MYB transcription factors and their responses to salt stress in *Casuarina equisetifolia*. *BMC Plant Biol.* 21 (1), 328. doi: 10.1186/s12870-021-03083-6

Wang, R., Zhao, P., Kong, N., Lu, R., Pei, Y., Huang, C., et al. (2018b). Genome-wide identification and characterization of the potato bHLH transcription factor family. *Genes (Basel)* 9(1):54. doi: 10.3390/genes9010054

Wu, J. Y., Wilf, P., Ding, S. T., An, P. C., and Dai, J. (2017). Late miocene *Cyclocarya* (Juglandaceae) from southwest China and its biogeographic implications. *Int. J. Plant Sci.* 178, 580–591. doi: 10.1086/692765

Xiong, L., Schumaker, K. S., and Zhu, J. K. (2002). Cell signaling during cold, drought, and salt stress. *Plant Cell* 14 Suppl (Suppl), S165–S183. doi: 10.1105/tpc.000596

Xu, G., Guo, C., Shan, H., and Kong, H. (2012b). Divergence of duplicate genes in exon-intron structure. *Proc. Natl. Acad. Sci. U.S.A.* 109 (4), 1187–1192. doi: 10.1073/pnas.1109047109

Xu, B., Sathitsuksanoh, N., Tang, Y., Udvardi, M., Zhang, J.-Y., Shen, Z., et al. (2012a). Overexpression of AtLOV1 in switchgrass alters plant architecture, lignin content, and flowering time. *PloS One* 7, e47399. doi: 10.1371/journal.pone.0047399

Yamaguchi-Shinozaki, K., and Shinozaki, K. (2005). Organization of cis-acting regulatory elements in osmotic- and cold-stress-responsive promoters. *Trends Plant Sci.* 10 (2), 88–94. doi: 10.1016/j.tplants.2004.12.012

Yang, J., Gao, M., Huang, L., Wang, Y., van Nocker, S., Wan, R., et al. (2017). Identification and expression analysis of the apple (*Malus* × *domestica*) basic helix-loop-helix transcription factor family. *Sci. Rep.* 7 (1), 28. doi: 10.1038/s41598-017-00040-y

Yao, X., Lin, Z., Jiang, C., Gao, M., Wang, Q., Yao, N., et al. (2015). *Cyclocarya paliurus* prevents high fat diet induced hyperlipidemia and obesity in sprague-dawley rats. *Can. J. Physiol. Pharmacol.* 93 (8), 677–686. doi: 10.1139/cjpp-2014-0477

Yue, H., Wang, M., Liu, S., Du, X., Song, W., and Nie, X. (2016). Transcriptome-wide identification and expression profiles of the WRKY transcription factor family in broomcorn millet (*Panicum miliaceum* l.). *BMC Genomics* 17, 343. doi: 10.1186/s12864-016-2677-3

Zhai, L. X., Ning, Z. W., Huang, T., Wen, B., Liao, C. H., Lin, C. Y., et al. (2018). *Cyclocarya paliurus* leaves tea improves dyslipidemia in diabetic mice: a lipidomics-based network pharmacology study. *Front. Pharmacol.* 9, 973. doi: 10.3389/fphar.2018.00973

Zhai, Y., Zhang, L., Xia, C., Fu, S., Zhao, G., Jia, J., et al. (2016). The wheat transcription factor, TabHLH39, improves tolerance to multiple abiotic stressors in transgenic plants. *Biochem. Biophys. Res. Commun.* 473 (4), 1321–1327. doi: 10.1016/j.bbrc.2016.04.071

Zhang, T., Bai, Y., Qi, X., Yu, X., Fang, H., Li, L., et al. (2022a). Cloning and expression analyses of *MhWRKY57* response to jasmonic acid in *Mentha canadensis*. *J. Nanjing For. Univ. (Nat. Sci. Ed.)* 46 (6), 279–287. doi: 10.12302/j.issn.1000-2006.202109036

Zhang, Y., Gao, W., Li, H., Wang, Y., Li, D., Xue, C., et al. (2020b). Genome-wide analysis of the bZIP gene family in Chinese jujube (*Ziziphus jujuba* mill.). *BMC Genomics* 21 (1), 483. doi: 10.1186/s12864-020-06890-7

Zhang, M., Liu, Y., Han, G., Zhang, Y., Wang, B., and Chen, M. (2020a). Salt tolerance mechanisms in trees: research progress. *Trees* 35 (3), 717–730. doi: 10.1007/s00468-020-02060-0

Zhang, Z., Liu, X., Wang, X., Zhou, M., Zhou, X., Ye, X., et al. (2012b). An R2R3 MYB transcription factor in wheat, TaPIMP1, mediates host resistance to *Bipolaris sorokiniana* and drought stresses through regulation of defense- and stress-related genes. *New Phytol.* 196 (4), 1155–1170. doi: 10.1111/j.1469-8137.2012.04353.x

Zhang, L., Zhang, Z., Fang, S., Liu, Y., and Shang, X. (2021). Integrative analysis of metabolome and transcriptome reveals molecular regulatory mechanism of flavonoid biosynthesis in *Cyclocarya paliurus* under salt stress. *Ind. Crops Prod.* 170. doi: 10.1016/j.indcrop.2021.113823

Zhang, L., Zhang, Z., Fang, S., Liu, Y., and Shang, X. (2022a). Metabolome and transcriptome analyses unravel the molecular regulatory mechanisms involved in photosynthesis of *Cyclocarya paliurus* under salt stress. *Int. J. Mol. Sci.* 23(3):1161. doi: 10.3390/ijms23031161

Zhang, Z., Zhang, L., Liu, Y., Shang, X., and Fang, S. (2022b). Identification and expression analysis of R2R3-MYB family genes associated with salt tolerance in *Cyclocarya paliurus*. *Int. J. Mol. Sci.* 23(7):3429. doi: 10.3390/ijms23073429

Zhang, L., Zhao, G., Jia, J., Liu, X., and Kong, X. (2012a). Molecular characterization of 60 isolated wheat *MYB* genes and analysis of their expression during abiotic stress. *J. Exp. Bot.* 63 (1), 203–214. doi: 10.1093/jxb/err264

Zhao, F., Li, G., Hu, P., Zhao, X., Li, L., Wei, W., et al. (2018). Identification of basic/helix-loop-helix transcription factors reveals candidate genes involved in anthocyanin biosynthesis from the strawberry white-flesh mutant. *Sci. Rep.* 8(1):2721. doi: 10.1038/s41598-018-21136-z

Zhao, Q., Ren, Y. R., Wang, Q. J., Yao, Y. X., You, C. X., and Hao, Y. J. (2016). Overexpression of *MdbHLH104* gene enhances the tolerance to iron deficiency in apple. *Plant Biotechnol. J.* 14 (7), 1633–1645. doi: 10.1111/pbi.12526

Zhou, M. M., Quek, S. Y., Shang, X. L., and Fang, S. Z. (2021). Geographical variations of triterpenoid contents in *Cyclocarya paliurus* leaves and their inhibitory effects on hela cells. *Ind. Crop Prod.* 162, 113314. doi: 10.1016/j.indcrop.2021.113314

frontiers | Frontiers in Plant Science

TYPE Original Research
PUBLISHED 10 March 2023
DOI 10.3389/fpls.2023.1063618

Check for updates

OPEN ACCESS

EDITED BY
Diaa Abd El Moneim,
Arish University, Egypt

REVIEWED BY
Shixian Sun,
Southwest Forestry University, China
Ismat Nawaz,
COMSATS Institute of Information Technology, Pakistan

*CORRESPONDENCE
Zahra Karimian
zkarimian@um.ac.ir

SPECIALTY SECTION
This article was submitted to Plant Abiotic Stress, a section of the journal Frontiers in Plant Science

RECEIVED 07 October 2022
ACCEPTED 14 February 2023
PUBLISHED 10 March 2023

CITATION
Karimian Z and Samiei L (2023) ZnO nanoparticles efficiently enhance drought tolerance in *Dracocephalum kotschyi* through altering physiological, biochemical and elemental contents.
Front. Plant Sci. 14:1063618.
doi: 10.3389/fpls.2023.1063618

COPYRIGHT
© 2023 Karimian and Samiei. This is an open-access article distributed under the terms of the Creative Commons Attribution License (CC BY). The use, distribution or reproduction in other forums is permitted, provided the original author(s) and the copyright owner(s) are credited and that the original publication in this journal is cited, in accordance with accepted academic practice. No use, distribution or reproduction is permitted which does not comply with these terms.

ZnO nanoparticles efficiently enhance drought tolerance in *Dracocephalum kotschyi* through altering physiological, biochemical and elemental contents

Zahra Karimian* and Leila Samiei

Department of Ornamental Plants, Research Center for Plant Sciences, Ferdowsi University of Mashhad, Mashhad, Iran

Using nanofertilizers in certain concentrations can be a novel method to alleviate drought stress effects in plants as a global climate problem. We aimed to determine the impacts of zinc nanoparticles (ZnO-N) and zinc sulfate ($ZnSO_4$) fertilizers on the improvement of drought tolerance in *Dracocephalum kotschyi* as a medicinal-ornamental plant. Plants were treated with three doses of ZnO-N and $ZnSO_4$ (0, 10, and 20 mg/l) under two levels of drought stress [50% and 100% field capacity (FC)]. Relative water content (RWC), electrolyte conductivity (EC), chlorophyll, sugar, proline, protein, superoxide dismutase (SOD), polyphenol oxidase (PPO) and, guaiacol peroxidase (GPO) were measured. Moreover, the concentration of some elements interacting with Zn was reported using the SEM-EDX method. Results indicated that foliar fertilization of *D. kotschyi* under drought stress with ZnO-N decreased EC, while $ZnSO_4$ application was less effective. Moreover, sugar and proline content as well as activity of SOD and GPO (and to some extent PPO) in treated plants by 50% FC, increased under the influence of ZnO-N. $ZnSO_4$ application could increase chlorophyll and protein content and PPO activity in this plant under drought stress. Based on the results, ZnO-N and then $ZnSO_4$ improved the drought tolerance of *D. kotschyi* through their positive effects on physiological and biochemical attributes changing the concentration of Zn, P, Cu, and Fe. Accordingly, due to the increased sugar and proline content and also antioxidant enzyme activity (SOD, GPO, and to some extent PPO) on enhancing drought tolerance in this plant, ZnO-N fertilization is advisable.

KEYWORDS

antioxidant enzyme activity, drought stress, nanoparticles, zinc fertilizers, elemental composition

1 Introduction

According to climate change and changes in global precipitation patterns, predictions and models have shown an increase in the size of deserts and xeric scrublands as the largest terrestrial biome (Guo et al., 2021). Every year, water scarcity and drought cause severe damage to agricultural products, green spaces, forests, and rangelands. In the past few years, these issues have resulted in a global decline in agricultural production (Bodner et al., 2015). In addition, water scarcity and drought contribute to the inhibition of crop growth and negatively impact plant quantitative and qualitative yield, as well as physiology and morphology (Bayat and Moghadam, 2019).

Applying fertilizers and nutritional compounds during the growth state is a crucial strategy to decrease the impact of drought on crops. Several studies have shown that micronutrients mitigate crops drought stress (Adrees et al., 2020; Bashir et al., 2020; Dimkpa et al., 2020). Zinc is a microelement, necessary for many plant activities, which plays a crucial role in protein, enzyme, and chlorophyll synthesis and the improvement of agricultural crop yield (Singh et al., 2018; Dimkpa et al., 2019). Furthermore, studies have confirmed the effect of Zn, in the form of zinc sulfate, zinc chelate, and Zn nanoparticle, on enhanced resistance to environmental stress by improving morphological, physiological, and biochemical factors in different plants (Mahdieh et al., 2018; Farooq et al., 2020; Faizan et al., 2021; Tariverdizadeh et al., 2021).

Nanoparticles (particles that are ≤100 nm in at least one dimension) play an essential role in altering different physiological processes in plants, nutrient absorption, plant growth, and increased plant resistance to abiotic stress (Jordan et al., 2018; Dimkpa et al., 2020). Moreover, nanoparticles are used in the form of micronutrients and fertilizers to improve qualitative and quantitative crop yield. Because of the limited and controlled release of nutrients, nanoparticles can contribute to plant growth and resistance to different types of stress (Adrees et al., 2020; Bashir et al., 2020).

Zn nanoparticle is a new plant fertilizer produced with the technology of nanoparticle synthesis, which has many benefits, such as increased tolerance to abiotic stress in some plants (Cicek and Nadaroglu, 2015; Rossi et al., 2018; Singh et al., 2018; Zhang et al., 2018; Farooq et al., 2020; Taghizadeh et al., 2020; Faizan et al., 2021; Tariverdizadeh et al., 2021). Studies have reported the positive effects of Zn nanoparticles on improved tomato (Faizan et al., 2021) and wheat (Bashir et al., 2021) yield under salinity and drought stress, respectively. In addition, Dimkpa et al. (2019) and Motyka et al. (2019) have approved increased yield of sorghum plants under drought stress and enhanced the situation of bryophytes under oxidative stress with the help of Zn nanoparticles. Moreover, different forms of zinc were applied to the coffee plant, compared to zinc sulfate, Zn nanoparticles could positively affect coffee plant growth and yield (Rossi et al., 2018).

Element interactions in plants can affect plant functions, such as growth, yield, and stress resistance. Studies have suggested that the Zn element has antagonistic and synergistic interactions with Cu, Fe, and P elements in absorption, transfer, and chemical reactions in the plant. It may vary depending on factors such as plant type, soil type, nutrition, and weather conditions (Fageria et al., 2012; Izsáki, 2014; Rietra et al., 2017). The impact of element interactions to nanoparticle form on abiotic stress resistance (e.g., drought) has been reported in some studies (Liu et al., 2020; Ahmed et al., 2022).

Dracocephalum kotschyi belongs to Lamiaceae and is one of the 60 species of the genus *Dracocephalum*. This species is endemic to Iran and is currently considered an endangered plant. *D. kotschyi* is known to have several medicinal properties (Muẓaffarīyān, 1996). This species is traditionally a medicine plant in Iran with several therapeutic effects such as analgesic, antispasmodic, and anticancer (Sharafi et al., 2014). *D. kotschyi* also was used in the treatment of headaches, congestion, stomach and liver disorders (Dorosti and Jamshidi, 2016). In addition to various pharmacological effects, it is used in industry, medicine, and food as a source of some valuable secondary metabolites. The most important secondary metabolites of this specimen include monoterpene glycosides, trypanocidal terpenoids (Saeidnia et al., 2004), flavonoids, rosmarinic acid (Fattahi et al., 2013), and some essential oils (Saeidnia et al., 2007). This herbaceous, beautiful, and aromatic wild-growing plant with a height of about 10-20 cm is grown in mountainous and highland areas of the central and northern regions of the country (Rechinger, 1986). In addition, *D. kotschyi* is used as an ornamental plant due to its aesthetic characteristics, such as abundant white and fragrant flowers, plant form, relatively fast growth, long flowering stage, and possible abiotic stress tolerance. Therefore, it can be used as a valuable ornamental plant in sustainable green space design in arid and semi-arid areas.

Climate change, especially consecutive years of drought, has been one of the critical extinctions treat of this valuable medical-ornamental plant. Notably, that most studies performed on this species have focused more on its phytochemical attributes, and few studies are available on strategies to enhance the abiotic stress tolerance of this species which could contribute to the cultivation development and survival of this plant.

The present study aimed to determine the effect of different concentrations of zinc in two forms of zinc oxide (ZnO-N) nanoparticles and zinc sulfate ($ZnSO_4$) on the drought tolerance of *D. kotschyi* plant. It is hypothesized that ZnO-N compared to $ZnSO_4$ might be more effective in alleviating the drought tolerance of *D. kotschyi* through its positive function on the physiological and biochemical processes of the plant.

2 Materials and methods

2.1 Plant growth conditions and treatments

Mature seeds of *D. kotschyi* were collected from its natural habitat in Semirom city (Isfahan province, Iran) with latitude and longitude of 31°49', 51° 59' ", respectively, and altitude of 2400 m above sea level. Seeds were grown in growth trays containing 80% cocopeat and 20% perlite. After germination, seedlings in the six-leaf stage were transferred to plastic pots containing sandy loam soil with a low organic matter (1.5%) and a pH of 7.2. Following ten

days of seedling transplanting, potted plants were regularly (twice a week) fed with an NPK fertilizer (20-20-20, 2g/l). After three weeks of growth in optimal conditions in the greenhouse, seedlings were divided in two groups: the first group (control) under well-watering (100% field capacity (FC)) and the second one (drought-stressed group) under limited watering (50% field capacity). According to the gravimetric method, soil moisture content was measured (Datta et al., 2009). It was monitored daily during the growth period using a soil moisture meter (EXTECH MO750, USA, probe length: 20 cm probe and max resolution: 0.1%). The pots are watered (when the humidity dropped below a certain level) to keep the moisture content at the desired level (100% and 50% FC).

Foliar fertilization with $ZnSO_4$ and ZnO-N at three concentrations of 0 (control), 10, and 20 mg/l was performed two times; first simultaneously with the start of drought stress and second three weeks after the start of drought stress (Rossi et al., 2018; Azmat et al., 2022). The control plants were watered up to 100% FC and received no fertilizer treatments ($ZnSO_4$ and ZnO-N).

ZnO-N were procured from Iranian Nanomaterials Pioneers Company, NANOSANY (Mashhad, Iran). Its characteristics, such as particle size, and purity, are presented in Figure 1 and Supplementary File 1. ZnO-N were added to deionized water and dispersed using ultra-sonication for 30 minutes. The treated plants were collected 45 days after the start of drought stress treatment, and leaf samples were immediately placed in liquid nitrogen and stored in a -80 freezer for later analysis.

2.2 Electrolyte conductivity and relative water content measurement

In order to measure EC, one gram of each leaf was added to 20 ml of distilled water and kept at room temperature (24°C) for 24 h. In addition, its electrical conductivity was measured by an EC meter as the initial EC (EC_1). After that, the samples were placed in an autoclave at 120°C for 15 min, and their secondary EC (EC_2) was determined. The following equation was exploited to calculate EC.

$$EC = (EC_1/EC_2) \times 100$$

Fresh weight (FW) of fully mature leaves was measured immediately after collection based on a method by (Ritchie et al., 1990). Afterward, they were placed in distilled water at 4°C for 24 h to determine the turgor weight (TW). In the next stage, samples were dried in an oven at 70°C for 48 hours, and the dry weight (DW) of each sample was recorded. The percentage of RWC was estimated using the equation below:

$$RWC = [(FW - DW)/(TW - DW) \times 100]$$

2.3 Photosynthetic pigments and soluble sugar determination

Leaf samples homogenized with 80% acetone were centrifuged for 5 min at 3000×g to calculate photosynthetic pigments (chlorophyll and carotenoid). Following that, optical absorbance of the supernatant solution was read at wavelengths of 470, 645, and 663 nm using a spectrophotometer (UV-VIS, Optima SP-3000 Plus, Bratislava, Slovakia). In the next stage, total chlorophyll and carotenoids were calculated in mg/g FW (Lichtenthaler, 1987).

Soluble sugar was determined using a phenol-sulfuric acid method based on acid hydrolysis of soluble sugars and furfural mixture creation (Kochert, 1978). After that, 100 µL of ethanol extract from the leaf sample, 300 µL of distilled water, and 1 mL 5% phenol were mixed while vortexed. In the next stage, 1 mL of concentrated sulfuric acid was added to the mixture, and adsorption was read at 485 nm against blanks after 30 min. In addition, the sugar content of the samples was assessed by using standard curves in mg/g FW.

2.4 Proline content determination and assay of total protein

Based on the technique by Bates et al. (1973), 200 µL of ninhydrin and glacial acetic acid reagents was added to 200 µL of extract from homogenized leaf sample and sulfuric acid. Afterward, the samples were placed in a hot water bath at a temperature of

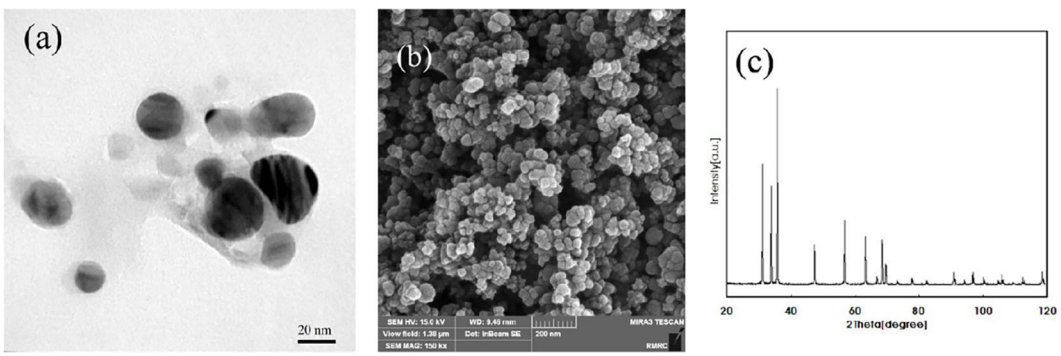

FIGURE 1
(A) Transmission Electron Micrograph (TEM), **(B)** SEM (Scanning electron microscope) and **(C)** X-ray diffraction (XRD) of Zinc oxide nanoparticles, Iranian Nanomaterials Pioneers Company, NANOSANY, 2020.

100°C for 30 min. Then, 600 µL of toluene was added to the samples following immediate rapid cooling and vortexed for 30 sec. After 20 minutes, the optical absorbance of the upper solution was read at 520 nm, and the concentration of proline in the solution was calculated in mg/g FW using the proline standard curve.

In order to assay total protein, 1 mL of extraction buffer (PBS) and EDTA with a concentration of 0.1 mM was added to powdered leaves using liquid nitrogen and homogenized. After that, the samples were centrifuged at 12000g for 10 minutes at 4°C. The supernatant was stored in a freezer at -80°C for protein and enzyme activity assay. In the next stage, 2.5 mL of Bradford solution was added to 50 µL of supernatant to determine the protein content of the extract. After 5 min, adsorption was read at a wavelength of 595 nm. Certain concentrations of bovine serum albumin (BSA) standard protein were prepared in order to draw a standard protein diagram (Bradford, 1976).

2.5 Assay of antioxidant enzyme activity

In this stage, 50 mM of PBS (pH=7), 0.02 M pyrogallol, and 50 µL enzymatic extract were prepared as the reaction mixture to assess the activity of polyphenol oxidase (PPO). Adsorption of all samples was measured based on the purpurogallin content at a wavelength of 420 nm in one min at a 5 second interval., Ultimately, the values obtained were calculated in Umg^{-1} protein (Raymond et al., 1993).

Superoxide dismutase (SOD) enzyme activity in the reaction mixture was assessed based on the measurement of inhibition of photochemical reduction of nitro blue tetrazolium. Reaction mixture encompasses BPS (50 mM, pH=7.8), methionine (13 mM), nitro blue tetrazolium (75 µM), riboflavin (2 µM), sodium carbonate (50 mM), triton X-100 (0.025%) and 50 µL of enzymatic extract. Sample adsorption was read at a wavelength of 560 nm against the blanks following exposure to light for 15 min. In addition, Blue Formazan production was expressed in Umg^{-1} protein by measuring the increase in absorption (Giannopolitis and Ries, 1977).

Guaiacol peroxidase (GPO) enzyme activity was assessed using (Hemeda and Klein, 1990) method. The reaction mixture included BPS (20 mM, pH=6), Guaiacol (5 mM), H_2O_2 (1 mM), and 50 µL of enzymatic extract. In addition, enzyme activity resulting from guaiacol oxidation with increased adsorption at 570 nm was determined. Alternation in adsorption was measured every five seconds for a minute and was expressed in Umg^{-1} protein.

2.6 SEM-elemental mapping and EDX analysis

Following the method by Pathan et al. (2010), intact and mature leaf samples separated from plants were powdered after drying at room temperature without any pretreatment and were used for SEM imaging. In addition, microanalysis of Zn, as well as Cu, Fe, and P elements as the most critical interactive elements with Zn, and elemental mapping was carried out using SEM-EDX (Energy-Dispersive X-ray). It is worth mentioning that all microscopic studies were done at Bu-Ali Research Institute, Mashhad University of Medical Sciences.

2.7 Statistical analysis

In the present study, a factorial experiment was conducted based on the completely randomized design with four replications (each pot represented one replication with two plants). Treatments were drought stress, including 50% FC and 100% FC and two zinc sources, $ZnSO_4$ and ZnO-N, at three concentrations of 0, 10, and 20 mg/l. The distribution normality of data was tested using the Anderson-Darling test prior to analysis. Analysis of variance (ANOVA) and means the comparison of measured attributes was performed using Minitab 16 software and Tukey's test at 5% probability level, respectively.

3 Results

3.1 EC and RWC measurement

It is evident from Table 1 that $ZnSO_4$ and ZnO-N and their interactions with drought stress had significant effects on EC in *D. kotschyi* ($P \leq 0.05$) (Table 1). In this respect, the EC of the samples (22.12%) decreased by 83%, compared to control (40.47%), by increasing the ZnO-N concentration. The lowest EC was observed in samples under drought stress and without drought stress receiving 20 mg of ZnO-N (18.4% and 25.84%). Foliar fertilization with $ZnSO_4$ at a concentration of 10 mg/l had a mitigating effect on the EC, such that the lowest EC was obtained in plants under drought stress and fertilized by 10 mg/l of $ZnSO_4$ (20.62%) (Figure 2, right).

Interaction of foliar fertilization of $ZnSO_4$ and ZnO-N with drought stress had a significant effect on changes in RWC content in *D. kotschyi* ($P \leq 0.05$) (Table 1). At both concentrations of 10 and 20 mg/l, $ZnSO_4$ increased RWC in plants under drought stress by up 10%, compared to plants under drought stress not treated with $ZnSO_4$ (Figure 2, left). This increase was about 3% in plants under drought stress fertilized with ZnO-N at two 10 and 20 mg/l concentrations, although these mitigating changes were not statistically significant. In addition, the highest RWC was related to control plants, which received no treatments, under full irrigation (78.46%) (Figure 2, left).

3.2 Photosynthetic pigment and soluble sugar content

The highest total chlorophyll content was obtained in plants under drought stress and foliar fertilization with $ZnSO_4$ at concentrations of 10 (1.22 mg/g FW) mg/l and then 20 (1.20

TABLE 1 Analysis variance of physiological and biochemical traits in treated *D. kotschyi* by $ZnSO_4$ and ZnO-N under drought stress.

P-Value										
Source	DF	RWC	EC	Chlorophyll	Sugar	Proline	Protein	SOD	GPO	PPO
(DS)	1	0.096	0.306	0.226	0.491	0.000	0.344	0.004	0.000	0.032
($ZnSO_4$)	2	0.553	0.002	0.975	0.026	0.000	0.237	0.000	0.086	0.046
(ZnO-N)	2	0.137	0.000	0.349	0.412	0.286	0.000	0.000	0.000	0.111
(DS)×($ZnSO_4$)	2	0.005	0.002	0.015	0.572	0.553	0.007	0.153	0.260	0.033
(DS)×(ZnO-N)	2	0.038	0.000	0.133	0.000	0.037	0.342	0.000	0.002	0.053
Error	44	–	–	–	–	–	–	–	–	–
Lack of fit	8	0.127	0.000	0.005	0.006	0.000	0.051	0.001	0.026	0.002
Total	52	–	–	–	–	–	–	–	–	–

DS, Drought stress; DF, degree of freedom.

mg/g FW) mg/l. The lowest amount of chlorophyll (1.07 mg/g FW) was observed in plants under drought stress and without zinc treatment. Moreover, the highest level of carotenoids (2 mg/g FW) was obtained in plants under drought stress. The other treatments had no significant effects on these contents (Table 1; Figure 3, left).

Drought stress and ZnO-N interaction had a significant effect on soluble sugar in leaf samples of *D. kotschyi* ($P \leq 0.05$) (Table 1). In addition, the highest sugar content (32.23 mg/g FW) was observed in plants under full irrigation treated with 10 mg/l of ZnO-N. Meanwhile, no significant difference was observed between these samples and the plants under drought stress treated with 20 mg/l of ZnO-N. In this regard, the lowest sugar content (19.16 mg/l FW) was observed in control samples and plants under full irrigation treated with 20 mg/l of ZnO-N (Figure 3, right).

3.3 Proline and protein content

In this study, drought stress, $ZnSO_4$ and interaction of drought stress with ZnO-N significantly affected proline content in *D. kotschyi* ($P \leq 0.05$) (Table 1). According to the results, proline content increased in plants under drought stress (213.87 µM/g FW) 50% more than plants under non-stressed conditions (142.32 µM/g FW). Furthermore, $ZnSO_4$ fertilization at a concentration of 10 mg/l (233.09 µM/g FW) led to a 136% increase in proline content, compared to plants not treated with this substance (98.67 µM/g FW). According to the results, the highest proline content (230.13 µM/g FW) was observed in plants under drought stress receiving $ZnSO_4$ fertilization at a concentration of 10 mg/l, which had a significant difference with plants under full irrigation (no drought stress) (Figure 4, left).

ZnO-N and also interaction of $ZnSO_4$ with drought stress had a significant effect on the protein content of *D. kotschyi* ($P \leq 0.05$). In this regard, the highest protein content (12.02 mg/g FW) was observed in the treated plants with 10 mg/l $ZnSO_4$ under drought stress. The lowest one was obtained in plants with 10 mg/l $ZnSO_4$ under full irrigation (Figure 4, right).

3.4 Activity of antioxidant enzymes

In this study, the activity levels of SOD, PPO, and GPO enzymes in *D. kotschyi* under drought stress increased by 20%, 90%, and 75%, respectively, compared to control samples. According to the results, the highest SOD and GPO enzyme activities were observed in plants under drought stress treated with 20 mg/l ZnO-N (Figure 5). Meanwhile, the use of 10 mg/l ZnO-N in plants under drought stress led to the highest activity of the PPO enzyme (Figure 5, right-above) under Drought Stress

3.5 Identification of the elemental composition

SEM-EDX analysis and elemental mapping were conducted to support our findings that Zn-nanoparticles could improve the drought tolerance in *D. kotschyi* by changing the concentrations of Cu, Fe, and P. As seen in Table 2, Fe and Cu percentages decreased with a decline in the concentration of Zn in plants, while an increase was observed in P percentage. According to Table 3, the concentrations of Zn, Cu, and Fe elements were respectively 5.5%, 5%, and 2.5% higher and the P element was 13% lower in plants treated with ZnO-N and $ZnSO_4$, compared to control plants. In addition, the concentration of Cu, Fe, and Zn elements in $ZnSO_4$ treatment was 1.5% higher, compared to ZnO-N, whereas the difference in P element concentration was 3.5% lower in this regard (Tables 2, 3).

TABLE 2 Scanning electron microscopy images, Zn maps of leaf surfaces and their EDX results of non-fertilized (control) and foliar fertilized with $ZnSO_4$ and ZnO-N in *D. kotschyi* under drought stress.

Source	Zn map	SEM image	EDX Analysis
Control	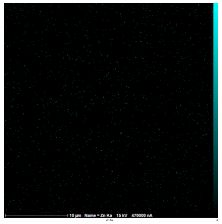	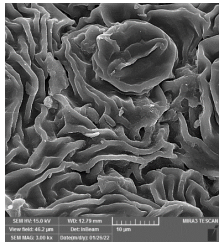	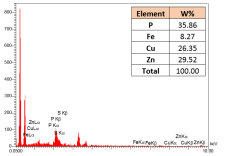
50% FC 10 mg $ZnSO_4$	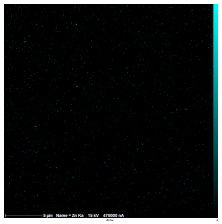	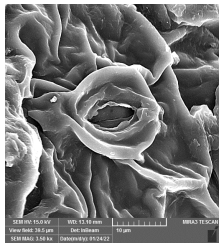	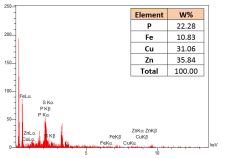
50% FC 20 mg $ZnSO_4$	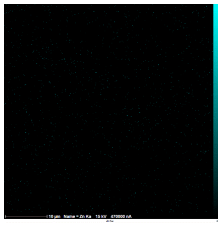	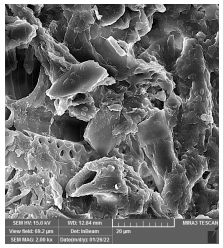	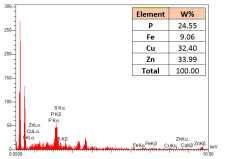
50% FC 10 mg $ZnSO_4$ 10 mg ZnO-N	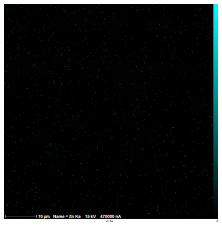	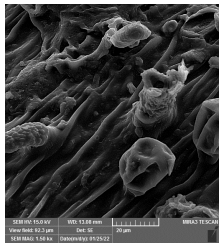	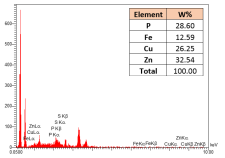

(Continued)

10.3389/fpls.2023.1063618

TABLE 2 Continued

Source	Zn map	SEM image	EDX Analysis
50% FC 20 mg $ZnSO_4$ 10 mg ZnO-N	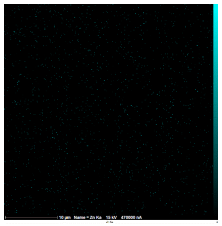	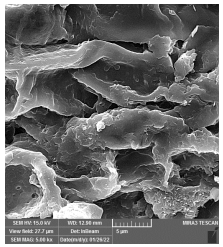	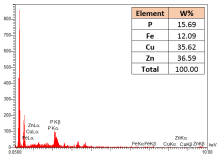
50% FC 10 mg ZnO-N	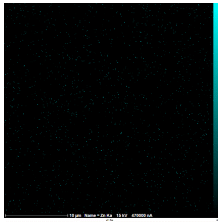	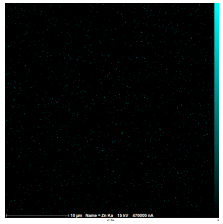	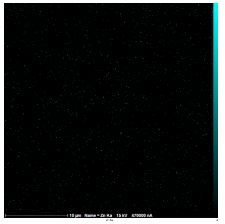
50% FC 20 mg $ZnSO_4$ 20 mg ZnO-N	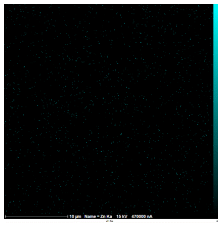	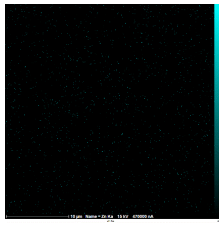	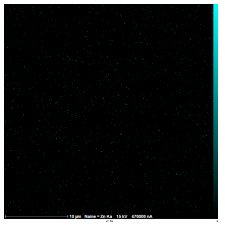
50% FC 20 mg ZnO-N	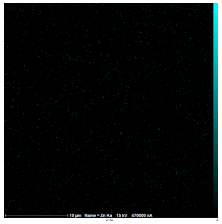	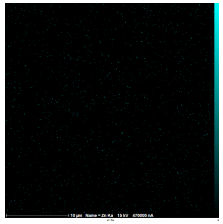	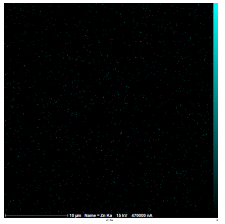

10.3389/fpls.2023.1063618

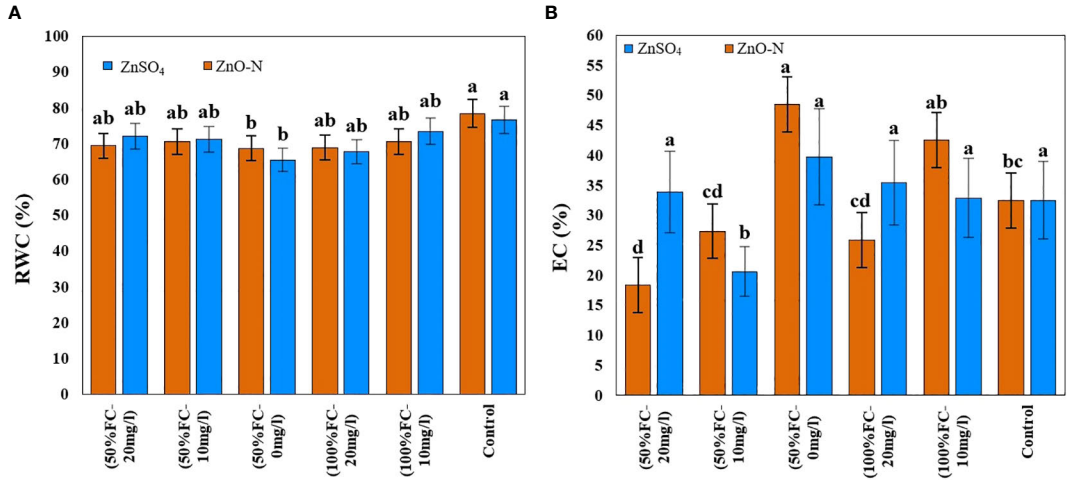

FIGURE 2
Impact of $ZnSO_4$ and ZnO-N on RWC **(A)** and EC **(B)** in *D Kotschyi* under Drought Stress. Means followed by the same letters did not differ significantly at $p \leq 0.05$, n = 4.

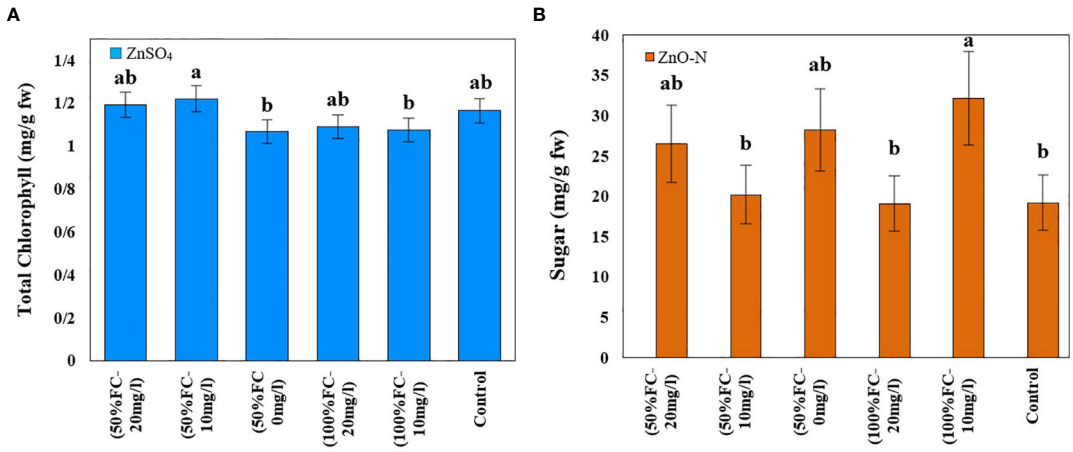

FIGURE 3
Impact of $ZnSO_4$ on total chlorophyll **(A)** and ZnO-N on sugar **(B)** in *D Kotschyi* under Drought Stress. Means followed by the same letters did not differ significantly at $p \leq 0.05$, n = 4.

4 Discussion

The present study aimed to increase the drought tolerance of *D. kotschyi* using ZnO-N and $ZnSO_4$ treatments. According to the results, ZnO-N reduced EC on the plants under drought stress, while the mitigating effect of $ZnSO_4$ on EC at the same conditions was less than ZnO-N. Meanwhile the highest sugar and proline content as well as the highest activity of SOD and GPO (and to some extent PPO) in *D. kotschyi* exposed to drought stress were at the same conditions observed by the application of ZnO-N. Using $ZnSO_4$ increased chlorophyll and protein content and also PPO activity in this plant under drought stress.

4.1 Changes in physiological, biochemical contents

RWC in plants indicates the amount of water stored in the leaves and the rate of transpiration. Stress (in particular drought stress) usually reduces electrical conductivity in plants, which leads to a decline in RWC (Ahluwalia et al., 2021). In this experiment, there was a significant decrease in RWC in plants under drought stress. Nonetheless, ZnO-N and $ZnSO_4$ treatments increased RWC in plants by 10% and 3%, respectively (although not statistically significant). Studies showed that using ZnO-N increases RWC in *Solanum melongena* (Semida et al., 2021) and *Triticum aestivum*

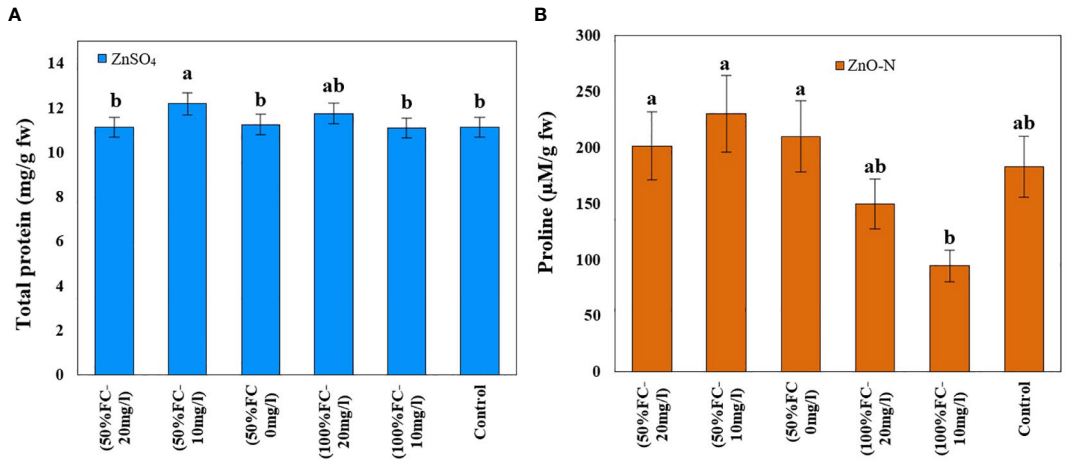

FIGURE 4
Impact of $ZnSO_4$ on total protein **(A)** and ZnO-N on proline **(B)** and in *D Kotschyi* under Drought Stress. Means followed by the same letters did not differ significantly at $p \leq 0.05$, n = 4.

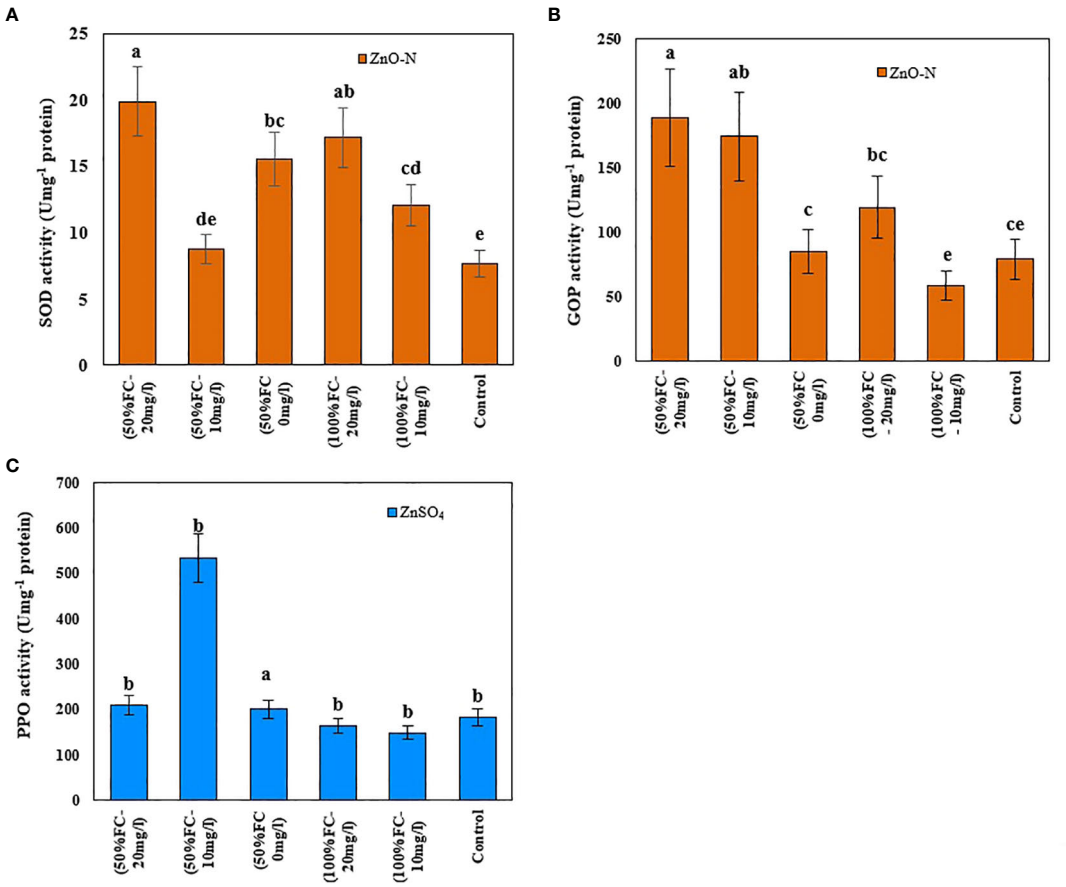

FIGURE 5
Impact of ZnO-N on SOD **(A)** and GPO **(B)**; $ZnSO_4$ on PPO **(C)** in *D Kotschyi* under Drought Stress. Means followed by the same letters did not differ significantly at $p \leq 0.05$, n = 4.

(Taran et al., 2017) under drought stress. Similarly, $ZnSO_4$ improved RWC in wheat (Sattar et al., 2022) and triticale (Kheirizadeh Arough et al., 2016) under stress. The Zn element affects water absorption and transport capacity in plants and decreases short-term adverse effects of environmental stresses (Kasim, 2007; Disante et al., 2010). On the other hand, regulation of gene expression affecting tolerance to environmental stress depends on the Zn element (Cakmak, 2000).

TABLE 3 Comparison of measured elements percentage with control (non-fertilized) in treated *D. kotschyi* by ZnSO4 and ZnO-N through SEM-EDX method under drought stress.

Source	P (%)	Fe (%)	Cu (%)	Zn (%)
Zn-Nanoparticle	24.85	10.47	30.30	34.37
$ZnSO_4$	21.37	11.01	31.83	35.78
Control	35.86	8.27	26.35	29.52

Different stresses, such as drought stress, damage cellular membrane in plants and lead to ion leakage, thereby increasing EC in the plant (Luo et al., 2012). Therefore, low EC in plants could be a criterion for resistance to environmental stresses (Blum, 2005). In this experiment, ZnO-N and to some extent $ZnSO_4$ reduced EC in plants under stress, respectively compared to the control plants. According to the results, a decline in EC of plants under stress was due to the use of ZnO-N in wheat (Adrees et al., 2020) and corn (Rizwan et al., 2019).

Results indicated that drought stress led to a decrease in total chlorophyll content in *D. kotschyi*, and $ZnSO_4$ was able to increase chlorophyll content in the plant under stress conditions. In support of this finding, Cakmak (2000) reported that zinc promotes chlorophyll synthesis by protecting sulfhydryl groups. In addition, it influences pigment content by creating a balance in the concentration and providing other elements involved in chlorophyll synthesis (N and Mg) (Movahhedi et al., 2017). According to various studies, Zn increases chlorophyll content under drought stress (Dimkpa et al., 2020; Faizan et al., 2021; Sun et al., 2021).

While drought treatment did not affect the sugar content of *D. kotschyi*, ZnO-N at 20 mg/l increased soluble sugar in the plants under drought stress, compared to the control plants. It is notable that Zn plays a role in carbohydrate metabolism and affects the activity of carbonic anhydrase, which regulates the CO_2-sensing pathway and improves drought tolerance in the plant (Tewari et al., 2019). The use of Zn in plants under drought stress led to an increase in the accumulation of soluble carbohydrates and increased drought tolerance in *Phaseolus vulgaris* (Mahdieh et al., 2018) and *Sesamum indicum* (Movahhedi et al., 2017). In the corn plant, the use of ZnO-N was associated with an improvement in drought tolerance of the plant through the regulation of the activity of key enzymes in carbohydrate metabolism (Sun et al., 2021).

In this experiment, proline accumulated in the plants in response to drought stress. Proline acts as an essential osmolyte and an efficient antioxidant in regulating cell osmosis and ROS scavenging in plants under stress. Proline maintains cellular turgidity, stabilizes the structure of enzymes and proteins, and protects the plant under stress. The increase in proline content in plants can be considered an as indicator of improved drought tolerance (Ahluwalia et al., 2021). Fertilization treatment with 10 mg/l ZnO-N increased proline content in plants under drought stress. Results of some previous studies were indicative of increased proline content as a result of ZnO-N (Noohpisheh et al., 2021) and Zn (Zengin, 2006) in *Trigonella foenum-graecum* and *Phaseolus vulgaris* under environmental stresses. According to our findings, in some plants under drought stress, the increase in protein concentration was associated with higher RWC (Sandhya et al., 2010; Silva et al., 2020). Moreover, Zn led to the accumulation of proline under drought stress, and proline accumulation resulted in the protection of osmoregulation enzymes and increased drought tolerance in the plant (Hasegawa et al., 2000). The exact mechanism of the role of proline on antioxidant enzymes has not been clarified (Haque et al., 2007). However, under environmental stress such as drought, the increase in the antioxidant enzymes' activity is usually accompanied by an increase in the proline content (Ghaffari et al., 2019).

The treatments of ZnO-N and $ZnSO_4$ led to increased protein content in plants under drought stress. This could be due to the increased level of photosynthesis, RWC, chlorophyll content, and also enzymes involved in synthesizing sugar in plants (Sun et al., 2021). The decrease in EC and improvement of damages caused by ion leakage in stress conditions could also be another reason for increased protein content in Zn- treated plants (Cakmak, 2000). Sugars and proteins are two key components in regulating plant responses to stresses. On the hand, transcription, translation, protein stability, and activity are the regulatory roles of sugars in plants (Rolland et al., 2006). On the other hand, various enzymes and proteins are involved in the sugar synthesis of plants (Pfister and Zeeman, 2016). Soluble sugars as osmoprotectors, stabilize proteins and cell membranes under environmental stresses lead to different expressions of some proteins related to sugar metabolism. Moreover, sugar signals enhance plant defense responses through some enzymes (like mitogen-activated protein kinase) signaling cascade (Kocal et al., 2008). In a study, a significant positive correlation between soluble proteins and sugars in the growth of two poplar species under drought stress was reported by Yang and Miao (2010). In this respect, our findings are congruent with the reports related to the use of Zn (as a nanoparticle or sulfate) in various plants under drought stress (Patra et al., 2013; Singh et al., 2018; Dimkpa et al., 2019; Motyka et al., 2019; Bashir et al., 2021).

In our study, drought stress significantly increased the activity of SOD, GPO, and PPO antioxidant enzymes in *D. kotschyi*. Studies show that antioxidant enzyme activities increase to improve plant tolerance in stress conditions. The SOD enzyme plays an important role in the cell's antioxidant defense system by converting peroxide radicals to hydrogen peroxide (Sharma et al., 2012). On the other hand, the PPO enzyme in the immune system of plants under environmental stress, prevents excessive reduction of electron transfer in photosynthesis (Islam et al., 2020). Meanwhile, GPO can convert H_2O_2 to water through oxidation (Dianat et al., 2016).

In the current research, ZnO-N increased the activities of SOD, GPO, and some extent PPO enzymes in *D. kotschyi* under drought

stress. Zn is a metal component and cofactor of many enzymes and increases the activity of antioxidant enzymes under drought stress conditions (Kheirizadeh Arough et al., 2016). The use of ZnO-N plays a role in modulating the activity of various enzymes, especially those related to plant adaptation to stress (Verma et al., 2020). In some previous studies, using ZnO-N intensified SOD enzyme activities in *Salvinia natan* (Hu et al., 2014) and *Gossypium hirsutum* (Priyanka and Venkatachalam, 2016). Bashir et al. (2021) reported that SOD and PPO activities increased in *Triticum aestivum* under oxidative stress conditions by using Zn nanoparticles. In addition, iron and Zn nanoparticles increased GPO activities in *Oryza sativa* (Upadhyaya et al., 2017) and *Dracocephalum moldavica* (Moradbeygi et al., 2020) under environmental stress.

Some reports are indicating the adverse effects of nanoparticles on biological systems and cellular components. ZnO-N are also shown to have some genotoxic effects on human epidermal cells (Sharma et al., 2009). It has been found that ZnO-N can be toxic for either normal or cancer cells (Ali et al., 2012). Moreover, it can cause oxidative DNA damage in human lung cells (Ng et al., 2017). Despite some reports showing the negative impact of ZnO-N on biological systems, there are other studies indicating that the toxicity of ZnO-N is not significant to human health and the environment. It has been found that ZnO-N are non-toxic up to a certain level but can be dangerous at higher concentrations (Nagara et al., 2022). In this regard, Amuthavalli et al. (2021) showed the moderate side effect of biosynthesized ZnO-N on rats and they reported that ZnO-N could be used as a multipurpose agent in the field of biomedical research (Amuthavalli et al., 2021). ZnO-N synthesized from plants (*Melia azedarach*) showed less toxicity compared to the one synthesized through the conventional method (Dinga et al., 2022). ZnO-N have a wide range of biomedical applications (Agarwal et al., 2017) and are also used in cosmetic products such as sunscreen creams (Hong et al., 2022). Recent studies have shown that the risks and benefits of zinc oxide nanoparticles depend on various factors including the concentration of ZnO-N, the synthesis method, and the tested organism (Czyżowska and Barbasz, 2022).

Increasing the concentration of Zn in the plant could cause poisoning by disrupting the balance of other nutrients and reducing photosynthesis (Kabata-Pendias, 2010). Meanwhile, nano-fertilizers have a lower chance of creating toxicity in the plant and soil with slower and more appropriate delivery of nutrients to the plant (Solanki et al., 2015). However, nano-fertilizers could be toxic at high concentrations, for instance, ZnO-N at high concentrations could inhibit growth *in Fagopyrum esculentum* (above 1000 mg/l) (Lee et al., 2013) and Radish (above 20 mg/l) (Lin and Xing, 2007). In this experiment, low concentrations of ZnO-N (10 and 20 mg/l) were applied on *D. kotschi* with the approach of ornamental/landscape use (not as an edible plant).

4.2 Changes in element concentration

According to the findings, there was a significant difference in the concentration of P, Cu, Fe, and Zn elements in treated plants with ZnO-N and $ZnSO_4$, compared to the control plants. However, no significant difference was observed between the treated plants with two fertilizers (ZnO-N and $ZnSO_4$) in terms of the element concentration. Double interactions between P, Fe, and Zn have long been recognized in plants, such that Cu and Fe concentrations increased with an increase in Zn concentration (Fan et al., 2021). Furthermore, studies have approved the antagonistic effect of Zn and Fe with P as a nutrient in some plants (Zheng et al., 2009). Overall, P, Cu, Fe, and Zn play a significant role in drought stress tolerance in plants (Marschner, 2012; Tripathi et al., 2018; Dimkpa et al., 2019).

In a previous study (Akbari et al., 2013), fertilization with Zn reduced drought stress through decreasing H_2O_2 content and lipid peroxidation, which resulted from increased antioxidant enzymes (CAT, GPX, and SOD). Fe regulates the unfavorable effects of drought, salinity, and heavy elements by controlling cellular redox states and the antioxidant defense mechanism, such as catalase and superoxide dismutase (Tripathi et al., 2018). Moreover, Cu increases drought tolerance by increasing the activity of SOD, ascorbate peroxidase enzymes, and anthocyanin levels (Van Nguyen et al., 2022). In addition, P increases water uptake and maintains cellular turgidity by improving root growth, thereby regulating stomatal conductance and ultimately increasing plant photosynthesis and drought tolerance (Waraich et al., 2011).

Compared to conventional fertilizers, nano fertilizers due to their higher absorption level and slower release rate are more efficient in plant processes, including improving tolerance to stresses (Manjunath et al., 2016; Bashir et al., 2020). In general, foliar spraying by nanoparticles has many paths for absorption in plants due to the small size of the particles. Nanoparticles can enter the leaves through stomata, endocytosis, leaf hydathodes, and direct absorption (Hong et al., 2021). In this experiment, the size of the ZnO-N was not larger than 20 nm, so according to the report of Alshaal and El-Ramady (2017), compared to $ZnSO_4$ it seems to be absorbed to a greater extent, and there was no limitation passing through the cell wall pores. In this regard, Rajemahadik et al. (2018) reported that nanoparticles because of dynamic properties have a high surface area, activity, and catalytic surface. Nanoparticles rapidly react and disperse and can absorb more water. These properties can make nanoparticle fertilizers perform better in plant functions than other forms of fertilizers.

The Efficiency of ZnO-N compared to $ZnSO_4$ (as two Zn fertilizers) on the growth of *Zea mays* was confirmed in the study of Subbaiah et al. (2016). Also, Rossi et al. (2018) by foliar spraying of ZnO-N and $ZnSO_4$ on coffee plants reported that ZnO-N significantly increased the photosynthesis rate and growth traits. Moreover, there are some studies on the positive effect of Zn-nanoparticles on enhancing tolerance to abiotic stresses (in particular drought) in *Solanum melongena* (Semida et al., 2021), *Triticum aestivum* (Taran et al., 2017), wheat (Adrees et al., 2020), corn (Rizwan et al., 2019), *Trigonella foenum-graecum* (Noohpisheh et al., 2021) and *Phaseolus vulgaris* (Zengin, 2006).

Moreover, given the equal leaf Zn level in the treated plants with ZnO-N and $ZnSO_4$ at the end of the experiment (EDX analysis), the toxicity of ZnO-N was not significant than $ZnSO_4$. In other words, it can be said that due to the use of low concentrations of ZnO-N (10 and 20 mg/l) in this experiment, no toxicity was observed using this fertilizer. Moreover, *D. kotschyi* can be considered as a model

organism to present reduced toxicity effects of ZnO-N through supplementary experiments related to toxicity assessments (Supplementary File 2 and Supplementary File 3).

5 Conclusion

Considering the drought problem, using compounds that could increase drought tolerance in plants plays an essential role in water management in agriculture and urban green space. This research has demonstrated that zinc nanoparticles (ZnO-N) improved drought tolerance in *Dracocephalum kotschyi* (a medicinal-ornamental endangered plant) under drought stress. Based on our findings, ZnO-N positively affected most of biochemical (sugar and proline) and physiological (electrolyte conductivity and to some extent relative water content) factors in drought conditions. Moreover, ZnO-N significantly increased the activity of antioxidant enzymes (SOD, GPO, and some extent PPO) in *D. kotschyi* exposed to drought stress. The positive effect of $ZnSO_4$ application on this plant under drought stress was achieved through increased EC, RWC, chlorophyll and protein content, and also POP activity. In addition, no significant difference was observed in the concentration of P, Cu, Fe, and Zn elements in plants treated with ZnO-N and $ZnSO_4$. Given the significant role of sugar and proline and also antioxidant enzymes (SOD, GPO, and to some extent PPO) in plants' defense systems and tolerance to environmental stresses, ZnO-N seems to be more efficient compared to $ZnSO_4$ in improving drought tolerance in *D. kotschyi*. Since there are some reports regarding the toxicity of ZnO-N at higher concentrations, it is recommended to use ZnO-N at a low level (less than 1000 mg/l).

Data availability statement

The original contributions presented in the study are included in the article/Supplementary Material. Further inquiries can be directed to the corresponding author.

Author contributions

All authors contributed to the study conception and design. Material preparation, experimental works and analysis were performed by ZK. The first draft of the manuscript was written by ZK. LS commented on preliminary versions of the manuscript. All authors contributed to the article and approved the submitted version.

Funding

This work was supported by a grant from Ferdowsi University of Mashhad-Iran [Grant number: 50779].

Conflict of interest

The authors declare that the research was conducted in the absence of any commercial or financial relationships that could be construed as a potential conflict of interest.

Publisher's note

All claims expressed in this article are solely those of the authors and do not necessarily represent those of their affiliated organizations, or those of the publisher, the editors and the reviewers. Any product that may be evaluated in this article, or claim that may be made by its manufacturer, is not guaranteed or endorsed by the publisher.

Supplementary material

The Supplementary Material for this article can be found online at: https://www.frontiersin.org/articles/10.3389/fpls.2023.1063618/full#supplementary-material

References

Adrees, M., Khan, Z. S., Ali, S., Hafeez, M., Khalid, S., Rehman, M. Z., et al. (2020). Simultaneous mitigation of cadmium and drought stress in wheat by soil application of iron nanoparticles. *Chemosphere* 238, 124681. doi: 10.1016/j.chemosphere.2019.124681

Agarwal, H., Venkat Kumar, S., and Rajeshkumar, S. (2017). A review on green synthesis of zinc oxide nanoparticles–an eco-friendly approach. *Res. Eff. Tech.* 3, 406–413. doi: 10.1016/j.reffit.2017.03.002

Ahluwalia, O., Singh, P. C., and Bhatia, R. (2021). A review on drought stress in plants: Implications, mitigation and the role of plant growth promoting rhizobacteria. *Res. Envir. Sustai.* 5, 100032. doi: 10.1016/j.resenv.2021.100032

Ahmed, T., Noman, M., Rizwan, M., Ali, S., Ijaz, U., Nazir, M. M., et al. (2022). Green molybdenum nanoparticles-mediated bio-stimulation of bacillus sp. strain ZH16 improved the wheat growth by managing in planta nutrients supply, ionic homeostasis and arsenic accumulation. *J. Hazard. Mater.* 423, 127024. doi: 10.1016/j.jhazmat.2021.127024

Akbari, G. A., Amirinejad, M., Baghizadeh, A., Allahdadi, I., and Shahbazi, M. (2013). Effect of zn and fe foliar application on yield, yield components and some physiological traits of cumin (*Cuminum cyminum*) in dry farming. *Int. J. Agro. Plant Prod.* 4, 3231–3237.

Ali, S. M. U., Fakhar-e-Alam, M., Wazir, Z., Kashif, M., Atif, M., Willander, M., et al. (2012). Cytotoxic effects of zinc oxide nanoflakes (ZNO NFS) in human muscle arcinoma. *Int. J. Med. Med. Sci.* 2, 053–058.

Alshaal, T., and El-Ramady, H. (2017). Foliar application: from plant nutrition to biofortification. *EBSS* 1, 71–83. doi: 10.21608/jenvbs.2017.1089.1006

Amuthavalli, P., Hwang, J. S., Dahms, H. U., Wang, L., Anitha, J., Vasanthakumaran, M., et al. (2021). Zinc oxide nanoparticles using plant lawsonia inermis and their mosquitocidal, antimicrobial, anticancer applications showing moderate side effects. *Sci. Rep.* 11, 8837. doi: 10.1038/s41598-021-88164-0

Azmat, A., Tanveer, Y., Yasmin, H., Hassan, M. N., Shahzad, A., Reddy, M., et al. (2022). Coactive role of zinc oxide nanoparticles and plant growth promoting rhizobacteria for mitigation of synchronized effects of heat and drought stress in wheat plants. *Chemosphere* 297, 133982. doi: 10.1016/j.chemosphere.2022.133982

Bashir, A., Rehman, M. Z., Hussaini, K. M., Adrees, M., Qayyum, M. F., Sayal, A. U., et al. (2021). Combined use of zinc nanoparticles and co-composted biochar enhanced wheat growth and decreased cd concentration in grains under cd and drought stress: A field study. *Environ. Technol. Innov.* 23, 101518. doi: 10.1016/j.eti.2021.101518

Bashir, M. A., Silvestri, C., Ahmad, T., Hafiz, I. A., Abbasi, N. A., Manzoor, A., et al. (2020). Osmotin: A cationic protein leads to improve biotic and abiotic stress tolerance in plants. *Plants (Basel)* 9, 992. doi: 10.3390/plants9080992

Bates, L. S., Waldren, R. P., and Teare, I. D. (1973). Rapid determination of free proline for water-stress studies. *Plant Soil* 39, 205–207. doi: 10.1007/BF00018060

Bayat, H., and Moghadam, A. N. (2019). Drought effects on growth, water status, proline content and antioxidant system in three *Salvia nemorosa* l. cultivars. *Acta Physiol. Plant* 41, 1–8. doi: 10.1007/s11738-019-2942-6

Blum, A. (2005). Drought resistance, water-use efficiency, and yield potential–are they compatible, dissonant, or mutually exclusive? *Aust. J. Agric. Res.* 56, 1159–1168. doi: 10.1071/AR05069

Bodner, G., Nakhforoosh, A., and Kaul, H. P. (2015). Management of crop water under drought: a review. *Agron. Sustain. Dev.* 35, 401–442. doi: 10.1007/s13593-015-0283-4

Bradford, M. M. (1976). A rapid and sensitive method for the quantitation of microgram quantities of protein utilizing the principle of protein-dye binding. *Anal. Biochem.* 72, 248–254. doi: 10.1016/0003-2697(76)90527-3

Cakmak, I. (2000). Tansley review no. 111: Possible roles of zinc in protecting plant cells from damage by reactive oxygen species. *New Phytol.* 146, 185–205. doi: 10.1046/j.1469-8137.2000.00630.x

Cicek, S., and Nadaroglu, H. (2015). The use of nanotechnology in the agriculture. *Adv. Nano. Res.* 3, 207–223. doi: 10.12989/anr.2015.3.4.207

Czyżowska, A., and Barbasz, A. (2022). A review: zinc oxide nanoparticles – friends or enemies? *Int. J. Environ. Health Res.* 32, 885–901. doi: 10.1080/09603123.2020.1805415

Datta, A., Sindel, B. M., Kristiansen, P., Jessop, R. S., and Felton, W. L. (2009). The effects of temperature and soil moisture on chickpea (*Cicer arietinum* l.) genotype sensitivity to isoxaflutole. *J. Agron. Crop Sci.* 195, 178–185. doi: 10.1111/j.1439-037X.2009.00362.x

Dianat, M., Saharkhiz, M. J., and Tavassolian, I. (2016). Salicylic acid mitigates drought stress in *Lippia citriodora* l.: Effects on biochemical traits and essential oil yield. *Biocatal. Agric. Biotechnol.* 8, 286–293. doi: 10.1016/j.bcab.2016.10.010

Dimkpa, C. O., Andrews, J., Sanabria, J., Bindraban, P. S., Singh, U., Elmer, W. H., et al. (2020). Interactive effects of drought, organic fertilizer, and zinc oxide nanoscale and bulk particles on wheat performance and grain nutrient accumulation. *Sci. Total. Environ.* 722, 137808. doi: 10.1016/j.scitotenv.2020.137808

Dimkpa, C. O., Singh, U., Bindraban, P. S., Elmer, W. H., Gardea-Torresdey, J. L., and White, J. C. (2019). Zinc oxide nanoparticles alleviate drought-induced alterations in sorghum performance, nutrient acquisition, and grain fortification. *Sci. Total. Environ.* 688, 926–934. doi: 10.1016/j.scitotenv.2019.06.392

Dinga, E., Mthiyane, M. N., Marume, U., Botha, T. L., Horn, S., Pieters, R., et al. (2022). Biosynthesis of ZnO nanoparticles using melia azedarach seed extract: Evaluation of the cytotoxic and antimicrobial potency. *OpenNano* 8, 100068. doi: 10.1016/j.onano.2022.100068

Disante, K. B., Fuentes, D., and Cortina, J. (2010). Sensitivity to zinc of Mediterranean woody species important for restoration. *Sci. Total. Environ.* 408, 2216–2225. doi: 10.1016/j.scitotenv.2009.12.045

Dorosti, N., and Jamshidi, F. (2016). Plant-mediated gold nanoparticles by dracocephalum kotschyi as anticholinesterase agent: synthesis, characterization, and evaluation of anticancer and antibacterial activity. *J. Appl. Biomed.* 14 (3), 235–245. doi: 10.1016/j.jab.2016.03.001

Fageria, N. K., Moreira, A., and Coelho, A. M. (2012). Nutrient uptake in dry bean genotypes. *Commun. Soil Sci. Plant Anal.* 43, 2289–2302. doi: 10.1080/00103624.2012.701689

Faizan, M., Bhat, J. A., Chen, C., Alyemeni, M. N., Wijaya, L., Ahmad, P., et al. (2021). Zinc oxide nanoparticles (ZnO-NPs) induce salt tolerance by improving the antioxidant system and photosynthetic machinery in tomato. *Plant Physiol. Biochem.* 161, 122–130. doi: 10.1016/j.plaphy.2021.02.002

Fan, X., Zhou, X., Chen, H., Tang, M., and Xie, X. (2021). Cross-talks between macro-and micronutrient uptake and signaling in plants. *Front. Plant* 12. doi: 10.3389/fpls.2021.663477

Farooq, M., Romdhane, L., Al Sulti, M. K. R. A., Rehman, A., Al-Busaidi, W. M., and Lee, D. J. (2020). Morphological, physiological and biochemical aspects of osmopriming-induced drought tolerance in lentil. *J. Agron. Crop Sci.* 206, 176–186. doi: 10.1111/jac.12384

Fattahi, M., Nazeri, V., Torras-Claveria, L., Sefidkon, F., Cusido, R. M., Zamani, Z., et al. (2013). Identification and quantification of leaf surface flavonoids in wild-growing populations of *Dracocephalum kotschyi* by LC-DAD-ESI-MS. *Food Chem.* 141, 139–146. doi: 10.1016/j.foodchem.2013.03.019

Ghaffari, H., Tadayon, M. R., Nadeem, M., Cheema, M., and Razmjoo, J. (2019). Proline-mediated changes in antioxidant enzymatic activities and the physiology of sugar beet under drought stress. *Acta Physiol. Plant* 41, 23. doi: 10.1007/s11738-019-2815-z

Giannopolitis, C. N., and Ries, S. K. (1977). Superoxide dismutases: II. purification and quantitative relationship with water-soluble protein in seedlings. *Plant Physiol.* 59, 315–318. doi: 10.1104/pp.59.2.315

Guo, X., Chen, R., Thomas, D. S. G., Li, Q., Xia, Z., and Pan, Z. (2021). Divergent processes and trends of desertification in inner Mongolia and Mongolia. *Land Degrad. Dev.* 32, 3684–3697. doi: 10.1002/ldr.3825

Haque, A. K., Yamaoka, N., and Nishiguchi, M. (2007). Cytosine methylation is associated with RNA silencing in silenced plants but not with systemic and transitive RNA silencing through grafting. *Gene* 396, 321–331. doi: 10.1016/j.gene.2007.04.003

Hasegawa, P. M., Bressan, R. A., Zhu, J. K., and Bohnert, H. J. (2000). Plant cellular and molecular responses to high salinity. *Annu. Rev. Plant Biol.* 51, 463–499. doi: 10.1146/annurev.arplant.51.1.463

Hemeda, H. M., and Klein, B. P. (1990). Effects of naturally occurring antioxidants on peroxidase activity of vegetable extracts. *J. Food Sci.* 55, 184–185. doi: 10.1111/j.1365-2621.1990.tb06048.x

Hong, H., Liu, Z., Li, S., Wua, D., Jiang, L., Li, P., et al. (2022). Zinc oxide nanoparticles (ZnO-NPs) exhibit immune toxicity to crucian carp (*Carassius carassius*) by neutrophil extracellular traps (NETs) release and oxidative stress. *Fish Shellfish Immunol.* 129, 22–29. doi: 10.1016/j.fsi.2022.07.025

Hong, J., Wang, C., Wagner, D. C., Gardea-Torresdey, J. L., He, F., and Rico, C. M. (2021). Foliar application of nanoparticles: mechanisms of absorption, transfer, and multiple impacts. *J. Rico Environ. Sci. Nano.* 8, 1196–1210. doi: 10.1039/D0EN01129K

Hu, C., Liu, X., Li, X., and Zhao, Y. (2014). Evaluation of growth and biochemical indicators of *Salvinia natans* exposed to zinc oxide nanoparticles and zinc accumulation in plants. *Environ. Sci. pollut. Res.* 21, 732–739. doi: 10.1007/s11356-013-1970-9

Islam, M., Kim, J., Begum, M., Abu, T., Sohel, M. A., and Lim, Y. S. (2020). Physiological and biochemical changes in sugar beet seedlings to confer stress adaptability under drought condition. *Plants* 9, 1511. doi: 10.3390/plants9111511

Izsáki, Z. (2014). Effects of phosphorus supplies on the nutritional status of maize (*Zea mays* l.). *Commun. Soil. Sci. Plant Anal.* 45, 516–529. doi: 10.1080/00103624.2013.863910

Jordan, J., Singh, K., and Cañas-Carrell, J. (2018). Carbon-based nanomaterials elicit changes in physiology, gene expression, and epigenetics in exposed plants: A review. *Curr. Opin. Environ. Sci. Health* 6, 29–35. doi: 10.1016/j.coesh.2018.07.007

Kabata-Pendias, A. (2010). *Trace elements in soils and plants* (CRC press), 548. doi: 10.1201/b10158

Kasim, W. A. (2007). Physiological consequences of structural and ultra-structural changes induced by zn stress in *Phaseolus vulgaris*. i. growth and photosynthetic apparatus. *Int. J. Bot.* 3, 15–22. doi: 10.3923/ijb.2007.15.22

Kheirizadeh Arough, Y., Seyed Sharifi, R., and Seyed Sharifi, R. (2016). Bio fertilizers and zinc effects on some physiological parameters of triticale under water-limitation condition. *J. Plant Interact.* 11, 167–177. doi: 10.1080/17429145.2016.1262914

Kocal, N., Sonnewald, U., and Sonnewald, S. (2008). Cell wall-bound invertase limits sucrose export and is involved in symptom development and inhibition of photosynthesis during compatible interaction between tomato and xanthomonas campestris pv vesicatoria. *Plant Physiol.* 148, 1523–1536. doi: 10.1104/pp.108.127977

Kochert, G. (1978). "Carbohydrate determination by the phenol-sulfuric acid method," in *Handbook of physiological methods. handb phycol methods, phycol biochem methods*. Eds. J. A. Helebust and J. S. Craig (Cambridge: Cambridge University Press), 95–97.

Lee, S., Kim, S., Kim, S., and Lee, I. (2013). Assessment of phytotoxicity of ZnO NPs on a medicinal plant, *Fagopyrum esculentum*. environ. *Sci. pollut. Res.* 20, 848–854. doi: 10.1007/s11356-012-1069-8

Lichtenthaler, H. K. (1987). Chlorophyll fluorescence signatures of leaves during the autumnal chlorophyll breakdown. *J. Plant Physiol.* 131, 101–110. doi: 10.1016/S0176-1617(87)80271-7

Lin, D., and Xing, B. (2007). Phytotoxicity of nanoparticles: inhibition of seed germination and root growth. *Environ. pollut.* 150, 243–250. doi: 10.1016/j.envpol.2007.01.016

Liu, Z., Liu, T., Liang, L., Li, Z., Hassan, M. J., Peng, Y., et al. (2020). Enhanced photosynthesis, carbohydrates, and energy metabolism associated with chitosan-induced drought tolerance in creeping bentgrass. *Crop Sci.* 60, 1064–1076. doi: 10.1002/csc2.20026

Luo, X., Bai, X., Zhu, D., Li, Y., Ji, W., Cai, H., et al. (2012). GsZFP1, a new Cys2/His2-type zinc-finger protein, is a positive regulator of plant tolerance to cold and drought stress. *Planta* 235, 1141–1155. doi: 10.1007/s00425-011-1563-0

Mahdieh, M., Sangi, M. R., Bamdad, F., and Ghanem, A. (2018). Effect of seed and foliar application of nano-zinc oxide, zinc chelate, and zinc sulphate rates on yield and growth of pinto bean (*Phaseolus vulgaris*) cultivars. *J. Plant Nutr.* 41, 2401–2412. doi: 10.1080/01904167.2018.1510517

Manjunath, S. B., Biradar, D. P., and Aladakatti, Y. R. (2016). Nanotechnology and its applications in agriculture: A review. *J. Farm. Sci.* 29 (1), 1–13. doi: 10.18782/2582-2845.8405

Marschner, P. (2012). *Marschner's mineral nutrition of higher plants* (Amsterdam, Netherlands: Elsevier/Academic Press), 684. doi: 10.1016/C2009-0-63043-9

Moradbeygi, H., Jamei., R., Heidari, R., and Darvishzadeh, R. (2020). Investigating the enzymatic and non-enzymatic antioxidant defense by applying iron oxide nanoparticles in *Dracocephalum moldavica* l. plant under salinity stress. *Sci. Hortic.* 272. doi: 10.1016/j.scienta.2020.109537

Motyka, O., Strbova, K., Olšovská, E., and Seidlerová, J. (2019). Influence of nano-ZnO exposure to plants on l-ascorbic acid levels: Indication of nanoparticle-induced oxidative stress. *J. Nanosci. Nanotechnol.* 19, 3019–3023. doi: 10.1166/jnn.2019.15862

Movahhedi, M. D., Misagh, M., Yadavi., A., and Merajipoor., M. (2017). Physiological responses of sesame (*Sesamum indicum* l.) to foliar application of boron and zinc under drought stress conditions. *J. Plant Proc. Func.* 6, 27–36.

Mużaffarīyān, W. (1996). *Dictionary of Iranian plant names* (Iran: Moaser-farhang publication).

Nagara, V., Singh, T., Tiwari, Y., Aseri, V., Pandit, P. P., Chopade, R. L., et al. (2022). ZnO nanoparticles: Exposure, toxicity mechanism and assessment. *Mater. Today: Proc. Press* 69, 56-63. doi: 10.1016/j.matpr.2022.09.001

Ng, C. T., Yong, L. Q., Hande, M. P., Ong, C. N., Yu, L. E., Bay, B. H., et al. (2017). Zinc oxide nanoparticles exhibit cytotoxicity and genotoxicity through oxidative stress responses in human lung fibroblasts and drosophila melanogaster. *Int. J. Nanomed.* 12, 1621–1637. doi: 10.2147/IJN.S124403.eCollection2017

Noohpisheh, Z., Amiri, H., Mohammadi, A., and Farhadi, S. (2021). Effect of the foliar application of zinc oxide nanoparticles on some biochemical and physiological parameters of *Trigonella foenum*-graecum under salinity stress. *Plant Biosyst.* 155, 267–280. doi: 10.1080/11263504.2020.1739160

Pathan, A. K., Bond, J., and Gaskin, R. E. (2010). Sample preparation for SEM of plant surfaces. *Mater* 12, 32–43. doi: 10.1016/S1369-7021(10)70143-7

Patra, P., Choudhury, S. R., Mandal, S., Basu, A., Goswami, A., Gogoi, R., et al. (2013). "Effect sulfur and ZnO nanoparticles on stress physiology and plant (Vigna radiata) nutrition," in *Advanced nanomaterials and nanotechnology* (Springer), 301–309. doi: 10.1007/978-3-642-34216-5_31

Pfister, B., and Zeeman, S. C. (2016). Formation of starch in plant cells. *Cell. Mol. Life. Sci.* 73 (14), 2781–2807. doi: 10.1007/s00018-016-2250-x

Priyanka, N., and Venkatachalam, P. (2016). Biofabricated zinc oxide nanoparticles coated with phycomolecules as novel micronutrient catalysts for stimulating plant growth of cotton. *Adv. Natural sci.: J. Nanosci. Nanotechnol.* 7, 45018. doi: 10.1088/2043-6262/7/4/045018

Rajemahadik, V. A., Chavan, S. A., More, V. G., Chavan, V. G., Chavan, A. P., and Shetye, V. N. (2018). Nanotechnology: Innovative approach in crop nutrition management. *Int. J. Agric. Sci.* 10 (8), 5826–5582.

Raymond, J., Rakariyatham, N., and Azanza, J. L. (1993). Purification and some properties of polyphenoloxidase from sunflower seeds. *Phytochemistry* 34, 927–931. doi: 10.1016/S0031-9422(00)90689-7

Rechinger, H. (1986). *Lora iranica, labiatae* Vol. 150 (Graz, Austria: Akademische Druck- und Verlagsanstalt).

Rietra, R. P. J. J., Heinen, M., Dimkpa, C. O., and Bindraban, P. S. (2017). Effects of nutrient antagonism and synergism on yield and fertilizer use efficiency. *Commun. Soil Sci. Plant Anal.* 48, 1895–1920. doi: 10.1080/00103624.2017.1407429

Ritchie, S. W., Nguyen, H. T., and Holaday, A. S. (1990). Leaf water content and gas-exchange parameters of two wheat genotypes differing in drought resistance. *Crop Sci.* 30, 105–111. doi: 10.2135/cropsci1990.0011183X003000010025x

Rizwan, M., Ali, S., Rehman, M. Z., Adrees, M., Arshad, M., Qayyum, M. F., et al. (2019). Alleviation of cadmium accumulation in maize (*Zea mays* l.) by foliar spray of zinc oxide nanoparticles and biochar to contaminated soil. *Environ. pollut.* 248, 358–367. doi: 10.1016/j.envpol.2019.02.031

Rolland, F., Baena-Gonzalez, E., and Sheen, J. (2006). Sugar sensing and signaling in plants: conserved and novel mechanisms. *Annu. Rev. Plant Biol.* 57, 675–709. doi: 10.1146/annurev.arplant.57.032905.105441

Rossi, L., Fedenia, L., Sharifan, H., Ma, X., and Lombardini, L. (2018). Effects of foliar application of zinc sulfate and zinc nanoparticles in coffee (*Coffea arabica* l.) plants. *Plant Physiol. Biochem.* 135, 160-166. doi: 10.1016/j.plaphy.2018.12.005

Saeidnia, S., Gohari, A., and Hadjiakhoondi, A. (2007). Bioactive compounds of the volatile oil of *Dracocephalum kotschyi*. *Z. Naturforsch. C. J. Biosci.* 62, 793–796. doi: 10.1515/znc-2007-11-1203

Saeidnia, S., Gohari, A., Uchiyama, N., Ito, M., Honda, G., and Kiuchi, F. (2004). Two new monoterpene glycosides and trypanocidal terpenoids from *Dracocephalum kotschyi*. *Chem. Pharm. Bull.* 52, 1249–1250. doi: 10.1248/cpb.52.1249

Sandhya, V., Ali, S. Z., Grover, M., Reddy, G., and Venkateswarlu, B. (2010). Effect of plant growth promoting pseudomonas spp. on compatible solutes, antioxidant status and plant growth of maize under drought stress. *Plant Growth Regul.* 62, 21–30. doi: 10.1007/s10725-010-9479-4

Sattar, A., Wang, X., Ul-Allah, S., Sher, A., Ijaz, M., Irfan, M., et al. (2022). Foliar application of zinc improves morpho-physiological and antioxidant defense mechanisms, and agronomic grain biofortification of wheat (*Triticum aestivum* l.) under water stress. *Saudi Sci. J. Biol. Sci.* 29, 1699–1706. doi: 10.1016/j.sjbs.2021.10.061

Semida, W. M., Abdelkhalik, A., Mohamed, G., El-Mageed, A., Taia, A., El-Mageed, A., et al. (2021). Foliar application of zinc oxide nanoparticles promotes drought stress tolerance in eggplant (*Solanum melongena* l.). *Plants* 10, 421. doi: 10.3390/plants10020421

Sharafi, A., Sohi, H. H., Azadi, P., and Sharafi, A. A. (2014). Hairy root induction and plant regeneration of medicinal plant *Dracocephalum kotschyi*. *Physiol. Mol. Biol. Plants* 20, 257–262. doi: 10.1007/s12298-013-0217-z

Sharma, P., Jha, A., Dubey, R., and Pessarakli, M. (2012). Reactive oxygen species, oxidative damage, and antioxidative defense mechanism in plants under stressful conditions. *J. Bot.* 2012. doi: 10.1155/2012/217037

Sharma, V., Shukla, R. K., Saxena, N., Parmar, D., Das, M., and Dhawan, A. (2009). DNA Damaging potential of zinc oxide nanoparticles in human epidermal cells. *Toxicol. Lett.* 185, 211–218. doi: 10.1016/j.toxlet.2009.01.008

Silva, V., Singh, R. K., Gomes, N., Soares, B. G., Silva, A., Falco, V., et al. (2020). Comparative insight upon chitosan solution and chitosan nanoparticles application on the phenolic content, antioxidant and antimicrobial activities of individual grape components of sousão variety. *Antioxidants* 9, 178. doi: 10.3390/antiox9020178

Singh, A., Singh, N. B., Afzal, S., Singh, T., and Hussain, I. (2018). Zinc oxide nanoparticles: a review of their biological synthesis, antimicrobial activity, uptake, translocation and biotransformation in plants. *J. Mater. Sci.* 53, 185–201. doi: 10.1007/s10853-017-1544-1

Solanki, P., Bhargava, A., Chhipa, H., Jain, N., and Panwar, J. (2015). "Nano-fertilizers and their smart delivery system," in *Nanotechnologies in food and agriculture* (Springer Cham), 81–101. doi: 10.1007/978-3-319-14024-7_4

Subbaiah, L. V., Prasad, T. N., Krishna, T. G., et al. (2016). Novel effects of nanoparticulate delivery of zinc on growth, productivity, and zinc biofortification in maize (*Zea mays* l.). *J. Agric. Food. Chem.* 64 (19), 3778–3788. doi: 10.1021/acs.jafc.6b00838

Sun, L., Song, F., Zhu, X., Liu, S., Liu, F., Wang, Y., et al. (2021). Nano-ZnO alleviates drought stress via modulating the plant water use and carbohydrate metabolism in maize. *Arch. Agron. Soil Sci.* 67, 245–259. doi: 10.1080/03650340.2020.1723003

Taghizadeh, M., Nasibi, F., Kalantari, K. M., and Benakashani, F. (2020). Callogenesis optimization and cell suspension culture establishment of *Dracocephalum polychaetum* bornm. and *Dracocephalum kotschyi* boiss.: An *in vitro* approach for secondary metabolite production. *S Afr. J. Bot.* 132, 79–86. doi: 10.1016/j.sajb.2020.04.015

Taran, N., Storozhenko, V., Svietlova, N., Batsmanova, L., Shvartau, V., and Kovalenko, M. (2017). Effect of zinc and copper nanoparticles on drought resistance of wheat seedlings. *Nanoscale Res. Lett.* 12, 1–6. doi: 10.1186/s11671-017-1839-9

Tariverdizadeh, N., Mohebodini, M., Chamani, E., and Ebadi, A. (2021). Iron and zinc oxide nanoparticles: An efficient elicitor to enhance trigonelline alkaloid production in hairy roots of fenugreek. *Ind. Crops Prod.* 162, 113240. doi: 10.1016/j.indcrop.2021.113240

Tewari, R. K., Kumar, P., and Sharma, P. N. (2019). An effective antioxidant defense provides protection against zinc deficiency-induced oxidative stress in zn-efficient maize plants. *J. Plant Nutr. Soil Sci.* 182, 701–707. doi: 10.1002/jpln.201800622

Tripathi, D. K., Singh, S., Gaur, S., Singh, S., Yadav, V., Liu, S., et al. (2018). Acquisition and homeostasis of iron in higher plants and their probable role in abiotic stress tolerance. *Front. Environ. Sci.* 5. doi: 10.3389/fenvs.2017.00086

Upadhyaya, H., Roy, H., Shome, S., Tewari, S., Bhattacharya, M. K., and Panda, S. K. (2017). Physiological impact of zinc nanoparticle on germination of rice (*Oryza sativa* l) seed. *J. Plant Sci. Phytopathol.* 1, 062–070. doi: 10.29328/journal.jpsp.1001008

Van Nguyen, D., Nguyen, H. M., Le, N. T., Nguyen, K. H., Nguyen, H. T., Le, H. M., et al. (2022). Copper nanoparticle application enhances plant growth and grain yield in maize under drought stress conditions. *J. Plant Growth Regul.* 41, 364–375. doi: 10.1007/s00344-021-10301-w

Verma, K. K., Song, X. P., Zeng, Y., Li, D. M., Guo, D. J., Rajput, V. D., et al. (2020). Characteristics of leaf stomata and their relationship with photosynthesis in *Saccharum officinarum* under drought and silicon application. *ACS omega* 5, 24145–24153. doi: 10.1021/acsomega.0c03820

Waraich, E. A., Ahmad, R., and Ashraf, M. Y. (2011). Role of mineral nutrition in alleviation of drought stress in plants. *Aust. J. Crop Sci.* 5, 764–777.

Yang, F., and Miao, L. F. (2010). Adaptive responses to progressive drought stress in two poplar species originating from different altitudes. *Silva Fennica* 44, 23–37. doi: 10.14214/sf.160

Zengin, F. K. (2006). The effects of Co^{2+} and Zn^{2+} on the contents of protein, abscisic acid, proline and chlorophyll in bean (*Phaseolus vulgaris* cv. strike) seedlings. *J. Environ. Biol.* 27, 441–448.

Zhang, Z., Szota, C., Fletcher, T. D., Williams, N. S. G., Werdin, J., and Farrell, C. (2018). Influence of plant composition and water use strategies on green roof stormwater retention. *Sci. Total Environ.* 625, 775–781. doi: 10.1016/j.scitotenv.2017.12.231

Zheng, L., Huang, F., Narsai, R., Wu, J., Giraud, E., He, F., et al. (2009). Physiological and transcriptome analysis of iron and phosphorus interaction in rice seedlings. *Plant Physiol.* 151, 262–274. doi: 10.1104/pp.109.141051

frontiers | Frontiers in Plant Science

TYPE Original Research
PUBLISHED 19 April 2023
DOI 10.3389/fpls.2023.1116863

Check for updates

OPEN ACCESS

EDITED BY
Mahmoud Magdy,
Ain Shams University, Egypt

REVIEWED BY
Rafael A. Cañas,
University of Malaga, Spain
Yizeng Lu,
Shandong Provincial Center of Forest and Grass Germplasm Resources, China
Dongna Ma,
Jiangnan University, China

*CORRESPONDENCE
Irene Cobo-Simón
irenecob@ucm.es

SPECIALTY SECTION
This article was submitted to Plant Abiotic Stress, a section of the journal Frontiers in Plant Science

RECEIVED 05 December 2022
ACCEPTED 30 March 2023
PUBLISHED 19 April 2023

CITATION
Cobo-Simón I, Gómez-Garrido J, Esteve-Codina A, Dabad M, Alioto T, Maloof JN, Méndez-Cea B, Seco JI, Linares JC and Gallego FJ (2023) *De novo* transcriptome sequencing and gene co-expression reveal a genomic basis for drought sensitivity and evidence of a rapid local adaptation on Atlas cedar (*Cedrus atlantica*). *Front. Plant Sci.* 14:1116863. doi: 10.3389/fpls.2023.1116863

COPYRIGHT
© 2023 Cobo-Simón, Gómez-Garrido, Esteve-Codina, Dabad, Alioto, Maloof, Méndez-Cea, Seco, Linares and Gallego. This is an open-access article distributed under the terms of the Creative Commons Attribution License (CC BY). The use, distribution or reproduction in other forums is permitted, provided the original author(s) and the copyright owner(s) are credited and that the original publication in this journal is cited, in accordance with accepted academic practice. No use, distribution or reproduction is permitted which does not comply with these terms.

De novo transcriptome sequencing and gene co-expression reveal a genomic basis for drought sensitivity and evidence of a rapid local adaptation on Atlas cedar (*Cedrus atlantica*)

Irene Cobo-Simón[1,2]*, Jèssica Gómez-Garrido[3], Anna Esteve-Codina[3], Marc Dabad[3], Tyler Alioto[3], Julin N. Maloof[4], Belén Méndez-Cea[2], José Ignacio Seco[1], Juan Carlos Linares[1] and Francisco Javier Gallego[2]

[1]Department of Physical, Chemical and Natural Systems. University Pablo de Olavide, Seville, Spain, [2]Department of Genetics, Physiology and Microbiology, Genetics Unit. Faculty of Biological Sciences, Complutense University of Madrid, Madrid, Spain, [3]Nacional Center for Genomic Analysis-Center for Genomic Regulation (CNAG-CRG), Centre for Genomic Regulation, Barcelona Institute of Science and Technology, Barcelona, Spain, [4]Department of Plant Biology, University of California at Davis, Davis, CA, United States

Introduction: Understanding the adaptive capacity to current climate change of drought-sensitive tree species is mandatory, given their limited prospect of migration and adaptation as long-lived, sessile organisms. Knowledge about the molecular and eco-physiological mechanisms that control drought resilience is thus key, since water shortage appears as one of the main abiotic factors threatening forests ecosystems. However, our current background is scarce, especially in conifers, due to their huge and complex genomes.

Methods: Here we investigated the eco-physiological and transcriptomic basis of drought response of the climate change-threatened conifer *Cedrus atlantica*. We studied *C. atlantica* seedlings from two locations with contrasting drought conditions to investigate a local adaptation. Seedlings were subjected to experimental drought conditions, and were monitored at immediate (24 hours) and extended (20 days) times. In addition, post-drought recovery was investigated, depicting two contrasting responses in both locations (drought resilient and non-resilient). Single nucleotide polymorphisms (SNPs) were also studied to characterize the genomic basis of drought resilience and investigate a rapid local adaptation of *C. atlantica*.

Results: *De novo* transcriptome assembly was performed for the first time in this species, providing differences in gene expression between the immediate and extended treatments, as well as among the post-drought recovery phenotypes. Weighted gene co-expression network analysis showed a regulation of stomatal closing and photosynthetic activity during the immediate drought, consistent

with an isohydric dynamic. During the extended drought, growth and flavonoid biosynthesis inhibition mechanisms prevailed, probably to increase root-to-shoot ratio and to limit the energy-intensive biosynthesis of secondary metabolites. Drought sensitive individuals failed in metabolism and photosynthesis regulation under drought stress, and in limiting secondary metabolite production. Moreover, genomic differences (SNPs) were found between drought resilient and sensitive seedlings, and between the two studied locations, which were mostly related to transposable elements.

Discussion: This work provides novel insights into the transcriptomic basis of drought response of *C. atlantica*, a set of candidate genes mechanistically involved in its drought sensitivity and evidence of a rapid local adaptation. Our results may help guide conservation programs for this threatened conifer, contribute to advance drought-resilience research and shed light on trees' adaptive potential to current climate change.

KEYWORDS

RNA-Seq, Atlas cedar, drought sensitiveness, eco-physiology, adaptive capacity, conifers, climate change, phenotypic diversity

1 Introduction

Forest ecosystems are key sources of important ecological, economic and social functions. However, the long-lived character and limited dispersal ability of trees make these complex ecosystems particularly concerning in facing major evolutionary challenges such as the current climate change (Jump and Peñuelas, 2005). Thus, knowledge of the molecular and functional mechanisms that control adaptation and resilience (Lloret et al., 2011) of trees to drought is key in the current context of a changing climate, since recurrent drought is one of the main climatic factors threatening forests, especially in the Mediterranean region (Alberto et al., 2013; Mencuccini et al., 2015). In fact, increasing severity, duration, and higher frequency of drought events as a consequence of climate change are increasing tree mortality and forest dieback worldwide (Schueler et al., 2021). Notwithstanding, this knowledge is scarce, especially in conifers, due to their huge and complex genomes (Klupczyńska and Ratajczak, 2021).

In particular, to predict future tree mortality and the carbon balance of forest ecosystems as well as to develop management strategies to help forests cope with this increasing drought occurrence, a better understanding is needed (i) of the physiological limits and traits connected to drought tolerance of individual trees (Sohn et al., 2013; Bennett et al., 2015; Trujillo-Moya et al., 2018), (ii) of the genetic diversity of traits related to drought resistance and avoidance (iii) of local adaptations and the adaptive capacity of single species (Schueler et al., 2021), for example, relicts (Hampe and Jump, 2011).

Relict species are populations left behind during climate-driven range shifts which persist in areas with benign but sub-optimal environmental conditions surrounded by an unfavorable regional climate (Hampe and Jump, 2011). Some adaptations to these sub-optimal habitats might be key to cope with the current changing climate (e.g. Kawecki, 2008; Sexton et al., 2009). Relicts usually have small population sizes, isolation and limited possibilities for migration, leading to reduced gene flow and genetic diversity, which make them unique experimental models to test the adaptive potential of trees to a changing environment (Hampe and Petit, 2005; e.g. Cobo-Simón et al., 2020; Cobo-Simón et al., 2021; Cobo-Simón et al., 2022). Despite this, some studies have found no evidence of decreasing population sizes or fitness (Hampe and Jump, 2011). Therefore, it has been hypothesized that they might retain genetic variants for some ecologically relevant traits (Kawecki, 2008).

Here we focus on *Cedrus atlantica*, a relict conifer endemic from North Africa (Algeria and Morocco), distributed in mountain ranges through altitudinal ecotones (Abel-Schaad et al., 2018). Despite its relatively wide tolerance to climate and soil type (Abel-Schaad et al., 2018), it is threatened by climate change, particularly by the projected temperature increase. Furthermore, its distribution range has undergone a dramatic reduction over the last decades due to the increasing aridity and human activities (Abel-Schaad et al., 2018). Its presence in Spain is product of a reforestation project carried out in southern Iberian Peninsula during the last century from natural stands of northern Morocco. This reforestation project further highlights *C. atlantica* wide tolerance to varied environmental conditions, since populations located at different regions, with remarkable differences in humidity and precipitation, do not show apparent differences in fitness. Hence, this reforestation project offers a natural experiment to investigate the molecular and functional mechanisms of adaptation to drought in conifers. To the best of our knowledge, it has never been performed in conifers.

The objective of this work is to investigate a possible rapid local adaptation to drought of *C. atlantica* populations at Southern Spain.

Moreover, we aim to investigate the molecular and functional basis of drought resilience in this climate change-threatened conifer. To this end, we study the mechanistic connection between gene expression/eco-physiology and drought resilience in two *C. atlantica* populations located in areas with contrasting differences in precipitation: Fiñana (Almería), characterized by strong droughts during the summer, and Dornajo (Granada), with higher precipitation rate. First, *C. atlantica* seedlings from both locations were subjected to controlled drought conditions, based on our field data (Linares et al., 2012; Sanchez-Salguero et al., 2015). Then, we investigated the differences in gene expression through the immediate (24 hours) and extended (20 days) drought responses and between two contrasting post-drought recovery phenotypes (resilient and sensitive) *via* RNA-seq within and between both studied populations. Single nucleotide polymorphisms (SNPs) between these contrasting phenotypes and the two locations were also analyzed to characterize their genomic basis and to investigate a rapid local adaptation. During the drought treatments and the post-drought recovery, two eco-physiological variables related to drought response were tracked (net photosynthesis and stomatal conductance) to investigate differences in the eco-physiological response to drought and post-drought recovery between locations.

We hypothesize a rapid local adaptation of the studied *C. atlantica* populations to the contrasting precipitation rates of both locations, supported by physiological, gene expression and genomic differences (SNPs). Furthermore, we hypothesize that contrasting gene expression is related to carbon and water balance variability in response to drought stress and causes the two contrasting post-drought recovery phenotypes in both locations. Given that resilient and sensitive individuals from both locations were subjected to the same drought treatment (extended), we expect SNPs as polymorphisms associated to their differentially expressed genes, and thus, related to their drought resilience. Although other molecular mechanisms might be acting (e.g. epigenetic regulation), their characterization is beyond the scope of this study.

2 Materials and methods

2.1 Plant material, growth conditions and drought stress experiment

A drought stress experiment was carried out using Atlas cedar seedlings germinated from seeds sampled in two afforested populations of southern Spain (Fiñana, F and Dornajo, D, respectively; Figures 1A, C). The reforestation project was performed with *C. atlantica* individuals from natural stands of northern Morocco during the last century. The study sites show contrasting climate conditions due to a longitudinal gradient, where aridity increases eastward, and due to elevation, where aridity increases downward. F site (Almería), is characterized by higher mean temperature and lower total precipitation, which determined increased summer drought, compared to D site (Figures 1B, D). During the period 2011-2015, air temperature (T) was registered hourly in both locations using a Hobo H8 data logger. Data loggers were placed inside open-bottom PVC cylinders situated at 1.5m from the ground and covered by sealing foam to prevent direct heating from the sun. Further, to obtain long-term climate data, monthly total precipitation (P) and T were downloaded from the EOBS database v23.1e for the period 1971–2021 (Haylock et al., 2008) using the Climate Explorer webpage (https://climexp.knmi.nl/). Local data of monthly total precipitation were also used to account for elevation gradients.

Seeds were obtained in the field from mature cones (Figure 1E) and germinated (Figure 1F) in the common garden of the University Pablo de Olavide (Seville, Spain). Both populations showed similar germination percentage (80.1% and 82.1%, for F and D, respectively), while seed dry weight was significantly higher in D site (Figure 1G). Seedlings grown in 0.77-liter pots with 38.5 cm^2 of surface exposed to evaporation, filled with sterile sand and perlite substrate in 3:1 ratio for about one year in the common garden. Environmental conditions in the common garden (temperature, relative humidity and PAR) were monitored using Onset Computing HOBO Pro v2 data loggers (HOBO U23-series). Mean annual air temperature was 17.9°C, 27.4°C in the hottest month (August), and 10.3°C in the coldest month, (January). Mean annual relative humidity was 68.3%, 55.9% in the drier month (July), and 81.2% in the wettest month (November). Mean PAR was 445.8 lux. Irrigation was provided to saturation. The seedlings were fertilized in pots with solid NPK synthetic fertilizer, containing 12.0% of total Nitrogen (N), of which 6.5% was nitric Nitrogen (N-NO_3), and 5.5% was ammoniacal Nitrogen (N-NH_4); Phosphorus pentoxide (P_2O_5) soluble in neutral ammonium citrate and water 12.0%, of which 6.0% was Phosphorus pentoxide (P_2O_5) water soluble; Sulfur trioxide (SO_3) total 15.0%, of which 12.0% was Sulfur trioxide (SO_3) water soluble; Magnesium Oxide (MgO) Total 2.0%, of which 1.5% was Magnesium oxide (MgO) water soluble; Potassium oxide (K_2O) water soluble 17.0%, Boron (B) total 0.02%, and Zinc (Zn) total 0.01%. Then, a subset of seedlings were randomly selected and introduced in controlled growth chambers (CGC) under constant conditions of humidity (70% relative humidity RH) and temperature (27°C). CGC air vapour pressure deficit (VPD, kPa) was calculated using temperature and relative humidity in the following equations (Sanchez-Salguero et al., 2015):

Saturated vapour pressure (svp) was calculated as: $svp = 0.66 \star e^{(0.06 \star T)}$

Then, VPD was obtained as: $VPD = (\frac{(100-RH)}{100}) \star svp$ where RH is the CGC air relative moisture (%), and T is the CGC air temperature (°C).

Independent of the following drought stress treatment, all seedlings stayed 15 days in CGC for acclimation, until the variables used to monitor control seedlings hydric status (net photosynthesis and stomatal conductance) showed high and stable values. Seedlings (both controls and those subjected to drought treatments) were monitored weekly by means of a gas exchange system provided with an infrared gas analyzer (IRGA) (LI-COR, LI-6400XT, EEUU). During this acclimation period, watering was carried out by adding 10 mL of water per day. After the acclimation, the variables used to monitor control seedlings (A and Gs) were relatively steady and averaged (± standard error) (A = 6.5 ± 0.5 µmol CO2·m^{-2}·s^{-1}, Gs = 110 ± 13 mmol H_2O cm^{-2} s^{-1}). Photoperiod was stablished between 7:00 AM and 19:00 PM

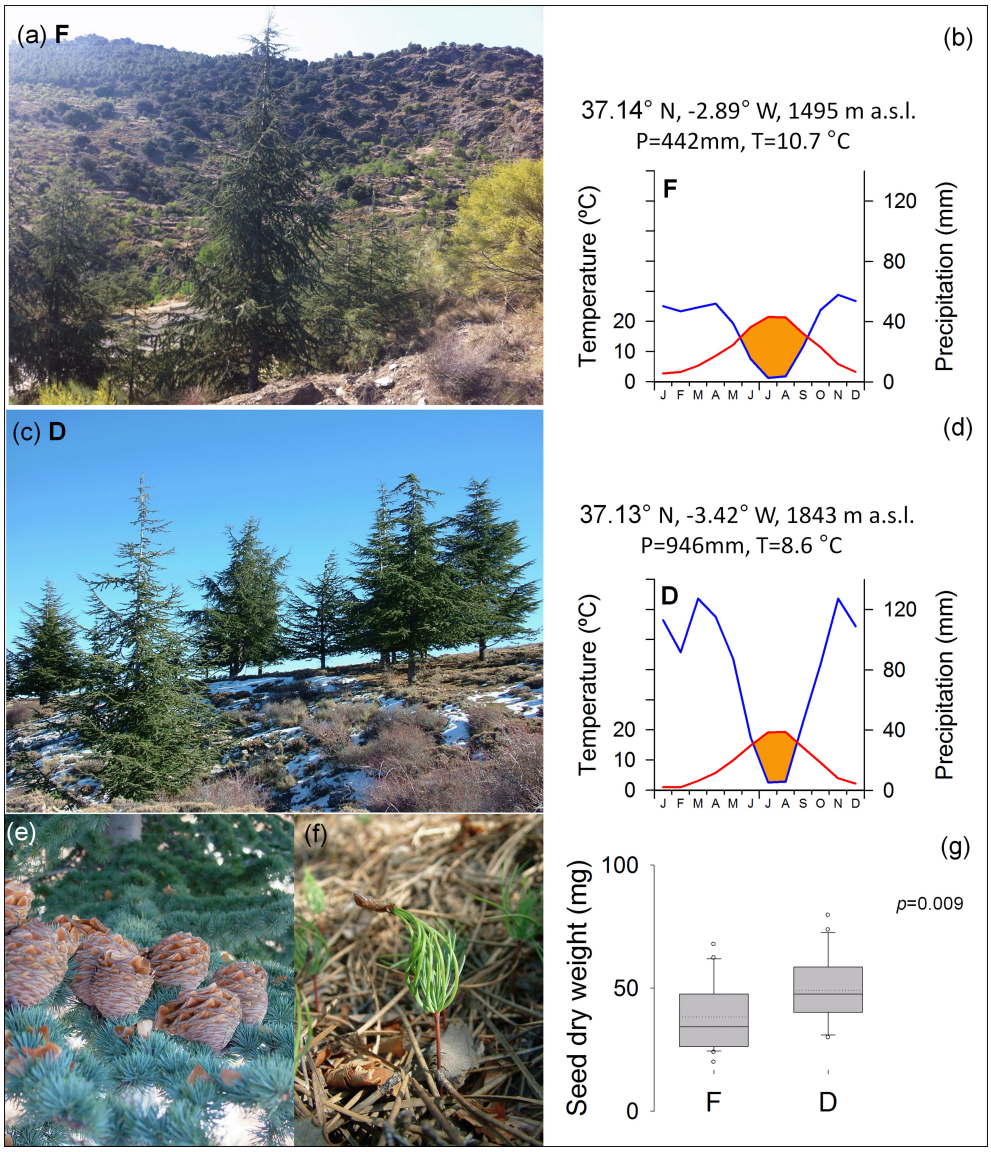

FIGURE 1
Atlas cedar (*Cedrus atlantica*) trees at Fiñana, F **(A)** and Dornajo, D **(C)** sites (Sierra Nevada range, south Spain). Sampling location (latitude N, longitude W, and elevation m a.s.l.) and mean climate for the period 1971-2021 are indicated for F **(B)** and D **(D)** sites, respectively. The blue lines indicate the monthly total precipitation, the red lines indicate the monthly mean temperature, the shaded orange area indicates the water deficit period; total annual precipitation (P, mm) and mean annual temperature (T, °C) are also noted. Mature cones with spreading seeds **(E)** and germinating seedlings **(F)** were highly viable in both sites. Mean seed dry weight **(G)**; the inset indicates the p value for ANOVA.

(12 hours light/12 hours darkness, light at 600 lux), while physiological measurements and further sampling for RNA extraction were performed between 10:00 AM and 1:00 PM, again, for both controls and seedlings subjected to the drought treatments.

Drought treatment (Figure 2) was applied to 38 seedlings by reducing the RH of the CGC up to 30%, which is equivalent to a VPD of 2.3 kPa, whereas 22 remained as control (RH=70%), which is equivalent to a VPD of 1.0 kPa. Both CGC maintained 27 °C of temperature and 10 mL per day of watering. Immediate drought response, extended drought response and drought resilience were assessed using gas exchange monitoring and gene expression by RNA extraction (Figure 2). This experimental design allows a quantification of drought effects at a molecular resolution for seedling subjected to experimental drought. Drought resilience was defined here as the capacity of a seedling to reach gas exchange rates (A and Gs) similar to those prior to drought treatment. Defined this way, drought resilience encompasses the capacity to cope with drought, that is, resistance, and the ability to return to prior gas exchange levels after drought, that is recovery (Lloret et al., 2011). We defined three sample types within the experiment (Figure 2): (i) Controls (C, n=11 from Dornajo and n=11 from Fiñana), seedlings were raised in CGC at 70% RH; (ii) immediate drought response treatment (I, n=8 from Dornajo and n=13 from Fiñana), seedlings were raised in CGC at 30% RH and needles for RNA extraction were collected 24 hours after; and (iii) extended drought response treatment (E, n=9 from Dornajo and

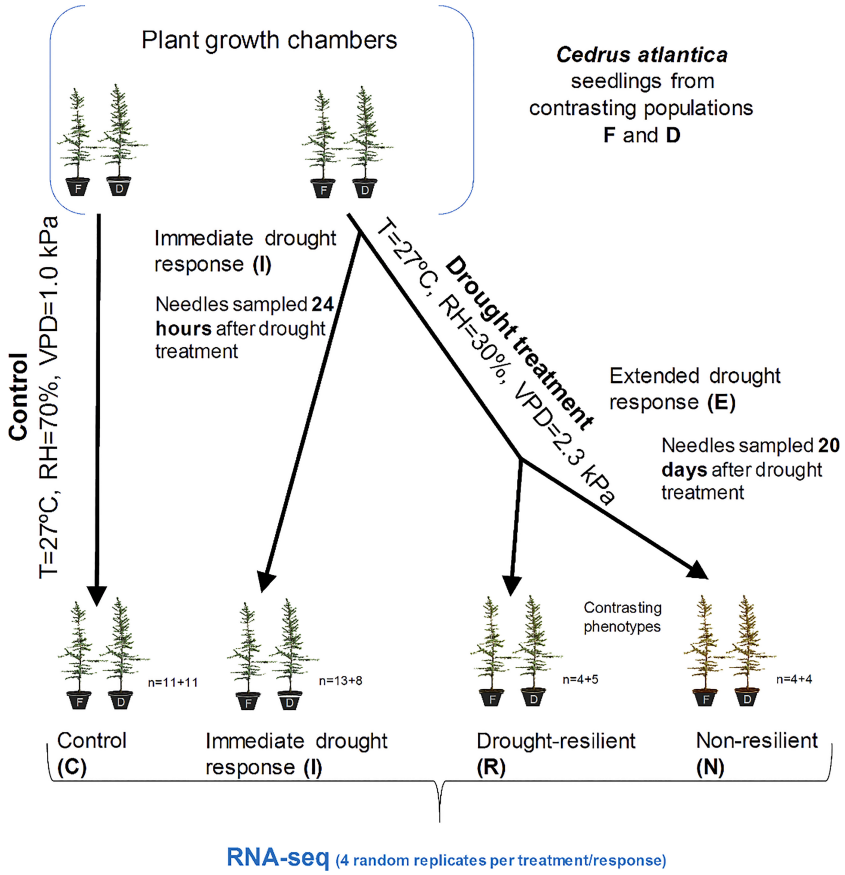

FIGURE 2
Drought treatment experimental design and sampling procedure. Net photosynthesis (A) and stomatal conductance (Gs) were monitored in controls (C), immediate drought (I, after 24 hours of drought treatment), and extended drought (E, after 20 days of drought treatment).The E group was divided into drought resilient seedlings (R) and non-resilient seedlings (N), based on recovery capacity after the extended drought. T, temperature; RH, relative humidity; VPD, vapor-pressure deficit; n indicates the number of individuals from Fiñana (F) and Dornajo (D), respectively (n=F+D).

n=8 from Fiñana), seedlings were raised in CGC at 30% RH and needles were collected for RNA extraction 20 days after the drought treatment started (Figure 2).

The recovering drought response treatment introduces the concept of drought resilience (Lloret et al., 2011). E treatment seedlings were returned to control conditions after 20 days of drought treatment (Figure 2). Then, recovery (regarding A and Gs values observed after drought) was monitored to quantify drought resilience (*sensu* Lloret et al., 2011). According to that, we defined two groups: drought resilient seedlings (R, n=4 from Fiñana; n=5 from Dornajo), defined as those E seedlings that reached, at least, the 30% of their A and Gs values in control conditions in less than 3 days; and non-resilient seedlings (N, n=4 from Fiñana, n=5 from Dornajo), defined as those E seedlings that died or did not manage to reach, at least, the 30% of their A and Gs values in control conditions in less than 3 days (Figure 2). We set this threshold (30%) based on our own experience on previous essays, where we determined that, overall, seedlings that are able to recover about 1/3 of their initial rates are thereafter able to survive after the drought conditions end. All collected needles were stored in a freezer at -80°C until RNA extraction was performed.

2.2 RNA extraction, cDNA library preparation and RNA-sequencing for transcriptome analysis

Four individuals belonging to each treatment/response (C, I, R, N) from each location (Fiñana and Dornajo) were selected for the RNA extraction to analyze the same quantity of biological replicates. Spectrum Plant Total RNA Kit (Sigma-Aldrich, Saint Louis, MO, USA) was used to carry out a total RNA extraction from the collected needles. The manufacturer's protocol was followed with one modification. 2% polyvinylpyrrolidone (PVP) K30 (Sigma-Aldrich) was added to the lysis buffer to enhance the extraction efficiency. Bioanalyzer 2100 (Agilent Technologies, Inc, Santa Clara, CA, USA) was used to test the quality of the extracted RNA. A ND-1000 Spectrophotometer (NanoDrop™, Thermo Fisher Scientific, Waltham, MA, USA) was used to measure its concentration. $1.8 \leq OD260/280 \leq 2.2$, $OD260/230 \geq 1.8$ and RNA Integrity Number (RIN) ≥ 7 were applied as quality standards. Then, all samples were sent to the National Center for Genomic Regulation (CNAG-CRG, Barcelona, Spain) for sequencing. There, quality control (QC) was performed by fluorescent-based

quantification (RiboGreen, Invitrogen™, Thermo Fisher Scientific) and integrity evaluation (2100 Bioanalyzer, Agilent Technologies, Santa Clara, CA, USA), followed by a cDNA library preparation (Illumina Stranded mRNA Prep) and RNA-sequencing by Illumina HiSeq2500 (Illumina, Inc, San Diego, CA, USA).

2.3 Bioinformatic analysis

2.3.1 *De novo* transcriptome sequencing and functional annotation

De novo transcriptome assemblies were performed for each treatment/response (C, I, R, N) in both studied populations (Fiñana and Dornajo) using Trinity (Grabherr et al., 2011) v2.8.4 and Bridger (Chang et al., 2015) version r2014-12-01, after performing read trimming and normalization using Trimmomatic (version 0.36, Bolger et al., 2014) and Trinity, respectively. Assembly quality for the obtained transcriptomes was compared in terms of contiguity (N50) and completeness with BUSCO (Simão et al., 2015) v3.0.2 using a plant specific dataset made of 956 genes. Finally, the Bridger approach was selected as the best one and RapClust (Trapnell et al., 2013) v0.1 was run on each of the Bridger assemblies in order to reduce redundancy before merging the four resulting transcriptomes together again with RapClust. In this process, a pseudoalignment is first performed with Sailfish (Li et al., 2010) v0.10.0 and then RapClust is used to cluster the assembled sequences into contained isoforms, in order to reduce redundancy and to cluster together all the isoforms that are likely to belong to the same gene. After obtaining the reference transcriptome, Open Reading Frames were annotated in the assembled transcripts with TransDecoder (Haas et al., 2013) v5.5.0 and functional annotation was performed on the annotated proteins with Blast2GO (Conesa et al., 2005) v 3.2. First, a BlastP (Altschul et al., 1990) search was made against the nr database from NCBI (last accessed January 2019) and InterProScan (Jones et al., 2014) 5.32-71.0 was run to detect protein domains on the annotated sequences. All these data were combined by Blast2GO which produced the final functional annotation results.

2.3.2 Atlas cedar RNA-seq data sets

Raw reads for each individual were trimmed in order to remove low quality reads (mean quality score<15; reads length<36) using Trimmomatic (version 0.36, Bolger et al., 2014). Then, FastQC (version 0.11.7, Andrews, 2014) was used to test read quality. Overrepresented sequences (adapters) were removed from all samples with Trimmomatic since they were abundant in all FastQC reports. The filtered reads quality was again tested using FastQC. The read from each pair-end showing the highest quality was selected to develop the following differential expression (DE) analysis based on single-end reads. Kallisto (version 0.44.0, Bray et al., 2016) was used to align the selected reads against the *de novo* sequenced reference transcriptome for *C. atlantica*. Genes in the reference with more than 10 reads in 3 or more samples were retained for subsequent analysis.

2.3.3 Differential expression analysis

The edgeR R package (Robinson et al., 2010; McCarthy et al., 2012) was used to perform a pairwise DE analysis at the gene level according to previously published protocols (Anders et al., 2013). TMM (Trimmed Mean of M Values) (Robinson and Oshlack, 2010) was applied as normalization method. Principal Component Analysis (PCA) between samples was performed to explore the data structure. DE analysis was conducted as follows: I versus C, using C as baseline, to find genes implied in the immediate drought response; E versus I, using I as baseline to obtain genes implied in the extended drought response; and R vs N, using N as baseline, to obtain potential candidate genes of drought resilience. The cut-off criteria of a false discovery rate (FDR)-adjusted P-value ≤ 0.05 was used to consider differentially expressed genes (DEG). Log fold change threshold = 0 was used to calculate up and down-regulated genes.

2.3.4 Gene co-expression network analysis

Gene co-expression network analysis was performed to cluster the reads into modules of highly co-expressed genes based on their expression similarity using the R package WGCNA (Langfelder and Horvath, 2008; Langfelder and Horvath, 2012). First, read alignments were normalized using "voom" fuction in limma R package (Bioconductor release 3.4, Law et al., 2014). Sample clustering was carried out to identify possible outliers. Genes were represented by nodes in the gene co-expression network. The similarity between expression profiles of paired genes was obtained by a Pearson correlation. To construct an adjacency matrix, a power function (β) was applied on the Pearson correlation matrix. To balance the scale-free property of the co-expression network and the sparsity of connections between genes, a value of 14 was given to the β. A signed co-expression network was constructed, in which modules correspond to positively correlated genes, since it is more accurate for this work. The obtained adjacency matrix was used to build a topographical overlap matrix (TOM). A hierarchical clustering was developed in order to group the genes based on dissimilarity of gene connectivity, defined as 1–TOM. Co-expression clusters were calculated by implementing the cutreeDynamic function with the following parameters: deepSplit = 2, pamRespectDendro = F, minClusterSize = 30. Finally, highly correlated clusters were merged to obtain modules in the network using mergeCloseModules function with a cutHeight set to 0.25 (see WGCNA code at Appendix 2).

An overlapping analysis between the genes belonging to the obtained modules and the DEGs was performed to select the most meaningful modules for our study. The DEGs were separated into up and down-regulated beforehand. The statistical significance of the overlap was calculated by Fisher's exact test. Modules with a statistically significant p-value (P<0.05) were selected for further analysis.

An expression-value heatmap was developed to cluster and visualize the log2 fold-change for gene expression of each selected module using the R package *pheatmap* (version 1, Kolde, 2012). Modules with the expected expression pattern, considering our experiment, were selected. We focused on highly connected genes

or hub genes per module because they are probably crucial components of the network, given their central location (Miao et al., 2017). Hub genes were identified by visualizing the modules and selecting the most interconnected genes in each module using Cytoscape version 3.9.1 (Shannon et al., 2003). The GO-seq package (Young et al., 2010) in R was used to perform GO term enrichment analysis to functionally annotate the hub genes and the selected modules for testing whether their functions were biologically meaningful. Only those GO terms with FDR-adjusted P-value< 0.05 were considered statistically significant. The GO term enrichment results were visualized using REVIGO (Supek et al., 2011).

2.3.5 Single nucleotide polymorphisms (SNP) calling

To investigate the existence of genetic variations (SNPs) associated with the differences in gene expression between the two post-drought phenotypes (R and N) and locations (Fiñana and Dornajo), variant detection was performed. This analysis was conducted to support the DE analysis and WGCNA results, since the low number of biological replicates was not enough to draw statistically robust conclusions. Paired-end reads were aligned with BWA program (version 0.7.17, Li and Durbin, 2009). Picard (version 2.9.2) was used to sort the alignments in genome order and to mark the pseudo-duplicates of DNA fragments which can occur during library preparation. Finally, Freebayes (version 1.3.4, Garrison and Marth, 2012) was used to call SNPs against the reference transcriptome. The resulting SNPs were plotted in a Principal Components Analysis (PCA). We filtered the SNP list to keep only those SNPs with fixed differences between all R and N samples, that is, those which are homozygous for one allele in all R samples and homozygous for a different allele in all N samples. To this end, we used BCFTOOLS (version 1.16, Li, 2011). We also filtered the SNP list to keep fixed SNPs between all Fiñana and Dornajo samples. Then, the GO-seq package (Young et al., 2010) in R was used to perform GO term enrichment analysis to functionally annotate the fixed SNPs between locations and responses to test whether their functions were biologically meaningful. Only those GO terms with FDR-adjusted P-value< 0.05 were considered statistically significant. The GO term enrichment results were visualized using REVIGO (Supek et al., 2011).

2.4 RNA validation with real-time quantitative pcr (qRT-PCR) of RNA-seq results

To confirm the results from the RNA-seq analysis, some DEGs were selected, and their expression levels were confirmed by qRT-PCR analysis. For the quantitative real-time PCR (qRT-PCR), a TB Green Advantage qPCR Premix (Takara, Japan) was used and run on a QuantStudio 7 Flex Real-Time PCR System (Thermofisher, USA). For each gene, the measurements were performed in four replicates, and the average cycle thresholds (Ct) were used to determine the fold-change. The expression ratio (Log2FC) change was calculated by the 2-ΔΔCT method. 18S rRNA gene was used as a reference gene to normalize the qRT-PCR data. All of the primers used for the qRT-PCR are listed in Table S1.

3 Results

3.1 Drought stress experiment

Net photosynthesis (A) and stomatal conductance (Gs) showed non-significant differences between populations, while drought treatment yielded a significant gas exchange decline (Figure 3; Supplementary Material, Table S2). During the post-drought recovery, R individuals showed significantly higher values of A and Gs, compared to N individuals, in both populations (Figure 3, Table S2; see ANOVA results at Appendix 1).

3.2 Bioinformatic analysis

3.2.1 *De novo* transcriptome sequencing

The final assembly was made of 452,220 assembled contigs with a contig N50 of 1835bp. The transcripts were clustered in a total of 115,334 genes, 89,137 of which were protein-coding. According to BUSCO, our reference transcriptome had 94.3% of complete genes, 1.2% fragmented genes and only a 4.5% of missing genes out of the 452,220 assembled contigs. Taking into account that not all the genes would be present in our samples, due to lack of expression (~80% of the genes of an organism are expected to be expressed), we can conclude that we obtained the complete transcriptome for our cases. 200,028 out of the 452,220 transcripts were annotated as protein coding, of which 196,133 (98%) were functionally annotated with protein descriptions and 172,977 (86%) with GO terms.

3.2.2 Atlas cedar RNA-seq data sets

Four biological replicates from each of the four treatments/responses (C, I, R and N) and from the two analyzed populations Dornajo (Granada) and Fiñana (Almería) were selected for RNA extraction (32 samples). However, a total of 17 RNA-seq libraries were successfully sequenced, 12 belonging to Fiñana and five belonging to Dornajo, since the RNA extraction was not successful in 11 individuals from Dornajo and four individuals from Fiñana. Thus, four RNA-seq libraries from C and I treatments, and two from R and N responses (each) were successfully sequenced for Fiñana samples. Two RNA-seq libraries from C, and one RNA-seq library from I, R and N treatments/responses (each) were successfully sequenced for Dornajo (Table 1).

17 cDNA libraries yielded approximately 528.94 million 76-bp single-end reads (Table S3). Quality trimming and filtration yielded 429.6 million cleaned reads that were mapped to the reference *C. atlantica de novo* transcriptome. A total of 452,220 counts were obtained after mapping reads against the reference transcriptome. After applying TMM normalization and the filtering criteria for defining an "expressed" gene (more than 10 reads in 3 or more samples) a total of 90,203 transcripts were obtained for all 17 samples.

10.3389/fpls.2023.1116863

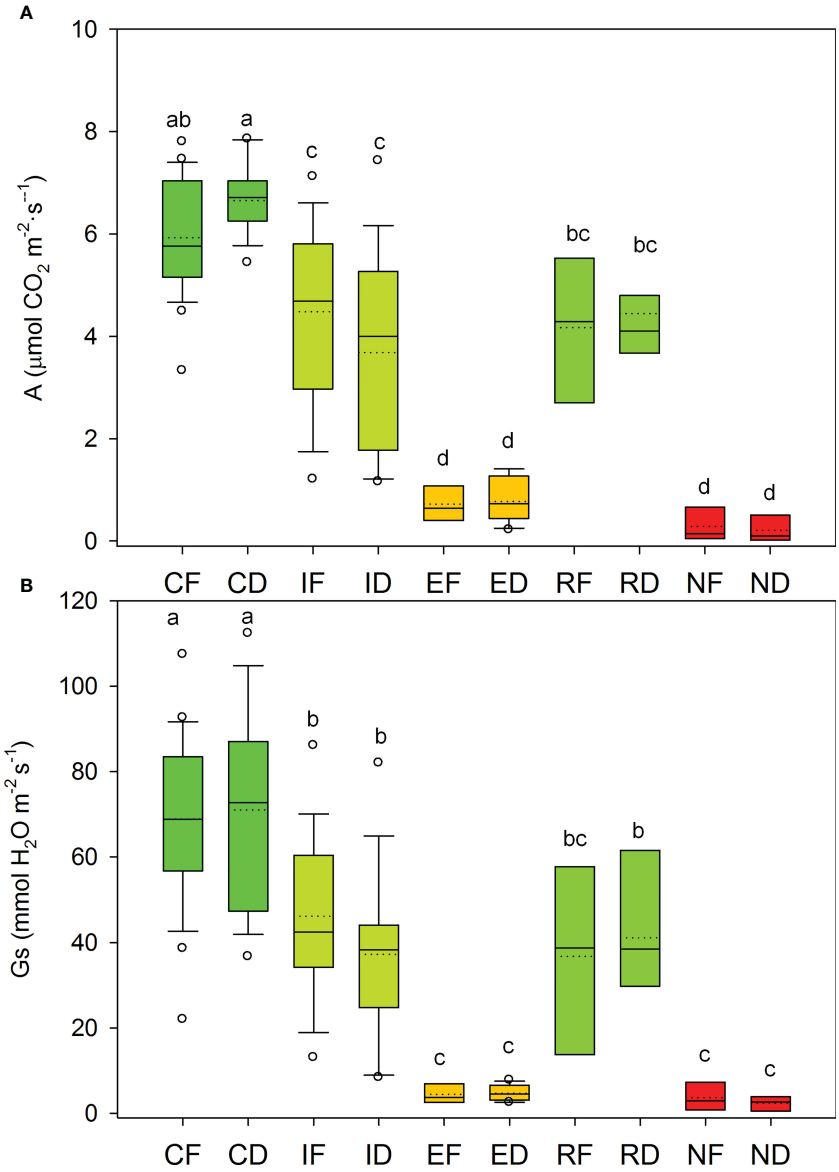

FIGURE 3
Net photosynthesis, A **(A)** and stomatal conductance, Gs **(B)** measured in seedlings from Fiñana (F) and Dornajo (D) subjected to treatments: control (C), immediate drought (I, after 24 hours of drought treatment), and extended drought (E, after 20 days of drought treatment).The E group was divided into drought resilient seedlings (R) and non-resilient seedlings (N), based on recovery capacity after the extended drought. Groups are noted by the treatment/response (C, I, E; R, N) and population codes (F, D). Different letters indicate significant diferenteces ($p<0.05$) by ANOVA.

TABLE 1 Differentially expressed genes between treatments/responses (FDR<0.05).

	I vs C	E vs I	R vs N
Fiñana (12 samples)			
Up-regulated	78 (0.093%)	3073 (3.6%)	3037 (3.6%)
Not significant	84,053	79,660	75,197
Down-regulated	181 (0.21%)	1579 (1.9%)	6078 (7.2%)
Fiñana + Dornajo (17 samples)			
Up-regulated	144 (0.16%)	5807 (6.4%)	6825 (7.6%)
Not significant	89,805	82,778	72,616
Down-regulated	254 (0.28%)	1618 (1.8%)	10762 (12%)

Log fold change threshold = 0 was used to calculate up and down-regulated genes. Fiñana: C = 4 samples, I=4 samples, R=2 samples, N=2 samples; Dornajo: C=2 samples, I= 1 sample, R=1 sample, N=1 sample.

3.2.3 Differential expression analysis

The Principal Component Analysis (PCA) between samples was plotted using a multi-dimensional scaling (Figure 4). The two studied locations (Fiñana and Dornajo) were clearly separated. Samples were not clustered by drought treatment (C, I, E) at any of the two locations; however, N response was clearly separated from the rest of samples in both locations. Furthermore, N individuals clustered between locations. Given the insufficient number of biological replicates per treatment/response, it was not possible to perform the DE analysis in Dornajo. Nevertheless, considering the clear separation between locations in the PCA, we decided to perform the DE analysis only in Fiñana population on the one hand, and combining both Fiñana and Dornajo populations on the other hand, in order to investigate the DEGs regardless the location. This Fiñana + Dornajo analysis is biologically meaningful since both locations were afforested with *C. atlantica* individuals from natural stands of northern Morocco. The results of both DE analyses (Fiñana and Fiñana + Dornajo) were consistent, showing the lowest number of DEGs during the I treatment, followed by E treatment, and finally, the highest number of DEGs were found between R and N responses (Table 1). Therefore, they showed a greater effect of the response compared to the drought treatment in the gene expression of *C. atlantica*. Nevertheless, it was remarkable that the percentage of DEGs in all three pairwise comparisons was higher when analyzing both populations together (Fiñana +Dornajo), compared to Fiñana samples (Table 1). To confirm the results from the RNA-seq analysis, some DEGs were selected, and their expression levels were confirmed by qRT-PCR analysis. The qRT-PCR results showed that the transcription levels of these genes were consistent with the previous RNA-seq analysis (Figure S1).

3.2.4 Drought stress-related gene modules

The clustering analysis did not show any outliers (Figure 5). Consistently with the PCA results, individuals from Fiñana and Dornajo populations were clearly separated with the exception of N individuals from both populations that clustered together. In addition, there was not clear separation among treatments/responses with the exception of N individuals from both populations. Given the high number of transcripts, genes were subset to retain the 36,359 ones with the highest variance across 12 Fiñana samples and the 12,060 ones across Fiñana + Dornajo samples (third quartile). WGCNA for Fiñana samples showed 466 modules, 194 after merging highly correlated ones (Figure 6A). WGCNA for Fiñana and Dornajo samples showed 64 modules, 15 after merging highly correlated ones (Figure 6B). To determine which modules were enriched in DEG, an overlapping table was constructed using the modules and the pairwise DEG, separately for up and down-regulated genes. 20 modules were significantly enriched in Fiñana (Figure 7A, Table 2) and 8 modules in Fiñana + Dornajo populations (Figure 7B, Table 2). Then, a heatmap was built for each significant module to select the most meaningful modules regarding their drought response pattern. Six significantly enriched modules showed an expression pattern of interest for Fiñana, related to the studied drought treatments and responses (Figure 8A). For Fiñana+Dornajo, two modules showed an expression pattern of interest, both related to the post-drought recovery response (Figure 8B). Consistently with Fiñana samples, uniquely expressed genes were found in N individuals, but not in R individuals. No modules showing an expression pattern related to the drought treatment (I or E) were found in Fiñana +Dornajo samples.

3.2.5 Selection of hub genes and functional annotation of hub genes and modules

Tables S4-S11 show the top most interconnected genes obtained using Cytoscape program (Shannon et al., 2003) for each of the six significantly enriched modules from Fiñana population (Tables S4-

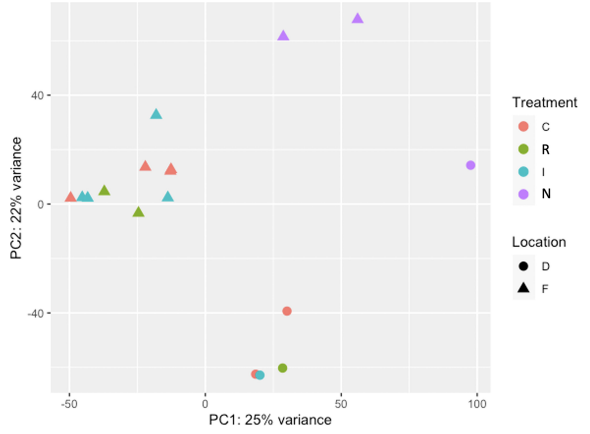

FIGURE 4
Principal Component Analysis (PCA) among the 17 normalized samples belonging to the four drought treatments/responses (Control C, immediate I, drought resilient R and non-resilient N) from Fiñana (F) and Dornajo (D) locations.

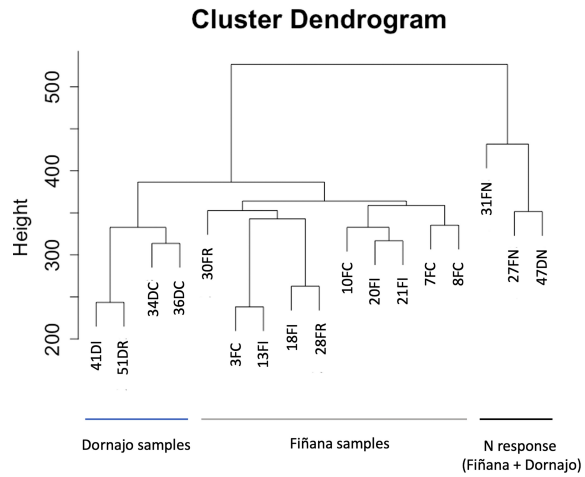

FIGURE 5
Dendrogram representing the clustering analysis of normalized samples (voom) subset for high variance with the objective of detecting outliers. Samples with a "D" after the number belong to Dornajo and with a F, to Fiñana. The last letters represent the treatment/response (C control, I immediate, R drought resilient, N non-resilient).

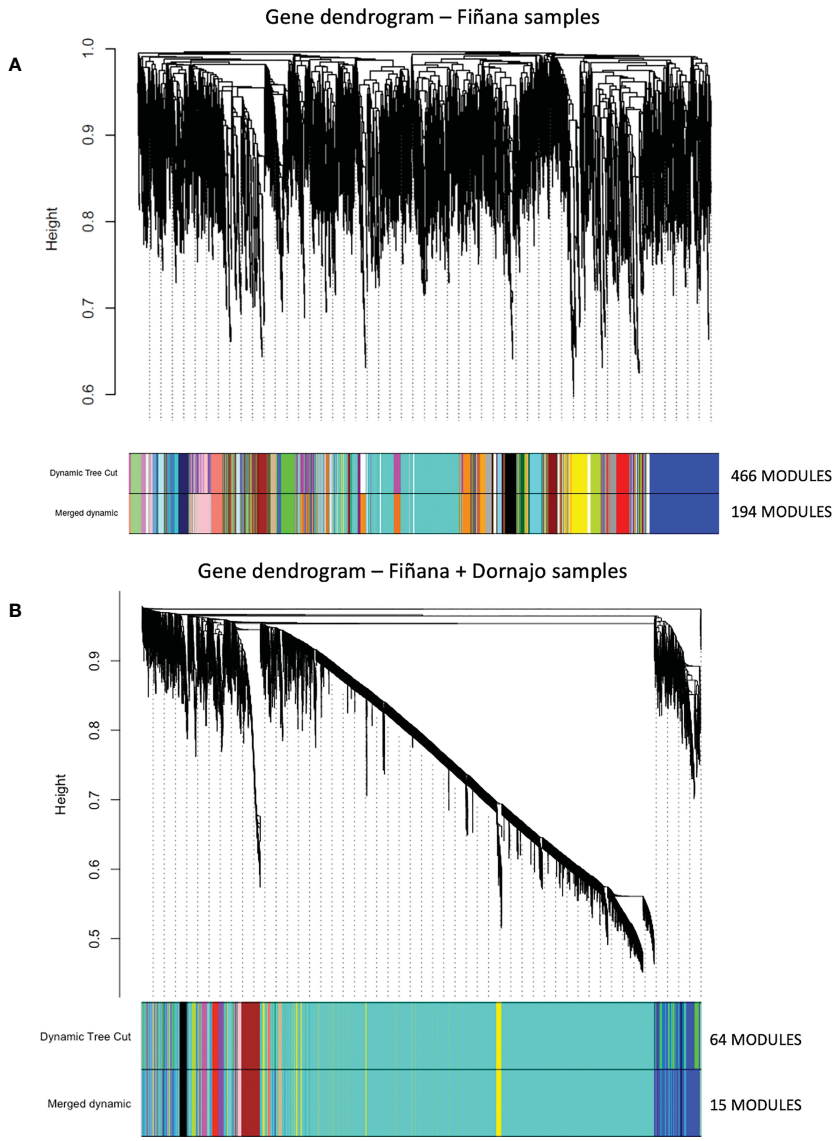

FIGURE 6
Hierarchical cluster dendrogram showing co-expression modules using weighted gene co-expression network analysis (WGCNA) of the counts to identify gene modules underlying drought stress at four different treatments and responses (C, I, R and N) in Fiñana **(A)** and Fiñana+Dornajo populations **(B)**. **(A)** 466 modules corresponding to branches are labelled with colours indicated by the colour bands underneath the tree. With 0.25 threshold merging, 194 modules were generated. **(B)** 64 modules corresponding to branches are labelled with colours indicated by the colour bands underneath the tree. With 0.25 threshold merging, 15 modules were generated.

S9) and the two modules from Fiñana+Dornajo populations (Tables S10-S11). All genes had a $\log_2$ Fold-Change (logFC) value above 2 and, in the majority of cases, was around or above 4, including the DEGs between R and N individuals from Fiñana, with two biological replicates each (Tables S8, S9). Hence, it can be concluded that the hub genes were highly expressed.

GO term enrichment analysis showed that the most abundant GO terms in all selected modules were biologically meaningful (Figure 9). Given the low number of DEGs, GO terms were very unspecific during I treatment, mostly related with metabolic activity among up-regulated genes and protein transport among the down-regulated (Figures 9A, B). Given the higher number of DEGs during E treatment, GO terms were more specific to plant drought response (Figure 9C). In particular, stomatal movement, potassium ion import, regulation of membrane potential, cell wall reorganization, sugar metabolism, cellular response to DNA damage stimulus, and protein ubiquitination GO terms were found among the up-regulated genes (Figure 9C). All these functions are related to plant response during drought stress (Kahur et al. 202, Tenhaken, 2015; Chen et al., 2021; Cobo-Simón et al., 2022, see DroughtDB Alter 2015, see Discussion). Among the down-regulated, the more prevalent GO terms were related to DNA/RNA biosynthesis and regulation, cell wall organization and anatomical structure development (Figure 9D), related to aerial plant growth inhibition, which can be observed during drought stress response in plants (Miao et al., 2017). Finally, the most prevalent GO terms among the up-regulated genes in N individuals were related to photosynthetic activity, cellular metabolism and

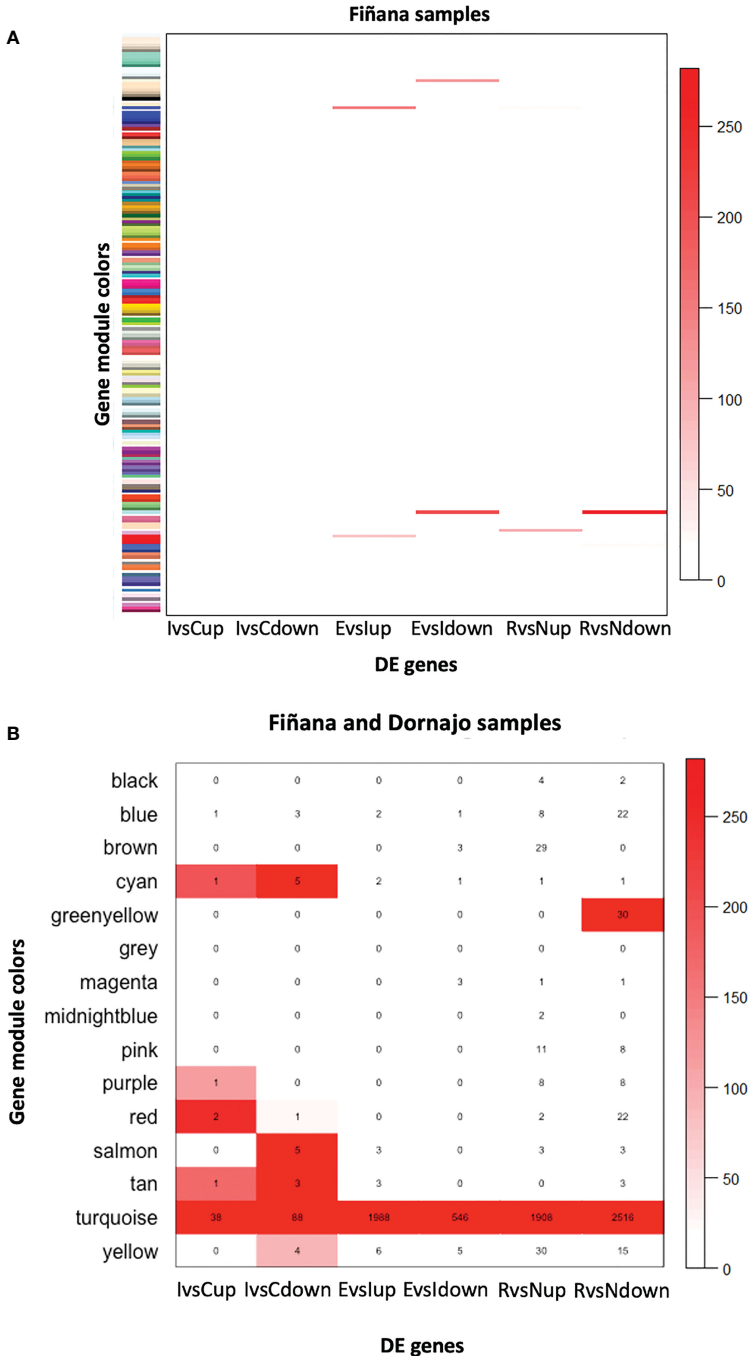

FIGURE 7
Heatmap showing the -log10(P-value) of the Fisher's exact test calculated between the genes belonging to the 194 obtained modules in Fiñana **(A)** and to the 15 obtained modules in Fiñana + Dornajo samples **(B)**, and the pairwise DE genes up and down-regulated (IvsC up, IvsC down, EvsI up, EvsI down, RvsN up, RvsN down). Given the low number of modules in Fiñana+Dornajo, it was possible to plot the number of overlapping genes in the heatmap **(B)**. 20 modules were found to be statistically significant in Fiñana **(A)**, and 8 modules in Fiñana + Dornajo **(B)**.

RNA activity (including methylation) in both Fiñana and Fiñana +Dornajo samples, as well as cell wall modification, aerial growth and response to oxidative stress in Fiñana+Dornajo samples, all of them related to drought stress response in plants (Figures 9E, G, see Discussion). The down-regulated genes in N individuals were mostly related to cell division and negative regulation of metabolism in Fiñana samples (Figure 9F), and metabolic and methylation activity in Fiñana + Dornajo samples (Figure 9H, see Discussion).

3.2.6 Genetic differences between responses and locations

SNP calling results, conducted in the two post-drought responses (R and N) and locations (Fiñana and Dornajo) (Tables

10.3389/fpls.2023.1116863

TABLE 2 Results of the enrichment analysis between pairwise DE up and down regulated genes and the 194 obtained modules in Fiñana samples, and the 15 modules in Fiñana+Dornajo samples.

Module	Pairwise comparison	Number of genes	P-value
Fiñana			
Aquamarine2	I vs C up	15	1.15×10^{-18}
Brown	I vs C up	5	0.03
Darkseagreen1	I vs C up	6	3.63×10^{-7}
Blue	I vs C down	4	6.69×10^{-4}
Darkolivegreen	I vs C down	2	1.9×10^{-3}
Lightblue3	I vs C down	6	1.15×10^{-12}
Mediumpurple4	I vs C down	3	1.1×10^{-4}
Blue	E vs I up	141	6.67×10^{-147}
Darkolivegreen	E vs I up	13	1.35×10^{-10}
Green.1	E vs I up	5	3×10^{-4}
Mediumpurple4	E vs I up	11	1.08×10^{-6}
Red	E vs I up	67	5.17×10^{-75}
Slateblue1	E vs I up	4	3.6×10^{-3}
Antiquewhite1	E vs I down	24	2.66×10^{-14}
Beige	E vs I down	104	4.42×10^{-118}
Darkgreen	E vs I down	10	0.01
Gold1	E vs I down	16	9.22×10^{-13}
Ivory1	E vs I down	9	4.03×10^{-10}
Lavenderblush4	E vs I down	15	5.75×10^{-8}
Mediumspringgreen	E vs I down	14	8.11×10^{-6}
Paleturquoise	E vs I down	161	4.76×10^{-199}
Pink.1	E vs I down	22	8.52×10^{-18}
Royalblue	E vs I down	10	0.02
Paleturquoise	R vs N up	166	2.84×10^{-282}
Royalblue	R vs N up	30	1.62×10^{-24}
Blue	R vs N down	31	1.09×10^{-23}
Darkolivegreen2	R vs N down	7	1.6×10^{-4}
Lavenderblush4	R vs N down	7	3.97×10^{-6}
Pink.1	R vs N down	51	2.94×10^{-95}
Fiñana+Dornajo			
Cyan	I vs C up	1	3.14×10^{-117}
Purple	I vs C up	1	6.45×10^{-76}
Red	I vs C up	2	1.34×10^{-219}
Tan	I vs C up	1	2.39×10^{-105}
Turquoise	I vs C up	38	3.28×10^{-221}
Cyan	I vs C down	5	2.31×10^{-232}
Red	I vs C down	1	1.42×10^{-30}

(Continued)

TABLE 2 Continued

Module	Pairwise comparison	Number of genes	P-value
Salmon	I vs C down	5	5.31×10^{-245}
Tan	I vs C down	3	7.48×10^{-230}
Turquoise	I vs C down	88	6.34×10^{-301}
Yellow	I vs C down	4	1.04×10^{-102}
Turquoise	E vs I up	1988	3.51×10^{-275}
Turquoise	E vs I down	546	2.34×10^{-250}
Turquoise	R vs N up	1908	5.68×10^{-234}
Greenyellow	R vs N down	30	2.23×10^{-220}
Turquoise	R vs N down	2516	4.50×10^{-280}

P-values were calculated by means of a Fisher's exact test. Only statistically significant modules (P<0.05) are shown.

S12, S13), were visualized by a Principal Component Analysis (PCA) (Figure 11). Although the number of biological replicates is not enough to draw statistically robust conclusions, principal component 1 (PC1) clearly separated the two locations, while principal component 2 (PC2) separated the N response from the rest of the individuals. These SNP-based results are clearly consistent with the PCA and the dendrogram based on gene expression differences (Figures 4, 5), which supports these results. We identified 48,002 SNPs with fixed alleles between R and N samples, located in 24,829 genes, 7,392 of which were successfully annotated (Table S13). Four of these fixed-allele genes were found among the down-regulated DEGs between R and N (Table 3) and six among the up-regulated DEGs (Table 4). 134,924 SNPs with fixed alleles were identified between Fiñana and Dornajo

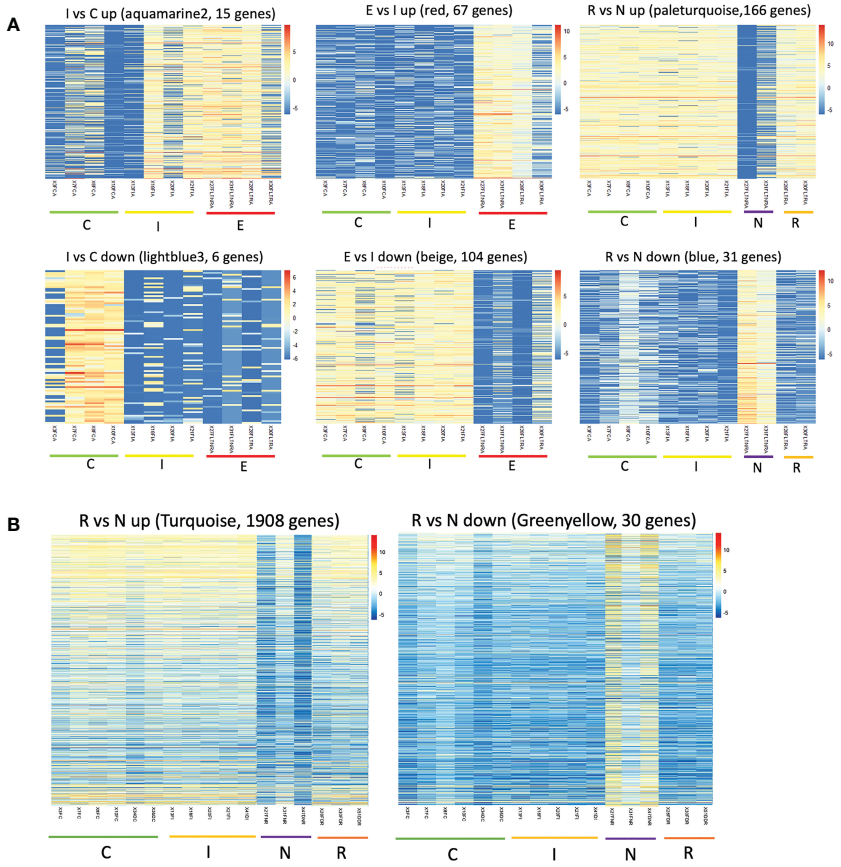

FIGURE 8
Heatmaps showing gene expression levels of the genes within the modules across three treatments (C, I, E) and responses (R, N). Warm colours represent up-regulated genes whereas cold colours represent down-regulated genes. The six modules that showed expression patterns related to the treatment/response are represented for Fiñana **(A)**, and the two modules related to the response for Fiñana + Dornajo **(B)**.

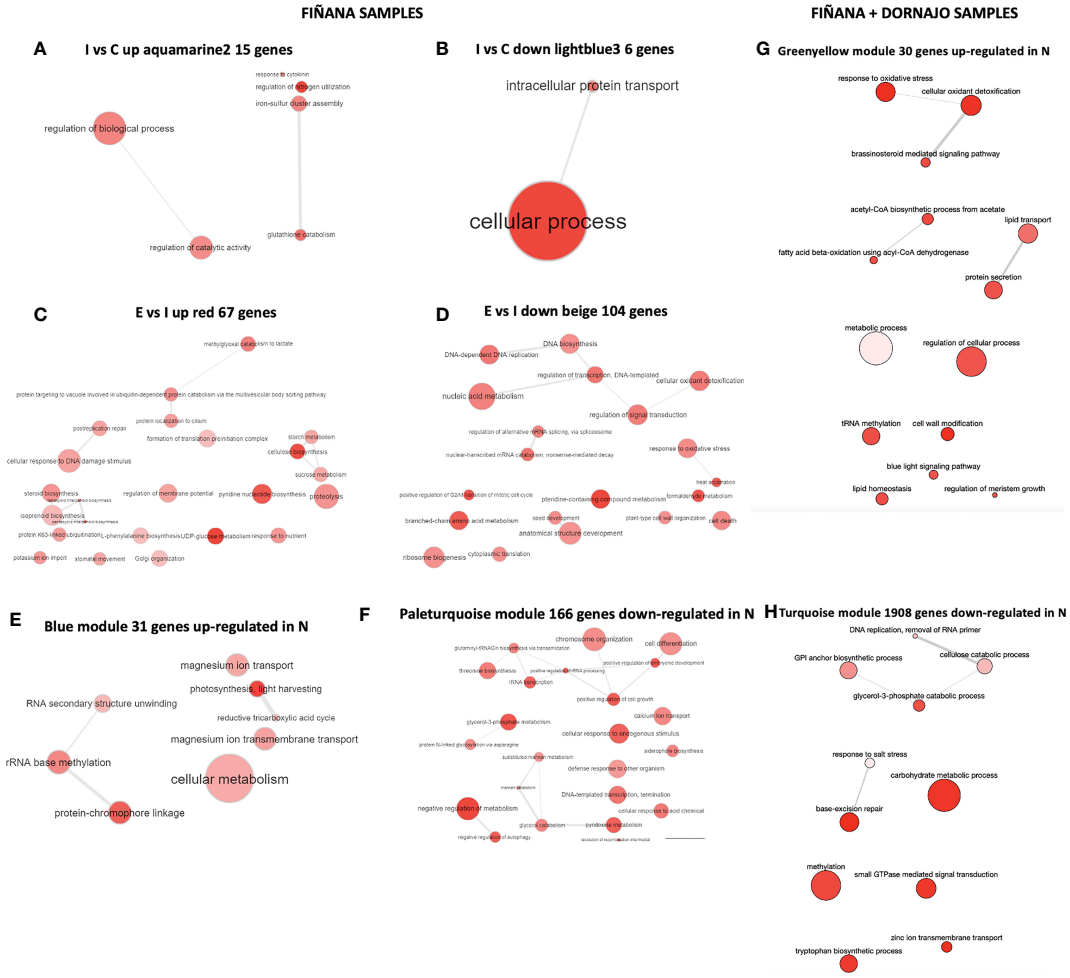

FIGURE 9
GO term enrichment results for the hub genes of the selected modules visualized using REVIGO. **(A)** Aquamarine module, I vs C up comparison (Fiñana samples). **(B)** Lightblue3 module, I vs C down comparison (Fiñana). **(C)** Red module, E vs I up comparison (Fiñana). **(D)** Beige module, E vs I down comparison (Fiñana). **(E)** Paleturquoise module, R vs N up comparison (Fiñana). **(F)** Blue module, R vs N down comparison (Fiñana). **(G)** Turquoise module, R vs N up comparison (Fiñana + Dornajo). **(H)** Greenyellow module, R vs N down comparison (Fiñana + Dornajo).

populations, located in 51,654 genes, of which 15,725 were successfully annotated (Table S12). It was remarkable the great abundance of transposon-related genes containing the fixed SNPs between responses and locations (Tables S12, S13). In particular, *Retrovirus-related Pol poly from transposon TNT 1-94* whose function is related to the catalytic activity to produce diphosphate from DNA/RNA (Grandbastien et al., 1989). This diphosphate-related catalytic activity can be observed in the GO term enrichment results (nucleoside triphosphate-diphosphate activity, Figure 10A; RNA phosphodiester bond hydrolysis, Figure 10B). Other functions related to drought response were found among the GO terms between locations (e.g. zinc ion binding, water channel activity, Figure 10A) and responses (e.g. abcisic acid activated signaling pathway, cellular oxidant detoxification, glucose import, Figure 10B) (see DroughtDB, Alter 2015), proving that the SNP-containing genes are biologically meaningful.

TABLE 3 Overlapping contigs between the fixed SNPs between N and R individuals and the down-regulated genes in N individuals.

Contig	GO function
ABIES09_047144T3	Pectinesterase 31
ABIES09_047752T1	spermidine synthase
ABIES09_057884T2	phosphatase 2C 57
ABIES09_061593T2	glutathione peroxidase, partial

4 Discussion

This work constitutes the first study in investigating the drought response and post-drought recovery in *Cedrus atlantica* from an

TABLE 4 Overlapping contigs between the fixed SNPs between N and R individuals and the up-regulated genes in N individuals.

Contig	GO function
ABIES09_011948T8	cannabidiolic acid synthase-like
ABIES09_014618T8	methyltransferase DDB_G0268948
ABIES09_016813T3	7-deoxyloganetin glucosyltransferase-like
ABIES09_037932T4	1-aminocyclopropane-1-carboxylate oxidase 5-like
ABIES09_041278T3	ORF124 (chloroplast)
ABIES09_065735T2	thaumatin, partial

'omics' perspective (RNA-seq). Moreover, we investigate its drought resilience by comparing the eco-physiology and gene expression patterns of two contrasting post-drought recovery phenotypes (drought resilient R and drought sensitive N). This comparison is key to understand the relative importance of drought response plasticity vs genetic differences in trees' drought resilience, whose underlying gene expression patterns are still largely unknown (Gailing et al., 2009; Neale and Kremer, 2011; Moran et al., 2017). This experimental design has been proved to be successful in identifying candidate genes of drought resilience in other relict conifers (e.g. Cobo-Simón et al., 2022). However, the main novelty of this work is the use of afforested populations as a natural experiment to investigate molecular and functional mechanisms that might contribute to rapid local adaptation to drought in conifers. To the best of our knowledge, it has never been performed in conifers.

Our study illustrates the dynamic response to drought in *C. atlantica*. Here, we describe the molecular responses that accompany the physiological response of *C. atlantica* needles to drought stress, and therefore, their gas exchange, and carbon and water balances. We hypothesized contrasting gene expression related to carbon and water balance variability in response to drought stress and causing the two contrasting post-drought recovery phenotypes in both locations. In addition, we hypothesized a rapid local adaptation in both populations. The lack of biological replicates per treatment/response prevented us from testing these hypotheses in Dornajo population. Nevertheless, we obtained enough biological replicates per population (five in Dornajo and ten in Fiñana) to draw statistically robust conclusions for a possible rapid local adaptation. In this sense, our transcriptomic results (Figures 4, 5) clearly separated both populations, supporting a rapid local adaptation and our initial hypothesis. Despite the low number of samples, our SNP-based results displayed a clearly consistent pattern with the DE analysis results (Figure 11), separating both locations. Thus, they give support to our results and help guide future adaptative potential research in conifers.

Another remarkable finding was the higher percentage of DEGs in all pairwise comparisons when analyzing both populations together, in comparison with Fiñana samples (Table 1). In contrast, we found more gene modules with expression patterns of interest, related to the treatment/responses, in Fiñana samples (Figures 8A, B). A possible explanation might be that, despite the higher number of DEGs when analyzing both populations together, these DEGs might contain more noisy data, as a consequence of the gene expression differences between populations (Figures 4, 5). This explanation is supported by the fact that the only gene modules with expression patterns of interest when analyzing both populations were found for N individuals (Figure 8B). Furthermore, N was the only treatment/response that clustered between populations based on gene expression (Figures 4, 5), supported by the SNP-based results (Figure 11). In contrast, when analyzing Fiñana samples, we obtained a gene module with an expression pattern of interest per each pairwise comparison, and for both up and down-regulated DEGs (Figure 8A), similarly to *A. pinsapo* (Cobo-Simón et al., 2022). All these results support, again, a rapid local adaptation, as well as a molecular singularity of N individuals in *C. atlantica*.

Rapid local adaptation to increasing drought has been previously reported in other relict coniferous species (e.g. Cobo-Simón et al., 2021). A rapid local adaptation might be possible due to the retention of genetic variants for some ecologically relevant traits, hypothesized for relicts (Kawecki, 2008). Nevertheless, this hypothetical rapid local adaptation was not supported by eco-physiological measures in this work (Figure 3). However, differences in other eco-physiological variables and/or traits, not measured in this study, might be possible, considering the contrasting environmental conditions to which both

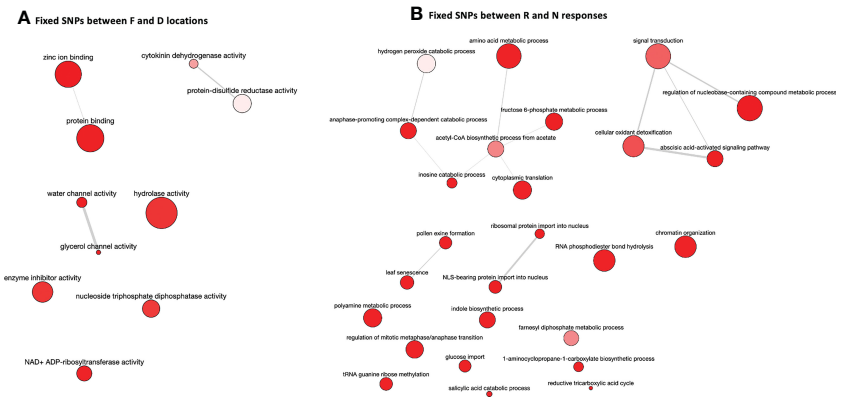

FIGURE 10
GO term enrichment results for genes containing fixed SNPs between F and D locations **(A)** and R and N responses **(B)** visualized using REVIGO.

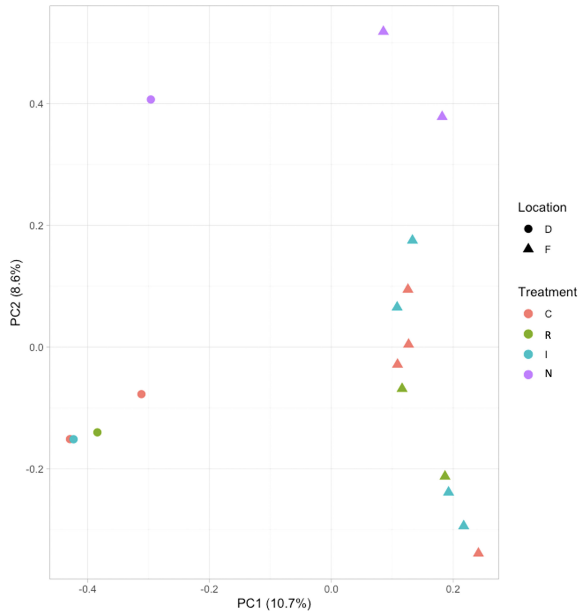

FIGURE 11
Principal component analysis (PCA) of the SNPs of the 17 samples from Fiñana and Dornajo populations.

populations are subjected in nature, without any apparent effect on fitness, and the transcriptomic and genomic differences observed in this study (Figures 4, 5, 11). In fact, morphological differences can be observed between both populations, such as leaf density or greenness, which are both higher in Dornajo individuals. Therefore, we strongly recommend to further investigate them in future studies. On the other hand, a study of the drought-response transcriptomic profile for Dornajo using, at least, three biological replicates per treatment/response is key to detect more detailed drought-related transcriptomic differences between both populations and confirm this hypothetical rapid local adaptation. Moreover, an analysis of molecular markers (e.g. SNPs) in both populations using a wider number of samples, integrating them with other omic data (e.g. metabolomic, epigenomic, proteomic) by applying multi-omic analysis, and associating them with other traits/environmental variables of interest (e.g. GWAS, GEA) would be advisable to further investigate the molecular basis of the observed drought-related gene expression and genomic differences in this work. Moreover, the metabolic pathways elucidated with these analyses will be useful to guide the search of potential phenotypic/physiological differences between these populations, and to better understand the mechanisms of rapid local adaptation in conifers. However, it is also worth noting that, although both locations were afforested using *C. atlantica* individuals from natural stands of northern Morocco, and the most probable explanation is a rapid local adaptation to drought (the afforestation project were performed during the last century, which is a short period of time for a long-lived species), we recommend to investigate these natural stands to better elucidate the cause of the genetic differences observed in F and D locations in this study. For instance, population structure or local adaptation in the populations of origin might also explain the observed differences. Notwithstanding, considering that the molecular differences found between locations in this study are drought-related, which is consistent with the contrasting precipitation rates between F and D locations, and given the lack of differences in fitness between F and D locations despite their contrasting precipitation rates, which points to a rapid local adaptation to these contrasting precipitation rates, the most plausible explanation would be a rapid local adaptation to the local environmental conditions.

Besides, we analyzed both populations together in order to examine drought-related gene expression patterns regardless the location. Contrasting gene expression significantly modulated their response to different drought intensities and their drought sensitiveness, supporting our initial hypotheses in both analyses (using only Fiñana and both populations). Nevertheless, it was remarkable the low number of DEGs during the immediate drought response (Table 1). These results contrasted with those obtained for the relict fir *Abies pinsapo* using a similar experimental design. They suggest a later molecular activation of the drought stress response in *C. atlantica*, compared to *A. pinsapo*, under the same drought stress conditions, supporting the wider drought stress tolerances in *C. atlantica* (Abel-Schaad et al., 2018).

N individuals from both populations, in addition to cluster together, constituted the only treatment/response clearly separated from the rest in the two PCAs (gene expression and SNP based, Figures 4, 11) and the gene expression-based dendrogram (Figure 5) in both populations. This molecular singularity of N individuals in *Cedrus atlantica*, which is another relevant finding of this study, was also supported by the uniquely up and down expressed genes found in N individuals from Fiñana population (Figure 8A), and when analyzing Fiñana and Dornajo populations together (Figure 8B). Again, further molecular, functional, eco-physiological and morphological research in these populations (e.g. multi-omics, GWAS) using more samples would be advisable to better understand the molecular singularity of N individuals, and thus, the mechanisms of drought resilience/sensitivity in *C. atlantica*.

These results contrast, again, with those obtained for the relict fir *Abies pinsapo* using a similar experimental design (Cobo-Simón et al., 2022). There, uniquely expressed genes were found for drought resilient individuals but not for sensitive ones, pointing to different molecular and functional strategies conferring drought resilience in these conifers. Moreover, *A. pinsapo* showed a clear separation of all treatments/responses in the gene expression-based PCA and cluster dendrograms (Cobo-Simón et al., 2022).

These circum-Mediterranean conifers (*A. pinsapo* and *C. atlantica*) are both relicts, located in altitudinal ecotones and climate-change threatened due to their susceptibility to drought (Linares, 2011; Abel-Schaad et al., 2018). Hence, both of them have been experiencing a population decline over the last decades due to climate change, together with human land use effects. Consequently, they are gradually migrating upwards in the mountain ranges where they inhabit (Linares, 2011; Abel-Schaad et al., 2018). In addition, previous studies have offered evidence of a common evolutionary history in North Africa (Scaltsoyiannes et al., 1999; Qiao et al., 2007; Linares, 2011; Alba-Sánchez et al., 2018). Hence, they have been likely subjected to very similar selective pressures. For these reasons, and given the similar experimental design of this and the previous work performed in *A. pinsapo* (Cobo-Simón et al., 2022), we consider pertinent to use *A. pinsapo* results to complement the discussion of

the results of this work. It is also worth noting that previous studies using genetics of circum-Mediterranean conifers reported that genetic differentiation between species seems to depend mainly on the individual biological history instead of a common vicariant phenomenon (Jaramillo-Correa et al., 2010; Liepelt et al., 2010). However, our results contradict this affirmation regarding their molecular adaptation to drought, since they show remarkably different molecular responses in *C. atlantica* and *A. pinsapo* related to their drought resilience. Although both species are considered sensitive to drought, *A. pinsapo* is extremely sensitive (Linares, 2011) whereas *C. atlantica* shows *a priori* wider tolerances (Abel-Schaad et al., 2018). Therefore, the different drought resilience-related molecular responses between *C. atlantica* and *A. pinsapo* might explain these differences in drought tolerance, shedding light on the molecular and functional mechanisms conferring drought resilience in conifers. Furthermore, the wider drought tolerances of *C. atlantica* are supported by the lack of separation between drought treatments observed in the PCAs and dendrogram (Figures 4, 5, 11) in this work, as well as the low number of DEGs during the immediate drought (Table 1). On the contrary, *A. pinsapo* exhibited a clear separation between treatments/responses and a higher number of DEGs (Cobo-Simón et al., 2022). A possible explanation might be that *C. atlantica* would exhibit a more constitutive gene expression pattern related to drought response and resilience than *A. pinsapo*, which would lead to its wider tolerances (Abel-Schaad et al., 2018). This possible explanation is supported by the molecular singularity of N individuals, based on both gene expression and SNPs (Figures 4, 5, 8, 11 Tables S8-S13). A constitutive expression of drought-related genes has been previously observed in drought tolerant individuals of *P. pinaster* (de María et al., 2020).

Another remarkable finding was the great prevalence of transposon-related genes among the SNPs found between both responses (R and N, Table S12) and the two locations (Fiñana and Dornajo, Table S13), which were absent among the DEGs (Tables S4-S11). These results point to a role of transposable elements (TEs) in the hypothetical rapid local adaptation and the constitutive molecular drought resilience of *C. atlantica*. TEs have been found to have a key role on genome and adaptive evolution of conifers, as an important force in shaping gene regulatory networks, their downstream metabolic and physiological outputs, and thus their phenotypes (Liu and El-Kassaby, 2019). Although the low number of samples analyzed in this work does not allow to draw robust conclusions based on SNPs, we strongly recommend to further investigate the potential role of TEs in the rapid local adaptation and constitutive drought response of *C. atlantica* in particular, and conifers in general.

4.1 *C. atlantica* seedlings regulate photosynthetic activity and stomatal closing during the first 24 hours of drought, consistent with an isohydric drought response

We obtained statistically significant DEGs during immediate treatment when analyzing only Fiñana, and Fiñana and Dornajo individuals together (Table 1). Nevertheless, given the lack of gene modules showing an expression pattern of interest when analyzing both populations (Figure 8B), we will focus the discussion of the *C. atlantica* seedling transcriptional profile after 24 hours of drought on Fiñana population.

Despite the low number of significantly up and down regulated genes in the two immediate drought gene modules (Figure 8A), they showed biologically meaningful functions (Figure 9A, B). *C. atlantica* is an isohydric tree regarding its physiological response to drought, characterized by its sensitivity to the atmospheric-moisture demand, which leads to a water-saving strategy by means of stomatal closure (Spinelli et al., 2011; Sanchez-Salguero et al., 2015; Lechuga et al., 2019). This stomatal closure is accomplished by increasing abscisic acid (ABA) concentrations (Moran et al., 2017). Consequently, it leads to a pronounced reduction of stomatal conductance (Gs) and limited carbon uptake by photosynthesis (A). This isohydric pattern has been observed in this work in *C. atlantica* seedlings through a progressive decrease of A and Gs values in both populations (Figure 3). These findings are similar to those obtained in *A. pinsapo* seedlings using the same study design (Cobo-Simón et al., 2022), whose physiological response to drought is also isohydric.

During the 24 hours of drought treatment (I), *C. atlantica* seedling transcriptional response showed consistencies with an isohydric profile. Among the hub genes, we observed several genes related to chloroplast activity and photosynthesis among the up (isoamylase 3 chloroplastic isoform X1, high chlorophyll fluorescent 107) and down-regulated genes (probable plastid-lipid-associated 8, chloroplastic, soluble inorganic pyrophosphatase 6, chloroplastic-like), including transcription factors (transcription termination factor MTERF4, chloroplastic) (Table S4), pointing to a regulation of photosynthetic activity.

Hub genes related with protein transport, protein kinase activity and protein phosphorylation pathways were observed among the up- (probable inactive serine threonine- kinase scy1, receptor kinase TMK1-like, GPI ethanolamine phosphate transferase 1, coatomer subunit delta, Tetratricopeptide repeat-containing domain) (Table S4) and down-regulated genes (leucine-rich repeat receptor-like serine threonine tyrosine-kinase, Table S5). Protein phosphorylation has been associated with drought-priming heat stress tolerance in plants (Zhang et al., 2020). Interestingly, protein kinases were also extremely abundant during both immediate and extended drought stress and both up and down regulated in *A. pinsapo* (Cobo-Simón et al., 2022). Protein kinases have been reported to be involved in core-stress signaling pathways related to abiotic stress, such as drought, salinity and extreme temperatures (Zhu, 2016), including ABA production and stomatal closing (Chen et al., 2021). Finally, hub genes related with transcription regulation (lncRNA, Table S4) and circadian clock regulation (XAP5 CIRCADIAN TIMEKEEPER, Table S4) were found among the up-regulated genes. Several evidence points that circadian clock contributes to plants' ability to tolerate different types of environmental stress, and to acclimate to them (Grundy et al., 2015), including, again, ABA production and stomatal responses under water stress (Kamrani et al., 2022).

4.2 *C. atlantica* seedlings perform cell wall and sugar distribution remodeling, and inhibit growth and flavonoid biosynthesis after 20 days of drought

After 20 days of drought stress (E treatment), *C. atlantica* seedlings showed a higher number DEGs, pointing to a stronger drought-related stress at this stage, compared to immediate drought response, in both analyses (using Fiñana and Fiñana+Dornajo individuals) (Table 1). Again, given the lack of gene modules showing an expression pattern of interest when analyzing both locations together, we will focus the discussion of the gene expression profile after 20 days of drought on Fiñana population. Similar to immediate response, *C. atlantica* transcriptional profile was consistent with an isohydric drought response (Figure 9C, D). Hub genes related to stomatal closure, ABA transportation (NRT1 PTR family-like proteins, Guo et al., 2003 Chiba et al., 2015; acetate butyrate ligases AAE7, Dong et al., 2018) (Table S6), and ABA homeostasis (probable E3 ubiquitin-ligase XERICO, Ko et al., 2006) (Table S6) were activated. In addition, hub genes related to photosynthesis (photosystem I reaction center subunit VI-1, chloroplastic; metal transporter Nramp3-like, Lanquar et al., 2010) (Table S7) and metabolism (mitochondrial adenine nucleotide transporter ADNT1 and phosphoglycerate kinase, both involved in ATP production; lysosomal Pro-X carboxypeptidase, involved in proteolysis; coatomer subunit delta, involved in Golgi function) (Table S7) were inhibited.

In addition, cell wall-related hub genes (probable E3 ubiquitin-ligase HIP1 isoform X1, Sun et al., 2009, exocyst complex component EXO70A1 Synek et al., 2006) (Table S6), together with carbohydrate/sugar metabolism and transportation-related genes (malate synthase, glyoxysomal, acetate butyrate ligase AAE7, peroxisomal, Allen et al., 2011, sugar transporter 7-like, which might contribute to the uptake and recycling of cell wall sugars, Rottmann et al., 2018) (Table S6) were activated in *C. atlantica* seedlings after 20 days of drought. Other plant growth-related hub genes were, conversely, inhibited (probable purine permease 11, Qi and Xiong, 2013; kinesin KIN-14I, Cooper et al., 2003; beta-tubulin, Eckardt, 2006; probable strigolactone esterase DAD2, involved in plant shoot branching, Hamiaux et al., 2012; cellulose synthase E6, involved in synthesis of cell wall cellulose) (Table S7), including plant polyamine biosynthesis-related genes (ornithine decarboxylase-like, Illingworth and Michael, 2012; Chen et al., 2019) (Table S7).

Sugar transport, distribution and signaling has a critical role in plants under drought stress conditions (Kaur et al., 2021). Abiotic stress and especially drought stress-mediated injury results in reprogramming of sugar distribution across the cellular and subcellular compartments (Kaur et al., 2021). Plant cell walls are composed of carbohydrate polymers, lignin and structural proteins in variable amounts (Tenhaken, 2015). Plants exposed to drought stress reduce shoot growth while maintaining root growth to improve water intake (Miao et al., 2017), a process requiring differential cell wall synthesis and remodeling (Tenhaken, 2015). A cell wall and sugar distribution remodeling in needles, where the RNA from this work was obtained, in order to allow further growth of stressed organs (roots) to improve water uptake under drought conditions, might explain these cell wall and sugar metabolism-related genes activation, and the inhibition of growth and cell division, in aerial tissues. Metabolic pathways implied in shoot: root ratio decrease were observed in *A. pinsapo* seedling needles, related to their drought resilience as well (Cobo-Simón et al., 2022). We do not have any measurements from this work to test this hypothetical decrease in the shoot:root ratio. Besides, the time spam of this experiment and the limited size of the plants pose limitations to reliably detect it. However, we strongly recommend to test the possible role of a shoot:root ratio decrease in the drought resilience of conifers in future studies, suggested by the results of this and previous works (Cobo-Simón et al., 2022).

Other activated hub genes were related to transcription regulation under environmental stress (regulator of nonsense transcripts 1 homolog, Shi et al., 2012, heavy metal-associated isoprenylated plant 23-like, Braga de Abreu-Neto et al., 2013), including TFs (LHY isoform X1, Moenga et al., 2020) and histone demethylases (FLOWERING LOCUS D isoform X1, related to the epigenetic regulation of flowering in *A. thaliana*, Luo et al., 2015). Since *C. atlantica* is a conifer, this histone demethylase might have another function in this species, probably related to the epigenetic regulation of drought response, which would need further investigation. Epigenetic regulation-related genes were also found in *A. pinsapo* seedlings, associated to their drought resilience (Cobo-Simón et al., 2022). In addition, a gene related to alternative splicing under salt stress response in *Arabidopsis* was inhibited (serine arginine-rich splicing factor 4-like, Table S7) since its overexpression produces hypersensitivity of salt stress (Li Y. et al., 2021)

Other genes related to water stress response were activated (water-stress inducible 1, partial, probable carboxylesterase 15, Cao et al., 2019, linked to drought stress response in *Abies alba* Behringer et al., 2015), including, again, protein phosphorylation (receptor kinase HAIKU2, associated with drought tolerance in *Sequoia sempervirens*, de la Torre et al., 2022), similar to the immediate drought treatment.

A gene related to GABA biosynthesis was found among the down-regulated hub genes (glutamate decarboxylase-like, Table S7). GABA has a protective role on plants subjected to abiotic stress. It enhances drought stress tolerance by improving photosynthesis, inhibiting reactive oxygen species (ROS) generation, activating antioxidant enzymes, and regulating stomatal opening (Li et al., 2021). However, its potential role in *C. atlantica* drought response requires further investigation, given its versatile role in plants (Li et al., 2021) and its down-regulation during drought stress in this species (Table S7). This down-regulation might be a consequence of the inhibition of polyamine biosynthesis-related genes, previously described, since GABA can be synthesized through the polyamine metabolic pathway (Li et al., 2021).

Flavonoid metabolism-related hub genes were inhibited after 20 days of drought stress (isoflavone reductase and flavonoid 3,5 -hydroxylase, Table S7). It has been suggested that flavonoids protect plants against abiotic stress, and thus, their accumulation is induced rapidly upon drought (Munné-Bosch et al., 2009; Nakabayashi et al., 2014). Nevertheless, flavonoid production has

been found to be inhibited in leaves during drought stress in several plants (Salekdeh et al., 2002, Pandey et al., 2010; Rani et al., 2012) including conifers (Fox et al., 2018). The pattern of down-regulation observed in our study may suggest that the plant limits the energy-intensive biosynthesis of secondary metabolites in favor of drought-related survival mechanisms.

Finally, mildew resistance locus o (Mlo) gene (MLO6), which loss-of-function confer broad-spectrum resistance to almost all known isolates of the fungal barley powdery mildew pathogen in plants (Acevedo-Garcia et al., 2014), was inhibited (Table S7). However, it is known that its function is not restricted to plant-powdery mildew interactions (Acevedo-Garcia et al., 2014). Therefore, a further investigation of its possible role in *C. atlantica* drought response would be advisable.

4.3 Drought sensitive individuals fail in metabolism and photosynthesis regulation under drought stress, and in limiting the energy-intensive biosynthesis of secondary metabolites

We hypothesized that differences in gene expression will cause the two contrasting post-drought recovery phenotypes (R and N). The identification of uniquely DEGs in drought sensitive individuals (N) was one of the main findings of this study (Table 1) and supports our initial hypothesis. In addition, we found gene modules showing an expected expression pattern based on our experiment and biologically meaningful functions in both analyses (using only Fiñana population, Figure 8A, 9E, F; and both populations, Figure 8B, 9G, H), up (Tables S9, S11) and down-regulated (Tables S8, S10). These results contrast with those obtained in *A. pinsapo* seedlings using a similar experimental design (Cobo-Simón et al., 2022), where uniquely DEGs were found for R individuals instead. These results suggest different molecular strategies conferring drought resilience in these drought sensitive and biogeographically related conifers (Scaltsoyiannes et al., 1999; Qiao et al., 2007; Linares, 2011; Alba-Sánchez et al., 2018), which would probably explain the wider drought stress tolerances in *C. atlantica* (Abel-Schaad et al., 2018).

Drought sensitive individuals from both analyses (F and F+D) showed an activation of flavonoid metabolism compared to drought resilient ones (isoflavone reductases, Table S9; Transparent testa 12, Debeaujon et al., 2001, Table S11; and a Transcription factor TT2, Table S9, which is involved in flavonoid metabolism when interacting with MYB TFs, Zimmermann et al., 2004). MYB TFs were found among the up-regulated genes in N individuals in both analyses as well (Tables S9 and S11). These results contrast with those obtained for the extended drought response, where the flavonoid metabolism was down-regulated. Hence, they support, again, that limiting the energy-intensive biosynthesis of secondary metabolites in favor of drought-related survival mechanisms might enhance drought resilience in this species. Moreover, an activation of terpene production-related hub genes was found in N individuals from both analyses (7-deoxyloganetin glucosyltransferase-like, involved in irioid biosynthesis, Asada et al., 2013), supporting this hypothesis.

Several hub genes related to ethylene production were up-regulated in N individuals from both analyses (1-aminocyclopropane-1-carboxylate oxidase 5-like, Qin et al., 2007) (Tables S9, S11), including TFs (ethylene-responsive transcription factor 2-like, ethylene-responsive transcription factor 1A-like) (Tables S9, S11). Ethylene is a phytohormone involved in the regulation of gene expression by stress factors and by components of stress signal transduction pathways (Fujimoto et al., 2000). In addition, several hub genes related to antifungal response were activated: chitinases (basic endochitinase, partial; chitinase 2-like, class VII chitinase), peroxidases/oxidoreductases ((R)-mandelonitrile lyase-like; blue copper-like, De Rienzo et al., 2000; cannabidiolic acid synthase-like, Taura et al., 2007), thaumatin-like proteins (Ruiz-Medrano et al., 1992; de Jesús-Pires et al., 2020), beta 1,3 glucanase, Balasubramanian et al., 2012), and others (wall-associated receptor kinase-like 20, Delteil et al., 2016, zinc finger ZAT5-like, zinc finger CCCH domain-containing 17, Gupta et al., 2012; TIR NBS LRR disease resistance, McHale et al., 2006) (Tables S9, S11). These anti-fungal proteins are usually co-expressed (Balasubramanian et al., 2012) and activated in plants by ethylene and other phytohormones under several biotic and abiotic stress conditions (e.g. Kasprzewska, 2003), like wounding, osmotic pressure, cold, heavy metal stress and salt in plants (e.g. Vaghela et al., 2022). Furthermore, ethylene has been found to induce flavonoid accumulation in plants (Lewis et al., 2011). All these findings point to ethylene as an important phytohormone in the drought sensitivity of this species, probably causing a failure in limiting the energy-intensive biosynthesis of secondary metabolites.

Other TFs and transcriptional regulation-related genes were activated in both populations (lncRNA, DRE-binding 2, Table S9; two-component response regulator ORR21 isoform X1, probable WRKY transcription factor 4, dynein light chain 1, cytoplasmic, Stelter et al., 2007; nuclear pore complex NUP 35, Table S11), including one related to epigenetic regulation (methyltransferase DDB_G0268948, Table S9). This methyltransferase supports, again, the role of epigenetic regulation during drought stress in this species, reported in *A. pinsapo* as well (Cobo-Simón et al., 2022). In addition, an E3 ubiquitin-ligase MIEL1 was up-regulated (Table S11), which mediates degradation of MYB-like TFs, weakening plant defense to pathogens (Marino et al., 2013). Therefore, the expression of this gene could also explain the drought sensitiveness of these individuals.

Furthermore, detoxification proteins were found among the up-regulated genes (detoxification 40-like, Li et al., 2002) (Tables S9,-S11) in N individuals, which might be a consequence of their higher levels of drought stress due to their sensitiveness to drought.

Finally, photosynthesis (probable 1-deoxy-D-xylulose-5-phosphate synthase 2, chloroplastic; ORF124), and metabolism-related pathways (probable fructokinase-4, Stein and Granot, 2018, cytochrome P450 82C4, mitochondrial; mitochondrial phosphate carrier 3, mitochondrial; glutamine–fructose-6-phosphate aminotransferase [isomerizing] 2 Vu et al., 2019; hydroquinone glucosyltransferase-like, glycosyl hydrolase; glycerol-3-phosphate dehydrogenase [NAD(+)] GPDHC1, cytosolic, Minic, 2008; acyl carrier 2, mitochondrial-like) were found among the up-regulated hub genes in N individuals when analyzing Fiñana and Dornajo populations (Table S11). Moreover, stomatal closure pathways were

activated (sphingosine kinase, Coursol et al., 2005; probable phosphatase 2C 76 isoform X2, Yang et al., 2018; Hsu et al., 2021) (Table S11). It is worth noting that a phosphatase 2C was related to drought resilience in *A. pinsapo* and was also up-regulated under drought stress conditions in *Pinus halepensis* (Fox et al., 2018). These findings suggest that drought sensitivity in *C. atlantica* might be caused by failing in down-regulating photosynthesis and metabolism under drought stress conditions, which will negatively affect the whole plant carbon status.

One of the main objectives of this work was the identification of candidate genes mechanistically involved in the drought resilience of *C. atlantica*. However, our findings provide a set of drought-sensitiveness candidate genes instead, since we found uniquely up and down regulated genes in non-resilient individuals. These drought-sensitiveness candidate genes are key for the design of conservation and management strategies, as well as breeding programs. To ensure their success, it is not only necessary to know the genes conferring tolerance, but those that we aim to avoid, that is, those conferring sensitivity.

4.4 Genetic differences between responses and locations point to a role of transposable elements in the local adaptation and drought resilience of *C. atlantica*

Given that both post-drought responses were subjected to the same drought treatment, we hypothesized SNPs as polymorphisms associated to their differentially expressed genes, and thus, related to their drought resilience. In addition, we hypothesized a drought-related rapid local adaptation in both *C. atlantica* locations given the lack of differences in their fitness despite the contrasting precipitation rates. Both hypotheses were supported by our results, showing genomic differences between responses and locations (Figure 11).

The lack of clear gene expression differences between treatments and responses, with the exception of N individuals (Figures 4, 5), in contrast with *A. pinsapo* results which showed a clear separation of all treatment/responses (Cobo-Simón et al., 2022), led us to hypothesize a more constitutive gene expression related to drought in *C. atlantica*, compared to *A. pinsapo*. This drought-related constitutive gene expression might lead to its wider drought tolerances (Abel-Schaad et al., 2018). The lack of genomic differences between treatments and responses, with the exception, again, of the molecular singularity of N individuals, based on the SNP results (Figure 11) supports this hypothesized constitutive gene expression conferring drought resilience on this species. In addition, the genomic differences between locations (Figure 11), consistent with their gene expression patterns (Figure 4, 5), support our hypothesis of a rapid local adaptation to the contrasting precipitation rates. This hypothetical rapid local adaptation might have been favored by this hypothesized drought-related constitutive genetic diversity. Evidence of local adaptation to drought has been found in other relict conifers (*A. pinsapo*, Cobo-Simón et al., 2021). Despite the low number of samples used in the SNP calling analysis, which prevents us to draw statistically robust conclusions based on SNPs, these findings point to enough adaptive potential of this species under a climate change scenario, although further investigation is needed to fully validate it.

As expected, few SNP genes were found among the DEGs (Tables 3, 4), since most of the causative variation of this DEGs is not located in the transcriptome, but in regulatory regions of the genome, both in *cis* and in *trans*. These results are similar to those obtained for *A. pinsapo* (Cobo-Simón et al., 2022). The annotation and GO term enrichment analysis of the SNP-related genes between responses (Table S12) and locations (Table S13) showed similar functions to the DEGs (Figure 10, Tables S4-S11). Nevertheless, the abundance of transposon-related genes in both comparisons, which were absent on the DEGs, was remarkable. These results point to a role of TEs in the local adaptation and the constitutive molecular response conferring drought resilience of *C. atlantica*.

TEs have been found to have a key role on genome and adaptive evolution of conifers, as an important force in shaping gene regulatory networks, their downstream metabolic and physiological outputs, and thus their phenotypes (Liu and El-Kassaby, 2019). In fact, the large genome size of conifers seems to result from the slow and steady accumulation of a diverse set of long-terminal repeat TEs, possibly due to a lack of an efficient elimination mechanism (Nystedt et al., 2013). TEs are DNA fragments that can move and amplify their copy number within a host genome (Casacuberta and González, 2013). As a result, they are a major and powerful source of genomic mutations, causing the evolution of new genes and their functionalities and generating novel regulatory sequences, such as promoters and enhancers (Liu and El-Kassaby, 2019). These *in cis* regulatory modifications change the regulatory and/or epigenetic environment, leading to modified gene expression (Mita and Boeke, 2016). Furthermore, TEs could generate genetic variation in response to environmental and genomic perturbations, which could facilitate adaptation (Casacuberta and González, 2013). Hence, it has been suggested that TEs may lead to adaptation to novel habitats in the face of limited genetic variation, such as invasive species (the so-called genetic paradox of invasive species, Stapley et al., 2015), which can also explain the local adaptation of relicts, such as *C. atlantica*. Hence, we strongly recommend to further investigate the potential role of TEs in rapid local adaptation and drought resilience of *C. atlantica* in particular, and conifers in general.

4.5 Future directions

Here we offer the first genomic resources for the climate change threatened relict *C. atlantica*, including its first *de novo* transcriptome assembly, drought-related transcriptomic profile and candidate genes of drought sensitiveness. Our results contrast with those obtained in a similar experimental design in the relict and biogeographically related fir *A. pinsapo* (Cobo-Simón et al., 2022), where uniquely expressed genes were found for drought resilient individuals instead. This finding is remarkable, specially from an evolutionary perspective, since it suggests two different molecular strategies to the same abiotic stress in both conifers

(drought), which would probably explain their different drought tolerances. In addition, our results suggest a constitutive molecular drought response conferring drought resilience in *C. atlantica* and a rapid local adaptation to drought in the two studied populations. TEs might play a key role in this rapid local adaptation and its standing genetic variation related to drought resilience, hypothesized for relict species (Kawecki, 2008). Thus, we recommend further research using a statistically robust number of biological replicates per treatment/response in Dornajo population to elucidate potential drought-related molecular and functional differences between populations. Moreover, we recommend further validation of this probable local adaptation suggested by our results, and the potential role of TEs, by using a wider sample size in both locations, by integrating multi-omic data (e.g. epigenomic, metabolomic) with other traits/environmental variables of interest (e.g. GWAS, GEA) and by studying the *C. atlantica* natural stands from northern Morocco.

Our findings, especially when complemented with those from *A. pinsapo* (Cobo-Simón et al., 2022), shed light on the adaptive potential of trees in general, and relict conifers in particular, to the projected increasing drought caused by current climate change, which is particularly concerning in Mediterranean and other semi-arid climates. This information will allow us better predict their future perspectives facing current global warming.

Finally, our results offer a diversity of drought-related genomic resources, including candidate genes of drought sensitiveness, which will help guide the design of conservation strategies and breeding programs for this climate-change threatened and drought-sensitive conifer. Furthermore, they can be used to advance future drought-resilience research, such as comparative genomic studies and functional transfer across species, which will also shed light on trees' molecular adaptive potential to current climate change.

Data availability statement

The datasets presented in this study can be found in online repositories. The names of the repository/repositories and accession number(s) can be found below: https://www.ncbi.nlm.nih.gov/, PRJNA668002.

Author contributions

IC-S wrote the manuscript. FG and JL conceived the idea. JL performed the field sampling. BM-C performed the RNA extraction. JS carried out the drought experiment. JL performed the eco-physiological analyses. JM, JG-G, AE-C, MD and TA carried out the *de novo* transcriptome sequencing and annotation. IC-S carried out the rest of bioinformatic analyses. ICS- conducted the results discussion. All authors contributed to the article and approved the submitted version.

Funding

IC-S was supported by a Predoctoral Grant BES-2014-070379 and a Predoctoral Mobility Grant EEBB-I-18-12943, Spanish Ministry of Economy. This study was supported by the projects CGL2013-48843-C2-2-R, Spanish Ministry of Economy; TED2021-129770B-C22 and PID2021-123675OB-C44, Spanish Ministry of Science and Innovation.

Conflict of interest

The authors declare that the research was conducted in the absence of any commercial or financial relationships that could be construed as a potential conflict of interest.

Publisher's note

All claims expressed in this article are solely those of the authors and do not necessarily represent those of their affiliated organizations, or those of the publisher, the editors and the reviewers. Any product that may be evaluated in this article, or claim that may be made by its manufacturer, is not guaranteed or endorsed by the publisher.

Supplementary material

The Supplementary Material for this article can be found online at: https://www.frontiersin.org/articles/10.3389/fpls.2023.1116863/full#supplementary-material

References

Abel-Schaad, D., Iriarte, E., López-Sáez, J. A., Pérez-Díaz, S., Sabariego Ruiz, S., Cheddadi, R., et al. (2018). Are *Cedrus atlantica* forests in the rif mountains of Morocco heading towards local extinction? *Holocene* 28 (6), 1023–1037. doi: 10.1177/0959683617752842

Acevedo-Garcia, J., Kusch, S., and Panstruga, R. (2014). Magical mystery tour: MLO proteins in plant immunity and beyond. *New Phytol.* 204, 273–281. doi: 10.1111/nph.12889

Alba-Sánchez, F., Abel-Schaad, D., López-Sáez, J. A., Sabariego, R., Pérez-Díaz, S., and González-Hernández, A. (2018). Paleobiogeografía de abies spp. y *Cedrus atlantica* en el mediterráneo occidental (península ibérica y marruecos). *Ecosistemas* 27 (1), 26–37. doi: 10.7818/ECOS.1441

Alberto, F. J., Aitken, S. N., Alia, R., Gonzalez-Martinez, S. C., Hanninen, H., Kremer, A., et al. (2013). Potential for evolutionary responses to climate change evidence from tree populations. *Global Change Biol.* 19, 1645–1661. doi: 10.1111/gcb.12181

Allen, E., Moing, A., Wattis, J. A. D., Larson, T., Maucourt, M., Graham, I. A., et al. (2011). Evidence that ACN1 (acetate non-utilizing 1) prevents carbon leakage from peroxisomes during lipid mobilization in *Arabidopsis* seedlings. *Biochem. J.* 437 (3), 505–513. doi: 10.1042/BJ20101764

Altschul, S. F., Gish, W., Miller, W., Myers, E. W., and Lipman, D. J. (1990). Basic local alignment search tool. *J. Mol. Biol.* 215, 403–410. doi: 10.1016/S0022-2836(05)80360-2

Anders, S., McCarthy, D. J., Chen, Y., Okoniewski, M., Smyth, G. K., Huber, W., et al. (2013). Count-based differential expression analysis of RNA sequencing data using r and bioconductor. *Nat. Protoc.* 8, 1765–1786. doi: 10.1038/nprot.2013.099

Andrews, S. (2014) *FASTQC. a quality control tool for high throughput sequence data*. Available at: http://www.bioinformatics.babraham.ac.uk/projects/fastqc/.

Asada, K., Salim, V., Masada-Atsumi, S., Edmunds, E., Nagatoshi, M., Terasaka, K., et al. (2013). A 7-deoxyloganetic acid glucosyltransferase contributes a key step in secologanin biosynthesis in Madagascar periwinkle. *Plant Cell.* 25 (10), 4123–4134. doi: 10.1105/tpc.113.115154

Balasubramanian, V., Vashisht, D., Cletus, J., and Sakthivel, N. (2012). Plant β-1,3-glucanases: their biological functions and transgenic expression against phytopathogenic fungi. *Biotechnol. Lett.* 34, 1983–1990. doi: 10.1007/s10529-012-1012-6

Behringer, D., Zimmermann, H., Ziegenhagen, B., and Liepelt, S. (2015). Differential gene expression reveals candidate genes for drought stress response in *Abies alba* (Pinaceae). *PloS One* 10 (4), e0124564. doi: 10.1371/journal.pone.0124564

Bennett, A. C., McDowell, N. G., Allen, C. D., and Anderson-Teixeira, K. J. (2015). Larger trees suffer most during drought in forests worldwide. *Nat. Plants* 28, 15139. doi: 10.1038/nplants.2015.139

Bolger, A. M., Lohse, M., and Usadel, B. (2014). Trimmomatic: A flexible trimmer for illumina sequence data. *Bioinformatics* 30(15), 2114–20. doi: 10.1093/bioinformatics/btu170

Bray, N., Pimentel, H., Melsted, P., and Pachter, L. (2016). Near-optimal RNA-seq quantification. *Nat. Biotechnol.* 34, 525–527. doi: 10.1038/nbt.3519

Cao, X., Duan, W., Wei, C., Chen, K., Grierson, D., and Zhang, B. (2019). Genome-wide identification and functional analysis of carboxylesterase and methylesterase gene families in peach (*Prunus persica* l. batsch). *Front. Plant Sci.* 10. doi: 10.3389/fpls.2019.01511

Casacuberta, E., and González, J. (2013). The impact of transposable elements in environmental adaptation. *Mol. Ecol.* 22, 1503–1517. doi: 10.1111/mec.12170

Chang, Z., Li, G., Liu, J., Zhang, Y., Ashby, C., Liu, D., et al. (2015). Bridger: a new framework for *de novo* transcriptome assembly using RNA-seq data. *Genome Biol.* 16, 30. doi: 10.1186/s13059-015-0596-2

Chen, X., Ding, Y., Yang, Y., Song, C., Wang, B., Yang, S., et al. (2021). Protein kinases in plant responses to drought, salt, and cold stress. *J. Integr. Plant Biol.* 63, 53–78. doi: 10.1111/jipb.13061

Chen, D., Shao, Q., Yin, L., Younis, A., and Zheng, B. (2019). Polyamine function in plants: Metabolism, regulation on development, and roles in abiotic stress responses. *Front. Plant Sci.* 9. doi: 10.3389/fpls.2018.01945

Chiba, Y., Shimizu, T., Miyakawa, S., Kanno, Y., Koshiba, T., Kamiya, Y., et al. (2015). Identification of *Arabidopsis thaliana* NRT1/PTR FAMILY (NPF) proteins capable of transporting plant hormones. *J. Plant Res.* 128, 679–686. doi: 10.1007/s10265-015-0710-2

Cobo-Simón, I., Maloof, J. N., Li, R., Amini, H., Méndez-Cea, B., García-García, I., et al. (2022). Contrasting transcriptomic patterns reveal a genomic basis for drought resilience in the relict fir *Abies pinsapo* boiss. *Tree Physiol.* 43(2), 315–334. doi: 10.1093/treephys/tpac115

Cobo-Simón, I., Méndez-Cea, B., Jump, A., Seco, J. I., Gallego, F. J., and Linares, J. C. (2020). Understanding genetic diversity of relict forests. linking long-term isolation legacies and current habitat fragmentation in *Abies pinsapo* boiss. *For. Ecol. Manage.* 461, 117947. doi: 10.1016/j.foreco.2020.117947

Cobo-Simón, I., Méndez-Cea, B., Seco, J. I., Wegrzyn, J., Linares, J. C., and Gallego, F. J. (2021). Gene frequency shift in relict *Abies pinsapo* forests associated with drought-induced mortality: Preliminary evidence of local-scale divergent selection. *Forests* 12 (9), 1220. doi: 10.3390/f12091220

Conesa, A., Gotz, S., Garcia-Gomez, J. M., Terol, J., Talon, M., and Robles, M. (2005). Blast2GO: a universal tool for annotation, visualization and analysis in functional genomics research. *Bioinformatics* 21, 3674–3676. doi: 10.1093/bioinformatics/bti610

Cooper, B., Hutchison, D., Park, S., et al. (2003). Identification of rice (*Oryza sativa*) proteins linked to the cyclin-mediated regulation of the cell cycle. *Plant Mol. Biol.* 53, 273–279. doi: 10.1023/B:PLAN.0000007001.30865.0f

Coursol, S., Le Stunff, H., Lynch, D. V., Gilroy, S., Assmann, S. M., and Spiegel, S. (2005). *Arabidopsis* sphingosine kinase and the effects of phytosphingosine-1-phosphate on stomatal aperture. *Plant Physiol.* 137 (2), 724–737. doi: 10.1104/pp.104.055806

de Abreu-Neto, J. B., Turchetto-Zolet, A. C., de Oliveira, L. F. V., Bodanese Zanettini, M. H., and Margis-Pinheiro, M. (2013). Heavy metal-associated isoprenylated plant protein (HIPP): characterization of a family of proteins exclusive to plants. *FEBS J.* 280, 1604–1616. doi: 10.1111/febs.12159

Debeaujon, I., Peeters, A. J., Léon-Kloosterziel, K. M., and Koornneef, M. (2001). The TRANSPARENT TESTA12 gene of *Arabidopsis* encodes a multidrug secondary transporter-like protein required for flavonoid sequestration in vacuoles of the seed coat endothelium. *Plant Cell.* 13 (4), 853–871. doi: 10.1105/tpc.13.4.853

de Jesús-Pires, C., Ferreira-Neto, J. R. C., Pacifico-Bezerra-Neto, J., Kido, E. A., de Oliveira-Silva, R. L., Pandolfi, V., et al. (2020). Plant thaumatin-like proteins: Function, evolution and biotechnological applications. *Curr. Protein Pept. Sci.* 21 (1), 36–51. doi: 10.2174/1389203720666190318164905

de la Torre, A. R., Sekhwal, M. K., Puiu, D., Salzberg, S. L., Scott, A. D., Allen, B., et al. (2022). Genome-wide association identifies candidate genes for drought tolerance in coast redwood and giant sequoia. *Plant J.* 109, 7–22. doi: 10.1111/tpj.15592

Delteil, A., Gobbato, E., Cayrol, B., Esteva, J., Michel-Romiti, C., Dievart, A., et al. (2016). Several wall-associated kinases participate positively and negatively in basal defense against rice blast fungus. *BMC Plant Biol.* 16, 17. doi: 10.1186/s12870-016-0711-x

de María, N., Guevara, M. A., Perdiguero, P., Vélez, M. D., Cabezas, J. A, López-Hinojosa, M., et al. (2020). Molecular study of drought response in the Mediterranean conifer pinus pinaster ait.: Differential transcriptomic profiling reveals constitutive water deficit-independent drought tolerance mechanisms. *Ecol. Evol.* 10, 9788–9807. doi: 10.1002/ece3.6613

De Rienzo, F., Gabdoulline, R., Menziani, M. C., and Wade, R. (2000). Blue copper proteins: A comparative analysis of their molecular interaction properties. *Protein Sci.* 9, 1439–1454. doi: 10.1110/ps.9.8.1439

Dong, H., Bai, L., Zhang, Y., Zhang, G., Mao, Y., Min, L., et al. (2018). Modulation of guard cell turgor and drought tolerance by a peroxisomal acetate-malate shunt. *Mol. Plant* 11 (10), 1278–1291. doi: 10.1016/j.molp.2018.07.008

Eckardt, N. A. (2006). Function of γ-tubulin in plants. *Plant Cell.* 18 (6), 1327–1329. doi: 10.1105/tpc.106.043976

Fox, H., Doron-Faigenboim, A., Kelly, G., Bourstein, R., Attia, Z., Zhou, J., et al. (2018). Transcriptome analysis of *Pinus halepensis* under drought stress and during recovery. *Tree Physiol.* 38 (3), 423–441. doi: 10.1093/treephys/tpx137

Fujimoto, S. Y., Ohta, M., Usui, A., Shinshi, H., and Ohme-Takagi, M. (2000). *Arabidopsis* ethylene responsive element binding factors act as transcriptional activators or repressors of GCC box mediated gene expression. *Plant Cell.* 12, 393–404. doi: 10.1105/tpc.12.3.393

Gailing, O., Vornam, B., Leinemann, L., and Finkeldey, R. (2009). Genetic and genomic approaches to assess adaptive genetic variation in plants: forest trees as a model. *Physiol. Plantarum* 137, 509–519. doi: 10.1111/j.1399-3054.2009.01263.x

Garrison, G., and Marth, G. (2012). Haplotype-based variant detection from short-read sequencing. *ArXiv. Genomics* (q-bio.GN); Quantitative Methods (q-bio.QM). doi: 10.48550/arXiv.1207.3907

Grabherr, M. G., Haas, B. J., Yassour, M., Levin, J. Z., Thompson, D. A., Amit, I., et al. (2011). Full-length transcriptome assembly from RNA-seq data without a reference genome. *Nat. Biotechnol.* 29, 644–652. doi: 10.1038/nbt.1883

Grandbastien, M. A., Spielmann, A., and Caboche, M. (1989). Tnt1, a mobile retroviral-like transposable element of tobacco isolated by plant cell genetics. *Nature* 337, 376–380. doi: 10.1038/337376a0

Grundy, J., Stoker, C., and Carré, I. A. (2015). Circadian regulation of abiotic stress tolerance in plants. *Front. Plant Sci.* 6. doi: 10.3389/fpls.2015.00648

Guo, F. Q., Young, J., and Crawford, N. M. (2003). The nitrate transporter AtNRT1.1 (CHL1) functions in stomatal opening and contributes to drought susceptibility in *Arabidopsis*. *Plant Cell* 15, 107–117. doi: 10.1105/tpc.006312

Gupta, S. K., Rai, A. K., Kanwar, S. S., and Sharma, T. R. (2012). Comparative analysis of zinc finger proteins involved in plant disease resistance. *PloS One* 7 (8), e42578. doi: 10.1371/journal.pone.0042578

Haas, B. J., Papanicolaou, A., Yassour, M., Grabherr, M., Blood, P. D., Bowden, J., et al. (2013). *De novo* transcript sequence reconstruction from RNA-seq using the trinity platform for reference generation and analysis. *Nat. Protoc.* 8, 1494–1512. doi: 10.1038/nprot.2013.084

Hamiaux, C., Drummond, R. S., Janssen, B. J., Ledger, S. E., Cooney, J. M., Newcomb, R. D., et al. (2012). DAD2 is an α/β hydrolase likely to be involved in the perception of the plant branching hormone strigolactone. *Curr. Biol.* 22 (21), 2032–2036. doi: 10.1016/j.cub.2012.08.007

Hampe, A., and Jump, A. S. (2011). Climate relicts: Past, present and future. *Annu. Rev. Ecol. Evol. Syst.* 42, 313–333. doi: 10.1146/annurev-ecolsys-102710-145015

Hampe, A., and Petit, R. J. (2005). Conserving biodiversity under climate change: the rear edge matters. *Ecol. Lett.* 8, 461–467. doi: 10.1111/j.1461-0248.2005.00739.x

Haylock, M. R., Hofstra, N., Klein Tank, A. M. G., Klok, E. J., Jones, P. D., and New, M. (2008). A European daily high-resolution gridded data set of surface temperature and precipitation for 1950–2006. *J. Geophys. Res.* 113 (D20), D20119. doi: 10.1029/2008JD010201

Hsu, P. K., Dubeaux, G., Takahashi, Y., and Schroeder, J. I. (2021). Signaling mechanisms in abscisic acid-mediated stomatal closure. *Plant J.* 105, 307–321. doi: 10.1111/tpj.15067

Illingworth, C., and Michael, A. J. (2012). Plant ornithine decarboxylase is not post-transcriptionally feedback regulated by polyamines but can interact with a cytosolic ribosomal protein S15 polypeptide. *Amino Acids* 42, 519–527. doi: 10.1007/s00726-011-1029-5

Jaramillo-Correa, J., Grivet, D., Terrab, A., Kurt, Y., De Lucas, A. I., Wahid, N., et al. (2010). The strait of Gibraltar as a major biogeographic barrier in Mediterranean conifers: a comparative phylogeographic survey. *Mol. Ecol.* 19, 5452–5468. doi: 10.1111/j.1365-294X.2010.04912.x

Jones, P., Binns, D., Chang, H. Y., Fraser, M., Li, W., McAnulla, C., et al. (2014). InterProScan 5: genome-scale protein function classification. *Bioinformatics* 30, 1236–1240. doi: 10.1093/bioinformatics/btu031

Jump, A. S., and Peñuelas, J. (2005). Running to stand still: adaptation and the response of plants to rapid climate change. *Ecol. Lett.* 8, 1010–1020. doi: 10.1111/j.1461-0248.2005.00796.x

Kamrani, Y. Y., Shomali, A., Aliniaeifard, S., Lastochkina, O., Moosavi-Nezhad, M., Hajinajaf, N., et al. (2022). Regulatory role of circadian clocks on ABA production and signaling, stomatal responses, and water-use efficiency under water-deficit conditions. *Cells* 11 (7), 1154. doi: 10.3390/cells11071154

Kasprzewska, A. (2003). Plant chitinases–regulation and function. *Cell Mol. Biol. Lett.* 8 (3), 809–824.

Kaur, H., Manna, M., Thakur, T., Gautam, V., and Salvi, P. (2021). Imperative role of sugar signaling and transport during drought stress responses in plants. *Physiol. Plantarum* 171, 833–848. doi: 10.1111/ppl.13364

Kawecki, T. J. (2008). Adaptation to marginal habitats. *Annu. Rev. Ecol. Evol. Syst.* 39, 321–342. doi: 10.1146/annurev.ecolsys.38.091206.095622

Klupczyńska, E. A., and Ratajczak, E. (2021). Can forest trees cope with climate change? - effects of DNA methylation on gene expression and adaptation to environmental change. *Int. J. Mol. Sci.* 22 (24), 13524. doi: 10.3390/ijms222413524

Ko, J. H., Yang, S. H., and Han, K. H. (2006). Upregulation of an *Arabidopsis* RING-H2 gene, XERICO, confers drought tolerance through increased abscisic acid biosynthesis. *Plant J.* 47, 343–355. doi: 10.1111/j.1365-313X.2006.02782.x

Kolde, R. (2012). *Pheatmap: pretty heatmaps* R Package Version 1.0.10. https://CRAN.R-project.org/package=pheatmap

Langfelder, P., and Horvath, S. (2008). WGCNA: an r package for weighted correlation network analysis. *BMC Bioinf.* 9, 559. doi: 10.1186/1471-2105-9-559

Langfelder, P., and Horvath, S. (2012). Fast r functions for robust correlations and hierarchical clustering. *J. Stat. Software* 46 (11), 1–17. doi: 10.18637/jssv046.i11

Lanquar, V., Ramos, M. S., Lelievre, F., Barbier-Brygoo, H., Krieger-Liszkay, A., Kraemer, U., et al. (2010). Export of vacuolar manganese by AtNRAMP3 and AtNRAMP4 is required for optimal photosynthesis and growth under manganese deficiency. *Plant Physiol.* 152, 1986–1999. doi: 10.1104/pp.109.150946

Law, C. W., Chen, Y., Shi, W., and Smyth, G. K. (2014). Voom: precision weights unlock linear model analysis tools for RNA-seq read counts. *Genome Biol.* 15 (2), R29. doi: 10.1186/gb-2014-15-2-r29

Lechuga, V., Carraro, V., Viñegla, B., Carreira, J. A., and Linares, J. C. (2019). Carbon limitation and drought sensitivity at contrasting elevation and competition of *Abies pinsapo* forests. does experimental thinning enhance water supply and carbohydrates? *Forests* 10 (12), 1132. doi: 10.3390/f10121132

Lewis, D. R., Ramirez, M. V., Miller, N. D., Vallabhaneni, P., Ray, W. K., Helm, R. F., et al. (2011). Auxin and ethylene induce flavonol accumulation through distinct transcriptional networks. *Plant Physiol.* 156 (1), 144–164. doi: 10.1104/pp.111.172502

Li, H. (2011). A statistical framework for SNP calling, mutation discovery, association mapping and population genetical parameter estimation from sequencing data. *Bioinformatics* 27 (21), 2987–2993. doi: 10.1093/bioinformatics/btr509

Li, Y., Guo, Q., Liu, P., Huang, J., Zhang, S., Yang, G., et al. (2021). Dual roles of the serine/arginine-rich splicing factor SR45a in promoting and interacting with nuclear cap-binding complex to modulate the salt-stress response in. *Arabidopsis New Phytol.* 230, 641–655. doi: 10.1111/nph.17175

Li, L., He, Z., Pandey, G. K., Tsuchiya, T., and Luan, S. (2002). Functional cloning and characterization of a plant efflux carrier for multidrug and heavy metal detoxification. *J. Biol. Chem.* 277, 5360–5368. doi: 10.1074/jbc.M108777200

Li, L., Na, D., Hui, Z., and Chunxia, W. (2021). The versatile GABA in plants. *Plant Signaling Behavior* 16, 3. doi: 10.1080/15592324.2020.1862565

Li, B., Ruotti, V., Stewart, R. M., Thomson, J. A., and Dewey, C. N. (2010). RNA-Seq gene expression estimation with read mapping uncertainty. *Bioinformatics* 26, 493–500. doi: 10.1093/bioinformatics/btp692

Li, H., and Durbin, R. (2009). Fast and accurate short read alignment with Burrows–Wheeler transform. *Bioinformatics* 25(14), 1754–1760. doi: 10.1093/bioinformatics/btp324

Liepelt, S., Mayland-Quellhorst, E., Lahme, M., and Ziegenhagen, B. (2010). Contrasting geographical patterns of ancient and modern genetic lineages in Mediterranean *Abies* species. *Plant Syst. Evol.* 284, 141–151. doi: 10.1007/s00606-009-0247-8

Linares, J. C. (2011). Biogeography and evolution of *Abies* (*Pinaceae*) in the Mediterranean basin. the roles of long-term climatic changes and glacial refugia. *J. Biogeogr.* 38, 619–630. doi: 10.1111/j.1365-2699.2010.02458.x

Linares, J. C., Covelo, F., Carreira, J. A., and Merino, J. (2012). Phenological and water-use patterns underlying maximum growing season length at the highest elevations: implications under climate change. *Tree Physiol.* 32, 161–170. doi: 10.1093/treephys/tps003

Liu, Y., and El-Kassaby, Y. A. (2019). Novel insights into plant genome evolution and adaptation as revealed through transposable elements and non-coding RNAs in conifers. *Genes (Basel)* 10 (3), 228. doi: 10.3390/genes10030228

Lloret, F., Keeling, E. G., and Sala, A. (2011). Components of tree resilience: effects of successive low-growth episodes in old ponderosa pine forests. *Oikos* 120, 1909–1920. doi: 10.1111/j.1600-0706.2011.19372.x

Luo, M., Tai, R., Yu, C. W., Yang, S., Chen, C. Y., Lin, W. D., et al. (2015). Regulation of flowering time by the histone deacetylase HDA5 in. *Arabidopsis Plant J.* 82, 925–936. doi: 10.1111/tpj.12868

Marino, D., Froidure, S., Canonne, J., Ben Khaled, S., Khafif, M., Pouzet, C., et al. (2013). *Arabidopsis* ubiquitin ligase MIEL1 mediates degradation of the transcription factor MYB30 weakening plant defence. *Nat. Commun.* 4, 1476. doi: 10.1038/ncomms2479

McCarthy, J. D., Chen, Y., and Smyth, K. G. (2012). Differential expression analysis of multifactor RNA-seq experiments with respect to biological variation. *Nucleic Acids Res.* 40 (10), 4288–4297. doi: 10.1093/nar/gks042

McHale, L., Tan, X., Koehl, P., and Michelmore, R. W. (2006). Plant NBS-LRR proteins: adaptable guards. *Genome Biol.* 7, 212. doi: 10.1186/gb-2006-7-4-212

Mencuccini, M., Minunno, F., Salmon, Y., Martínez-Vilalta, J., and Hölttä, T. (2015). Coordination of physiological traits involved in drought-induced mortality of woody plants. *New Phytol.* 208, 96–409. doi: 10.1111/nph.13461

Miao, Z., Han, Z., Zhang, T., Chen, S., and Ma, C. (2017). A systems approach to a spatio-temporal understanding of the drought stress response in maize. *Sci. Rep.* 7, 6590. doi: 10.1038/s41598-017-06929-y

Minic, Z. (2008). Physiological roles of plant glycoside hydrolases. *Planta* 227 (4), 723–740. doi: 10.1007/s00425-007-0668-y

Mita, P., and Boeke, J. D. (2016). How retrotransposons shape genome regulation. *Curr. Opin. Genet. Dev.* 37, 90–100. doi: 10.1016/j.gde.2016.01.001

Moenga, S. M., Gai, Y., Carrasquilla-Garcia, N., Perilla-Henao, L. M., and Cook, D. R. (2020). Gene co-expression analysis reveals transcriptome divergence between wild and cultivated chickpea under drought stress. *Plant J.* 104, 1195–1214. doi: 10.1111/tpj.14988

Moran, E., Lauder, J., Musser, C., Stathos, A., and Shu, M. (2017). The genetics of drought tolerance in conifers. *New Phytol.* 216, 1034–1048. doi: 10.1111/nph.14774

Munné-Bosch, S., Falara, V., Pateraki, I., López-Carbonella, M., Cela, J., and Kanellis, A. K. (2009). Physiological and molecular responses of the isoprenoid biosynthetic pathway in a drought-resistant Mediterranean shrub, *Cistus creticus* exposed to water deficit. *J. Plant Physiol.* 166 (2), 136–145. doi: 10.1016/j.jplph.2008.02.011

Nakabayashi, R., Yonekura-Sakakibara, K., Urano, K., Suzuki, M., Yamada, Y., Nishizawa, T., et al. (2014). Enhancement of oxidative and drought tolerance in *Arabidopsis* by overaccumulation of antioxidant flavonoids. *Plant J.* 77 (3), 367–379. doi: 10.1111/tpj.12388

Neale, D., and Kremer, A. (2011). Forest tree genomics: growing resources and applications. *Nat. Rev. Genet.* 12, 111–122. doi: 10.1038/nrg2931

Nystedt, B., Street, N. R., Wetterbom, A., Zuccolo, A., Lin, Y. C., Scofield, D. G., et al. (2013). The Norway spruce genome sequence and conifer genome evolution. *Nature* 497 (7451), 579–584. doi: 10.1038/nature12211

Pandey, A., Rajamani, U., Verma, J., Subba, P., Chakraborti, N., Datta, A., et al. (2010). Identification of extracellular matrix proteins of rice (*Oryza sativa* l.) involved in dehydration-responsive network: A proteomic approach. *J. Proteome Res.* 9, 3443–3464. doi: 10.1021/pr901098p

Qi, Z., and Xiong, L. (2013). Characterization of a purine permease family gene OsPUP7 involved in growth and development control in rice. *J. Integr. Plant Biol.* 55 (11), 1119–1135. doi: 10.1111/jipb.12101

Qiao, C. Y., Ran, J. H., Li, Y., and Wang, X. Q. (2007). Phylogeny and biogeography of *Cedrus* (*Pinaceae*) inferred from sequences of seven paternal chloroplast and maternal mitochondrial DNA regions. *Ann. Bot.* 100 (3), 573–580. doi: 10.1093/aob/mcm134

Qin, Y. M., Hu, C. Y., Pang, Y., Kastaniotis, A. J., Hiltunen, J. K., and Zhu, Y. X. (2007). Saturated very-Long-Chain fatty acids promote cotton fiber and *Arabidopsis* cell elongation by activating ethylene biosynthesis. *Plant Cell.* 19 (11), 3692–3704. doi: 10.1105/tpc.107.054437

Rani, A., Singh, K., Ahuja, P. S., and Kumar, S. (2012). Molecular regulation of catechins biosynthesis in tea [*Camellia sinensis* (L.) o. kuntze]. *Gene* 495, 205–210. doi: 10.1016/j.gene.2011.12.029

Robinson, M. D., McCarthy, D. J., and Smyth, G. K. (2010). edgeR: a bioconductor package for differential expression analysis of digital gene expression data. *Bioinformatics* 26 (1), 139–140. doi: 10.1093/bioinformatics/btp616

Robinson, M. D., and Oshlack, A. (2010). A scaling normalization method for differential expression analysis of RNA-seq data. *Genome Biol.* 11, R25. doi: 10.1186/gb-2010-11-3-r25

Rottmann, T., Klebl, F., Schneider, S., Kischka, D., Rüscher, D., Sauer, N., et al. (2018). Sugar transporter STP7 specificity for l-arabinose and d-xylose contrasts with the typical hexose transporters STP8 and STP12. *Plant Physiol.* 176 (3), 2330–2350. doi: 10.1104/pp.17.01493

Ruiz-Medrano, R., Jimenez-Moraila, B., Herrera-Estrella, L., and Rivera-Bustamante, R. F. (1992). Nucleotide sequence of an osmotin-like cDNA induced in tomato during viroid infection. *Plant Mol. Biol.* 20 (6), 1199–1202. doi: 10.1007/BF00028909

Salekdeh, G. H., Siopongco, J., Wade, L. J., Ghareyazie, B., and Bennett, J. (2002). Proteomic analysis of rice leaves during drought stress and recovery. *Proteomics* 2, 1131–1145. doi: 10.1002/1615-9861(200209)2:9<1131::AID-PROT1131>3.0.CO;2-1

Sanchez-Salguero, R., Ortíz, C., Covelo, F., Ochoa, V., García-Ruíz, R., Seco, J. I., et al. (2015). Regulation of water use in the southernmost European fir (*Abies pinsapo* boiss.): Drought avoidance matters. *Forests* 6, 2241–2260. doi: 10.3390/f6062241

Scaltsoyiannes, A., Tsaktsira, M., and Drouzas, A. D. (1999). Allozyme differentiation in the Mediterranean firs (*Abies*, pinaceae). a first comparative study with phylogenetic implications. *P1. Syst. Evol.* 216, 289–307. doi: 10.1007/BF01084404

Schueler, S., George, J. P., Karanitsch-Ackerl, S., Mayer, K., Klumpp, R. T., and Grabner, M. (2021). Evolvability of drought response in four native and non-native conifers: Opportunities for forest and genetic resource management in Europe. *Front. Plant Sci.* 12. doi: 10.3389/fpls.2021.648312

Sexton, J. P., McIntyre, P. J., Angert, A. L., and Rice, K. J. (2009). Evolution and ecology of species range limits. *Annu. Rev. Ecol. Evolution Systematics* 40, 415–436. doi: 10.1146/annurev.ecolsys.110308.120317

Shannon, P., Markiel, A., Ozier, O., Baliga, N. S., Wang, J. T., Ramage, D., et al. (2003). Cytoscape: a software environment for integrated models of biomolecular interaction networks. *Genome Res.* 13 (11), 2498–2504. doi: 10.1101/gr.1239303

Shi, C., Baldwin, I. T., and Wu, J. (2012). *Arabidopsis* plants having defects in nonsense-mediated mRNA decay factors UPF1, UPF2, and UPF3 show photoperiod-dependent phenotypes in development and stress responses. *J. Integr. Plant Biol.* 54, 99–114. doi: 10.1111/j.1744-7909.2012.01093.x

Simão, F., Waterhouse, R. M., Ioannidis, P., Kriventseva, E. V., and Zdobnov, E. M. (2015). BUSCO: assessing genome assembly and annotation completeness with single-copy orthologs. *Bioinformatics* 31 (19), 3210–3212. doi: 10.1093/bioinformatics/btv351

Sohn, J. A., Ammer, C., Bauhus, J., Häberle, K.-H., Matyssek, R., and Grams, T. E. E. (2013). Mitigation of drought by thinning: short-term and long-term effects on growth and physiological performance of Norway spruce (*Picea abies*). *For. Ecol. Manage.* 308, 188–197. doi: 10.1016/j.foreco.2013.07.048

Spinelli, F., Cellini, A., Marchetti, L., Nagesh, K. M., and Piovene, C. (2011). "Emission and function of volatile organic compounds in response to abiotic stress," in *Abiotic stress inplants-mechanisms and adaptations*. Eds. A. Shanker and B. Venkateswarlu (West Palm Beach: InTech).

Stapley, J., Santure, A. W., and Dennis, S. R. (2015). Transposable elements as agents of rapid adaptation may explain the genetic paradox of invasive species. *Mol. Ecol.* 24, 2241–2252. doi: 10.1111/mec.13089

Stein, O., and Granot, D. (2018). Plant fructokinases: Evolutionary, developmental, and metabolic aspects in sink tissues. *Front. Plant Sci.* 9. doi: 10.3389/fpls.2018.00339

Stelter, P., Kunze, R., Flemming, D., Höpfner, D., Diepholz, M., Philippsen, P., et al. (2007). Molecular basis for the functional interaction of dynein light chain with the nuclear-pore complex. *Nat. Cell Biol.* 9, 788–796. doi: 10.1038/ncb1604

Sun, S. Y., Chao, D. Y., Li, X. M., Shi, M., Gao, J. P., Zhu, M. Z., et al. (2009). OsHAL3 mediates a new pathway in the light-regulated growth of rice. *Nat. Cell Biol.* 11, 845–851. doi: 10.1038/ncb1892

Supek, F., Bošnjak, M., Škunca, N., and Šmuc, T. (2011). REVIGO summarizes and visualizes long lists of gene ontology terms. *PloS One* 6 (7), e21800. doi: 10.1371/journal.pone.0021800

Synek, L., Schlager, N., Eliáš, M., Quentin, M., Hauser, M.-T., and Žárský, V. (2006). AtEXO70A1, a member of a family of putative exocyst subunits specifically expanded in land plants, is important for polar growth and plant development. *Plant J.* 48, 54–72. doi: 10.1111/j.1365-313X.2006.02854.x

Taura, F., Sirikantaramas, S., Shoyama, Y., Yoshikai, K., Shoyama, Y., and Morimoto, S. (2007). Cannabidiolic-acid synthase, the chemotype-determining enzyme in the fiber-type *Cannabis sativa*. *FEBS Lett.* 581 (16), 2929–2934. doi: 10.1016/j.febslet.2007.05.043

Tenhaken, R. (2015). Cell wall remodeling under abiotic stress. *Front. Plant Sci.* 5. doi: 10.3389/fpls.2014.00771

Trapnell, C., Hendrickson, D. G., Sauvageau, M., Goff, L., Rinn, J. L., and Pachter, L. (2013). Differential analysis of gene regulation at transcript resolution with RNA-seq. *Nat. Biotechnol.* 31, 46–53. doi: 10.1038/nbt.2450

Trujillo-Moya, C., George, J. P., Fluch, S., Geburek, T., Grabner, M., Karanitsch-Ackerl, S., et al. (2018). Drought sensitivity of Norway spruce at the species' warmest fringe: quantitative and molecular analysis reveals high genetic variation among and within provenances. *G3 (Bethesda)* 8, 1225–1245. doi: 10.1534/g3.117.300524

Vaghela, B., Vashi, R., Rajput, K., and Joshi, R. (2022). Plant chitinases and their role in plant defense: A comprehensive review. *Enzyme Microb. Technol.* 159, 110055. doi: 10.1016/j.enzmictec.2022.110055

Vu, K. V., Jeong, C. Y., Nguyen, T. T., Dinh, T. T. H., Lee, H., and Hong, S. W. (2019). Deficiency of AtGFAT1 activity impairs growth, pollen germination and tolerance to tunicamycin in arabidopsis. *J. Exp. Botany* 70 (6), 1775–1787. doi: 10.1093/jxb/erz055

Yang, Q., Liu, K., Niu, X., Wang, Q., Wan, Y., Yang, F., et al. (2018). Genome-wide identification of PP2C genes and their expression profiling in response to drought and cold stresses in *Medicago truncatula*. *Sci. Rep.* 8, 1284. doi: 10.1038/s41598-018-29627-9

Young, M. D., Wakefield, M. J., Smyth, G. K., and Oshlack, A. (2010). Gene ontology analysis for RNA-seq: accounting for selection bias. *Genome Biol.* 11, R14. doi: 10.1186/gb-2010-11-2-r14

Zhang, X., Zhuang, L., Liu, Y., Yang, Z., and Huang, B. (2020). Protein phosphorylation associated with drought priming-enhanced heat tolerance in a temperate grass species. *Horticulture Res.* 7, 207. doi: 10.1038/s41438-020-00440-8

Zhu, J. K. (2016). Abiotic stress signaling and responses in plants. *Cell* 167 (2), 313–324. doi: 10.1016/j.cell.2016.08.029

Zimmermann, I. M., Heim, M. A., Weisshaar, B., and Uhrig, J. F. (2004). Comprehensive identification of arabidopsis thaliana MYB transcription factors interacting with R/B-like BHLH proteins. *Plant J.* 40, 22–34. doi: 10.1111/j.1365-313X.2004.02183.x

frontiers | Frontiers in Plant Science

TYPE Original Research
PUBLISHED 21 April 2023
DOI 10.3389/fpls.2023.1164151

Check for updates

OPEN ACCESS

EDITED BY
Mehdi Rahimi,
Graduate University of Advanced Technology, Iran

REVIEWED BY
Vijay Sheri,
East Carolina University, United States
Yunhe Jiang,
China Agricultural University, China

*CORRESPONDENCE
Dali Liu
daliliu_hlju@163.com
Wang Xing
xyjiayou_086@163.com

†These authors have contributed equally to this work

SPECIALTY SECTION
This article was submitted to Plant Abiotic Stress, a section of the journal Frontiers in Plant Science

RECEIVED 12 February 2023
ACCEPTED 31 March 2023
PUBLISHED 21 April 2023

CITATION
Li J, Liu X, Xu L, Li W, Yao Q, Yin X, Wang Q, Tan W, Xing W and Liu D (2023) Low nitrogen stress-induced transcriptome changes revealed the molecular response and tolerance characteristics in maintaining the C/N balance of sugar beet (*Beta vulgaris* L.). *Front. Plant Sci.* 14:1164151. doi: 10.3389/fpls.2023.1164151

COPYRIGHT
© 2023 Li, Liu, Xu, Li, Yao, Yin, Wang, Tan, Xing and Liu. This is an open-access article distributed under the terms of the Creative Commons Attribution License (CC BY). The use, distribution or reproduction in other forums is permitted, provided the original author(s) and the copyright owner(s) are credited and that the original publication in this journal is cited, in accordance with accepted academic practice. No use, distribution or reproduction is permitted which does not comply with these terms.

Low nitrogen stress-induced transcriptome changes revealed the molecular response and tolerance characteristics in maintaining the C/N balance of sugar beet (*Beta vulgaris* L.)

Jiajia Li[1,2†], Xinyu Liu[1,2,3], Lingqing Xu[1,2], Wangsheng Li[1,2], Qi Yao[1,2,3], Xilong Yin[1,2], Qiuhong Wang[1,2], Wenbo Tan[1,2], Wang Xing[1,2*] and Dali Liu[1,2*†]

[1]National Beet Medium-term Gene Bank, Heilongjiang University, Harbin, China, [2]Key Laboratory of Sugar Beet Genetics and Breeding, Heilongjiang Province Common College/College of Advanced agriculture and ecological environment, Heilongjiang University, Harbin, China, [3]Key Laboratory of Molecular Biology, School of Life Sciences, Heilongjiang University, Harbin, China

Nitrogen (N) is an essential macronutrient for plants, acting as a common limiting factor for crop yield. The application of nitrogen fertilizer is related to the sustainable development of both crops and the environment. To further explore the molecular response of sugar beet under low nitrogen (LN) supply, transcriptome analysis was performed on the LN-tolerant germplasm '780016B/12 superior'. In total, 580 differentially expressed genes (DEGs) were identified in leaves, and 1,075 DEGs were identified in roots ($\log_2^{|FC|} \geq 1$; q value < 0.05). Gene Ontology (GO), protein–protein interaction (PPI), and Kyoto Encyclopedia of Genes and Genomes (KEGG) analyses clarified the role and relationship of DEGs under LN stress. Most of the downregulated DEGs were closely related to "photosynthesis" and the metabolism of "photosynthesis-antenna proteins", "carbon", "nitrogen", and "glutathione", while the upregulated DEGs were involved in flavonoid and phenylalanine biosynthesis. For example, *GLUDB* (glutamate dehydrogenase B) was identified as a key downregulated gene, linking carbon, nitrogen, and glutamate metabolism. Thus, low nitrogen-tolerant sugar beet reduced energy expenditure mainly by reducing the synthesis of energy-consuming amino acids, which in turn improved tolerance to low nitrogen stress. The glutathione metabolism biosynthesis pathway was promoted to quench reactive oxygen species (ROS) and protect cells from oxidative damage. The expression levels of nitrogen assimilation and amino acid transport genes, such as *NRT2.5* (high-affinity nitrate transporter), *NR* (nitrate reductase [NADH]), *NIR* (ferredoxin-nitrite reductase), *GS* (glutamine synthetase leaf isozyme), *GLUDB, GST* (glutathione transferase) and *GGT3* (glutathione hydrolase 3) at low nitrogen levels play a decisive role in nitrogen utilization and may affect the conversion of the carbon skeleton. *DFRA* (dihydroflavonol 4-reductase) in roots was negatively correlated with *NIR* in leaves (coefficient = −0.98, $p < 0.05$), suggesting that there may be corresponding remote regulation between "flavonoid biosynthesis" and

"nitrogen metabolism" in roots and leaves. *FBP* (fructose 1,6-bisphosphatase) and *PGK* (phosphoglycerate kinase) were significantly positively correlated ($p < 0.001$) with Ci (intercellular CO_2 concentration). The reliability and reproducibility of the RNA-seq data were further confirmed by real-time fluorescence quantitative PCR (qRT–PCR) validation of 22 genes ($R^2 = 0.98$). This study reveals possible pivotal genes and metabolic pathways for sugar beet adaptation to nitrogen-deficient environments.

KEYWORDS

sugar beet, low nitrogen stress, transcriptome, photosynthesis, carbon and nitrogen balance, nitrogen assimilation and transport

1 Introduction

The current world population is 7.7 billion, and China accounts for 1/5 of the total population (O'Sullivan, 2021). Increasing crop yield has been one of the key objectives to meet the needs of China's growing population and global agricultural production. Nitrogen (N) is an important mineral element essential for plant life activities and a major limiting factor for crop yield, especially for sugar beet (*Beta vulgaris* L.). In both developed and developing countries, large amounts of nitrogen fertilizers are applied to meet crop demand (Zhang et al., 2015). However, such operations have led to serious biodiversity and environmental pollution problems and threaten human health (Xu et al., 2017; Ren et al., 2021). As an essential sugar and economic crop (Peleman and van der Voort, 2003; Simões et al., 2016), sugar beet is mainly distributed in northeast, northwest, and north China (Chen et al., 2017). N provides beets with nutrients, and proper N application has attracted increasing attention in recent years for high yield and sugar production of taproots.

In plants, N limitation causes leaf yellowing and plant biomass reduction. Low N application was found to reduce total plant nutrient accumulation and adversely affect yield (Pan et al., 2016). However, Yin et al. (2019) found that N deficiency optimized the distribution of N within wheat and therefore maintained or increased the yield of the grain. This indicates that nitrogen regulation and utilization is a complex process, and different plants in different nitrogen-deficient environments may have similar and different response mechanisms.

Photosynthesis is an important biological process that affects the accumulation of energy and dry matter in plants. The photosystem consists of two parts, photosystem II (PSII) and photosystem I (PSI), including a complex of proteins and photosynthetic pigments (e.g., chlorophyll) that absorb, transmit, and convert light energy. Transcriptome analysis revealed that low nitrogen stress reduced the expression levels of genes related to the apple antenna system, light absorption, and electron transfer (Wen et al., 2022). A reduction in photosynthesis ultimately leads to a decrease in biomass production and yield (Shi et al., 2022). Glycolysis, the pentose phosphate pathway (PPP), and the tricarboxylic acid (TCA) cycle are the major metabolic pathways in plants and are influenced by nitrogen supply, providing energy and carbon skeletons for other metabolic pathways. Carbon (C) metabolism and nitrogen metabolism in plants are closely coordinated, and their balance is crucial.

The C metabolism and N metabolism of plants are closely coordinated with each other (Bao et al., 2015) and require a common reducing power, ATP, and carbon skeleton (Sweetlove et al., 2010). Under stress conditions, they exhibit complex and diverse responses to abiotic stresses by altering gene and protein expression as well as primary and secondary metabolites (Bhatotia et al., 2015; Onaga and Wydra, 2016). During nitrogen starvation, various defective response genes act to maintain plant survival by altering root architecture (Li et al., 2023), improving nitrogen assimilation (Imamura et al., 2009), and increasing lignin content (Tian et al., 2022). The phenylpropanoid metabolic pathway is closely related to lignin synthesis (Cong et al., 2013), whose pathway is closely related to photosynthetic carbon utilization (Zhang et al., 2018c). Phenylpropanoid polymers such as lignin are mechanical supports for plant growth and facilitate the long-distance transport of water and nutrients (Zhao, 2016). Studies have shown that the enzymatic activities of *PAL*, *4CL*, *CAD*, and *POD* and their corresponding gene expression in lignified tissues affect lignin biosynthesis in bamboo shoots, indicating that these enzymes play key roles in lignin biosynthesis (Zheng et al., 2020). Naringenin is a member of the flavonoid family and is the starting point for the synthesis of a variety of other flavonoid molecules. Drought stress induces the expression of the flavonoid structural genes *CHS*, *CHI*, *FLS*, and *DFR*, which leads to the accumulation of flavonoids such as anthocyanins and improves the tolerance of ginkgo to drought (Yu et al., 2022). Plant flavonoid compounds, especially anthocyanins and rutin, also play a crucial role under nitrogen deficiency conditions (Shen et al., 2022). Carbon metabolism provides the carbon source and energy for nitrogen metabolism (Nunes-Nesi et al., 2010), while nitrogen metabolism provides enzymes and photosynthetic pigments for carbon metabolism. Glutamate is used for the synthesis of N compounds such as proteins and nucleic acids. When the GS/GOGAT cycle assimilates NH_3, the carbon skeleton needs to be continuously replenished to meet the demand for N associated with plant growth (Liao et al., 2022). Thus, glutamate metabolism can directly link nitrogen to carbon metabolism.

In recent years, continuous progress in sequencing technologies has provided an efficient way to identify functional genes and study their regulatory mechanisms, and the sugar beet genome has also been extensively developed (Dohm et al., 2014; Wascher et al., 2022). Previously, we explored the tolerance and adaptation characteristics of different sugar beet germplasms at both morphological and physiological levels under low N (LN) environments (Li et al., 2022; Li et al., 2023). However, there are still some important phenomena in this process that need to be explained through relevant molecular regulation. Thus, in this study, the sugar beet low N-tolerant germplasm '780016B/12 superior' was subjected to both low N and normal N conditions. Using RNA-seq, we attempted to identify possible metabolic pathways and clarify the functions of candidate genes of sugar beet involved in the response to nitrogen deficiency. This study will help to improve the understanding of the mechanism of the sugar beet response to low N stress and provide a theoretical basis for proper N utilization in sugar beet.

2 Materials and methods

2.1 Plant materials and growing conditions

The experiment was conducted at the National Beet Medium-Term Gene Bank (Harbin, China) using '780016B/12 superior' sugar beet germplasm as the test material. The intact and uniform seeds were sterilized in ethanol (75%) for 1 min and then washed three times in distilled water. Subsequently, they were sown in seedling trays containing vermiculite. After 9 days of cultivation, seedlings with consistent growth were selected and grown in Hoagland nutrient solution. There were two N-level treatments, LN treatment (0.5 mmol/L N) and normal N (CV, 5 mmol/L N), which were adjusted by the dose of KNO_3 and $Ca(NO_3)_2$ in the modified Hoagland nutrient solution. Seedlings with two pairs of fully expanded leaves (approximately 2 weeks) were subjected to LN. After 12 h of treatment, samples were immediately frozen in liquid nitrogen and then refrigerated at −80°C until RNA was extracted. The hydroponic conditions were 25°C/18°C (day/night) with a 14 h light/10 h dark cycle, 45%–55% relative humidity, and a light intensity of 200 μmol/(m^2·s^{-1}). Each treatment was repeated three times.

2.2 Determination of physiological indexes

A CI-340 photosynthesis instrument (Sidi Ecological Instrument Co., Ltd., Beijing, China) was used to determine the net photosynthetic rate (Pn), transpiration rate (Tr), stomatal conductivity (Gs), and intercellular CO_2 concentration (Ci). The second pair of fully expanded true leaves of sugar beet seedlings was measured. Five seedlings of each treatment were dried, and the roots and leaves were ground separately into powder. First, 0.1 g of the sample was digested with potassium sulfate and copper sulfate as catalysts and concentrated sulfuric acid (sulfuric acid), and the nitrogen content was determined using a Hanon K1100 automatic Kjeldahl nitrogen tester (Hanon Instrument Co., Ltd., Shandong, China). The N content (N uptake) was presented as mg per plant.

Correlations between nitrogen-stressed photosynthetic indexes and differentially expressed genes (DEGs) under LN were analyzed using Pearson's correlation statistics. Independent samples t-tests were performed using SPSS statistical software (version 26.0, SPSS, Chicago, IL, USA). All analyses were performed with $p < 0.05$, 0.01, or 0.001 as the significance levels.

2.3 Illumina sequencing, data analysis, and DEG annotation

After the determination of RNA concentration, purity, and integrity, the cDNA libraries were sequenced using the Illumina high-throughput sequencing platform (NovaSeq 6000, San Diego, CA, USA). The raw reads with low quality, junction contamination, and high content of unknown bases were filtered to obtain clean reads and analyzed for guanine–cytosine (GC) content, Q20, and Q30. HISAT2 was used to align clean reads to the sugar beet reference genome RefBeet-1.2.2. Fragments per kilobase per million fragments localized transcripts (FPKM) values were calculated for each gene in the samples using StringTie software to quantify its expression abundance and variation. EdgeR software (available online: http://www.r-project.org/) was used to screen for DEGs q value <0.05, $\log_2^{|FC|} \geq 1$) (Cosgrove, 2016). Functional enrichment of DEGs was determined using the Gene Ontology (GO) (available online: http://www.r-project.org/) and Kyoto Encyclopedia of Genes and Genomes (KEGG) database (available online: http://kobas.cbi.pku.edu.cn/). We used p-values calculated by hypergeometric tests and corrected by FDR with FDR ≤0.05 as the threshold to identify significant functional categories and metabolic pathways.

2.4 Protein interaction network construction

The protein–protein interaction (PPI) network of DEG-encoded proteins identified by transcriptomic analysis was constructed using the STRING v11.5 online database (https://string-db.org/). PPI networks were constructed by targeting upregulated and downregulated DEGs. The core genes were further screened using Cytoscape software v3.9.1 (http://www.cytoscape.org/). The nodes represent proteins, and the connected edges illustrate the relevant interactions between proteins in the PPI network.

2.5 Bioinformatics analysis

The amino acid sequences of sugar beet BvGLUDB (BVRB_3g056180) and BvDFRA (BVRB_1g007170) were used to identify homologous sequences in the NCBI database. The alignment and domain analyses of proteins were performed using Espript3.

2.6 Real-time fluorescence quantitative PCR

Total RNA was extracted from sugar beet roots and leaves using RNA-easy Isolation Reagent (Vazyme R701, Nanjing Novozymes Biotech Co., Nanjing, China). RNA concentration and the OD_{260}/OD_{230} and OD_{260}/OD_{280} were determined. The cDNA was reverse transcribed according to the TranScript One-Step gDNA Removal and cDNA Synthesis SuperMix protocol (AT311, Beijing All Style Gold Biotechnology Co., Beijing, China). qPCR was performed on a real-time fluorescence quantitative PCR instrument (Thermo Fisher Scientific Instruments, Shanghai, China; QuantStudio™ 1 Plus) using the SuperReal PreMix Plus kit (Tiangen Biochemical Technology Co., Beijing, China; version FP210831). The PCR procedure was as follows: predenaturation at 95°C for 15 min; 40 cycles of denaturation at 95°C for 10 s, annealing at 60°C for 20 s, and extension at 72°C for 32 s; and a melting curve at 65°C–95°C. *BvGAPDH* (NC_ 024800) was selected as the internal reference gene. The primers were designed using the NCBI database tool (Supplementary Table 1). The real-time fluorescence quantitative PCR (qRT–PCR) analysis was repeated three times for each sample. Correlation coefficients of RNA-seq and qRT–PCR data were plotted and calculated using Origin (version 2021) graphing software.

3 Results

3.1 Transcriptome sequencing and alignment

To clarify the regulatory profile of genes related to nitrogen metabolism in sugar beet seedlings under LN stress, the transcriptional changes in the LN-tolerant germplasm (780016B/12 superior) were investigated by RNA sequencing after 0.5 mmol/L N treatment for 12 h. A total of 1,130,329,346 raw reads and 1,088,994,086 clean reads (Supplementary Table 2) were obtained. The GC content ranged from 41.08% to 43.15%, and the Q20 and Q30 values were >97.01% and >92.66%, respectively. Compared with the sugar beet reference genome (RefBeet-1.2.2), the alignment rate within each treatment group was > 98%. Therefore, the depth of this sequencing was sufficient. Principal component analysis (PCA) of the transcriptome showed a high degree of similarity between the three biological replicates within each treatment group. A clear separation of CV_R and LN_R data was observed, while a closer distance between CV_L and LN_L was detected (Figure 1). This indicated that short-term N deficiency influenced more transcription products in roots than in leaves.

3.2 Differentially expressed genes in leaves and roots of sugar beet seedlings under LN

The transcript levels of the DEGs were measured using FPKM as a metric, which takes into account the effects of sequencing depth and gene length on fragment count. LN-responsive genes were further screened ($\log_2^{|FC|} \geq 1$; q value < 0.05). A total of 580 DEGs were identified in leaves, of which 91 were upregulated and 489 were downregulated (Figure 2A). A total of 1,075 DEGs were found in roots, of which 689 were upregulated and 386 were downregulated (Figure 2B). The number of DEGs in roots was greater and more significant than those in leaves, which might be because roots were the first to respond to stress stimuli.

In the top 20 significantly upregulated ($\log_2^{FC} \geq 1$; q value < 0.05) and downregulated ($\log_2^{FC} \leq -1$; q value < 0.05) DEGs (Figure 3, Supplementary Table 3), the differential expression fold changes were all above 5; in roots, between 6.115 and 9.814 were upregulated and between −14.907 and −7.112 were downregulated; and in leaves, between 6.792 and 13.464 were upregulated and between −13.562 and −5.424 were downregulated. Among them, vacuolar sorting protein 39 (*VPS39*, XM_019250064.1) and cytochrome P450 (*CYP76AD1*, XM_010697501.2/CYP72A397, and XM_010685350.2/XM_010685351.2/XM_010678432.2) were transcribed at high levels in both leaves and roots of sugar beet and might play important roles in LN tolerance in sugar beet.

The transcription factors BIM2 (*BIM2*, XM_019249651.1) and bHLH67 (*BHLH67*, XM_019251340.1) were found to be upregulated in leaves ($\log_2^{FC}$ = 12.620 and $\log_2^{FC}$ = 10.580). In addition, 6,7,8-trihydroxycoumarin synthase (*CYP71AZ3*, XM_010672674.2) and arginine—tRNA ligase, chloroplastic/mitochondrial (*EMB1027*, XM_010680324.2) were also upregulated in leaves ($\log_2^{FC}$ = 7.814 and $\log_2^{FC}$ = 7.028); quinolinate synthase, chloroplastic (*QS*, XM_019247621.1) and gibberellin 3-beta-dioxygenase 1 (*GA3OX1*, XM_010692935.2) were downregulated in leaves ($\log_2^{FC}$ = −6.023 and $\log_2^{FC}$ = −6.224). In roots, NRT1/PTR FAMILY 7.3-like (XM_010694132.1) was upregulated ($\log_2^{FC}$ = 9.815); DEGs encoding amino acids were also transcribed in roots: primary amine oxidase (*AMO*, XM_010677915.2) and aspartyl protease family protein 1 (*APF1*, XR_002039854.1) were upregulated ($\log_2^{FC}$ = 6.701) and downregulated ($\log_2^{FC}$ = −8.342), respectively.

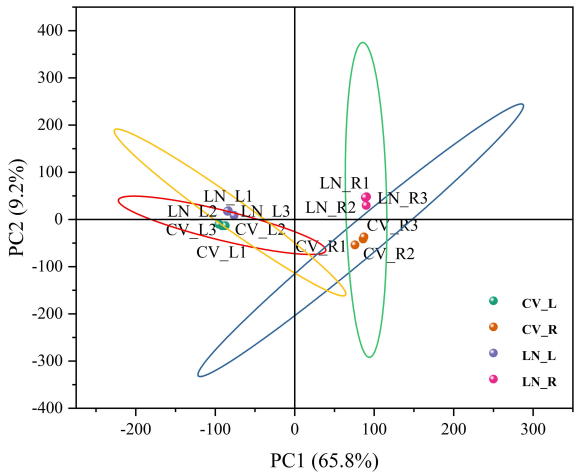

FIGURE 1
PCA plot of transcriptomes under low N stress in sugar beet. CV_R, control group, root; CV_L, control group, leaf; LN_R, low N group, root; LN_L, low N group, leaf; PCA, principal component analysis. The same abbreviations are used below.

10.3389/fpls.2023.1164151

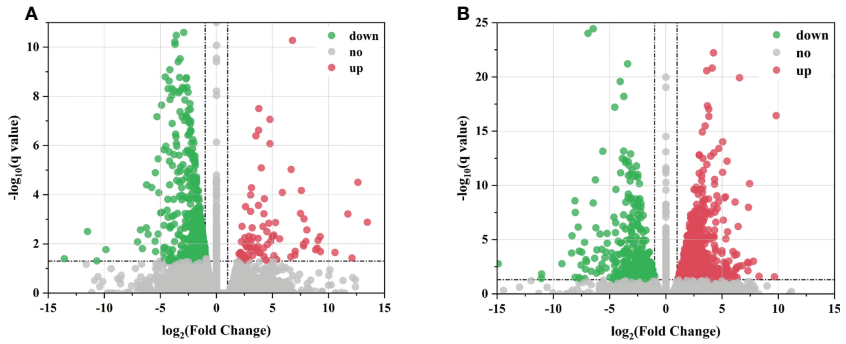

FIGURE 2
Differentially expressed genes (DEGs) of sugar beet under LN treatment. **(A, B)** Volcano plot of DEGs in leaves and roots between the control and low N treatments, respectively. The x-axis represents changes in gene expression ploidy across LN stress; the y-axis represents statistically significant differences in gene expression. Scattered dots represent individual genes; gray dots indicate no significant differences in transcripts, red dots indicate significant differences in downregulated genes, and green dots indicate significant differences in upregulated genes.

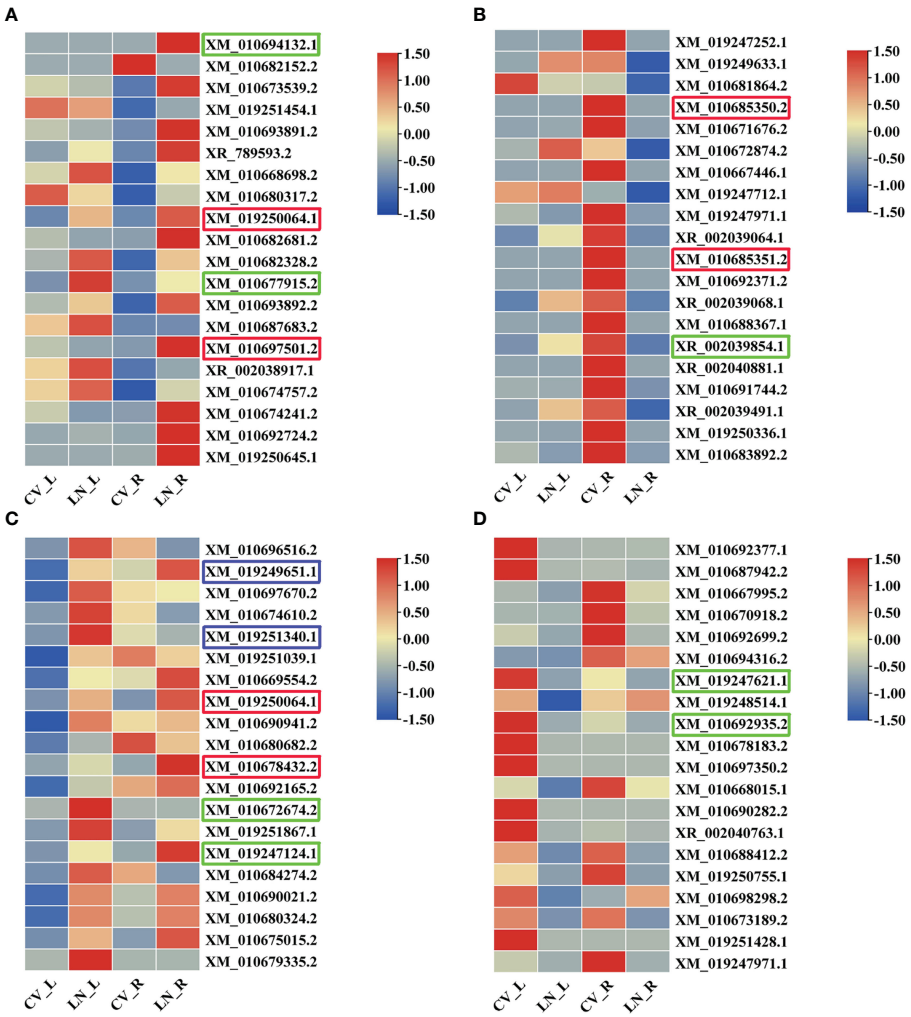

FIGURE 3
Heatmap of the top 20 significantly upregulated (**A**, roots; **C**, leaves) and downregulated (**B**, roots; **D**, leaves) DEGs responsive to LN in sugar beet. The redder the color, the more pronounced the expression of that transcript. DEGs, differentially expressed genes.

10.3389/fpls.2023.1164151

3.3 The transcript pattern, biological processes, and pathways of DEGs

GO enrichment analysis of DEGs was performed using GOSeq, topGO, and hmmscan (Release 2.12) (Young et al., 2010). GO terms with FDRs less than 0.05 were considered significantly enriched for DEGs. In leaves, a total of 165 DEGs ($\log_2^{|FC|} \geq 1$, q value < 0.05) were significantly enriched in two biological process (BP), five cellular component (CC), and two molecular function (MF) categories (Figure 4A). They were "photosynthesis, light harvesting (GO:0009765)" and "protein-chromophore linkage (GO:0018298)" in BP. The top three of the CC category were "photosystem I (GO:0009522)", "chloroplast thylakoid membrane (GO:0009535)", and "photosystem II (GO:0009523)". In the MF category, "manganese ion binding (GO:0030145)" and "chlorophyll binding (GO:0016168)" were significantly enriched. A total of 526 DEGs ($\log_2^{|FC|} \geq 1$, q value < 0.05) in the roots were obtained in one BP, three CC, and two MF categories (Figure 4B), and they were mainly related to "negative regulation of translation (GO:0017148)", "cell wall (GO:0005618)", "extracellular region (GO:0005576)", "apoplast (GO:0048046)", "channel activity (GO:0015267)", and "rRNA N-glycosylase activity (GO:0030598)". These results suggested that the DEGs involved in low nitrogen stress were mainly related to photosynthesis, transport, and stimulus response to stress.

In organisms, genes usually perform their biological functions in coordination with each other. The important biochemical metabolic and signal transduction pathways in which specific genes are involved (Kanehisa et al., 2008) can be identified by KEGG enrichment analysis. FDR ≤ 0.05 was defined as pathways significantly enriched in DEGs, and we used KOBAS (v2.0) (Mao et al., 2005) for pathway enrichment analysis. Seven and nine pathways were significantly enriched in LN-treated leaves and roots, respectively (Figures 4C, D). The enriched pathways were "photosynthesis (bvg00195)", "photosynthesis-antenna proteins (bvg00196)", "metabolic pathways (bvg01100)", "carbon fixation in photosynthetic organisms (bvg00710)", "glyoxylate and dicarboxylate metabolism (bvg00630)", "carbon metabolism (bvg01200)", and "porphyrin metabolism (bvg00860)" in leaves and "biosynthesis of secondary metabolites (bvg01110)", "metabolic pathways (bvg01100)", "flavonoid biosynthesis (bvg00941)", "nitrogen metabolism (bvg00910)", "phenylpropanoid biosynthesis (bvg00940)", "cutin, suberine and wax biosynthesis (bvg00073)", "fatty acid elongation (bvg00062)", "ABC transporters (bvg02010)", and "glutathione metabolism (bvg00480)" in roots. These results indicated that photosynthesis

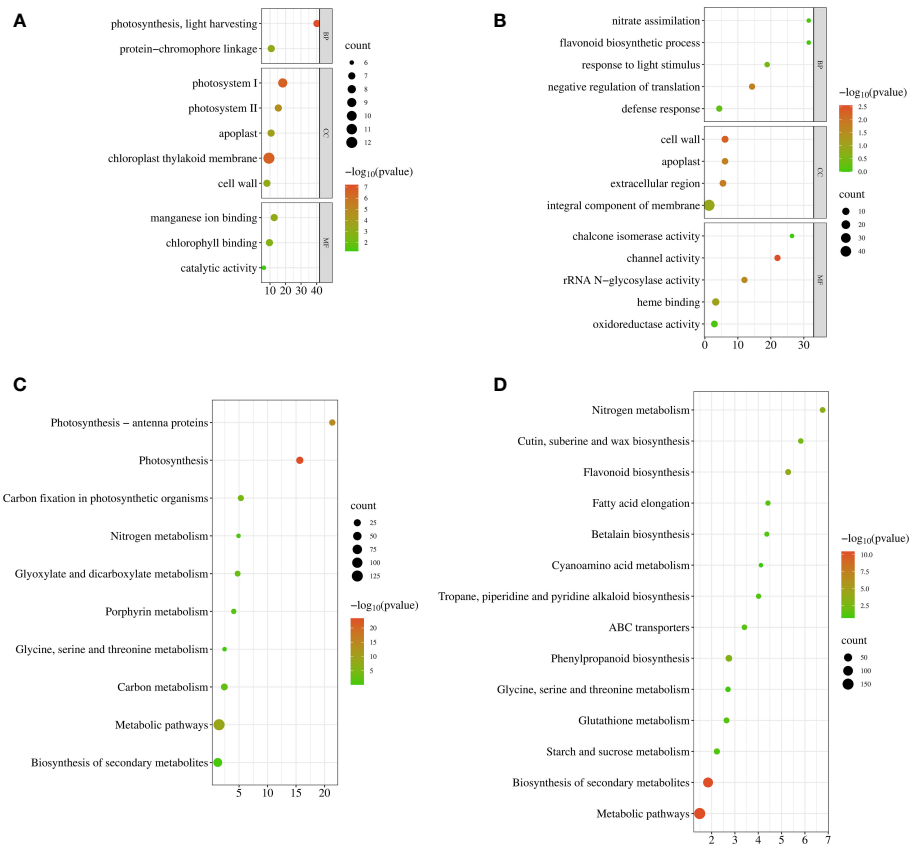

FIGURE 4
Functional enrichment of DEGs of sugar beet under low N stress. **(A, B)** Scatter plot of GO functional enrichment in leaves and roots. **(C, D)** Scatter plot of KEGG enrichment in leaves and roots. The x-axis is the enrichment factor; the y-axis is the enrichment of entries. The size of the bubbles represents the number of DEGs on the annotated items; the color represents the enrichment degree $-\log_{10}^{(p\text{-value})}$. DEGs, differentially expressed genes; GO, Gene Ontology; KEGG, Kyoto Encyclopedia of Genes and Genomes.

and synthesis of secondary metabolites were key pathways for sugar beet in response to LN.

3.4 Response of differentially expressed hub genes to LN stress

PPI networks were constructed using DEGs ($\log_2^{|FC|} > 1$, q value < 0.05) in LN-tolerant germplasm to explain the importance of these interactions in physiological biochemistry and signal transduction. Differential expression was screened for hub genes of each pathway using Cytoscape (Figure 5, Supplementary Table 4). Among the downregulated DEGs, the core genes associated with photosynthesis were photosystem II core complex proteins psbY, chloroplastic (*PsbY*, BVRB_6g147470) (Figure 5Aa), and chlorophyll *a*–*b* binding protein 4, chloroplastic (*CAB4/Lhca4*, BVRB_5g114540) (Figure 5Ab). The essential genes associated with carbon metabolism are fructose 1,6-bisphosphatase, cytosolic (*FBP*, BVRB_1g011460) (Figure 5Ad), and phosphoglycerate kinase, chloroplastic (*PGK*, BVRB_2g038200) (Figure 5Ae). Ferredoxin-nitrite reductase, chloroplastic (*NIR*, BVRB_4g087070), and nitrate reductase [NADH] (*NR*, BVRB_1g000370) (Figure 5Ah) are the core genes associated with nitrogen metabolism. Phosphoglycolate phosphatase 1A, chloroplastic (*PGLP1A*, BVRB_4g074740) (Figure 5Af), is highly associated with the glyoxylate and dicarboxylic acid metabolic pathways. Magnesium protoporphyrin IX methyltransferase, chloroplastic (*CHLM*, BVRB_7g180360) (Figure 5Ag), is a key gene for secondary metabolite biosynthesis. In conclusion, the downregulated DEGs were mainly closely related to photosynthesis, C/N metabolism, and secondary metabolite synthesis under low N stress in sugar beet.

For upregulated DEGs, the key genes in the secondary metabolic biosynthesis and metabolic pathways are likely cinnamyl alcohol dehydrogenase 6 (*CAD6*, BVRB_005400) (Figure 5Ba), and proline dehydrogenase 2, mitochondrial (*POX2*, BVRB_2g025900 (Figure 5Bb). Chalcone-flavanone isomerase (*CHI*, BVRB_2g036880), chalcone-flavanone isomerase (*CHI*, BVRB_2g036940), and dihydroflavonol 4-reductase (*DFRA*, BVRB_1g007170) (Figure 5Bc) play key roles in flavonoid biosynthesis. The key gene for phenylpropanoid biosynthesis is spermidine hydroxycinnamoyl transferase (*SHT*, BVRB_2g034560) (Figure 5Bd). Cytochrome P450 86A1 (*CYP86A1*, BVRB_7g172510) is vital for keratin, cork, and wax key genes in the biosynthetic pathway. It can be speculated that the upregulated DEGs involved in secondary metabolite synthesis and flavonoid and phenylpropanoid biosynthesis fulfill crucial functions in the sugar beet response to LN.

3.5 Correlation analysis between low nitrogen stress and the expression levels of key genes

To understand the relationship between DEGs and LN stress, we analyzed the correlation between them using Pearson's correlation analysis (Figure 6). Nitrogen accumulation in plants was positively correlated with *DFRA* in the roots (coefficient = 0.99, $p < 0.01$). *PsbY* and *CAB4* in the leaves were coregulated with four

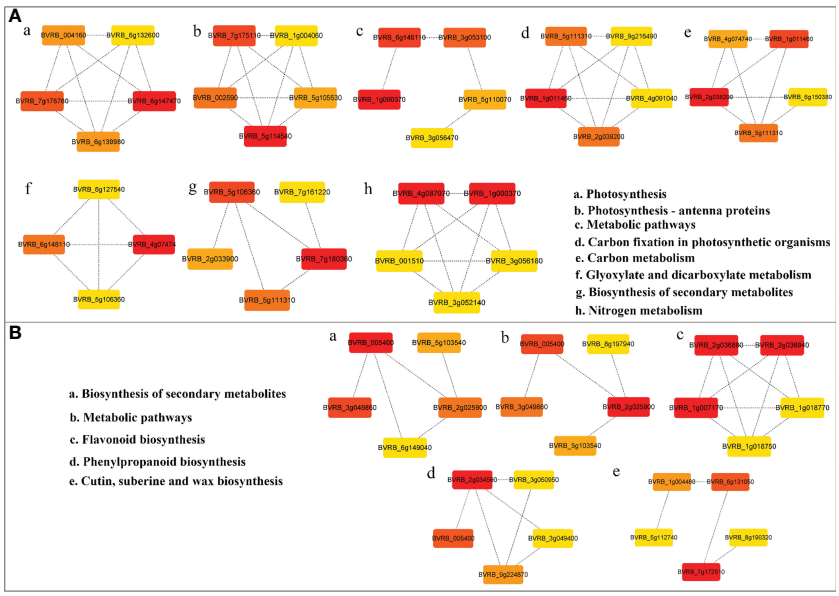

FIGURE 5
PPI network of primary and secondary metabolism of DEGs in sugar beet under LN stress. **(A, B)** PPI network diagram of downregulated and upregulated DEGs, respectively. Proteins are represented as nodes, and interactions are represented as edges. The color of the proteins indicates the strength of the protein interactions; the redder the color, the stronger the interactions. Only pathways with categories in error incidence rate (FDR) <0.01 were considered (Supplementary Table 4). PPI, protein–protein interaction; DEGs, differentially expressed genes; FDR, false discovery rate.

10.3389/fpls.2023.1164151

DEGs, *FBP*, *PGK*, *PGLP1A*, and *CHLM* (coefficient ≥ 0.95, $p < 0.05$), and the coefficients equal to 1 indicated a stronger correlation with each other. *PGK*, *GLP1A*, and *CHLM* had positive correlations with each other ($p < 0.05$). *DFRA* in the roots was negatively correlated with NIR in the leaves (coefficient = −0.98, $p < 0.05$). There may be remote regulation between flavonoid biosynthesis and nitrogen metabolism in sugar beet roots and leaves.

3.6 Abundant DEGs involved in primary metabolism under LN stress

In the KEGG analysis, photosynthesis was found to be the most regulated pathway in the transcriptome. We annotated 48 genes involved in photosynthesis (Supplementary Table 5), and 15 of them were associated with photosynthesis - antenna protein. All of these genes were significantly downregulated in response to LN. This was similar to genes involved in photosynthesis in *Arabidopsis*, which were found to be downregulated at the mRNA level under nitrogen starvation conditions (Peng et al., 2007; Kiba et al., 2011). Under LN stress, DEGs involved in PSII (*PsbO*, *PsbP*, *PsbQ*, *PsbY*, and *Psb27-1*) were all significantly downregulated in sugar beet (Figure 7A, Supplementary Table 5, q value < 0.01). In LHC II, Lhcb1, Lhcb2, Lhcb3, Lhcb4, Lhcb5, and Lhcb6 involved in the photosynthetic antenna protein pathway were also significantly downregulated (Figure 7B, Supplementary Table 5, q value < 0.01). *PetE*, *PetF*, and *PetH* mediating electron transfer between PS II and PS I were found to be downregulated (Figure 7A, Supplementary Table 5, q value < 0.05). The other downregulated DEGs included photosystem I reaction center subunits (*PsaE*, *PsaF*, *PsaG*, *PsaH*, *PsaK*, *PsaL*, *PsaN*, and *PsaO*) (Figure 7A, Supplementary Table 5, q value < 0.01) and *Lhca1*, *Lhca 2*, *Lhca 3*, *Lhca 4*, and *Lhca 5*, which are involved in photosynthetic antenna proteins in LHC I (Figure 7B, Supplementary Table 5, q value < 0.01). These data suggested that the light-dependent function of photosynthesis was diminished in 780016B/12 superior leaves due to LN supply.

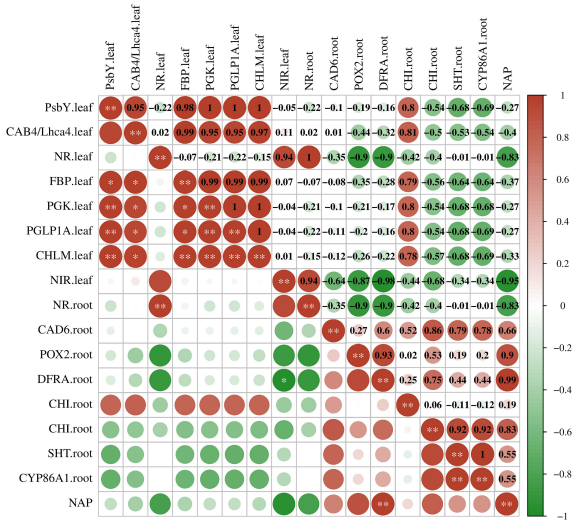

FIGURE 6
Pearson's correlation coefficient (r) of the expression level of key genes. PSBY. leaf, photosystem II core complex proteins psbY, chloroplastic; CAB4/Lhca4. leaf, chlorophyll *a*−*b* binding protein 4; NR. leaf, nitrate reductase [NADH]; FBP. leaf, fructose 1,6-bisphosphatase, cytosolic; PGK. leaf, phosphoglycerate kinase, chloroplastic; PGLP1A. leaf, phosphoglycolate phosphatase 1A; CHLM. leaf, magnesium protoporphyrin IX methyltransferase; NIR. leaf, ferredoxin-nitrite reductase; CAD6. root, probable cinnamyl alcohol dehydrogenase 6; POX2. root, proline dehydrogenase 2, mitochondrial; DFRA. root, dihydroflavonol 4-reductase; CHI. root, chalcone-flavanone isomerase; SHT. root, spermidine hydroxycinnamoyl transferase; CYP86A1. root, cytochrome P450 86A1; NAP, nitrogen accumulation in plants. Scale: bright blue to bright red represents negative to positive correlations. *p < 0.05, **p < 0.01.

In sugar beet, a large number of genes involved in carbon (C) metabolic pathways were significantly transcriptionally altered during nitrogen starvation. Of the 50 DEGs annotated (Supplementary Table 6), 15 are associated with carbon fixation in photosynthetic organisms, and 22 and 12 genes are within carbon metabolic and nitrogen metabolic pathways, respectively. Rubisco (ribulose-1,5-bisphosphate carboxylase/oxygenase) is an important carboxylase and an indispensable oxygenase in photorespiration in C_3 plants. The transcript of the small subunit (*RBCS*) was downregulated under LN treatment (Figure 8, Supplementary Table 6), indicating that N deficiency influenced the N use efficiency for N fixation. C_3 is the basic pathway for carbon assimilation, which can synthesize a variety of organic substances, such as sugars and starch. Starch can also be hydrolyzed in leaves to produce fructose and glucose, which need to be phosphorylated to enter glycolysis mediated by phosphofructokinase. Fructose 1,6-bisphosphatase (*FBP*), fructose-bisphosphate aldolase (*FBA5*, *FBA1*), phosphoglycerate kinase (*PGK*), and glyceraldehyde-3-phosphate dehydrogenase (*GAPA*, *GAPB*) were all downregulated under LN conditions (Figure 8, Supplementary Table 6). Decreases in phosphoglycerate lyase and phosphofructokinase are an important basis for the decrease in the C backbone of amino acid biosynthesis (Diop and Gallois, 2022; Fei et al., 2022). Sugar beet nitrogen-tolerant germplasms have less glucose entering the respiratory pathway, which may facilitate starch synthesis to maintain nocturnal leaf metabolism and support the production of other polysaccharides or glycoproteins (Meng et al., 2021).

During nitrogen starvation, genes directly involved in nitrogen metabolism were differentially transcribed. *NRT2.5, GS, GS1, NR, NIR, GLUDB* were significantly downregulated (Figure 8, Supplementary Table 6, q value < 0.05). This downregulation under LN was accompanied by extensive changes in cellular transport and was necessary for plant cells to maintain homeostatic growth (Cai et al., 2012). Glutathione (*GSH*) plays an important role in detoxification, antioxidant response, and redox homeostasis (Yamazaki et al., 2019). Under nitrogen deficiency, GST23 (*GST23*), glutathione S-transferase (*GSTU7*, *GSTU9*, and *GSTU17*), and L-ascorbate peroxidase 3 (*APX3*) were detected as significantly upregulated transcripts (Figure 8, Supplementary Table 6, q value < 0.01).

10.3389/fpls.2023.1164151

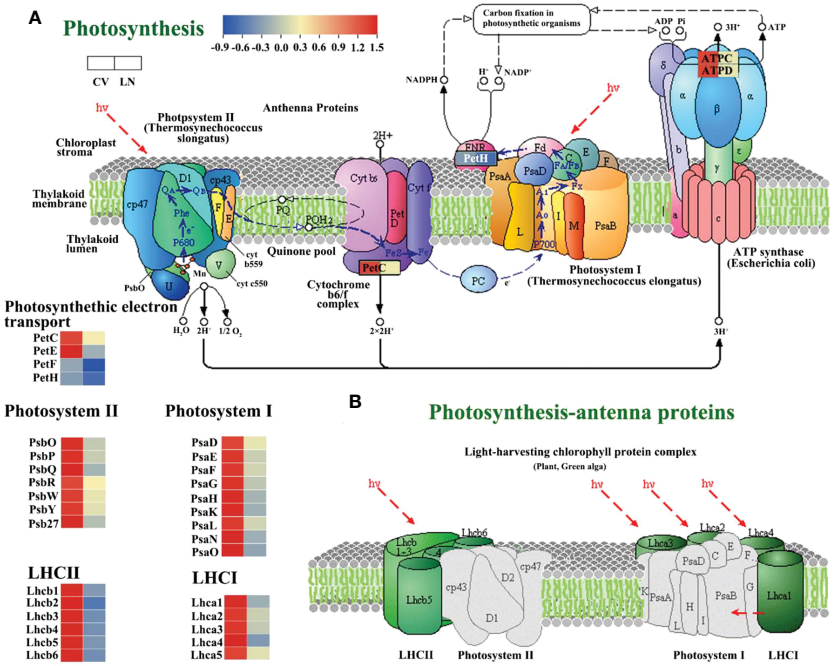

FIGURE 7
Significantly downregulated expression of photosynthesis-regulated genes under low N stress in sugar beet (Supplementary Table 5). **(A)** Photosynthetic pathway. **(B)** Photosynthetic antenna protein (Kanehisa et al., 2016; Kanehisa et al., 2017).

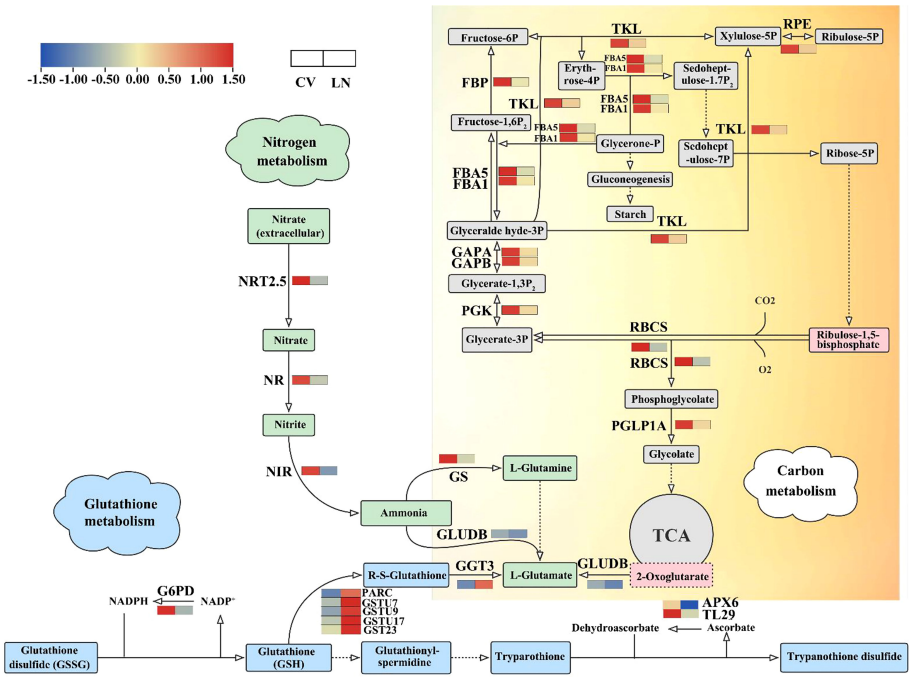

FIGURE 8
DEGs in C, N, and glutathione metabolism biosynthetic pathways under LN. The red to blue colors indicate upregulated to downregulated tendencies. Same as below. DEGs, differentially expressed genes.

3.7 Essential DEGs in phenanthrene metabolism and flavonoid biosynthesis

In secondary metabolism, phenylpropane metabolism and flavonoid biosynthesis were found to be the most regulated pathways. In sugar beet, 30 and 13 DEGs were derived from phenylpropanoid metabolism and flavonoid biosynthesis, respectively (Supplementary Table 7). Sixteen peroxidase genes (*PER*, 13 upregulated and three downregulated) were transcriptionally altered due to nitrogen deficiency. The peroxidase multigene family encodes secreted glycoproteins involved in lignin biosynthesis, cell elongation, cell wall construction and differentiation, and pathogen defense responses (Passardi et al., 2004; Silva et al., 2022; Yang et al., 2022) (Figure 9, Supplementary Table 7). Members of the 4-coumarate-CoA ligase (*4CL*) family are key enzymes in lignin biosynthesis (Liang et al., 2021). In this study, *4CL2* was found to be upregulated for the synthesis of phenylpropanoid derivatives, such as lignin. *CAD6* was also upregulated, and it is required for the final step in stimulating lignin biosynthesis (Hirano et al., 2012). Thus, lignin formation and cell wall modification are regulated by morphological changes in the roots in response to nitrogen starvation signals (Liang et al., 2021). A total of five beta-glucosidase genes (*BGLU*, four upregulated and one downregulated) were observed in response to LN stress in this study. *BGLU13* is a defense protein that plays a key role in fighting against plant protection from salinity stress (Jia et al., 2019). β-Glucosidases are active in many metabolic processes, such as hydrolysis of derived oligosaccharides on the cell wall, as well as controlling the reactivity and biological activity of plant secondary metabolites and phytohormones, which regulate plant growth and development (Gan et al., 2022).

Flavonoids are derived from the phenylpropanoid metabolic pathway and are induced by C metabolism (Zhang et al., 2018b). In sugar beet, genes involved in flavonoid biosynthesis (*CHS*, *CHI*, *F3H*, *SHT*, *HST*, *DFRA*, and *FLS1*) were significantly upregulated under LN, but *SAT* was downregulated (Figure 9, Supplementary Table 7, q value < 0.05). Members of CHIs interact with chalcone synthase (*CHS*), flavonol synthase/flavanone 3-hydroxylase (*FLS*), naringin, and 2-oxoglutarate 3-dioxygenase (*F3H*) to form heterodimers, which may jointly play a regulatory role and participate in the flavonoid pathway (Wan et al., 2022).

3.8 Effect of low nitrogen stress on the photosynthetic characteristics of sugar beet seedlings

Furthermore, we detected the net photosynthetic rate (Pn), transpiration rate (Tr), stomatal conductivity (Gs), and intercellular CO_2 concentration (Ci) of sugar beet under LN conditions. As shown in Supplementary Figures 1A, C, in sugar beet, both Pn and Gs showed significant decreases ($p < 0.01$) of 42.7% and 21.9%, respectively, under low-N stress conditions; Ci decreased significantly ($p < 0.05$) (Supplementary Figure 1D). *FBP* and *PGK* were significantly positively correlated with Ci and significantly negatively correlated ($p < 0.001$) with Pn (Supplementary Figure 1E). Tr and Gs exhibited significant negative correlations ($p < 0.001$) with *CHLM*, *PSBY*, and *PGLP1A*. Tr and Gs were negatively correlated with CHLM, *PSBY*, and *PGLP1A* ($p < 0.001$). This result suggested that the changes in photosynthetic gas exchange parameters under N deficiency might be determined by some photosynthetic DEGs in sugar beet.

3.9 Validation of RNA sequencing data by real-time fluorescence quantitative PCR

Gene fold changes between low nitrogen-stressed tissues and control treatments were confirmed using correlation analysis of qRT–PCR and RNA-seq data. A total of 22 genes were selected for qRT–PCR, including eight upregulated genes and 14 downregulated genes (Figure 10, Supplementary Table 1). There was a strong positive correlation coefficient ($R^2 = 0.98$) for all these genes under low nitrogen stress, which confirmed the reliability and reproducibility of the RNA-seq data.

4 Discussion

4.1 The crucial role of downregulated DEGs in the photosynthesis of sugar beet suffering from N deficiency

Photosynthesis provides the carbon skeleton and energy for nitrogen assimilation and other metabolic processes (Meng et al.,

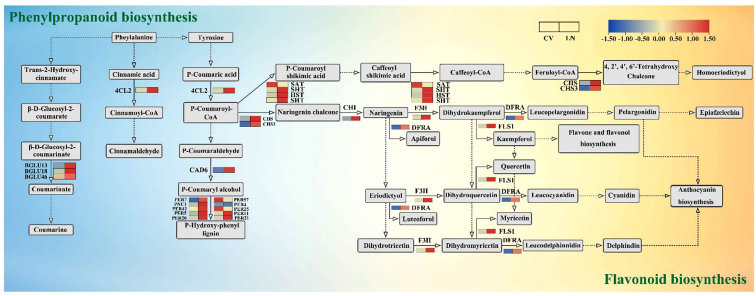

FIGURE 9
DEGs in the metabolic pathways of phenylpropanoid metabolism and flavonoid biosynthesis under LN. DEGs, differentially expressed genes.

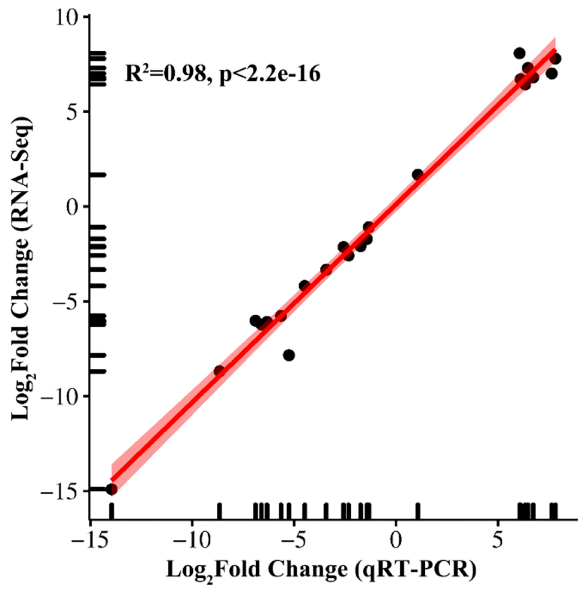

FIGURE 10
qRT–PCR validation of sugar beet RNA-seq results.

2021). In the present study, LN stress caused a significant decrease in Pn, Ci, and Gs (Supplementary Figure 1, $p < 0.05$). It was shown that the reduction in photosynthetic capacity was mainly attributed to stomatal or non-stomatal limitation (Erel et al., 2015), which may depend on the changes in Pn, Ci, and Gs. In plants grown under nitrogen-deficient conditions, coordination between PSII activity and CO_2 assimilation is important to maintain photosynthesis efficiency (Sun et al., 2022). In sugar beet, most of the DEGs involved in photosynthesis and photorespiration, including PSI, PSII, ATP synthase, and Rubisco, were downregulated (Figure 7, Supplementary Table 5). The reason for this may be that Rubisco breaks down under low nitrogen stress, plant photosynthetic activity is reduced, and ultimately plant growth may be inhibited (Curci et al., 2017). It was deduced that the downregulated *PetE*, *PetF*, and *PetH* in sugar beet under low nitrogen stress reduced the energy provided by photosynthetic biocarbon fixation due to the decreased Calvin cycle activity and NADPH consumption, resulting in reduced ATP (ATPC and ATPD downregulation) utilization (Figure 7A, q value < 0.01). Some of these genes have been proven to be of general importance for photosynthesis and plant growth, including PSII dissolved oxygen enhancing proteins, cytochrome b6/f complex proteins, PSI subunits, FNRs, and Rubisco (Ermakova et al., 2019; Meng et al., 2021), which is consistent with our hypothesis that the identified DEGs in sugar beet played key roles in nitrogen use efficiency (NUE) under low nitrogen conditions.

Many studies have reported that low nitrogen stress affects photosynthesis by affecting light and dark reactions in chloroplasts (Sultana et al., 2020; Tantray et al., 2022). Excited energy captured by the LHC is transferred to the core antenna complex and ultimately used in PSI and PSII reaction centers (RCs) for photochemical reactions. Both PSII and PSI in sugar beet have an antenna system (Pan et al., 2020) that includes a series of membrane proteins binding chlorophyll and carotenoids and belongs to the light-harvesting complex (LHC) superfamily, including LHCII and LHCI. Lhcb proteins are important components of the PSII-related light-harvesting complex (LHCII), which is composed of the minor antenna complex Lhcb4 (*CP29*), Lhcb5 (*CP26*), and Lhcb6 (*CP24*) and the major antenna complex containing homodimeric and heterodimeric trimers of the Lhcb1, Lhcb2, and Lhcb3 gene products (Boekema et al., 1995; Damkjær et al., 2009). In this study, all chlorophyll *a–b* binding proteins interacting with low nitrogen regulation were downregulated (Supplementary Table 5), which may be due to the decrease in chlorophyll content. Lhca encodes the LHCI protein and binds to the PSI core complex to form the PSI-LHCI supercomplex (BenShem et al., 2003; Ozawa et al., 2018). Consistent with the study of wheat varieties under nitrogen stress (Sultana et al., 2020), the expression of LHC components in PSII and PSI was significantly reduced in the current study (Figure 7B, Supplementary Table 5).

The identification of functional genes for improving low nitrogen tolerance is a feasible way to improve nitrogen use efficiency. In higher plants, *PsbO*, *PsbP*, and *PsbQ* in PSII have been identified as exogenous proteins required for optimal oxygen release (Bricker et al., 2012). PsbP proteins are important cofactors of PSII and are involved in key processes such as calcium binding and photosynthesis (Kakiuchi et al., 2012). In addition, PsbP proteins can act as signaling response factors in response to various adverse external environments (Liu et al., 2012; Ding et al., 2022). Inhibition of *PsbP* results in slower growth and some defects in PSII function, such as lower oxygen-evolving activity (oxygen-evolving), lower quantum yield, and slower electron transfer rate on the PSII donor side (Yi et al., 2007; Yi et al., 2009). Allahverdiyeva et al. found that *PPD1* is essential at the early stages of seedling development (Allahverdiyeva et al., 2013). In the present study, the PsbP structural domain-containing protein 1 (*PPD1*) gene, a member of the *PsbP* gene family, was significantly downregulated in sugar beet leaves under low nitrogen stress.

The core genes of the photosynthetic pathway are *PsbY* (Figure 5Aa) and *CAB4/Lhca4* (Figure 5Ab). Both *PsbY1* and *PsbY2* were identified in spinach (Gau et al., 1998). The *PsbY* protein of *Arabidopsis* photosystem II plays an important role in the redox regulation of cytochrome b559 (*PsbE* and *PsbF*) (Lotta et al., 2016). The *PsbY* gene was similarly found to be repressed in maize under low nitrogen stress (Du et al., 2021). According to Supplementary Table 4, two *PsbY* proteins are likely present in PSII of sugar beet, as in spinach. This hypothesis requires further confirmation.

Fe is a major element in the photosynthetic process and is involved in plant C metabolism (Quan et al., 2017). *PetF* is the major photosynthetic iron oxygen returning protein in chloroplasts and plays a role in electron transfer between PSI and FNR (Schmitter et al., 1988; Terauchi et al., 2009). Lin et al. found that overexpression of *PetF* increases the efficiency of chloroplasts in scavenging reactive oxygen species, thus conferring heat tolerance to plants (Lin et al., 2013). However, the results of the present study showed that *PetF* in sugar beet leaves was downregulated under low nitrogen stress. Its role is to reduce trivalent Fe(III) to divalent Fe (II) (Li et al., 2019), and thus, Fe may function in maintaining homeostasis in sugar beet under low nitrogen stress.

4.2 DEG performance on the balance of C and N metabolism in sugar beet under low N supply

The maintenance of coordinated carbon and nitrogen metabolism and the proper C/N balance is important for plant growth, development, and yield (Krapp and Traong, 2006). In sugar beet, as shown in the genes in Figure 8 and Supplementary Table 6, carbon, nitrogen, and glutamate metabolism were found to play important roles in response to nitrogen deficiency, and the downregulation of glutamate dehydrogenase B (*GLUDB*) was a pivotal link between these processes, similar to the results of Li et al. (2018). Sequence alignment showed that BvGLUDB was highly homologous with GDHs in *Arabidopsis* (Fontaine et al., 2012). They share the same conserved structural domain of Glu/Leu/Phe/Val dehydrogenase, dimerization domain (InterPro: IPR006097) (Supplementary Figure 2A). In the *gdh1-2-3* mutation, the main physiological function of NADH-GDH is to provide 2-oxoglutarate for the tricarboxylic acid cycle by altering primary C and N metabolism (Fontaine et al., 2012). In the present study, BvGLUDB was found to be downregulated in leaves, which is speculated that the cycle of the metabolites Glu and 2-oxoglutarate is weakened. GDH controls the levels of C and N metabolites by changing the structure of heterohexamers (Tercé-Laforgue et al., 2013), and the related metabolic pathways play a major role in nitrogen assimilation (Tercé-Laforgue et al., 2015).

Rubisco and 2-oxoglutarate act as carbon and nitrogen starvation signals, respectively (Laurent et al., 2005). Carbon and nitrogen metabolism are fundamental metabolic processes in plants, and nitrogen assimilation requires carbon metabolism to provide energy and a carbon skeleton, which is mainly formed by α-ketoglutarate. α-Ketoglutarate changes significantly under low nitrogen treatment (Li et al., 2018), and it affects the conversion pathway to glutamate as a carbon source. Glutamate has been reported to exhibit considerable stability in amino acid profile changes, suggesting its homeostasis function in plants (Liao et al., 2022). The expression levels of nitrogen assimilation and amino acid transport genes play a decisive role in nitrogen utilization. In this study, we found that the *NRT2.5*, *NR*, *NIR*, *GS*, *GLUDB*, *GST*, and *GGT3* genes are involved in the regulation of homeostasis in sugar beet seedlings under low nitrogen application. They were significantly downregulated except for *GST* and *GGT3*, which were significantly upregulated. Reduced expression levels of *NRT2.5* lead to decreased high-affinity nitrate uptake (Lezhneva et al., 2014). *NR* and *NIR* are mainly responsible for the conversion of NO_3^- to nitrite and nitrite to NH_4^+, respectively (Rana et al., 2010), and *GLUDB* mediates the conversion of NH_4^+ to glutamate. *GSTU* and *GGT3* participate in glutathione (*GSH*) to *R-S*-glutathione to L-glutamate conversion. Glutamate is used as an amino donor for the synthesis of many other amino acids, such as proline, arginine, and lysine. This indicates that a low supply of nitrogen significantly promotes the glutathione metabolic biosynthetic pathway to quench reactive oxygen species (ROS) and protect cells from oxidative damage under short-term stress (Kumar and Trivedi, 2018).

Under stress conditions, different levels of regulation exist in cells to maintain a properly balanced metabolic ratio between carbon and nitrogen, which is necessary to avoid metabolic inefficiencies (Zhang et al., 2018a). In plants, photosynthesis is the energy source for carbon and nitrogen metabolism, and nitrogen deficiency has been reported to significantly reduce the photosynthetic capacity of plants (Tantray et al., 2022). Low nitrogen significantly attenuated the expression of genes controlling nitrogen metabolism (Figure 8, Supplementary Table 6). As a result, it competes with photosynthetic carbon sources for ATP and NADPH, increasing the photosynthetic electron transport burden while reducing the overall activity of PSII in sugar beet. Increasing nitrogen application can alleviate this competitive relationship and make it easier to balance carbon and nitrogen metabolism. In the present study, the transcript levels of ribulose bisphosphate carboxylase small subunit (*RBCS*) and phosphoglycolate phosphatase 1A (*PGLP1A*) were significantly downregulated (Figure 8), which may inhibit glycolate as a carbon backbone to synthesize other amino acids such as glutamate, interfering with the fixation or assimilation of photosynthetic carbon in sugar beet seedlings under low N conditions. When N is insufficient, plants can enhance the regulation of carbon metabolism in the roots. Phosphoglycerate kinase (*PGK*) catalyzes the first ATP production of the glycolytic pathway (Bowler, 2013). Glyceraldehyde-3-phosphate dehydrogenase (*GAPA*, *GAPB*), fructose-bisphosphate aldolase (*FBA1*, *FBA5*), and *PGK* were all downregulated, indicating that the intermediate steps of glycolysis were inhibited. *FBP* catalyzes the production of fructose-6P (*F6P*) from fructose-1,6P2 (*FDP*) in the gluconeogenesis pathway (Li et al., 2020). *FBP* was significantly downregulated under low nitrogen stress in sugar beet, indicating that the fructose phosphate pathway in glycolysis was inhibited. Therefore, the fructose content in sugar beet seedlings may be related to their tolerance to LN stress. Transketolase (*TKL*) was downregulated (Figure 8); it catalyzes reversible reactions in the carbon skeleton and plays a large role in carbon metabolism. We hypothesized that the conversion of the carbon skeleton is disturbed by nitrogen deficiency. Therefore, nitrogen deficiency not only leads to a decrease in nitrogen and carbon metabolism but also inhibits the synthesis of most amino acids to some extent (Hao et al., 2021). *DFRA* in the roots was found to be negatively correlated with *NIR* in the leaves (coefficient = −0.98, $p < 0.05$). Regulation of carbon and nitrogen balance can promote uptake, assimilation, and metabolic efficiency of carbon- and nitrogen-containing nutrients, which is a guide to improving low nitrogen tolerance in crops.

4.3 DEGs involved in conservative secondary metabolic regulatory networks in sugar beet in response to nitrogen starvation

In terms of energy and substrate availability, C status is considered to be a key factor in the accumulation of secondary metabolites (Beshir et al., 2019). Phenylpropanoids are an important metabolic pathway in which a large number of phenylalanine or tyrosine secondary metabolites, such as flavonoids and isoflavonoids, are produced. These important

molecules are involved in many biological processes in plants (Betti et al., 2014). The phenylpropanoid metabolic pathway is closely related to lignin synthesis (Cong et al., 2013). Lignin is a major component of the plant skeleton and functions in plant root growth (Guo et al., 2001). Peroxidase superfamily protein (*PER*) is one of the key proteins involved in lignin synthesis and is able to catalyze lignin monomer precursors to produce *p*-hydroxyphenyl lignin (Figure 9). In the present study, 4-coumarate-CoA ligase 2 (*4CL2*) and probable cinnamyl alcohol dehydrogenase 6 (*CAD6*) were significantly upregulated and were speculated to be the major enzymes involved in lignin synthesis under low nitrogen application in sugar beet. Among the genes encoding peroxidase in this pathway, DEGs (*PER4*, *PER5*, *PER7*, *PER11*, *PER20*, *PER21*, and *PER42*) were upregulated compared to the downregulated *PER25* and *PER57* genes (Figure 9, Supplementary Table 7). This is different from previous results in rice (Guo et al., 2001) and oilseed rape (Qin et al., 2019). The reason is speculated to be that the reduction in *PER25* and *PER57* transcripts further triggered the response of sugar beet to a low nitrogen environment, but LN stress seems to promote lignin biosynthesis, which could contribute to the response of plants to various abiotic stresses (Dong and Lin, 2021).

The expression of beta-glucosidases (*BGLU13*, *BGLU18*, and *BGLU46*) involved in phenylalanine biosynthesis was upregulated under low nitrogen stress, and *BGLU13* catalyzed the conversion of β-D-glucosyl-2-coumarate to β-D-glucosyl-2-coumarinate and then to coumarin (Figure 9, Supplementary Table 7). Recent studies have shown that *BGLU13* is involved in glucose synthesis under saline stress (Jia et al., 2019). Han et al. (2020) found that BGLU18 in *Arabidopsis* is abundant in the petiole and localized mainly in the endoplasmic reticulum (ER), suggesting its involvement in defense against biotic stresses in the petiole. *BGLU46* is mainly located in the primary xylem (Baiya et al., 2018) and functions in the lignification process with *4CL2* (Figure 9). *Os4BGlu18* was found to be closely associated with *Arabidopsis BGLU46* in the rice genome (Opassiri et al., 2006). Further detailed examination of the distribution of *BGLU* needs to be verified in aboveground tissues of sugar beet (mainly leaves and petioles). Thus, *BGLUs* may be defense proteins in response to stress, and their upregulation may protect sugar beet from low nitrogen stress. The upregulated *POX2* and *APX* (Supplementary Tables 6, 7) can alleviate low nitrogen stress and improve LN tolerance, which is consistent with previous findings (Hao et al., 2021; Zhang et al., 2023). These results confirm that oxidative damage and compositional changes are sensitive responses for sugar beet to cope with low nitrogen stress.

Although a number of studies have investigated the effect of C or N on flavonoid biosynthesis, the mechanism by which C/N interactions affect flavonoid metabolism remains unclear (Klem et al., 2022). Chalcone synthase (CHS) is involved in the biosynthesis of precursor molecules for flavonoids and isoflavones (García-Calderón et al., 2020), generating naringenin chalcone with *p*-coumaroyl-CoA. Naringenin can also be catalyzed by chalcone isomerase (CHI) as a precursor of other flavonoids. The present study found that *CHS*, *F3H*, and *p*-coumaroyl-CoA were used as precursors of other flavonoids in sugar beet (Figure 9). *CHS*, *F3H*, *DFRA*, *FLS*, and *CHI* interacted with each other and played important roles in flavonoid biosynthesis (Figures 5Bc, 9). *CHI* in the roots was closely associated with *PsbY*, *CAB4*, *PGK*, and *PGLP1A* involved in the photosynthetic carbon pathway (coefficient ≥ 0.8, $p < 0.05$, Figure 6), suggesting that dynamic changes in beet carbon metabolism directly affect the expression of genes related to photosynthesis (Sweetlove and Fernie, 2013; García-Calderón et al., 2020). *CHS* provides the basic carbon shelf structure for flavonoids and is a key step in the synthesis of flavonols, flavanones, and other substances. Upregulation of *CHS* and *CHI* facilitates the accumulation of naringenin and high-sage phenols (Figure 9) (Chen et al., 2021).

Flavonoids act as antioxidants to reduce oxidative damage caused by ROS accumulation due to abiotic stresses (Nakabayashi and Saito, 2015; Jia et al., 2019; Jiao et al., 2020). 2-Oxoglutarate 3-dioxygenase (*F3H*) has been shown to be a key gene for cold stress tolerance in tomatoes (Hu et al., 2019). F3H catalyzed the oxidation of the 3′ position of naringenin to produce dihydrokaempferol and catalyzed eriodictyol to dihydrotricetin and subsequently dihydromyricetin (Figure 9). They were then catalyzed by dihydroflavonol 4-reductase (*DFRA*) to produce leucocyanidin, anthocyanin, and leucodelphinnidin; flavonol synthase/flavanone 3-hydroxylase (*FLS1*) was used to produce kaempferol, quercetin, and myricetin (Figure 9). The upregulated flavonoid biosynthesis genes could increase the accumulation of flavonoids and thus reduce oxidative damage, thus improving the tolerance of sugar beet to low nitrogen stress. Amino acid sequence analysis revealed the presence of a common conserved structural domain in both sugar beet BvDFRA and AtDFR, the putative NADP binding site (Supplementary Figure 2B). It has been shown that the *AtDFR* gene ectopic expression determines the increase of anthocyanins and thus confers salt stress tolerance in *Brassica napus* L. (Kim et al., 2017). It is known that low nitrogen stress interferes with redox homeostasis in plant cells, which induces ROS production and leads to oxidative stress. DFRi transgenic plants by downregulation of *IbDFR* expression have reduced antioxidant capacity and are more sensitive to abiotic stress, implying an important biological role of flavonoids such as anthocyanins against oxidative stress *in vivo* (Wang et al., 2013).

5 Conclusion

The molecular tolerance and adaptation mechanisms of sugar beet to low nitrogen stress were identified by comprehensive transcriptome analysis. In summary, DEGs were extensively involved in the network of sugar beet primary and secondary metabolism (Figure 11). Low nitrogen stress suppressed the transcription of various genes involved in photosynthesis and C, N, and glutathione metabolism by regulating them in both leaves and roots. More C skeleton is used in secondary metabolism in sugar beet, which contributed to the increased expression of functional genes in phenylalanine and flavonoid biosynthesis. The present study contributed to the understanding of responsive

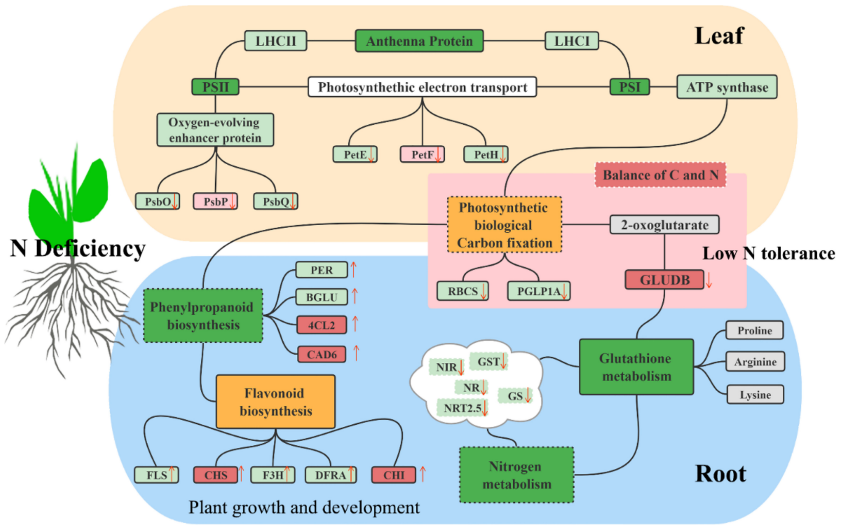

FIGURE 11
Modeling the response of sugar beet seedlings to low N stress.

relationships of gene networks related to the nitrogen metabolic pathway in sugar beet under low N conditions and provided a series of excellent genes for the improvement of sugar beet.

Data availability statement

The datasets presented in this study can be found in online repositories. The names of the repository/repositories and accession number(s) can be found below: NCBI SRA database, accession number SRP422868.

Author contributions

JL and DL conceived and designed the experiments, analyzed the data, wrote and reviewed the manuscript, and approved the final draft. WL and QY produced the graphs. XL provided reagents, materials, and analytical tools. JL, LX, and XY performed the experiments. Revisions were performed by QW, WT, and WX. All authors contributed to the article and approved the submitted version.

Funding

This research was funded by the Natural Science Foundation of Heilongjiang Province of China (LH2019C057), the Youth Program of the National Nature Science Foundation of China (31601229), the National Sugar Industry Technology System Project (CARS-170102), the Ministry of Agriculture and Rural Affairs Project (19221878, 19211031, and 19210911), and the Innovative Training Plan for Young Talents in Heilongjiang Ordinary Undergraduate Colleges and Universities (UNPYSCT-2020).

Conflict of interest

The authors declare that the research was conducted in the absence of any commercial or financial relationships that could be construed as a potential conflict of interest.

Publisher's note

All claims expressed in this article are solely those of the authors and do not necessarily represent those of their affiliated organizations, or those of the publisher, the editors and the reviewers. Any product that may be evaluated in this article, or claim that may be made by its manufacturer, is not guaranteed or endorsed by the publisher.

Supplementary material

The Supplementary Material for this article can be found online at: https://www.frontiersin.org/articles/10.3389/fpls.2023.1164151/full#supplementary-material

References

Allahverdiyeva, Y., Suorsa, M., Rossi, F., Pavesi, A., Kater, M. M., Antonacci, A., et al. (2013). Arabidopsis plants lacking PsbQ and PsbR subunits of the oxygen-evolving complex show altered PSII super-complex organization and short-term adaptive mechanisms. *Plant J.* 75, 671–684. doi: 10.1111/tpj.12230

Baiya, S., Mahong, B., Lee, S., Jeon, J., and Cairns, J. R. K. (2018). Demonstration of monolignol β-glucosidase activity of rice Os4BGlu14, Os4BGlu16 and Os4BGlu18 in *Arabidopsis thaliana bglu45* mutant. *Plant Physiol. Bioch.* 127, 223–230. doi: 10.1016/j.plaphy.2018.03.026

Bao, A., Zhao, Z., Ding, G., Shi, L., Xu, F., and Cai, H. (2015). The stable level of *glutamine synthetase 2* plays an important role in rice growth and in carbon-nitrogen metabolic balance. *Int. J. Mol. Sci.* 16, 12713–12736. doi: 10.3390/ijms160612713

BenShem, A., Frolow, F., and Nelson, N. (2003). Crystal structure of plant photosystem I. *Nature* 426, 630–635. doi: 10.1038/nature02200

Beshir, W. F., Tohge, T., Watanabe, M., Hertog, M. L., Hoefgen, R., Fernie, A. R., et al. (2019). Non-aqueous fractionation revealed changing subcellular metabolite distribution during apple fruit development. *Hortic. Res.* 6, 98. doi: 10.1038/s41438-019-0178-7

Betti, M., García-Calderón, M., Pérez-Delgado, C. M., Credali, A., Pal'ove-Balang, P., Estivill, G., et al. (2014). Reassimilation of ammonium in *Lotus japonicus*. *J. Exp. Bot.* 65, 5557–5566. doi: 10.1093/jxb/eru260

Bhatotia, K., Khatodia, S., and Khurana, S. (2015). Abiotic stress specific phosphorylation in plant proteins: a review. *Curr. Adv. Agric. Sci. (An Int. Journal)* 7, 95–100. doi: 10.5958/2394-4471.2015.00024.6

Boekema, E. J., Hankamer, B., Bald, D., Kruip, J., Nield, J., Boonstra, A. F., et al. (1995). Supramolecular structure of the photosystem II complex from green plants and cyanobacteria. *Proc. Natl. Acad. Sci. U.S.A.* 92, 175–179. doi: 10.1073/pnas.92.1.175

Bowler, M. W. (2013). Conformational dynamics in phosphoglycerate kinase, an open and shut case? *FEBS J.* 587, 1878–1883. doi: 10.1016/j.febslet.2013.05.012

Bricker, T. M., Roose, J. L., Fagerlund, R. D., Frankel, L. K., and Eaton-Rye, J. J. (2012). The extrinsic proteins of photosystem II. *Biochim. Biophys. Acta Bioenerg.* 1817, 121–142. doi: 10.1016/j.bbabio.2011.07.006

Cai, H., Lu, Y., Xie, W., Zhu, T., and Lian, X. (2012). Transcriptome response to nitrogen starvation in rice. *J. Biosci.* 37, 731–747. doi: 10.1007/s12038-012-9242-2

Chen, Y., Li, Y., Yu, L., Wang, Y., and Ni, H. (2017). Analysis of the development of the sugar beet industry in china's three main production areas. *Sugar Crops China* 39, 74–76 + 80. doi: 10.13570/j.cnki.scc.2017.04.024

Chen, C., Zhou, G., Chen, J., Liu, X., Lu, X., Chen, H., et al. (2021). Integrated metabolome and transcriptome analysis unveils novel pathway involved in the formation of yellow peel in cucumber. *Int. J. Mol. Sci.* 22, 1494. doi: 10.3390/ijms22031494

Cong, F., Diehl, B. G., Hill, J. L., Brown, N. R., and Tien, M. (2013). Covalent bond formation between amino acids and lignin: cross-coupling between proteins and lignin. *Phytochemistry* 96, 449–456. doi: 10.1016/j.phytochem.2013.09.012

Cosgrove, D. J. (2016). Plant cell wall extensibility: connecting plant cell growth with cell wall structure, mechanics, and the action of wall-modifying enzymes. *J. Exp. Bot.* 67, 463–476. doi: 10.1093/jxb/erv511

Curci, P. L., Aiese Cigliano, R., Zuluaga, D. L., Janni, M., Sanseverino, W., and Sonnante, G. (2017). Transcriptomic response of durum wheat to nitrogen starvation. *Sci. Rep.* 7, 1–14. doi: 10.1038/s41598-017-01377-0

Damkjær, J. T., Kereïche, S., Johnson, M. P., Kovacs, L., Kiss, A. Z., Boekema, E. J., et al. (2009). The photosystem II light-harvesting protein Lhcb3 affects the macrostructure of photosystem II and the rate of state transitions in arabidopsis. *Plant Cell* 21, 3245–3256. doi: 10.1105/tpc.108.064006

Ding, G., Cao, L., Zhou, J., Li, Z., Lai, Y., Liu, K., et al. (2022). DNA Methylation correlates with the expression of drought-responsive genes and drought resistance in rice. *Agronomy* 12, 1445. doi: 10.3390/agronomy12061445

Diop, M., and Gallois, J. (2022). Exploring new routes for genetic resistances to potyviruses: the case of the *Arabidopsis thaliana* phosphoglycerates kinases (PGK) metabolic enzymes. *Viruses* 14, 1245. doi: 10.3390/v14061245

Dohm, J. C., Minoche, A. E., Holtgräwe, D., Capella-Gutiérrez, S., Zakrzewski, F., Tafer, H., et al. (2014). The genome of the recently domesticated crop plant sugar beet *(Beta vulgaris)*. *Nature* 505, 546–549. doi: 10.1038/nature12817

Dong, N. Q., and Lin, H. X. (2021). Contribution of phenylpropanoid metabolism to plant development and plant–environment interactions. *J. Integr. Plant Biol.* 63, 180–209. doi: 10.1111/jipb.13054

Du, Q., Juan, Y., Sadiq, S., Yang, R., Yu, J., and Li, W. (2021). Comparative transcriptome analysis of different nitrogen responses in low-nitrogen sensitive and tolerant maize genotypes. *J. Integr. Agric.* 20, 2043–2055. doi: 10.1016/S2095-3119(20)63220-8

Erel, R., Yermiyahu, U., Ben-Gal, A., Dag, A., Shapira, O., and Schwartz, A. (2015). Modification of non-stomatal limitation and photoprotection due to K and Na nutrition of olive trees. *J. Plant Physiol.* 177, 1–10. doi: 10.1016/j.jplph.2015.01.005

Ermakova, M., LopezCalcagno, P. E., Raines, C. A., Furbank, R. T., and von Caemmerer, S. (2019). Overexpression of the rieske FeS protein of the cytochrome b6f complex increases C_4 photosynthesis in setaria viridis. *Commun. Biol.* 2, 1–12. doi: 10.1038/s42003-019-0561-9

Fei, X., Hu, H., Luo, Y., Shi, Q., and Wei, A. (2022). Widely targeted metabolomic profiling combined with transcriptome analysis provides new insights into amino acid biosynthesis in green and red pepper fruits. *Food Res. Int.* 160, 111718. doi: 10.1016/j.foodres.2022.111718

Fontaine, J.-X., Tercé-Laforgue, T., Armengaud, P., Clément, G., Renou, J.-P., Pelletier, S., et al. (2012). Characterization of a NADH-dependent glutamate dehydrogenase mutant of arabidopsis demonstrates the key role of this enzyme in root carbon and nitrogen metabolism. *Plant Cell* 24, 4044–4065. doi: 10.1105/tpc.112.103689

Gan, L., Chen, M., Zhang, J., Fan, J., and Yan, X. (2022). A novel beta-glucosidase gene for plant type was identified by genome-wide association study and gene Co-expression analysis in widespread bermudagrass. *Int. J. Mol. Sci.* 23, 11432. doi: 10.3390/ijms231911432

García-Calderón, M., Pérez-Delgado, C. M., Palove-Balang, P., Betti, M., and Márquez, A. J. (2020). Flavonoids and isoflavonoids biosynthesis in the model legume lotus japonicus; connections to nitrogen metabolism and photorespiration. *Plants* 9, 774. doi: 10.3390/plants9060774

Gau, A., Thole, H., Sokolenko, A., Altschmied, L., Herrmann, R., and Pistorius, E. (1998). PsbY, a novel manganese-binding, low-molecular-mass protein associated with photosystem II. *Mol. Genet. Genom.* 260, 56–68. doi: 10.1007/s004380050870

Guo, D., Chen, F., Inoue, K., Blount, J. W., and Dixon, R. A. (2001). Downregulation of caffeic acid 3-o-methyltransferase and caffeoyl CoA 3-o-methyltransferase in transgenic alfalfa: impacts on lignin structure and implications for the biosynthesis of G and s lignin. *Plant Cell* 13, 73–88. doi: 10.1105/tpc.13.1.73

Han, Y., Watanabe, S., Shimada, H., and Sakamoto, A. (2020). Dynamics of the leaf endoplasmic reticulum modulate β-glucosidase-mediated stress-activated ABA production from its glucosyl ester. *J. Exp. Bot.* 71, 2058–2071. doi: 10.1093/jxb/erz528

Hao, J., Li, Q., Yu, H., Wang, H., Chai, L., Miao, T., et al. (2021). Comparative proteomic analysis of cucumber fruits under nitrogen deficiency at the fruiting stage. *Hortic. Plant J.* 7, 59–72. doi: 10.1016/j.hpj.2020.12.002

Hirano, K., Aya, K., Kondo, M., Okuno, A., Morinaka, Y., and Matsuoka, M. (2012). *OsCAD2* Is the major *CAD* gene responsible for monolignol biosynthesis in rice culm. *Plant Cell Rep.* 31, 91–101. doi: 10.1007/s00299-011-1142-7

Hu, T., Wang, Y., Wang, Q., Dang, N., Wang, L., Liu, C., et al. (2019). The tomato 2-oxoglutarate-dependent dioxygenase gene *S1F3HL* is critical for chilling stress tolerance. *Hortic. Res.* 6, 45. doi: 10.1038/s41438-019-0127-5

Imamura, S., Kanesaki, Y., Ohnuma, M., Inouye, T., Sekine, Y., Fujiwara, T., et al. (2009). R2R3-type MYB transcription factor, CmMYB1, is a central nitrogen assimilation regulator in *Cyanidioschyzon merolae*. *Proc. Natl. Acad. Sci.* 106, 12548–12553. doi: 10.1073/pnas.090279010

Jia, X., Zhu, Y., Hu, Y., Zhang, R., Cheng, L., Zhu, Z., et al. (2019). Integrated physiologic, proteomic, and metabolomic analyses of *Malus halliana* adaptation to saline–alkali stress. *Hortic. Res.* 6, 91. doi: 10.1038/s41438-019-0172-0

Jiao, C., Sørensen, I., Sun, X., Sun, H., Behar, H., Alseekh, S., et al. (2020). The *Penium margaritaceum* genome: hallmarks of the origins of land plants. *Cell* 181, 1097–1111. doi: 10.1016/j.cell.2020.04.019

Kakiuchi, S., Uno, C., Ido, K., Nishimura, T., Noguchi, T., Ifuku, K., et al. (2012). The PsbQ protein stabilizes the functional binding of the PsbP protein to photosystem II in higher plants. *Biochim. Biophys. Acta Bioenerg.* 1817, 1346–1351. doi: 10.1016/j.bbabio.2012.01.009

Kanehisa, M., Araki, M., Goto, S., Hattori, M., Hirakawa, M., Itoh, M., et al. (2008). KEGG for linking genomes to life and the environment. *Nucleic Acids Res.* 36, D480–D484. doi: 10.1093/nar/gkm882

Kanehisa, M., Furumichi, M., Tanabe, M., Sato, Y., and Morishima, K. (2017). KEGG: new perspectives on genomes, pathways, diseases and drugs. *Nucleic Acids Res.* 45, D353–DD61. doi: 10.1093/nar/gkw1092

Kanehisa, M., Sato, Y., Kawashima, M., Furumichi, M., and Tanabe, M. (2016). KEGG as a reference resource for gene and protein annotation. *Nucleic Acids Res.* 44, D457–DD62. doi: 10.1093/nar/gkv1070

Kiba, T., Kudo, T., Kojima, M., and Sakakibara, H. (2011). Hormonal control of nitrogen acquisition: roles of auxin, abscisic acid, and cytokinin. *J. Exp. Bot.* 62, 1399–1409. doi: 10.1093/jxb/erq410

Kim, J., Lee, W. J., Vu, T. T., Jeong, C. Y., Hong, S.-W., and Lee, H. (2017). High accumulation of anthocyanins *via* the ectopic expression of AtDFR confers significant salt stress tolerance in *Brassica napus* l. *Plant Cell Rep.* 36, 1215–1224. doi: 10.1007/s00299-017-2147-7

Klem, K., Oravec, M., Holub, P., Šimor, J., Findurová, H., Surá, K., et al. (2022). Interactive effects of nitrogen, UV and PAR on barley morphology and biochemistry are associated with the leaf c: n balance. *Plant Physiol. Bioch.* 172, 111–124. doi: 10.1016/j.plaphy.2022.01.006

Krapp, A., and Traong, H. (2006). Regulation of C/N interaction in model plant species. *J. Crop Improv.* 15, 127–173. doi: 10.1300/J411v15n02_05

Kumar, S., and Trivedi, P. K. (2018). Glutathione s-transferases: role in combating abiotic stresses including arsenic detoxification in plants. *Front. Plant Sci.* 9. doi: 10.3389/fpls.2018.00751

Laurent, S., Chen, H., Bédu, S., Ziarelli, F., Peng, L., and Zhang, C. (2005). Nonmetabolizable analogue of 2-oxoglutarate elicits heterocyst differentiation under repressive conditions in anabaena sp. PCC 7120. *Proc. Natl. Acad. Sci. U.S.A.* 102, 9907–9912. doi: 10.1073/pnas.050233710

Lezhneva, L., Kiba, T., FeriaBourrellier, A. B., Lafouge, F., BoutetMercey, S., Zoufan, P., et al. (2014). The arabidopsis nitrate transporter NRT 2.5 plays a role in nitrate acquisition and remobilization in nitrogen-starved plants. *Plant J.* 80, 230–241. doi: 10.1111/tpj.12626

Li, J., Li, W., Xu, L., Wang, M., Zhou, W., Li, S., et al. (2022). Acclimation of sugar beet in morphological, physiological and Bv*AMT1. 2* expression under low and high nitrogen supply. *PloS One* 17, e0278327. doi: 10.1371/journal.pone.0278327

Li, J., Liu, X., Yao, Q., Xu, L., Li, W., Tan, W., et al. (2023). Tolerance and adaptation characteristics of sugar beet *(Beta vulgaris* l.) to low nitrogen supply. *Plant Signal. Behav.* 18, 2159155. doi: 10.1080/15592324.2022.2159155

Li, M., Xu, J., Wang, X., Fu, H., Zhao, M., Wang, H., et al. (2018). Photosynthetic characteristics and metabolic analyses of two soybean genotypes revealed adaptive strategies to low-nitrogen stress. *J. Plant Physiol.* 229, 132–141. doi: 10.1016/j.jplph.2018.07.009

Li, Y., Ye, Q., He, D., Bai, H., and Wen, J. (2020). The ubiquity and coexistence of two FBPases in chloroplasts of photosynthetic eukaryotes and its evolutionary and functional implications. *Plant Divers.* 42, 120–125. doi: 10.1016/j.pld.2019.09.002

Li, L., Ye, L., Kong, Q., and Shou, H. (2019). A vacuolar membrane ferric-chelate reductase, OsFRO1, alleviates fe toxicity in rice *(Oryza sativa* l.). *Front. Plant Sci.* 10. doi: 10.3389/fpls.2019.00700

Liang, T., Yuan, Z., Fu, L., Zhu, M., Luo, X., Xu, W., et al. (2021). Integrative transcriptomic and proteomic analysis reveals an alternative molecular network of glutamine synthetase 2 corresponding to nitrogen deficiency in rice *(Oryza sativa* l.). *Int. J. Mol. Sci.* 22, 7674. doi: 10.3390/ijms22147674

Liao, H., Chung, Y., and Hsieh, M. (2022). Glutamate: a multifunctional amino acid in plants. *Plant Sci.* 318, 111238. doi: 10.1016/j.plantsci.2022.111238

Lin, Y., Pan, K., Hung, C., Huang, H., Chen, C., Feng, T., et al. (2013). Overexpression of ferredoxin, PETF, enhances tolerance to heat stress in chlamydomonas reinhardtii. *Int. J. Mol. Sci.* 14, 20913–20929. doi: 10.3390/ijms141020913

Liu, J., Yang, H., Lu, Q., Wen, X., Chen, F., Peng, L., et al. (2012). PsbP-domain protein1, a nuclear-encoded thylakoid lumenal protein, is essential for photosystem I assembly in *Arabidopsis*. *Plant Cell* 24, 4992–5006. doi: 10.1105/tpc.112.106542

Lotta, v. S., Serena, S., Jörg, M., Christiane, F., Fikret, M., and Wolfgang, P. S. (2016). The PsbY protein of arabidopsis photosystem II is important for the redox control of cytochrome *b559*. *Biochim. Biophys. Acta Bioenerg.* 1857, 1524–1533. doi: 10.1016/j.bbabio.2016.05.004

Mao, X., Cai, T., Olyarchuk, J. G., and Wei, L. (2005). Automated genome annotation and pathway identification using the KEGG orthology (KO) as a controlled vocabulary. *Bioinformatics* 21, 3787–3793. doi: 10.1093/bioinformatics/bti430

Meng, X., Wang, X., Zhang, Z., Xiong, S., Wei, Y., Guo, J., et al. (2021). Transcriptomic, proteomic, and physiological studies reveal key players in wheat nitrogen use efficiency under both high and low nitrogen supply. *J. Exp. Bot.* 72, 4435–4456. doi: 10.1093/jxb/erab153

Nakabayashi, R., and Saito, K. (2015). Integrated metabolomics for abiotic stress responses in plants. *Curr. Opin. Plant Biol.* 24, 10–16. doi: 10.1016/j.pbi.2015.01.003

Nunes-Nesi, A., Fernie, A. R., and Stitt, M. (2010). Metabolic and signaling aspects underpinning the regulation of plant carbon nitrogen interactions. *Mol. Plant* 3, 973–996. doi: 10.1093/mp/ssq049

Onaga, G., and Wydra, K. (2016). Advances in plant tolerance to abiotic stresses. *Plant Genomics* 10, 229–272. doi: 10.5772/64350

Opassiri, R., Pomthong, B., Onkoksoong, T., Akiyama, T., Esen, A., and Ketudat Cairns, J. R. (2006). Analysis of rice glycosyl hydrolase family 1 and expression of Os4bglu12 β-glucosidase. *BMC Plant Biol.* 6, 1–19. doi: 10.1186/1471-2229-6-33

O'Sullivan, J. (2021). "Chapter 12 - climate change and world population," in *The impacts of climate change*. Ed. T. M. Letcher (Australia: Elsevier), 313–350.

Ozawa, S.-I., Bald, T., Onishi, T., Xue, H., Matsumura, T., Kubo, R., et al. (2018). Configuration of ten light-harvesting chlorophyll a/b complex I subunits in chlamydomonas reinhardtii photosystem I. *Plant Physiol.* 178, 583–595. doi: 10.1104/pp.18.00749

Pan, X., Cao, P., Su, X., Liu, Z., and Li, M. (2020). Structural analysis and comparison of light-harvesting complexes I and II. *Biochim. Biophys. Acta Bioenerg.* 1861, 148038. doi: 10.1016/j.bbabio.2019.06.010

Pan, S., Liu, H., Mo, Z., Patterson, B., Duan, M., Tian, H., et al. (2016). Effects of nitrogen and shading on root morphologies, nutrient accumulation, and photosynthetic parameters in different rice genotypes. *Sci. Rep.* 6, 1–14. doi: 10.1038/srep32148

Passardi, F., Longet, D., Penel, C., and Dunand, C. (2004). The class III peroxidase multigenic family in rice and its evolution in land plants. *Phytochemistry* 65, 1879–1893. doi: 10.1016/j.phytochem.2004.06.023

Peleman, J. D., and van der Voort, J. R. (2003). Breeding by design. *Trends Plant Sci.* 8, 330–334. doi: 10.1016/S1360-1385(03)00134-1

Peng, M., Hannam, C., Gu, H., Bi, Y. M., and Rothstein, S. J. (2007). A mutation in *NLA*, which encodes a RING-type ubiquitin ligase, disrupts the adaptability of *Arabidopsis* to nitrogen limitation. *Plant J.* 50, 320–337. doi: 10.1111/j.1365-313X.2007.03050.x

Qin, L., Walk, T. C., Han, P., Chen, L., Zhang, S., Li, Y., et al. (2019). Adaption of roots to nitrogen deficiency revealed by 3D quantification and proteomic analysis. *Plant Physiol.* 179, 329–347. doi: 10.1104/pp.18.00716

Quan, X., Zeng, J., Han, Z., and Zhang, G. (2017). Ionomic and physiological responses to low nitrogen stress in Tibetan wild and cultivated barley. *Plant Physiol. Bioch.* 111, 257–265. doi: 10.1016/j.plaphy.2016.12.008

Rana, N. K., Mohanpuria, P., Kumar, V., and Yadav, S. K. (2010). A CsGS is regulated at transcriptional level during developmental stages and nitrogen utilization in *Camellia sinensis* (L.) o. kuntze. *Mol. Biol. Rep.* 37, 703–710. doi: 10.1007/s11033-009-9559-6

Ren, C., Jin, S., Wu, Y., Zhang, B., Kanter, D., Wu, B., et al. (2021). Fertilizer overuse in Chinese smallholders due to lack of fixed inputs. *J. Environ. Manage.* 293, 112913. doi: 10.1016/j.jenvman.2021.112913

Schmitter, J., Jacquot, J., Frédéric, D. L., Beauvallet, C., Dutka, S., Gadal, P., et al. (1988). Purification, properties and complete amino acid sequence of the ferredoxin from a green alga, *Chlamydomonas reinhardtii*. *Eur. J. Biochem.* 172, 405–412. doi: 10.1111/j.1432-1033.1988.tb13901.x

Shen, X., Yang, L., Han, P., Gu, C., Li, Y., Liao, X., et al. (2022). Metabolic profiles reveal changes in the leaves and roots of rapeseed *(Brassica napus* l.) seedlings under nitrogen deficiency. *Int. J. Mol. Sci.* 23, 5784. doi: 10.3390/ijms23105784

Shi, Y., Guo, E., Cheng, X., Wang, L., Jiang, S., Yang, X., et al. (2022). Effects of chilling at different growth stages on rice photosynthesis, plant growth, and yield. *Environ. Exp. Bot.* 203, 105045. doi: 10.1016/j.envexpbot.2022.105045

Silva, F. A., Albuquerque, L. M., Martins, T. F., de Freitas, J. A., Vasconcelos, I. M., de Freitas, D. Q., et al. (2022). A peroxidase purified from cowpea roots possesses high thermal stability and displays antifungal activity against *Colletotrichum gloeosporioides* and *Fusarium oxysporum*. *Biocatal. Agric. Biotechnol.* 42, 102322. doi: 10.1016/j.bcab.2022.102322

Simões, W. L., Yuri, J. E., Guimarães, M. J., Santos, J., and Araújo, E. F. (2016). Beet cultivation with saline effluent from fish farming. *Rev. Bras. Eng. Agr. Amb.* 20, 62–66. doi: 10.1590/1807-1929/agriambi.v20n1p62-66

Sultana, N., Islam, S., Juhasz, A., Yang, R., She, M., Alhabbar, Z., et al. (2020). Transcriptomic study for identification of major nitrogen stress responsive genes in Australian bread wheat cultivars. *Front. Genet.* 11. doi: 10.3389/fgene.2020.583785

Sun, H., Shi, Q., Zhang, S., and Huang, W. (2022). The response of photosystem I to fluctuating light is influenced by leaf nitrogen content in tomato. *Environ. Exp. Bot.* 193, 104665. doi: 10.1016/j.envexpbot.2021.104665

Sweetlove, L. J., Beard, K. F., Nunes-Nesi, A., Fernie, A. R., and Ratcliffe, R. G. (2010). Not just a circle: flux modes in the plant TCA cycle. *Trends Plant Sci.* 15, 462–470. doi: 10.1016/j.tplants.2010.05.006

Sweetlove, L. J., and Fernie, A. R. (2013). The spatial organization of metabolism within the plant cell. *Annu. Rev. Plant Biol.* 64, 723–746. doi: 10.1146/annurev-arplant-050312-120233

Tantray, A. Y., Hazzazi, Y., and Ahmad, A. (2022). Physiological, agronomical, and proteomic studies reveal crucial players in rice nitrogen use efficiency under low nitrogen supply. *Int. J. Mol. Sci.* 23, 6410. doi: 10.3390/ijms23126410

Terauchi, A. M., Lu, S., Zaffagnini, M., Tappa, S., Hirasawa, M., Tripathy, J. N., et al. (2009). Pattern of expression and substrate specificity of chloroplast ferredoxins from chlamydomonas reinhardtii. *J. Biol. Chem.* 284, 25867–25878. doi: 10.1074/jbc.M109.023622

Tercé-Laforgue, T., Bedu, M., Dargel-Grafin, C., Dubois, F., Gibon, Y., Restivo, F. M., et al. (2013). Resolving the role of plant glutamate dehydrogenase: II. physiological characterization of plants overexpressing the two enzyme subunits individually or simultaneously. *Plant Cell Physiol.* 54, 1635–1647. doi: 10.1093/pcp/pct108

Tercé-Laforgue, T., Clément, G., Marchi, L., Restivo, F. M., Lea, P. J., and Hirel, B. (2015). Resolving the role of plant NAD-glutamate dehydrogenase: III. overexpressing individually or simultaneously the two enzyme subunits under salt stress induces changes in the leaf metabolic profile and increases plant biomass production. *Plant Cell Physiol.* 56, 1918–1929. doi: 10.1093/pcp/pcv114

Tian, H., Song, H., Wu, X., and Zhang, Z. (2022). Responses of cell wall components to low nitrogen in rapeseed roots. *Agronomy* 12, 1044. doi: 10.3390/agronomy12051044

Wan, Q., Bai, T., Liu, M., Liu, Y., Xie, Y., Zhang, T., et al. (2022). Comparative analysis of the chalcone-flavanone lsomerase genes in six citrus species and their expression analysis in sweet orange *(Citrus sinensis)*. *Front. Genet.* 13:848141. doi: 10.3389/fgene.2022.848141

Wang, H., Fan, W., Li, H., Yang, J., Huang, J., and Zhang, P. (2013). Functional characterization of dihydroflavonol-4-reductase in anthocyanin biosynthesis of purple sweet potato underlies the direct evidence of anthocyanins function against abiotic stresses. *PloS One* 8, e78484. doi: 10.1371/journal.pone.0078484

Wascher, F. L., Stralis-Pavese, N., McGrath, J. M., Schulz, B., Himmelbauer, H., and Dohm, J. C. (2022). Genomic distances reveal relationships of wild and cultivated beets. *Nat. Commun.* 13, 2021. doi: 10.1038/s41467-022-29676-9

Wen, B., Gong, X., Chen, X., Tan, Q., Li, L., and Wu, H. (2022). Transcriptome analysis reveals candidate genes involved in nitrogen deficiency stress in apples. *J. Plant Physiol.* 279, 153822. doi: 10.1016/j.jplph.2022.153822

Xu, C., Huang, S., Tian, B., Ren, J., Meng, Q., and Wang, P. (2017). Manipulating planting density and nitrogen fertilizer application to improve yield and reduce environmental impact in Chinese maize production. *Front. Plant Sci.* 8. doi: 10.3389/fpls.2017.01234

Yamazaki, S., Ochiai, K., and Matoh, T. (2019). Rice plants have three homologs of glutathione synthetase genes, one of which, OsGS2, codes for hydroxymethyl-glutathione synthetase. *Plant direct* 3, e00119. doi: 10.1002/pld3.119

Yang, T., Zhang, P., Pan, J., Amanullah, S., Luan, F., Han, W., et al. (2022). Genome-wide analysis of the peroxidase gene family and verification of lignin synthesis-related genes in watermelon. *Int. J. Mol. Sci.* 23, 642. doi: 10.3390/ijms23020642

Yi, X., Hargett, S. R., Frankel, L. K., and Bricker, T. M. (2009). The PsbP protein, but not the PsbQ protein, is required for normal thylakoid architecture in *Arabidopsis thaliana*. *FEBS Lett.* 583, 2142–2147. doi: 10.1016/j.febslet.2009.05.048

Yi, X., Hargett, S. R., Liu, H., Frankel, L. K., and Bricker, T. M. (2007). The PsbP protein is required for photosystem II complex assembly/stability and photoautotrophy in *Arabidopsis thaliana*. *J. Biol. Chem.* 282, 24833–24841. doi: 10.1074/jbc.M705011200

Yin, L., Xu, H., Dong, S., Chu, J., Dai, X., and He, M. (2019). Optimised nitrogen allocation favours improvement in canopy photosynthetic nitrogen-use efficiency: evidence from late-sown winter wheat. *Environ. Exp. Bot.* 159, 75–86. doi: 10.1016/j.envexpbot.2018.12.013

Young, M. D., Wakefield, M. J., Smyth, G. K., and Oshlack, A. (2010). Gene ontology analysis for RNA-seq: accounting for selection bias. *Genome Biol.* 11, R14. doi: 10.1186/gb-2010-11-2-r14

Yu, W., Liu, H., Luo, J., Zhang, S., Xiang, P., Wang, W., et al. (2022). Partial root-zone simulated drought induces greater flavonoid accumulation than full root-zone simulated water deficiency in the leaves of *Ginkgo biloba*. environ. *Exp. Bot.* 201, 104998. doi: 10.1016/j.envexpbot.2022.104998

Zhang, X., Davidson, E. A., Mauzerall, D. L., Searchinger, T. D., Dumas, P., and Shen, Y. (2015). Managing nitrogen for sustainable development. *Nature* 528, 51–59. doi: 10.1038/nature15743

Zhang, X., Gong, X., Yu, H., Su, X., Cheng, S., Huang, J., et al. (2023). The proline-rich protein MdPRP6 confers tolerance to salt stress in transgenic apple *(Malus domestica)*. *Sci. Hortic.* 308, 111581. doi: 10.1016/j.scienta.2022.111581

Zhang, X., Misra, A., Nargund, S., Coleman, G. D., and Sriram, G. (2018c). Concurrent isotope-assisted metabolic flux analysis and transcriptome profiling reveal responses of poplar cells to altered nitrogen and carbon supply. *Plant J.* 93, 472–488. doi: 10.1111/tpj.13792

Zhang, Q., Tang, D., Liu, M., and Ruan, J. (2018b). Integrated analyses of the transcriptome and metabolome of the leaves of albino tea cultivars reveal coordinated regulation of the carbon and nitrogen metabolism. *Sci. Hortic.* 231, 272–281. doi: 10.1016/j.scienta.2017.11.026

Zhang, C., Zhou, C., Burnap, R. L., and Peng, L. (2018a). Carbon/nitrogen metabolic balance: lessons from cyanobacteria. *Trends Plant Sci.* 23, 1116–1130. doi: 10.1016/j.tplants.2018.09.008

Zhao, Q. (2016). Lignification: flexibility, biosynthesis and regulation. *Trends Plant Sci.* 21, 713–721. doi: 10.1016/j.tplants.2016.04.006

Zheng, J., Li, S., Maratab, A., Huang, Q., Zhneg, X., and Pang, L. (2020). Effects of UV-b treatment on controlling lignification and quality of bamboo *(Phyllostachys prominens)* shoots without sheaths during cold storage. *J. Integr. Agric.* 19, 1387–1395. doi: 10.1016/S2095-3119(20)63170-7

frontiers | Frontiers in Plant Science

TYPE Original Research
PUBLISHED 30 May 2023
DOI 10.3389/fpls.2023.1163939

Check for updates

OPEN ACCESS

EDITED BY
Diaa Abd El Moneim,
Arish University, Egypt

REVIEWED BY
Klára Kosová,
Crop Research Institute (CRI), Czechia
Zahoor Ahmad,
University of Central Punjab, Pakistan

*CORRESPONDENCE
Hongmei Zeng
zenghongmei@caas.cn

RECEIVED 11 February 2023
ACCEPTED 26 April 2023
PUBLISHED 30 May 2023

CITATION
Yan J, Ninkuu V, Fu Z, Yang T, Ren J, Li G, Yang X and Zeng H (2023) OsOLP1 contributes to drought tolerance in rice by regulating ABA biosynthesis and lignin accumulation.
Front. Plant Sci. 14:1163939.
doi: 10.3389/fpls.2023.1163939

COPYRIGHT
© 2023 Yan, Ninkuu, Fu, Yang, Ren, Li, Yang and Zeng. This is an open-access article distributed under the terms of the Creative Commons Attribution License (CC BY). The use, distribution or reproduction in other forums is permitted, provided the original author(s) and the copyright owner(s) are credited and that the original publication in this journal is cited, in accordance with accepted academic practice. No use, distribution or reproduction is permitted which does not comply with these terms.

OsOLP1 contributes to drought tolerance in rice by regulating ABA biosynthesis and lignin accumulation

Jianpei Yan, Vincent Ninkuu, Zhenchao Fu, Tengfeng Yang, Jie Ren, Guangyue Li, Xiufen Yang and Hongmei Zeng*

State Key Laboratory for Biology of Plant Diseases and Insect Pests, Institute of Plant Protection, Chinese Academy of Agricultural Sciences, Beijing, China

Rice, as a major staple crop, employs multiple strategies to enhance drought tolerance and subsequently increase yield. Osmotin-like proteins have been shown to promote plant resistance to biotic and abiotic stress. However, the drought resistance mechanism of osmotin-like proteins in rice remains unclear. This study identified a novel osmotin-like protein, OsOLP1, that conforms to the structure and characteristics of the osmotin family and is induced by drought and NaCl stress. CRISPR/Cas9-mediated gene editing and overexpression lines were used to investigate the impact of OsOLP1 on drought tolerance in rice. Compared to wild-type plants, transgenic rice plants overexpressing OsOLP1 showed high drought tolerance with leaf water content of up to 65%, and a survival rate of 53.1% by regulating 96% stomatal closure and more than 2.5-fold proline content promotion through the accumulation of 1.5-fold endogenous ABA, and enhancing about 50% lignin synthesis. However, OsOLP1 knockout lines showed severely reduced ABA content, decreased lignin deposition, and weakened drought tolerance. In conclusion, the finding confirmed that OsOLP1 drought-stress modulation relies on ABA accumulation, stomatal regulation, proline, and lignin accumulation. These results provide new insights into our perspective on rice drought tolerance.

KEYWORDS

OsOLP1, drought tolerance, rice, abscisic acid, lignin

Introduction

Drought is a significant environmental stress that adversely affects plant growth, development, and rhythm. Climate uncertainty leads to water deficits, and crops coordinate diverse signaling cascades and osmotic adjustments to resist drought, maintain extrinsic metabolism, and increase production to ensure food supply worldwide (Hu and Xiong, 2014). Rice is an essential commodity that is consumed by about half of the global population (Wei and Huang, 2019). However, rice is also an extremely water-consuming

crop owing to its tiny root architecture and rapid stomatal aperture. Drought constrains rice growth and yield enhancement (Sahebi et al., 2018).

When plants suffer from water shortages in the external environment, signaling commences adopting various strategies to avoid physiological water imbalances in the osmotic potential of cells, thereby preventing drought damage (Hu and Xiong, 2014; Gupta et al., 2020). Abscisic acid (ABA) is an essential regulatory hormone that is responsive to adverse abiotic factors. Under drought conditions, ABA signals activate downstream resistance components that participate in water regulation (Gupta et al., 2020). Plants mainly lose water through transpiration *via* stomata on their leaves. Stomata contain two specialized guard cells whose density and movement determine the rate of transpiration. Previous studies have demonstrated that plants can enhance drought tolerance by mediating water utilization through stomata, as evidenced by the overexpression of *ERECTA*, *ENHANCED DROUGHT TOLERANCE1/HOMEODOMAIN GLABROUS11* (*EDT1/HDG11*) in Arabidopsis, and *stress-induced protein kinase gene 1* (*SIK1*), and *transcription factor 1-like* (*TF1L*) from rice (Masle et al., 2005; Ouyang et al., 2010; Zhu et al., 2016; Bang et al., 2019). The accumulation of intracellular solutes decreases osmotic potential, allowing plants to maintain turgor stress. Proline can act as an osmolyte to cope with unfavorable conditions faced by plants. Plant lignification can reflect the degree of drought tolerance, and synthetic lignin content can express the degree of lignification (Bang et al., 2019; Bang et al., 2022). Lignin helps maintain the osmotic balance of cells by controlling osmosis and transpiration through the cell wall. Additionally, lignin is deposited on specific tissue walls to enhance mechanical support and water impermeability (Ninkuu et al., 2023; Bang et al., 2022; Li et al., 2022).

Osmotins and osmotin-like proteins (OLPs) are widely found in plants and named for their ability to adapt to low osmotic environments. This family of proteins belongs to the pathogenesis-related protein 5 (PR5) and is responsive to biotic and abiotic stressors (Chowdhury et al., 2017; Hakim et al., 2018; Bashir et al., 2020). Initial studies have shown that osmotins could be induced by salinity and drought conditions and adapt well to low water potential (Hakim et al., 2018; Bashir et al., 2020). Further research has demonstrated that osmotins and OLPs mediate plant tolerance to abiotic stress. Overexpression of *SnOLP* in soybean significantly improved the physiological state and plant yield under water shortage (Weber et al., 2014). *SindOLP* overexpression promoted the recovery of sesame plants after prolonged exposure to drought and salt stress (Chowdhury et al., 2017). Osmotin-expressing seedlings of apoplastically secreted tobacco osmotin in cotton slowed down the wilting rate following the termination of dry conditions (Parkhi et al., 2009). The above evidence indicates that osmotin family proteins play a protective role against drought conditions.

There are a few reports on osmotins or osmotin-related proteins in rice in terms of stress tolerance. The rice osmotin gene *OsOSM1* conferred immunity against rice sheath blight (Xue et al., 2016). Overexpression of the osmotin protein TlOsm from *Tripogon loliiformis* in rice enhances cold, drought, and salinity tolerance (Le et al., 2018). Overexpression of osmotin promoter binding protein 1 (OPBP1) from tobacco in rice enhances salt stress and defense against belly rot (*Rhizoctonia solani*) and rice blast (*Magnaporthe oryzae*) (Chen and Guo, 2008). The above reports indicate that osmotins or osmotin-related proteins can affect rice stress response. However, relatively little research has been conducted on osmotins or OLPs from rice. There are more than 40 osmotins or OLPs in the rice genome (https://www.genome.jp), designing further studies to characterize their roles in drought tolerance would provide an insight into attempts for drought-tolerant rice transformation.

This study reported a new osmotin-like protein, OsOLP1, identified from rice and demonstrated its involvement in mediating drought tolerance through CRISPR/Cas9 knockout and overexpression techniques. The results showed that overexpression of *OsOLP1* gene enhanced drought tolerance through ABA accumulation, which caused the closure of leaf stomata and the proline enrichment, to alleviate water loss in rice. In addition, OsOLP1 promoted the lignification of vascular tissue and maintained the balance between water and ion distribution. In contrast, CR-*OsOLP1* knockout lines showed more sensitivity to drought. Our data indicated that OsOLP1 is a drought-tolerance protein that can address plant tolerance to external stress.

Materials and methods

Plasmid construction, rice transformation, and detection of transgenic plants

The rice gene *OsOLP1* (GenBank accession number: Os01g0839900) was used in the present study. The gene has no intron in its coding region. To generate *OsOLP1* knockout mutant, a gene editing vector for *OsOLP1* was constructed using the CRISPR/Cas9 method (Ma et al., 2015). To improve the targeting efficiency of CRISPR, two sites in the coding region of OsOLP1, T1 (ACCTTGGTCCGGCCGCAT'TGG) and T2 (AGTTGCCGG CCCTCGTGC'GGG) were selected and ligated to *OsU6a* and *OsU6b* promoters by overlapping PCR, and sgRNA was ligated to the end of the target site to construct the "OsU6a-T1-sgRNA-OsU6b-T2- sgRNA" expression cassette, and assembled into the binary pYLCRISPR/Cas9 Pubi-H vectors (digested with *Bsa I*) to generate transgenic rice plants. The target sites and primers (Supplementary Table 1) required for vector construction were selected using CRISPR-GE(http://skl.scau.edu.cn/).

To generate *OsOLP1* overexpression line, the full-length coding sequence of *OsOLP1* was amplified from *Oryza sativa* (japonica Nipponbare cultivar) using the All-in-one First-Strand cDNA synthesis SuperMix and TransStart® FastPfu Fly DNA polymerase (TransGene Biotech, Beijing, China) and inserted into the pRHV-cHA (He et al., 2018) vector carrying the *Ubi* promoter and C-terminal HA tag. Supplementary Table 1 shows the primer pairs required for construction of the vector.

The *Agrobacterium tumefaciens* EHA105 transformation was performed as described previously (Hiei et al., 1994; Clough and Bent, 1998). All constructed vectors were transferred to *A.*

tumefaciens EHA105 *via* chemical transformation. 1 µg of recombinant plasmid DNA was added to EHA105 competent cells, placed on ice for 5 min, in liquid nitrogen for 5 min, at 37°C for 5 min, and on ice for 5 min, 700 mL of antibiotic-free LB medium was added and incubated for 2-3 h with shaking, followed by centrifugation to collect the cells, and 100 µL of the suspension was spread on LB plates with 50 µg/mL kanamycin and 25 µg/mL rifampicin. *A. tumefaciens* was co-incubated with callus tissues induced from mature rice seeds, and the desired rice lines were obtained by hygromycin resistance screening and differentiation.

For the identification of CR-*OsOLP1* lines, DNA was extracted from five-week-old leaves, and the coding region of OsOLP1 was amplified using the Cas-*OsOLP1* primer pairs (Supplementary Table 1). The PCR products were then sequenced and aligned using DNAMAN. RNA was also extracted from the selected lines (CR-*OsOLP1*#20 and #27), and the expression levels of *OsOLP1* were analyzed by qRT-PCR.

OsOLP1 overexpression lines (OE-*OsOLP1*) were determined by immunobloting and qRT-PCR. Total protein was extracted from five-week-old leaves in the OE-*OsOLP1* lines using a plant protein extraction kit (Solarbio life science, Beijing, China) according to the manufacturer's instructions. Rice leaves were extracted with extraction buffer to obtain total protein and then subjected to SDS-PAGE analysis. Samples were incubated with anti-HA antibodies (1:1000) and anti-rabbit (1:5000) and then exposed and photographed with Tanon Chemiluminescence Imaging System. Wild-type seedlings were used as the negative controls. Staining of total proteins with Ponceau S was used as the control. The leaves of the selected lines (OE-*OsOLP1*#28 and #38) were sampled for qRT-PCR analysis. Primer pairs used for the PCR are listed in Supplementary Table 1.

Plant growth and stress treatment

Sterilization of experimental rice seeds consisting of *OsOLP1* overexpressing and *OsOLP1* knockout lines was accomplished by immersing them in 75% ethanol for 15 minutes, and residual ethanol was removed by rinsing seven times. Rice seeds were spread out on a Petri dish containing moistened filter paper and germinated in a growth chamber at 28°C under 16 h light and 8 h in darkness. Sprouted seedlings were transplanted and grown under the same conditions for five weeks. Each pot contains equal amounts of breathable vermiculite and nutrient soil. Samples were quick-frozen in liquid nitrogen and stored temporally at -80°C until analysis.

For the treatment of drought tolerance, five-week-old rice seedlings were continuously deprived of water for 5 days to test for their drought tolerance rate. The seedlings were rewatered for 7 days until the plants recovered, and plant survival was determined by the color and appearance of new leaves. The survival rate was determined by calculating the ratio of total survived seedlings to the total number of seedlings subjected to drought stress. Three replicates of each experiment with 20 seedlings per replicate were performed. To calculate the soil water content (SWC), a 1 ml pipette tip was inserted into the culture soil and vertical sampling of the soil was performed at different (0, 1, 2, 3, 4, 5) days of the drought treatment and SWC was calculated using the formula below. To calculate the relative water content (RWC) of leaves, the full-expanded leaves of *OsOLP1* knockout and overexpression line, and WT were sampled at 0 and 5 days, and RWC was analyzed using the formula below.

$$\mathrm{SWC}\,\% = \frac{(\mathrm{Sf\text{-}Sd})}{\mathrm{Sd}} \times 100 \quad \text{and} \quad \mathrm{RWC}\,\% = \frac{(\mathrm{Wf\text{-}Wd})}{(\mathrm{Ws\text{-}Wd})} \times 100$$

where Sf represents soil fresh weight, Sd represents soil dry weight, Wf represents the fresh weight of rice leaves, Wd represents the dry weight, and Ws represents the saturated weight of leaves after immersion in sterile water for 6 h.For the treatment of NaCl, irrigated water was discarded from five-week-old rice seedlings cultured normally, and then the seedlings were watered with water containing 150 mM NaCl. The rice tissues were sampled at different time points to determine the level of gene transcription.

Total RNA isolation, cDNA synthesis

Triplicate samples of *OsOLP1* overexpression lines, *OsOLP1* knockout lines, and WT were obtained. Total RNA was extracted from related plant tissues (roots, stems, leaves, nodes, and leaf sheaths for *OsOLP1* expression pattern analysis; leaves for CR-*OsOLP1* and OE-*OsOLP1* identification, transcript analysis of ABA and proline synthesis genes) using the EasyPure® Plant RNA Kit (TransGen Biotech, Beijing, China). 1 µg of total RNA was reverse-transcribed into first-strand cDNA using All-in-One First-Strand cDNA Synthesis SuperMix (TransGen Biotech, Beijing, China).

Quantitative real-time PCR analysis

qRT-PCR primers pairs (Supplementary Table 1) were designed using the primer premier 5 and the 2×RealStar Fast SYBR green qRT-PCR Mix purchased from GenStar, Beijing, China. 20 microliters (µl) of the qRT–PCR mix was prepared following the manufacturer's description, and analysis was carried out using the 96-well desktop QuantStudio 5 real-time PCR system. *Osactin1* (*LOC_Os03g50885*) was used as the internal control for normalization. The relative expression analysis was calculated using the $2^{-\Delta\Delta Ct}$ method as previously performed (Livak and Schmittgen, 2001).

Quantification of ABA levels

ABA concentration analysis was performed following Ding et al. approach (Ding et al., 2011). About 0.2 g of 3-week-old rice leaves were ground with liquid nitrogen to obtain a fine powder. 500 µL of extraction buffer (90% (v/v) methanol containing 200 mg/L diethydithiocarbamic acid sodium salt) was added and mixed them thoroughly. The extracts were transferred to glass tubes and incubated at 4°C overnight, then centrifuged for 10 min at 8000 g. The supernatant was evaporated to dryness in a new centrifuge tube, and the residue was dissolved with 500 µL of

methanol tris buffer. Each experiment included 3 replicates. ABA content was determined using an ABA ELISA Kit following the manufacturer's instructions (Mlbio, Shanghai, China).

Scanning electron microscopy of stomata morphology

Five-week-old rice leaves (before and 2 h after drought treatment) were fixed in a fixative buffer containing 2.5% glutaraldehyde overnight at 4°C. The fixative solution was discarded, and samples were washed three times with PBS buffer. After removing excess PBS buffer, samples were desiccated in a serially graded ethanol of 30%, 40%, 50%, 70%, 90%, and 100% for 15 min each. The leaf samples were dried in a vacuum desiccator, mounted on a metal stub with two-sided tape, and sprayed with gold. The stomata were examined using Zeiss Gemini 500 field emission scanning microscope (Gemini 500 FESEM). X500 magnification was used to count the number of stomata per square millimeter, and X1500 magnification to count the percentage of stomata opening and closing from six plants for each line.

Determination of proline concentration

The proline concentration was determined using Lee et al. method (Lee et al., 2013). 0.2 g of five-week-old leaf tissue was placed in a 2 ml tube and pulverized using a tissue lyser after quickly freezing the samples in liquid nitrogen. 3% sulfosalicylic acid was added to the extract. The samples were boiled at 100°C for 10 minutes and centrifuged at 10,000 g for 10 minutes at room temperature. The supernatant was pipetted into a fresh centrifuge tube, and glacial acetic acid (1 ml) and acidic ninhydrin solutions (1 ml) were added after cooling and after boiling for 1 h. The wavelength of the sample was determined at 520 nm using a spectrophotometer. Each experiment included three replicates. Proline content was calculated using the L-proline concentration standard curve.

Lignin quantification

Plant growth and preparation were the same as above. The thioglycolic acid (TGA) of lignin content determination method was carried out as previously described (Suzuki et al., 2009). Samples pulverization was the same as performed for proline content analysis. The powdered samples were oven-dried at 60°C for 1 h. 1.8 ml of methanol was added and extracted at 60°C for 20 min. The extract was centrifuged at 16100 g for 10 min at room temperature. The supernatant was discarded, and the extraction step was repeated with methanol. 1 ml of 3 N HCl and 0.1 ml of thioglycolic acid were added, and the samples were heated at 80°C for 3 h and centrifuged at 16100 g for 10 min. The supernatant was carefully removed and discarded, and 1 ml of distilled water was added to the pellet and vortexed for 30 s to mix. The samples were centrifuged as above, and the pellet was resuspended in 1 ml of 1 N NaOH and then vertically rocked for 16 h at 80 rpm. After centrifugation at 16100 g for 10 min at room temperature, the supernatant (about 1 ml) was transferred into a new 1.5 ml tube and acidified with 0.2 ml concentrated HCl. After freezing at 4°C for 4 h, the samples were centrifuged at 16,100 g for 10 min at room temperature. The supernatant was removed, and the pellet was dissolved in 1 ml of 1 N NaOH. After a 50-fold dilution with 1 N NaOH, the absorbance of the solution at 280 nm was measured using the spectrophotometer. Each experiment included four replicates. The lignin concentration was computed using the lignin standard curve as a reference.

Phloroglucinol-HCl staining of lignin

Cross-sections of rice roots were stained as previously described (Pradhan Mitra and Loque, 2014). The cross-sections were obtained from the roots of five-week-old rice seedlings and incubated in 50% alcohol for 2 h. The sections of root tissues were embedded in an embedding medium, then cut into 100 mm sections with a cryostat, and stained with phloroglucinol-HCl solution (one volume of 37 N HCl to two volumes of 3% phloroglucinol in ethanol). The prepared sections were observed and photographed using the OLYMPUS BX61 microscope at 10X magnifications.

Data analysis

The amino acid sequence, signal peptide, and disulfide bond analysis of the protein were performed by phytozome (https://phytozome-next.jgi.doe.gov/) and Uniprot (https://www.uniprot.org/); amino acid sequence alignment by DNAMAN 9; gene expression profiling was performed by RiceXPro (https://ricexpro.dna.affrc.go.jp/) and Rice Expression Database (http://expression.ic4r.org/index); Analysis of the spider plot is performed by Hiplot (https://hiplot.cn/).

Data sets from the experiments were subjected to analysis of variance and graphs plotted on the GraphPad Prism, version 9.0.0. Data significance analysis was performed using one-way ANOVA and Tukey's multiple comparison test. Each bar represents the means and standard deviations from each observation determined at a 95% significance level.

Results

OsOLP1 is an osmotic-inducible protein

To ascertain that OsOLP1 has the characteristics of osmotins and OLPs, we performed cluster analysis of 40 osmotins and OLPs from rice. The result confirmed that OsOLP1 formed a cluster with multiple rice osmotins and OLPs (Figure 1A). By Uniprot and phytozome analysis, OsOLP1 was identified as a secreted protein with an N-terminal signal peptide containing 22 amino acids. Without signal peptide, the molecular weight of the mature

protein was 24 kDa. The amino acid sequence alignment indicated that the protein has 16 cysteines and is capable of forming eight disulfide bonds (Supplementary Figure 1), whose position could be obtained by Uniprot analysis. Furthermore, relative quantification of OsOLP1 revealed transcript abundance in various rice tissues, especially in the leaf nodes (Figure 1B). RiceXpro study revealed that *OsOLP1* expression was present throughout the rice life cycle and was highest during the blooming stage. Rice Expression Database exhibited changes in OsOLP1 under various stresses, and environment Ontology indicated that OsOLP1 was associated with desiccation/dehydration stress response. (Supplementary Figure 2). Therefore, Drought and NaCl were used to treat rice to explore whether the transcript levels of OsOLP1 respond to osmotic stress. After rice seedlings were exposed to drought and NaCl (150 mM) stress for 12 and 24 hours, the expression level of *OsOLP1* was high in the roots, stems, and leaves (Figures 1C, D). These results suggest that OsOLP1 is widely expressed in tissues and responds to different osmotic stresses.

CRISPR/Cas9-mediated mutagenesis and overexpression lines of *OsOLP1*

The genetic regulatory activities of OsOLP1 in drought-stressed rice seedlings were further ascertained by constructing *OsOLP1* knockout plants by the CRISPR/Cas9 system and overexpressing plants. The *OsOLP1* knockout mutant was generated using two targets in the coding sequence (CDS) regions of *OsOLP1* driven by *OsU6a* and *OsU6b* promoters were ligated to sgRNA to generate sgRNA expression cassettes. Then the cassettes were inserted into the pYLCRISPR/Cas9Pubi-H vector for gene editing in wild-type rice, and 48 transgenic lines were obtained. DNA from all the lines was extracted, and the region *OsOLP1* located was amplified and sequenced to determine knockout efficiency. However, only specific target fragments from three lines, #20, #27, and #31, were amplified. Sequencing analysis showed that all three lines were homozygous with a deletion of 206 base pairs between the two sites (Figure 2A). The transcript level of *OsOLP1* determined by qRT-PCR was found to be lower in the *OsOLP1* gene editing lines (CR-*OsOLP1*#20 and #27) (Figure 2B); therefore, these two lines were selected for further evaluation of drought stress.

Meanwhile, the coding sequence of *OsOLP1* was fused with a 4HA tag driven by the *Ubi* promoter to generate overexpressing rice plants (Figure 2C). The expression of *OsOLP1* in overexpression lines OE-*OsOLP1*#28 and #38 was successfully detected by immunoblot analysis using HA antibodies (Figure 2D). *OsOLP1* expression levels of OE-*OsOLP1*#28 and #38 were 7-10-fold higher than that of wild-type (Figure 2E). The generation of CR-*OsOLP1* and OE-*OsOLP1* helped us to evaluate further the effect of OsOLP1 on drought tolerance in rice.

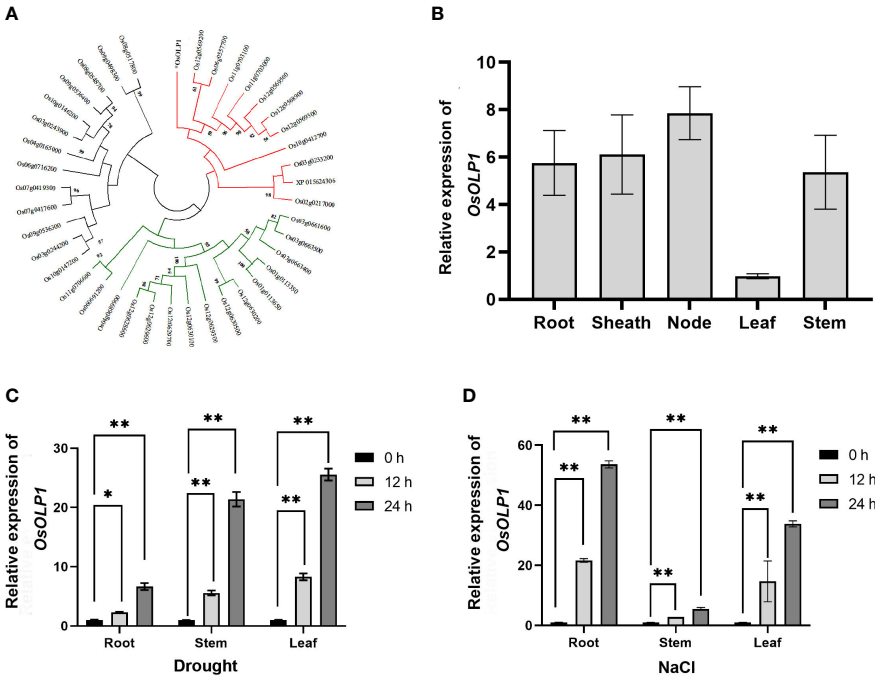

FIGURE 1
Characteristics and expression patterns of OsOLP1. **(A)** The phylogenetic tree was created using the neighbor-joining method with amino acid sequences of the rice osmotin and osmotin-like proteins. The number of nodes at the phylogenetic tree represents the bootstrap value. **(B)** Quantitative expression of *OsOLP1* in different tissues during vegetative growth in rice. The *Osactin1* was the internal control for quantitative real-time PCR (qRT–PCR) analysis. **(C, D)** show the expression levels of *OsOLP1* in rice after drought and NaCl (150 mM) treatments at 12 h and 24 h, respectively. The *Osactin1* was the internal control for qRT–PCR analysis. Bars denote mean ± SD (n = 3). Asterisks denote the significance level determined by one-way ANOVA followed by Tukey's multiple comparison tests [$p \leq 0.05$ (*) and $p \leq 0.01$ (**)].

10.3389/fpls.2023.1163939

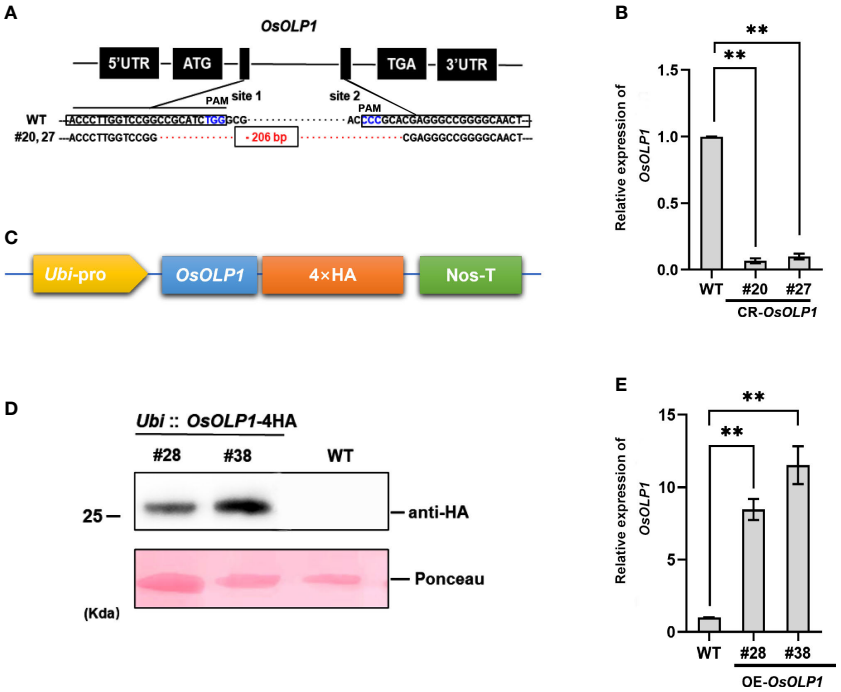

FIGURE 2
CRISPR/Cas9-mediated mutagenesis and overexpression of *OsOLP1*. **(A)** *OsOLP1* was knocked out by CRISPR/cas9 editing. The black boxes show the targeting sequences, site 1(T1) and site 2(T2), which are driven by promoters and linked to sgRNA for targeting. Both sites are located in the coding region of *OsOLP1*. The PAM area is shown in blue; The 206 base pairs deleted in CR-*OLP1*#20 and #27 are shown in red. **(B)** The relative expression level of *OsOLP1* in CR-*OsOLP1*#20 and #27 lines. The bars denote mean ± SD (n = 3). **(C)** Schematic diagram of the vector pRHV driven by the *Ubi* promoter and containing a 4HA tag at the C-terminus for *OsOLP1* overexpression. **(D)** The expression of *OsOLP1* in OE-*OsOLP1* was analyzed using anti-HA antibodies with the immunoblot method. **(E)** Analysis of *OsOLP1* expression levels in OE-*OsOLP1* lines by qRT-PCR (#28, 38). The *Osactin1* was used as an internal control for qRT-PCR analysis. Bars denote mean ± SD (n = 3). Asterisks denote the significance level determined by one-way ANOVA followed by Tukey's multiple comparison tests [$p \leq 0.01$ (**)].

OsOLP1 contributes to drought tolerance in rice

Although OsOLP1 also conforms to the structural characteristics of osmotin-like proteins, its role in drought conditions still needs to be verified. Five-week-old seedlings from the CR-*OsOLP1* and OE-*OsOLP1* lines were removed from the irrigation water and subsequently subjected to a 5-day drought without watering. After 5 days, the soil water content was reduced to about 30%, and the plants were in a severe state of water loss (Figure 3B). The survival rates of rice were calculated after recovery of 7 days of watering. After five days of drought treatment, the wild type showed survival rates of 28%. Compared to wild type, CR-*OsOLP1* knockout lines showed lower average survival rates of 8.2%, exhibiting more sensitive to water loss, significant drought-induced symptoms, such as leaf curling and wilting, as well as significantly lower recovery rates after rehydration. However, OE-*OsOLP1* lines grew better and maintained an average high survival rate of 53.1% after rehydration (Figures 3A, D). In addition, the relative water content of OE-*OsOLP1* (~65%) was higher than that of WT (51.4%), whereas that of CR-*OsOLP1* was lower (~ 25%) (Figures 3C). In a nutshell, *OsOLP1* overexpression can avoid rapid water loss and improve rice drought tolerance.

OsOLP1 influences ABA accumulation

ABA can respond to the osmotic stress faced by plants and utilize water rationally. The dehydration signal leads to ABA accumulation and activation of downstream stress-resistance signaling pathways. Therefore, variation in ABA content can be used as the barometer for plant drought tolerance assessment. The ABA content in CR-*OsOLP1*, OE-*OsOLP1*, and WT was analyzed. Under normal condition, no difference in ABA concentration among OE-*OsOLP1*, CR-*OsOLP1* and WT. However, when subjected to a one-day drought, the ABA level in the CR-*OsOLP1* knockout lines decreased by 50%, while that in the OE-*OsOLP1* lines increased by 50% (Figure 4A).

However, the question of how OsOLP1 promotes endogenous ABA synthesis was raised. Zeaxanthin epoxidase (ZEP) and 9-*cis*-epoxycarotenoid dioxygenase (NCED) are crucial to ABA synthesis. ZEP1 is the initial enzyme in the ABA synthesis pathway, and NCED3 regulates ABA synthesis under water deficit, and their expression contributes to ABA-mediated drought tolerance. The transcript levels of these two enzymes were quantified by qRT-PCR. The results showed consistency with the ABA content above. The relative transcript abundance of *OsZEP1* and *OsNCED3* in OE-*OsOLP1* lines were significantly up-regulated under drought

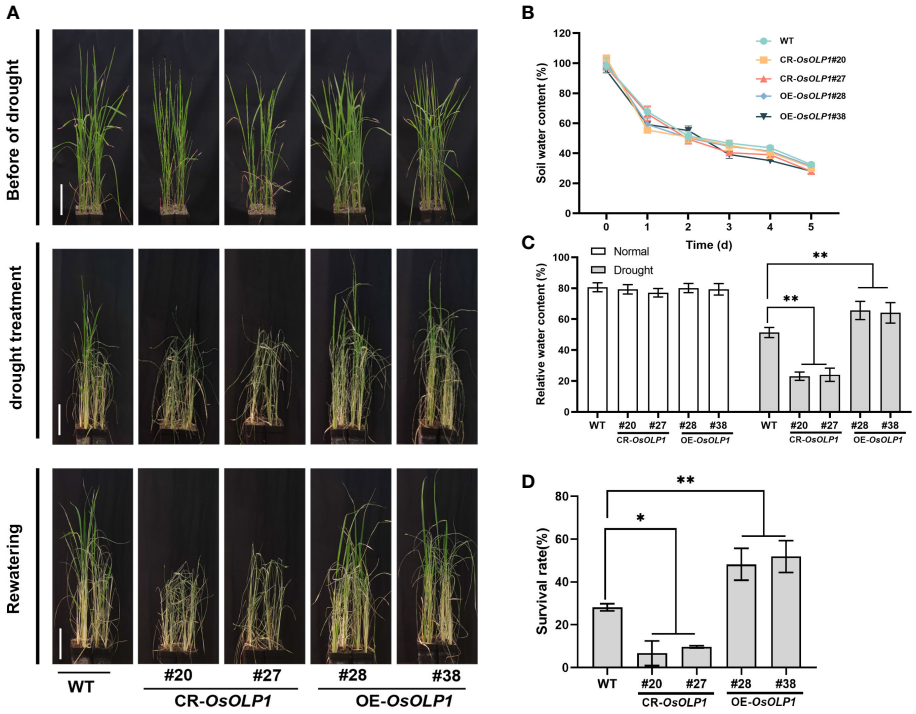

FIGURE 3
OsOLP1 contributes to drought tolerance in rice seedlings. **(A)** WT, CR-*OsOLP1*, and OE-*OsOLP1* lines phenotypes before drought treatment, after exposure to drought for five days, followed by water recovery. Scale bar, 10 cm. **(B)** Soil water content at different time points under drought stress. Data denotes mean ± SD (n =5). **(C)** Relative water content of leaves of WT, CR-*OsOLP1*, and OE-*OsOLP1* plants before and after drought stress. Data denotes mean ± SD (n =4). **(D)** Survival rates of WT, CR-*OsOLP1*, and OE-*OsOLP1* lines were calculated after rewatering. Data denotes mean ± SD (n = 3). Asterisks denote the significance level determined by one-way ANOVA followed by Tukey's multiple comparison tests [$p \leq 0.05$ (*) and $p \leq 0.01$ (**)].

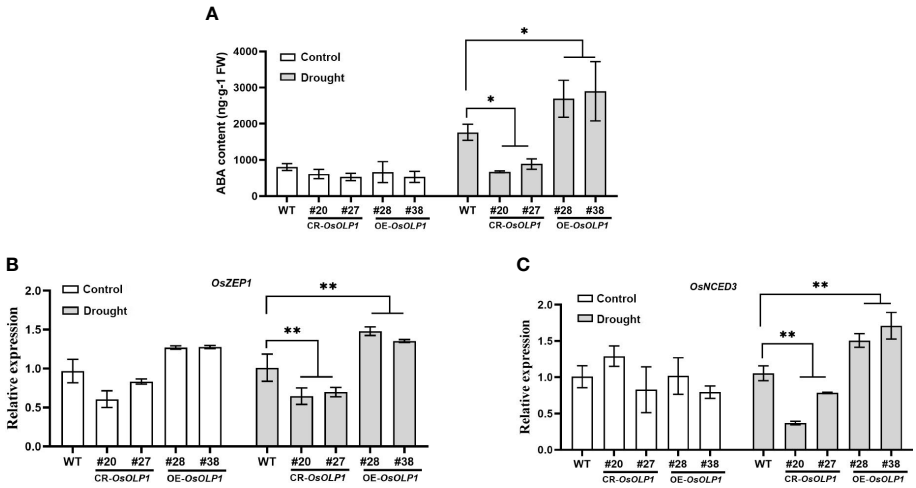

FIGURE 4
OsOLP1 positively regulated ABA accumulation. **(A)** ABA content in WT, CR-*OsOLP1*, and OE-*OsOLP1* under control and drought-stressed conditions for one day. Data denotes mean ± SD (n = 4). **(B, C)** Transcript abundance of key ABA-encoding genes (*OsZEP1* and *OsNCED3*) in WT, CR-*OsOLP1*, and OE-*OsOLP1* subjected to normal growth conditions and drought treatment. The bars denote mean ± SD (n = 3). Asterisks denote the significance level determined by one-way ANOVA followed by Tukey's multiple comparison tests [$p \leq 0.05$ (*) and $p \leq 0.01$(**)].

conditions, while vice versa was observed in CR-*OsOLP1* lines (Figures 4B, C). Thus, OsZEP1 and OsNCED3 mediated the OsOLP1-enhanced ABA deposition under drought.

OsOLP1 modulates stomatal movement under drought

The stomata are enclosed by specialized pairs of guard and subsidiary cells for mechanical support. The stomata regulate water utilization in higher plants through transpiration, and the density and closure of stomata are critical factors for plant drought tolerance. Therefore, we observed the closure and density of epidermal stomata in rice leaves using the scanning electron microscopy technique. As shown in Figures 5A, B, there was no significant difference in stomatal density per square millimeter between CR-*OsOLP1*, OE-*OsOLP1*, and WT. Then, after 2 hours of drought exposure, we calculated the percentage of stomatal closure per square millimeter using Figure 5C as the standard. The percentage of stomatal closure in CR-*OsOLP1*, OE-*OsOLP1*, and WT lines was not significantly different before drought treatment. However, after drought exposure, the percentage of stomatal closure was 85.6% in the wild type and ~80% in knockout CR-*OsOLP1*, indicating that CR-*OsOLP1* had less stomatal closure than the wild type, while overexpression plants OE-*OsOLP1* showed more stomatal closure numbers of ~96% (Figure 5D), suggesting that OsOLP1 can reduce water loss in rice by regulating stomatal apparatus to maintain water balance.

Overexpression of *OsOLP1* promotes proline accumulation

When plants suffer from unfavorable external conditions, they usually adapt by accumulating protective components. Among these protective components, proline accumulation is characteristic for plant stress defense. It was determined that the proline level was low under normal conditions. However, compared with WT, its levels rapidly increased by 2.7-6.1-fold in the *OsOLP1* overexpression lines and decreased by 1.9-4.4-fold in the *OsOLP1* knockout lines under water deficit conditions (Figure 6A). Consistent with this result, the transcript levels of genes encoding delta-1-pyrroline-5-carboxylate synthase (OsP5CS1 and OsP5CS2) involved in the proline synthesis were significantly increased by about 1 to 10 folds in OE-*OsOLP1* lines (Figures 6B, C). In addition, the transcription level of the proline-degrading protein proline dehydrogenase (OsPDH1) was significantly increased in CR-*OsOLP1* lines compared to WT (Figure 6D). Proline accumulation levels in our report are partly attributable to these regulatory genes' expression.

Overexpression of *OsOLP1* contributes to lignin deposition

Deposition of lignin leads to the lignification of plant tissues, which often strengthens plants against abiotic stresses. The degree of lignification is proportional to the lignin content. We measured

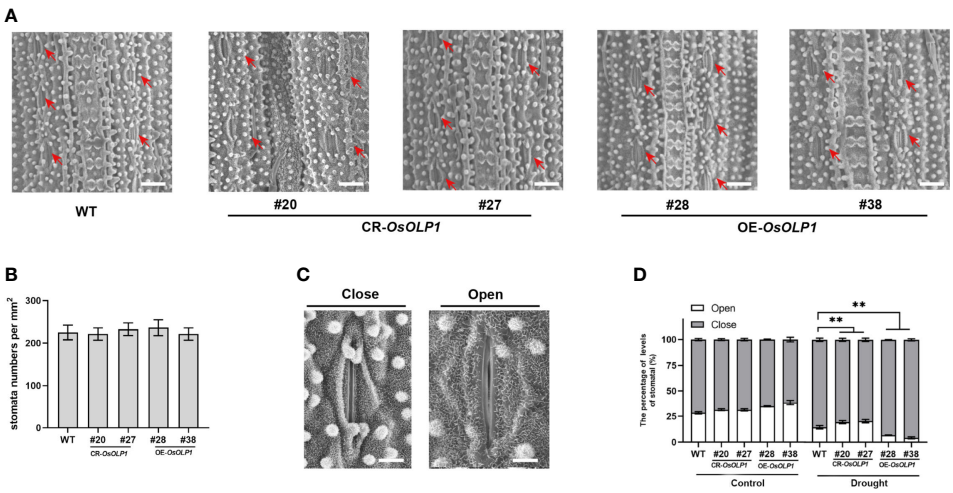

FIGURE 5
Stomatal distribution and movement in WT, CR-*OsOLP1*, and OE-*OsOLP1* plants. **(A)** Stomatal distribution of WT, CR-*OsOLP1*, and OE-*OsOLP1* plants. The stomatal locations are shown by red arrows. Scale bar, 100 μm. **(B)** Stomatal density per square millimeter was measured in the transgenic plants, CR-*OsOLP1*, and OE-*OsOLP1* lines. Data denote mean ± SD (n = 6). **(C)** Stomatal opening and closing levels of rice were observed by scanning electron microscopy. Scale bar, 10 μm. **(D)** Percentage of stomatal opening and closing of transgenic plants CR-*OsOLP1* and OE-*OsOLP1* lines under normal conditions and after drought exposure. The bars denote the mean ± SD (n = 6). Asterisks denote the significance level determined by one-way ANOVA followed by Tukey's multiple comparison tests $p \leq 0.01$(**).

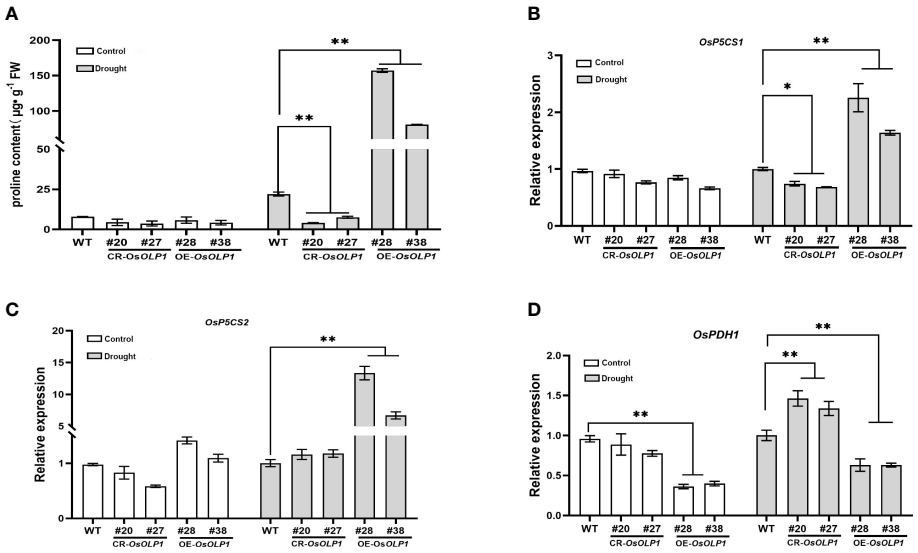

FIGURE 6
OsOLP1 promotes proline accumulation. **(A)** proline content in transgenic plants CR-*OsOLP1* and OE-*OsOLP1* lines under control conditions and after drought exposure. Bars denote mean ± SD (n = 3). **(B–D)** Expression levels of key proline regulatory genes involved in synthesis (*OsP5CS1* and *OsP5CS*) and degradation (*OsPDH1*) in transgenic plants, CR-*OsOLP1* and OE-*OsOLP1* under normal and drought conditions. The *Osactin1* was used as an internal control for qRT-PCR analysis. Bars denote mean ± SD (n = 3). Asterisks denote the significance level determined by one-way ANOVA followed by Tukey's multiple comparison tests [$p \leq 0.05$ (*) and $p \leq 0.01$(**)].

the lignin content of CR-*OsOLP1*, OE-*OsOLP1*, and WT lines using the Thioglycolic acid (TGA) method. The results revealed that *OsOLP1* deletion adversely affects lignin content in rice. However, the lignin concentration of the *OsOLP1*-overexpression lines was significantly 1.3-1.6-fold higher than that of WT (Figure 7A). Lignin-specific (Phloroglucinol-HCl) staining of rice roots also visually showed the degree of lignification of CR-*OsOLP1* and OE-*OsOLP1* lines. The sclerenchyma tissues and vasculature in

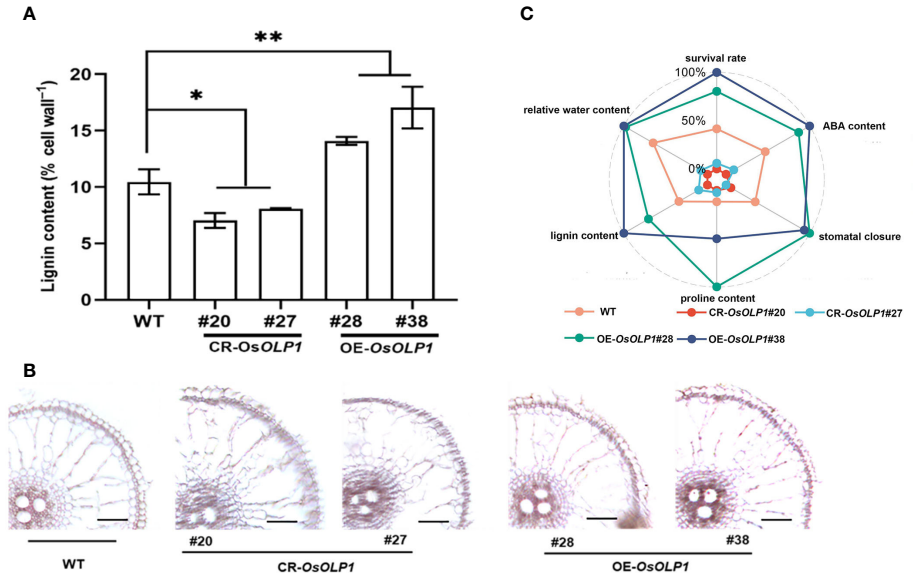

FIGURE 7
Lignin accumulation in WT and transgenic plants of CR-*OsOLP1* and OE-*OsOLP1*. **(A)** Lignin content was determined in five-week-old seedlings of WT and transgenic plants CR-*OsOLP1* and OE-*OsOLP1*. The bars denote the mean ± SD (n = 4). **(B)** The transverse sections of WT and transgenic plant CR-*OsOLP1* and OE-*OsOLP1* showed roots stained with phloroglucinol-HCl. The vascular tissue of OE-*OsOLP1* lines showed highly lignified. Asterisks denote the significance level determined by one-way ANOVA followed by Tukey's multiple comparison tests [$p \leq 0.05$ (*) and $p \leq 0.01$(**)]. **(C)** A spider plot was used to describe the levels of ABA, proline, lignin, stomatal closure, relative water content, and survival rate in OE-*OsOLP1*, CR-*OsOLP1* and WT under drought condition.

OE-*OsOLP1* lines were highly lignified, whereas WT and CR-*OsOLP1* lines were less lignified (Figure 7B). Taken together, OsOLP1 may have mediated the synthesis of lignin.

Finally, a spider plot was used to normalize the effects of OsOLP1 on rice survival rate, relative water content, ABA and proline contents, stomatal closure, and lignin accumulation under drought conditions (Figure 7C). The evenly distributed spokes on the wheel showed that CR-*OsOLP1*#20 and *CR-OsOLP1*#27 were closer toward the center (0%), and therefore weakened their tolerance to drought stress. However, OE-*OsOLP1*#28# and OE-*OsOLP1*#38 showed strong drought tolerance as most of their spokes were far from the center on the wheel.

Discussion

The process of drought tolerance is an integrated response in which plants use various metabolites, hormones, and signaling molecules to activate a series of downstream components through receptor sensing, transduction, and transcriptional regulatory cascades to ensure plant growth and reproduction in arid environments (Singh et al., 2022). Traditional breeding relies on natural genetic variation in related plants, which is rice's primary strategy for drought-tolerant breeding. At the same time, the development of genomics and precise gene editing tools have made it possible to manipulate plant traits in a targeted manner, which has also greatly improved plant yields under stressful environments (Gupta et al., 2020). Here, *OsOLP1* was investigated as a rice drought tolerance gene that can be used as a complement to the high-quality genetic resources of rice.

Similar to Bowman-Birk trypsin inhibitors, osmotins are cysteine-rich proteins (CRPs), such proteins are evolutionarily conserved to promote plant growth and coordinate stress tolerance (Marshall et al., 2011; Liu et al., 2017; Srivastava et al., 2021). It has been shown that osmotins are involved in plants' biotic and abiotic stress regulation. Osmotin levels were reported to be maintained at low levels in cells without osmotic treatment (Singh et al., 1985; Anil Kumar et al., 2015). OsOLP1, an osmotin-like protein, is natively expressed in various tissues and abundantly induced in treatments with low water potential (drought and salinity). Kononowicz et al. have reported that the osmotin promoter is spatiotemporally specific in mediating the development of plants after exposure to stress (Kononowicz et al., 1992; Raghothama et al., 1997). We also found that drought and salinity induced different transcriptional profiles of *OsOLP1*, which may be related to the osmotin promoter region and activity (Figures 1C, D). Rice, a water-demanding crop, is particularly sensitive to changes in osmotic pressure in the external environment and is often exposed to stresses such as drought in nature. Osmotin-like proteins have also been reported to improve drought tolerance in plants (Weber et al., 2014; Chowdhury et al., 2017). In rice, osmotin-like proteins have not been extensively studied as a genetic resource for drought tolerance. We knocked out and overexpressed *OsOLP1* based on gene editing and genetic transformation techniques and found that overexpression of *OsOLP1* could significantly increase rice survival rate and reduce water loss under drought conditions (Figures 2, 3). Prolonged drought can lead to senescence, abscission of leaves, and even death of the entire plant, which severely hampers crop quality and yield. OsOLP1 also partially delayed or alleviated the development of these symptoms in rice.

The ABA signaling pathway is essential in the drought regulation of plants. The receptor elements of plants sense drought signals causing the accumulation of ABA, and the ABA receptor is phosphorylated and binds to other co-receptors to participate in the regulation of downstream resistance genes by transcription factors (Zhu, 2016; Takahashi et al., 2020). We observed that overexpression of *OsOLP1* under drought conditions increased endogenous ABA content, which is necessary to improve drought tolerance in rice (Figure 4A). Transcript abundance of ZEP1 and NCED3, two rate-limiting enzymes of ABA synthesis, was also increased (Figures 4B, C), and it has been reported that ZEP and NCED can enhance drought tolerance in plants by regulating ABA synthesis (Iuchi et al., 2001; Park et al., 2008; Zhang et al., 2008; Hwang et al., 2010; Frey et al., 2012; Tong et al., 2017). Similar results have been shown in other studies involved in the overexpression of drought-regulated genes, such as Pyrabactin resistance1-like/Regulatory components of ABA receptors 10 (OsPYL10) (Verma et al., 2019), chloroplastic β-glucosidase isoenzyme (Os3BGlu6) (Wang et al., 2020) and other drought-inducible proteins, such as OsASR1 (Park et al., 2019). These studies proposed that OsOLP1 stimulates the expression of ABA synthesis genes and thus enhances rice's tolerance to water loss stress. In addition, an osmotin OSM34 from Arabidopsis can interact with an F-box SKP2A in the ABA response pathway, suggesting that osmotin not only mediates ABA synthesis but also is responsible for ABA signaling pathway (Park and Kim, 2021). In contrast, a PR5-like receptor kinase, AtPR5K, which belongs to the same family as osmotin, controls plant drought tolerance by negatively regulating the ABA signaling pathway (Baek et al., 2019), and the reason for this difference is related to the phosphorylation of PR5K, whereas osmotin does not have a phosphokinase domain.

Under drought conditions, plant roots first sense the water loss in the soil. That signal is transported from roots to plant's above-ground parts *via* CLE25 peptide, and leaves regulate drought resistance dependent on stomatal closure (Christmann and Grill, 2018; Gupta et al., 2020). Stomata are located at the interface between the plant leaves and the atmosphere, and stomatal closure restricts the inflow of carbon dioxide and transpiration to reduce water loss (Matsuda et al., 2016; Durand et al., 2019; Lu et al., 2020). The degree of circulation between stomata and the environment can be described by density and degree of aperture. EPIDERMAL PATTERNING FACTOR 1 (OsEPF1) is responsible for maintaining the density and spacing of stomatal precursor cells, and overexpression of OsEPF1 significantly reduced stomatal density and conductance, further enhancing crop tolerance and yield in drought and high temperature (Caine et al., 2019). We observed that knockout and overexpression of *OsOLP1* had little effect on stomatal density and mainly affected stomatal closure (Figure 5), thus avoiding water loss due to transpiration, which was similar to the manner of OsTF1L (Bang et al., 2019). Closure of

stomata is a rapid response to ABA synthesis after plants face drought, so we speculate that OsOLP1 positively regulates ABA synthesis to promote stomatal closure and thus further reduce the damage caused by water loss.

Solute accumulation in the cytoplasm maintains cell expansion pressure and promotes water absorption, a strategy that plants use for drought tolerance. Proline is an osmolyte that has been extensively studied under various adverse conditions, and its accumulation is of great significance for plant drought resistance. Furthermore, proline is not only an osmoprotectant but also functions as a metal chelator, antioxidant defense molecule, and signaling molecule, which also contributes to the stress tolerance of higher plants (Ghosh et al., 2022). Increased intracellular proline content has been observed in the overexpression of drought-tolerance genes, such as *ornithine delta-aminotransferase* (*OsOAT*) and *ORANGE* (*OR*) (You et al., 2012; Ali et al., 2022). Osmotin overexpression in transgenic tobacco, carrots, and olives showed high proline accumulation under osmotic stress (Barthakur et al., 2012; Annon et al., 2014; Silvestri et al., 2017). P5CS is a rate-limiting enzyme for the synthesis of proline, and *AtP5CS1* has been identified to be induced and activated by an ABA-dependent regulatory pathway in response to osmotic stress (Savoure et al., 1997; Strizhov et al., 2003; Szabados and Savoure, 2010). However, PDH transcription can be inhibited by dehydration and activated by rehydration, thus preventing proline degradation during abiotic stresses (Kiyosue et al., 1996; Szabados and Savoure, 2010). We suggested that OsOLP1-mediated enhancement of drought tolerance in rice is caused by ABA-regulated proline accumulation, which avoids drought damage through intracellular solute accumulation and reactive oxygen species scavenging.

Controlling the hydraulic conductivity of vascular tissues through lignin accumulation can be seen as another protective mechanism of plants against drought (Zhou et al., 2020). Lignin is a cell wall-strengthening secondary metabolite produced by the phenylpropanoid pathway. Lignin maintains the mechanical support of plants and reduces cell wall water leakage and evaporation (Monties and Fukushima, 2005; Bang et al., 2022). Transgenic rice overexpressing Cinnamoyl-CoA reductase *10* (*OsCCR10*) and *OsTF1L* showed drought tolerance by promoting lignin accumulation (Bang et al., 2019; Bang et al., 2022). Similar results were found in other crops, such as the PdNF-YB21 transcription factor in poplar, IbLEA14 in sweet potato, PoCCoAOMT in tobacco, and VlbZIP30 in grapevine (Park et al., 2011; Tu et al., 2020; Zhou et al., 2020; Zhao et al., 2021). Our study revealed that *OsOLP1* deletion reduced lignin accumulation, whereas overexpression of *OsOLP1* increased lignin content and enhanced the lignification of vascular tissues (Figure 7). Therefore,

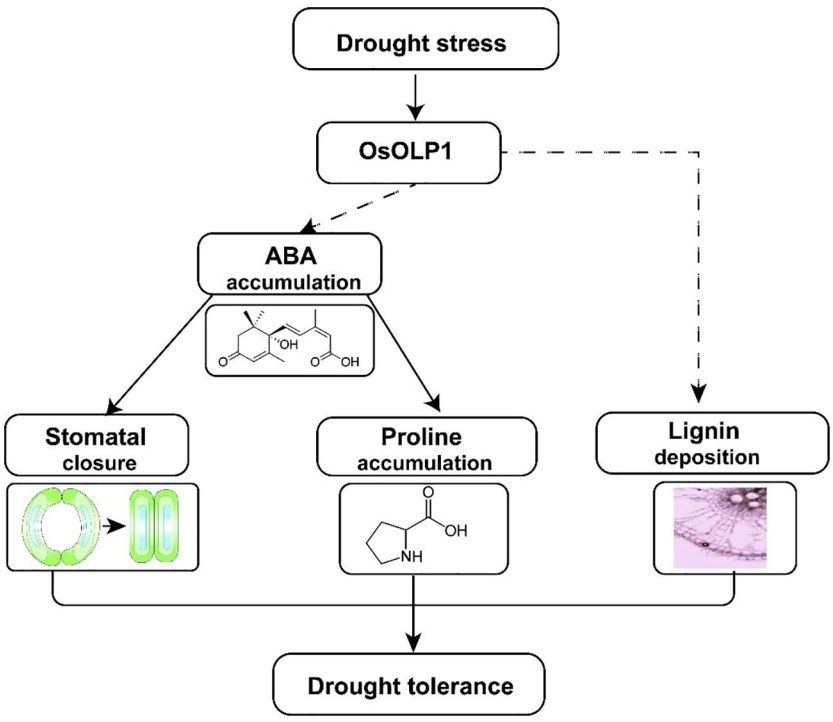

FIGURE 8
A model illustrating how OsOLP1 mediates drought tolerance in rice. Under drought conditions, up-regulated expression of OsOLP1 activated the ABA synthesis pathway, resulting in the accumulation of ABA, which acts as a signaling molecule to promote the closure of rice epidermal stomata and the synthesis of intracellular proline, thereby reducing water loss and maintaining cell expansion pressure. In addition, OsOLP1 also caused the deposition of lignin, which would make rice better drought tolerance.

OsOLP1 may promote water balance and plant rigidity by increasing lignin levels and delaying the damage caused by drought.

Conclusion

In the present study, we identified a new osmotin-like protein, OsOLP1, which has a positive regulatory effect on drought tolerance in rice. OsOLP1 induced the accumulation of endogenous ABA under drought conditions, activated the expression of downstream tolerance genes through the ABA signaling pathway, further reduced water loss by closing stomata, and increased proline content to maintain cellular osmotic pressure. In addition, OsOLP1 directly or indirectly regulates lignin accumulation to enhance plant vascular tissue toughness and ensure water transport (Figure 8). However, the regulatory mechanisms of OsOLP1 on ABA synthesis and lignin deposition need to be investigated in depth. The effect of OsOLP1 on rice yield under drought conditions should also be further clarified in the field. The elucidation of the function of OsOLP1 will provide a new perspective for rice stress tolerance breeding.

Data availability statement

The original contributions presented in the study are included in the article/Supplementary Material. Further inquiries can be directed to the corresponding author.

Author contributions

HZ and JY designed the project, VN, ZF, and TY prepared the materials and data analysis, JY conducted the experiments and drafted the manuscript, and JR, GL, XY, and HZ revised the manuscript. All authors read and approved the final manuscript.

Funding

This Work was supported by the National Key Research and Development Program of China (2017YFD0200900).

Conflict of interest

The authors declare that the research was conducted in the absence of any commercial or financial relationships that could be construed as a potential conflict of interest.

Publisher's note

All claims expressed in this article are solely those of the authors and do not necessarily represent those of their affiliated organizations, or those of the publisher, the editors and the reviewers. Any product that may be evaluated in this article, or claim that may be made by its manufacturer, is not guaranteed or endorsed by the publisher.

Supplementary material

The Supplementary Material for this article can be found online at: https://www.frontiersin.org/articles/10.3389/fpls.2023.1163939/full#supplementary-material

References

Ali, F., Wang, Q., Fazal, A., Wang, L. J., Song, S., Kong, M. J., et al. (2022). The dnaj-like zinc finger protein ORANGE promotes proline biosynthesis in drought-stressed arabidopsis seedlings. *Int. J. Mol. Sci.* 23 (7), 3907. doi: 10.3390/ijms23073907

Anil Kumar, S., Hima Kumari, P., Shravan Kumar, G., Mohanalatha, C., and Kavi Kishor, P. B. (2015). Osmotin: a plant sentinel and a possible agonist of mammalian adiponectin. *Front. Plant Sci.* 6. doi: 10.3389/fpls.2015.00163

Annon, A., Rathore, K., and Crosby, K. (2014). Overexpression of a tobacco osmotin gene in carrot (*Daucus carota* l.) enhances drought tolerance. *In Vitro Cell. Dev. Biol.-Plant* 50 (3), 299–306. doi: 10.1007/s11627-013-9590-0

Baek, D., Kim, M. C., Kumar, D., Park, B., Cheong, M. S., Choi, W., et al. (2019). AtPR5K2, a PR5-like receptor kinase, modulates plant responses to drought stress by phosphorylating protein phosphatase 2Cs. *Front. Plant Sci.* 10. doi: 10.3389/fpls.2019.01146

Bang, S. W., Choi, S., Jin, X., Jung, S. E., Choi, J. W., Seo, J. S., et al. (2022). Transcriptional activation of rice cinnamoyl-CoA reductase 10 by OsNAC5, contributes to drought tolerance by modulating lignin accumulation in roots. *Plant Biotechnol. J.* 20 (4), 736–747. doi: 10.1111/pbi.13752

Bang, S. W., Lee, D. K., Jung, H., Chung, P. J., Kim, Y. S., Choi, Y. D., et al. (2019). Overexpression of OsTF1L, a rice HD-zip transcription factor, promotes lignin biosynthesis and stomatal closure that improves drought tolerance. *Plant Biotechnol. J.* 17 (1), 118–131. doi: 10.1111/pbi.12951

Barthakur, S., Babu, V., and Bansa, K. C. (2012). Over-expression of osmotin induces proline accumulation and confers tolerance to osmotic stress in transgenic tobacco. *J. Plant Biochem. Biotechnol.* 10 (1), 31–37. doi: 10.1007/bf03263103

Bashir, M. A., Silvestri, C., Ahmad, T., Hafiz, I. A., Abbasi, N. A., Manzoor, A., et al. (2020). Osmotin: a cationic protein leads to improve biotic and abiotic stress tolerance in plants. *Plants-Basel* 9 (8), 992. doi: 10.3390/plants9080992

Caine, R. S., Yin, X., Sloan, J., Harrison, E. L., Mohammed, U., Fulton, T., et al. (2019). Rice with reduced stomatal density conserves water and has improved drought tolerance under future climate conditions. *New Phytol.* 221 (1), 371–384. doi: 10.1111/nph.15344

Chen, X., and Guo, Z. (2008). Tobacco OPBP1 enhances salt tolerance and disease resistance of transgenic rice. *Int. J. Mol. Sci.* 9 (12), 2601–2613. doi: 10.3390/ijms9122601

Chowdhury, S., Basu, A., and Kundu, S. (2017). Overexpression of a new osmotin-like protein gene (*SindOLP*) confers tolerance against biotic and abiotic stresses in sesame. *Front. Plant Sci.* 8. doi: 10.3389/fpls.2017.00410

Christmann, A., and Grill, E. (2018). Peptide signal alerts plants to drought. *Nature* 556 (7700), 178–179. doi: 10.1038/d41586-018-03872-4

Clough, S. J., and Bent, A. F. (1998). Floral dip: a simplified method for *Agrobacterium*-mediated transformation of *Arabidopsis thaliana*. *Plant J.* 16 (6), 735–743. doi: 10.1046/j.1365-313x.1998.00343.x

Ding, Y., Avramova, Z., and Fromm, M. (2011). The arabidopsis trithorax-like factor ATX1 functions in dehydration stress responses *via* ABA-dependent and ABA-independent pathways. *Plant J.* 66 (5), 735–744. doi: 10.1111/j.1365-313X.2011.04534.x

Durand, M., Brendel, O., Bure, C., and Le Thiec, D. (2019). Altered stomatal dynamics induced by changes in irradiance and vapour-pressure deficit under drought: impacts on the whole-plant transpiration efficiency of poplar genotypes. *New Phytol.* 222 (4), 1789–1802. doi: 10.1111/nph.15710

Frey, A., Effroy, D., Lefebvre, V., Seo, M., Perreau, F., Berger, A., et al. (2012). Epoxycarotenoid cleavage by NCED5 fine-tunes ABA accumulation and affects seed dormancy and drought tolerance with other NCED family members. *Plant J.* 70 (3), 501–512. doi: 10.1111/j.1365-313X.2011.04887.x

Ghosh, U. K., Islam, M. N., Siddiqui, M. N., Cao, X., and Khan, M. A. R. (2022). Proline, a multifaceted signalling molecule in plant responses to abiotic stress: understanding the physiological mechanisms. *Plant Biol. (Stuttg)* 24 (2), 227–239. doi: 10.1111/plb.13363

Gupta, A., Rico-Medina, A., and Cano-Delgado, A. I. (2020). The physiology of plant responses to drought. *Science* 368 (6488), 266–269. doi: 10.1126/science.aaz7614

Hakim,, Ullah, A., Hussain, A., Shaban, M., Khan, A. H., Alariqi, M., et al. (2018). Osmotin: a plant defense tool against biotic and abiotic stresses. *Plant Physiol. Biochem.* 123, 149–159. doi: 10.1016/j.plaphy.2017.12.012

He, F., Zhang, F., Sun, W., Ning, Y., and Wang, G.-L. (2018). A versatile vector toolkit for functional analysis of rice genes. *Rice* 11 (1), 27. doi: 10.1186/s12284-018-0220-7

Hiei, Y., Ohta, S., Komari, T., and Kumashiro, T. (1994). Efficient transformation of rice (*Oryza sativa* l.) mediated by *Agrobacterium* and sequence analysis of the boundaries of the T-DNA. *Plant J.* 6 (2), 271–282. doi: 10.1046/j.1365-313x.1994.6020271.x

Hu, H., and Xiong, L. (2014). Genetic engineering and breeding of drought-resistant crops. *Annu. Rev. Plant Biol.* 65 (1), 715–741. doi: 10.1146/annurev-arplant-050213-040000

Hwang, S.-G., Chen, H.-C., Huang, W.-Y., Chu, Y.-C., Shii, C.-T., and Cheng, W.-H. (2010). Ectopic expression of rice OsNCED3 in arabidopsis increases ABA level and alters leaf morphology. *Plant Sci.* 178 (1), 12–22. doi: 10.1016/j.plantsci.2009.09.014

Iuchi, S., Kobayashi, M., Taji, T., Naramoto, M., Seki, M., Kato, T., et al. (2001). Regulation of drought tolerance by gene manipulation of 9-*cis*-epoxycarotenoid dioxygenase, a key enzyme in abscisic acid biosynthesis in arabidopsis. *Plant J.* 27 (4), 325–333. doi: 10.1046/j.1365-313x.2001.01096.x

Kiyosue, T., Yoshiba, Y., Yamaguchi-Shinozaki, K., and Shinozaki, K. (1996). A nuclear gene encoding mitochondrial proline dehydrogenase, an enzyme involved in proline metabolism, is upregulated by proline but downregulated by dehydration in arabidopsis. *Plant Cell* 8 (8), 1323–1335. doi: 10.1105/tpc.8.8.1323

Kononowicz, A. K., Nelson, D. E., Singh, N. K., Hasegawa, P. M., and Bressan, R. A. (1992). Regulation of the osmotin gene promoter. *Plant Cell* 4 (5), 513–524. doi: 10.1105/tpc.4.5.513

Le, T. T. T., Williams, B., and Mundree, S. G. (2018). An osmotin from the resurrection plant *Tripogon loliiformis* (TlOsm) confers tolerance to multiple abiotic stresses in transgenic rice. *Physiol. Plant* 162 (1), 13–34. doi: 10.1111/ppl.12585

Lee, B.-R., Muneer, S., Park, S.-H., Zhang, Q., and Kim, T.-H. (2013). Ammonium-induced proline and sucrose accumulation, and their significance in antioxidative activity and osmotic adjustment. *Acta Physiol. Plant* 35 (9), 2655–2664. doi: 10.1007/s11738-013-1297-7

Li, D., Yang, J., Pak, S., Zeng, M., Sun, J., Yu, S., et al. (2022). PuC3H35 confers drought tolerance by enhancing lignin and proanthocyanidin biosynthesis in the roots of *Populus ussuriensis*. *New Phytol.* 233 (1), 390–408. doi: 10.1111/nph.17799

Liu, X., Zhang, H., Jiao, H., Li, L., Qiao, X., Fabrice, M. R., et al. (2017). Expansion and evolutionary patterns of cysteine-rich peptides in plants. *BMC Genomics* 18 (1), 610. doi: 10.1186/s12864-017-3948-3

Livak, K. J., and Schmittgen, T. D. (2001). Analysis of relative gene expression data using real-time quantitative PCR and the 2(-delta delta C(T)) method. *Methods* 25 (4), 402–408. doi: 10.1006/meth.2001.1262

Lu, Y., Duursma, R. A., Farrior, C. E., Medlyn, B. E., and Feng, X. (2020). Optimal stomatal drought response shaped by competition for water and hydraulic risk can explain plant trait covariation. *New Phytol.* 225 (3), 1206–1217. doi: 10.1111/nph.16207

Ma, X. L., Zhang, Q. Y., Zhu, Q. L., Liu, W., Chen, Y., Qiu, R., et al. (2015). A robust CRISPR/Cas9 system for convenient, high-efficiency multiplex genome editing in monocot and dicot plants. *Mol. Plant* 8 (8), 1274–1284. doi: 10.1016/j.molp.2015.04.007

Marshall, E., Costa, L. M., and Gutierrez-Marcos, J. (2011). Cysteine-rich peptides (CRPs) mediate diverse aspects of cell–cell communication in plant reproduction and development. *J. Exp. Bot.* 62 (5), 1677–1686. doi: 10.1093/jxb/err002

Masle, J., Gilmore, S. R., and Farquhar, G. D. (2005). The ERECTA gene regulates plant transpiration efficiency in arabidopsis. *Nature* 436 (7052), 866–870. doi: 10.1038/nature03835

Matsuda, S., Takano, S., Sato, M., Furukawa, K., Nagasawa, H., Yoshikawa, S., et al. (2016). Rice stomatal closure requires guard cell plasma membrane atp-binding cassette transporter RCN1/OsABCG5. *Mol. Plant* 9 (3), 417–427. doi: 10.1016/j.molp.2015.12.007

Monties, B., and Fukushima, K. (2005). Occurrence, function, and biosynthesis of lignins. *Biopolymers Online*., 1–64. doi: 10.1002/3527600035.bpol1001

Ninkuu, V., Yan, J., Fu, Z., Yang, T., Ziemah, J., Ullrich, M. S., et al. (2023). Lignin and its pathway-associated phytoalexins modulate plant defense against fungi. *J. Fungi (Basel)* 9 (1), 52. doi: 10.3390/jof9010052

Ouyang, S.-Q., Liu, Y.-F., Liu, P., Lei, G., He, S.-J., Ma, B., et al. (2010). Receptor-like kinase OsSIK1 improves drought and salt stress tolerance in rice (*Oryza sativa*) plants. *Plant J.* 62 (2), 316–329. doi: 10.1111/j.1365-313X.2010.04146.x

Park, E. J., and Kim, T. H. (2021). Arabidopsis OSMOTIN 34 functions in the aba signaling pathway and is regulated by proteolysis. *Int. J. Mol. Sci.* 22 (15), 7915. doi: 10.3390/ijms22157915

Park, S. C., Kim, Y. H., Jeong, J. C., Kim, C. Y., Lee, H. S., Bang, J. W., et al. (2011). Sweetpotato late embryogenesis abundant 14 (IbLEA14) gene influences lignification and increases osmotic- and salt stress-tolerance of transgenic calli. *Planta* 233 (3), 621–634. doi: 10.1007/s00425-010-1326-3

Park, S. I., Kim, J. J., Shin, S. Y., Kim, Y. S., and Yoon, H. S. (2019). ASR enhances environmental stress tolerance and improves grain yield by modulating stomatal closure in rice. *Front. Plant Sci.* 10. doi: 10.3389/fpls.2019.01752

Park, H. Y., Seok, H. Y., Park, B. K., Kim, S. H., Goh, C. H., Lee, B. H., et al. (2008). Overexpression of arabidopsis ZEP enhances tolerance to osmotic stress. *Biochem. Biophys. Res. Commun.* 375 (1), 80–85. doi: 10.1016/j.bbrc.2008.07.128

Parkhi, V., Kumar, V., Sunilkumar, G., Campbell, L. M., Singh, N. K., and Rathore, K. S. (2009). Expression of apoplastically secreted tobacco osmotin in cotton confers drought tolerance. *Mol. Breed.* 23 (4), 625–639. doi: 10.1007/s11032-009-9261-3

Pradhan Mitra, P., and Loque, D. (2014). Histochemical staining of *Arabidopsis thaliana* secondary cell wall elements. *J. Vis. Exp.* (87), e5318. doi: 10.3791/51381

Raghothama, K. G., Maggio, A., Narasimhan, M. L., Kononowicz, A. K., Wang, G., D'Urzo, M. P., et al. (1997). Tissue-specific activation of the osmotin gene by ABA, C2H4 and NaCl involves the same promoter region. *Plant Mol. Biol.* 34 (3), 393–402. doi: 10.1023/a:1005812217945

Sahebi, M., Hanafi, M. M., Rafii, M. Y., Mahmud, T. M. M., Azizi, P., Osman, M., et al. (2018). Improvement of drought tolerance in rice (*Oryza sativa* l.): genetics, genomic tools, and the WRKY gene family. *BioMed. Res. Int.* 2018, 3158474. doi: 10.1155/2018/3158474

Savoure, A., Hua, X. J., Bertauche, N., Van Montagu, M., and Verbruggen, N. (1997). Abscisic acid-independent and abscisic acid-dependent regulation of proline biosynthesis following cold and osmotic stresses in *Arabidopsis thaliana*. *Mol. Gen. Genet.* 254 (1), 104–109. doi: 10.1007/s004380050397

Silvestri, C., Celletti, S., Cristofori, V., Astolfi, S., Ruggiero, B., and Rugini, E. (2017). Olive (*Olea europaea* l.) plants transgenic for tobacco osmotin gene are less sensitive to *in vitro*-induced drought stress. *Acta Physiol. Plant* 39 (10), 229. doi: 10.1007/s11738-017-2535-1

Singh, N. K., Handa, A. K., Hasegawa, P. M., and Bressan, R. A. (1985). Proteins associated with adaptation of cultured tobacco cells to NaCl. *Plant Physiol.* 79 (1), 126–137. doi: 10.1104/pp.79.1.126

Singh, P. K., Indoliya, Y., Agrawal, L., Awasthi, S., Deeba, F., Dwivedi, S., et al. (2022). Genomic and proteomic responses to drought stress and biotechnological interventions for enhanced drought tolerance in plants. *Curr. Plant Biol.* 29, 100239. doi: 10.1016/j.cpb.2022.100239

Srivastava, S., Dashora, K., Ameta, K. L., Singh, N. P., El-Enshasy, H. A., Pagano, M. C., et al. (2021). Cysteine-rich antimicrobial peptides from plants: the future of antimicrobial therapy. *Phytother. Res.* 35 (1), 256–277. doi: 10.1002/ptr.6823

Strizhov, N., Ábrahám, E., Ökrész, L., Blickling, S., Zilberstein, A., Schell, J., et al. (2003). Differential expression of two P5CS genes controlling proline accumulation during salt-stress requires ABA and is regulated by ABA1, ABI1 and AXR2 in arabidopsis. *Plant J.* 12 (3), 557–569. doi: 10.1111/j.0960-7412.1997.00557.x

Suzuki, S., Suzuki, Y., Yamamoto, N., Hattori, T., Sakamoto, M., and Umezawa, T. (2009). High-throughput determination of thioglycolic acid lignin from rice. *Plant Biotechnol.* 26 (3), 337–340. doi: 10.5511/plantbiotechnology.26.337

Szabados, L., and Savoure, A. (2010). Proline: a multifunctional amino acid. *Trends Plant Sci.* 15 (2), 89–97. doi: 10.1016/j.tplants.2009.11.009

Takahashi, Y., Zhang, J., Hsu, P. K., Ceciliato, P. H. O., Zhang, L., Dubeaux, G., et al. (2020). MAP3Kinase-dependent SnRK2-kinase activation is required for abscisic acid signal transduction and rapid osmotic stress response. *Nat. Commun.* 11 (1), 12. doi: 10.1038/s41467-019-13875-y

Tong, S. M., Xi, H. X., Ai, K. J., and Hou, H. S. (2017). Overexpression of wheat TaNCED gene in arabidopsis enhances tolerance to drought stress and delays seed germination. *Biol. Plant* 61 (1), 64–72. doi: 10.1007/s10535-016-0692-5

Tu, M., Wang, X., Yin, W., Wang, Y., Li, Y., Zhang, G., et al. (2020). Grapevine VlbZIP30 improves drought resistance by directly activating VvNAC17 and promoting lignin biosynthesis through the regulation of three peroxidase genes. *Hortic. Res.-England* 7, 150. doi: 10.1038/s41438-020-00372-3

Verma, R. K., Santosh Kumar, V. V., Yadav, S. K., Pushkar, S., Rao, M. V., and Chinnusamy, V. (2019). Overexpression of ABA receptor PYL10 gene confers drought and cold tolerance to indica rice. *Front. Plant Sci.* 10. doi: 10.3389/fpls.2019.01488

Wang, C., Chen, S., Dong, Y., Ren, R., Chen, D., and Chen, X. (2020). Chloroplastic Os3BGlu6 contributes significantly to cellular ABA pools and impacts drought tolerance and photosynthesis in rice. *New Phytol.* 226 (4), 1042–1054. doi: 10.1111/nph.16416

Weber, R. L., Wiebke-Strohm, B., Bredemeier, C., Margis-Pinheiro, M., de Brito, G. G., Rechenmacher, C., et al. (2014). Expression of an osmotin-like protein from *Solanum nigrum* confers drought tolerance in transgenic soybean. *BMC Plant Biol.* 14, 343. doi: 10.1186/s12870-014-0343-y

Wei, X., and Huang, X. (2019). "origin, taxonomy, and phylogenetics of rice," in Rice, *4th* ed. Ed. J. Bao (AACC International Press), 1–29. doi: 10.1016/B978-0-12-811508-4.00001-0

Xue, X., Cao, Z. X., Zhang, X. T., Wang, Y., Zhang, Y. F., Chen, Z. X., et al. (2016). Overexpression of OsOSM1 enhances resistance to rice sheath blight. *Plant Dis.* 100 (8), 1634–1642. doi: 10.1094/pdis-11-15-1372-re

You, J., Hu, H., and Xiong, L. (2012). An ornithine delta-aminotransferase gene OsOAT confers drought and oxidative stress tolerance in rice. *Plant Sci.* 197, 59–69. doi: 10.1016/j.plantsci.2012.09.002

Zhang, Y., Yang, J., Lu, S., Cai, J., and Guo, Z. (2008). Overexpressing SgNCED1 in tobacco increases ABA level, antioxidant enzyme activities, and stress tolerance. *J. Plant Growth Regul.* 27 (2), 151–158. doi: 10.1007/s00344-008-9041-z

Zhao, D., Luan, Y., Shi, W., Zhang, X., Meng, J., and Tao, J. (2021). A *Paeonia ostii* caffeoyl-CoA O-methyltransferase confers drought stress tolerance by promoting lignin synthesis and ROS scavenging. *Plant Sci.* 303, 110765. doi: 10.1016/j.plantsci.2020.110765

Zhou, Y., Zhang, Y., Wang, X., Han, X., An, Y., Lin, S., et al. (2020). Root-specific NF-y family transcription factor, PdNF-YB21, positively regulates root growth and drought resistance by abscisic acid-mediated indoylacetic acid transport in populus. *New Phytol.* 227 (2), 407–426. doi: 10.1111/nph.16524

Zhu, J. K. (2016). Abiotic stress signaling and responses in plants. *Cell* 167 (2), 313–324. doi: 10.1016/j.cell.2016.08.029

Zhu, Z., Sun, B., Xu, X., Chen, H., Zou, L., Chen, G., et al. (2016). Overexpression of *AtEDT1/HDG11* in Chinese kale (*Brassica oleracea* var. *alboglabra*) enhances drought and osmotic stress tolerance. *Front. Plant Sci.* 7. doi: 10.3389/fpls.2016.01285

frontiers | Frontiers in Plant Science

TYPE Original Research
PUBLISHED 02 June 2023
DOI 10.3389/fpls.2023.1167145

Check for updates

OPEN ACCESS

EDITED BY
Mehdi Rahimi,
Graduate University of Advanced Technology, Iran

REVIEWED BY
Milan Kumar Lal,
Central Potato Research Institute (ICAR), India
Chengguo Jia,
Jilin University, China
Sun Jin,
Nanjing Agricultural University, China

*CORRESPONDENCE
Hongbo Gao
hongbogao@hebau.edu.cn

RECEIVED 16 February 2023
ACCEPTED 10 April 2023
PUBLISHED 02 June 2023

CITATION
Wu X, Yuan D, Bian X, Huo R, Lü G, Gong B, Li J, Liu S and Gao H (2023) Transcriptome analysis showed that tomato-rootstock enhanced salt tolerance of grafted seedlings was accompanied by multiple metabolic processes and gene differences.
Front. Plant Sci. 14:1167145.
doi: 10.3389/fpls.2023.1167145

COPYRIGHT
© 2023 Wu, Yuan, Bian, Huo, Lü, Gong, Li, Liu and Gao. This is an open-access article distributed under the terms of the Creative Commons Attribution License (CC BY). The use, distribution or reproduction in other forums is permitted, provided the original author(s) and the copyright owner(s) are credited and that the original publication in this journal is cited, in accordance with accepted academic practice. No use, distribution or reproduction is permitted which does not comply with these terms.

Transcriptome analysis showed that tomato-rootstock enhanced salt tolerance of grafted seedlings was accompanied by multiple metabolic processes and gene differences

Xiaolei Wu[1], Ding Yuan[1], Xinyu Bian[1], Ruixiao Huo[1], Guiyun Lü[1], Binbin Gong[1], Jingrui Li[1], Sichao Liu[2] and Hongbo Gao[1]*

[1]College of Horticulture, Hebei Agricultural University, Key Laboratory of North China Water-saving Agriculture, Ministry of Agriculture and Rural Affairs, Hebei Key Laboratory of Vegetable Germplasm Innovation and Utilization, Collaborative Innovation Center of Vegetable Industry in Hebei, Baoding, China, [2]Chengde Vegetable Technology Promotion Station, Chengde, China

Introduction: Grafting is a commonly used cultural practice to counteract salt stress and is especially important for vegetable production. However, it is not clear which metabolic processes and genes are involved in the response of tomato rootstocks to salt stress.

Methods: To elucidate the regulatory mechanism through which grafting enhances salt tolerance, we first evaluated the salt damage index, electrolyte permeability and Na^+ accumulation in tomato (*Solanum lycopersicum* L.) leaves of grafted seedlings (GSs) and nongrafted seedlings (NGSs) subjected to 175 $mmol \cdot L^{-1}$ NaCl for 0-96 h, covering the front, middle and rear ranges.

Results: Compared with the NGS, the GSs were more salt tolerant, and the Na^+ content in the leaves decreased significantly. Through transcriptome sequencing data analysis of 36 samples, we found that GSs exhibited more stable gene expression patterns, with a lower number of DEGs. *WRKY* and *PosF21* transcription factors were significantly upregulated in the GSs compared to the NGSs. Moreover, the GSs presented more amino acids, a higher photosynthetic index and a higher content of growth-promoting hormones. The main differences between GSs and NGSs were in the expression levels of genes involved in the BR signaling pathway, with significant upregulation of *XTHs*. The above results show that the metabolic pathways of "photosynthetic antenna protein", "amino acid biosynthesis" and "plant hormone signal transduction" participate in the salt tolerance response of grafted seedlings at different stages of salt stress, maintaining the stability of the photosynthetic system and increasing the contents of amino acids and growth-promoting hormones

(especially BRs). In this process, the transcription factors *WRKYs, PosF21* and *XTHs* might play an important role at the molecular level.

Discussion: The results of this study demonstrates that grafting on salt tolerant rootstocks can bring different metabolic processes and transcription levels changes to scion leaves, thereby the scion leaves show stronger salt tolerance. This information provides new insight into the mechanism underlying tolerance to salt stress regulation and provides useful molecular biological basis for improving plant salt resistance.

KEYWORDS

transcriptome, NaCl stress, grafting, Na + transportation, amino acid accumulation, plant hormone signal transduction

Introduction

Soil salinization is one of the main abiotic stresses affecting plant growth and development worldwide, with an estimated 833 million hectares of land currently affected by salinity, accounting for 8.7% of the Earth's area and 20% of irrigated land (Said et al., 2022; Zhang et al., 2022). In recent years, the protected vegetable industry has developed vigorously, but current environmental conditions and overapplication of chemical fertilizers have caused secondary soil salinization to increase daily. Investigations have shown that the total salt content of protected vegetable fields is on average 69.3% higher than that of open-field vegetable fields in China (Huang et al., 2016). Therefore, it is particularly important for protected crops to explore ways to alleviate salt stress.

Na^+ and Cl^- are not essential mineral but are the main ions causing salt stress injury to plants (Ramesh et al., 2015). Soil salinity can hinder plant productivity and inhibit physiological and biochemical processes (Marschner, 1995; Shi et al., 2022), including photosynthesis and membrane integrity. Soil salinity can also lead to chlorophyll degradation, membrane lipid peroxidation, and ion balance disruption, thereby reducing membrane fluidity and selectivity (Bulgari et al., 2019; Hashem et al., 2019; Essalimi et al., 2022; Desoky et al., 2019; Sitohy et al., 2020). Therefore, improving the salt tolerance of plants has become a popular research topic in recent years. This research mainly focuses on the selection and breeding of salt-tolerant varieties, the application of exogenous substances and the use of reasonable irrigation systems. Among these methods, the screening and utilization of salt-tolerant varieties is the most effective way to improve the salt tolerance of greenhouse-grown crops. Compared with cultivated varieties, rootstock varieties are usually more salt tolerant (Penella et al., 2017), but there are few studies on the mechanism underlying the salt tolerance of and identifying salt-tolerant rootstock varieties.

Grafting, which was first applied in melon production, is a commonly used cultural practice to counteract salt stress in practical production (Tian et al., 2012). Cucumber and watermelon were used as experimental materials to improve the salt tolerance of vegetables by grafting. Grafting can enhance the salt tolerance of plants at multiple levels, including regulating the absorption and distribution of K^+ and Na^+ (Estan et al., 2005). After grafting, more Na^+ is stored in the root system, and the selective absorption capacity of K^+ strengthens (Goreta et al., 2008). Tomato (*Solanum lycopersicum* L.) is one of the most widely cultivated, moderately salt-sensitive horticultural crop species worldwide, and it can be used for the development of the vegetable industry in saline-alkali areas after variety improvement or cultivation technology innovation. Therefore, it is of great significance to explore the salt-alkali tolerance mechanism of tomato and improve the salt-alkali tolerance of tomato for the development of the vegetable industry in saline-alkali areas. Compared with that of melon rootstocks, the screening and utilization of tomato rootstocks and the production and application of grafted seedlings (GSs) occurred later, and the improvement of the salt tolerance of tomato seedlings by grafting is manifested through many physiological factors. However, there have been few reports on the research and utilization of tomato rootstock salt tolerance mechanisms in grafted tomato seedlings. Therefore, it is important to determine which metabolic processes and genes are involved in the response of tomato rootstocks to salt stress to analyze the mechanism of stress resistance of grafting.

The development of molecular biological technology, particularly transcriptome sequencing (RNA-seq) technology, makes it possible to understand the salt resistance mechanism of tomato and provides a technical means for understanding salt tolerance mechanisms at the molecular level. At present, a large number of genes induced in response to salt stress have been isolated and identified (Seo et al., 2012; Safdar et al., 2013), mainly sodium ion transport-related genes, including members of the NHX (Na^+/H^+ antiporter) family, and osmotic stress resistance-related genes, including the zinc finger protein-coding gene and the trehalose-6-phosphate synthase gene (Li et al., 2013; Sun et al., 2014). It is reported that multiple hormone regulatory networks during grafting involve auxin, cytokinin, abscisic acid, and gibberellic acid pathways, as well as a variety of transcription factors, which are involved in complex growth induction processes. However, there are few studies on how various hormones change and gene changes during signal transduction under salt stress(Chen et al.,

2020). Moreover, it is not clear which metabolic pathway genes are differentially expressed to elicit the differences in leaf salt stress damage between GSs of salt-tolerant rootstocks and NGS.

To explore the molecular and physiological mechanism of salt tolerance induced by grafting tomato with salt-tolerant rootstock under salt stress, we investigated differences in the salt stress response and Na^+ content of GSs and NGSs. Furthermore, the transcriptome profiles of both of these materials under salt stress were analyzed. The main enriched metabolic pathway products were determined by verifying the significantly differentially expressed genes (DEGs). The objective of this article is to clarify the main metabolic processes and differential gene expression patterns involved in the process of improving salt tolerance in tomato seedlings through grafting.

Materials and methods

Plant material and treatments

The salt-sensitive tomato variety Zhongza 9 and the strongly salt-tolerant tomato rootstock variety QZ-006 (selected by the research group in the early stage) were used as experimental materials and were purchased from the Vegetable and Flower Institute of the Chinese Academy of Agricultural Sciences (Beijing, CHN) and Beijing Kaixingelin Agricultural Technology Co., Ltd. (Beijing, CHN).

The experiment was conducted at the scientific research base of Hebei Agricultural University. (38° 10 '- 40° 00' N, 113° 40 '- 116° 20' E). When the tomato seedlings developed four leaves and one heart, the split grafting method was used to obtain GSs. We selected GSs and NGS that were uniform and displayed good growth, rinsed the roots, used Hoagland's nutrient solution formula for hydroponic cultivation, and used an oxygen pump to supplement oxygen to maintain the normal growth of the grafted tomato seedlings for 15 days after grafting. After 3 days of precultivation, the two types of seedlings were subjected to 175 mmol·L^{-1} NaCl, which was added to Hoagland's nutrient solution. This concentration is the concentration that has significant phenotypic differences in plants selected in previous experiments. (Wu et al., 2020).

In terms of cultivation, the temperature was maintained at 20°C, the pH value of the nutrient solution was maintained at 6.5, and samples were taken at different times after treatment to determine the growth and various physiological indexes of the seedlings. The samples were taken at 8:00 a.m. The leaves of the treated seedlings were harvested at 0 (control), 6, 12, 24, 48 and 96 h for transcriptome sequencing and obtained 12 sets of samples (Three biological replicates for each group of samples, totaling 36 samples). Then the same samples were used for physiological index determination (three biological replicates per treatment). All the samples were immediately placed in liquid nitrogen and stored at -80°C until use.

Physiological measurements

The grading standard of the salt damage index was the same as that of *Liu* et al. (Liu et al., 2007). The electrolyte leakage rate of tomato seedling leaves was measured by a conductivity meter (Thermo Orion, MA, USA) according to the methods of *Dionisio Sese* and *Tobita* (Dionisio-Sese and Tobita, 1998). The leaves of the seedlings of every sample was added to 5 mL of HNO_3 (65%~68%) after they were heated in a microwave digestion system for 2~3 hours. The Na^+ content was determined by inductively coupled plasma-mass spectrometry (ICP-MS; PerkinElmer, Inc., Elan DRC-e) (Chen et al., 2010).

RNA-seq and data analysis

Frozen leaves of 36 samples were sent to Novogene Bioinformatics Technology Co. (Beijing, China) for RNA-seq. Total RNA was isolated using an RNeasy Mini Kit (Qiagen, Germany) according to the manufacturer's instructions and then analyzed with 1% agarose gel electrophoresis to determine the RNA integrity and the presence of DNA contaminants. qRT-PCR was used to quantify the effective concentration of the library after the insert size met expectations (the effective concentration of the library was higher than 2 nM) to ensure the quality of the library.

RNA-seq libraries were sequenced on an Illumina HiSeq X Ten platform. After filtering the adapters and low-quality sequences, the clean reads were mapped to the tomato SL 2.0 genome (https://www.ncbi.nlm.nih.gov/genome/7?genome_assembly_id=393272) using HISAT (Kim et al., 2015). DEGs were identified using the DESeq R package (version 1.10.1; http://www.bioconductor.org/packages/release/bioc/html/DESeq.html) based on |log2(fold change)| ≥1 and false discovery rate (FDR) < 0.05.

qRT-PCR validation

We randomly selected 28 genes for qRT-PCR testing to verify the accuracy of transcriptome. The relative expression level of the candidate genes was analyzed by using the Actin-7 gene as an internal reference, the sequence of which was retrieved from GenBank (GenBank accession number X58253). Gene-specific primers (Table S1) were designed; the primers were synthesized by staff at Shanghai Bioengineering Company. qRT-PCR was performed according to the instructions of a Fast Super EvaGreen qPCR Master Mix Kit (US Everbright®, Inc.). The experimental results were analyzed by the $2^{-\Delta\Delta CT}$ method, and each sample included three technical replicates.

Determination of amino acid contents, photosynthetic indexes and hormone contents

The amino acid contents in the tomato leaves were calculated by the external standard method (Deng et al., 2014). The chlorophyll of the seedlings was extracted with acetone-ethanol (1:1) (Zhang, 1986).

The photosynthetic parameters were measured with an LI-6400 (LI-COR, USA) portable photosynthesis apparatus during sunny days from 9:00 to 11:00 a.m. The potential water use efficiency

(*WUEi*) was calculated using the methods of Ashraf et al. (Ashraf, 2003). The chlorophyll fluorescence parameters were measured with a FluorCam open chlorophyll fluorescence imaging system (Czech Republic) on the 3rd leaf from the top of the plants. The chlorophyll fluorescence parameters included the initial fluorescence (*F0*), *Fm* (maximum fluorescence), *Fv/Fm* (maximum photochemical efficiency), actual quantum efficiency of photosystem II (PSII)), photosynthetic electron transfer rate (*ETR*), photochemical quenching coefficient (*qp*), and nonphotochemical quenching coefficient (*NPQ*). The following parameters were calculated (Demmig-Adams et al., 1996; Lang et al., 1996): PSII potential photochemical efficiency (*Fv/F0*); antenna conversion efficiency (*Fv'/Fm'*); PSII excitation energy pressure (1-*qp*); chlorophyll fluorescence decay rate (*Rfd=(Fm-Fs)/Fs*); and proportion of antenna heat dissipation (*D*=1-*Fv'/Fm'*).

An indirect enzyme-linked immunosorbent assay (ELISA) was used to determine auxin (IAA), gibberellin (GA), cytokinin (ZR), brassinolide (BR), abscisic acid (ABA), jasmonic acid (JA) and salicylic acid (SA) contents, and kit purchased from ThermoFisher Scientific Co., Ltd. (USA). Endogenous ethylene (ETH) was collected, fixed and determined according to the methods of *Ling* (Ling et al., 2008) using a Shimadzu 2010 gas chromatograph equipped with a hydrogen flame ion detector. ETH standard gas was purchased from Sigma Company.

Statistical analysis

Statistical analysis was carried out by Excel2010 software and SPSS 22.0 software. Duncan's method was used for data variance analysis and difference significance comparison ($P<0.05$). The data was expressed as mean ± S.E.M.

Results

Physiological investigation of GSs

The salt damage index of the seedlings indicated that the capacity to withstand salinity stress was significantly weaker for the NGSs than for the GSs (Table 1). With a salt damage index of 3.33%, NGSs showed symptoms of salt damage at 12 h, but that of the GSs was still 0. Afterwards, the salt damage index of the NGSs was always significantly higher than that of the GSs, reflected by a 40.1%-117.5% improvement from 24-96 h. The electrolyte leakage in the leaves of the NGSs was always significantly higher than that in those of controls and GSs from 12-96 h, suggesting more membrane damage during salt stress in the NGSs than in the GSs (Table 2). The Na^+ content in the leaves increased significantly with prolonged salt stress time (Table 3). Compared with the NGSs, the GSs presented significantly lower Na^+ accumulation, which ranged from 16.4%-35.2%. However, there was no significant difference in the sodium ion content between the two types of seedlings under the normal treatment.

Transcriptome analysis under salt stress

We obtained ~271 Gb (clean bases) of quality-filtered sequence data (error rate ≤ 0.03) by RNA-seq, and the alignment rate (mapping rate) ranged from 82.53% to 97.26%, with >92.25% of the bases having a quality score of Q30 or higher (Table S2). The percentage of reads aligned to the unique location of the tomato genome (unique mapping rate) ranged from 80.63% to 95.58%, and the percentage of reads aligned to the positive and negative chains was higher than 40.30% (Table S3). As shown in Figure S1, a strong correlation ($R^2>0.92$) was observed across all the treatments, which indicated that the biological replicates were reliable in this study. In total, 6578/6300, 5141/7176, 2441/7057, 3688/6438 and 4040/5054 genes were differentially regulated at 6, 12, 24, 48, and 96 h, respectively, compared with the control (0 h) (Figure 1A). Venn diagram analysis indicated that many salt-responsive genes were detected at different times under salt stress, which may account for the differences in salt tolerance between the GSs and NGSs (Figure 1B). Notably, 154 DEGs were detected at all salt stress time points, which we called 'core DEGs'. More DEGs were observed at early stress time points, such as 6 and 12 h (Figure 1C).

Several stress-related GO terms were commonly found, such as 'response to abiotic stimulus', 'response to auxin', 'response to endogenous stimulus' and 'response to hormone' (Figure 2A, B). Gene Ontology (GO) enrichment analysis of the GSs revealed several terms related to amino acid biosynthesis and metabolic processes. There were significant differences in DEG-enriched pathways between the GSs and NGSs at different time points (Figure S2). At the initial time of salt stress, the GO terms were enriched in 'photosynthesis' at 6 and 12 h. Taken together, these results suggested that the initial stage of the response to salt stress mainly involves several important genes associated with photosynthesis.

We conducted a Kyoto Encyclopedia of Genes and Genomes (KEGG) enrichment analysis based on the DEGs detected in the GS vs. GC and NGS vs. NGC comparison groups (Figures 3A, B). The

TABLE 1 Salt injury index of grafted and non-grafted tomato seedlings under salt stress.

Type	Treatment	Salt injury index(%)				
		6 h	12 h	24 h	48 h	96 h
Grafted	Control	0	0	0	0	0
	NaCl	0	0	5.67±2.31b	20.33±4.62 b	43.33±2.31 b
Non-Grafted	Control	0	0	0	0	0
	NaCl	0	3.33±2.31 a	12.33±2.31a	36.67±2.31a	60.67±2.31a

TABLE 2 Leaf electrolyte leakage of grafted and non-grafted tomato seedlings under salt stress.

Type	Treatment	Electrolyte leakage(%)				
		6 h	12 h	24 h	48 h	96 h
Grafted	Control	5.33±0.42b	5.85±0.55c	5.92±0.64c	6.11±0.85c	5.24±0.62c
	NaCl	6.05±0.59ab	8.21±0.44b	10.12±1.22b	15.53±1.72b	23.41±2.31b
Non-Grafted	Control	5.24±0.47b	5.38±0.56c	6.13±0.54c	6.26±0.75c	5.87±0.57c
	NaCl	8.11±0.72a	10.43±1.22a	15.27±1.51a	22.37±2.91a	30.25±2.31a

TABLE 3 Na^+ accumulation in leaves of grafted and non-grafted tomato seedlings under salt stress.

Type	Treatment	Na^+ content($mg \cdot g^{-1}$ DW)				
		6 h	12 h	24 h	48 h	96 h
Grafted	Control	6.63±0.25c	6.55±0.24c	6.29±0.35c	6.42±0.21c	6.22±0.22c
	NaCl	7.01±0.23b	8.12±0.30b	8.83±0.38b	9.41±0.27b	10.03±0.41b
Non- Grafted	Control	6.48±0.16c	6.42±0.22c	6.36±0.27c	6.60±0.22c	6.32±0.23c
	NaCl	8.23±0.34a	9.47±0.33a	10.37±0.32a	10.87±0.42a	13.56±0.53a

most significantly enriched pathways of the GSs included 'MAPK signaling'; 'plant hormone signal transduction'; 'alanine, aspartate and glutamate 'metabolism'; and 'plant-pathogen interaction', all of which mainly involve signal transduction and amino acid metabolism. KEGG enrichment analysis of the NGSs also revealed a focus on photosynthesis, in addition to signal transduction and amino acid metabolism. To determine which pathway genes are responsible for the differences in salt tolerance between the two types of seedlings at different stages of salt stress, we analyzed the KEGG pathways at each time point. The significantly enriched pathways at each time point were evaluated. Under salt stress, most of these pathway genes were downregulated at each time point. The DEGs upregulated at 6 h and 12 h were significantly enriched in 'circadian rhythm - plant', while the DEGs downregulated at 6 h were enriched in 'carbon metabolism', 'biosynthesis of amino acids', and 'carbon fixation in photosynthetic organisms', where the DEGs enriched in 'ribosome' and 'photosynthesis - antenna proteins' at 12 h were downregulated (Figures 4A, B). The genes differentially expressed at 24 h were enriched in 'photosynthesis - antenna proteins', 'photosynthesis', 'porphyrin and chlorophyll metabolism', etc., all of which are related to photosynthesis and were downregulated (Figure 4C). At 48 h, DEGs enriched in 'ribosome' and 'DNA replication' pathways were downregulated, and those enriched in the 'MAPK signaling pathway-plant' were upregulated (Figure 4D). At 96 h, there were three pathways whose enriched DEGs were upregulated: 'plant-pathogen interaction', 'phenylalanine metabolism' and 'MAPK signaling pathway-plant', while those enriched in 'plant hormone signal transduction' were downregulated (Figure 4E).

To assess the reliability of the RNA-seq data, qPCR was used to analyze the expression patterns of 31 randomly selected genes (Figures 5A, 6A). The correlation coefficients (R^2 = 0.9267, R^2 = 0.9072) implied that the RNA-seq data were reliable (Figures 5B, 6B). The temporal and spatial expression patterns of 154 core DEGs are presented in a heatmap (Figure 7). There were 4 transcription factor-encoding genes among the 154 core genes coenriched within the two types of seedlings under salt stress in our study, including *WRKY* (LOC101255501, LOC101247012, LOC543855) transcription factors and the basic leucine zipper type (*bZIP*) transcription factor *PosF21* (LOC101250636). Moreover, in terms of expression level, these four genes in the GSs exhibited increased expression most of the time after salt stress, suggesting that they play important roles in transcriptional regulation that contributes to the salt tolerance of tomato. Other DEGs exhibited similar expression patterns, indicating that these genes were commonly induced in this species in response to salinity stress.

Amino acid contents and related gene expression levels

On the basis of the results of the KEGG pathway enrichment analysis, which revealed enrichment of amino acid-related pathways at 6 h and 96 h, we carried out a detailed analysis of amino acid metabolism pathway genes. Figure 8 shows the amino acid biosynthesis pathways and the general pattern of the relative changes in related metabolites in the GS and NGS genotypes under salt stress conditions. The content of most free amino acids considered osmotic regulatory substances significantly increased in both genotypes, implying that the accumulation of free amino acids is crucial in the response to salt stress. Obviously, the accumulation rate of many free amino acids and related compounds (including alanine, asparagine, glutamate, glycine, leucine, lysine, methionine, phenylalanine, proline, γ-aminobutyrate (GABA), serine, threonine, tyrosine, and valine) was higher in the GSs than in the NGSs, which

10.3389/fpls.2023.1167145

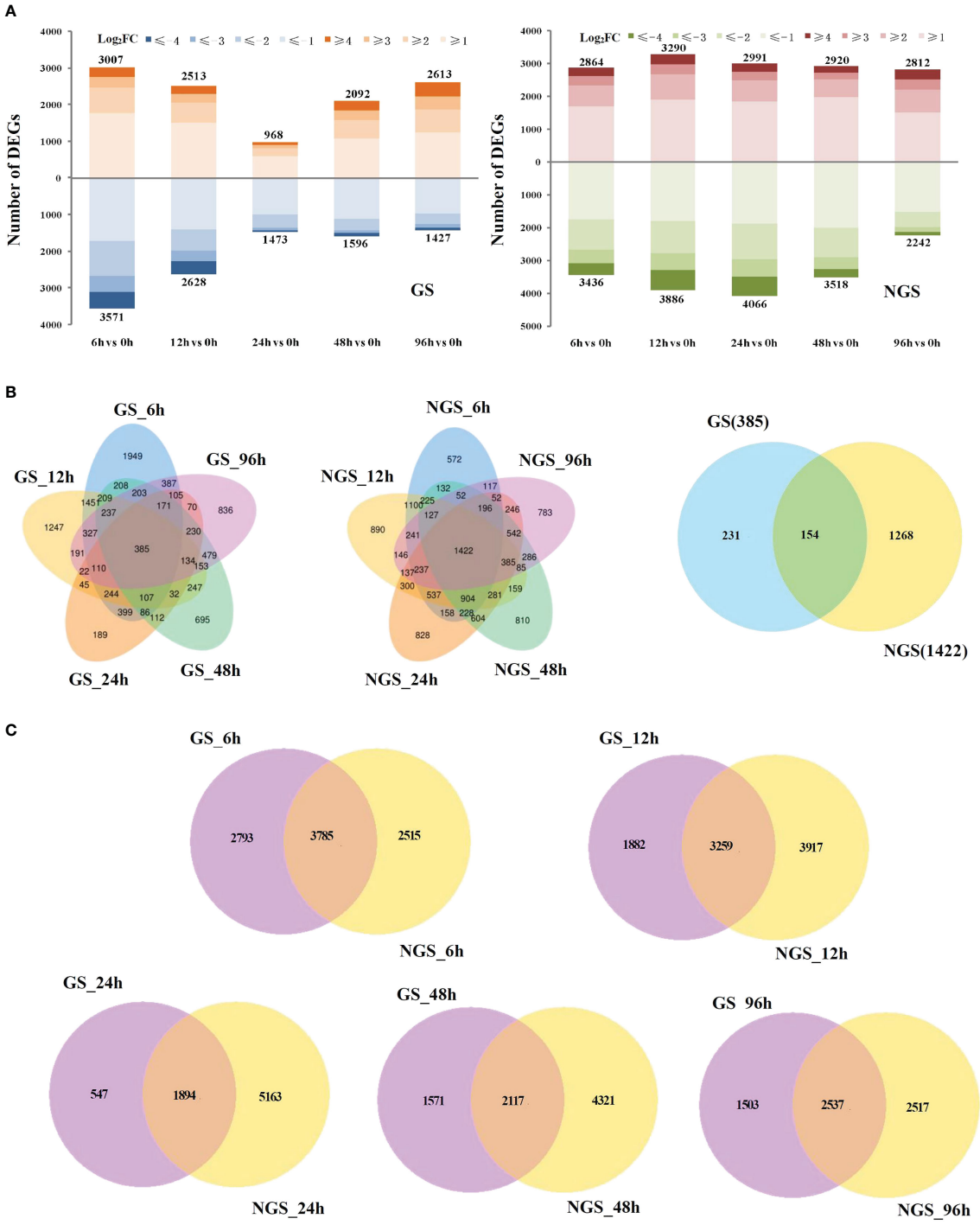

FIGURE 1
Differentially expressed genes (DEGs) in GS and NGS in response to salt stress. Numbers of DEGs in GS and NGS at different salt stress time points **(A)**. Venn diagrams of DEGs among different salt stress time points in GS and NGS **(B)** and between both genotypes at 6, 12, 24, 48 and 96h **(C)**, respectively.

may be a positive feature for withstanding salinity stress by the GS genotype. The change in most free amino acids was detected mainly from 6-24 h, but the contents of proline and GABA, which are major stress-related amino acids, changed markedly from 48-96 h.

The expression of genes related to the amino acid metabolism pathway also changed significantly, as shown in Figure 8B. Most of the genes involved in the biosynthesis of these amino acids and related compounds, such as asparagine, aspartate, alanine, arginase and GABA, were upregulated in both genotypes under salt stress. At the same time, there was also a trend towards downregulation of several genes that encode related enzymes, such as those involved in the arginine, glutamate, and cysteine pathways, but most of these genes did not encode synthetases. Several genes, such as those encoding the arginine biosynthesis bifunctional protein *ArgJ*

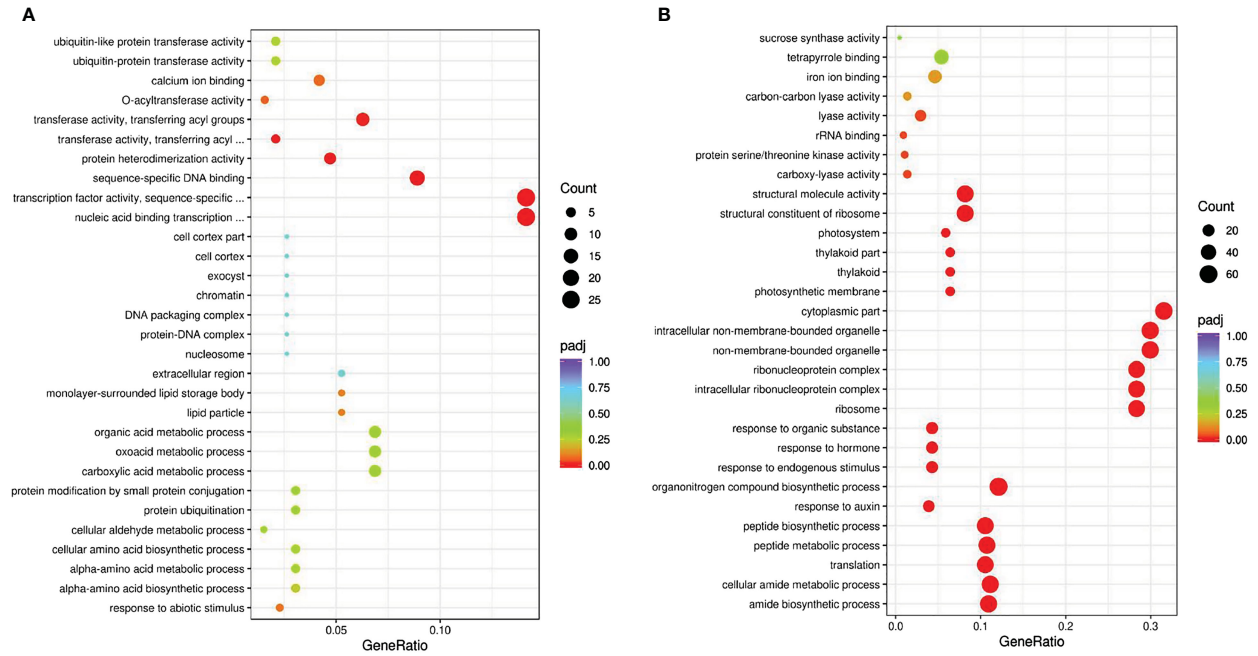

FIGURE 2
GO enrichment analysis of DEGs in leaves. GS vs GC **(A)** and NGS vs NGC **(B)**.

(LOC101265059), glutamate synthase 1 (NADH; chloroplastic; LOC101254281), and S-adenosylmethionine synthase 2 (LOC101247506), showed higher expression changes in the GSs than in the NGSs at 12 h to 48 h after salt stress. In addition to those involving amino acids, genes and products related to organic acid metabolism, especially that of citrate and 2-oxoglutarate, were also significantly upregulated. Moreover, the expression of the gene encoding glutamate decarboxylase (LOC544313), which is involved in the GABA biosynthesis pathway, was upregulated markedly, explaining the rise in GABA levels. Overall, the integration of the two omics datasets showed that amino acid metabolism strongly promoted the salt tolerance of tomato, especially in the GS genotype.

Photosynthesis and related gene expression levels during salinity stress

Considering that photosynthesis has been shown to play vital roles in the abiotic stress response in the initial stage and middle stage of salt stress, we focused on 24 DEGs enriched in the 'photosynthesis - antenna proteins' pathway (Figure 9A). In general, the expression of the genes encoding antenna pigment proteins showed a general downwards trend after salt stress. Notably, the gene expression in the GS genotype was higher than that in the NGS genotype, especially at 12 h, which may be a positive feature for withstanding salinity stress in the GS genotype. LHCI is the major light-trapping pigment protein of photosystem I (PSI). The expression levels of the genes encoding chlorophyll a-b binding protein 6A (LOC101253380) and the chlorophyll a/b binding protein precursor (LOC544310) in the GSs were significantly higher than those in the NGSs at 12 h. *Lhcb1* is one of the genes encoding chlorophyll a/b binding protein in PSII. The gene encoding chlorophyll a/b binding protein 3A (LOC101267774) showed an increase in expression in the GSs at 12 h. At 24 h of stress, all photosynthetic antenna pigment protein pathway-related genes were significantly downregulated in both the GSs and the NGSs.

We calculated the related photosynthesis indexes and found that the photosynthesis of the seedlings of both genotypes was inhibited under salt stress (Figure 9B). However, compared with the NGSs, the GSs presented better photosynthesis-related indexes. The chlorophyll content in the GSs was significantly higher than that in the NGSs, and the chlorophyll a/b ratio was significantly lower in the GSs than in the NGSs, especially at 24 h. The *Pn*, *Tr*, *Gs* and *Ci* of the tomato seedlings decreased continuously with the prolongation of NaCl stress. The *Pn* and *Ci* of the GSs were significantly higher than those of the NGS at 24 h. With prolonged NaCl stress time, the chlorophyll fluorescence parameters of both genotypes showed a downwards trend. The parameters of the GSs, such as *F0*, *Fm*, *Fv/F0*, *Fv/Fm*, *Fv'/Fm'*, *φPSII*, *qp*, *ETR* and *1-qp*, were significantly higher than those of the NGSs. However, the *NPQ*, *D* and R_{fd} of the GSs were significantly lower than those of the NGSs.

Hormone signal transduction pathway DEGs and hormone contents during salinity stress

The 'plant hormone signal transduction' KEGG pathway was shown to be enriched in DEGs during almost the whole stress process, and plant hormones have been shown to play vital roles in

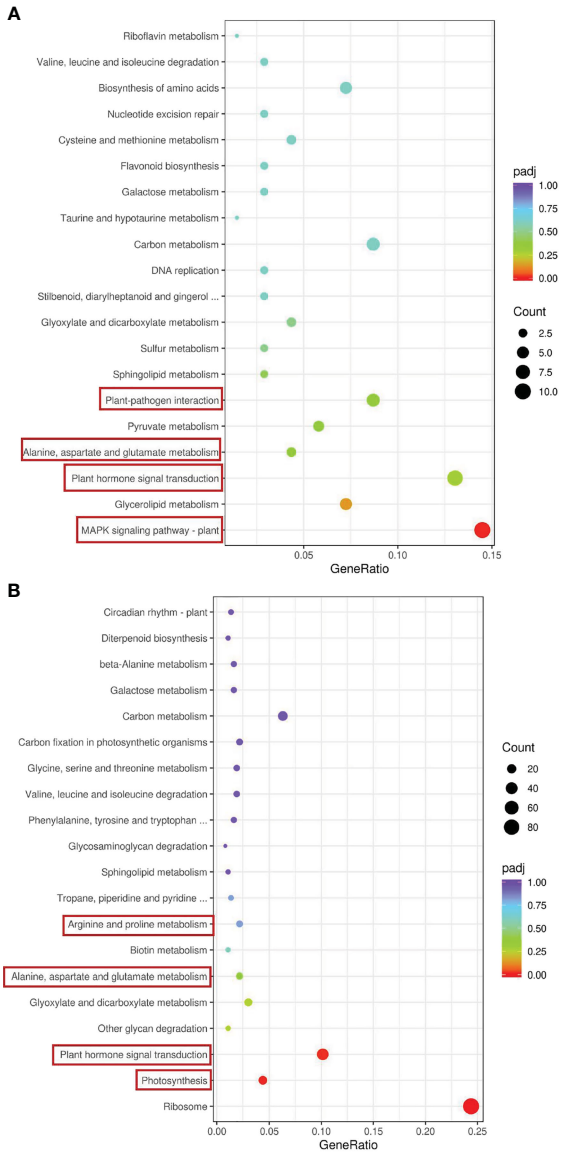

FIGURE 3
KEGG enrichment analysis of DEGs in leaves. GS vs GC **(A)** and NGS vs NGC **(B)**.The red border indicates that this article focuses on metabolic pathways.

the abiotic stress response. We focused on 87 DEGs enriched in the 'plant hormone signal transduction' pathway from 12-96 h (Figure 10). The expression of DEGs in the two genotypes was different. In particular, several genes involved in the IAA, ZR, GA, brassinosteroid, and JA pathways, such as those encoding probable indole-3-acetic acid-amido synthetase *GH3.1* (LOC101246970), histidine-containing phosphotransfer protein 1 (LOC101253938), DELLA protein GAI (LOC101265384), xyloglucan endotransglucosylase-hydrolase *XTH3* (LOC543914), probable xyloglucan endotransglucosylase/hydrolase protein 23 (LOC101258345, LOC101258926 and LOC101258632), jasmonate ZIM-domain protein 1 (LOC100134911) and protein TIFY 10b-like (LOC101247936), showed higher levels in the GSs than in the NGSs after exposure to salt. Moreover, the difference in BR signaling pathway genes between the two materials was the most significant. These genes are mainly involved in promoting beneficial hormones involved in stress resistance, which together may be one of the reasons for the increased salt tolerance of the GSs.

We selected two time points with significant gene enrichment to determine leaf hormone contents (Figure 11). The hormone change range in the NGSs was larger than that in the GSs. Between the two genotypes, the contents of IAA, ZR, gibberellic acid (GA), BR, methyl jasmonate (MeJA) and SA, which are considered to be positively related to stress tolerance, showed a downwards trend. However, the time points at which the various hormones in the GSs occurred sooner than those in the NGSs. Among them, the BR content decrease of NGSs was greater than that of other hormones, with more than 50%. However, the BR content of GSs decreased by only 15% and 21.3%. The ABA and ETH contents increased, and the increases in the GSs were less drastic than they were in the NGSs. In addition, salt stress also affected the hormone balance in the two types of seedlings. The ratios of IAA, ZR and GA to ABA also decreased significantly in both genotypes, but these decreases were still greater in the NGSs than in the GSs.

Discussion

Salt-tolerant rootstock grafting inhibits the accumulation of Na^+ in the leaves

The damage to plant cells and the resulting growth inhibition under salt stress are mainly caused by the excessive absorption and accumulation of Na^+ (Flowers and Colmer, 2015). Under salt stress, the absorption of Na^+ by plant roots is significantly increased. Na^+ is translocated from the roots and stems to the leaves, causing ion toxicity in leaf cells and osmotic stress, which disrupts the structure and function of the membrane system (Tian et al., 2012), causing plants to display obvious salt stress symptoms. The salt tolerance of nonhalophytes mainly depends on the ability of their root system to selectively absorb salt ions and control the transport of those ions into the roots from the soil (Yang et al., 2015). Our previous study showed that the growth potential of GSs is significantly different due to different rootstocks and that the salt tolerance of GSs is mainly determined by the resistance of the root systems of rootstocks (Jia et al., 2020).

The results of the present experiments show that salt stress leads to a gradual increase in Na^+ content in the two types of tomato seedlings. The Na^+ content in the leaves of GSs was found to be significantly lower than that in the leaves of NGSs, and the salt stress index of the leaves of NGSs was higher than that of the leaves of GSs. This is because salt-tolerant rootstocks have a strong ability to avoid and reject sodium. Less Na^+ is absorbed by salt-tolerant roots than by salt-sensitive roots, and more Na^+ is trapped in the roots to reduce the transport of Na^+ to the leaves, alleviating the damage caused by salt stress to seedlings. However, which metabolic processes related to the salt stress response are accompanied by rootstocks inhibiting the accumulation of sodium ions on the leaves, thus alleviating the salt stress damage on the leaves?

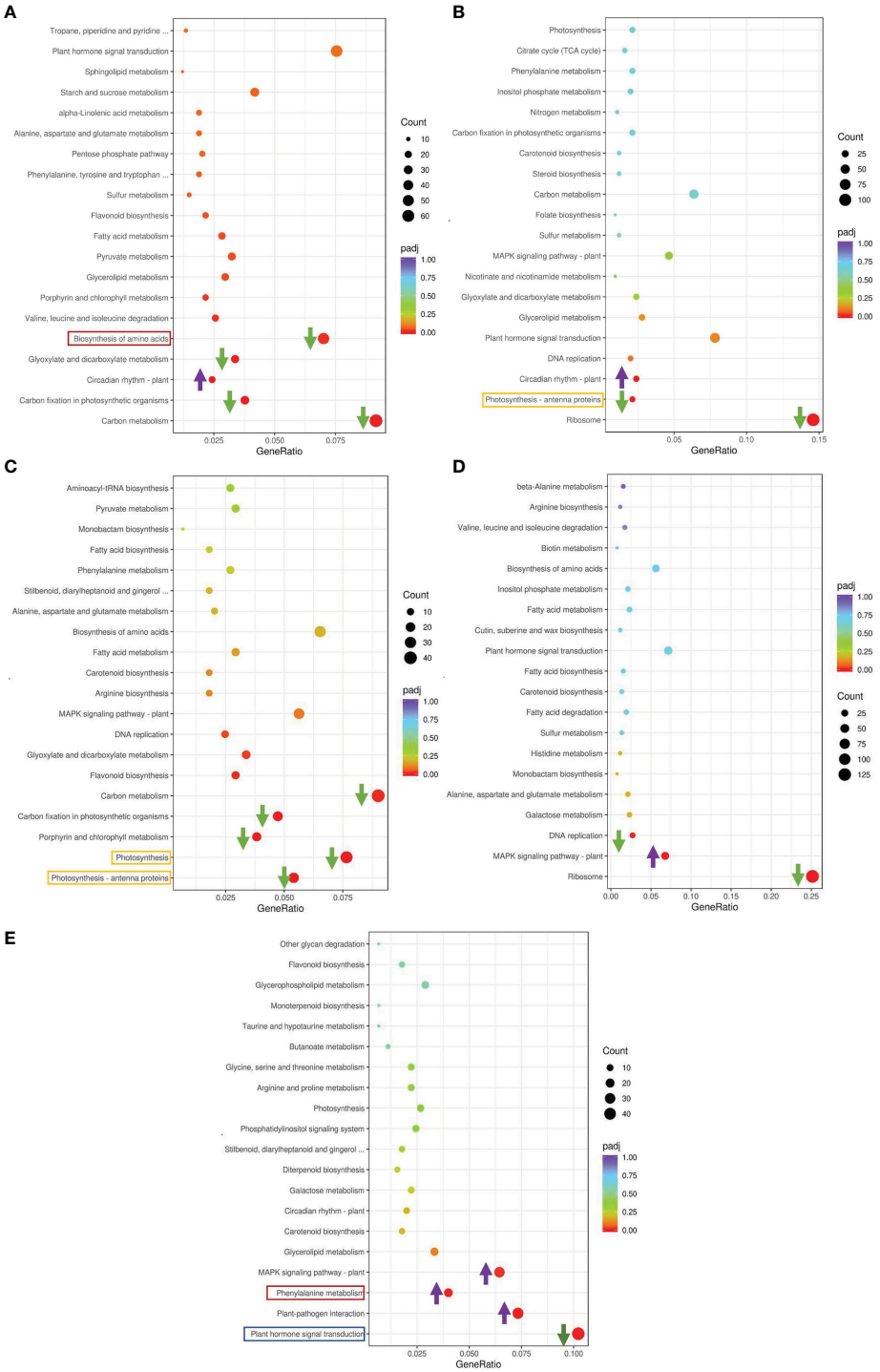

FIGURE 4
KEGG enrichment analysis of DEGs in leaves. GS_6h vs NGS_6h **(A)**, GS_12h vs NGS_12h **(B)**, GS_24h vs NGS_24h **(C)**, GS_48h vs NGS_48h **(D)**, GS_96h vs NGS_96h **(E)**.

GSs stabilize the number of genes expressed and have different expression modes

With the development of molecular biology technology, it has been found that there is a wide range of genetic material exchange and interactions that occur in grafts, including those involving mRNAs, sRNAs, proteins and so forth (Lewsey et al., 2016; Lu et al., 2020; Wang et al., 2020). Transcriptome sequencing of disease-resistant and nondisease-resistant rootstocks in tomato showed that the former were less sensitive to virus-induced injury (Spanò et al., 2020). In the present study, the total number of DEGs in the GSs was significantly

10.3389/fpls.2023.1167145

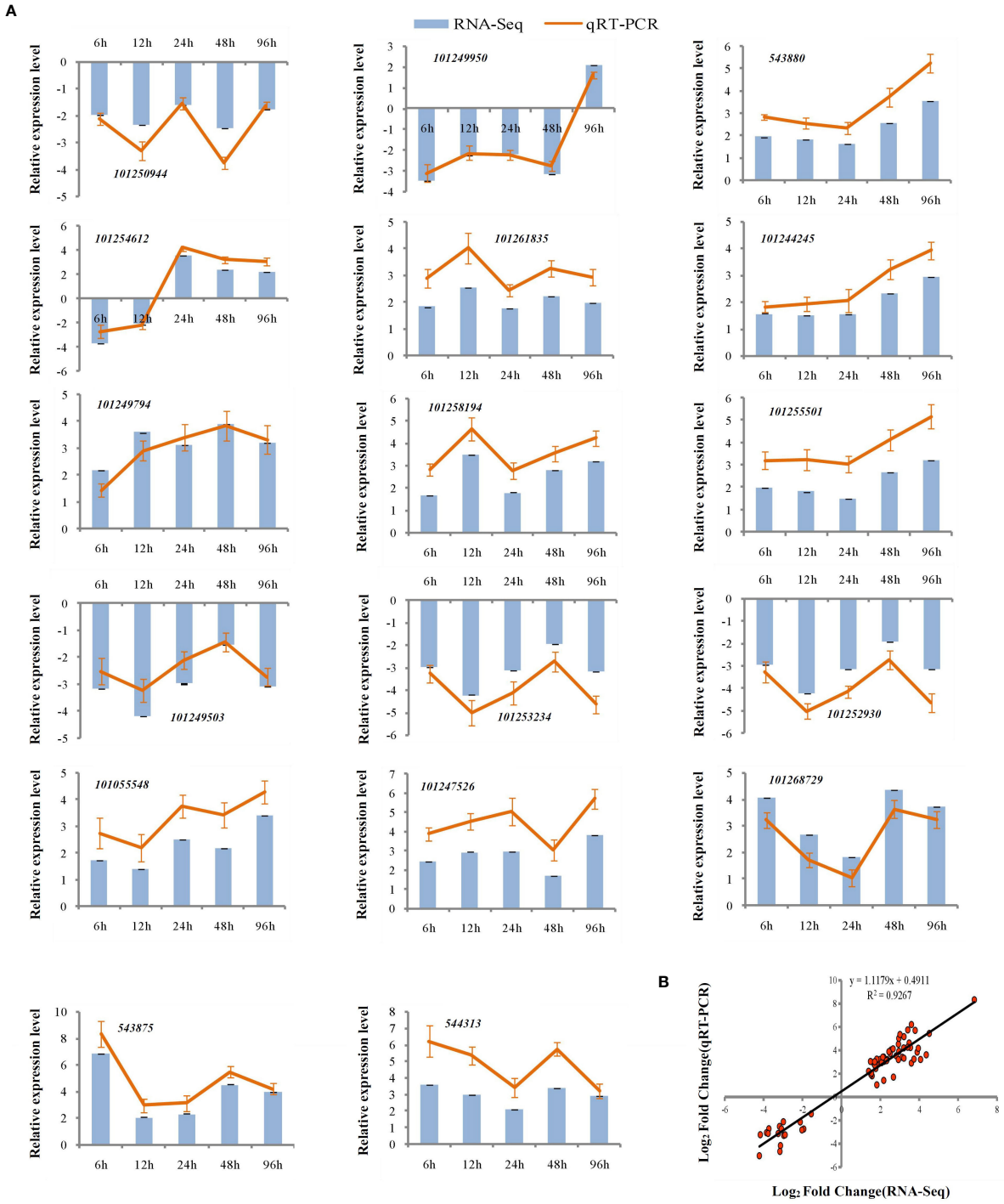

FIGURE 5
qRT-PCR validation of expression profiles obtained by RNA-seq in GS under salt stress. qRT-PCR analysis of 17 selected genes. The Y-axis represents the relative expression levels, the X-axis shows the time of 175 mM NaCl treatment in GS **(A)**. The correlation of $\log_2$ Fold Change obtained by qRT-PCR (Y-axis) and RNA-seq (X-axis) in GS **(B)**.

lower than that in the NGSs throughout the whole process of salt stress (Figure 2A), with ratios equal to 0.72, 0.35, 0.57 and 0.80. Moreover, the variation trend of the expression of DEGs in the GSs and NGSs at the different time points was also different. The number of DEGs in the GSs was highest at 6 h and decreased to the lowest value at 24 h. However, the number of DEGs in the NGSs decreased gradually after peaking at both 12 h and 24 h. These results indicate that the GS gene response was faster than the NGS gene response and that maintaining the stability of gene expression may underpin the molecular basis for inducing salt tolerance in GSs with salt-tolerant rootstocks.

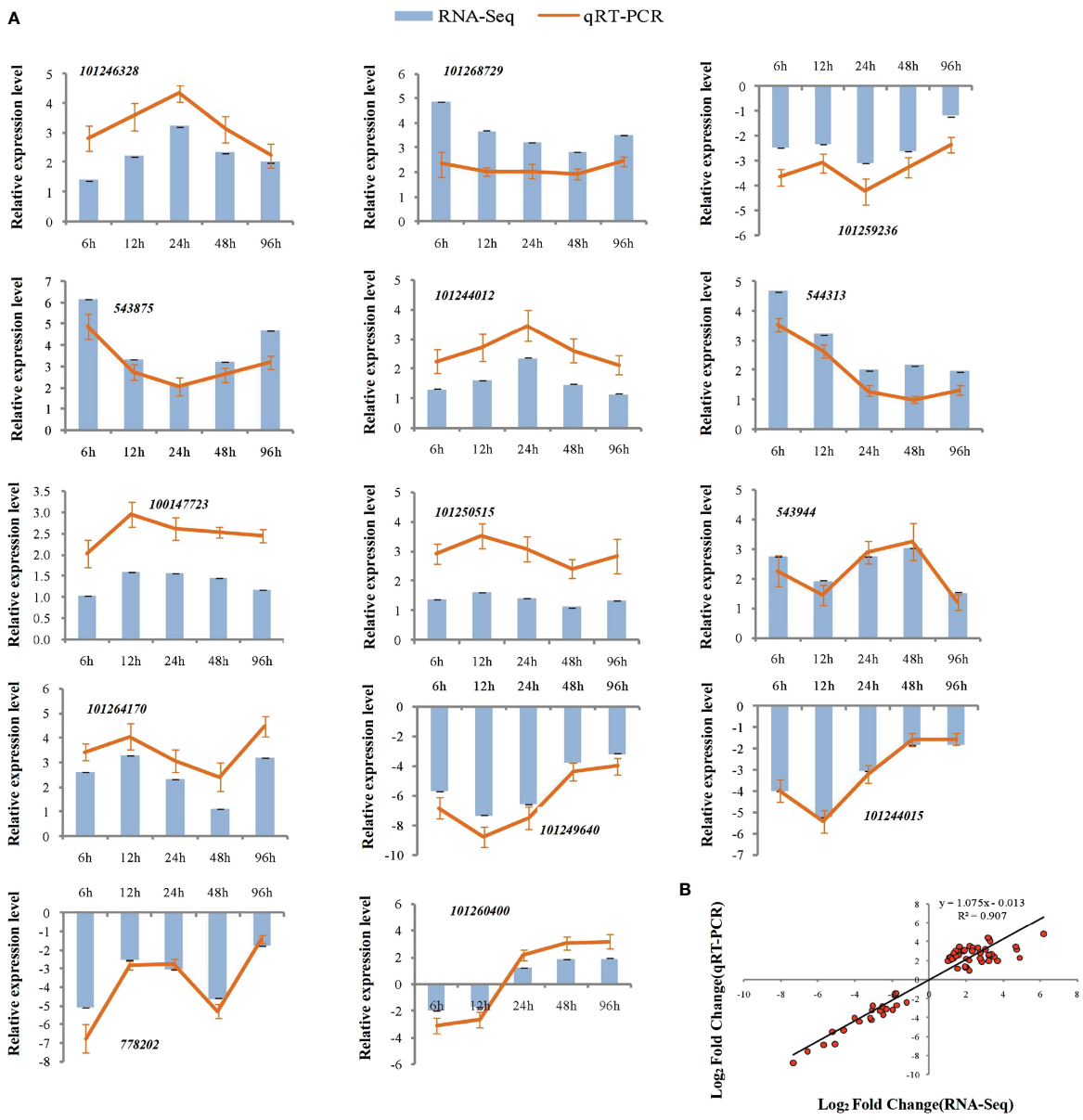

FIGURE 6
qRT-PCR validation of expression profiles obtained by RNA-seq in NGS under salt stress. qRT-PCR analysis of 14 selected genes. The Y-axis represents the relative expression levels, the X-axis shows the time of 175 mM NaCl treatment in NGS **(A)**. The correlation of log2 Fold Change obtained by qRT-PCR (Y-axis) and RNA-seq (X-axis) in NGS **(B)**.

Based on the phenotypic and physiological data, we considered the time spanning 6 and 12 h as the initial stage of salt stress, the time spanning 24 h and 48 h as the middle phase of salt stress, and 96 h as the later stage of salt stress. Generally, the change trend of the expression of DEGs in the two types of seedlings at each time point was mainly downwards, especially in the early and middle stages of stress. Photosynthetic pathway gene enrichment mainly occurred during the above two periods. Amino acid metabolic pathways were mainly enriched in the early and late stages of stress, while hormone signal transduction was enriched throughout the whole process of stress. These three pathways are closely related to salt stress, and further studies are necessary.

Previous studies have shown that many important salt tolerance-related genes are directly regulated by transcription factors related to the stress response. *ABI4* in Arabidopsis regulates the expression of the *HKT1* gene (Shkolnik-Inbar et al., 2013). *NAC* transcription factors are induced in response to salt stress and participate in the regulation of salt tolerance-related genes in the root system of pumpkin rootstocks (Cao et al., 2017). The *WRKY* transcription factor family is one of the largest transcription factor families in plants. *WRKY* members participate in the plant response to biotic/abiotic stress, growth and development and are important components of the plant regulatory network (Xu et al., 2016). The three *WRKY* genes selected in this study were *WRKY33A*, *WRKY7* and *WRKY17*. *AtWRKY33*

10.3389/fpls.2023.1167145

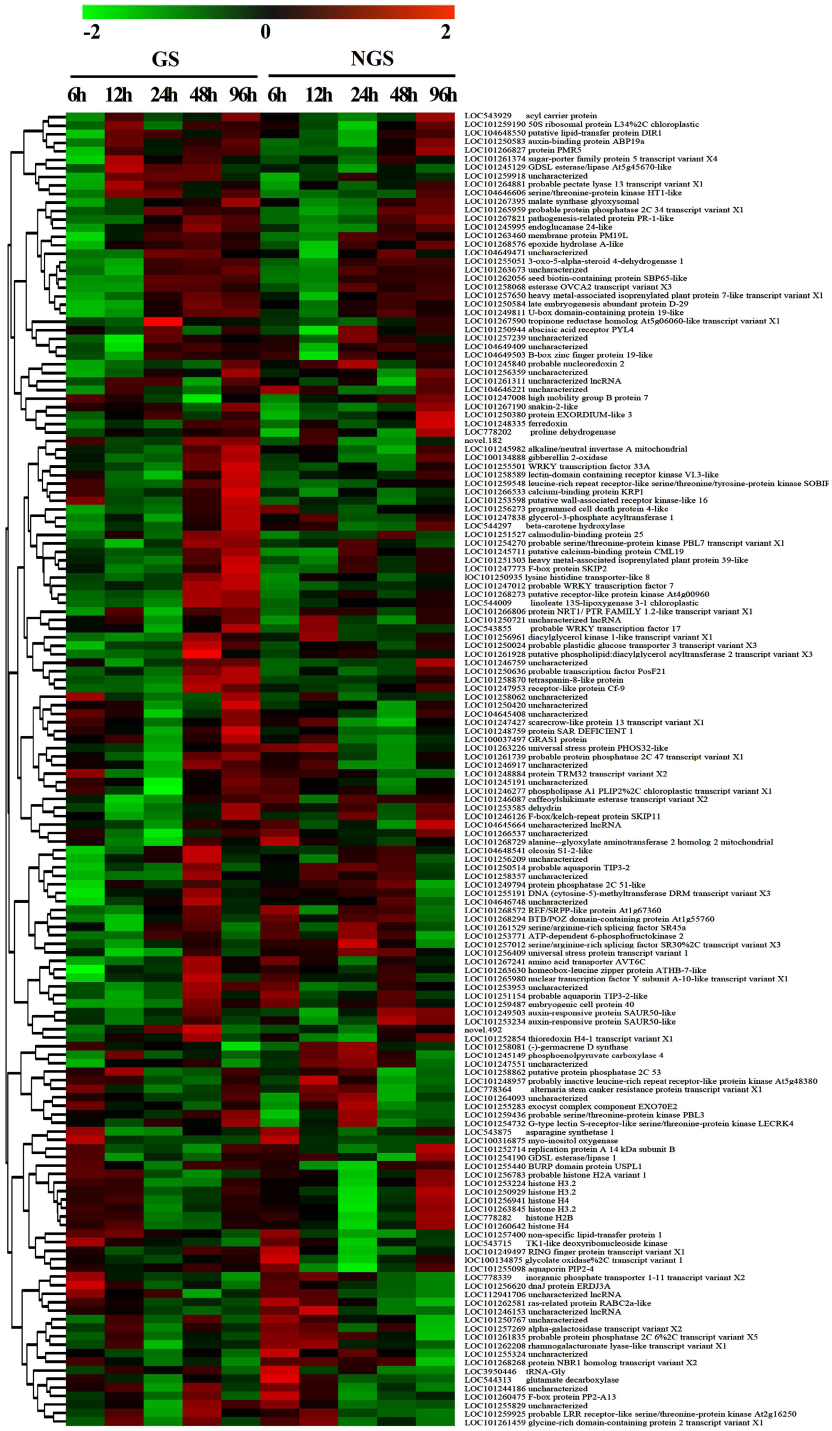

FIGURE 7
Heatmap of analysis of 154 core DEGs in GS and NGS at different salt stress time points. X-axis, samples; Y-axis, differentially expressed gene names with annotations.

controls the formation of an extracellular barrier in Arabidopsis roots by regulating the cytochrome P450 gene, thus improving salt tolerance (Krishnamurthy et al., 2020). *WRKY7* may be involved in the response of rice to bacterial blight (Zheng, 2018), and *WRKY17* regulates osmotic stress and ABA-induced stomatal closure. In addition, *PosF21* plays a positive regulatory role in the ABA signaling pathway, which may be related to salt stress tolerance (Zhong, 2016). Therefore, we speculate that the abovementioned transcription factors are important, and the regulatory mechanism needs to be further verified.

10.3389/fpls.2023.1167145

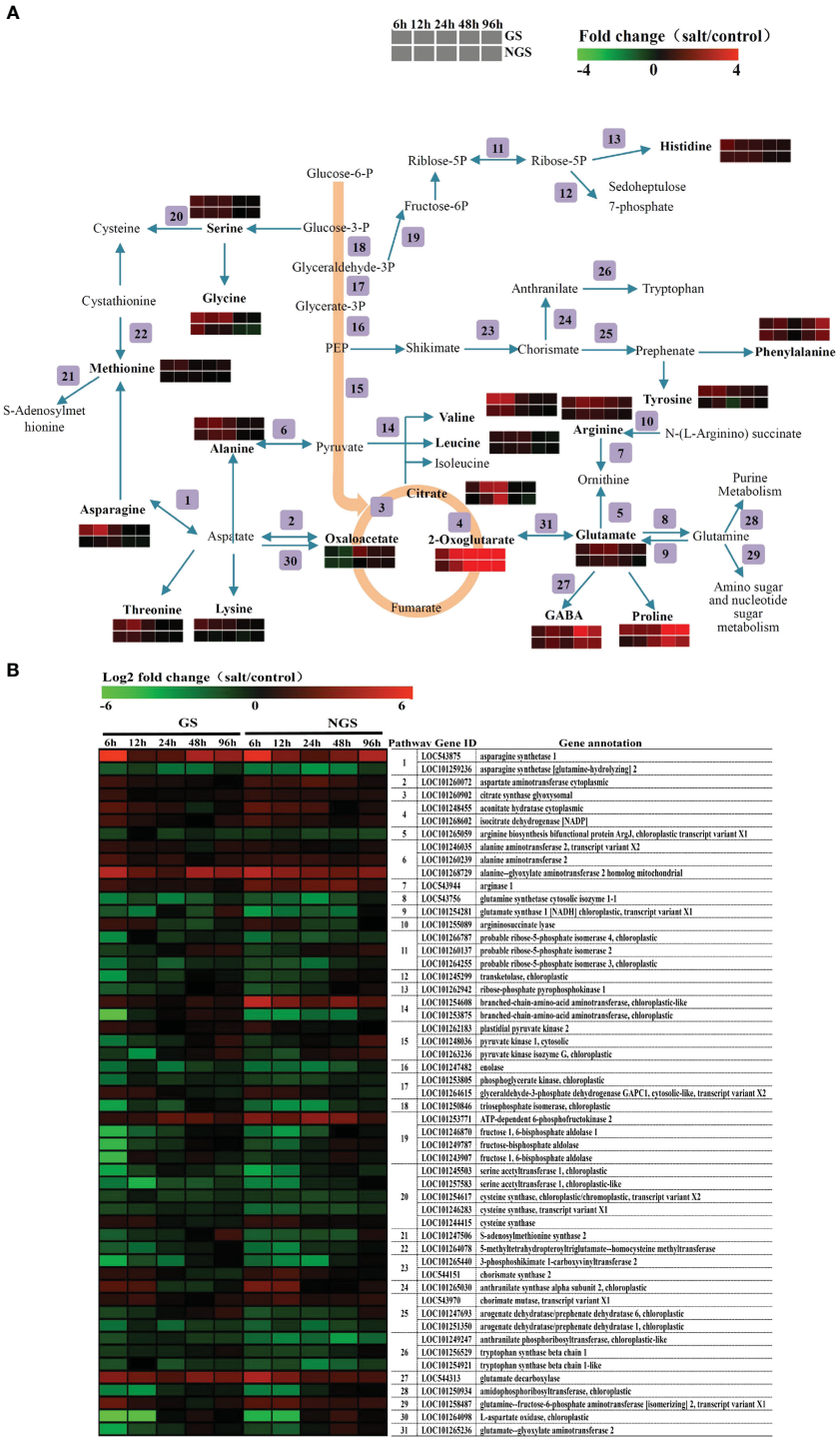

FIGURE 8
Adaptive changes in amino acid metabolism in GS and NGS during salinity stress. Amino acid metabolic pathways and the general pattern of metabolites changes associated with the pathways in GS and NGS at 6 h to 96 h after salinity stress **(A)**. Expression changes of the genes involved in metabolic pathways in GS and NGS at different salt stress time points. The pathway ID column indicates the gene product in relation to metabolic pathway **(B)**.

Leaves of GSs accumulate more amino acids

In addition to inhibiting plant growth, salt stress also causes plants to initiate metabolic changes, in which the osmotic regulation of amino acids plays an important role in improving plant salt tolerance (Zhang et al., 2017). An increase in amino acid content can also improve the adaptability of plants to salt stress. Previous studies have shown that amino acid synthesis is one of the adaptive responses of plants to NaCl stress (Misra and Gupta,

10.3389/fpls.2023.1167145

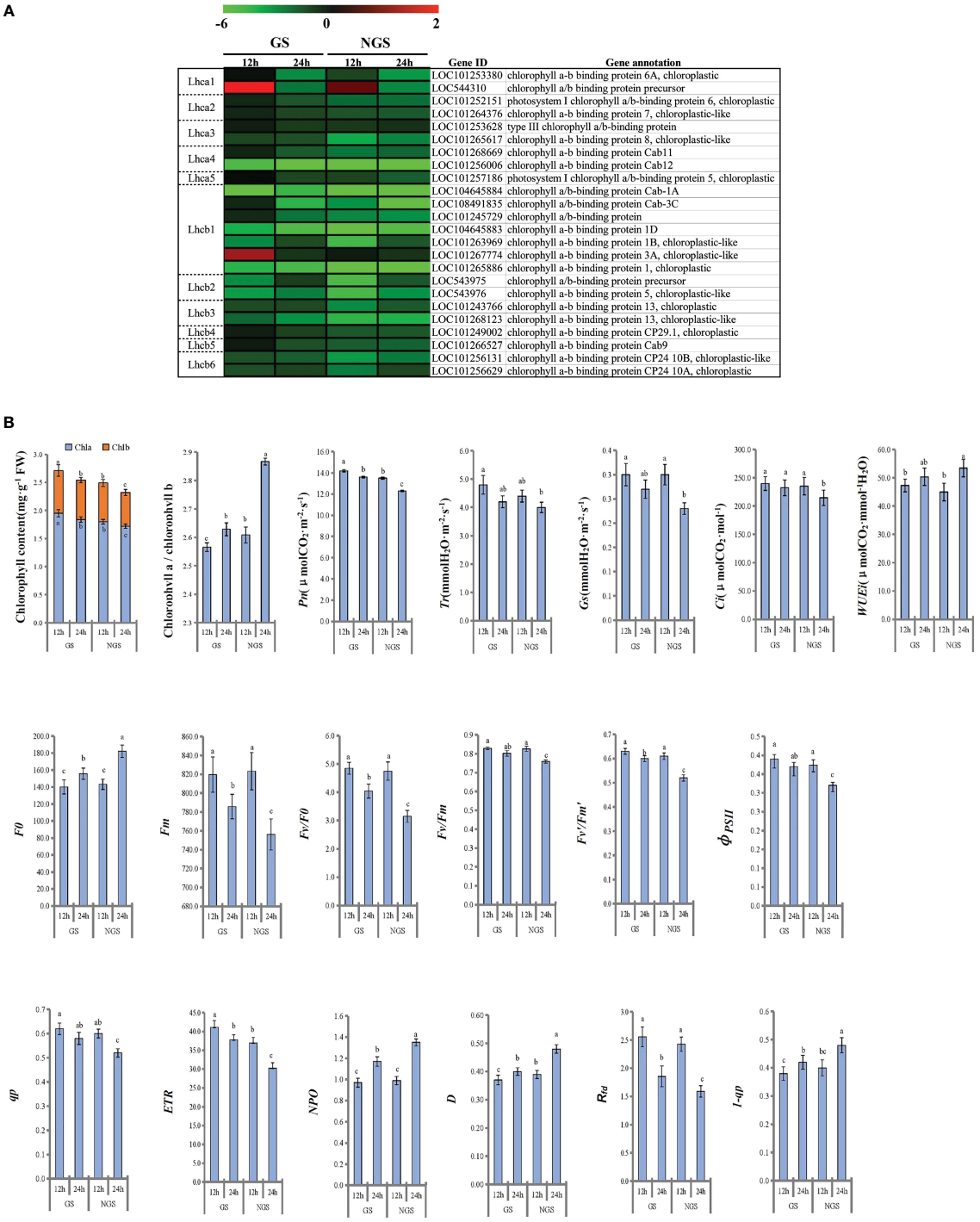

FIGURE 9
Photosynthetic antenna protein related genes of leaves at 12 h and 24 h after salinity stress **(A)**. Photosynthesis and fluorescence related parameters of leaves at 12 h and 24 h after salinity stress **(B)**.

2005). Moreover, previous studies have mostly focused on the relationships between salt stress and total proline and free amino acid contents. The salt tolerance of grafted tomato seedlings can be improved by inducing an increase in the free proline content (Chen et al., 2005). Free amino acids may be important osmotic pressure regulators in the cytoplasm of plant cells, perhaps due to the accumulation of toxic NH_4^+ in plants under salt stress, and it is possible to increase the tolerance of some plants to salt stress (Xu et al., 2016).

In this study, the contents of 16 main amino acids and 3 metabolic intermediates involved in the tricarboxylic acid (TCA) cycle in the leaves of tomato seedlings under salt stress were analyzed. Although the contents of most amino acids increased, their peak accumulation occurred mainly in the early stage of stress

10.3389/fpls.2023.1167145

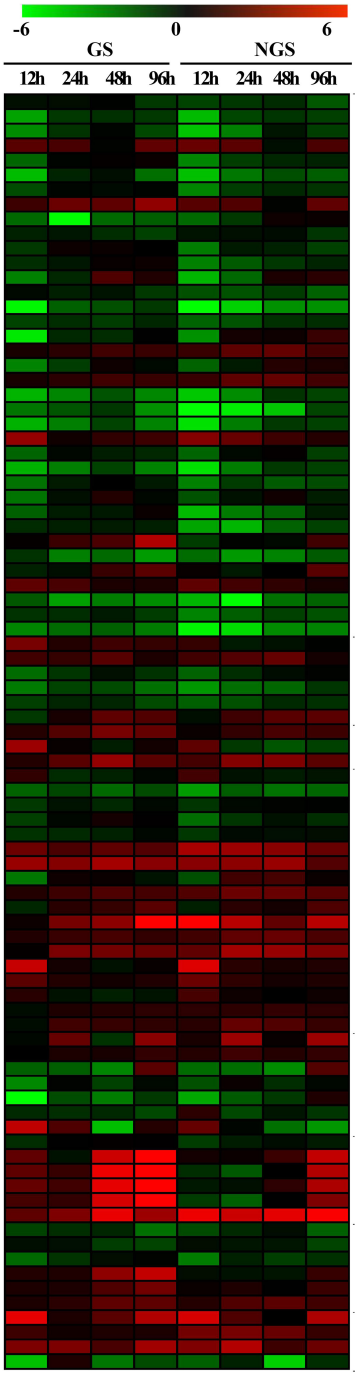

Pathway	Gene ID	Gene annotation
Auxin	LOC100736540	protein LAX1
	LOC101255303	auxin-responsive protein IAA4
	LOC101055550	IAA22
	LOC101055556	IAA36
	LOC101055541	IAA1
	LOC101055542	IAA2, transcript variant X1
	LOC101055547	IAA14
	LOC101055548	protein IAA8
	LOC101055549	IAA19
	LOC543541	auxin-regulated IAA27
	LOC543542	IAA7 protein
	LOC543543	auxin responsive protein IAA16
	LOC543544	IAA10 protein
	LOC100191131	auxin response factor 7, transcript variant X1
	LOC101253537	Auxin_inducible
	LOC101245895	auxin-induced protein 6B
	LOC101055583	small auxin-up protein 58
	LOC101263158	auxin-responsive protein SAUR32
	LOC101246226	auxin-responsive protein SAUR32
	LOC101250847	auxin-responsive protein SAUR50-like
	LOC101253234	auxin-responsive protein SAUR50-like
	LOC101244440	auxin-responsive protein SAUR21-like
	LOC101249503	auxin-responsive protein SAUR50-like
	LOC101255313	auxin-responsive protein SAUR71
	LOC101243817	auxin-induced protein 15A
	LOC112941374	auxin-induced protein 15A-like
	LOC104645434	auxin-induced protein 15A-like
	LOC101268587	uncharacterized LOC101268587, transcript variant X1
	LOC101247499	auxin-responsive protein SAUR50
	LOC101246270	auxin-responsive protein SAUR36-like
	LOC101246970	probable indole-3-acetic acid-amido synthetase GH3.1
	LOC101258277	indole-3-acetic acid-amido synthetase GH3.10-like
	LOC101262636	indole-3-acetic acid-amido synthetase GH3.6
	LOC101258198	indole-3-acetic acid-amido synthetase GH3.6-like
	LOC101252930	auxin-responsive protein SAUR50-like
	LOC104645435	auxin-induced protein 15A-like
	LOC101251725	auxin-responsive protein SAUR50
Cytokinine	LOC101253938	histidine-containing phosphotransfer protein 1
	LOC101252689	two-component response regulator ORR26, transcript variant X2
	LOC101247174	two-component response regulator ARR9
	LOC101248058	two-component response regulator ORR9
	LOC101244285	two-component response regulator ARR5
	LOC101265701	two-component response regulator ORR3-like
Gibberellin	LOC100736493	putative GID1-like gibberellin receptor
	LOC101265384	DELLA protein GAI
	LOC101267355	transcription factor PIF3, transcript variant X4
Abscisic acid	LOC101258963	abscisic acid receptor PYL4
	LOC101250944	abscisic acid receptor PYL4
	LOC101246807	abscisic acid receptor PYL9
	LOC101246907	abscisic acid receptor PYL2-like
	LOC101245998	abscisic acid receptor PYL4-like
	LOC101261835	probable protein phosphatase 2C 6,transcript variant X5
	LOC101249794	protein phosphatase 2C 51-like
	LOC101265524	protein phosphatase 2C 53, transcript variant X2
	LOC100316894	protein phosphatase 2C ABI2 homolog, transcript variant X5
	LOC101268450	probable protein phosphatase 2C 75, transcript variant X1
	LOC101258071	protein phosphatase 2C
	LOC101248778	protein phosphatase 2C 37
	LOC100316895	protein phosphatase 2C AHG3 homolog
	LOC101251432	serine/threonine-protein kinase SRK2I, transcript variant X2
	LOC100820704	ABA responsive transcription factor, transcript variant X3
	LOC101253950	abscisic acid-insensitive 5-like protein 2, transcript variant X1
	LOC544204	AREB-like protein，transcript variant X2
	LOC101263766	abscisic acid-insensitive 5-like protein 7
Ethylene	LOC543834	ethylene receptor
	LOC543946	MAPKK
	LOC101249950	ethylene insensitive 3-like 3 protein,transcript variant X2
	LOC606712	ethylene-responsive transcription factor 1
	LOC101246590	ethylene-responsive transcription factor 1B
	LOC101267105	ethylene-responsive transcription factor 1B
	LOC101247461	ethylene response factor C.3
Brassinosteroid	LOC101251509	serine/threonine-protein kinase BSK2
	LOC543914	xyloglucan endotransglucosylase-hydrolase XTH3
	LOC101258345	probable xyloglucan endotransglucosylase/hydrolase protein 23
	LOC101258926	probable xyloglucan endotransglucosylase/hydrolase protein 23
	LOC101258632	probable xyloglucan endotransglucosylase/hydrolase protein 23
	LOC101245668	xyloglucan endotransglucosylase/hydrolase protein 24-like
Jasmonic acid	LOC101268624	jasmonic acid-amido synthetase JAR1-like, transcript variant X1
	LOC101262053	jasmonic acid-amido synthetase JAR1, transcript variant X1
	LOC543601	Pto-responsive gene 1 protein
	LOC100134911	jasmonate ZIM-domain protein 1
	LOC101247936	protein TIFY 10b-like
	LOC544165	transcription factor MYC2
Salicylic acid	LOC101246001	BLADE-ON-PETIOLE protein BOP3
	LOC101251993	transcription factor TGA9, transcript variant X2
	LOC101247526	transcription factor TGA2.3-like
	LOC544083	PR-1a1 protein

FIGURE 10
Heatmap of genes involved in hormone signal transduction in GS and NGS at 12 h-96 h after salinity stress. X-axis, samples; Y-axis, differentially expressed gene names with annotations.

but then decreased slowly. However, in contrast to the KEGG data, this increase in amino acid content continued from the initial stage to the late stage of salt stress. Compared with those of the other amino acids and related compounds, the degree of increase and duration of proline and GABA were higher and longer, which played an important role in alleviating salt stress injury in the grafted tomato seedlings. Moreover, glutamate, which is the precursor of proline and GABA and is an important intermediate of carbon and energy metabolism (Dent et al., 1947), also presented sustained accumulation. However, at the gene level, the two genotypes showed no similar change trend. Only for a few biosynthesis-related genes was the expression level in the GSs higher than that in the NGSs. We speculate that in addition to the increase in the expression level of enzymes related to the amino acid synthesis pathway, GSs may employ other mechanisms to regulate amino acid contents *in vivo*, for example, inhibiting the

10.3389/fpls.2023.1167145

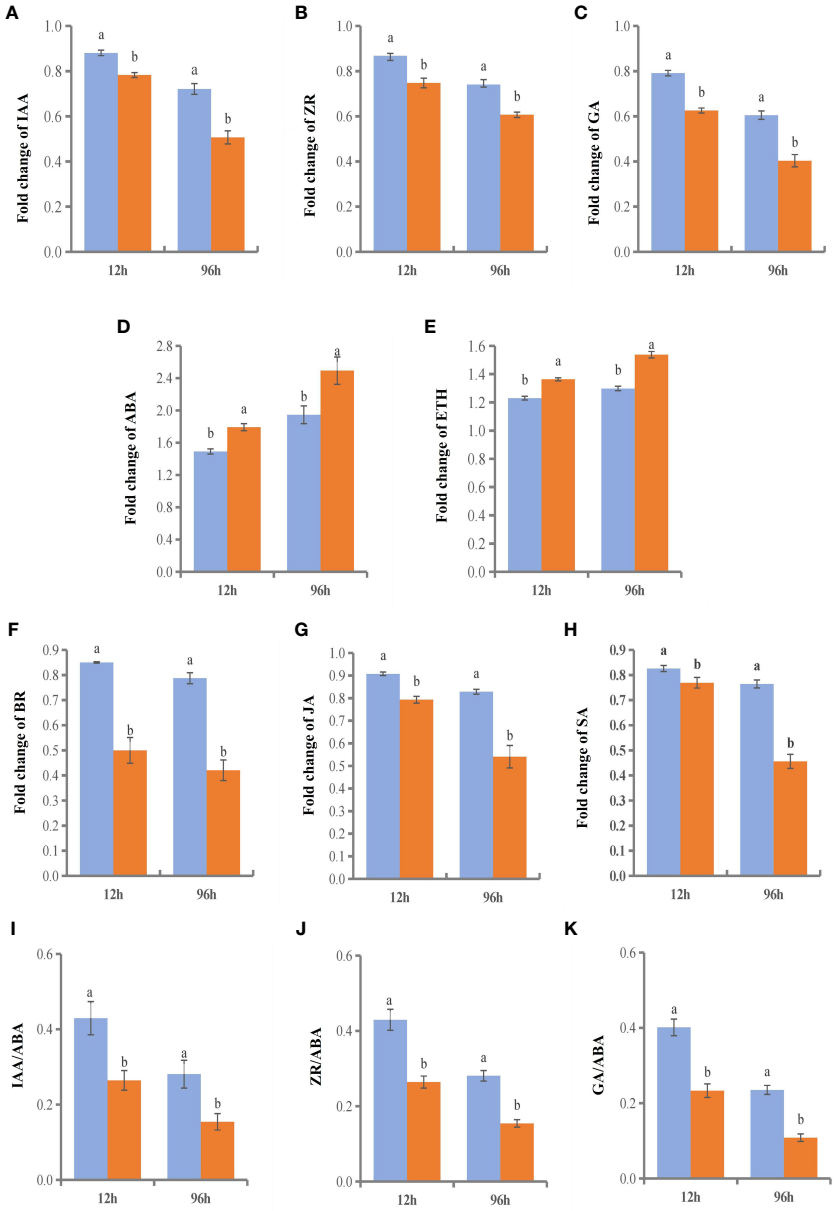

FIGURE 11
Hormone content and ratio of leaves in GS and NGS at 12 h and 96 h after salinity stress. A-H represents levels of different hormone content. I-K represents the ratio of different hormones.

decomposition of amino acids. The significant increase in multiple amino acids in GS leaves should be the result of improved salt tolerance by grafting. Specifically, it has stronger osmoregulation ability and improves the tolerance to sodium ion stress.

Photosynthesis of GSs remained relatively stable

In higher plants, PSI and PSII, which are the two different light energy conversion systems on the thylakoid membranes, have their own light harvesting pigment protein complexes. The complex associated with PSI is the light harvesting pigment protein complex LHCI, which is composed of various LHCA antenna protein subunits (Huang et al., 2018). The complex associated with PSII is the light harvesting pigment protein complex LHCII, which is composed of various LHCB antenna protein subunits. LHCII is the most important pigment protein complex; LHCII accounts for nearly 50% of the pigment total content and approximately 1/3 of the protein embedded in the photosynthetic membranes. LHCII plays an important role in the capture, transmission and transformation of light energy (Ruban et al., 2022).

Our research revealed that both types of tomato seedlings presented decreases in chlorophyll content and photosynthetic indicators during the early and middle stages of stress, but the inhibition of photosynthesis of the NGSs was significantly greater than that of the GSs. By comparing the expression of genes involved in the photosynthesis - antenna protein pathway, we found that the

expression in the GSs remained relatively stable at 12 hours compared with that of the NGSs, even if the gene level was downregulated. Lhca1 and Lhcb1, the main light harvesting chlorophyll a/b binding proteins composing the photosystems, are the most abundant members of the light harvesting antenna family and play important roles in the capture, transmission and transformation of light energy. We observed that the two genes (chlorophyll A-B binding protein 3A and chlorophyll a/b binding protein precursor) encoding these proteins were upregulated at 12 h, and the expression level in the GSs was significantly higher than that in the NGSs, partly alleviating the damage to PSI and PSII caused by salt stress. We believe that the difference in the photosynthetic response of the two types of seedlings under salt stress is caused by the different salt tolerances of the roots. In addition to that of antenna proteins, maintenance of the homeostasis of the proteins active in photosynthesis in GSs must also rely on the joint action of other relevant genes, and key genes need to be further identified.

GSs maintain the content of growth-promoting hormones, and some transcription factors may play an important role

Plant hormones are organic trace substances that accumulate in response to specific environmental signals, and at low concentrations, they can regulate plant physiological reactions (Yu et al., 2020). It has been reported that many hormones are involved in the molecular signaling response to salt stress. Plant hormones are classified according to their function in plant growth and in response to stress, with IAA, ZR, GA, BR, and strigolactones (SLs) classified as growth-promoting hormones and ABA, SA, JA and ETH considered stress response hormones (Verma et al., 2016; Shu et al., 2022). Growth-promoting hormones play important roles in maintaining plant growth under salt stress, and ABA and other signaling compounds are also important in the response to stress, as these play roles mainly through signal transduction pathways (Yang and Guo, 2018). We found that the changes in the contents of various hormones under salt stress were in accordance with reported regulatory patterns, with a higher content of growth-promoting hormones in the GSs than in the NGSs and lower ABA and ETH contents. This difference in hormone contents is also one of the reasons why the phenotype of the GSs under salt stress is better than that of the NGSs. Notably, 8 transcription factors were identified that are involved in the GA, ABA, SA, JA and ETH pathways. The expression of transcription factor-encoding genes involved in all of these pathways was significantly upregulated except in the case of ETH-related transcription factors.

Previous studies on hormone responses to salt stress have focused on the ABA signaling pathway (Verslues and Zhu, 2004). There was a significant difference in the expression patterns of different genes involved in the BR pathway between GSs and NGSs in our study, with the xyloglucan endotransglucosylase-hydrolase *XTH3* (LOC543914) and probable xyloglucan endotransglucosylase/hydrolase protein 23 (LOC101258345, LOC101258926, LOC101258632) expression levels in the GSs being significantly higher than those in the NGSs. *Xths* acts on the microfilament-matrix interface during cell elongation (Vissenberg et al., 2005a; Vissenberg et al., 2005b), maintaining the thickness, integrity and strength of the cell wall (Vissenberg et al., 2001; Rose et al., 2002; Jimenez et al., 2006). In *Arabidopsis thaliana*, *XTH* affects the growth of the main roots and stems and participates in light morphogenesis; gene expression is regulated by many plant hormones. The expression of *AtXTH3* and *AtXTH23* is induced by BR signaling (Keuskamp et al., 2011; Song et al., 2018). There are 25 *XTH* genes in the tomato genome. Previous studies on this topic have mainly focused on pectin metabolism (Muñoz-Bertomeu et al., 2013; Tsuchiya et al., 2015); however, little attention has been given to its relation to stress. The results of our study suggested that the upregulation of several *Xth* genes in the leaves of grafted tomato seedlings increased BR signal transduction. These findings provide a new idea for the mechanism underlying the salt tolerance of grafted tomato.

Conclusion

In summary, the leaves of tomato seedlings grafted with salt tolerant rootstocks obtained higher salt tolerance than before grafting. At the transcriptional level, GS leaves showed a more stable

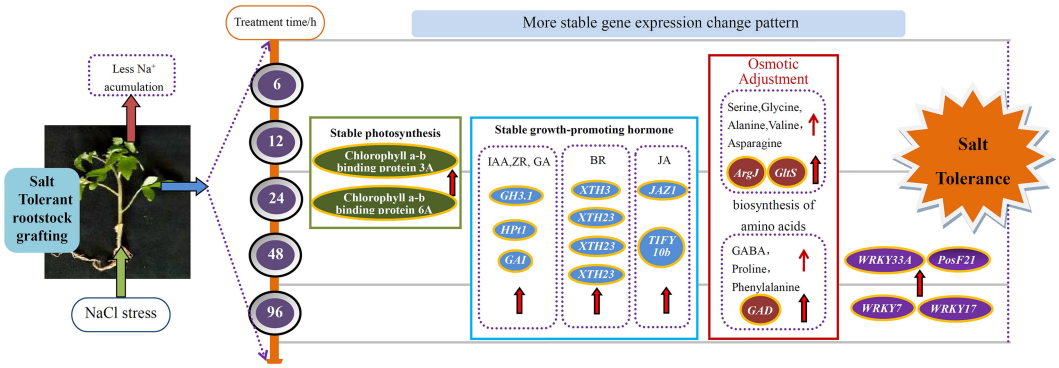

FIGURE 12
A model for mechanisms underlying the enhanced salt tolerance of grafted tomato.

pattern of gene expression changes under salt stress. The differences in leaf genes between the two types of seedlings mainly focus on pathways such as amino acid synthesis, photosynthetic antenna proteins, and hormone signal transduction. Among them, transcription factors such as WRKY, PosF21, and XTH are the most significant in the BR signaling pathway. The tolerance of grafted seedlings to salt stress may be due to the synergistic effect of the entire regulatory network, including the physiological regulatory mechanisms, amino acids, various TFs, and hormones of grafted seedlings of tomato salt tolerant rootstocks (Figure 12). It is certain that grafting on salt tolerant rootstocks can bring different metabolic processes and transcriptional level changes to the scion leaves, thereby making the scion leaves show stronger salt tolerance. Further comprehensive research is needed to further verify the role of key genes in metabolism.

Data availability statement

The data presented in the study are deposited in NCBI, accession number GSE233233.

Author contributions

XW and HG conceived and designed the research. XW, XB, RH, and DY conducted the experiments. GL, BG, JL, and SL contributed new reagents and analytical tools. All authors contributed to the article and approved the submitted version.

Funding

This work was financially supported by Natural Science Foundation of Hebei Province. (C2021204006), Hebei Facility vegetables Innovation Team of Modern Agro-industry Technology (HBCT2021030213), and the Key Research and Develop Program of Hebei (22327214D).

Conflict of interest

The authors declare that the research was conducted in the absence of any commercial or financial relationships that could be construed as a potential conflict of interest.

Publisher's note

All claims expressed in this article are solely those of the authors and do not necessarily represent those of their affiliated organizations, or those of the publisher, the editors and the reviewers. Any product that may be evaluated in this article, or claim that may be made by its manufacturer, is not guaranteed or endorsed by the publisher.

Supplementary material

The Supplementary Material for this article can be found online at: https://www.frontiersin.org/articles/10.3389/fpls.2023.1167145/full#supplementary-material

References

Ashraf, M. (2003). Relationships between leaf gas exchange characteristics and growth of differently adapted populations of blue panicgrass (*Panicum antidotale* retz.) under salinity or waterlogging. *Plant Sci.* 165 (1), 69–75. doi: 10.1016/S0168-9452(03)00128-6

Bulgari, R., Franzoni, G., and Ferrante, A. (2019). Biostimulants application in horticultural crops under abiotic stress conditions. *Agronomy* 9 (6), 306. doi: 10.3390/agronomy9060306

Cao, H., Wang, L., Nawaz, M. A., Niu, M. L., Sun, J. Y., Xie, J. J., et al. (2017). Ectopic expression of pumpkin *NAC* transcription factor *CmNAC1* improves multiple abiotic stress tolerance in arabidopsis. *Front. Plant Sci.* 8. doi: 10.3389/fpls.2017.02052

Chen, Y. H., An, X. H., Zhao, D. Y., Li, E. M., Ma, R. P., Li, Z., et al. (2020). Transcription profiles reveal sugar and hormone signaling pathways mediating tree branch architecture in apple (Malus domestica borkh.) grafted on different rootstocks. *PloS One* 15 (7), e0236530. doi: 10.1371/journal.pone.0236530

Chen, L., Wu, F. H., Liu, T. W., Chen, J., Li, Z. J., Pei, Z. M., et al. (2010). Soil acidity reconstruction based on tree ring information of a dominant species *Abies fabri* in the subalpine forest ecosystems in southwest China. *Environ. pollut.* 158, 3219–3224. doi: 10.1016/j.envpol.2010.07.005

Chen, S. F., Zhu, Y. L., Liu, Y. L., and Li, S. J. (2005). Effects of NaCl stress on activities of protective enzymes, contents of osmotic adjustment substances and photosynthetic characteristics in grafted tomato seedlings. *Acta Hortic. Sinica.* 32 (4), 609–613. doi: 10.16420/j.issn.0513-353x.2005.04.009

Demmig-Adams, B., Adams, III W W, Barker, D. H., Logan, B. A., and Verhoeven, A. S. (1996). Using chlorophyll fluorescencethe fraction of absorbed light allocated to the thermal dissipation of excitation. *Physiol. Plant.* 98 (2), 253–264. doi: 10.1034/j.1399-3054.1996.980206.x

Deng, Y. C., Deng, B. Y., Yang, J., Jiang, X. Y., Xia, Y. Q., Tai-Gang, M. O., et al. (2014). Comparing the nutritional ingredients of salt tolerance tomato with others. *Food Sci. Technol.* 39, 73–77. doi: 10.13684/j.cnki.spkj.2014.01.016

Dent, C. E., Stepka, W., and Steward, F. C. (1947). Detection of the free amino-acids of plant cells by partition chromatography. *Nature* 160 (4072), 682. doi: 10.1038/160682a0

Desoky, E. S. M., ElSayed, A. I., Merwad, A. R. M. A., and Rady, M. M. (2019). Stimulating antioxidant defenses, antioxidant gene expression, and salt tolerance in pisum sativum seedling by pretreatment using licorice root extract (LRE) as an organic biostimulant. *Plant Physiol. Bioch.* 142, 292–302. doi: 10.1016/j.scienta.2020.109495

Dionisio-Sese, M. L., and Tobita, S. (1998). Antioxidant response of rice seedlings to salinity stress. *Plant Sci.* 135, 1–9. doi: 10.1016/S0168-9452(98)00025-9

Essalimi, B., Esserti, S., Rifai, L. A., Koussa, T., Makroum, K., Belfaiza, M., et al. (2022). Enhancement of plant growth, acclimatization, salt stress tolerance and verticillium wilt disease resistance using plant growth-promoting rhizobacteria (PGPR) associated with plum trees (Prunus domestica). *Sci. Hortic.* 291, 110621. doi: 10.1016/j.scienta.2021.110621

Estan, M. T., Martinez-Rodriguez, M. M., Perez-Alfocea, F., Flowers, T. J., and Bolarin, M. C. (2005). Grafting raises the salt tolerance of tomato through limiting the transport of sodium and chloride to the shoot. *J. Exp. Bot.* 56 (412), 703–712. doi: 10.1093/jxb/eri027

Flowers, T. J., and Colmer, T. D. (2015). Plant salt tolerance: adaptations in halophytes. *Ann. Bot-London.* 115 (3), 327–331. doi: 10.1093/aob/mcu267

Goreta, S., Bucevic-Popovic, V., Selak, G. V., Pavela-Vrancic, M., and Perica, S. (2008). Vegetative growth, superoxide dismutase activity and ion concentration of salt-stressed watermelon as influenced by rootstock. *J. Agric. Sci.* 146 (6), 695–704. doi: 10.1017/S0021859608007855

Hashem, H. A., Mansour, H. A., El-Khawas, S. A., and Hassanein, R. A. (2019). The potentiality of marine macro-algae as bio-fertilizers to improve the productivity and salt stress tolerance of canola (*Brassica napus* l.) plants. *Agronomy* 9 (3), 146. doi: 10.3390/agronomy9030146

Huang, S. W., Guo, W., Tang, J. W., and Li, C. H. (2016). Total salt content and ion composition in tillage layer of soils in the main vegetable production regions of China. *J. Plant Nutr.* 22, 965–977. doi: 10.11674/zwyf.15010

Huang, W., Yang, Y. J., Zhang, S. B., and Liu, T. (2018). Cyclic electron flow around photosystem I promotes ATP synthesis possibly helping the rapid repair of photodamaged photosystem II at low light. *Front. Plant Sci.* 9. doi: 10.3389/fpls.2018.00239

Jia, Q. Y., Wu, X. L., Ji, S. X., Chu, X. P., liu, H. L., Gong, B. B., et al. (2020). Effects of *Solanum lycopersicum* rootstock on biomass,amnio acid content and reactive oxygen species metabolism of grafted seedlings under salt stress. *Cina. J. Appl. Ecol.* 31 (9), 3075–3084. doi: 10.13287/j.1001-9332.202009.024

Jimenez, T., Martin, I., Labrador, E., and Dopico, B. (2006). The immunolocation of a xyloglucan endotransglucosylase/hydrolase specific to elongating tissues in *Cicer arietinum* suggests a role in the elongation of vascular cells. *J. Exp. Bot.* 57 (15), 3979–3988. doi: 10.1093/jxb/erl169

Keuskamp, D. H., Sasidharan, R., Vos, I., Peeters, A. J. M., Voesenek, L. A. C. J., and Pierik, R. (2011). Blue-light-mediated shade avoidance requires combined auxin and brassinosteroid action in *Arabidopsis* seedlings. *Plant* 67, 208–217. doi: 10.1111/j.1365-313X.201104597.x

Kim, D., Langmead, B., and Salzberg, S. L. (2015). HISAT: a fast spliced aligner with low memory requirements. *Nat. Methods* 12 (4), 357–360. doi: 10.1038/nmeth.3317

Krishnamurthy, P., Vishal, B., Ho, W. J., Lok, F. C. J., Lee, F. S. M., and Kumar, P. P. (2020). Regulation of a cytochrome P450 gene *CYP94B1* by *WRKY33* transcription factor controls apoplastic barrier formation in roots to confer salt tolerance. *Plant Physiol.* 184, 2199–2215. doi: 10.1104/pp.20.01054

Lang, M., Lichtenthaler, H. K., Sowinska, M., Heisel, F., and Miehé, J. A. (1996). Fluorescence imaging of water and temperature stress in plant leaves. *J. Plant Physiol.* 148 (5), 613–621. doi: 10.1016/S0176-1617(96)80082-4

Lewsey, M. G., Hardcastle, T. J., Melnyk, C. W., Molnarc, A., Vallic, A., Uricha, M. A., et al. (2016). Mobile small RNAs regulate genome-wide DNA methylation. *PNAS* 113 (6), E801–E810. doi: 10.1073/pnas.1515072113

Li, J., Sima, W., Ouyang, B., Luo, Z. D., Yang, C. X., Ye, Z. B., et al. (2013). Identification and expression pattern of a ZPR1 gene in wild tomato (*Solanum pennellii*). *Plant Mol. Biol. Rep.* 31, 409–417. doi: 10.1007/s11105-012-0509-4

Ling, Z., Zheng, S. F., Wu, P., and Li, W. (2008). Study on the determination method of plant endogenous ethylene tissue localization. *Henan Agric. Sci.* 04), 51–52+63. doi: 10.15933/j.cnki.1004–3268.2008.04/003

Liu, X., Xu, M., and Li, Z. W. (2007). Study on salt tolerance index in seedlings of tomato. *Northern horticult.* 26 (03), 4–7. doi: 10.3969/j.issn.1001-0009.2007.03.002

Lu, X. H., Liu, W. Q., Wang, T., Zhang, J. L., and Zhang, W. N. (2020). Systemic long-distance signaling and communication between rootstock and scion in grafted vegetables. *Front. Plant Sci.* 11. doi: 10.3389/fpls.2020.00460

Marschner, H. (1995). *Mineral nutrition of higher plants. 2nd edn* (Germany: Institute of Plant Nutrition University of Hohenheim).

Misra, N., and Gupta, A. K. (2005). Effect of salt stress on proline metabolism in two high yielding genotypes of green gram. *Plant Sci.* 169 (2), 331–339. doi: 10.1016/j.plantsci.2005.02.013

Muñoz-Bertomeu, J., Miedes, E., and Lorences, E. P. (2013). Expression of xyloglucan endotransglucosylase/hydrolase (*XTH*) genes and XET activity in ethylene treated apple and tomato fruits. *J. Plant Physiol.* 170 (13), 1194–1201. doi: 10.1016/j.jplph.2013.03.015

Penella, C., Nebauer, S. G., López-Galarza, S., Quiñones, A., Bautista, A. S., and Calatayud, Á. (2017). Grafting pepper onto tolerant rootstocks: an environmental-friendly technique overcome water and salt stress. *Sci. Hortic.* 226, 33–41. doi: 10.1016/j.scienta.2017.08.020

Ramesh, S. A., Tyerman, S. D., Xu, B., Bose, J., Kaur, S., Conn, V., et al. (2015). GABA signalling modulates plant growth by directly regulating the activity of plant-specific anion transporters. *Nat. Commun.* 6, 7879. doi: 10.1038/ncomms8879

Rose, J. K. C., Braam, J., Fry, S. C., and Nishitani, K. (2002). The *XTH* family of enzymes involved in xyloglucan endotransglucosylation and endohydrolysis:Current perspectives and a new unifying nomenclature. *Plant Cell Physiol.* 43 (12), 1421–1435. doi: 10.1093/pcp/pcf171

Ruban, A. V., Wilson, S., and Li, D. (2022). Chlorophyll excimers in LHCII complex. *BBA-Bioenergetics* 1863, 148834. doi: 10.1016/j.bbabio.2022.148834

Safdar, N., Mirza, B., and Ullah, N. (2013). Comparative physiological responses of the yeast halotolerance genes expressed in transgenic lines of tomato cv Rio grande under saline conditions. *Acta Physiol. Plant* 35, 919–929. doi: 10.1007/s11738-012-1135-3

Said, I., Salman, S. A., and Elnazer, A. A. (2022). Salinization of groundwater during 20 years of agricultural irrigation, luxor, Egypt. *Environ. Geochem Health* 44 (11), 3821–3835. doi: 10.1007/s10653-021-01135-2

Seo, Y. S., Choi, J. Y., Kim, S. J., Kim, E. Y., Shin, J. S., and Kim, W. T. (2012). Constitutive expression of *CaRma1H1*, a hot pepper ER-localized RING E3 ubiquitin ligase, increases tolerance to drought and salt stresses in transgenic tomato plants. *Plant Cell Rep.* 31, 1659–1665. doi: 10.1007/s00299-012-1278-0

Shi, L. N., Lu, L. X., Ye, J. R., and Shi, H. M. (2022). The endophytic strain ZS-3 enhances salt tolerance in arabidopsis thaliana by regulating photosynthesis, osmotic stress, and ion homeostasis and inducing systemic tolerance. *Front. Plant Sci.* 13. doi: 10.3389/fpls.2022.820837

Shkolnik-Inbar, D., Adler, G., and Bar-Zvi, D. (2013). *ABI4* downregulates expression of the sodium transporter *HKT1*; 1 in arabidopsis roots and affects salt tolerance. *Plant J.* 73 (6), 993–1005. doi: 10.1111/tpj.12091

Shu, P., Li, Y., Li, Z., Sheng, J. P., and Shen, L. (2022). *SlMAPK3* enhances tolerance to salt stress in tomato plants by scavenging ROS accumulation and up-regulating the expression of ethylene signaling related genes. *Environ. Exp. Bot.* 104698. doi: 10.1016/j.envexpbot.2021.104698

Sitohy, M. Z., Desoky, E. S. M., Osman, A., and Rady, M. M.. (2020). Pumpkin seed protein hydrolysate treatment alleviates salt stress effects on phaseolus vulgaris by elevating antioxidant capacity and recovering ion homeostasis. *Sci. Hortic.* 271, 109495. doi: 10.1016/j.scienta.2020.109495

Song, L., Valliyodan, B., Prince, S., Wan, J. R., and Nguyen, H. T. (2018). Characterization of the *XTH* gene family: new insight to the roles in soybean flooding tolerance. *Int. J. Mol. Sci.* 19 (9), 2705–2705. doi: 10.3390/ijms19092705

Spanò, R., Ferrara, M., Montemurro C Mulè, G., Gallitelli, D., and Mascia, T. (2020). Grafting alters tomato transcriptome and enhances tolerance to an airborne virus infection. *Sci. Rep.* 10 (1), 2538. doi: 10.1038/s41598-020-59421-5

Sun, W. H., Liu, X. Y., Wang, Y., Hua, Q., Song, X. M., Gu, Z., et al. (2014). Effect of water stress on yield and nutrition quality of tomato plant overexpressing *StAPX*. *Biol. plant.* 58 (1), 99–104. doi: 10.1007/s10535-013-0360-y

Tian, X. M., Wei, M., Liu, Q., Dong, C. Q., Wang, X. F., Shi, Q. H., et al. (2012). Physiological responses of cucumber seedlings grafted on different salt-tolerant rootstocks to NaCl stress. *Cina. J. Appl. Ecol.* 23 (1), 147-153. doi: 10.13287/j.1001-9332.2012.0020

Tsuchiya, M., Satoh, S., and Iwai, H. (2015). Distribution of *XTH*, expansin, and secondary-wall-related CesA in floral and fruit abscission zones during fruit development in tomato (*Solanum lycopersicum*). *Front. Plant Sci.* 6. doi: 10.3389/fpls.2015.00323

Verma, V., Ravindran, P., and Kumar, P. P. (2016). Plant hormone-mediated regulation of stress responses. *BMC Plant Biol.* 16 (1), 1–10. doi: 10.1016/j.scienta.2022.111302

Verslues, P. E., and Zhu, J. K. (2004). Before and beyond ABA: upstream sensing and internal signals that determine ABA accumulation and response under abiotic stress. *Biochem. Soc. T.* 33, 375–379. doi: 10.1042/BST0330375

Vissenberg, K., Fry, S. C., Pauly, M., Höfte, H., and Verbelen, J. P. (2005a). *XTH* acts at the microfibril-matrix interface during cell elongation. *J. Exp. Bot.* 56, 673–683. doi: 10.1093/jxb/eri048

Vissenberg, K., Fry, S. C., and Verbelen, J. (2001). Root hair initiation is coupled to a highly localized increase of xyloglucan endotransglycosylase action in *Arabidopsis* roots. *Plant Physiol.* 127 (3), 1125–1135. doi: 10.1104/pp.010295

Vissenberg, K., Oyama, M., Osato, Y., Yokoyama, R., Verbelen, J. P., and Nishitani, K. (2005b). Differential expression of AtXTH17, AtXTH18, *AtXTH19* and *AtXTH20* genes in *Arabidopsis* roots. physiological roles in specification in cell wall construction. *Plant Cell Physiol.* 46 (1), 192–200. doi: 10.1093/pcp/pci013

Wang, Y., Wang, L., Xing, N., Wu, X., and Wang, Y. (2020). A universal pipeline for mobile mRNA detection and insights into heterografting advantages under chilling stress. *Hortic. Res-England.* 7 (1), 76. doi: 10.1038/s41438-020-0313-5

Wu, X., Jia, Q., Ji, S., Gong, B., Li, J., Lü, G., et al. (2020). Gamma-aminobutyric acid (GABA) alleviates salt damage in tomato by modulating na^+ uptake, the GAD gene, amino acid synthesis and reactive oxygen species metabolism. *BMC Plant Biol.* 20 (1), 465. doi: 10.1186/s12870-020-02669-w

Xu, H., Watanabe, K. A., Zhang, L., and Shen, Q. J. (2016). *WRKY* transcription factor genes in wild rice *Oryza nivara*. *DNA Res.* 23 (4), 311–323. doi: 10.1093/dnares/dsw025

Xu, Y., Xiao, H. Y., Zheng, N. J., Zhang, Z. Y., and Zhai, L. L. (2016). Progress on responding of free amino acid in plants to salt stress. *Environ. Sci. Technol.* 39 (7), 40–47. doi: 10.3969/j.issn.1003-6504.2016.07.008

Yang, Y., and Guo, Y. (2018). Unraveling salt stress signaling in plants. *Integr. Plant Biol.* 60, 796–804. doi: 10.1111/jipb.12689

Yang, Y. J., Guo, S. R., and Yu, W. J. (2015). Effect of rootstock-grafting on the contents and distributions of ions and endogenous hormones in watermelon seedlings under NaCl stress. *Northwest Bot. J.* 35 (3), 0500–0507. doi: 10.7606/j.issn.1000-4025.2015.03.050

Yu, Z., Duan, X., Luo, L., Dai, S. J., Ding, Z. J., and Xia, G. M. (2020). How plant hormones mediate salt stress responses. *Trends Plant Sci.* 25 (11), 1117–1130. doi: 10.1016/j.tplants.2020.06.008

Zhang, X. Z. (1986). Determination of chlorophyll content of plants-acetone and ethanol mixture method. *Liaoning Agric. Sci.* 3, 26–28.

Zhang, Y., Hou, K., Qian, H., Gao, Y., Fang, Y., Xiao, S., et al. (2022). Characterization of soil salinization and its driving factors in a typical irrigation area of Northwest China. *Sci. Total Environ.* 837, 155808. doi: 10.1016/j.scitotenv

Zhang, Z., Mao, C. Y., Shi, Z., and Kou, X. H. (2017). The amino acid metabolic and carbohydrate metabolic pathway play important roles during salt-stress response in tomato. *Front. Plant Sci.* 8. doi: 10.3389/fpls.2017.01231

Zheng, C. (2018). Study on the mechanism of *WRKY7* transcription factor regulating white leaf blight in rice. *Zhejiang Normal University*, 33-35.

Zhong, B. (2016). Arabidopsis *POSF21* and ABA receptor PYR/PYL protein interaction and functional analysis. *Graduate School Chin. Acad. Sciences(Wuhan Bot. Garden)*, 25-26.

frontiers | Frontiers in Plant Science

TYPE Original Research
PUBLISHED 07 June 2023
DOI 10.3389/fpls.2023.1109460

Check for updates

OPEN ACCESS

EDITED BY
Diaa Abd El Moneim,
Arish University, Egypt

REVIEWED BY
MHM Borhannuddin Bhuyan,
Bangladesh Agricultural Research Institute, Bangladesh
Nita Lakra,
Chaudhary Charan Singh Haryana Agricultural University, India

*CORRESPONDENCE
Min Yan
yanmin75@163.com

RECEIVED 27 November 2022
ACCEPTED 09 May 2023
PUBLISHED 07 June 2023

CITATION
Zhang E, Zhu X, Wang W, Sun Y, Tian X, Chen Z, Mou X, Zhang Y, Wei Y, Fang Z, Ravenscroft N, O'Connor D, Chang X and Yan M (2023) Metabolomics reveals the response of hydroprimed maize to mitigate the impact of soil salinization.
Front. Plant Sci. 14:1109460.
doi: 10.3389/fpls.2023.1109460

COPYRIGHT
© 2023 Zhang, Zhu, Wang, Sun, Tian, Chen, Mou, Zhang, Wei, Fang, Ravenscroft, O'Connor, Chang and Yan. This is an open-access article distributed under the terms of the Creative Commons Attribution License (CC BY). The use, distribution or reproduction in other forums is permitted, provided the original author(s) and the copyright owner(s) are credited and that the original publication in this journal is cited, in accordance with accepted academic practice. No use, distribution or reproduction is permitted which does not comply with these terms.

Metabolomics reveals the response of hydroprimed maize to mitigate the impact of soil salinization

Enying Zhang[1], Xingjian Zhu[1], Wenli Wang[1], Yue Sun[1], Xiaomin Tian[1], Ziyi Chen[1], Xinshang Mou[1], Yanli Zhang[1], Yueheng Wei[1], Zhixuan Fang[1], Neil Ravenscroft[1,2,3], David O'Connor[1,2], Xianmin Chang[1,2] and Min Yan[1]*

[1]College of Agronomy, Qingdao Agricultural University, Qingdao, China, [2]School of Agriculture, Food and Environment, Royal Agricultural University, Cirencester, United Kingdom, [3]International Agriculture University, Tashkent, Uzbekistan

Soil salinization is a major environmental stressor hindering global crop production. Hydropriming has emerged as a promising approach to reduce salt stress and enhance crop yields on salinized land. However, a better mechanisitic understanding is required to improve salt stress tolerance. We used a biochemical and metabolomics approach to study the effect of salt stress of hydroprimed maize to identify the types and variation of differentially accumulated metabolites. Here we show that hydropriming significantly increased catalase (CAT) activity, soluble sugar and proline content, decreased superoxide dismutase (SOD) activity and peroxide (H_2O_2) content. Conversely, hydropriming had no significant effect on POD activity, soluble protein and MDA content under salt stress. The Metabolite analysis indicated that salt stress significantly increased the content of 1278 metabolites and decreased the content of 1044 metabolites. Ethisterone (progesterone) was the most important metabolite produced in the roots of unprimed samples in response to salt s tress. Pathway enrichment analysis indicated that flavone and flavonol biosynthesis, which relate to scavenging reactive oxygen species (ROS), was the most significant metabolic pathway related to salt stress. Hydropriming significantly increased the content of 873 metabolites and significantly decreased the content of 1313 metabolites. 5-Methyltetrahydrofolate, a methyl donor for methionine, was the most important metabolite produced in the roots of hydroprimed samples in response to salt stress. Plant growth regulator, such as melatonin, gibberellin A8, estrone, abscisic acid and brassinolide involved in both treatment. Our results not only verify the roles of key metabolites in resisting salt stress, but also further evidence that flavone and flavonol biosynthesis and plant growth regulator relate to salt tolerance.

KEYWORDS

land degradation, soil salinization, hydropriming, progesterone, metabolomics analysis

1 Introduction

Soil salinization is a major environmental stressor hindering global crop production, risking food security and weakening global efforts towards the Sustainable Development Goals (Wang et al., 2022). Because saline soil affects seed germination and seedling establishment (Farooq et al., 2015), priming crop seeds before germination has emerged as a promising approach to reduce seedling salt stress and enhance crop yields on salinized land (Hussain et al., 2023).

Seed priming involves exposing crop seeds to natural and/or synthetic compounds (Hernandez-Apaolaza, 2022) that cause the activation of early germination events. This makes primed seeds more resilient to environmental stressors, leading to increased survival rates. Seed priming methods include invasive (hydro-, osmo-, halo-, solid matrix, bio- or nano-priming) and non-invasive (magneto, UV-irradiation, γ-radiation, cold plasma, electron and laser priming) processes (Hernandez-Apaolaza, 2022). Among these, hydropriming offers a sustainable and low-cost means to improve seed germination and seedling emergence in salt affect soil (Yan, 2016; Yaghoubian et al., 2022).

Maize (Zea mays) is a globally critical cereal crop that is sensitive to salinized soil conditions (Farooq et al., 2015). Several studies have focused on the effectiveness of priming maize seeds to mitigate salt stress, highlighting the physical-biochemical response in its germination and establishment (Chattha et al., 2022; Hamna et al., 2022; Samra et al., 2022). However, little attention has been paid so far to the metabolic response of hydroprimed maize under salt stress in the early development stage. A systematic assessment of endogenous plant metabolites (metabolomics) can help unravel metabolic networks and shed light on interactions between plants and the environment (Abideen et al., 2022). Roots are in close contact with the soil solution, they are first to confront excessive salinity and are the first places of "line of defence". Therefore, differences among roots may (partially) underlie distinguishing salt tolerances(Rewald et al., 2013)

In this study, we used a metabolomics approach to study the effect of salt stress of hydroprimed maize to identify the types and variation of differentially accumulated metabolites in roots with the objective to provide a scientific basis for enhancing salt tolerant traits.

2 Materials and methods

2.1 Hydropriming

Maize seeds (cv Tiantai 316, a high-quality and high-yielding maize variety) were surface sterilized and soaked in deionized water under dark conditions (24 hours; 20 °C). After soaking, the seeds were rinsed (×3) with deionized water and then air-dried (48 hours; room temperature) to back their initial moisture content.

2.2 Germination tests

Germination tests (3 replicates; 20 seeds per replicate) involved placing seeds in transparent germination boxes on filter paper wetted with saline water (15 mL; 150 mM NaCl), or deionized water (15 mL) as a control. The seeds were allowed to germinate under light/dark cycles (12/12 hour) at 25 °C for 7 days. Germination was considered to occur when the radicle protruded through the seed coat, with the number germinated seeds recorded daily. The germination potential was calculated as $\Sigma(Gn/Tn)$ where Gn is the number of germinated seeds on day n and Tn is day n.

Then, the seedling were divided into two parts. One part was oven dried (80°C; 24 hours) and the seedling, root and shoot dry weight recorded. The roots of the other part were immediately used for biochemical and metabolite analyses.

2.3 Biochemical analyses

2.3.1 Hydrogen peroxide analysis

Peroxide (H_2O_2) levels were determined according to Sergiev et al. (1997). In brief, root sample (0.5 g fresh weight) was homogenized in trichloroacetic acid (5 mL; 0.1% w/v) and centrifuged (12,000 rpm; 15 min). The supernatant (0.5 mL) was mixed with potassium phosphate (0.5 ml; 10 mM; pH7.0) and potassium iodide (1 mL; 1 M) before being allowed to develop for 1 hour in dark conditions. The H_2O_2 concentration was then measured spectrophotometrically at 390 nm.

2.3.2 Antioxidant enzymes, lipid peroxidation, and soluble protein analysis

Root samples were first treated with liquid nitrogen and mixed with potassium phosphate buffer (50 mM; pH 7.0) containing Na-EDTA (2 mM) and then centrifuged. Superxoide dismutase (SOD) activity was then measured in the supernatant by its ability to inhibit the reduction of nitroblue tetrazolium at 560 nm (Dhindsa et al., 1981). Peroxidase (POD) activity was assayed according to Chance and Maehly (1955). CAT activity was measured as described by Aebi (1984). Malondialdehyde (MDA) was determined according to the thiobarbituric acid assay described by Heath and Packer (1968). Soluble proteins were measured according to Bradford (1976).

2.3.3 Soluble sugars and proline analysis

Soluble sugars were measured using the anthrone method (Irigoyen et al., 1992) and proline was determined according to Bates et al. (1973).

2.3.4 Sodium and potassium analysis

Roots samples were washed with deionized water followed by air and oven drying(24 hours; 80°C). Dried powder samples (0.1 g) were treated with concentrated nitric acid (10 mL) for 12 h. Each digested material was then diluted with deionized water to a definite volume

(100 mL). The contents of Na^+ and K^+ were determined by flame photometry according to the method described by Williams and Twine (1960).

2.4 Metabolite analyses

2.4.1 Metabolite extraction

Frozen root samples (3 replicates; ~50 mg per replicate) were transferred to Eppendorf tubes (2 mL). Then, methanol/acetonitrile/water (1 mL; 2:2:1 v/v/v) containing ribitol (20 μL; 1 mg/mL) was added as an internal standard. The samples were vortexed (30 s), homogenized using a ground powder system (45 Hz; 10 min), subjected to supersonic processing in ice water (10 min), cultured (-20 °C; 1 hour) and centrifuged (12,000 rpm; 15 min; 4 °C). Then the supernatant (500 μL) was transferred to an Eppendorf tube and dried in a vapor concentrator. The samples were dissolved in acetonitrile/water (160 μL; 1:1 v/v), vortexed (30 s), sonicated (10 min) and centrifuged (12,000 rpm; 15 min; 4 °C). The supernatant (120 μL) was dispensed into glass vials and 10 μL of each sample was mixed into a QC sample for assay analysis.

2.4.2 LC-MS/MS analysis

A Waters Acquity I-Class PLUS ultra-high performance liquid tandem Waters Xevo G2-XS QTOF high-resolution mass spectrometer installed with a Waters Acquity UPLC HSS T3 (1.8μm 2.1*100mm) column was used for metabolomics analyses. The following parameters were applied:

Positive ion mode: mobile phase A: 0.1% formic acid aqueous solution; mobile phase B: 0.1% formic acid acetonitrile. Negative ion mode: mobile phase A: 0.1% formic acid aqueous solution; mobile phase B: 0.1% formic acid acetonitrile. The step elution program was as follows: 0 min, 98% A; 0.25 min, 98% A; 10 min, 2% A; 13 min, 2% A; 13.1 min, 98% A; 15 min, 98% A; the injection volume was 1 μL. MS/MS profiles were obtained using triple TOF-MS based on information acquisition technique (IDA). MS databases were continuously collected and evaluated by acquisition software with full scan survey (Analyst TF 1.7, AB Sciex), and MS/MS spectra were acquired depending on preset parameters. Within each cycle, precursor ions with strengths above 100 were picked and then fragmented at 30 V collision energy (CE) (15 MS/MS events every 50 ms). The electrospray ionization (ESI) source was set to 60 PSI nebulizer pressure, 60 PSI auxiliary gas pressure, 30 PSI air curtain pressure, 650 °C source temperature, and ion spray voltage float (ISVF) of 5000 or -4000 V in positive and negative patterns, respectively.

Primary and secondary mass spectrometry data were collected in MSe mode (MassLynx V4.2, Waters). In each data acquisition cycle, dual-channel data acquisition was performed on both low collision energy and high collision energy at the same time. The low collision energy was 2V, the high collision energy range was 10~40V, and the scanning frequency was 0.2 seconds for a mass spectrum. The parameters of the ESI ion source are as follows: Capillary voltage: 2000V (positive ion mode) or -1500V (negative ion mode); cone voltage: 30V; ion source temperature: 150°C; desolvent gas temperature 500°C; backflush gas flow rate: 50L/h; Desolventizing gas flow rate: 800L/h.

2.4.3 Data analysis

Firstly, peak areas were normalized to the total peak area. Then, principal component analysis and Spearman correlation analysis were used to assess the repeatability of the samples. Identified compounds were searched for classification and pathway information in KEGG, HMDB and lipidmaps databases. T-tests were performed to determine significant differences between each compound. R (programming language) with the ropls software package was used to perform principal component analysis (PCA) and OPLS-DA modeling, with 200 permutations performed to verify the reliability of the model. VIP values were calculated using multiple cross-validation. The difference multiple, P value and the VIP value of the OPLS-DA model was used to screen the differential metabolites (criteria = FC > P<0.05 and VIP > 1). Difference of metabolites of KEGG pathway enrichment significance were calculated using a hypergeometric distribution test.

2.5 Validation of metabonomics data by quantitative real-time reverse transcription polymerase chain reaction

To validate our data, four genes (*delta-1-pyrroline-5-carboxylate synthase 2* (*P5CS*, Gene ID:100280719), *caffeic acid 3-O-methyltransferase* (*COMT*, Gene ID:100125646), *catalase isozyme 2* (*CAT2*, Gene ID:542230) and *steroid reductase DET2*(Gene ID:100283443) were selected for qRT-PCR assay, with three biological replicates used for each analysis. The primer used for one internal reference gene (*Actin*) and the four selected genes are shown in Table S1. Total RNA was extracted from the maize roots samples treated with either 150 mMNaCl or water by the RNA extraction kit (Monad Biotech, Suzhou, China) following the manufacturer's instructions. The concentration and integrity of each RNA samples was examined by BioPhotometer measurement and 1% agarose gel. Based on the recommendation of the TUREscript 1st Stand cDNA SYNTHESIS Kit (Aidlab, Beijing, China), 2 μg total RNA was measured to perform the cDNA synthesis. The PCR reactions were performed on the analytik Jena-qTOWER2.2 Real-Time QPCR System using the following program: denaturation at 95°C for 3min followed by 39 cycles of 95 °C for 10 s and 60°C for 30 s, and terminated at 72°C for 60 s. Dissociation curve analysis was performed to determine the target specificity. The $2^{-\Delta\Delta CT}$ method was used to calculation of the relative expression of selected genes normalized to a maize *Actin* gene.

2.6 Statistical analysis

A statistical analysis was carried out using SPSS 19.0 software (IBM). Germination percentage data were arcsine transformed before an analysis of variance. Mean comparisons were performed using a Duncan test (5% probability).

3 Results

3.1 Effect of salt stress on germination and seedling traits

The effect of salt stress on germination and seedling traits is illustrated in Figures 1, 2; Figure S1. Salt stress severely inhibited the germination of unprimed samples and significantly decreased the germination traits [germination percentage (Figure 2A) and germination potential (Figure 2B)] and early seedling growth [seedling fresh weight (Figure 2C), seedling dry weight (Figure 2D), root dry weight (Figure 2E) and shoot dry weight (Figure 2F)] compared to the control. In comparison, hydroprimed sample displayed significantly improved germination and early seedling growth in all aspects apart from shoot dry weight. The germination percentage (Figure 2A) and root dry weight (Figure 2E) of hydroprimed samples achieved level not significantly different to the control (i.e., unhindered by salt conditions). Furthermore, the germination potential of primed samples actually superseded that of the control (Figure 2B). However, the shoot dry weight of primed samples was not significantly different to unprimed samples under salt stress (Figure 2F).

3.2 Effect of salt stress and hydropriming on physiological and biochemical traits

The effect of salt stress on the physiological and chemical traits of unprimed and hydroprimed samples is shown in Figures 3, 4. We found that salt stress had no significant effect on CAT activity of the unprimed samples, while hydroprimed samples had significantly increased CAT activity under salt stress (Figure 3A). Salt stress decreased POD activity of unprimed samples under salt stress, while hydropriming treatment had no significant effect on POD activity under salt stress (Figure 3B). For unprimed samples, SOD activity (Figure 3C), H_2O_2 (Figure 3D), MDA (Figure 3E) levels all significantly increased under salt stress. SOD activity of hydroprimed samples was lower than the unprimed one and significantly higher than the control (i.e., not salt stress effect) (Figure 3C). The H_2O_2 content of hydroprimed samples was lower than the unprimed one and not significantly different to the control (i.e., not salt stress effect) (Figure 3D). MDA content of hydroprimed samples was not significantly different to the unprimed samples (Figure 3E).

Soluble protein (Figure 4A), soluble sugars (Figure 4B), proline (Figure 4C) levels all significantly increased under salt stress, hydropriming treatment had no significant effect on soluble protein under salt stress (Figure 4A). Soluble sugars (Figure 4B) and proline (Figure 4C) levels in primed samples increased. Salt stress decreased K^+/Na^+ ration of unprimed samples under salt stress, while hydropriming treatment had no significant effect on K^+/Na^+ ratio under salt stress (Figure 4D).

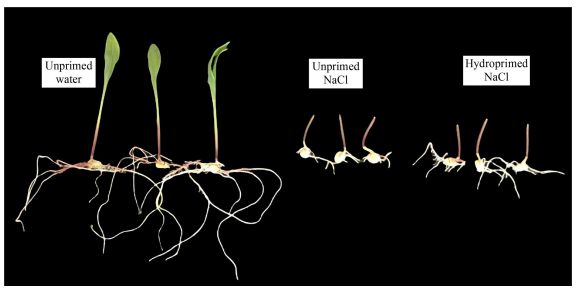

FIGURE 1
Comparative growth of seedlings of unprimed and hydroprimed samples under salt stress (NaCl) and control (unprimed water) on 7th day.

3.3 Change in metabolites and metabolic pathways in unprimed samples in response to salt stress

A total of 3418 intracellular metabolites were detected(Table S2), for which we compared the differences between the roots of unprimed samples with and without salt stress by a multivariate statistical analysis. The PCA score plot shows two principal components accounting for 86.1% of the variability (Figure 5A), while the OPLS-DA score plot ($R^2 = 0.94$; $Q^2 = 0.998$) shows a clear distinction in the metabolite profiles between the salt-stressed roots and the control (Figure 5B).

We screened 2322 differential metabolites between the roots from unprimed seeds under control and salt stress condition (VIP > 1; $p < 0.05$) (Table S3). Among them, 1278 metabolites significantly increased and 1044 metabolites significantly decreased in the NaCl-stressed samples compared to the control (Table S3). VIP scores obtained from PLS-DA and OPLS-DA analyses indicated that some metabolites made important contribution to the separation of the salt stresses samples from control. The 10 most important metabolites identified from VIP and PCA scores were in the order of: Ethisterone (progesterone); Menadione (Vitamin K3); 10-Deacetyl-2-debenzoylbaccatin III; Neomycin B; Pelargonidin 3-O-(6-caffeoyl-beta-D-glucoside); 5-O-beta-D-glucoside; 6-Gingerol; Dexamethasone, N6-(L-1,3-Dicarboxypropyl)-L-lysine; Tacrolimus and Quinate (Table S3).

We identified 256 metabolic pathways with 421 differential metabolites. Among these pathways, Flavone and flavonol biosynthesis, CoA biosynthesis, Vitamin B6 metabolism, Terpenoid backbone biosynthesis and Histidine metabolism were the top five predominant metabolic pathway (Figure 6).

Flavone and flavonol biosynthesis was the only pathway that was significantly ($p<0.05$) affected by salt stress with an increase for 10 metabolites and a decrease for 2 metabolites. The concentration of Luteolin 7-O-beta-D-glucoside (prunin), 3,7,4'-Tri-O-methylquercetin, Chrysoeriol, Scolymoside(luteolin 7-O-rutinoside), Kaempferol 3-O-glucoside, 3,7-Di-O-methylquercetin, Luteolin 7-O-glucuronide, Quercetin 3-methyl ether, Rutin, Quercetin 3-O-glucoside increased 18.44-fold, 18.38-fold, 11.37-fold, 4.36-fold, 3.73-fold, 3.60-fold, 3.20-fold, 3.06-fold, 2.30-fold, 2.06-fold, respectively. Kaempferol and Acacetin decreased.

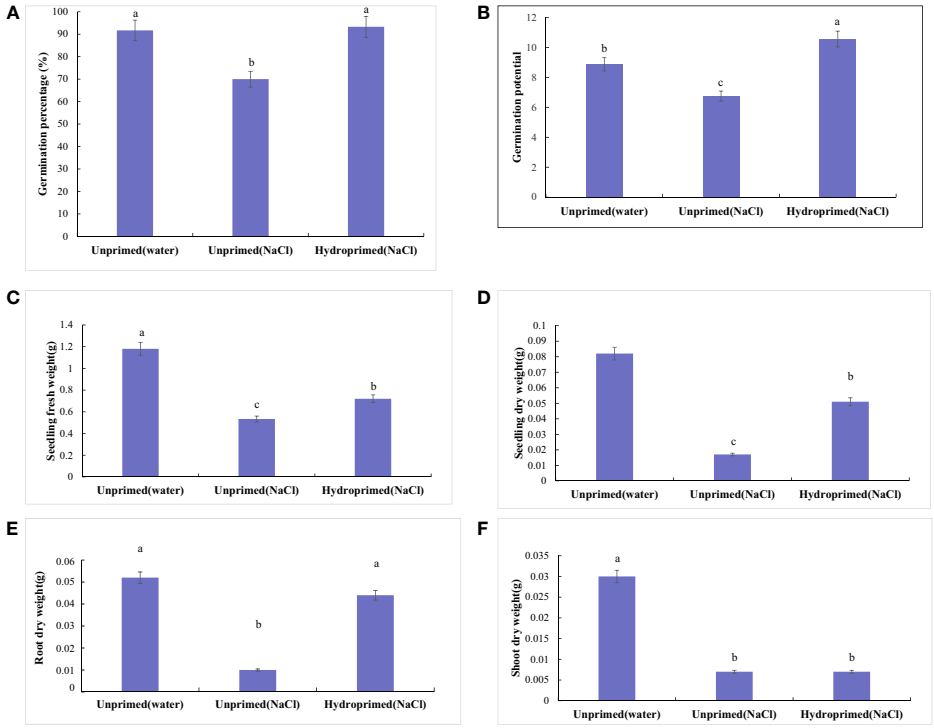

FIGURE 2
Influence of salt stress and hydropriming treatment on germination [Germination percentage **(A)** and Germination potential **(B)**] and seedling traits [Seedling fresh weight **(C)**, Seedling dry weight **(D)**, Root dry weight **(E)** and Shoot dry weight **(F)**] of maize. Different letters (a and b) indicate significant differences among treatments according to Duncan's test ($p < 0.05$). Error bars indicate ± SE of mean (n = 3).

3.4 Change in metabolites and metabolic pathways in hydroprimed samples in response to salt stress

For hydroprimed samples, the results of the PCA score plot showed that the samples were clearly separated by two principal components, which explained 82.4% of the variability (Figure 7A). The OPLS-DA score plot (R^2 = 0.908; Q^2 = 0.994) also shows a clear distinction in the metabolite profile of unprimed and hydroprimed samples under salt stress (Figure 7B).

A total of 2186 differential metabolites were screened (VIP > 1; $p < 0.05$), between the roots from unprimed and hydroprimed seeds under salt stress condition (Table S4). Among them, 873 metabolites significantly increased and 1313 metabolites significantly decreased in the hydroprimed samples compared to the control (Table S4). VIP scores obtained from PLS-DA analysis and loading plots from OPLS-DA (Figure not presented) analysis indicated that 5-Methyltetrahydrofolate and some metabolites were of important contributing to the separation of the hydropriming treatment samples from control. The top 10 most important contributory obtained from VIP and PCA scores were 5-Methyltetrahydrofolate, 24-Hydroxy-beta-amyrin, Dethiobiotin, 3alpha,7alpha-Dihydroxy-5beta-cholestane, Piperideine, (S)-Autumnaline, Formononetin 7-O-glucoside-6''-O-malonate, 2-Heptyl-4(1H)-quinolone, 2-Hydroxycinnamic acid, Lupinine, 2-Methylglutaric acid (Table S4).

Among the 2186 differential metabolites, 374 differential metabolites involved in 254 metabolic pathways. Flavone and flavonol biosynthesis, Valine,leucine and isoleucine degradation, Toluene degradation, Dopaminergic synapse, Polycyclic aromatic hydrocarbon degradation were the top five predominant metabolic pathway (Figure 8). Thus, none of these metabolic pathways was significantly affected by hydropriming treatment.

3.5 Shared features of salt stress and hydropriming treatment on metabolites

The metabolites between salt stress and hydropriming treatment maize roots were compared in this study. Between the salt stress and hydropriming treatment group, 422 increased (Table S5) and 379 decreasd (Table S6) overlapping metabolites were identified (Figure 9). We noticed that plant growth regulator, such as melatonin, gibberellin A8 and estrone increased, while abscisic acid and brassinolide decreased in both treatment.

3.6 Expression of selected genes

The effects of salt stress on the expression of four genes of unprimed and hydroprimed samples is shown in Figures S2 and 10. We found that salt stress had no significant effect on the expression

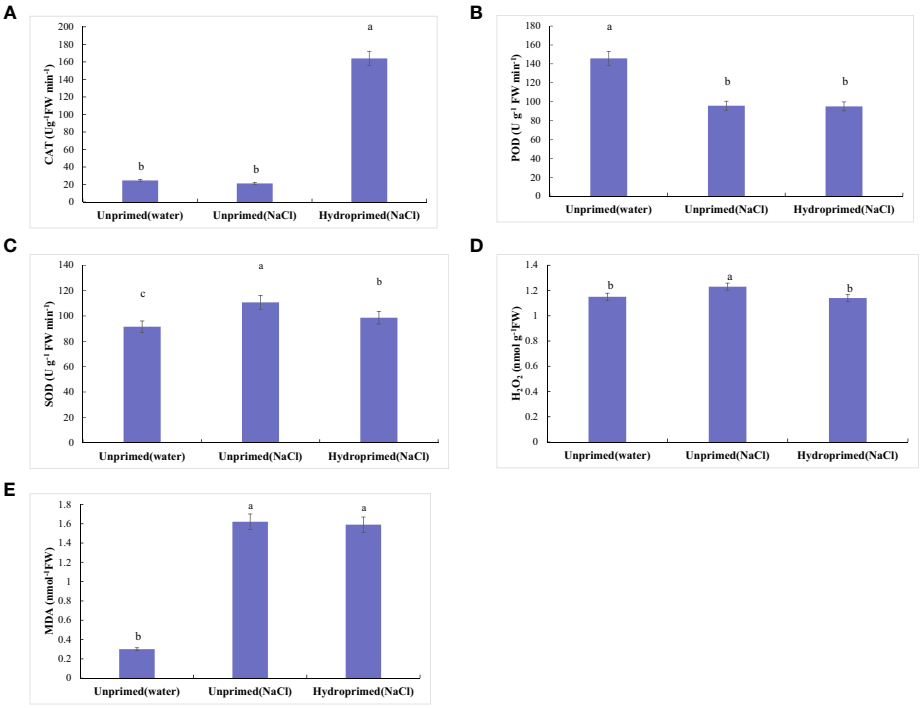

FIGURE 3
Influence of salt stress and hydropriming treatment on the activities of CAT **(A)**, POD **(B)**, SOD **(C)**, and content of H_2O_2 **(D)**, MDA **(E)** in maize roots. Different letters (a and b) indicate significant differences among treatments according to Duncan's test ($p < 0.05$). Error bars indicate ± SE of mean (n = 3).

of *P5CS*, *COMT* and *steroid reductase DET2* in the unprimed samples (Figures 10A, B, D), and increased the expression of *CAT2* (Figure 10C). Hydroprimed samples had significantly increased the expression of four genes under salt stress (Figures 10A–D).

4 Discussion

4.1 Effects of salt stress and hydropriming treatment on germination and early seedling growth

Exogenous and endogenous factors including salinity affect maize germination and seedling growth (Mahara et al., 2022). The present study indicated that 150 mmol.L^{-1} NaCl significantly inhibited germination and seedling growth. The germination traits (germination percentage and germination potential) and seedling traits (seedling dry weight, root dry weight and shoot dry weight) of unprimed seeds significantly decreased under salt stress. We found that hydropriming treatment significantly improved germination and seedling growth of maize under salt stress, which is in agreement with previous research (Mahara et al., 2022). The dry weight of seedlings and shoots of hydroprimed samples were higher than those of seedlings from unprimed seeds under salt stress, but lower than those of seedlings from unprimed seeds. Thus, the dry weight of roots from hydroprimed seeds reach the level of that of unprimed seeds under non-salt stress conditions, which means that the improvement in seedling growth mainly manifested in promoting root growth.

4.2 Physiology and biochemical responding to salt stress and hydropriming

Previous studies have indicated that salt stress often leads to excessive production of reactive oxygen species (ROS), such as superoxide ($O_2^{\bullet-}$), hydroxyl radical ($^{\bullet}OH$) and hydrogen peroxide (H_2O_2), which attack biomacromolecules and results in lipid peroxidation, protein degradation and membrane damage (Choudhary et al., 2020). The antioxidant enzymes SOD, CAT and POD are crucial to alleviating oxidative damage by scavenging ROS (Choudhary et al., 2020). SOD is the first line of antioxidant defense and transforms superoxide radicals to H_2O_2 and form hydroxyl radicals (Choudhary et al., 2020; Hai et al., 2022). In this study, we found that SOD activity significantly increased under salt stress. MDA is an index of lipid peroxidation and accumulates when the antioxidant defenses fail to maintain ROS levels (Choudhary et al., 2020). We found that MDA levels increased in salt stressed roots, attributed to excessive H_2O_2. Importantly, hydropriming significantly decreased H_2O_2 levels under salt stress and curtailed an increase MDA. The positive effect of hydropriming is likely related to increased antioxidant CAT activity, which detoxifies H_2O_2 to oxygen and water (Choudhary et al., 2020). However, due to the decrease of SOD activity, MDA content of primed samples was significantly higher than unprimed samples under salt stress.

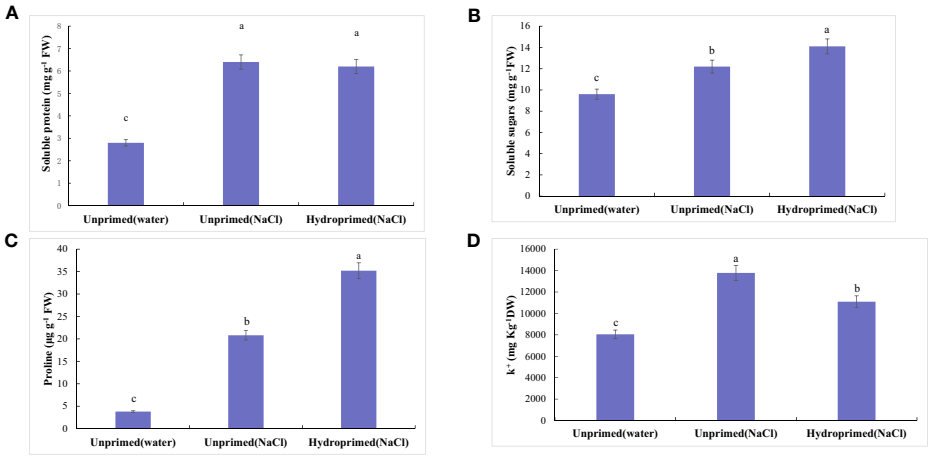

FIGURE 4
Influence of salt stress and hydropriming treatment on soluble protein **(A)**, soluble sugars **(B)**, proline **(C)**, K^+/Na^+ ration **(D)** in maize roots. Different letters (a and b) indicate significant differences among treatments according to Duncan's test ($p < 0.05$). Error bars indicate ± SE of mean (n = 3).

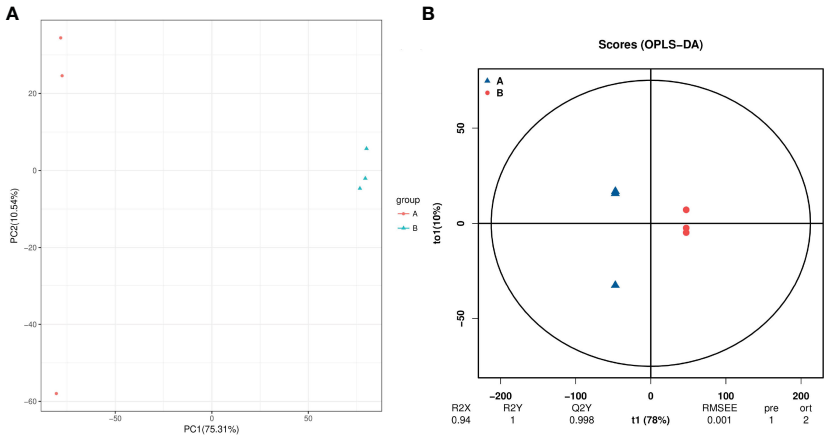

FIGURE 5
PCA **(A)** and PLS-DA **(B)** analyses of metabolic profiles of roots from unprimed maize seeds under with and without salt stress. group A, roots from unprimed maize seeds without salt stress; group B, roots from unprimed maize seeds under salt stress.

In present study, the expression of *CAT2* increased while catalase activity remained unchanged in salt stress roots, which may be caused by the decreased expression of other isoenzymes of catalase. In hydropeimed roots, increased CAT activity appeared linked to the increase expression of *CAT2*.

The influence of salt stress on soluble protein content generally relates to salt tolerance of plants (Gandonou et al., 2011). Previous studies of sugarcane plants have indicated that salt stress leads to an increase in soluble proteins in salt tolerant cultivars and a decrease in salt sensitive cultivars (Gandonou et al., 2011). The increase is probably related to stress proteins, which play important roles in osmotic adjustment under stress conditions (Timperio et al., 2008). The present findings elucidated that salt treatment significantly increased soluble protein content in maize seedlings under salt stress. Hydropriming did not increase further the amount of soluble protein produced under salt stress.

Plants also accumulate proline and sugars under water stress (Boughalleb et al., 2020). Soluble sugars are involved in osmo-regulation in plants exposed to osmotic stress (Boughalleb et al., 2020). Proline has been considered a compatible osmoregulator, contributing to cellular osmotic adjustment and cellular and physiological homeostasis maintenance in salt-stressed plants (Boughalleb et al., 2020). The present findings indicated that salt stress in unprimed and hydroprimed samples significantly augmented proline and sugar content. This is in agreement with previous data showing enhanced proline and sugar content contributing to mitigating adverse effects of salt stress (Boughalleb et al., 2020).

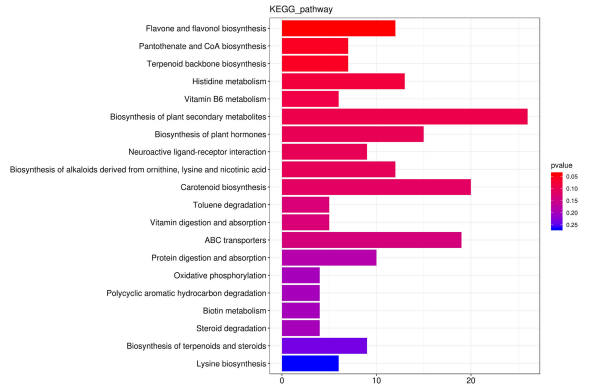

FIGURE 6
The top 20 the Kyoto Encyclopedia of Genes and Genomes (KEGG)-enriched metabolism pathway of differential metabolites between roots from unprimed maize seeds under with and without salt stress.

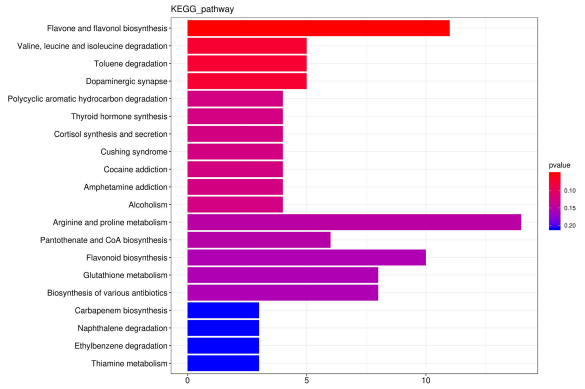

FIGURE 8
The top 20 the Kyoto Encyclopedia of Genes and Genomes (KEGG)-enriched metabolism pathway of differential metabolites between roots from unprimed and hydroprimed maize seeds under salt stress.

Delta-1-pyrroline-5-carboxylate synthase 2 (*P5CS*) encoding delta1 -pyrroline-5-carboxylate synthase (P5CS) has been reported as the main responsible gene in proline biosynthesis (Lutts et al., 1999). In present study, the interesting point is the differences between high proline content and low expression levels of *ZmP5CS2* in salt stressed roots, which indicated that the accumulation of proline can not be only a result of increased stress-induced expression of *ZmP5CS2*. In the meantime, the accumulation of proline accompanying with the increase expression of *ZmP5CS2* in hydroprimed roots showed *ZmP5CS2* seem to relate to salt tolerance.

K^+/Na^+ ratio is often used as a salt tolerance criterion and higher K^+/Na^+ ration accompanied with better growth under salt stress (Chen et al., 2023). Present study indicated the K^+/Na^+ ratio decreased under salt stress, while hydropriming treatment had no significant effect on K^+/Na^+ under salt stress. This suggests that the enhanced salt tolerance of hydropriming treatment was not caused by ion homeostasis.

4.3 Metabolites and metabolic pathway responding to salt stress

We found that Ethisterone (progesterone) was the most important metabolite produced in the roots grown from unprimed seeds in response to salt stress. Progesterone is a steroid hormone and ubiquitous in plants at low levels (Li et al., 2022), which enhances antioxidant enzyme activity and affects the K^+/Na^+ ratio and pigment content (Li et al., 2022). The amount of progesterone in the roots of unprimed samples significantly decreased under salt stress, while it significantly increased in hydroprimed samples, in accord with previous results (Li et al., 2022).

Menadione is a superoxide-releasing compound and generates ROS through redox cycling (Loor et al., 2010). The metabolite in the roots of unprimed samples significantly increased in response to salt stress. Hydropriming also significantly increased it. We interpret

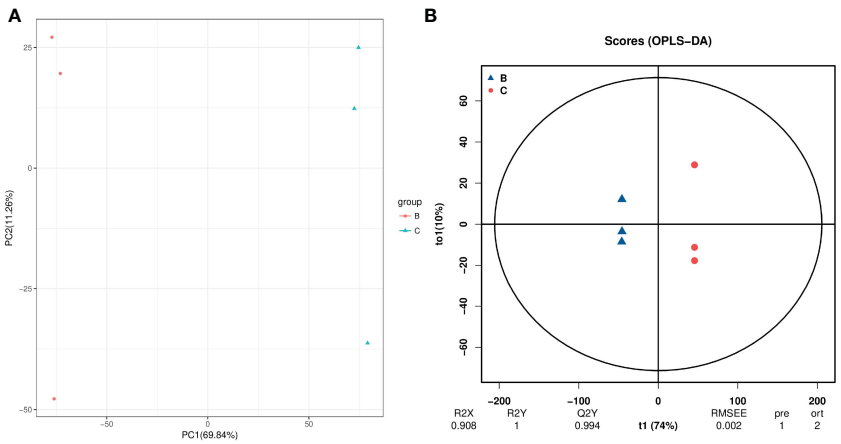

FIGURE 7
PCA **(A)** and PLS-DA **(B)** analyses of metabolic profiles of roots from unprimed and hydroprimed maize seeds under salt stress. group B, roots from unprimed maize seeds under salt stress; group C, roots from hydroprimed maize seeds under salt stress.

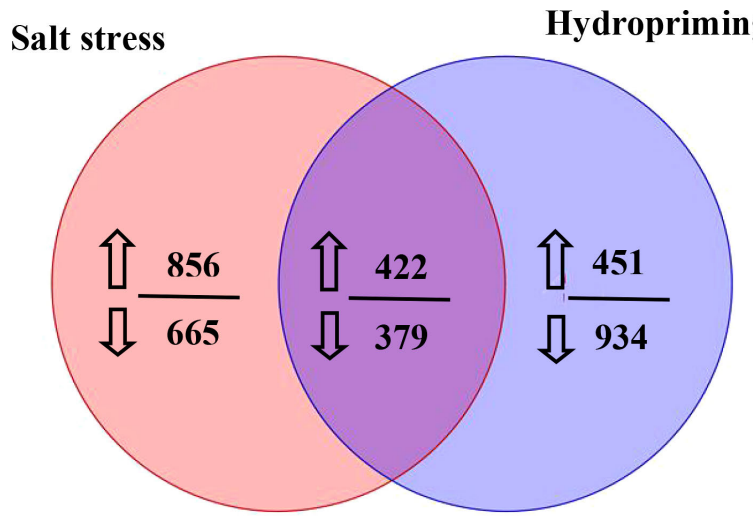

FIGURE 9
Venn diagram showing the number of metabolites that increased or decreased in the salt stressed and hydroprimed seedlings. The numbers next to up and down arrows indicated the number of upregulated and downrugulated differentially metabolites.

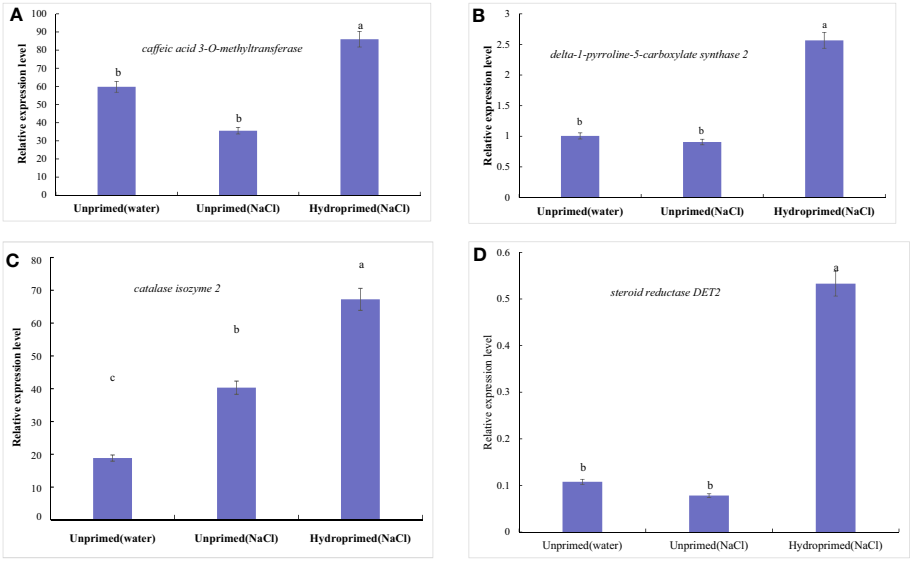

FIGURE 10
Influence of salt stress and hydropriming treatment on relative expression levels of *delta-1-pyrroline-5-carboxylate synthase 2* **(A)**, *caffeic acid 3-O-methyltransferase* **(B)**, *catalase isozyme 2* **(C)** and *Steroid reductase DET2* **(D)** by qRT-PCR. Different letters (a and b) indicate significant differences among treatments according to Duncan's test ($p < 0.05$). Error bars indicate ± SE of mean (n = 3).

that the accumulation of ROS resulting from salt stress and hydropriming signals the production of antioxidant enzymes such as catalase to scavenge ROS, which otherwise accumulates to potentially damaging levels. Previous research has shown that exogenous application of menadione inducing a mild oxidative stress, leading to chilling tolerance in maize seedlings (Prasad et al., 1994).

10-deacetyl-2-debenzoylbaccatin III (10-DAB III) is an important precursor for taxol synthesis (Yu et al., 2021). Salt stress tolerance requires microtubule disassembly (Zhou et al., 2017a), however, the stability of microtubule with taxol reduces the survival of seedlings under salt stress (Zhou et al., 2017a). We found that 10-Deacetyl-2-debenzoylbaccatin III significantly decreased under salt stress. The decrease in 10-Deacetyl-2-debenzoylbaccatin III may result in the decrease of taxol (not detected) and lead to the depolymerization of the cortical microtubule, which increased the survival of seedlings under salt stress.

Neomycin B is an aminoglycoside antibiotic, which displaces divalent metal ions bound to RNA and inhibits translation in prokaryotes (Waldsich et al., 1998). We found that Neomycin B significantly decreased due to salt stress and hydropriming. The decreased of Neomycin B results in an increase of translation, which is consistent with the increase of soluble proteins under salt stress and hydropriming.

Pelargonidin 3-O-(6-caffeoyl-beta-D-glucoside) 5-O-beta-D-glucoside is a acylated anthocyanin, stimulated by increasing concentrations of NaCl in seedlings (Eryilmaz, 2006).It has been shown to confer significant salt stress tolerance in *Brassica napus* L (Kim et al., 2017). We found that salt stress and hydropriming treatment both significantly increased the content of Pelargonidin 3-O-(6-caffeoyl-beta-D-glucoside) 5-O-beta-D-glucoside.

[6]-gingerol possess strong antioxidant properties, decreases peroxidation of phospholipid liposomes in the presence of iron(III) and ascorbate (Aeschbach et al., 1994). We found a decrease of [6]-Gingerol accompanying the increase of H_2O_2 under salt stress. Hydropriming significantly increased [6]-Gingerol with the decrease of H_2O_2.

Dexamethasone is a potent glucocorticoid receptor agonist and dexamethasone treatments leading to the activation of mitogen-activated protein kinase3 (MPK3) and MPK6, and depolymerization of the cortical microtubules (Zhou et al., 2017b). Zhou et al. (2017) reported that the activation of MPK3 and MPK6 affects the stability of microtubules, which significantly increased the surviving of seedlings under salt stress (Zhou et al., 2017b). We found that dexamethasone decreased under salt stress for unprimed samples and increased for hydroprimed samples. The variation trend of dexamethasone was consistent with that of seed germination and early seedling growth.

*N*6-(L-1,3-dicarboxypropyl)-L-lysine is a key intermediate in the α-amino adipate pathway for L-lysine biosynthesis (Kiyota et al., 2015), whereas lysine significantly represses proline and pipecolic acid synthesis (Kiyota et al., 2015). We found that *N*6-(L-1,3-dicarboxypropyl)-L-lysine and L-lysine both decreased and proline increased due to salt stress for unprimed and hydroprimed samples.

Tacrolimus is a calcineurin pathway inhibitor (Ma et al., 2005). Calcineurin is a conserved Ca^{2+}-calmodulin-dependent serine-threonine-specific protein phosphatase and has multiple functions including regulating ionic homeostasis (Ma et al., 2005). Previous research indicated that the expression of mouse calcineurin protein improved the salt stress tolerance of rice, partly due to limiting Na^+ accumulation in the roots (Ma et al., 2005). We found a decrease of tacrolimus under salt stress, which likely decreased the inhibition of calcineurin and, thus, increased seedling survival under salt stress.

Quinate is an important marker of salt stress involved in the shikimate pathway in biosynthesis of aromatic amino acid, including tyrosine, phenylalanine and tryptophan (Shelden et al., 2016). We found that quinate significantly increased in the roots of unprimed and hydroprimed samples under salt stress. Tyrosine and phenylalanine both significantly decreased under salt stress. Changes in tryptophan were not obvious. Thus, increased quinate levels may relate to decrease used as a precursor for aromatic amino acid synthesis.

Salt stress also influences metabolic pathways. We found that flavone and flavonol biosynthesis was the most significantly affected among 256 pathways affected by NaCl stress. Related metabolites, including Luteolin 7-O-beta-D-glucoside, 3,7,4'-Tri-O-methylquercetin, Chrysoeriol, Scolymoside, Kaempferol 3-O-glucoside, 3,7-Di-O-methylquercetin, Luteolin 7-O-glucuronide, Quercetin 3-methyl ether, Rutin, Quercetin 3-O-glucoside were significantly increased under salt stress. In contrast, the content of Acacetin and Kaempferol significantly decreased under salt stress. Among the 12 differential metabolites, 10 metabolites increased and 2 metabolites decreased, suggesting that salt stress activated this pathway in seedlings. Luteolin-7-O-beta-D-glucoside(Luteoloside) exhibited strong scavenging effect on active oxygens and increase under salt stress (Cai et al., 2020). 3,7,4'-Tri-O-methylquercetin was regarded as a contributor to the antioxidant of *Phragmites* under copper stress (Wu et al., 2022). Chrysoeriol possess a potent antioxidant activity and regarded as an important biomarker for salt tolerance in hulless barley (Wang et al., 2019). Scolymoside (luteolin 7-O-rutinoside) exhibited higher antioxidant activity than that of L-ascorbic acid and significantly increased under water-stressed conditions (Kim et al., 2000). Kaempferol 3-O-glucoside possess in vitro antioxidant properties (Taiwo et al., 2019). Griesser et al. (2015) discovered that prolonged drought stress leads to an increase of kaempferol-3-*O*-glucoside. 3,7-Di-O-methylquercetin was found to be related to flavonoids biosynthesis, which involves in plant defense against pathogens, herbivores, and environmental stress (Treutter, 2005). Luteolin-7-O-glucuronide possesses antioxidant activities and may act as reactive oxygen species scavengers, which was associated with the protective role in olive trees under field drought conditions (Araújo et al., 2021). Quercetin 3-methyl ether is the active antioxidant principle in the fruits and stems of Opuntia ficus-indica and markedly inhibited lipid peroxidation and scavenged free radicals (Dok-Go et al., 2003). Rutin scavenged hydroxyl radical and prevented K^+ leak in quinoa and broad beans under salinity treatment (Ismail et al., 2015). Quercetin 3-O-glucoside exhibits high antioxidant effect and moderate salinity induce the synthesis of quercetin-3-*O*-glucoside (Sgherri et al., 2017). Our results are consistent with previous studies which reported that flavones and flavonol accumulated in plants exposed to salt stress, and that they enhanced plant salinity tolerance *via* scavenging ROS (Zhang et al., 2017). Pathway diagrams are portrayed in Figure 11.

4.4 Metabolites and metabolic pathway responding to hydropriming under salt stress

We found that 5-Methyltetrahydrofolate was the most important metabolite produced in the roots of hydroprimed samples under salt stress. As a methyl donor, the methyl group of 5-methyltetrahydrofolate was transform to l-homocysteine resulting in the formation of methionine (Xu et al., 2010). Methionine is used in proteins synthesis or converted into *S*-adenosylmethionine. The methyl group of *S*-adenosylmethionine is applied to DNA and RNA modification and the synthesis of plant

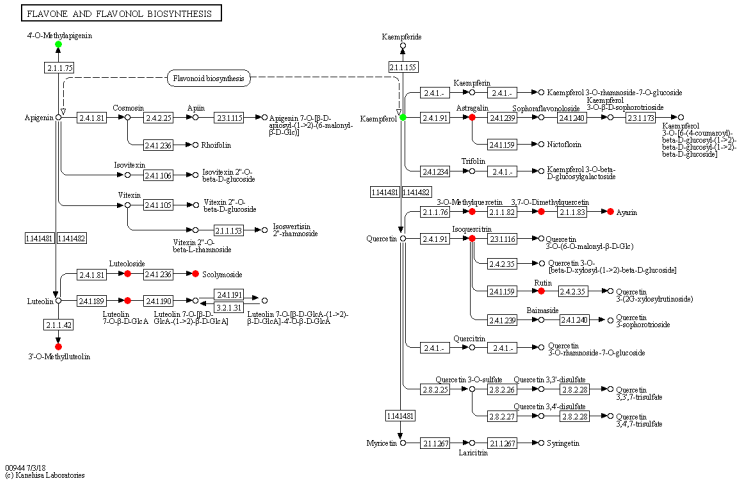

FIGURE 11
Changes in metabolic pathways of maize roots responding to salt stress. Red-marked metabolites indicated that the metabolite concentration increased significantly under salt stress($p<0.05$). Green-marked metabolites indicated that the metabolites concentration decreased significantly under salt stress($p<0.05$). Black-marked metabolites showed no significant change.

structural components (Xu et al., 2010). The carbon part of *S*-adenosylmethionine is used to generate ethylene and polyamines (Xu et al., 2010). Ethylene is a pivotal regulator of salt stress tolerance in plants (Riyazuddin et al., 2020). Polyamines can regulate the replication of DNA and cell division and the content of polyamines significantly increased under salt stress (Flores et al., 1989). Our results indicate that hydropriming significantly increased the level of endogenous 5-methyltetrahydrofolate under salt stress, in agreement with previous research (Riyazuddin et al., 2020).

24-Hydroxy-beta-amyrin is the precursor of soyasapogenol B (Tamura et al., 2018). Soyasapogenol B is a plant metabolite belonging to the group of triterpenoid saponins and is reported to stimulate germination of barley seeds (Evidente et al., 2011). We found that hydropriming significantly increased 24-OH-β-amyrin in maize roots under salt stress.

Dethiobiotin is the precursor of biotin (Wienhausen et al., 2022). Biotin is a water-soluble vitamin and required for normal cellular function and growth (McMahon, 2002). Biotin addition can enhance salt tolerance (shown in *Torulopsis mogii*) by accumulating glycerol and trehalose, improving fatty acid synthesis with longer chains and higher saturation, which enhances the stability of the cell structure, increasing PM-ATPase activity, and decreasing the ratio of K^+/Na^+(Chen et al., 2015). It is known that the relative proportions of saturated and unsaturated fatty acids affect the fluidity and permeability of the cell membrane (Chiang et al., 2005).

3α, 7α-dihydroxy-5β-cholestane is the intermediate bile acid synthesis (Kimura et al., 1988). In the presence of iron ions, hydrophobic bile acids may enhance lipid peroxidation (Sreejayan and Ritter, 1998). We found that 3α,7α-Dihydroxy-5β-cholestane increased in roots of unprimed and hydroprimed samples under salt stress, with no bile acid was detected, which indicates that the increase of 3α,7α-Dihydroxy-5β-cholestane was due to decreased synthesis of bile acid. A decrease of bile acid may result in a decrease of lipid peroxidation.

(S)-autumnaline is the precursor of cadaverine, which affects growth and development under normal and stress environments (Kuznetsov et al., 2007). Cadaverine decreases salt-induced impact, which is attributed to its antioxidative function scavenging of free radicals. We found that hydropriming significantly increased (S)-autumnaline and colchicine in mazie roots under salt stress, which was in accordance with the observed decrease in H_2O_2.

Formononetin 7-O-glucoside-6''-O-malonate is an intermediate in the elicitor-induced formation of pterocarpan phytoalexins, whose synthesis is known to be induced by biotic and abiotic stress factors (Dixon and Paiva, 1995). We found that hydropriming significantly increased Formononetin 7-O-glucoside-6''-O-malonate in maize roots under salt stress.

2-heptyl-4(1H)-quinolone is the core structure of several alkaloids and may act as a messenger molecule in a cell-cell-communication pathway (Déziel et al., 2004). It also acts as co-inducer of the transcriptional regulator PqsR (Xiao et al., 2006). We found that hydropriming significantly increased 2-Heptyl-4(1H)-quinolone in maize roots under salt stress.

2-Hydroxycinnamic acid is a derivative of hydroxycinnamic acids, which is involved in the regulation of plant growth and development and response to environmental stress (Luo et al., 2009). We found that that hydropriming significantly increased 2-Hydroxycinnamic acid in maize roots under salt stress.

Lupinine is a piperidine alkaloid whose concentration increases in plants under stress situations (Gill and Tuteja, 2010). We found

that hydropriming significantly increased piperideine and lupinine in maize roots under salt stress.

2-Methylglutaric acid is the precursor of acetic acid (Scott, 1967). Previous research indicates that acetic acid priming may mitigate salt stress to plants by modulating lipid metabolism (Hu et al., 2021). We found that hydropriming significantly increased 2-Methylglutaric acid in maize roots under salt stress.

Plant growth regulators play critical roles in regulating plant responses to stress at extremely low concentration (Fariduddin et al., 2019). Melatonin is regarded as a candidate phytohormone that affects responses to biotic and abiotic stresses (Li et al., 2019). Rapid accumulation of melatonin in plants enhances salt resistance *via* its actions on antioxidants, photosynthesis, ion regulation and stress signaling (Li et al., 2019). Present study indicated that melatonin increased in salt-stressed and hydroprimed maize roots, which is agreement with previous result of Li et al. (2019).

Caffeic acid 3-O-methyltransferase(*COMT*) encodes caffeic acid O-methyltransferase, which is a multifunctional enzyme responsible for lignin and flavonoid biosynthesis (Kim et al., 2006). Caffeic acid O-methyltransferase can catalyse *N*-acetylserotonin into melatonin, suggestive of alternative melatonin pathways in plants (Chang et al., 2021). In present study, melatonin increased in salt-stressed and hydroprimed maize roots, while the expression of *COMT* remained unchanged in salt-stressed roots and increased in hydroprimed maize roots. Present study suggested the gene products (caffeic acid O-methyltransferase) is not the rate-limiting enzyme for melatonin synthesis, which is in accord with the result of Byeon et al. (2015).

Caffeic acid O-methyltransferase is also known as flavone 3'-O-methyltransferase and responsible for flavonoid biosynthesis. Flavone 3'-O-methyltransferase can transfer the methyl group specifically to the 3'-hydroxyl group of quercetin and luteolin, resulting in the formation of 3'-O-methylquercetin and 3'-O-methylluteolin (chrysoeriol). 3'-O-methylquercetin is further methylated to 3,7-Di-O-methylquercetin and ayarin (3,7,4'-Tri-O-methylquercetin) (Kim et al., 2006). In present study, 3'-O-methylquercetin remained unchanged in salt-stressed roots and decreased in hydroprimed maize roots. 3,7-Di-O-methylquercetin and ayarin increased in salt-stressed roots and decreased in hydroprimed maize roots. Chrysoeriol increased in salt-stressed and hydroprimed maize roots. While the expression of *COMT* remained unchanged in salt-stressed roots and increased in hydroprimed maize roots. Present study suggested flavone 3'-O-methyltransferase is not the rate-limiting enzyme for ayarin and chrysoeriol synthesis. The increase of chrysoeriol in hydroprimed maize roots may be related with increased expression of *Flavone 3'-O-methyltransferase* (*Caffeic acid O-methyltransferase*).

The alteration of endogenous levels of gibberellins is regulated by both developmental and environmental stimuli (Ryu and Cho, 2015). The triggering of gibberellins by salinity was depending on NaCl dosage, Gibberellins 8 was down accumulated at lower dosage and up accumulated at high dosage (Benjamin et al., 2019). Present results indicated that Gibberellins 8 increased under salt stress, which was in accord with previous results of Benjamin et al. (2019). Present study also indicated that Gibberellin A8 increased in hydroprimed roots, which is in accord with Ryu and Cho (2015) who found that GA application could be helpful to improve crop yields under salt stress condition.

Estrone is a steroid estrogen, which inhibit plant growth at high levels and promoted plant growth at low levels (Adeel et al., 2018). Present results indicated estrone decreased in salt-stressed and hydroprimed samples, which means maize adapted to salt stress by reducing estrogen content and hydropriming treatment promotes growth of maize under salt stress by reducing estrogen content. Present results is in agreement with the discover of Adeel et al. (2018).

Abscisic acid(ABA) is a phytohormone enabling plants to survive salt stresses (Costa et al., 2007). Cramer and Quarrie (2002) observed a negative relationship between leaf growth and ABA concentration under salt stress. Costa et al. (2007) observed that higher ABA is related to increased resistance to salt stress. The difference between the two results could attribute to differences in experimental methodology and differences in the range of ABA concentrations observed. Costa et al. (2007) spectulated that the growth-promotiing effect of low concentration ABA in plants under salt stress was dominant over its growth-inhibiting effect. Present results indicated ABA decreased in salt-stressed and hydroprimed samples, which means maize adapted to salt stress by reducing ABA content and hydropriming treatment promotes growth of maize under salt stress by reducing ABA content. Present results is in agreement with the spectulation of Costa et al. (2007).

Previous study indicated that brassinolide affects potato root growth in a dose-dependent manner (Hu et al., 2016). Low brassinolide concentrations promoted root elongation and lateral root development, whereas high brassinolide concentrations restrained root elongation (Hu et al., 2016). Present study showed that brassinolide decreased due to salt stress and hydropriming treatment. We speculated that maize may promote root elongation by reducing brassinosteroids concentration.

As reported, steroid reductase DET2 catalyzes the conversion of campestanol to castasterone, a major rate-limiting step in brassinolide biosynthesis (Li et al., 2023). In present study, the expression of *steroid reductase DET2* remind unchange in salt stressed roots and significantly increased in hydroprimed roots. Castasterone, the product of steroid reductase DET2 decreased in salt stressed roots and significantly increased in hydroprimed roots. Therefore, we speculated that the decreased of brassinolide in salt stress and hydropriming treatment was due to its degradation.

5 Conclusions

Soil salinization can significantly hamper germination and growth of maize crops. To combat salt stress, maize increases SOD activity and accumulates soluble sugar, soluble protein and proline. We found that maize also adjusts its metabolism. Our metabolite analysis indicates that salt stress significantly increased the content of 1278 metabolites and decreased the content of 1044 metabolites. Ethisterone(progesterone), a steroid hormone, was the most important metabolite produced in the roots grown from unprimed seeds in response to salt stress. Pathway enrichment analysis indicated the flavone and flavonol biosynthesis, which relates to scavenging reactive oxygen species (ROS), was the only

significantly metabolic pathway affected by salt stress and activated by salt stress. Hydropriming significantly alleviated the adverse effects of salt stress and enhanced germination and seedling growth of maize under salt stress. Hydropriming significantly increased CAT activity, soluble sugar and proline content, decreased H_2O_2 under salt stress. Hydropriming significantly increased the content of 873 metabolites and significantly decreased the content of 1313 metabolites compared to the control. 5-Methyltetrahydrofolate, a methyl donor for methionine, was the most important metabolite produced in the roots of hydroprimed samples in response to salt stress. None of metabolic pathways were significantly affected by hydropriming treatment. Our results not only verified the important roles of some metabolites in resisting salt stress, but also further evidenced that flavone and flavonol biosynthesis and plant growth regulator relate to salt tolerance. The functions of other contributory metabolites related to salt stress amelioration in hydroprimed crops are not yet clear and warrants further analysis.

Data availability statement

The original contributions presented in the study are included in the article/Supplementary Material. Further inquiries can be directed to the corresponding author.

Author contributions

EZ: Conceptualization, Investigation, Data curation. XZ: Investigation, Methodology. WW: Investigation, Methodology. YS: Investigation. XT: Investigation. ZC: Investigation. XM: Investigation. YZ: Investigation. YW: Investigation. ZF: Investigation. NR: Writing-review and editing. DO'C: Writing-review and editing. XC: Formal analysis, Writing-review and editing. MY: Funding acquisition, Supervision, Visualization, Conceptualization, Writing- review and editing. All authors contributed to the article and approved the submitted version.

Funding

This work was financially supported by the Foundation of LuYu science and technology cooperation (2020LYXZ032, 2021LYXZ004) and project from department of foreign experts affairs, ministry of science and technology of China (G2021025001).

Conflict of interest

The authors declare that the research was conducted in the absence of any commercial or financial relationships that could be construed as a potential conflict of interest.

Publisher's note

All claims expressed in this article are solely those of the authors and do not necessarily represent those of their affiliated organizations, or those of the publisher, the editors and the reviewers. Any product that may be evaluated in this article, or claim that may be made by its manufacturer, is not guaranteed or endorsed by the publisher.

Supplementary material

The Supplementary Material for this article can be found online at: https://www.frontiersin.org/articles/10.3389/fpls.2023.1109460/full#supplementary-material

References

Abideen, Z., Hanif, M., Munir, N., and Nielsen, B. L. (2022). Impact of nanomaterials on the regulation of gene expression and metabolomics of plants under salt stress. *Plants (Basel Switzerland).* 11, 691. doi: 10.3390/plants11050691

Adeel, M., Yang, Y. S., Wang, Y. Y., Song, X. M., Ahmad, M. A., and Rogers, H. J. (2018). Uptake and transformation of steroid estrogens as emerging contaminants influence plant development. *Environ. Pollut.* 243, 1487–1497. doi: 10.1016/j.envpol.2018.09.016

Aebi, H. (1984). Catalase in vitro. *Methods Enzymol.* 105, 121–126. doi: 10.1016/S0076-6879(84)05016-3

Aeschbach, R., Loliger, J., Scott, B. C., Murcia, A., Butler, J., and Halliwell, B. (1994). Antioxidant actions of thymol, carvacrol, 6-gingerol, zingerone and hydroxytyrosol. *Food. Chem. Toxicol.* 32, 31–36. doi: 10.1016/0278-6915(84)90033-4

Araújo, M., Prada, J., Mariz-Ponte, N., Santos, C., Pereira, J. A., Pinto, D. C. G. A., et al. (2021). Antioxidant adjustments of olive trees (*Olea europaea*) under field stress conditions. *Plants* 10, 684. doi: 10.3390/plants10040684

Bates, L. E., Waldren, R. P., and Teare, I. D. (1973). Rapid determination of free proline for water stress studies. *Plant Soil.* 39, 205–207. doi: 10.1007/BF00018060

Benjamin, J. J., Lucini, L., Jothiramshekar, S., and Parida, A. (2019). Metabolomic insights into the mechanisms underlying tolerance to salinity in different halophytes. *Plant Physiol. Bioch.* 135, 528–545. doi: 10.1016/j.plaphy.2018.11.006

Boughalleb, F., Abdellaoui, R., Mahmoudl, M., and Bakhshanden, E. (2020). Changes in phenolic profile, soluble sugar, proline, and antioxidant enzyme activities of *Polygonum equisetiforme* in response to salinity. *Turk. J. Bot.* 44, 25–35. doi: 10.3906/bot-1908-2

Bradford, M. M. (1976). A rapid and sensitive method for the quantitation of microgramquantities of protein utilizing the principle of protein-dye binding. *Anal. Biochem.* 72 (1-2), 248–254. doi: 10.1016/0003-2697(76)90527-3

Byeon, Y., Choi, G. H., Lee, H. Y., and Back, K. (2015). Melatonin biosynthesis requires *N*-acetylserotonin methyltransferase activity of caffeic acid *O*-methyltransferase in rice. *J. Exp. Bot.* 66, 6917–6925. doi: 10.1093/jxb/erv396

Cai, Z., Chen, H., Chen, J., Yang, R., Zou, L., Wang, C., et al. (2020). Metabolomics characterizes the metabolic changes of lonicerae japonicae flos under different salt stresses. *PloS One* 15, e0243111. doi: 10.1371/journal.pone.0243111

Chance, B., and Maehly, C. (1955). Assay of catalase and peroxidases. *Methods Enzymology.* 11, 764–775. doi: 10.1016/S0076-6879(55)02300-8

Chang, J., Guo, Y., Yan, J., Zhang, Z., Yuan, L., Wei, C., et al. (2021). The role of watermelon caffeic acid *O*-methyltransferase-methyltransferase (*ClCOMT1*) in melatonin biosynthesis and abiotic stress tolerance. *Hortic. Res.* 8, 210. doi: 10.1038/s41438-021-00645-5

Chattha, M. U., Hassan, M. U. U., Khan, I., Nawaz, M., Shah, A. N., Sattar, A., et al. (2022). Hydrogen peroxide priming alleviates salinity induced toxic effect in maize by improving antioxidant defense system, ionic homeostasis, photosynthetic efficiency and hormonal crosstalk. *Mol. Biol. Rep.* 49, 5611–5624. doi: 10.1007/s11033-022-07535-6

Chen, Q., Xu, K., Xu, Y., Ji, D., Chen, C., Xie, C., et al. (2023). Na^+ /K^+- ATPase regulates the k^+ /Na^+ homeostasis in the intertidal macroalgae, *Neoporphyra haitanensis*, in response to salt stress. *Front. Plant Sci.* 13. doi: 10.3389/fpls.2022.1040142

Chen, X., Yan, M., Xie, F. L., Dai, J., Li, D. S., Wang, Z., et al. (2015). Biotin enhances salt tolerance of *Torulopsis mogii*. *Ann. Microbiol.* 65, 393–398. doi: 10.1007/s13213-014-0871-6

Chiang, M. L., Yu, R. C., and Chou, C. C. (2005). Fatty acid composition, cell morphology and responses to challenge by organic acid and sodium chloride of heat-shocked *Vibrio parahaemolyticus*. *Int. J. Food. Microbiol.* 104, 179–187. doi: 10.1016/j.ijfoodmicro.2005.02.007

Choudhary, A., Kumar, A., and Kaur, N. (2020). ROS and oxidative burst: roots in plant development. plant. *Divers* 42, 33–43. doi: 10.1016/j.pld.2019.10.002

Costa, W. D., Zörb, C., Hartung, W., and Schubert, S. (2007). Salt resistance is determined by osmotic adjustment and abscisic acid in newly developed maize hybrids in the first phase of salt stress. *Physiol. Plantarum* 131, 311–321. doi: 10.1111/j.1399-3054.2007.00962.x

Cramer, G. R., and Quarrie, S. A. (2002). Abscisic acid is correlated with the leaf growth inhibition of four genotypes of maize differing in their response to salinity. *Funct. Plant Biol.* 29, 111–115. doi: 10.1071/PP01131

Déziel, E., Lépine, F., Milot, S., He, J., Mindrinos, M. N., Tompkins, R. G., et al. (2004). Analysis of *Pseudomonas aeruginosa* 4-hydroxy-2-alkylquinolines (HAQs) reveals a role for 4-hydroxy-2-heptylquinoline in cell-to-cell communication. *Proc. Natl. Acad. Sci. U.S.A.* 101, 1339–1344. doi: 10.1073/pnas.0307694100

Dhindsa, R. S., Dhindsa, P. P., and Thorpe, T. A. (1981). Leaf senescence correlated with increased levels of membrane permeability and lipid-peroxidation and decreased levels of superoxide dismutase and catalase. *J. Exp. Bot.* 32, 93–101. doi: 10.1093/jxb/32.1.93

Dixon, R. A., and Paiva, N. L. (1995). Stress induced phenylpropanoid metabolism. *Plant Cell.* 7. doi: 10.3389/fpls.2022.874590

Dok-Go, H., Lee, K. H., Kim, H. J., Lee, E. H., Lee, J., Song, Y. S., et al. (2003). Neuroprotective effects of antioxidative flavonoids, quercetin, (+)-dihydroquercetin and quercetin 3-methyl ether, isolated from Opuntia ficus-indica Var Saboten. *Brain Res.* 965, 130–136. doi: 10.1016/S0006-8993(02)04150-1

Eryilmaz, F. (2006). The relationships between salt stress and anthocyanin content in higher plants. *Biotechnol. Biotechnol. Eq.* 20, 47–52. doi: 10.1104/pp.010818

Evidente, A., Cimmino, A., Fernández-Aparicio, M., Rubiales, D., Andolfi, A., and Melck, D. (2011). Soyasapogenol b and trans-22-dehydrocam- pesterol from common vetch (*Vicia sativa* l.) root exudates stimulate broomrape seed germination. *Pest. Manage. Sci.* 67, 1015–1022. doi: 10.1002/ps.2153

Fariduddin, Q., Zaid, A., and Mohammad, F. (2019). "Plant growth regulators and salt stress: mechanism of tolerance trade-off," in *Salt stress, microbes, and plant interactions: causes and solution*. Ed. M. Akhtar (Singapore: Springer). doi: 10.1007/978-981-13-8801-9_4

Farooq, M., Hussain, M., Wakeel, A., and Siddique, K. H. M. (2015). Salt stress in maize: effects, resistance mechanisms, and management. a review. *Agron. Sustain. Dev.* 35, 461–481. doi: 10.1007/s13593-015-0287-0

Flores, H. E., Protacio, C. M., and Signs, M. W. (1989). Primary and secondary metabolism of polyamines in plants. plant nitrogen metabolism. *Recent Adv. Phytochemistry.* 23, 329–393. doi: 10.1007/978-1-4613-0835-5_10

Gandonou, C. B., Bada, F., Abrini, J., and Skali-Senhaji, N. (2011). Free proline, soluble sugars and soluble proteins concentration as affected by salt stress in two sugarcane (*Saccharum sp.*) cultivars differing in their salt tolerance. *Int. J. Biol. Chem. Sci.* 5, 2441–2453. doi: 10.4314/ijbcs.v5i6.23

Gill, S. S., and Tuteja, N. (2010). Polyamines and abiotic stress tolerance in plants. *Plant Signal. Behav.* 5, 26–33. doi: 10.4161/psb.5.1.10291

Griesser, M., Weingart, G., Schoedl-Hummel, K., Neumann, N., Becker, M., Varmuza, K., et al. (2015). >Severe drought stress is affecting selected primary metabolites, polyphenols, and volatile metabolites in grapevine leaves (*Vitis vinifera* cv. Pinot noir). *Plant Physiol. Bioch.* 88, 17–26. doi: 10.1016/j.plaphy.2015.01.004

Hai, X., Mi, J., Zhao, B., Zhang, B., Zhao, Z., and Liu, J. (2022). Foliar application of spermidine reduced the negative effects of salt stress on oat seedlings. *Front. Plant Sci.* 13. doi: 10.3389/fpls.2022.846280

Hamna, A. H., Aeman, S., Danish, W., Shehla, T., Muhammad, U., and Shaheed, S. Z. (2022). Profiling of energy compartmentalization in photosystem II (PSII), light harvesting complexes and specific energy fluxes of primed maize cultivar (P1429) under salt stress environment. *Plant Physiol. Bioch.* 170, 296–306. doi: 10.1016/j.plaphy.2021.12.015

Heath, R. L., and Packer, I. (1968). Photoperoxidation in isolated chloroplasts. i. kinetics and stoichiometry of fatty acid peroxidation. *Arch. Biochem. Biophys.* 125, 189–198. doi: 10.1016/0003-9861(68)90654-1

Hernandez-Apaolaza, L. (2022). Priming with silicon: a review of a promising tool to improve micronutrient deficiency symptoms. *Front. Plant Sci.* 13. doi: 10.3389/fpls.2022.840770

Hu, Q., Cui, H., Ma, C., Li, Y., Yang, C., Wang, K., et al. (2021). Lipidomic metabolism associated with acetic acid priming-induced salt tolerance in carex rigescens. *Plant Physiol. Bioch.* 167, 665–677. doi: 10.1016/j.plaphy.2021.08.045

Hu, Y., Xia, S., Su, Y., Wang, H., Luo, W., Su, S., et al. (2016). Brassinolide increases potato root growth in vitro in a dose-dependent way and alleviates salinity stress. *BioMed. Res. Int.* 2016, 8231873. doi: 10.1155/2016/8231873

Hussain, S., Ahmed, S., Akram, W., Li, G., and Yasin, N. (2023). Selenium seed priming enhanced the growth of salt-stressed Brassica rapa L. through improving plant nutrition and the antioxidant system. *Front. Plant Sci.* 13, 1050359. doi:10.3389/fpls.2022.1050359

Irigoyen, J. J., Emerich, D. W., and Sanchez-Diaz, M. (1992). Water stress induced changes in concentrations of proline and total soluble sugars in nodulated alfalfa (*Medicago sativa*) plants. *Physiol. Plantarum.* 84, 55–60. doi: 10.1111/j.1399-3054.1992.tb08764.x

Ismail, H., Maksimović, J. D., Maksimović, V., Shabala, L., Živanović, B. D., Tian, Y., et al. (2015). Rutin, a flavonoid with antioxidant activity, improves plant salinity tolerance by regulating k^+ retention and na^+ exclusion from leaf mesophyll in quinoa and broad beans. *Funct. Plant Biol.* 43, 75–86. doi: 10.1071/FP15312

Kim, B. G., Lee, Y., Hur, H. G., Lim, Y., and Ahn, J. H. (2006). Flavonoid 3'-o-methyltransferase from rice: cDNA cloning, characterization and functional expression. *Phytochemistry* 67 (4), 387–394. doi: 10.1016/j.phytochem.2005.11.022

Kim, J., Lee, W. J., Vu, T. T., Jeong, C. Y., Hong, S. W., and Lee, H. (2017). High accumulation of anthocyanins *via* the ectopic expression of AtDFR confers significant salt stress tolerance in *Brassica napus* l. *Plant Cell. Rep.* 36, 1215–1224. doi: 10.1007/s00299-017-2147-7

Kim, N. M., Kim, J., Chung, H. Y., and Choi, J. S. (2000). Isolation of luteolin 7-O-rutinoside and esculetin with potential antioxidant activity from the aerial parts of Artemisia montana. *Arch. Pharm. Res.* 23 (3), 237–239. doi: 10.1007/BF02976451

Kimura, K., Ogura, Y., and Ogura, M. (1988). Increased rate of cholic acid formation from 3α, 7α-dihydroxy-5β-cholestane in perfused livers from diabetic rats. *Acta (BBA)-Lipids Lipid Metab.* 963, 329–332. doi: 10.1016/0005-2760(88)90298-6

Kiyota, E., Pena, I. A., and Arruda, P. (2015). The saccharopine pathway in seed development and stress response of maize. *Plant Cell. Environ.* 38, 2450–2461. doi: 10.1111/pce.12563

Kuznetsov, V., Shorina, M., Aronova, E., Stetsenko, L., Rakitin, V., and Shevyakova, N. (2007). NaCl- and ethylene-dependent cadaverine accumulation and its possible protective role in the adaptation of the common ice plant to salt stress. *Plant Sci.* 172, 363–370. doi: 10.1016/j.plantsci.2006.09.012

Li, H., Chen, L., Chen, H., Xue, R., Wang, Y., and Song, J. (2022). The role of plant progesterone in regulating growth, development, and biotic/abiotic stress responses. *Int. J. Mol. Sci.* 23, 10945. doi: 10.3390/ijms231810945

Li, Y., Hua, J., Hou, X., Qi, N., Li, C., Wang, C., et al. (2023). Brassinosteroids is involved in methane-induced adventitious root formation *via* inducing cell wall relaxation in marigold. *BMC Plant Biol.* 23, 2. doi: 10.1186/s12870-022-04014-9

Li, J., Liu, J., Zhu, T., Zhao, C., Li, L., and Chen, M. (2019). The role of melatonin in salt stress responses. *Int. J. Mol. Sci.* 20 (7), 1735. doi: 10.3390/ijms20071735

Loor, G., Kondapalli, J., Schriewer, J. M., Chandel, N. S., Hoek, T. L. V., and Schumacker, P. T. (2010). Menadione triggers cell death through ROS-dependent mechanisms involving PARP activation without requiring apoptosis. *Free. Radical. Bio. Med.* 49, 1925–1936. doi: 10.1016/j.freeradbiomed.2010.09.021

Luo, J., Fuell, C., Parr, A., Hill, L., Bailey, P., Elliott, K., et al. (2009). A novel polyamine acyltransferase responsible for the accumulation of spermidine conjugates in *Arabidopsis* seed. *Plant Cell.* 21, 318–333. doi: 10.1105/tpc.108.063511

Lutts, S., Majerus, V., and Kinet, J. M. (1999). NaCl Effects on proline metabolism in rice (*Oryza sativa*) seedlings. *Physiol. Plant* 105, 450–458. doi: 10.1034/j.1399-3054.1999.105309.x

Ma, X., Qian, Q., and Zhu, D. (2005). Expression of a calcineurin gene improves salt stress tolerance in transgenic rice. *Plant Mol. Biol.* 58, 483–495. doi: 10.1007/s11103-005-6162-7

Mahara, G., Bam, R., Kandel, M., Timilsina, S., Chaudhary, D., Lamichhane, J., et al. (2022). Seed priming with NaCl improves germination in maize under saline soil conditions. *Eurasian. Soil.* 11, 151–156. doi: 10.18393/ejss.1027558

McMahon, R. J. (2002). Biotin in metabolism and molecular biology. *Annu. Rev. Nutr.* 22, 221–239. doi: 10.1146/annurev.nutr.22.121101.112819

Prasad, T. K., Anderson, M. D., Martin, B. A., and Stewart, C. R. (1994). Evidence for chilling-induced oxidative stress in maize seedlings and a regulatory role for hydrogen peroxide. *Plant Cell.* 6, 65–74. doi: 10.1105/tpc.6.1.65

Rewald, B., Shelef, O., Ephrath, J. E., and Rachmilevitch, S. (2013). "Adaptive plasticity of salt-stressed root systems," in *Ecophysiology and responses of plants under salt stress*. Eds. P. Ahmad, M. Azooz and M. Prasad (New York, NY: Springer). doi: 10.1007/978-1-4614-4747-4_6

Riyazuddin, R., Verma, R., Singh, K., Nisha, N., Keisham, M., Bhati, K. K., et al. (2020). Ethylene: a master regulator of salinity stress tolerance in plants. *Biomolecules* 10, E959. doi: 10.3390/biom10060959

Ryu, H., and Cho, Y. G. (2015). Plant hormones in salt stress tolerance. *J. Plant Biol.* 58, 147–155. doi: 10.1007/s12374-015-0103-z

Samra, Y. H., Muhammad, A., Muhammad, A., and Muhammad, S. (2022). Seed priming with silicon and chitosan for alleviating water stress effects in maize (*ZEA MAYS* l.) by improving antioxidant enzyme activities, water status and photosynthesis. *J. Plant Nutr.* 45, 2263–2276. doi: 10.1080/01904167.2022.2046070

Scott, T. A. (1967). A method for the degradation of radioactive nicotinic acid. *Biochem. J.* 102, 87–93. doi: 10.1042/bj1020087

Sergiev, I., Alexieva, V., and Karanov, E. (1997). Effect of spermine, atrazine and combination between them on some endogenous protective systems and stress markers in plants. *Compt. Rend. Acad. Bulg. Sci.* 51, 121–124. doi: 10.1046/j.1365-3040.2001.007

Sgherri, C., Pérez-López, U., Micaelli, F., Miranda-Apodaca, J., Mena-Petite, A., Muñoz-Rued, A., et al. (2017). Elevated CO_2 and salinity are responsible for phenolics-enrichment in two differently pigmented lettuces. *Plant Physiol. Bioch.* 115, 269–278. doi: 10.1016/j.plaphy.2017.04.006

Shelden, M. C., Dias, D. A., Jayasinghe, N. S., Bacic, A., and Roessner, U. (2016). Root spatial metabolite profiling of two genotypes of barley (*Hordeum vulgare L*) reveals differences in response to short-term salt stress. *J. Exp. Bot.* 67, 3731–3745. doi: 10.1093/jxb/erw059

Sreejayan, N., and Ritter, C. V. (1998). Effect of bile acids on lipid peroxidation: the role of iron. free. *Radical. Bio. Med.* 25, 50–56. doi: 10.1016/S0891-5849(98)00045-8

Taiwo, F. O., Oyedeji, O., and Osundahunsi, M. T. (2019). Antimicrobial and antioxidant properties of kaempferol-3-O-glucoside and 1-(4-Hydroxyphenyl)-3-phenylpropan-1-one isolated from the leaves of *Annona muricata* (Linn.). *J. Pharm. Res. Int.* 26, 1–13. doi: 10.9734/jpri/2019/v26i330138

Tamura, K., Yoshida, K., Hiraoka, Y., Sakaguchi, D., Chikugo, A., Mochida, K., et al. (2018). The basic helix-loop-helix transcription factor gubhlh3 positively regulates soyasaponin biosynthetic genes in *Glycyrrhiza uralensis*. *Plant Cell. Physiol.* 59, 778–791. doi: 10.1093/pcp/pcy075

Timperio, A. M., Egidi, M. G., and Zolla, L. (2008). Proteomics applied on plant abiotic stresses: role of heat shock proteins (HSP). *J. Proteomics.* 71, 391–411. doi: 10.1016/j.jprot.2008.07.005

Treutter, D. (2005). Significance of flavonoids in plant resistance and enhancement of their biosynthesis. *Plant Biol. (Stuttg).* 7, 581–591. doi: 10.1055/s-2005-873009

Waldsich, C., Semrad, K., and Schroeder, R. (1998). Neomycin b inhibits splicing of the td intron indirectly by interfering with translation and enhances missplicing *in vivo*. *RNA* 4, 1653–1663. doi: 10.1017/S1355838298981444.

Wang, W., Pang, J., Zhang, F., Sun, L., Yang, L., and Siddique, K. H. M. (2022). Transcriptomic and metabolomics-based analysis of key biological pathways reveals the role of lipid metabolism in response to salt stress in the root system of *Brassica* napus. *Plant Growth. Regul.* 97, 127–141. doi: 10.1007/s10725-021-00788-4

Wang, Y., Zeng, X., Xu, Q., Mei, X., Yuan, H., Jiabu, D., et al. (2019). Metabolite profiling in two contrasting Tibetan hulless barley cultivars revealed the core salt-responsive metabolome and key salt-tolerance biomarkers. *AoB Plants.* 11, plz021. doi: 10.1093/aobpla/plz021

Wienhausen, G., Bruns, S., Sultana, S., Dlugosch, L., Groon, L. A., Wilkes, H., et al. (2022). The overlooked role of a biotin precursor for marine bacteria-desthiobiotin as an escape route for biotin auxotrophy. *ISME. J.* 16, 2599–2609. doi: 10.1038/s41396-022-01304-w

Williams, V., and Twine, S. (1960). "Flame photometric method for sodium, potassium and calcium," in *Modern methods of plant analysis*. Eds. K. Peach and M. V. Tracey (Berlin: Springer-Verlag), 3–5.

Wu, J., Gao, T., Zhao, L., Bao, H., Yu, C., Hu, J., et al. (2022). Investigating phragmites ustralis response to copper exposure using physiologic, Fourier transform infrared and metabolomic approaches. *Funct. Plant Biol.* 49, 365–381. doi: 10.1071/FP21258

Xiao, G., Déziel, E., He, J., Lépine, F., Lesic, B., Castonguay, M. H., et al. (2006). MvfR, a key *Pseudomonas aeruginosa* pathogenicity LTTR-class regulatory protein, has dual ligands. *Mol. Microbiol.* 62, 1689–1699. doi: 10.1111/j.1365-2958.2006.05462.x

Xu, C., Sibicky, T., and Huang, B. (2010). Protein profile analysis of salt-responsive proteins in leaves and roots in two cultivars of creeping bentgrass differing in salinity tolerance. *Plant Cell. Rep.* 29, 595–615. doi: 10.1007/s00299-010-0847-3

Yaghoubian, I., Antar, M., Ghassemi, S., Modarres-Sanavy, S. A. M., and Smith, D. L. (2022). The effects of hydro-priming and colonization with *Piriformospora indica* and *Azotobacter chroococcum* on physio-biochemical traits, flavonolignans and fatty acids composition of milk thistle (*Silybum marianum*) under saline conditions. *Plants* 11 (10), 1281. doi: 10.3390/plants11101281

Yan, M. (2016). Hydro-priming increases seed germination and early seedling growth in two cultivars of napa cabbage (*Brassica rapa* subsp. *pekinensis*) grown under salt stress. *J. Hortic. Sci. Biotech.* 91, 421–426. doi: 10.1080/14620316.2016.1162031

Yu, C., Zhang, C., Xu, X., Huang, J., Chen, Y., Luo, X., et al. (2021). Omic analysis of the endangered taxaceae species *Pseudotaxus chienii* revealed the differences in taxol biosynthesis pathway between *Pseudotaxus* and *Taxus yunnanensis* trees. *BMC Plant Biol.* 21. doi: 10.3389/fpls.2022.846280

Zhang, H., Wu, Z., Suo, Y., Wang, J., Zheng, L., and Wang, Y. (2017). Gene expression and flavonol biosynthesis are induced by ultraviolet-b and salt stresses in *Reaumuria trigyna*. *Biol. Plant* 61, 246–254. doi: 10.1007/s10535-017-0725-8

Zhou, S., Chen, Qi., Li, X., and Li, Y. (2017a). MAP65-1 is required for the depolymerization and reorganization of cortical microtubules in the response to salt stress in arabidopsis. *Plant Sci.* 264, 112–121. doi: 10.1016/j.plantsci.2017.09.004

Zhou, S., Chen, Q., Sun, Y., and Li, Y. (2017b). Histone H2B monoubiquitination regulates salt stress-induced microtubule depolymerization in *Arabidopsis*. *Plant Cell Environ.* 40, 1512–1530. doi: 10.1111/pce.12950

frontiers | Frontiers in Plant Science

TYPE Original Research
PUBLISHED 12 June 2023
DOI 10.3389/fpls.2023.1088537

Check for updates

OPEN ACCESS

EDITED BY
Mohammad Golam Mostofa,
Department of Biochemistry and Molecular Biology, Michigan State University, United States

REVIEWED BY
Ujjal Jyoti Phukan,
University of Arizona, United States
Yunpeng Cao,
Wuhan Botanical Garden (CAS), China

*CORRESPONDENCE
Jun-Shan Gao
gaojsh@ahau.edu.cn

RECEIVED 03 November 2022
ACCEPTED 10 April 2023
PUBLISHED 12 June 2023

CITATION
Owusu AG, Lv Y-P, Liu M, Wu Y, Li C-L, Guo N, Li D-H and Gao J-S (2023) Transcriptomic and metabolomic analyses reveal the potential mechanism of waterlogging resistance in cotton (*Gossypium hirsutum* L.).
Front. Plant Sci. 14:1088537.
doi: 10.3389/fpls.2023.1088537

COPYRIGHT
© 2023 Owusu, Lv, Liu, Wu, Li, Guo, Li and Gao. This is an open-access article distributed under the terms of the Creative Commons Attribution License (CC BY). The use, distribution or reproduction in other forums is permitted, provided the original author(s) and the copyright owner(s) are credited and that the original publication in this journal is cited, in accordance with accepted academic practice. No use, distribution or reproduction is permitted which does not comply with these terms.

Transcriptomic and metabolomic analyses reveal the potential mechanism of waterlogging resistance in cotton (*Gossypium hirsutum* L.)

Anane Gideon Owusu, Yin-Ping Lv, Man Liu, Yong Wu, Cheng-Lin Li, Ning Guo, Da-Hui Li and Jun-Shan Gao*

School of Life Sciences, Anhui Agricultural University, Hefei, China

Introduction: Cotton (*Gossypium hirsutum* L.) is susceptible to long-term waterlogging stress; however, genomic information of cotton response mechanisms toward long days of waterlogging is quite elusive.

Methods: Here, we combined the transcriptome and metabolome expression level changes in cotton roots after 10 and 20 days of waterlogging stress treatment pertaining to potential resistance mechanisms in two cotton genotypes.

Results and discussion: Numerous adventitious roots and hypertrophic lenticels were induced in CJ1831056 and CJ1831072. Transcriptome analysis revealed 101,599 differentially expressed genes in cotton roots with higher gene expression after 20 days of stress. Reactive oxygen species (ROS) generating genes, antioxidant enzyme genes, and transcription factor genes (*AP2*, *MYB*, *WRKY*, and *bZIP*) were highly responsive to waterlogging stress among the two genotypes. Metabolomics results showed higher expressions of stress-resistant metabolites sinapyl alcohol, L-glutamic acid, galactaric acid, glucose 1-phosphate, L-valine, L-asparagine, and melibiose in CJ1831056 than CJ1831072. Differentially expressed metabolites (adenosine, galactaric acid, sinapyl alcohol, L-valine, L-asparagine, and melibiose) significantly correlated with the differentially expressed *PRX52*, *PER1*, *PER64*, and *BGLU11* transcripts. This investigation reveals genes for targeted genetic engineering to improve waterlogging stress resistance to enhance abiotic stress regulatory mechanisms in cotton at the transcript and metabolic levels of study.

KEYWORDS

cotton, waterlogging stress, transcriptomics, metabolomics, differentially expressed genes, transcription factors

Introduction

Waterlogging is a major type of flooding problem, depending on the water level encountered by plant species (Jia et al., 2021). It primarily causes oxygen deficiency in soil in plant roots, resulting in morphological, physiological, molecular, and anatomical changes in plant tissues that affect plant growth and development. Typically, major damage from waterlogging stress is similar but species-specific. However, very common intrinsic disruptive substances and reactive oxygen species, such as hydrogen peroxides (H_2O_2) (Xu et al., 2013) and superoxide anion radical ($O_2^{\cdot-}$) (Wang et al., 2018a) and malondialdehyde (MDA) (Tian et al., 2019), usually accumulate under oxidative conditions posed by waterlogging. These substances are detrimental to plant growth and development because they reduce plant photosynthesis by causing leaf chlorosis, root death, and a reduction in chlorophyll content and chloroplast damage (Parent et al., 2008; Broughton et al., 2015; Zhang et al., 2022). In contrast, when these substances are activated during waterlogging, plants also use defensive mechanisms and counteract them by adapting to anaerobic conditions. Adaptive mechanisms are normally characterized morphologically, biochemical, anatomically, and molecularly, with the aim of discovering resistance mechanisms for plant survival. Popularly reported morphological defensive mechanisms mainly include adventitious root formation (Broughton et al., 2015), hypertrophic lenticel formation (Le Provost et al., 2016), aerenchyma air space formation (Chávez-Arias et al., 2019), radial oxygen loss spaces (Dodd et al., 2013), and formation of apical meristem (Blokhina et al., 2001). Biochemical defensive mechanisms consist of the production of enzymatic scavengers such as peroxidase (POD), superoxide dismutase (SOD), dehydroascorbate reductase (DHAR), catalase (CAT), monodehydroascorbate reductase, (MDHAR), glutathione reductase (GR), and non-enzymatic scavengers, such as proline (Zhang et al., 2016; Chávez-Arias et al., 2019; Hasanuzzaman et al., 2020; Park et al., 2020). In addition, hormone biosynthesis, such as ethylene abscisic acid, gibberellins, and auxin biosynthesis, has been reported to help in plant signaling and resistance to waterlogging stress (Coutinho et al., 2018; Zhao et al., 2018).

Cotton is a prevalent crop due to its chief source of high-quality fiber, making it an important asset to mankind. It is largely cultivated in more than 80 countries worldwide, including China, India, the USA, and Pakistan (Zahra et al., 2019). However, it is commonly known to be susceptible to waterlogging stress (Bange et al., 2004). Waterlogging stress damages cotton plant growth and development, as well as nutrient uptake (Dodd et al., 2013), resulting in yield reduction (Cao et al., 2012; Najeeb et al., 2015). Existing research on cotton tolerance mechanisms has proven that cotton adapts to waterlogging using three primary mechanisms: escape, quiescence adaptation, and self-regulation and compensation (Zhang et al., 2020). The plant uses the escape strategy under short-term waterlogging stress by increasing adventitious root growth, producing aerenchyma, and accelerating stem elongation (Hussain et al., 2014). Self-regulation and compensation strategies include indeterminate growth habits, compensatory abilities, and the acceleration of plant growth and development after stress recovery (Sadras, 1995; Zhang et al., 2017). Finally, the quiescent adaptation strategy involves changes in the activity of protective enzyme systems, changes in hormone concentration and distribution, differential expression of genes (Zhang et al., 2020), and hydrogen peroxide H_2O_2 signaling (Zhao et al., 2018). In China, areas closer to the Yangtze River and the Yellow River along the middle and lower plains have high potential for supporting plantations of fast-growing plants in the future. However, these places are highly flooded (Gong et al., 2007). Moreover, in the context of China's global climate change records, flooding is a frequently occurring abiotic stress, in addition to drought, which poses yearly threats to agricultural productivity (Qian et al., 2020). Furthermore, an extreme number of reports on cotton tolerance mechanisms have centered on escape strategies, self-regulatory strategies, and compensational waterlogging stress adaptability strategies (Yin et al., 2010). However, research on quiescence adaptability, which involves more molecular studies by coupling transcriptomics and metabolomics resistance mechanisms, is minimal. In addition, there is lesser information of cotton-tolerant responses to long-term waterlogging. Therefore, the objectives of this study were to observe the morphological changes in "CJ1831056" and "CJ1831072" cotton genotypes during long-term waterlogging stress and primarily the potential tolerance mechanisms of cotton at the transcriptome and metabolome profiles in response to waterlogging stress. To attain this goal, we first revealed induced waterlogging-responsive genes through the analysis of differentially expressed genes. Subsequently, we classified differentially expressed metabolites during long-term waterlogging using metabolomics analysis. Our results can provide a system-level context for advanced studies on the potential mechanism of waterlogging resistance in cotton and further contribute to the breeding of waterlogging-tolerant lines.

Abbreviations: AAO, L-Ascorbate oxidase; ADH, Alcohol dehydrogenase; APX, L-Ascorbate peroxidase; BGLU, Beta-glucosidase; CAD, Cinnamyl alcohol dehydrogenase; CAT, Catalase; CYP98A3, Cytochrome P450, family 98, subfamily A, polypeptide 3; DEGs, Differentially expressed genes; ERF, Ethylene responsive factor; FAH, Ferulic acid 5-hydroxylase; FC, Fold change; GR, Glutathione reductase; KEGG, Kyoto Encyclopedia of Genes and Genomes; LC-MS/MS, Liquid chromatography–mass spectrometry; MDA, Malondialdehyde; MDAR, Monodehydroascorbate reductase; MT, Metallothionein; NEG, Negative ion mode; PAL, PHE ammonia lyase; PCO, Plant cysteine oxidase; PDC, Pyruvate decarboxylase; POD, Peroxidase; POS, Positive ion mode; RBOH, Respiratory burst oxygen homolog; ROS, Reactive oxygen species; SOD, Superoxide dismutase; SUS, Sucrose synthase; TFs, Transcription factors; XTH, Xyloglucan endotransglucosylase/hydrolase.

Materials and methods

Plant material

Two cotton (*Gossypium hirsutum* L.) lines "CJ1831056 and CJ1831072" were chosen for this study. Seed materials were sourced from the Institute of Cotton Research, Chinese Academy of Agricultural Sciences (ICRCAAS). Cotton seeds were planted in a

controlled environment (greenhouse) under natural lighting and temperature (22.2°C/day and 18.2°C/night) and relative humidity ranging from 70% to 85%.

Waterlogging stress treatment and sampling

After seed emergence, seedlings were treated with a modified Hoagland nutrient solution containing 5 mM nitrate (NO_3^-), as described previously (Sharma et al., 2019). After 30 days of culturing seedlings, plants were screened at a 0-day treatment as a control and at 5-, 10, 15-, and 20-day treatments to determine the ideal time points for waterlogging for subsequent experiments, where pots were kept in 5-cm-deep tap water (waterlogged, WL). After waterlogging stress time-point screening, vigorous physio-morphological changes in cotton leaves, stems, and roots were observed at both 10 and 20 days of stress. Hence, control (CK) experiments at 0 days and treated groups at 10 and 20 days of waterlogging time points were used. The primary roots, lateral roots, and adventitious roots were collected from each plant, frozen separately in liquid nitrogen, and stored at −80°C.

RNA-seq library preparation

A total of l μg of RNA per sample was used as the input material for the RNA sample preparations. Sequencing libraries were generated using the NEBNext® Ultra™ RNA Library Prep Kit for Illumina (NEB, USA) following the manufacturer's recommendations. Index codes were added to attribute sequences to each sample. mRNA was purified from total RNA using poly-T oligo-attached magnetic beads. Fragmentation was carried out using divalent cations at elevated temperatures in NEBNext First Strand Synthesis Reaction Buffer (5×). First-strand cDNA was synthesized using random hexamer primers and M-MuLV Reverse Transcriptase. To synthesize the second cDNA strand, the first cDNA strand was combined with DNA Polymerase I and RNaseH. The remaining overhangs were converted into blunt ends via exonuclease and polymerase activities. After adenylation of the 3′ ends of the DNA fragments, the NEBNext Adaptor with a hairpin loop structure was ligated to prepare for hybridization. To select cDNA fragments that were preferentially 250–300 bp in length, the library fragments were purified with the AMPure XP system (Beckman Coulter, Beverly, USA). Then, 3 μl of USER Enzyme (NEB, USA) was used with size-selected, adaptor-ligated cDNA at 37°C for 15 min, followed by 5 min at 95°C before PCR. PCR was then performed with Phusion High-Fidelity DNA polymerase, universal PCR primers, and Index(X) Primer. Finally, PCR products were purified (AMPure XP system), and library quality was assessed using the Agilent Bioanalyzer 2100 system. The clustering of the index-coded samples was performed on a cBot cluster generation system using the TruSeq PE Cluster Kit v3-cBot-HS (Illumina), according to the manufacturer's instructions. After cluster generation, the library preparations were sequenced on an Illumina NovaSeq platform, and 150-bp paired-end reads were generated.

RNA-seq analysis

Reference genome and gene model annotation files were downloaded directly from the Cotton Genome website. The index of the reference genome was built using Hisat2 v2.0.5, and paired-end clean reads were aligned to the reference genome using Hisat2 v2.0.5. Feature Counts v1.5.0-p3 was used to count the read numbers mapped to each gene. The fragments per kilobase of exon per million mapped (FPKM) of each gene was calculated based on the length of the gene and the read count mapped to this gene. Based on the raw count data, differential expression analysis between samples was performed using the DESeq2 R package (1.16.1). The resulting P-values were adjusted using Benjamini and Hochberg's approach to controlling the false discovery rate. Genes with an adjusted P-value<0.05 found by DESeq2 were assigned as differentially expressed.

GO and KEGG enrichment analyses

Gene Ontology (GO) enrichment analysis of differentially expressed genes was implemented using the cluster Profiler R package, in which gene length bias was corrected. GO terms with a corrected P value of less than 0.05 were considered significantly enriched by differentially expressed genes. KEGG is a database resource for understanding high-level functions and utilities of the biological system, such as the cell, organism, and ecosystem, from molecular-level information, especially large-scale molecular datasets generated by genome sequencing and other high-throughput experimental technologies (http://www.genome.jp/kegg/). We used the cluster Profiler R package to test the statistical enrichment of differentially expressed genes (DEGs) in the KEGG pathways.

Metabolite extraction, LC-MS/MS analysis, and metabolite quantification

For metabolite extraction, 20 mg of the sample was weighted onto an EP tube after grinding with freeze-drying, and 1000 μl of extract solution (methanol: water = 3: 1, with isotopically labeled internal standard mixture) was added. Then, the samples were homogenized at 35 Hz for 4 min and sonicated for 5 min in an ice water bath. The homogenization and sonication cycles were repeated three times. The samples were then incubated at −40°C for 1 h before being centrifuged at 12,000 rpm (RCF = 13,800*g*, R = 8.6 cm) for 15 min at 4°C. The resulting supernatant was transferred to a fresh glass vial for analysis. The quality control (QC) sample was prepared by mixing an equal aliquot of supernatants from all samples. LC-MS/MS analyses were performed using an UHPLC system (Vanquish, Thermo Fisher Scientific) with a UPLC HSS T3 column (2.1 mm × 100 mm, 1.8 μm) coupled to a Q Exactive HF-X mass spectrometer (Orbitrap MS, Thermo). To visualize group separation and find significantly changed metabolites, supervised orthogonal projections to latent structures-discriminate analysis (OPLS-DA) were applied. Then, a sevenfold cross validation was performed to calculate the

values of R2 and Q2. R2 indicates how well the variation of a variable is explained, and Q2 indicates how well a variable can be predicted. To check the robustness and predictive ability of the OPLS-DA model, 200 permutations were conducted. Afterward, the R2 and Q2 intercept values were obtained. Here, the intercept value of Q2 represents the robustness of the model, the risk of overfitting, and the reliability of the model, which will be better the smaller the intercept value. Furthermore, in the OPLS-DA, the value of variable importance in projection (VIP) of the first principal component was obtained. It summarizes the contribution of each variable to the model. The metabolites with VIP >1 and P< 0.05 (Student t test) were considered significantly changed metabolites. In addition, commercial databases, namely, KEGG (http://www.genome.jp/kegg/) and MetaboAnalyst (http://www.metaboanalyst.ca/), were used for pathway enrichment analysis.

Validation of RNA-seq by qRT-PCR

Quantitative real-time PCR (qRT-PCR) was conducted using six genes, namely, *XTH9*, *PER1*, *RAP2-3*, metallothionein (*MT1*), *RbohD*, and *ADH*. Respective qRT-PCR primers are listed in Supplementary Table S6. Total RNA was extracted from upland cotton fiber using TRIzol Reagent. cDNA synthesis was performed using an RT reagent kit (Tiangen, China). qRT-PCR was analyzed in a 20-µl reaction system (including 10 µl SYBR Premix Ex Taq™ II (2×), 2 µl cDNA, and 0.8 µl upstream and downstream primers) and a simple procedure (50°C for 2 min; 40 cycles at 95°C for 30 s, 95°C for 5 s, and 60°C for 20 s; and a final extension at 72°C for 10 min). Three biological repeats were included for each condition, and the GhUBQ gene was used as a control. The relative expression levels were calculated using the $2^{-\Delta\Delta Ct}$ method.

Results

Morphological variations of the two cotton genotypes to waterlogging stress

Morphological changes between CJ1831056 and CJ1831072 genotypes following 0 days of no stress and then 10 and 20 days of waterlogging stress were assessed. At 10 days of waterlogging compared with the control, the two cotton genotypes displayed green leaves and no signs of damage (Figures 1A, B). Formation of hypertrophic lenticel and few adventitious roots on cotton stems and roots were observed at 10 days of stress in both genotypes (Figures 1A, B). Although cotton leaves of both genotypes turned yellow and chlorotic at 20 days of stress, formation of hypertrophic lenticel and adventitious roots was vigorous in CJ1831056 and CJ1831072 (Figures 1A, C).

Transcriptome analysis

Here, a total of 18 qualified libraries were established. Clean reads were obtained by removing low-quality reads. Approximately 800 million clean reads were obtained with a total of 120.07 Gb of sequence data. Clean readings at Q20 and Q30 were over 98% and 93%, respectively (Supplementary Table 1). Principal component analysis (PCA) revealed that replicated biological samples significantly clustered together. This shows that biological replicates, consistent samples, and sequencing results were reliable (Figure 1B). Pearson's correlation coefficient (PC) analysis was performed to check the correlation between all samples (Figure 1C). Results show a higher correlation at 10 and 20 days of replicated samples compared with 0 days. Furthermore, transcriptomics differentially expressed genes revealed 101,599 genes. To effectively analyze and interpret the DEGs, a P-value< 0.05 and |log2 fold change| ≥2 were used to effectively analyze and interpret DEGs as visualized among comparisons (9) (Figure 1D). In general, CJ56T10 vs. CJ56T0 and CJ56T20 vs. CJ56T0 had 41,832 DEGs higher than 8,306 DEGs in CJ72T10 vs. CJ72T0, and CJ72T20 vs. CJ72T0 during waterlogging stress (Figure 1D). This shows that the CJ1831056 genotype has a stronger response to waterlogging than the CJ1831072 genotype at the transcription level. Moreover, 33,547 DEGs were assigned for gene regulation analysis using a Venn diagram. A total of 1,862 upregulated and 843 downregulated DEGs were shared among all four comparisons (Figure 1E). This revealed that upregulated genes were more responsive to waterlogging than downregulated genes. Hence, CJ56T10 vs. CJ56T0, CJ56T20 vs. CJ56T0, CJ72T10 vs. CJ72T0, and CJ72T20 vs. CJ72T0 comparisons were selected for further analysis. For GO analysis, the total annotated number of genes was 43,894, into three ontologies (Supplementary Table 2; Additional File 1). In the biological process category, metabolic (17,784), cellular (15,675), and single-organism processes (10,731) were recorded to have a significantly expressed number of genes. The cellular component category was mainly cell (4,972), cell parts (4,972), and organelles (3,445). Molecular function categories included binding (25,575) and catalytic activity (17,034), as highly represented (Supplementary Table 2). For subsequent analysis, the assembled gene functions were evaluated through a search against the KOG database for functional prediction and classification (Supplementary Table 2).

Pathway analysis of DEGs

Pathway analysis of DEGs was conducted by using the Kyoto Encyclopedia of Genes and Genomes (KEGG) pathway database. Various pathways were induced in cotton roots by waterlogging stress (Supplementary Table 3). The top enriched KEGG pathways among upregulated and downregulated DEGs in CJ1831056 and CJ1831072 are shown in Supplementary Table 3. A higher differentially expressed gene count was recorded in phenylpropanoid biosynthesis, glycolysis, gluconeogenesis, and starch and sucrose metabolism pathways (Figures 2A–D and Supplementary Table 3). The phenylpropanoid biosynthesis pathway, popularly known to regulate under hypoxia and waterlogging conditions (Zhang et al., 2017; Yu et al., 2020), revealed a higher expression of peroxidases (EC: 1.11.1.7) and beta glucosidases (EC: 3.2.1.21) (Figure 2E). This is a clear indication of ROS scavenging and activation of the plant defense system, hormone production, and cell wall lignification (Kongdin et al., 2021). In the glycolysis pathway, phosphofructokinase (EC: 2.7.1.11), alcohol dehydrogenase (EC: 1.1.1.1), and pyruvate decarboxylase-2

10.3389/fpls.2023.1088537

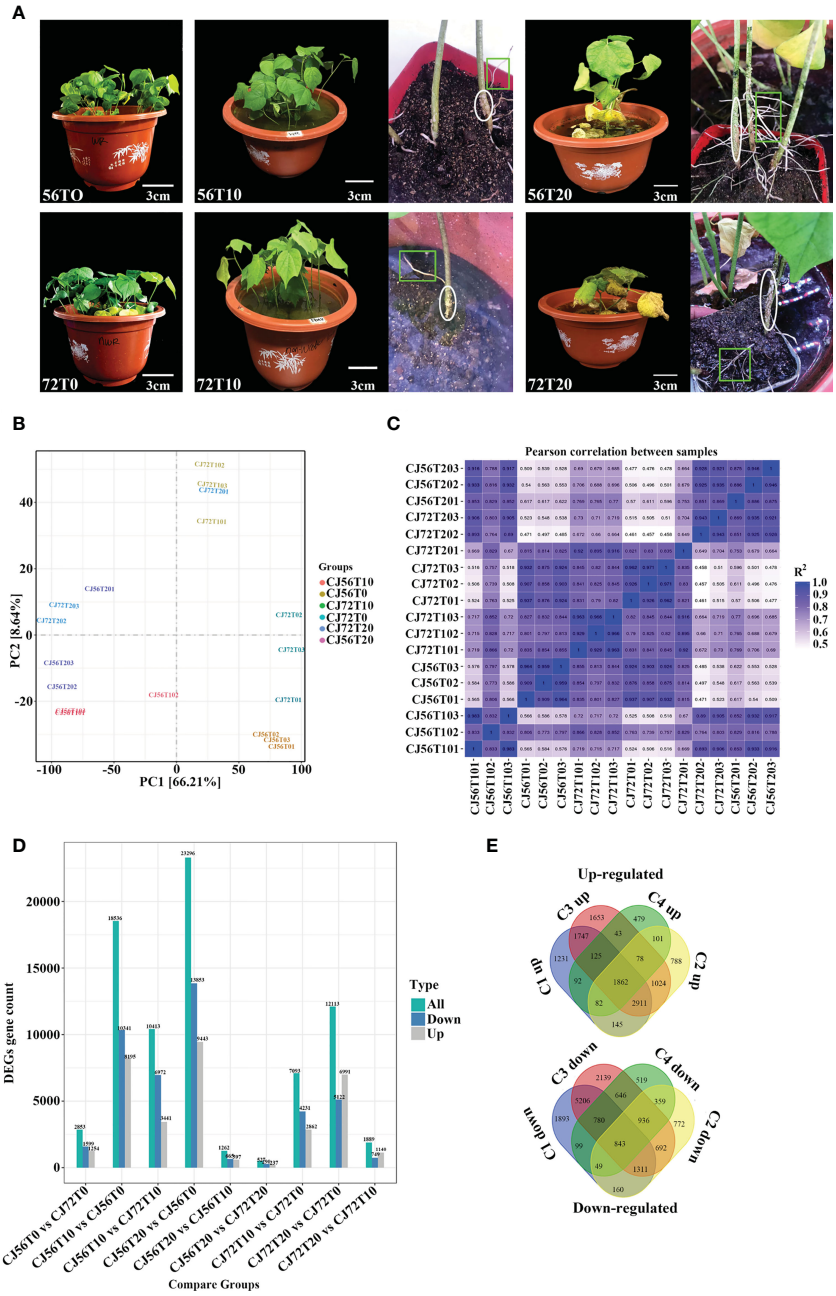

FIGURE 1
Observable morphological changes and gene expression analysis of "CJ1831072" and "CJ1831056" genotypes under waterlogging stress. **(A)** Cotton seedling morphological changes after 30 days of culture in 5 cm of water depth above the soil surface for 10 and 20 days, with 0 days as the control. Circles indicate hypertrophic lenticels, whereas squares/rectangles show adventitious roots. Scale bar: 3 cm. **(B)** Principal component analysis (PCA) between samples. **(C)** Correlation between samples obtained for cotton genotypes under the waterlogging treatment. The color of the box represents the degree of correlation; deep blue represents the highest degree of correlation, and light blue represents the lowest degree of correlation. **(D)** Total differentially expressed genes. **(E)** Venn diagram of both upregulated and downregulated genes. C1up/down, C2up/down, C3up/down, and C4up/down denote CJ656T10vsCJ56T0, CJ72T20vsCJ72T0, CJ56T20vsCJ56T0, and CJ72T10vsCJ72T0, respectively.

(EC: 4.1.1.1) genes were significantly expressed in CJ1831072 than in CJ1831056 (Figure 2F). Starch and sucrose metabolism pathways are known to be induced by waterlogging stress (Loreti et al., 2018). Similarly, starch synthase (EC: 2.4.1.21) SS4, sucrose synthase (EC: 2.4.1.13), chloroplast beta-amylase (EC: 3.2.1.2), and hexokinase (EC: 2.7.1.1) genes significantly responded to waterlogging in both cotton genotypes (Figure 2G).

Effect of differentially expressed ROS gene and related antioxidant protection

Identification of ROS and antioxidant and redox-sensing mechanisms plays a key role in waterlogging tolerance mechanisms. The ROS-generating *RBOH-D* (107905423) gene showed higher upregulation at 20 days of waterlogging in

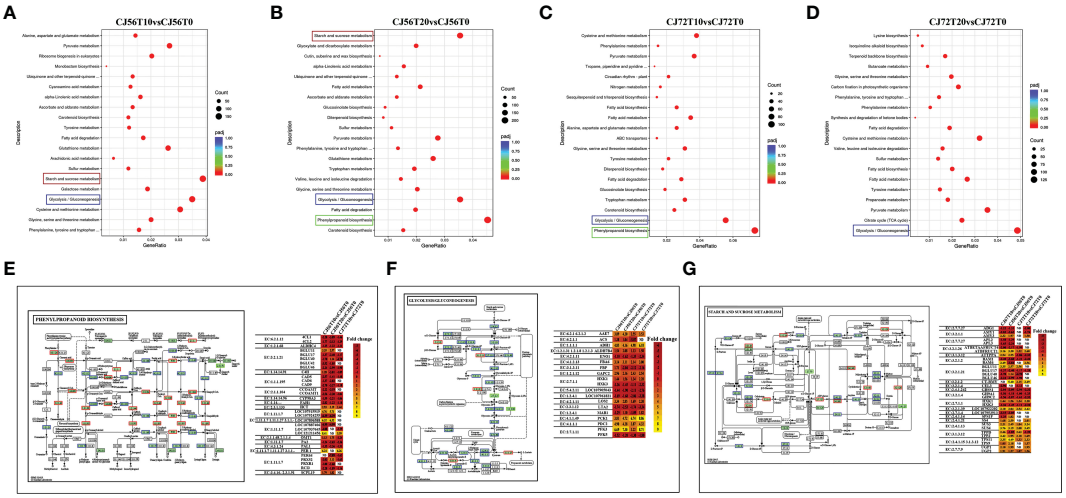

FIGURE 2
Pathway analysis. **(A–D)** KEGG enrichment analysis of top 20 most significant enrichment pathways in CJ1831056 and CJ1831072 at 10 and 20 days of stress. **(E)** Pattern diagram of the phenylpropanoid biosynthesis pathway with the relative expression level of DEGs. **(F)** Pattern diagram of the glycolysis and gluconeogenesis pathways with the relative expression level of DEGs. **(G)** Pattern diagram of the starch and sucrose metabolism pathways with the relative expression level of DEGs. Yellow color represents upregulated genes, red color represents downregulated genes, and blue represents both upregulated and downregulated genes. Respective relative expression levels of DEGs measured by log2 ratio (fold change between waterlogging treatment and control). Positive fold-change values (yellow) indicate upregulation, whereas negative fold-change values (red) indicate downregulation. ND indicates no detected expression.

CJ1831056 than in CJ1831072 (Figure 3). Moreover, two *CAT* genes (107905765 and 107905725) were more upregulated in CJ1831056 than in CJ1831072 at 20 days of waterlogging, compared to the control (Figure 3). Peroxidase DEGs played a role in antioxidant signaling under waterlogging stress in cotton. For instance, 1-*Cys peroxiredoxin* (107916248) and *1-Cys peroxiredoxin-like* (107896588) were upregulated more after 10 and 20 days of waterlogging in both genotypes compared with the control. Four SOD genes were also induced in ROS scavenging in defense against waterlogging stress. Among DEGs involved in SOD, superoxide dismutase (FE) % chloroplastic 2C was more upregulated in CJ1831072 than in CJ1831056 at 10 days of waterlogging, whereas superoxide dismutase (MN) % mitochondrial was more upregulated in CJ1831056 than in CJ1831072. *GR* genes (107924091 and 107923983), *DHAR* genes (107925966 and 107959887), L-ascorbate oxidase (*AAO*) genes (107943178, 107951678, and 121209663), and L-ascorbate peroxidase (*APX*) genes were also induced by waterlogging in cotton roots (Figure 3).

Analysis of DEGs for TFs induced by waterlogging

To further understand the potential tolerant mechanism of cotton toward genes waterlogging stress, highly responsive TFs were identified and analyzed. Interestingly, a considerable number of differentially expressed TFs were recorded. For instance, TFs such as *MYB DNA-binding*, *AP2*, *NB-ARC*, *NAM*, *bHLH*, *WRKY*, *LRRNT2*, *GRAS*, and *bZIP* were induced at 0, 10, and 20 days (Figure 4). However, among the two cotton lines, CJ1831056 genotypes showed higher recorded TFs than CJ1831072 genotypes. Parallel tendencies were also found, as DEGs downregulated were significantly higher than upregulated DEGs (Figure 4). Furthermore, among the TF families, differentially expressed *AP2* (2), *bZIP* (3), *bHLH* (1), *MYB* (1), *NAM* (1), and *WRKY* (2) were significantly upregulated in both genotypes. On the other hand, two *AP2*s, one *bZIP*, two *MYB*s, one *NAM*, and one *WRKY* gene were significantly downregulated (Table 1). However, similar genes of the same TF family showed a differential expression between the two genotypes.

Metabolome analysis of cotton root under waterlogging stress

For the UHPLC system, OPLS-DA and PCA were used to reduce dimensionality from metabolomics data groups generated by LC-MS/MS analyses. The ionization source of the QE platform is electrospray ionization, which comprises both positive ion modes (POS) and negative ion modes (NEG). The explanation and predictability values were measured for the first two principal components (PCs) for POS (23.3% and 20%) and NEG (30.6% and 19.7%). In general, S56T10 and S72T10 have strong relationships with quality control (QC). However, the treated groups for 20 days were more significant in POS and NEG (Figure 5A). In addition, the OPLS-DA score chart differences between all groups of samples were significant (within the 95% confidence interval), confirming that the OPLS-DA results were valid (Figure 5B). The separation of control groups from treated groups and variation within treated groups indicate clear differences in metabolite accumulation between samples. Metabolite studies also show more differentially expressed metabolites (DEM) of 171 DEM

10.3389/fpls.2023.1088537

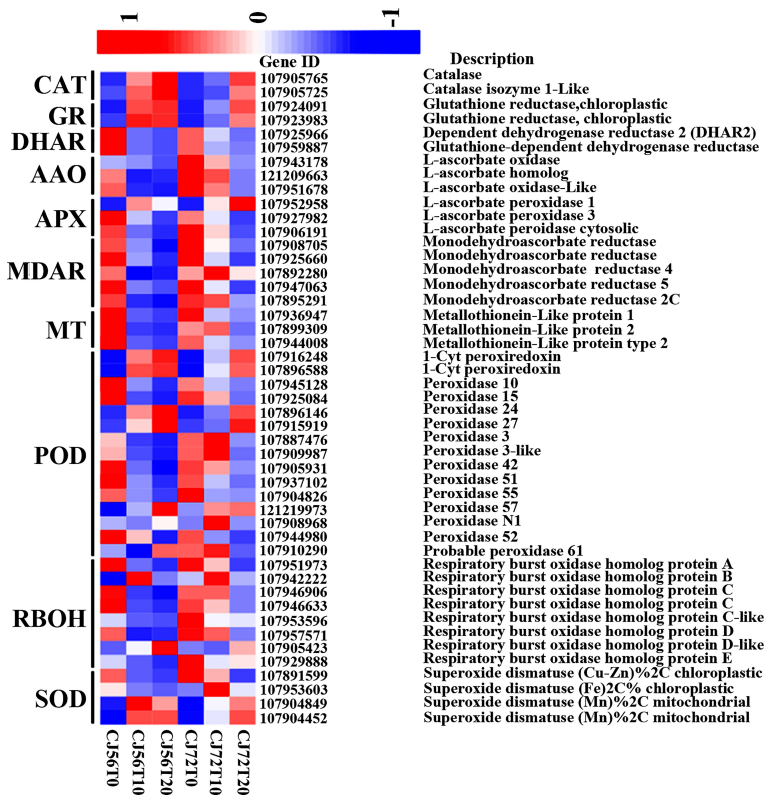

FIGURE 3
Heatmap analysis of DEGs involved in ROS and antioxidant signaling. The bar represents the scale of the expression levels of each gene (log2 FPKM) in each sample, as indicated by red/blue rectangles. Red rectangles represent the high expression of genes, and blue rectangles represent the low expression.

at 20 days and 52 DEM at 10 days of stress compared to 51 DEM at 0 days of no stress in both POS and NEG metabolite detection coverage (Figure 5C). As shown in Table 2, top 20 significantly accumulated metabolites were selected by their respective fold change values and OPLS-DA methods (Table 2). Zero days of waterlogging stress revealed two significantly upregulated metabolites (dibutyl phthalate 1.6 FC and equol 1.1 FC) and one downregulated metabolite (15-KETE −1.5 FC) (Table 2). At 10 days of waterlogging, phenylpropanoids and polyketides (nobiletin −3.1 FC), organoheterocyclic (urocanic acid −2.3 FC), and benzenoids

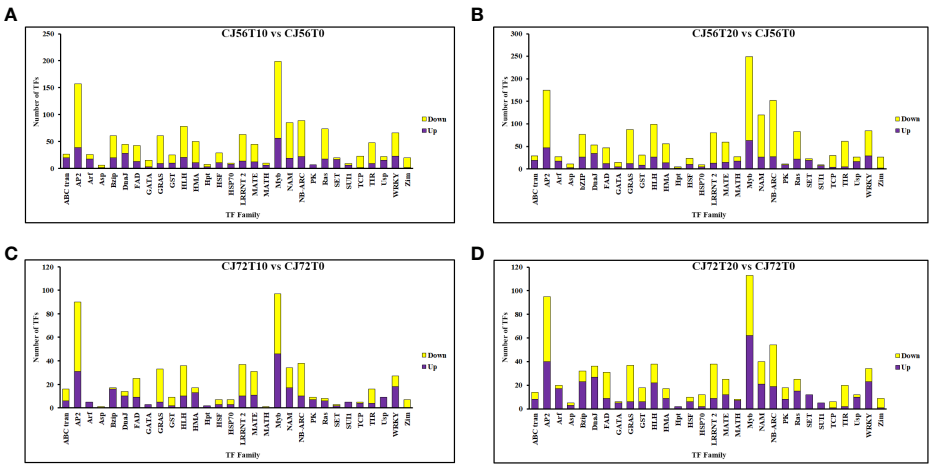

FIGURE 4
Differentially expressed transcription factor gene count in cotton roots during waterlogging. **(A)** CJ56T10 vs. CJ56T0 combination. **(B)** CJ56T20 vs. CJ56T0 combination. **(C)** CJ72T10 vs. CJ72T0 combination; **(D)** CJ72T20 vs. CJ72T0 combination.Yellow denotes downregulation, and purple denotes upregulation.

10.3389/fpls.2023.1088537

TABLE 1 Comparisons of the expression levels of DEG transcription factors induced in "CJ1831056" and "CJ1831072" varieties. 'ND' represents not detected.

	Gene ID	56T10 vs. 56T0	56T20 vs. 56T0	Gene description	72T10 vs. 72T0	72T20 vs. 72T0
TF category		Log2FC	Log2FC		Log2FC	Log2FC
AP2	LOC107889672	5.7	6.5	Ethylene-responsive transcription factor ABR1-like	3.3	5.4
AP2	LOC107917284	5.0	5.1	Ethylene-responsive transcription factor ERF071	4.9	6.1
AP2	LOC121220769	−3.9	−6.8	AP2-like ethylene-responsive transcription factor	−8.0	−7.8
AP2	LOC107929210	−5.8	−2.0	Ethylene-responsive transcription factor ERF027-like	ND	−2.2
bZIP_1	LOC107913052	4.0	3.2	bZIP transcription factor 11-like	3.0	3.4
bZIP_1	LOC107901213	3.2	2.5	bZIP transcription factor 2-like	2.4	2.6
bZIP_1	LOC107946949	2.4	2.3	bZIP transcription factor 59	1.5	4.1
bZIP_1	LOC107951428	−3.4	−5.0	Transcription factor TGA3-like	ND	ND
bHLH	LOC107889526	3.2	3.3	Transcription factor bHLH130	2.0	3.1
Myb	LOC107946442	5.3	4.7	Transcription factor HHO2 (early flowering Myb)	1.7	3.4
Myb	LOC107889761	−3.7	−5.4	Transcription factor DIVARICATA	ND	ND
Myb	LOC107922466	−4.1	−6.2	Myb-related protein 308	ND	ND
NAM	LOC121231838	−4.0	−2.8	NAC domain-containing protein 4-like	ND	ND
WRKY	LOC107923243	3.4	2.7	Probable WRKY transcription factor 27	2.6	2.7
WRKY	LOC107918521	2.0	2.2	Probable WRKY transcription factor 57	1.3	2.7
WRKY	LOC107920274	−1.1	−1.3	Probable WRKY transcription factor 2	ND	−1.1

(sinapyl alcohol −1.8 FC) were significantly downregulated metabolites responsive to waterlogging. In contrast, an organic acid compound, galactaric acid 3.0 FC, was significantly upregulated at 10 days (Table 2). Moreover, 20 days of waterlogging revealed highly significantly upregulated metabolites including lipids and lipid-like molecules (gamma-linolenic acid 1.1 FC and testosterone 2.0 FC), organic acids, and derivatives (L-asparagine 1.5 FC, pyrrolidonecarboxylic acid 1.3 FC, and L-valine 1.1 FC) (Table 2). Conversely, significantly repressed metabolites responsive to 20 days of waterlogging were organoheterocyclic (E,E-trichostachine −3,6FC), nucleosides, nucleotides, analogue compound (adenosine monophosphate), organic acids and derivatives (N-acetyl-L-phenylalanine −1.9 FC and citric acid −1.7 FC), organic oxygen compounds (melibiose −1.2 FC), benzenoid (carmine red −2.0 FC), and phenylpropanoids and polyketides (procyanidin B2 −1.6 FC) (Table 2).

Correlation analysis between DEGs and metabolite in phenylpropanoid biosynthesis during waterlogging

To investigate the relationship of DEGs and differentially accumulated metabolites in cotton under long-term waterlogging, a correlation analysis was performed between DEGs in CJ56T20 vs. CJ56T0 and CJ72T10 vs. CJ72T0 and between POS and NEG highly expressed metabolites with their respective KEEG ID. The correlation of each DEG–metabolite pair was assessed at a correlation coefficient of 0.89. The details of the representative phenylpropanoid DEG–metabolite correlation analysis are listed in Additional file 2. In addition, the correlations of representative DEG–metabolites are visualized in Figure 6. In CJ56T20 vs. CJ56T0, POS metabolites correlated with DEGs; adenosine, L-asparagine, L-valine, and testosterone metabolites had a considerably negative correlation with DEGs, such as *PA2*, *PAL1*, *PAL2*, *BGLU42*, *C4H*, *CYP98A3*, and *FAH1*. In contrast, melibiose, positively correlated with *PRX52* whereas sinapyl alcohol correlated positively with *PER64* (Figure 6A). In the NEG CJ56T20 vs. CJ56T0 comparison with metabolites, galactaric acid forms a significant negative correlation with DEGs, such as *CYP98A3*, *BGLU42*, *BGLU46*, *PAL1*, *PA2*, *PRX52*, and *RCI3* (Figure 6A). Conversely, hypoxanthine metabolites formed significant positive correlations with *CYP98A3*, *BGLU42*, *PAL1*, *PRX52*, and *RCI3* (Figure 6A). Furthermore, in CJ72T10 vs. CJ72T0, DEGs *BGLU40*, *BGLU46*, *107937102*, *107936009*, *107926676*, *CAD9*, and *CAD5* were significantly positively correlated with procyanidin B2 metabolite. However, these DEGs were negatively correlated with adenosine, L-valine, L-asparagine, and testosterone metabolites (Figure 6B).

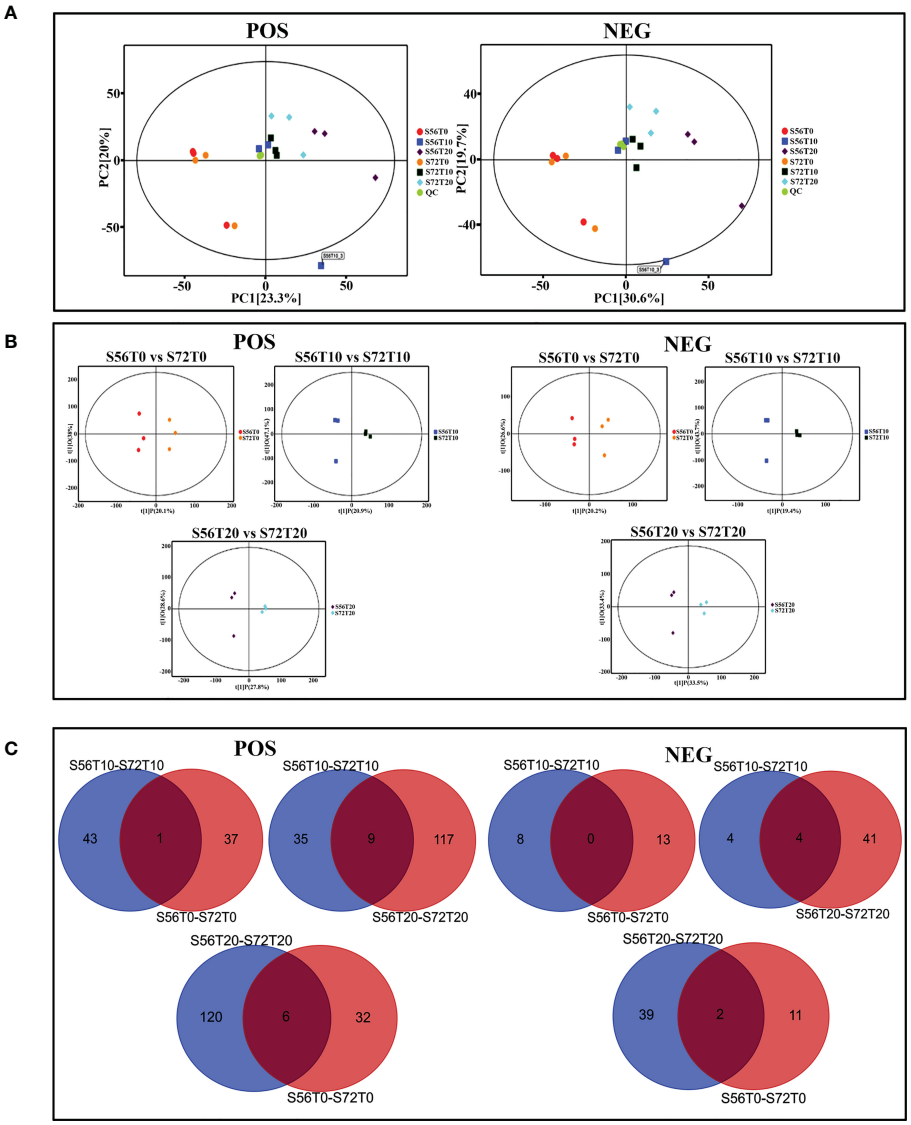

FIGURE 5
PCA score plot, OPLS-DA scatter plot, and Venn diagram analysis. **(A)** PC1 and PC2 coordinates for both POS and NEG coordinates. Each scatter point represents a sample, and the color and shape of the scatter point represent different groups. **(B)** OPLS-DA models of positive/negative ion modes for S56T0 vs. S72T0, S56T10 vs. S72T10, and S56T20 vs. S72T20. Ordinate t(1)P denotes the predicted principal component score for the first principal component, whereas ordinate t(1)O represents orthogonal principal component scores. All samples are within the 95% confidence interval (Hotelling's T-square eclipse). **(C)** Venn diagram showing differentially upregulated and downregulated metabolites. POS denotes positive ion mode, and NEG denotes negative ion mode.

Conversely, *RHS19*, *RCI3*, *121215291*, *121214674*, *121209489*, and *121202811* DEGs significantly positively correlated with metabolites, carmine red (Figure 6B).

DEGs validation by qRT-PCR

To verify the accuracy of the DEGs, qRT-PCR analysis was conducted to compare the consistency in the expression of some genes (Wang et al., 2022). Six differentially expressed genes, namely, *ADH-class-P-like* (107910431), *PER1* (107916248), *RbohD* (107957571), *RAP2-3* (107896651), *MT1* (107936947), and *XTH9* ((107959252), were randomly chosen (Figure 7). As shown in Figure 7, *ADH-class-P-like* and *XTH9* genes had significant expression levels during 10 days of waterlogging stress in CJ1831056 than in CJ1831072, whereas the relative expression levels in *RbohD*, *RAP 2-3*, and *MT1* were significantly higher in CJ1831072 than in CJ1831056 (Figure 7). In addition, the relative expression levels of *PER1* and *ADH-class-P-like* were significantly higher at 20 days of waterlogging in CJ1831056 than in CJ1831072, whereas in *RAP 2-3* and *MT1* genes at 20 days of waterlogging, significant expressions were observed in CJ1831072 than CJ1831056 (Supplementary Table 6 and Figure 7). The expression patterns of five out six genes were consistent with RNA-seq data (Figure 7). These results highly confirm the credibility of the RNA-seq results.

TABLE 2 Top 20 important POS/NEG metabolites with their kyoto encyclopedia of genes and genomes identifier number (KEGG ID/PubChem CID/Metabolite ID) and molecular formula (MF), identified through significant analysis of metabolites (SAM) and orthogonal partial least square discrepant analysis (OPLS-DA) in CJ1831056 and CJ1831072 cotton genotypes.

Stress time	Metabolite name	Compound ID	Compound class	Molecular formula	VIP	FC	Metabolite type
	Dibutyl phthalate	C14214	Benzenoids	C_9H_7NO	2.21	1.6	POS
Zero stress	Equol	C14131	Phenylpropanoids and polyketides	$C_{15}H_{14}O_3$	2.07	1.1	POS
	15-KETE	C00457	Lipids and lipid-like molecules	$C_{20}H_{30}O_3$	1.93	−1.5	NEG
10 days	Nobiletin	C10112	Phenylpropanoids and polyketides	$C_{21}H_{22}O_8$	1.66	−3.1	POS
	Urocanic acid	C00785	Organoheterocyclic compounds	$C_6H_6N_2O_2$	2.00	−2.3	POS
	Sinapyl alcohol	C02325	Benzenoids	$C_{11}H_{14}O_4$	1.36	−1.8	POS
	Galactaric acid	C00879	Organic oxygen compounds	$C_6H_{10}O_8$	2.06	3.0	NEG
20 days	(E,E)-Trichostachine	C10174	Organoheterocyclic compounds	$C_{16}H_{17}NO_3$	1.54	−3.6	POS
	L-Asparagine	C00152	Organic acids and derivatives	$C_4H_8N_2O_3$	1.71	1.5	POS
	L-Valine	C00183	Organic acids and derivatives	$C_5H_{11}NO_2$	1.89	1.1	POS
	Adenosine monophosphate	C00020	Nucleosides, nucleotides, and analogues	$C_{10}H_{12}N_5O_6P$	1.52	−2.7	NEG
	N-Acetyl-L-phenylalanine	C03519	Organic acids and derivatives	$C_{11}H_{13}NO_3$	1.01	−1.9	NEG
	Citric acid	C00158	Organic acids and derivatives	$C_6H_8O_7$	1.15	−1.7	NEG
	Gamma-linolenic acid	C06426	Lipids and lipid-like molecules	$C_{18}H_{30}O_2$	1.56	1.1	NEG
	Carmine red	C11254	Benzenoids	$C_{22}H_{20}O_{13}$	1.32	−2.0	NEG
	Procyanidin B2	C17639	Phenylpropanoids and polyketides	$C_{30}H_{26}O_{12}$	1.30	−1.8	POS
	Melibiose	C05402	Organic oxygen compounds	$C_{12}H_{22}O_{11}$	1.70	−1.2	POS
	Testosterone	C00535	Lipids and lipid-like molecules	$C_{19}H_{28}O_2$	2.21	2.0	POS
	Pyrrolidonecarboxylic acid	C02237	Organic acids and derivatives	$C_5H_7NO_3$	1.62	1.3	NEG

Discussion

Morphological tolerant mechanisms in waterlogged cotton

Plants' tolerance against flooding has always been extensively studied. However, the ability of plants to form adventitious roots and hypertrophic lenticel are major keys to tolerance against flooding (Else et al., 2009; Shimamura et al., 2010). Formation of adventitious roots at the hypocotyl internodes or at the stem base during waterlogging stress facilitates gas exchange and nutrition absorption (Qi et al., 2019). To a greater extent, these root tissues usually replace primary roots that die as a result of hypoxic stress, allowing normal growth and development to progress (Eysholdt-Derzsó and Sauter, 2019). In the present investigation, vigorous formation adventitious roots were found on waterlogged cotton root and stems. However, formation was numerous in the CJ1831056 genotype at 20 days of stress (Figure 1A). This illustrates that waterlogged cotton may use root and stem adventitious root formation as an escape tolerance strategy for subsequent respiration. Moreover, hormones play a vital role in adventitious root growth in plants' tolerance against waterlogging. For example, in cucumber, both auxins and ethylene were found to induce adventitious root growth under waterlogged conditions (Qi et al., 2019). Similarly, our present study showed a higher expression of differentially expressed auxins and ethylene genes in CJ1831056 genotypes in comparison with CJ1831072 genotypes (Figure S1). We hypothesized that both hormones may have a significant role in cotton tolerance against waterlogging stress. A recent report showed that a putative cell-wall-loosening enzyme xyloglucan endotransglucosylase/hydrolase (XTH) may be involved in cell wall metabolism during flooding-induced aerenchyma and adventitious root growth. Although the *XTH* gene family is thought to play a major role in cell wall remodeling, it is also proven to play a significant role in plants' tolerance against abiotic stresses such as flooding (Song et al., 2018). For instance in barley, upregulation of xyloglucan endotransglucosylase/hydrolase in roots improves waterlogging resistance (Luan et al., 2018). In cotton, Gh*XTH1* and Gh*XTH3* were upregulated in the roots of tolerant waterlogged genotypes (Zhang et al., 2020). Similarly in transgenic soybean, overexpression of the *AtXTH31* gene induced more adventitious roots in tolerance against flooding stress at the early seedling growth stage (Song et al., 2018). Clearly, our results showed the expression of four *XTH* DEGs (*XTH9*, *XTH22*, *XTH30*, and *XTH21*)

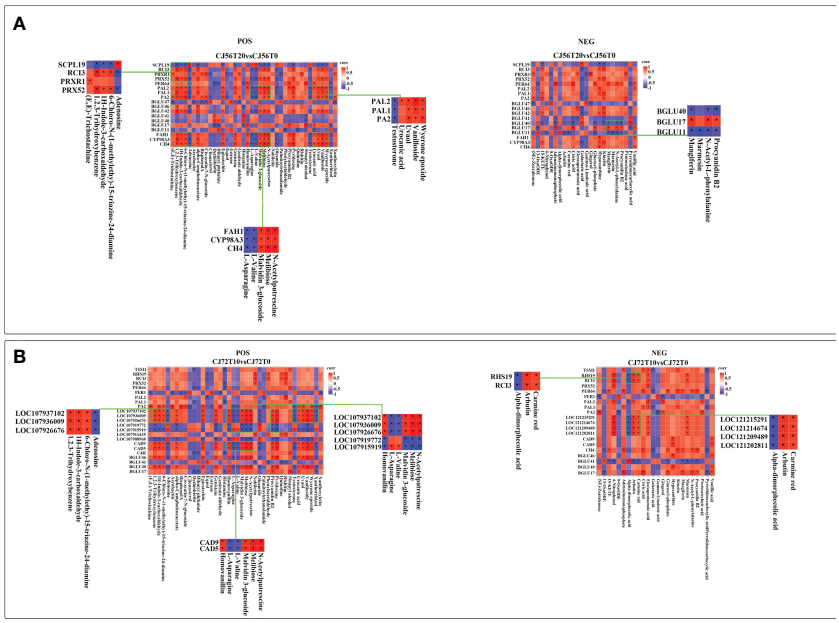

FIGURE 6
Spearman correlation analysis of DEGs in the phenylpropanoid biosynthesis pathway–accumulated POS and NEG metabolite modes. **(A)** Correlation between DEGs in CJ56T20 vs. CJ56T0 and metabolites in POS and NEG modes. **(B)** Correlation between DEGs in CJ72T10 vs. CJ72T0 and metabolites in POS and NEG modes. Each square of the heat map indicates a correlation coefficient score resulting from a Spearman correlation coefficient of 0.89. Red indicates a positive correlation, whereas blue indicates a negative correlation. An asterisk * indicates a significant correlation.

(Supplementary Table 4). We hypothesized that XTH-mediated cell wall adjustment may have a role in cotton adaptation to waterlogging stress, along with a useful gene family to develop flooding tolerance lines through molecular transgenic breeding study. Hypertrophic lenticel formation is a sign of tolerance in flooding conditions. Previous reports show that it regulates oxygen transport to the root by acting as a conduit through the cambium layer for gaseous uptake (Le Provost et al., 2016). As shown in Figure 1, 20 days of stress showed vigorous lenticel organs in the CJ1831056 cotton genotype than CJ1831072. This shows that induction of hypertrophic lenticel organs may play a vital role in cotton tolerance against waterlogging stress.

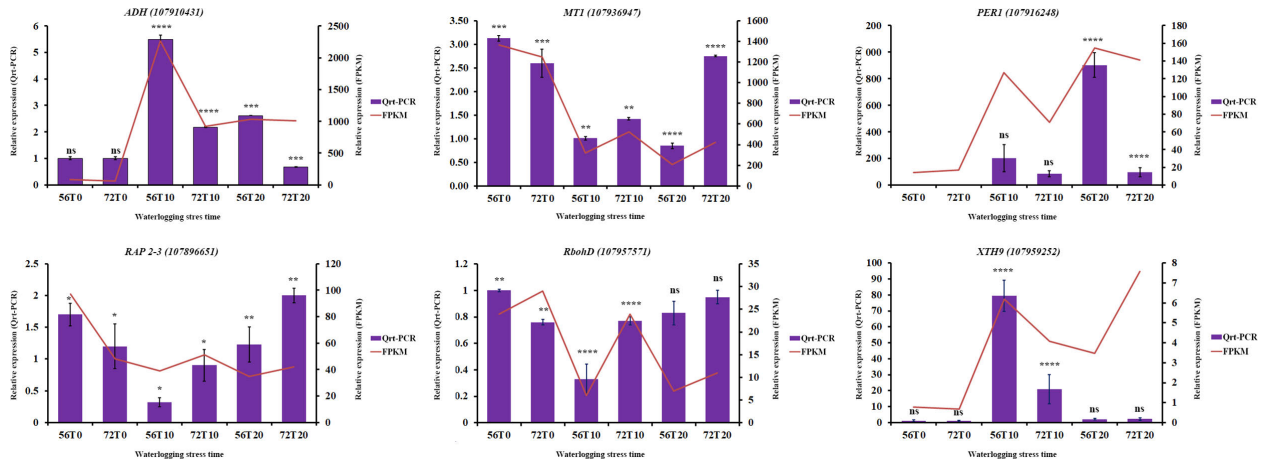

FIGURE 7
qRT-PCR verification of some key genes with RNA-seq expression. Bars represent qRT-PCR expression, and zigzags represent FPKM expression. Each bar represents the mean ± SD. Asterisk *, ***, and **** represent the significant differences (P< 0.1 to<0.05 two-way ANOVA with Tukey's HSD post-hoc test), whereas ns indicates no significance, respectively. 56T0/72T0, 56T10/721T0, and 56T20/72T20 denote 0 days of no waterlogging, 10 days of waterlogging, and 20 days of waterlogging, respectively.

Mechanism of ROS and antioxidant tolerance in waterlogged cotton

The incidence of abiotic stress activates ROS overproduction. ROS accumulation is usually regulated by the respiratory burst homolog D (*RbohD*) which enhances ROS production and then acts as a sensory signal for other cells to increase their ROS production (Mansoor et al., 2022). In high quantities, ROS negatively affects plant growth but, when minimized, is capable of inducing defense and hypersensitive responses and protein signaling (Qi et al., 2019; Fardus et al., 2021). In the present study, *RhohD* (107957571) was induced by waterlogging in both genotypes. However, it was more repressed in CJ1831056 than in CJ1821072 (Figure 3), indicating that ROS production may have played a significant role in waterlogged cotton tolerance, and moreover, CJ1831056 may have a tendency to withstand waterlogging stress by repressing ROS accumulation. A clear signal of high production of harmful ROS substance is proportional to the high production of antioxidant scavenging enzymes. In the present study, antioxidant scavenging enzymes such as PODs, DHARs, SODs, MDHAR, AAOs, CATs, MTs and APXs significantly expressed to reduce the harmful effects of ROS (Figure 3). According to existing reports, the CAT enzyme catalyzes the conversion of the ROS compound (H_2O_2) into water and oxygen (Kaushal et al., 2018). In addition, SOD is popularly known to remove ROS in anaerobic organisms based on the type of metal cofactor, and POD also catalyzes the reduction of hydrogen peroxide and alkyl hydroperoxides against oxidative damage (Nevalainen, 2010; Cheng et al., 2015). Clearly, this present study showed significant expressions of CAT and POD DEGs at 10 and 20 days in CJ1831056 than in CJ1831072, respectively (Figure 3). In addition, *MnSOD* and *FeSOD* gene expressions were significant in CJ1831056 than in CJ1831072 at 10 days of waterlogging, but the *FeSOD* gene was poorly induced at 20 days in both genotypes (Figure 3). We hypothesized that this could contribute to waterlogging resistance in the CJ1831072 genotype at 10 days of waterlogging (Figure 1A). Metallothionein (MT) is a small cysteine-rich protein that plays a role in ROS scavenging in biotic and abiotic stresses (Patankar et al., 2019). Although the role of MTs in waterlogging resistance is minimal, in maize, downregulation of the *MT1* gene is thought to play a role in the regulation of aerenchyma formation in the root cortex (Rajhi et al., 2011). Similarly, in the present study, *MT1* was highly downregulated in both genotypes, with a higher expression in the CJ1831056 at the designated waterlogging time points (Figure 3). Our findings clearly suggest that MTs may not only play a role in ROS scavenging but also determines the fate of inducible aerenchyma formation in cotton genotypes under waterlogging stress. Sucrose synthase, catalyzing sucrose to UDP-glucose and fructose, plays a fundamental role in providing an adequate sugar supply during anoxic stress, Zeng and colleagues recently demonstrated that waterlogging for 5–10 days reduced sucrose synthase activities, most likely due to changes in gene expression in starch and sucrose metabolism (Zeng et al., 2021). Contrarily, the presence of sucrose in anoxic conditions significantly alleviated meristem death and was capable of restoring root tip viability (Springer et al., 1986). Here, the starch and sucrose pathways were significantly expressed, and related genes were significantly downregulated in both genotypes (Figure 2G and Figure S2B). We speculated that the downregulation of numerous sucrose synthase genes in response to waterlogging may have played a role in root chlorosis and leaf dropping in cotton genotypes (Figure 1A).

Differentially expressed TF responses in waterlogged cotton roots

Stress-responsive TFs play critical roles in abiotic stress responses and waterlogging stress tolerance in plants including members of the *AP2/ERF*, *MYB*, *bHLH*, *NAC*, *WRKY*, and *bZIP* families (Yoon et al., 2020; Zhang et al., 2022). Similar expressions of these TFs were discovered in this study (Figure 4). N-end pathway TFs are popularly known as oxygen-sensing mechanisms thought to trigger responses that destabilize proteins in oxygen-deprived environments (Perata and Dongen, 2011). Key N-end rule pathway DEGs, such as *RAP2.12*, *RAP2.3*, *HRE2*, *PCO1*, and *PCO2*, were upregulated by waterlogging and downregulated by reoxygenation in both tolerant and resistant chrysanthemum cultivars (Zhao et al., 2018). However, in the present study, all *RAP2-3* and *RAP2-12* DEGs were significantly upregulated at 0 days of no stress but repressed at waterlogging for 10 and 20 days (Figure S2). Based on the present results, we speculated that VII ERFs played a significant role in tolerance, but expression could be relative to the plant species. PCO activity is known as a signaling response to changes in oxygen availability. According to recent reports, during submergence, PCO activity drops, resulting in increased stabilization of ERF-VIIs (Taylor-kearney and Flashman, 2021). However, in this study, PCO DEGs were highly expressed during waterlogging stress but suppressed at no stress in CJ1831056, compared with CJ1831072. We speculated that the higher expression of PCO genes could be a result of ERF-VII instability. Among other TFs, APETALA2 (AP2) domain *ABR1*-like genes and ethylene-responsive transcription factor *ERF071* were significantly induced. *ABR1* acts as a repressor of ABA (Chen et al., 2020). However, *ERF71* is believed to contribute to tolerance in anoxia stress condition by increasing anaerobic gene expression and adventitious root growth under hypoxia (Licausi et al., 2010; Eysholdt-Derzsó and Sauter, 2017). In this study, both *ABR1*-like and *ERF71* genes were significantly upregulated (Table 1). We hypothesized that both genes may play a significant role in cotton tolerance to waterlogging in ABA repression and adventitious root growth. WRKY TFs play important roles, mainly in the innate immune system of plants. For instance, recent reports have shown that the expression of *GhWRKY27* was induced by leaf senescence in early-aging cotton (Gu et al., 2019). A similar result in this study showed that the WRKY27 gene was more expressed in the CJ1831056 than CJ1831072 genotype at 10 days of waterlogging, but at 20 days of waterlogging, expression in the CJ1831056 genotype decreased as expression in the CJ1831072 genotype increased (Table 1). This shows that the WRKY27 senescence gene was significantly enhanced in CJ1831072 compared with CJ1831056, as waterlogging time increased.

Responsive metabolites in waterlogged cotton root

Metabolomics studies in cotton genotypes, CJ1831056 and CJ1831072, significantly induced phenylpropanoid biosynthesis, purine metabolism, and galactose metabolism pathways (Supplementary Table 5). Zhang et al. (2021) explained that phenylpropanoid biosynthesis and purine metabolism are the major pathways that respond to abiotic conditions (Zhang et al., 2021). Similar to the current investigation, phenylpropanoid biosynthesis and purine metabolism pathways were highly influenced at the metabolite level of study in responses to waterlogging stress. Moreover, adenosine and sinapyl alcohol metabolites were highly accumulated in these pathways at 10 days of waterlogging (Supplementary Table 3). Sinapyl alcohol metabolite acts as an antioxidant against oxidative injury (Takahama et al., 1996). In the present study, sinapyl alcohol was upregulated in CJ1831072 but downregulated in CJ1831056 (Figure S3B). We speculated that the early accumulation of sinapyl alcohol may play a role in the phenotypic resistance observed at 10 days of stress (Figure 1B). Adenosine, produced from hypoxic and damaged tissues, reduces proinflammatory activities by facilitating anti-inflammatory activities (Ohta, 2016). Adenosine metabolite accumulation observed in this study was upregulated in CJ1831056 but downregulated in CJ1831072 (Figure S3B). First, we hypothesized that accumulation of adenosine was triggered by ROS in both genotypes at 10 days of waterlogging; however, it had high-tolerance responses in CJ1831056 than CJ1831072.

Furthermore, two metabolites, galactaric acid and nobiletin, were highly accumulated metabolites under 10 days of waterlogging, with fold change values of 3.0 and −3.1, respectively (Figures S3B, S4B). Galactaric acid has been shown to be involved in osmoprotection and stress signaling under drought (Marczak and Augustyniak, 2016). Therefore, its upregulation in CJ1831056 and downregulation in CJ1831072 may support the notion that the CJ1831056 genotype was protected from osmotic stress more than CJ1831072 (Figure S4B). Wang et al. (2018b) further reported that nobiletin phytochemicals protect *Saccharomyces cerevisiae* cells from the oxidative damage imposed by H_2O_2 (Wang et al., 2018b). We speculated that nobiletin metabolites also contributed to antioxidant protection at 10 days of waterlogging in cotton. However, its expression was downregulated in CJ1831056 and upregulated in CJ1831072 (Figure S4B). In response to several kinds of abiotic stressors, plants greatly increase their accumulation of free amino acids and sugar compounds. In this study, valine, leucine, and isoleucine biosynthesis and galactose metabolism pathways were the two main pathways that responded to 20 days of waterlogging in cotton (Supplementary Table 5). Amino acid accumulation is evident in enhancing stress elasticity in plants (Fardus et al., 2021). In this study, L-glutamic acid, L-

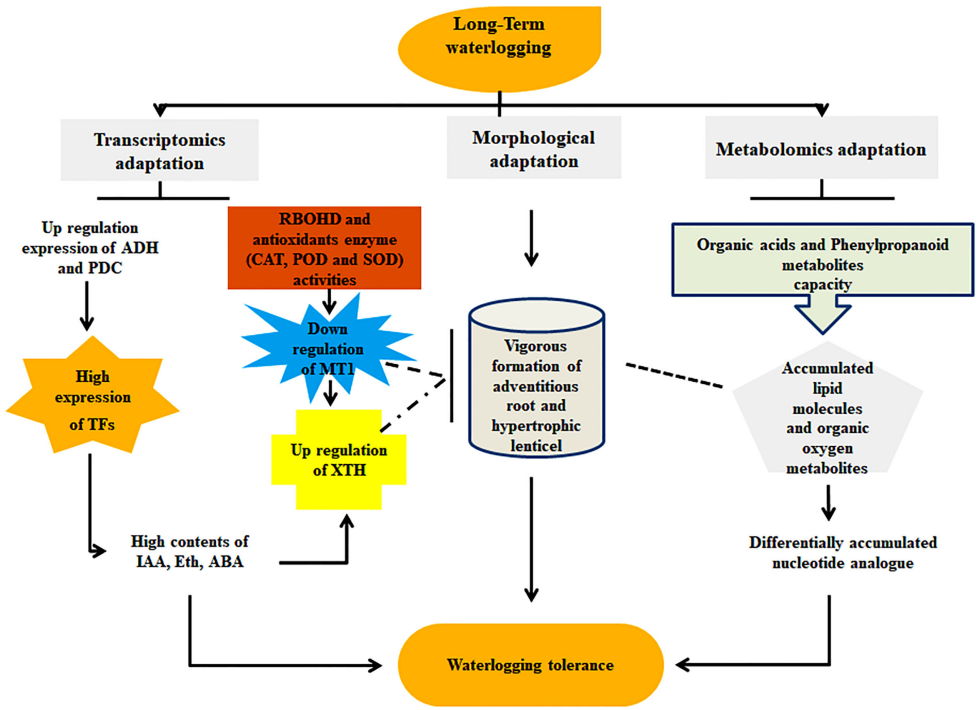

FIGURE 8
Molecular and morphological adaptation strategies of cotton in response to waterlogging stress. Molecular adaption denoted transcriptomic expression of genes (ADH: alcohol dehydrogenase, PDC: pyruvate decarboxylase, XTH: xyloglucanendo-transglucosylase/hydrolase, RBOHD: respiratory burst oxidase homolog protein D, CAT: catalase, SOD: superoxide dismutase, POD: peroxidase, MT1: metallothionein 1, TFs: transcription factors, IAA: indole-3-acetic acid, Eth: ethylene and ABA: abscisic acid) and metabolic expression of metabolites (organic acid, phenylpropanoid, organic oxygen, and nucleotide analogue). Morphological adaptation represents adventitious roots and hypertrophic lenticels formation.

asparagine, and L-valine metabolites were induced at 20 days of waterlogging (Figures S3C and S4C). Reports have confirmed that exogenous applications of glutamate and glutamic acid enhance drought and salt tolerance in radish and Lens culinaris Medik., respectively (Fardus et al., 2021). These findings suggest that L-glutamic acid may play a role by increasing stress tolerance in plants, indicating that L-glutamic acid metabolite accumulation might regulate "arginine and proline metabolism" and "glutathione" pathways in this study (Supplementary Table 5). Additionally, at 20 days of waterlogging, amino acid metabolites, such as malic acid and citric acid, were both upregulated in CJ1831072 and downregulated in CJ1831056. Other metabolites, such as vanillic acid, gamma-linolenic acid, procyanidin C1, 9-OxoODE, and procyanidin B2, also accumulated significantly at 20 days of waterlogging (Figure S4C).

Conclusion

The combination of metabolomic and transcriptomic analyses revealed the potential mechanism of long-term waterlogging resistance between the cotton genotypes CJ1831056 and CJ1831072. Transcriptomic analysis with RNA-seq revealed significant genes such as *PER1*, *PRX52*, *PER64*, *ADH*, *PDC*, *MT1*, *XTH*, and *SUS* to be the key genes highly contributing to waterlogging resistance and highly expressed in CJ1831056 than in CJ1831072. Moreover, innately resistant TFs, including *WRKY*, *AP2/ERF*, and *MYB*, were significantly induced in waterlogged CJ8131056 genotype roots, which hypothetically show signs of tolerance in response to waterlogging. Contrarily, metabolomics studies with metabolites revealed significant variations between the two genotypes after 10 to 20 days of waterlogging duration. Stress-tolerant metabolites, including sinapyl alcohol, adenosine, L-glutamic acid, galactaric acid, nobiletin, and L-asparagine, were significantly expressed in CJ1831056 than in CJ1831072 in response to long-term waterlogging. Based on these findings, a schematic model of cotton adaptable mechanisms to long-term waterlogging durations (Figure 8) is presented. These analyses provide comprehensive knowledge on the molecular understanding of cotton's response to long-term waterlogging, providing effective guidance for future breeding techniques in cotton production.

Data availability statement

The original contributions presented in the study are publicly available. This data can be found here: NCBI, PRJNA911339.

Author contributions

Conceived and designed the experiments: J-SG and AGO. Experiments: AGO and Y-PL. Data analysis: AGO, J-SG, Y-PL, ML, YW, C-LL, NG, and D-HL. Main authors: AGO, Y-PL, and J-SG. Manuscript revision: J-SG and AGO. All authors contributed to the article and approved the submitted version.

Funding

This research was supported by the Key Research and Development Plan of Anhui province (No. 202004e11020002), and this work was partially supported by the Anhui Provincial College Students Innovation and Entrepreneurship Training Program (S202010364227). The funding bodies were not involved in the design of the study.

Acknowledgments

We particularly appreciate the guidance of the editor and reviewers on the refinement of the manuscript.

Conflict of interest

The authors declare that the research was conducted in the absence of any commercial or financial relationships that could be construed as a potential conflict of interest.

Publisher's note

All claims expressed in this article are solely those of the authors and do not necessarily represent those of their affiliated organizations, or those of the publisher, the editors and the reviewers. Any product that may be evaluated in this article, or claim that may be made by its manufacturer, is not guaranteed or endorsed by the publisher.

Supplementary material

The Supplementary Material for this article can be found online at: https://www.frontiersin.org/articles/10.3389/fpls.2023.1088537/full#supplementary-material

SUPPLEMENTARY FIGURE 1
Number of hormone DEGs in cotton roots during waterlogging stress. (A) DEGs in CJ56T10vsCJ56T0. (B) DEGs in CJ56T20vsCJ56T0. (C) DEGs in CJ72T10vsCJ72T0. (D) DEGs in CJ72T20vsCJ72T0.

SUPPLEMENTARY FIGURE 2
Heat map clustering analysis of DEGs. **(A)** Clustering analysis of DEGs involved in the N-end rule pathway. **(B)** Clustering analysis of DEGs involved in carbohydrate metabolism. The bar represents the scale of the expression levels of each gene (log2 FPKM) in each sample, as indicated by red/blue rectangles. Red rectangles represent the high expression of genes, and blue rectangles represent the low expression.

SUPPLEMENTARY FIGURE 3
Analysis of accumulated metabolites at 10 days of waterlogging in cotton waterlogged roots. **(A)** Metabolites absolute value of the fold change. **(B)** The bubble plot represents a metabolic pathway. **(C)** Hierarchical cluster analysis. The abscissa represents the different experimental groups, the ordinate represents the comparative metabolites of the group, and the color blocks

at different positions represent the relative expression amount of the metabolites at the corresponding positions. Red indicates high expression of the substance, and blue indicates low expression.

SUPPLEMENTARY FIGURE 4
Analysis of accumulated metabolites at 20 days of waterlogging in cotton waterlogged roots. **(A)** Metabolites' absolute value of the fold change (waterlogging/Control) at 20 days in cotton roots. **(B)** The bubble plot represents a metabolic pathway. **(C)** Hierarchical cluster analysis. The abscissa represents the different experimental groups, the ordinate represents the comparative metabolites of the group, and the color blocks at different positions represent the relative expression amount of the metabolites at the corresponding positions. Red indicates high expression of the substance, and blue indicates low expression.

References

Bange, M. P., Milroy, S. P., and Thongbai, P. (2004). Growth and yield of cotton in response to waterlogging. *F. Crop Res.* 88, 129–142. doi: 10.1016/j.fcr.2003.12.002

Blokhina, O. B., Chirkova, T. V., and Fagerstedt, K. V. (2001). Anoxic stress leads to hydrogen peroxide formation in plant cells. *J. Exp. Bot.* 52, 1179–1190. doi: 10.1093/jxb/52.359.1179

Broughton, S., Zhou, G., and Teakle, N. L. (2015). Waterlogging tolerance is associated with root porosity in barley (Hordeum vulgare l). *Mol. Breed.* 35, 1–15. doi: 10.1007/s11032-015-0243-3

Cao, G., Wang, X., Liu, Y., and Luo, W. (2012). Effect of water logging stress on cotton leaf area index and yield. *Proc. Eng.* 28, 202–209. doi: 10.1016/j.proeng.2012.01.706

Chávez-Arias, C. C., Gómez-Caro, S., and Restrepo-Díaz, H. (2019). Physiological, biochemical and chlorophyll fluorescence parameters of physalis peruviana l. seedlings exposed to different short-term waterlogging periods and fusarium wilt infection. *Agronomy* 9, 1–20. doi: 10.3390/agronomy9050213

Chen, L., Zhang, D., Song, C., Wang, H., Tang, X., and Chang, Y. (2020). Transcriptomic analysis and specific expression of transcription factor genes in the root and sporophyll of dryopteris fragrans (L.) schott. *Int. J. Mol. Sci.* 21, 1–20. doi: 10.3390/ijms21197296

Cheng, X., Yu, M., Zhang, N., Zhou, Z., Xu, Q., Mei, F., et al. (2015). Reactive oxygen species regulate programmed cell death progress of endosperm in winter wheat (triticum aestivum l .) under waterlogging. *Springer* 2, 1–17. doi: 10.1007/s00709-015-0811-8

Coutinho, I. D., Henning, L. M. M., Döpp, S. A., Nepomuceno, A., Moraes, L. A. C., Marcolino-Gomes, J., et al. (2018). Flooded soybean metabolomic analysis reveals important primary and secondary metabolites involved in the hypoxia stress response and tolerance. *Environ. Exp. Bot.* 153, 176–187. doi: 10.1016/j.envexpbot.2018.05.018

Dodd, K., Guppy B, C. N., Lockwood, P. V., and Rochester, I. J. (2013). Impact of waterlogging on the nutrition of cotton (Gossypium hirsutum l.) produced in sodic soils. *Crop Pasture Sci.* 64, 816–824. doi: 10.1071/CP13093

Else, M. A., Janowiak, F., Atkinson, C. J., and Jackson, M. B. (2009). Root signals and stomatal closure in relation to photosynthesis, chlorophyll a fluorescence and adventitious rooting of flooded tomato plants. *Ann. Bot.* 103, 313–323. doi: 10.1093/aob/mcn208

Eysholdt-Derzsó, E., and Sauter, M. (2017). Root bending is antagonistically affected by hypoxia and ERF-mediated transcription *via* auxin signaling. *Plant Physiol.* 175, 412–423. doi: 10.1104/pp.17.00555

Eysholdt-Derzsó, E., and Sauter, M. (2019). Hypoxia and the group VII ethylene response transcription factor HRE2 promote adventitious root elongation in arabidopsis. *Plant Biol.* 21, 103–108. doi: 10.1111/plb.12873

Fardus, J., Hossain, S., and Fujita, M. (2021). Modulation of the antioxidant defense system by exogenous l -glutamic acid application enhances salt tolerance in lentil (lens culinaris medik .). *Biomolecules* 11, 1–15. doi: 10.3390/biom11040587

Gong, J. R., Zhang, X. S., Huang, Y. M., and Zhang, C. L. (2007). The effects of flooding on several hybrid poplar clones in northern China. *Agrofor. Syst.* 69, 77–88. doi: 10.1007/s10457-006-9019-4

Gu, L., Dou, L., Guo, Y., Wang, H., Li, L., Wang, C., et al. (2019). The WRKY transcription factor GhWRKY27 coordinates the senescence regulatory pathway in upland cotton (gossypium hirsutum l .). *BMC Plant Biol.* 19, 1–14. doi: 10.1186/s12870-019-1688-z

Hasanuzzaman, M., Bhuyan, M. H. M. B., Zulfiqar, F., Raza, A., and Fotopoulos, V. (2020). Reactive oxygen species and antioxidant defense in plants under abiotic Stress: revisiting the crucial role of a universal defense regulator. *Antioxid. (Basel).* 9, 1–52. doi: 10.3390/antiox9080681

Hussain, A., Zafar, Z. U., and Athar, H. ur R. (2014). Flooding tolerance in cotton (Gossypium hirsutum l.) at early vegetative and reproductive growth stages. *Pakistan J. Bot.* 46, 1001–1009.

Jia, W., Ma, M., Chen, J., and Wu, S. (2021). Molecular sciences plant morphological, physiological and anatomical adaption to flooding stress and the underlying molecular mechanisms. *Int. J. Mol. Sci.* 22, 1088. doi: 10.3390/ijms22031088

Kaushal, J., Singh, S. G., and Arya, S. K. (2018). Catalase enzyme: application in bioremediation and food industry. *Biocatal. Agric. Biotechnol.* 16, 192–199. doi: 10.1016/j.bcab.2018.07.035

Kongdin, M., Mahong, B., Lee, S. K., Shim, S. H., Jeon, J. S., and Ketudat Cairns, J. R. (2021). Action of multiple rice β-glucosidases on abscisic acid glucose ester. *Int. J. Mol. Sci.* 22, 1–14. doi: 10.3390/ijms22147593

Le Provost, G., Lesur, I., Lalanne, C., Da Silva, C., Labadie, K., Aury, J. M., et al. (2016). Implication of the suberin pathway in adaptation to waterlogging and hypertrophied lenticels formation in pedunculate oak (Quercus robur l.). *Tree Physiol.* 36, 1330–1342. doi: 10.1093/treephys/tpw056

Licausi, F., Van Dongen, J. T., Giuntoli, B., Novi, G., Santaniello, A., Geigenberger, P., et al. (2010). HRE1 and HRE2, two hypoxia-inducible ethylene response factors, affect anaerobic responses in arabidopsis thaliana. *Plant J.* 62, 302–315. doi: 10.1111/j.1365-313X.2010.04149.x

Loreti, E., Valeri, M. C., Novi, G., and Perata, P. (2018). Gene regulation and survival under hypoxia requires starch availability and Metabolism. *Plant Physiol.* 176, 1286–1298. doi: 10.1104/pp.17.01002

Luan, H., Guo, B., Pan, Y., Lv, C., Shen, H., and Xu, R. (2018). Morpho-anatomical and physiological responses to waterlogging stress in different barley (Hordeum vulgare L.) genotypes. *Plant Growth Regul.* 85, 399–409. doi: 10.1007/s10725-018-0401-9

Mansoor, S., Wani, O. A., Lone, J. K., Manhas, S., Kour, N., Alam, P., et al. (2022). Reactive oxygen species in Plants: from source to sink. *Antioxidants* 11, 1–14. doi: 10.3390/antiox11020225

Marczak, Ł., and Augustyniak, A. (2016). Water deficit affects primary metabolism differently in two lolium multiflorum / festuca arundinacea introgression forms with a distinct capacity for photosynthesis and membrane regeneration. *Front. Plant Sci.* 7. doi: 10.3389/fpls.2016.01063

Najeeb, U., Bange, M. P., Tan, D. K. Y., and Atwell, B. J. (2015). Consequences of waterlogging in cotton and opportunities for mitigation of yield losses. *AoB Plants.* 7, 1–18. doi: 10.1093/aobpla/plv080

Nevalainen, T. J. (2010). 1-cysteine peroxiredoxin: a dual-function enzyme with peroxidase and acidic Ca2+-independent phospholipase A2 activities. *Biochimie* 92, 638–644. doi: 10.1016/j.biochi.2010.01.019

Ohta, A. (2016). A metabolic immune Checkpoint: adenosine in tumor microenvironment. *Front Immunol* 7, 109. doi: 10.3389/fimmu.2016.00109

Parent, C., Berger, A., Folzer, H., Dat, J., Crevècoeur, M., Badot, P., et al. (2008). A novel nonsymbiotic hemoglobin from oak: cellular and tissue specificity of gene expression. *New Phytol.* 177, 142–154. doi: 10.1111/j.1469-8137.2007.02250.x

Park, S., Lee, C., Kim, S., Lim, Y., Lee, H., Nam, S., et al. (2020). Plant physiology and biochemistry selection of flooding stress tolerant sweetpotato cultivars based on biochemical and phenotypic characterization. *Plant Physiol. Biochem.* 155, 243–251. doi: 10.1016/j.plaphy.2020.07.039

Patankar, H. V., Al-Harrasi, I., Al Kharusi, L., Jana, G. A., Al-Yahyai, R., Sunkar, R., et al. (2019). Overexpression of a metallothionein 2A gene from date palm confers abiotic stress tolerance to yeast and arabidopsis thaliana. *Int. J. Mol. Sci.* 20, 1–21. doi: 10.3390/ijms20122871

Perata, P., and Dongen, J. T. (2011). Rule pathway for protein destabilization. *Nature* 479, 419–422. doi: 10.1038/nature10536

Qi, X., Li, Q., Ma, X., Qian, C., Wang, H., Ren, N., et al. (2019). Waterlogging-induced adventitious root formation in cucumber is regulated by ethylene and auxin through reactive oxygen species signalling. *Plant Cell Environ.* 42, 1458–1470. doi: 10.1111/pce.13504

Qian, L., Chen, X., Wang, X., Huang, S., and Luo, Y. (2020). The effects of flood, drought, and flood followed by drought on yield in cotton. *Agronomy* 10, 1–18. doi: 10.3390/agronomy10040555

Rajhi, I., Yamauchi, T., Takahashi, H., Nishiuchi, S., and Shiono, K. (2011). Identification of genes expressed in maize root cortical cells during lysigenous aerenchyma formation using laser microdissection and microarray analyses. *New Phytol.* 190, 351–368. doi: 10.1111/j.1469-8137.2010.03535.x

Sadras, V. O. (1995). Field crops research review compensatory growth in cotton after loss of reproductive organs. *F. Crop Res.* 40, 1–18. doi: 10.1016/0378-4290(94)00088-T

Sharma, A., Shahzad, B., Rehman, A., Bhardwaj, R., and Landi, M. (2019). Response of phenylpropanoid pathway and the role of polyphenols in plants under abiotic stress. *Molecules* 24, 1–22. doi: 10.3390/molecules24132452

Shimamura, S., Yamamoto, R., Nakamura, T., Shimada, S., and Komatsu, S. (2010). Stem hypertrophic lenticels and secondary aerenchyma enable oxygen transport to roots of soybean in flooded soil. *Ann. Bot.* 106, 277–284. doi: 10.1093/aob/mcq123

Song, L., Valliyodan, B., Prince, S., Wan, J., and Nguyen, H. T. (2018). Characterization of the XTH gene family: new insight to the roles in soybean flooding tolerance. *Int. J. Mol. Sci.* 19, 1–20. doi: 10.3390/ijms19092705

Springer, B., Werr, W., Starlinger, P., Bennett, D. C., Zokoliea, M., and Freeling, M. (1986). The shrunken gene on chromosome 9 of zea mays l is expressed in various plant tissues and encodes an anaerobic protein. *Mol. Gen. Genet.* 4, 461–468. doi: 10.1007/BF00338083

Takahama, U., Oniki, T., and Shimokawa, H. (1996). *A possible mechanism for the oxidation of sinapyl alcohol by peroxidase- dependent reactions in the Apoplast: enhancement of the oxidation by hydroxycinnamic acids and components of the apoplast*. Kitakyushu, Japan: Plant Cell Physiology, Kyushu Dental College, Vol. 37. 499–504. doi: 10.1093/oxfordjournals.pcp.a028972

Taylor-kearney, L. J., and Flashman, E. (2021). Targeting plant cysteine oxidase activity for improved submergence tolerance. *Plant J.* 109, 1–10. doi: 10.1111/tpj.15605

Tian, L., Bi, W., Liu, X., Sun, L., and Li, J. (2019). Effects of waterlogging stress on the physiological response and grain-filling characteristics of spring maize (Zea mays l.) under field conditions. *Acta Physiol. Plant* 41, 1–14. doi: 10.1007/s11738-019-2859-0

Wang, G., Li, Q., Dzakpasu, M., Gao, X., Yuwen, C., and Wang, X. C. (2018a). Impacts of different biochar types on hydrogen production promotion during fermentative co-digestion of food wastes and dewatered sewage sludge. *Waste Manage.* 80, 73–80. doi: 10.1016/j.wasman.2018.08.042

Wang, M., Meng, D., Zhang, P., Wang, X., Brennan, C., Li, S., et al. (2018b). Antioxidant protection of nobiletin , 5-demethylnobiletin , tangeretin , and 5-demethyltangeretin from citrus peel in saccharomyces cerevisiae. *J. Agric. Food Chem.* 66, 3155–3160. doi: 10.1021/acs.jafc.8b00509

Wang, T., Wang, Y., Liu, X., Gao, X., and Hu, K. (2022). Combined transcriptomics and metabolomics analyses in grass carp under anesthetic stress. *Front. Cell. Infect. Microbiol.* 12. doi: 10.3389/fcimb.2022.931696

Xu, Q. T., Yang, L., Zhou, Z. Q., Mei, F. Z., Qu, L. H., and Zhou, G. S. (2013). Process of aerenchyma formation and reactive oxygen species induced by waterlogging in wheat seminal roots. *Planta* 238, 969–982. doi: 10.1007/s00425-013-1947-4

Yin, D., Chen, S., Chen, F., Guan, Z., and Fang, W. (2010). Morpho-anatomical and physiological responses of two dendranthema species to waterlogging. *Environ. Exp. Bot.* 68, 122–130. doi: 10.1016/j.envexpbot.2009.11.008

Yoon, Y., Seo, D. H., Shin, H., Kim, H. J., Kim, C. M., and Jang, G. (2020). The role of stress-responsive transcription factors in modulating abiotic stress tolerance in plants. *Agronomy* 10, 1–23. doi: 10.3390/agronomy10060788

Yu, F., Tan, Z., Fang, T., Tang, K., Liang, K., and Qiu, F. (2020). A comprehensive transcriptomics analysis reveals long non-coding RNA to be involved in the key metabolic pathway in response to waterlogging stress in maize. *Genes (Basel).* 11, 1–19. doi: 10.3390/genes11030267

Zahra, R., Id, N., Id, S. S. Z., Mukhtar, M. S., Amin, I., Mishra, B., et al. (2019). Transcriptomic analysis of cultivated cotton gossypium hirsutum provides insights into host responses upon whitefly-mediated transmission of cotton leaf curl disease. *PloS One* 14, 1–21. doi: 10.1371/journal.pone.0210011

Zeng, R., Chen, T., Wang, X., Cao, J., Li, X., Xu, X., et al. (2021). Physiological and expressional regulation on photosynthesis , starch and sucrose metabolism response to waterlogging stress in peanut. *Front. Plant Sci.* 12. doi: 10.3389/fpls.2021.601771

Zhang, C., Chen, J., Huang, W., Song, X., and Niu, J. (2021). Transcriptomics and metabolomics reveal purine and phenylpropanoid metabolism response to drought stress in dendrobium sinense , an endemic orchid species in hainan island. *Front. Genet.* 12. doi: 10.3389/fgene.2021.692702

Zhang, Y., Chen, Y., Lu, H., Kong, X., Dai, J., Li, Z., et al. (2016). Growth, lint yield and changes in physiological attributes of cotton under temporal waterlogging. *F. Crop Res.* 194, 83–93. doi: 10.1016/j.fcr.2016.05.006

Zhang, Y., Kong, X., Dai, J., Luo, Z., Li, Z., Lu, H., et al. (2017). Global gene expression in cotton (Gossypium hirsutum l.) leaves to waterlogging stress. *PloS One* 12, 1–24. doi: 10.1371/journal.pone.0185075

Zhang, H., Li, G., Yan, C., Zhang, X., Cao, N., Le, M., et al. (2022). Elucidating the molecular responses to waterlogging stress in cucumis melo by comparative transcriptome profiling. *Horticulturae* 8, 891. doi: 10.3390/horticulturae8100891

Zhang, Y., Liu, G., Dong, H., and Li, C. (2020). ScienceDirect waterlogging stress in cotton: damage, adaptability, alleviation strategies, and mechanisms. *Crop J.* 2, 1–14. doi: 10.1016/j.cj.2020.08.005

Zhao, N., Li, C., Yan, Y., Cao, W., Song, A., Wang, H., et al. (2018). Comparative transcriptome analysis of waterlogging-sensitive and waterlogging-tolerant chrysanthemum morifolium cultivars under waterlogging stress and reoxygenation conditions. *Int. J. Mol. Sci.* 19, 1–21. doi: 10.3390/ijms19051455

10.3389/fpls.2023.1088537

Appendix A. Supporting information

Additional supporting information may be found online in the supporting information section at the end of the article.

frontiers | Frontiers in Plant Science

TYPE Original Research
PUBLISHED 17 July 2023
DOI 10.3389/fpls.2023.1164534

Check for updates

OPEN ACCESS

EDITED BY
Diaa Abd El Moneim,
Arish University, Egypt

REVIEWED BY
Yunhe Jiang,
China Agricultural University, China
Emanuela Pedrazzini,
National Research Council (CNR), Italy

*CORRESPONDENCE
Jinmin Fu
turfcn@qq.com

†These authors have contributed equally to this work

RECEIVED 13 February 2023
ACCEPTED 27 June 2023
PUBLISHED 17 July 2023

CITATION
Shao A, Xu X, Amombo E, Wang W, Fan S, Yin Y, Li X, Wang G, Wang H and Fu J (2023) CdWRKY2 transcription factor modulates salt oversensitivity in bermudagrass [*Cynodon dactylon* (L.) Pers.]. *Front. Plant Sci.* 14:1164534. doi: 10.3389/fpls.2023.1164534

COPYRIGHT
© 2023 Shao, Xu, Amombo, Wang, Fan, Yin, Li, Wang, Wang and Fu. This is an open-access article distributed under the terms of the Creative Commons Attribution License (CC BY). The use, distribution or reproduction in other forums is permitted, provided the original author(s) and the copyright owner(s) are credited and that the original publication in this journal is cited, in accordance with accepted academic practice. No use, distribution or reproduction is permitted which does not comply with these terms.

CdWRKY2 transcription factor modulates salt oversensitivity in bermudagrass [*Cynodon dactylon* (L.) Pers.]

An Shao†, Xiao Xu†, Erick Amombo, Wei Wang, Shugao Fan, Yanling Yin, Xiaoning Li, Guangyang Wang, Hongli Wang and Jinmin Fu*

Coastal Salinity Tolerant Grass Engineering and Technology Research Center, Ludong University, Yantai, Shandong, China

Common bermudagrass [*Cynodon dactylon* (L.) Pers.] has higher utilization potential on saline soil due to its high yield potential and excellent stress tolerance. However, key functional genes have not been well studied partly due to its hard transformation. Here, bermudagrass "Wrangler" successfully overexpressing *CdWRKY2* exhibited significantly enhanced salt and ABA sensitivity with severe inhibition of shoot and root growth compared to the transgenic negative line. The reduced auxin accumulation and higher ABA sensitivity of the lateral roots (LR) under salt stress were observed in *CdWRKY2* overexpression *Arabidopsis* lines. IAA application could rescue or partially rescue the salt hypersensitivity of root growth inhibition in *CdWRKY2*-overexpressing *Arabidopsis* and bermudagrass, respectively. Subsequent experiments in *Arabidopsis* indicated that CdWRKY2 could directly bind to the promoter region of *AtWRKY46* and downregulated its expression to further upregulate the expression of ABA and auxin pathway-related genes. Moreover, *CdWRKY2* overexpression in *mapk3* background *Arabidopsis* could partly rescue the salt-inhibited LR growth caused by *CdWRKY2* overexpression. These results indicated that CdWRKY2 could negatively regulate LR growth under salt stress *via* the regulation of ABA signaling and auxin homeostasis, which partly rely on AtMAPK3 function. CdWRKY2 and its homologue genes could also be useful targets for genetic engineering of salinity-tolerance plants.

KEYWORDS

bermudagrass, WRKY, auxin, ABA, salt stress, lateral roots

1 Introduction

Breeding and selection of salt-tolerant plant germplasm is a requisite for developing and utilizing saline-alkali land. Common bermudagrass [*Cynodon dactylon* (L.) Pers.] is an extensively used turfgrass and forage species due to its high stress tolerance level and high yield potential (Ackerson and Youngner, 1962). Despite having salt tolerance

ability, the genetic mechanism underlying the salt response in bermudagrass is poorly understood, greatly limiting its utilization in saline soil. Therefore, it is necessary to isolate potential salt-responsive genes of bermudagrass and intensively investigate their salt-responsive function to provide useful gene resources for conducting high salt-tolerant and agronomical desirable bermudagrass varieties (lines).

WRKY transcription factors (TFs), named after their conserved amino acid sequences WRKYGQK, are vital for plant environmental stress response primarily by binding to the W-box elements at the promoter regions of downstream genes and then activating or inhibiting their transcription to active the following stress response cascade (Jiang et al., 2017). In model plants such as *Arabidopsis*, hormones such as abscisic acid (ABA) and auxin have previously been reported to play critical roles in environmental abiotic stress response. Also, a series of TFs could function in stress response *via* an ABA-dependent manner and regulation of auxin homeostasis including WRKY TFs (Zhou et al., 2008; Jiang and Deyholos, 2009; Lavenus et al., 2013; Cai et al., 2017; Jiang et al., 2017). For instance, AtWRK18, AtWRKY60, and AtWRKY40 interact physically and functionally to bind to the promoters of ABA response genes *ABI4* and *ABI5* (ABA-Insensitive 4 and 5) to suppress their expression (Liu et al., 2012). The *wrky18* and *wrky60* mutants exhibited a reduced ABA and salt sensitivity (Chen et al., 2010). The overexpression of *AtWRKY33* in *Arabidopsis* improves the salt-resistant ability of plants through the SOS (salt overly sensitive) pathway and increases plants' sensitivity to ABA. The AtWRKY33 can also directly bind to the promoters of key enzymes encoding genes involved in ethylene biosynthesis (ACS2 and ACS6) to promote their expression, and then regulate ethylene biosynthesis induced by glutathione under salt conditions (Datta et al., 2015). Furthermore, other WRKY TFs have been reported to respond to salt stress *via* an ABA-independent manner. For example, under high salt stress in *Arabidopsis*, an AtWRKY8 directly binds to the W-box of the stress-responsive marker gene *RD29A* and promotes its expression to offset the Na^+ and K^+ homeostasis. The VQ9 can interact with AtWRKY8 and adversely affect its transcription activation function. However, compared to the wild type, salt stress significantly changes the expression of ABA response-related genes in *wrky8* and *vq9* mutants (Hu et al., 2013), suggesting that the effect of WRKY8 on salt tolerance does not depend on the ABA pathway. A recent study showed that a WRKY TF, AtWRKY46, binds to the promoter of genes involved in auxin conjugation and inhibits their expression to increase the active auxin accumulation in roots and maintain roots growth under salt stress (Korasick et al., 2013; Ding et al., 2015). Moreover, ABA and auxin pathways may have a combined effect in a wide range when modulating plant growth response to environmental stress (Smet et al., 2006). For example, ABA might regulate lateral root (LR) growth by affecting auxin transport (Brady et al., 2003; Deak and Malamy, 2005). Furthermore, ABI4 limits the expression of the auxin-efflux carrier protein PIN1 to inhibit the transporting of auxin to LR and mediates ABA-dependent inhibition of LR formation (Shkolnik-Inbar and Bar-Zvi, 2010). AtWRKY46 has also been reported to bind directly to the *ABI4* promoter to reduce its expression in *AtWRKY46* overexpression *Arabidopsis* plants grown in osmotic/salt stress conditions, suggesting that AtWRKY46 mediates the regulation of LR growth under osmotic/salt stress *via* effects on ABA signaling and modulation of auxin distribution in the roots (Ding et al., 2015).

MAPK (mitogen-activated protein kinase) cascade plays a vital role in plant response to stress including salt (Asai et al., 2002; Kim and Zhang, 2004; Andreasson et al., 2005). Generally, the signal molecules upstream activate MAPK cascade and lead to the phosphorylation of MAPKs to further activate them. The activated MAPKs often induce their translocation from the cytoplasm into the nucleus, where they can phosphorylate and activate sets of stress-resistant TFs (Shen et al., 2012). Some WRKY TFs have been reported to act downstream of MAPK cascades in plants. The binding ability of WRKY to the W-box motif of downstream genes can be enhanced or activated to further function in various physiological responses (Kim and Zhang, 2004). Among those MAPKs, MAPK3 and MAPK6 are the two main kinases that mediate downstream signaling in *Arabidopsis*. A previous study revealed that 26 out of 72 WRKY members of *Arabidopsis* interacted with MAPK3 (Sharma et al., 2013). For instance, in *Arabidopsis*, AtWRKY22 and AtWRKY29 function downstream of the MEKK1-MKK4/5-MPK3/6 cascade in response to elicitation by flagellin (Asai et al., 2002). AtWRKY33 can be directly phosphorylated by AtMPK3/AtMPK6 to regulate the expression level of genes that participated in camalexin biosynthesis in response to *Botrytis cinerea* infection. The mutation of the phosphorylation sites of AtWRKY33 compromises its camalexin induction ability (Mao et al., 2011).

Considering the crucial role of WRKY TFs in salt response, efforts have been made to investigate the potential function of WRKY genes in crops. For example, transgenic *Arabidopsis* overexpressing soybean *GmWRKY54* or wheat *TaWRKY2* in *Arabidopsis* induced the expression level of stress-responsive genes and thus elevated their salt tolerance ability (Zhou et al., 2008; Tao et al., 2011; Niu et al., 2012). Also, overexpressing cotton *GhWRKY34* in *Arabidopsis* could improve the salt tolerance of transgenic plants by protecting ionic balance and maintaining the stability of the intracellular environment (Zhou et al., 2015). Overexpressing *NbWRKY79* in tomatoes could reduce the accumulation of reactive oxygen and malonaldehyde, enhance the activity of antioxidant enzyme, and ultimately improve the salt tolerance (Nam et al., 2017). Recently, some crops expressing *WRKY* genes under salt stress followed the ABA signaling pathways. For instance, rice overexpressing *OsWRKY45-1* exhibited an induced expression of ABA signal-related and stress-responsive-related genes, which enhanced salt tolerance in the transgenic lines (Tao et al., 2011). Also, *Nicotiana* overexpressing a cotton *GhWRKY17* exhibited an enhanced salt and drought sensitivity by reducing ABA level and downregulating the expression of a series of ABA-inducible genes (Yan et al., 2014). Transgenic *Arabidopsis* overexpressing a GhWRKY6-like TF showed an improved salt tolerance by activating the ABA signaling pathway and decreasing the content of reactive oxygen species (Ullah et al., 2018). Overexpressing the maize *ZmWRKY17* in *Arabidopsis* enhanced salt sensitivity and decreased ABA sensitivity of transgenic plants by regulating ABA- and stress-

responsive genes (Cai et al., 2017). Soybean GmWRKY16 promoted both salt and drought tolerance of transgenic *Arabidopsis* plants through an ABA-mediated pathway (Ma et al., 2019).

Generally, in tandem with their upstream regulators and interacting proteins, the WRKY TFs can modulate plants' salt response by activating or repressing the expression of downstream salt-responsive genes, regulating hormone-related pathways, or inducing physiological responses (Jiang et al., 2017). Partly due to the lack of full genomic sequence information and its hard transformation, the functional study of salt-responsive *WRKY* genes in bermudagrass for potential cultivation in saline soil has been limited. Therefore, in this study, based on the efficient and stable genetic transformation system established in our laboratory, the salt-responsive function and possible molecular mechanism of a salt-induced WRKY TF encoding bermudagrass *CdWRKY2* gene was intensively investigated. Transgenic bermudagrass and *Arabidopsis* plants overexpressing *CdWRKY2* showed higher salt-induced inhibition of LR growth, decreased salt tolerance, and increased ABA sensitivity compared to the negative control plants. Our results demonstrated that CdWRKY2 and its homologues can be useful targets for genetic engineering of salinity-tolerance varieties to achieve salt-tolerant germplasm breeding.

2 Materials and methods

2.1 Plant materials

The bermudagrass variety "Wrangler" was used to isolate gene sequence and check gene expression pattern and was used for transgenic donor. The wild type Col-0 and *mapk3* mutant were used to create the overexpression *Arabidopsis* lines. The *DR5::GUS* lines were used to cross with the *CdWRKY2* overexpression line to generate *DR5::GUS* lines under the *CdWRKY2* overexpression background.

2.2 Gene identification and phylogenetic analysis

The sequence of the *CdWRKY2* coding sequence was identified and isolated from our transcriptome data by using the primers supplied in Table S1. Using ClustalX 2.0, CdWRKY2 and WRKY proteins from other species were aligned (Thompson et al., 2002). Using the neighbor-joining method, phylogenetic trees were conducted and were displayed using the MEGA 5.0 software (Tamura et al., 2011).

2.3 Vector construction and transformation of plants

The *CdWRKY2* coding region was inserted into an entry vector PGWC to construct *PGWC-CdWRKY2* using the homologous recombination method. Then, the entry clone *PGWC-CdWRKY2* was mixed with a Gateway® vector *pUbi-6B* for LR reaction to generate expression vector *pUbi::CdWRKY2*. The construct was then transformed into immature embryos of the bermudagrass variety "Wrangler". To generate the *p35S::CdWRKY2* construct, the *CdWRKY2* coding sequence was cloned into the *pRI101-AN* vector. An *Agrobacterium* strain GV3101 containing the constructed vector was then transformed into *Arabidopsis via* a floral dip method. The homozygous T3 seedlings of independent transgenic lines were used for further experiments. The primers used for vector construction for transformation are listed in Table S1.

2.4 Hydroponic culture of bermudagrass

The uniform stolons of the bermudagrass wild-type "Wrangler" and overexpression bermudagrass lines were planted in solid medium (sand with nutrient solution/1/2 Hogland) for a month. For the RT-qPCR analysis of salt response, the seedlings were washed clean and transferred into CK (1/2 Hogland with 0 mM NaCl) and salt stress (1/2 Hogland with 200 mM NaCl) for 0, 6, or 12 h in the shoots and roots, and the seedlings were transferred into CK (0 mM NaCl) and salt stress (200 mM NaCl) for 0, 6, or 12 h, respectively. For the expression analysis of ABA response, the seedlings were then transferred into 1/2 Hogland with 0 μM ABA or 100 μM ABA added for 0, 3, 6, 12, or 24 h, respectively. For phenotype characterization, after being planted in a single branch of the wild type, overexpression lines were planted in solid medium for approximately 7–10 days. The roots of each plant were washed clean and then supplied with 0 mM NaCl (CK) or 200 mM NaCl (Salt) for approximately 20 days in hydroponic culture. The hydroponic culture was processed in a growth chamber. The growth conditions were set as follows: 65% relative humidity, 400 μmol m^{-2} s^{-1} photons and 22/18°C (16-h day/8-h night). The roots and shoots from three biological replicate plants under control and salt conditions were harvested separately for the analysis of physiological parameters and root morphology. Before treatment and after treatment, the biomass of individual samples was measured and the total PR length, total root length, and number were determined using Win-RHIZO software (Regent Instruments Canada Inc., Ottawa, ON, Canada) to further calculate the relative increment of these parameters. In a separate experiment, the seedlings were transferred to 1/2 Hogland containing 200 mM NaCl (Salt), 200 mM NaCl with 10 nM IAA (Salt+IAA), or 100 μM ABA and grown for approximately 2 weeks to determine the relative increase of root growth parameters, respectively.

2.5 Pot experiment of bermudagrass

The wild-type "Wrangler" and transgenic bermudagrass lines were cut to the same height. The experiment consisted of control and salt treatment conditions, each of which had three biological replications. For salt treatment of bermudagrass, the plants were treated with 200 mM NaCl for 4 weeks. For the control condition, the plants were supplied with water without NaCl. The plant height and biomass of every individual plant from the three biological

replicates was detected and the leaves and roots were harvested separately to determine the physiological parameters. The electrolyte leakage (EL), malondialdehyde (MDA), and the activities of antioxidant enzymes were measured based on the previous description (Shao et al., 2020).

2.6 Plant growth conditions of *Arabidopsis*

CK (0 mM NaCl or ABA) represents normal growth conditions for *Arabidopsis*, and Salt (100 mM NaCl) or ABA (10 μM) represents stress treatment. Briefly, the stratified *Arabidopsis* seeds were cultured on nutritious medium (one-half-strength Murashige and Skoog) containing 1.0% agar for 4 days. The seedlings were then transferred to CK, Salt, and ABA medium and were cultured vertically for 7–10 days in a growth chamber, which was set at 22°C with a 16-h/8-h (light/dark) cycle. The numbers of visible lateral roots were counted manually. After salt treatment, the shoots of Col-0 and transgenic *Arabidopsis* lines were collected to measure their shoots' fresh weight. The root samples of Col-0 and transgenic lines were collected for gene expression analysis. In a separate experiment, the seedlings were transferred to 1/2 MS containing 100 mM NaCl (Salt) or 100 mM NaCl with 0.1 μM IAA (Salt+IAA) for shoot fresh weight and LR number measurement, respectively.

2.7 Yeast transformation

For the trans-activation assay, the coding region of *CdWRKY2* was amplified and cloned into the *pGBKT7* vector (Clontech) to generate a *pGBKT7-CdWRKY2* construct and was then transformed into yeast strain AH109 competent cells. The empty *pGBKT7* vector was transformed individually as a negative control. The transformed yeast cells were cultured on SD/-Trp/-His/-Ade to check their growth status. For DNA binding activity, three W-box (CGTTGACC) and three mutated W-box (mW-box) (CGTAGACG) were constructed into the *pAbAi* vector, respectively, and were grown on growth medium containing 800 ng/ml AbAi. For yeast two-hybrid, the *pGBKT7-CdWRKY2* and *pGADT7-MAPK3* (or *pGADT7-AtWRKY46*) vectors were co-transformed into Y2H gold strain competent cells. The *pGBKT7-53* and *pGADT7-T* vector pair was co-transformed as a positive interaction control. The transformed yeast cells were grown on SD/-Trp/-Leu and SD/-Trp/-Leu/-Ade/-His plates, respectively. For yeast one-hybrid, the W-box-containing region of *ABI4*, *UGT84B2*, and *AtWRKY46* promoter sequence was cloned into *pAbAi* yeast vector to construct *pABI4-AbAi*, *pUGT84B2-AbAi*, and *pAtWRKY2-AbAi* vectors. The *pGADT7-CdWRKY2/pABI4-AbAi* (or *pUGT84B2-AbAi* or *pAtWRKY46*) vector pair was co-transformed into Y1H yeast strains, respectively. Furthermore, the *pGADT7-AtWRKY2* and *pAtWRKY46* vector pair was co-transformed into Y1H yeast strains. All the yeast cells were streaked on SD/-Leu and SD/-Leu+AbAi plates (200 ng/ml), respectively, and were placed at 28°C under dark conditions for 3–5 days to check their growth state.

2.8 GUS staining and GUS quantitative assay

DR5::GUS staining in *Arabidopsis* samples was conducted as previously described (Ma et al., 2014). Samples were stained in solution containing 50 mM $NaPO_4$, 0.4 mM $K_3Fe(CN)_6$, 0.4 mM $K_4Fe(CN)_6$, 1 mM X-gluc, and 0.1% Triton X-100 incubated at 37°C for 8 h in the dark. After GUS staining, the stained samples were washed with 70% ethanol three times and then microscopically imaged. GUS activities were measured as previously described (Liu et al., 2015). Briefly, seedlings of each sample were collected in Eppendorf tubes (100 mg per measurement) and homogenized with steel beads in buffer (50 mM potassium phosphate buffer, pH 7, 1 mM EDTA, 0.1% SDS, and 0.1% Triton X-100). The supernatant was used for measurement after centrifuging at 12,000 rpm for 15 min at 4°C and the protein concentrations were quantified using a Micro BCA Protein Assay Kit (Vigorous). Enzyme activity was calibrated by the concentration of 4-methylumbelliferone (Sigma-Aldrich). The fluorescence of the samples was measured on 96-well plates on a Fluoroskan Ascent FL fluorometer (excitation wavelength of 365 nm and emission wavelength of 455 nm) after incubating with 4-methylumbelliferyl-β-D-glucuronide hydrate (Sigma-Aldrich). Measurements were read when stopped by adding stop buffer (0.2 M Na_2CO_3) at 0, 15, 45, and 60 min, and the standard curve was fitted.

2.9 Gene expression analysis

Total RNA of different tissues was extracted (RNAeasy kit, QIAGEN) and the commensurable RNA of each sample was reverse-transcribed to first-strand cDNA and were diluted to the same multiples for the template for gene expression analysis (TaqMan reverse transcription kit, Applied Biosystems). The qPCR system containing 10 μl of SYBR Green mix (Roche, Mannheim, Germany), 2 μl of template, and 0.2 μM primers was conducted using the ABI real-time PCR system (Applied Biosystems, Foster City, CA). Three technical replicates of each reaction were performed. Transcript levels of each sample were determined and normalized with respect to the internal control gene using the ΔΔCt method (Czechowski et al., 2005; Schmittgen and Livak, 2008; Chen et al., 2015). The specific primers used for RT-qPCR are shown in Table S2.

2.10 Statistical analysis of data

SPSS22 software for Windows (SPSS Inc., Chicago, Illinois, US) was used for one- or two-way analysis of variance (ANOVA tests,

Tukey's post-hoc test). The individual p level of comparison is shown in Tables S3, S4, and S5.

3 Results

3.1 Identification, expression, and DNA binding activity analysis of CdWRKY2

Here, a *CdWRKY2* gene, containing a complete open reading frame (ORF) of 2,025 bp, was cloned from bermudagrass. The CdWRKY2 contained two WRKYGQK motifs (Figure 1A) and a C_2HC-type zinc finger and belonged to the group I WRKY subfamily (Figure S1). Homology search and phylogenetic analysis of the WRKY-related proteins against the GenBank database showed that CdWRKY2 was homologous to AtWRKY2 TF of *Arabidopsis* (Figure 1B). A transcriptional activity assay using yeast one-hybrid method indicated that CdWRKY2 possesses no transcriptional activation activity in the yeast. This was deduced from the observation that only the positive control yeast cells could grow on the SD/-Trp/-His/-Ade, which was converse to the negative control and the cells transformed with *pGBKT7-CdWRKY2* (Figure 1C). However, CdWRKY2 had a putative role as a WRKY TF binding to the W-box of target genes because the *pAbAi-W-box/pGADT7-CdWRKY2* co-transformation yeast cells could grow on SD/-Leu (containing 800 ng/ml AbA) medium whereas the *pAbAi-mW-box/pGADT7-CdWRKY2* (mW represents mutated W-box) co-transformation yeast cells could not grow (Figure 1D). A quantitative real-time PCR (RT-qPCR) analysis indicated that the *CdWRKY2* was expressed in both the roots and shoots (Figure 1E). Also, the investigation of expression pattern in response to salt revealed a strong upregulation of *CdWRKY2* expression in the shoots and roots after NaCl exposure for 6 h or 12 h (Figure 1E).

3.2 Overexpressing *CdWRKY2* in bermudagrass increases plants' salt sensitivity

By transforming the bermudagrass cultivar "Wrangler" with *pUbi::CdWRKY2*, eight overexpression lines were successfully obtained (Figure S2) and two lines (CdOE13 and CdOE12) with higher *CdWRKY2* expression levels were selected for subsequent investigation under control and salt conditions (Figures 2A; S2). In the pot experiment, the plant height of the two overexpression lines (CdOE13 and CdOE12) and the negative control plants (WT) showed no significant difference. However, under salt conditions, overexpression of *CdWRKY2* in bermudagrass significantly decreased plant height compared to the negative control plants (Figure 2B). The salt tolerance-related physiological indicators were further measured. We observed that the EL (Figure 2C) and MDA content (Figure 2D) of *CdWRKY2* overexpression lines were

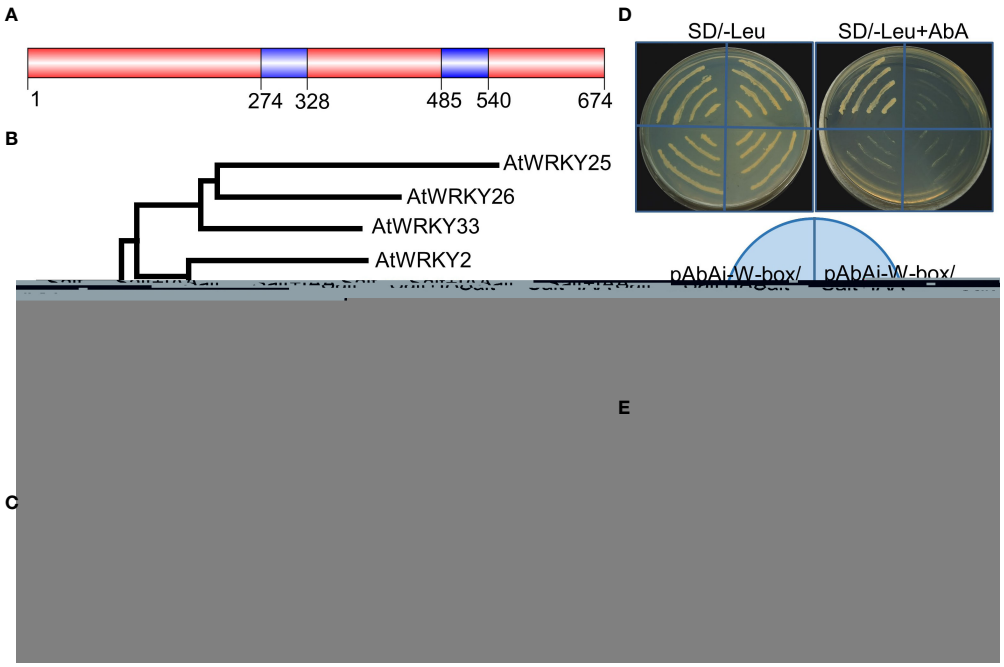

FIGURE 1
Sequence analysis, transcription activation activity, DNA binding activity, and gene expression of CdWRKY2. **(A)** The protein structure of CdWRKY2 with two WRKY domains. **(B)** Phylogenetic tree constructed with CdWRKY2 and other WRKY proteins in *Arabidopsis* by the MEGA 5.0 program with neighbor-joining method. **(C)** Transcriptional activation analysis of CdWRKY2 in yeast cells. The negative control vector was *pGBKT7*. **(D)** W-box and mutated W-box (mW-box) was constructed into *pAbAi* vector, respectively, and were used to check DNA binding activity of CdWRKY2 using the yeast one-hybrid method. RT-qPCR analysis of *CdWRKY2* expression in the shoots and roots under salt condition (200 mM NaCl for 0, 6, and 12 h) **(E)**. The internal control gene used for salt treatment was *CdPP2A*. Data are represented as means ± SD of three independent replicates, and different letters indicate significant differences at $p < 0.05$ by two -way analysis of variance (ANOVA tests) with Tukey's post-hoc test.

10.3389/fpls.2023.1164534

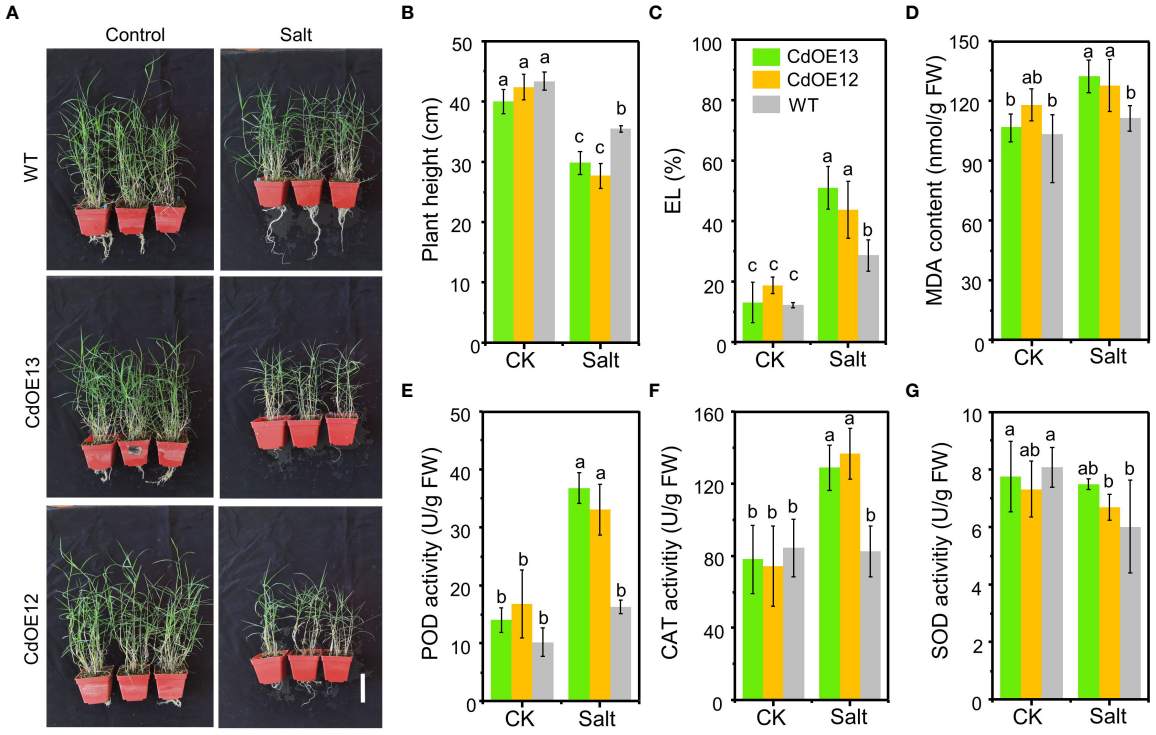

FIGURE 2
The phenotype of *CdWRKY2* overexpression transgenic bermudagrass plants. The same number of branches of the *CdWRKY2* overexpression lines (CdOE13 and CdOE12) and the transgenic negative control line (WT) were planted in soil for about 1 month. The plants were cut to the same height and supplied with 0 mM NaCl (CK) or 200 mM NaCl (Salt) and then treated for 4 weeks. **(A)** Images of the overexpression lines and control line grown under CK and salt conditions. Bar = 10 cm. **(B)** Plant height after treatments. **(C)** EL. **(D)** MDA content. **(E)** POD activity. **(F)** CAT activity. **(G)** SOD activity. Data are the means ± SD of three independent biological replicates containing at least 10 plants. Different letters represent statistically significant differences at $p < 0.05$. Two-way ANOVA test was used and the data were further compared by Tukey's post-hoc multiple range test. Different letters on histograms indicate that means were statistically different at the $p < 0.05$ level.

significantly higher than those of the negative control plants under salt conditions. Moreover, we determined the degree of lipid peroxidation and the activities of antioxidant enzymes of the leaves. Under salt stress, the activities of peroxidase (POD) (Figure 2E) and catalase (CAT) (Figure 2F) were greater than those of the negative control plants while the superoxide dismutase (SOD) activities remained statistically unchanged (Figure 2G). The phenotypic and physiological indicators of plants observed and detected under salt stress suggested that overexpression of *CdWRKY2* could increase the sensitivity of bermudagrass to salt stress.

3.3 *CdWRKY2* overexpression inhibits the salt-induced root growth of bermudagrass

In the soil experiment, we noticed that salt stress notably induced the root growth of negative control plants while there was no obvious induction of root growth of overexpression lines (Figure 2A). To further confirm the inhibition of root growth in *CdWRKY2* overexpression lines, we hydroponically investigated the root growth difference. The results showed that under salt conditions, both the CdOE13 and CdOE12 lines exhibited a lower increase of biomass (Figure 3A) and a higher withering rate (Figure 3B) than the negative control plants, which was consistent with the soil experiment. Concretely, the negative control plants showed significantly increased total root length (Figure 3F) and total root number (Figure 3G) when exposed to salt conditions compared to the control condition. However, total root length and number of *CdWRKY2* overexpression lines showed no significant salt-induced increase under salt stress compared to the control condition (Figures 3F, G). In addition, under salt stress, the *CdWRKY2* overexpression-induced inhibition degree on the primary roots (PR) was relatively lower than that of the LR, as the salt-induced relative increment of total PR length (Figure 3E) and total root length (Figure 3F) of the overexpression lines was approximately 70% and 10% that of the wild type, respectively. This observation suggested that the salt-induced total root length increment might stem from the contribution of LR increase and the inhibition effect of overexpressing *CdWRKY2* on root growth under salt stress might be mainly derived from LR inhibition.

3.4 Overexpression of *CdWRKY2* inhibits LR growth and increases salt sensitivity in *Arabidopsis*

To investigate the possible salt-induced mechanism underlying the root growth inhibition of *CdWRKY2* overexpression lines

10.3389/fpls.2023.1164534

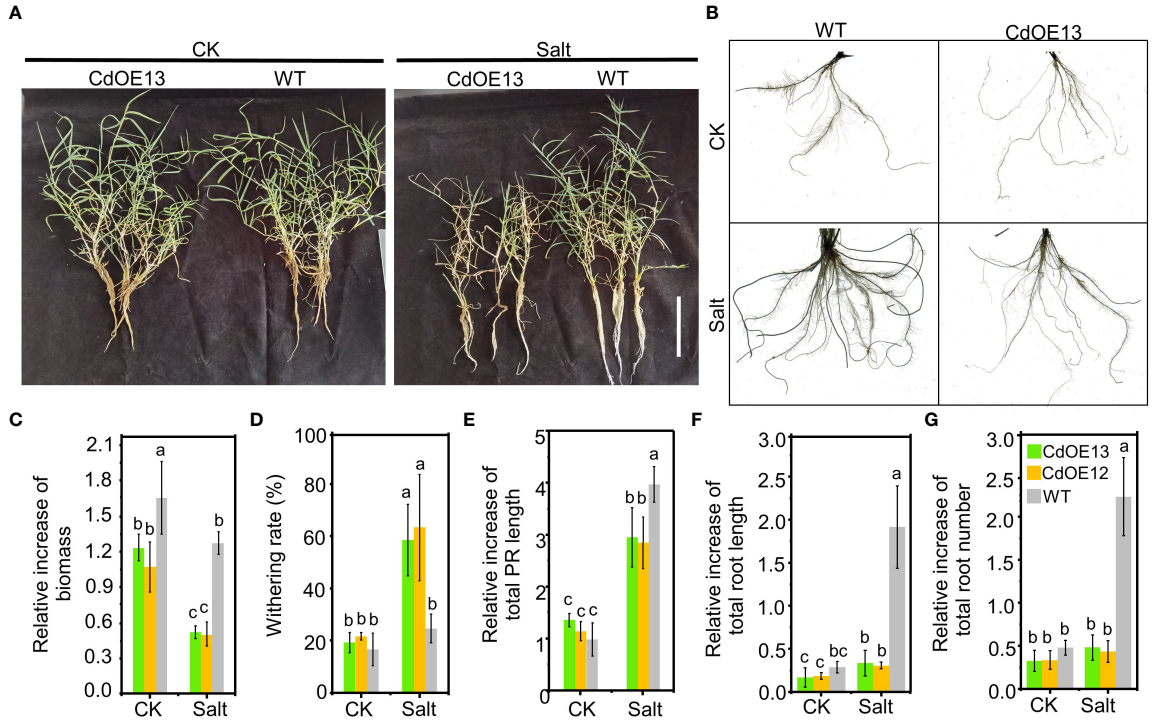

FIGURE 3
The phenotype of *CdWRKY2* overexpression transgenic bermudagrass grown in hydroponic culture. A single branch of the *CdWRKY2* overexpression lines (CdOE13 and CdOE12) and the transgenic negative control line (WT) was planted in soil for approximately 7 days. The roots of each plant were washed clean and then supplied with 0 mM NaCl (CK) or 200 mM NaCl (Salt) for 20 days in hydroponic culture. **(A)** Images of the overexpression lines and control line grown under CK and salt conditions. Bar = 10 cm. **(B)** Images of roots of plants under CK and salt conditions. **(C)** Relative increment of biomass before and after treatment. **(D)** Withering rate. **(E)** Relative increase of total PR length before and after treatment. **(F)** Relative increase of total roots length before and after treatment. **(G)** Relative increase of total roots number before and after treatment. Data are the means ± SD of three biological replicates. Two-way ANOVA test was used and the data were further compared by Tukey's post-hoc test. Significant differences at $p < 0.05$ were shown by different letters above the columns.

(AtOE10-4 and AtOE6-1), we studied the growth pattern of transgenic *Arabidopsis* lines overexpressing this gene (Figures 4A, B). Under salt conditions, the shoot and root growth of AtOE10-4 was obviously decreased than that of the wild type (Col-0) (Figure 4A). The results showed that both the AtOE10-4 and AtOE6-1 lines had lower shoot fresh weight (Figure 4D) compared to the wild type under salt treatment. Furthermore, salt treatment significantly decreased the number of visible LR in transgenic lines relative to the wild type (Figure 4E). Reports showed that the stress-induced LR inhibition can be realized by interfering with auxin-related response (Lavenus et al., 2013). Therefore, we added IAA (1 μM) into the growth media. Interestingly, we observed that IAA application could significantly rescue the salt hypersensitivity of salt-treated *CdWRKY2* transgenic *Arabidopsis* lines (Figure 4C), as the inhibition of LR growth (Figure 4F) and shoot growth (Figure 4G) showed no significant difference between overexpression lines and the wild type after IAA application. In bermudagrass, IAA application could partially rescue the salt hypersensitivity of root growth in *CdWRKY2*-overexpressing bermudagrass lines, as the salt-inhibited total root length and total root number were slightly decreased compared with the wild type (Figures S3C, D). From the results in bermudagrass together with *Arabidopsis*, CdWRKY2 was proved to participate in the inhibition of salt-induced LR growth in bermudagrass and in the salt-inhibited LR growth in *Arabidopsis*. Moreover, preliminary results indicated that CdWRKY2 might negatively affect LR development under salt stress and increase the salt sensitivity of plants *via* the regulation of auxin homeostasis.

3.5 IAA accumulation decreases in *CdWRKY2* overexpression *Arabidopsis*

To determine the possible contribution of auxin distribution in salt-induced *CdWRKY2* inhibitory role to LR development, the expression pattern of *DR5::GUS* (Ulmasov et al., 1997) was investigated in both the wild type (Col-0) and *CdWRKY2* overexpression background (AtOE10-4) plants grown under both control and salt conditions. We observed that the overexpression line AtOE10-4 exhibited a weaker GUS staining in LR primordia (LRP) (Figure 5A), non-emerged LR tip (Figure 5B), and the visible LR tip (Figure 5C) compared with the wild type under salt stress. However, under normal conditions, GUS staining in LR showed no obvious difference between transgenic line and wild type (Figure 5). The relative GUS activity of roots expressing *DR5::GUS* in AtOE10-4 presented a significant lower salt-inhibited value compared to the wild type (Figure S4). The expression of auxin synthesis gene *YUC1* and *YUC4* was higher in overexpression lines under both control and

10.3389/fpls.2023.1164534

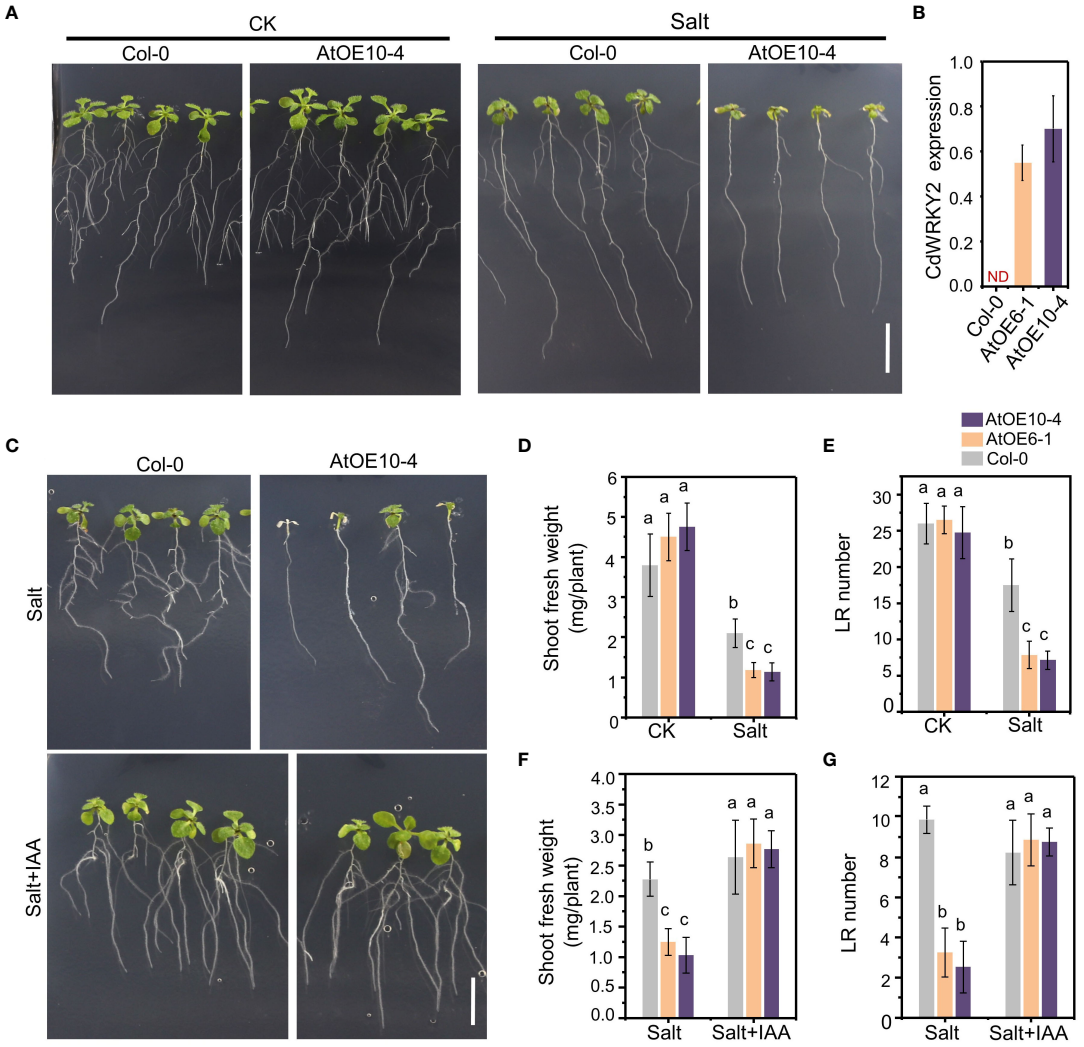

FIGURE 4
The phenotype of the *CdWRKY2* transgenic *Arabidopsis* lines. The seeds of wild type (Col-0) and *CdWRKY2* overexpression lines (AtOE10-4 and AtOE6-1) were germinated and grown for 4 days on 1/2 MS. The seedlings were transferred to 1/2 MS containing 0 mM NaCl (CK), 100 mM NaCl (Salt), or 100 mM NaCl with 0.1 μM IAA (Salt+IAA), respectively. The morphological parameters were measured after being grown vertically for 7 days. **(A)** Images of overexpression line (AtOE10-4) and wild type (Col-0) grown 7 days on CK and salt conditions. Bar = 1 cm. **(B)** Relative expression of *CdWRKY2* in AtOE10-4 and AtOE6-1. **(C)** Images of AtOE10-4 and Col-0 grown 7 days on 1/2 MS containing salt and salt plus 0.1 μM IAA, respectively. Bar = 1 cm. **(D)** Shoot fresh weight of overexpression and wild-type plants grown under CK and salt conditions. **(E)** Visible LR number of overexpression and wild-type plants grown under CK and salt conditions. Shoot fresh weight **(F)** and visible LR number **(G)** of overexpression and wild-type plants grown under salt and salt plus IAA conditions. Data are represented as means ± SD of at least 15 seedlings from three independent treatments. Two-way ANOVA test was used and the data were further compared by Tukey's post-hoc test. Different letters displayed represent significant differences at $p < 0.05$ statistically.

salt conditions and significantly decreased by salt (Figures 5D, E). Furthermore, the expression of auxin transporter encoding gene *PIN1* in the transgenic lines was higher under normal conditions but decreased significantly under salt conditions (Figure 5F). *PIN3* was upregulated in the overexpression line under both control and salt conditions (Figure S5A). However, under both control and salt conditions, the expression of other auxin transport-related genes such as *PIN2*, *PIN7*, *PID* (Figures S5B–D), and other auxin synthesis-related genes *TAA1* and *TAR2* (Figures S5E, F) remained statistically unchanged in wild-type and transgenic lines. Moreover, salt significantly induced the expression of the auxin conjugation-related gene *UGT84B2* and had a higher level in *CdWRKY2* overexpression lines under both control and salt conditions (Figure 5G). Other auxin conjugation-related genes such as *IAGLU* and *GH3.1* showed no difference between wild-type and transgenic lines under both control and salt conditions (Figures 5G, H).

3.6 Root ABA sensitivity increases in *CdWRKY2* overexpression lines

To investigate the role of ABA on salt-induced *CdWRKY2* overexpression, we compared the LR growth of wild type and *CdWRKY2* overexpression *Arabidopsis* lines on a medium containing 10 μM ABA. Results indicated that overexpression lines

10.3389/fpls.2023.1164534

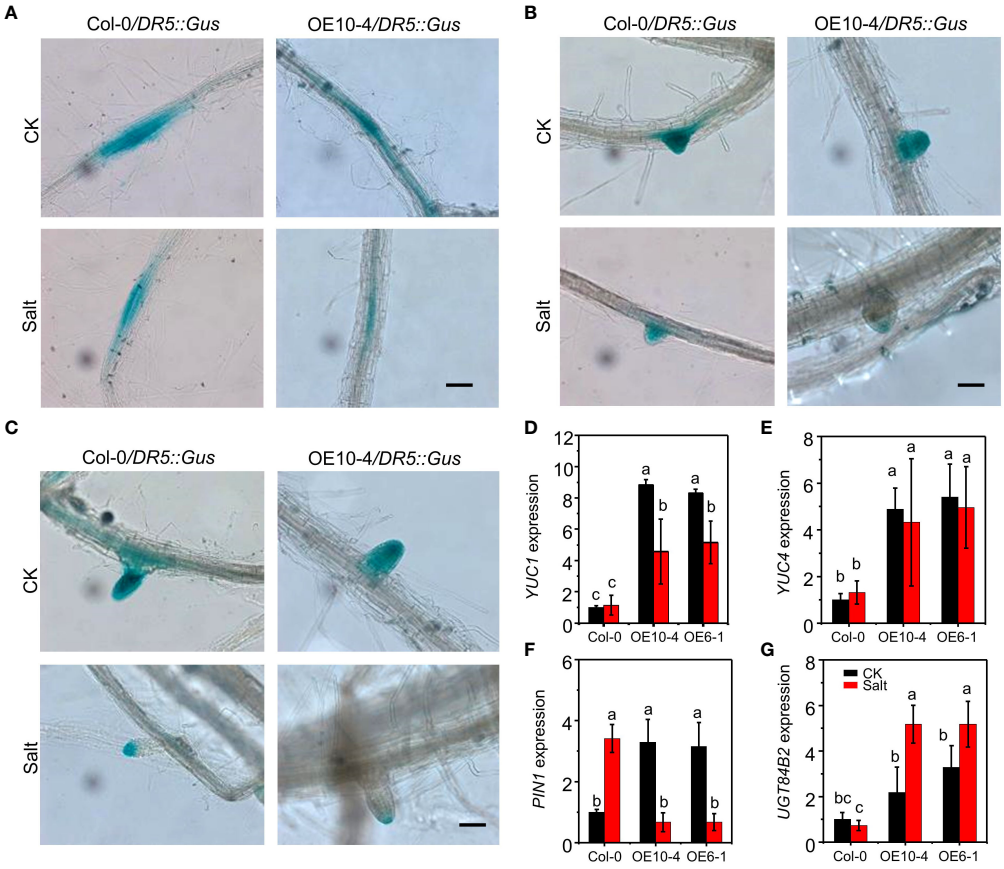

FIGURE 5
GUS staining and auxin pathway-related gene expression of Col-0 and the *CdWRKY2* overexpression background. The seeds of wild type (Col-0), *CdWRKY2*-overexpressing line (AtOE10-4), plants expressing *DR5::GUS* in Col-0 and AtOE10-4 background were germinated for 4 days. The seedlings were transferred to 1/2 MS that contained either 0 mM NaCl (CK) or 100 mM NaCl (Salt) for 7 days. GUS staining in LR primordia (LRP) **(A)**, emerged LR tip **(B)**, and visible LR **(C)**. Bar = 1000 μm. Gene expression of *YUC1* **(D)**, *YUC4* **(E)**, *PIN1* **(F)**, and *UGT84B2* **(G)** in Col-0 and AtOE10-4 roots under CK and salt conditions were determined by RT-qPCR using *UBQ10* as an internal control reference gene. Transcript levels of each sample were normalized to the expression of untreated wild-type plants. Three independent replicates were performed. Two-way ANOVA test was used and the data were further compared by Tukey's post-hoc test. Different letters represent significant differences at $p < 0.05$.

exhibited higher ABA sensitivity with less LR number (Figures 6A, B). In bermudagrass, the upregulated expression in the roots by ABA was observed especially after ABA application for 6 h and 12 h (Figure S3B). The ABA sensitivity *CdWRKY2* overexpression line also showed significant elevation compared to the wild type with decreased root length and root number (Figures S3C, D). In the *CdWRKY2* overexpression *Arabidopsis* lines, the expression of ABA-responsive genes such as *ABI4* (Figure 6C), *ABI5* (Figure 6D), *ABI3* (Figure 6E), and *ABF1* (Figure 6F) was upregulated compared to wild type under control conditions, which might contributed to the ABA hypersensitive phenotype of *CdWRKY2* overexpression lines. The *ABI4* (Figure 6C) gene was highly expressed in *CdWRKY2* overexpression lines compared to the wild type under both control and salt conditions. Under salt stress, the expression of *ABI5* (Figure 6D) and *ABF1* (Figure 6F) decreased in the *CdWRKY2* overexpression lines compared to that in the wild type, while under control conditions, the expression of *ABF2* (Figure 6G) and *ABF3* (Figure 6H) declined in the *CdWRKY2* overexpression lines compared to that in the wild type. In contrast, in transgenic lines, the expression of *ABI1* and *ABI2* showed higher salt inhibition degree compared to the wild type (Figures S6A, B). *ABI4* or *UGT84B2* was reported to act downstream of AtWRKY46 to play a critical role in LR growth under salt stress (Ding et al., 2015). Therefore, using the yeast one-hybrid system, we investigated the interaction of CdWRKY2 with their promoter regions, which contained several W-box (Figure 6I). However, *pGADT7-CdWRKY2* and *pABI4-AbAi* (or *pUGT84B2-AbAi*) co-transformed yeast cells could not grow on -Leu plates containing 200 ng/ml AbAi, the same as control vector pairs (*pGADT7-AD/pABI4-AbAi* or *pGADT7-AD/pUGT84B2-AbAi*), suggesting that there was no interaction *in vitro* (Figure 6J). However, in *CdWRKY2* overexpression lines, the *AtWRKY46* expression level was significantly inhibited compared to wild type (Figure 6K). Subsequently, yeast two-hybrid and yeast one-hybrid experiments showed that CdWRKY2 had no protein interaction with AtWRKY46 (Figure S7) but could bind to the promoter region of *AtWRKY46* (Figure 6J). Moreover, in the yeast one-hybrid assay, no interaction was observed between AtWRKY2 protein (the orthologs of CdWRKY2) and the promoter of *AtWRKY46*, suggesting that AtWRKY2 and CdWRKY2 might not be direct counterparts during salt-induced root inhibition (Figure 6J).

10.3389/fpls.2023.1164534

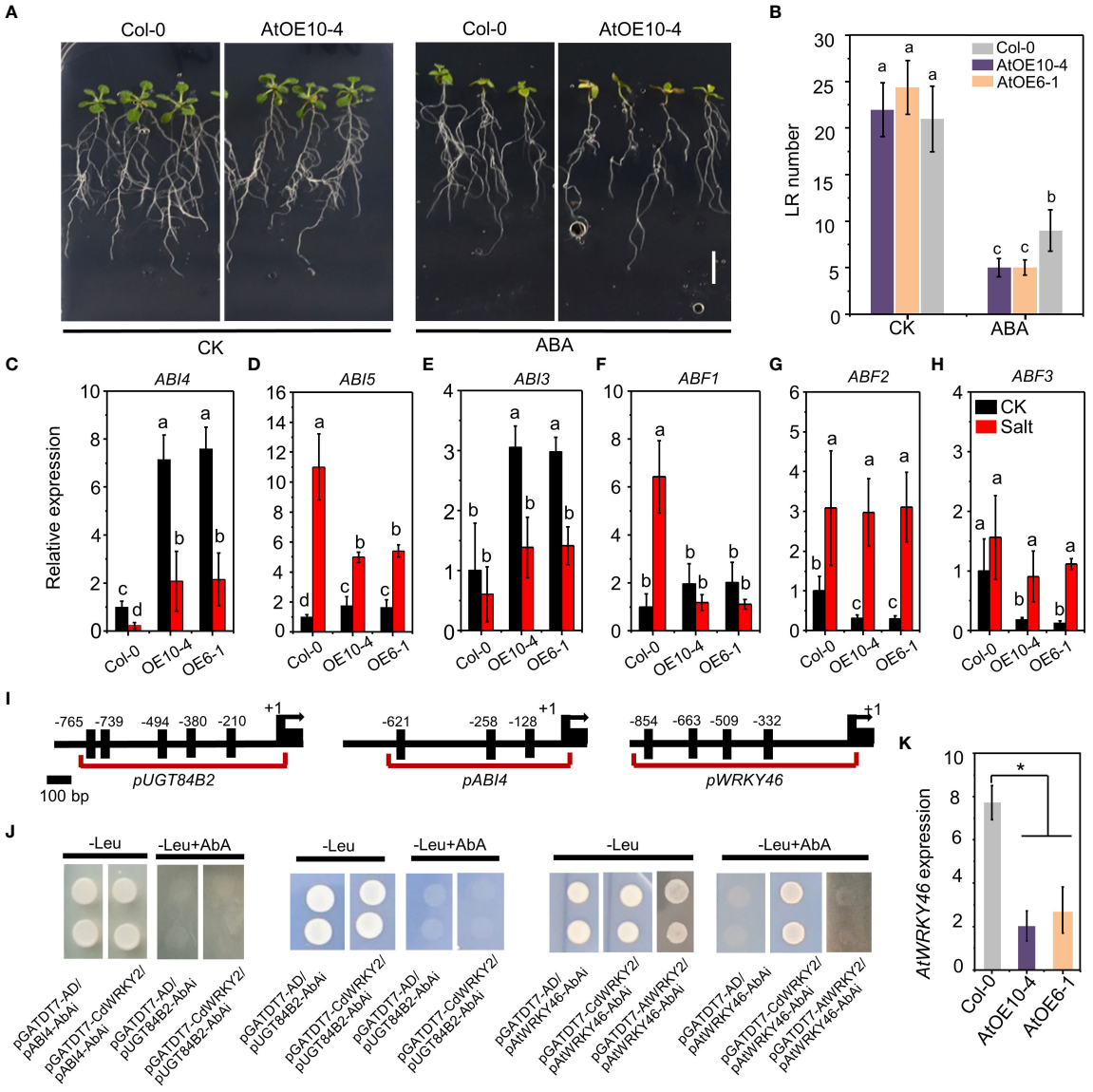

FIGURE 6
The ABA sensitive phenotype of the *CdWRKY2* overexpression *Arabidopsis* lines. The seeds of wild type (Col-0), *CdWRKY2* overexpression lines (AtOE10-4 and AtOE6-1) were germinated for 4 days on 1/2 MS and the seedlings were then transferred to 1/2 MS containing 0 mM ABA (CK) or 10 μM ABA (ABA), respectively. After being grown vertically for 10 days, morphological parameters were measured. **(A)** Images of overexpression line (AtOE10-4) and wild type (Col-0) grown 10 days on CK and ABA conditions. Bar = 1 cm. **(B)** Visible LR number of overexpression lines and wild-type plants grown under CK and ABA conditions. **(C–F)** Relative expression of ABA-responsive genes in the roots of Col-0 and overexpression lines under control and salt conditions of three independent replicates. *ABI4* **(C)**, *ABI5* **(D)**, *ABI3* €, *ABF1* **(F)**, *ABF2* **(G)**, *ABF3* **(H)**. *UBQ10* was used as an internal control reference gene. Transcript levels of each sample were normalized to the expression of untreated wild-type plants. Three independent replicates were performed. Two-way ANOVA test was used and the data were further compared by Tukey's post-hoc test. Different letters on histograms indicate that means were statistically different at the $p < 0.05$ level. **(I)** Illustration of the *ABI4*, *UGT84B2*, and *AtWRKY46* promoter regions showing the presence of consensus motif W-box. Shown are 2-kb upstream sequences of genes. **(J)** Yeast one-hybrid analysis of the binding of CdWRKY2 to the promoters. The promoter region of *ABI4*, *UGT84B2*, and *AtWRKY46* containing multiple W-box was constructed into pAbAi vector, respectively, and was used to check DNA binding activity of CdWRKY2 using yeast one-hybrid method. The promoter region of *AtWRKY46* was then used to check the DNA binding activity of AtWRKY2. **(K)** The relative expression level of *AtWRKY46* in *CdWRKY2* overexpression lines. Data are represented as means ± SD of three independent replicates, and * indicates significant difference between Col-0 and overexpression lines at $p < 0.05$ by one-way analysis of variance with Tukey's post-hoc test.

3.7 *CdWRKY2* functions in elevating salt sensitivity in *Arabidopsis* partially *via* AtMAPK3

Several reports have shown that WRKY TFs may function downstream of MAPK cascades. Rice OsWRKY30, which is the direct homologue of CdWRKY2, could interact with AtMAPK3 and was proved to play a vital role in drought tolerance of rice (Shen et al., 2012). Here, using the yeast two-hybrid method, we observed that CdWRKY2 could interact with AtMAPK3 in the yeast cell (Figure 7A). The expression level of CdWRKY2 was not detectable in Col-0 and *mapk3* (Figure 7B). Overexpression of *CdWRKY2* in

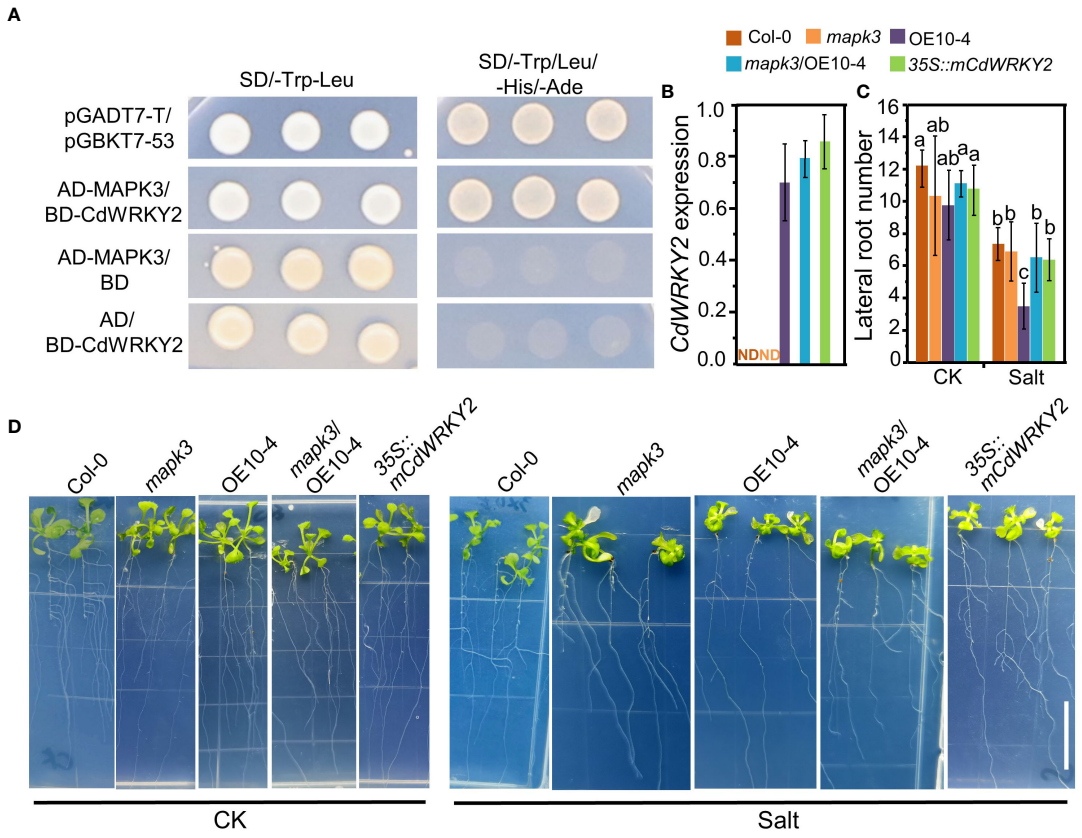

FIGURE 7
CdWRKY2 functions in LR growth inhibition under salt stress in *Arabidopsis via* the function of MAPK3. **(A)** Interactions between AtMAPK3 and CdWRKY2 in the yeast cell. Transformants transferred with different construct pair growth on SD/-Trp-Leu and SD/-Trp-Leu-His-Ade plates. *pGADT7-T/pGBKT7-53* was used as a positive control vector pair. **(B)** The seeds of Col-0, *mapk3* mutant, AtOE10-4 (*CdWRKY2* overexpression line), *mapk3*/AtOE10-4 (*CdWRKY2* overexpression in *mapk3* mutant background), and *35S::mCdWRKY2* (mutated *CdWRKY2* overexpression line) were germinated and grown for 4 days on 1/2 MS. The seedlings were transferred to 1/2 MS containing 0 mM NaCl (CK) and 100 mM NaCl (Salt), respectively. The morphological parameters were measured and the gene expression was analyzed after being grown vertically for 7 days. Total RNAs were extracted from the roots of seedlings of these genotypes and gene expression was determined by RT-qPCR using *AtActin2* mRNA as internal reference. Three independent repeats were done. The expression of *CdWRKY2* in Col-0 and *mapk3* was not detectable (ND). **(C)** LR number of different plant samples grown under control and salt conditions. Three independent experiments containing at least 10 plants were performed. Two-way ANOVA test was used and the data were further compared by Tukey's post-hoc test and statistically significant differences at $p < 0.05$ were displayed by different letters. **(D)** Image of different genotypes of plants samples grown under control and salt conditions. Bar = 1 cm.

the *mapk3* background *Arabidopsis* could partly rescue the salt oversensitive phenotype of LR grown on salt condition (Figures 7C, D) by statistical analysis of LR number between *CdWRKY2* overexpression lines in wild type and *mapk3* mutant background (Figure 7C). In the CdWRKY2 protein sequence, there are six potential SP (serine proline) phosphorylation sites (Figure S8). To identify the necessity of SP sites for the function of *CdWRKY2*, we mutated the first two SP sites (SP site into alanine proline site) and constructed an m*CdWRKY2* overexpression line in *Arabidopsis*. Results showed that the salt sensitivity of *mCdWRKY2* overexpression lines had no significant difference with the wild type (Figures 7C, D). These preliminary results suggested that the function of elevated salt sensitivity of *CdWRKY2* might partially be dependent on the function of MAPK3. Also, the SP sites of CdWRKY2 might play a critical role in the process of CdWRKY2 performing its function in elevating the salt sensitivity in *Arabidopsis*.

4 Discussion

WRKY has been reported to play multiple roles in plant development and abiotic responses including salt stress (Ülker and Somssich, 2004; Rushton et al., 2012). However, little progress in bermudagrass has been made because of its complex transformation and lack of genomic reference. In this study, a salt-induced *CdWRKY2* was cloned based on a reference sequence obtained by stitching two RNA-Seq data of bermudagrass (Hu et al., 2015; Shao et al., 2021). To investigate its function in salt response, we successfully obtained eight overexpression lines by transforming bermudagrass cultivar "Wrangler" with *pUbi::CdWRKY2* and two transgenic lines (CdOE13 and CdOE12) were further used for further study. Results showed that the overexpression lines exhibited enhanced salt sensitivity compared with the negative control lines (Figure 2), suggesting that CdWRKY2 might act as a negative regulator of salt tolerance in bermudagrass (Vanderauwera et al., 2012). We noticed that the root growth of control

lines was significantly induced by salt compared to the control condition (Figure 3). This can be attributed to the relative salt-tolerant cultivar used in this study. However, under salt treatment, bermudagrass overexpressing *CdWRKY2* had a lower root growth rate than the negative control counterparts (Figure 3). We also noticed that the inhibition degree of overexpressing *CdWRKY2* on the primary root was relatively lower than that of the LR. To investigate the possible mechanism underlying the salt-induced LR inhibition of *CdWRKY2* overexpression lines, we then conducted overexpressed *Arabidopsis* lines of *CdWRKY2* (Figures 4A, B). The statistical results showed that both the AtOE10-4 and AtOE6-1 lines had less LR number (Figure 4E) than the wild type under salt treatment. However, the PR length was not obviously altered. Taken together, we speculated that the salt-induced inhibitory role of CdWRKY2 might be mainly exerted on the development of LR growth, which was reported to be a main determinant of plant root architecture (Péret et al., 2009).

Previous studies have shown that auxin metabolism plays an important role in LR development (Lavenus et al., 2013). To determine the possible effect of auxin distribution in salt-induced inhibitory on LR growth, we investigated the expression pattern of auxin-indicator gene *DR5::GUS* (Ulmasov et al., 1997) in the wild type (Col-0) and *CdWRKY2*-overexpressing (AtOE10-4) background *Arabidopsis* grown under both control and salt treatment. Compared with the wild type, the AtOE10-4 line displayed a weaker GUS staining in LR (Figure 5) especially under salt stress. To explore the possible mechanism, the expression of genes that participated in the major auxin synthesis pathway named IPA pathway was detected (Won et al., 2011; Zhao, 2012). We observed that the expression of auxin synthesis gene *YUC1* was highly expressed in *CdWRKY2*-overexpressing lines under both control and salt conditions and significantly decreased under salt conditions (Figure 5D). The expression of other auxin synthesis genes *TAA1*, *TAR2*, and *YUC4* had no obvious difference between the wild type and *CdWRKY2*-overexpressing lines under both control and salt conditions (Figure 5E; S5E, F). We also observed that *PIN3* was upregulated in *CdWRKY2*-overexpressing lines under both control and salt conditions. *PIN3* is expressed in the pericycle where LR is generated to function in auxin transportation (Friml et al., 2002). Thus, in this study, the upregulation of *PIN3* in *CdWRKY2*-overexpressing lines might also be a stimulus response during LR growth inhibition in *CdWRKY2*-overexpressing lines. In this study, CdWRKY2 could directly bind to the promoter of *AtWRKY46*, which was required for LR development under osmotic/salt stress by directly regulating the expression of auxin conjugation (to produce inactive forms of auxin to accurately modulate their endogenous auxin levels)-related gene *UGT84B2* and *GH3* in *Arabidopsis* (Staswick et al., 2005; Westfall et al., 2010; Korasick et al., 2013; Ding et al., 2015). The expression of *UGT84B2* was higher in *CdWRKY2*-overexpressing lines under both control and salt conditions (Figure 5G). However, *GH3.1* expression remained unchanged between the wild type and *CdWRKY2*-overexpressing lines under both control and salt conditions (Figure S5H), which might be probably because CdWRKY2 not only regulated the expression of *AtWRKY46* but also affected other modules to further neutralize the gene expression change of *GH3.1*.

ABA has previously been shown to play important roles in plants' response to abiotic stress. Also, a series of TFs could function in abiotic response in an ABA-dependent manner including WRKY TFs (Zhou et al., 2008; Jiang and Deyholos, 2009; Cai et al., 2017). ABA has also been shown to play critical roles in mediating osmotic stress-dependent LR inhibition (Deak and Malamy, 2005). Here, we found that ABA significantly induced *CdWRKY2* expression in the roots of bermudagrass (Figure S3B) and the roots of *CdWRKY2*-overexpressing bermudagrass showed higher ABA sensitivity compared to their transgenic negative control (Figures S3A, C, D). To deduce whether CdWRKY2 elevated salt sensitivity of plants through the ABA pathway, we investigated the expression pattern of some well-characterized ABA-responsive genes in the roots of transgenic *Arabidopsis* lines (Lopez-Molina et al., 2001). We observed that *CdWRKY2* overexpression lines exhibited a remarkable altered expression of ABA-responsive genes (Figures 6C–H), suggesting an ABA-dependent function (Merlot et al., 2001; Reeves et al., 2011; Rushton et al., 2012). Reports indicate that ABI4 functions downstream of ABA signaling and plays important roles in ABA and cytokinin-mediated inhibition of LR formation by limiting *PIN1* expression, and thus reduces the polar auxin transport (Finkelstein et al., 1998; Signora et al., 2001; Shkolnik-Inbar and Bar-Zvi, 2010). A previous study also showed that AtWRKY46 could directly regulate the expression of *ABI4* in *Arabidopsis* to participate in LR development especially under osmotic/salt stress (Ding et al., 2015). Here, under both control and salt conditions, *ABI4* was highly expressed in transgenic lines compared to the wild type under both control and salt conditions (Figure 6C). In contrast to the salt condition, the expression of *PIN1* in the transgenic line was higher under normal conditions (Figure 5F). These results demonstrated that the *ABI4*-mediated limitation of auxin transport in the roots might be another route for LR growth inhibition and increased salt sensitivity. However, the *ABI4* expression was not significantly induced by salt, which might partly be due to the different sampling time used in this study. Together with the previous studies, here, CdWRKY2 and AtWRKY46 lacked protein interaction (Figure S7), but still CdWRKY2 might inhibit the expression level of *AtWRKY46*, which could further regulate several target genes downstream such as *ABI4* and *UGT84B2* to inhibit polar auxin transport and decrease root endogenous auxin levels especially under salt stress and lead to the inhibited LR growth (Ding et al., 2015).

MAPK cascade plays a critical role in plant stress response including salt stress (Cobb and Goldsmith, 2000). Several reports have shown that WRKY TFs may function downstream of MAPK cascades to participate in various physiological responses in plants (Asai et al., 2002; Kim and Zhang, 2004; Andreasson et al., 2005). In this study, we observed that CdWRKY2 could interact with AtMAPK3 in the yeast (Figure 7A). Furthermore, although the mutation of the *MAPK3* gene did not significantly inhibit the growth of LR in *Arabidopsis* under salt stress, overexpression of *CdWRKY2* in the *mapk3* background could partly rescue the salt oversensitive phenotype of LR grown on salt conditions (Figures 7C, D). A previous study showed that rice *OsWRKY30*, the orthologous gene of *CdWRKY2* (Figure S9) can be phosphorylated by OsMAPK3 to play vital roles in drought tolerance (Shen et al., 2012). The substrates of MAPK often contain several consecutive SP (serine proline) sites (Menke et al., 2005; Shen et al., 2012) and the mutation at SP site of

the MAPK substrate could result in the loss of function WRKY in rice (Shen et al., 2012). In this study, we mutated the first two SP sites and constructed m*CdWRKY2* overexpression lines in *Arabidopsis*. The root salt sensitivity of *mCdWRKY2* overexpression lines remained statistically indifferent relative to the wild type. Also, there was no significant increase in LR number in the *mapk3* mutant compared to wild type under control and salt conditions (Figures 7C, D). These results at least suggested that the elevated LR salt sensitivity *via CdWRKY2* might partially be dependent on the function of MAPK3, and these SP sites might be the potential phosphorylation sites of MAPK3. Thus, whether the interaction between CdMAPK3 and CdWRKY2 exists in bermudagrass or not, as well as the phosphorylation of CdWRKY2, remains to be further examined. Moreover, whether OsWRKY30 has the same function as CdWRKY2 and whether knocking out *OsWRKY30* in rice could elevate the salt tolerance ability of mutants should be further investigated in rice. Moreover, phylogenetic analysis revealed that CdWRKY2 was the ortholog of AtWRKY2 in *Arabidopsis* (Figures 1B; S1). A previous study reported that the expression of *AtWRKY2* could be induced by NaCl and mannitol treatments, suggesting that AtWRKY2 might be involved in osmotic stress (Jiang and Yu, 2010). However, in the yeast one-hybrid assay, results showed that there was no interaction between the AtWRKY2 protein and the promoter of AtWRKY46 (Figure 6J), suggesting that AtWRKY2 and CdWRKY2 might not be direct counterparts during salt-induced root inhibition. However, based on the salt-response function of CdWRKY2, whether AtWRKY2 could participate in salt stress response in *Arabidopsis via* other pathways and the molecular mechanism in-depth should also be studied in the future.

In summary, we identified and overexpressed a salt-induced *WRKY* gene *CdWRKY2* in bermudagrass, which plays a negative role in salt-induced LR growth under salt stress. In *Arabidopsis*, CdWRKY2 could negatively regulate LR growth *via* the regulation of auxin homeostasis and ABA signaling-related genes while partly relying on the function of AtMAPK3 (Figure S10). Taken together, our results indicated that *CdWRKY2* and its homologue genes in other plant species should be useful targets for genetic engineering of salinity-tolerant plants to better utilize saline-alkali land.

Data availability statement

The original contributions presented in the study are included in the article/Supplementary Material. Further inquiries can be directed to the corresponding author.

Author contributions

AS and XX performed most of the experiments and wrote the article with contributions of all the authors. EA modified the manuscript. WW and SF provided technical assistance. YY, XL, GW, and HW provided experiment assistance. JF supervised the experiments. All authors contributed to the article and approved the submitted version.

Funding

This study was supported by the National Natural Science Foundation of China (grant no. 31801892), the National Key R&D Program of China (grant no. 2019YFD0900702), and the Agricultural Variety Improvement Project of Shandong (grant no. 2019LZGC010).

Acknowledgments

We thank Prof. Shuhua Yang's laboratory (China Agricultural University) for providing the seeds of the *mapk3* mutant. We thank Prof. Yiping Tong's laboratory (Institute of Genetics and Developmental Biology) for giving the vectors used for yeast one-hybrid and yeast two-hybrid. We thank Prof. Chunxiang Fu's laboratory (Qingdao Institute of Biomass Energy and Bioprocess) for giving the vectors used for constructing overexpression bermudagrass lines. We thank the Genovo company (Tianjin) for developing the knocking out lines of rice.

Conflict of interest

The authors declare that the research was conducted in the absence of any commercial or financial relationships that could be construed as a potential conflict of interest.

Publisher's note

All claims expressed in this article are solely those of the authors and do not necessarily represent those of their affiliated organizations, or those of the publisher, the editors and the reviewers. Any product that may be evaluated in this article, or claim that may be made by its manufacturer, is not guaranteed or endorsed by the publisher.

Supplementary material

The Supplementary Material for this article can be found online at: https://www.frontiersin.org/articles/10.3389/fpls.2023.1164534/full#supplementary-material

References

Ackerson, R. C., and Youngner, V. B. (1962). Responses of bermudagrass to salinity. *Agron. J.* 67, 678–681. doi: 10.2134/agronj1975.00021962006700050024x

Andreasson, E., Jenkins, T., Brodersen, P., Thorgrimsen, S., and Mundy, J. (2005). The MAP kinase substrate MKS1 is a regulator of plant defense responses. *EMBO J.* 67, 2579–2589. doi: 10.1038/sj.emboj.7600737

Asai, T., Tena, G., Plotnikova, J., Willmann, M. R., Chiu, W.-L., Gomez-Gomez, L., et al. (2002). MAP kinase signalling cascade in *Arabidopsis* innate immunity. *Nature* 67, 977–983. doi: 10.1038/415977a

Brady, S. M., Sarkar, S. F., Bonetta, D., and Mccourt, P. (2003). The *ABSCISIC INSENSITIVE3* (*ABI3*) gene is modulated by farnesylation and is involved in auxin signalling and lateral root development in *Arabidopsis*. *Plant J.* 34, 67–75. doi: 10.1046/j.1365-313X.2003.01707.x

Cai, R., Dai, W., Zhang, C., Wang, Y., Wu, M., Zhao, Y., et al. (2017). The maize WRKY transcription factor ZmWRKY17 negatively regulates salt stress tolerance in transgenic *Arabidopsis* plants. *Planta* 246, 1215–1231. doi: 10.1007/s00425-017-2766-9

Chen, H., Lai, Z., Shi, J., Xiao, Y., Chen, Z., and Xu, X. (2010). Roles of *Arabidopsis* WRKY18, WRKY40 and WRKY60 transcription factors in plant responses to abscisic acid and abiotic stress. *BMC Plant Biol.* 10, 281. doi: 10.1186/1471-2229-10-281

Chen, Y., Tan, Z., Hu, B., Yang, Z., Xu, B., Zhuang, L., et al. (2015). Selection and validation of reference genes for target gene analysis with quantitative RT-PCR in leaves and roots of bermudagrass under four different abiotic stresses. *Physiol. Plantarum* 155, 138–148. doi: 10.1111/ppl.12302

Cobb, M. H., and Goldsmith, E. J. (2000). Dimerization in MAP-kinase signaling. *Trends Biochem. Sci.* 25, 7–9. doi: 10.1016/S0968-0004(99)01508-X

Czechowski, T., Stitt, M., Altmann, T., Udvardi, M. K., and Scheible, W. R. (2005). Genome-wide identification and testing of superior reference genes for transcript normalization in arabidopsis. *Plant Physiol.* 139, 5–17. doi: 10.1104/pp.105.063743

Datta, R., Kumar, D., Sultana, A., Hazra, S., Bhattacharyya, D., and Chattopadhyay, S. (2015). Glutathione regulates 1-aminocyclopropane-1- carboxylate synthase transcription *via* WRKY33 and 1-aminocyclopropane-1 -carboxylate oxidase by modulating messenger RNA stability to induce ethylene synthesis during stress. *Plant Physiol.* 169, 2963–2981. doi: 10.1104/pp.15.01543

Deak, K. I., and Malamy, J. (2005). Osmotic regulation of root system architecture. *Plant J.* 43, 17–28. doi: 10.1111/j.1365-313X.2005.02425.x

Ding, Z. J., Yan, J. Y., Li, C. X., Li, G. X., Wu, Y. R., and Zheng, S. J. (2015). Transcription factor WRKY46 modulates the development of *Arabidopsis* lateral roots in osmotic/salt stress conditions *via* regulation of ABA signaling and auxin homeostasis. *Plant J.* 84, 56–69. doi: 10.1111/tpj.12958

Finkelstein, R. R., Wang, M. L., Lynch, T. J., Rao, S., and Goodman, H. M. (1998). The *Arabidopsis* abscisic acid response locus ABI4 encodes an APETALA2 domain protein. *Plant Cell.* 10, 1043–1054. doi: 10.1105/tpc.10.6.1043

Friml, J., Wiśniewska, J., Benková., E., Mendgen, K., and Palme, K. (2002). Lateral relocation of auxin efflux regulator PIN3 mediates tropism in arabidopsis. *Nature* 415, 806–809. doi: 10.1038/415806a

Hu, Y., Chen, L., Wang, H., Zhang, L., Wang, F., and Yu, D. (2013). *Arabidopsis* transcription factor WRKY8 functions antagonistically with its interacting partner VQ9 to modulate salinity stress tolerance. *Plant J.* 74, 730–745. doi: 10.1111/tpj.12159

Hu, L., Li, H., Chen, L., Lou, Y., Amombo, E., and Fu, J. (2015). RNA-Seq for gene identification and transcript profiling in relation to root growth of bermudagrass (*Cynodon dactylon*) under salinity stress. *BMC Genomics* 16, 575. doi: 10.1186/s12864-015-1799-3

Jiang, Y., and Deyholos, M. K. (2009). Functional characterization of *Arabidopsis* NaCl-inducible WRKY25 and WRKY33 transcription factors in abiotic stresses. *Plant Mol. Biol.* 69, 91–105. doi: 10.1007/s11103-008-9408-3

Jiang, J., Ma, S., Ye, N., Jiang, M., Cao, J., and Zhang, J. (2017). WRKY transcription factors in plant responses to stresses. *J. Integr. Plant Biol.* 59, 86–101. doi: 10.1111/jipb.12513

Jiang, W. B., and Yu, D. Q. (2010). *Arabidopsis WRKY2* transcription factor may be involved in osmotic stress response. *Acta Bot. Yunnanica* 31, 427–432. doi: 10.3724/SP.J.1143.2009.09046

Kim, C. Y., and Zhang, S. (2004). Activation of a mitogen-activated protein kinase cascade induces WRKY family of transcription factors and defense genes in tobacco. *Plant J.* 38, 142–151. doi: 10.1111/j.1365-313X.2004.02033.x

Korasick, D. A., Enders, T. A., and Strader, L. C. (2013). Auxin biosynthesis and storage forms. *J. Exp. Bot.* 64, 2541–2555. doi: 10.1093/jxb/ert080

Lavenus, J., Goh, T., Roberts, I., Guyomarch, S., Lucas, M., De, S. I., et al. (2013). Lateral root development in *Arabidopsis*: fifty shades of auxin. *Trends Plant Sci.* 18, 450–458. doi: 10.1016/j.tplants.2013.04.006

Liu, W., Li, R. J., Han, T. T., Cai, W., Fu, Z. W., Lu, Y. T., et al. (2015). Salt stress reduces root meristem size by nitric oxide-mediated modulation of auxin accumulation and signaling in Arabidopsis. *Plant Physiol* 168, 343–356. doi: 10.1104/pp.15.00030

Liu, Z. Q., Yan, L., Wu, Z., Mei, C., Lu, K., Yu, Y. T., et al. (2012). Cooperation of three WRKY-domain transcription factors WRKY18, WRKY40, and WRKY60 in repressing two ABA-responsive genes *ABI4* and *ABI5* in *Arabidopsis*. J. *Exp. Bot.* 63, 6371–6392. doi: 10.1093/jxb/ers293

Lopez-Molina, L., Sébastien, M., and Chua, N. H. (2001). A postgermination developmental arrest checkpoint is mediated by abscisic acid and requires the ABI5 transcription factor in *Arabidopsis*. proc. *Natl. Acad. Sci. U.S.A.* 98, 4782–4787. doi: 10.1073/pnas.081594298

Ma, W., Li, J., Qu, B., He, X., Zhao, X., Li, B., et al. (2014). Auxin biosynthetic gene *TAR2* is involved in low nitrogen-mediated reprogramming of root architecture in *Arabidopsis*. *Plant J.* 78, 70–79. doi: 10.1111/tpj.12448

Ma, Q., Xia, Z., Cai, Z., Li, L., Cheng, Y., Liu, J., et al. (2019). GmWRKY16 enhances drought and salt *tolerance thro*ugh an ABA-mediated pathway in *Arabidopsis thaliana*. front. *Plant Sci.* 9, 1979. doi: 10.3389/fpls.2018.01979

Mao, G., Meng, X., Liu, Y., Zheng, Z., Chen, Z., and Zhang, S. (2011). Phosphorylation of a WRKY transcription factor by two pathogen-responsive MAPKs drives phytoalexin biosynthesis in *Arabidopsis*. *Plant Cell.* 23, 1639–1653. doi: 10.1105/tpc.111.084996

Menke, F. L., Kang, H. G., Chen, Z., Park, J. M., Kumar, D., and Klessig, D. F. (2005). Tobacco transcription factor WRKY1 is phosphorylated by the MAP kinase SIPK and mediates HR-like cell death in tobacco. *Mol. Plant Microbe* 18, 1027–1034. doi: 10.1094/MPMI-18-1027

Merlot, S., Gosti, F., Guerrier, D., Vavasseur, A., and Giraudat, J. (2001). The ABI1 and ABI2 protein phosphatases 2C act in a negative feedback regulatory loop of the abscisic acid signalling pathway. *Plant J.* 25, 295–303. doi: 10.1046/j.1365-313x.2001.00965.x

Nam, T. N., Thia, L. H., Mai, D. S., and Tuan, N. V. (2017). Overexpression of *NbWRKY79* enhances salt stress tolerance in *Nicotiana benthamiana*. acta. *Physiol. Plant* 39, 121. doi: 10.1007/s11738-017-2423-8

Niu, C. F., Wei, W., Zhou, Q. Y., Tian, A. G., and Chen, S. Y. (2012). Wheat *WRKY* genes *TaWRKY2* and *TaWRKY19* regulate abiotic stress tolerance in transgenic *Arabidopsis* plants. *Plant Cell Environ.* 35, 1156–1170. doi: 10.1111/j.1365-3040.2012.02480.x

Péret, B., Rybel, B. D., Casimiro, I., Benková, E., Swarup, R., Laplaze, L., et al. (2009). *Arabidopsis* lateral root development: an emerging story. *Trends Plant Sci.* 14, 399–408. doi: 10.1016/j.tplants.2009.05.002

Reeves, W. M., Lynch, T. J., Mobin, R., and Finkelstein, R. R. (2011). Direct targets of the transcription factors ABA-insensitive (ABI)4 and ABI5 reveal synergistic action by ABI4 and several bZIP ABA response factors. *Plant Mol. Biol.* 75, 347–363. doi: 10.1007/s11103-011-9733-9

Rushton, D. L., Tripathi, P., Rabara, R. C., Lin, J., Ringler, P., Boken, A. K., et al. (2012). WRKY transcription factors: key components in abscisic acid signalling. *Plant Biotechnol. J.* 10, 2–11. doi: 10.1111/j.1467-7652.2011.00634.x

Schmittgen, T. D., and Livak, K. J. (2008). Analyzing real-time PCR data by the comparative C(T) method. *Nat. Protoc.* 3, 1101–1108. doi: 10.1038/nprot.2008.73

Shao, A., Sun, Z., Fan, S., Xu, X., Wang, W., Amombo, E., et al. (2020). Moderately low nitrogen application mitigate the negative effects of salt stress on annual ryegrass seedlings. *Peer J.* 8, e10427. doi: 10.7717/peerj.10427

Shao, A., Wang, W., Fan, S., Xu, X., Yin, Y., Erick, A., et al. (2021). Comprehensive transcriptional analysis reveals salt stress- regulated key pathways, hub genes and time-specific responsive gene categories in common bermudagrass (*Cynodon dactylon* (L.) pers.) roots. *BMC Plant Biol.* 21, 175. doi: 10.1186/s12870-021-02939-1

Sharma, S., Giri, P., Taj, G., and Kumar, A. (2013). WRKY transcription factor-the interactor of MAPK cascade. *Int. J. Agric. Environ. Biotechnol.* 6, 341. doi: 10.5958/j.2230-732X.6.3.001

Shen, H., Liu, C., Zhang, Y., Meng, X., Zhou, X., Chu, C., et al. (2012). OsWRKY30 is activated by MAP kinases to confer drought tolerance in rice. *Plant Mol. Biol.* 80, 241–253. doi: 10.1007/s11103-012-9941-y

Shkolnik-Inbar, D., and Bar-Zvi, D. (2010). ABI4 mediates abscisic acid and cytokinin inhibition of lateral root formation by reducing polar auxin transport in *Arabidopsis* CW. *Plant Cell.* 22, 3560–3573. doi: 10.1105/tpc.110.074641

Signora, L., De Smet, I., Foyer, C., and Zhang, H. (2001). ABA plays a central role in mediating the regulatory effects of nitrate on root branching in *Arabidopsis*. *Plant J.* 28, 655–662. doi: 10.1046/j.1365-313x.2001.01185.x

Smet, I. D., Zhang, H., Inzé, D., and Beeckman, T. (2006). A novel role for abscisic acid emerges from underground. *Trends Plant Sci.* 11, 434–439. doi: 10.1016/j.tplants.2006.07.003

Staswick, P. E., Serban, B., Rowe, M., Tiryaki, I., Maldonado, M. T., Maldonado, M. C., et al. (2005). Characterization of an *Arabidopsis* enzyme family that conjugates amino acids to indole-3-acetic acid. *Plant Cell.* 17, 616–627. doi: 10.1105/tpc.104.026690

Tamura, K., Peterson, D., Peterson, N., Stecher, G., Nei, M., and Kumar, S. (2011). MEGA5: molecular evolutionary genetics analysis using maximum likelihood, evolutionary distance, and maximum parsimony methods. *Mol. Biol. Evol.* 28, 2731–2739. doi: 10.1093/molbev/msr121

Tao, Z., Kou, Y., Liu, H., Li, X., Xiao, J., and Wang, S. (2011). OsWRKY45 alleles play different roles in abscisic acid signalling and salt stress tolerance but similar roles in drought and cold tolerance in rice. *J. Exp. Bot.* 62, 4863–4874. doi: 10.1093/jxb/err144

Thompson, J. D., Gibson, T. J., and Higgins, D. G. (2002). Multiple sequence alignment using ClustalWand ClustalX. *Curr. Protoc. Bioinf.* 2, 2.3.

Ülker, B., and Somssich, I. E. (2004). WRKY transcription factors: from DNA binding towards biological function. *Curr. Opin. Plant Biol.* 7, 491–498. doi: 10.1016/j.pbi.2004.07.012

Ullah, A., Sun, H., Hakim.,, Yang, X., and Zhang, X. (2018). A novel cotton WRKY gene, *GhWRKY6*-like, improves salt tolerance by activating the ABA signaling pathway and scavenging of reactive oxygen species. *Physiol. Plant* 162, 439–454. doi: 10.1111/ppl.12651

Ulmasov, T., Murfett, J., Hagen, G., and Guilfoyle, T. J. (1997). Aux/IAA proteins repress expression of reporter genes containing natural and highly active synthetic auxin response elements. *Plant Cell.* 9, 1963–1971. doi: 10.2307/3870557

Vanderauwera, S., Vandenbroucke, K., Lnze, A., Cotte, B. V. D., Muhlenbock, P., Rycke., R. D., et al. (2012). AtWRKY15 perturbation abolishes the mitochondrial stress response that steers osmotic stress tolerance in *Arabidopsis.* proc. *Natl. Acad. Sci. U.S.A.* 109, 20113–20118. doi: 10.1073/pnas.1217516109

Westfall, C. S., Herrmann, J., Chen, Q., Wang, S., and Jez, J. M. (2010). Modulating plant hormones by enzyme action: the GH3 family of acyl acid amido synthetases. *Plant Signal. Behav.* 5, 1607–1612. doi: 10.4161/psb.5.12.13941

Won, C., Shen, X., Mashiguchi, K., Zheng, Z., Dai, X., Cheng, Y., et al. (2011). Conversion of tryptophan to indole-3-acetic acid by TRYPTOPHAN AMINOTRANSFERASES OF ARABIDOPSIS and YUCCAs in *Arabidopsis.* proc. *Natl. Acad. Sci. U.S.A.* 108, 18518–18523. doi: 10.1073/pnas.1108436108

Yan, H., Jia, H., Chen, X., Hao, L., An, H., and Guo, X. (2014). The cotton WRKY transcription factor GhWRKY17 functions in drought and salt stress in transgenic *Nicotiana benthamiana* through ABA signaling and the modulation of reactive oxygen species production. *Plant Cell Physiol.* 55, 2060–2076. doi: 10.1093/pcp/pcu133

Zhao, Y. (2012). Auxin biosynthesis: a simple two-step pathway converts tryptophan to indole-3-acetic acid in plants. *Mol. Plant* 5, 334–338. doi: 10.1093/mp/ssr104

Zhou, Q. Y., Tian, A. G., Zou, H. F., Xie, Z. M., Lei, G., Huang, J., et al. (2008). Soybean WRKY-type transcription factor genes, *GmWRKY13*, *GmWRKY21*, and *GmWRKY54*, confer differential tolerance to abiotic stresses in transgenic *Arabidopsis* plants. *Plant Biotechnol. J.* 6, 486–503. doi: 10.1111/j.1467-7652.2008.00336.x

Zhou, L., Wang, N. N., Gong, S. Y., Lu, R., Li, Y., and Li, X. B. (2015). Overexpression of a cotton (*Gossypium hirsutum*) *WRKY* gene, *GhWRKY34*, in *Arabidopsis* enhances salt-tolerance of the transgenic plants. *Plant Physiol. Biochem.* 96, 311–320. doi: 10.1016/j.plaphy.2015.08.016

frontiers | Frontiers in Plant Science

TYPE Original Research
PUBLISHED 19 July 2023
DOI 10.3389/fpls.2023.1167238

Check for updates

OPEN ACCESS

EDITED BY
Fernanda Fidalgo,
University of Porto, Portugal

REVIEWED BY
Cristiano Fortuna Soares,
University of Porto, Portugal
Viviana Martins,
University of Minho, Portugal

*CORRESPONDENCE
Sakil Mahmud
sakilbmb@bau.edu.bd
Mohammad Golam Mostofa
mostofam@msu.edu

†These authors have contributed equally to this work

RECEIVED 16 February 2023
ACCEPTED 25 May 2023
PUBLISHED 19 July 2023

CITATION
Mahmud S, Kamruzzaman M, Bhattacharyya S, Alharbi K, Abd El Moneim D and Mostofa MG (2023) Acetic acid positively modulates proline metabolism for mitigating PEG-mediated drought stress in Maize and Arabidopsis. *Front. Plant Sci.* 14:1167238. doi: 10.3389/fpls.2023.1167238

COPYRIGHT
© 2023 Mahmud, Kamruzzaman, Bhattacharyya, Alharbi, Abd El Moneim and Mostofa. This is an open-access article distributed under the terms of the Creative Commons Attribution License (CC BY). The use, distribution or reproduction in other forums is permitted, provided the original author(s) and the copyright owner(s) are credited and that the original publication in this journal is cited, in accordance with accepted academic practice. No use, distribution or reproduction is permitted which does not comply with these terms.

Acetic acid positively modulates proline metabolism for mitigating PEG-mediated drought stress in Maize and Arabidopsis

Sakil Mahmud[1*†], Mohammad Kamruzzaman[2,3†], Sabarna Bhattacharyya[4], Khadiga Alharbi[5], Diaa Abd El Moneim[6] and Mohammad Golam Mostofa[7,8*]

[1]Department of Biochemistry and Molecular Biology, Bangladesh Agricultural University, Mymensingh, Bangladesh, [2]Department of Plant Breeding, Institute of Crop Science and Resource Conservation, University of Bonn, Bonn, Germany, [3]Plant Breeding Division, Bangladesh Institute of Nuclear Agriculture (BINA), Mymensingh, Bangladesh, [4]Plant Cell Biology, Institute of Cellular and Molecular Botany, University of Bonn, Bonn, Germany, [5]Department of Biology, College of Science, Princess Nourah bint Abdulrahman University, Riyadh, Saudi Arabia, [6]Department of Plant Production (Genetic Branch), Faculty of Environmental Agricultural Sciences, Arish University, El-Arish, Egypt, [7]Department of Energy Plant Research Laboratory, Michigan State University, East Lansing, MI, United States, [8]Department of Biochemistry and Molecular Biology, Michigan State University, East Lansing, MI, United States

Introduction: Osmotic imbalance is one of the major consequences of drought stress, negatively affecting plant growth and productivity. Acetic acid has modulatory roles in osmotic balance in plants; however, the mechanistic insights into acetic acid-mediated osmotic adjustment under drought stress remains largely unknown.

Methods: Here, we investigated how seed priming and seedling root treatment with acetic acid enabled maize plants overcoming polyethylene glycol (PEG)-induced drought effects.

Results: Maize seeds primed with acetic acid showed better growth performance when compared with unprimed seeds under PEG application. This growth performance was mainly attributed to improved growth traits, such as fresh weight, dry weight, length of shoots and roots, and several leaf spectral indices, including normalized difference vegetation index (NDVI) and chlorophyll absorption in reflectance index (MCARI). The levels of oxidative stress indicators hydrogen peroxide (H_2O_2) and malondialdehyde (MDA) did not alter significantly among the treatments, but proline content as well as the expression of proline biosynthetic gene, *Δ1-PYRROLINE-5-CARBOXYLATE SYNTHETASE 1* (*P5CS1*) was significantly elevated in plants receiving acetic acid under PEG-treatments. On the other hand, treating the seedlings root with acetic acid led to a significant recovery of maize plants from drought-induced wilting. Although growth traits remained unchanged among the treatments, the enhancement of leaf water content, photosynthetic rate, proline level, expression of *P5CS1*, and antioxidant enzyme activities along with reduced level of H_2O_2 and MDA in acetic acid-supplemented drought plants indicated a positive regulatory role of acetic

acid in maize tolerance to drought. Moreover, the high expression of *P5CS1* and the subsequent elevation of proline level upon acetic acid application were further validated using wild type and proline biosynthetic mutant *p5cs1* of Arabidopsis. Results showed that acetic acid application enabled wild type plants to maintain better phenotypic appearance and recovery from drought stress than *p5cs1* plants, suggesting a crosstalk between acetic acid and proline metabolism in plants under drought stress.

Discussion: Our results highlight the molecular and intrinsic mechanisms of acetic acid conferring plant tolerance to drought stress.

KEYWORDS

acetic acid, antioxidant defense, maize (*Zea mays* L.), osmotic stress, proline metabolism

Introduction

Ever changing environments are often stressful for growth and development of plants. Drought is considered as a major abiotic stress, affecting plant ecological distribution, growth, and productivity worldwide (Gupta et al., 2020). Drought causes osmotic stresses that lead to rapid changes in gene expression and metabolic alterations, some of which help plants to cope with such stresses (Kamruzzaman et al., 2022; Mahmud et al., 2022). Osmotic stress can directly interrupt stomatal regulation, resulting in poor photosynthetic performance in plants (Mittler et al., 2022). Reactive oxygen species (ROS) accumulation is a secondary response in plants under osmotic-related stresses, including water-shortage. However, an imbalance between production and scavenging of ROS, such as hydrogen peroxide (H_2O_2), superoxide radicals ($O_2^{\cdot-}$), singlet oxygen ($^1O_2$), and hydroxyl radicals ($HO^{\bullet}$) may initiate a cascade of oxidative reactions that result in membrane lipid peroxidation, chlorophyll degradation, protein denaturation, and DNA strand breakage (Claeys and Inze, 2013; Lei et al., 2021; Mittler et al., 2022). Plants have evolved sophisticated antioxidant mechanisms to counter the damaging effects of ROS. The antioxidant system includes non-enzymatic compounds, such as tocopherols, glutathione, ascorbate, and carotenoids, as well as enzymes, including catalase (CAT, EC: 1.11.1.6), ascorbate peroxidase (APX, EC: 1.11.1.11), peroxidase (POD, EC: 1.11.1.7), and superoxide dismutase (SOD, EC 1.15.1.1) (Nikoleta-Kleio et al., 2020; Mittler et al., 2022).

Plants accumulate an array of osmolytes to adjust their intracellular osmotic potential under stressful conditions. Osmolytes are known to stabilize the protein structure and are ubiquitous in living organisms. The major organic osmolytes include amino acids (e.g., proline), methylamines (e.g., betaine and trimethylamine-N-oxide), polyamines (e.g., spermidine), sugars (e.g., trehalose), and polyols (e.g., sorbitol) (Ozturk et al., 2021; Singh et al., 2021). Among these osmolytes, proline has cardinal importance in plants, both as structural unit of protein and osmolyte for osmoprotection (Moukhtari et al., 2020; Alvarez et al., 2022; Spormann et al., 2023). When plants are exposed to osmotic stress, proline accumulates in the cytoplasm and acts as an osmoprotectant for stabilizing cellular membranes and maintaining turgor pressure. This helps plant prevent damage to cellular components, allowing plants to continue to grow and function maximally despite the stress. In addition to its role as an osmoprotectant, proline has been shown to enhance the expression of stress-responsive genes, which are involved in plant responses to stress (Shrestha et al., 2021; Kamruzzaman et al., 2022). Besides its role as an osmolyte, proline has been further reported to scavenge ROS under drought stress (Moukhtari et al., 2020). Nonetheless, proline accumulation alone cannot provide tolerance rather other pathways activated upon different abiotic stresses are linked to its effect on plants (Chun et al., 2018; Ozturk et al., 2021). Under drought stress, synthesis of proline in the cytosol derived from the precursor glutamate in two-sequential steps catalyzed by δ-pyrroline-5-carboxylate synthetase (P5CS) and δ-pyrroline-5-carboxylate reductase (P5CR) (Adamipour et al., 2020). *P5CS* expression increases upon exposure to drought while low or no increase in *P5CR* expression depending on plant species (Chen et al., 2021).

Maize (*Zea mays* L.) is a major agricultural crop cultivated across the world. Despite having wide genetic variation, most of the maize varieties are moderately sensitive to drought stress, especially seedling stage of maize is more sensitive to water-shortage (Badr et al., 2020; Sheoran et al., 2022). The negative effects of drought stress on maize plants are involved with changes in morphological and physiological parameters, including shoot and root growth, photosynthetic activity, stomatal features, proline accumulation, and abscisic acid levels in the whole plant (Salika and Rifat, 2021; Sheoran et al., 2022). Reports suggest that invisible wilting symptoms induced by high osmotic potential may lead to 60% yield losses in maize (Avramova et al., 2015; Farooq et al., 2015). Thus, developing maize varieties with better osmotic stress tolerance potential continues to be an important strategy in sustaining maize production in arid and semi-arid areas globally. Endogenous level of proline accumulation is enhanced in maize root upon low water potential, which has been reported to be a tolerance mechanism against the osmotic stress (Kang et al., 2022). Besides, exogenously applied proline in maize plants can enhance

the antioxidant activity, better growth performance, and prevent water loss upon osmotic stresses induced by drought and salinity (Mosaad et al., 2020; Ibrahim et al., 2022). Polyethylene glycol (PEG)-mediated elevation of osmotic potential inhibits apical shoot growth while increasing lateral root formation, suggesting a potential mechanism of maize plants to combat water deficiency (Ji et al., 2014).

Recently, there has been increasing interest in using plant growth-promoting compounds, such as acetic acid, to mitigate osmotic stress in plants. Acetic acid is a naturally occurring organic acid that has been shown to have various positive effects on plant growth and stress tolerance by improving water and nutrient uptake and photosynthesis rate (Kim et al., 2017; Rahman et al., 2019; Mendiburu, 2019). Several studies reported the potential aspects of acetic acid in enhancing plant resistance to a variety of abiotic stresses, including salinity and drought. For example, application of acetic acid potentiated drought tolerance mechanisms in cereal crops rice (*Oryza sativa*), maize, and wheat (*Triticum aestivum*) through the activation of various physiological and molecular mechanisms (Kim et al., 2017; Ogawa et al., 2021). A low dose (<50 mM) of acetic acid has been suggested to be effective in mitigating drought adversities in cassava (*Manihot esculenta*) (Utsumi et al., 2019) and mung bean (*Vigna radiata*) (Rahman et al., 2019). Although the beneficial effects of acetic acid on osmotic stress tolerance are already quite recognized, the regulatory mechanism is still not fully understood. Moreover, acetic acid-induced proline accumulation varies upon different plants and abiotic stresses. For example, proline level was elevated with the application of acetic acid under salt stress in mung bean (Rahman et al., 2019), whereas the level was lowered upon drought stress in soybean (*Glycine max*) (Rahman et al., 2020). Thus, how acetic acid application regulates cellular level of proline for rendering osmotic stress tolerance is yet to be studied at genetic level in plants.

In the current study, we attempted to explore the functions of acetic acid in mitigation of PEG-induced osmotic stress by studying several morphological, physiological, and biochemical features in maize. We compared the seed priming and seedling treatment modes of acetic acid to understand common pathway(s) elicited by acetic acid for conferring drought tolerance in maize. We also validated our findings by conducting a complementary functional study using the model plant *A. thaliana* wild-type and its proline biosynthetic mutant *p5cs1*. Our comprehensive study using both maize and Arabidopsis provided an in-depth understanding of how acetic acid modulates cellular intrinsic mechanisms to make plants more resilient to osmotic stress.

Materials and methods

Experimental design and treatments

The seeds of maize (*Zea mays* L., cv Baden seed corn; kindly provided by Kiepenkerl, Blooming, Germany) were surface sterilized with 70% (v/v) ethanol treatment for 1 min followed by 0.5% (v/v) sodium hypochlorite solution for 10 minutes. Seeds were then washed 5 times with distilled water (dH_2O). For priming, the treatments were as follows: Ctrl (Control, dH_2O), PEG (20% w/v polyethylene glycol-6000), AA (500 µM acetic acid), and PEG + AA (20% w/v PEG and 500 µM AA). The dose of AA (500 µM) was selected based on the trial with the different concentrations of AA that did not negatively impact the germination percentage without influencing proline content (Supplementary Figures 1A–C). Seeds were soaked overnight with above-mentioned solutions and allowed for germination on a wet filter paper. Growth assessment and biochemical analyses of germinated seedlings were performed after growing in commercial hydroponic nutrient solution (Flora Series® nutrient system: Floragro® (total nitrogen (N): 2%, available phosphate (P_2O_5): 1%, soluble potash (K_2O): 6%, magnesium (Mg): 0.5%), Floramicro® (total nitrogen (N): 5%, soluble potash (K_2O): 1%, calcium (Ca): 5%, boron (B): 0.01%, cobalt (Co): 0.0005%, copper (Cu): 0.01%, iron (Fe): 0.1%, manganese (Mn): 0.05%, molybdenum (Mo): 0.0008%, zinc (Zn): 0.015%) and Florabloom® (available phosphate (P_2O_5): 5%, soluble potash (K_2O): 4%, magnesium (Mg): 1.5%, sulfur (S): 1%), USA, 2 ml/2 L distilled water) for 10 days. All the above experiments were repeated three times to ensure the reproducibility of the experiment.Similarly, the treatments for root application at the seedlings stage were Ctrl (hydroponic nutrient solution), PEG (20% w/v), AA (25 mM), and PEG + AA (treatment with 20% w/v PEG and 25 mM AA). The dose of acetic acid (25 mM) was selected based on the findings of Kim et al. (2017). Solution of 'Ctrl' treatment was used as a solvent to prepare other treatments. Properly germinated seedlings in the wet filter paper were grown for 12 days in 'Ctrl' solution followed by subjecting to different treatments for 48 h. After the treatment period, leaves were harvested to assess various morphological, physiological, and biochemical parameters. Morphological parameters included shoot fresh weight (SFW), root fresh weight (RFW), shoot dry weight (SDW), root dry weight (RDW), root length (RL), shoot length (SL), root volume, and average root diameter. The biochemical parameters were proline, MDA, H_2O_2, CAT, POD, and APX.

In both priming and exogenous treatment experiments, plants were grown in a growth chamber (Bronson Climate, LW Zaltbommel, the Netherlands) set at 26° C with 12/12 h dark/light cycle in white fluorescent light up to 600 µmol m^{-2} s^{-1} and 55-60% relative humidity. A handmade system, made of nylon mesh and glass jar, was adopted for seedlings growth in this study (Figures 1A, C). The treatment solutions were replaced in every 48 h on a regular basis. All of the above experiments were repeated three times.

For Arabidopsis (*A. thaliana*) experiment, wild-type Columbia ecotype (Col-0) and *p5cs1* T-DNA insertion mutant seeds (Funck et al., 2012) were surface sterilized using 5.25% sodium hypochlorite for 1 min and then washed 5 times with sterilized dH_2O. Sterilized seeds were placed on the petri-plates containing Murashige and Skoog medium (MS; Duchefa Biochemie) with 1% (w/v) sucrose and 0.6% (w/v) phytagel (Sigma-Aldrich, Inc.) for germination and properly germinated seedlings were grown for 14 days. Properly grown plants were then placed in liquid culture (Rivero et al., 2013) containing different treatments in a sterile plastic box with gentle rotation (120 rpm) on an orbital shaker (Innova 2000, New

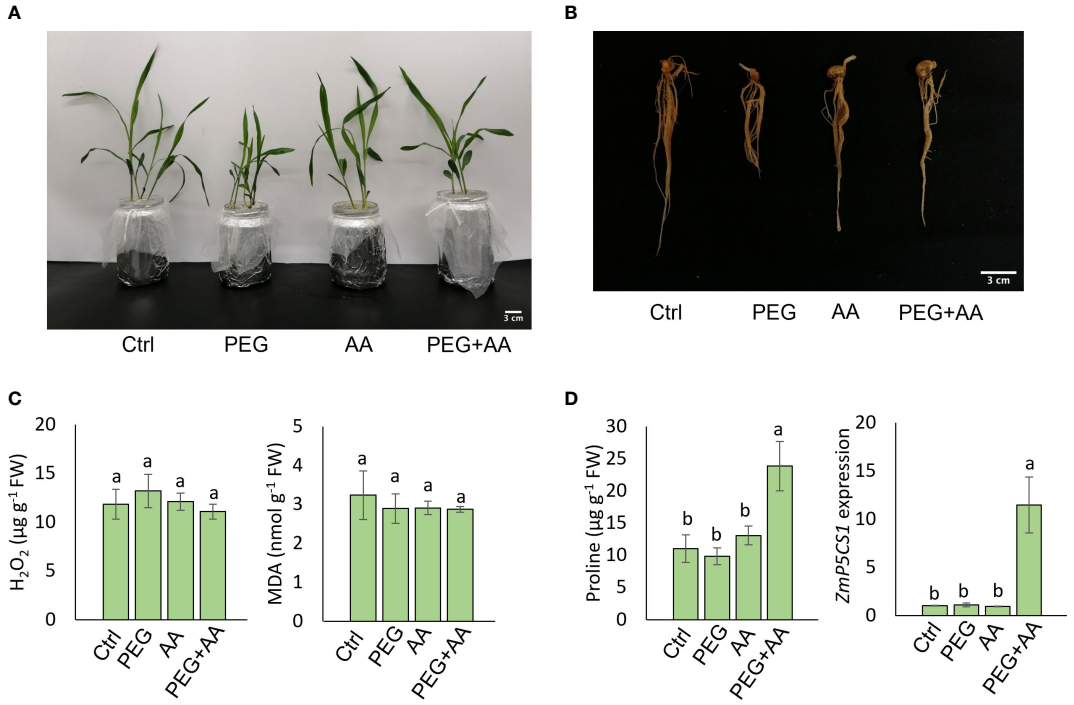

FIGURE 1
Seed priming effect of acetic acid on maize growth and oxidative stress parameters in response to PEG treatments. **(A, B)** Phenotype of shoots **(A)** and roots **(B)** of maize plants grown for 10 days after seed priming with the treatments for overnight. **(C, D)** The levels of oxidative stress markers hydrogen peroxide (H_2O_2) and malondialdehyde (MDA) **(C)**, and proline content and relative expression of *ZmP5CS1* **(D)** in 10 days old maize leaves recorded after seed priming. Data represent mean ± SE of six individual replicates (n=6) for H_2O_2, MDA and proline content and three individual replicates (n=3) for *ZmP5CS1* expression, and different alphabetical letters indicate significant variations among the treatments following Tukey's *Post-Hoc* HSD test (P<0.05). FW, fresh weight. Ctrl, PEG (20%), AA (500 µM), and PEG+AA represent treatments with distilled water (dH_2O), 20% polyethylene glycol, 500 µM acetic acid, and 20% polyethylene glycol + 500 µM acetic acid, respectively. FW, fresh weight.

Brunswick Scientific, USA). The dose of AA (500 µM) was selected based upon trial with the different concentrations of acetic acid and that did not negatively impact the germination percentage with a steady increase of proline content compared to non-treated plants (Supplementary Figures 2A, B). Immediately, after 48 h of treatment, seedlings were re-placed into petri-plates containing MS with 1% (w/v) sucrose and 0.6% (w/v) phytagel and were grown for another seven days to observe the growth. For biochemical analysis, the whole shoot of the plants was collected immediately after 48 h of treatment in the liquid culture. If not otherwise stated, plants were cultured in growth chambers with long day conditions (16 h/8 h light/dark) at 22°C and up to 100 µmol photons m^{-2} s^{-1} and 60% relative humidity. Phenotypic experiment was repeated two times and biochemical assays were repeated three times.

Assessment of morphological traits and leaf spectral indices

Root and shoot fresh weights were recorded by a digital balance and then dried into an oven at 70°C for 3 days to measure the dry weights. Leaf water status was estimated through relative water content (RWC) according to Ghoulam et al. (2002). Tip of flag leaves were cut into 5-6 small pieces and the fresh weight (FW) was recorded. Then, the leaf pieces were dipped into 10 mL deionized water into a falcon tube for 24 h at room temperature. After 24 h, the leaves were wiped with a paper towel and the turgid weight (TW) was recorded. Dry weight was recorded after oven drying at 70°C for 72 h. RWC was estimated as (FW-DW)/(TW-DW) ×100. Three measurements were taken from each leaf. A portable infrared gas exchange analyzer (LI-6400 XT; LI-COR) was used (at 15:00 pm, when light was on) to measure the photosynthetic parameters, namely stomatal conductance (g_s), transpiration rate (E), intercellular CO_2 concentration (Ci), and photosynthesis rate (A) from flag leaves according to previous studies (Siddiqui et al., 2021; Fang et al., 2022). The internal ambient CO_2 level was 400 ppm.

Leaf spectral reflectance was also measured on the flag leaves with at least three plants using a PolyPen RP410 device (PSI, Drasov). Three points were measured from each leaf of each plant, and then the average of the three points was computed as described in previous study by Begum et al. (2020). Among various vegetation indices, Normalized Difference Vegetation Index (NDVI) = (RNIR – RRED)/(RNIR + RRED) (Rouse et al., 1973);, Chlorophyll Absorption in Reflectance Index (MCARI) = [(R700 – R670) – 0.2 * (R700 – R550)] x (R700/R670) (Daughtry et al., 2000), Simple Ratio Pigment Index (SPRI), Carter Indices (Ctr1), Lichtenthaler Indices (Lic2), Greenness Index (GI), Photochemical Reflectance Index (PRI) and Normalized Pigment Chlorophyll Index (NPCI) were recorded. In all equations, R

indicates the reflectance at a given wavelength of light. Roots were scanned using an Epson scanner (Perfection LA24000) with a resolution of 600 dots per inch and root images were analyzed using the WinRhizo software (Regent Instruments Inc., Quebec, Canada) to record the root architectural traits including average root diameter (mm), and root volume (cm^3) from 6 individuals. SFW, SDW, RFW, RDW, SL, and RL were averaged from 6 individual replicates. A normal measuring ruler was used to measure the lengths.

Proline, MDA, and H_2O_2 determination

First, fully expanded leaf of six maize and whole shoot of six Arabidopsis were used for proline, MDA, and H_2O_2 determination. Proline was determined according to the method described by Bates et al. (1973). Samples were ground in liquid nitrogen and 90-100 mg powdered tissue was homogenized in 1.5 mL of 3% sulphosalicylic acid (w/v). The suspension was centrifuged at 12,000 g for 5 min and 200 µL of sample supernatant was added with 200 µL acetic acid and 200 µL ninhydrin reagents. This mixture was incubated at 95°C temperature for 60 min and the reaction was immediately stopped by putting it into ice for 3-5 min. Then, 600 µL of pure toluene was mixed and incubated at room temperature for 30 min. The chromatophore readings were recorded at 520 nm wavelength with 10 reads per well through 96 well plastic plates using a microplate reader (TECAN Infinite 200 Pro, TECAN Group Limited, Switzerland). Proline content was estimated using standard curve method and expressed in µg/g FW.

Hydrogen peroxide (H_2O_2) was determined according to the previously described method (Sergiev et al., 1997; Velikova et al., 2000). Samples were grounded into powder using liquid nitrogen and 90-100 mg powder was homogenized into 500 µL 0.1% (w/v) trichloroacetic acid (TCA) and centrifuged at 12,000 g for 10 min. Then, 200 µL supernatant was added to 200 µL of 10 mM potassium phosphate buffer (pH 7.0 and 1 M 400 µL potassium iodide and mixed through vortexing. The sample absorbance was recorded at 390 nm through a microplate reader (TECAN Infinite 200 Pro, TECAN Group Limited, Switzerland). H_2O_2 level was determined by developing standard curve with known concentration of H_2O_2 and expressed in µg/g FW.

Lipid membrane damage was estimated by determining malondialdehyde (MDA) content using thiobarbituric acid (TBA) method (Hodges et al., 1999) adapted to a microplate-based protocol. Samples were homogenized in liquid nitrogen and 100 mg of pulverized powder was added to 1.5 mL of 0.1% (w/v) trichloroacetic acid (TCA) followed by centrifugation at 14,000 g for 15 min at 4°C. Then, 500 µl supernatant was mixed with reaction solution I (0.01% w/v 2,6-di-tert-butyl-4-methyl phenol (BHT) in 20% w/v TCA) and reaction solution II (0.65% w/v TBA, 0.01% w/v BHT in 20% w/v TCA) in a 1:1 ratio. The sample mix was then incubated at 95°C for 30 min. The reaction was stopped by putting on ice for five minutes, and the reaction mix was centrifuged at 8000 g for 10 min at 4°C. The absorbance of the supernatant was measured at 440, 532, and 600 nm using a microplate reader (TECAN Infinite 200 Pro, TECAN Group Limited, Switzerland). MDA content was expressed as nanomoles per gFW.

Assay of antioxidant enzyme activity

Leaf samples (500 mg/sample) were ground into powder through liquid nitrogen and then homogenized into 1 mL of 50 mM ice-cold potassium phosphate (K-P) buffer, pH 7.0 (100 mM potassium chloride (w/v), 5 mM β-mercaptoethanol and 10% glycerol v/v). The homogenized tissue was centrifugated at 11,500 g for 2 min, and the collected supernatant was used for measuring protein content and enzyme activities.

To determine the activity of catalase (CAT, EC: 1.11.1.6), we monitored the decline of absorbance for 1 minute at 240 nm, following the method of Rahman et al. (2019). The reaction mixture consisted of K-P buffer (50 mM, pH 7.0), H_2O_2 (15 mM), and enzyme extract (5 µL), with a final volume of 700 µL. CAT activity was calculated using an extinction coefficient of 39.4 M^{-1} cm^{-1}.

The activity of APX was assessed according to the method of Nakano and Asada, 1981 by recording absorbance change at 290 nm for 1 minute. The reaction mixture contained K-P buffer (50 mM, pH 7.0), ascorbate (AsA, w/v) (0.5 mM), ethylenediaminetetraacetic acid (EDTA, 0.1 mM), H_2O_2 (0.1 mM), and enzyme extract (5 µL), with a final volume of 700 µL. APX activity was estimated using an extinction coefficient of 2.8 M^{-1} cm^{-1}.

The activity of peroxidase was assessed using the method of Hemeda and Klein (1990). The reaction mixture contained K-P buffer (25 mM, pH 7.0), guaiacol (0.05%, v/v), H_2O_2 (10 mM), and enzyme extract (5 µL), with a final volume of 700 µL. An increase in absorbance was recorded at 470 nm for 1 min, and the extinction coefficient of 26.6 mM^{-1} cm^{-1} was used to calculate POD activity.

Total protein from the enzyme extract was measured using Coomassie Bradford protein assay kit (cat. 23200, Thermo Scientific USA) according to manufacturer's instructions.

P5CS1 expression analysis in maize and Arabidopsis using RT-qPCR

Fully expanded leaves of three maize and whole shoot of three Arabidopsis seedlings were homogenized in liquid nitrogen, and RNA was extracted using Monarch RNA miniprep kit (New England Biolabs, USA) following the manufacturer's instruction. The RNA concentration and quality were determined by a nanodrop (NanoDrop 2000c, Thermo Fischer Scientific, USA). cDNA was synthesized using Luna Script super RT mix (New England Biolabs, USA) following the manufacturer's instruction. Quantitative real-time PCR (RT-qPCR) was performed in 96-well plates using a 7500 fast real-time PCR system (Applied Biosystems, USA). A SYBR green-based Luna Universal qPCR master mix was used in the assay with three technical replicates per sample. The qPCR run was set to initial denaturation at 95°C for 3 min followed by 40 cycles (95°C for 15 s, 60°C for 1 min). Specific amplification was analyzed using a melt curve (95°C for 15 s, 60°C for 1 min, 95°C

for 15 s). Primers were designed by using the Oligo Calculator, version 3.27 (http://biotools.nubic.northwestern.edu/OligoCalc.html). Primer efficiency was estimated before running the qPCR reaction (0.936 for *Actin2* and 0.946 for *AtP5CS1* in Arabidopsis, and 0.921 for 19 *α-zein* and 0.932 for *ZmP5CS1* in maize). Relative mRNA expression of *P5CS1* was normalized to the reference, 19 *α-zein* in maize and *Actin2* in Arabidopsis and calculated based on the $2^{-\Delta\Delta Ct}$ method. Primers used in the study are listed in the Supplementary Table 2.

Statistical analysis

Statistical significance was analyzed using open-access statistical computing and statistical platform RStudio (version 4.0.3). All the statistical analysis was performed with one-way ANOVA followed byTukey's PostHoc HSD test except a two-way ANOVA for Figure 1D. For one-way ANOVA and Tukey's PostHoc HSD test the package agricolae (Mendiburu, 2019) and tidyverse (Wickham, 2021), respectively, were used. All codes were designed on a R script (version 4.0.3). Bar plots with error bars were generated in Microsoft Excel (version 16.69.1).

Results

Maize seed priming

Seed priming with acetic acid improved morphological attributes of PEG-primed maize plants

Maize seeds were primed with 500 µM acetic acid (AA) or/and with PEG (PEG+AA) and germinated seedlings were grown in the non-treated hydroponic solutions to observe the priming effect of acetic acid under drought stress. Our observations revealed stunted shoot and root growth in plants treated with PEG, while no visible differences were observed in 'AA' compared to 'Ctrl' (Figures 1A, B). However, a similar pattern of shoot and root growth was observed between 'PEG+AA' and 'Ctrl' (Figures 1A, B). The shoot and root growth parameters, specifically SFW, SDW, RFW, and RDW were significantly decreased by 22%, 20%, 40%, and 43%, respectively, under 'PEG' compared with 'Ctrl'. However, these reductions were recovered in 'PEG+AA', where SFW, SDW, RFW, and RDW showed a decrease of 12%, 5% (not significant), 19%, and 13%, respectively, compared with 'Ctrl' (Table 1). The growth parameters in 'AA' did not exhibit significant variation when compared to the 'Ctrl', which is consistent with the results of visual observations.

Under 'PEG', both shoot and root length showed a significant reduction of 29% and 41%, respectively, when compared to 'Ctrl'. However, no significant changes were observed among 'PEG+AA', 'AA', and 'Ctrl' (Table 1). Interestingly, the trend was opposite for total root volume and average diameter, which showed a significant increase of 55% and 20%, respectively, in 'PEG' compared to 'Ctrl'. Nevertheless, there were no noticeable differences observed among 'PEG+AA', 'AA', and 'Ctrl' for these parameters.

Seed priming with acetic acid improved leaf spectral indices of PEG-primed maize plants

Plants were also studied for leaf spectral reflectance indices. Out of several parameters detected, significant differences were found in Normalized Difference Vegetation Index (NDVI), Simple Ratio Pigment Index (SPRI), Chlorophyll Absorption in Reflectance Index (MCARI), Carter Indices (Ctr1) and Lichtenthaler Indices (Lic2) in the 'PEG' compared to 'Ctrl' (Table 1). NDVI and SPRI significantly decreased by 33% and 23%, respectively, in the 'PEG'. In contrast, MCARI, Ctr1 and Lic2 showed significant increase of 60%, 22% and 11%, respectively, in the 'PEG'. However, there was no significant variations among 'PEG+AA', 'AA', and 'Ctrl' for these indices except slightly decrease of Lic2 in 'PEG+AA' and 'AA' compared with 'Ctrl' (Table 1). Under 'PEG+AA' and 'AA', Lic2 was decreased by 8% and 3%, respectively, as compared with 'Ctrl'.

Seed priming with acetic acid stimulated the proline content of PEG-primed maize plants without influencing the oxidative stress indicators

To monitor the plant status under different conditions, oxidative stress related biochemical and physiological parameters were assessed. Here we observed no significant differences in H_2O_2 and MDA levels among the treatments (Figure 1C), but interestingly, the proline content was highest in 'PEG+AA' and significantly increased by 110% as compared with 'Ctrl' while proline accumulation in other treatments remained unchanged (Figure 1D). In line that, the expression of the proline biosynthetic gene *ZmP5CS1* did not show significant differences among the treatments 'Ctrl', 'AA', and 'PEG', but it was approximately 10-fold higher in 'PEG+AA' compared to the 'Ctrl' and other treatments (Figure 1D). The RWC of shoot showed no variation among the treatments (Table 1).

Overall, our data indicates that pre-treating seeds with acetic acid can modify the response of several morphological and biochemical attributes to drought stress in comparison with non-treated plants.

Exogenous root treatment of maize seedlings

Exogenous acetic acid reduced PEG-mediated negative effects on water content

The above-mentioned morphological study was further devised with exogenous application through root uptake in the 12 days old non-treated seedlings. PEG-treated plants showed severe wilting symptoms in 48 hours after the treatment (Figure 2A). As similar to priming plants, exogenous application of acetic acid didn't employ any visible difference. Intriguingly, the wilting nature of PEG-treatment was recovered in the 'PEG + AA' (Figure 2A). The severity of PEG-treatment was further demonstrated by measuring the shoot RWC. After 48 h of treating the plants, RWC was declined nearly to 60% in 'PEG' while it remained nearly 98% both in 'Ctrl' and 'AA' (Figure 2B). However, the rate of decline was lower (80%) in the 'PEG+AA' (Figure 2B). Moreover, RWC after 4 days declined to 20% in 'PEG'. While no variation was

10.3389/fpls.2023.1167238

TABLE 1 Effect of acetic acid on leaf spectral reflectance indices of maize plants subjected to seed primed PEG treatments*.

Parameters		Ctrl	PEG	AA	PEG+AA
SFW (mg)	Mean	1022.17^{a}	792.17^{b}	1043.17^{a}	899.50^{ab}
	SD	163.42	27.19	163.55	22.32
RFW (mg)	Mean	609.66^{a}	364.17^{b}	550.33^{a}	490.66^{ab}
	SD	38.87	22.48	95.68	182.22
SDW (mg)	Mean	80.33^{a}	64.50^{b}	81.33^{a}	75.83^{a}
	SD	8.43	7.40	4.84	3.87
RDW (mg)	Mean	44.43^{a}	25.28^{b}	41.32^{a}	38.51^{ab}
	SD	1.02	0.95	2.05	1.75
SL (cm)	Mean	34.50^{a}	24.60^{b}	32.66^{a}	34.16^{a}
	SD	2.35	3.76	1.75	2.86
RL (cm)	Mean	15^{a}	8.83^{b}	14.17^{a}	14.83^{a}
	SD	3.03	1.47	2.32	3.49
Total root volume (cm^3)	Mean	0.289^{b}	0.45^{a}	0.28^{b}	0.33^{b}
	SD	0.07	0.04	0.05	0.07
Total root avg. diam (mm)	Mean	0.82^{b}	0.98^{a}	0.80^{b}	0.89^{b}
	SD	0.06	0.065	0.02	0.06
RWC (%)	Mean	97.59^{a}	96.60^{a}	96.72^{a}	96.53^{a}
	SD	0.39	0.978	1.77	0.52
NDVI	Mean	0.57^{a}	0.38^{b}	0.58^{a}	0.55^{a}
	SD	0.03	0.01	0.01	0.01
MCARI	Mean	0.10^{b}	0.16^{a}	0.10^{b}	0.10^{b}
	SD	0.001	0.0077	0.0103	0.004
SPRI	Mean	0.98^{a}	0.75^{b}	0.97^{a}	0.97^{a}
	SD	0.014	0.015	0.022	0.016
Ctr1	Mean	1.27^{b}	1.56^{a}	1.30^{b}	1.33^{b}
	SD	0.05	0.028	0.082	0.05
Lic2	Mean	0.89^{b}	0.99^{a}	0.86^{bc}	0.82^{c}
	SD	0.022	0.081	0.017	0.034
Germination Percentage	Mean	100^{a}	99^{a}	99^{a}	100^{a}
	SD	3	2	4	5

*Data represented as mean, standard deviation (SD) of six individual replicates along with the alphabetical letters representing different levels of statistical significance calculated with one-way ANOVA and Tukey's Post-Hoc HSD test (P<0.05). SFW, shoot fresh weight; RFW, root fresh weight; SDW, shoot dry weight; RDW, root dry weight; SL, shoot length; RL, root length; RWC, relative water content; NDVI, Normalized Difference Vegetation Index; MCARI, Chlorophyll Absorption in Reflectance Index; SPRI, Simple Ratio Pigment Index; Ctr1, Carter Indices; Lic2, Lichtenthaler Indices.

found in 'AA', the water content was still nearly 60% in the 'PEG +AA' (Figure 2B).

Exogenous acetic acid reduced PEG-mediated negative effects on photosynthesis

Two photosynthetic parameters- *A* and *Ci* were significantly reduced by 98% and 45% respectively, in 'PEG'. However, there were no significant variation found among 'Ctrl', 'AA' and 'PEG +AA' (Figures 3A, B). Transpiration related parameters g_s and *E* followed a reciprocal trend compared to photosynthetic parameters with significant up-regulation by 120% and 25% respectively in 'PEG' (Figures 3C, D). Similar to photosynthetic parameters, no significant variation was found among 'Ctrl', 'AA' and 'PEG+AA'. (Figures 3A, B). However, the leaf spectral reflectance indices those showed variation in the seed priming plants were remained unaltered albeit changes of three indices- Photochemical

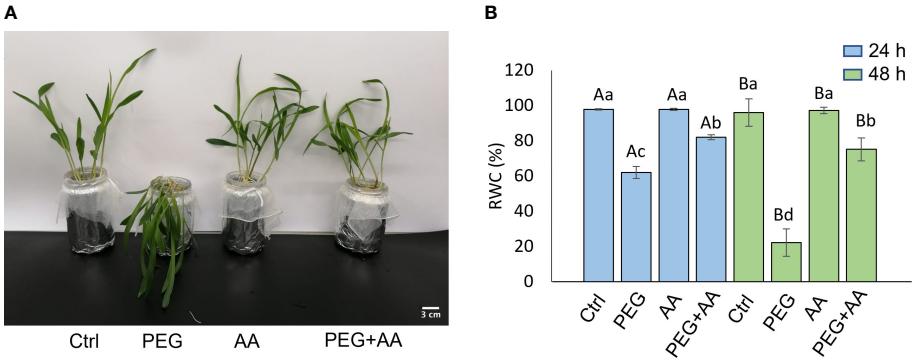

FIGURE 2
Effects of acetic acid on growth and water content of exogenously treated maize seedlings exposed to PEG-treatments. **(A, B)** Shoot growth **(A)** and relative water content (RWC) **(B)** of maize plants treated with exogenous acetic acid under PEG-treatment. Shoot phenotype was photographed after 24 h of treatments, whereas RWC was recorded after 24 h and 48 h of treatments. Data represent mean ± SE of six individual replicates (n=6) and different alphabetical letters indicate significant variations among the treatments following two-way ANOVA including Tukey's *Post-Hoc* HSD test ($P<0.05$). Ctrl, PEG (20%), AA (25 mM), and PEG+AA represent treatments with distilled water (dH_2O), 20% polyethylene glycol, 25 mM acetic acid, and 20% polyethylene glycol + 25 mM acetic acid, respectively.

Reflectance Index (PRI), Normalized Pigment Chlorophyll Index (NPCI) and Greenness Index (GI) (Supplementary Table 1) in the 'PEG'. Significant decrease of PRI (70%) and GI (17%) was observed in 'PEG' compared to 'Ctrl'. No significant alteration of PRI and GI were found in 'AA' and 'PEG+AA' compared to 'Ctrl' (Supplementary Table 1). NPCI showed a significant increase (85%) in the 'PEG' compared with 'Ctrl'. However, the indices had no significant variation in 'AA' and 'PEG+AA' compared with 'Ctrl' (Supplementary Table 1).

Exogenous acetic acid stimulated antioxidant activity to scavenge ROS

We measured the content of H_2O_2, MDA, and proline content in the different treatments. H_2O_2 content was abruptly increased in the 'PEG' by 304% compared to 'Ctrl' (Figure 4A). This substantial increase was declined almost nearly to the level of 'Ctrl' in the 'PEG +AA' and no significant variation found in the 'AA' compared to 'Ctrl'. MDA content increased significantly by 160% upon 'PEG' while no significant variation was found in 'AA' and 'PEG+AA' compared to 'Ctrl' (Figure 4B). On antioxidant activity furthermore, we measured the catalytic activity of 3 antioxidant enzymes. CAT, POD and APX activity was significantly increased by 176%, 121% and 31% respectively in the 'PEG'. However, although there was no significant variation in 'AA', all of them had significantly higher activity by 466%, 260% and 137% in the 'PEG+AA' compared to 'Ctrl' (Figure 4C).

Moreover, substantial increase (416%) of proline content was observed in the 'PEG' compared to 'Ctrl' (Figure 5A). Intriguingly, the content was significantly higher by 148% in 'AA' and an abrupt increase of 2560% in 'PEG+AA' was observed compared 'Ctrl'. To extend our observations on proline biosynthesis, we checked the expression of *ZmP5CS1*, responsible for the biosynthesis of proline (Figure 5B). Expression followed a similar trend to proline content with the increase of around 10-, 4-and 20-fold in the 'PEG', 'AA' and 'PEG+AA', respectively compared to 'Ctrl'.

Overall, our data indicates that exogenous root treatment with acetic acid can ameliorate the negative effects of drought stress by positively regulating the antioxidant activity.

Arabidopsis

Acetic acid regulated ROS and proline levels in Arabidopsis similar to maize

To observe the regulation of proline biosynthesis by acetic acid we further analyzed H_2O_2, proline and MDA accumulation in the model plant Arabidopsis under above-mentioned treatments. Similar to the trend of maize plant, H_2O_2 content followed an significant increase of 106% in 'PEG' compared with 'Ctrl'. Although there was no significant variation in 'AA' but 40% increase was found in 'PEG+AA' compared to 'Ctrl' that is almost 2-fold lower than 'PEG' (Figure 6A). MDA content was also enhanced significantly by 148% upon 'PEG' while no variation found among 'AA', 'PEG+AA' and 'Ctrl' (Figure 6B). Moreover, proline content was significantly increased by 98% in the 'PEG' while the increase was even higher (98%) in the 'PEG+AA' compared to 'Ctrl' (Figure 6C). A slight but significant increase of 62% in 'AA' was found compared with 'Ctrl' which is similar to the observation in maize. Moreover, the observation was confirmed through similar 10-, 5- and 20-fold higher expression of proline biosynthetic gene *AtP5CS1* in 'PEG', 'AA' and 'PEG+AA' respectively compared with 'Ctrl' (Figure 6D).

Functional validation of Arabidopsis *P5CS1* in acetic acid-mediated proline accumulation under PEG-treatment

As proline plays the potential role for acetic acid induced tolerance, we wanted to check the performance of the mutant disrupted in proline biosynthesis. We collected one T-DNA insertion line of proline biosynthetic gene, *P5CS1* and compared

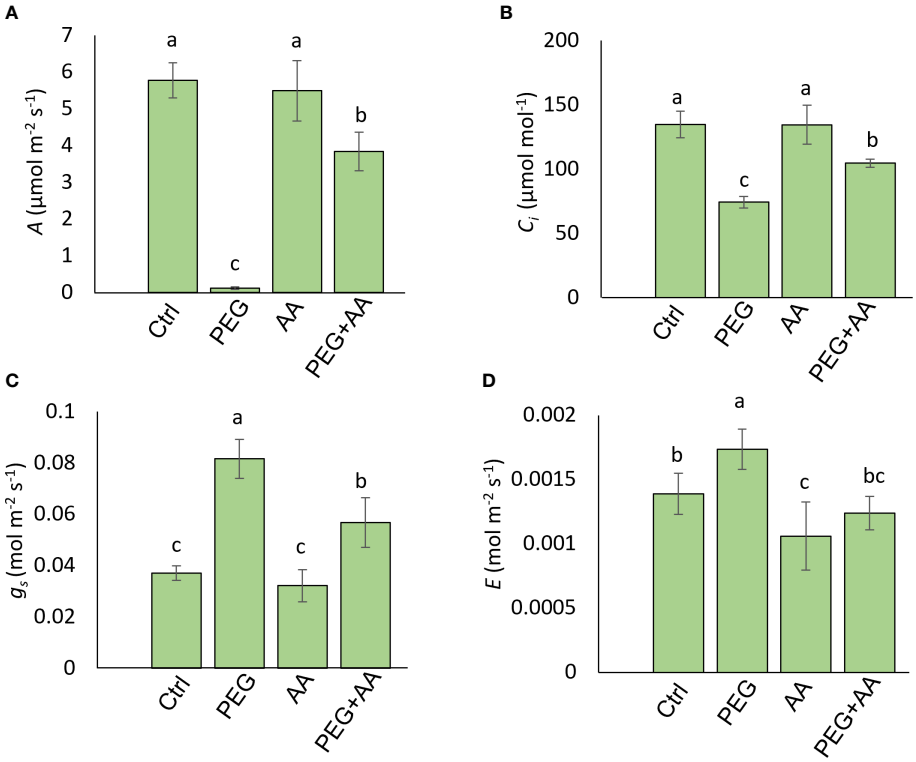

FIGURE 3
Effects of acetic acid on photosynthetic attributes of exogenously treated maize seedlings exposed to PEG-treatments. **(A-D)**, Photosynthetic parameters, including photosynthetic rate (*A*) **(A)**, internal CO_2 concentration (*Ci*) **(B)**, stomatal conductance (g_s), **(C)** and transpiration rate (*E*) **(D)** were recorded in maize leaves after 48 h of treatments. Data represent mean ± SE of six individual replicates (n=6) and different alphabetical letters indicate significant variations among the treatments following Tukey's *Post-Hoc* HSD test ($P<0.05$). Ctrl, PEG (20%), AA (25 mM), and PEG+AA represent treatments with distilled water (dH_2O), 20% polyethylene glycol, 25 mM acetic acid, and 20% polyethylene glycol + 25 mM acetic acid, respectively.

its performance with wild-type (Col-0) under the above-mentioned treatments. From the visual observations, no phenotypic differences were detected between 'Ctrl' and 'AA' (Figure 7). However, both wild-type and *p5cs1* mutant suffered terribly under 'PEG' and wilted to pale-colored leaves. Intriguingly, *p5cs1* mutant was negatively affected in 'PEG+AA'. On the other hand, Col-0 plants still grew better than the others with slightly yellowish and narrower leaves (Figure 7). Overall, our data on Arabidopsis suggests a positive regulation of exogenous acetic acid on proline regulation to reduce the negative effects of drought stress.

Discussion

Drought stress has negative consequences on leaf epinasty, stomatal closure, and photosynthesis, resulting in detrimental effects on plant physiology and growth. Plants have evolved adaptive mechanisms to survive under drought stress (Farooq et al., 2009; Gill and Tuteja, 2010; Claeys and Inze, 2013). Several reports suggested the positive effect of acetic acid in counteracting osmotic stress, especially caused by drought and salinity (Kim et al., 2017; Utsumi et al., 2019; Rahman et al., 2020). In our study, we employed two main approaches to find the potential roles of acetic acid in mitigation of PEG-induced osmotic effects, including i) priming of maize seeds with acetic acid (500 µM) and grown under PEG (20%) and ii) application of exogenous acetic acid (25 mM) to maize seedlings grown under PEG.

Seed priming with PEG resulted in stunted growth that was also consistent with the shoot and growth parameters. The stunted growth of maize plants was almost recovered in 'PEG+AA', although acetic acid alone did not exhibit any positive modulation (Figure 1A). We did not find any variation in the germination percentage of maize seeds among the treatments (Supplementary Table 1). Previous studies reported that germination rate of osmo-primed seeds was decreased in sorghum (Zhang et al., 2015) and in model plant *A. thaliana* (Alavilli et al., 2016). However, the stunted growth recovery in 'PEG+AA' might be due to stress memory transmission. This induced memory perhaps is transmitted from seed germination to seedling stage to induce the growth defects in 'PEG' and ultimately provided lesser canopy to combat the transpirational water loss. Several studies reported PEG- or water deficiency-induced shoot and root growth inhibition or growth parameters reduction while acetic acid application enhanced the recovery (Rahman et al., 2019; Utsumi et al., 2019; Rahman et al., 2020), which was also in parallel with our current findings (Figures 1A, B) Although the root length was much smaller, but the total root volume was higher in 'PEG' while both root length and root volume were almost similar in 'PEG +AA' compared with 'Ctrl' (Table 1). In corroboration with our findings, a previous study also suggested that the root tip growth

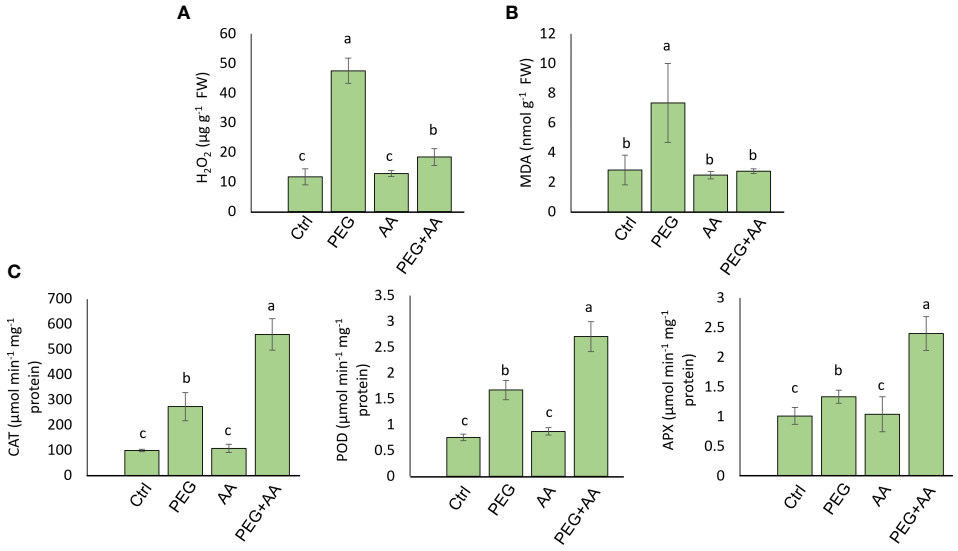

FIGURE 4
Effects of acetic acid on oxidative stress parameters and antioxidant enzyme activities of exogenously treated maize seedlings exposed to PEG-treatments. **(A, B)** The levels of oxidative stress markers hydrogen peroxide (H_2O_2) **(A)** and malondialdehyde (MDA) **(B)**, and the activities of catalase (CAT), ascorbate peroxidase (APX) and peroxidase (POD) **(C)** in the maize leaves were recorded after 48 h of treatments. Data represent mean ± SE of six individual replicates (n=6) and different alphabetical letters indicate significant variations among the treatments following Tukey's *Post-Hoc* HSD test (P<0.05). Ctrl, PEG (20%), AA (25 mM), and PEG+AA represent treatments with distilled water (dH_2O), 20% polyethylene glycol, 25 mM acetic acid, and 20% polyethylene glycol + 25 mM acetic acid, respectively. FW, fresh weight.

was enhanced upon PEG treatment, resulting in a more enhanced diameter (Ji et al., 2014). However, similar root length and volume in 'PEG+AA' to 'Ctrl' suggest the alleviating capacity of acetic acid to overcome PEG-induced negative effects.

Variation was also observed for several leaf spectral indices, including NDVI, SPRI, MCARI, Ctr1, and Lic2 among different treatments. These indices are generally used to detect the effects of environmental stresses on different leaf parameters, such as leaf fluorescence and chlorophyll status (Li et al., 2018). In the current study, NDVI and SPRI had a decreasing trend while MCARI, Ctr1, and Lic2 increased under 'PEG' (Table 1). PEG-induced variation in the indices has not been explored comprehensively; however, our findings are well supported by recent findings on bread wheat under drought (Rustamova et al., 2021; Siddiqui et al., 2021). Increasing NDVI and SPRI, and decreasing MCARI, Ctr1, and Lic2 in 'PEG +AA' plants correlated with morphological parameters, indicating a growth promoting effect of acetic acid in maize (Figures 1A, B). NDVI and SPRI are broadband indices associated with plant biomass production and are often used to indirectly estimate the net primary productivity and photosynthetic capacity (Main et al.,

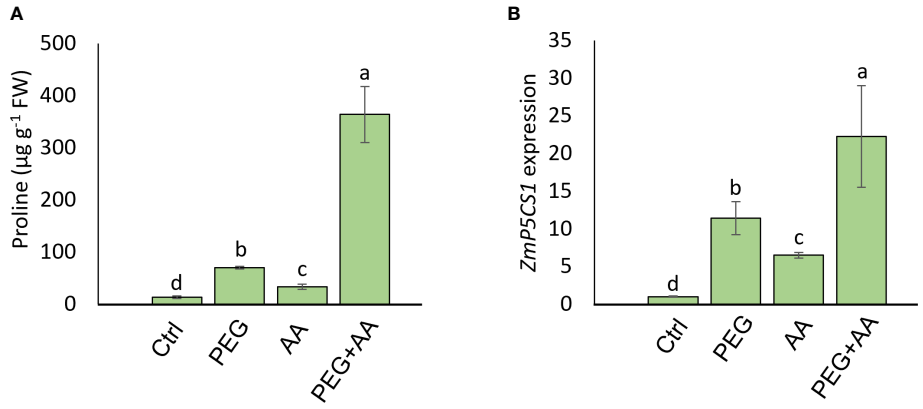

FIGURE 5
Effects of acetic acid on proline accumulation and transcript level of *ZmP5CS1* of exogenously treated maize seedlings exposed to PEG-treatments. **(A, B)** proline content **(A)** and relative expression of *ZmP5CS1* **(B)** in maize leaves recorded after 48 h of treatments. Data represent mean ± SE of six individual replicates (n=6) and three individual replicates (n=3) for proline and *ZmP5CS1* expression respectively, and different alphabetical letters indicate significant variations among the treatments following Tukey's *Post-Hoc* HSD test (P<0.05). FW, fresh weight. Ctrl, PEG (20%), AA (25 mM), and PEG+AA represent treatments with distilled water (dH_2O), 20% polyethylene glycol, 25 mM acetic acid, and 20% polyethylene glycol + 25 mM acetic acid, respectively. FW, fresh weight.

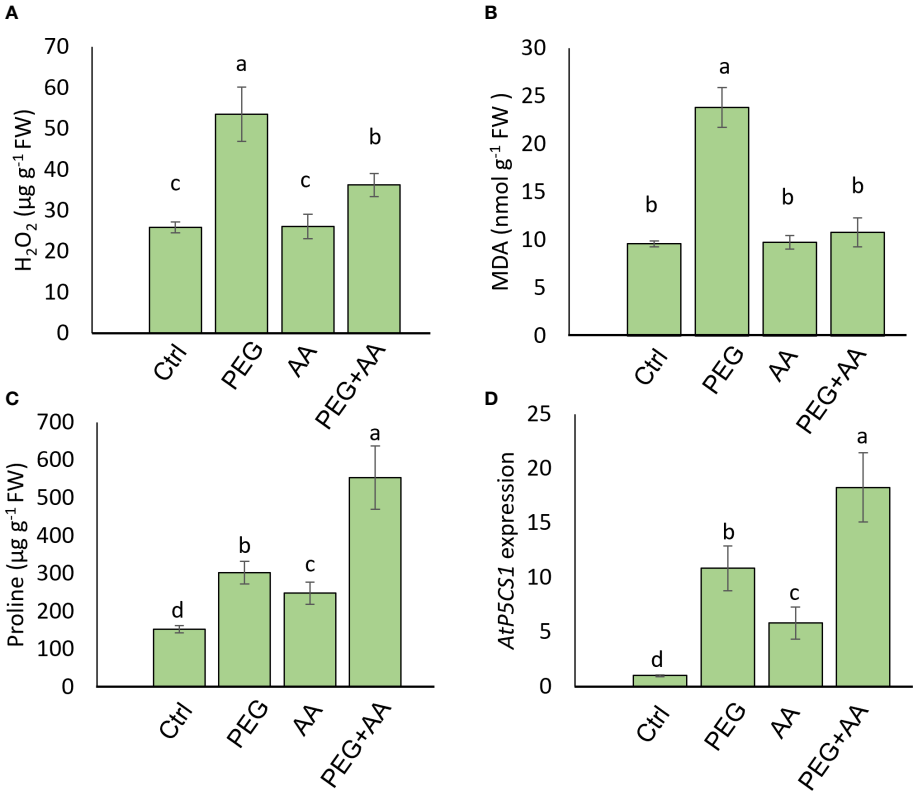

FIGURE 6
Effects of acetic acid on the accumulation of oxidative stress parameters, proline accumulation, and the transcript level of *AtP5CS1* in Arabidopsis plants exposed to PEG-treatments. **(A, B)** The levels of oxidative stress markers hydrogen peroxide (H_2O_2) **(A)** and malondialdehyde (MDA) **(B)**, and **(C, D)** proline content **(C)** and relative expression of *AtP5CS1* **(D)** in Arabidopsis leaves were recorded after 48 h of treatments. Data represent mean ± SE of six individual replicates (n=6) for H2O2, MDA and proline content and three individual replicates (n=3) for *AtP5CS1* expression, and different alphabetical letters indicate significant variations among the treatments following Tukey's *Post-Hoc* HSD test (P<0.05). FW, fresh weight. Ctrl, PEG (20%), AA (500 µM), and PEG+AA represent treatments with distilled water (dH_2O), 20% polyethylene glycol, 500 µM acetic acid, and 20% polyethylene glycol + 500 µM acetic acid, respectively. FW, fresh weight.

2011; Begum et al., 2020). As stress index, intrinsic MCARI indicates the relative abundance of chlorophyll, generally a low MCARI value indicates high leaf chlorophyll content (Li et al., 2018), which was also observed in 'PEG+AA' compared with 'PEG' in the current study (Table 1). However, an increase in Ctr1 index suggests a change in reflectance, which might have occurred due to a shift in carotenoid to chlorophyll ratio (Penuelas et al., 1995). Under stress conditions, chlorophyll degrades at a faster rate compared to carotenoids (Penuelas et al., 1995; Liu et al., 2011), which partially substantiated stunted growth in 'PEG' even though no wilting symptoms were found (Table 1). Notably, the Lic2 index is significantly correlated with plant growth and grain yield and generally a lower value indicates high biomass (Begum et al., 2020) which was observed in 'PEG+AA' compared to 'PEG' (Table 1).

Alteration in leaf spectral indices in the root treated seedlings was not conspicuous albeit significant variation in three indices, including GI, PRI, and NPCI. GI and PRI were decreased in 'PEG' while remaining similar in 'PEG+AA' when compared with 'Ctrl' (Supplementary Table 1). On the other hand, NPCI followed the reciprocal trend (Supplementary Table 1). GI and PRI determine the activity of the photosynthetic apparatus under stress conditions (Gamon et al., 1997), which is in line with the wilting symptoms and low water content in 'PEG' plants while no changes recorded in 'PEG+AA' plants (Figures 2A, B). An increase in NPCI often indicates chlorophyll degradation (Peñuelas et al., 1994), and thus the increase of NPCI in 'PEG' plants and no change in 'PEG+AA' plants highlighted the control of acetic acid over photosynthetic capacity in maize. Moreover, results of gas exchange parameters revealed that PEG-mediated stress perturbed photosynthetic performance with reduced photosynthetic rate and net carbon content, which also coincided with the findings related to severe wilting symptoms (Figure 1C). In contrast, an improved photosynthetic rate in 'PEG+AA' plants despite having declined stomatal conductance and reduced transpiration rate (Figure 3) indicated an intrinsic mechanism employed by acetic acid to sustain maize photosynthetic ability under water-shortage conditions. Similar findings were also reported mung bean plants under salinity stress (Rahman et al., 2019). It is likely that higher transpiration rate and subsequent loss of leaf turgidity were responsible for greater susceptibility to PEG-mediated osmotic stress. By contrast, reduced transpiration rate and stomatal conductance were observed in 'PEG+AA' plants, which coincided with higher RWC and less wilting (Figures 2A, B). Overall, it is pertinent that acetic acid application adjusted the balance between

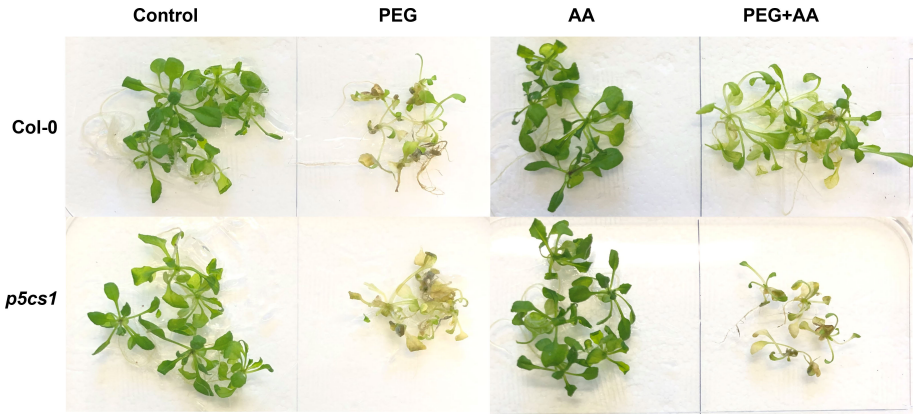

FIGURE 7
Phenotypic variation of Arabidopsis wild-type (Col-0) and *p5cs1* mutant line upon treatment with exogenous acetic acid under PEG treatments. 14 days old seedlings were subjected to exogenous treatments for 48 hours, brought back to the normal MS plate and subsequently grown for another seven days. Ctrl, PEG (20%), AA (500 µM), and PEG+AA represent treatments with dH_2O, 20% polyethylene glycol, 500 µM acetic acid, and 20% polyethylene glycol + 500 µM acetic acid, respectively. FW, fresh weight. This photo is a representative of 3-time experiments.

transpirational loss and photosynthetic capacity, which ultimately led to enhanced tolerance to PEG-mediated osmotic stress.

A vibrant antioxidant system is pre-requisite to detoxify excessive ROS under different types of abiotic stress (Sade et al., 2011; Choudhury et al., 2017; Sehar et al., 2021). In this study, significant increase in MDA and H_2O_2 were observed in 'PEG' plants in comparison with 'Ctrl' plants, suggesting that PEG treatment led to a generation of oxidative stress (Figures 4A, B). On the other hand, reduction of MDA and H_2O_2 contents was positively correlated with the enhanced activities of antioxidant enzymes, including CAT, POD and APX in 'PEG+AA' plants (Figure 4C). These results imply that acetic acid boosted maize antioxidant mechanism by enhancing the activities of key antioxidant enzymes, which ultimately contributed to the alleviation of drought-caused oxidative stress. Intriguingly, proline content was elevated even under acetic acid treatment alone (Figure 5A). Although there was no variation in the H_2O_2 and MDA contents in priming treatments, the amount of proline was increased in 'PEG+AA' plants (Figure 1D), suggesting that stimulation of proline accumulation may be a putative function of acetic acid to fight against drought stress in plants. Like our findings, mung bean plants treated with acetic acid in presence or absence of salt stress displayed an enhanced accumulation of endogenous proline in the leaves (Rahman et al., 2019). It is likely that the lower level of proline in the 'PEG' plants was not sufficient to surpass the PEG-induced osmotic effects, eventually aggravating oxidative damage in maize. Our RT-qPCR data also showed that the enhanced transcript levels of *ZmP5CS1* positively correlated with proline accumulation in 'PEG+AA' plants (Figures 1D, 5B). These results suggest that acetic acid regulates proline level by upregulating the expression of *P5CS1* in plants. We further examined the role of acetic acid in proline metabolism by investigating the drought tolerance of wild-type and *p5cs1* plants of Arabidopsis. PEG-treatment resulted in severe damage in both wild-type and *p5cs1* plants, while under acetic acid application only wild-type survived through severe drought stress but *p5cs1* exhibited profound damage and less recovery (Figure 7). These results underpin that the inability of *p5cs1* to perceive acetic acid treatment through proline accumulation resulted in severe damage under drought stress. Indeed, these results were well-supported by our findings on maize plants primed and treated with acetic acid during seed germination and seedling developments, respectively. Based on this, it appears that acetic acid-mediated high proline accumulation aided maize plants overcoming drought effects.

Conclusions

The present study provides a mechanistic insight into the role of acetic acid in mediating PEG-induced drought tolerance in maize. Drought stress mitigation strategy of acetic acid application was plausibly correlated with the accumulation of endogenous proline through the upregulation of *P5CS1* in plants. Our complementary study using proline biosynthetic mutant *p5cs1* provided additional evidence on the regulatory roles of acetic acid on proline biosynthesis and accumulation under osmotic stress conditions in plants. The overexpression of *P5CS1* upon AA treatment could also underly other metabolic mechanisms associated to the formation of the product P5C that is highly linked to the glutamate and ornithine pathways. Although rigorous study is still needed for proper understanding of acetic acid-mediated drought tolerance, the present study underpinned a vital clue on the potential molecular mechanism of acetic acid in alleviating osmotic stress effects on plants. Because acetic acid is cheap, ecofriendly, and easily accessible, it could provide a dramatic solution for management of drought stress effects on plants in drought-prone areas worldwide.

Data availability statement

The original contributions presented in the study are publicly available. This data can be found here: https://www.ncbi.nlm.nih.gov/

nuccoreMaize: 19 α-zein (NM_001152088), P5CS1(NM_001352327). Arabidopsis: Actin2 (At3g18780), AtP5CS1 (At2g39800).

Author contributions

SM designed the research. SM and MK performed the research. SM and MM analyzed the data and prepared the figures. KA, DAM, and MK acquired funding. SM, MM, and MK wrote the paper with the input from all authors. All authors contributed to the article and approved the submitted version.

Funding

This research was funded by Princess Nourah bint Abdulrahman University Researchers Supporting Project number (PNURSP2023R188), Princess Nourah bint Abdulrahman University, Riyadh, Saudi Arabia. We also gratefully acknowledge the financial support from the National Agricultural Technology Project (NATP), Phase-II, PIU, Bangladesh Agricultural Research Council to MK for this research outcome.

Acknowledgments

Princess Nourah bint Abdulrahman University Researchers Supporting Project number (PNURSP2023R188), Princess Nourah bint Abdulrahman University, Riyadh, Saudi Arabia. We are grateful to Dr. Dietmar Funck, Chemical and Synthetic Biology of Nucleic Acids Chemistry Department, University of Konstanz for providing *p5cs1* seeds.

Conflict of interest

The authors declare that the research was conducted in the absence of any commercial or financial relationships that could be construed as a potential conflict of interest.

Publisher's note

All claims expressed in this article are solely those of the authors and do not necessarily represent those of their affiliated organizations, or those of the publisher, the editors and the reviewers. Any product that may be evaluated in this article, or claim that may be made by its manufacturer, is not guaranteed or endorsed by the publisher.

Supplementary material

The Supplementary Material for this article can be found online at: https://www.frontiersin.org/articles/10.3389/fpls.2023.1167238/full#supplementary-material

SUPPLEMENTARY FIGURE 2
Dose-specific effect of acetic acid on Arabidopsis seed germination and proline content. **(A, B)** Germination percentage calculated **(A)** and the level of proline content **(B)** from the 3 days old germinated seedlings after plating them into MS medium containing **(A)** or treating 48 h with **(B)** different concentration of acetic acid. Data represent mean ± SE of three individual replicates (n=3) with 100 individual seeds for germination percentage and six individual replicates (n=6) for proline content, and different alphabetical letters indicate significant variations among the treatments following Tukey's *Post-Hoc* HSD test ($P<0.05$).

References

Adamipour, N., Khosh-Khui, M., Salehi, H., Razi, H., Karami, A., and Moghadam, A. (2020). Metabolic and genes expression analyses involved in proline metabolism of two rose species under drought stress. *Plant Physiol. Biochem.* 155, 105–113. doi: 10.1016/j.plaphy.2020.07.028

Alavilli, H., Awasthi, J. P., Rout, G. R., Sahoo, L., Lee, B. H., and Panda, S. K. (2016). Overexpression of a barley aquaporin gene, HvPIP2; 5 confers salt and osmotic stress tolerance in yeast and plants. *Front. Plant Sci.* 7. doi: 10.3389/fpls.2016.01566

Alvarez, M. E., Savouré, A., and Szabados, L. (2022). Proline metabolism as regulatory hub. *Trends Plant Sci.* 27 (1), 39–55. doi: 10.1016/j.tplants.2021.07.009

Avramova, V., Elgawad, H., Zhang, Z., Fotschki, B., Casadevall, R., and Vergauwen, L. (2015). Drought induces distinct growth response, protection, and recovery mechanisms in the maize leaf growth zone. *Plant Physiol.* 169, 1382–1396. doi: 10.1104/pp.15.00276

Badr, A., El-Shazly, H. H., Tarawneh, R. A., and Börner, A. (2020). Screening for drought tolerance in maize (*Zea mays* l.) germplasm using germination and seedling traits under simulated drought conditions. *Plants* 9, 565. doi: 10.3390/plants9050565

Bates, L. S., Waldren, R. P., and Teare, I. D. (1973). Rapid determination of free proline for water-stress studies. *Plant Soil.* 39, 205–207. doi: 10.1007/BF00018060

Begum, H., Alam, M. S., Feng, Y., Koua, P., Ashrafuzzaman, M., Shrestha, A., et al. (2020). Genetic dissection of bread wheat diversity and identification of adaptive loci in response to elevated tropospheric ozone. *Plant Cell Environ.* 43, 2650–2665. doi: 10.1111/pce.13864

Chen, C., Cui, X., Zhang, P., Wang, Z., and Zhang, J. (2021). Expression of the pyrroline-5-carboxylate reductase (P5CR) gene from the wild grapevine *Vitis yeshanensis* promotes drought resistance in transgenic *Arabidopsis.* plant physiol. *Biochem.* 168, 188–201. doi: 10.1016/j.plaphy.2021.10.004

Choudhury, F. K., Rivero, R. M., Blumwald, E., and Mittler, R. (2017). Reactive oxygen species, abiotic stress and stress combination. *Plant J.* 90, 856–867. doi: 10.1111/tpj.13299

Chun, S. C., Paramasivan, M., and Chandrasekaran, M. (2018). Proline accumulation influenced by osmotic stress in arbuscular mycorrhizal symbiotic plants. *Front. Plant Sci.* 9. doi: 10.3389/fmicb.2018.02525

Claeys, H., and Inze, D. (2013). The agony of choice: how plants balance growth and survival under water limiting conditions. *Plant Physiol.* 162, 1768–1779. doi: 10.1104/pp.113.220921

Daughtry, C. S. T., Walthall, C. L., Kim, M. S., Brown, E. C., and McMurtrey, J. E. (2000). Estimating corn leaf chlorophyll concentration from leaf and canopy reflectance. *Remot. Sens. Env.* 74, 229–239. doi: 10.1016/S0034-4257(00)00113-9

de Mendiburu, F. (2019) *Agricolae: statistical procedures for agricultural research. r package version 1.* Available at: https://CRAN.R-project.org/package=agricolae.

Fang, L., Yin, X., Peter, E. L., Martre, P., and Struik, P. C. (2022). Drought exerts a greater influence than growth temperature on the temperature response of leaf day respiration in wheat (*Triticum aestivum*). *Plant Cell Environ.* 45, 2062–2077. doi: 10.1111/pce.14324

Farooq, M., Hussain, M., Wakeel, A., and Siddiqui, K. H. M. (2015). Salt stress in maize: effects, resistance mechanisms, and management: a review. *Agron. Sustain. Dev.* 35, 461–481. doi: 10.1007/s13593-015-0287-0

Farooq, M., Wahid, A., Kobayashi, N., Fujita, D., and Barsa, S. M. A. (2009). Plant drought stress: effects, mechanisms and management. *Agron. Sustain. Dev.* 29, 185–212. doi: 10.1051/agro:2008021

Funck, D., Winter, G., Baumgarten, L., and Forlani, G. (2012). Requirement of proline synthesis during *Arabidopsis* reproductive development. *BMC Plant Biol.* 12, 191. doi: 10.1186/1471-2229-12-191

Gamon, J., Serrano, L., and Surfus, J. (1997). The photochemical reflectance index: an optical indicator of photosynthetic radiation use efficiency across species, functional types, and nutrient levels. *Oecologia.* 112, 492–501. doi: 10.1007/s004420050337

Ghoulam, C., Fours, A., and Fares, K. (2002). Effects of salt stress on growth, inorganic ions and proline accumulation in relation to osmotic adjustment in five sugar beet cultivars. *Environ. Exp. Bot.* 47, 39–50. doi: 10.1016/S0098-8472(01)00109-5

Gill, S. S., and Tuteja, N. (2010). Reactive oxygen species and antioxidant machinery in abiotic stress tolerance in crop plants. *J. Plant Physiol.* 48, 909–930. doi: 10.1016/j.plaphy.2010.08.016

Gupta, A., Rico-Medina, A., and Cano-Delgado, A. I. (2020). The physiology of plant responses to drought. *Science* 368, 266–269. doi: 10.1126/science.aaz7614

Hemeda, H. M., and Klein, B. P. (1990). Effects of naturally occurring antioxidants on peroxidase activity of vegetable extracts. *J. Food Sci.* 55, 184 185. doi: 10.1111/j.1365-2621.1990.tb06048.x

Hodges, D., DeLong, J., Forney, C., and Prange, R. K. (1999). Improving the thiobarbituric acid-reactive-substances assay for estimating lipid peroxidation in plant tissues containing anthocyanin and other interfering compounds. *Planta.* 207, 604–611. doi: 10.1007/s00425-017-2699-3

Ibrahim, A. A., Mageed, A. E. T., Abohamid, Y., Abdallah, H., El-Saadony, M., and AbuQamar, S. (2022). Exogenously applied proline enhances morph-physiological responses and yield of drought-stressed maize plants grown under different irrigation systems. *Front. Plant Sci.* 13. doi: 10.3389/fpls.2022.897027

Ji, H., Liu, L., Li, K., Xie, Q., Wang, Z., Zhao, X., et al. (2014). PEG-mediated osmotic stress induces premature differentiation of the root apical meristem and outgrowth of lateral roots in wheat. *J. Exp. Bot.* 65, 4863–4872. doi: 10.1093/jxb/eru255

Kamruzzaman, M., Beyene, M. A., Siddiqui, M. N., Ballvora, A., Léon, J., and Naz, A. A. (2022). Pinpointing genomic loci for drought-induced proline and hydrogen peroxide accumulation in bread wheat under field conditions. *BMC Plant Biol.* 22, 584. doi: 10.1186/s12870-022-03943-9

Kang, J., Peng, Y., and Xu, W. (2022). Crop root responses to drought stress: molecular mechanisms, nutrient regulations, and interactions with microorganisms in the rhizosphere. *Int. J. Mol. Sci.* 23, 9310. doi: 10.3390/ijms23169310

Kim, J. M., To, T., Matsui, A., Tanoi, K., Kobayashi, N. I., Matsuda, F., et al. (2017). Acetate-mediated novel survival strategy against drought in plants. *Nat. Plants.* 3, 17097. doi: 10.1038/nplants.2017.97

Lei, C., Bagavathiannan, M., Wang, H., Sharpe, S. M., Meng, W., and Yu, J. (2021). Osmopriming with polyethylene glycol (PEG) for abiotic stress tolerance in germinating crop seeds: a review. *Agron.* 11, 2194. doi: 10.3390/agronomy11112194

Li, M., Chu, R., Yu, Q., Islam, A. R. M., Chou, S., and Shen, S. (2018). Evaluating structural, chlorophyll-based and photochemical indices to detect summer maize responses to continuous water stress. *Water* 10, 500. doi: 10.3390/w10040500

Liu, C. C., Liu, Y. G., Guo, K., Fan, D. Y., Li, G. G., Zheng, Y., et al. (2011). Effect of drought on pigments, osmotic adjustment and antioxidant enzymes in six woody plant species in karst habitats of south- western China. *Env. Exp. Bot.* 71, 174–183. doi: 10.1016/j.envexpbot.2010.11.012

Mahmud, S., Ullah, C., Kortz, A., Bhattacharyya, S., Yu, P., Gershenzon, J., et al. (2022). Constitutive expression of *JASMONATE RESISTANT 1* induces molecular changes that prime the plants to better withstand drought. *Plant Cell Environ.* 45, 2906–2922. doi: 10.1111/pce.14402

Main, R., Cho, M. A., Mathieu, R., O'Kennedy, M. M., Ramoelo, A., and Koch, S. (2011). An investigation into robust spectral indices for leaf chlorophyll estimation. *ISPRS J. Phot. Remo. Sens.* 66, 751–761. doi: 10.1016/j.isprsjprs.2011.08.001

Mittler, R., Zandalinas, S. I., Fichman, Y., and Breusegem, F.V. (2022). Reactive oxygen species signalling in plant stress responses. *Nat. Rev. Mol. Cell. Biol.* 23, 663–679. doi: 10.1038/s41580-022-00499-2

Mosaad, I. S. M., Ayman, H. I. S., Moustafa-Farag, M., and Seadh, A. K. (2020). Effect of exogenous proline application on maize yield and the optimum rate of mineral nitrogen under salinity stress, J. *Plant Nutr.* 43, 354–370. doi: 10.1080/01904167.2019.1676901

Moukhtari, A., Cabassa-Hourton, C., Farissi, M., and Savoure, A. (2020). How does proline treatment promote salt stress tolerance during crop plant development? *Front. Plant Sci.* 11. doi: 10.3389/fpls.2020.01127

Nakano, Y., and Asada, K. (1981). Hydrogen peroxide is scavenged by ascorbate-specific peroxidase in spinach chloroplasts. *Plant Cell Physiol.* 22, 867–880. doi: 10.1093/oxfordjournals.pcp.a076232

Nikoleta-Kleio, D., Theodoros, D., and Roussos, P. A. (2020). Antioxidant defense system in young olive plants against drought stress and mitigation of adverse effects through external application of alleviating products. *Sci. Hortic.* 259, 108812. doi: 10.1016/j.scienta.2019.108812

Ogawa, D., Suzuki, Y., Yokoo, T., Katoh, E., Teruya, M., Muramatsu, M., et al. (2021). AA-acid-induced jasmonate signaling in root enhances drought avoidance in rice. *Sci. Rep.* 11, 6280. doi: 10.1038/s41598-021-85355-7

Ozturk, M., Turkyilmaz, U. B., García-Caparrós, P., Khursheed, A., Gul, A., and Hasanuzzaman, M. (2021). Osmoregulation and its actions during the drought stress in plants. *Physol. Plant* 172, 1321–1335. doi: 10.1111/ppl.13297

Peñuelas, J., Gamon, J., Fredeen, A., Merino, J., and Field, C. (1994). Reflectance indices associated with physiological changes in nitrogen-and water-limited sunflower leaves. *Remote Sens. Environ.* 48, 135–146. doi: 10.1016/0034-4257(94)90136-8

Penuelas, J., Baret, F., and Filella, I. (1995). Semiempirical indexes to assess carotenoids chlorophyll-a ratio from leaf spectral reflectance. *Photosynthetica* 31, 221–230.

Rahman, M., Mostofa, M. G., Keya, S. S., Rahman, A., Das, A. K, Islam, R., et al. (2020). Acetic acid improves drought acclimation in soybean: an integrative response of photosynthesis, osmoregulation, mineral uptake and antioxidant defense. *Physiol. Plant* 172, 334–350. doi: 10.1111/ppl.13191

Rahman, M. M., Mostofa, M. G., Rahman, M. A., Islam, M.R., Keya, S.S., Das, A.K., et al. (2019). Acetic acid: a cost-effective agent for mitigation of seawater-induced salt toxicity in mung bean. *Sci. Rep.* 9, 15186. doi: 10.1038/s41598-019-51178-w

Rivero, L., Scholl, R., Holomuzki, N., Crist, D., Grotewold, E., and Brkljacic, J. (2013). Handling *Arabidopsis* plants: growth, preservation of seeds, transformation, and genetic crosses. *Methods Mol. Biol.* 1062, 3–25. doi: 10.1007/978-1-62703-580-4_1

Rouse, J. W., Haas, R. H., Schell, J. A., and Deering, D. W. (1973). "Monitoring vegetation systems in the great plains with ERTS," in *Proceedings of 3rd earth resources technology satellite symposium, Greenbelt, SP-351*. 309–317.

Rustamova, S., Shreshtha, A., Naz, A. A., and Huseynova, I. (2021). Expression profiling of DREB1 and evaluation of vegetation indices in contrasting wheat genotypes exposed to drought stress. *Plant Gene.* 25, 266. doi: 10.1016/j.plgene.2020.100266

Sade, B., Soylu, S., and Yetim, E. (2011). Drought and oxidative stress. *Afric. J. Biotech.* 10, 11102–11109. doi: 10.5897/AJB11.1564

Salika, R., and Rifat, J. (2021). Abiotic stress responses in maize: a review. *Acta Physiol. Plant* 43, 130. doi: 10.1007/s11738-021-03296-0

Sehar, Z., Jahan, B., Masood, A., Anjum, N. A., and Khan, N. A. (2021). Hydrogen peroxide potentiates defense system in presence of sulfur to protect chloroplast damage and photosynthesis of wheat under drought stress. *Physiol. Planta.* 172, 922–934. doi: 10.1111/ppl.13225

Sergiev, I., Alxieva, V., and Karanov, E. (1997). Effect of spermone, atrazine and combination between them on some endogenous protective systems and stress markers in plants. *Comp. Rend. Acad. Bulg. Sci.* 51, 121–124.

Sheoran, S., Kaur, Y., Kumar, S., Shukla, S., Rakshit, S., and Kumar, R. (2022). Recent advances for drought stress tolerance in maize (*Zea mays* l.): present status and future prospects. *Front. Plant Sci.* 13. doi: 10.3389/fpls.2022.872566

Shrestha, A., Cudjoe, D. K., Kamruzzaman, M., Siddique, S., Fiorani, F., Léon, J., et al. (2021). Abscisic acid-responsive element binding transcription factors contribute to proline synthesis and stress adaptation in *Arabidopsis*. J. *Plant Physiol.* 261, 153414. doi: 10.1016/j.jplph.2021

Siddiqui, M. N., Teferi, T. J., Ambaw, A. M., Gabi, M. T., Koua, P., Léon, J., et al. (2021). New drought-adaptive loci underlying candidate genes on wheat chromosome 4B with improved photosynthesis and yield responses. *Physiol. Planta.* 173, 2166–2180. doi: 10.1111/ppl.13566

Singh, C. K., Rajkumar, B. K., and Kumar, V. (2021). Differential responses of antioxidants and osmolytes in upland cotton (*Gossypium hirsutum*) cultivars contrasting in drought tolerance. *Plant Stress.* 2, 100031. doi: 10.1016/j.stress.2021.100031

Spormann, S., Nadais, P., Sousa, F., Pinto, M., Martins, M., Sousa, B., et al. (2023). Accumulation of proline in plants under contaminated soils–are we on the same page? *Antioxidants* 12 (3), 666. doi: 10.3390/antiox12030666

Utsumi, Y., Chikako, U., Maho, T., Chien, V. H., Takahashi, S., Matsui, A., et al. (2019). Acetic acid treatment enhances drought avoidance in cassava (*Manihot esculenta*). *Front. Plant Sci.* 10, 521. doi: 10.3389/fpls.2019.00521

Velikova, V., Yordanov, I., and Edreva, A. (2000). Oxidative stress and some antioxidant systems in acid rain-treated bean plants: protective role of exogenous polyamines. *Plant Sci.* 151, 59–66. doi: 10.1016/S0168-9452(99)00197-1

Wickham, H., Averick, M., Bryan, J., Chang, W., McGowan, L.D., François, R., et al (2021). Wecome to tydyverse. *J. Open Source Softw.* 4, 1686. doi: 10.21105/joss.01686

Zhang, F., Yu, J., Johnston, C. R., Wang, Y., Zhu, K., Lu, F., et al. (2015). Seed priming with polyethylene glycol induces physiological changes in sorghum (*Sorghum bicolor* l. moench) seedlings under suboptimal soil moisture environments. *PloS One* 10, 10. doi: 10.1371/journal.pone.0140620

frontiers | Frontiers in Plant Science

TYPE Original Research
PUBLISHED 11 August 2023
DOI 10.3389/fpls.2023.1155441

Check for updates

OPEN ACCESS

EDITED BY
Mahmoud Magdy,
Ain Shams University, Egypt

REVIEWED BY
Tamir Klein,
Weizmann Institute of Science, Israel
Hagar Elhifnawy,
Ain Shams University, Egypt

*CORRESPONDENCE
Francisco Javier Gallego
fjgalleg@ucm.es

RECEIVED 31 January 2023
ACCEPTED 19 July 2023
PUBLISHED 11 August 2023

CITATION
Méndez-Cea B, García-García I, Linares JC and Gallego FJ (2023) Warming appears as the main risk of non-adaptedness for western Mediterranean relict fir forests under expected climate change scenarios. *Front. Plant Sci.* 14:1155441. doi: 10.3389/fpls.2023.1155441

COPYRIGHT
© 2023 Méndez-Cea, García-García, Linares and Gallego. This is an open-access article distributed under the terms of the Creative Commons Attribution License (CC BY). The use, distribution or reproduction in other forums is permitted, provided the original author(s) and the copyright owner(s) are credited and that the original publication in this journal is cited, in accordance with accepted academic practice. No use, distribution or reproduction is permitted which does not comply with these terms.

Warming appears as the main risk of non-adaptedness for western Mediterranean relict fir forests under expected climate change scenarios

Belén Méndez-Cea[1], Isabel García-García[1], Juan Carlos Linares[2] and Francisco Javier Gallego[1]*

[1]Dpto. Genética, Fisiología y Microbiología, Unidad Docente de Genética, Facultad de CC Biológicas, Universidad Complutense de Madrid, Madrid, Spain, [2]Dpto. Sistemas Físicos, Químicos y Naturales, Universidad Pablo de Olavide, Sevilla, Spain

Circum-Mediterranean firs are considered among the most drought-sensitive species to climate change. Understanding the genetic basis of trees' adaptive capacity and intra-specific variability to drought avoidance is mandatory to define conservation measures, thus potentially preventing their extinction. We focus here on *Abies pinsapo* and *Abies marocana*, both relict tree species, endemic from south Spain and north Morocco, respectively. A total of 607 samples were collected from eight nuclei: six from Spanish fir and two from Moroccan fir. A genotyping by sequencing technique called double digestion restriction site-associated DNA sequencing (ddRAD-seq) was performed to obtain a genetic matrix based on single-nucleotide polymorphisms (SNPs). This matrix was utilized to study the genetic structure of *A. pinsapo* populations and to carry out selection signature studies. In order to understand how Spanish fir and Moroccan fir cope with climate change, genotype–environment associations (GEAs) were identified. Further, the vulnerability of these species to climate variations was estimated by the risk of non-adaptedness (RONA). The filtering of the *de novo* assembly of *A. pinsapo* provided 3,982 SNPs from 504 out of 509 trees sequenced. Principal component analysis (PCA) genetically separated Grazalema from the rest of the Spanish populations. However, F_{ST} values showed significant differences among the sampling points. We found 51 *loci* potentially under selection. Homolog sequences were found for some proteins related to abiotic stress response, such as dehydration-responsive element binding transcription factor, regulation of abscisic acid signaling, and methylation pathway. A total of 15 associations with 11 different *loci* were observed in the GEA studies, with the maximum temperature of the warmest month being the variable with the highest number of associated *loci*. This temperature sensitivity was also supported by the risk of non-adaptedness, which yielded a higher risk for both *A. pinsapo* and *A. marocana* under the high emission scenario (Representative Concentration Pathway (RCP) 8.5). This study sheds light on the response to climate change of these two endemic species.

KEYWORDS

circum-Mediterranean firs, selection signature, genotype-environment associations, risk of non-adaptedness, Sierra de las Nieves, Grazalema, Talassemtane

1 Introduction

The frequency and intensity of drought events are increasing worldwide, triggering extensive growth decline, dieback, and mortality in many forest ecosystems (DeSoto et al., 2020; McDowell et al., 2020). At a regional scale, the Mediterranean basin is highly vulnerable to ongoing warming, a trend that is predicted to worsen (Ozturk et al., 2015). Consequently, drought-sensitive forests are likely to be increasingly stressed, as water shortage impairs the functioning of trees by reducing their photosynthesis and growth rates (Choat et al., 2018). The circum-Mediterranean firs can be considered among the most sensitive tree species to climate change (Aussenac, 2002; Linares, 2011; Caudullo and Tinner, 2016; Sánchez-Salguero et al., 2017). Furthermore, they are mainly represented by relict tree species, which causes several uncertainties concerning their future prospects (Hampe and Jump, 2011). Ecological and evolutionary factors determine the population dynamics of these endangered tree species, while several underlying genetic responses remain elusive to our knowledge (Alberto et al., 2013). Thus, a proper understanding of key physiological and genetic mechanisms involved in the populations' persistence becomes imperative for maintaining forest biodiversity and ecosystem services (Anderegg et al., 2013).

Here, we focus on *Abies marocana* Trab. and *Abies pinsapo* Boiss., the westernmost circum-Mediterranean fir species, endemic from north Morocco and south Spain, respectively (Linares, 2011; Ben-Said, 2022). Both species are included in the International Union for Conservation of Nature (IUCN) Red List of Threatened Species as endangered species, with climate change one of the main threats to their conservation (Alaoui et al., 2011; Arista et al., 2011). Events of forest dieback and mortality have been mainly reported for *A. pinsapo* (Linares et al., 2009; Navarro-Cerrillo et al., 2020a; Navarro-Cerrillo et al., 2022; Cortés-Molino et al., 2023), while the sensitivity to climate change of *A. marocana* has been also pointed out (Esteban et al., 2010; Navarro-Cerrillo et al., 2020b; Alaoui et al., 2021). Despite the increasing concern regarding the apparent rising mortality rates of these relict tree species in the context of pervasive environmental changes and habitat loss, the genetic mechanisms underlying contrasting vulnerability among individuals are still poorly understood. However, some efforts have been made to shed light on this issue (e.g., Cobo-Simón et al., 2021; Cobo-Simón et al., 2023b). Furthermore, a better understanding of the climatic factors affecting species' vulnerability, such as the risk of non-adaptedness, may allow for better predictions of the success of species to track changing climates (Rellstab et al., 2016; Pina-Martins et al., 2019).

Previous genetic studies performed in *A. pinsapo* and *A. marocana* focused mainly on molecular markers of the nucleus and cytoplasm, namely, chloroplast and mitochondria, but not on the entire genome. The main reasons are related to the intrinsic characteristics of the conifer genomes, characterized by their large size (18–20 Gbp), a high number of repetitive sequences, and the absence of reference genomes for most species (Neale and Wheeler, 2019; García-García et al, 2022). Hence, there are studies determining genetic diversity and population structure using chloroplast microsatellites (cpSSRs) (Terrab et al., 2007); developing new molecular markers such as nuclear microsatellites (nSSRs) (Sánchez-Robles et al., 2012); describing genetic differentiation between *A. pinsapo* and *Abies alba* using SSRs (Jaramillo-Correa et al., 2010; Dering et al., 2014); determining the genetic diversity of several Spanish fir populations using SSRs, intermicrosatellites (ISSRs), and single-nucleotide polymorphisms (SNPs) (Cobo-Simón et al., 2020); characterizing drought response genes of *A. pinsapo* applying SNPs (Cobo-Simón et al., 2021; Cobo-Simón et al., 2023a); or performing biogeographic studies with several species of *Abies* taxa (Litkowiec et al., 2021). Nonetheless, current advances in next-generation sequencing (NGS) and in bioinformatics open a wide range of possibilities to perform studies with conifer genomes. Furthermore, transcriptomes can be used as an alternative reference. Hence, in the case of *A. pinsapo*, Pérez-González et al. (2018) obtained a *de novo* transcriptome, and recently, Ortigosa et al. (2022) published other transcriptome with the aim to determine intraspecific variations.

In this work, a genotyping by sequencing (GBS) technique named double digestion restriction site-associated DNA sequencing (ddRAD-seq) was used to obtain a genetic matrix based on SNPs. Our specific aims were i) to study the genetic structure of *A. marocana* and *A. pinsapo* populations and to determine the presence of loci under selection based on the obtained SNPs, ii) to identify genotype–environment associations (GEAs) based on local climate variables and population genetics, and iii) to assess the vulnerability of *A. marocana* and *A. pinsapo* to future climate change scenarios based on the risk of non-adaptedness (RONA).

2 Materials and methods

2.1 Species of study and field sampling

A. pinsapo is a sub-dioicous fir with a pyramidal shape, which can grow up to 30 m. Spanish fir is located on north-facing slopes between 1,000 and 1,800 m a.s.l. (Linares et al., 2009). This location allows *A. pinsapo* to maintain optimum conditions of humidity, which is the most relevant issue to this species' survival. Spanish fir is a relict species whose distribution is restricted to the South of Spain. There are three nuclei, which are placed in Sierra de las Nieves with an area of approximately 5,800 ha, Sierra Bermeja with 1,212 ha, and Sierra de Grazalema with approximately 2,000 ha.

A total of 571 leaf samples from six populations of *A. pinsapo* were collected (Figure 1). The studied populations located in the National Park of Sierra de las Nieves were Saucillo (SA), with 126 samples collected; Caucón (CA), with 259 samples; Ánimas (AN), with 51 samples; Pilones (PI), with 29 samples; and Pilar de Tólox (PT), with 16. Additionally, 90 samples were sampled from the Biosphere Reserve Sierra de Grazalema (GR). Not all the samples collected were sequenced (Table 1). To assess the genetic differences between saplings and old trees, individuals of these two cohorts were collected from three nuclei: SA, CA, and AN (Table 1).

A. marocana is a monoecious species that appears in the high peaks between 1,500 and 2,000 m a.s.l. (Ben-Said, 2022). As it was

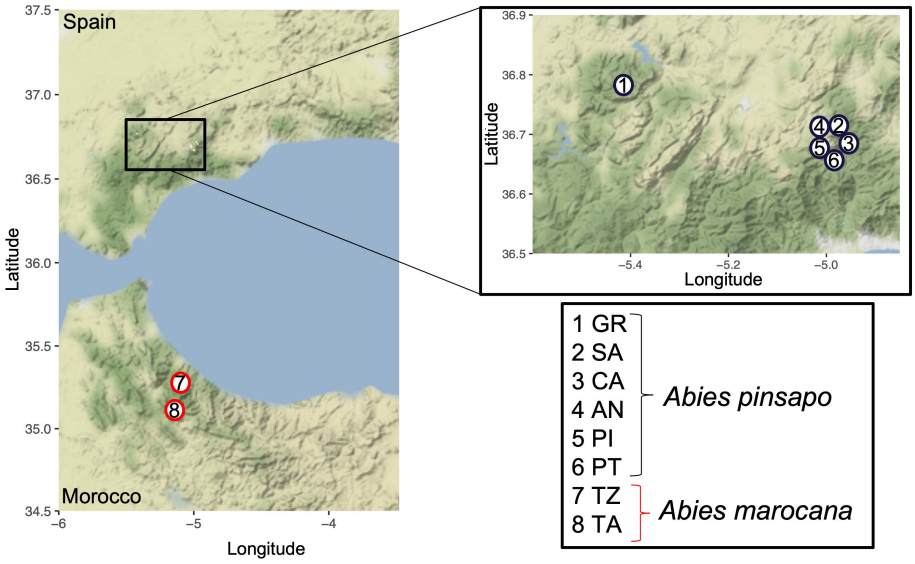

FIGURE 1
Geographical localization of the nuclei used to carry out the genetic structure of *Abies pinsapo* populations. In addition, the map shows the two places occupied by *Abies marocana*.

described for Spanish fir, this species is usually present in the north slope because it needs humid environments to survive due to its drought sensitivity (Aussenac, 2002). Moroccan fir is a relict species whose range distribution is in Northern Morocco.

In terms of *A. marocana*, two populations located in Talassemtane National Park were studied. Talassemtane (TA) accounts for approximately 2,000 ha, and Jebel Tazaot (TZ), which is the mountain range of Talassemtane, is approximately 1,000 ha (Ben-Said, 2022; Ben-Said et al., 2022). The number of collected samples was 101, with 53 from TA and 45 from TZ (Figure 1). As it was described for *A. pinsapo* populations, saplings and old trees were collected from these two populations (Table 1).

2.2 DNA extraction and ddRAD-seq

The extraction starts with the lyophilization of 100 mg of each fresh leaf sample. Then, total DNA extraction was carried out by using DNeasy Plant Mini Kit (Qiagen®, Berlin, Germany) following the manufacturer's instructions with some modifications. DNA concentration was measured on a NanoDrop™ spectrophotometer, and the integrity of the extracted samples was determined by electrophoresis in 1% agarose gel. Only those samples that reached the requirements for the ddRAD-seq technique (Peterson et al., 2012) were selected for genotyping (Table 1). In this case, a total of 509 samples of Spanish fir and 98 of Moroccan fir were optimum for the technique. Subsequently, ddRAD-seq (Peterson et al., 2012) libraries were constructed using *Ape*KI/*Pst*I double digestion and sequenced by LGC Genomics (Berlin, Germany). To know more about the methodology, please see Méndez-Cea et al. (2023a).

Due to the lack of Spanish and Moroccan firs reference genomes, a *de novo* assembly of the obtained paired-end sequences was performed. However, there is an available transcriptome of *A. pinsapo*, which allowed us to carry out a reference assembly. This transcriptome was previously obtained by our group (for more details, please see Pérez-González et al., 2018). Both assemblies and the SNP callings were performed using ipyrad v.0.9.65 (Eaton and Overcast, 2020). Several filtering steps were carried out using VCFtools v0.1.16 (Danecek et al., 2011). With the aim to retain only quality biallelic SNPs, the following parameters were used: a minor allele frequency (MAF) of 5% and maximum missingness of 50%, and, to avoid linkage disequilibrium, only one SNP per locus was maintained. Moreover, a final step removing those individuals with information for less than 50% of the filtered SNPs was performed. Several genetic matrixes were obtained depending on the dataset used in the filtration steps.

The following sections are summarized as a workflow in Figure 2.

2.3 Genetic structure of populations

Two approaches were used to study the genetic structure of *A. pinsapo* populations: principal component analysis (PCA) and sparse non-negative matrix factorization (sNMF) analysis. PCA was performed to describe the inter- and intrapopulation structures, while sNMF was used to estimate ancestry coefficients (Frichot et al., 2014). PCA was carried out using the plink2 2.00a2.3 software (Chang et al., 2015) with the ––pca option, and then a graphic representation was obtained using the R v4.1.2 (R Core Team, 2022) package called ggplot2 v3.3.5 (Wickham, 2016). For the second approach, a cross-entropy study was carried out using the snmf function of the LEA package v3.4.0 (Frichot and François, 2015) in R to determine the most probable number of ancestry populations (K) that best explains the structure of the populations. In addition,

10.3389/fpls.2023.1155441

TABLE 1 Characteristics of each nucleus of study.

Species	Nucleus	Country	Abbreviation	Latitude (°N)	Longitude (°W)	Elevation (m a.s.l.)	Mean annual temperature (°C)	Mean annual precipitation (mm)	Population (n)	Saplings (n)	Old trees (n)
Abies pinsapo	Caucón	Spain	CA	36.71	−4.96	1,114	12.0	975.0	226	24	25
	Saucillo	Spain	SA	36.72	−4.98	1,352	11.2	1,261.6	110	12	12
	Grazalema	Spain	GR	36.78	−5.40	1,085	12.0	1,277.5	79	–	–
	Pilar de Tólox	Spain	PT	36.68	−5.00	1,669	10.2	1,647.6	16	–	–
	Pilones	Spain	PI	36.69	−5.02	1,700	10.3	1,659.3	28	–	–
	Ánimas	Spain	AN	36.70	−5.01	1,637	10.3	1,616.6	50	18	17
Abies marocana	Talassemtane	Morocco	TA	35.17	−5.18	1,694	10.1	1,821.0	53	23	30
	Tazaot	Morocco	TZ	35.23	−5.10	1,677	10.5	1,644.3	45	26	19

It is indicated which species is located in each region, the name of the area, their localization (latitude and longitude), elevation, and mean annual temperature and precipitation. The last three columns are related to the total number of samples genotyped with ddRAD-seq and the number of saplings and old trees genotyped of those populations in which two ages were collected.
ddRAD-seq, double digestion restriction site-associated DNA sequencing.

the admixture coefficients were calculated too. For this analysis, a total of 10 repetitions for each K from 1 to 8 was performed. Then, a graphic representation of the admixture results was performed using the pong software package (Behr et al., 2016).

Several statistical analyses of each genetic matrix were performed using GenAlEx v6.5 (Peakall and Smouse, 2006; Peakall and Smouse, 2012) and GenoDive v3.06 (Meirmans, 2020). Parameters such as fixation indexes (F_{ST}), to determine population differentiation, and migration rate (Nm), to describe the presence or not of gene flow among populations, were estimated. Nei's genetic distance among populations was also determined. Heterozygosity, private alleles, and polymorphic loci were obtained too. Finally, the Shannon index was calculated to infer genetic diversity.

In addition, a molecular variance analysis (AMOVA) with 9,999 permutations was carried out with the aim to determine the proportion of genetic variation attributable to differences among and within populations.

2.4 Selection signatures

BayeScan 2.1 software (Foll and Gaggiotti, 2008) was used to identify selection signatures. Default parameters were applied. For more details, please see Méndez-Cea et al. (2023a). The significance threshold was established at 5%. The complete sequence containing the significative SNPs was queried against the nucleotide database and, in the case of the matrixes obtained from reference assembly, against the transcriptome shotgun assembly (TSA) database using, in both cases, BLASTn (National Center for Biotechnology Information (NCBI); Altschul et al., 1990). When a match was obtained, a BLASTx (NCBI; Gish and States, 1993) against the non-redundant protein database was performed too.

2.5 Genotype–environment associations

The 19 bioclimatic variables from the WorldClim database (Fick and Hijmans, 2017) with a resolution of 30 s were used to identify GEAs. These variables were obtained using the freeware QGIS 3.18 (Quantum Geographic Information System) (QGIS Development Team, 2022) for each location. Highly correlated variables were removed based on their Pearson's correlation values ($r > 0.9$), which were calculated with the Hmisc package v4.7-0 (Frank and Harrell, 2022) in R. Since this correlation needs a minimum of four populations to be estimated, the coefficient could be obtained depending on the used genetic matrix. On the other hand, an imputation step was conducted by using the LEA R package v3.4.0 (Frichot and François, 2015) to fill in all the missing data of the genetic matrix before performing the GEA study.

The lfmm (latent factor mixed models) function of the LEA R package v3.4.0 (Frichot and François, 2015) was used to perform GEA studies. Each run was repeated 20 times with 100,000 iterations and a burn-in of 50,000. The used K value was the one obtained from the cross-entropy analysis. The p-value results were corrected to q-values using a false discovery rate (FDR), and the significance threshold was set to 5%. The complete sequences,

10.3389/fpls.2023.1155441

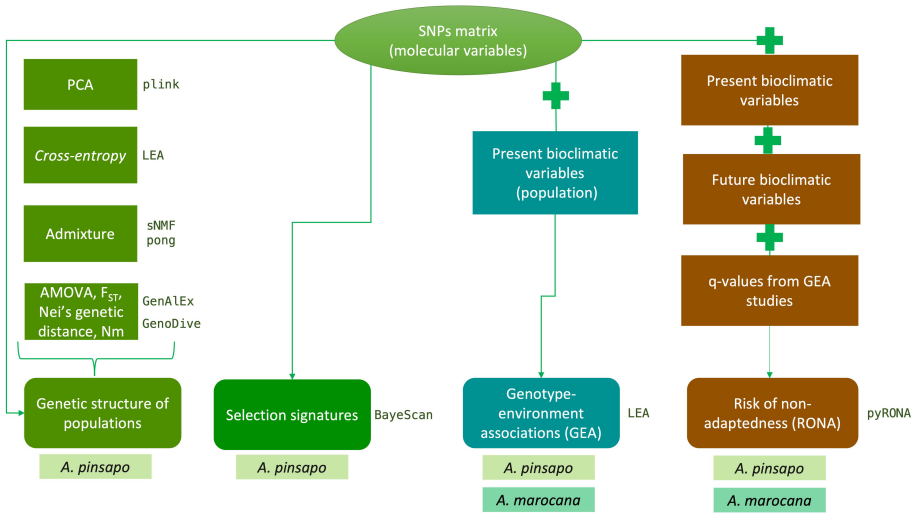

FIGURE 2
Description of the workflow followed to perform the different studies. The species used for each analysis are indicated.

which include the SNPs that showed significant associations with one or more bioclimatic variables, were queried against the nucleotide and protein NCBI database as it was described above.

2.6 Risk of non-adaptedness

The RONA value indicates the theoretical percentage of change in allele frequency at loci associated with environmental variables, which is required for a given population to cope with future changes in that variable, allowing it to survive (Rellstab et al., 2016; Pina-Martins et al., 2019). The estimation of this value is based on the average absolute difference of the changes in allele frequencies between the current and future climate conditions of those loci, which showed associations with environment variables. Low values of RONA predict a greater predisposition to adapt to new environmental conditions.

pyRona v0.3.6 (Pina-Martins et al., 2019) for lfmm results was used to calculate the RONA value at the population level. Two different climate scenarios, which are predicted to take place by the end of this century (2081–2100), were studied: low emissions (Representative Concentration Pathway (RCP) 2.6), which limits the increase of global mean temperature to 2°C, and high emissions (RCP8.5), whose limitation is 4.9°C. A total of 19 bioclimatic variables of each scenario were tested. These variables were downloaded from the WorldClim database as it was described in the GEA section.

3 Results

3.1 Genetic structure of *A. pinsapo* populations

The filtering of the *de novo* assembly of the Spanish fir nucleus dataset maintained 504 individuals and 3,982 SNPs. The first axis of PCA separated GR from the rest of the Spanish populations with an explanation percentage of 27.2% (Figure 3). AN, PI, and PT are very similar, while CA shows a gradient ranging from SA to the rest of the populations. The cross-entropy analysis, which was carried out for K values ranging from 1 to 8, did not provide much information, as the lowest obtained value was 8. However, the graphical representation of the admixture results showed that K = 3 seemed to be the best explanation for our results. In this case, GR showed its own gene pool again, SA and CA composed the second group, and the rest of the Spanish populations were grouped.

The AMOVA results of *A. pinsapo* nuclei showed the greatest differences within individuals (55.2%) and the lowest among individuals (4.3%) with a high significance (p-value = 0.000). In addition, significant differences among populations were found (40.5%).

Pairwise population F_{ST} values ranged from 0.007 to 0.062, with high significance in all the cases (p-values = 0.000), indicating the presence of genetic differences among all nucleus pairs (Table 2).

The percentages of polymorphic loci were high in all populations, reaching 100% in CA. The average was 97.49% ± 1.07%. The Shannon index (I) of each population ranged from 0.467 to 0.501. The minimum appeared in PT and the maximum in CA. In this case, no private alleles were found. Finally, all Nm values are very high, which indicates that the populations of study have a strong gene flow among them. An extremely high value was found between CA and SA (35.923), and the lowest was among SA and PT (5.287).

Nei's genetic distance showed values near 0 (from 0.006 to 0.045), indicating that all *A. pinsapo* nuclei are very similar. However, it is remarkable that GR showed the highest values, which indicates that this population is the most genetically different.

The Spanish fir dataset from the reference assembly filtering retained 494 individuals and 1,642 SNPs. PCA results showed that GR separated from the rest of the populations with an explanation percentage of 24.7% (Figure 4). The cross-entropy study, which was carried out with a range from 1 to 8, did not provide much information

10.3389/fpls.2023.1155441

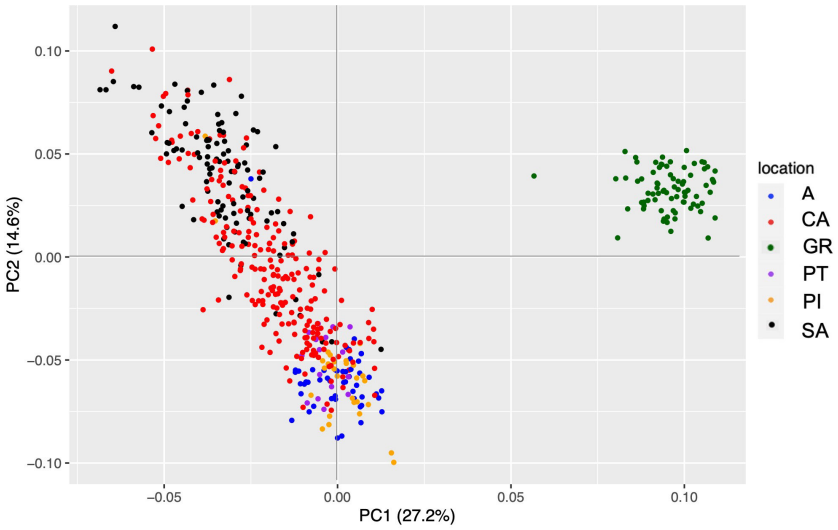

FIGURE 3
PCA representation with the *de novo* assembly dataset of *Abies pinsapo* populations. Each of them has a different color, which is indicated in the legend. PCA, principal component analysis.

as in the case of the *de novo* assembly. The admixture results were interpreted by the PCA results, and K = 3 was the best value to explain the genetic structure of our populations. In this case, GR had its own gene pool, SA and CA conformed to other groups, and the rest of the populations were grouped. However, there are several genetic differences among populations as indicated above.

Predictably, the statistical analyses showed the same results, which were obtained with the *de novo* assembly dataset. However, the Nm value between CA and SA was higher (42.561) than the estimated value with the *de novo* assembly. In addition to Nei's genetic distance ranging from 0.005 to 0.037, the higher value of the range was lower than the estimated value with the *de novo* assembly dataset.

3.2 Selection signatures

BayeScan analysis with the *de novo* assembly of *A. pinsapo* nuclei showed 51 loci under selection (q-value < 5%). The complete sequence of the 10 SNPs, which had the lowest q-values, and those that showed associations with bioclimatic variables in GEA studies were queried against the databases. Homolog sequences were found for nine of these sequences, and six of them obtained protein hits (Table S1). It is remarkable that two of the used scaffolds gave the same result for both the nucleotide sequence and the proteins. A protein whose function is involved in the dark reaction photosynthesis was obtained (Table S1). However, the most interesting proteins found are those that are related to abiotic stress response such as dehydration-responsive element binding transcription factor and the late embryogenesis abundant protein (LEA3-1), which is produced during the seed embryogenesis (Table S1).

The Spanish fir reference dataset showed 24 loci under selection. The 10 complete sequences analyzed matched sequences in the NCBI database. However, only four of them obtained hits with proteins (Table S2). Two proteins are enzymes involved in photosynthesis and the Calvin cycle. Another homology is found with serine/arginine-rich splicing factor SR45, which is

TABLE 2 Pairwise population F_{ST} obtained from the *Abies pinsapo de novo* assembly dataset.

Pairwise population F_{ST} values						
CA	SA	GR	PT	AN	PI	
0.000						CA
0.007*	**0.000**					SA
0.052*	0.062*	**0.000**				GR
0.018*	0.034*	0.063*	**0.000**			PT
0.020*	0.031*	0.059*	0.027*	**0.000**		AN
0.020*	0.032*	0.059*	0.024*	0.016*	**0.000**	PI

A higher index was obtained between GR and PT. The presence of the asterisk indicates significant differences (p-value < 0.001). The numbers in bold indicate the results obtained when the comparative was done within the same population. For this reason, the value is 0 which means that is a single population.

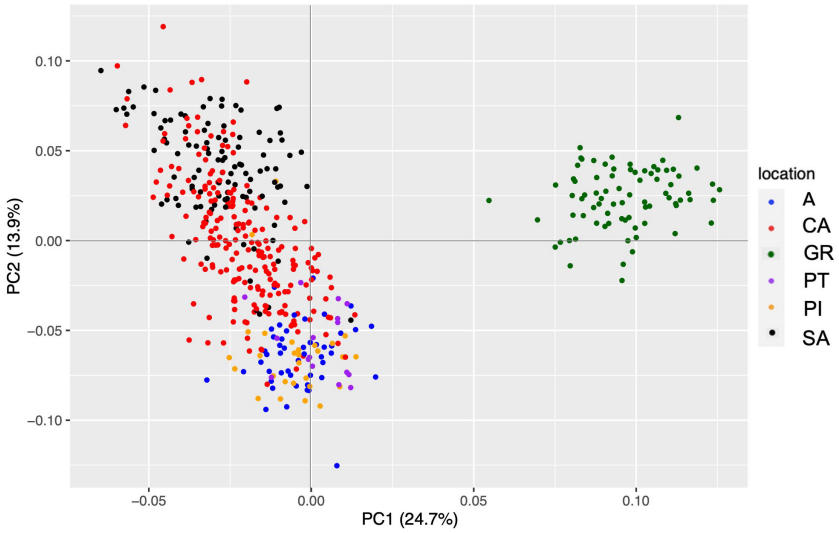

FIGURE 4
PCA representation of the genetic matrix obtained from the reference assembly with *Abies pinsapo* populations. The meaning of the colors is indicated in the legend. PCA, principal component analysis.

related to the regulation of abscisic acid (ABA) signaling and methylation pathway (Table S2).

3.3 Genotype–environment associations

The genetic matrix of the *A. pinsapo* populations assembly with the *de novo* approach was used to perform a GEA study. First, after calculating Pearson's correlation, only those bioclimatic variables that did not show high correlations were used to perform the association study, which were as follows: isothermality (BIO3), maximum temperature of the warmest month (BIO5), temperature annual range (BIO7), precipitation of wettest quarter (BIO16), and precipitation of driest quarter (BIO17). A total of 15 associations with 11 different loci were observed, with the most numerous at the maximum temperature of the warmest month (BIO5) with five loci. Some associations were shared between two or more bioclimatic variables.

Once the alignments were performed, nine sequences matched nucleotide sequences, and six of them gave us information about homologies with other proteins. Some of these found proteins are related to transmembrane transport, transcription regulation, or abiotic stress response (Table S3). Six of these loci were under selection including the locus involved in abiotic stress response. The allele frequencies of some loci were calculated for three *A. pinsapo* populations, which had the two age cohorts (adults and saplings), as follows: CA, SA, and AN. The results indicated that CA and SA populations are very similar to each other, while they are different from AN. The allele frequencies estimated by separating the individuals of these populations into old trees and saplings were slightly different within the CA and SA populations for SNP 448, within the SA population for SNP 2400 and SNP 2528, and within the AN population for SNP 3808 (Figure 5).

The GEA study with the reference assembly carried out with *A. pinsapo* populations' genetic matrix showed 12 associations. The bioclimatic variable called isothermality (BIO3) did not show associations with any locus. This study was performed with the same five bioclimatic variables, which were used with the *de novo* matrix. The highest number of associations was observed with BIO7 (seven loci). The complete sequences of all these loci hit against the nucleotide database, but only five of them matched proteins. Some of their functions were involved in ubiquitination, transmembrane transport, or stomatal closure (Table S4).

The GEA study with Moroccan fir populations was carried out with the 19 bioclimatic variables since Pearson's correlation could not be performed because this genetic matrix had only two populations. The same locus (SNP 5594) was associated with all the variables, and the alignment results showed homology with a protein whose function is related to protein phosphorylation (LRK1). Méndez-Cea et al. (2023b) identified this locus under selection too, so the allele frequencies of each nucleus were calculated. TA had an allele frequency of the reference variant of 0.97, while TZ showed 0.41 for the same allele. When the two sites were separated by age, the saplings from TZ showed a higher allele frequency of the alternative one (0.67) than the adults (0.5), while TA did not show differences for this locus between age groups (Figure 5).

3.4 Risk of non-adaptedness

The obtained allele frequency change rate value in the low emission scenario for *A. pinsapo* nuclei ranged from 0.01 to 0.47, while in the high emission scenario, the range was 0.02–0.97. In the case of Moroccan fir, the change rate value was between almost 0 to 0.39 for the low emission expected scenario, ranging from

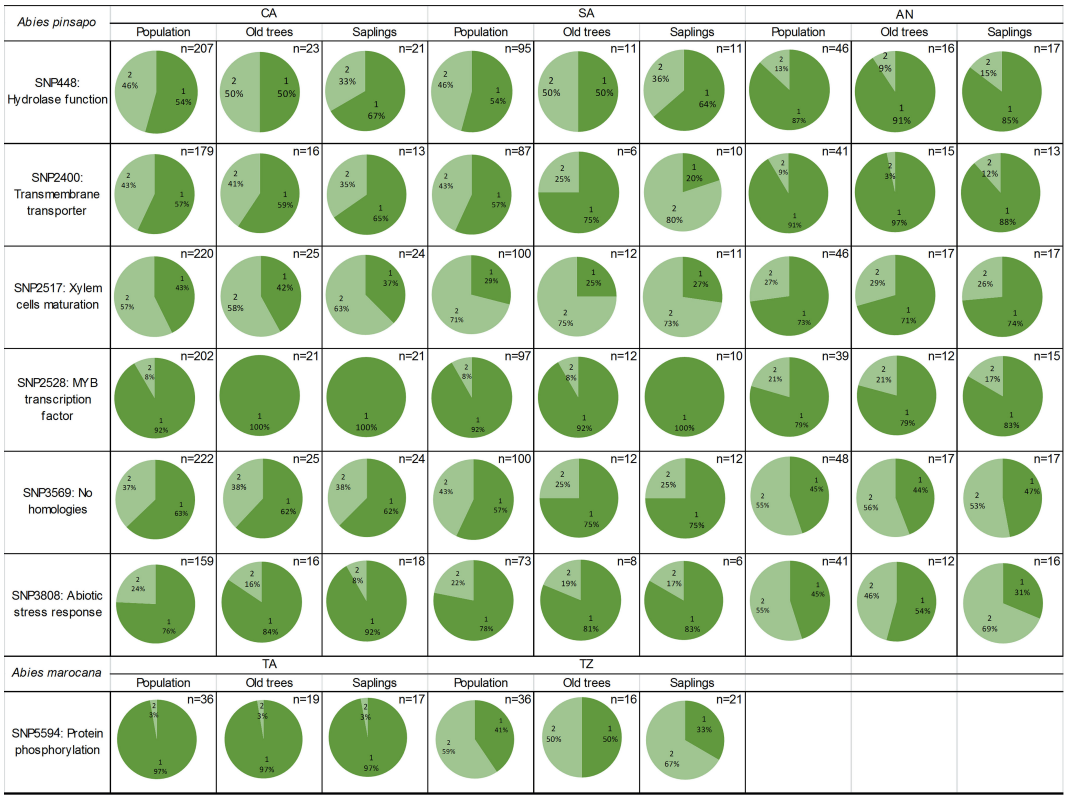

FIGURE 5
Frequencies of reference allele (1) and alternative allele (2) in SNPs associated with bioclimatic variables in the GEA study of *Abies pinsapo* (CA, SA, and AN populations) and *Abies marocana* (TA and TZ populations). Allele frequencies are shown for the whole population, old trees, and saplings. SNPs, single-nucleotide polymorphisms; GEA, genotype–environment association.

approximately 0.02 to 0.90. Considering these results, the high emission scenario showed a higher risk for the Spanish and Moroccan firs' survival than the other scenario, as expected.

The isothermality (BIO3) showed the maximum change rates for each of the Spanish fir populations in the low emission scenario except for GR and PI populations, which displayed high values in the temperature annual range (BIO1) (Figure 6A). The Moroccan fir populations reached higher rates with temperature annual range (BIO1), like GR and PI. However, the annual precipitation (BIO12) was the bioclimatic variable related to precipitations, which showed the maximum change rate value in both species and scenarios (Figure 6B).

In terms of the high emission scenario, *A. pinsapo* and *A. marocana* showed the maximum rates with temperature annual range (BIO1). Depending on the Spanish fir population, the second bioclimatic variable, which needs a higher change rate value, was related to temperature (SA, CA, and PT) or precipitation (PI). The second maximum value obtained with Moroccan fir populations (TA and TZ) was always related to annual range precipitation (BIO12).

4 Discussion

The development of new genotyping techniques based on NGS technology, such as the ddRAD-seq used in this work, allows to increase the genomic knowledge regarding tree species, which was poorly investigated previously. The number of SNPs detected by ddRAD-seq varied depending on the molecular marker density in the genome of the study (Shirasawa et al., 2016). The number of SNPs maintained after filtering steps was always higher with the *de novo* assembly than with reference. This could be explained by the representation of those SNPs in the reads obtained. Due to the large-size genome of this species (García-García et al., 2022), the likelihood of obtaining the same fragment in most of the individuals sequenced is low. Hence, SNPs are likely to be less represented, and they cannot be retained.

The lack of a reference genome but the availability of Spanish fir transcriptomes gave us the chance to perform two different assembly approaches. Using a transcriptome as a reference allowed us to obtain functional information since all the SNPs described are placed in genes (Card et al., 2014). However, the absence of a correct annotation prevents us to know in some cases the putative biological function of the regions of interest.

Regarding the genetic differences observed among populations, F_{ST} values over 0.15 are usually interpreted as an indicator of significant divergences (Frankham et al., 2002). Hence, considering the low F_{ST} values obtained (<0.15), the six *A. pinsapo* populations might behave as in complete panmixia. Nevertheless, the p-values were significant, indicating that these nuclei showed differences among them. In the light of our results, the locality of GR seems to

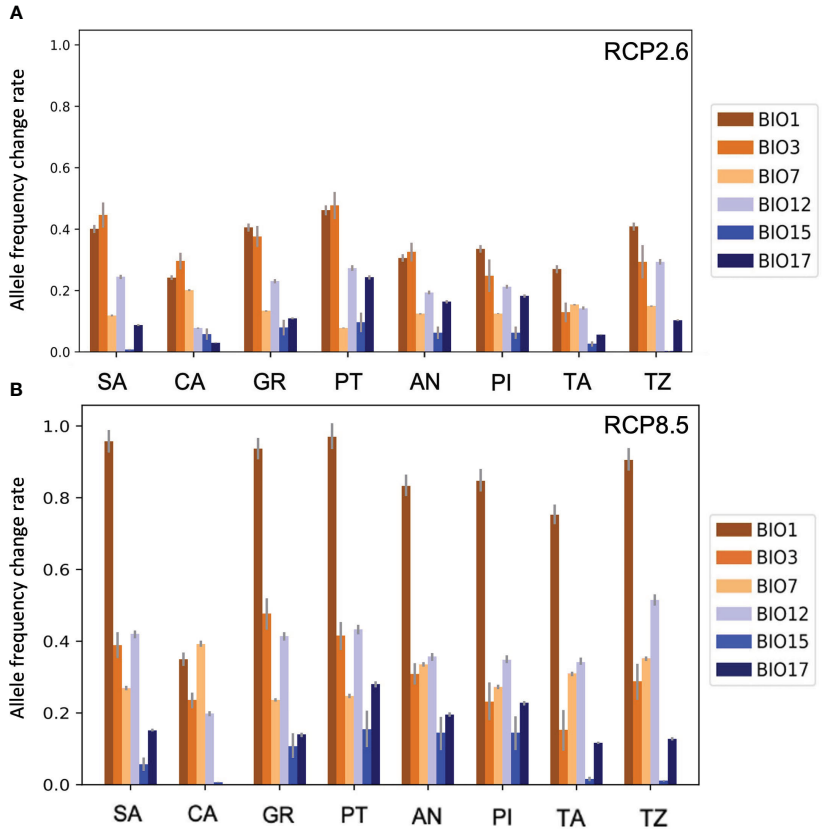

FIGURE 6
RONA results. Change rate values of each Spanish and Moroccan fir population studied for the low emission scenario **(A)** and the high emission scenario **(B)**. The bioclimatic variables related to temperature are colored in orange, and those related to precipitation appear in blue. The x-axis indicates the nucleus of study, and the y-axis indicates the allele frequency change rate required to respond to the perturbations in each studied variable. RONA, risk of non-adaptedness.

be the most dissimilar one. Indeed, previous studies carried out with cpSSRs showed differences between GR and Sierra de las Nieves (Terrab et al., 2007; Sánchez-Robles et al., 2012; Cobo-Simón et al., 2020), which is congruent with the present work.

Despite that all the study sites were characterized by a Mediterranean mountain climate, with a summer drought period, the local climate is influenced by elevation and longitude (distance to the Atlantic Ocean). Thus, the mean annual temperature decreases by an average of 0.72°C for every 100 m of elevation, while annual rainfall decreased toward the east by an average of 173 mm for every 10 km and increased by an average of 81 mm for every 100 m of elevation (Linares et al., 2011). As a result, most of the annual rainfall, carried by low-pressure systems coming from Atlantic depressions, falls on the western part of the study area and decreases toward the eastern part, such that high mean precipitation values occur in the westernmost population of Grazalema (GR), as compared to the easternmost population of Sierra de las Nieves (Figure 1). This longitudinal differentiation was also reflected in the demographic history inferred by nSSR and cpSSR markers (Sánchez-Robles et al., 2012; Cobo-Simón et al., 2020), indicating that potential adaptive divergence of easternmost and westernmost populations should be subject to further research. Hence, the individuals from GR may have their own genetic pool because they do not have to cope with very harsh drought stress conditions (Cobo-Simón et al., 2020). In addition, the low dispersion of the *A. pinsapo* pollen (lower than 3 km) (Arista and Talavera, 1994; Alba-Sánchez et al., 2010) could act as a limiting factor to genetic exchange.

The noticeable dispersion observed in the PCA for the CA population could be explained by the fact that it is a rear edge of *A. pinsapo* distribution. Since the individuals of this population are under limiting climatic conditions, drier and hotter than average due to low elevation and eastern location, they should have some genetic pressure to cope with them (Cobo-Simón et al., 2020; Cobo-Simón et al., 2021). This is confirmed by the 100% polymorphic loci found in the CA population and by the Shannon index, which showed the highest value among our dataset.

Regarding the loci under selection obtained with *A. pinsapo* populations, one of them also showed associations in the GEA studies, increasing the robustness of the results and highlighting the possible adaptive relevance of this locus. The putative protein homolog identified for this locus, which was under selection and associated with bioclimatic variables, is a dehydration-responsive element binding transcription factor (DREB). Generally, the expression of DREBs is induced by abiotic stresses, such as extreme temperatures, drought, and salinity. Due to this involvement in abiotic stressors responses, the DREB genes of several economically important organisms have been modified

with the aim to increase their resistance, such as freezing tolerance in potatoes (i.e., Behnam et al., 2007) and dehydration tolerance in soybean (i.e., de Paiva Rolla et al., 2014) or rice (i.e., Zhao et al., 2010). In terms of studies with angiosperms, Chen et al. (2009) have described the role of DREB genes involved in the responses to cold, drought, and salt in *Populus euphratica* Olivier. Regarding conifers, the involvement of DREB in the drought stress response of *Picea abies* (L.) Karst (Haas et al., 2020) has been reported. Therefore, this locus might be promising for future studies.

Since temperature increase and extreme drought events have been reported in the range of *A. pinsapo* and *A. marocana* (Linares et al., 2009; IPCC, 2022; Méndez-Cea et al., 2023b), the GEA results provide insights into the genetic response of these relict species to the ongoing climate change. *A. pinsapo* populations showed associations with temperature and precipitation variables, indicating that both are important to its development (Alba-Sánchez et al., 2010; López-Tirado and Hidalgo, 2014), while recent studies performed on *A. marocana* pointed out to the main role of temperature (Alaoui et al., 2021; Méndez-Cea et al., 2023b).

Drought events are causing widespread tree mortality across many forest biomes with profound effects on the ecosystem dynamics and carbon balance (Anderegg et al., 2013; McDowell et al., 2020). Our results suggest that the effect of future droughts will almost certainly be worsened by increases in air temperature associated with global warming (Figure 6).

The results obtained by comparing saplings and old trees gave a higher number of loci under selection in these two age groups than within the whole population. These contrasting selection signatures may be reflecting the fact that the studied young trees could have been subjected to a selective pressure, as they have been established under a warmer and dryer climate scenario, compared to old trees, which were mainly established around the 19th century. Old trees play key roles in forests and can be disproportionately important to ecosystem carbon storage (McDowell et al., 2020). However, the saplings' cohorts depict the forest of the future, including the coming allele frequency structure (Figure 5). Droughts may have a more detrimental impact on the growth and mortality of old, usually larger, trees (DeSoto et al., 2020). This pronounced drought sensitivity of larger trees might be related to greater inherent vulnerability to hydraulic failure and the higher evaporative demand experienced by their towering crowns (Bennett et al., 2015). Assuming that future extreme drought events, whose frequency is expected to worsen, will have a more detrimental impact on the growth and mortality of old trees, it should be expected to exacerbate feedback to climate change, affecting forest biodiversity and ecosystem services (Anderegg et al., 2013; McDowell et al., 2020).

Reducing uncertainty about tree vulnerability and mortality projections should be founded on robust physiological processes (Anderegg et al., 2012). However, the proposed mechanisms of drought-induced mortality, including hydraulic failure and carbon starvation, are still unresolved (Choat et al., 2018). To that extent, some protein homologies obtained here may provide useful insights into the physiological processes underlying drought-induced tree mortality. One of the homology proteins identified with the *de novo A. pinsapo* dataset in the GEA studies was a transcription factor of the MYB family. This is one of the most relevant and abundant families responsible for plant abiotic stress response/tolerance, and they are often implied in the ABA response, so much so that there are studies that have reported gene expression changes of these transcription factors family during drought stress response in conifer species (Lorenz et al., 2011; Du et al., 2018; de María et al, 2020).

The protein related to stomatal closure, which showed an association between the reference Spanish fir dataset and temperature annual range (BIO7), is called aluminum-activated malate transporter 12-like. In *Arabidopsis thaliana* (L.) Heynh., it is expressed in the guard cells, and as a response to drought stress, this protein induced the stomatal closure as a response to ABA (Meyer et al., 2010). This function is very interesting because most of the gymnosperms, such as *A. pinsapo*, which is an isohydric species, close their stomata to avoid water loss in dry conditions (Brodribb et al., 2014).

In the case of Moroccan fir, the identification of only one locus associated with all the bioclimatic variables, which is also under selection, gave us an insight into the relevance that its genomic region could have. The allele frequency variations found among populations and between ages could indicate that the selection pressure is acting. In addition, a protein homology was identified with a leucine-rich repeat serine/threonine-protein kinase (LRK1). This protein kinase family can be involved in the abiotic stress response (Shiu and Bleecker, 2003). For this reason, this region could be an interesting target for future genotyping in Moroccan fir populations.

Finally, the RONA studies allowed us to describe the genetic vulnerability of the species under future scenarios. Simulating the local adaptation at the population level and their adaptative potential to future conditions is very useful to determine the risk of the species. The use of this kind of study, such as RONA, allows us to integrate the current and future environment data with genetic information to obtain a robust prediction of species adaptation (Feng and Du, 2022). Conifers, as Spanish and Moroccan firs, are long-lived species with long generation times. These characteristics cause them to show a lag in their adaptation to current and future environmental perturbations (Browne et al., 2019). Therefore, the faster climate change is, the greater adaptation lag occurs (Jump and Peñuelas, 2005). Previous studies suggested that conifer species may have difficulty coping with rapid climate change (Dauphin et al., 2021).

Despite recent observational, experimental, and modeling studies suggesting increased vulnerability of relict trees to hotter drought, to our knowledge, this is the first estimation of climate change-induced vulnerability based on genetics and future climate scenarios in *A. pinsapo* and *A. marocana*. RONA modeling supports that warming might be the main limiting factor for the survival of *A. pinsapo* and *A. marocana*, according to several studies performed on drought-sensitive species (e.g., Williams et al., 2013; Allen et al., 2015). Our results support that *A. pinsapo* and *A. marocana* should overcome the high risk of non-adaptedness under any warming climate scenario (Figure 6). Previous studies in trees showed that if the change values were less than 0.1 per decade, the

species might cope with the climate alterations, while if these changes were higher than the range from 0.1 to 0.2 per decade, the species showed a lag between allele frequencies and environment perturbations (Jump et al., 2006). Dauphin et al. (2021) estimated that the allele frequency variation rate of the conifer species *Pinus cembra* L. was 1.23×10^{-2} per generation. Furthermore, the maximum RONA value obtained with *P. cembra* was 0.10 (Dauphin et al., 2021), which is considerably lower than the maximum values estimated for Spanish fir and Moroccan fir. For this reason, both species studied here are likely to have several difficulties coping with the environmental alterations (Esteban et al., 2010; but see also Cortés-Molino et al., 2023). Interestingly, the Moroccan fir population from TZ, with a drier climate, showed the highest vulnerability to variations in annual precipitation at both emission scenarios, suggesting some relationship between the local climate and genetic structure.

Similar results were obtained by dendrochronological studies and climate growth for the whole circum-Mediterranean fir group (Sánchez-Salguero et al., 2017; Méndez-Cea et al., 2023b). Regarding *A. marocana*, previous studies aimed at the potential distribution of Moroccan fir, based on species distribution models (SDMs), showed that the main variables conditioning the presence of *A. marocana* were the average temperature of the warmest quarter and the maximum temperature of the warmest month (Alaoui et al., 2021). Further, similar methodological approaches performed for *A. pinsapo* also obtained a significant effect on temperatures (Alba-Sánchez et al., 2010; López-Tirado and Hidalgo, 2014). Notwithstanding, it is noteworthy that these SDMs are reported as the most important bioclimatic variable driving the modern distribution of *A. pinsapo* winter rainfall, instead of temperature. This disagreement shows that the interpretation of the vulnerability of the species is not straightforward. Temperature (that is, global warming) could change our expectations based on niche suitability and future range distribution of endangered species, such as the circum-Mediterranean firs (Lerner et al., 2023).

Understanding the ecological and evolutionary processes driving the species' range limits is of particular interest for relict trees owing to their limited distribution and long-term genetic isolation (Hampe and Jump, 2011). Recent studies investigating the underlying forces limiting the range of several tree species support an association of range-edge hotspots with steep spatial climatic gradients (Lerner et al., 2023). Both Spanish and Moroccan firs have a limited distribution, strongly linked to the spatial heterogeneity of climate micro-refugia (Linares, 2011). Thus, the vulnerability of relict trees, as well as those of some isolated range-limit populations, might be hindered because of steep climatic gradients. Further, we present here likely genetic vulnerability drivers, which were, to date, scarcely known. Overall, we obtained estimations of change in allele frequencies higher than 0.1, so both species are at risk because they might not keep pace with climate change due to their change rates being slower than those of the expected environmental shift. The RONA values obtained for *Quercus suber* L. at a high emission scenario (RCP8.5) ranged from 0.07 to 0.38 (Pina-Martins et al., 2019). The estimated values for both Spanish and Moroccan firs in our study at the RCP8.5 scenario (0.97) were higher than the ones in *Q. suber*. Hence, these species are apparently more vulnerable to climate change.

Additional methodological approaches whose relevance is increasing are based, for instance, on machine learning as a promising way to assess the vulnerability of populations in forest species (Ellis et al., 2012). This technology allows us to make predictions at different spatial–temporal scales and can estimate the individual response of SNPs to different environmental variations (Fitzpatrick and Keller, 2015). Furthermore, the development of new genotyping technologies based on NGS that reduce the genome complexity, such as ddRAD-seq, permits to perform genetic studies in conifer species. However, the use of a transcriptome as a reference may give the opportunity to identify SNPs located in genes. In terms of the genetic structure, the *A. pinsapo* populations have shown that all the nuclei behave as in complete panmixia, with existing gene flow among them (see also Sánchez-Robles et al., 2012; Cobo-Simón et al., 2020). Despite this, GR has its own genetic pool that differentiates it from the rest of the populations. GEA results indicated that temperatures and precipitations have effects on both species.

It is widely assumed that warming will lead to hotter droughts and non-linear increasing atmospheric moisture demand. As a result, tree mortality may occur faster as stressful water shortages become more frequent, according to eco-physiological observations and modeling (Linares et al., 2012; Sánchez-Salguero et al., 2015; Choat et al., 2018). As a result, understanding the genetic basis driving the contrasting vulnerability observed among individuals is mandatory. In this context, some studies have described gene expression differences between individuals under drought stress in Mediterranean conifers such as *A. pinsapo* and *Cedrus atlantica* (Endl.) Manetti ex Carrière (Cobo-Simón et al., 2023a; Cobo-Simón et al., 2023b) and in *Pinus halepensis* Mill. (Fox et al., 2018). However, additional studies focused on temperature are still needed. In this sense, our results highlight urgent challenges for research, management, and policy-making communities. The combined analysis of genome-wide single-nucleotide polymorphisms and local environmental data provided genetically based evidence of tree-level sensitivity to climate, estimations of the risk of non-adaptedness, and preliminary evidence of shifting allele frequencies in young cohorts. Notwithstanding, the molecular mechanisms of adaptation remain largely unknown for long-lived tree species. Nonetheless, *A. pinsapo* and *A. marocana* showed high vulnerability to, mainly, temperature variations. The RONA value estimation indicated that both species are at risk because they might not keep pace with climate change. Deciphering such patterns will enable a proper understanding of how endangered tree species are responding to the current changing climate, as well as provide guidelines for future conservation strategies.

Data availability statement

The raw data presented in the study are deposited in the NCBI's Sequence Read Archive (SRA) repository, BioProject accesion number PRJNA1000741 (http://www.ncbi.nlm.nih.gov/bioproject/1000741).

Author contributions

BM-C: investigation, formal analysis, writing—original draft, and writing—review and editing. IG-G: investigation and writing—review and editing. JCL: conceptualization, funding acquisition, formal analysis, and writing—review and editing. FJG: conceptualization, funding acquisition, and writing—review and editing. All authors contributed to the article and approved the submitted version.

Funding

BM-C is a recipient of a UCM Santander predoctoral fellowship (CT42/18-CT43/18). This research was funded by TED2021-129770B-C22, Spanish Ministry of Science and Innovation, and PID2021-123675OB-C44, Spanish Ministry of Science and Innovation.

Conflict of interest

The authors declare that the research was conducted in the absence of any commercial or financial relationships that could be construed as a potential conflict of interest.

Publisher's note

All claims expressed in this article are solely those of the authors and do not necessarily represent those of their affiliated organizations, or those of the publisher, the editors and the reviewers. Any product that may be evaluated in this article, or claim that may be made by its manufacturer, is not guaranteed or endorsed by the publisher.

Supplementary material

The Supplementary Material for this article can be found online at: https://www.frontiersin.org/articles/10.3389/fpls.2023.1155441/full#supplementary-material

References

Alaoui, M. L., Knees, S., and Gardner, M. (2011) *Abies pinsapo var. marocana* (The IUCN Red List of Threatened Species) (Accessed 05 September 2022).

Alaoui, A., Laaribya, S., Ayan, S., Ghallab, A., and López-Tirado, J. (2021). Modelling spatial distribution of endemic Moroccan fir (*Abies marocana* Trabut) in Talassemtane National Park, Morocco. *Austrian J. For. Sci.* 138 (2), 73–94.

Alba-Sánchez, F., López-Sáez, J. A., Benito-de Pando, B., Linares, J. C., Nieto-Lugilde, D., and López-Merino, L. (2010). Past and present potential distribution of the Iberian Abies species: a phytogeographic approach using fossil pollen data and species distribution models. *Divers. Distrib.* 16 (2), 214–228. doi: 10.1111/j.1472-4642.2010.00636.x

Alberto, F. J., Aitken, S. N., Alía, R., González-Martínez, S. C., Hänninen, H., Kremer, A., et al. (2013). Potential for evolutionary responses to climate change evidence from tree populations. *Glob. Change Biol.* 19, 1645–1661. doi: 10.1111/gcb.12181

Allen, C. D., Breshears, D. D., and McDowell, N. G. (2015). On underestimation of global vulnerability to tree mortality and forest die-off from hotter drought in the Anthropocene. *Ecosphere* 6 (8), 129. doi: 10.1890/ES15-00203.1

Altschul, S. F., Gish, W., Miller, W., Myers, E. W., and Lipman, D. J. (1990). Basic local alignment search tool. *J. Mol. Biol.* 215, 403–410. doi: 10.1016/S0022-2836(05)80360-2

Anderegg, W. R. L., Berry, A., Smith, D. D., and Field, C. B. (2012). The roles of hydraulic and carbon stress in a widespread climate-induced forest die-off. *PNAS* 109, 233–237. doi: 10.1073/pnas.1107891109

Anderegg, W. R. L., Kane, J. M., and Anderegg, L. D. L. (2013). Consequences of widespread tree mortality triggered by drought and temperature stress. *Nat. Clim. Change* 3, 30–36. doi: 10.1038/nclimate1635

Arista, A., Alaoui, M. L., Knees, S., and Gardner, M. (2011). Abies pinsapo. *IUCN Red List Threatened Species*, e.T42295A10679577. doi: 10.2305/IUCN.UK.2011-2.RLTS.T42295A10679577.en

Arista, M., and Talavera, S. (1994). Pollen dispersal capacity and pollen viability of *abies pinsapo* boiss. *Silvae Genet.* 43, 155–158.

Aussenac, G. (2002). Ecology and ecophysiology of circum-Mediterranean firs in the context of climate change. *Ann. For. Sci.* 59, 823–832. doi: 10.1051/forest:2002080

Behnam, B., Akira Kikuchi, A., Toprak, F. C., Kasuga, M., Yamaguchi-Shinozaki, K., and Watanabe, K. N. (2007). Arabidopsis rd29A::DREB1A enhances freezing tolerance in transgenic potato. *Plant Cell Rep.* 26, 1275–1282.

Behr, A. A., Liu, K. Z., Liu-Fang, G., Nakka, P., and Ramachandran, S. (2016). pong: fast analysis and visualization of latent clusters in population genetic data. *Bioinformatics* 32 (18), 2817–2823. doi: 10.1093/bioinformatics/btw327

Bennett, A., McDowell, N., Allen, C., and Anderson-Teixeira, K. J. (2015). Larger trees suffer most during drought in forests worldwide. *Nat. Plants* 1, 15139. doi: 10.1038/nplants.2015.139

Ben-Said, M. (2022). The taxonomy of Moroccan fir Abies marocana (Pinaceae): conceptual clarifications from phylogenetic studies. *Mediterr. Bot.* 43, e71201. doi: 10.5209/mbot.71201

Ben-Said, M., Linares, J. C., Carreira, J. A., and Taïqui, L. (2022). Spatial patterns and species coexistence in mixed Abies marocana-Cedrus atlantica forest in Talassemtane National Park. *For. Ecol. Manage.* 506, 119967. doi: 10.1016/j.foreco.2021.119967

Brodribb, T. J., McAdam, S. A. M., Jordan, G. J., and Martins, S. C. V. (2014). Conifer species adapt to low-rainfall climates by following one of two divergent pathways. *PNAS* 111, 14489–14493. doi: 10.1073/pnas.1407930111

Browne, L., Wright, J. W., Fitz-Gibbon, S., Gugger, P. F., and Sork, V. L. (2019). Adaptational lag to temperature un valley oak (*Quercus lobata*) can be mitigated by genome-informed assisted gene flow. *PNAS* 116 (50), 25179–25185. doi: 10.1073/pnas.1908771116

Card, D. C., Schield, D. R., Reyes-Velasco, J., Fujita, M. K., Andrew, A. L., Oyler-McCance, S. J., et al. (2014). Two low coverage bird genomes and a comparison of reference-guided versus *de novo* genome assemblies. *PloS One* 9 (9), e106649. doi: 10.1371/journal.pone.0106649

Caudullo, G., and Tinner, W. (2016). "*Abies* - Circum-Mediterranean firs in Europe: distribution, habitat, usage and threats," in *European Atlas of Forest Tree Species*. Eds. J. San-Miguel-Ayanz, D. de Rigo, G. Caudullo, T. Houston Durrant and A. Mauri (Luxembourg: Publ. Off. EU).

Chang, C. C., Chow, C. C., Tellier, L. C. A. M., Vattikuti, S., Purcell, S. M., and Lee, J. J. (2015). Second-generation PLINK: rising to the challenge of larger and richer datasets. *GigaScience* 4.

Chen, J., Xia, X., and Yin, W. (2009). Expression profiling and functional characterization of a DREB2-type gene from Populus euphratica. *Biochem. Biophys. Res. Commun.* 378, 483–487. doi: 10.1016/j.bbrc.2008.11.071

Choat, B., Brodribb, T. J., Brodersen, C. R., Duursma, R. A., López, R., Medlyn, B. E., et al. (2018). Triggers of tree mortality under drought. *Nature* 558, 531–539. doi: 10.1038/s41586-018-0240-x

Cobo-Simón, I., Gómez-Garrido, J., Esteve-Codina, A., Dabad, M., Alioto, T., Maloof, J. N., et al. (2023b). *De novo* transcriptome sequencing and gene co-

expression reveal a genomic basis for drought sensitivity and evidence of a rapid local adaptation on Atlas cedar (*Cedrus atlantica*). *Front. Plant Sci.* 14. doi: 10.3389/fpls.2023.1116863

Cobo-Simón, I., Maloof, J. N., Li, R., Amini, H., Méndez-Cea, B., García-García, I., et al. (2023a). Contrasting transcriptomic patterns reveal a genomic basis for drought resilience in the relict fir *Abies pinsapo* Boiss. *Tree Physiol.* 43 (2), 315–334. doi: 10.1093/treephys/tpac115

Cobo-Simón, I., Méndez-Cea, B., Jump, A. S., Seco, J., Gallego, F. J., and Linares, J. C. (2020). Understanding genetic diversity of relict forests. Linking long-term isolation legacies and current habitat fragmentation in *Abies pinsapo* Boiss. *For. Ecol. Manag* 461, 117947. doi: 10.1016/j.foreco.2020.117947

Cobo-Simón, I., Méndez-Cea, B., Seco, J. I., Wegrzyn, J., Linares, J. C., and Gallego, F. J. (2021). Gene frequency shift in relict *abies pinsapo* forests associated with drought-induced mortality: preliminary evidence of local-scale divergent selection. *Forests* 12 (9), 1220. doi: 10.3390/f12091220

Cortés-Molino, Á., Linares, J. C., Viñegla, B., Lechuga, V., Salvo-Tierra, A. E., Flores-Moya, A., et al. (2023). Unexpected resilience in relict *Abies pinsapo* forests to dieback and mortality induced by climate change. *Front. Plant Sci.* 13. doi: 10.3389/fpls.2022.991720

Danecek, P., Auton, A., Abecasis, G., Albers, C. A., Banks, E., DePristo, M. A., et al. (2011). The variant call format and VCFtools. *Bioinformatics* 27, 2156–2158. doi: 10.1093/bioinformatics/btr330

Dauphin, B., Rellstab, D., Schmid, M., Zoller, S., Narger, D. N., Brodbeck, S., et al. (2021). Genomic vulnerability to climate warming in a tree species with a long generation time. *Glob. Change Biol.* 27, 1181–1195. doi: 10.1111/gcb.15469

de Maríia, N., Guevara, M.Aí., Perdiguero, P., Vélez, M. D., Cabezas, J. A., López-Hinojosa, M., et al. (2020). Molecular study of drought response in the Mediterranean conifer Pinus pinaster Ait.: differential transcriptomic profiling reveals constitutive water deficit-independent drought tolerance mechanisms. *Ecol. Evol.* 10, 9788–9807. doi: 10.1002/ece3.6613

de Paiva Rolla, A. A., Carvalho, J. D. F. C., and Fuganti-Pagliarini, R. (2014). Phenotyping soybean plants transformed with rd29A: AtDREB1A for drought tolerance in the greenhouse and field. *Transgenic Res.* 23, 75–87. doi: 10.1007/s11248-013-9723-6

Dering, M., Sękiewicz, K., Boratyńska, K., Litkowiec, M., Iszkulo, G., Romo, A., et al. (2014). Genetic diversity and inter-specific relations of western Mediterranean relic Abies taxa as compared to the Iberian *A. alba*. *Flora* 209, 367–374. doi: 10.1016/j.flora.2014.03.011

DeSoto, L., Cailleret, M., Sterck, F., Jansen, S., Kramer, K., Robert, E. M. R., et al. (2020). Low growth resilience to drought is related to future mortality risk in trees. *Nat. Commun.* 11, 545. doi: 10.1038/s41467-020-14300-5

Du, M., Ding, G., and Cai, Q. (2018). The transcriptomic responses of *Pinus massoniana* to drought stress. *Forests* 9 (6), 326. doi: 10.3390/f9060326

Eaton, D. A. R., and Overcast, I. (2020). ipyrad: Interactive assembly and analysis of RADseq datasets. *Bioinformatics* 36, 2592–2594. doi: 10.1093/bioinformatics/btz966

Ellis, N., Smith, S. J., and Pitcher, C. R. (2012). Gradient forests: calculating importance gradients on physical predictors. *Ecology* 93, 156–168. doi: 10.1890/11-0252.1

Esteban, L., De Palacios, P., and Aguado, L. (2010). *Abies pinsapo* forests in Spain and Morocco: Threats and conservation. *Oryx* 44 (2), 276–284. doi: 10.1017/S0030605310000190

Feng, L., and Du, F. K. (2022). Landscape genomics in tree conservation under a changing environment. *Front. Plant Sci.* 13. doi: 10.3389/fpls.2022.822217

Fick, S. E., and Hijmans, R. J. (2017). WorldClim 2: new 1km spatial resolution climate surfaces for global land areas. *Int. J. Clim.* 37, 4302–4315. doi: 10.1002/joc.5086

Fitzpatrick, M. C., and Keller, S. R. (2015). Ecological genomics meets community-level modelling of biodiversity: mapping the genomic landscape of current and future environmental adaptation. *Ecol. Lett.* 18, 1–16. doi: 10.1111/ele.12376

Foll, M., and Gaggiotti, O. E. (2008). A genome scan method to identify selected loci appropriate for both dominant and codominant markers: A Bayesian perspective. *Genetics* 180, 977–993. doi: 10.1534/genetics.108.092221

Fox, H., Doron-Faigenboim, A., Kelly, G., Bourstein, R., Attia, Z., Zhou, J., et al. (2018). Transcriptome analysis of *Pinus halepensis* under drought stress and during recovery. *Tree Physiol.* 38 (3), 423–441. doi: 10.1093/treephys/tpx137

Frank, E., and Harrell, Jr. (2022). *Hmisc: harrell miscellaneous* (R package version 4), 7–0. Available at: https://CRAN.R-project.org/package=Hmisc.

Frankham, R., Ballou, J. D., and Briscoe, D. A. (2002).). *Introduction to conservation genetics* (Cambridge: Cambridge University Press). doi: 10.1017/CBO9780511808999

Frichot, E., and François, O. (2015). LEA: an R package for landscape and ecological association studies. *Methods Ecol. Evol.* 6, 925–929. doi: 10.1111/2041-210X.12382

Frichot, E., Mathieu, F., Trouillon, T., Bouchard, G., and François, O. (2014). Fast and efficient estimation of individual ancestry coefficients. *Genetics* 196 (4), 973–983. doi: 10.1534/genetics.113.160572

Garciía-Garciía, I., Meíndez-Cea, B., Martiín-Gaílvez, D., Seco, J. I., Gallego, F. J., and Linares, J. C. (2022). Challenges and perspectives in the epigenetics of climate change-induced forests decline. *Front. Plant Sci.* 12. doi: 10.3389/fpls.2021.797958

Gish, W., and States, D. J. (1993). Identification of protein coding regions by database similarity search. *Nat. Genet.* 3, 266–272. doi: 10.1089/cmb.1994.1.39

Haas, J. C., Vergara, A., Serrano, A. R., Mishra, S., Hurry, V., and Street, N. R. (2020). Candidate regulators and target genes of drought stress in needles and roots of Norway spruce. *Tree Physiol.* 41, 1230–1246. doi: 10.1093/treephys/tpaa178

Hampe, A., and Jump, A. S. (2011). Climate relicts: Past, present, future. *Annu. Rev. Ecol. Evol. Sys.* 42 (1), 313–333. doi: 10.1146/annurev-ecolsys-102710-145015

Jaramillo-Correa, J. P., Grivet, D., Terrab, A., Kurt, A., De-Lucas, A. I., Wahid, N., et al. (2010). The Strait of Gibraltar as a major biogeographic barrier in Mediterranean conifers: A comparative phylogeographic survey. *Mol. Ecol.* 19, 5452–5468. doi: 10.1111/j.1365-294X.2010.04912.x

Jump, A. S., Hunt, J. M., Martinez-Izquierdo, J. A., and Peñuelas, J. (2006). Natural selection and climate change: Temperature-linked spatial and temporal trends in gene frequency in Fagus sylvatica. *Mol. Ecol.* 15, 3469–3480. doi: 10.1111/j.1365-294X.2006.03027.x

Jump, A. S., and Peñuelas, J. (2005). Running to stand still: adaptation and the response of plants to rapid climate change. *Ecol. Lett.* 8, 1010–1020. doi: 10.1111/j.1461-0248.2005.00796.x

Lerner, D., Martínez, M. F., Livne-Luzon, S., Belmaker, J., Peñuelas, J., Klein, T., et al. (2023). A biome-dependent distribution gradient of tree species range edges is strongly dictated by climate spatial heterogeneity. *Nat. Plants* 9, 544–553. doi: 10.1038/s41477-023-01369-1

Linares, J. C. (2011). Biogeography and evolution of *Abies* (Pinaceae) in the Mediterranean Basin. The roles of long-term climatic changes and glacial refugia. *J. Biogeogr.* 38, 619–630. doi: 10.1111/j.1365-2699.2010.02458.x

Linares, J. C., Camarero, J. J., and Carreira, J. A. (2009).). Interacting effects of changes in climate and forest cover on mortality and growth of the southernmost European fir forests. *Glob. Ecol. Biogeogr.* 18 (4), 485–497. doi: 10.1111/j.1466-8238.2009.00465.x

Linares, J. C., Covelo, F., Carreira, J. A., and Merino, J. (2012). Phenological and water-use patterns underlying maximum growing season length at the highest elevations: implications under climate change. *Tree Physiol.* 32, 161–170. doi: 10.1093/treephys/tps003

Linares, J. C., Delgado-Huertas, A., and Carreira, J. A. (2011). Climatic trends and different drought adaptive capacity and vulnerability in a mixed Abies pinsapo–Pinus halepensis forest. *Climatic Change* 105, 67–90. doi: 10.1007/s10584-010-9878-6

Litkowiec, M., Sękiewicz, K., Romo, A., Ok, T., Dagher-Kharrat, M. B., Jasińska, A. K., et al. (2021). Biogeography and relationships of the Abies taxa from the Mediterranean and central Europe regions as revealed by nuclear DNA markers and needle structural characters. *For. Ecol. Manage.* 479, 118606. doi: 10.1016/j.foreco.2020.118606

López-Tirado, J., and Hidalgo, P. J. (2014). A high resolution predictive model for relict trees in the Mediterranean-mountain forests (*Pinus sylvestris* L., *P. nigra* Arnold and *Abies pinsapo* Boiss.) from the south of Spain: A reliable management tool for reforestation. *For. Ecol. Manage.* 330, 105–1114. doi: 10.1016/j.foreco.2014.07.009

Lorenz, W. W., Alba, R., Yu, Y. S., Bordeaux, J. M., Simoães, M., and Dean, J. F. D. (2011). Microarray analysis and scale-free gene networks identify candidate regulators in drought-stressed roots of loblolly pine (*P. taeda* L.). *BMC Genomics* 12, 264. doi: 10.1186/1471-2164-12-264

McDowell, N. G., Allen, C. D., Anderson-Teixeira, K., Aukema, B. H., Chini, L., Clark, J. S., et al. (2020).). Pervasive shifts in forest dynamics in a changing world. *Science* 368 (6494), eaaz9463. doi: 10.1126/science.aaz9463

Meirmans, P. G. (2020). Genodive version 3.0: Easy-to-use software for the analysis of genetic data of diploids and polyploids. *Mol. Ecol. Resour.* 20 (4), 1126–1131. doi: 10.1111/1755-0998.13145

Méndez-Cea, B., García-García, I., Gazol, A., Camarero, J. J., González de Andrés., E., Colangelo, M., et al. (2023a). Weak genetic differentiation but strong climate-induced selective pressure toward the rear edge of mountain pine in north-eastern Spain. *Sci. Total Environ.* 858, 159778. doi: 10.1016/j.scitotenv.2022.159778

Méndez-Cea, B., García-García, I., Sánchez-Salguero, R., Lechuga, V., Gallego, F. J., and Linares, J. C. (2023b). Tree-level growth patterns and genetic associations depict drought legacies in the relict forests of *abies marocana*. *Plants* 12, 873. doi: 10.3390/plants12040873

Meyer, S., Mumm, P., Imes, D., Endler, A., Weder, B., Al-Rasheid, K. A. S., et al. (2010). AtALMT12 represents an R-type anion channel required for stomatal movement in Arabidopsis guard cells. *Plant J.* 63, 1054–1062. doi: 10.1111/j.1365-313x.2010.04302.x

Navarro-Cerrillo, R. M., Gazol, A., Rodríguez-Vallejo, C., Manzanedo, R. D., Palacios-Rodríguez, G., and Camarero, J. J. (2020a). Linkages between Climate, Radial Growth and Defoliation in *Abies pinsapo* Forests from Southern Spain. *Forests* 11 (9), 1002. doi: 10.3390/f11091002

Navarro-Cerrillo, R. M., González-Moreno, P., Ruiz-Gómez, F. J., Sánchez-Cuesta, R., Gazol, A., and Camarero, J. J. (2022). Drought stress and pests increase defoliation and mortality rates in vulnerable *Abies pinsapo* forests. *For. Ecol. Manage.* 504, 119824. doi: 10.1016/j.foreco.2021.119824

Navarro-Cerrillo, R. M., Manzanedo, R. D., Rodriguez-Vallejo, C., Gazol, A., Palacios-Rodríguez, G., and Camarero, J. J. (2020b). Competition modulates the response of growth to climate in pure and mixed *Abies pinsapo* subsp. *maroccana* forests in northern Morocco. *For. Ecol. Manage.* 459, 117847. doi: 10.1016/j.foreco.2019.117847

Neale, D. B., and Wheeler, N. C. (2019). *The conifers: genomes, variation and evolution* (Suiza: Springer). doi: 10.1007/978-3-319-46807-5

Ortigosa, F., Ávila, C., Rubio, L., Álverez-Garrido, L., Carreira, J. A., Cañas, R. A., et al. (2022). Transcriptome analysis and intraspecific variation in spanish fir (*Abies pinsapo* boiss.). *Int. J. Mol. Sci.* 23, 9351. doi: 10.3390/ijms23169351

Ozturk, T., Ceber, Z. P., Türkeş, M., and Kurnaz, M. L. (2015). Projections of climate change in the Mediterranean Basin by using downscaled global climate model outputs. *Int. J. Climatol.* 35, 4276–4292. doi: 10.1002/joc.4285

Peakall, R., and Smouse, P. E. (2006). GENALEX 6: genetic analysis in Excel. Population genetic software for teaching and research. *Mol. Ecol. Notes* 6, 288–295. doi: 10.1111/j.1471-8286.2005.01155.x

Peakall, R., and Smouse, P. E. (2012). GenAlEx 6.5: genetic analysis in Excel. Population genetic software for teaching and research-an update. *Bioinformatics* 28, 2537–2539. doi: 10.1093/bioinformatics/bts460

Pérez-González, A., Marconi, M., Cobo-Simón, I., Méndez-Cea, B., Perdiguero, P., Linacero, R., et al. (2018). *Abies pinsapo* boiss. Transcriptome sequencing and molecular marker detection: A novel genetic resources for a relict mediterranean fir. *For. Sci.* 64 (6), 609–617. doi: 10.1093/forsci/fxy022

Peterson, B. K., Weber, J. N., Kay, E. H., Fisher, H. S., and Hoekstra, H. E. (2012). Double digest RADseq: an inexpensive method *for de* novo SNP discovery and genotyping in model and non-model species. *PloS One* 7, e37135. doi: 10.1371/journal.pone.0037135

Pina-Martins, F., Baptista, J., Pappas, G.Jr., and Paulo, O. S. (2019). New insights into adaptation and population structure of cork oak using genotyping by sequencing. *Glob. Change Biol.* 25, 337–350. doi: 10.1111/gcb.14497

QGIS Development Team (2022). *QGIS geographic information system* (Open Source Geospatial Foundation Project). Available at: http://qgis.osgeo.org.

R Core Team (2022). *R: A language and environment for statistical computing*.

Rellstab, C., Zoller, S., Walthert, L., Lesur, I., Pluess, A. R., Graf, R., et al. (2016). Signatures of local adaptation in candidate genes of oaks (*Quercus* spp.) with respect to present and future climatic conditions. *Mol. Ecol.* 25, 5907–5924. doi: 10.1111/mec.13889

Sánchez-Robles, J. M., Balao, F., García-Castaño, J. L., Terrab, A., Navarro-Sampedro, L., and Talavera, S. (2012). Nuclear microsatellite primers for the endangered relict fir, Abies pinsapo (Pinaceae) and cross-amplification in related Mediterranean Species. *Int. J. Mol. Sci.* 13 (11), 14243–14250. doi: 10.3390/ijms131114243

Sánchez-Salguero, R., Camarero, J. J., Carrer, M., Gutiérrez, E., Alla, A. Q., Andreu-Hayles, L., et al. (2017). Climate extremes and predicted warming threaten Mediterranean Holocene fir forest refugia. *PNAS* 114 (47), E10142–E10150. doi: 10.1073/pnas.1708109114

Sánchez-Salguero, R., Ortíz, C., Covelo, F., Ochoa, V., García-Ruíz, R., Seco, J. I., et al. (2015). Regulation of water use in the Southernmost European fir (*Abies pinsapo* boiss.): drought avoidance matters. *Forests* 6, 2241–2260. doi: 10.3390/f6062241

Shirasawa, K., Hirakawa, H., and Isobe, S. (2016). Analytical workflow of double-digest restriction site-associated DNA sequencing based on empirical and in *silico* optimization in tomato. *DNA Res.* 23 (2), 145–153. doi: 10.1093/dnares/dsw004

Shiu, S. H., and Bleecker, A. B. (2003). Expansion of the receptor-like kinase/Pelle gene family and receptor-like proteins in *Arabidopsis*. *Plant Physiol.* 132, 530–543. doi: 10.1104/pp.103.021964

Terrab, A., Talavera, S., Arista, M., Paun, O., Stuessy, T. F., and Tremetsberger, K. (2007). Genetic diversity and geographic structure at chloroplast microsatellites (cpSSRs) in endangered west Mediterranean firs (*Abies* spp., Pinaceae). *Taxon* 56 (2), 409–416.

Wickham, H. (2016). *ggplot2: elegant graphics for data analysis* (New York: Springer-Verlag). Available at: https://ggplot2.tidyverse.org

Williams, A. P., Allen, C. D., Macalady, A. K., Griffin, D., Woodhouse, C. A., Meko, D. M., et al. (2013). Temperature as a potent driver of regional forest drought stress and tree mortality. *Nat. Clim. Change* 3, 292–297. doi: 10.1038/nclimate1693

Zhao, L., Hu, Y., Chong, K., and Wang, T. (2010). ARAG1, an ABA-responsive DREB gene, plays a role in seed germination and drought tolerance of rice. *Ann. Bot.* 105, 401–409. doi: 10.1093/aob/mcp303

Frontiers in
Plant Science

Cultivates the science of plant biology and its applications

The most cited plant science journal, which advances our understanding of plant biology for sustainable food security, functional ecosystems and human health.

Discover the latest Research Topics

See more →

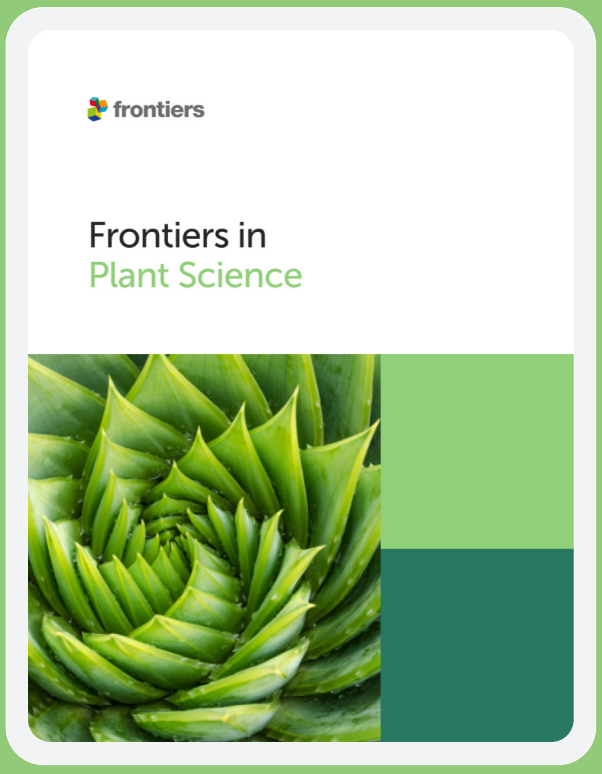

Frontiers

Avenue du Tribunal-Fédéral 34
1005 Lausanne, Switzerland
frontiersin.org

Contact us

+41 (0)21 510 17 00
frontiersin.org/about/contact